

THE JOURNAL OF PHYSICAL CHEMISTRY

Volume 69, Number 2 February 1965

Low-Temperature Thermodynamic Properties of <i>n</i> -Propyl, <i>n</i> -Butyl, and <i>n</i> -Decyl-Substituted Cyclopentanes John F. Messerly, Samuel S. Todd, and Herman L. Finke	353
The Radiation-Induced Decomposition of the Alkali and Alkaline Earth Perchlorates. I. Product Yields and Stoichiometry L. A. Prince and E. R. Johnson	359
The Radiation-Induced Decomposition of the Alkali and Alkaline Earth Perchlorates. II. Mechanism of the Decomposition L. A. Prince and E. R. Johnson	377
Lattice Energies of Ionic Crystals. II. Some Group I-A and II-A Salts Arthur Finch and P. J. Gardner	384
Effect of Hydrostatic Pressure on Gases Dissolved in Water T. Enns, P. F. Scholander, and E. D. Bradstreet	389
The Catalytic Cracking of Hexadecane—Effects of Impurities, Olefins, and Steam. W. F. Pansing	392
Diffusion-Conductance Relations and Free Volume in Molten Salts C. A. Angell	399
Infrared Spectra of Nitrilotriacetate Chelates in Aqueous Solution Yuko Tomita, Takeshi Ando, and Keihei Ueno	404
The Kinetics of the Hydrogen-Fluorine Reaction. II. The Oxygen-Inhibited Reaction Joseph B. Levy and B. K. Wesley Copeland	408
The Effect of Molecular Weight on the Melting Temperature and Fusion of Polyethylene J. G. Fatou and L. Mandelkern	417
The Kinetics of the Thermal Isomerization of Ethylcyclopropane Marcel L. Halberstadt and John P. Chesick	429
Volta Potential Studies of the Aging of Gold Surfaces R. C. Plumb and N. Thakkar	439
Pyrolysis of Magnesium Oxalate: Kinetics and Stoichiometry Peter E. Yankwich and Petros D. Zavitsanos	442
Simultaneous Independent Hydrogen-Bonding Equilibria and Self-Association in Some Halomethanes and Haloethanes A. L. McClellan and S. W. Nicksic	446
The Thermal Decomposition of Cadmium Hydroxide M. J. D. Low and A. M. Kamel	450
The Catalytic Vapor Phase Oxidation of <i>o</i> -Methylbenzyl Alcohol Theodor Vrbaški and Walter K. Mathews	457
Fast Reactions Involving Hydrogen Bonding in 2,2-Disubstituted Malonic Acids Melvin H. Miles, Edward M. Eyring, William W. Epstein, and Richard E. Ostlund	467
Cleavage Reactions in Cross-Linked Urethane Elastomers A. V. Tobolsky, V. Johnson, and W. J. MacKnight	476
The Shapes and Close-Pack Areas of Oriented Long-Chain Dipoles at the Water-Octane Interface Joseph J. Jasper and Robert D. Van Dell	481
Proton Magnetic Resonance Studies of Ten Diolefins David F. Koster and Alfred Danti	486
Generation of Catalytic Activity in Silica Gel by Ionizing Radiation. C. Barter and C. D. Wagner	491
Analytical Expressions for the Zero Pressure Thermodynamic Properties of Nitrogen Gas Including Corrections for the Latest Values of the Atomic Constants and the New Carbon-12 Atomic Weight Scale Robert E. Barieau	495
The Wien Effect in Uranyl Ion Solutions. I. Uranyl Nitrate and Perchlorate from 5 to 65°. Negative Wien Effects Joseph F. Spinnler and Andrew Patterson, Jr.	500
The Wien Effect in Uranyl Ion Solutions. II. Uranyl Fluoride from 5 to 65° Joseph F. Spinnler and Andrew Patterson, Jr.	508
The Wien Effect in Uranyl Ion Solutions. III. Uranyl Sulfate from 5 to 65° Joseph F. Spinnler and Andrew Patterson, Jr.	513

METAL

TRIFLUOROACETYLACETONATES

- Examples of these chelates have been known for some time^{1,2}, and the synthesis and spectral properties summarized³ for the Cr, Co, Rh, Al, Ga, In, Mn and Fe complexes.
- Solvent extraction studies of Zr and Hf have been reported^{4,5}, and the extractability of Cu, Fe, Al, Ni, Mn, Cr, Mg and Zn from aqueous solution studied⁶.

● GLC elution of trifluoroacetylacetonates of Be (II), Al (III), Ga (III), In (III), Sc (III), Cr (III), Fe (III), Cu (II), Rh (III), Zr (IV) and Hf (IV), has been reported by Sievers, Moshier, and others^{7,8}, and the efficient resolution of multicomponent mixtures demonstrated. Quantitative aspects of tri- and hexafluoroacetylacetonate gas chromatography have been examined by Hill and Gesser⁹, and Ross and others^{10,11}. A thorough study of this promising new method of metal analysis will be found in "Gas Chromatography of Metal Chelates" by R. W. Moshier and R. E. Sievers.¹²

● The rare earth chelates are expected to be of interest in laser studies. Gas phase reduction of others shows promise in the vapor deposition of metals at modest temperatures; as an example, copper is plated satisfactorily at only 250°C.¹³

1. R. A. Staniforth, Doctoral Dissertation, Ohio State Univ., 1943. 2. H. W. Crandall, J. R. Thomas, and J. C. Reid, U. S. At. Energy Comm. CN 2657 (1945). 3. R. C. Fay and T. S. Piper, JACS 85 500 (1963). 4. E. M. Larsen and G. A. Terry, JACS 75 1560 (1953). 5. B. G. Schultz and E. M. Larsen, JACS 72 3610 (1950). 6. William G. Scribner, private communication. 7. R. W. Moshier, J. E. Schwarberg, M. L. Morris, and R. E. Sievers, Pittsburgh Conference, March 1963. 8. R. E. Sievers, B. W. Ponder, M. L. Morris, and R. W. Moshier, Inorganic Chemistry, 2 693 (1963). 9. R. D. Hill and H. Gesser, J. Gas Chromatog. 1 10 (1963). 10. W. D. Ross, Anal. Chem. 35 1596 (1963). 11. W. D. Ross and G. Wheeler, Anal. Chem. 36 266 (1964). 12. Pergamon Press, Oxford; to be published Summer, 1965. 13. R. E. Sievers, R. W. Moshier and L. B. Spendlove, private communication.

These trifluoroacetylacetonates are prepared in high purity, and are suitable as standards for gas chromatography:

Fe (III), Cu (II), Co (II), Ni (II), Al (III), or Mg (II): \$20/25g.
60/100g.
Kit MTF-6, 5 grams each of the above: \$25.00

The following fluorinated β -Diketones are offered in the highest available purity:

	25g.	100g.
Benzoyltrifluoroacetone (BTA)	\$ 4.50	\$ 10.00
Ethyl Trifluoroacetoacetate (ETAA)	12.00	36.00
Hexafluoroacetylacetone (HFA)	12.00	36.00
2-Naphthoyltrifluoroacetone (NTA)	60.00	180.00
Thenoyltrifluoroacetone (TTA)	5.00	11.00
Trifluoroacetylacetone (TFA)	12.00	36.00
Kit TFL-6 25g. each of the above		\$80.00

(References cited imply no approval or endorsement by the investigator.)



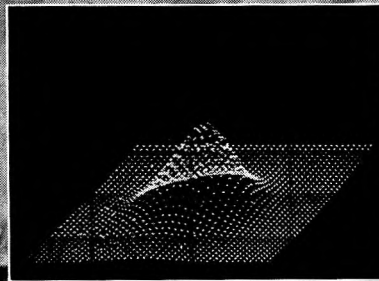
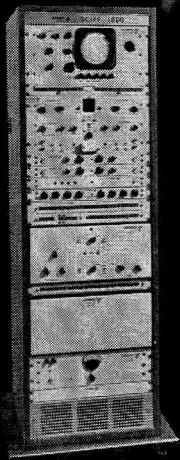
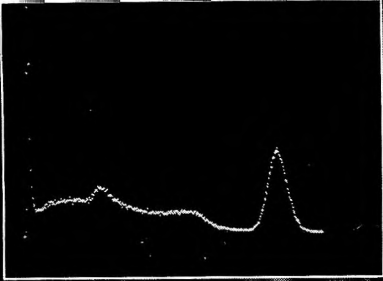
PIERCE CHEMICAL COMPANY
P.O. Box 117 Rockford, Illinois
PHONE 815-965-8013 TWX 815-398-0006

Viscosity and Self-Diffusion of Liquid Thallium from Its Melting Point to About 1300°K.	J. A. Cahill and A. V. Grosse	518
Chemical Reactions in Chromatographic Columns	John M. Matsen, John W. Harding, and Ellington M. Magee	522
Nuclear Magnetic Resonance Studies of Boron Trifluoride Addition Compounds. III. Rates and Mechanism for the Exchange of Boron Trifluoride between Ethyl Ether-Boron Trifluoride and Tetrahydrofuran-Boron Trifluoride and between Ethyl Ether-Boron Trifluoride and Ethyl Sulfide-Boron Trifluoride	A. C. Rutenberg and A. A. Palko	527
Ion Exchange on the Mineral Clinoptilolite	Darryl G. Howery and Henry C. Thomas	531
Vacuum Ultraviolet Photochemistry. VIII. Propylene	D. A. Becker, H. Okabe, and J. R. McNesby	538
Tetrapropylammonium Bromide: Ion Size Parameters in Solution and in the Solid State	H. K. Bodenseh and J. B. Ramsey	543
The Role of Copper(I) in the Kinetics of Hydrogen Reduction of Aqueous Cupric Sulfate Solutions	E. A. von Hahn and E. Peters	547
The Hydration of Tricalcium Silicate	S. A. Greenberg and T. N. Chang	553
The Use of Large Anodic Galvanostatic Transients to Evaluate the Maximum Adsorption on Platinum from Formic Acid Solutions	S. B. Brummer	562
Ionic Reactions in Gaseous Acetylene	M. S. B. Munson	572
The Nuclear Magnetic Resonance Spectra of Some 1,4-Diheterocyclohexanes	William B. Smith and Ben A. Shoulders	579
The Kinetics of Calcium Formate Pyrolysis in Potassium Bromide Matrix	K. O. Hartman and I. C. Hisatsune	583
The Dehydration of Ethanol on Aluminas of Various Specific Surface Areas	William H. Wade, Shiichiro Teranishi, and Jack L. Durham	590
The Electronegativity of Noble Gases	Bing-Man Fung	596
Sorption Rates Indicative of Structural Changes in Solid Polypeptides	W. W. Brandt and R. S. Budrys	600
Irregular Solutions of Iodine	Kozo Shinoda and Joel H. Hildebrand	605
Studies of Ions and Ion Pairs in Tetrahydrofuran Solution. Alkali Metal Salts of Tetraphenylboride	D. N. Bhattacharyya, C. L. Lee, J. Smid, and M. Szwarc	608
Reactivities and Conductivities of Ions and Ion Pairs in Polymerization Processes	D. N. Bhattacharyya, C. L. Lee, J. Smid, and M. Szwarc	612
Alternative Paths in Anionic Propagation of Ion Pairs. Effect of Solvent and Counterion	D. N. Bhattacharyya, J. Smid, and M. Szwarc	624
Electron Affinities of Aromatic Hydrocarbons in Tetrahydrofuran Solution	J. Jagur-Grodzinski, M. Feld, S. L. Yang, and M. Szwarc	628
The Conformation of the Pyranose Rings in Mono-, Di-, and Polysaccharides at High pH by Proton Magnetic Resonance Studies	V. S. R. Rao and Joseph F. Foster	636
Dye-Sensitized Photopolymerization Processes. I. The Thionine-Nitritoltripropionamide-Acrylamide System	S. Chaberek, A. Shepp, and R. J. Allen	641
Dye-Sensitized Photopolymerization Processes. II. A Comparison of the Photoactivities of Thionine and Methylene Blue	S. Chaberek and R. J. Allen	647

NOTES

An Addition Complex between Carbohydrates and Dimethyl Sulfoxide as Revealed by Proton Magnetic Resonance	V. S. R. Rao and Joseph F. Foster	656
The Wien Effect in Mixed Electrolyte Solutions. I. Reference Electrolytes	Joseph F. Spinnler and Andrew Patterson, Jr.	658
Charge-Transfer Complexes of Titanium Tetrachloride, Titanium Tetrabromide, and Vanadium Oxytrichloride with Aromatic Hydrocarbons	C. Dijkgraaf	660
The Role of Silver Nitrate Ion Pairs in the Alkyl Halide-Silver Nitrate Reaction	G. D. Parfitt, A. L. Smith, and A. G. Walton	661

expandable...



SCIPP SERIES ANALYZERS

Expandability feature, exclusive with Victoreen SCIPP series, enables user to expand SCIPP 400 single-parameter pulse height analyzers to 1600-channel single-parameter or 1600-channel multiparameter operation as his requirements dictate.

▽ Now — for the first time — there is no need to buy an analyzer with a built-in obsolescence factor. New Victoreen SCIPP series analyzers are designed to grow as your needs grow. SCIPP 400A can perform precision pulse height analysis...yet can be expanded readily to SCIPP-1600TP for multiparameter operation...or can perform other analyses. Other important features of SCIPP series analyzers: 8MC digitizing rate; silicon semi-conductors used throughout. Full details on request. Meantime check condensed specification data below.

8MC DIGITIZING RATE • PATCH PROGRAMMABLE

400, 1600, 10,000 words (word length 10^6 , decimal).

Patch program can be changed to meet virtually any requirement.

Built-in address and data register.

Random parallel access.

Serial and parallel outputs.

On-line data handling.

Memory subgrouping, transfer and overlap capability.

Digital factor-of-two display of memory live, static, static/live.

Single or dual ADC units available —

parallel transfer from ADC address register to memory address register.

Analog function of pulse input ADC's.

High-speed readout and readin.

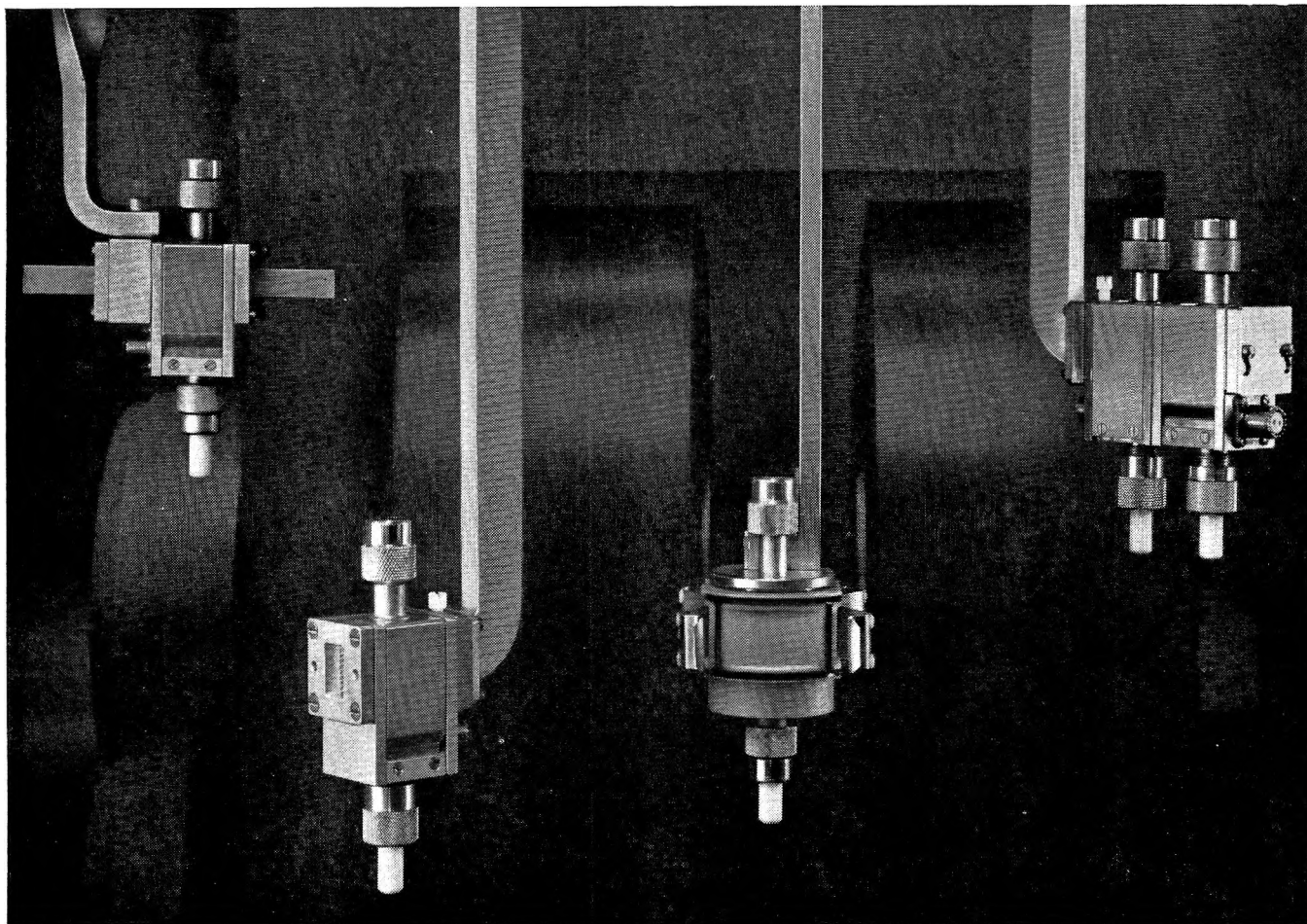
TULLAMORE



A DIVISION OF

THE VICTOREEN INSTRUMENT COMPANY
5857 West 95th Street • Oak Lawn, Illinois, U. S. A.

The Reaction of Methyl Radicals with Methyl and Methylene Fluoride	G. O. Pritchard, J. T. Bryant, and R. L. Thommarson	664
γ -Radiation-Induced Isomerization of Cyclohexanone to 5-Hexenal in the Liquid Phase	Ajit Singh and Gordon R. Freeman	666
Effects of Charge and Nickel Ion on Proton Chemical Shifts of Glycyl Peptides	Raj Mathur and R. Bruce Martin	668
The Reduction Principle in Linear Viscoelasticity	Hershel Markovitz	671
Prediction of the Heats of Activation for Viscous Flow in Simple Nonmetallic Liquids	J. O'M. Bockris and S. R. Richards	671
The Proton Nuclear Magnetic Resonance Spectrum of 2,2'-Bipyridine	F. Axtell Kramer, Jr., and Robert West	673
Dielectric Relaxation of Mixtures of Dipolar Liquids	Surendra K. Garg and Prasad K. Kadaba	674
The Mechanism of Photochromism in Metal Carbonyl Solutions	G. R. Dobson	677
Radiolysis of Cyanogen-Cyclohexane Mixtures	J. A. Knight, R. A. Stokes, and David Bowen	678
Activity Coefficients of Cadmium Chloride in Mixed Aqueous Solution with Benzyltrimethylammonium Chloride	E. Lyndol Harris	681
An Infrared Study of Complexes of Ethylamine with Ethylammonium and Copper Ions in Montmorillonite	V. C. Farmer and M. M. Mortland	683
Kinetics of Base-Catalyzed Hydrolysis of Urea	K. R. Lynn	687
Depolarization of Scattered Light by Optically Active Systems.	P. F. Mijnlief and H. Zeldenrust	689
Electric Moment of Isonicotinamide in Benzene and Dioxane Solutions	William P. Purcell and Judith A. Singer	691
The Infrared Spectra of Perfluorocyclopropane and <i>cis</i> - and <i>trans</i> -Perfluorobutene-2	Julian Heicklen, Francis Wachi, and Vester Knight	693
Multistate Dissociation and the Effect of Pressure on the Equilibrium on Magnesium Sulfate	F. H. Fisher	695
Dissociation Studies in High Dielectric Solvents. II. Conductance of Some 2-2 Salts in Formamide at 25°	Gyan P. Johari and P. H. Tewari	696
Isotope Effects in the Radiolysis and Photolysis of H ₂ O-D ₂ O Mixtures.	M. Anbar and D. Meyerstein	698
Pure Acetic Acid and Acetic Anhydride and the Electrical Conductance and Dielectric Constant of This System	R. Thomas Myers	700
On the Polarizability of Rare Gas Atoms	Ralph L. Amey	702
The Conductance of Some Alkali Metal Salts in Hydrogen Cyanide	R. H. Davies and E. G. Taylor	704



GREATER EPR VERSATILITY

WITH INTERCHANGEABLE CAVITIES

The ultimate usefulness of an EPR spectrometer depends largely on the variety of experiments you can perform with the instrument. That's why Varian designed an EPR system with four interchangeable sample cavities and a large number of cavity accessories. Each of the cavities and accessories extends the total capabilities of the system and provides optimum performance over a wide range of applications.

As new uses for EPR are discovered, Varian will continue to develop compatible cavities and accessories designed to give you the very best in system performance. We call this our "Living Instrument" policy. It's your assurance that the Varian Spectrometer bought today will still be the most versatile spectrometer available tomorrow.

Please write or call the Analytical Instrument office nearest you for complete information.

V-4531 MULTI-PURPOSE CAVITY. Will accept sample tubes with diameters up to 11 mm. Permits experiments with accessories such as aqueous sample cell, liquid mixing chamber, liquid nitrogen Dewar, electrolytic cell, and variable temperature accessory. Samples can be irradiated continuously with either u-v or visible light.

V-4532 DUAL SAMPLE CAVITY. Allows simultaneous observation of two samples. Provides a method for determining precise g value and line widths as well as hyperfine splittings and the relative and absolute number of electron spins in an unknown.

V-4534 OPTICAL-TRANSMISSION CAVITY. Allows simultaneous observation of changes in sample optical density, and observation of paramagnetic resonance, as well as simultaneous irradiation of the sample from two light sources of different wave lengths.

V-4533 ROTATING CAVITY. Particularly useful in single crystal studies with a rotating electromagnet. Compatible with Varian liquid nitrogen and variable temperature accessories. Irradiation is possible from above or below this cavity. Provides improved sensitivity for many types of samples.

 **VARIAN ASSOCIATES**
ANALYTICAL INSTRUMENT DIVISION
611 HANSEN WAY, PALO ALTO, CALIF.
In Europe: Varian A. G., Zug, Switzerland

THE JOURNAL OF PHYSICAL CHEMISTRY

Registered in U. S. Patent Office © Copyright, 1965, by the American Chemical Society

VOLUME 69, NUMBER 2 FEBRUARY 15, 1965

Low-Temperature Thermodynamic Properties of *n*-Propyl-, *n*-Butyl-, and *n*-Decyl-Substituted Cyclopentanes

by John F. Messerly, Samuel S. Todd, and Herman L. Finke

Contribution No. 135 from the Thermodynamics Laboratory of the Bartlesville Petroleum Research Center, Bureau of Mines, U. S. Department of the Interior, Bartlesville, Oklahoma (Received October 1, 1964)

The heat capacities in the range 12–370°K., heats of fusion, triple points, and purity of *n*-propylcyclopentane, *n*-butylcyclopentane, and *n*-decylcyclopentane were measured in an adiabatic calorimeter. From these data the thermodynamic functions, $(G_s - H^{\circ}_0)/T$, $(H_s - H^{\circ}_0)/T$, $H_s - H^{\circ}_0$, S_s , and C_s , were calculated for the solid and liquid states at selected temperatures in the range 10–370°K. The entropies of these compounds in the ideal gas state at 298.15°K. were calculated using a Cox equation fitted to vapor pressure data from the literature. The average entropy increments per methylene group from *n*-butyl- through *n*-decylcyclopentane in the liquid and ideal gas states were found to be 7.76 and 9.33 cal. deg.⁻¹ mole⁻¹, respectively, in close agreement with the constant value for higher members of the normal alkane series of hydrocarbons.

Introduction

In the continuing program of thermodynamics research on hydrocarbons and related substances conducted in this laboratory, the low-temperature thermal properties of a number of homologous series of compounds have been determined. Because the effects of systematic errors can be minimized by utilizing the same apparatus and methods in all the measurements, the low-temperature studies yield incremental results of greater precision than those derivable from the determinations of a number of different investigators. Measurements on nine *n*-paraffins by Finke, *et al.*,¹ and on seven selected 1-olefins from C₆ to C₁₆ by McCullough, *et al.*,² have shown that the entropy increment per methylene group in the liquid state at 298.15°K. is a constant within the limits of precision of the meas-

urements. Person and Pimentel³ have shown the same relation to hold for the ideal gas state for the *n*-paraffins C₈ through C₁₆. From the entropy of *n*-heptane,⁴ the entropies of the *n*-alkanes from C₈ to C₁₆,¹ and unpublished data on *n*-pentane, *n*-hexane, *n*-heptadecane, and *n*-octadecane, the entropy increment per methylene group in *n*-alkanes from C₅ to C₁₈ has been found to be essentially constant. With the view of verifying the

(1) H. L. Finke, M. E. Gross, G. Waddington, and H. M. Huffman, *J. Am. Chem. Soc.*, **76**, 333 (1954).

(2) J. P. McCullough, H. L. Finke, M. E. Gross, J. F. Messerly, and G. Waddington, *J. Phys. Chem.*, **61**, 289 (1957).

(3) W. B. Person and G. C. Pimentel, *J. Am. Chem. Soc.*, **75**, 532 (1953).

(4) J. P. McCullough and J. F. Messerly, U. S. Bureau of Mines Bulletin 596, U. S. Government Printing Office, Washington, D. C., 1961.

constancy of the value of the entropy increment for higher members of other *n*-alkyl series, studies were undertaken on several series of *n*-alkyl-substituted ring compounds. The results of the first of these investigations on the substituted cyclopentanes are presented in this paper. As the first members of the series show irregular increments in both the liquid and ideal gas states, the *n*-propyl, *n*-butyl, and *n*-decyl substituents were chosen for these studies.

Discussion

From the heat capacities and heats of fusion of the three compounds studied, the entropies in the liquid phase at 298.15°K. were calculated. From these values, together with the vapor pressure and the entropy of vaporization, the entropies of the compounds in the ideal gas state at 1 atm. were calculated. These entropy values are presented in Table I with the average entropy increment per methylene group, $\Delta S/\text{CH}_2$.

Table I: Molal Entropies at 298.15°K. (cal. deg.⁻¹ mole⁻¹)

Compound	Liquid		Ideal gas	
	S°	$\Delta S/\text{CH}_2$	S°	$\Delta S/\text{CH}_2$
<i>n</i> -Propylcyclopentane	74.29	7.89	99.06	9.40
<i>n</i> -Butylcyclopentane	82.18	7.76	108.46	9.33
<i>n</i> -Decylcyclopentane	128.71		164.45	

It will be noted in Table I that the increment from *n*-propyl to *n*-butyl, 7.89 cal. deg.⁻¹ mole⁻¹, is somewhat larger than the average increment from *n*-butyl to *n*-decyl, 7.76 cal. deg.⁻¹ mole⁻¹. This latter value agrees quite well with the average increment of 7.74 cal. deg.⁻¹ mole⁻¹ found for the liquid *n*-paraffins from C₅ to C₁₈ in this laboratory. For the ideal gas, the average methylene increment from *n*-butyl- through *n*-decylcyclopentane is 9.33 cal. deg.⁻¹ mole⁻¹, in close agreement with the average value of the methylene increment of 9.31 cal. deg.⁻¹ mole⁻¹ calculated for the C₈ to C₁₆ normal paraffins in the ideal gas state by Person and Pimentel.³ For alkyl cyclopentanes lower than *n*-butylcyclopentane in both the liquid and ideal gas states, the entropy differences per CH₂ group at 298.15°K. are irregular.

Experimental

Apparatus and Physical Constants. The low-temperature calorimetric measurements were made with apparatus described by Huffman and co-workers.⁵ The "1951 International Atomic Weights"⁶ and values of the fundamental physical constants⁷ were used. Measurements of temperature were made with platinum re-

sistance thermometers calibrated in terms of the International Temperature Scale of 1948⁸ from 90 to 400°K., and Celsius temperatures were converted to Kelvin temperatures by the addition of 273.15°.⁹ From 11 to 90°K., temperature measurements were made in terms of the provisional scale of the National Bureau of Standards.¹⁰ Energy was measured in joules and converted to calories by the relation, 1 calorie = 4.184 (exactly) joules. Measurements of mass, electrical potential, and resistance were made in terms of standard devices calibrated at the National Bureau of Standards.

Some of the results in this paper were originally calculated with physical constants and temperatures related to the definition 0° = 273.16°K. Temperatures reported here are in terms of the newer definition,⁹ but only part of the experimental results were recalculated; however, numerical inconsistencies less than the precision of the experimental data may have been introduced by this procedure.

Materials. All of the samples used in this study were American Petroleum Institute Research hydrocarbons.¹¹ The samples were frozen in the ampoules as received, and the liquid just above the melting point was found to show no traces of ice. Each sample was transferred to the calorimeter without exposure to oxygen or water.

Results

Heat Capacities in the Solid and Liquid States. The heat capacities of *n*-propylcyclopentane and *n*-butylcyclopentane were measured in the solid and liquid states over the approximate range 12 to 370°K. The values of heat capacity in the liquid and solid states for *n*-decylcyclopentane were measured from 12 to 320°K. The observed values of heat capacity at saturation pressure, C_s , are recorded for each compound in Table II. The temperature increments used in the measurements were small enough to obviate

(5) H. M. Huffman, *Chem. Rev.*, **40**, 1 (1947); H. M. Huffman, S. S. Todd, and G. D. Oliver, *J. Am. Chem. Soc.*, **71**, 584 (1949); D. W. Scott, D. R. Douslin, M. E. Gross, G. D. Oliver, and H. M. Huffman, *ibid.*, **74**, 883 (1952).

(6) E. Wichers, *ibid.*, **74**, 2447 (1952).

(7) F. D. Rossini, F. T. Gucker, Jr., H. L. Johnston, L. Pauling, and G. W. Vinal, *ibid.*, **74**, 2699 (1952).

(8) H. F. Stimson, *J. Res. Natl. Bur. Std.*, **42**, 209 (1949).

(9) H. F. Stimson, *Am. J. Phys.*, **23**, 614 (1955).

(10) H. J. Hoge and F. G. Brickwedde, *J. Res. Natl. Bur. Std.*, **22**, 351 (1939).

(11) These samples of American Petroleum Institute Research hydrocarbons were made available through the American Petroleum Institute Research Project 44 on the "Collection, Analysis and Calculation of Data on Properties of Hydrocarbons" and were purified by the American Petroleum Institute Research Project 6 on the "Analysis, Purification, and Properties of Hydrocarbons."

corrections for nonlinear variation of C_s with T and were omitted, except as noted in Table II. The precision uncertainty of the results was, in general, less than 0.1%, and above 30°K. the accuracy uncertainty should

Table II: Heat Capacity (cal. deg.⁻¹ mole⁻¹)

T^a	C_s^b	T^a	C_s^b	T^a	C_s^b
<i>n</i> -Propylcyclopentane					
Crystal					
12.12	0.873	28.39	5.748	93.84	20.084
12.37	0.936	29.56	6.114	94.37	20.168
13.16	1.124	32.58	7.078	99.59	20.900
13.52	1.203	36.00	8.129	105.61	21.719
14.32	1.415	39.64	9.180	111.40	22.498
14.82	1.552	43.86	10.335	117.43	23.287
15.62	1.763	48.56	11.551	119.73	23.568
16.26	1.941	53.35	12.687	123.71	24.087
17.08	2.189	55.78	13.244	124.85	24.193
17.88	2.412	58.43	13.828	125.05	24.226
18.76	2.679	60.90	14.369	129.78	24.841
19.57	2.935	66.20	15.444	130.04	24.843
20.68	3.282	71.55	16.419	135.08	25.490
21.55	3.563	77.01	17.380	135.67	25.564
23.41	4.159	82.61	18.363	141.79	26.389 ^c
23.96	4.334	88.36	19.284	144.46	26.730 ^c
25.81	4.934	88.38	19.303	149.13	27.831 ^c
26.70	5.210				
Liquid					
162.15	41.560	220.45	44.474	300.27	51.912
166.52	41.702	230.96	45.257	302.37	52.147
168.15	41.768	241.73	46.137	310.88	53.103
173.51	41.934	252.32	47.057	321.68	54.337
175.10	41.997	262.70	48.018	332.26	55.544
181.44	42.251	272.89	49.031	343.00	56.792
189.76	42.628	282.90	50.050	353.89	58.061
199.82	43.166	292.72	51.109	364.57	59.367
210.21	43.780				
<i>n</i> -Butylcyclopentane					
Crystal					
11.34	0.884	28.31	6.216	102.73	23.936
11.80	1.020	28.73	6.363	108.67	24.851
12.47	1.170	32.48	7.669	114.39	25.724
13.14	1.353	36.44	9.001	119.91	26.555
13.83	1.532	42.93	11.059	125.17	27.311
14.41	1.704	49.70	13.039	125.70	27.419
15.43	1.978	53.83	14.146	132.25	28.361
15.74	2.065	54.46	14.308	132.70	28.445
17.26	2.519	58.55	15.349	132.79	28.442
18.11	2.775	63.85	16.651	139.07	29.366
19.00	3.065	69.45	17.875	140.14	29.561
20.90	3.696	75.11	19.033	140.62	29.630
20.93	3.693	80.81	20.188	140.77	29.636
23.10	4.431	86.03	21.205	145.14	30.359
23.10	4.440	86.59	21.298	147.92	30.800
25.61	5.307	91.68	22.163	150.48	31.286 ^d
25.62	5.298	97.06	23.027	154.28	32.152 ^d

Table II Continued

T^a	C_s^b	T^a	C_s^b	T^a	C_s^b
Liquid					
167.87	48.315	229.71	51.688	298.75	58.699
173.24	48.471	239.51	52.516	307.68	59.788
181.25	48.795	249.16	53.392	317.35	60.967
190.45	49.158	259.09	54.340	327.43	62.200
190.91	49.197	269.26	55.384	337.31	63.454
199.88	49.653	279.26	56.464	347.58	64.763
209.65	50.248	289.09	57.568	357.66	66.026
219.76	50.928	298.24	58.654	367.57	67.262
<i>n</i> -Decylcyclopentane					
Crystal					
11.30	1.148	78.55	30.720	171.21	53.102
12.68	1.616	85.11	32.852	171.37	53.202
12.79	1.641	86.26	33.180	171.53	53.188
14.38	2.214	88.72	33.911	172.72	53.463
14.75	2.359	91.90	34.789	175.07	54.043
16.15	2.919	92.79	34.993	179.97	55.201
16.75	3.160	94.68	35.446	180.24	55.306
18.08	3.741	99.05	36.646	183.65	56.127
19.01	4.168	99.47	36.726	186.36	56.644
20.44	4.853	106.26	38.483	188.43	57.266
21.44	5.356	114.00	40.354	188.67	57.376
23.17	6.206	122.20	42.291	193.97	58.629
23.77	6.510	128.82	43.654	197.02	59.484
25.90	7.602	130.42	44.157	200.55	60.414
26.19	7.744	137.18	45.577	201.46	60.676
28.54	8.953	139.04	46.061	203.42	61.374
28.78	9.088	144.72	47.262	208.74	62.869
32.05	10.830	147.33	47.903	209.49	63.149
35.99	12.943	147.42	47.818	215.79	65.120
39.99	15.037	152.47	49.029	223.11	67.779
44.51	17.454	154.99	49.608	223.76	68.007
49.54	19.856	155.05	49.470	227.41	69.350
54.71	22.140	158.64	50.192	229.40	69.227
54.77	22.112	159.97	50.719	229.73	70.518
55.04	22.258	162.85	51.369	233.07	71.952 ^e
59.79	24.063	163.15	51.488	239.04	74.934 ^e
60.71	24.419	166.18	51.972	241.07	76.553 ^e
65.43	26.238	169.10	52.566	246.41	82.426 ^e
71.83	28.450				
Liquid					
258.18	97.041	271.95	98.228	299.44	102.107
258.37	97.070	273.87	98.446	301.64	102.534
264.82	97.506	282.67	99.591	311.43	104.163
265.34	97.554	292.04	100.968	321.40	105.967

^a T is the mean temperature (in °K.) of each heat capacity measurement. ^b C_s is the heat capacity of the condensed phase at saturation pressure. Values of C_s for crystals are *not* corrected for effects of premelting caused by impurities. ^{c,d,e} The temperature increments of these measurements are in the order of increasing T , °K.: (c) 6.446, 4.768, 4.611; (d) 5.275, 6.246; (e) 9.090, 9.790, 6.912, 4.941.

not exceed 0.2%, except in regions near phase transformations. Near phase changes, data for the solid

Table III: Equations for Heat Capacity of Liquid Using $C_s = A + BT + CT^2 + DT^3$ (cal. deg. $^{-1}$ mole $^{-1}$)

Compound	A	B	$C \times 10^4$	$D \times 10^7$	Range, °K.	Av. dev., cal.	Max. dev., cal.
<i>n</i> -Propylcyclopentane	54.288	-0.20145	8.9720	-8.4105	175-365	0.01	0.03
<i>n</i> -Butylcyclopentane	67.971	-0.28063	11.710	-11.2270	210-370	0.01	0.02
<i>n</i> -Decylcyclopentane	398.61	-3.1295	104.27	-109.63	260-320	0.02	0.04

state may be less precise and less accurate owing to rapid changes in C_s with T , slow equilibration, or uncertainties caused by the presence of impurities.

Empirical equations were obtained to represent the heat capacity of each compound in the liquid state. The constants for these equations are listed in Table III, together with values of the deviations from observed data as an estimate of reliability.

Heats of Fusion, Triple Point Temperatures, and Purity of Samples. The heats of fusion, ΔH_m , were determined from the heat capacity data and enthalpy measurements made over finite temperature intervals that included the triple point temperature. The average of two or more measurements for each compound is listed in Table IV.

Table IV: Triple Point Temperatures, Heats of Fusion, and Cryoscopic Constants

Compound	T_{tp} , °K.	ΔH_m , cal. mole $^{-1}$	A, deg. $^{-1}$	B, deg. $^{-1}$
<i>n</i> -Propylcyclopentane	155.79	2398 ± 5^a	0.04971	0.00360
<i>n</i> -Butylcyclopentane	165.18	2704 ± 2^a	0.04987	0.00340
<i>n</i> -Decylcyclopentane	251.02	7917 ± 10^a	0.06323	0.00330

^a The uncertainty indicated is the maximum deviation from the mean.

The triple point temperature and sample purity for each compound were determined from studies of the equilibrium melting temperature as a function of the fraction of sample melted.¹² The resulting melting point summaries are given for the three compounds in Table V. In all cases the equilibrium temperatures, T_F , were plotted as functions of $1/F$, the reciprocal of the fraction of the total sample in the liquid state. The triple point temperatures, T_{tp} , were determined by linear extrapolations to zero value of $1/F$. If the impurities form ideal solutions in the liquid phase and are insoluble in the solid phase, the relation between mole fraction of total impurity, N_2^* , and melting point depression, $\Delta T = T_{tp} - T_F$, is¹³

$$-\ln(1 - N_2) = A\Delta T(1 + B\Delta T + \dots) \quad (1)$$

where $N_2 = N_2^*/F$. The cryoscopic constants, $A = \Delta H_m/RT_{tp}^2$ and $B = 1/T_{tp} - \Delta C_m/2\Delta H_m$, were calculated from the values of ΔH_m and T_{tp} in Table IV and from the values of ΔC_m , the difference between the heat capacities of the compound in the solid and liquid states at the triple point, obtained from data in Table VI (discussed in the following section). Values of A and B are included in Table IV. Impurity values given in Table V were calculated using eq. 1 in its simplified form (for $N_2^* \ll 1$), $N_2^* = A_F\Delta T$.

Table V: Melting Point Summaries

F	1/F	T_F , °K.	T_{calcd} , °K.
<i>n</i> -Propylcyclopentane (impurity = 0.05 mole %)			
0.1107	9.033	155.6938 ^a	155.6938
0.2628	3.805	155.7480	155.7480
0.5006	1.998	155.7667	155.7667
0.7045	1.419	155.7748	155.7727
0.9084	1.101	155.7760 ^a	155.7760
1.000	1.000		155.7770
Pure	0		155.7874
<i>n</i> -Butylcyclopentane (impurity = 0.02 mole %)			
0.1093	9.149	165.1471 ^a	165.1471
0.2639	3.789	165.1644 ^a	165.1644
0.5073	1.971	165.1695	165.1703
0.7064	1.416	165.1716	165.1721
0.9054	1.104	165.1750	165.1731
1.0000	1.000		165.1734
Pure	0		165.1766
<i>n</i> -Decylcyclopentane (impurity = 0.10 mole %)			
0.0827	12.086	250.8765	250.8267
0.2319	4.312	250.9576	250.9517
0.4918	2.033	250.9883 ^a	250.9883
0.7085	1.411	250.9982	250.9983
0.9251	1.081	251.0036 ^a	251.0036
1.0000	1.000		251.0049
Pure	0		251.0210

^a Straight lines through these points were extrapolated to $1/F = 0$ to calculate triple point temperature.

(12) J. P. McCullough and G. Waddington, *Anal. Chim. Acta*, **17**, 80 (1957).

(13) A. R. Glasgow, Jr., A. J. Streiff, and F. D. Rossini, *J. Res. Natl. Bur. Std.*, **35**, 355 (1945).

Chemical Thermodynamic Properties in the Solid and Liquid States. The low-temperature data for *n*-propylcyclopentane, *n*-butylcyclopentane, and *n*-decylcyclo-

Table VI: Thermodynamic Functions for Condensed Phases^a (Units: cal., mole, °K.)

<i>T</i> , °K.	$-(G_s - H^{\circ}_s)/T$, cal. deg. ⁻¹ mole ⁻¹	$(H_s - H^{\circ}_s)/T$, cal. deg. ⁻¹ mole ⁻¹	$(H_s - H^{\circ}_s)$, cal. mole ⁻¹	<i>S_s</i> , cal. deg. ⁻¹ mole ⁻¹	<i>C_s</i> , cal. deg. ⁻¹ mole ⁻¹
<i>n</i> -Propylcyclopentane					
Crystal					
10	0.043	0.128	1.283	0.171	0.511
15	0.143	0.416	6.239	0.559	1.589
20	0.324	0.889	17.786	1.213	3.068
25	0.584	1.485	37.11	2.069	4.670
30	0.912	2.148	64.43	3.060	6.254
35	1.296	2.848	99.67	4.144	7.827
40	1.723	3.562	142.47	5.285	9.278
45	2.184	4.273	192.29	6.457	10.629
50	2.669	4.974	248.67	7.643	11.901
60	3.697	6.321	379.2	10.018	14.173
70	4.767	7.588	531.1	12.355	16.144
80	5.859	8.768	701.4	14.627	17.909
90	6.956	9.877	888.9	16.833	19.542
100	8.051	10.915	1,091.5	18.966	20.959
110	9.137	11.890	1,307.8	21.027	22.302
120	10.212	12.812	1,537.4	23.024	23.600
130	11.272	13.690	1,779.6	24.962	24.841
140	12.318	14.529	2,034.0	26.847	26.023
150	13.348	15.335	2,300.2	28.683	27.204
155.79	13.938	15.788	2,459.6	29.726	27.883
Liquid					
155.79	13.938	31.181	4,857.7	45.119	41.38
160	14.77	31.45	5,032	46.22	41.50
170	16.69	32.05	5,448	48.74	41.82
180	18.54	32.60	5,868	51.14	42.19
190	20.32	33.12	6,292	53.44	42.64
200	22.03	33.61	6,721	55.64	43.17
210	23.68	34.08	7,156	57.76	43.76
220	25.28	34.53	7,597	59.81	44.44
230	26.82	34.98	8,045	61.80	45.18
240	28.32	35.42	8,501	63.74	45.99
250	29.77	35.86	8,965	65.63	46.85
260	31.19	36.30	9,438	67.49	47.76
270	32.57	36.74	9,920	69.31	48.74
273.15	33.00	36.88	10,074	69.88	49.06
280	33.91	37.19	10,413	71.10	49.75
290	35.23	37.64	10,915	72.87	50.80
298.15	36.28	38.01	11,333	74.29	51.69
300	36.51	38.10	11,429	74.61	51.89
310	37.77	38.56	11,953	76.33	53.00
320	39.00	39.03	12,489	78.03	54.14
330	40.21	39.50	13,036	79.71	55.29
340	41.39	39.99	13,595	81.38	56.44
350	42.56	40.47	14,165	83.03	57.61
360	43.70	40.97	14,747	84.67	58.80
370	44.84	41.46	15,341	86.30	59.98

Table VI *Continued*

<i>T</i> , °K.	$-(G_s - H^{\circ}_s)/T$, cal. deg. ⁻¹ mole ⁻¹	$(H_s - H^{\circ}_s)/T$, cal. deg. ⁻¹ mole ⁻¹	$(H_s - H^{\circ}_s)$, cal. mole ⁻¹	<i>S_s</i> , cal. deg. ⁻¹ mole ⁻¹	<i>C_s</i> , cal. deg. ⁻¹ mole ⁻¹
<i>n</i> -Butylcyclopentane					
Crystal					
10	0.054	0.162	1.619	0.216	0.640
15	0.178	0.509	7.629	0.687	1.852
20	0.393	1.030	20.605	1.423	3.383
25	0.690	1.670	41.75	2.360	5.090
30	1.057	2.381	71.43	3.438	6.798
35	1.480	3.137	109.79	4.617	8.522
40	1.949	3.913	156.53	5.862	10.155
45	2.455	4.692	211.14	7.147	11.688
50	2.989	5.464	273.17	8.453	13.111
60	4.119	6.959	417.5	11.078	15.718
70	5.299	8.378	586.4	13.677	17.988
80	6.506	9.707	776.5	16.213	20.023
90	7.722	10.961	986.4	18.683	21.885
100	8.938	12.135	1,213.4	21.073	23.500
110	10.147	13.239	1,456.2	23.386	25.050
120	11.344	14.287	1,714.4	25.631	26.570
130	12.527	15.289	1,987.5	27.816	28.036
140	13.696	16.252	2,275.2	29.948	29.522
150	14.849	17.190	2,578.4	32.039	31.150
160	15.988	18.117	2,898.7	34.105	32.92
165.18	16.574	18.597	3,072	35.171	33.86
Liquid					
165.18	16.574	34.966	5,776	51.540	48.23
170	17.58	35.34	6,008	52.92	48.38
180	19.62	36.08	6,493	55.70	48.73
190	21.59	36.75	6,983	58.34	49.15
200	23.49	37.39	7,477	60.88	49.66
210	25.33	37.98	7,976	63.31	50.28
220	27.11	38.56	8,482	65.67	50.95
230	28.84	39.11	8,996	67.95	51.72
240	30.51	39.66	9,517	70.17	52.56
250	32.14	40.19	10,047	72.33	53.47
260	33.73	40.72	10,587	74.45	54.44
270	35.28	41.24	11,136	76.52	55.47
273.15	35.76	41.41	11,312	77.17	55.80
280	36.79	41.77	11,696	78.56	56.55
290	38.26	42.30	12,267	80.56	57.68
298.15	39.44	42.74	12,742	82.18	58.64
300	39.71	42.83	12,850	82.54	58.86
310	41.12	43.37	13,444	84.49	60.07
320	42.50	43.91	14,051	86.41	61.29
330	43.86	44.46	14,670	88.32	62.52
340	45.20	45.00	15,302	90.20	63.79
350	46.51	45.56	15,946	92.07	65.07
360	47.80	46.12	16,603	93.92	66.32
370	49.08	46.68	17,273	95.76	67.58
<i>n</i> -Decylcyclopentane					
Crystal					
10	0.069	0.207	2.07	0.276	0.820
15	0.229	0.661	9.92	0.890	2.440
20	0.511	1.370	27.40	1.881	4.635

Table VI Continued

$T, ^\circ\text{K.}$	$-(G_s - H^\circ_s)/T,$ cal. deg. ⁻¹ mole ⁻¹	$(H_s - H^\circ_s)/T,$ cal. deg. ⁻¹ mole ⁻¹	$(H_s - H^\circ_s),$ cal. mole ⁻¹	$S_s,$ cal. deg. ⁻¹ mole ⁻¹	$C_s,$ cal. deg. ⁻¹ mole ⁻¹
25	0.910	2.271	56.77	3.181	7.135
30	1.414	3.295	98.85	4.709	9.715
35	2.004	4.406	154.21	6.410	12.425
40	2.668	5.571	222.85	8.239	15.035
45	3.394	6.772	304.8	10.166	17.690
50	4.170	7.984	399.2	12.154	20.060
60	5.836	10.352	621.1	16.188	24.135
70	7.602	12.592	881.5	20.194	27.826
80	9.423	14.708	1,176.7	24.131	31.20
90	11.272	16.716	1,504.4	27.988	34.26
100	13.14	18.604	1,860.4	31.74	36.88
110	14.99	20.381	2,241.9	35.37	39.39
120	16.84	22.065	2,647.8	38.90	41.77
130	18.66	23.67	3,077	42.33	44.06
140	20.47	25.21	3,529	45.68	46.28
150	22.27	26.68	4,003	48.95	48.48
160	24.04	28.11	4,498	52.15	50.65
170	25.78	29.50	5,016	55.28	52.85
180	27.50	30.87	5,556	58.37	55.24
190	29.21	32.21	6,121	61.42	57.67
200	30.90	33.55	6,710	64.45	60.26
210	32.57	34.89	7,327	67.46	63.26
220	34.22	36.26	7,976	70.48	66.61
230	35.86	37.66	8,661	73.52	70.40
240	37.49	39.12	9,388	76.61	75.30
250	39.13	40.71	10,179	79.84	84.30
251.02	39.29	40.90	10,267	80.19	85.84
Liquid					
251.02	39.29	72.44	18,184	111.73	96.69
260	41.85	73.28	19,052	115.13	97.16
270	44.63	74.18	20,028	118.81	98.00
273.15	45.50	74.45	20,338	119.95	98.36
280	47.34	75.05	21,014	122.39	99.22
290	49.99	75.91	22,013	125.90	100.65
298.15	52.11	76.60	22,839	128.71	101.94
300	52.58	76.76	23,027	129.34	102.24
310	55.11	77.61	24,058	132.72	103.99
320	57.59	78.46	25,107	136.05	105.72

^a The values tabulated are the Gibbs energy function, enthalpy function, enthalpy, entropy, and heat capacity of the condensed phases at saturation pressure.

pentane were used in calculating values of the Gibbs energy function, enthalpy function, enthalpy, entropy, and heat capacity for the compounds in the solid and liquid states at selected temperatures from 10 to 370°K. The values at 10°K. were calculated from Debye functions, the parameters of which were evaluated from the heat capacity data between 11 and 20°K.¹⁴ Thermodynamic properties above 10°K. were calculated from values of heat and temperature of phase changes and from appropriate integration of smoothed values of C_s at regular intervals. The results are in Table VI. Corrections for the effects of premelting were applied as necessary in computing the "smoothed" data in Table VI.

Vapor Pressures and Calculation of Heats of Entropies of Vaporization. In order to calculate the entropy and enthalpy of the compounds in the ideal gas state at 298.15°K., values of the heat of vaporization and vapor pressure were required for each compound. For *n*-propylcyclopentane the value of Osborne and Ginnings¹⁵ was used. For the other compounds studied, experimentally determined heats of vaporization were not available. To obtain more reliable heats of vaporization, Cox equations were fitted to the experimentally determined vapor pressures from the literature. Unpublished results from this laboratory have shown that the Cox equation can be fitted to the experimental data and extrapolated with more precision than the Antoine equation as used by Rossini and co-workers.¹⁶ From the Clapeyron equation and the value of dp/dT determined from the Cox equation, the heats and entropies of vaporization were calculated. Corrections for

Table VIII: Heats and Entropies of Vaporization at 298.15°K.

Compound	Calcd.		Lit. ΔH_{vap} , cal. mole ⁻¹
	ΔH_{vap} , cal. mole ⁻¹	ΔS_{vap} , cal. deg. ⁻¹ mole ⁻¹	
<i>n</i> -Propylcyclopentane	9,802	32.88	9820.4 ¹⁶
<i>n</i> -Butylcyclopentane	10,949	36.72	
<i>n</i> -Decylcyclopentane	17,873	59.95	

Table VII: Vapor Pressure Expressed by the Cox Equation, $\log p$ (mm.) = $A(1 - B/T)^a$

Compound	$B, ^\circ\text{K.}$	a	$b \times 10^3$	$c \times 10^6$	Dev. from obsd. data, mm.		
					Av.	Max.	Range, mm.
<i>n</i> -Propylcyclopentane	404.099	0.841060	-0.631123	0.539617	0.04	+0.28	48-780
<i>n</i> -Butylcyclopentane	429.750	0.885910	-0.791049	0.714893
<i>n</i> -Decylcyclopentane	552.526	0.968115	-0.735153	0.489083	0.06	0.11	52-758

^a B is n.b.p. in °K. and A is defined by $\log A = a + bT + cT^2$, $T, ^\circ\text{K.}$

effects of gas imperfection were negligible and omitted. The constants for the Cox equation and maximum and average deviations from the experimentally observed data are given for the three compounds in Table VII.

The heats of vaporization at 298.15°K. calculated for the compounds are given in Table VIII, together with the experimentally determined value of Osborne and Ginnings¹⁵ for *n*-propylcyclopentane.

Acknowledgments. The assistance of Mrs. M. E. Gross, Mrs. T. C. Kincheloe, and Dr. J. P. McCullough

with some of the measurements is gratefully acknowledged.

(14) The number of degrees of freedom used and the characteristic Debye temperature, respectively, were determined as follows: *n*-propylcyclopentane, 6.0 and 121.8°; *n*-butylcyclopentane, 5.0 and 105.9°; *n*-decylcyclopentane, 7.5 and 111.8°.

(15) N. S. Osborne and D. C. Ginnings, *J. Res. Natl. Bur. Std.*, **39**, 468 (1947).

(16) (a) *n*-Propylcyclopentane: A. F. Forziati, W. R. Norris, and F. D. Rossini, *ibid.*, **43**, 55 (1949); (b) *n*-decylcyclopentane: D. L. Camin, A. F. Forziati, and F. D. Rossini, *J. Phys. Chem.*, **58**, 440 (1954); (c) *n*-butylcyclopentane: unpublished data, American Petroleum Institute Research Project 44.

The Radiation-Induced Decomposition of the Alkali and Alkaline Earth Perchlorates. I. Product Yields and Stoichiometry^{1a}

by L. A. Prince and E. R. Johnson^{1b}

Chemistry Department, Stevens Institute of Technology, Hoboken, New Jersey (Received March 5, 1964)

The radiation-induced decomposition of the alkali and alkaline earth perchlorates has been studied. ClO_3^- , ClO_2^- , ClO_2 , ClO^- , Cl^- , O_2 , and metal oxide (or superoxide), and possibly some ClO_3 , are the products. Good stoichiometry has been obtained. The order of decreasing $G_{\text{ClO}_4^-}^0$ is $\text{Cs} > \text{Rb} > \text{Mg} > \text{Sr} > \text{Na} > \text{Ca} > \text{K} > \text{Li} > \text{Ba}$.

Previous studies on the radiation-induced decomposition of the solid inorganic perchlorates have indicated that chlorine in almost all of its oxidation states appears in the products of the decomposition. Heal² identified chloride, chlorate, and oxygen, and indicated the possible presence of hypochlorite and chlorite as products in the radiolysis of solid KClO_4 by X-rays. He found a G value of about 5 for perchlorate decomposition. Bakerkin³ found a G value of 1.1 for chlorate yield from the radiolysis of KClO_4 by cobalt-60 γ -rays. Heller and Cole⁴ reported on the presence, as determined by electron spin resonance, of ClO_2 and ClO_3 in single crystals of KClO_4 irradiated with X-rays and γ -rays.

More extensive work has been done on the radiolysis of the inorganic chlorates. Heal⁵ has reported chloride, hypochlorite, chlorite, oxygen, Cl_2O_6 , and ClO_2 in the

radiolysis of KClO_3 . Bakerkin,⁶ however, reported only the presence of chlorite, chloride, and oxygen as products. Burchill,⁷ who studied the decomposition of NaClO_3 , KClO_3 , and $\text{Ba}(\text{ClO}_3)_2$ by cobalt-60 γ -rays

(1) (a) Research supported by A.E.C. contract AT-30-1-1824; (b) National Standard Reference Data Program, National Bureau of Standards, Washington 25, D. C.

(2) H. G. Heal, *Can. J. Chem.*, **37**, 979 (1959).

(3) A. S. Bakerkin, *Tr. 1-go Vses. Soveshch. po Radiation, Khim., Akad. Nauk SSSR Otd. Khim. Nauk*, 1957, 167 (1958).

(4) (a) C. Heller and T. Cole, *Chem. Eng. News*, **39**, 38 (1961); (b) T. Cole, *Proc. Natl. Acad. Sci. U. S. A.*, **46**, 506 (1960).

(5) H. G. Heal, *Can. J. Chem.*, **31**, 91 (1953).

(6) A. S. Bakerkin, "The Action of Ionizing Radiation on Inorganic and Organic Systems," Moscow, Academy of Sciences of the U.S.S.R. Press, 1958, p. 187.

(7) C. E. Burchill, *Nature*, 191, 194 (1962) (reported by P. F. Patrick and K. J. McCallum).

reports chlorite, chloride, oxygen, hypochlorite, chlorine dioxide, and perchlorate as the products.

The wide variations found in both products and yields by different workers for the decomposition of oxychlorine compounds may possibly be attributed to the instability of the products and to the analytical procedures used to identify them. This systematic study of the perchlorates was undertaken in the hope of elucidating these discrepancies. A preliminary investigation has already been discussed.⁸

Experimental

Sodium, magnesium, calcium, strontium, and barium perchlorates were obtained by dissolving a "purified" grade in distilled water made slightly acid with perchloric acid and filtering through a fine fritted-glass disk. The solutions contained in a 96% silica glass beaker were partially evaporated in a drying oven and the crystals which separated on cooling were filtered off, washed with distilled water, and then recrystallized four times.

Rubidium and cesium perchlorates were prepared by addition of excess perchloric acid to the chlorides and nitrates and heated until dense perchloric acid fumes were evolved for several minutes. The resulting perchlorates were recrystallized four times from distilled water.

Potassium perchlorate was prepared by double recrystallization of analytical reagent grade crystals from distilled water.

Lithium perchlorate was prepared by adding reagent grade lithium carbonate to dilute perchloric acid, boiling the resulting solution to remove carbon dioxide, and crystallizing the salt in the usual manner.

The hydrated perchlorates were dried in a vacuum oven at 200° until constant weight was obtained. (In the case of calcium perchlorate it was necessary to pass through a molten hydrate state in order to obtain the anhydrous salt.)

The radiation source, 800 curies of cobalt-60, has been previously described.⁹ All irradiations were carried out at room temperature.

Dosimetry. The Fricke ferrous sulfate dosimeter was employed for all dose determinations. Appropriate temperature corrections were made for the ferric iron absorbance. A value of 15.45 (± 0.11) molecules of ferric ions produced per 100 e.v. absorbed was used in all dose calculations. Correction for photoelectric absorption was not made.

Analytical Procedures. The analytical procedures used in the determination of O_2 , Cl^- , ClO^- , ClO_2^- , ClO_2 , ClO_3^- , and ClO_4^- were largely developed in the course of the investigation. Because of the necessary

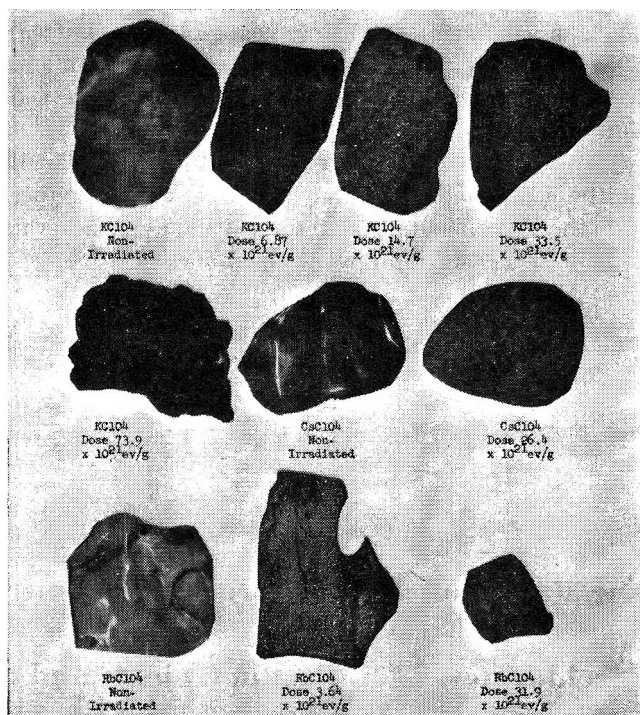


Figure 1. Photomicrographs of nonirradiated and irradiated crystals of $KClO_4$, $RbClO_4$, and $CsClO_4$; magnification 400 \times .

research to establish the validity of these methods, an adequate description is quite lengthy and has been the subject of separate publications.^{10,11}

Results and Discussion

General. All of the perchlorates studied become colored upon irradiation. Colors are cream (Mg), yellow (Na, Li, Ba), yellow-orange (Ca, Sr), and golden brown (K, Rb, Cs), the color fading somewhat with time. Beyond a certain absorbed dose, ranging from about 1×10^{21} e.v./g. (Sr, Cs) to over 20×10^{21} e.v./g. (Na, Li), gas evolution from the crystals occurs, as evidenced by weight loss on irradiation, and in some instances (Cs, Rb) by powdering. $KClO_4$ crystals irradiated to a high dose erupt with an audible crackling noise when pressed gently with a spatula. Photomicrographs of irradiated $KClO_4$, $RbClO_4$, and $CsClO_4$ show gas pockets and a dendritic structure produced by the escaping gas (see Figure 1).

After long exposure to radiation, all the perchlorates have associated with them a chlorine-like odor, which has been identified as being due to ClO_2 . There is also

(8) L. A. Prince and E. R. Johnson, 2nd International Conference on Radiation Research, Harrogate, England, Aug. 1962.

(9) T. Chen and E. R. Johnson, *J. Phys. Chem.*, **66**, 2249 (1962).

(10) L. A. Prince, *Anal. Chem.*, **36**, 613 (1964).

(11) L. A. Prince, *Chem. Analyst*, **53**, 11 (1964).

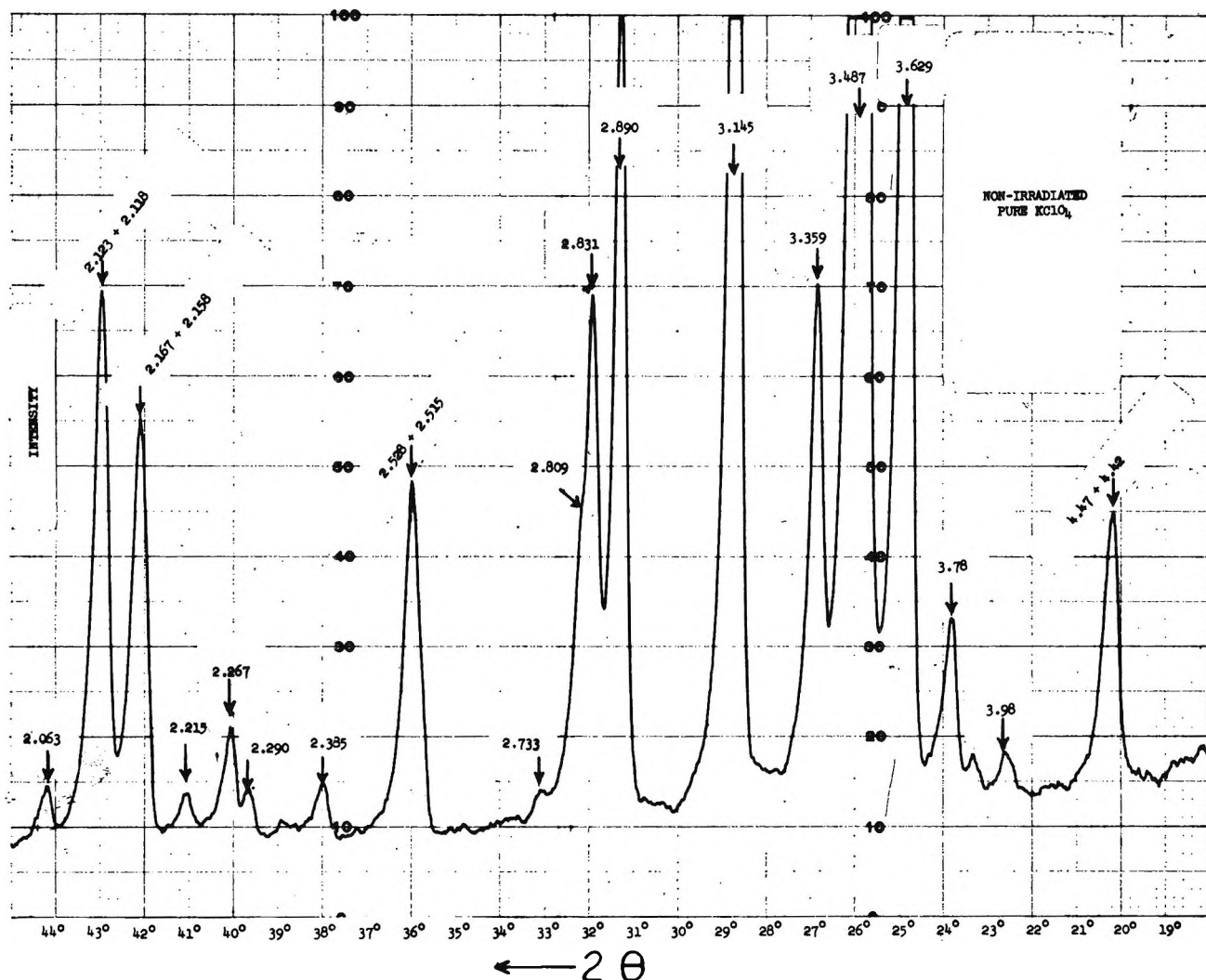


Figure 2. Automatically recorded X-ray diffraction pattern of nonirradiated KClO_4 , $-100 + 325$ mesh, from $2\theta = 18$ to 45° , using nickel-filtered copper radiation; scanning speed $1^\circ 2\theta/\text{min}$.

a general correlation between color intensity and ClO_2 yields, perchlorates with high ClO_2 yields displaying more intense coloration.

The crystal structure of irradiated KClO_4 is only very slightly altered at an absorbed dose of 13.0×10^{21} e.v./g., corresponding to 10% decomposition. At an absorbed dose of 25.1×10^{21} e.v./g., about 17% decomposition, the crystal structure is drastically altered, but the structures of the decomposition products are not yet evident; however, at an absorbed dose of 73.9×10^{21} e.v./g. (over 35% decomposition), significant regrouping occurs, and the structures of KCl and KClO_3 and the restored KClO_4 structure are apparent (see Figures 2, 3, 4, and 5).

Products of Decomposition. The products of decomposition that have been definitely established are ClO_3^- ,

ClO_2 , ClO_2^- , ClO^- , Cl^- , O_2 , and metallic oxide. Identification was determined by infrared and X-ray examination of the irradiated crystals, by chemical analysis, and by the ultraviolet absorption spectra of aqueous solutions of the irradiated salts.

The separate ultraviolet absorption spectra of ClO_4^- , ClO_3^- , ClO_2^- , ClO^- , Cl^- , and ClO_2 , dissolved in 0.01 *M* borax, show that the ClO_2^- absorption maximum is at $261 \text{ m}\mu$, ClO^- at $290 \text{ m}\mu$, and ClO_2 at $360 \text{ m}\mu$, in agreement with the literature.^{12,13} Figure 6 shows the ultraviolet spectra at various times of a sample of LiClO_4 irradiated to a total dose of 24.6×10^{21} e.v./g.

(12) H. L. Friedman, *J. Chem. Phys.*, **21**, 319 (1953).

(13) F. Stith, S. Friedlander, H. J. Lewis, and F. E. Young, *Anal. Chem.*, **26**, 1479 (1954).

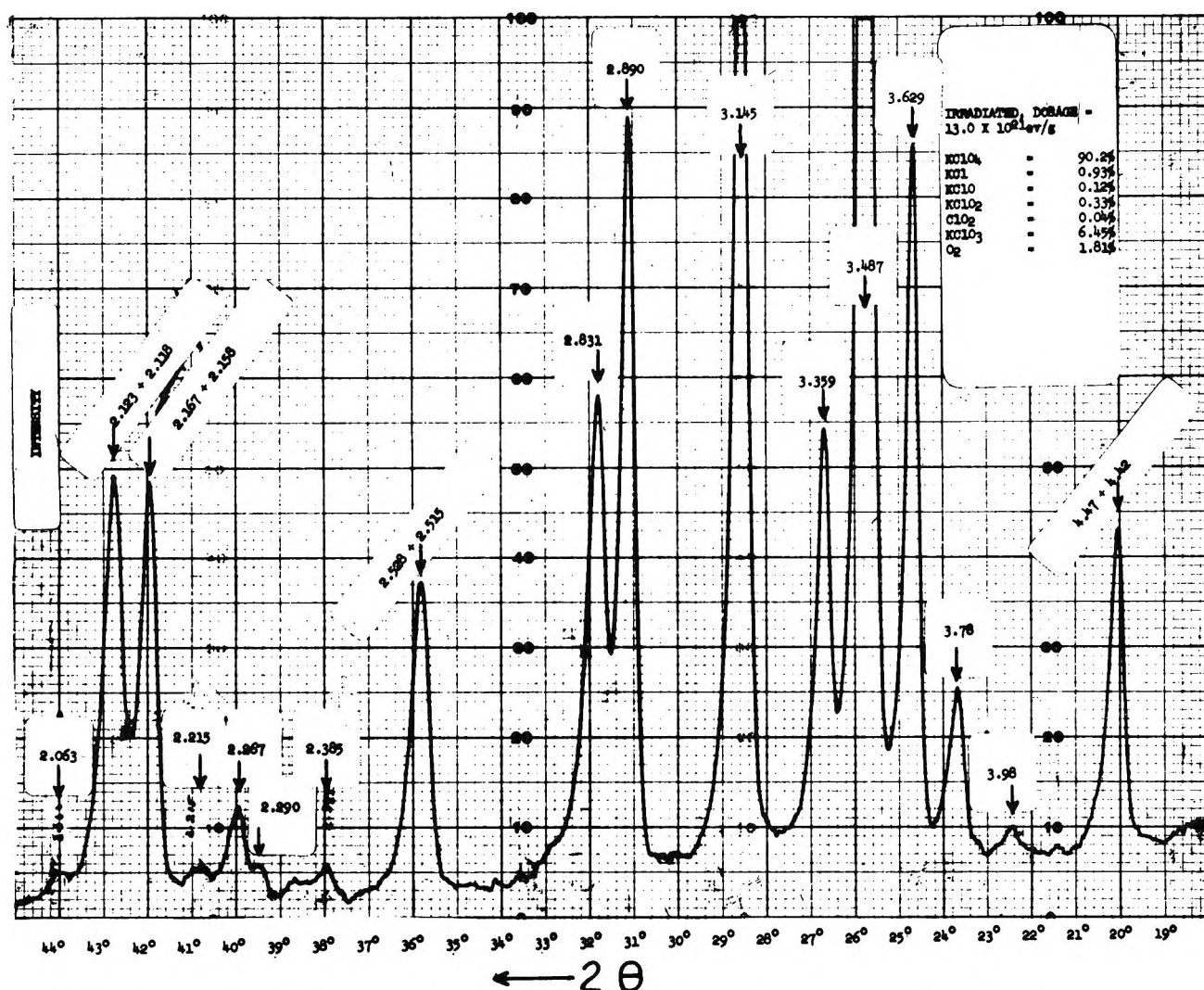


Figure 3. Automatically recorded X-ray diffraction pattern of irradiated KClO_4 , $-100 + 325$ mesh, dosage 13.0×10^{21} e.v./g., from $2\theta = 18$ to 45° , using nickel-filtered copper radiation; scanning speed $1^\circ 2\theta/\text{min}$.

Absorption peaks corresponding to those of ClO^- , ClO_2^- , and ClO_2 are clearly evident. The photosensitive ClO_2 is seen to decompose completely in 20 min. ClO_2 has also been identified by sweeping an aqueous solution of the irradiated perchlorates with argon and passing the liberated gases through a KI solution at different pH. A characteristic reaction of ClO_2 in this system was observed, *i.e.*, one-fifth of the molecule reacting in the KI solution at pH 9, and a complete reaction at pH 1.5. This result is also good evidence for the absence of O_3 or free Cl_2 , since either O_3 or Cl_2 would alter the 1:5 ratio by reacting completely with KI at pH 9 or 1.5.

ClO_3^- has been positively identified in the dry crystals by X-ray and infrared analysis. Figure 7 shows a comparison between the infrared spectra of irradiated

and nonirradiated KClO_4 . The KClO_3 bands at 20.6 and 10.3μ are clearly discernable. The X-ray diffraction pattern of irradiated KClO_4 (Figure 5) shows the KClO_3 crystal constants $d = 2.32 \text{ \AA}$. and $d = 2.79 \text{ \AA}$. clearly present. Also in Figure 5 are the KCl crystal constants $d = 2.224 \text{ \AA}$. and $d = 3.146 \text{ \AA}$. which are unresolvable because of the KClO_4 constants of $d = 2.215 \text{ \AA}$. and $d = 3.145 \text{ \AA}$., but can be discerned by comparison by the relative enhancement of these KClO_4 peaks obtained with nonirradiated KClO_4 .

The presence of oxygen is easily established by evolution of the gas when the crystals are dissolved in de-aerated H_2O and subsequently combined with H_2 in a vacuum apparatus, and by the quantitative oxidation of divalent manganese.¹¹

It has been found that thermal decomposition of the

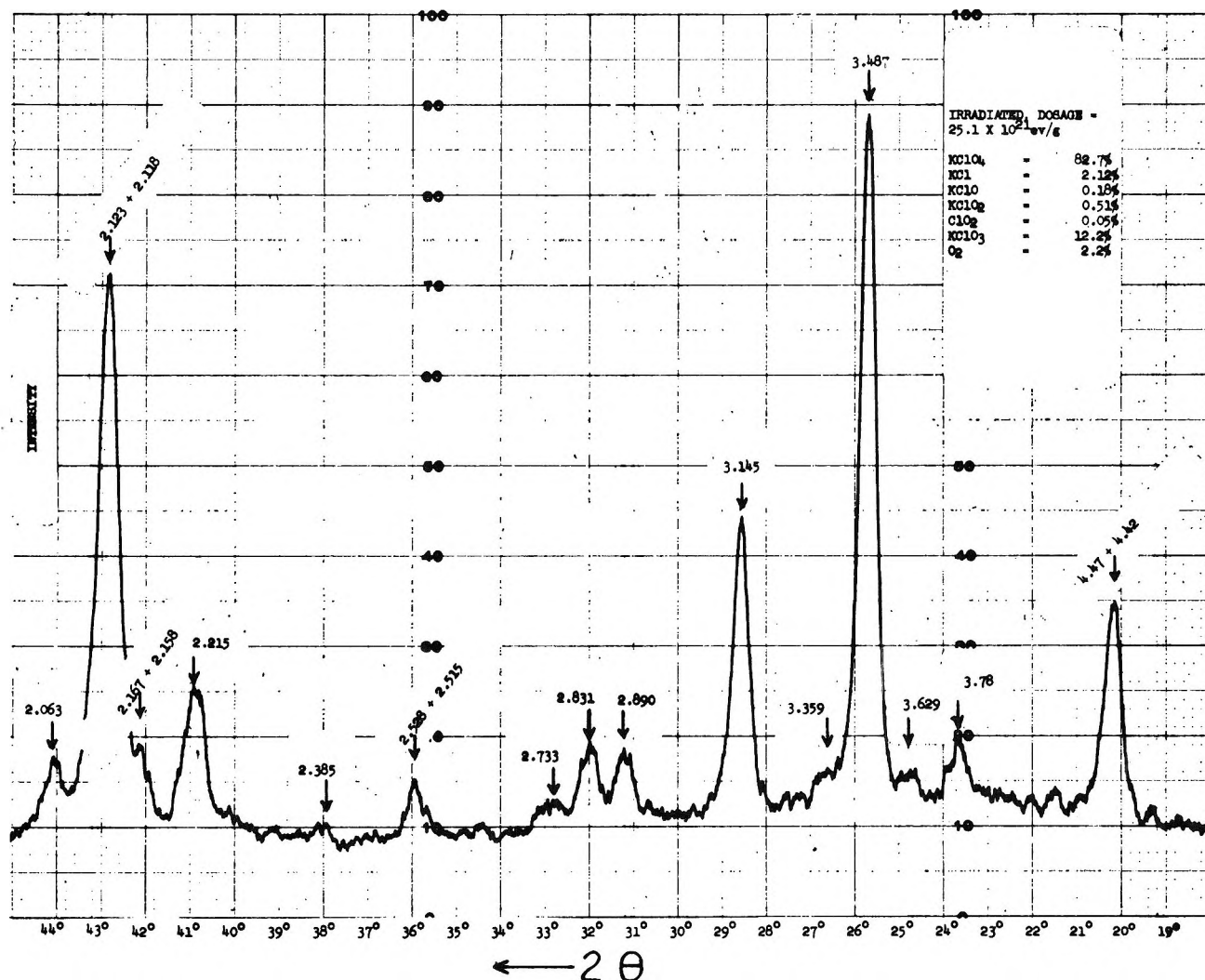


Figure 4. Automatically recorded X-ray diffraction pattern of irradiated KClO_4 , $-100 + 325$ mesh, dosage 25.1×10^{21} e.v./g., from $2\theta = 18$ to 45° , using nickel-filtered copper radiation; scanning speed $1^\circ 2\theta/\text{min}$.

products of the irradiation-induced decomposition occurs at room temperatures, and that the rate of this thermal decomposition depends on the nature of the salt and has a complicated concentration dependence. This subject will be treated in a separate communication. It suffices to state here that, in the discussion that follows, all initial G values have been corrected for thermal decomposition of the products; however, the data shown in Figures 8–16 are not corrected for the thermal decomposition that took place during irradiation.

In Table I are summarized initial G values, molecules formed or decomposed per 100 e.v. of energy absorbed, for the alkali and alkaline earth perchlorates. All of the data shown were obtained from room temperature radiolysis and have been corrected for electron density. It is apparent from Table I that there is considerable

variation in the initial yields of perchlorate disappearance, but that this variation is not as dramatic as that found for the radiation-induced decomposition of the

Table I: G^0 Values of Alkali and Alkaline Earth Perchlorates Irradiated at Room Temperature and Pressure

Salt	$-G_{\text{ClO}_4^-}$	$G_{\text{ClO}_3^-}$	$G_{\text{ClO}_2^-}$	G_{ClO_2}	G_{ClO^-}	G_{Cl^-}	G_{O_2}
Li	3.76	2.80	0.15	0.59	0.10	0.12	2.15
Na	4.36	3.57	0.17	0.11	0.09	0.42	2.96
K	3.83	2.99	0.18	0.12	0.09	0.45	2.68
Rb	5.27	4.06	0.20	0.12	0.14	0.75	3.84
Cs	6.84	5.28	0.22	0.10	0.17	1.07	5.28
Mg	4.67	4.29	0.14	0.07	0.03	0.15	2.62
Ca	4.15	3.44	0.00	0.51	0.08	0.12	1.99
Sr	4.53	3.90	0.19	0.14	0.11	0.19	2.61
Ba	3.20	1.76	0.84	0.42	0.12	0.06	2.18

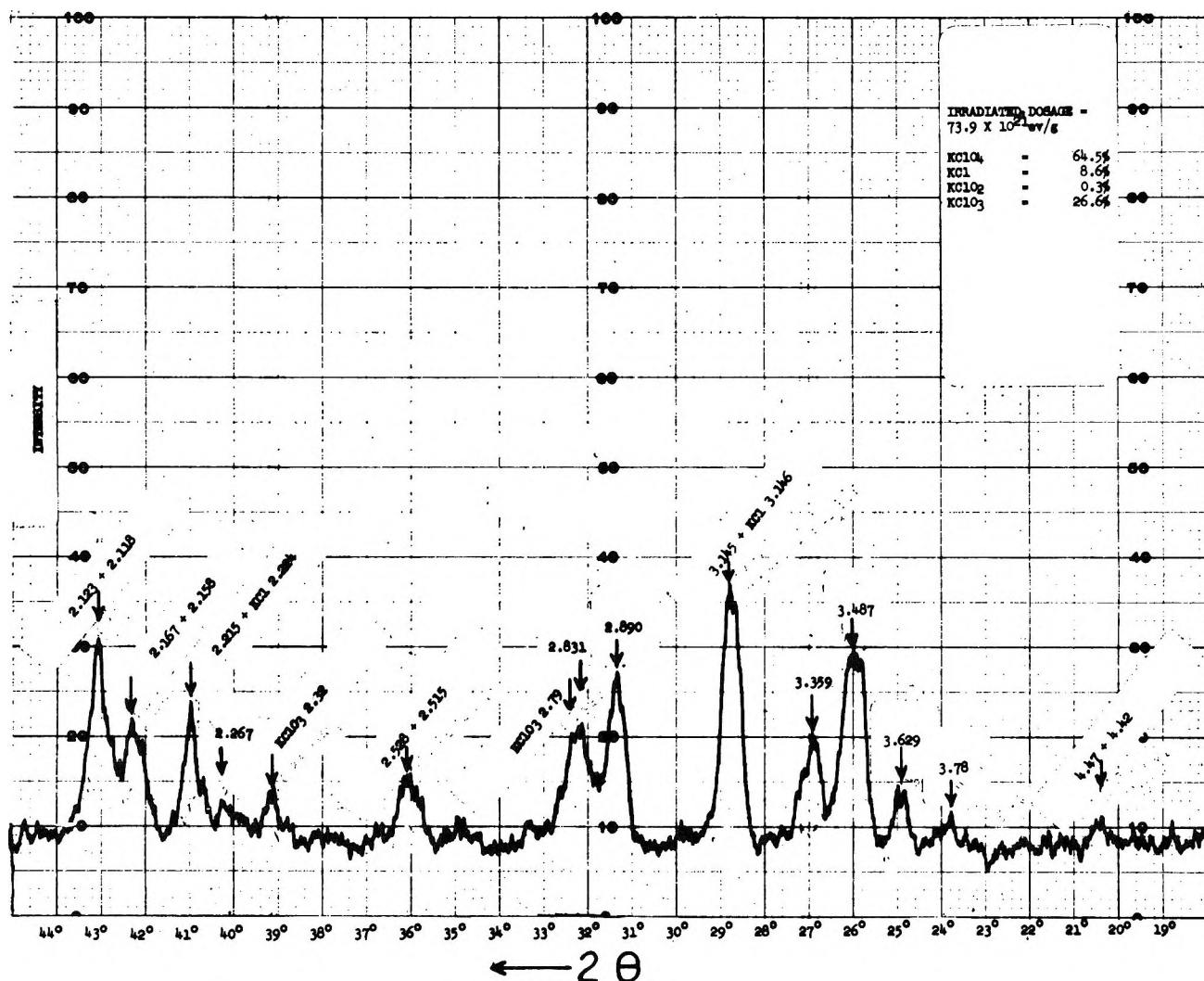


Figure 5. Automatically recorded X-ray diffraction pattern of irradiated KClO_4 , -100 +325 mesh, dosage 73.9×10^{21} e.v./g., from $2\theta = 18$ to 45° , using nickel-filtered copper radiation; scanning speed $1^\circ 2\theta/\text{min}$.

alkali or alkaline earth nitrates whose G^0 values range between 0.11 and 1.7.

In Figures 8 through 16 are shown the variations in product yields as a function of dose.

Stoichiometry. A simple calculation from G^0 values serves to determine stoichiometry. A summation of $\frac{1}{2}G^0_{\text{ClO}_3^-} + G^0_{\text{ClO}_2^-} + G^0_{\text{ClO}_2} + \frac{3}{2}G^0_{\text{ClO}^-} + 2G^0_{\text{Cl}^-}$ should equal $G^0_{\text{O}_2}$, if the oxygen liberated is present only as free O_2 trapped in the crystal lattice.

A comparison of the calculated and experimental initial G values for oxygen for the radiolysis of the alkali and alkaline earth perchlorates is summarized in Table II, calculating all oxygen fragments as free O_2 . As can be seen, within experimental error a stoichiometric relationship between experimental and calculated $G^0_{\text{O}_2}$ values for NaClO_4 , KClO_4 , RbClO_4 , CsClO_4 , and $\text{Sr}(\text{ClO}_4)_2$ is found, but not for LiClO_4 , $\text{Ba}(\text{ClO}_4)_2$, and

$\text{Ca}(\text{ClO}_4)_2$. (No accurate experimental value of $G^0_{\text{O}_2}$ for $\text{Mg}(\text{ClO}_4)_2$ has been obtained due to the inaccu-

Table II: A Comparison of Experimental and Calculated Initial G Values of Oxygen Calculating All Oxygen Fragments as Free Oxygen

Compound	$G^0_{\text{O}_2}$, exptl.	$G^0_{\text{O}_2}$, calcd.	Variation, %
LiClO_4	2.15	2.54	+18
NaClO_4	2.96	3.04	+3
KClO_4	2.68	2.84	+6
RbClO_4	3.84	4.05	+6
CsClO_4	5.28	5.33	+1
$\text{Mg}(\text{ClO}_4)_2$		2.68	
$\text{Ca}(\text{ClO}_4)_2$	1.99	2.59	+30
$\text{Sr}(\text{ClO}_4)_2$	2.61	2.81	+8
$\text{Ba}(\text{ClO}_4)_2$	2.18	2.44	+12

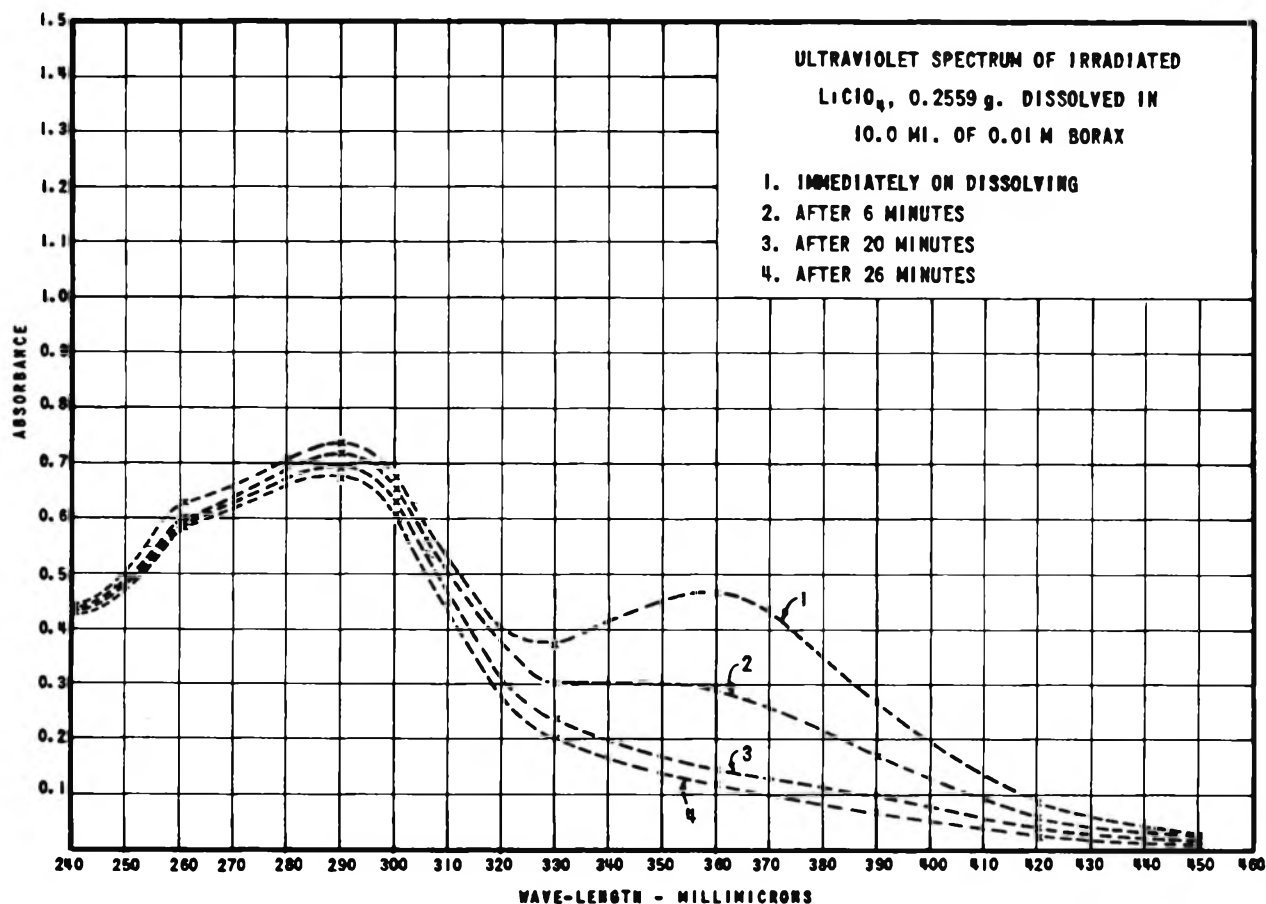


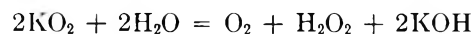
Figure 6. Ultraviolet spectrum of irradiated LiClO₄ in 0.01 M borax.

racies caused by the extreme hygroscopic nature of this salt.)

A possible explanation for the poor stoichiometry in these salts may be found by comparison of the results summarized in Table II with those shown in Table I. Those salts with the highest $G^0_{\text{ClO}_2}$ values show the poorest agreement between the experimental and the calculated $G^0_{\text{O}_2}$ values. Thus CsClO₄ with $G^0_{\text{ClO}_2} = 0.08$ shows the least variation (1%); NaClO₄, KClO₄, and RbClO₄, with $G^0_{\text{ClO}_2} = 0.10, 0.11,$ and $0.10,$ respectively, show variations from 3 to 6%; Sr(ClO₄)₂, with $G^0_{\text{ClO}_2} = 0.12,$ shows a variation of 8%; and Ba(ClO₄)₂, Ca(ClO₄)₂, and Li(ClO₄)₂, with $G^0_{\text{ClO}_2} = 0.35, 0.45,$ and $0.52,$ respectively, show variations of from 12 to 30%, indicating a possible correlation between $G^0_{\text{ClO}_2}$ and the lack of stoichiometry as calculated by the method described above. There are two possible explanations for this. The first is that a significant amount of ClO₂ may be converted to Cl⁻ in the course of the chemical analysis for chloride content; however, careful tests showed only a negligible conversion to chloride when a ClO₂ solution was treated as in the chemical

analysis. The second explanation, and the one which appears most likely, is that the residual oxygen initially associated with ClO₂ in the ClO₄⁻ ion is not all available as gaseous O₂. Considerations of electrical neutrality would favor the simultaneous formation of a metal oxide, peroxide, or superoxide with ClO₂.

The reactions of a metal oxide or superoxide in an irradiated perchlorate lattice, on dissolution in water, are uncertain. According to George,¹⁴ half of the oxygen contained in a superoxide is liberated as gaseous O₂ on dissolving in water. For example



Summarized in Table III is a comparison of experimental $G^0_{\text{O}_2}$ values with those calculated by assuming that only half of the residual oxygen produced on ClO₂ formation is included in the oxygen analysis. As can be seen, there is considerable improvement in stoichiometry. (In the case of Ca(ClO₄)₂, there still remains a large discrepancy which we believe is probably due to

(14) P. George, *Discussions Faraday Soc.*, 2, 196 (1947).

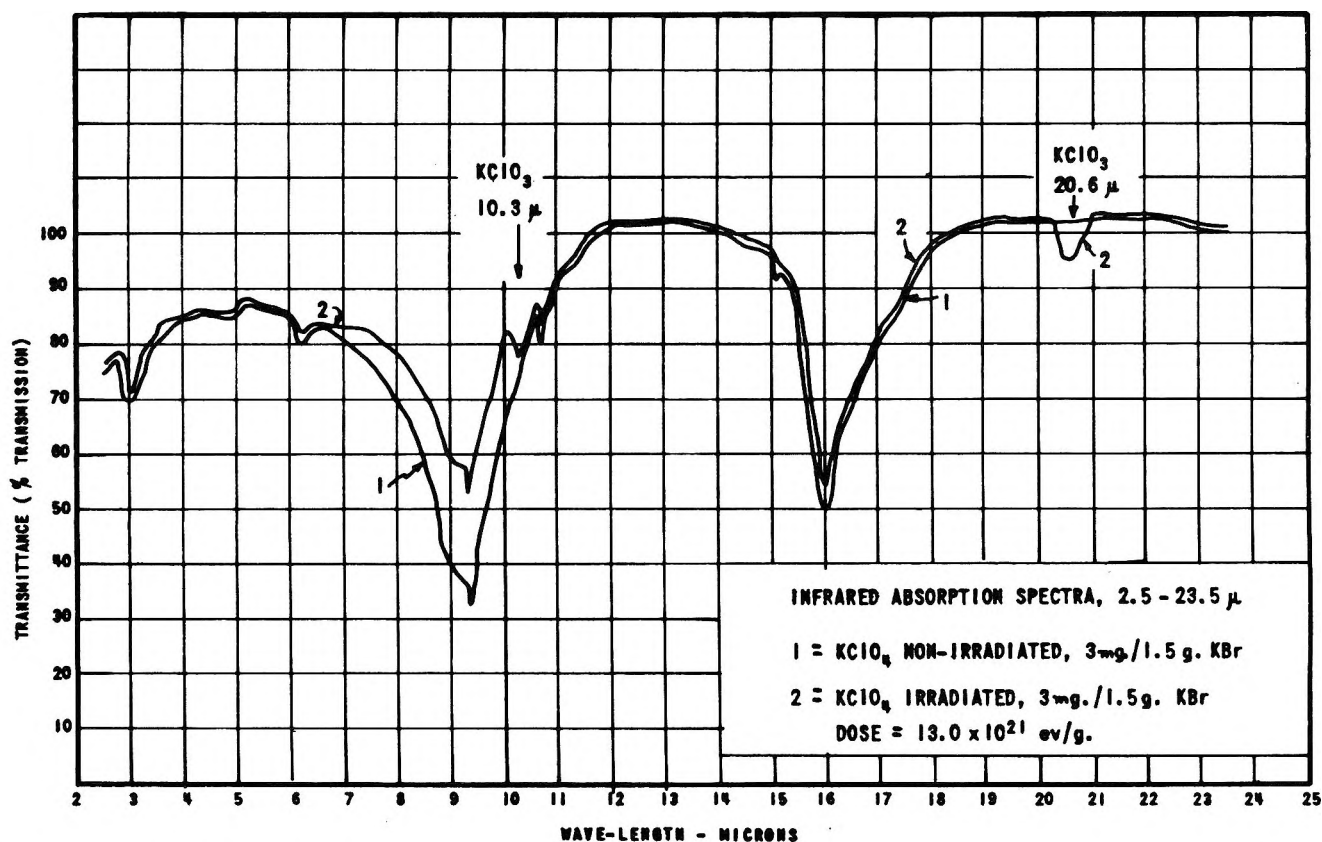


Figure 7. Infrared absorption spectra of irradiated and nonirradiated KClO_4 .

experimental error because of its hygroscopic nature. Next to $\text{Mg}(\text{ClO}_4)_2$, it is the most hygroscopic perchlorate.)

Experimental confirmation of the presence of metal oxides in these salts with high $G_{\text{ClO}_2}^0$ values is found by determining the pH of aqueous solutions of the irradiated perchlorates. Table IV summarizes the results of pH measurements obtained by dissolving 0.2 g. of sample in 50 ml. of distilled water at pH 7.0 while de-

Table IV: pH of Aqueous Solutions of Nonirradiated and Irradiated Alkali and Alkaline Earth Perchlorates

Salt	Dose, e.v./g. $\times 10^{-21}$	pH	pH after annealing 17 hr. at 170°
LiClO_4	Nil	7.0	
	1.25	8.9	7.2
NaClO_4	Nil	7.0	
	1.12	7.8	7.0
KClO_4	Nil	7.0	
	1.28	8.2	7.0
RbClO_4	Nil	7.0	Not determined
	0.93	6.4	
CsClO_4	Nil	7.0	Not determined
	0.96	7.0	
$\text{Mg}(\text{ClO}_4)_2$	Nil	8.5	Not determined
	1.38	8.5	
$\text{Ca}(\text{ClO}_4)_2$	Nil	6.9	
	1.23	8.3	7.0
$\text{Sr}(\text{ClO}_4)_2$	Nil	7.0	
	1.46	7.8	7.0
$\text{Ba}(\text{ClO}_4)_2$	Nil	7.0	
	1.38	8.9	7.2

Table III: A Comparison of Experimental and Calculated $G_{\text{O}_2}^0$ Values, Assuming Half of the Oxygen Fragment from ClO_2 Formation Is Not Free Oxygen

Compound	$G_{\text{O}_2}^0$, exptl.	$G_{\text{O}_2}^0$, calcd.	Variation, %
LiClO_4	2.15	2.24	+4
NaClO_4	2.96	2.98	+1
KClO_4	2.68	2.78	+4
RbClO_4	3.84	3.99	+4
CsClO_4	5.28	5.28	0
$\text{Mg}(\text{ClO}_4)_2$		2.64	
$\text{Ca}(\text{ClO}_4)_2$	1.99	2.33	+17
$\text{Sr}(\text{ClO}_4)_2$	2.61	2.74	+5
$\text{Ba}(\text{ClO}_4)_2$	2.18	2.23	+2

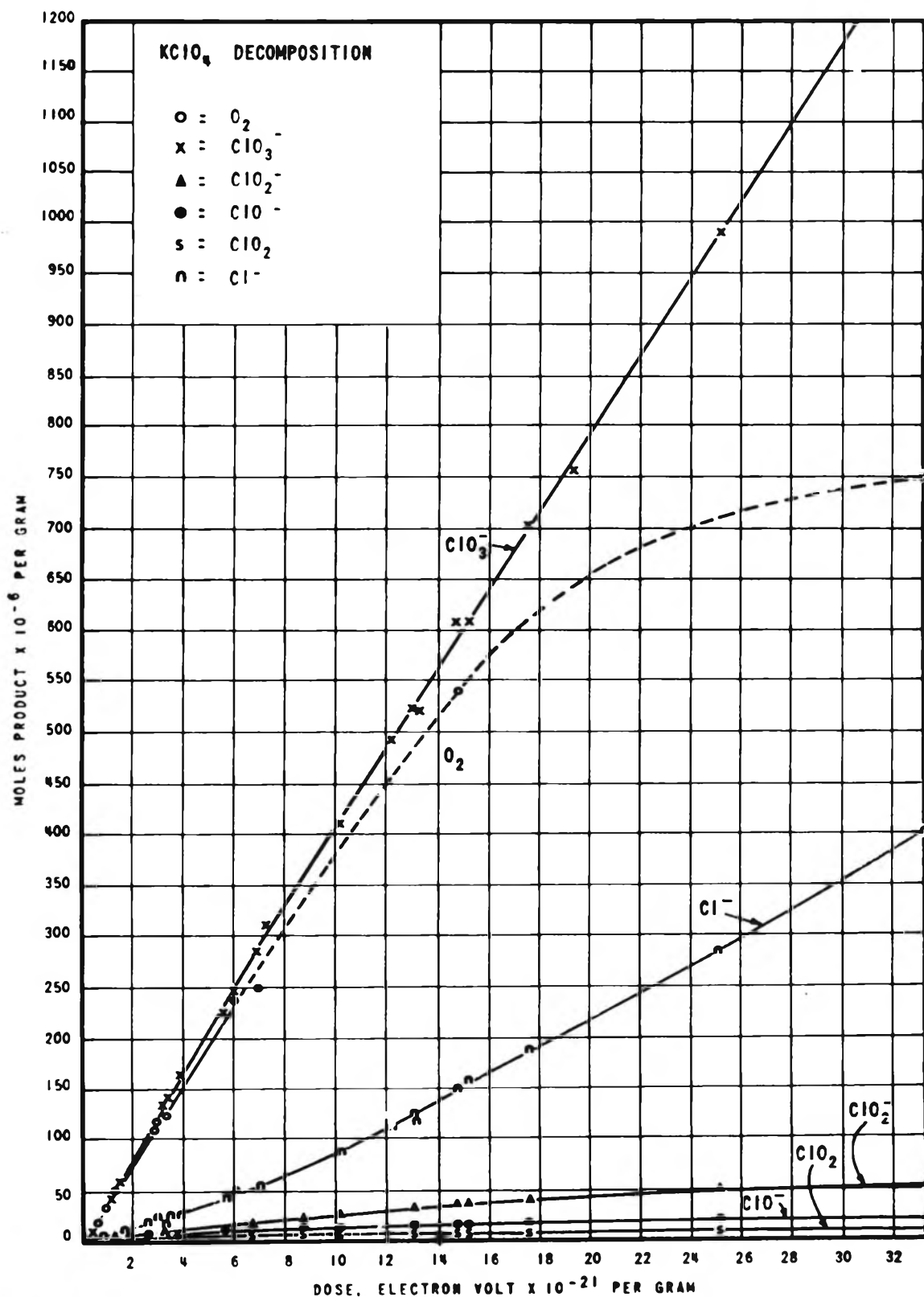


Figure 8. Yields of KClO₄ decomposition products as functions of dose.

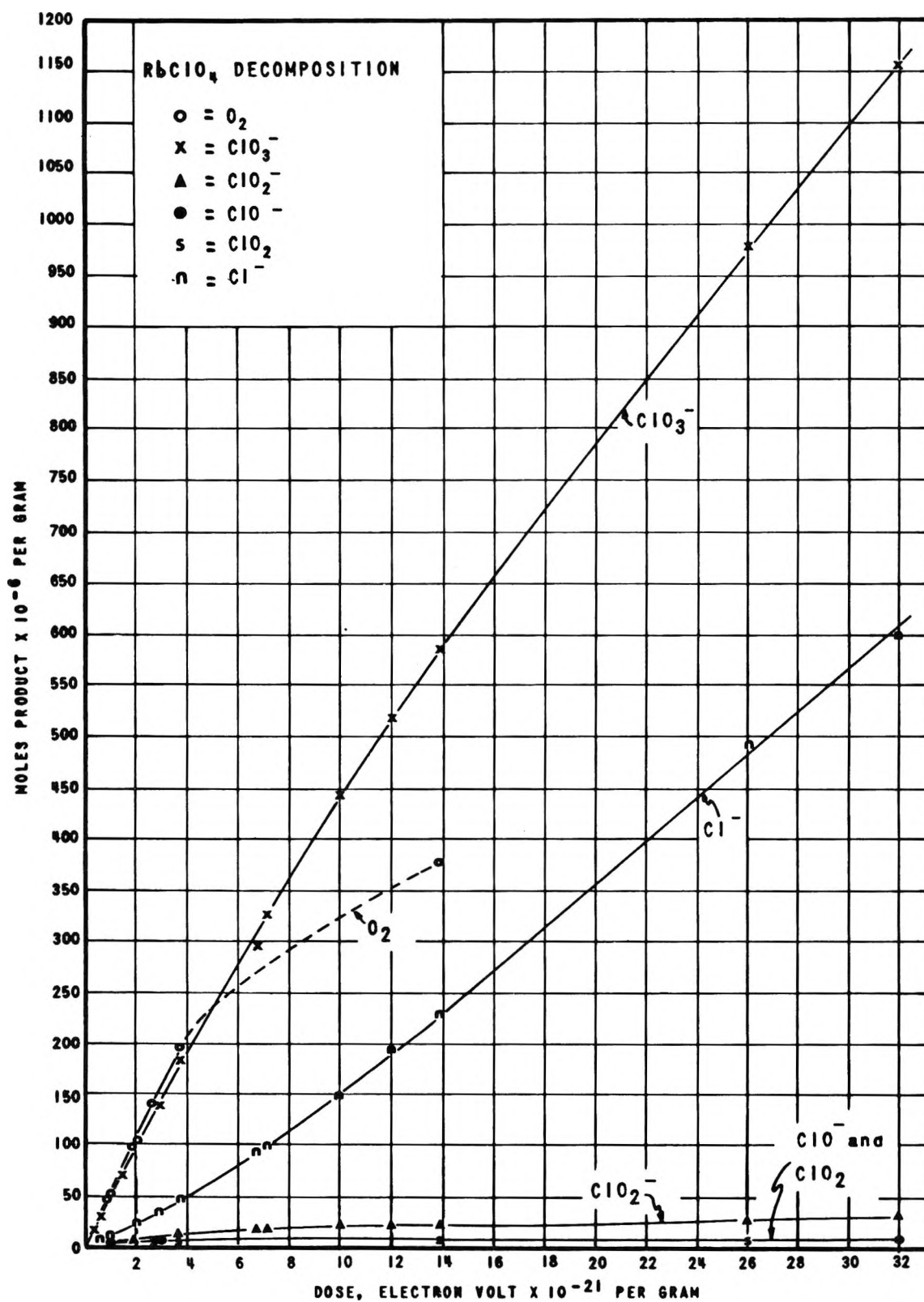


Figure 9. Yields of RbClO₄ decomposition products as functions of dose.

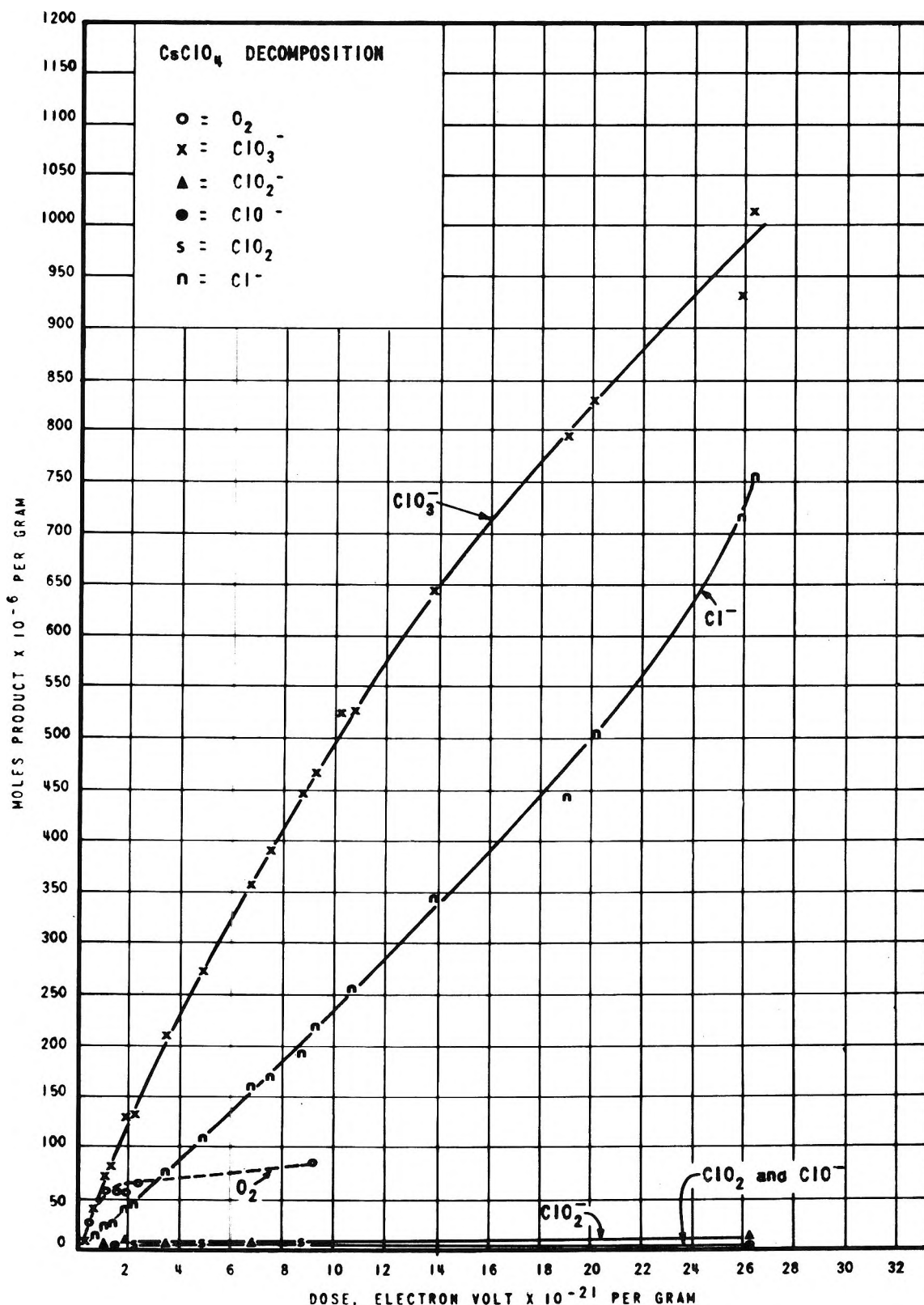


Figure 10. Yields of CsClO₄ decomposition products as functions of dose.

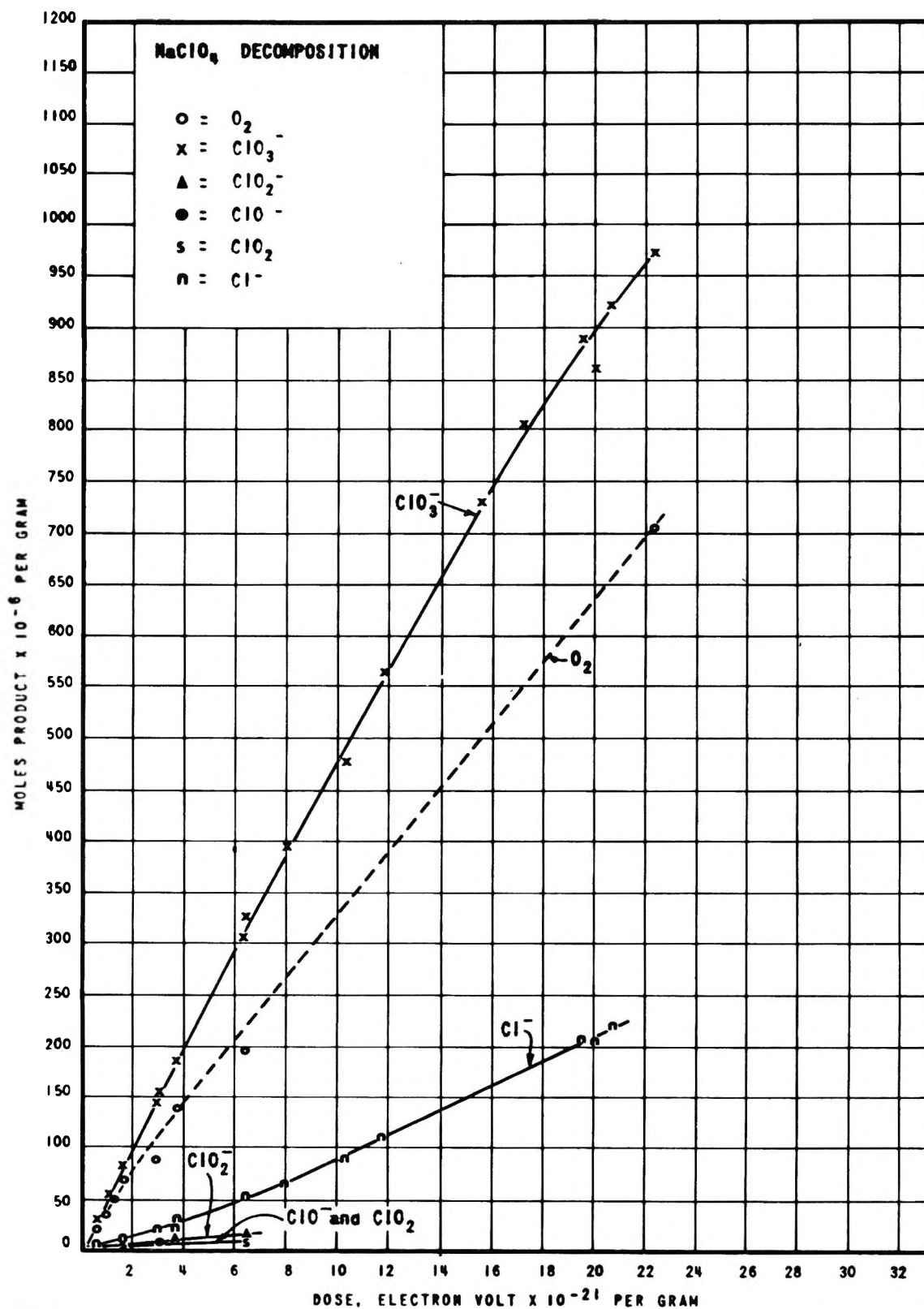


Figure 11. Yields of NaClO₄ decomposition products as functions of dose.

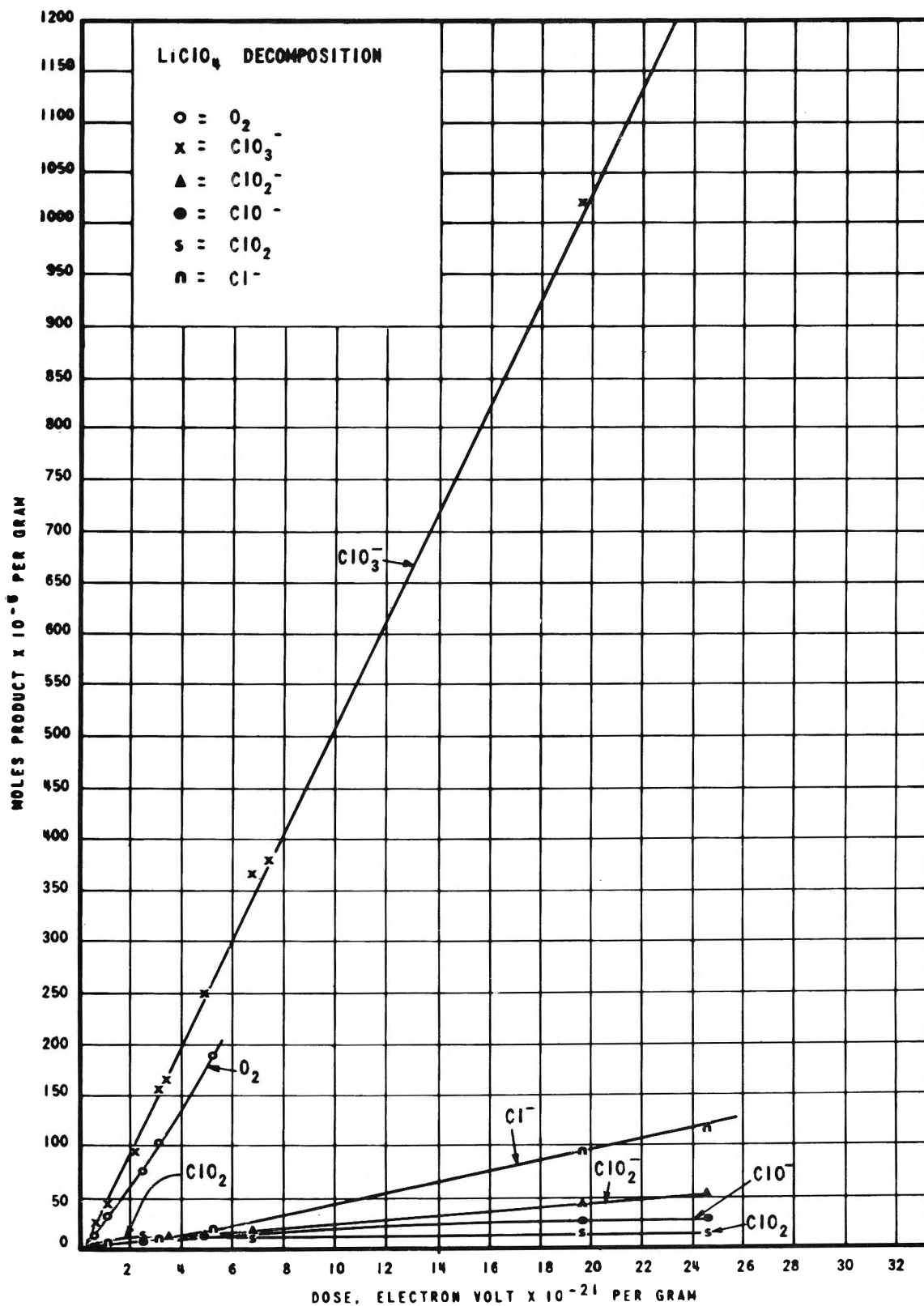


Figure 12. Yields of LiClO₄ decomposition products as functions of dose.

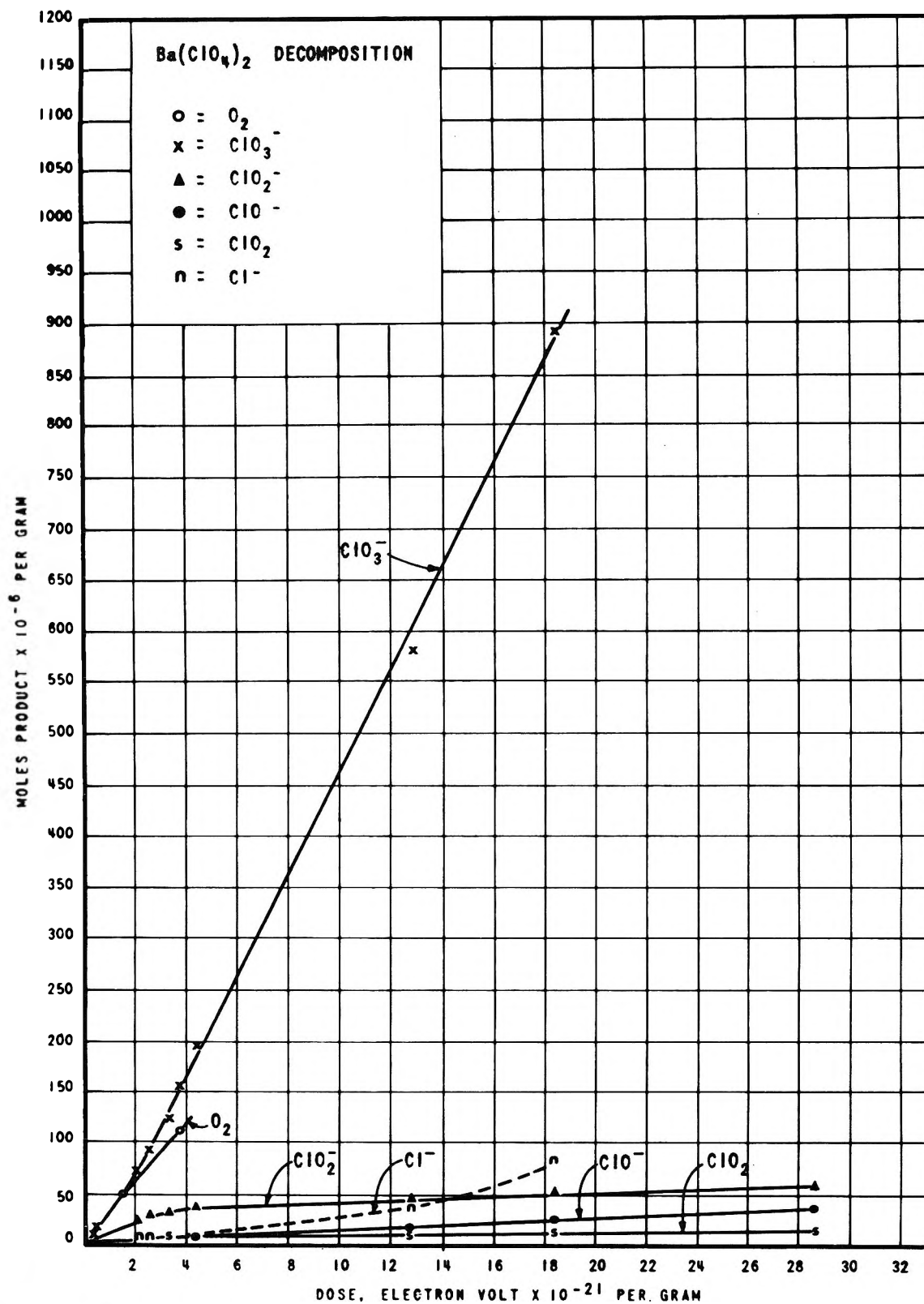


Figure 13. Yields of Ba(ClO₄)₂ decomposition products as functions of dose.

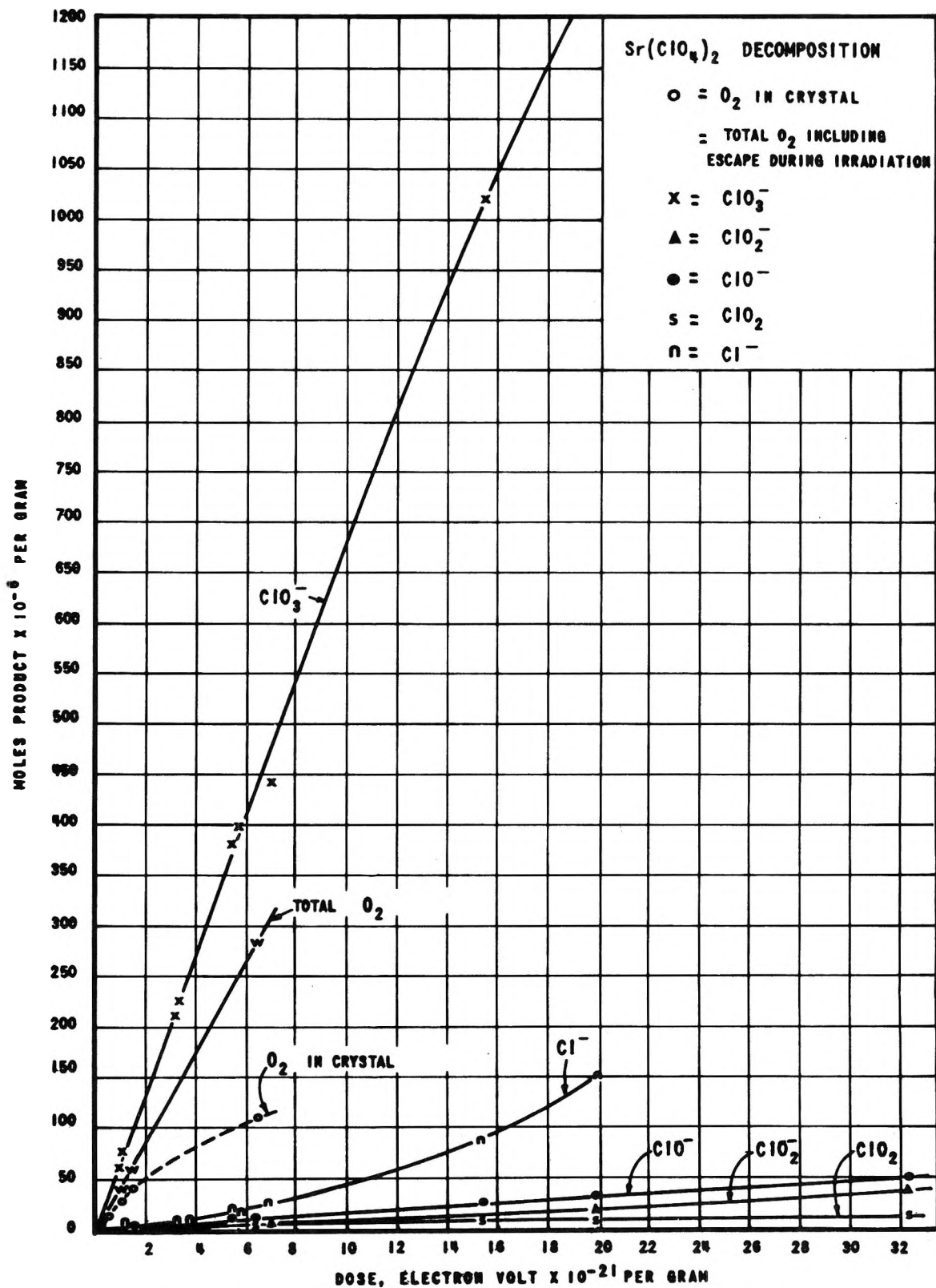


Figure 14. Yields of Sr(ClO₄)₂ decomposition products as functions of dose.

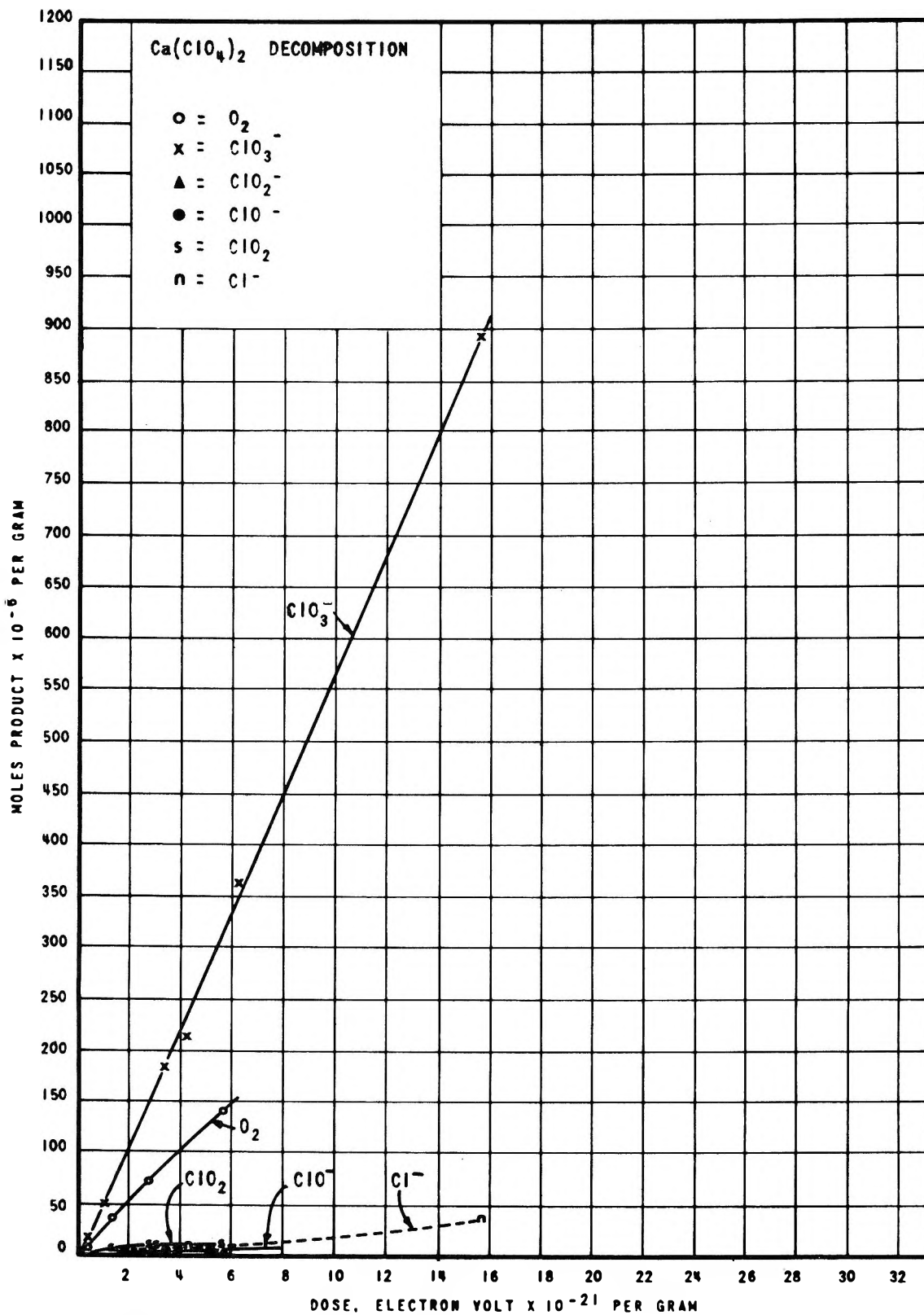


Figure 15. Yields of Ca(ClO₄)₂ decomposition products as functions of dose.

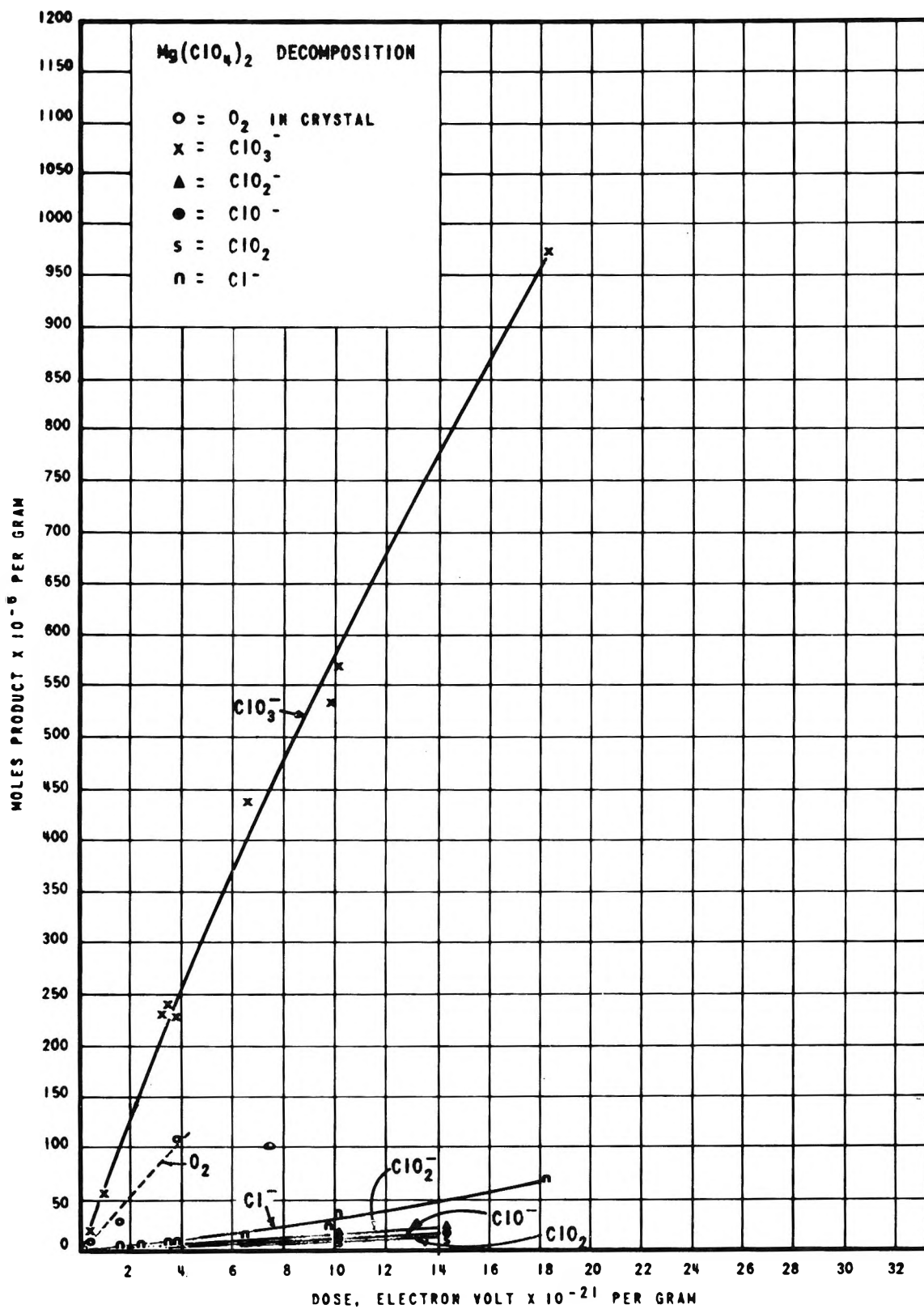


Figure 16. Yields of Mg(ClO₄)₂ decomposition products as functions of dose.

gassing with a stream of pure argon. It is seen that those perchlorates with the highest $G^0_{\text{ClO}_2}$ values, *viz.*, Li, Ca, and Ba, show the greatest increase in pH on irradiation. (Calculation and actual experimental measurement show that hydrolysis of chlorite and hypochlorite is negligible and cannot account for the observed increase in pH.) It is also seen from Table IV that neutrality is restored on annealing the irradiated salts at 170°.

Effect of Pressure. The effect of pressure on the radiolysis of the perchlorates is summarized in Table V. This was determined in a manner essentially similar to that employed by Chen and Johnson.⁹ Argon gas was used to maintain pressures of 1000 and 2000 p.s.i. No differences in G values from irradiation at 1 atm. pressure were obtained with any of the nine perchlorates studied. The only differences observed were lower weight losses (escape of O_2 from the lattice) on irradiation with Sr, Rb, and Cs perchlorates.

Table V: Comparison of Weight Loss in RbClO_4 , CsClO_4 , and $\text{Sr}(\text{ClO}_4)_2$ Irradiated at 14.7 p.s.i. (1 atm.) and at 2000 p.s.i.

Sample	Dose, e. v./g. $\times 10^{-21}$	Pressure, p.s.i.	Weight loss on irradiation, % by weight
RbClO_4	6.64	2000	0.14
RbClO_4	6.64	14.7	0.43
CsClO_4	6.69	2000	1.14
CsClO_4	6.68	14.7	1.25
$\text{Sr}(\text{ClO}_4)_2$	5.68	2000	0.25
$\text{Sr}(\text{ClO}_4)_2$	5.67	14.7	0.60

Other Products. There is at least one other radiolysis product, though minor, which has the chemical properties of ClO_3 (or Cl_2O_6). To appreciate the following discussion, reference to the analytical procedure for the determination of ClO_2 , ClO_2^- , and ClO^- must be made.

Briefly, this procedure is in two parts. In part 1, the sample is introduced to a solution of KI at pH 9 and the absorbance of liberated iodine is determined. At this pH, ClO^- reacts (2 equivalents) to form I_3^- and Cl^- , and ClO_2 reacts (1 of 5 equivalents) to form I_3^- and ClO_2^- . The alkaline solution is then acidified (pH 1.5) and the I_3^- absorbance is redetermined. This second absorbance now includes I_3^- liberated by the ClO_2^- (4 equivalents) originally in the sample, and by the ClO_2 (4 of the remaining 5 equivalents) from the ClO_2 which reacted with the KI at pH 9. In part 2, ClO_2 is removed (by flash boiling) and the absorbances at pH 9 and pH 1.5 repeated as in part 1. Thus, if ClO^- , ClO_2^- , and ClO_2 were the only components of the

sample to liberate iodine, the two pH 9 absorbances should differ by the contribution of the 1 equivalent of the ClO_2 , and the two pH 1.5 absorbances by the 5 equivalents of ClO_2 , *i.e.*, the differences in absorbances should be in a 1:5 ratio, and this has been confirmed with synthetic mixtures of ClO^- , ClO_2^- , and ClO_2 .

Of the irradiated alkali metal perchlorates, this 1:5 ratio was obtained only with NaClO_4 ; a somewhat greater than the 1:5 ratio was obtained with the others. This discrepancy is attributed to the presence of an unidentified fragment, which must have the properties of reacting with KI at pH 9 with no further reaction of pH 1.5, and it must be volatile or destroyed by flash boiling in such a manner as not to react with KI. This would be the expected reaction for a ClO_3 (or Cl_2O_6) or possibly a ClO_4 radical to form the corresponding anion ClO_3^- or ClO_4^- . G^0 values for this substance, calculated as ClO_3 , are 0.1 for each of KClO_4 , RbClO_4 , and CsClO_4 , 0.2 for LiClO_4 , and nil for NaClO_4 .

Similar calculations for the alkaline earth perchlorates revealed no substance of this type; however, it was noticed that except for $\text{Mg}(\text{ClO}_4)_2$ there appeared to be some minor product which reacted with KI only after the flash boiling procedure as described in part 2 of the analytical procedure for ClO^- , ClO_2^- , and ClO_2 . This product increased with increased dosage but was not identified.

Discussion

As mentioned earlier ClO^- , ClO_2^- , and ClO_2 undergo thermal decomposition to yield primarily Cl^- . There is some exception to this, which will be discussed in a subsequent communication. It suffices to say here that the increase observed in G_{Cl^-} for the several perchlorates cannot be accounted for entirely on the basis of the thermal decomposition of the products, and one must conclude that the increases in G_{Cl^-} with increased absorbed dose are attributable to changes which are occurring in the lattice.

Low temperature radiolysis of the perchlorates show that the primary products are ClO_3^- , ClO_2^- , ClO_2 , and Cl^- . The hypochlorite appears to arise from the decomposition of ClO_2 and/or ClO_2^- . The increase observed in G_{Cl^-} is a direct one, that is, it is due to an increase in the rate of formation of this product. A full detailed discussion of the mechanism of the decomposition will be made in a future communication.

Conclusion

The alkali and alkaline earth perchlorates decompose under the action of ionizing radiation to yield ClO_3^- , ClO_2 , ClO_2^- , ClO^- , Cl^- , O_2 , a metal oxide, and possibly

a small amount of ClO_3 . Good stoichiometry has been obtained.

Acknowledgment. The authors wish to extend their thanks to Mr. I. H. S. Fraser, Dr. W. Forgeng, and associates, Union Carbide Corporation, Metals Division,

Niagara Falls, N. Y., for their assistance in obtaining the infrared, ultraviolet, and X-ray diffraction data. We also wish to express our appreciation to the Union Carbide Corporation, Linde Division, for many courtesies, including provision of the apparatus and gases employed in the high pressure radiation experiments.

The Radiation-Induced Decomposition of the Alkali and Alkaline Earth

Perchlorates. II. Mechanism of the Decomposition^{1a}

by L. A. Prince and E. R. Johnson^{1b}

Chemistry Department, Stevens Institute of Technology, Hoboken, New Jersey (Received August 6, 1964)

The mechanism of the radiation-induced decomposition of the alkali and alkaline earth perchlorates is discussed. Evidence is presented to show that ClO_3^- , Cl^- , ClO_2^- , ClO_2 , and oxygen are the primary products and that ClO^- is not, its appearance being concomitant with a decrease in the yield of ClO_2 and ClO_2^- . The yields of $(\text{ClO}_2 + \text{ClO}_2^-)$ and Cl^- are related and appear to originate from a competitive primary reaction. Data are presented on the thermal decomposition of the products in the irradiated crystals. It is shown that ClO_2^- and ClO^- thermally decompose to yield Cl^- , whereas ClO_2 undergoes a neutralization reaction.

In a previous communication,^{1c} we have reported on the products and stoichiometry of the radiation-induced decomposition of lithium, sodium, potassium, rubidium, cesium, magnesium, calcium, barium, and strontium perchlorates. The results and discussions were confined to establishing the products, methods of analysis, and G values. It was shown that ClO_3^- and O_2 are always the principal products, followed by Cl^- , ClO_2 , or ClO_2^- , depending upon the particular salt, then ClO^- . Evidence was also given for the presence of a minor product found only in the alkali perchlorates, tentatively identified as ClO_3 , and also for the presence of a metal oxide. In this communication, we discuss the kinetics and mechanism of the decomposition.

Experimental

The radiation source and methods of analysis have been discussed previously. There were no other excep-

tional experimental methods employed which require further discussion other than that which is found in the text.

Kinetics. In Figure 1 is shown a semilog plot of undecomposed ClO_4^- vs. dose for the alkali and alkaline earth perchlorates. The dashed lines represent a first-order plot and the solid lines experimental values. For low percentages of decomposition, all the perchlorates appear to follow first-order kinetics. This seems to be true for most radiation-induced inorganic solid decompositions.²⁻⁴ The degree of departure from first-order kinetics varies considerably among the different per-

(1) (a) Research supported by A.E.C. contract AT-30-1-1824; (b) National Standard Reference Data Program, National Bureau of Standards, Washington 25, D. C.; (c) L. A. Prince and E. R. Johnson, *J. Phys. Chem.*, **69**, 359 (1965).

(2) T. Chen and E. R. Johnson, *ibid.*, **66**, 2249 (1962).

(3) J. Cunningham, *ibid.*, **65**, 628 (1961).

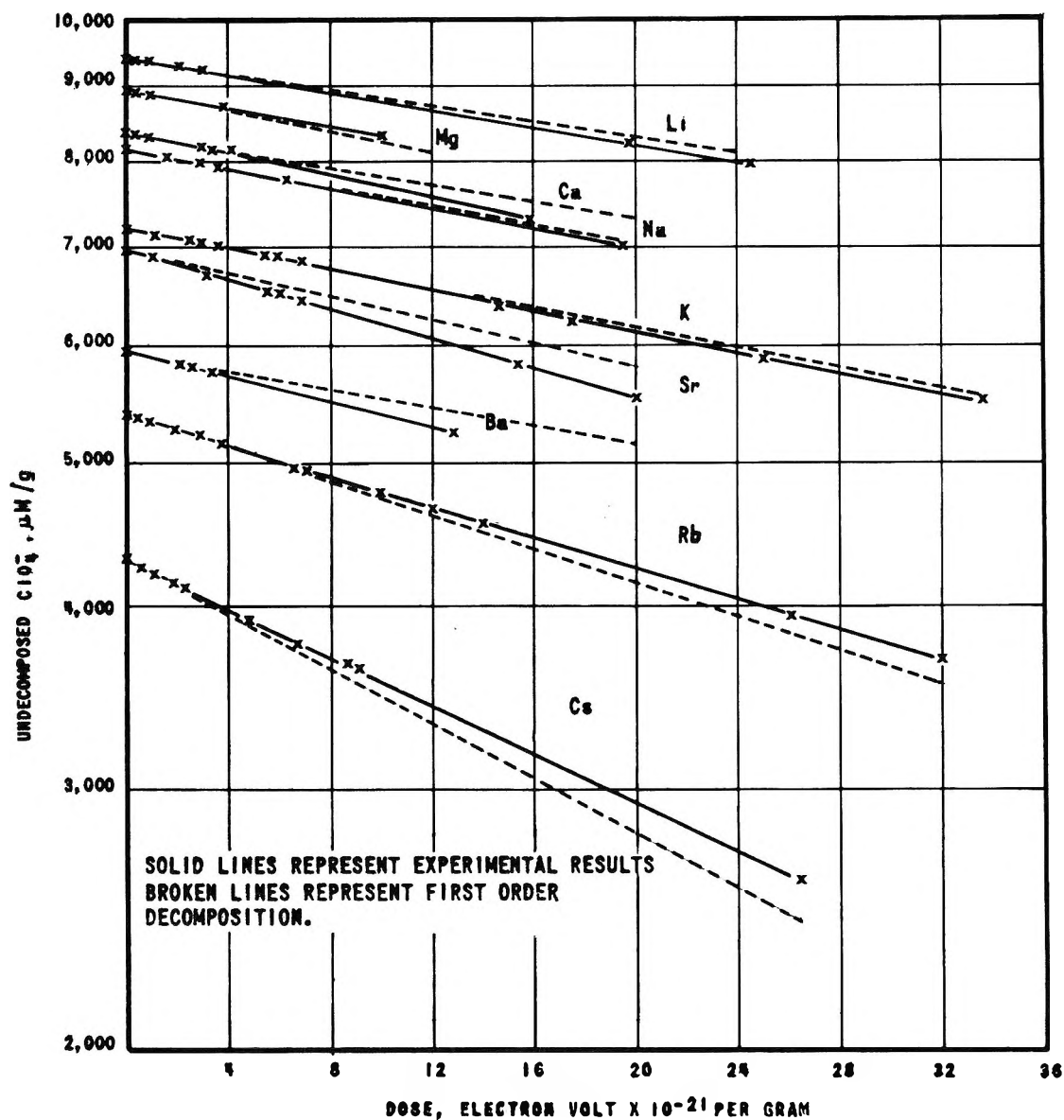


Figure 1. Semilog plot of undecomposed ClO_4^- concentrations in irradiated alkali and alkaline earth perchlorates as functions of dose.

chlorates, and there is good evidence to indicate that this is due to the different degrees of back reaction which occurs.

Effect of Temperature. In Table I are summarized the results for the decomposition of KClO_4 irradiated at different temperatures. The effect of temperature on the radiation-induced decompositions of the other perchlorates was not studied. As can be seen from Table I, the appearance of hypochlorite as a product is concurrent with a decrease in the G value for ClO_2 and ClO_2^- . It appears also that, within experimental error for analysis at these low concentrations, the sum of the concentrations of $\text{ClO}_2 + \text{ClO}^-$ is approximately constant up

to about 20° . At the higher temperatures, ClO^- is no longer observed as a product. $G_{\text{Cl}^-}^0$ is relatively constant up to 72° where there is an abrupt increase due, as will be shown later, to the thermal decomposition of ClO_2^- and ClO^- to Cl^- .

Both $-G_{\text{ClO}_4^-}^0$ and $G_{\text{ClO}_3^-}^0$ remain relatively constant except at 72 and 260° . Whether or not any significance can be attached to the increases at these temperatures cannot be determined at this writing. Certainly, stoichiometry is good at 72° , as there is ex-

(4) G. E. Boyd, E. W. Graham, and Q. V. Larson, *J. Phys. Chem.* 66, 300 (1962).

Table I: G^0 Yields of KClO_4 Irradiated at Various Temperatures and Atmospheric Pressure

Temp., °C.	$-G^0_{\text{ClO}_4^-}$	$G^0_{\text{ClO}_3^-}$	$G^0_{\text{ClO}_2^-}$	$G^0_{\text{ClO}_2}$	$G^0_{\text{ClO}^-}$	$G^0_{\text{Cl}^-}$	$G^0_{\text{O}_2}$
-196	4.0	2.7	0.58	0.18	0.00	0.5	3.0
-80	4.0	2.8	.49	.17	.00	.6	2.7
-16	3.7	2.8	.26	.06	.06	.5	2.4
-8	3.5	2.6	.26	.09	.06	.5	2.6
0	3.4	2.6	.20	.70	.06	.5	2.2
19	3.7	2.9	.20	.10	.06	.5	
20	3.7	2.9	.19	.09	.08	.5	2.5
72	4.1	3.3	.19	.09	.00	.5	2.7
260	4.9	4.2	.00	.00	.00	.7	2.0
295	3.8	2.9	.00	.00	.00	.9	1.0

cellent agreement between the experimental O_2 value and O_2 calculated from the radiolytic fragments. ($-G^0_{\text{ClO}_4^-}$ values are determined by difference.)

The G values for ClO_2^- and ClO_2 show the widest variation with temperature. At -196° , $G^0_{\text{ClO}_2^-}$ is 0.58 and $G^0_{\text{ClO}_2}$ is 0.18; at room temperature $G^0_{\text{ClO}_2^-}$ is 0.19 and $G^0_{\text{ClO}_2}$ is 0.09. The fact that ClO^- is not a product at -196° and that its appearance is accompanied by a decrease in ClO_2 and ClO_2^- , suggest that its origin may be associated with some reaction or reactions of these molecules. This will be discussed in more detail later.

Thermal Decomposition of Reaction Products. A comparison of the data in Tables II and III shows the relative stability of ClO^- , ClO_2^- , and ClO_2 in the different lattices. More extensive data on the thermal decomposition of the perchlorates can be found by consulting ref. 5. It is seen, for instance, that ClO^- is generally more stable in the alkaline earth lattices than in the alkali lattices, and that ClO_2^- and ClO_2 are least stable in the cesium and rubidium lattices. A kinetic plot of the thermal decomposition of ClO^- , ClO_2^- , and ClO_2 in irradiated perchlorate lattices does not reveal any simple order. There is a very complicated concentration dependence of these components for thermal decompositions at room temperature and at elevated temperatures. The kinetics of the thermal decomposition of these species are such that it has not been possible to obtain even a crude number for an activation energy for decomposition of any of the species.

In Table IV are summarized the results of annealing irradiated KClO_4 at different temperatures. Within experimental error, it appears that the increase in Cl^- can be accounted for by the disappearance of ClO^- and ClO_2^- . If ClO_2 is included in the Cl^- increase, there is a disparity in chlorine balance which is beyond experimental error (the ClO_3^- ion is stable at the temperatures used in these studies).

Table II: Thermal Decomposition of the Reaction Products of the Alkali Perchlorates Irradiated and Stored at Room Temperature

Sample	Dose, e.v./ g. $\times 10^{-21}$	Time, days	ClO^- , $\mu\text{moles/g.}$	ClO_2^- , $\mu\text{moles/g.}$	ClO_2 , $\mu\text{moles/g.}$
RbClO_4	31.9	0	7.3	30.8	8.0
		3	6.7	21.6	3.4
		17	1.9	14.0	1.6
CsClO_4	1.37	0	2.0	2.1	1.5
		109	0.1	0.6	0.1
CsClO_4	26.4	0	0.7	7.1	1.5
		3	0.8	5.2	1.0
		17	0.1	1.7	0.0
LiClO_4	2.35	0	3.3	5.0	9.2
		112	2.8	7.0	5.6
		112	0.9	1.9	1.3
NaClO_4	0.75	0	0.9	2.0	0.8
		112	0.9	2.0	0.8
		112	0.9	2.0	0.8
KClO_4	33.5	0	18.2	52.7	8.8
		3	16.4	52.6	4.7
		17	8.2	38.9	2.9
KClO_4	6.87	0	8.5	17.7	4.9
		113	5.5	17.0	3.7
		113	5.5	17.0	3.7

Table III: Thermal Decomposition of the Reaction Products of the Alkaline Earth Perchlorates Irradiated and Stored at Room Temperature

Sample	Dose, e.v./g. $\times 10^{-21}$	Time, days	ClO^- , $\mu\text{moles/g.}$	ClO_2^- , $\mu\text{moles/g.}$	ClO_2 , $\mu\text{moles/g.}$
$\text{Mg}(\text{ClO}_4)_2$	1.45	0	0.7	2.8	1.5
		109	0.6	2.8	1.0
$\text{Ca}(\text{ClO}_4)_2$	2.66	0	2.4	0.0	8.1
		114	2.6	1.6	4.8
$\text{Sr}(\text{ClO}_4)_2$	32.3	0	50	37	13
		3	48	36	13
		17	45	36	0
$\text{Ba}(\text{ClO}_4)_2$	28.8	0	35	56	13
		3	32	52	13
		17	28	49	5

There is evidence that in room temperature thermal decomposition, some ClO_2 is converted to ClO_2^- . This is rather difficult to detect, since ClO_2^- is also somewhat unstable, and generally a sample which has undergone thermal decomposition contains less ClO_2^- than was initially present. However, there are several instances where this has been detected.⁵ Examples are to be found in Tables II and III. The irradiated LiClO_4 sample contained more ClO_2^- after 112 days than was present immediately after removal from the radiation chamber. The irradiated $\text{Ca}(\text{ClO}_4)_2$ sample, in which initially no ClO_2^- was detected, contained some ClO_2^-

(5) L. A. Prince, Dissertation, Stevens Institute of Technology, Hoboken, N. J., June 1963.

Table IV: Analysis of Irradiated KClO₄ Heated at Different Temperatures

Dose, e.v./g. × 10 ⁻²¹	Temp., °C.	Heating time, min.	O ₂ , μmoles/g.	Cl ⁻ , μmoles/g.	ClO ⁻ , μmoles/g.	ClO ₂ ⁻ , μmoles/g.	ClO ₂ , μmoles/g.	ClO ₃ ⁻ , μmoles/g.	ClO ₄ ⁻ , μmoles/g.	Wt. loss, %
33.5	R.t.	0	562 ± 6	409 ± 6	18.2 ± 1.0	52.7 ± 1.0	8.8 ± 0.2	1269 ± 13	5644 ± 20	
	51	5498	552 ± 6	442 ± 5	2.7 ± 0.1	31.2 ± 0.6	0.8 ± 0.1	1273 ± 13	5648 ± 20	0.16
	84	2401	369 ± 4	464 ± 5	0.0	9.5 ± 0.2	0.5 ± 0.1	1267 ± 13	5647 ± 20	0.94
	151	210	244 ± 3	469 ± 5	0.0	0.3	0.0	1278 ± 13	5650 ± 20	1.43
14.7	R.t.	0	543 ± 6	149 ± 2	11.8 ± 0.3	33.7 ± 0.7	5.3 ± 0.1	611 ± 6	6410 ± 10	
	51	5498	555 ± 6	162 ± 2	5.3 ± 0.1	26.5 ± 0.5	1.2 ± 0.1	604 ± 6	6422 ± 10	0.03
5.90	R.t.	0	238 ± 3	48.8 ± 1.0	6.2 ± 0.1	14.8 ± 0.3	4.8 ± 0.1	245 ± 3	6898 ± 5	
	84	2401	239 ± 3	54.4 ± 1.0	3.0 ± 0.1	12.8 ± 0.3	1.6 ± 0.1	245 ± 3	6901 ± 5	0.00
	151	210	233 ± 3	60.5 ± 1.2	0.3	7.3 ± 0.2	0.8	247 ± 3	6902 ± 5	0.02
6.87	R.t.	0		54.8 ± 0.8	8.5 ± 0.1	17.7 ± 0.4	4.9 ± 0.1			
	52	1110		57.5 ± 0.8	6.8 ± 0.1	17.7 ± 0.4	4.1 ± 0.1			

after 112 days. The sample of KClO₄ of high absorbed dose showed no decrease in ClO₂⁻ content for the first 3 days, and nearly half of the ClO₂ decomposed during the same period, whereas there is a disproportionate drop in ClO₂⁻ content after an additional 14 days.

The principal thermal reaction of ClO₂ in the lattice above room temperature is believed to be associated with a neutralization reaction. Experimental evidence was obtained^{1c} to show that in the radiation-induced decomposition of the perchlorates there is simultaneously produced with ClO₂ an alkaline fragment MO or MO₂. It was also shown that solutions of irradiated perchlorates containing high ClO₂ contents are alkaline, and annealing irradiated perchlorates at 170° produced a neutralization reaction which removed the alkaline fragment. Since chlorine balance studies can account for ClO₂⁻ and ClO⁻, it appears that ClO₂ is the species most likely associated with the neutralization reaction.

Variation of Yields with Crystal Parameters. It has been a trend in solid inorganic salt decompositions to compare *G* values with "free space."^{3,4} Free space is defined as the difference between the volume of the crystal per ion pair and the combined volumes of the ions as calculated from accepted ionic radii. In the calculation of free space, a volume of 33.2 Å³ (rather than a 29.1 Å³ obtained from atomic volume summation) was used for the perchlorate ion, obtained by considering the perchlorate ion as a nearly regular tetrahedron with chlorine at the center and a mean Cl-O distance of 1.46 Å.³ In Figure 2 are shown the variations of $-G^0_{\text{ClO}_4^-}$, $G^0_{\text{ClO}_2^-}$, $G^0_{\text{ClO}_2}$, G^0_{ClO} , $G^0_{\text{O}_2}$, and G^0_{Cl} with free space, and in Table V is summarized a comparison of $-G^0_{\text{ClO}_4^-}$, free space, and some physical properties of the perchlorates studied. In Figure 3 are shown O₂ concentrations in the lattice of irradiated perchlorates at doses at which crystal rupture occurs, as functions of free space. The oxygen content at crystal

rupture was determined in a very simple manner: as the absorbed dose increases, a point is reached where oxygen diffuses out of the lattice, as evidenced by weight loss; by extrapolating to zero loss, the dose at which crystal rupture occurs is determined. All data were taken at room temperature.

Table V: A Comparison of Perchlorate *G*⁰ Values with Some Physical Properties and with Free Space

	$-G^0_{\text{ClO}_4^-}$	Free space per ion pair, Å ³	Exptl. density	Cation radii, Å.	Total lattice energy, kcal./mole
Ba(ClO ₄) ₂	3.20	36.4	3.69	1.43	
LiClO ₄	3.76	37.5	2.40	0.78	
Ca(ClO ₄) ₂	4.15	38.2	2.68	1.06	
Mg(ClO ₄) ₂	4.67	41.1	2.46	0.78	
NaClO ₄	4.36	43.0	2.49	0.98	156.4
Sr(ClO ₄) ₂	4.53	45.6	2.86	1.27	
KClO ₄	3.83	47.8	2.51	1.33	150.2
RbClO ₄	5.27	54.6	3.01	1.49	145.3
CsClO ₄	6.84	64.1	3.32	1.65	142.4

In Table VI are summarized the volumes of the various species produced during irradiation, calculated from atomic and ionic volumes (they are to be compared with a ClO₄⁻ volume of 29.1 Å³ similarly calculated). As can be seen, decomposition into Cl⁻ + 2O₂ requires the largest volume (the only volume increase), while decomposition into ClO₂ or ClO₂⁻ + O₂ requires the smallest volume. One would expect, therefore, a correlation between the yields of these various species and free space. It is apparent from Figure 2 that there is some correlation between these parameters, but there are some significant exceptions. There is essentially no variation in the total *G*⁰ value of ClO₂ + ClO₂⁻ of

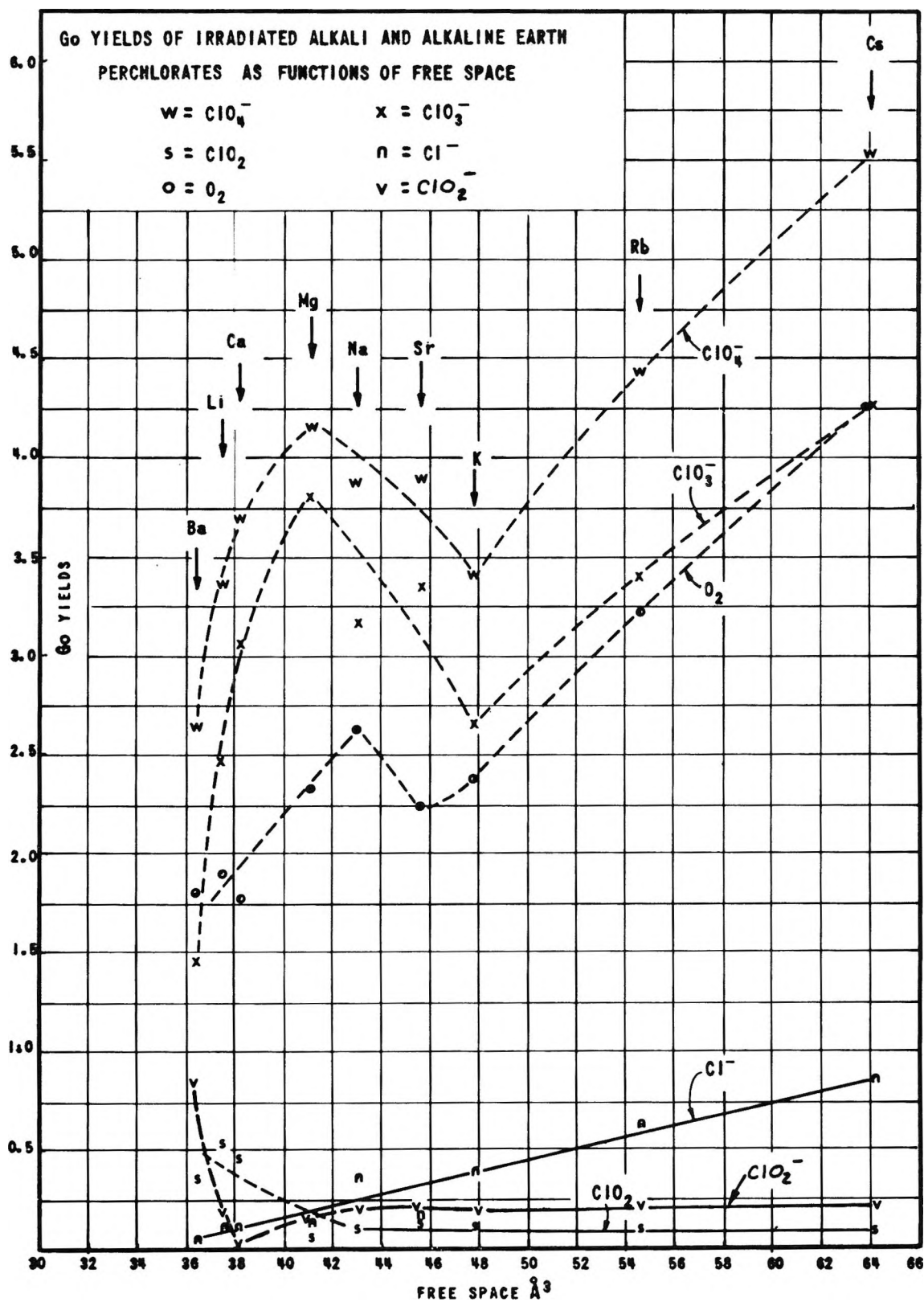


Figure 2. G⁰ yields of irradiated alkali and alkaline earth perchlorates as functions of free space.

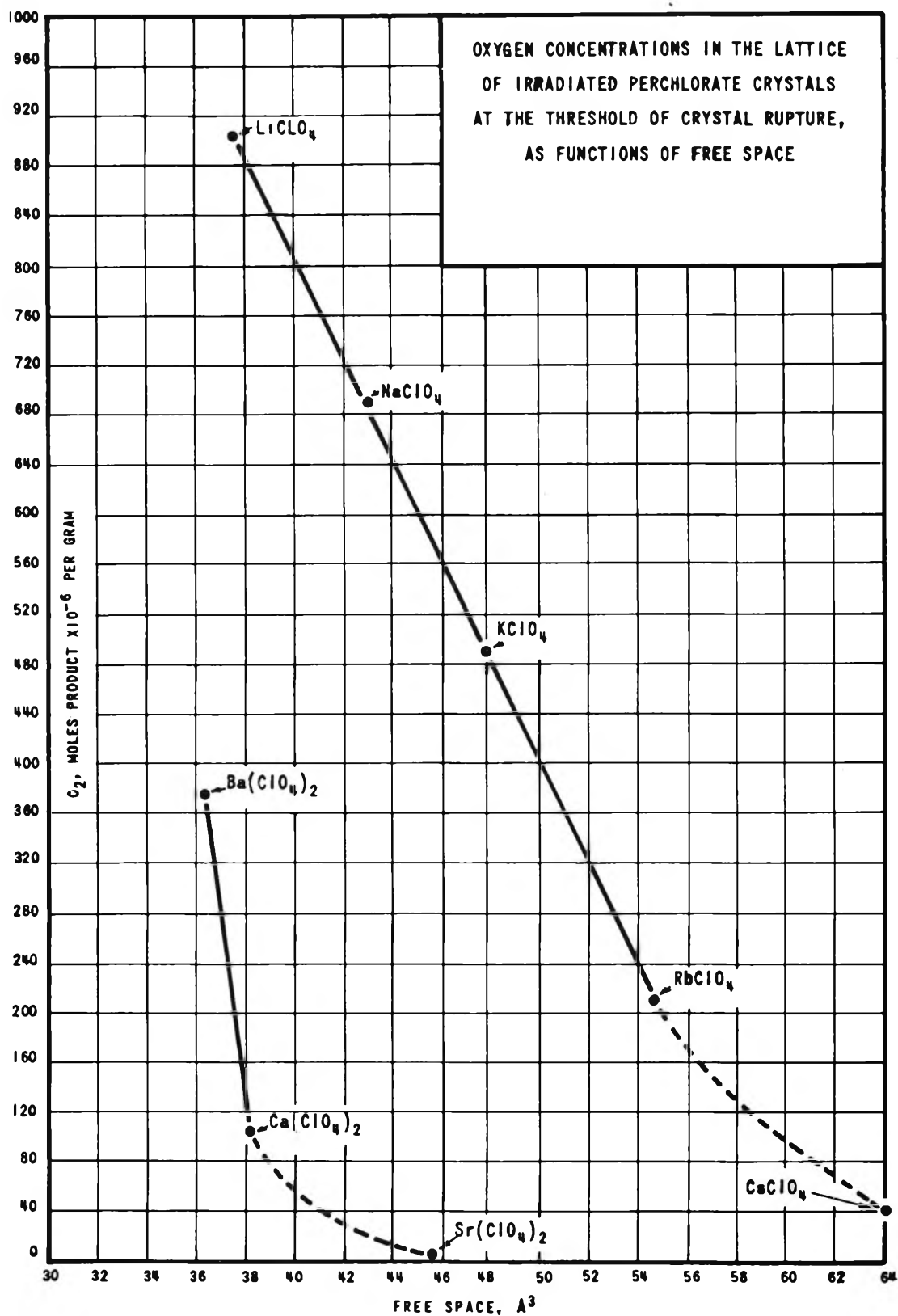


Figure 3. Oxygen concentrations in the lattice of irradiated perchlorate crystals at the threshold of crystal rupture, as functions of free space.

NaClO_4 , $\text{Sr}(\text{ClO}_4)_2$, KClO_4 , RbClO_4 , and CsClO_4 , yet there is approximately a 35% change in free space.

Table VI: Volumes of Fragments from the Radiolytic Decomposition of the Perchlorate Ion

Fragments	Approximate total volume, \AA^3
$\text{Cl}^- + 2\text{O}_2$	32
$\text{ClO}_3^- + \text{O}$	25
$\text{ClO}_2^- + \text{O}_2$	19
$\text{ClO}_2 + \text{O} + \text{O}^-$	13
$\text{ClO}_2 + \text{O}_2^-$	13
$\text{ClO}_3 + \text{O}^-$	13
$\text{ClO}^- + \text{O}_2 + \text{O}$	13

Free space is only one aspect of the over-all factors governing ease of decomposition of the perchlorates; like the nitrates, these factors are dependent on crystal structure, impurities, and previous history; *i.e.*, the immediate environment of the decomposing species.⁶ If free space *per se* is the deciding factor in solid inorganic decomposition, then cage effects should be operable at all times—which they are not—and one should observe substantial isotope effects in these decompositions. G^0 values for perchlorate decomposition correlate equally well with lattice energies and ease of crystal rupture as they do with free space. From Figure 3 it is apparent that those lattices which contain the smallest free space can withstand the largest internal pressure.

The factor which is believed to be the most important in deciding relative ease of decomposition in a homologous series like the perchlorates, nitrates, bromates, etc., is the relative ease of transfer of electronic excitation energy to the vibrational modes in the crystal.

Changes in Product Yields with Radiation. Examination of dose-yield curves in ref. 1c shows that very definite changes in yields of the products occur as the per cent decomposition increases.

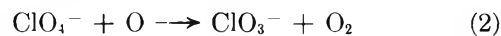
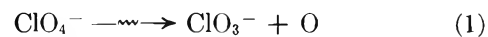
To determine whether changes in yields could be explained by the depletion of perchlorate ions and the decomposition of the products, a study was made comparing the actual composition of irradiated samples of KClO_4 , RbClO_4 , and CsClO_4 with the composition calculated from G^0 values, making an appropriate correction for ClO_4^- depletion.⁵ With KClO_4 the total decrease in $\text{ClO}_3^- + \text{ClO}_2^- + \text{ClO}_2 + \text{ClO}^-$ concentrations was considerably less than the increase in the Cl^- concentration, as compared with the calculated values. Since decomposition of the products alone cannot account for the G_{Cl^-} increase, it must arise directly from $\text{ClO}_4^- \rightarrow \text{Cl}^- + 2\text{O}_2$. However, with both RbClO_4 and

CsClO_4 the total decrease in $\text{ClO}_3^- + \text{ClO}_2^- + \text{ClO}_2 + \text{ClO}^-$ concentrations was very much greater than the increase in the Cl^- concentration (by nearly a factor of 2). Here one must assume recombination of $\text{ClO}_3^- + \text{O}$ to form ClO_4^- , or the less likely prospect of increased ability of the lattice to dissipate the absorbed energy in a manner which does not cause decomposition.

The recombination of the $\text{ClO}_3^- + \text{O}$ to form ClO_4^- is supported by the observation of Burchill,⁷ who found ClO_4^- in γ -irradiated sodium, potassium, and barium chlorates. Perchlorate was also found in pile-irradiated sodium chlorate by Sharman and McAllum.⁸

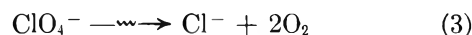
Mechanism of the Decomposition. The decomposition of the perchlorates is most certainly a very complicated process since it involves changes in product yields, back reaction, and thermal decomposition. However, it is possible to indicate certain reaction paths which must occur.

The fact that ClO_3^- is the major primary product in all perchlorate decompositions would indicate that the reactions



are important in the decomposition.

Chloride yields appear to be independent of temperature, indicating that thermal activation is not necessary for its formation. This would indicate a direct decomposition to $\text{Cl}^- + 2\text{O}_2$.



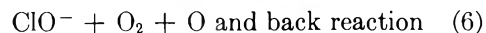
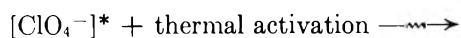
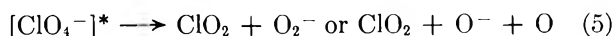
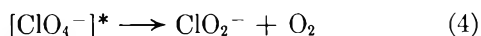
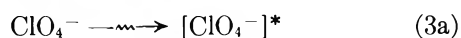
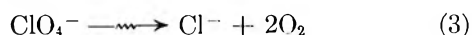
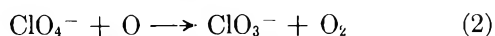
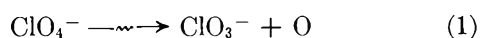
The appearance of ClO^- with a simultaneous decrease in ClO_2^- and ClO_2 suggests that there may be a relationship between these molecules. There appears also to be some connection between ($G_{\text{ClO}_2}^0 + G_{\text{ClO}_2^-}^0$) and $G_{\text{Cl}^-}^0$. Referring to Figure 2, it appears that these two quantities are inversely related, *i.e.*, high $G_{\text{Cl}^-}^0$ values are associated with low ($G_{\text{ClO}_2}^0 + G_{\text{ClO}_2^-}^0$) values. These considerations favor the idea of some common primary species, such as $[\text{ClO}_4^-]^*$, ClO_4^{-2} , or ClO_4 . Of these, the available data would favor $[\text{ClO}_4^-]^*$ or ClO_4^{-2} , since the ClO_4 radical would be expected to yield $\text{ClO}_2 + \text{O}_2$, or $\text{Cl} + 2\text{O}_2$, which would lead to further speculation as to the lack of Cl_2 in the decomposition products, and to the origin of the alkaline fragment shown to be associated with ClO_2 .

Considering these facts, an over-all mechanism for perchlorate decomposition, exclusive of thermal decomposition of the products, would be

(6) J. Cunningham, *J. Am. Chem. Soc.*, **85**, 3716 (1963).

(7) C. E. Burchill, *Nature*, **191**, 194 (1962).

(8) L. J. Sharman and K. J. McAllum, *J. Chem. Phys.*, **23**, 597 (1955).



Acknowledgment. The authors wish to extend their thanks to the Research Division of the Atomic Energy Commission for their support of this research and to the Union Carbide Corporation, Linde Division, for the many courtesies extended to them.

Lattice Energies of Ionic Crystals. II. Some Group I-A and II-A Salts

by Arthur Finch and P. J. Gardner

Royal Holloway College, University of London, Englefield Green, Surrey, United Kingdom
(Received April 15, 1964)

The lattice energies of group I-A bromates and iodates and of group II-A hydroxides, nitrates, and chlorates have been calculated using an established correlation between combined ion hydration enthalpy and an anion parameter. The electron affinities of various XO_3 radicals have been estimated.

Introduction

The determination of the lattice energies of crystals by direct calculation is restricted to simple systems for which extensive structural data are available.^{1,2} In the absence of detailed structural information and to avoid the force-field assumptions implicit in such term-by-term calculations, the usual procedure is application of the Born-Haber cycle (method a). The major restriction to this approach is the nonavailability of the electron affinities of anions other than halides. Use is therefore made of less fundamental methods such as (b) a semiempirical equation, as in Kapustinkii's³ approach, (c) extrapolation or interpolation from known data of a series, as in a Karapet'yants⁴ graph, or (d) the empirical estimation of combined ion hydration enthalpies which, on combination with enthalpy of solution data, yield values for lattice enthalpies. These methods have been extensively exploited⁵ for uni-univalent systems and, to a lesser extent

(except approach d), for di-univalent systems. For the salts considered in this work, neither structural nor electron affinity data are available; we have, therefore, applied methods b and d, supplemented when necessary by (c), to derive lattice energy values. We report also (experimental) solution enthalpy data for group II-A chlorates in order to use approach d.

Experimental

(a) *Calorimeter.* A glass dewar, constant temperature environment calorimeter⁶ was used for solution en-

(1) T. C. Waddington, *Advan. Inorg. Chem. Radiochem.*, **1**, 157 (1959).

(2) D. Cubicciotti, *J. Chem. Phys.*, **31**, 1646 (1959).

(3) A. F. Kapustinkii, *Quart. Rev. (London)*, **10**, 283 (1956).

(4) M. Karapet'yants, *Zh. Fiz. Khim.*, **28**, 1136 (1954). (See also ref. 5b.)

(5) (a) D. F. C. Morris, *J. Inorg. Nucl. Chem.*, **6**, 295 (1958); (b) *Rec. trav. chim.*, **78**, 150 (1959).

(6) A. Finch and P. J. Gardner, *J. Chem. Soc.*, 2985 (1964).

thalpy determinations. The calorimeter was totally immersed in a thermostat maintained at $25 \pm 0.01^\circ$, and temperature differences were measured to $\pm 1 \times 10^{-3}^\circ$ using an F53 thermistor (Standard Telephones and Cables Ltd.). The temperature variation for each run was monitored using a miniature platinum resistance thermometer coupled to a 15.24-cm. potentiometric recorder, the trace from which was used to estimate thermal leakage. Calibration was electrical, and samples were contained in fragile glass ampoules.

(b) *Materials.* Commercial samples (British Drug Houses) of magnesium, calcium, strontium, and barium chlorates were obtained as hydrates. Barium chlorate was recrystallized from water, and all chlorates were dehydrated at 100° and 14 mm. Unfortunately, magnesium chlorate was found to decompose before dehydration. Subsequent to dehydration, samples were handled in a nitrogen-filled drybox. Analysis for chlorate was by conventional procedures [calcium chlorate, 99.1%; strontium chlorate, 99.2%; barium chlorate, 99.7% of the calculated value].

(c) *Units.* All enthalpy changes are expressed in terms of the thermochemical calorie defined by 1 calorie = 4.1840 absolute joules.

If N is the ratio of the number of moles of H_2O to the number of moles of $\text{M}^{\text{II}}(\text{ClO}_3)_2$ and T is the mean temperature of the solution period, the experimental enthalpy changes for reaction 1 are shown in Table I.

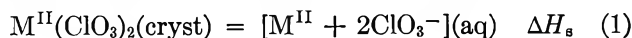


Table I

M^{II}	$T, ^\circ\text{C.}$	N	$\Delta H_s, \text{kcal. mole}^{-1}$	ΔH_s (accepted), kcal. mole^{-1}
Ba	24.1	555	5.62	5.64 ± 0.05
	24.8	497	5.71	
	24.6	305	5.67	
	24.7	473	5.58	
Sr	24.7	453	0.64	0.61 ± 0.05
	24.6	381	0.58	
Ca	24.2	525	-5.59	-5.60 ± 0.02
	25.1	977	-5.61	
Mg	25	-17.5 ± 2.0^a

^a Estimated value; see Method of Calculation and Results.

Method of Calculation and Results

Kapustinkii³ (method b) found empirically that the change in the reduced Madelung constant was proportional to the change in the interatomic distance in passing from one lattice type to another. In effect, the

isoenergetic rebinding of an unknown crystal into a rock salt lattice is envisaged, the lattice energy of the unknown crystal being given by eq. 2 in terms of rock salt lattice parameters.

$$U^\circ_{\text{K}} = \frac{287.2\nu z_+ z_-}{(r_c + r_A)} \left[1 - \frac{0.345}{(r_c + r_A)} \right] \quad (2)$$

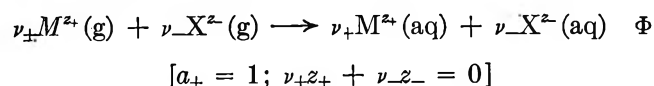
where r_c are r_A = Goldschmidt cationic and anionic radii, ν = number of ions per molecule, z_+ and z_- = cationic and anionic charges. Experimentally, it has been found that lattice energies derived from Kapustinkii's equation are generally lower than those obtained by extended calculation. Accordingly, Yatsimirskii⁷ has modified Kapustinkii's equation to the form

$$U^\circ_{\text{KY}} = \frac{287.2\nu z_+ z_-}{(r_c + r_A)} \left[1 - \frac{0.345}{(r_c + r_A)} \right] + 2.5\nu z_+ z_- \quad (3)$$

The radius of a complex anion (r_A) is either obtained by estimation of the repulsion envelope^{8,9} or by utilizing Yatsimirskii's "thermochemical radii." Values of lattice energies calculated by this method are listed in subsequent tables under the heading U°_{KY} .

Karapet'yants' method c involves constructing a graph of the lattice energies of a known complete series (say, $U(\text{M}^{\text{I}}\text{Cl})$ or $U(\text{M}^{\text{II}}\text{Cl}_2)$) vs. the lattice energies of an incomplete series (e.g., $U(\text{M}^{\text{I}}\text{X})$ or $U(\text{M}^{\text{II}}\text{X}_2)$) and interpolating or extrapolating the required unknown values. This is used in estimation of relevant functions for iodates.

Method d, which is probably the most reliable for complex systems, combines an empirically determined combined ion hydration enthalpy Φ , defined by a relationship of the type



with an experimentally determined solution enthalpy, ΔH_s° , via

$$\Delta H_s^\circ = \Delta H_L^\circ + \Sigma \phi_i \quad (4)$$

where ϕ_i is the ion hydration enthalpy of the i th species, and ΔH_L° is the lattice enthalpy at 25° . The lattice energy U° is then calculated by substitution in

$$U^\circ = \Delta H_L^\circ - \nu RT \quad (5)$$

To determine the combined ion hydration enthalpy, two empirical correlations (i) between Φ and anion

(7) K. B. Yatsimirskii, *Russ. J. Inorg. Chem.*, **6**, 265 (1961).

(8) P. Gray and T. C. Waddington, *Proc. Roy. Soc. (London)*, **A235**, 481 (1956).

(9) T. C. Waddington, *Trans. Faraday Soc.*, **54**, 25 (1958).

radius (r_-) and (ii) between Φ and anion lyotropic number (N_1) are established. Anion radii are usually based on the Pauling scale, and for complex anions some assumptions regarding ion symmetry are necessary. Lyotropic number is a concept introduced by Buchner,¹⁰ which expressed quantitatively the position of an ion in the Hofmeister series. However lyotropic data for only a restricted number of ions are available. The correlation graphs of $\Phi(MX)$ vs. r_- and $\Phi(MX)$ vs. N_1 are well established for the group I-A halides. For this series $\Phi(MX)$ was determined by substituting experimentally known ΔH_s° and calculated $\Delta H_L^\circ(MX)$ values¹¹ into eq. 4 and 5. Corresponding $\Delta H_L^\circ(MX_2)$ values are not available, but evidence has been presented¹² for the validity of interpolation graphs for group II-A salts using hydration enthalpy data calculated by Noyes.¹³ Values of lattice energies calculated from this method are listed in subsequent tables under the heading U° , and it is from these values that ΔH_f° (anion gas) figures are derived.

Results. A. Alkali Metal Bromates. Interpolating a value of 9.5 for $N_1(\text{BrO}_3^-)$ the results in Table II are obtained.

Table II

	ΔH_s°	Φ (M^+ - BrO_3^-)	ΔH_L°	U°	ϕ (BrO_3^-)	U°_{KY}	ΔH_f° (BrO_3^-) (g)
LiBrO ₃	0.34	-212.0	+212.3	211	-91	212	-33.7
NaBrO ₃	6.35	-186.5	+192.8	192	-91.5	182	-35.1
KBrO ₃	9.70	-168.5	+178.2	177	-92.5	163	-32.9
RbBrO ₃	11.7	-161.5	+173.2	172	-92.5	157	-34.0
CsBrO ₃	12.0	-154.5	+166.0	165	-92	149	-33.6

The ΔH_s° values are those of Boyd and Vaslow,¹⁴ ΔH_L° and U° are obtained from eq. 4 and 5 and U°_{KY} from (3) using a thermochemical radius of 1.91 Å. for BrO_3^- .

$\phi(\text{BrO}_3^-)$ is obtained from

$$\Phi(MX) = \Sigma \phi_i \quad (6)$$

using $\phi(M^+)$ data of Latimer, *et al.*¹⁵ Data for $\Delta H_f^\circ(\text{BrO}_3^-)(g)$ are obtained from

$$\Delta H_L^\circ = \Delta H_f^\circ(M^+)(g) + \Delta H_f^\circ(X^-)(g) - \Delta H_L^\circ(MX)(\text{cryst}) \quad (7)$$

using the National Bureau of Standards Circular 500 values for $\Delta H_f^\circ(M^+)(g)$ and those of Boyd,¹⁴ *et al.*, for $\Delta H_f^\circ(MX)(\text{cryst})$. An independent check of the assumption of the ionic nature of the series is provided by the very satisfactory consistency of the values of $\Delta H_f^\circ(\text{BrO}_3^-)(g)$ from salt to salt.

B. Group I-A Iodates. Solution enthalpy and ΔH_f° data are lacking for rubidium and cesium salts. Values of ΔH_L° were obtained directly from a Karapet'yants-type plot (Figure 1). This method provides only very crude estimates of ΔH_L° . The linearity of such graphs is illustrated in Figure 1 for nitrates and bromates. The error in the extrapolated iodate data arises from

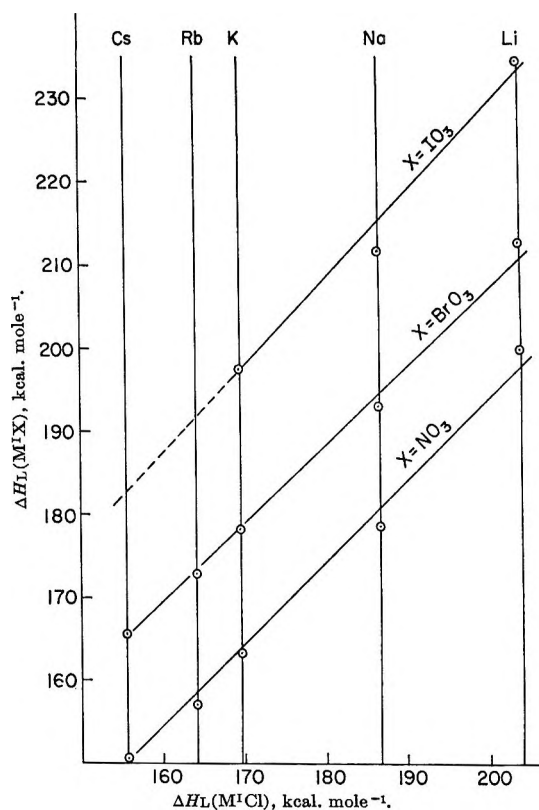


Figure 1. Karapet'yants-type graph for the extrapolation of approximate data for the lattice enthalpies of rubidium and cesium iodates.

the extrapolation error and the intrinsic error of the extrapolation data. The former is of the order of ± 3 kcal. mole⁻¹, and the latter is considered in the Discussion. A better procedure is to estimate ΔH_s° values for these salts from a graph of ΔH_s° vs. $\phi(M^+)$, using values taken from Latimer. Values for ΔH_L° are, however, in good agreement by both methods and are

- (10) See A. Voet, *Chem. Rev.*, **20**, 169 (1937).
 (11) M. L. Huggins, *J. Chem. Phys.*, **5**, 143 (1937).
 (12) A. Finch and P. J. Gardner, *J. Inorg. Nucl. Chem.*, in press.
 (13) R. M. Noyes, *J. Am. Chem. Soc.*, **84**, 513 (1962).
 (14) G. E. Boyd and F. Vaslow, *J. Chem. Eng. Data*, **7**, 237 (1962).
 (15) W. M. Latimer, K. S. Pitzer, and C. M. Slansky, *J. Chem. Phys.*, **7**, 108 (1939).

included in Table III with corresponding data for other metal iodates.

The ΔH_s° data for sodium and potassium iodates are from Hepler,¹⁶ and those for lithium are from Murgulescu.¹⁷ The lyotropic number for the iodate anion is 6.3, and a thermochemical radius of 1.82 Å. was used to calculate U_{KY}° .

Table III

	ΔH_s°	Φ ($M^I IO_3$)	ΔH_L°	U°	U_{KY}°	ΔH_f° (IO_3^-)(g)	$\phi(IO_3^-)$
LiIO ₃	1.59	-233	234.6	233	208	-49.2	-112
NaIO ₃	4.83	-207	211.8	211	187	-51.1	-112
KIO ₃	6.5	-191	197.5	196	167	-46.9	-115
RbIO ₃	8.3 ^a	-182	(191) ^b (190.3) ^c	189	160	...	-113
CsIO ₃	9.1 ^a	-175	(182) ^b (184.1) ^c	182	154	...	-113

^a Extrapolated from Figure 2. ^b Extrapolated from Figure 1. ^c From eq. 4 and extrapolated Figure 2 data.

C. Group II-A Hydroxides. For group II-A crystals, interpolated Φ -data were obtained from plots of $\Phi(MX_2)$ ($X = \text{halogen}$) vs. r_- or N_1 , the validity of the correlation graphs having been previously established.¹² No lyotropic data are available for the hydroxide ion, and Goubeau's estimate¹⁸ of the crystal radius of 1.47 Å. was used for interpolation; Yatsimirskii's "thermochemical radius" of 1.40 Å. was used in calculating U_{KY}° .

D. Group II-A Nitrates. Similar data for the group II-A nitrates are shown in Table V, interpolating

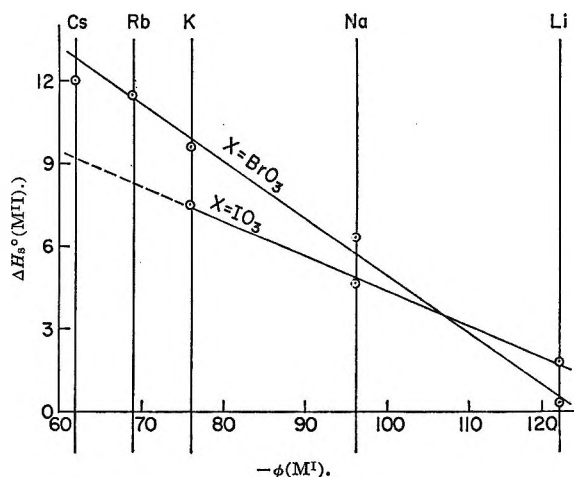


Figure 2. Graph of standard enthalpy of solution vs. cationic hydration enthalpy (ref. 15) to extrapolate approximate data for $\Delta H_s^\circ(\text{RbIO}_3)$ and $\Delta H_s^\circ(\text{CsIO}_3)$.

Table IV

	ΔH_s° ^a	Φ [M ^{II} - (OH) ₂]	ΔH_L°	U°	U_{KY}°	$\phi(\text{OH}^-)$	ΔH_f° (OH ⁻) (g)
Be(OH) ₂							
α-form	13.8	-819	832.8	831	809	-105.5	-49.2
Mg(OH) ₂	0.7	-684	687.7	686	680	-105.4	-49.4
Ca(OH) ₂	-3.9	-605	601.1	599	617	-105.3	-49.0
Sr(OH) ₂	-11.0	-570	559.0	557	577	-105.4	-49.0
Ba(OH) ₂	-12.4	-536	513.6	512	550	-105.3	-54.1

^a ΔH_s° data from NBS Circular 500.

for Φ and using $N_1(\text{NO}_3^-) = 11.6$; U_{KY}° was calculated using a "thermochemical radius" of 1.89 Å.

Table V

	ΔH_s° ^a	Φ [M ^{II} - (NO ₃) ₂]	ΔH_L°	U°	U_{KY}°	ϕ (NO ₃ ⁻)	ΔH_f° (NO ₃ ⁻) (g)
Mg(NO ₃) ₂	-20.43	-612	591.6	590	593	-69.4	-79.5
Ca(NO ₃) ₂	-4.51	-534	529.5	528	542	-69.8	-79.1
Sr(NO ₃) ₂	4.23	-498	502.2	500	520	-69.4	-79.4
Ba(NO ₃) ₂	9.65	-464	473.6	472	500	-69.3	-79.6

^a ΔH_s° data from NBS Circular 500.

E. Group II-A Chlorates. For group II-A chlorates, a lyotropic number of 10.7 was used for interpolation, ΔH_s° data were as recorded in the Experimental section, and "thermochemical radius" of 2.00 Å. was used. A value of $\Delta H_s^\circ[\text{Mg}(\text{ClO}_3)_2]$ was extrapolated from a $\phi(\text{M}^{\text{II}})$ vs. $\Delta H_s^\circ[\text{M}^{\text{II}}(\text{ClO}_3)_2]$ plot as $\text{Mg}(\text{ClO}_3)_2$

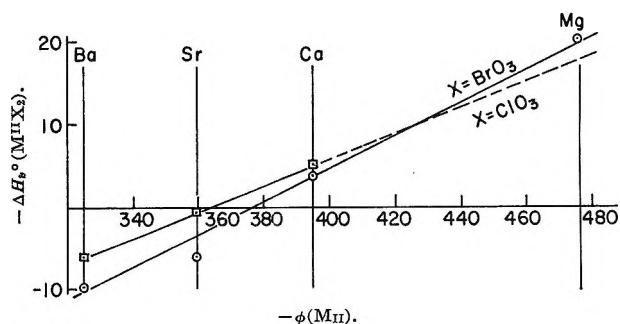


Figure 3. Graph of standard enthalpy of solution vs. cationic hydration enthalpy (ref. 13) to extrapolate an approximate datum for $\Delta H_s^\circ[\text{Mg}(\text{ClO}_3)_2]$.

(16) L. G. Hepler and J. G. Spencer, *J. Phys. Chem.*, **64**, 499 (1960).

(17) I. G. Murgulescu and E. Tomus, *Analele Univ. "C. I. Parhon," Ser. Stiint. Nat.*, **10**, 13 (1961).

(18) J. Goubeau, *Z. physik. Chem. (Leipzig)*, **334**, 432 (1936).

Table VI

	ΔH_s°	Φ [M^{II}] (ClO_3) ₂	ΔH_L°	U°	U°_{KY}	ϕ (ClO_3^-)	ΔH_f° (ClO_3^-) (g)
$Mg(ClO_3)_2$	-17.5	-626	608	606	580	-76.3	-64 ± 3
$Ca(ClO_3)_2$	-5.6	-548	542	540	525	-76.7	-52.0
$Sr(ClO_3)_2$	0.6	-512	513	511	505	-76.5	-45.8
$Ba(ClO_3)_2$	5.6	-479	485	483	476	-76.7	-40.4

was not obtainable in anhydrous form (see Figure 3 and Table VI). To calculate $\Delta H_f^\circ(ClO_3^-)(g)$ from eq. 7, values of $\Delta H_f^\circ[M^{II}(ClO_3)_2](cryst)$ are required. These are not available from the literature so estimates were made using the relationship

$$\Delta H_f^\circ[M^{II}(ClO_3)_2](cryst) = 2\Delta H_f^\circ(ClO_3^-)(aq) + \Delta H_f^\circ[M^{II}](aq) - \Delta H_s^\circ \quad (8)$$

with standard enthalpies of formation of aqueous ions taken from NBS Circular 500.

Discussion

Of the empirical methods for the determination of lattice energy outlined in the Introduction, method d is most fully exploited in this paper. A general discussion of the accuracy of the method is therefore in order. In using eq. 4, 5, and 6 to determine lattice energies, the Φ -term generally contributes over 90% of the final result. For group I-A halides this term is as accurate as the calculated^{2,11} lattice energies. For group II-A halides, the Φ -term is as accurate as Noyes' data for ϕ_i .¹² For any other anion, the accuracy of Φ depends on the accuracy of the data for N_1 or r_- . The correlation graphs of Φ vs. N_1 are generally linear whereas Φ vs. r_- plots exhibit shallow curvature. With the exception of group II-A hydroxides, interpolation is *via* the former graph. The bulk of the lyotropic number data was recorded by Buchner and Klein¹⁹ working with agar-agar sols and by Buchner and Postma,²⁰ who used gelatin sols. According to these authors, no special precautions were taken to ensure that experimental conditions of the determinations were reproducible. Lyotropic numbers have recently been recalculated²¹ from the original data; arbitrary limits of error of ±0.2 were assigned to lyotropic data independently checked, and to data obtained from one sol only were assigned limits of error of ±1.0.

The gradients of the lyotropic interpolation graphs are 14 and 6 kcal. per lyotropic unit, respectively, for group I-A and II-A halides.

Mean values of $\Delta H_f^\circ(X^-)(g)$ and $\phi(X^-)$ are collected in Table VII and compared with literature values.

(i) A value for $\Delta H_f^\circ(ClO_3)(g)$ is not quoted because

Table VII^a

	$\Delta H_f^\circ(X^-)(g)$	$\Delta H_f^\circ(X^-)(g)$ [lit.]	$\phi(X^-)$	$\phi(X^-)$ [lit.] ^b
ClO_3	...	-47 ^c	-76	-69
BrO_3	-34	...	-92	...
IO_3	-49	-77 ^c	-113	...
OH	-49	-50 ^d	-105	-122
NO_3	-79	-79 ^c	-70	-74

^a Units are kcal. mole⁻¹. ^b See ref. 22. ^c See ref. 5a. ^d See ref. 1.

the results obtained (Table VI) are not sufficiently consistent. This is probably because $\Delta H_f^\circ[M^{II}(ClO_3)_2]$ data, on which $\Delta H_f^\circ(ClO_3^-)(g)$ depends, were estimated from eq. 8 which implies a wholly ionic model. Values from heat capacity data are not available. (ii) The excellent agreement between these and literature sources for ΔH_f° values of hydroxide and nitrate ions give some confidence in the new and different values for $\phi(NO_3^-)$ and $\phi(OH^-)$. Literature values²² for this latter function are due to "best" values selected from the literature up to 1960. Very wide divergence in quoted values for ϕ is a feature of this parameter. (iii) The new figure for $\Delta H_f^\circ(IO_3^-)(g)$ differs greatly from the current literature value. The reference given for this^{5a} is derivative.

It is of interest to estimate values of the electron affinities (E) of the radicals XO_3 (X = halogen). An estimate of $\Delta H_f^\circ(XO_3)(g)$ is required, and only for $X = Cl$ is the species XO_3 more than transiently stable. Consequently, bond energy data $E(X-O)$ in XO_3 is lacking. Although an isolated datum for $\Delta H_f^\circ(ClO_3)(g)$ is available, it was decided to recalculate $\Delta H_f^\circ(XO_3)(g)$ assuming $E(X-O)$ in $XO_3 \sim D(X-O)$ and using Durie and Ramsay's data²³ for bond dissociation energies of halogen-oxygen bonds. Results from eq. 9 and 10 are shown in Table VIII.

$$\Delta H_f^\circ(XO_3)(g) = \Delta H_f^\circ(X)(g) + 3\Delta H_f^\circ(O)(g) - 3D(X-O) \quad (9)$$

$$E = \Delta H_f^\circ(XO_3)(g) - \Delta H_f^\circ(XO_3^-)(g) \quad (10)$$

The ionic systems studied in this paper are all of the

(19) E. H. Buchner and D. Klein, *Proc. Acad. Sci. Amsterdam*, **30**, 740 (1927).

(20) E. H. Buchner and G. Postma, *Proc. Koninkl. Acad. Wetenschap.*, **34**, 699 (1931).

(21) P. J. Gardner, Thesis, University of London, 1963.

(22) V. P. Vasil'ev, E. K. Zolotarev, A. F. Kapustinkii, K. P. Mischenko, E. A. Podgornaya, and K. B. Yatsimirskii, *Zh. Fiz. Khim.*, **34**, 1763 (1960).

(23) R. A. Durie and D. A. Ramsay, *Can. J. Phys.*, **36**, 35 (1958).

Table VIII

	$\Delta H_f^\circ (\text{XO}_3) (\text{g})$	$\Delta H_f^\circ (\text{XO}_3^-) (\text{g})$	E
ClO_3	17.7 ± 0.1	-47	65 ± 0.5
BrO_3	39.8 ± 0.2	-34	74 ± 0.5
IO_3	78 ± 15	-49	127 ± 16

general formula $\text{M}^{\text{I}}\text{X}^{\text{I}}$ or $\text{M}^{\text{II}}\text{X}^{\text{I}}_2$, for this is the form of the template graphs used for interpolation. Extension of the method to cover systems of the type $\text{M}^{\text{I}}_2\text{X}^{\text{II}}$ and $\text{M}^{\text{II}}\text{X}^{\text{II}}$ is discussed in a further publication.

Acknowledgments. It is a pleasure to thank the American Chemical Society (Petroleum Research Fund) for partial financial support.

Effect of Hydrostatic Pressure on Gases Dissolved in Water

by T. Enns, P. F. Scholander, and E. D. Bradstreet

University of California, San Diego, La Jolla, California^{1a,b} (Received May 1, 1964)

The effect of hydrostatic pressure on equilibrium pressures of a gas dissolved in water has been determined by direct measurement. At approximately 100 atm. hydrostatic pressure the equilibrium pressure increase was approximately 13% for helium, 16% for carbon dioxide, and 14% for nitrogen, oxygen, and argon. Extrapolation of the data indicates that when dissolved surface gases are carried to a depth of 10,000 m., their equilibrium partial pressure increases by a factor of 4.

Several species of deep water fish have swim bladders in which partial pressures of nitrogen gas up to 10 atm. have been observed. As the apparent source of this gas is the atmosphere, the gas pressure must have increased correspondingly. Before determining the role played by the fish in inflating its swim bladder at high pressures, it is necessary to determine the equilibrium pressure for dissolved gases at various depths.

The literature gives no direct data on such gas equilibrium pressures. An attempt to calculate the pressures from the partial molal volume data of Kritchevsky and Iliinskaya² has been made by Klotz,³ but, contrary to existing information, the implication in the equations is that gas diffusion equilibrium exists between surface and ocean deeps. Considerable information is available on the solubility of gases at high pressures applied to both gas and liquid. The data of Wiebe, Gady, and Heins⁴ for nitrogen at 75 and 100 atm. when inserted in eq. 4 below give a partial molal volume of 32.1 cm.³ which agrees with the values in Table I.

Water equilibrated with gas at or near atmospheric pressure has been subjected to hydrostatic pressures up to approximately 100 atm., and the resultant gas equilibrium pressure has been determined directly. In nitrogen, oxygen, and argon the gas equilibrium pressure increase was approximately 14%/100 atm. Helium showed a slightly smaller and carbon dioxide a slightly greater equilibrium pressure increase.

Simple thermodynamic calculations extrapolate the data to give equilibrium pressures of gases dissolved at the surface and carried to ocean depths. The same calculations yield new values of partial molal volumes

(1) (a) Contribution from the Scripps Institution of Oceanography, University of California, San Diego; (b) this work was supported by Research Grants RG 5979 and GM 10521 from the U. S. Public Health Service.

(2) I. Kritchevsky and A. Iliinskaya, *Acta Physicochim. URSS*, 20, 327 (1945).

(3) I. M. Klotz, *Limnol. Oceanog.*, 8, 149 (1963).

(4) R. Wiebe, V. L. Gady, and J. Heins, *J. Am. Chem. Soc.*, 55, 947 (1933).

Table I^a

Gas	p in mm. at $P = 102$ atm.	p in mm. at $P = 68$ atm.	p in mm. at $P = 34$ atm.	p in mm. at $P = 0$	\ln ($p_{102}/$ p_0)	δ , cm. ³ / mole
O ₂	839.5	805	771	734.5	0.133	31.9
	892	855	819	781	.133	31.9
	410.5	390	373	359	.1345	32.2
	508	484	464	443	.135	32.3
O ₂ at 0.5°	789			682	.1457	32.0
O ₂ in sea water	842	806	775	737	.131	31.7
N ₂	843	803	773	733	.1385	33.2
	811	777	744	705	.1385	33.2
	844	806.5	769	732	.140	33.5
N ₂ in detergent	811	774	742	712	.133	31.9
Ar	849	814	779	741	.135	32.3
	839	803	771	734	.134	32.1
He	815 ^b	779	748	719	.124	29.7
	828.5	797.5	765	732	.124	29.7
CO ₂	817	779	742	705	.1475	35.3
	849.5	811.5	774	737	.143	34.3

^a P = Hydrostatic pressure; p = gas equilibrium pressure.
^b P = 102.7 atm.

for the dissolved gases comparable to those reported by Kritchevsky and Iliinskaya.²

The gas equilibrium pressures were determined by a null point measurement of gas pressure developed inside a Teflon tube inserted in a pressure chamber containing the desired gas solutions. The nominal dimensions of the Teflon were 0.3 mm. i.d. and 0.23 mm. wall thickness. The length of the tube varied from 10 cm. for relatively insoluble gases to 30 cm. for more soluble gases. The Teflon tube will withstand external pressure of at least 150 atm. without collapsing.

Procedure

Water was gas extracted repeatedly. Gas at the desired pressure was dissolved in it at controlled temperature. Distilled water was used except as noted. The equilibration vessel was shaken during the gas uptake, and the process was complete after 0.5 to 1 hr. The solution was then transferred anaerobically to a 100-cc. syringe through a short section of 0.32-cm. i.d. vacuum tubing. This tubing remained attached to the syringe after filling and was sealed with a screw clamp.

One end of the gas-sensing Teflon tube was closed with a slightly tapered glass rod. The other end was forced over the end of a stainless steel tube (no. 26 needle tubing) about 12 cm. long. This tubing passed through a seal in the lid of the pressure tank near the middle of its length.

The apparatus (Figure 1) was assembled by loosening the clamp on the syringe, inserting the Teflon in the

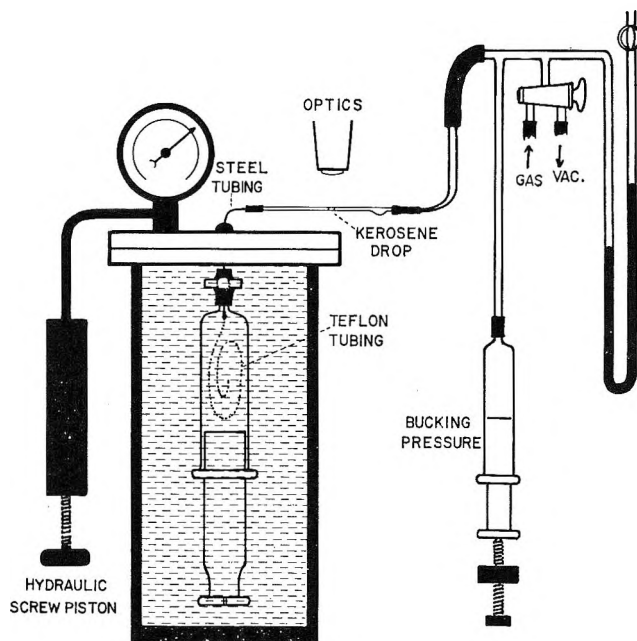


Figure 1. Pressure chamber and gas pressure measurement apparatus.

syringe until the stainless steel tube was inside the rubber tube, and then clamping the rubber tightly. This seal was checked by pushing on the syringe plunger. The syringe was then taped to a support on the pressure chamber lid, and the lid was placed on the water-filled pressure chamber so that the syringe was inside the chamber and all air was expelled from the chamber. The external end of the stainless steel tube was immediately connected to the gas-handling system; the Teflon tube was evacuated and then filled with the appropriate gas at atmospheric pressure.

Measurements were made in the following manner. The end of the stainless steel tube was connected to the gas-handling system by a glass tube about 5 cm. long with a 0.5 mm. i.d. A kerosene drop was introduced into this tube and observed on the scale of a microscope. The movement of this drop was timed, and the bucking pressure was adjusted until the drop did not move. Pressures were read on a mercury manometer (Figure 1). Stirring of the solution was found unnecessary because the null measurements moved only negligible amounts of gas in or out of the solutions.

In each experiment, gas equilibrium pressure determinations were made consecutively at 1500 (102 atm.), 1000, 500, and 0 p.s.i.g. pressure, in that order. Checks gave the same values when the sequence was reversed. The gauge used in these experiments was calibrated against a dead weight gauge.

In all experiments except one, the water temperature

was 25°. One experiment was conducted with a detergent solution having a surface tension equal to 30% of that of water.

Results

For all gases examined, the equilibrium pressure inside the Teflon tube was increased by about 14% when the hydrostatic pressure increased from 0 to 1500 p.s.i. (gauge). Water vapor readily crosses the Teflon tube walls; hence, the vapor pressure corresponding to the water temperatures was subtracted from all gas pressure values.

In each experiment natural logarithms of gas pressures were plotted as abscissas, and water gauge pressures, as ordinates. Straight lines were drawn to best fit the points, and the differences between their intercepts on the abscissa and at 102 atm. were recorded under $\ln(p_{102}/p_0)$ in Table I. Figure 2 shows plots of all data obtained at 25° and approximately atmospheric pressure. For each gas, data from different runs are superimposed for best agreement by arbitrary displacement of abscissas.

The effect of reduced surface tension of water was probably not significant. Hence, it must be concluded that surface tension plays no major role in the observed hydrostatic effect on gas equilibrium.

From eq. 3 derived below the partial molal volumes of the gases were calculated and are shown in the last column of Table I.

Discussion

If the dissolved gas is considered an ideal gas within the accuracy of this experiment, the measured equilibrium pressure is proportional to the activity and to the fugacity of the gas. The effect of pressure on the latter is given by⁵

$$\left(\frac{\partial \ln f}{\partial P}\right)_{T,x} = \frac{\bar{v}}{RT} \quad (1)$$

where f = fugacity, P = hydrostatic pressure, \bar{v} = partial molal volume, R = gas constant (82.06 atm./°K.), T = absolute temperature, and x = dissolved gas concentration.

If \bar{v} is assumed constant over the range of the experiment, integration between hydrostatic pressures P_1 and P_2 gives

$$\ln(f_1/f_2) = \bar{v} \frac{(P_1 - P_2)}{RT} \quad (2)$$

where f_1 and f_2 are the fugacities corresponding to P_1 and P_2 .

Substituting the ratio of the equilibrium partial pressures p_1 and p_2 for the ratio of the fugacities

$$\ln(p_1/p_2) = \frac{\bar{v}(P_1 - P_2)}{RT} \quad (3)$$

It may be added that, since these experiments were conducted at constant x , the pressure dependence of the Henry's law constant, $k = p/x$, is given by

$$\ln(k_1/k_2) = \frac{\bar{v}(P_1 - P_2)}{RT} \quad (4)$$

The data indicate that the effect of hydrostatic pressure on the activity of dissolved gases is essentially the same for oxygen, argon, and nitrogen. Helium and carbon dioxide show a slight difference. The same conclusion applies to the partial molal volumes which average approximately 33 cc. for nitrogen, 32 cc. for oxygen and argon, 29.7 cc. for helium, and 35 cc. for carbon dioxide.

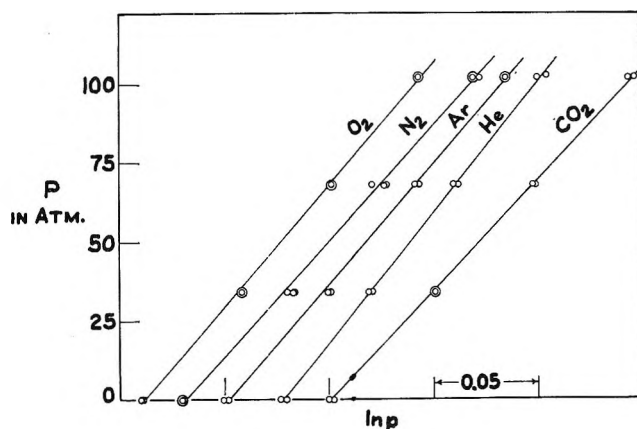


Figure 2. Effect of hydrostatic pressure on equilibrium pressure of dissolved gases. Abscissas arbitrarily displaced.

The values of partial molal volumes reported here are average values based on straight lines drawn as in Figure 2. Actually, all gases except helium give slightly curved plots indicating a decrease in partial molal volume with increase in hydrostatic pressure.

The data may be extended to calculate equilibrium partial pressure of gas at ocean depths. For dissolved gases which have their origin in water equilibrated with the atmosphere at the surface, eq. 3 gives the gas pressures at depths. At 10,000 m. depth the pressures so calculated are approximately four times as great as at the surface. It may be noted that marine organisms living at this depth may be exposed to an oxygen activity four times that of the atmosphere.

(5) G. N. Lewis and M. Randall, "Thermodynamics," revised by K. S. Pitzer and L. Brewer, McGraw-Hill Book Co., Inc., New York, N. Y., 1961, p. 204.

The Catalytic Cracking of Hexadecane—Effects of Impurities, Olefins, and Steam

by W. F. Pansing

American Oil Company, Whiting, Indiana (Received May 7, 1964)

The nature of hexadecane cracking on silica-alumina catalyst was investigated to provide a better understanding of activity and selectivity. At low temperatures (343–399°) in the absence of trace impurities or olefins to act as initiators, an induction period occurred. Apparently, cracking was initiated on Lewis acid sites until olefinic products activated Brønsted acid sites. Trace impurities or added olefins eliminated the induction period and markedly increased initial cracking rates. At higher temperatures (482°), thermal olefins acted as initiators, and no induction period was observed. However, hexadecane cracking was autocatalyzed by olefin products as indicated by a constant rate of cracking up to at least 50% conversion even though initial rates were essentially first order. With increasing octene-1 additions, initial cracking rates of hexadecane reached a maximum with about 20% octene-1 present. Higher concentrations of octene-1 decreased the cracking rate by competing with the hexadecane for adsorption. In general, the effect of olefin addition depended on the conversion level of the hexadecane. Compared to helium dilution, steam dilution decreased initial rates of cracking of hexadecane but at higher conversions increased the rate of cracking. Steam increased cumene cracking rates at all conversions. Apparently, hydrated Lewis sites have sufficient protonic acidity to crack cumene but are not sufficiently active to form carbonium ions capable of extracting a hydride ion from hexadecane. At higher conversions of hexadecane, steam increases cracking rates probably by reducing chemisorption of reaction products which compete for chemisorption on cracking sites.

Although much of the chemistry of catalytic cracking can be explained by the carbonium ion theory,¹⁻⁴ the nature of paraffin cracking, particularly its initiation, is one of the least understood reactions. The classical notion that the sites on silica-alumina are protonic or Brønsted acids requires the presence of trace olefins to initiate the formation of carbonium ions. After carbonium ions are formed, a paraffin can become a carbonium ion by transferring a hydride ion to another carbonium ion.

In recent years, spectroscopic studies suggested that when molecules such as triphenylmethane were adsorbed at very low pressures and near room temperatures, carbonium ions were formed by hydride ion abstraction on Lewis acid type sites.⁵ These ions appeared to be readily formed or destroyed by the removal or addition of water.

Spectroscopic studies of ammonia adsorbed on silica-alumina also indicated the presence of Lewis acid sites. However, the formation of adsorbed ammonium ions on addition of water suggested that Lewis sites could become hydrated and act like protonated or Brønsted type sites.⁶

The acidities of silica-alumina also have been measured by nonaqueous titration using Hammett indicators

- (1) B. S. Greensfelder, H. H. Voge, and G. H. Good, *Ind. Eng. Chem.*, **41**, 2573, 2945 (1949).
- (2) M. W. Tamele, *Discussions Faraday Soc.*, **8**, 270 (1950).
- (3) C. L. Thomas, *Ind. Eng. Chem.*, **41**, 2564 (1949).
- (4) H. H. Voge, "Catalysis," Vol. VI, P. H. Emmett, Ed., Reinhold Publishing Corp., New York, N. Y., 1958, Chapter 5.
- (5) H. P. Leftin and W. K. Hall, *Actes Congr. Intern. Catalyse, 2e, Paris*, 1353 (1961).
- (6) J. E. Mapes and R. P. Eischens, *J. Phys. Chem.*, **58**, 1059 (1954).

and arylmethanols as indicators. This work appears to support the view that the acidity is caused by Brønsted sites.^{7,8}

Relatively little work has been done to investigate the influence of water and olefins on the actual cracking of high-boiling paraffins. These studies should provide inferences about the nature of the active sites. Studies with butane and isobutane indicate that there may be an optimum degree of hydration of a catalyst for isomerization and cracking although isobutane adsorption decreased continuously with hydration.⁹⁻¹³ A thoroughly dehydrated catalyst was inactive for cumene cracking but was readily activated by water addition.¹⁴ Olefins accelerated the exchange of hydrogen between deuterated catalyst and isobutane¹¹ and accelerated the cracking of *n*-butane in a static reaction system.¹⁵ However, it has also been stated that admixture of olefins with paraffins such as hexadecane does not appreciably accelerate cracking.⁴

There is some evidence for autocatalysis or an induction period in paraffin cracking. In the cracking of 2-methylpentane in a batch reactor, Franklin and Nicholson¹⁵ observed that the rate constants in the first two minutes were 50% lower than steady-state rates. Van Hook and Emmett¹⁶ observed that the rate of conversion of hexadecane at 372° was 3.5 times greater in an integral reactor at high conversions than in a differential reactor at low conversions.

The present study was undertaken to investigate the effects of olefins, water, and trace impurities on hexadecane cracking rates. Initial rates, in particular, were studied because they provide insight into the mechanism of paraffin cracking. The observed phenomena are explained in terms of the action of Lewis and Brønsted sites on the catalyst.

Experimental

Cracking data were obtained in a small, versatile reactor system.^{17,18} Most of the studies were made with normal hexadecane and silica-alumina catalyst.

Materials. Hexadecane obtained from Humphrey-Wilkinson, Inc., was purified by percolation through at least three times its volume of silica gel. Depending on the degree of activation of the silica gel, the hexadecane was obtained in two different purities. In the first case, 60- to 200-mesh gel was heated overnight in shallow dishes in a large forced-circulation oven at 538° and allowed to cool to 93° in the oven. This gel picked up some moisture from the air. In the second case, gel was heated for 6 hr. at 538° in a muffle furnace, removed, and bottled hot to prevent pickup of moisture. Comparative ultraviolet and infrared analyses of hexadecane percolated through either type of activated gel

showed no detectable olefin or aromatic compound, but a trace impurity which appeared to be a carbonyl compound was detected in the hexadecane percolated through the first gel. Hereafter, hexadecane will be termed "impure" or "pure" depending on whether the trace impurity was present.

Although the concentration of impurity was not known, tests proved that the technique for activating the silica gel was the critical factor in affecting cracking rates. Comparative runs were made with two feeds. The first was percolated through silica gel activated in a circulating oven which permitted moisture pickup on cooling, and the second was percolated through silica gel which had been activated in a muffle furnace but was then allowed to stand out in the room for several hours before use. Both gels produced a hexadecane which gave essentially the same cracking rates at 343°, while the hexadecane percolated through gel heated in the muffle furnace and bottled hot gave a much lower cracking rate, as explained later.

Octene-1 (Phillips, Research grade), pentene-1 (Phillips, Pure grade), and cumene (Eastman, White Label grade) were percolated through silica gel which had been activated overnight in a muffle furnace at 538° and bottled hot. The cumene was also percolated through Floridian clay, which had been calcined at 538°, to ensure removal of cumene peroxides.

Two different samples of a fluid grade of Cyanamid silica-alumina catalyst containing 25% alumina were used. One was fresh catalyst which had been steamed for 16 hr. at 650° before use to reduce its activity to a level that would be reached very quickly under commercial conditions. The second sample was taken from a commercial unit and was thoroughly regenerated in air for 16 hr. at 538°. Both catalysts had average

- (7) A. E. Hirschler, *J. Catalysis*, **2**, 428 (1963).
- (8) H. A. Benesi, *J. Phys. Chem.*, **61**, 970 (1957).
- (9) A. N. Webb, *Actes Congr. Intern. Catalyse, 2e, Paris*, 1298 (1960).
- (10) R. G. Haldeman and P. H. Emmett, *J. Am. Chem. Soc.*, **78**, 2917, 2922 (1956).
- (11) R. C. Hansford, P. G. Waldo, L. C. Drake, and R. E. Honig, *Ind. Eng. Chem.*, **44**, 1108 (1952).
- (12) S. G. Hindin, A. G. Oblad, and G. A. Mills, *J. Am. Chem. Soc.*, **77**, 535 (1955).
- (13) D. S. MacIver, P. H. Emmett, and H. S. Frank, *J. Phys. Chem.*, **62**, 935 (1958).
- (14) K. V. Topchieva, G. M. Panchenkov, M. A. Kaliko, A. V. Agafonov, L. I. Figusova, N. M. Kamakin, and Ya. V. Mirsky, *World Petrol. Congr., Proc., 5th, N. Y.*, 133 (1959).
- (15) J. L. Franklin and D. E. Nicholson, *J. Phys. Chem.*, **60**, 59 (1956).
- (16) W. A. Van Hook and P. H. Emmett, *J. Am. Chem. Soc.*, **84**, 4410 (1962).
- (17) W. F. Pansing and J. B. Malloy, *Chem. Eng. Progr.*, **58**, No. 12, 53 (1962).
- (18) W. F. Pansing and J. B. Malloy, to be published.

particle sizes of about 80 μ . Other characteristics of the steamed, fresh catalyst and the commercially used catalyst were, respectively, surface area, 500 and 130 m.²/g.; pore volume, 0.67 and 0.45 cc./g.; particle density (by Hg displacement), 0.78 and 1.14 g./cc.; sodium content, 0.02 and 0.02 wt. %; and Fe₂O₃, 0.04 and 0.44 wt. %.

Procedure

The catalyst, mixed with inert Vycor granules to provide a uniform bed volume, was loaded in a reactor about 10.16 cm. in length and 0.95 cm. in i.d. A 2.54-cm. zone of Vycor was provided ahead of the catalyst for final preheat. The reactor was heated within 30 to 60 min., depending on the desired temperature, and then held for about 20 min. while it was continuously purged with dry helium. For feed partial pressures below 1 atm., either helium was metered into the reactor or steam was generated in the preheater by water pumped at the desired rate with a hypodermic syringe. With steam dilution, the catalyst was pre-treated at reaction temperature for 30 min. before the hydrocarbon feed was started.

Eight samples of the reactor effluent, each about 0.2 μ l. as liquid, were taken over a 30- or 40-min. reaction period and analyzed to obtain the conversion. Conversion declined slightly during the first 5 min. and then remained constant. The average conversion was based on the analyses of the seven samples taken during the period of constant activity.

In most runs, the reactor was operated as a differential reactor to provide very low conversions, from 2 to 5%. In other runs, it was operated as an integral reactor to provide conversions up to 30%. The material balance governing both types of reactors is $Fdx = r dW$ or

$$r = \frac{Fdx}{dW} = \frac{dx}{d(1/S)} \quad (1)$$

where r is the cracking rate, F the feed rate, x the fraction conversion, W the weight of catalyst, and S the space velocity. The cracking rate, which varies with conversion, is obtained from the slope of the curve of conversion *vs.* $1/S$ as indicated by eq. 1. However, at very low conversions the concentration of the reactant remains essentially constant, so the differentials in eq. 1 can be replaced by Δ 's. Thus, a single measure of conversion establishes the initial rate of cracking from

$$r = \frac{Fx}{W} = xS \quad (2)$$

Product samples were analyzed in a gas chromatography column providing a separation equivalent to

an analytical distillation.¹⁸ A flame ionization detector was used on the column effluent. Since the cracking of hexadecane predominantly results in C₂ to C₆ hydrocarbons,⁴ over 90% of the cracked products were made to come through the column as unresolved low-boiling peaks whose total weight was obtained by electronic integration of the detector output. Negligible amounts of intermediate products between about C₁₀ and the unreacted hexadecane were obtained. Hence, there was no problem in distinguishing cracked products from unreacted feed in the gas chromatograph.

When the effects of olefins (primarily octene-1) on hexadecane cracking were studied, unreacted olefin and its cracked products came through the chromatograph mixed with the products from the cracking of hexadecane. The amount of olefin added to the feed was checked in triplicate chromatographic analyses, and an appropriate correction was applied to the total product analysis to give the net conversion of hexadecane in the presence of olefin. Octene-1 was cracked alone at 399 and 482°, and the products were examined for materials heavier than the feed. No significant amounts of products heavier than octene were found.

Thermal conversions of hexadecane were measured under conditions like those used in measuring catalytic cracking rates, except that the reactor was filled with Vycor diluent. In most cases, particularly at low partial pressures with high helium dilution rates, thermal conversion was practically negligible compared to catalytic conversion; the maximum thermal conversion was 0.9% at 482° and 1.0 atm. Thermal conversion was subtracted from total conversion to give catalytic conversion.

Paraffin Cracking Initiation

Trace impurities or 1.0% pentene-1 in pure hexadecane markedly accelerated the initial cracking rates.

Table I: Effects of Impurities and Olefins on Initial Cracking Rates of Hexadecane^a

Impurities	—343° ($S = 40$) ^b —		—482° ($S = 150$) ^b —	
	Conv., wt. %	Cracking rate, mmoles/hr. g.	Conv., wt. %	Cracking rate, mmoles/hr. g.
None detectable	0.5	0.2	2.0	2.9
Trace impurities	2.5	0.9	2.0	3.1
1% pentene-1	3.2	1.3	2.0	3.5

^a Steamed, fresh silica-alumina catalyst; hexadecane partial pressure, 0.16 atm. ^b Approximate space velocity, mmoles/hr. g.

As shown in Table I, at 343° the respective increases were 350 and 550%. At 482°, the increases were relatively small because thermal olefins must have masked the effects of impurities or added pentene-1.

The effect of the extent of conversion of the hexadecane on its cracking rate at 399° is shown in Figure 1. An induction period is clearly evident. At conversions below 1% the rate was essentially constant at 1.6 mmoles/hr. g. At higher conversions it rather suddenly increased and became relatively constant again at 4.8 mmoles/hr. g.

No induction period was evident in the presence of trace impurities at low temperatures or at 482° where significant concentrations of thermal olefins were present. The rate of 4.8 mmoles/hr. g. in Figure 1 for pure feed agrees with the value of 4.7 mmoles/hr. g. for impure feed determined by interpolation on Figure 2 where the data showed no induction period and rates were calculated from αS for a single measure of conversion, α .

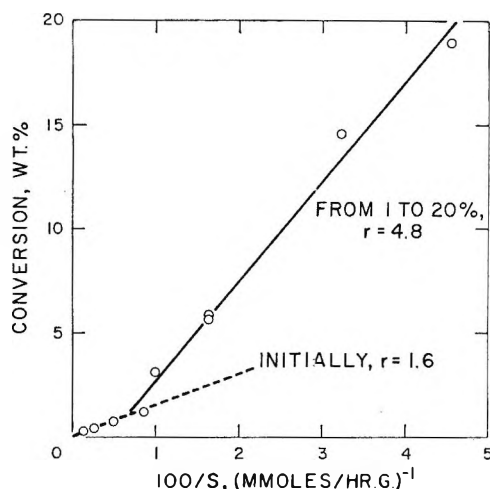


Figure 1. Induction period in catalytic cracking of pure hexadecane on steamed, fresh catalyst at 399° and 0.4 atm.

The acceleration of initial rates by impurities or added olefins indicates the presence of Brønsted sites, which require carbonium ion precursors to catalyze paraffin cracking. However, cracking in the absence of thermal olefins or impurities is probably initiated on Lewis sites by hydride ion abstraction from the hexadecane to form a carbonium ion. When sufficient olefins are generated to form carbonium ions on Brønsted sites, hexadecane can crack by hydride ion transfer to these ions. With thermal olefins or impurities present, apparently both sites start functioning immediately. From the rates in Figure 1, cracking on the Lewis sites

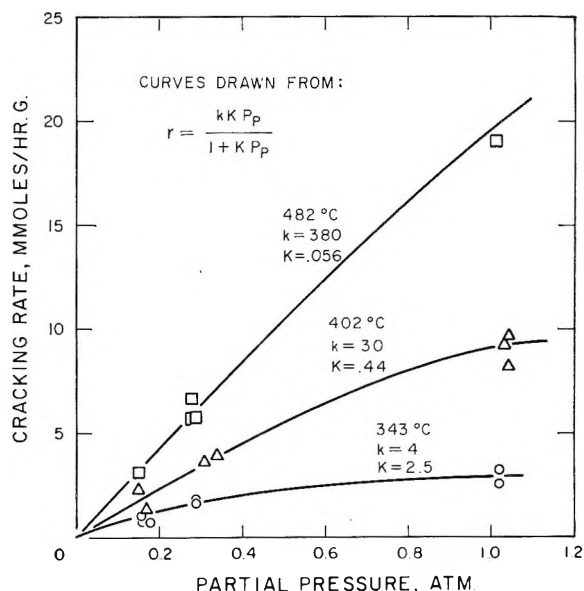


Figure 2. Effect of hexadecane pressure on initial cracking rate with steamed, fresh catalyst and impurities present in feed.

appears to be about one-half as fast as on the Brønsted sites.

Effects of Olefins

Effect of Olefin Concentration. Olefin concentrations from 10 to 40% in pure hexadecane had very pronounced effects on initial rates of cracking of hexadecane beyond merely eliminating an induction period. The effects were determined at 399 and 482° using octene-1 and a thoroughly regenerated commercial equilibrium catalyst. The partial pressure of hexadecane was held constant while the partial pressure of octene-1 was varied, and helium was added to keep the total pressure at 1 atm. Conversions were generally around 2 to 5% and directly proportional to $1/S$ at otherwise constant conditions, which indicates no induction period. Hence, each rate was determined from a single run using eq. 2.

As shown in Figure 3, at 399° the addition of up to 15% of octene-1 to pure hexadecane greatly increased the initial rate of cracking. At higher octene-1 concentrations, the rate decreased. As shown in Figure 4, at 482° the addition of octene-1 also sharply increased the initial rate. However, a rather flat maximum was reached at about 30% octene-1.

The initial rate of cracking of hexadecane appears to depend on the concentration of carbonium ions on the catalyst. Increasing the olefin partial pressure increases the carbonium ion concentration up to a point, beyond which the olefins begin to monopolize the active sites and prevent adsorption of hexadecane.

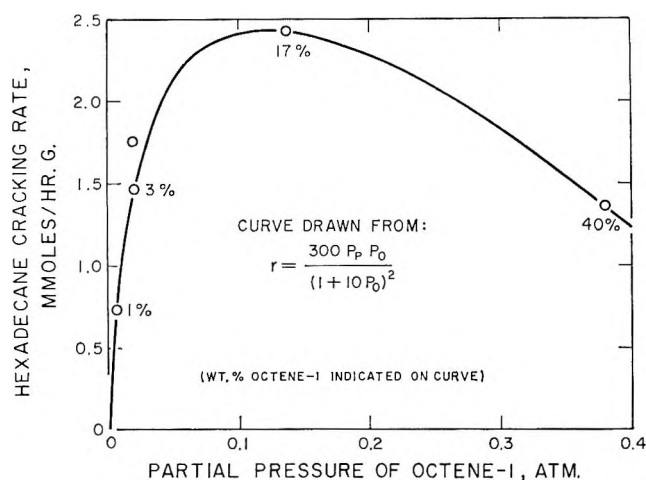


Figure 3. Effect of octene-1 on initial cracking rate of pure hexadecane on commercially used catalyst at 399° and 0.3 atm. of hexadecane pressure.

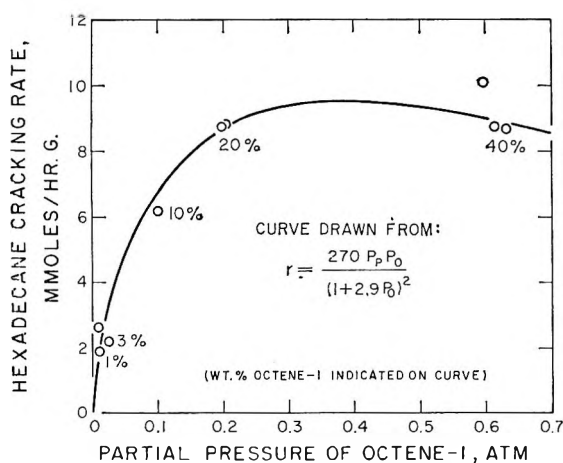


Figure 4. Effect of octene-1 on initial cracking rate of pure hexadecane on commercially used catalyst at 482° and 0.4 atm. of hexadecane pressure.

Based on Langmuir type kinetics, the following equation was developed¹⁹

$$r = \frac{kK_P K_O P_P P_O}{(1 + K_P P_P + K_O P_O)^2} \quad (3)$$

where k is the specific reaction velocity constant for the decomposition of the adsorbed activated complex, K_P and K_O are the adsorption equilibrium constants for the paraffin and the olefin, and P_P and P_O are their respective partial pressures.

Evaluation of k , K_P , and K_O would require extensive data on the effects of both the hexadecane and octene-1 partial pressures on cracking rates. However, as is frequently the case with this type of mechanism, one component is much more strongly adsorbed than

the other. In this case, the hexadecane adsorption equilibrium constant was apparently so small compared to the octene-1 adsorption constant that the rate equation could be fitted to the data in the approximate form

$$r = \frac{kK_P K_O P_P P_O}{(1 + K_O P_O)^2} \quad (4)$$

The constants are summarized in Table II.

Table II: Effect of Temperature on the Reaction Constants for Cracking Hexadecane Containing Octene-1

Temp., °C.	$kK_P K_O$, mmoles/hr. g. atm. ²	K_O , atm. ⁻¹	kK_P , mmoles/hr. g. atm.
399	300	10	30
482	270	2.9	93

From the effect of temperature on K_O , the apparent heat of adsorption¹⁹ is 15,300 cal./mole. The constants k and K_P cannot be separated with the available data. However, the increase in k with temperature more than compensates for the decrease in K_P . Actual and calculated initial rates of cracking at 399° agree well over a wide range of octene-1 and hexadecane partial pressures, as shown in Table III.

Table III: Comparisons of Observed and Calculated Hexadecane Cracking Rates for Various Octene-1 and Hexadecane Pressures

Partial pressure, atm.		Hexadecane cracking rate, mmoles/hr. g.	
Octene-1	Hexadecane	Calcd.	Obsd.
0.0044	0.21	0.25	0.25
0.0074	0.35	0.68	0.73
0.012	0.20	0.55	0.61
0.018	1.00	3.90	3.22
0.019	0.32	1.28	1.75
0.021	0.34	1.44	1.46
0.14	0.33	2.41	2.42
0.37	0.28	1.34	1.35

In the absence of added olefins, the model predicts a zero initial hexadecane cracking rate. Experimentally this is not true because Lewis sites catalyze the cracking in the absence of olefins. Attempts to account for the unpromoted cracking by adding a term involving the partial pressure of hexadecane alone

(19) K. J. Laidler, "Catalysis," Vol. I, P. H. Emmett, Ed., Reinhold Publishing Corp., New York, N. Y., 1954, Chapter 4.

were unsuccessful; as indicated by the above comparisons, there is no independent effect of hexadecane partial pressure in the presence of octene-1 other than that accounted for by the model. At 482° where thermal olefins were present there was little difference between the rate with no olefin addition and the rates with 1 and 3% octene-1 additions.

Effect of Conversion. The initial cracking rates of pure hexadecane were markedly accelerated by the additions of relatively large amounts of octene-1, whereas at about 30% conversion, the rates at constant conditions decreased. The effects of 5 and 20% octene-1 at 482° and 0.35 atm. with steamed fresh catalyst are shown in Figure 5 with the conversion-space velocity relation for pure hexadecane. In the vicinity of 30% conversion at constant space velocity and hexadecane partial pressure, the conversion of hexadecane increased by about 5% with 5% octene-1 but decreased by about 16% with 20% octene-1.

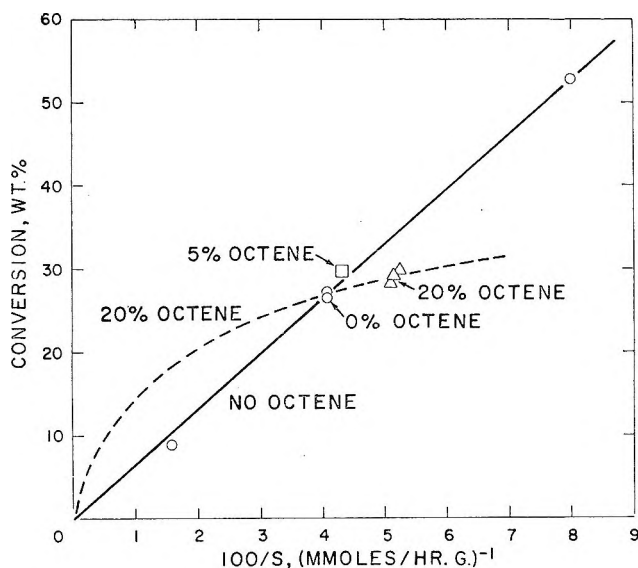


Figure 5. Effect of octene-1 at various conversion levels of pure hexadecane with steamed fresh catalyst at 482° and 0.35 atm. of hexadecane pressure.

Since instantaneous cracking rates are determined by the slope of the plot of conversion *vs.* $1/S$ at any conversion level, the cracking rate of hexadecane is essentially constant up to at least 50% conversion without olefin added to the feed; or in other words, the rate is constant along the length of the reactor. However, with 20% octene-1 added, which is near optimum for accelerating initial rates, the initial rate is four times higher (as estimated from increase with commercially used catalyst in Figure 4), but then it steadily decreases as conversion increases along the length of the reactor

until, eventually, the rate with olefin added is less than that without olefin addition. Thus, with the optimum amount of olefin in the feed for accelerating initial rates of hexadecane cracking, the olefins formed from cracking began to retard the rate because of competition for active sites.

In the absence of added olefins, the relatively constant cracking rate of pure hexadecane up to 50% conversion must result from the promotion of cracking by product olefins. Theoretically, if the cracking reaction is first order, the curve of conversion *vs.* $1/S$ should bend over at higher conversions because the concentration driving force is decreasing as feed is cracked and diluted with 3.6 moles of product per mole of feed cracked.⁴ Thus, at 50% conversion the initial 0.35-atm. partial pressure of the feed is reduced by 65%. Hence, the cracking rate should be reduced by 65%. Instead, the rate is relatively constant from 0 to 50% conversion. Apparently, the decrease in concentration is offset by the promotional effect of the product olefins.

Kinetics of Hexadecane Cracking

A model for hexadecane cracking should take into account the effect of impurities on initial cracking rates. However, if impurities or thermal olefins eliminate the induction period without any further effects on cracking rates, a reproducible kinetic model for the initial cracking period can be developed. The effects of feed partial pressure on the initial cracking rates of hexadecane, containing sufficient impurity to eliminate any induction period, were determined for steamed, fresh catalyst at 343, 402, and 482°. The results are shown in Figure 2.

A Langmuir type of kinetic model, assuming a simple surface-reaction controlling, fits the data¹⁹

$$r = \frac{kKP}{1 + KP} \quad (5)$$

where r is the cracking rate, k the specific reaction velocity constant for decomposition of the paraffin complex on the surface of the catalyst, K an adsorption equilibrium constant for hexadecane, and P the partial pressure of hexadecane. The constants were determined by plotting $1/r$ *vs.* $1/P$, which produced a straight line with slope $1/kK$ and ordinate intercept $1/k$. The constants at 482° were evaluated by the least-squares technique because the intercept was too close to the origin to evaluate graphically.

The effect of temperature on k and K is shown in Figure 6. From the slope of the reaction velocity constant line, the intrinsic activation energy was found to be 30,800 cal./mole; from the slope of the adsorption

equilibrium constant line, the apparent heat of adsorption was found to be 25,200 cal./mole.

Although the model adequately represents the initial stages of cracking, it does not apply at higher conversions. The rate should decrease with increasing conversion because the reactant partial pressure decreases. Actually, rates were constant up to at least 50% conversion. The model will need to be modified to include the promotional effects of olefinic products at higher conversions.

Effect of Steam

Compared to helium, steam as a diluent at a constant partial pressure markedly decreased the initial cracking rates of hexadecane but at higher conversions increased the effective cracking rates. As shown in Table IV,

Table IV: Effects of Steam and Dry Helium on Hexadecane Cracking with Steamed Fresh Catalyst

Temp., °C.	Dry helium		Steam			
	S , mmoles/hr. g.	Conv., wt. %	r , mmoles/hr. g.	S , mmoles/hr. g.	Conv., wt. %	r , mmoles/hr. g.
Differential reactor, 0.30 atm. impure feed						
343	47	3.76	1.78	31	3.49	1.07
	60	2.91	1.75			
482	296	1.93	5.73	201	1.58	3.18
	393	1.46	5.73	201	1.39	2.80
	829	0.79	6.56	279	1.12	3.13
				295	1.25	3.71
Integral reactor, 0.35 atm. pure feed						
482	24.6	26.6		24.6	33.5	
	24.6	27.2		24.6	39.4	
				24.6	39.6	

in a differential reactor at 343 and 482°, steam reduced the initial cracking rates by about 40%. However, at about 30% conversion in an integral reactor at 482°, steam increased conversion by 40% at constant space velocity. In general, initial rates were not a function of conversion level, and, hence, no induction period was evident. Further, the severe steaming of the catalyst before use eliminates any effects of steam on surface area during the reaction period.

With cumene cracking, which is generally believed to occur on Brønsted or protonic acid sites, steam increased cracking rates. As shown in Table V, compared to helium as a diluent, steam increased conversion by about 40% at all conversion levels.

Steam may reduce initial cracking rates of hexadecane by hydrating the Lewis sites to form protonic type

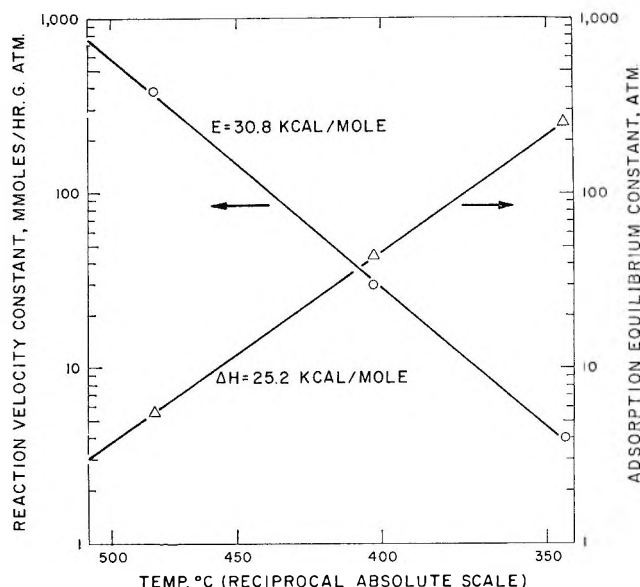


Figure 6. Effect of temperature on rate constant and adsorption equilibrium constant for initial cracking of impure hexadecane.

Table V: Effects of Steam on Cumene Cracking at 482°

Catalyst	Diluent	Feed partial press., atm.	S , mmoles/hr. g.	Conv., wt. %
Commercial eqm., calcined	Helium	0.7	790	4.2
	Steam	0.7	830	5.8
Fresh, steamed	Helium	0.5	3100	24.4
	Steam	0.5	3040	32.2
	Helium	0.3	6510	8.2
	Steam	0.3	5620	12.9

acid sites which, although not capable of initiating hexadecane cracking, are capable of cracking cumene. The hexadecane used to measure initial rates contained trace impurities and thermal olefins at 482° to initiate cracking on Brønsted sites. Hence, if hydrated Lewis sites were equivalent to Brønsted sites, the cracking of hexadecane should not be retarded. Apparently, hydrated Lewis sites are not sufficiently active to form carbonium ions capable of extracting a hydride ion from hexadecane even though these sites are sufficiently active to crack cumene. If hydrated Lewis sites are inactive for hexadecane cracking, the initial rate should be reduced by 33%, based on the rates for the two sites from Figure 1. This reduction agrees favorably with the 40% reduction in initial rates actually observed. At higher conversions of hexadecane, steam may increase cracking rates by reducing the chemisorption of reaction products on cracking sites.

Conclusion

The concept of both Lewis and Brønsted sites on a cracking catalyst is very helpful for explaining the observed rate phenomena. A Langmuir type of kinetics adequately describes initial rates of cracking under various conditions. However, the apparent auto-catalytic effect of product olefins in sustaining the cracking rate up to high conversions requires further investigation to develop a kinetic model valid over

the whole range of conversions. Determining whether the adsorption equilibrium constants derived from kinetic data have any physical significance will require further studies with other paraffins and other types of hydrocarbons.

Acknowledgment. The author gratefully acknowledges helpful discussions with H. S. Seelig, J. B. Malloy, and W. F. Johnston.

Diffusion-Conductance Relations and Free Volume in Molten Salts

by C. A. Angell*

Department of Metallurgy, University of Melbourne, Parkville N.2, Victoria, Australia (Received May 27, 1964)

Departures from the Nernst-Einstein equation for a variety of pure molten salts are correlated by means of "glass transition-based" corresponding temperatures suggested by a recent free volume model of transport in molten salts. Coupled with molar volume data, these correlations are consistent with the view that mutual ionic interference, rather than paired vacancy diffusion, causes the breakdown of the Nernst-Einstein equation in these liquids.

The Nernst-Einstein equation

$$\lambda_i = \frac{F^2}{RT} z_i D_i \quad (1)$$

(where λ_i is the equivalent conductance, D_i the diffusion coefficient, and z_i the charge of species i , F is the Faraday constant, and T the absolute temperature), which relates diffusion and electrical conductance transport processes for cases where the moving species translate under identical local conditions,¹ has been shown by a number of studies to be inaccurate for molten salts. The observed discrepancies so far have not been related to any other properties of the salts or their constituent ions. Here we wish to examine these discrepancies in the light of a recent attempt² to interpret transport in fused salts in terms of a free volume model.

Equation 1 is known to apply accurately in the case of very dilute solutions,³ where only the ion-solvent inter-

action is important in both processes. It is also obeyed within experimental error for certain instances of transport in ionic crystals,⁴ where the density of current carriers is so small that both processes may be considered to involve only interaction between the mobile species and the lattice.⁵ In these cases it is necessary to take lattice-dependent correlation factors

* Argonne National Laboratory, Argonne, Ill.

(1) (a) W. Nernst, *Z. physik. Chem.*, **2**, 613 (1888); (b) N. F. Mott and R. W. Gurney, "Electronic Processes in Ionic Crystals," Oxford University Press, Oxford, 1940; 2nd Ed., Oxford, 1948.

(2) (a) C. A. Angell, *J. Phys. Chem.*, **68**, 218 (1964); (b) C. A. Angell, *ibid.*, **68**, 1917 (1964).

(3) R. Mills and E. W. Godbole, *J. Am. Chem. Soc.*, **82**, 2395 (1960).

(4) (a) D. H. Mapother, N. Crookes, and R. Maurer, *J. Chem. Phys.*, **18**, 1231 (1950); (b) W. D. Compton and R. Maurer, *J. Phys. Chem. Solids*, **1**, 191 (1956).

(5) The validity of the Nernst-Einstein equation in the cases of aqueous solutions and ionic crystals has been discussed in detail by R. W. Laity, *J. Chem. Phys.*, **30**, 682 (1959).

for the tracer diffusion coefficients into account in relating the measured diffusion coefficients to the conductance.⁶

A third case in which adherence to the Nernst–Einstein equation may be expected is that of ionic glass-forming liquids in the vicinity of the glass transition temperature, since here also the density of actual current carriers (moving ions)⁵ should be so small that interaction between the moving species will not be significant.

By application of the free volume concepts of Cohen and Turnbull⁷ to the analysis of transport data, it has recently been shown² that molten salts as a whole behave as if they would undergo a glass transition if they could be undercooled sufficiently without crystallization occurring. We therefore propose, as a basis for the following discussion, that a characteristic temperature, T_0 , may be assigned to each salt at and near which the (metastable) liquid would obey the Nernst–Einstein equation. The value of T_0 can evidently be predicted approximately from the electrostatic field strengths of the ions in the melt (see Figure 9 in ref. 2b).

From this viewpoint the relation between electrical conductance and diffusion in a typical molten salt may be seen by considering the effect of reheating a salt which has been cooled by some unspecified procedure to a temperature below T_0 without crystallization having occurred. At temperatures up to T_0 , the mobility of the ions is, ideally, zero. About T_0 , the generation of "free volume"⁸ commences with a rapid increase in the expansion coefficient to a value characteristic of the liquid state, and diffusive motion of the ions becomes possible. While the free volume, and therefore the concentration of moving ions, is very small, the Nernst–Einstein equation should be fulfilled, but as the current carrier density increases and interference between mobile charge species becomes significant, the probability of motion in the direction of the field will fall below the Nernst–Einstein value. A coupled vacancy type mechanism⁸ may also contribute to the lowering of the measured electrical mobility relative to the diffusion mobility. The over-all magnitude of the interference will be dependent on the concentration of moving ions; hence, with rising temperature, the electrical mobility will fall progressively behind the diffusion mobility. Thus the temperature coefficient for conductance should be lower than the corresponding value for diffusion, *i.e.*, following eq. 1, $dD_i/dT > d(\lambda_i T)/dT$, or, expressing the temperature coefficients by means of "activation energies,"⁹ $E_{D_i} > E_{\lambda_i} + RT$. The mathematical necessity of including RT in the comparison of "Arrhenius coefficients" for diffusion and electrical conductance has often been overlooked. Since "Arrhenius

coefficients" for cations and anions in the same salt have proved to be the same within experimental error, the above line of thought leads us to expect that $E_{D_{\pm}} > E_A + RT$, where E_A is the "Arrhenius coefficient" for equivalent conductance of the salt. Examination of the available data for molten salts, Table I, columns 9 and 10, shows this is indeed the case, with the apparent exception of AgNO_3 .¹⁰ Fischer, *et al.*,¹¹ also have noted this trend in the data.

Since the model thus far provides a satisfactory qualitative explanation of the relative magnitudes of E_D and E_A , it is of interest to examine the deviations from the Nernst–Einstein equation displayed by the different salts. From the above reasoning it seems that the higher the temperature of measurement is above T_0 , the greater should be the observed departure from the Nernst–Einstein equation. The model at present does not enable one to predict the magnitude of the deviation for a given salt, since this would require some specific knowledge of the factors determining the degree of interference between different cations and anions.

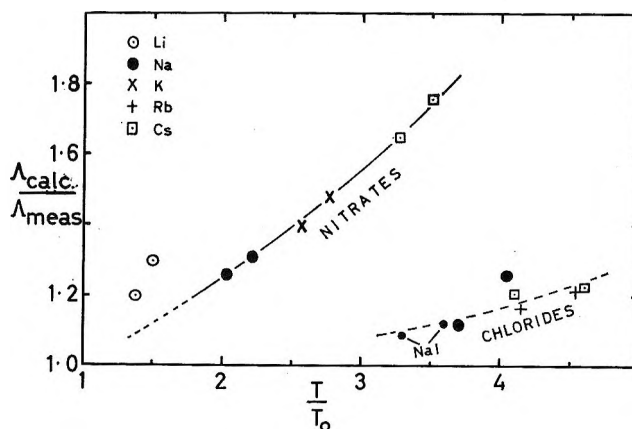


Figure 1. Dependence of Nernst–Einstein equation deviations on T/T_0 .

(6) A. B. Lidard, "Handbuch der Physik," Vol. XX, S. Flugge, Ed., Springer-Verlag, Berlin, 1957, p. 325.

(7) M. H. Cohen and D. Turnbull, *J. Chem. Phys.*, **31**, 1164 (1959).

(8) J. O'M. Bockris and G. W. Hooper, *Discussions Faraday Soc.*, **32**, 218 (1962).

(9) Conventional activation energies for transport, when measured accurately, generally show a temperature dependence which this model attributes to T_0 rather than 0°K . being the theoretical point of zero probability of ionic motion. For this reason, it has been suggested that the term "activation energy" for the "constant" in the Arrhenius equation for transport processes is misleading and should be replaced by the term "Arrhenius coefficient" referred to a given temperature range.

(10) The experimental uncertainty in the E_D values of Tricklebank, *et al.*, for NaI is ± 0.7 kcal. (S. V. Tricklebank, L. Nanis, and J. O'M. Bockris, *J. Phys. Chem.*, **68**, 58 (1964)) and, as these values apparently supersede earlier measurements by Bockris and Hooper,⁸ it is probable that NaI is no longer an exception to the general finding.

(11) W. Fischer, K. Heinziger, W. Herzog, and A. Klemm, *Z. Naturforsch.*, **17a**, 799 (1962).

Table I

Salt	$T_m, ^\circ\text{C.}$	$T_0, ^\circ\text{K.}^a$	$T_m, ^\circ\text{K.}/T_0$	E_D		E_A^b		$-E_D \pm EA + RT^c$		$\Lambda_{\text{calcd}}/\Lambda_{\text{measd}}^d$	
				+	-	T_m	$T_m + T$	+	-	T_m	$T_m + T$
LiNO ₃	252	385	1.37	5.49 ^e	6.34 ^e	4.22 ^f	3.17	0.44	1.29	1.20	1.30
NaNO ₃	307	285	2.03	4.97 ^e	5.08 ^e	3.37 ^g	3.16	0.50	0.61	1.26	1.31
KNO ₃	334	237	2.56	5.53 ^e	5.76 ^e	4.06 ^f	3.70	0.36	0.59	1.40	1.48
RbNO ₃	310	225	2.59
CsNO ₃	414	210	3.27	5.61 ^e	6.28 ^e	3.3 ^h	3.1	1.0	1.7	1.65	1.76
AgNO ₃	210	225	2.15	3.73 ^e	3.84 ^e	{ 3.70 ^f	2.95	-0.62	-0.51	1.29	1.27
						{ 3.40 ⁱ	2.88 ⁱ	{ -0.44	-0.33		
LiCl	613	390	2.27	2.04	2.04
NaCl	801	290	3.7	8.4 ^j	7.9 ^j	2.79 ^k	2.88	3.2	2.7	1.12	1.26
KCl	776	250	4.2	3.62 ^k	3.33
RbCl	722	240	4.15	7.4 ^j	8.0 ^j	4.71 ^k	4.37	0.7	1.4	1.16	1.21
CsCl	646	220	4.2	7.8 ^j	7.3 ^j	5.74 ^k	5.18	0.8	0.3	1.20	1.22
NaI	659	285	3.3	5.0 ^l	7.2 ^l	3.14 ^k	3.16	-0.2	2.0	1.09	1.12
TlCl	430	240	2.93	4.5 ^m	4.6 ^m	3.18 ⁿ	3.18	0.0	0.1	1.88	1.88
PbCl ₂	501	385	2.01	7.9 ^m	8.2 ^m	5.0 ^o	3.8	1.9	2.2	1.25	1.48
CdCl ₂	568	400	2.10	~6 ^p	~6 ^p	2.43 ^q	2.43	1.88	..
ZnBr ₂	394	450	1.48	16.9 ^r	17.0 ^e	17.7 ^q	14.1	1.6	1.7	2.2 ^t	..

^a T_0 values are estimated to $\pm 5^\circ$ for nitrates and $\pm 10^\circ$ for chlorides, from Figure 9 of ref. 2b, using Pauling crystal radii. ^b $T = 50^\circ$ for nitrates for which the temperature range of measurement has been small, 100° for other salts. ^c $E_A + RT$ values used are the mean values from T_m to $T_m + 50^\circ$ for nitrates, and T_m to $T_m + 100^\circ$ for other salts. ^d Λ_{calcd} is the equivalent conductance calculated by eq. 1 from the diffusion coefficients, Λ_{measd} is the experimental value. ^e A. S. Dworkin, R. B. Escue, and E. R. Van Artsdalen, *J. Phys. Chem.*, **64**, 872 (1960). ^f H. C. Cowen and H. J. Axon, *Trans. Faraday Soc.*, **52**, 242 (1956). ^g J. Byrne, A. Fleming, and F. E. W. Wetmore, *Can. J. Chem.*, **30**, 922 (1952). ^h F. M. Jaeger and B. Kapma, *Z. anorg. allgem. Chem.*, **113**, 27 (1920). ⁱ R. L. Spooner and F. E. W. Wetmore, *Can. J. Chem.*, **29**, 777 (1951). ^j J. O'M. Bockris and G. W. Hooper, *Discussions Faraday Soc.*, **32**, 218 (1962). ^k I. S. Jaffe and E. R. Van Artsdalen, *J. Phys. Chem.*, **60**, 1125 (1956). ^l S. V. Tricklebank, L. Nanis, and J. O'M. Bockris, *J. Phys. Chem.*, **68**, 58 (1964). ^m C. A. Angell and J. W. Tomlinson, in press. ⁿ C. Tubandt and E. Lorenz, *Z. physik. Chem.*, **87**, 513 (1914). ^o H. Bloom and E. Heymann, *Proc. Roy. Soc. (London)*, **A188**, 392 (1947). ^p C. A. Angell and J. W. Tomlinson, *Discussions Faraday Soc.*, **32**, 237 (1962). ^q J. O'M. Bockris, H. Bloom, E. H. Crook, and N. E. Richards, *Proc. Roy. Soc. (London)*, **A255**, 558 (1960). ^r C.-A. Sjöblom and A. Lunden, *Z. Naturforsch.*, **18a**, 942 (1963). ^s C.-A. Sjöblom, *ibid.*, **18a**, 1247 (1963). ^t This result is considered improbable. Independent measurements of $D_{Zn^{2+}}$ in ZnBr₂ (L. Wallin and A. Lunden, *Z. Naturforsch.*, **14a**, 262 (1959)) indicate a higher value (~ 4.5), more in keeping with the highly associated nature of the zinc halides.

However, since correlations obtained in ref. 2b among conductance data for various molten salts and salt mixtures suggested that a scale of corresponding temperatures based on T_0 values may prove useful to the interpretation of transport data for fused salts, it is reasonable to hope that the application of such corresponding temperatures in the comparison of deviations from the Nernst-Einstein equation for different salts may lead to correlations of analytical value. While conductance data are generally available, systematic studies of diffusion have unfortunately only been made for group I nitrates¹² and some alkali metal halides.^{8,10} For these salts, the deviations from the Nernst-Einstein equation noted in Table I in the form of the ratio, $\Lambda_{\text{calcd}}/\Lambda_{\text{measd}}$, are plotted in Figure 1 against the appropriate T/T_0 values, where T_0 in each case refers to the value for the particular salt (Table I).

Despite the limited amount of systematic data available, it appears from Figure 1 that a correlation does

exist for the alkali metal nitrates on the one hand and for the halides on the other. Greater weight may be placed on the plot for the nitrates since (a) the T/T_0 values are lower than for the halides, hence are closer to the temperature range, $< 1.7T_0$, in which the general equation of the free volume model

$$D = AT^{1/2} \exp(-k/(T - T_0)) \quad (2)$$

where A and k are constants, applies accurately; (b) difficulty in obtaining reproducibility has been experienced with the method used for measuring the diffusion coefficients in the halides, further measurements on NaI with the same method¹⁰ having led to a revision of previous values. In view of the correlation for Cs, K, and Na nitrates, some explanation for the discrepancy in the case of LiNO₃ is required; one interesting possibility will be discussed below.

(12) See footnote *e* in Table I.

It is tempting to extrapolate the plots in Figure 1 to pass through the origin to accord with the suggestion made in the introduction that the Nernst–Einstein equation should be obeyed at the glass transition temperature ($T/T_0 = 1$). This extrapolation may not be correct, however, since at low concentrations of moving ions near $T/T_0 = 1$, some form of correlation correction to the tracer diffusion coefficients would probably be required, though this factor could not be calculated directly as in the case of crystalline solids. The data could be represented almost as well by linear plots which would yield, at $T/T_0 = 1$, $\Lambda_{\text{calcd}}/\Lambda_{\text{measd}}$ values of 0.8–0.9, corresponding to correlation corrections similar to those required for diffusion in f.c.c. and h.c.p. lattices.

Accepting Figure 1 at face value, the correlations suggest that T_0 is the only parameter required to predict the relative deviations at a given temperature from the Nernst–Einstein equation in the alkali nitrate or chloride series. Since T_0 itself is obtained from an experimental correlation based on cation radii, the prime dependence of the deviation for a given salt in the series would be on the cation radius. Thus $\Lambda_{\text{calcd}}/\Lambda_{\text{measd}}$ should, and does, correlate reasonably well with the product $T(^{\circ}\text{K})r_{\text{cation}}$, though the plot differs somewhat from Figure 1 due to the fact that the T_0 dependence on $1/r_{\text{cation}}$ does not pass through the origin (Figure 9 in ref. 2b).

On the other hand, according to Figure 1 the Nernst–Einstein deviations are markedly greater for nitrates than for halides. Two alternative explanations for the breakdown of the Nernst–Einstein equation for fused salts have been advanced. One of these, explicitly used in the development of this paper, involves the concept of mutual interference¹³ between ions moving in opposite directions under the influence of an applied field. The other⁸ proposes that large holes of approximately twice the ion size arising in the natural thermal distribution of hole sizes in the liquid¹⁴ provide a currentless diffusion path analogous to the paired vacancy mechanism in ionic crystals. Figure 1, together with estimates of packing densities of ions in the salts, permits some comments on the plausibility of these alternative proposals. In Table II, packing densities for the nitrates and halides are represented by the ratio of the molar volumes, V_m , at the designated temperature to the (assumed unchanging) total volumes per mole of the ions themselves, V_i . Where necessary, V_m/V_i ratios were obtained by extrapolation of the linear density–temperature equations. To judge by the findings of Dietzel and Poegel¹⁵ for glass-forming nitrate melts, this procedure should be valid down to T_0 .

In computing the values for the nitrate series it has

been assumed that the nitrate ion rotates freely and hence behaves as a spherical ion. This is probably close to the truth since even in the crystalline state various degrees of rotation are possible in most nitrates of univalent cations, and in ammonium nitrate complete freedom of rotation is found.¹⁶ (See also footnote 21.)

Table II

Salt	V_i^a	T_m	V_m/V_i^b		
			$T/T_0 = 1$	$T/T_0 = 2$	$T/T_0 = 3$
LiNO ₃	27.05	1.43	1.37	1.58	1.78
NaNO ₃	28.7	1.54	1.40	1.55	1.72
KNO ₃	32.4	1.66	1.45	1.58	1.73
CsNO ₃	38.7	1.87	1.51	1.65	1.79
LiCl	15.43	1.83	1.60	1.80	2.00
NaCl	17.1	2.20	1.75	1.90	2.05
KCl	20.8	2.34	1.80	1.95	2.10
RbCl	23.1	2.34	1.80	1.95	2.10
CsCl	27.1	2.21	1.81	1.94	2.07
NaI	27.4	1.97	1.61	1.77	1.92

^a The volumes of the halide and alkali metal ions were calculated from the Pauling radii, and that of NO₃⁻ from the radius of 2.19 Å. used by O. Kleppa and L. S. Hersh, *J. Chem. Phys.*, **34**, 351 (1961). ^b Density data were obtained from G. P. Smith, G. F. Peterson, and W. M. Ewing, U. S. Atomic Energy Commission Reports ORNL-2762 (1959) (for nitrates) and footnote *k*, Table I (for halides).

It appears that the packing density is markedly greater in the nitrates than in the halides, the difference being most clearly defined when the comparison is made at equal T/T_0 values. "Double" holes originating purely from a thermal distribution of unoccupied space in the liquid would therefore be expected to arise more frequently in the looser chloride melts, thus the paired vacancy-type argument would lead one to expect greater Nernst–Einstein deviations for the chlorides than for the nitrates, which Figure 1 shows is not the case. On the other hand, it is reasonable to expect interference between moving ions to be greatest in the more densely packed salts. Therefore, unless (i) special assumptions concerning the distribution of hole sizes can be justified, or (ii) it can be demonstrated that, at

(13) R. W. Laity, *Discussions Faraday Soc.*, **32**, 172 (1962).

(14) This model has the advantage that such holes become more probable with increasing temperature, thus accounting for the increase in Nernst–Einstein deviation with temperature, an effect which could not be readily understood if a special stability were attributed to paired holes as is done in the case of ionic crystals.

(15) A. Dietzel and H. J. Poegel, Proceedings of the 3rd International Glass Congress, Venice, 1953, p. 219.

(16) A. F. Wells, "Structural Inorganic Chemistry," 2nd Ed., Oxford, 1950, p. 138.

least for transport considerations, the nitrate ion does not rotate freely enough to behave as a spherical ion, then it seems that an interference mechanism provides a more consistent explanation of the observed deviations.

It is worth emphasizing the similar values of V_m/V_i within the nitrate and chloride groups obtained at equal T/T_0 values (Table II). Within each group the relative V_m/V_i values do not change rapidly with T/T_0 , except for the lithium salts. It would be consistent with the interference mechanism, favored by the above discussion, to link the similar packing densities at equal T/T_0 with the equal Nernst-Einstein deviations at equal T/T_0 suggested by Figure 1, although the intermediate position of NaI seems to rule out the possibility that the deviations are any simple function of packing density.

Data on salts of divalent cations are only available for PbCl_2 and ZnBr_2 , and the latter salt is apparently extensively associated in the liquid state.¹⁷ To judge by the value of $\Delta_{\text{calcd}}/\Delta_{\text{measd}}$ for PbCl_2 , the interference between Pb^{+2} and Cl^- is greater than between the alkali metal cations and Cl^- , which might be expected in view of the double charge on the cation.

It is of interest to note that by comparison of the T_m/T_0 values of Table I with the reduced melting points, τ_m , quoted by Reiss, *et al.*,¹⁸ in their theory of corresponding states for fused salts, one obtains reduced glass transition temperatures τ_0 . This comparison for the chlorides of Na, K, Rb, and Cs yields $\tau_0 = 0.79 \pm 0.02$, compared with $\tau_m = 3.2 \pm 0.1$, *i.e.*, the estimates of τ_0 by use of Figure 9 of ref. 2b are constant to about the same degree as the τ_m . This seems reasonable since glass transition temperatures for molecular liquids of the same class are constant on the reduced temperature scale.⁷ One concludes that the basis for the correlations discussed in this paper, *viz.*, the slope of the T_0 -ionic strength plot (see above) is not inconsistent with fused salts corresponding states theory and what is already known about glass formation in molecular liquids.

Finally, we consider the case of LiNO_3 , which, according to the present analysis of results, behaves abnormally. Since other attempts,^{18,19} notably that of Reiss, *et al.*,¹⁸ to correlate properties of uni-univalent molten salts of alkali metal cations by means of Pauling ionic radii, have found exceptional behavior in the case of lithium salts, the present instance should cause little surprise, and an attempt to explain the discrepancy is probably premature.

However, the recent work of Stokes,²⁰ who pointed out that ionic radii *in vacuo* should be considerably

larger than the corresponding crystal radii and proceeded with striking success to apply his concept of van der Waals ionic radii to the calculations of ionic hydration energies and crystal lattice energies for a wide variety of halides, is very suggestive. In molten LiNO_3 , anion-anion contact must occur, the radius of the holes between close-packed rotating²¹ nitrate groups of effective radius 2.19 Å,²² being 0.92 Å. compared with the Pauling radius of 0.60 Å. Following Stokes, there may therefore be some value in the notion that the Li^+ ion in molten LiNO_3 expands toward its "in vacuo" radius of 1.14 Å.^{20b} to fill the holes between the nitrate ions; *i.e.*, a sort of Parkinson's law "ions expand to fill the available volume" may apply to small ions. The deviation from the Nernst-Einstein equation for LiNO_3 at T_m would in fact correlate with the results for other nitrates in Figure 1 if the T_0 value for LiNO_3 were 290° , which corresponds to a radius of approximately 0.9 Å. The transport data for LiNO_3 are consistent in this respect since it is possible to show that E_A and its dependence on temperature (Table I) are also more appropriate to a Li^+ radius of approximately 0.9 Å. Against the "swollen" Li^+ ion idea, however, must be counted the correlations achieved by Kleppa and Hersh²² for heat of mixing data for alkali metal nitrates by use of Pauling radii for the cations and possibly also the X-ray data for LiI ²³ in which the anion size is comparable with that of the nitrate ion. Concerning the latter data, however, some difficulty is encountered in interpretation of the radial distribution functions for LiI and LiBr ,^{23,24} which could be taken to indicate an Li^+ radius greater than the Pauling value. There is, at least, good reason to expect the extreme ion radius ratio in LiNO_3 to lead to abnormal transport behavior.

(17) R. W. Laity, *Ann. N. Y. Acad. Sci.*, **79**, 997 (1960).

(18) H. Reiss, S. W. Mayer, and J. L. Katz, *J. Chem. Phys.*, **35**, 820 (1961).

(19) C. Thomas and J. Braunstein, *J. Phys. Chem.*, **68**, 957 (1964).

(20) (a) R. H. Stokes, *J. Am. Chem. Soc.*, **86**, 979 (1964); (b) R. H. Stokes, *ibid.*, **86**, 982 (1964).

(21) J. Zarzycki (*Discussions [Faraday Soc.*, **32**, 38 (1962)) has given reasons for doubting that free anion rotation occurs in molten Li_2CO_3 and Li_2SO_4 . On the other hand, the entropy of fusion of LiNO_3 is higher than the fusion plus solid state transition entropies for the other alkali metal nitrates (N. J. Davis, S. E. Rogers, and A. R. Ubbelohde, *Proc. Roy. Soc. (London)*, **A220**, 14 (1953)) rather than lower as would be expected if nitrate rotation were absent in the case of the lithium salt.

(22) See footnote a, Table II.

(23) H. A. Levy, R. A. Agron, and M. A. Bredig, *Ann. N. Y. Acad. Sci.*, **79**, 762 (1960).

(24) K. Furukawa, *Discussions Faraday Soc.*, **32**, 53 (1962).

Infrared Spectra of Nitrilotriacetate Chelates in Aqueous Solution

by Yuko Tomita, Takeshi Ando, and Keihei Ueno

Contribution No. 65 from the Department of Organic Synthesis, Faculty of Engineering, Kyushu University, Fukuoka, Japan (Received June 8, 1964)

The nitrilotriacetic acid chelates of magnesium and copper in aqueous solution have been studied at various pH values by infrared spectroscopy using deuterium oxide as the solvent. On the basis of the antisymmetric stretching bands of the ionized, un-ionized, and coordinated carboxyl groups, the schemes of the chelate formation reactions are proposed. In the case of the magnesium chelate, the stability constant has been estimated from the effect of pH upon the spectra.

Introduction

Recently, the applications of infrared spectroscopy to the study of metal chelates in aqueous solution have provided new information.¹⁻³ In our previous paper,⁴ the chelating behavior of nitrilotriacetic acid (NTA) was investigated by infrared spectroscopy in the solid state as well as in solution, and the antisymmetric carbonyl stretching frequencies of NTA in aqueous solution were utilized to determine the state of the carboxyl group.

In this investigation, the infrared spectra of NTA-metal chelates in aqueous solution were taken as a function of the pH to supplement the information obtained by potentiometric measurements.

The metal chelates chosen in this study are magnesium- and copper(II)-NTA, because they are sufficiently soluble in deuterium oxide for the infrared spectral measurement. On the bases of the spectral changes with pH and of our previous knowledge of the metal-NTA chelates, the coordinating structures of NTA with these metal ions in solution and a new method of determining their chelate stability constant are proposed.

Experimental

Infrared Spectra. The infrared spectra in aqueous solution were observed using a cell with calcium fluoride windows. The measurements were made with a Nippon Koken Model DS 301 double-beam spectrophotometer equipped with sodium chloride optics.

Preparation of Metal Chelates and pH Measurements. Solutions of metal-NTA chelates were prepared by dissolving equimolar amounts of NTA free acid and

metal chloride in deuterium oxide (99.5%) at concentrations approximately 5-10% by weight. The inorganic salts used in preparing the complexes were reagent grade in all cases. The free acid of NTA (donated by Dojindo and Co.) was analytical grade and was used without further purification. The pH values of the solutions were controlled by the careful addition of concentrated NaOD solution from a microburet.

Table I: Antisymmetric Carboxyl Absorption Bands (cm.⁻¹)

Mg-NTA complex				
pH	COOH	NH ⁺ - CH ₂ COO ⁻	COO-Mg	Pre-dominant species
3.2	1730	1625		I
4.2		1625		II
5.5-10.0		1625	1610	II, V
11.6			1610	V
Cu-NTA complex				
pH	COOH	NH ⁺ - CH ₂ COO ⁻	COO-Cu	Pre-dominant species
1.6	1730	1625		I
1.8-11.0			1615	V

(1) (a) K. Nakamoto, Y. Morimoto, and A. E. Martell, *J. Am. Chem. Soc.*, **84**, 2081 (1962); (b) *ibid.*, **85**, 309 (1963).

(2) D. T. Sawyer and J. E. Tackett, *ibid.*, **85**, 314, 2390 (1963).

(3) D. Chapman, D. R. Llund, and R. H. Prince, *J. Chem. Soc.*, 3645 (1963).

(4) Y. Tomita and K. Ueno, *Bull. Chem. Soc. Japan*, **36**, 1069 (1963).

The pH values listed were obtained from the solutions of the duplicate run using ordinary water and were measured with a Hitachi-Horiba Model P pH meter. Therefore, the pD values of the deuterium oxide solution used for spectral measurements may be slightly different from the conventional pD values, which are obtained from the equation, $pD = \text{meter reading} + 0.40$, but they are within the tolerances required for meaningful interpretation of the results.

Results and Discussion

When NTA is mixed with a metal ion in aqueous solution, the extent of their interaction is governed mainly by the solution pH and the kind of metal ion. The possible ionic species existing in the solution are schematically shown in Figure 1, and the antisymmetric carboxyl stretching frequencies of NTA-metal chelates are listed in Table I.

It has been known that the antisymmetric stretching band of the carboxyl group of NTA in aqueous solution occurs in different frequency regions according to the state of the carboxyl group, and the band due to $>N-CH_2COOH$, $>NH^+-CH_2COO^-$, or $>N-CH_2COO^-$ appears at 1730–1700, 1630–1620, or 1585–1575 cm^{-1} , respectively.^{1a} The similar investigation on the metal chelates of NTA has revealed that the coordinated carboxyl group gives rise to a band at 1615–1605 cm^{-1} .⁴

This information, together with the knowledge of the potentiometric titration,⁵ allows one to follow the scheme of reaction which occurs during the chelate formation.

Magnesium-NTA Chelate. The carboxylate absorption band of magnesium-NTA chelates is shown as a function of solution pH in Figure 2. At pH 3.2 two peaks at 1730 and 1625 cm^{-1} are observed. As the pH is increased, the weak band at 1730 cm^{-1} dis-

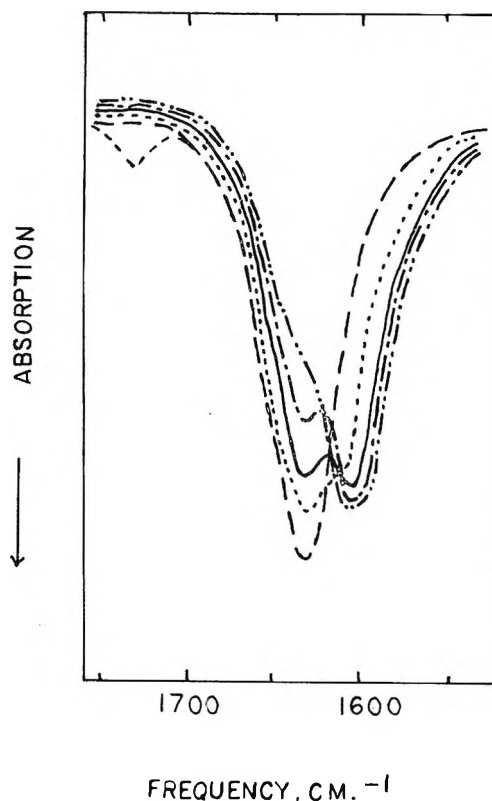


Figure 2. Infrared spectra of Mg-NTA complex in D_2O solutions: - - - -, pH 3.2; — — —, pH 4.2; - - - - -, pH 5.5; — — — —, pH 6.8; - · - · - ·, pH 10.0; — · — · — ·, pH 11.6.

appears, and a single strong band at 1625 cm^{-1} is observed. With the further increase of pH, a new band appears at 1610 cm^{-1} which grows in intensity at the expense of the 1625- cm^{-1} peak. Finally, at the most basic pH value, only the peak at 1610 cm^{-1} remains.

According to Nakamoto and others, two bands at 1720 cm^{-1} (vw) and 1623 cm^{-1} (m) which appeared in a solution of pH 2–3, were assigned to the COOH and $NH^+-CH_2COO^-$ groups, respectively, of the monovalent NTA anion (H_2A^-).^{1a} As the spectrum of magnesium-NTA at pH 3.2 is quite similar to that observed by Nakamoto for the free ligand in the low pH region, it is apparent that there occurs little interaction between the ligand and magnesium ion at this pH value (I in Figure 1).

With the increase of pH, NTA is known to dissociate to give a divalent anion (HA^{2-}), which shows only one band at 1625 cm^{-1} . Since the change of spectrum of magnesium-NTA chelate from pH 3.2 to 4.2 is identical with that of free ligand in the same pH range, no coordination of NTA with magnesium ion is indicated in this pH region, and the predominant species existing

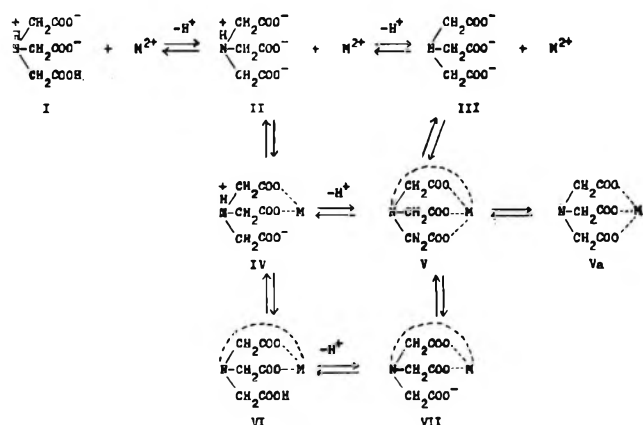


Figure 1. The solution equilibria of NTA-metal complex.

(5) G. Schwarzenbach, E. Kampitsch, and R. Stener, *Helv. Chim. Acta*, **28**, 828 (1945).

in the solution are the divalent ligand anion and free metal ion (II in Figure 1). This conclusion is also supported by the titration data of magnesium-NTA chelate since no appreciable pH drop is observed in this pH region.

When the solution pH becomes higher than 4.2, a new band at 1610 cm^{-1} is observed. This band, which is not observed in the free ligand over the entire pH range investigated but is found in the NTA-metal chelates, has been assigned to a coordinated carboxyl group.⁴ Since the two bands at 1610 and 1625 cm^{-1} are observed in the solution of pH 4.2 or higher, the ionic species existing in this pH range may be an equilibrium mixture of the divalent ligand anion, free metal ion, and the tetracoordinated chelate⁶ (II and V, respectively, in Figure 1), and the last component (tetracoordinated magnesium-NTA chelate) exists as a single ionic species only at the relatively high pH region, where a single band at 1610 cm^{-1} is observed.

The increase in absorption at 1610 cm^{-1} and the decrease in absorption at 1625 cm^{-1} with increasing pH indicate that the intensities of these peaks may be proportional to the concentration of ionic species II and V, respectively.

Although the peak at 1625 cm^{-1} could be associated with a complex containing an acidic hydrogen, such as IV, the pH titration study appears to rule out any appreciable amount of such a complex above pH 4.⁷

As is known from the titration data, the chelate formation between NTA and magnesium ion occurs in the pH region higher than 4.8.⁵ Thus, the main equilibria involved in the pH region of 4.2 or higher are



However, eq. 2 will be valid only in the relatively high pH region, as the third dissociation constant of NTA is $10^{-9.73}$. Therefore, the main equilibrium, which is effective at pH 4-8, will be represented by eq. 1, and the equilibrium constant can be given as

$$K = \frac{(\text{MA}^-)(\text{H}^+)}{(\text{HA}^{2-})(\text{M}^{2+})} = K_{\text{MA}}K_3 \quad (3)$$

where K_{MA} and K_3 are the stability constants of magnesium-NTA chelate and the third acid dissociation constant of NTA, respectively.

As previously noted, it is reasonable to assume that the intensity of the 1610- and 1625- cm^{-1} peaks are proportional to the concentrations of ionic species MA^- and HA^{2-} , respectively. Then, the relative concentrations of MA^- and HA^{2-} can be derived according to the usual treatment in the spectrophotometric

determination of two components mixtures. As the spectra at pH 3.2 and 11.6 are believed to represent the divalent ligand anion (HA^{2-}) and the tetracoordinated magnesium-NTA chelate, respectively, molecular extinction coefficients for both components can be obtained from their spectra. Thus, the concentrations of both components in a solution of given pH value may be calculated from the peak intensities of 1610- and 1625- cm^{-1} bands in the spectra of intermediate pH value. Plots of such concentrations in terms of the absorption intensity against pH are shown in Figure 3.

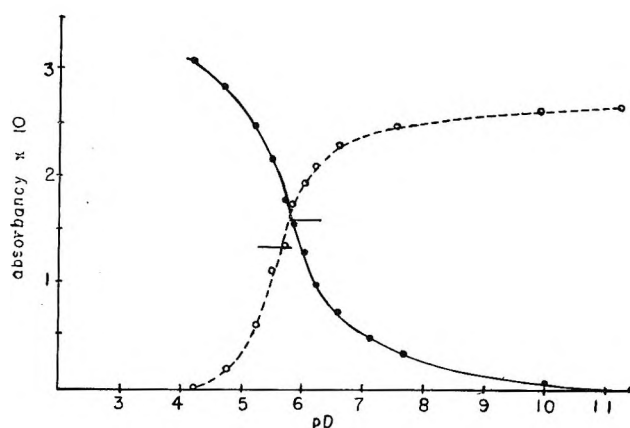


Figure 3. Absorbance of carboxylate bands of Mg-NTA complex as function of pH: —, 1625- cm^{-1} band; ---, 1610- cm^{-1} band.

At the pH values where the intensity of the peak is one-half of the original intensity, the concentrations of HA^{2-} and MA^- become equal, as the spectral measurements were made on the equimolar mixture of metal ion and the ligand. Then, eq. 3 can be rewritten as

$$\log K_{\text{MA}} = \text{p}K_3 - \text{pH} - \log (\text{M}^{2+}) \quad (4)$$

The pH value which satisfies this condition is determined from Figure 3 as 5.65 (1610- cm^{-1} peak) or 5.9 (1625- cm^{-1} peak). Although the agreement of values obtained from the two different peaks is not completely satisfactory, the mean pH value 5.75 is used for the calculation of the stability constant described as follows. To determine the stability constant, K_{MA} , the value of $\text{p}K_3$ must be corrected for D_2O solutions.

(6) Although there is no positive evidence for the presence of a N-Mg bond in the Mg-NTA chelate, a recent n.m.r. study proved the existence of nitrogen-metal bonds in the EDTA chelates of alkaline earth metals [R. J. Kula, D. T. Sawyer, S. I. Chan, and C. M. Finly, *J. Am. Chem. Soc.*, 85, 2930 (1963)]. Therefore, it is likely that the Mg-NTA chelate exists as V rather than as Va in Figure 1.

(7) G. Schwarzenbach and E. Freitag, *Helv. Chim. Acta*, 34, 1492 (1951).

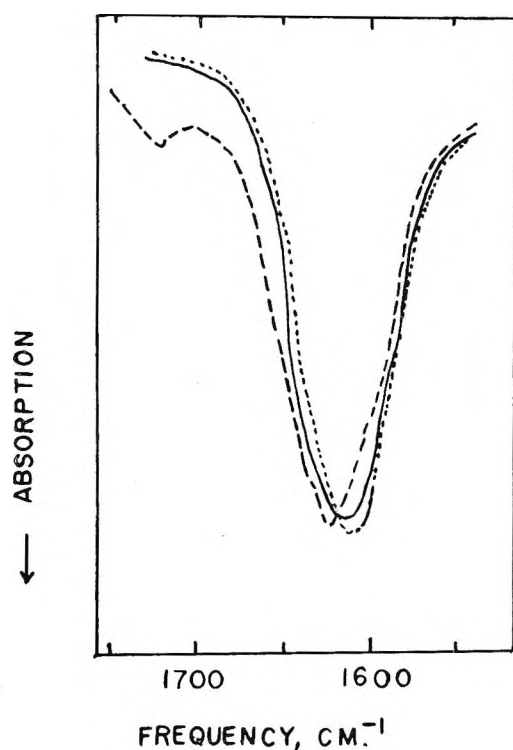


Figure 4. Infrared spectra of Cu-NTA complex in D₂O solutions: ----, pH 1.6; —, pH 1.8; - · - · -, pH 2.3.

This can be done using the equations proposed by Li, Tang, and Mathur,⁸ to give a calculated value for pK_3 of 10.13. The free metal ion concentration (M^{2+}) in this condition is equal to $0.5C_M$, where C_M is the total concentration of metal ion and $\log(M^{2+})$ is calculated as -0.86 .

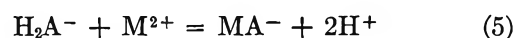
Then, one could calculate the stability constant K_{MA} from eq. 4. Although the calculated value $\log K_{MA} = 5.24$ does not agree very well with the literature values ($\log K_{MA} = 5.41$),⁶ it is indicative of the validity of determining chelate stability constants from infrared absorption measurements.

Copper-NTA Chelate. Infrared spectra of copper(II)-NTA chelate are shown in Figure 4 as a function of solution pH. At pH 1.6, two peaks at 1730 and 1625 cm^{-1} are observed. However, when the pH is increased to 1.8, a new band appears at 1615 cm^{-1} , the 1730- cm^{-1} peak has completely disappeared, and

the 1625- cm^{-1} peak can be observed only as a very weak shoulder. With further increase of pH, the new band at 1615 cm^{-1} becomes a well-defined, single band which does not change up to pH 11.0.

The two bands at 1730 and 1625 cm^{-1} , which are observed at pH 3.2 in the spectrum of the magnesium-NTA chelate, can be assigned to COOH and $\text{NH}^+\text{-CH}_2\text{COO}^-$, respectively; both are characteristic of the free ligand in the low pH region. Thus, it is clear that NTA does not interact with copper(II) ion at pH 1.6.

However, in the solution of pH 1.8 or higher, copper(II)-NTA shows only one peak at 1615 cm^{-1} , which is characteristic of the coordinated carboxyl group. As no other band is observed in this pH region, it is fair to conclude that the predominant species existing in the solution is a tetradentate normal chelate (V in Figure 1). Thus, in the case of copper, the chelate formation reaction represented by the equation



occurs instantaneously in a fairly low pH region. Since no intermediate stage of chelate formation is observed for the copper(II)-NTA chelate, the stability constant cannot be derived in this case. Finally, it is interesting to note that the copper(II)-NTA chelate shows only one carboxyl band at 1615 cm^{-1} . Coordination to the metal of the nitrogen atom and three carboxylate groups cannot result in a planar $\begin{matrix} \text{N} \\ \diagup \quad \diagdown \\ \text{O} \quad \text{Cu} \quad \text{O} \\ \diagdown \quad \diagup \\ \text{O} \end{matrix}$ configuration. The absence of a free COO^- band in the 1585–1575- cm^{-1} region of the spectrum suggests that the nitrogen atom and three carboxylate groups occupy four octahedral coordination sites around the copper atom in aqueous solution.

Acknowledgment. The authors are grateful to Dr. K. Nakamoto of the Illinois Institute of Technology, who gave valuable suggestions at the early stage of this investigation. They also thank the Ministry of Education, Japanese Government, for the financial support for this work.

(8) N. C. Li, P. Tang, and R. Mathur, *J. Phys. Chem.*, **65**, 1074 (1961).

The Kinetics of the Hydrogen-Fluorine Reaction. II.

The Oxygen-Inhibited Reaction¹

by Joseph B. Levy and B. K. Wesley Copeland

Atlantic Research Corporation, Alexandria, Virginia (Received June 9, 1964)

The kinetics of the thermal, gaseous hydrogen-fluorine reaction have been investigated by a colorimetric technique. The reaction has been found to be inhibited by oxygen and the inhibited reaction was studied mainly at 132°, but also from 122 to 162°. The experiments have been performed at a total pressure of about 645 mm., with oxygen varying from about 85 to 500 mm. Nitrogen and helium have been used to maintain the total pressure at the desired value. Hydrogen and fluorine pressures have been in the general range of ~20–80 mm. It has been found that the rate decreases with added oxygen but reaches a limiting value unaffected by further oxygen addition. The limiting rate obeys the expression $-d(F_2)/dt = k(F_2)(H_2)^{1/2}$ fairly well, but the curves of the integrated forms are linear only for about the first 50% of reaction, dropping off thereafter. The Arrhenius plot for the rates from 132 to 162° is linear, yielding an activation energy of 16.7 kcal./mole. The results are discussed in terms of a chain reaction involving the propagation steps, $H + F_2 \rightarrow HF + F$; $F + O_2 + M \rightarrow FOO + M$; and $FOO + H_2 \rightarrow HF + O_2 + H$. Evidence is presented for an activation energy of 5–7 kcal./mole for the reaction $F + H_2 \rightarrow HF + H$ and for a heat of formation for the FOO species of +3.5 kcal./mole.

Introduction

We have recently reported² the results of a study of the kinetics of the thermal hydrogen-fluorine reaction in a magnesium flow reactor at 110° in which a stream of hydrogen was mixed with a stream of nitrogen containing 1–5% fluorine. The reaction rate was followed by titrating the effluent fluorine iodometrically. The results showed the reaction rate to be independent of surface area to volume ratio and hydrogen concentration, and to be first order in fluorine. We concluded that the reaction was a chain reaction with initiation and termination occurring on the walls. References to earlier work on this system are given in that report.

We report here on a further study of this system in which we have followed the rate of disappearance of fluorine continuously by making use of its absorption peak at 2849 Å. The bulk of the results reported here were determined at 132° in the presence of oxygen. A few measurements have been made at higher temperatures.

Experimental

Chemicals. The nitrogen used in this work was Southern Oxygen Co. prepurified grade specified as 99.998% nitrogen with the remainder oxygen. The hydrogen used was Southern Oxygen Co. dry electrolytic grade, containing no more than 0.2% impurities, including nitrogen and oxygen. The fluorine used was General Chemical Co. fluorine. It was freed of hydrogen fluoride by passage through a potassium fluoride trap. The helium used was Southern Oxygen Co. helium specified as 99.997% pure grade A.

Apparatus. The Reaction Cells. Two magnesium cells have been used in the experiments reported here. Each was made from a block of pure magnesium, and each was designed to fit into the cell compartment of the Beckman DK spectrophotometer. The cell shape in

(1) This work was supported by the Air Force Office of Scientific Research of the Office of Aerospace Research under Contract No. AF 49(638)-1131.

(2) J. B. Levy and B. K. W. Copeland, *J. Phys. Chem.*, **67**, 2156 (1963).

each case was that of a cylinder which lay in the cell compartment on its side, so that the axis was parallel to the light path. One cell, which we call cell I, had two axial cylindrical passages machined in it to line up with the two light paths in the spectrophotometer. One cell path was 1.8 cm. in diameter and the other was 0.9 cm. in diameter. Cell II had only one light path. The diameter of this light path was 3.7 cm. except at the very ends where magnesium end plates were welded on to accommodate cell windows, 2.54 cm. in diameter. The path lengths in the cells were 10 cm. Access was gained to these volumes by drilling 0.32-cm. holes from the top of the cylinder. Magnesium tubing, 0.64 cm. o.d., was welded to the tops of the holes and Teflon valves were swage-locked to these tubes. Fused sapphire windows were compression-sealed to the ends of the cell through Teflon gaskets. (No sign of attack on these windows can be detected even after months of use.) The cells were found to be vacuum tight. The cells were wrapped with nichrome wire for heating. Five thermocouple holes were spaced along the cylinder from one end to the other; the holes were drilled to within 0.16 cm. of the chamber and the temperature was monitored by the thermocouple readings. Temperature uniformity was very good—the differences between the readings of the various thermocouples did not exceed 0.2° . Temperature control was accomplished manually by controlling the voltage and temperatures were maintained constant to $\pm 0.5^\circ$.

Apparatus for Filling the Cells. From the cell valve, a Teflon tube was split to four Teflon tubes by means of Teflon tee units attached by Swagelok fittings. One line went to a mixing vessel, one to the fluorine cylinder, one to a glass manifold, and one to a vacuum pump. The manifold was fitted with a mercury manometer of sufficient length to allow measurement of about 1000 mm. pressure. The manometer arm connected to the manifold was twenty times the diameter of the other arm so that essentially all the pressure change occurred in the narrow arm. The mercury in the wide arm was protected by a layer of Fluorolube oil.

Two types of mixing vessels were used. One was a cylindrical Teflon cup 6.3 cm. in diameter and 13.5 cm. deep of about 400-cc. capacity. It was sealed by fitting a circular 0.013-cm. sheet of Teflon to the top, placing a Viton O-ring on the sheet and a 1.27-cm. thick glass plate on the O-ring, and compressing the plate against the O-ring mechanically. Access was gained to the cup by a Teflon side arm which was threaded into the side of the cup. The cup was vacuum tight. It was fitted with a perforated rectangular Teflon paddle which rode in a depression in the bottom of the cup and had a

small bar magnet sealed in the top. The cup contents could be stirred by rotating a permanent magnet above the glass plate. The other mixing vessel was a 300-cc. glass bulb containing a Teflon-clad magnet in the shape of a football, and about twenty pieces of Teflon tubing, about 2.5 cm. in length and 0.64 cm. i.d. Agitation of the bulb contents was effected by a magnetic stirrer. The Teflon tubing was thrown around vigorously.

Procedure. Rate measurements have been made in this work by two techniques. One will be referred to as the direct admission technique and the other as the premixed technique.

The Direct Admission Technique. In the direct admission technique, the components were metered directly into the evacuated thermostated cell. Fluorine was always added first and hydrogen last. The fluorine pressure was read on the manometer and at the same time determined optically. After the fluorine had been added, the cell valve was closed, the system exterior to the cell evacuated, flushed with the next component to be added, and the pressure built up to the value desired with the next component. The cell valve was then opened and the pressure on the manometer brought to the desired value by the addition of more gas. This effectively prevented diffusion out of the cell, as evidenced by the constancy of the spectrophotometer reading. The remaining components were added in the same way.

The Premixed Technique. In this method, fluorine was added simultaneously to the mixing vessel, which was kept at room temperature, and the cell. This allowed us to read the pressure optically and on the manometer. The mixing vessel was then shut off and the system exterior to it was evacuated. The remaining components were then added to the mixing bulb by the technique described above for filling the cell. When all the components had been added, the mixing bulb contents were agitated for 10 min. (see below) and the contents expanded into the evacuated cell. The ratio of the fluorine pressure, determined optically, as found on expansion into the cell to that measured when the mixing vessel was filled was 0.85 ± 0.01 for the 1.8-cm. i.d. cell compartment at 132° . This agreed with the value found for blank experiments in which the above procedure was repeated, omitting the hydrogen, but making the pressure up to 1 atm. in the mixing vessel with helium. For the 0.9- and 3.7-cm. i.d. vessels the ratios at 132° were 0.86 and 0.73, respectively.

The Beer's law constants were measured each day that experiments were performed for the pressures 50, 100, 150, and 200 mm. The pressures were measured on the manometer at room temperature while the cell

was at its higher temperature. The constants were reproducible and the values calculated from the above individual points agreed to about 0.5%. At 132°, the absorbance, $\log I_0/I$, for the given path length of 10 cm., was 0.244 for $P = 100$ mm. In the following discussion, it seems most convenient to refer to absorbances rather than pressures and we shall use the letter A to denote absorbance. For purposes of conversion, the Beer's law constant of 0.00244 can be used for 132°.

Results

The Inhibiting Effect of Oxygen. We first applied the colorimetric method by the direct admission technique to mixtures of fluorine, nitrogen, and hydrogen at 72°. Unless otherwise specified, the results discussed refer to the 1.8-cm. i.d. compartment in the magnesium cell. Smooth rates of disappearance of fluorine were observed, but the results were not very reproducible. Some typical data are shown in Figure 1 where the absorbance is plotted *vs.* time. Runs A and B represent experiments with identical compositions performed at different times. The divergence between the curves is typical of the degree of reproducibility.

Since we could not get quantitative reproducible results, we performed an experiment with a large amount of oxygen to see if the method would reveal a qualitative effect. Run C in Figure 1 differs from the other two only in that oxygen has replaced nitrogen as the third gas. The rate has been drastically di-

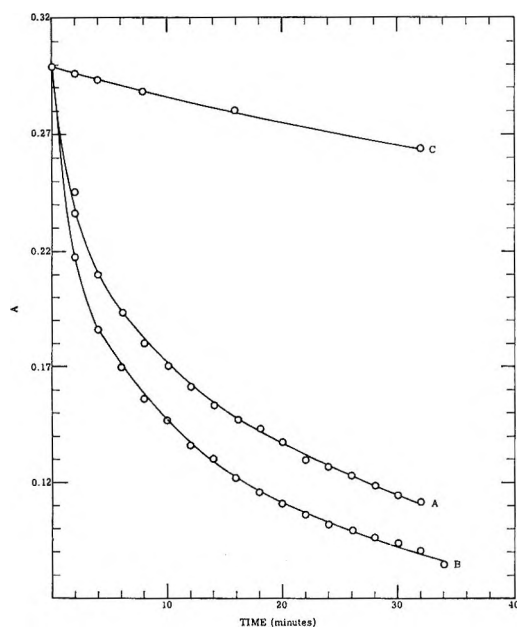


Figure 1. The hydrogen-fluorine reaction at 72°: A and B, $(F_2)^0 = (H_2)^0 = 100$ mm., $(N_2) = 560$ mm.; C, $(F_2)^0 = (H_2)^0 = 100$ mm., $(O_2) = 560$ mm. Total pressure is 760 mm.

minished, well beyond the range of scatter of the other runs, indicating an inhibiting effect of oxygen.

We then investigated the possibility of premixing our gases at room temperature with oxygen present. The inhibiting effect of oxygen suggested the possibility that, in the presence of oxygen, hydrogen and fluorine could be premixed at room temperature. We felt that if the gases could be premixed, a procedure that would be an improvement over the direct admission technique could be developed. We therefore investigated this possibility.

A series of experiments were performed in the evacuated Teflon cup described in the Experimental part. Measured amounts of fluorine, helium, oxygen, and hydrogen, in the order named, were added to the evacuated cup to a total pressure of 1 atm. and were stirred for 5 min. The mixture was then expanded into the evacuated colorimeter cell and the fluorine concentration was determined. The results are shown in Table I.

Table I: Premixing F_2 - O_2 -He- H_2 Mixtures at 25°

Pressures in mm. at 25° as made up in cup				Results
F_2	H_2	He	O_2	
50	50	...	660	No reaction in mixer
50	50	560	100	No reaction in mixer
50	50	610	50	No reaction in mixer
50	50	635	25	About 5-10% reaction in mixer
50	50	650	10	Reaction complete in mixer

In the last experiment in Table I, a faint click was heard as the hydrogen was admitted to the mixer. Experiments similar to those of Table I were then performed in which the mixing vessel was a 300-cc. Pyrex bulb, equipped with a stopcock lubricated with Kel-F stopcock grease. The results agreed with those of Table I. Since the Pyrex bulb mixer was more convenient, it was used in the experiments described below. In each experiment, comparison of the absorbance registered when the bulb was filled to that registered when it was expanded into the cell (see Procedure) served to check whether reaction occurred in the mixing bulb. No reaction was observed for any of the experiments reported below.

The Hydrogen-Fluorine Reaction in the Presence of Oxygen at 132°. At the time that these experiments were performed, we felt that the lack of reproducibility illustrated by Figure 1 was due to the importance of surface effects. The inhibiting effect of oxygen suggested that termination of chains would be homogeneous with

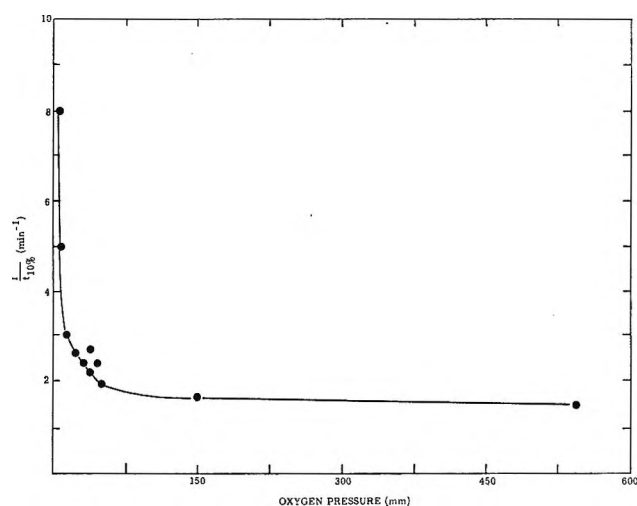


Figure 2. The effect of oxygen on the rate of the hydrogen-fluorine reaction at 132° : $(F_2)^0 = (H_2)^0 = 50$ mm. Total pressure = 760 mm. Inert gas is helium.

oxygen present. Since homogeneous initiation would be favored at higher temperatures, we felt that a completely homogeneous reaction might be attained if the temperature could be raised. This could be done in the presence of oxygen and we found that at 132° the reaction could be studied conveniently in the presence of oxygen. We have therefore done most of our work at that temperature.

General Nature of the Effect of Oxygen at 132° . The results of a series of experiments performed by the direct admission technique are shown in Figure 2. In these experiments the hydrogen and fluorine pressures were standardized at 50 mm. each and the pressure was kept at 1 atm. with helium and oxygen. The reciprocal of the time for 10% of the fluorine to be consumed has been taken as a measure of the rate and plotted vs. the oxygen pressure. It is clear that while small additions of oxygen sharply diminish the rate, after about 100 mm. has been added, further additions have little effect, *i.e.*, the curve slopes off very slowly, if at all.

We shall refer to the flat position of the curve as the region of the inhibited reaction. The remainder of the results reported here deal with the kinetics of the inhibited reaction, studied by the premixed method.

The Inhibited Reaction at 132° . The Nature of the Reaction Products. In the experiments described thus far, we have assumed that the rate of disappearance of fluorine corresponded strictly to the reaction of fluorine with hydrogen to form hydrogen fluoride. It seemed overwhelmingly probable to us that the same assumption could be made for the reaction in the presence of oxygen. We have two types of evidence to confirm this. In Table II of the following section there are

experimental results that show that when fluorine is present in excess over hydrogen, the drop in absorbance for complete reaction corresponds, within experimental error, to the amount of hydrogen present. In addition to this evidence, we have compared the quantity of hydrogen fluoride formed, in a reaction of a hydrogen-fluorine-oxygen-helium mixture, with the fluorine consumed and we have found agreement. This was done by cooling the cell to room temperature after reaction at 132° , inserting it in a Perkin-Elmer Model 21 infrared spectrometer, and determining the absorbance at 3880 cm^{-1} . The intensity was compared to that of standard pressures of hydrogen fluoride and the pressure of hydrogen fluoride formed was found by interpolation. The ratio of hydrogen fluoride found to twice the fluorine consumed was 1.03. We conclude that the rate of consumption of fluorine measures the rate of reaction of fluorine with hydrogen.

Reproducibility of Results with Premixed Method. Before assessing reproducibility, it is necessary to point out the level of accuracy that the spectrophotometer affords. The level of stability of the instrument and the scale of the chart are such that we assign a probable error of ± 0.25 division for any reading. For the range of absorbances ($\log I_0/I$) involved here, this leads to an error of $\pm 1\%$ in the absorbance.

In examining the reproducibility of our results, we found that it was necessary to stir the mixing bulb contents for at least 5 min. to ensure homogeneity. This was revealed by the results of a group of experiments wherein the initial hydrogen pressure was set at one-fourth that of the fluorine, and the reaction was allowed to proceed until the absorbance became constant.

Table II: The Effect of Stirring Time on Homogeneity of Mixtures^a

Stirring time, min.	Initial fluorine pressure, mm.	Absorbance		Change in absorbance/ 0.25 \times initial absorbance
		Initial	Final	
2	163	0.398	0.285	1.13
5	181	.441	.332	0.99
5	182	.442	.327	1.04
10	171	.417	.309	1.04

^a $t = 132^\circ$; initial $H_2 = 0.25 \times$ initial F_2 ; $O_2 = 212$ mm.; $He = 222$ mm.

The last three readings in the right-hand column are equal to unity within the accuracy of our experiments. The first reading exceeds unity by an amount well beyond experimental error. Since hydrogen was the last

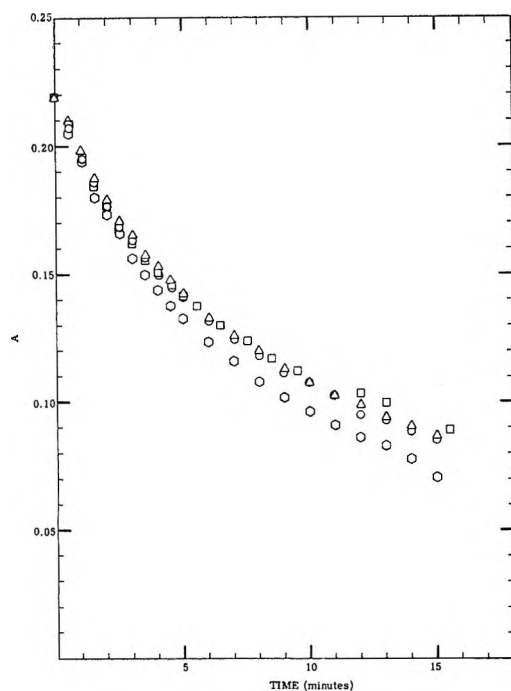


Figure 3. Reproducibility of the data by the premixed technique at 132° : \circ , A: first run in series; Δ , B: second run in series; \circ , C: third run in series; \square , D: second run in a series made at a later date; $(F_2)^0 = (H_2)^0 = 85$ mm., $(O_2) = 425$ mm., $(N_2) = 50$ mm. in all runs.

component added to the mixer, the high value for the drop in absorbance is interpreted to mean that mixing was incomplete and that the gas that expanded into the cell was richer in hydrogen than the average composition. A stirring time of 10 min. was adopted for the standard procedure.

We then performed experiments in which a series of consecutive identical runs were made and the results compared. We found that in any series of experiments, *i.e.*, a group performed after a lapse of time during which the cell was left filled with fluorine, good reproducibility was attained from the second run on; the first run in a series usually was faster than the rest. This is illustrated by Figure 3, where four runs of identical starting compositions are shown. The first run of a series of three, run A, showed faster decrease in absorbance than B or C, which in turn agreed well with each other. Run D was the second run in a series taken a few days later and illustrates the reproducibility attained for different series.

The Effect of Light. The effect of the amount of light in the spectrophotometer beam was checked by comparing data obtained when the reactants were exposed continuously to the beam and when they were protected from the beam by a shutter except for the brief period

required to take a reading. No difference in reaction rate was observed and we conclude that the beam has no effect.

The Kinetics of the Reaction at 132° . We have performed a number of experiments with large pressures of oxygen in an attempt to establish the kinetics for the inhibited reaction. The results are summarized in Table III.

Table III: The Kinetics of the Hydrogen-Fluorine Reaction at 132° ^a

No.	Initial pressure, mm. F ₂	H ₂	Initial concentrations in absorbance units, a.u.		P _{O₂} , k _{1.5} , a.u. ^{-1/2} mm.	min. ⁻¹
1	20.5	20.5	0.050	0.050	512	0.14
2	42.5	42.5	0.104	0.104	425	0.14
3	83.0	83.0	0.203	0.203	425	0.14
4	42.5	85.0	0.104	0.208	425	0.16
5	85.0	42.5	0.208	0.104	425	0.15
6	42.5	170	0.104	0.416	425	0.18
7	42.5	255	0.104	0.624	340	0.20
8	42.5	340	0.104	0.832	255	0.26
9	170	42.5	Explosion on ad-		425	
10	241	40.5	mitting mix- ture to cell		340	

^a Total $P = 645$ mm. Inert gas = N₂.

The first three entries of Table III represent experiments with equal concentrations of reagents. The range within which these concentrations could be varied was limited on the lower side by the loss of accuracy in reading the instrument at lower absorbances, and on the high side by the occurrence of explosions at higher concentrations.

Our procedure was to plot the absorbance-time curves for these experiments and to attempt to determine the reaction order from initial slopes. The results from entries 1-3 of Table III suggested a total order of 1.5 and we have plotted the data in the integrated form for these experiments in Figure 4, *viz.*, $(A_t)^{-1/2} - (A_0)^{-1/2} = (k/2)t$.

The curves in Figure 4 for the two higher pressures of reagents, $P_0 = 42.5$ mm. and $P_0 = 85$ mm., are virtually coincident for the first 10 min. ($\sim 40\%$ reaction). The curve for $P_0 = 21.2$ mm. lies above these but parallel to them; a sharp initial spurt has raised this curve. The curves for the higher two pressures drop off above 50% reaction while that for the lower pressure is quite linear. The rate constants calculated from the initial linear portions of the curves for Tables II and III are 0.14 absorbance unit^{-1/2} min.⁻¹. A similar value is found for entry no. 1 for the region $t = 1.5$ min. to $t =$

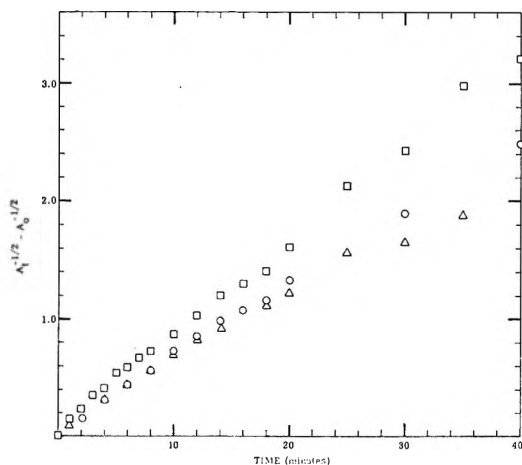


Figure 4. Three-halves-order curves for $(F_2) = (H_2)$ at 132° : $(F_2)^0 = 20.5$ mm., \square ; $(F_2)^0 = 42.5$ mm., \circ ; $(F_2)^0 = 83.0$ mm., Δ . Oxygen = 425 mm. Total pressure kept at 645 mm. with N_2 .

30 min. (8% reaction to 58% reaction). These values are shown in Table III in the last column.

Experiments in which $(H_2)^0 \neq (F_2)^0$ were also performed. The absorbance-time curves showed consistent behavior only for the expression $-d(F_2)/dt = k(F_2)(H_2)^{1/2}$ and the data were plotted for the integrated forms.

These are

$$kt = \frac{2}{\sqrt{(F_2)^0 - (H_2)^0}} \left(\tan^{-1} \frac{\sqrt{(H_2)^0}}{\sqrt{(F_2)^0 - (H_2)^0}} - \tan^{-1} \frac{\sqrt{(H_2)^t}}{\sqrt{(F_2)^0 - (H_2)^0}} \right); (F_2)^0 > (H_2)^0$$

and

$$kt = \frac{2.303}{\sqrt{(H_2)^0 - (F_2)^0}} \times \left(\log \frac{\sqrt{(H_2)^0} - \sqrt{(H_2)^0 - (F_2)^0}}{\sqrt{(H_2)^0} + \sqrt{(H_2)^0 - (F_2)^0}} - \log \frac{\sqrt{(H_2)^t} - \sqrt{(H_2)^0 - (F_2)^0}}{\sqrt{(H_2)^t} + \sqrt{(H_2)^0 - (F_2)^0}} \right); (H_2)^0 > (F_2)^0$$

In Figure 5 the appropriate functions are plotted for the cases $(H_2)^0 = 2(F_2)^0$ and $(F_2)^0 = 2(H_2)^0$. The former gives a more linear plot than the latter. The rate constants found from the initial portions of the curves were $0.16 \text{ a.u.}^{-1/2} \text{ min.}^{-1}$ for $(H_2)^0 = 2(F_2)^0$ and $0.15 \text{ a.u.} \text{ min.}^{-1}$ for $(F_2)^0 = 2(H_2)^0$. These values are also shown in Table III. The rate constants obtained in a similar manner for more extreme variations are also shown in Table III. The rates tend to increase with

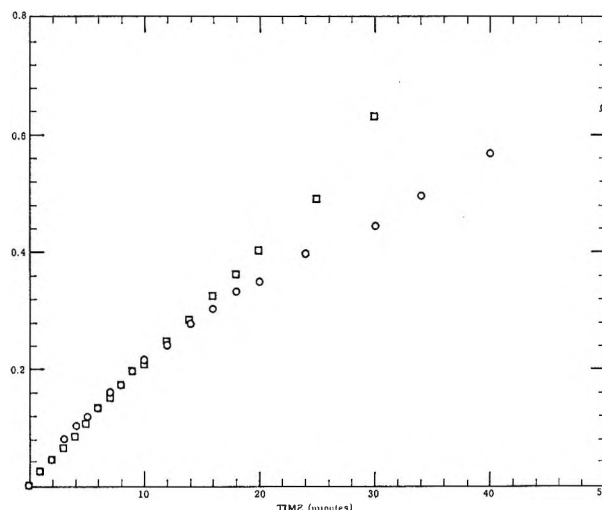


Figure 5. Experiments with $(F_2) = (H_2)$ at 132° : $(O_2) = 425$ mm. Total pressure is kept at 645 mm. with N_2 . \square , $(H_2)^0 = 85.0$ mm., $(F_2)^0 = 42.5$ mm. Ordinate is

$$\log \frac{\sqrt{(H_2)^t} - \sqrt{(H_2)^0 - (F_2)^0}}{\sqrt{(H_2)^t} + \sqrt{(H_2)^0 - (F_2)^0}} - \log \frac{\sqrt{(H_2)^0} - \sqrt{(H_2)^0 - (F_2)^0}}{\sqrt{(H_2)^0} + \sqrt{(H_2)^0 - (F_2)^0}}$$

\circ , $(H_2)^0 = 42.5$ mm., $(F_2)^0 = 85.0$ mm. Ordinate is

$$\tan^{-1} \sqrt{\frac{(H_2)^t}{(F_2)^0 - (H_2)^0}} - \tan^{-1} \sqrt{\frac{(H_2)^0}{(F_2)^0 - (H_2)^0}}$$

higher hydrogen pressures, no. 6, 7, and 8. Attempts to prepare mixtures with large $(F_2):(H_2)$ values, no. 9 and 10, resulted in explosions.

Experiments with Varying Oxygen Pressure. We have employed the integrated 1.5-order expression to check the effect of oxygen pressure for experiments with $(F_2)^0 = (H_2)^0$. In Figure 6 are shown plots for experiments with $(F_2)^0 = (H_2)^0 = 42.5$ and $O_2 = 425, 212,$ and 85 mm. The curves for the two higher oxygen pressures are practically coincident while that for the lowest pressure yields a distinctly higher rate. The curve of rate *vs.* P_{O_2} for these reagent pressures thus does become horizontal at $85 \text{ mm.} < P_{O_2} < 212 \text{ mm.}$

Temperature Dependence of the Rate. We have performed experiments at $122^\circ, 142^\circ, 152^\circ,$ and 162° with equal reagent concentrations for comparison with the results at 132° . In all the experiments we have adjusted the fluorine pressure to give an initial absorbance of 0.104, which corresponds to 42.5 mm. at 132° . The hydrogen pressure has been kept equal to the fluorine pressure. The use of equal initial absorbances means that the initial concentrations were the same though the initial pressures varied somewhat. The total pressure in the mixer was kept at 1 atm. with nitrogen and the oxygen pressure at ten times the fluorine pressure so that

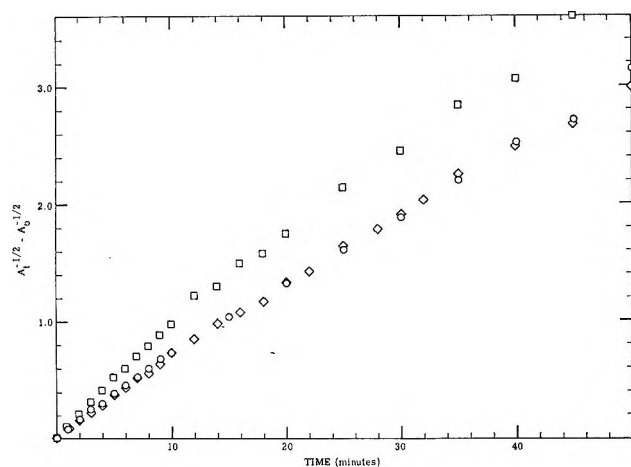


Figure 6. The effect of oxygen on the 1.5-order rate. $(F_2)^0 = (H_2)^0 = 42.5$ mm. Total pressure is kept at 645 mm. with nitrogen. \diamond , $O_2 = 425$ mm.; \circ , $O_2 = 212$ mm.; \square , $O_2 = 85$ mm.

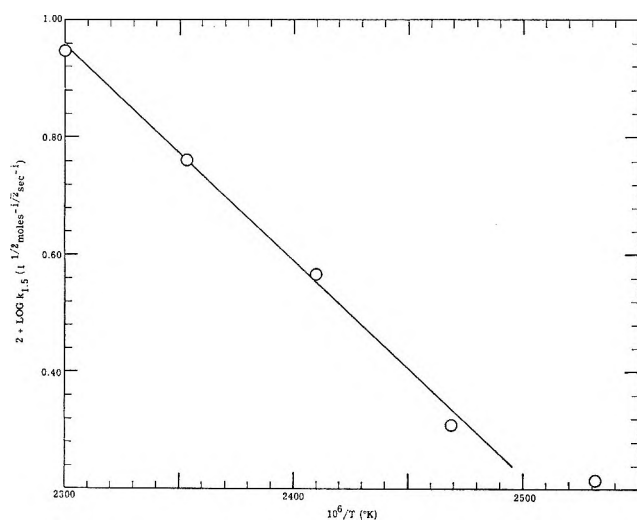


Figure 7. Temperature dependence of the 1.5-order rate.

in all the experiments the oxygen pressure was close to 425 mm. and the total pressure close to 645 mm. Rate constants were found from the initial linear portions of the $(A_t)^{-1/2} - (A_0)^{-1/2}$ vs. t curves. The results, summarized in Table IV, are plotted as the Arrhenius function in Figure 7.

The data for the higher four temperatures fall on a good straight line while the point for 122° falls well off. The line drawn through the points for 132 – 162° yields

$$k_{1.5} = 10^{7.4} \exp \frac{-16,700 \pm 1000}{RT} \text{ l.}^{1/2} \text{ mole}^{-1/2} \text{ sec.}^{-1}$$

The indicated precision in the activation energy is based on slopes of various lines drawn visually through the above points.

Table IV: Temperature Dependence of the 1.5-Order Rate Constant, $k_{1.5}$

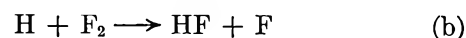
Temp., °K.	$k_{1.5}$, a.u. min.^{-1}	$k_{1.5}$, $\text{l.}^{1/2} \text{ mole}^{-1/2} \text{ sec.}^{-1}$
395	0.13	0.017
405	0.15 ± 0.01	0.020 ± 0.001
415	0.28	0.037
425	0.44	0.058
435	0.68	0.089

The Effect of Surface Area:Volume Ratio. We have performed experiments in the 0.9-cm. i.d. compartment of cell I and the 3.7-cm. i.d. compartment of cell II and compared the results with those obtained in the 1.8-cm. compartment of cell I where the bulk of our experiments have been performed. The mixture compositions were the same as those of entry 2 of Table III. The curves obtained for the $(A_t)^{-1/2} - (A_0)^{-1/2}$ vs. t function were similar in shape to those obtained in the 1.8-cm. cell; see Figure 4. The rate constants calculated from these curves were $0.13 \text{ a.u.}^{-1/2} \text{ min.}^{-1}$ for the 0.9-mm. i.d. cell and $0.16 \text{ a.u.}^{-1/2} \text{ min.}^{-1}$ for the 1.8-cm. i.d. cell. These results are barely outside the experimental scatter of our data and indicate a possible heterogeneous contribution to the rate of around 5%.

Discussion

The following results from this paper and the preceding one² must be considered: (a) at 110° , in the absence of oxygen and in a dilute stream, the rate of the hydrogen-fluorine reaction is independent of the hydrogen concentration and the surface area concentration and is first order in fluorine; (b) the reaction is inhibited by oxygen and the inhibition is such that, for given hydrogen and fluorine pressures, the rate reaches a limiting value at some oxygen pressure and does not decrease further with further oxygen addition; (c) in the region where the rate has leveled off, the kinetics are expressed by $-d(F_2)/dt = k(F_2)(H_2)^{1/2}$ for about the first 50% of reaction; (d) over the temperature range 132 – 162° , an activation energy of about 17 kcal./mole is found.

The Nature of the Inhibition by Oxygen. In our earlier paper,² we proposed that the uninhibited reaction at 110° was a chain reaction in which initiation and termination occurred at the walls, and the chain propagation steps were



We feel this is still a valid conclusion. The most reasonable explanation for the inhibiting effect of oxygen is

that it interferes in some way with the above steps and we consider the two alternatives



and



Step c is a well-known reaction. Step d is written on the basis of analogy with (c) and with the similar step which has been written for the chlorine atom³ and, like them, is assigned a zero energy of activation. We shall present evidence below that ΔH_f for FO_2 is about +3.5 kcal./mole so that step d would be exothermic by about 15 kcal./mole. It should therefore be a rapid reaction. The inhibition then consists of step c competing with step b or step d competing with step a.

If the above description for the reaction were complete, the reaction rate would drop off steadily as oxygen was added and would not level off. One possible explanation for the observed behavior is that in the region where the rate levels off, all chains have been suppressed and the residual reaction is occurring completely on the surface. The experiments in which the surface area:volume ratio was varied indicated a small heterogeneous contribution to the rate but were not consistent with the entire reaction proceeding on the walls. We therefore reject this explanation.

We feel that the most plausible explanation is that in the region where the rate is independent of oxygen, the inhibiting step is much faster than the step it competes with; *i.e.*, step d is much faster than step a or step c is much faster than step b, so that further oxygen addition does not lower the rate. The fact that the limiting value of the rate is not zero requires that the species formed in either step c or step d continue the chain.

Activation Energy Calculations for Elementary Reactions. Before discussing this point, let us consider the consequences of the proposal that the inhibiting step is much faster than its competitor in the region where the rate is independent of oxygen. If we consider steps a and d, then we may say that for $(\text{O}_2)/(\text{H}_2) = 5$, step d is roughly 100 times faster than step a, *i.e.*

$$k_d(\text{F}) \times (\text{O}_2) \times (\text{M}) = 100k_a(\text{F}) \times (\text{H}_2)$$

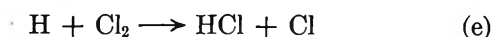
then

$$k_a = 0.05k_d \times (\text{M})$$

It seems reasonable to assign the same value to k_a as has been reported for k_c , *i.e.*, $10^{8.1} \text{ l.}^2 \text{ mole}^{-2} \text{ sec.}^{-1}$.⁴ Since (M) in these experiments was about 0.03 mole/l., $k_a \approx 10^{5.3} \text{ l. mole}^{-1}$. If we take $10^9 \text{ l. mole}^{-1} \text{ sec.}^{-1}$ as a reasonable pre-exponential factor for k_a ,⁵ we arrive at an activation energy of 7 kcal./mole for reaction a. If

the multiplying factor above is 10 rather than 100, a value of 5 kcal./mole is found. If we proceed in a similar way for the competition between steps b and c, we conclude that step b has an activation energy of 5–7 kcal./mole.

Of these two alternatives, the former is more attractive on theoretical grounds. If we consider the chlorine atom analog of step b



we find that there is good evidence for an activation energy of 2–4 kcal./mole.⁶ Although it is not possible to predict activation energies, it is generally observed that in closely related reactions, such as (b) and (e), the reaction in which the bond broken is weaker⁷ or in which the exothermicity is greater⁸ has the lower activation energy. The F–F bond dissociation energy is 37 kcal./mole,⁹ compared to 58 kcal./mole for Cl–Cl.¹⁰ Step b is exothermic by 98 kcal./mole compared to 45 for step e. On either basis, then, we would expect step b to have an activation energy of 0–3 kcal./mole rather than 5–7 kcal./mole.

On the other hand, it is of interest to compare step a to some related reactions. This is done in Table V.

Table V: Comparison of Atom Reactions with H_2

Reaction	Exothermicity, kcal./mole	Activation energy, kcal./mole
$\text{D} + \text{H}_2 \rightarrow \text{HD} + \text{H}^a$	0	5.5
$\text{Cl} + \text{H}_2 \rightarrow \text{HCl} + \text{H}^b$	-1 (endothermic)	5.0
$\text{OH} + \text{H}_2 \rightarrow \text{H}_2\text{O} + \text{H}^c$	15	5.9–10
$\text{F} + \text{H}_2 \rightarrow \text{HF} + \text{H}$	30	5–7

^a See ref. 5. ^b P. G. Ashmore and J. Chanmugam, *Trans. Faraday Soc.*, **49**, 254 (1953). ^c F. Kaufman and F. P. Del-Greco, Ninth Symposium (International) on Combustion, Academic Press, New York, N. Y., 1960, p. 659.

It is interesting that in these reactions, where the bond broken is the same in each case, the activation

(3) S. W. Benson and J. H. Buss, *J. Chem. Phys.*, **27**, 1382 (1957).

(4) S. W. Benson, "The Foundations of Chemical Kinetics," McGraw-Hill Book Co., Inc., New York, N. Y., 1960, p. 310.

(5) See ref. 4, p. 292.

(6) See ref. 4, p. 340.

(7) J. O. Hirschfelder, *J. Chem. Phys.*, **9**, 645 (1941).

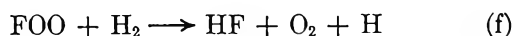
(8) N. N. Semenov, "Some Problems in Chemical Kinetics and Reactivity," Vol. I, Princeton University Press, Princeton, N. J., 1958, pp. 29–33.

(9) A. L. G. Rees, *J. Chem. Phys.*, **26**, 1567 (1957).

(10) L. Pauling, "The Nature of the Chemical Bond," 3rd Ed., Cornell University Press, Ithaca, N. Y., 1960, p. 85.

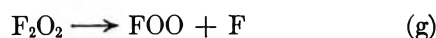
energies are similar even though the exothermicities vary rather widely. The assignment of the value of 5–7 kcal./mole to the activation energy of step a thus seems quite plausible.^{11–13}

We therefore proceed on the assumption that step d is the inhibiting step and propose that the species FOO may continue the chain *via* the reaction



The inhibition thus consists of replacing the chain carrier F by the less active chain carrier FOO.

The Heat of Formation of FOO. In order to assess the plausibility of step f, it is necessary to consider its thermochemistry, which in turn necessitates an estimate for ΔH_f of FOO. To make this estimate, we start with the molecule F_2O_2 for which, it has recently been found,¹⁴ the structure is F–O–O–F. The heat of formation for F_2O_2 has been measured as $+4.73 \pm 0.030$ kcal./mole.¹⁵ If we consider the dissociation



it is clear that we can find ΔH_f for FOO if we can estimate the enthalpy change for reaction g. For this we turn to the results of Schumacher and Frisch¹⁶ on the thermal decomposition of F_2O_2 . They reported the reaction to be first order and to yield the expression $k = 5.9 \times 10^{12} \exp -17,300/RT$ sec.⁻¹. The most reasonable rate-determining step for this reaction is the above step g; we therefore estimate the enthalpy change in step g as $\sim +17.3$ kcal./mole, and hence the heat of formation of FOO as $+3.5$ kcal./mole. As we mentioned earlier, this figure leads to a value of 15 kcal./mole for the O–F bond in FOO. These figures are much lower than would be expected by comparison with the related compound OF_2 . There the average bond strength is about 45 kcal./mole,¹⁵ while the thermal decomposition of this species has an activation energy of 40.6 ± 3 kcal./mole.¹⁷ This latter value can plausibly be assigned to the dissociation energy of the first O–F bond. However, the O–F bond distance in F_2O_2 is substantially greater than that in OF_2 , 1.58 Å. *vs.* 1.41 Å,¹⁴ indicating that the O–F bonds in the former are much weaker than those in the latter. The assignment of 17.3 kcal./mole for the enthalpy change of step

g is thus consistent with the relation of the O–F bond lengths in the two fluorine oxides.

We now return to reaction f. The above value for the heat of formation of FOO, combined with the values -64 kcal./mole for HF and $+52$ kcal./mole for H,¹⁰ allow us to calculate the enthalpy change of reaction f. It is exothermic by 15.5 kcal./mole and is therefore a reasonable chain-propagating step. If we compare it to step a we find the latter to be the more exothermic (30 kcal./mole *vs.* 15.5 kcal./mole). In addition, two bonds are broken in step f while only one is broken in step a. It is thus reasonable that replacement of step a by step f in the chain propagation sequence should lower the rate substantially.

General Comments on the Reaction Mechanism. We thus conclude that the chain-propagating steps for the oxygen-inhibited hydrogen–fluorine reaction are steps b, d, and f. We are not prepared at this time to write the initiation and termination steps and hence do not propose a complete mechanism for the reaction. The principal difficulty is that the experimental data, particularly for the region beyond 50% reaction, do not obey the rate expression written earlier, $-d(\text{F}_2)/dt = k(\text{F}_2)(\text{H}_2)^{1/2}$ as precisely as would be desired. Thus the kinetics do not offer a clear test for any proposed mechanism. It is quite possible that a more complex expression would represent the data better. In the absence of a mechanism, also, we do not feel that a detailed interpretation of the observed activation energy is possible. The observed value is certainly consistent with a chain reaction. We hope that further study of this reaction will allow us to establish conditions where the kinetics can be determined unequivocally.

(11) Schumacher¹² derived an energy of activation of 7.5 kcal./mole for reaction a by deductions from data reported by Bodenstein and Jokusch¹³ for the photochemical reaction. In this derivation it was assumed that H reacted with F_2 at every collision.

(12) H. J. Schumacher, "Chemische Gasreaktionen," Theodor Steinkopff, Leipzig, 1938, p. 443.

(13) M. Bodenstein and H. Jokusch, *Z. anorg. allgem. Chem.*, **231**, 24 (1937).

(14) R. H. Jackson, *J. Chem. Soc.*, 4585 (1962).

(15) A. D. Kirshenbaum, A. V. Grosse, and J. G. Aston, *J. Am. Chem. Soc.*, **81**, 6398 (1959).

(16) H. J. Schumacher and P. Frisch, *Z. physik. Chem.*, **B24**, 332 (1934).

(17) W. Koblitz and H. J. Schumacher, *ibid.*, **B25**, 283 (1934).

The Effect of Molecular Weight on the Melting Temperature and Fusion of Polyethylene¹

by J. G. Fatou and L. Mandelkern

Department of Chemistry and Institute of Molecular Biophysics, Florida State University, Tallahassee, Florida
(Received June 22, 1964)

The fusion process, melting temperature, density, and wide-angle X-ray diffraction of carefully crystallized molecular weight fractions of linear polyethylene encompassing a molecular weight range from 3×10^3 to 1.5×10^6 have been investigated. For molecular weights less than 50,000 the densities at room temperature are very close to the value of the unit cell, and the wide-angle X-ray diffraction patterns are typified by very sharp reflections and the absence of the usual halo. Above this molecular weight a monotonic decrease of the density with molecular weight is observed. The reflections in the X-ray pattern broaden and the halo appears. These results can be given a consistent explanation in terms of the relation of the crystallite size to the extended chain length and the coexistence of amorphous regions in the higher molecular weight range. The melting temperatures also depend on molecular weight and reach an asymptotic value of 138.5° . The difference between the observed melting temperature and that calculated for equilibrium also depends on molecular weight and can be explained, over the complete range, by assuming crystallite sizes in the chain direction comparable to those of the nuclei from which they are formed. To obtain quantitative agreement, however, nucleation theory pertinent to chains of finite length must be employed. Independent confirmation of the crystallite sizes that are calculated is obtained from other reports dealing with low-angle X-ray diffraction and electron microscopic examination of fracture surfaces. For the lowest molecular weights the fusion curves are broad as expected, become extremely sharp in the range 12,500 to 50,000, and then significantly broaden as the molecular weight is increased. The question as to whether the breadth of melting, characteristic of the higher molecular weight species, is attributable to the coexisting amorphous regions or the nature of the crystallites remains at present unresolved.

Introduction

The crystallization of long-chain molecules from the melt results in a polycrystalline substance of rather complex morphology. Despite these complexities, the kinetics of the crystallization process has been shown to adhere remarkably well to the general mathematical formulation for the kinetics of phase changes, and the fusion process has been successfully treated as a first-order phase transition.^{2a,b} With rare exception, most of these studies have been accomplished with unfractionated polymers possessing a very broad molecular weight distribution. In the few exceptions where molecular weight fractions have been utilized, the

range of molecular weights studied has been limited. The recent investigation by Chiang and Flory³ has emphasized the importance of molecular weight fractions on the sharpness of the fusion process and on the observed melting temperature. In order to further explore the role played by molecular weight homogeneity in the fusion process and in the morphological nature

(1) This work was supported by a grant from U. S. Army Research Office (Durham) and a contract with the Division of Biology and Medicine, Atomic Energy Commission.

(2) (a) P. J. Flory, *Science*, **124**, 53 (1956); (b) L. Mandelkern, "Crystallization of Polymers," McGraw-Hill Book Co., New York, N. Y., 1964.

(3) R. Chiang and P. J. Flory, *J. Am. Chem. Soc.*, **83**, 2857 (1961).

of the crystalline state of long-chain molecules, we have investigated these properties over a molecular weight range of 3×10^3 to 1.5×10^6 . In addition, following the theoretical discussion of Flory and Vrij,⁴ a connection can be made between the melting of the molecular crystals formed by the *n*-paraffins and the crystals formed by polymers. Although our major concern in the present report is the fusion process, cognizance must be taken of the crystallization kinetics and mechanisms from the melt, to avoid the complication of comparing indiscriminate and poorly crystallized specimens. To this end, all our samples were isothermally crystallized from the melt at comparable high temperatures under prescribed and reproducible conditions. All subsequent cooling and heating processes are carefully detailed since they influence the results significantly.

Experimental

Materials. Molecular weight fractions of the linear polyethylene were obtained from either unfractionated Marlex-50 or a polymer obtained from the Union Carbide Co. or from a polymer prepared by the decomposition of diazomethane using boron ester catalysts.⁵ The fractionation of the commercial whole polymers was accomplished by utilizing conventional elution column techniques.⁶⁻⁸ *p*-Xylene and hydroxyethyl butyl ether were used as solvent and nonsolvent, respectively, and the fractionation was carried out at 127°. In decalin at 135°, the intrinsic viscosity of the whole polymer was 1.95 g.⁻¹ 100 ml. This corresponds to a molecular weight of 180,000 according to the relation, $[\eta] = 2.55 \times 10^{-4} M_w^{0.74}$, given by Billmeyer and De la Cuesta⁹ for unfractionated linear polyethylene. Twenty-four fractions were obtained from each of these fractionations. The viscosity average molecular weights of the fractions were obtained from intrinsic viscosity measurements in decalin at 135° using a Ubbelohde type viscometer as modified by Flory, Ciferri, and Chiang.¹⁰ The relation $[\eta] = 6.2 \times 10^{-4} M_w^{0.70}$ as established by Chiang¹¹ was used, and it was not necessary to apply any kinetic energy corrections. Because of the theoretical uncertainty in accurately determining molecular weights in the low molecular weight range, from relations of the type cited above, number-average molecular weights were also determined for fractions having a molecular weight less than 10,000. A Mechrolab Model 302 vapor pressure osmometer, utilizing decalin as a solvent at 130°, was utilized for this purpose.¹² The number-average molecular weights in this molecular weight range agreed, within 10%, with those calculated from intrinsic viscosity measurements. The molecular weights of the fractions obtained from

the above sources ranged from 1×10^3 to 4×10^6 . The typical very broad molecular weight distribution for Marlex-50 with its high proportion of low molecular weight components was observed.

In decalin at 135°, the intrinsic viscosity of the polymer prepared from diazomethane was 11.65 g.⁻¹ 100 ml., which corresponds to a molecular weight of approximately 2×10^6 . After extracting the lowest molecular weight fractions with a mixture of *p*-xylene-hydroxyethyl butyl ether at 127°, the column fractionation was carried out at 140° using tetralin and hydroxyethyl butyl ether as the solvent-nonsolvent mixture. Twelve fractions were obtained with molecular weights (determined by intrinsic viscosity) ranging from 5×10^5 to 1.5×10^6 . In the fractionation of this polymer there appears to be some overlapping of the fractions, and, hence, the efficiency of the fractionation is not deemed so good as that for the lower molecular weight samples.

A summary of the samples used in this work and their molecular weights is given in Table I. The designations R-2 and R-3 correspond to the two different fractionations of Marlex-50 while PM refers to the fractionation of the polymer prepared by the decomposition of diazomethane.

Procedures. The dilatometric techniques utilized in studying the fusion process, by means of observing the changes in the density of the specimens, have been previously described in detail.^{13,14} After being dried *in vacuo* for 48 hr. at 50°, the samples were pressed into the form of thin sheets by compression molding and then cut into thin strips. A sample weighing from 0.2 to 0.5 g. was inserted into the dilatometer which used mercury as a confining fluid. To convert the dilatometer capillary readings into specific volumes, the volumes of the mercury and polymer samples were computed from their weights. The specific volume of the liquid polymer, which served as a convenient refer-

- (4) P. J. Flory and A. Vrij, *J. Am. Chem. Soc.*, **85**, 3548 (1963).
- (5) L. Mandelkern, M. Hellman, D. W. Brown, D. E. Roberts, and F. A. Quinn, Jr., *ibid.*, **75**, 4093 (1953).
- (6) P. S. Francis, R. G. Cook, and J. H. Elliot, *J. Polymer Sci.*, **31**, 453 (1958).
- (7) P. M. Henry, *ibid.*, **36**, 3 (1959).
- (8) R. Chiang, private communication.
- (9) M. O. De la Cuesta and F. W. Billmeyer, *J. Polymer Sci.*, **A1**, 1712 (1963).
- (10) P. J. Flory, A. Ciferri, and R. Chiang, *J. Am. Chem. Soc.*, **83**, 1023 (1961).
- (11) R. Chiang, *J. Polymer Sci.*, **36**, 91 (1959).
- (12) L. Westermann, private communication; we wish to thank Dr. Westermann for so kindly performing these measurements for us.
- (13) P. J. Flory, L. Mandelkern, and H. K. Hall, *J. Am. Chem. Soc.*, **73**, 2532 (1951).
- (14) L. Mandelkern and P. J. Flory, *ibid.*, **73**, 3206 (1951).

Table I: Molecular Weights and Crystallization Times for Samples Studied

Sample	M_n	Crystallization time at 130°, days	Crystallization half-time, min.
R-2-6	3,300	10 ^a	2650
R-2-8	5,300	4 ^b	1250
R-2-9	12,500	28	5000
R-2-10	20,000	5	470
R-2-11	47,000	13	350
R-3-8	200,000	3	200
R-3-9	425,000	4	1000
PM-3	1,000,000	22	
PM-9	1,300,000	22	7000
PM-11	1,470,000	22	7300
PM-12	1,550,000	22	6400

^a Crystallized at 126°. ^b Crystallized at 127°.

ence point, was provided by the relationship given by Chiang and Flory.³ In certain specific experiments the specimens were isothermally crystallized from the melt in vacuum-sealed tubes for 40 days at 130° and then cooled to room temperature over a 24-hr. period. The densities of the specimens were measured at 25° in a toluene-dioxane solvent gradient column which had been previously calibrated with glass floats to give a density range of 1.002 to 0.9398 (± 0.0001) g./cm.³. The agreement between the densities thus observed, with corresponding samples in the dilatometer which underwent an identical crystallization and thermal cycle was better than 3 parts per 1000 in every case.

The degrees of crystallinity of the samples, $1 - \lambda$, were calculated from the observed specific volumes assuming the additive contribution of the specific volume of the crystalline and amorphous portions. The appropriate specific volume-temperature relations for the completely crystalline and completely amorphous polymers are available from the previously cited data of Chiang and Flory.³

With the exception of R-2-6 and R-2-8, all of the fractions were crystallized from the melt, in a dilatometer at 130° for a sufficient length of time so that essentially no further crystallization would occur at this temperature. The time required to accomplish this was predetermined through studies of the isothermal crystallization kinetics of the various molecular weight fractions.¹⁵ For this set of experiments, studies of the fusion process were then initiated without any further lowering of the temperature. Fraction R-2-6 was crystallized at 126° (crystallization at an elevated temperature being impracticable, despite the large amount of time invested), and fraction R-2-8 was crystallized at 127° for the same reason. A summary

of the time required for the crystallization at 130° is also given in Table I, as are the half-times for crystallization at this temperature.

In another set of experiments, after completion of the crystallization process at 130°, the dilatometers were cooled to room temperature over a period of 24 hr. As has been indicated previously, the densities calculated dilatometrically agreed quite well with those directly measured. In these experiments the fusion studies were initiated at room temperature.

For certain specific cases, after the cessation of crystallization at 130° the dilatometers were quickly transferred to a thermostat at 125°, and the decrease in specific volume was studied as a function of time. A stationary value in the specific volume was attained in approximately 24 hr. This process was repeated by lowering the temperature in 5° intervals to 25°.

The fusion process of the samples crystallized in the manner described above was studied by investigating the specific volume-temperature relation upon heating. Starting at either 25 or 130°, depending on the previous crystallization history, the temperature was raised according to a fixed schedule. For experiments where the temperature was initially 130°, the temperature was raised from 130 to 135° at the rate of 1° per day and from 135° to the melting temperature at 0.5° per day. The samples were held at the melting temperature for 24 hr., and the liquidus was established by heating a few degrees above it. For the dilatometers which had been lowered to room temperature, the heating process followed the schedule previously reported,^{16a} 15° per day from 25 to 100°, 5° per day from 100 to 125°, 1° per day from 125 to 137°, and 0.5° per day above 137° until completion of melting. In certain specific experiments the temperature interval from 70 to 100° was traversed at the slower rate of 5° per day. As has been previously indicated,^{3,4,16b} for samples crystallized in the manner indicated above recrystallization processes were not observed during the heating cycle. The specific volume of the sample increased rapidly to a constant value after each successive elevation of the temperature. However, for temperatures within 3° of the melting point, the time required was more prolonged, and at least 24 hr. was required for a constant specific volume to be reached.

Results

Density and Degree of Crystallinity. The densities of the various molecular weight fractions after crystal-

(15) J. G. Fatou and L. Mandelkern, to be published.

(16) (a) F. A. Quinn, Jr., and L. Mandelkern, *J. Am. Chem. Soc.*, **80**, 3178 (1958); (b) L. Mandelkern, *Rubber Chem. Technol.*, **32**, 1392 (1959).

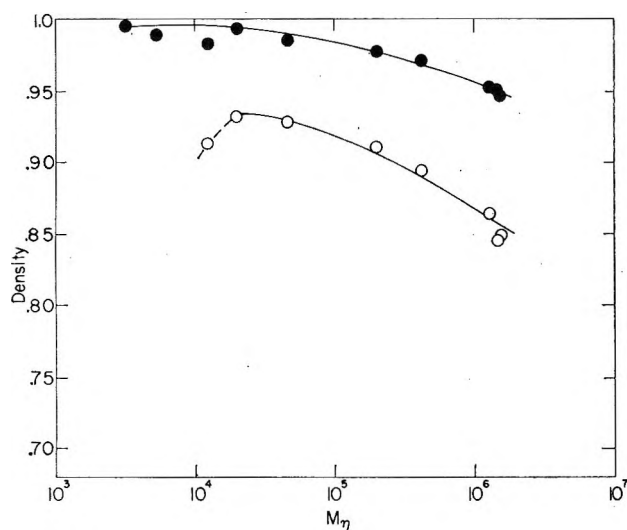


Figure 1. Plot of density as a function of molecular weight for linear polyethylene fractions: O, after crystallization at 130°; ●, after subsequent cooling to room temperature.

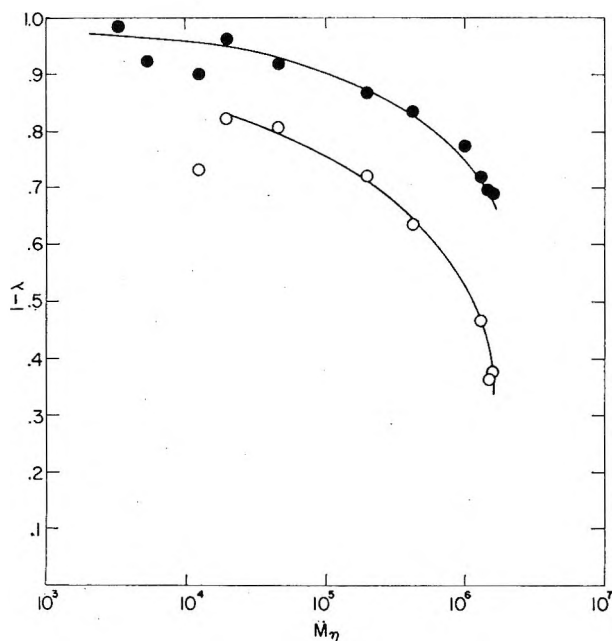


Figure 2. Plot of degree of crystallinity, $1 - \lambda$, as a function of molecular weight for linear polyethylene fractions: O, after crystallization at 130°; ●, after subsequent cooling to room temperature.

lization from the melt at 130°¹⁷ for a requisite length of time, to ensure no further crystallization at this temperature, are plotted in Figure 1, as are the densities observed after subsequently cooling the samples to room temperature. After crystallization at 130°, a maximum density of 0.9313 is reached for $M_n = 2 \times$

10⁴; the density then decreases monotonically with increasing molecular weight to a value of 0.8477 for $M_n = 1.55 \times 10^6$. As is indicated in Figure 2, this corresponds to a variation in the degree of crystallinity from 82 to 37%, the latter being a significantly low value for polyethylene resulting from the extremely high molecular weights employed.

The densities of the samples, after cooling to room temperature over a 24-hr. period, follow a similar pattern, as far as their dependence on molecular weight is concerned. We note that, for $M \leq 20,000$, densities very close to unity are observed, unity being the density of the unit cell. In particular, for $M = 20,000$, a density of 0.9935 is achieved which corresponds to a degree of crystallinity of 96.5%. This appears to be among the highest values reported for polyethylene crystallized in the bulk. The degree of crystallinity, at room temperature, for the lower molecular weight samples also lies in this range. The intensity and degree of crystallinity upon cooling increase progressively with an increase in molecular weight. For a molecular weight of 1.5×10^6 , the degree of crystallinity increases from 37 to 70% while, for $M = 20,000$, the increase is proportionately less. The general trend of the decreasing density with molecular weight is similar to that reported by others,^{3,18,19} but is now seen to encompass a very much larger molecular weight range.

In another set of experiments, the density increase upon cooling was investigated in more detail. For several fractions the temperature was lowered in 5° intervals, from 130° to room temperature, and the change in the density with time was observed at each temperature. After thermal equilibrium was reached at a given temperature, the isothermal density increase had a sigmoidal shape characteristic of the kinetics of a phase transition. This phenomenon is illustrated in Figure 3 for a fraction $M = 1.47 \times 10^6$. At temperatures below 100°, the density decreases so rapidly with time that it is not possible to observe experimentally the kinetics of the process. However, even at these temperatures, a definite increase in the density and in the level of crystallinity is observed.

X-Ray Diffraction. Wide-angle X-ray diffraction patterns of three representative samples ($M_n = 12,500$, 425,000, and 1,000,000) which were crystallized at 130°

(17) As has been previously noted, owing to unfavorable crystallization rates, molecular weight fractions (M_n) of 3300 and 5300 were initially crystallized at 126 and 127°, respectively, and then cooled to room temperature.

(18) (a) W. Banks, M. Gordon, R. J. Roe, and A. Sharples, *Polymer*, **4**, 61 (1963); (b) L. H. Tung and S. Bukser, *J. Phys. Chem.*, **62**, 1530 (1958).

(19) H. Kojima and K. Yamaguchi, *Kobunshi Kagaku*, **19**, 715 (1962).

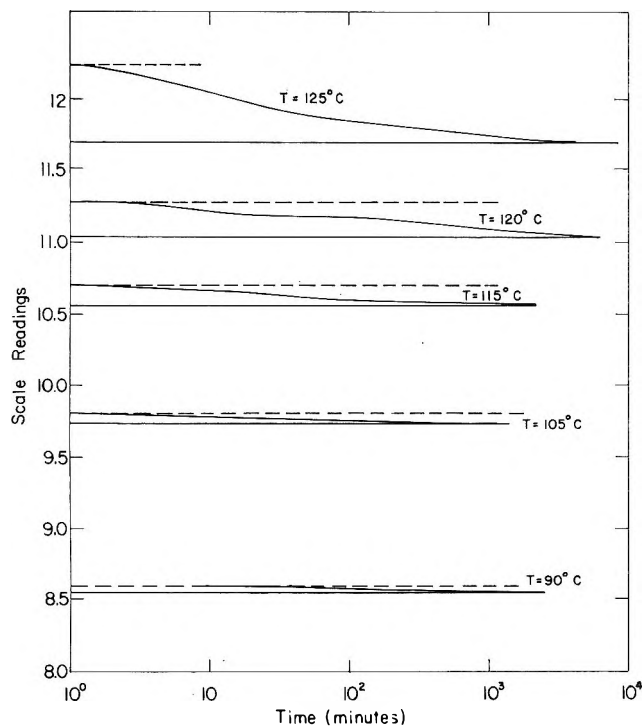


Figure 3. Dilatometer scale readings in cm. as a function of log time for successively lower cooling temperatures. Molecular weight is 1.47×10^6 , initially crystallized at 130° .

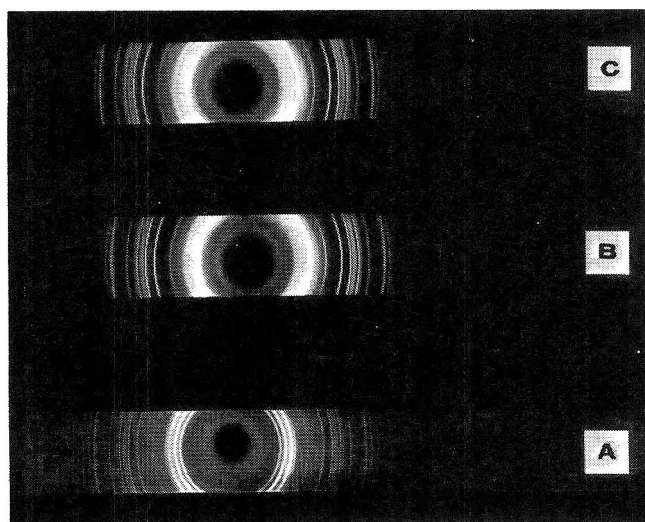


Figure 4. Wide-angle X-ray diffraction patterns, at room temperature, for polyethylene fractions crystallized from melt at 130° for 40 days: A, $M = 12,500$; B, $M = 425,000$; C, $M = 10^6$.

for 40 days and cooled to room temperature in 24 hr. are shown in Figure 4. All the Bragg spacings utilized by Bunn²⁰ in the determination of the orthorhombic structure are observed, as are six additional reflections

previously reported by others²¹⁻²³ and attributed by Teare and Holmes²¹ to a triclinic structure. Of particular interest in this set of patterns are the very sharp reflections in the lowest molecular weight sample and the complete absence of the broad halo usually observed in crystalline polymers. Similar patterns to the one for $M = 12,500$ are also observed for the lower molecular weight samples. However, as the molecular weight increases, the reflections progressively broaden, and the usual well-developed halo appears.

The Fusion Process and Melting Temperature. Subsequent to the development of all the crystallinity that will form at 130° , the various molecular weight fractions were heated according to the schedule previously described. The results are given in Figure 5 as a plot of the degree of crystallinity as a function of tempera-

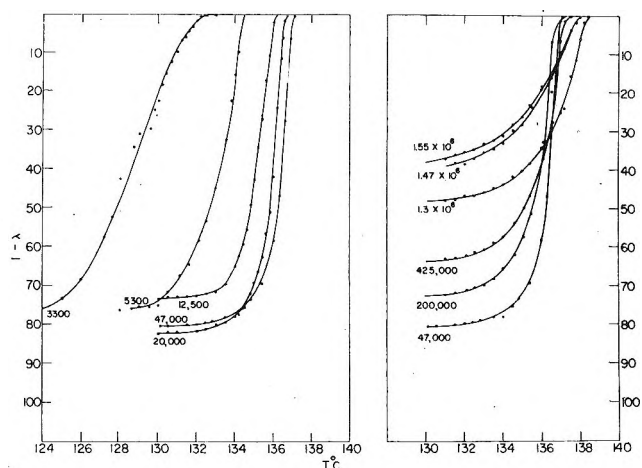


Figure 5. Plot of degree of crystallinity, $1 - \lambda$ (after crystallization at a high temperature), as a function of temperature for molecular weights indicated.

ture. For the two lowest molecular weight samples, the fusion process is relatively broad, the curve is sigmoidal in character, and changes in the amount of crystallinity are observed over the whole temperature range. On the other hand, in the molecular weight range 12,500–47,000 the melting curves become much sharper. For example, for $M = 20,000$ the degree of crystallinity decreases from 72 to 0% in a 2° interval in which 88% of the total transformation is observed. Molecular weight fractions 12,500 and 47,000 behave similarly, and the very sharp fusion process in this

(20) C. W. Bunn, *Trans. Faraday Soc.*, **35**, 482 (1939).

(21) P. W. Teare and D. R. Holmes, *J. Polymer Sci.*, **24**, 496 (1957).

(22) S. S. Pollack, W. H. Robinson, R. Chiang, and P. J. Flory, *J. Appl. Phys.*, **33**, 237 (1962).

(23) A. T. Jones, *J. Polymer Sci.*, **62**, S-53 (1962).

molecular weight range is in accord with the results previously reported by Chiang and Flory.³ However, as the molecular weight is further increased, the fusion curves begin to broaden once again. For example, for $M = 425,000$ only 40% of the crystallinity disappears in the last 2° below the melting temperature. The situation becomes much more accentuated for the highest molecular weight analyzed. Here, the fusion process resembles that of a copolymer or a homopolymer fraction of low molecular weight since less than half of the total transformation occurs over the final 2°. In the molecular weight range greater than 12,500, there appears to be, at least superficially, a general correlation between the level of crystallinity and the breadth of the fusion process.

Although the fusion process is diffuse for the extremes in molecular weight, well-defined melting temperatures can be delineated and are summarized in Tables II and III. The melting temperatures are ob-

Table II: Calculated Values of Crystallite and Nuclei Sizes

M_n	$T_{m,e}^a$	T_m^b	ζ_{total}	ζ_{eq}	ζ	ζ^{*c}
12,500	138.8	136.2	893	835	512	537
20,000	141.0	136.7	1,429	1,350	523	538
47,000	143.7	137.2	3,357	3,000	528	533
200,000	145.0	137.5	14,286	13,000	535	531
425,000	145.4	138.0	30,357	28,000	572	530
1,300,000	145.5	138.5	92,857	87,000	614	530

^a Calculated equilibrium melting temperature for $\sigma_e = 4600$ cal./mole. ^b Melting temperature subsequent to crystallization at 130°. ^c For crystallization at 130°.

Table III: Calculated Crystallite and Nuclei Sizes and Melting Temperatures for Low Molecular Weight Fractions

M_n	T_c^a	T_m	ζ_{total}	ζ^{*b}	σ_{ec}^c	$T_{m,e}^d$
3300	123	132.5	256	222	1556	133.8
	126	133		223	1704	134.1
5300	127	134.5	379	345	2831	134.8
	130	135.0		353	2386	135.8

^a Crystallization temperature. ^b Calculated at crystallization temperature with $\sigma_e = 4600$ cal./mole. ^c Calculated from eq. 3 under assumption that $\zeta = \zeta^*$. ^d Calculated from eq. 1 with interfacial energies of preceding columns.

served to increase progressively with molecular weight. Between $M_n = 12,500$ and 1.5×10^6 a 2° difference in melting temperature is noted, with an asymptotic value of 138.5° being achieved in accord with previous

reports.³ For molecular weight $M_n = 5600$, a melting temperature of 135.0° is observed after crystallization at 130° for 70,000 min. (resulting in 26% crystallization). After crystallization at 127°, the melting temperature is 134.5°. For the lowest molecular weight sample studied ($M = 3300$), the melting temperature was 132.5° after crystallization at 123 and 133° subsequent to crystallization at 126°. For these low molecular weight fractions, the crystallization times and undercoolings at which the crystallizations were conducted were comparable to those for the high molecular weight fraction.

The fusion curves for three representative molecular weights, after cooling to room temperature, are given in Figure 6. For comparative purposes, the fusion curves for the same specimens from Figure 5 are also given and are represented by the dashed lines. For the two lowest molecular weight samples the degree of crystallinity at 130° is now slightly greater than that obtained upon isothermal crystallization at this tem-

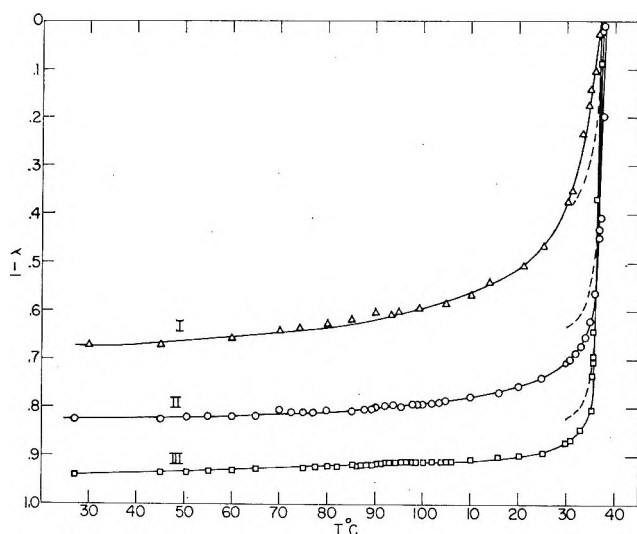


Figure 6. Plot of degree of crystallinity $1 - \lambda$ (after cooling to room temperature), as a function of temperature: curve I, $M = 1.47 \times 10^6$; curve II, $M = 425,000$; curve III, $M = 20,000$.

perature. The fusion curves are still relatively sharp and virtually identical in shape above 130°. The level of crystallinity at 130° is slightly less for the highest molecular weight sample, and the increased level of crystallinity has brought about a very marked broadening of the fusion curve above 90°.

Discussion

Melting Temperature. In order to discuss the dependence of the observed melting temperatures on

molecular weight, we first establish equilibrium models from which the theoretically expected melting temperatures can be calculated. The experimental results can then be discussed in terms of these results by taking into account additional nonequilibrium effects that might be pertinent. As a first consideration, we examine the model recently treated by Flory and Vrij.⁴ The system of long-chain molecules is taken to consist of molecules of precisely uniform chain length, there being x carbon atoms per chain. Molecular crystals are formed, in that complete molecules participate in the crystallization. The chains are arranged end to end with the terminal group juxtaposed in successive layers of the crystal lattice. Thus, the end groups are paired from one molecule to its colinear neighbor, and the sequence of ordered chain units is perpetuated from one molecule to the next. We shall refer to this model as one of "end-pairing." Based on the thermodynamic data for the fusion of the low molecular weight n -paraffins, the melting temperature-molecular weight relation for long-chain polyethylene molecules was calculated.⁴ The results of this calculation are plotted in Figure 7. The melting temperature T_m° for the infinite molecular weight chain is found theoretically to be $145 \pm 0.5^\circ$. Melting point data for low molecular weight n -paraffins, as tabulated by Broadhurst,²⁴ are plotted coincident with this curve. Here structural analysis indicates that the end-paired molecular type crystals are indeed formed. It has also been shown that it is possible, even for a collection of chains absolutely uniform in length, for an intermediate state of order to be more favored thermodynamically. In particular, the case has been considered⁴ where the end-pairing is disrupted, and a partial unpeeling or disordering occurs from the ends of the molecules. In this instance the number of ordered chain units in a crystalline sequence, ζ , is less than x . Theoretical analysis indicates⁴ that the choice of the more stable of the two models is dependent on the chain length and the magnitudes of the quantity $(2\sigma_e + \Delta G_e)$. The interfacial free energy per mole of units emerging from the 001 crystal face (*i.e.*, normal to the c -axis) is σ_e , while ΔG_e is the free energy change for the destruction of the end-group layers. The quantity ΔG_e has been determined from the analysis of the n -paraffins and is found to be a negative quantity.⁴ ($\Delta H_e = -2100$ cal. mole⁻¹, and $\Delta S_e = 2.7$ e.u./mole.) According to three independent experiments, the relatively large value of 4600 cal./mole can be associated with σ_e . This assignment is based on studies of the nucleation rate of small polyethylene droplets,²⁵ the analysis of the melting behavior of random polyethylene copolymers,²⁶ and an interpretation of the dependence of the low-angle X-ray spacings on

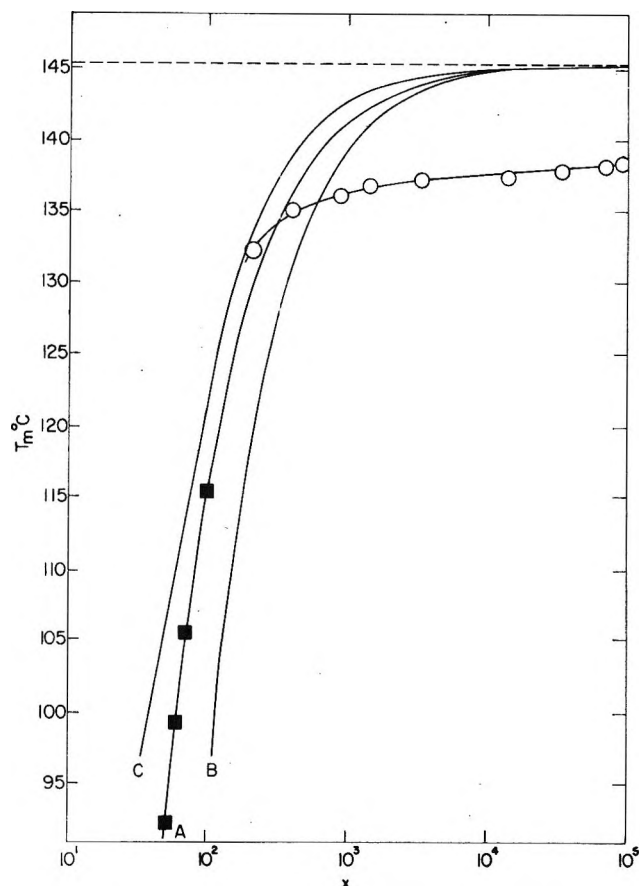


Figure 7. Plot of melting temperatures as a function of the number of carbon atoms in a chain: curve A, theoretical curve for end-pairing model; curves B and C, theoretical curves for unpeeled model with $\sigma_e = 1200$ and 4600, respectively; ■, values for n -paraffins; ○, experimental values of polyethylene fractions.

the crystallization temperature of polyethylene.²⁷ Based on the above values for the parameters involved, the conclusion is reached that, for polyethylene chains have x approximately equal to or less than 10^4 , molecular crystals with the end pairing would be most stable thermodynamically. For greater chain length the "unpeeled" model, with crystallites having dimension $\zeta < x$, would be favored.²⁸ Theoretical equilibrium melting temperature-molecular weight relations for the "unpeeled" model can be calculated according to^{4,29}

(24) M. G. Broadhurst, *J. Chem. Phys.*, **36**, 2578 (1962).

(25) R. L. Cormia, F. P. Price, and D. Turnbull, *ibid.*, **37**, 1333 (1962).

(26) M. J. Richardson, P. J. Flory, and J. B. Jackson, *Polymer*, **4**, 221 (1963).

(27) L. Mandelkern, A. S. Posner, A. F. Diorio, and D. E. Roberts, *J. Appl. Phys.*, **33**, 237 (1962).

(28) It was also pointed out⁴ that under equilibrium conditions, if ζ approached x for chains of finite length, a smaller value of σ_e could be anticipated.

$$\frac{1}{T_{m,e}} - \frac{1}{T_m^\circ} = \frac{R}{\Delta H_u} \left(\frac{1}{x} - \frac{1}{x - \zeta_e + 1} \right) \quad (1)$$

and

$$2\sigma_e = RT_m \left\{ \frac{\zeta_e}{x - \zeta_e + 1} + \ln \left(\frac{x - \zeta_e + 1}{x} \right) \right\} \quad (2)$$

where $T_{m,e}$ is the equilibrium melting temperature of the finite chain, characterized by the equilibrium crystallite length, ζ_e , and ΔH_u is the heat of fusion per CH_2 unit. Plots of this calculation are also given in Figure 7 for values of σ_e of 4600 and 1200 cal./mole, respectively. The stable form (highest T_m) must clearly depend on the value assigned to σ_e . For $\sigma_e = 4600$ the end-paired model is more stable up to $x = 10^4$; for higher molecular weights the unpeeled model becomes stable since it possesses slightly higher melting temperatures. However, if σ_e is assigned the value 1200, then the unpeeled model will be stable for all molecular weights.

The above analysis has been predicated on the assumption that a perfect system of uniform chain length exists. If this condition is not met, then the end-paired molecular crystal cannot be considered to be a legitimate model. Complete uniformity of chain length has been achieved up to $x = 100$. However, a collection of real polymer chains, no matter how well fractionated, cannot be represented as a system of absolutely uniform chain length. Hence, the end-paired model cannot be taken to depict a real system. We, therefore, assume that the unpeeled model represents a fractionated polymer system at equilibrium. Small deviations from monodispersity can be tolerated by this model. Numerical calculations, utilizing eq. 1 and 2 and $\sigma_e = 4600$, show that ζ_e represents about 93% of the complete molecule. Therefore, the configurational properties of the chain units in the intercrystalline regions³⁰ which would restrict the consideration of this crystallite model are, in the main, alleviated. The experimentally observed melting temperatures for the polyethylene fractions are also plotted in Figure 7.

In discussing the experimental results in terms of equilibrium theory, it is convenient to consider first the molecular weight range equal to or greater than 12,500. In this range the observed melting temperatures are significantly less than the equilibrium requirements. In particular, for $\sigma_e = 4600$ the difference between observed and calculated melting temperatures increases with increasing molecular weight. These deviations range from 2.6° for $M = 12,500$ to 7° for $M = 1.3 \times 10^6$. Low-angle X-ray diffraction^{22,27} and the examination of replicas of fracture surfaces by electron microscopy³¹ indicate that the crystalline regions in poly-

ethylene occur characteristically as thin lamellae with the chain axes being directed normal to their wide faces. On the basis of these morphological observations, we examine the possibility that the depression of the melting temperature results from a restricted crystal growth in the chain directions. Thus, in the crystallite that forms, ζ will be less than the required ζ_e . It is easily shown^{4,29} that the melting temperature for a system, where ζ does not attain its equilibrium value, is given by the relation

$$\frac{1}{T_m} - \frac{1}{T_m^\circ} = \frac{-R}{\Delta H_u} \left\{ \frac{\ln D}{\zeta} + \frac{1}{\zeta} \ln \left[\frac{x - \zeta + 1}{x} \right] \right\} \quad (3)$$

where $D = \exp(-2\sigma_e/RT)$. The values of ζ consistent with the observed melting temperatures calculated according to eq. 3 are listed in Table II. Also given are the total number of units per molecule and the value required for ζ_e if total equilibrium were to prevail. These calculated values of ζ increase slightly with increasing molecular weight. For molecular weights of 12,500 and 20,000 the values of ζ are comparable to the total number of units per molecule and the number required for equilibrium. As the molecular weight is increased, however, ζ becomes extremely small when compared to the extended length of the molecule. A premise of the calculation is that only the finite size of the crystallites contribute to the depression of the melting temperature.

A direct estimate of the crystallites sizes involved can also be made from several independent lines of investigation. From the examination, at room temperatures of replicas of the fracture surfaces of a polyethylene fraction, $M = 11,900$, which was crystallized at 128° for 10 days, Anderson³² observed that the thickness of the lamellae ranged from 500 to 1050 Å. with an average size of 700 Å. This average size corresponds to a crystallite which is 560 units long. Comparison with Table II shows that this average dimension agrees very well with the values calculated for ζ . (Part of the breadth of the crystallite sizes that are observed at room temperature can be attributed to the increased crystallization that occurs on cooling to room temperature from the crystallization temperature. Slightly greater values for the calculated ζ can be obtained by utilizing slightly higher values σ_e .)

Flory and Vrij⁴ have estimated, from the low-angle X-ray diffraction spacings for specimens of molecular

(29) P. J. Flory, *J. Chem. Phys.*, **17**, 223 (1949).

(30) P. J. Flory, *J. Am. Chem. Soc.*, **84**, 2857 (1962).

(31) (a) R. Eppe, E. W. Fischer, and H. A. Stuart, *J. Polymer Sci.*, **34**, 721 (1959); (b) P. H. Geil, *ibid.*, **44**, 449 (1960); **47**, 65 (1960).

(32) F. R. Anderson, *ibid.*, **3C**, 123 (1963); *J. Appl. Phys.*, **35**, 64 (1964).

weights 126,000 and 360,000²² crystallized at 131.3°, that the crystallites are approximately 720 units long. After crystallization at 130°, for comparison with the present data, a 10 to 15% reduction in the crystallite size would be expected. (See below.) This estimated length is still somewhat greater than the values calculated from the melting point depression in this molecular weight range. Other nonequilibrium defects, besides restricted size, could, of course, be contributing to the melting point depression. On the other hand, complete quantitative agreement could be obtained, over the molecular weight range where crystallite size data are available, by assuming that σ_e increases slightly with molecular weight. To a first approximation, however, satisfactory agreement is obtained between the directly observed sizes and those calculated from eq. 3 utilizing $\sigma_e = 4600$ cal./mole independent of molecular weight.

It is also of interest to calculate the number of chain units, ζ^* , that are required to form a nucleus of critical size. By utilizing homogeneous nucleation theory appropriate to chains of finite length, it is found that ζ^* must satisfy the relation³³

$$\frac{\zeta^*}{2} \left[\Delta f_u - \frac{RT}{x} + \frac{RT}{x - \zeta^* + 1} \right] = 2\sigma_e - RT \ln \left(\frac{x - \zeta^* + 1}{x} \right) \quad (4)$$

Here Δf_u is the free energy of fusion per repeating unit of an infinite molecular weight chain. The values of ζ^* , that are calculated according to eq. 4, by utilizing $\sigma_e = 4600$ cal./mole for isothermal crystallization at 130° are listed in the last column of Table II. It is of significance to note that the calculated values for ζ and ζ^* are comparable to one another. Moreover, for the lower molecular weights in this table, these two quantities are virtually identical within the experimental uncertainty. If a slightly higher melting temperature were taken or a slightly higher value of σ_e assigned, ζ and ζ^* would agree exactly and, as has been noted above, would correspond with the directly observed crystallite sizes.³⁴ For the higher molecular weights, the required value of ζ to satisfy eq. 3 is about 20% greater than that calculated for ζ^* . A consistent interpretation of the observed melting temperatures for molecular weights greater than 12,500 can, thus, be obtained if it is postulated that the depression from the equilibrium values is due to the reduced crystallite size in the chain direction. Moreover, the size that is required is comparable to or slightly larger than that which is calculated for the formation of a stable nucleus.

This latter postulate has previously been invoked³⁵

to explain the dependence of the melting temperature (subsequent to fast heating) on the isothermal crystallization temperature for natural rubber and polychlorotrifluoroethylene. However, the theories of melting and nucleation that were used in these instances were in the approximation of infinite molecular weight chains. When the interfacial energies for the nucleus and the mature crystallite are equated in this approximation, the depression of the equilibrium melting temperature equals one-half the value of the undercooling at which the crystallization is conducted. This approximation is seen to be adequate for the very high molecular weight sample, $M = 1.3 \times 10^6$, where a melting point depression of 7° is observed, and the simple calculation predicts a depression of 7.8°.³⁶ However, for the lower molecular weights the infinite molecular weight approximation becomes obviously inadequate. If the calculated undercooling is based on the equilibrium melting temperature of the finite chain, the melting point depression is overestimated by 2°. If the simple relation indicated above is used and the undercooling is reckoned from the melting temperature of the infinite chain, the depression is underestimated by approximately 2°. However, as the data in Table II indicate, the utilization of eq. 3 and 4 with the same physical assumption, namely, the equality of nucleus and crystallite sizes, leads to quantitative agreement of the melting point depression over the complete molecular weight range.

The values of ζ^* have been calculated independent of any melting point data or direct observations of crystallite size. However, the calculations are predicated on homogeneous nucleation theory. It can, in principle, be questioned as to whether a homogeneous nucleation process could be operative at such relatively high crystallization temperatures. The close agreement of ζ^* with both the calculated and the observed crystallite size could either represent a unique coincidence or be of physical significance. We can note,

(33) L. Mandelkern, J. G. Farrow, and C. Howard, *J. Phys. Chem.*, **68**, 3386 (1964).

(34) It should be noted that in this calculation the interfacial energies of a nucleus and a mature crystallite have been equated. In general, this can be considered to be a restrictive assumption.

(35) (a) L. Mandelkern, *J. Polymer Sci.*, **47**, 494 (1960); (b) J. D. Hoffman and J. J. Weeks, *J. Res. Natl. Bur. Std.*, **A66**, 13 (1962).

(36) A slight dilemma exists in this interpretation of the observed melting points of the high molecular weight samples. Since in these cases ζ is such a small fractional part of the total chain length, a significant portion of the chain trajectories which emanate from a crystal face must return to it.³⁰ Hence, the nature of the crystallite, as well as its associated interfacial region, will be quite different from that of the nucleus from which it is formed. The apparent adequacy of the calculation must reside in a compensation between the size and interfacial energy of a crystallite compared to those for a nucleus.

parenthetically, that a similar situation was encountered in the analyses of the dependence of the low-angle diffraction spacing on crystallization temperature.²⁷ If we rule out the possibility of coincidence and seek a physical explanation, at least two possibilities suggest themselves. In the nucleation of long-chain molecules we are concerned with an asymmetric nucleation problem in which at least two distinctly different surfaces and interfacial energies are involved. Hence, nucleation catalysts need not affect all surfaces in the same manner. Theoretically, therefore, it is not necessary for all of the critical dimensions of a nucleus to be altered by the presence of heterogeneities. Hence, it is possible for the actual critical nucleus size in the chain direction to be comparable to that calculated from homogeneous nucleation theory while the free energy and rate of nucleus formation could be governed by a heterogeneous process. Alternatively, it could be argued that ζ^* is much smaller than is calculated, but ensuring growth in the chain direction increases the size to that observed.

The results for the two lowest molecular weight samples present a rather special and interesting situation. The observed melting temperatures are substantially greater than those required for equilibrium in terms of the model employed and the value of σ_e characteristic of the high molecular weight samples. Moreover, the melting temperature of the lowest molecular weight fraction, $M = 3300$, is even greater than that for the hypothetical end-paired model. Nuclei sizes, calculated according to eq. 4, with $\sigma_e = 4600$, give values of ζ^* for the different crystallization temperatures which are very close to the total number of units contained in the chain. These calculated values are summarized in the fifth column of Table III. Anderson³² has also observed that for samples of molecular weights 2960 and 5890, crystallized under comparable conditions, the average thickness of the lamellae can, within experimental error, be identified with the extended length of the molecules. With this excellent agreement between the calculated nuclei sizes and those observed for the crystallites, we can only conclude that in this molecular weight range the interfacial energy characteristic of the crystallite must be less than that of the nucleus from which it is formed. From the observed melting temperature and crystallite size the interfacial energy, σ_{ec} , can be calculated from eq. 3. The values thus obtained are also listed in Table III and are seen to be less than 4600 cal./mole assigned to the nucleus. A lower value for this interfacial energy for a mature crystallite is to be expected when almost the complete molecule is incorporated into a crystallite because the severe configurational re-

straints typical of the interfacial layer of the higher molecular weights will be significantly reduced. The equilibrium melting temperatures consistent with the calculated interfacial energies of the crystallite can also be calculated. These values are listed in the last column of Table III and are seen to be very close to those actually measured.

For molecular weights up to 20,000, a consistent interpretation between the melting temperatures and the observed and calculated crystallite sizes is obtained on the assumption of an extended chain configuration within the crystallite. Important in this interpretation is the utilization of a value of the nucleus interfacial energy of 4600 cal./mole. This molecular weight corresponds to about 1500 chain bonds for polyethylene and will reflect a much higher molecular weight for other types of chain-repeating units. These conclusions preclude the assumptions that a regularly folded structure is an equilibrium requirement for the crystallization of long-chain molecules³⁷ or that stable nuclei of long-chain molecules must be regularly folded.³⁸ We note also that in this molecular weight range densities approaching that of the unit cell and the concomitant high levels of crystallinity are attained.

For the higher molecular weights, the crystallite sizes that are compatible with the observed melting temperature represent only a very small fraction of the extended length of the molecule. Interfacial and interzonal difficulties that arise in accommodating the long, noncrystalline, randomly coiled sequences will necessitate the return of a proportion of the chains to the crystal from which they originated.³⁰ A lamellae crystalline structure of finite thickness will thus result with there being no *a priori* requirement for the chains to be regularly folded. Folding or the re-entry of chain sequences must obviously occur. However, the apparent independence of the nucleation interfacial energy with molecular weight indicates that this does not occur as a result of a regularly folded nucleation process. As has been previously indicated, besides internal imperfections, the nonregular interfacial region of such a crystal structure makes difficult an exact calculation of the melting of finite size crystals in this molecular weight range. It is in this range of molecular weights ($M_n \geq 47,000$) where the degree of crystallinity begins to decrease monotonically with increasing chain length.

Fusion Curves. As has been previously noted, for heating processes subsequent to crystallization at 130°,

(37) A. Peterlin and E. W. Fischer, *Z. Physik*, **159**, 272 (1960); A. Peterlin, E. W. Fischer, and C. Reinhold, *J. Chem. Phys.*, **37**, 1403 (1962).

(38) J. S. Hoffman and J. I. Lauritzen, *J. Res. Natl. Bur. Std.*, **A64**, 73 (1960); **A65**, 297 (1961).

the sharpness or breadth of the fusion curves is strongly dependent on the molecular weight. The sharpest curves are found in the molecular weight range 12,500–47,000 and begin to resemble the expectations of a classical first-order phase transition. The crystallite length for these cases represents a significant portion of the extended length of the molecule, and the concentration of chain ends, *per se*, should not be sufficient to cause a perceptible melting point depression with a change in the relative proportion of the two phases. The much broader melting range for $M = 5300$ and 3300 can be attributed to the decreasing concentration of chain ends as fusion progresses. However, the breadth of melting for $M = 12,500$, which is of the order of $2-4^\circ$, in this range, does not comply with expectations. If an extension of the theory used to calculate ζ were used to calculate the melting range, essentially hypersharp melting would be expected, even for ζ substantially less than the required equilibrium length.²⁹ For example, for $M = 12,500$ and $\zeta = 512$, the last 15% of crystallinity should disappear in about 0.1° . Experimentally, a 0.4° interval is observed. Although, if a value for ζ of 491 was assumed, this fusion range could be accounted for, the experimental results would not be reconciled at slightly higher levels of crystallinity. At 30% crystallinity, the deviations would again become about 0.5° . More serious than the slightly enhanced broadening observed for the fusion of $M = 12,500-47,000$ is the fact that the theory predicts that the melting process should become sharper as the molecular weight is increased, even for non-equilibrium values of ζ . This expectation is clearly contrary to the experimental observations. Hence, despite the fact that the crystallite size can be calculated, which is independently confirmed and accounts for the experimental melting point depression-molecular weight relationship, the theory does not adequately predict the level of crystallinity below the melting temperature, even at temperatures close to melting temperature. This discrepancy is quite marked for the higher molecular weights.

Various qualitative explanations can be offered for the melting range and the significant broadening that is observed as the molecular weight increases. Obviously, either the nature of the crystallites, the influence of the coexisting amorphous regions, or both are involved. In Figure 5, for $M \geq 12,500$, the fusion curves become much broader as the level of crystallinity decreases. It might be concluded that contributions from the amorphous regions are most significant in broadening melting.³⁹ However, changes in the level of the crystallinity in these experiments are obtained at the expense of varying molecular weight. It

is possible that increasing the molecular weight could be affecting the crystallites, in terms of internal imperfection and a broader distribution of crystallite sizes. Hence, it would not be proper, at this point, to attribute the broadening solely to the interzonal amorphous regions. The effect of polydispersity in chain length has not, as yet, been investigated in detail. As was pointed out in the Experimental portion, although we are dealing with fractionated material, the higher molecular weight samples are expected to be more polydisperse.

The results for fusion, after cooling to room temperature as is illustrated in Figure 6, point out some of the complexities in attributing the broadening solely to the amorphous regions. For $M = 20,000$ the breadth of melting is unaffected by the cooling and subsequent heating. However, for the higher molecular weight fraction, the melting range becomes broader (even above 130°) with the crystallization that accompanies the cooling to room temperature.

Density. The variation of the densities of the samples at the isothermal crystallization temperature appears to be quite intimately connected with the influence of molecular weight on the crystallization kinetics and mechanisms. Characteristic changes in the crystallization isotherms from the melt^{15,18a} are found in the same molecular weight range where the monotonic decrease of density is observed. The extremely low densities observed in the highest molecular weight range preclude chain ends being a factor and demonstrate an inherent effect of molecular weight in limiting the level of crystallinity that can be attained.

The argument could be advanced that the low density does not reflect the level of crystallinity but instead is caused, in general, by a large set of internal defects.^{40,41} The nature of these defect structures would, thus, have to be very molecular weight dependent, and their concentration would have to be extraordinarily high to account for a density of 0.85, which is characteristic of the higher molecular weights. In addition, the crystallization isotherms display all the major characteristics of an incomplete phase transition. Moreover, since there is nothing inherently unique about the analysis of the density at 130° , we note a substantial increase in density on cooling to room temperature. Formally, these observations could be interpreted as the disappearance of defect structures with decreasing temperature or the development of further crystallinity from the residual

(39) (a) L. H. Tung and S. Bukser, *J. Phys. Chem.*, **62**, 1530 (1958); (b) R. J. Roe, K. J. Smith, Jr., and W. R. Krigbaum, *J. Chem. Phys.*, **35**, 1306 (1961).

(40) H. A. Stuart, *Ann. N. Y. Acad. Sci.*, **93**, 3 (1959).

(41) D. A. Zaukelies, *J. Appl. Phys.*, **33**, 2797 (1962).

amorphous regions as the temperature is lowered. The former of these interpretations would be difficult to reconcile with the thermodynamic stability of non-equilibrium defects while the latter, besides not violating any fundamental principles, is given strong confirmation by the data of Figure 3. In the typical example illustrated, the dilatometer scale heights, which are directly related to the density, decrease with time, isothermally, in a manner which is in accord with the occurrence of a phase change.

At 25° the densities for $M \leq 20,000$ are very close to the value calculated for the macroscopic crystal. The differences between the observed and calculated densities are 0.006 or less. These differences could be attributed to contributions from the interfacial regions, internal defects, or some residual, noncrystalline chain units. A differentiation as to the probable contributory effects cannot be made at present. These contributions to the density could be expected to be at levels of crystallinity of the order of 90%, which is typified by the molecular weight range of 50,000 or less. It is in this molecular weight range, characterized by levels of crystallinity of the order of unity, that we calculate nuclei and crystallite sizes that are comparable to the extended length of the molecule. The high levels of crystallinity, both at the crystallization temperature and at room temperature, can be attributed to this fact. The occurrence of nonequilibrium defect structures is to be expected in all crystalline substances, those formed from long-chain molecules included. However, there is no reason for these structures to be formed at the expense of the coexisting noncrystalline regions that have been shown to exist in appreciable proportion for molecular weights greater than 50,000. In this connection we note, in an extension of Anderson's observations,^{35b} that samples of molecular weight equal to or less than 50,000, crystallized in the manner described, can easily be fractured at room temperature.

However, the higher molecular weight fractions, with their lower density and decreasing level of crystallinity, can only be fractured with some difficulty at liquid nitrogen temperatures. These observations are indicative of the presence of an appreciable amorphous content which is the intercrystalline regions. Fracture can, thus, be attained only below the glass temperature of the amorphous regions.

X-Ray Diffraction Patterns. The very sharp reflections and the absence (or extreme diminution) of a halo in the X-ray diffraction patterns at room temperature for molecular weights $\leq 20,000$ are in accord with the discussion given above for the observed densities and calculated degrees of crystallinity between 0.90 and 1.00. Close scrutiny of these results gives evidence that for polyethylene the density measurement is a more sensitive detector of the crystalline state. The complete absence of a halo in the X-ray pattern for $M = 12,500$, for example, would lead to the expectation that the density of the sample should be that of the unit cell. Small deviations from this value have already been noted. The correlation between the wide-angle X-ray diffraction pattern and sample density is further seen as the molecular weight is increased. The reflections begin to broaden, and a very definite halo appears which becomes more intense with increasing molecular weight.

A detailed report of the temperature requirements for the formation and disappearance of the polymorphic form (to which the six extra reflections can be attributed) will be given shortly.⁴² The present volume-temperature data do not unequivocally show a transition or discontinuity that could be attributed to the disappearance of this form.⁴³

(42) J. G. Fatou, C. Baker, and L. Mandelkern, to be published.

(43) R. Boyer, *Rubber Chem. Technol.*, **36**, 1303 (1963).

The Kinetics of the Thermal Isomerization of Ethylcyclopropane^{1a}

by Marcel L. Halberstadt and John P. Chesick^{1b}

Sterling Chemistry Laboratory, Yale University, New Haven, Connecticut (Received July 6, 1964)

Ethylcyclopropane simultaneously undergoes an isomerization to 1-pentene, *cis*- and *trans*-2-pentene, and 2-methyl-1-butene and a decomposition to butadiene and methane. The reaction has been studied in the gas phase by static methods from 454 to 484° and over a pressure range of 84 to 5×10^{-2} mm.; under these conditions, the isomerization to the pentenes was found to be a homogeneous unimolecular process. The decomposition to butadiene may be taking place *via* a free-radical process or by a unimolecular disproportionation reaction. The lifetime of the activated molecule is about a factor of 10 longer than that of the methylcyclopropane decomposition reaction as evidenced by a shift of the $\log k/k_{\infty}$ vs. $\log P$ curve to lower pressures for ethylcyclopropane. All degrees of freedom appear to participate in increasing the lifetime of the activated molecule. The Marcus extension of the Rice-Ramsperger-Kassel theory is applied to this reaction. The high pressure rate constant for isomerization to pentenes may be expressed as $k_{i\infty} = 10^{14.40} \exp\{-61.3 \pm 1.4\} \text{ kcal./RT} \text{ sec.}^{-1}$.

Introduction

The detailed model provided by Slater² for calculation of the rate and pressure dependence of a unimolecular reaction has served as a great spur to experimental and theoretical activity on this subject. Both the Slater model, which assumed no intramolecular energy transfer between collisions, and the Rice-Ramsperger-Kassel (RRK) treatment, assuming free intramolecular energy transfer, yielded results which were quite similar considering the presence of adjustable parameters or unevaluable quantities in the two approaches. Thus, experimental studies turned to examination of substituent effects on a parent molecule or to chemical activation by various means. Such tests were provided, for example, by Chesick³ and Butler and Kistiakowsky⁴ who studied the isomerization of methylcyclopropane and "hot" methylcyclopropane, respectively. The latter authors found that the composition of product butenes did not vary when methylene was added to cyclopropane or to propylene. This was interpreted to mean that the energy of the excited molecules migrates freely among the normal modes of vibration of methylcyclopropane within the time interval between their formation and rearrangement, in contradiction to the assumptions of the Slater theory.

The study of the thermal isomerization of methylcyclopropane was undertaken by Chesick to study the effect of additional degrees of freedom on the lifetime of the reactant molecule. Chesick found that the addition of the methyl group increased the lifetime of the molecule by a factor of about 30. The data were fitted quite well by a curve calculated from the Kassel expression with the number of effective degrees of freedom now equal to 19. The change in lifetime with shift of the $\log k$ vs. $\log P$ curve to lower pressure was calculated and found to be in good agreement with experiments using the Marcus⁵ quantum formulation of the RRK approach.

It was of interest to learn if the addition of still more degrees of freedom to the molecule by replacing

(1) (a) This paper is abstracted, in part, from the dissertation submitted by M. L. H. to the Graduate School of Yale University, 1963, in partial fulfillment of the requirements for the Ph.D. degree; (b) to whom requests for reprints should be directed at Department of Chemistry, Haverford College, Haverford, Pa.

(2) N. B. Slater, "Theory of Unimolecular Reactions," Cornell University Press, Ithaca, N. Y., 1959. A comprehensive list of references to the original literature may be found in this book.

(3) J. P. Chesick, *J. Am. Chem. Soc.*, **82**, 3277 (1960).

(4) J. M. Butler and G. B. Kistiakowsky, *ibid.*, **82**, 759 (1960); **83**, 1324 (1961).

(5) G. M. Wieder and R. A. Marcus, *J. Chem. Phys.*, **37**, 1835 (1962).

the methyl with an ethyl group would cause the high pressure rate constant drop-off at a still lower pressure. The substitution of a methyl group for a hydrogen atom on the ring would be expected to affect the energetics and details of the reaction in the ring considerably more than the further addition of another methyl group once removed from the ring (as opposed to addition of a second methyl group to the ring as in 1,1-dimethylcyclopropane). Furthermore, if a given amount of energy is distributed among a small number of normal modes, the average amount in each may be sufficiently large that there is a significant amount of coupling. Energy may then flow readily between the modes, and the RRK assumption will apply. But, if the number of modes is large, each vibration will occur mainly in the harmonic region; there may then be little coupling, and the Slater assumption that reaction can occur only if the vibrations come suitably into phase becomes more reasonable.⁶ It was thus possible that the additional vibrational modes in ethylcyclopropane might cause little or no effect and that the fall-off behavior would be similar to that of methylcyclopropane. A study of the thermal isomerization of ethylcyclopropane was, therefore, undertaken.

Experimental

Ethylcyclopropane was prepared by the addition of diazomethane to Matheson C.P. grade 1-butene in the presence of cuprous chloride catalyst,⁷ the reaction mixture being cooled in an ice-salt bath to approximately -20° . The product mixture was warmed to 0° , and the butene was allowed to evaporate. The fraction distilling through a Vigreux column in the range $35-36.2^{\circ}$ was bubbled through saturated solutions of iodine, bromine, and potassium hydroxide and was distilled into storage flasks on the vacuum manifold after trapping over Ascarite and Drierite to remove carbon dioxide and water. No detectable impurity was found in this ethylcyclopropane upon passage through a g.l.p.c. column consisting of a 3.2-m. section of silver nitrate in glycerol on firebrick coupled with a 20.3-cm. section packed with Dow Corning 703 silicone oil on firebrick. Infrared and mass spectra compared favorably with those in the literature.^{8,9} This material is taken to be more than 99.9% pure.

The following chemicals were used: ethane, Matheson C.P. grade; ethylene, Phillips research grade; propane, Phillips research grade; propylene, Matheson C.P. grade; allene, Columbia Organic Chemicals, 99%; butane, Matheson instrument grade; butene-1, *cis*- and *trans*-butene-2, isobutene, all Matheson C.P.

grade; 1,3-butadiene, Matheson instrument grade; pentene-1, Phillips, 99%; pentene-2, Phillips, 99%; *cis*-pentene-2, Phillips, 95%; 2-methylbutene-1, Phillips, 99%; cyclopropane, Matheson, 99.5%; helium, Matheson high purity; nitrogen, Matheson prepurified; nitric oxide, Matheson, 99%. Samples of methylcyclopropane and methylenecyclopropane prepared in this laboratory were also used. Many of the hydrocarbons listed above were purified further by gas chromatography; many were used only for comparison and identification purposes during calibration of the gas chromatography column and detector. Nitrogen used for the inert gas runs was liquefied under pressure in a U-trap that was kept at liquid nitrogen temperature, and gas was taken from this liquid to leave frozen any condensable impurities.

The vacuum system used in this work has been described previously.³ Mercury float valves were used in that part of the line where hydrocarbon mixtures were prepared and transferred to prevent absorption by stopcock grease. Stopcocks were provided with mercury cutoffs to avoid contact of hydrocarbon mixtures with stopcock grease. The storage flask from which gas was expanded into the reaction vessel was fitted with a magnetically driven paddle stirrer for mixture preparation. Each run was terminated by expansion of the reaction vessel products through a three-loop product trap which was immersed in liquid nitrogen; trapping of products from noncondensable gases which were pumped off was efficient. Pressure measurements were made with a 15-mm. bore mercury differential manometer with a mirror scale or a calibrated McLeod gauge.

A 1500-ml. quartz reaction vessel of 10-cm o.d. was coated on the inside with a mirror of silicon metal by thermal decomposition of silane.¹⁰ It had been reported that a coating of metallic silicon reduced reactions at the walls of the vessel¹¹ in the pyrolysis of sensitive compounds. Preliminary runs with a Pyrex reaction vessel had indicated that many products were formed from the decomposition of ethylcyclopropane or its isomerization products, and the silicon-coated

(6) E. K. Gill and K. J. Laidler, *Proc. Roy. Soc. (London)*, **A250**, 121 (1959).

(7) P. Gaspar, Ph.D. Thesis, Yale University, 1961.

(8) American Petroleum Institute Research Project 44, Infrared Spectrum No. 881.

(9) American Petroleum Institute Research Project 44, Mass Spectrum No. 1652.

(10) We express our gratitude to Dr. E. P. Blanchard of the Central Research Division, E. I. du Pont de Nemours and Co., Wilmington, Del., for his kindness in furnishing us with an ample supply of silane and the directions for use.

(11) H. E. Simmons, private communication.

quartz vessel was used in an attempt to reduce the unwanted side products. The nature and abundance of products, in fact, remained unchanged with the substitution of the coated vessel. Temperature control and measurement were as previously described.²

Product Analysis. Extreme care was necessary in sampling the product mixtures because of the large difference in volatility of some of the components. If aliquot samples were to be taken, the total product mixture was vaporized in a storage flask and mixed, and a representative gas sample was taken. Repetitive sampling established that uniform samples were being obtained.

The silver nitrate-silicone oil combination column was used for the bulk of the runs. Varying lengths of silicone oil and dimethylformamide columns were used to confirm g.l.p.c. peak identities and homogeneities. Calibration mixtures of authentic compounds were prepared for detector calibrations.

Results

Primary and Secondary Products. The chromatogram of a run which had gone to about 10% conversion of the ethylcyclopropane showed nine clearly distinguishable product peaks. These were pentene-1, *trans*-pentene-2, 2-methylbutene-1, *cis*-butene-2, butadiene, and minor peaks which were identified as propane, ethylene, and an incompletely resolved peak consisting of butene-1 and *cis*-butene-2. Some products arise from decomposition of product pentenes. A correction can be made to the percentage of pentenes formed to take into account this decomposition. The possibility existed, however, that some products might be formed from ethylcyclopropane decomposition reactions occurring in parallel with the isomerization to the four pentenes.

Several runs were made with either a mixture of pentenes or 1-pentene as the reactant instead of ethylcyclopropane, under conditions similar to those for the runs using ethylcyclopropane, so that a direct comparison could be made between the yields of butadiene in all cases. These runs clearly showed that there was more butadiene formed in the ethylcyclopropane decomposition than could be accounted for by the secondary decomposition of the pentenes, and thus butadiene was indicated as a primary product.

A number of runs was then made at various conversions from 15 to 60%, starting with approximately the same initial pressure of ethylcyclopropane (25 mm.) with duplicate analyses for each run. The results are shown graphically in Figure 1 in which a plot is made of product per cent *vs.* per cent conversion for each of the reaction products. Extrapolation to

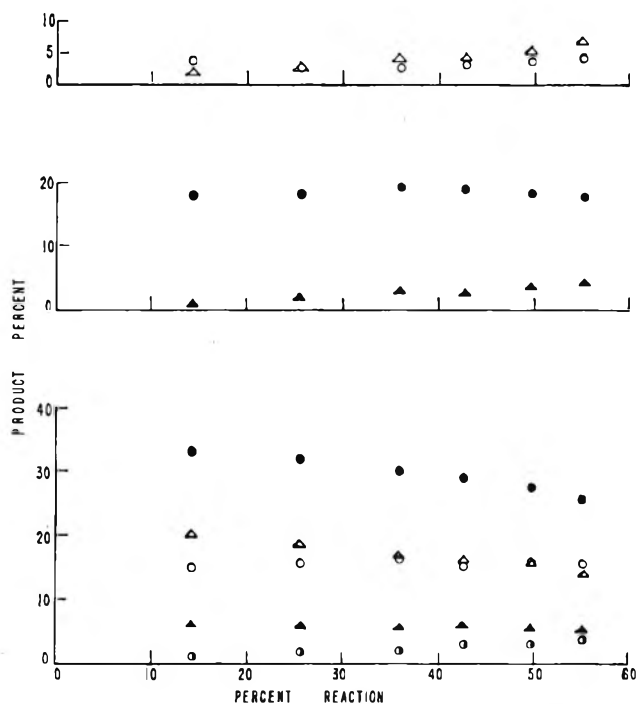


Figure 1. Determination of primary products at 467.8°. Top: O, ethylene; Δ, propylene. Middle: ●, butadiene; ▲, butenes. Bottom: ●, 1-pentene; Δ, *cis*-2-pentene; ○, *trans*-2-pentene; ▲, 2-methyl-1-butene; ○, propane.

0% reaction enables us to determine which products are primary. Compounds such as propane, propylene, and butene extrapolate to the origin and, therefore, are secondary. The pentenes and butadiene, on the other hand, extrapolate to finite values on the "product" axis. Butadiene, therefore, is a primary product formed to the extent of about 20% of all the products. Addition of the extrapolated product fractions to 99% serves as a check on the extrapolation procedure. Ethylene appears as a small shoulder on the tail of the ethylcyclopropane peak, and the extrapolation for ethylene is somewhat uncertain. It is probable that it is also a secondary product, allowing for the uncertainty in measurement. In a study of the pyrolysis of pentenes in a flow system at 800°, it was found¹² that the main products from the reaction of 1-pentene were ethylene, propylene, butene, and butadiene, while those from 2-pentene were butadiene, ethylene, and propylene. Thus, the secondary products can be accounted for, and some of the butadiene is probably also formed as a secondary product. Butadiene is known to undergo condensation and polymerization reactions at the temperatures employed here. Using

(12) E. Gorin, A. G. Oblad, and R. F. Schmuck, *Ind. Eng. Chem.*, **38**, 1187 (1946).

the rate constant of Rowley and Steiner¹³ for the dimerization of butadiene in the range 400–600°, we calculate that only 1–2% of the butadiene would be consumed in dimerization at the low conversions of ethylcyclopropane employed in this work. The same authors also studied the Diels–Alder condensation of butadiene and ethylene to give cyclohexene and showed that the process was very similar energetically to the dimerization of butadiene. Although it is possible that butadiene and pentene can react in this fashion, only a small percentage of each will be consumed in such a reaction at the low pressures employed here. It may be that the slight curvature in the plot for butadiene in Figure 1 is caused by these effects: first, there is a slight positive slope caused by the addition of the butadiene from pentene decomposition to that produced directly from the ethylcyclopropane, and, second, there is a decrease in the relative percentage of butadiene above 40% reaction owing to its consumption by condensation or polymerization. The over-all disappearance of ethylcyclopropane is a first-order process, at least to over 55% conversion. After this, decomposition of the pentenes becomes a problem in determination of total reaction.

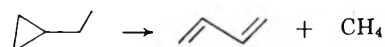
Butadiene–Methane Balance. Small amounts of noncondensable gas were formed; this was usually pumped away during product freeze out. However, samples were trapped for mass spectral analysis by expansion of the noncondensable gas through the cold trap into a calibrated and evacuated 2-l. bulb. The pressure of gas in the bulb was measured, and a mass spectrum showed that the gas in the bulb was mostly methane with small traces of C₂ and C₃ hydrocarbons and hydrogen amounting to about one-twelfth of the methane. Analysis of the condensable products for butadiene and comparison with the amount of noncondensable gas for two separate runs gave the results in Table I. These

Table I

Pressure, mm.	Total per cent reaction	Moles of butadiene	Moles of gas
43.6	9.9	2.0×10^{-5}	2.3×10^{-5}
84.2	10.3	2.45×10^{-5}	2.5×10^{-5}

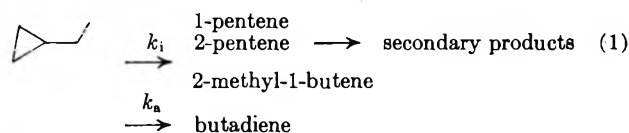
runs were made in the vessel when it was packed with glass tubing to test for surface effects. The agreement may be somewhat fortuitous because one would expect some of the methane to be occluded in the frozen condensables.¹² This loss may be balanced by the methane which is produced by the decomposition of the

pentenes; this decomposition probably accounts for the small amounts of hydrogen¹² found in the mass spectrum of the noncondensables. The mass balance, thus, appears to be reasonably good. It is, therefore, concluded that methane and butadiene are formed in the ratio 1:1 in the reaction



The mechanism of this reaction will be discussed later.

Rate Constants. The following reaction scheme may be formulated for the first-order processes at low conversions when the contributions from secondary processes are negligible.



The rate for the over-all reaction can be written

$$-d(\text{ethylcyclopropane})/dt = (k_i + k_d)(\text{ethylcyclopropane}) = k(\text{ethylcyclopropane}) \quad (2)$$

Therefore

$$[\text{pentenes}]/[\text{butadiene}] = k_i/k_d \quad (3)$$

and

$$k_i = k/(1 + 1/a) \quad (4)$$

where $a = [\Sigma \text{pentenes}]/[\text{butadiene}]$.

Pressure Dependence of Rate Constant. Table I shows the results for a number of runs in the vicinity of 467.8° which were made with initial pressures ranging from 65 to 0.005 mm. of ethylcyclopropane. In each case, k_i was calculated with eq. 4, a correction being applied for small temperature deviations from 467.8°. It will be noted that the ratio [pentenes]/[butadiene] is near enough to being constant to warrant the use of eq. 4. There is, perhaps, a significant increase in the quantity [pentenes]/[butadiene] with decreasing pressure, as shown in Figure 2. It should be noted, however, that the runs, for which the ratio is in the vicinity 3.5–4, are from one series while those for which the ratio is 5–7 are from two other series. Since the starting material was treated identically in all cases and since the reaction vessel had not been opened to the atmosphere, either during or between the series or even before the first one (*i.e.*, it was “seasoned”), this observation cannot be explained. The extent of the reaction (percentage of reactant consumed) was calculated by the determi-

(13) D. Rowley and H. Steiner, *Discussions Faraday Soc.*, 10, 198 (1951).

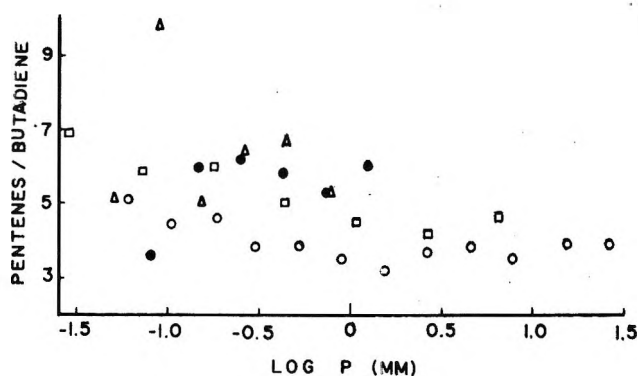


Figure 2. Pentenes/butadiene as a function of pressure at 467.8°: O, group A; ●, group B; △, group C; □, runs in the presence of added nitrogen.

nation of the total amounts of C₃, C₄, and C₅ hydrocarbons in the products from the chromatograms. The usual dead volume correction was applied to the percentage of ethylcyclopropane left unreacted. Figure 3 is a plot of $\log k_i/k_{i\infty}$ vs. $\log P$, and it shows a definite decrease of the first-order rate constant from its high pressure value. This falloff does not begin until the pressure has been lowered to less than 1 mm., and at 0.05 mm. the rate constant has only decreased by about 25%.

The scatter of the data in this work resulted chiefly from the low conversions necessary to minimize pentene decomposition, and the best estimates of high pressure rate constants were obtained by taking the mean of the rate constants of those runs in which the initial pressure was greater than 1 mm. These high pressure values are probably valid to $\pm 5\%$.

Addition of an Inert Gas. A series of runs was made in which nitrogen was added to ethylcyclopropane in the ratio of 17.6:1 to verify that an energy transfer phenomenon was responsible for the decrease in $k_i/k_{i\infty}$ with a decrease in pressure. Initial pressures of reactant varied from 6.42 to 0.03 mm. The results are shown in a plot of $\log k_i/k_{i\infty}$ vs. $\log P$ in Figure 3. The

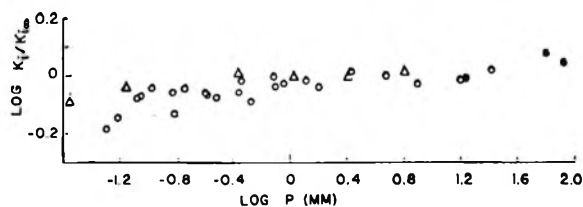


Figure 3. Behavior of first-order rate constant for the isomerization of ethylcyclopropane to pentenes as a function of pressure at 467.8°: O, silicon-coated quartz vessel; ●, packed vessel; △, nitrogen added (nitrogen/ethylcyclopropane = 17.6:1).

Table II: Variation of Rate Constant with Pressure at 467.8°

Pressure, mm.	% conversion	[Pentenes]/[butadiene]	$k_i \times 10^4$, sec. ⁻¹
26.5	10.5	3.92	1.77
15.5	7.2	3.96	1.63
7.85	6.9	3.52	1.58
4.56	7.1	3.85	1.69
2.66	7.3	3.70	1.75
1.56	7.3	3.23	1.54
1.26	6.8	6.02	1.62
0.89	6.7	3.50	1.58
0.78	6.6	5.34	1.54
0.748	6.5	5.32	1.67
0.52	6.2	3.87	1.37
0.450	7.0	6.68	1.63
0.425	6.0	5.86	1.48
0.30	6.6	3.85	1.42
0.256	6.5	6.38	1.45
0.252	6.3	6.22	1.47
0.177	6.5	4.63	1.53
0.151	6.1	5.01	1.26
0.147	6.6	5.96	1.48
0.104	7.4	4.46	1.53
0.088	6.8	9.72	1.44
0.081	7.6	3.63	1.41
0.060	7.4	5.35	1.21
0.050	5.5	5.12	1.11

Runs with nitrogen added^a

Ethylcyclopropane pressure, mm.			
6.42	7.0	4.65	1.76
2.66	8.4	4.18	1.68
1.08	8.6	4.53	1.68
0.439	8.6	5.02	1.73
0.178	8.0	5.96	1.56
0.071	8.4	5.86	1.53
0.028	11.5	6.88	1.38

^a $T = 467.8^\circ$; [nitrogen]/[ethylcyclopropane] = 17.6.

efficiency of the nitrogen relative to the ethylcyclopropane in maintaining the high pressure rate can now be calculated to be 0.20 ± 0.05 on a pressure basis from an estimate of a shift of the values of $k_i/k_{i\infty}$ on the $\log P$ axis. The [pentene]/[butadiene] ratio is also shown in Figure 2. The slight upward trend with a decrease in pressure seems to be real.

Packed Vessel. The reaction vessel was packed with thin-walled, 2-mm. o.d. Pyrex tubing increasing the surface-volume ratio by a factor of 20. The average value of k_i for six runs at 467.8° and at pressures between 17 and 63 mm. was 10% higher than the average of values for runs above 1 mm. in the unpacked vessel. The average of the [pentene]/

[butadiene] ratio was 7.6, which seems significantly higher than that observed in the unpacked vessel as shown in Figure 2.

Nitric Oxide Addition. The addition of nitric oxide at pressures between 6 and 300% of the reactant pressure did not inhibit the reaction and may, in fact, accelerate it somewhat at the higher levels. Butadiene formation was not significantly affected. It is concluded that the decomposition to pentenes is probably a homogeneous unimolecular isomerization; the mode of butadiene formation is, however, uncertain.

Arrhenius Plot. An Arrhenius plot for data in the temperature range 446.1–479.3° is presented in Figure 4. The pressure was above 15 mm. in all cases in the

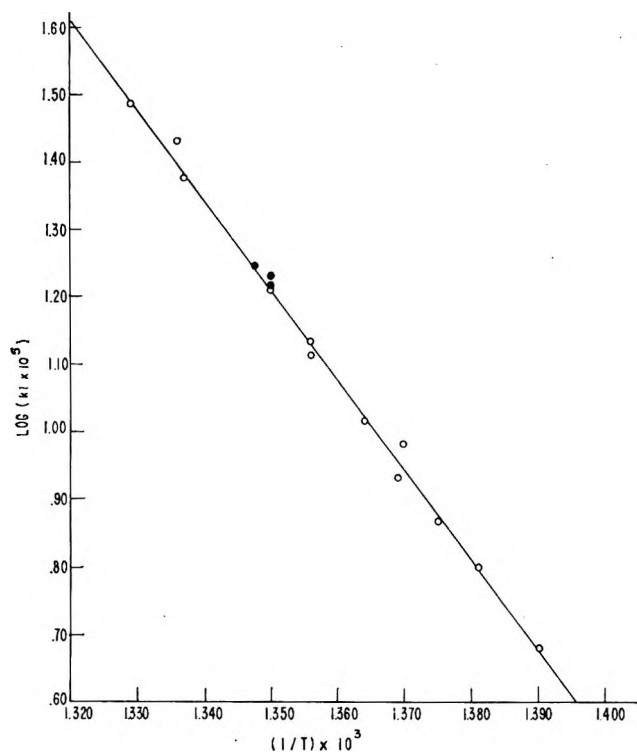


Figure 4. Arrhenius plot for ethylcyclopropane decomposition: O, silicon-coated quartz vessel; ●, packed vessel.

high pressure region. A least-square fit of the data yields a value of 61.6 ± 1.4 kcal. for the activation energy of the isomerization reaction. Using the value of 1.70×10^{-4} sec.⁻¹ for the high pressure rate constant at 467.8°, we obtain $k_{im} = 10^{14.40} \exp[(-61.6 \pm 1.4) \text{ kcal./RT}]$.

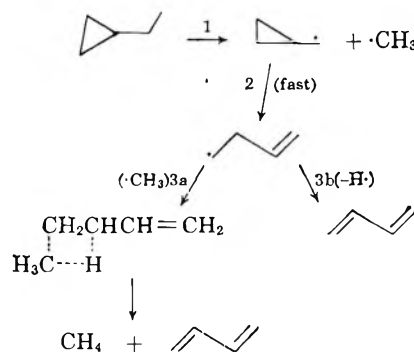
Product Ratios. Pentene product ratios are shown as a function of pressure in Figure 5. There are no obvious trends to be noticed with variations in temperature and pressure. The ratio of 2-methyl-1-

butene to 1-pentene increases somewhat with an increase in extent of reaction; this is probably due to the greater thermal instability of pentene-1.¹⁴

Discussion

Mechanism of Decomposition. The thermal isomerization of ethylcyclopropane at 446–479° is complicated by the simultaneous decomposition to butadiene and methane, as well as secondary decomposition of pentenes to butadiene and lower hydrocarbons. It has been shown that the secondary products can be accounted for by the decomposition of the primary pentenes that are formed from the opening of the ring in a manner analogous to the isomerization of cyclopropane to propylene or methylcyclopropane to the isomeric butenes.

The formation of the butadiene, however, poses the question of the mechanism of its formation. Since the cyclopropane ring may have some double-bond character,¹⁵ it is possible that the bond β to the ring is somewhat weakened¹⁶ and initially breaks into two fragments in step 1.



The methylcyclopropyl radical would probably then rearrange in a fast step (2) to form the butenyl radical. Such a process would be analogous to a mechanism proposed by Roberts, *et al.*,¹⁷ to explain the products of the photochlorination of methylcyclopropane. They suggested that the methylcyclopropyl radical rearranges to the butenyl radical which then attacks chlorine to give one of the observed products. Alternatively, they suggested that the butenyl radical may not be formed at all and that a homoallylic radical may be the species which reacts with chlorine to give chloromethylcyclopropane and 4-chlorobutene-1. The methyl and

(14) M. J. Molera and F. J. Stubbs, *J. Chem. Soc.*, 381 (1951).

(15) E. E. Royals, "Advanced Organic Chemistry," Prentice-Hall, New York, N. Y., 1954.

(16) F. O. Rice and K. K. Rice, "The Aliphatic Free Radicals," Johns Hopkins Press, Baltimore, Md., 1935; cited by M. Taniowski, *Proc. Roy. Soc. (London)*, A265, 519 (1962).

(17) E. Renk, P. R. Shafer, W. H. Graham, R. A. Mazur, and J. D. Roberts, *J. Am. Chem. Soc.*, 83, 1987 (1961).

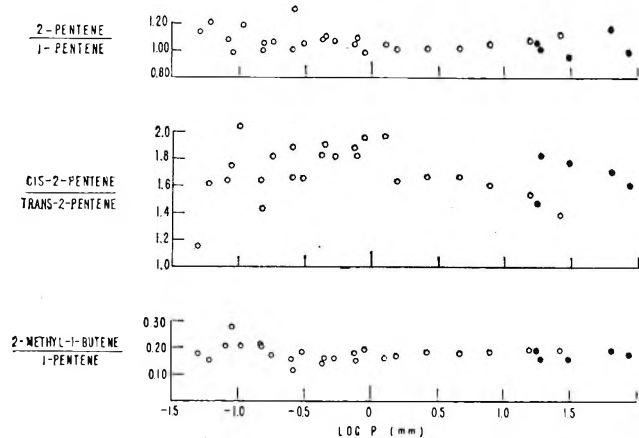


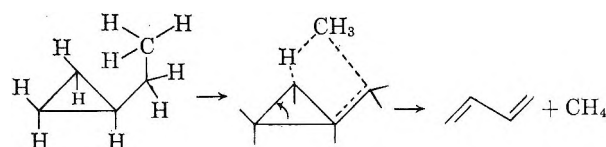
Figure 5. Pentene ratios as a function of pressure at 467.8°C: O, silicon-coated quartz vessel; ●, packed vessel.

butenyl radicals would be the radicals present in greatest concentrations in the present work. These could disproportionate in step 3a to give methane and butadiene. I² disproportionation needs a third body, as has been suggested,¹⁸ it is difficult to explain the observation that yield of butadiene does not fall off markedly at low pressures.

An alternative mechanism is the loss of a hydrogen atom (3b) by the butenyl radical to give butadiene. Alkyl radicals smaller than pentyl decompose to yield either a hydrogen atom or a methyl or ethyl radical.¹⁹ An estimate of the heat of this reaction can be made as follows. The strength of the primary C-H bond in propane and butane is about 100 kcal./mole²⁰ and is here assumed to be the same for 1-butene. The heats of formation of 1-butene and atomic hydrogen are -0.03 and +52.1 kcal./mole, respectively.²¹ This gives a heat of formation of the 4-butenyl radical of 47.9 kcal./mole. (This radical is much less favored than the 3-butenyl radical if it is actually to be formed by hydrogen abstraction from 1-butene.²²) With a value for the heat of formation of butadiene of 26.3 kcal./mole,²¹ we obtain a ΔH of 30.5 kcal. for reaction 3b above. A similar figure is obtained if one uses the value of 37 kcal./mole calculated by Kerr and Trotman-Dickenson¹⁹ for ΔH for the loss of a hydrogen atom by *n*-propyl. On subtracting from this the 6 kcal./mole stabilization energy of butadiene relative to 1-butene,²³ we obtain 31 kcal./mole, in good agreement with the previous calculation. Reaction 3b is, thus, endothermic by about 31 kcal. Some of this energy may be furnished by the exothermicity of the isomerization of the cyclopropyl to butenyl resulting from the difference between the 60-65 kcal./mole gained from double-bond formation (calculated from

heats of hydrogenation of olefins to corresponding hydrocarbons) and the 54 kcal./mole as the ΔH for rupture of the cyclopropane ring.²⁴ This gives ΔH for the cyclopropylmethyl to butenyl isomerization of about -6 to -11 kcal., in good agreement with the value of -7.86 kcal./mole found for the heat of isomerization of cyclopropane to propylene.²⁵ The loss of a hydrogen atom to give butadiene, thus, will still require about 20 kcal. of additional energy. The unimolecular decomposition of a butenyl radical at *ca.* 470° with an energy barrier of this magnitude might be a significant reaction. The atomic hydrogen produced would produce H₂ by abstraction from ethylcyclopropane at low conversions and would add to the pentenes at reactant conversions above 1-3%. Methyl radicals would then have to recombine to form ethane or would recombine and disproportionate with C₃ radicals reducing the CH₄/C₄H₆ ratio well below unity. The product analyses and CH₄/C₄H₆ balance make this an unlikely reaction sequence.

Another possible mechanism for the formation of butadiene and methane would not entail a free-radical process. It has been suggested¹⁸ that unimolecular disproportionation processes probably occur in hydrocarbon pyrolyses but are masked by the considerable chain length of the concurrent free-radical process. Such a process may be taking place in the ethylcyclopropane decomposition. The configuration in which the ethyl group is over the ring permits a transition state in which the leaving methyl group is accompanied by a hydrogen, and butadiene is formed in the same step.



Pyrolysis of a mixture of ethylcyclopropane and ethylcyclopropane-*d*₁₀ with mass spectral analysis of the

(18) K. J. Laidler and B. W. Wojciekowi, "The Transition State," Special Publication No. 16, The Chemical Society, London, 1962.

(19) J. A. Kerr and A. F. Trotman-Dickenson, "Progress in Reaction Kinetics," Vol. I, Pergamon Press, Inc., New York, N. Y., 1961, p. 120.

(20) T. L. Cottrell, "The Strengths of Chemical Bonds," Academic Press, New York, N. Y., 1954.

(21) "Selected Values of the Properties of Hydrocarbons," American Petroleum Institute Research Project 44.

(22) J. R. McNesby and A. S. Gordon, *J. Am. Chem. Soc.*, **79**, 5902 (1957).

(23) M. J. S. Dewar and H. N. Schmeising, *Tetrahedron*, **11**, 96 (1960).

(24) S. W. Benson, *J. Chem. Phys.*, **34**, 521 (1961).

(25) J. W. Knowlton and F. D. Rossini, *J. Res. Natl. Bur. Std.*, **43**, 113 (1949).

methane produced would provide an unambiguous choice of the molecular or free-radical processes for butadiene and methane production.

Pentene-1, pentene-2, and 2-methylbutene-1 are produced at high pressures in the relative yields 1.0:1.0:0.19, in close agreement with the butene-1, butene-2, and isobutene relative yields of 1.0:0.9:0.16 found for the methylcyclopropane decomposition.² A slight deviation is found in the ratios of *cis*- to *trans*-pentene-2 isomers. Chesick observed this ratio to be approximately 2 in the opposite direction from the ratio of thermodynamic stability; the ratio of about 1.6 obtained here is slightly lower, but the *cis* isomer still predominates. These ratios are probably influenced by factors too subtle to be explained at present since the *trans*-2-pentene should also have greater thermodynamic stability than the *cis* form.

Comparisons of Pressure Dependencies of Cyclopropane Reactions. The effect of additional degrees of freedom in the homologous series, cyclopropane, methylcyclopropane, and ethylcyclopropane, is shown quite dramatically in Figure 6, in which curves have been drawn through the experimental points³ for the fall of rate constant with the pressure for the three previously mentioned compounds. Strictly speaking, for such a comparison to be made the activation energies for the three reactions should be unchanged. Such is the case for the first two for which the activation energies for isomerization were found to be identical within experimental error (65.0 kcal.). The presence of the methyl group did not appear to have disturbed appreciably the energetics of the reaction.² The substitution of an ethyl for the methyl group obviously changes the aspect of the reaction to some extent as evidenced by the unexpected formation of butadiene. The activation energy for isomerization is calculated to be 61.6 ± 1.4 kcal. so it may be as high as 63 kcal. In spite of the slight differences in the energetics of the reaction, the comparison of the fall-off curves is considered to be significant. The methylcyclopropane curve has been shifted to lower pressures by 1.60 log units relative to cyclopropane, while ethylcyclopropane is shifted still further by an additional 0.95 to 1.0 log units. Therefore, the lifetime of an activated methylcyclopropane molecule is some 40 times greater than cyclopropane, and that of ethylcyclopropane, 400 times. The curve for ethylcyclopropane is for $T = 468^\circ$ while those for the other two molecules are for 490° . For the higher temperature, the ethylcyclopropane curve should be shifted only slightly to the right of the position in which it is drawn. Thus, we can conclude that intramolecular energy flow takes place in the activated molecule and that the entire molecule acts

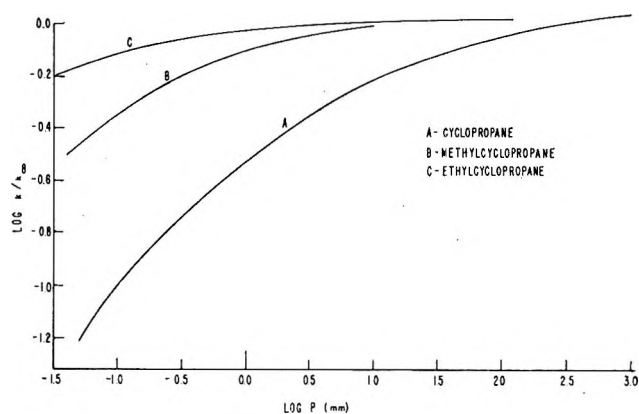


Figure 6. Comparison of falloff of first-order rate constant with pressure for cyclopropane, methylcyclopropane, and ethylcyclopropane isomerization.

as a sink for the activating energy it receives upon collision. The conclusions of Chesick³ that Slater's theory (assuming classical harmonic oscillators) cannot be reconciled with the results of the methylcyclopropane work are emphatically supported by these results, and further increase in the number of oscillators not directly attached to the ring does not favor the Slater formulation. A similar increase in lifetime of activated molecules was found by Flowers and Frey²⁶ in the isomerization of 1,1-dimethylcyclopropane. They do not list any data in their paper, but points estimated from their Figure 3 give a curve that is only slightly more to the right on the log P axis than the curve shown here for ethylcyclopropane.

Classical KRR Theory. The data for the behavior of the rate constant as a function of pressure can be compared with the theoretical predictions of the classical KRR theory by making use of the values of the Kassel integral listed by Schlag, Rabinovitch, and Schneider,²⁷ using interpolations for values of the adjustable parameters between those tabulated. Taking 5.5 Å. as the collision diameter, s , the number of classical oscillators, effective as sources or sinks of energy, was found to be between 21 and 23 for ethylcyclopropane.

An estimate of the number of oscillators contributing to a reaction can be made by comparison with cyclopropane,²⁸ in which 12 or 13 modes out of 21 are effective, and methylcyclopropane,² in which 19 modes out of 30 are found to contribute. Since ethylcyclopro-

(26) M. C. Flowers and H. M. Frey, *J. Chem. Soc.*, 1157 (1962).

(27) E. W. Schlag, B. S. Rabinovitch, and F. W. Schneider, *J. Chem. Phys.*, **32**, 1599 (1960).

(28) H. O. Pritchard, R. G. Sowden, and A. F. Trotman-Dickenson, *Proc. Roy. Soc. (London)*, **A217**, 563 (1953).

pane has 39 modes of vibration, it was estimated that 23–25 of them would contribute as “classical modes” to the isomerization if the ratio of effective to total modes was similar to that for each of the two smaller molecules. Flowers and Frey²⁶ also found that the fall-off curves for the isomerization of (isomeric) 1,1-dimethylcyclopropane could be fitted by curves calculated from the Kassel expression with $s = 23$ when the molecular diameter was taken as 5.9 Å.

Thus, it is reasonable to conclude that, although there is still some doubt as to what value of s gives the best agreement with experiment, the ratio of effective (in the classical oscillator model) to total degrees of vibration is similar to that found in the other cyclopropanes.

Marcus-Wieder Extension of RRK Theory. This modification of the classical coupled oscillator model, in which consideration is made for the contribution of quantum effects to the course of the reaction, has been quite successful in calculating the pressure dependencies of a variety of unimolecular reactions^{5,29} from the high pressure Arrhenius parameters and a vibrational analysis of the reactant molecule.

As our model we choose a “rigid” activated complex, *i.e.*, one that is defined⁵ as having all the attributes of the isomerizing or decomposing molecule except that one of the degrees of freedom is an internal translation which has replaced a vibrational or internal rotational mode of the reactant. The expression for the unimolecular rate constant as a function of pressure reduces to⁵

$$k = \alpha \frac{k_B T P_1^+}{h P_1 P_2} e^{-E_a/RT} \times \int_0^\infty \sum_{E_v^+ \leq E^+} \frac{P(E_v^+) e^{-E^+/RT}}{1 + k_a/k_2 P} d(E^+/RT) \quad (5)$$

where

$$k_a = \frac{\alpha \sigma_1}{h P \sigma_1^+} \sum_{E_v^+ \leq E^+} \frac{P(E_v^+)}{N^+(E_a + E^+ + E_0)} \quad (6)$$

The same symbols have been defined in detail elsewhere.⁵

Since the formation of 2-methyl-1-butene, which is present as only about 10% of the pentenes, requires a higher activation energy than the formation of the straight-chain pentenes, this reaction was neglected in order to simplify the calculations. The formations of 1- and 2-pentene were treated as one unimolecular reaction since they are produced with approximately the same activation energy. These assumptions are analogous to those made by Wieder for methylcyclopropane.²⁹

The vibrational assignments used for ethylcyclopropane were those of Sverdlov and Krainov.³⁰ An assignment of 237 cm.⁻¹ for the methyl torsional frequency was made by analogy with the 1-butene spectrum.³¹

The W–M theory treatment is comparatively insensitive to selection of the reaction coordinate and to moderate variations in structure and frequency of the activated complex where these give adequate correspondence with the observed high pressure frequency factor A_∞ , *i.e.*, with ΔS^* .³² The reaction coordinate was chosen to be a partial H-migration combined with ring deformation, and the activated complex has eight isomers as in methylcyclopropane.²⁸ Thus, for this activated complex, $\sigma^+ = 1$ and $\alpha = 8$.

Vibrational assignments for the activated complex were made by eliminating one of the C–H stretching frequencies (which becomes an internal translation, the reaction coordinate) and lowering some of the ring frequencies until the internal entropy of the activated complex, as calculated from this assignment, agrees with the value calculated from the observed entropy of activation and the entropy of the reactant molecule calculated from the spectroscopic vibrational assignment. The experimental entropy of activation is found to be 3.44 e.u. which leads to an experimental value for the internal entropy S_v^+ of the activated complex of 35.09 e.u. The vibrational assignment, 0.83×5 , 2.49×7 , 3.32×10 , 4.15×7 , 8.30×9 , gives a value of S_v^* (calculated) = 35.07. Here the vibrational frequencies, in kcal./mole, are grouped in multiples of the lowest frequency to facilitate computation of $P(E_v^+)$. An attempt was made to assign the frequencies as closely as possible to the geometric means of groups of the reactant frequencies. There is considerable leeway in making and grouping these assignments, and one might say that this comes close to being an “adjustable parameter” in the Wieder–Marcus treatment.

The quantity k_2 is taken to be equal to the bimolecular collision rate constant in pressure units calculated using a value of 5.5 Å. for the collision diameter of ethylcyclopropane. It is multiplied by λ , the collisional efficiency for energy transfer and deactivation. This quantity assumes the properties of an adjustable parameter; a value of about 0.20 was found to fit the

(29) G. M. Wieder, Ph.D. Thesis, Polytechnic Institute of Brooklyn, 1961.

(30) L. M. Sverdlov and E. P. Krainov, *Opt. Spectry.* (USSR), **7**, 296 (1959).

(31) N. Sheppard, *J. Chem. Phys.*, **17**, 74 (1949).

(32) F. W. Schneider and B. S. Rabinovitch, *J. Am. Chem. Soc.*, **84**, 4215 (1962).

data for cyclopropane, cyclobutane, and methylcyclopropane.⁵

The semiclassical expression⁵ used to calculate the quantity $N^*(E_a + E^+ + E_0)$ was

$$N^*(E_a + E^+ + E_0) = \frac{\sum_{n=0}^{n \leq \epsilon/b} Cn(\epsilon - nb)^{s-m-1}}{\Gamma(s-m)\pi \prod_{i=1}^m h\nu_i^*} \quad (7)$$

where the asterisk refers to the active molecule, $\epsilon = E_a + E^+ + E_0 - E_0'$, $E_0 = \sum_{i=1}^s h\nu_i/2 = 83.56$ kcal./mole, $E_0' = \sum_{i=1}^m h\nu_i^*/2 = 42.87$ kcal./mole, $s =$ number of vibrational frequencies of reactant = 39, $m =$ number of vibrational frequencies of the C-H stretching modes of reactant = 10, $b =$ geometric mean of the ten C-H stretching frequencies = 8.57 kcal./mole, and $Cn =$ number of ways of distributing n quanta among m degenerate oscillators.

The rate constant K was evaluated at various pressures by a piecewise integration of eq. 1 over the ranges, $E_1^+ = 0$ to $E_2^+ = h\nu^+$, $E_2^+ = h\nu^+$ to $E_3^+ = 2h\nu^+$, etc., where ν^+ is the lowest frequency of the activated complex corresponding here to $h\nu^+ = 0.83$ kcal./mole. In each of the above intervals in which $P(E_{\nu^+})$ is constant, $N^*(E_a + E^+ + E_0)$ was treated as a constant by using the average value of E^+ in each range. The integration was cut off at an upper limit for which the error in neglecting further terms is small; after 50 terms, the error is 0.17%. These calculations were run from a Fortran program used with an IBM 709 computer. Before the calculations were made for ethylcyclopropane, the program was checked by repeating Wieder's calculations for methylcyclopropane:

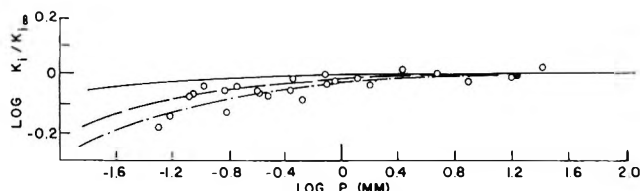


Figure 7. Comparison of falloff of first-order rate constant for isomerization of ethylcyclopropane with pressure at 467.8° with theoretical prediction of the Marcus-Wieder treatment: —, collision efficiency (λ) = 1; ---, λ = 0.09; - · - · - ·, λ = 0.04.

Figure 7 shows a plot comparing the results of the application of the Wieder-Marcus treatment to the experimental data. It is seen that a value of λ between 0.04 and 0.09 gives the best fit for the data. This would indicate that the pressure falloff is a bit greater than expected from the Marcus-Wieder model since it is probable that the collision efficiency for ethylcyclopropane should be similar to the value of 0.20 giving the best fit for cyclopropane and methylcyclopropane.⁵ The discrepancy can be explained, however, on the basis of a 1.4-kcal. error in the activation energy which, in turn, causes the values of $\log A$ to be in error by 0.40 for a given value of the rate constant. As detailed in Appendix IV of ref. 5, this will cause a shift along the $\log P$ axis of about 0.3 ($\theta = 0.3$, $\gamma = 10^{0.4}$) so that the deviation of the collision efficiency from 0.20 is within experimental error.

Acknowledgments. This work was supported by a grant from the Chemical Science Division, Air Force Office of Scientific Research, Contract AF 49(638)722, Yale University. M. L. H. acknowledges the receipt of Loomis and Monsanto Summer Fellowships from Yale University. We thank Miss Patricia Cundall and Miss Susan Flory for help in programming for the computer.

Volta Potential Studies of the Aging of Gold Surfaces¹

by R. C. Plumb and N. Thakkar

Division of Chemistry, Worcester Polytechnic Institute, Worcester, Massachusetts (Received July 7, 1964)

Volta potential measurements have demonstrated that gold surfaces may quickly become contaminated with oxides of impurity metals if a source of such impurities, either from the gold itself or from the supporting substrate, is available. It is likely that the aging of gold surfaces observed by other investigators results from the formation of these oxides. No changes in Volta potential owing to oxidation or adsorption are observed when the sources of impurities are eliminated.

Introduction

It would be expected from the instability of Au_2O with respect to decomposition into Au and Au_2O_3 and from the large positive free energy of formation of Au_2O_3 from the elements (39 kcal./mole)² that metallic gold would not be covered by oxide films. There is considerable evidence that gold surfaces prepared by cutting and polishing and etching or by evaporation under vacuum are not clean and free of oxide films. Early investigations of gas adsorption³ showed that gold prepared by reduction of C.P. gold chloride adsorbed oxygen strongly at temperatures of 130–150°. Both the quantity of oxygen taken up and the rate of adsorption increased with increasing temperature. Recently, Carpenter, Clark, Main, and Dickson,⁴ studying changes of the pressure of oxygen in contact with 883° gold surfaces of variable purity, concluded that metallic impurities in the gold are oxidized, suggesting that gold surfaces are contaminated by surface films of metallic impurities from the gold. Shishakov,⁵ from electron diffraction studies at room temperature, concluded that gold heated at 500° in oxygen at atmospheric pressure is coated with gold peroxide. Shishakov's electron diffraction patterns gave no evidence for base metal oxides, and he maintained that the work of Dickson, *et al.*, did not provide adequate evidence for impurity oxide films. In a subsequent publication, Dickson, *et al.*,⁶ stated that the electron diffraction patterns which they attributed to base metal oxides on gold surfaces were unchanged by electrochemical reduction under conditions which would decompose gold oxide so that they felt that the oxides they observed must have been from impurities.

Antes and Hackerman,⁷ in one of the earliest investigations of the behavior of the contact potential of evaporated metal films, observed changes in the Volta potential of gold of the order of several tenths of 1 v. over times of the order of 30 min. after exposure of gold films to oxygen-containing atmospheres. The potential changes were interpreted by them as resulting from physical adsorption of oxygen on the gold surfaces. Bewig and Zisman^{8a,b} have examined the problem of the stability of the contact potential of gold and platinum surfaces. They found that gold and platinum surfaces prepared by polishing, etching, and heating in a reducing flame showed aging effects when placed in a nitrogen atmosphere of 1% relative humidity. The changes in potential amounted to several tenths of 1 v. in times of 10 or more hr.⁹ Water adsorption on the electrodes could account for the changes in potential which they observed although their studies of the effects of humidity were made in the range of 10 to

(1) This research was supported in part by Atomic Energy Commission Research Contract AT(30-1) 2479.

(2) W. M. Lattimer, "Oxidation Potentials," 2nd Ed., Prentice-Hall, New York, N. Y., 1952.

(3) A. F. Benton and J. C. Elgin, *J. Am. Chem. Soc.*, **49**, 2426 (1927).

(4) L. D. Carpenter, D. E. Clark, W. H. Main, and T. Dickson, *Trans. Faraday Soc.*, **55**, 1924 (1959).

(5) M. A. Shishakov, *J. Phys. Chem.*, **64**, 1580 (1960).

(6) D. Clark, T. Dickson, and W. N. Main, *ibid.*, **65**, 1470 (1961).

(7) L. L. Antes and N. Hackerman, *J. Appl. Phys.*, **22**, 1395 (1951).

(8) (a) K. W. Bewig and W. A. Zisman, *Advances in Chemistry Series*, No. 33, American Chemical Society, Washington, D. C., 1961, p. 100; (b) K. W. Bewig and W. A. Zisman, *J. Phys. Chem.*, **67**, 130 (1963).

(9) See ref. 8a and Figure 2.

90% relative humidity. Bewig and Zisman later stated^{8b} that polished platinum surfaces gave reproducible potentials when prepared in a room ventilated with air freed of adsorbable organic vapors and having controlled temperature and humidity but they described no aging studies on the surfaces, which may have been coated with oxides when the measurements were made.¹⁰

This investigation was designed to determine whether or not oxide films form on gold at room temperature and to explore the aging of gold surfaces observed with Volta potential measurements.

Experimental

The vibrating capacitor consisted of a perforated wheel, electroplated with gold, which was rotated by a synchronous motor over a probe, causing a change in capacitance at 450 c.p.s. The signal was fed to an amplifier having an input impedance of 10^{11} ohms, beat against a standard signal of 452 c.p.s., and displayed on an oscilloscope. Balance of the potentials of the rotor and probe was achieved with a sensitivity of a few millivolts.

The vibrating capacitor was enclosed and flushed at a rate of 0.1 volume of system/min. with a specially purified atmosphere. The atmosphere consisted of dry, compressed air which had been freed of condensable vapors by passing it through a high-capacity metal trap at Dry Ice temperature and rehumidified by bubbling it through sulfuric acid. The atmosphere purification train and vibrating capacitor enclosure were constructed of glass and metal. The probe was inserted into the system and adjusted through an air lock permitting manipulation with a minimum of contamination from the room air.

The metal films were formed by evaporation from tungsten baskets (previously freed of contamination by heating under vacuum) at pressures of about 5×10^{-6} torr in a separate system. About 100 sec. elapsed between the end of the evaporations and the time when the probes were in position for measurement.

Using the same equipment under similar conditions, transients of several hundred millivolts caused by the oxidation of aluminum and copper evaporated films were observed.¹¹ The transients on aluminum and copper are reproducibly different from each other and from the behavior of gold which will be described. The facts (1) that the aging effects on different metals are reproducibly different and (2) that the aging effects on gold, as will be shown, can be varied by controlling the substrate beneath the metal film as a source of impurity show that contamination of the surfaces by adsorp-

tion of organic material from the atmosphere is not the cause of the observed changes in potential.

The probe was designed to minimize stray fields at the edges of the evaporated films so that the potentials were independent of the distance between the probe and the rotating wheel.¹¹

The potential measurements are reported as electric potentials of the probes relative to the gold-plated wheel in the absence of impressed voltage, that is, the negative of the impressed voltage required to produce a null in the signal. The gold-plated wheel was cleaned occasionally by wiping it with a clean, grease-free polishing cloth, and, providing care was taken to allow a few hours for stabilization after cleaning, it served as a suitable reference surface. Measurements on surfaces prepared by similar procedures were reproducible within 20 mv. A long-term drift of ~ 100 mv. over ~ 3 years was corrected by a thorough vigorous polishing of the wheel and a few days' aging. Relative to the wheel, an oxidized copper surface gives a potential between 0.08 and 0.09 v.

Three grades of gold—99.5 and 99.999% pure as wire^{12a} and spectroscopically pure as sponge,^{12b} containing less than 3 p.p.m. of silver and calcium and less than 1 p.p.m. of copper, iron, magnesium, and sodium—were used. Electrolytic copper and polished Lucite were used as substrates. The copper probes were ion-bombarded with argon to minimize interfacial oxide layers. Film thicknesses were determined by weighing films deposited on slips of mica.

Results

In preliminary experiments using gold films, which were several thousand Ångstroms thick, evaporated on brass probes, it was found that the Volta potential, within a few hours of evaporation, changed to a potential similar to that of an oxidized copper surface.

A series of experiments were performed which demonstrated that the surfaces of the gold films became contaminated by copper diffusing through the films from the substrates. Films of different thicknesses were deposited upon copper substrates, and the changes in Volta potential were followed for 3 days. Results of five experiments are shown in Figures 1 and 2. The Volta potentials were constant for an initial period which depended upon the film thickness. Then they

(10) In their recent work (*J. Chem. Phys.*, **68**, 1804 (1964)) published after this paper was submitted for publication, Bewig and Zisman point out that no aging is observed on gold and platinum surfaces prepared by their grinding and polishing technique.

(11) J. E. Boggio, unpublished results obtained at the Worcester Polytechnic Institute.

(12) (a) Obtained from A. D. MacKay Co., New York, N. Y.; (b) obtained from Jarrell-Ash Co.

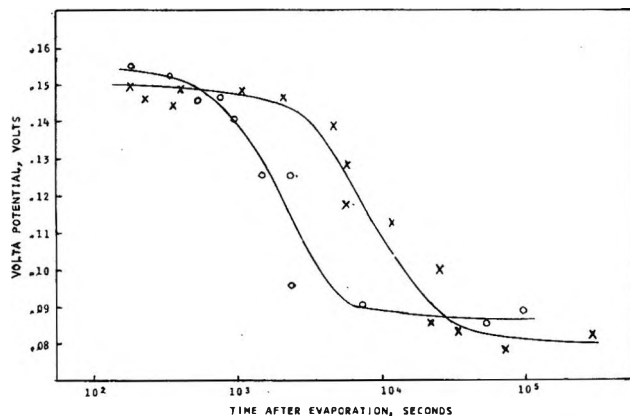


Figure 1. Aging in air of gold films evaporated from 99.5% pure gold charge onto copper substrate. Volta potentials determined relative to well-aged, electroplated gold surface: O, 500 Å.; X, 1500 Å.

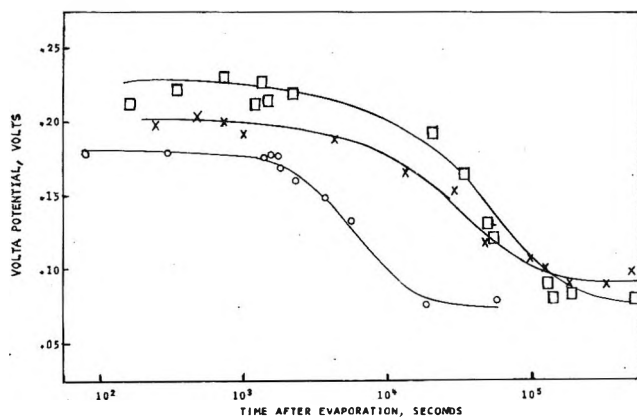


Figure 2. Aging in air of gold films evaporated from 99.999% pure gold charge onto copper substrate. Volta potentials determined relative to well-aged, electroplated gold surface: O, 950 Å.; X, 5000 Å.; □, 9500 Å.

changed, rather abruptly, to a new value. The initial values and the final values varied somewhat with the film thickness, but the time required, before the change of potential occurred, depended markedly upon the film thickness. One concludes that the principal process observed is diffusion of the copper through the gold. The final potentials are within 20 mv. of those observed with oxidized copper probes.

One may estimate the diffusion coefficient of copper in gold from these measurements. The time elapsed between the evaporation of the gold film and the completion of the transient may be interpreted as the time

required for diffusion of sufficient copper through the gold to form a monolayer of copper oxide. Assuming that no copper is present in the gold immediately after it is condensed on the copper substrate and assuming that the copper reaching the gold-air interface is immediately converted to copper oxide so that the concentration of copper at that interface is always zero, the diffusion equation was solved for the time required to produce a monolayer of copper oxide as a function of the diffusion coefficient and film thickness. From the observed times the diffusion coefficient of copper in the films of gold was determined to be about 10^{-18} cm.²/sec. The diffusion coefficient of copper in gold has been determined in the temperature range of 300–500° by Jost.¹³ Assuming the activation energy for the diffusion process at room temperature is the same as that at elevated temperatures, the diffusion coefficient calculated for room temperature from Jost's measurements is about 10^{-20} cm.²/sec. The higher diffusivity determined from our measurements probably results from the imperfect structure of the evaporated films employed in our work. From these results, one anticipates that any gold sample which contains as much as 0.01% copper and which is thick enough to contain enough copper to form a monolayer (about 10,000 Å. for 0.01% copper) will rapidly become coated with a layer of copper oxide.

Stable gold surfaces were prepared by evaporating films from spectroscopically pure gold onto polished Lucite substrates. These films exhibited no aging effects within a limit of detection of about 5 mv. during the period from 10^2 to 10^7 sec. after exposure to the atmosphere. Aging effects of films on Lucite prepared from impure gold charges were observed but not studied in detail because of the lack of knowledge of the chemical composition of the condensed films.

Conclusions

We find no evidence of aging of pure gold surfaces prepared by evaporation. If there is physical adsorption of oxygen, it takes place in times too short for us to observe. If there is formation of gold oxide films, it is completed much more rapidly than it is on aluminum. It appears that the aging of gold surfaces, which has been observed in other contact potential measurements,^{3,4} results from diffusion of impurity metals to the surfaces where they are oxidized.

(13) W. Jost, *Z. physik. Chem.*, B16, 123 (1932).

Pyrolysis of Magnesium Oxalate: Kinetics and Stoichiometry

by Peter E. Yankwich and Petros D. Zavitsanos

Noyes Laboratory of Chemistry, University of Illinois, Urbana, Illinois (Received July 8, 1964)

The stoichiometry of the pyrolytic decomposition of anhydrous magnesium oxalate has been studied over the temperature range 350–500°; the kinetics, between 404 and 472°. The stoichiometry corresponds very closely to $\text{MgC}_2\text{O}_4 = \text{MgO} + \text{CO} + \text{CO}_2$, the maximum deviation being of the order of 1%. The kinetics results indicate that there are two phases in the decomposition: (a) an initial acceleratory period ($\alpha < \text{ca. } 0.3$) during which reaction is due primarily to the growth of nuclei formed during the dehydration of the $\text{MgC}_2\text{O}_4 \cdot 2\text{H}_2\text{O}$ from which the anhydrous starting material is prepared and (b) a decay period ($\alpha > \text{ca. } 0.5$) in which similar elementary processes operate. If random nucleation contributes significantly to the rate, it does so apparently only in phase a.

Introduction

In this paper we report the results of experiments on the kinetics and stoichiometry of the thermal decomposition of anhydrous magnesium oxalate. This work was undertaken as an extension of earlier investigations of the pyrolyses of lead,¹ zinc,² and manganous³ oxalates.

Several studies,^{4–8} usually involving thermogravimetry, have shown that the principal reaction occurring during the pyrolysis of magnesium oxalate is $\text{MgC}_2\text{O}_4(\text{s}) = \text{MgO}(\text{s}) + \text{CO}(\text{g}) + \text{CO}_2(\text{g})$, but insufficient data are given to define the limits of this stoichiometry. Reports on the kinetics of the decomposition^{9–11} are fragmentary. The experiments reported here were undertaken to gain information of potential utility in the interpretation of the carbon kinetic isotope effects accompanying the pyrolysis.

Experimental

Preparation of Magnesium Oxalate Dihydrate. Aqueous solutions of equal volume of 0.50 M magnesium chloride and of 0.55 M sodium oxalate (reagent grade chemicals in deionized water) were brought to their boiling points, and the former was added rapidly to the latter. The mixture was stirred occasionally as it cooled to room temperature. The crystals of the dihydrate formed in this way are fine (particle size 12–16 μ) and rather uniform in appearance. The precipitate was washed several times with distilled water, air dried for 2–3 hr. at 110°, and stored over magnesium perchlorate in a desiccator.

Apparatus and Procedure. The apparatus and procedures employed in the kinetics and stoichiometry experiments have been described in detail in an earlier publication from this laboratory.² In this work, the sample size was approximately 0.25 mmole; the product gases were separated and trapped during the stoichiometry runs but remained in contact with the solid phases during the kinetics runs. Check comparisons showed no effect of gas–solid contact on the gaseous product composition.

It is important to note that the anhydrous magnesium oxalate used in each run was prepared *in vacuo* from the dihydrate in the initial part of each experi-

- (1) P. E. Yankwich and J. L. Copeland, *J. Am. Chem. Soc.*, **79**, 2081 (1957).
- (2) P. E. Yankwich and P. D. Zavitsanos, *J. Phys. Chem.*, **68**, 457 (1964).
- (3) P. E. Yankwich and P. D. Zavitsanos, *Pure Appl. Chem.*, **8**, 287 (1964).
- (4) T. Duval and C. Duval, *Anal. Chim. Acta*, **2**, 45 (1948). See also C. Duval, "Inorganic Thermogravimetric Analysis," Elsevier Publishing Co., New York, N. Y., 1953, pp. 101, 102.
- (5) J. Robin, *Bull. soc. chim. France*, 1078 (1953).
- (6) Y. A. Ugai, *Zh. Obshch. Khim.*, **24**, 1315 (1954).
- (7) L. Erdey and F. Paulik, *Magy. Tud. Akad. Kem. Tud. Oszt. Kozlemen.*, **5**, 461 (1955).
- (8) H. G. Wiedemann and D. Nehring, *Z. anorg. allgem. Chem.*, **304**, 137 (1960).
- (9) V. Ponec and V. Danes, *Collection Czech. Chem. Commun.*, **25**, 17 (1960).
- (10) V. Danes, *Probl. Kinetiki i Kataliza, Akad. Nauk SSSR*, **4**, 450 (1960).
- (11) G. M. Zhabrova and V. A. Gordeeva, *Kinetika i Kataliz, Akad. Nauk SSSR, Sb. Statei*, **31** (1960).

ment. This procedural feature was adopted to avoid handling and "atmosphere" effects, but it complicates evaluation of the quality of our results on the basis of "reproducibility." However, the general characteristics of a solid decomposition are often apparent from examination of the results obtained in a single experiment, and the quality of the kinetic activation parameters (being based on data obtained at several temperatures) is not necessarily dependent upon a demonstration of reproducibility of α - t curves at a single temperature, α being the degree of decomposition and t the time.

Results

Stoichiometry. Gaseous products were collected separately in seven runs, four at 400° and one each at 350, 415, and 500°. With manometric error included, the ratios (CO₂/CO), temperature-ascending, were found to be 1.02 ± 0.01, 1.02 ± 0.01, 0.99 ± 0.01, and 1.02 ± 0.01. In each case, the solid product was soluble in dilute aqueous hydrochloric acid and appeared to consist of pure magnesium oxide. The stoichiometry of the decomposition is very closely that indicated above—the mean deviation being 1 ± 1% (compared with 4 ± 3% for manganous oxalate³ and 7 ± 1% for the zinc salt²).

Kinetics. The α - t data were obtained in single, consecutive kinetics runs at several temperatures—451, 472, 458, 452, 469, 404, and 437° (in that order); the first and fourth runs may be regarded as replicates. The α - t data pairs used in subsequent calculations were obtained from a smooth curve through the original data; typically, 85% of the points lay on the curve, none were deviant by more than twice the manometric error, and none of the conclusions reached below are affected if the calculations are based only on the original data pairs. Values of $d\alpha/dt$ were taken from the curves by means of a prismatic tangent meter.

Except for the runs at 404 and 437° (which exhibit no acceleratory phase), the α - t curves are sigmoid in shape, which is indicative of an initial acceleratory phase in the decomposition and a final deceleratory phase. Where it is observed that the acceleratory phase is rather brief, inflection occurring after 7–12% decomposition.

Four functional representations of the rate results were selected for trial from numerous possibilities¹²: (i) a "power of t " relation, expected to describe the acceleratory phase of the decomposition

$$\alpha = (k_m t)^m \quad (1)$$

(ii) the "contracting-sphere" equation¹³

$$1 - (1 - \alpha)^{1/3} = (k/a)_{CS} t \quad (2)$$

expected to hold in the deceleratory phase; (iii) a rate law of order n

$$\frac{d\alpha}{dt} = k_n (1 - \alpha)^n \quad (3)$$

applicable also to the deceleratory phase; (iv) the Avrami equation¹⁴ in asymptotic form

$$-\ln(1 - \alpha) = (k_A t)^{n_A} \quad (4)$$

which might obtain for $\alpha > 0.5$.

The main part of Table I is a listing of the kinetic parameters obtained (by graphical means) for these four relations, together with the ranges of α (r_α) over which they obtain; the first line of the table proper shows the α of the first nonzero data point (α_F) and of the last point before "infinite" time (α_L). In Table II there are collected the values of the Arrhenius-like parameters E and A associated with the several rate constants in Table I.

Discussion

Acceleratory Phase. A simple power law seems to fit the data for 0.05 < α < 0.2. In three runs where observations were made for $\alpha < 0.05$, these early points do not lie on the linear portion of a plot of $\ln \alpha$ vs. $\ln t$. Further, there is no system to the values of m observed at the several temperatures of the experiments. The fact that the highest m is not associated with the highest temperature indicates that sluggish establishment of thermal equilibrium is not responsible for the seemingly arbitrary m values. (Also, in this regard, it is worthy of note that, in view of the separate dehydration of the samples, the correspondence of the various kinetic parameter values, except m for the runs at 451 and 452°, is quite good.) As in the cases of the manganous and zinc oxalate decompositions, the m observed here may be a mean value arising in the parallel operation of two or more modes of nucleation.^{15a,b} The indefinite temperature dependence of

(12) In reply to a referee ref. 14, *vide infra*, describes four families of equations which preliminary examination showed were less closely applicable to the results reported here than the representations cited; they are equations which account for a "slow growth period," exponential rate laws, relations based on autocatalytic nucleation and/or nucleus growth, and equations which account for overlapping and ingestion of growing nuclei.

(13) k (cm. sec.⁻¹) is the linear rate of inward motion of the reaction interface; a is the initial mean radius of the spherical particles assumed to comprise the decomposing solid.

(14) M. Avrami, *J. Chem. Phys.*, 9, 177 (1941).

(15) (a) P. W. M. Jacobs and F. C. Tompkins in "Chemistry of the Solid State," W. E. Garner, Ed., Academic Press, Inc., New York, N. Y., 1955, Chapter 7; (b) C. Bagdassarian, *Acta Physicochim. URSS*, 20, 441 (1945).

Table I: MgC₂O₄ Decomposition Kinetics Parameters and Their Ranges of Validity

Run temp., °C.	404	437	451	452	458	469	472
$\alpha_{F-\alpha_L}$	0.02-0.82	0.06-0.75	0.03-0.95	0.05-0.98	0.04-0.90	0.07-0.93	0.28-0.99
(i) Acceleratory phase							
m	0.69	1.05	1.31	1.90	1.89	1.42	...
k_m , sec. ⁻¹	1.24×10^{-5}	2.57×10^{-4}	5.77×10^{-4}	6.90×10^{-4}	8.29×10^{-4}	1.27×10^{-3}	...
τ_α	0.05-0.33	0.06-0.21	0.10-0.25	0.05-0.19	0.10-0.22	0.07-0.33	...
(ii) Contracting-sphere equation							
$(k/a)_{CS}$, sec. ⁻¹	4.44×10^{-6}	8.90×10^{-6}	1.84×10^{-4}	1.57×10^{-4}	1.75×10^{-4}	4.47×10^{-4}	5.49×10^{-4}
	2.85×10^{-6}	3.13×10^{-5}	1.21×10^{-4}	8.57×10^{-5}	1.18×10^{-4}	2.14×10^{-4}	2.95×10^{-4}
	1.95×10^{-6}				7.37×10^{-6}		
τ_α	0.28-0.47	0.06-0.44	0.10-0.48	0.05-0.57	0.22-0.58	0.07-0.67	0.28-0.75
	0.47-0.79	0.61- α_L	0.48-0.76	0.64-0.85	0.68-0.82	0.82-0.91	0.80-0.98
	0.75- α_L				0.86- α_L		
(iii) Deceleratory phase							
n	1.33	1.73	1.08	1.00	1.11	1.25	1.36
k_1 , sec. ⁻¹	1.13×10^{-6}	1.35×10^{-4}	4.28×10^{-4}	4.43×10^{-4}	5.96×10^{-4}	1.34×10^{-3}	2.08×10^{-3}
τ_α	0.47- α_L	0.65- α_L	0.68- α_L	0.50-0.85	0.50-0.86	0.67-0.91	0.28-0.98
(iv) Avrami equation							
n_A	0.73	0.79	0.92	1.00	1.00	1.00	1.00
k_A , sec. ⁻¹	1.66×10^{-4}	2.41×10^{-4}	5.34×10^{-4}	4.44×10^{-4}	5.61×10^{-4}	1.38×10^{-3}	1.69×10^{-3}
τ_α	0.02- α_L	0.39- α_L	0.48- α_L	0.32-0.90	0.32- α_L	0.46- α_L	0.68-0.93

Table II: Arrhenius-Like Parameters Associated with X

X	E, kcal. mole ⁻¹	A, sec. ⁻¹
k_m	70 ± 6	9.1×10^{17}
$(k/a)_{CS}$	78 ± 5	2.9×10^{19}
k_1	75 ± 3	1.6×10^{19}
k_A	60 ± 3	5.0×10^{14}

m and the relative shortness of the τ_α leave us without insight into the details.

Deceleratory Phase. Comparison of parts iii and iv of Table I shows that the Avrami exponent n_A is unity for most of the runs, equivalent to a first-order law

$$-\ln(1 - \alpha) = k_1 t + \text{constant} \quad (5)$$

However, k_1 and k_A differ significantly. Except, perhaps, for the very last part of the decomposition, a first-order law is a satisfactory representation of the rate for $\alpha > 0.5$. Random nucleation¹⁶ and uniform growth of randomly situated "original" nuclei¹⁷ both lead to first-order kinetics.

The contracting-sphere equation apparently applies, separately, to early, middle, and late phases of the decomposition. Equation 2 ordinarily is not found to describe data below $\alpha = 0.3$; typically, it holds for $0.3 < \alpha < 0.9$.^{18,19} The longest ranges of fit to eq. 2 occur near the start of the reaction, as shown in part

ii of Table I. The apparent activation energies associated with the early, middle, and late phase representations are all the same, within experimental error; the pre-exponential factor shown in Table II is that for the middle phase.

Zhabrova and Gordeeva¹¹ suggest the applicability of the contracting-sphere equation to the decomposition kinetics of magnesium carbonate, hydroxide, and oxalate but point to the indistinguishability of fit to it and to a first-order rate equation in the range $0.2 < \alpha < 0.7$. Both the contracting-sphere and first-order laws arise from the growth of established nuclei, provided there is no random nucleation during the reaction.^{15a,17,20} The fit of our results to both eq. 2 and 5 at high α suggests relative unimportance of random nucleation—a difference from the zinc and manganous oxalate pyrolyses.

Apparent Activation Energy and Pre-exponential Factor. Some of the rate constants in eq. 1-5 are those associated with elementary processes; others are composite. Where $m \neq 1$, k_m is related to both k_1' , the probability (sec.⁻¹) for one of the events leading to the

(16) K. L. Mampel, *Z. physik. Chem.*, **A187**, 43, 235 (1940).

(17) S. Z. Roginskii and O. M. Todes, *Izv. Akad. Nauk SSSR, Otd. Khim. Nauk*, 475(1940).

(18) S. J. Gregg and R. I. Razouk, *J. Chem. Soc.*, S36 (1949).

(19) W. D. Spencer and B. Topley, *ibid.*, 2633 (1929).

(20) O. M. Todes, *Zh. Fiz. Khim.*, **14**, 1224 (1940).

formation of a growth nucleus, and k_2 , the (linear) rate of growth of such a nucleus. It would be difficult to interpret the pre-exponential factor in k_m , but the related activation energy is a linear combination of E_1' and E_2 . The k in $(k/a)_{CS}$ is related to k_2 ; since we do not have measurements of a (which is a mean effective quantity) for the *anhydrous* oxalate, we can interpret the E derived from the temperature dependence of $(k/a)_{CS}$ but not the A . If random nucleation does not occur (and we believe it does not, here), the $k_n = k_1$ of eq. 3 and 5 is or is related to k_2 but is k_1' if random nucleation does occur; in either case, E is well defined, but A is only so in the latter. In the asymptotic form of the Avrami equation, k_A is equivalent to k_2 when nucleus growth is three-dimensional and $n_A = 3$; where n_A is smaller, the equivalence is probable, especially if the data for low α are excluded.

A striking feature of the data collected in Table II is the similarity among the calculated activation energies (not including that derived from k_A), in spite of the varying makeup of the k values with which they are associated. The values for the pre-exponential factors are similar also (again excepting that derived from k_A) and are very high. If our surmise concerning the relative unimportance of random nucleation is correct, the similarity of the activation parameters arises because all actually pertain to k_2 .

This similarity of kinetic parameters was noted earlier for the decompositions of zinc and manganous oxalates. In Table III are collected average values of these parameters. The span of the values of $\log A$

points to significant differences in the nature of the nucleation and growth processes among the three compounds. The values of E and $\log A$ exhibit approximate inverse correlation to the squares of the metal ion radii—whatever that may mean.

Table III: Average Values of Kinetic Parameters

Pyrolyte	E , kcal. mole ⁻¹	$\log (A, \text{sec.}^{-1})$
MgC ₂ O ₄ ^a	71 ± 5	17.8 ± 1.1
MnC ₂ O ₄ ^b	43 ± 3	11.1 ± 0.2
ZnC ₂ O ₄	50 ± 3	14.6 ± 0.5

^a Parameters from k_A included for comparability. ^b Parameters of the Prout-Tompkins constant excluded.

Conclusions

The stoichiometry of the magnesium oxalate pyrolysis *in vacuo* differs by 1% or less from $\text{MgC}_2\text{O}_4 = \text{MgO} + \text{CO} + \text{CO}_2$. As with zinc and manganous oxalates, the deviation is in the direction of excess carbon dioxide in comparison with monoxide.

Our kinetics results indicate that random nucleation processes are important only in the very early phases of the decomposition, if at all; apparently, the reaction proceeds primarily through the growth of nuclei formed during dehydration of the magnesium oxalate dihydrate.

Acknowledgment. This research was supported by the U. S. Atomic Energy Commission.

Simultaneous, Independent Hydrogen-Bonding Equilibria and Self-Association in Some Halomethanes and Haloethanes

by A. L. McClellan and S. W. Nicksic

California Research Corporation, Richmond Laboratory, Richmond, California (Received July 20, 1964)

The n.m.r. shifts of 18 chloro- and bromomethanes and -ethanes and 8 related compounds have been measured for the pure compounds and for 5% solutions in dimethyl sulfoxide, cyclohexane, and CCl_4 . A more extensive study of some 1,1,2-trihaloethanes in dimethyl sulfoxide is reported. The various results can be summarized by three general statements. (a) Hydrogen bonding between 1,1,2-trihaloethanes and dimethyl sulfoxide can be adequately accounted for by assuming that each type of hydrogen acts independently to form a 1:1 complex with the sulfoxide. (b) All the halogenated compounds are self-associated to about the same extent when grouped according to the number of protons per carbon atom. (c) The hydrogen-bond shift for the various compounds in dimethyl sulfoxide solution is roughly proportional to the diamagnetic shielding, as measured by their resonance frequencies in cyclohexane solution.

Introduction

Following our study of chloroform-dimethyl sulfoxide,¹ we looked at all the chloromethanes and -ethanes, a number of the bromo analogs, and a few similar compounds, to see if there were any unusual effects. In particular, we were looking for large self-associations or strong interactions with proton acceptors. All the observed data are presented first; then the case of independent equilibria is considered.

Experimental

The same general procedure and equipment were used as in our previous work.¹ The irradiating frequency was 60 Mc.p.s. In these present experiments, the reagents were generally Eastman White Label quality used without further purification. Tetramethylsilane was used as an internal standard so magnetic susceptibility correction was not needed.

Results

Table I gives the results. Figure 1 shows a plot of the chemical shift for these halogenated hydrocarbons in cyclohexane (considered inert) vs. the hydrogen-bond shift in dimethyl sulfoxide. The line in the figure is the least-squares best fit for compounds 1-20 and 25. Its equation is

$$Y = A + 0.23X$$

where Y = hydrogen-bonding shift = resonance in dimethyl sulfoxide minus the resonance in cyclohexane, in c.p.s.; X = resonance in cyclohexane, in c.p.s.; $A = -27.8$ c.p.s.

There is a rough correlation between these variables. Those resonances which occur farthest from the tetramethylsilane reference point show the largest hydrogen-bond shift. One interpretation is that these compounds have an electron configuration in which the electrons around the proton are considerably displaced. As the dimethyl sulfoxide approaches such a "polarized" proton, it then exerts a large effect on it, and a large hydrogen-bonding shift is observed.

The third and eighth columns in Table I show that, although the proton resonances occur over a wide region (120-440 c.p.s.), the shift on dilution in cyclohexane is roughly the same for all. The data in Figure 2, although rather widely scattered, suggest a trend for both the self-association and hydrogen-bonding shifts to decrease as the number of protons per carbon goes from 1 to 3. This is a rough way to allow for the successively greater activation of the protons as addi-

(1) A. L. McClellan, S. W. Nicksic, and J. C. Guffy, *J. Mol. Spectry.*, **11**, 340 (1963).

Table I: N.m.r. Shifts (from Tetramethylsilane) at $27 \pm 2^\circ$

Compd. no.	Compound	Proton resonance, c.p.s.				Shift, c.p.s.		
		Pure	95% DMSO	95% C ₆ H ₁₂	95% CCl ₄	DMSO—C ₆ H ₁₂	Pure—C ₆ H ₁₂	Pure—CCl ₄
1	Chloromethane	^a	183	172	186	11
2	Dichloromethane	321	344.5	309.1	318.2	35.4	11.9	3
3	Chloroform	436	498	426	436	72.0	10.0	0
4a	Chloroethane, H _a ^b	86	85	83	90	2	3	-4
4b	Chloroethane, H _b ^c	208	220	205	211	15	3	-3
5a	1,1-Dichloroethane, H _a	122.5	120.8	118.3	134.2	2.5	4.2 ^d	-12
5b	1,1-Dichloroethane, H _b	357	385.8	345.6	352.2	40.2	11.4	5
6	1,2-Dichloroethane	226	234.2	214.5	221.7	19.7	11.5	4
7	1,1,1-Trichloroethane	163.8	171	158.3	165	12.7	5.5 ^d	-1
8a	1,1,2-Trichloroethane, H _a	239.0	253.2	228.9	236	24.3	10.1	3
8b	1,1,2-Trichloroethane, H _b	350.6	394	336.8	344	57.2	13.8	7
9	1,1,1,2-Tetrachloroethane	258.5	287.5	249.5	256.5	38	9.0	2
10	1,1,2,2-Tetrachloroethane	360	416.5	347	355.5	69.5	13	5
11	Pentachloroethane	367	449.5	358.5	367	91	8.5	0
12	1,1,2-Trichloroethylene	386	440	380	388	60	6	-2
13	Bromochloromethane	314	332	301	309	31	13	5
14	Dibromomethane	300	324	288	297	36	12	3
15	Bromoform	409	462	404	410	58	5	-1
16a	Bromoethane, H _a	96	103	96	100	7	0	-4
16b	Bromoethane, H _b	205	211	196	205	15	9	0
17	1,2-Dibromoethane	221	228	210	216	18	11	5
18	1,1,2,2-Tetrabromoethane	368	414	356	363	58	12	5
19	1-Bromo-2-chloroethylene	223	232	212	221	20	11	2
20	1,2-Dibromoethylene	409	438	391	409	47	18	0
21a	1,2-Dibromopropane, CH ₃	108	104	112	110	-8	-4	-2
21b	1,2-Dibromopropane, CH ₂	222	229	213	222	16	9	0
21c	1,2-Dibromopropane, CH	250	270	242	246	8	28	4
22a	1,3-Dibromopropane ^g	140.5	138	142	142	-4	-1.5	-1
22b	1,3-Dibromopropane ^f	213	218	207	212.5	11	6	0
23	Dibromoacetonitrile	355	418 ^g	342	349	76	13	6
24	Dichloroacetonitrile	385	446 ^g
25a	1,1,2-Tribromoethane, H _a	249	259	238	245	21	11	4
25b	1,1,2-Tribromoethane, H _b	346	384	333	339	51	13	7
26a	1-Chloro-2-phenylethane ^h	167	181.5	177	181	4.5	-10	-14
26b	1-Chloro-2-phenylethane ^f	204	231	212.5	217	18.5	-8.5	-13

^a Gas at room temperature. ^b H_a refers to the proton on the carbon having more protons. ^c H_b refers to the proton on the carbon having fewer protons. ^d Methyl protons. ^e Proton on carbon 2. ^f Proton nearer halogen atom. ^g 10% in DMSO. ^h Proton nearer phenyl group.

tional electronegative substituents are added to the molecule. The same trend is observed for bromo and chloro derivatives.

Such curves indicate that chloroform (compound 3) is not particularly outstanding as a proton donor. A similar conclusion was reached by Allerhand² for infrared studies of C-H stretching frequency. For example, the relative hydrogen-bonding shifts for CHCl₃, Cl₂CH-CN, and Br₂CHCN were 29, 66, 80 cm.⁻¹ when the compounds were very much diluted in dimethyl sulfoxide-*d*₆. N.m.r. showed a smaller variation of hydrogen-bond shifts, namely 72, 61, 76 c.p.s. in dimethyl sulfoxide.

The data of Table I allow a further comparison of

the differing effects of dilution in CCl₄ or cyclohexane. We might expect cyclohexane to be inert, merely breaking up association by dilution, while CCl₄ would offer chlorine atoms for hydrogen bonding similar to the self-association present in the pure compound. If these expectations are realized, the shift on dilution with cyclohexane should be larger than that in CCl₄. A comparison of the last two columns in Table I shows that usually such is the case. Occasionally, a negative value of shift is found. According to the interpretation above, a negative number means that bonding to the added solvent is greater than self-association.

(2) A. Allerhand, Dissertation, Princeton University, 1963, p. 94.

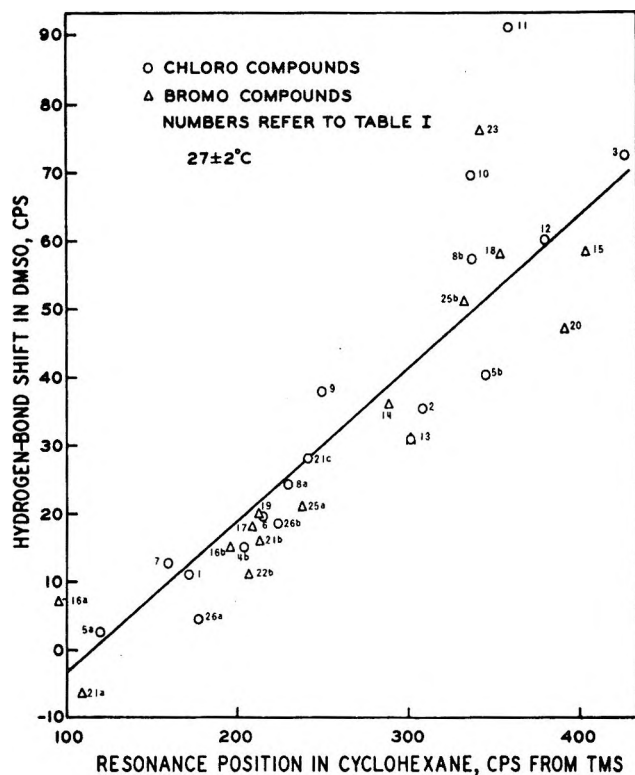


Figure 1. Hydrogen-bond shift vs. resonance position in cyclohexane.

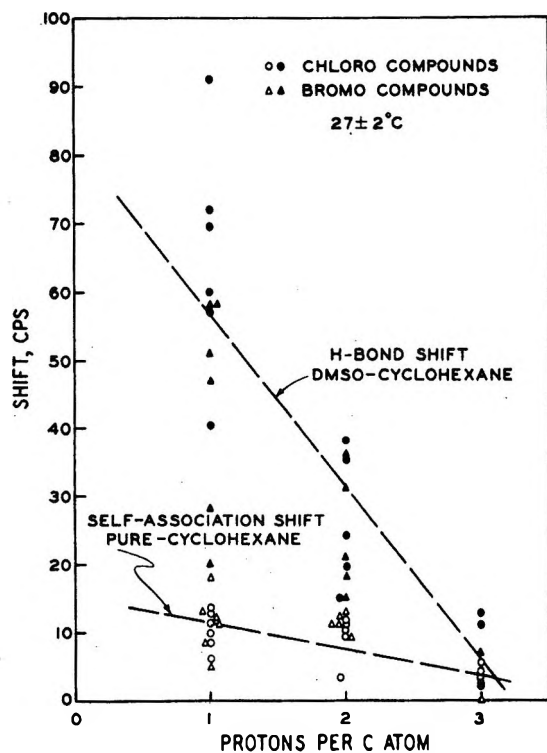


Figure 2. Hydrogen-bonding and self-association shifts vs. protons per carbon atom.

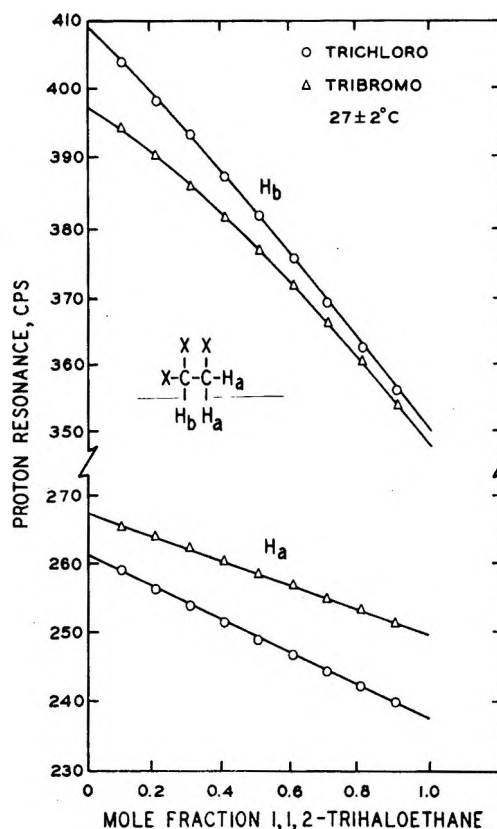


Figure 3. Hydrogen-bonding shifts for 1,1,2-trihaloethane protons in dimethyl sulfoxide.

Compounds with Two Types of Protons. Chloro-, 1,1-dichloro-, and 1,1,2-trichloroethane and the corresponding bromo compounds each have two types of protons with different electronic environments, and the n.m.r. spectra reflect this by showing two proton resonances. The dilution shifts of the two different protons in cyclohexane still fit the trend shown in Figure 2. A similar effect on hydrogen bonding is also noted. The results of a more extensive study of 1,1,2-trihaloethane-dimethyl sulfoxide mixtures at room temperature are shown as the circles and triangles in Figure 3. The data are corrected for self-association as in our previous work.¹ The lines represent trends calculated as subsequently discussed.

Preliminary calculations were based on the assumption, suggested by data of the type in Figure 2, that the H_b proton would form the stronger hydrogen bond. The equilibrium between sulfoxide and the H_a proton is imagined as somewhat weaker. The resulting equations, derived as outlined earlier,¹ were complicated and did not give the observed dependence of n.m.r. resonance position upon concentration. After considering and rejecting various schemes, involving as many as five equilibria, we found that the observed

shifts can be adequately explained by assuming that there are two complexing equilibria each forming a 1:1 complex. If we symbolize the haloethane as H_aCH_b to emphasize the two different protons and dimethyl sulfoxide as S, then we can write



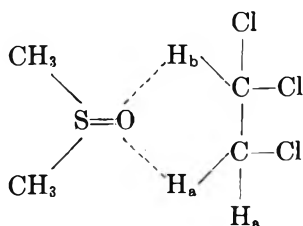
With the further assumption that these equilibria are satisfied *independently*, we can calculate shifts following our previous work.¹ The equilibrium constants used to make these calculations, as well as some on 1,1,2,2-tetrachloroethane, are given in Table II for which ν -values were found by the method of Huggins, Pimentel, and Shoolery.³

Table II: Summary of Equilibrium Calculations at $27 \pm 2^\circ$

	ν_{free} , c.p.s.	ν_{bonded} , c.p.s.	10^2k , M^{-1}
Chloroform (from ref. 1)	426	516	30
1,1,2-Trichloroethane, H_a	238	261.5	1.4
1,1,2-Trichloroethane, H_b	346.5	409	1.4
1,1,2-Tribromoethane, H_a	250.1	272.2	5.6
1,1,2-Tribromoethane, H_b	347.4	397.8	5.6
1,1,2,2-Tetrachloroethane	360	416	5.6

We see the same variation in k as shown for hydrogen-bonding shift in Figure 1. Chloroform forms a considerably stronger hydrogen bond than the haloethanes. The uncertainty of the k values is moderate, being perhaps $\pm 1 M^{-1}$.

There still remains the intuitive feeling that the two types of proton should have different hydrogen-bonding equilibrium constants. Why is this not found in the calculations? One answer may be simply that the bonds are so weak that small differences are not detected by the technique used. In addition, the data and calculations do not exclude another possibility. That is that the two different protons form hydrogen bonds at the same time to the oxygen atom of the sulfoxide group. Such a complex could be shown diagrammatically as



For this complex, we would expect weak bonding since the $C-H \cdots O$ angle is high (about 100°). Pimentel and McClellan⁴ discuss the problem of bent hydrogen-bond configurations, and, for the very simple view adopted there, bending is calculated to have little effect. As they point out, no great weight can be attached to their computation, but it is perhaps indicative that such complexing is possible. In a similar way, we can argue that the finding of the same k value for H_a and H_b in the same molecule is compatible with, but not a compelling argument for, simultaneous formation of two hydrogen bonds.

Nuclear magnetic resonance spectra were recorded for the 1,1,2-trichloroethane-dimethyl sulfoxide mixtures at 2.5° , the lowest temperature which did not freeze some of the samples. The data for H_a shift lies essentially on the line observed at 27° (Figure 3). For H_b the points are higher by about 2 c.p.s., an amount just outside experimental error. The trend of the H_b line is the same as at 27° so we cannot detect a change in the k values. This behavior would be expected for the cyclic 1:1 complex, lending some additional support for this proposed structure. N.m.r. spectra were not measured at higher temperatures because the k values, which are already small at room temperature, would be still smaller, and differences could not be detected.

Perhaps it is best to say that chemical intuition suggests the two types of protons should have different equilibrium constants, but our observations are fit more easily by the assumption that they do not. The difference may be too small for observation, or a 1:1 complex with two hydrogen bonds from the same haloethane molecule may somehow "average out" the properties of the two protons.

Summary

We have observed an example in which two types of protons in the same molecules form hydrogen bonds independently in the same mixtures of 1,1,2-trihaloethane-dimethyl sulfoxide. We have noted hydrogen-bond shifts of 26 halogenated hydrocarbons in dimethyl sulfoxide, cyclohexane, and CCl_4 and have shown a relation between self-association shifts and the number of protons per carbon atom.

Acknowledgments. We appreciate the thoughtful discussions with Dr. L. L. Ferstandig and the permission of California Research Corp. to publish this work.

(3) C. M. Huggins, G. C. Pimentel, and J. N. Shoolery, *J. Chem. Phys.*, **23**, 1244 (1955).

(4) G. C. Pimentel and A. L. McClellan, "The Hydrogen Bond," W. H. Freeman and Co., San Francisco, Calif., 1960, p. 243.

The Thermal Decomposition of Cadmium Hydroxide

by M. J. D. Low and A. M. Kamel

School of Chemistry, Rutgers, The State University, New Brunswick, New Jersey (Received July 21, 1964)

Differential thermal and thermogravimetric analyses of $\text{CdO}\cdot 1.65\text{H}_2\text{O}$ showed that four processes were involved in the thermal decomposition. Isothermal weight loss determinations showed that, at 300° and above, the decomposition to $\text{CdO}_{0.80}$ was continuous. The composition of intermediates is uncertain because of the rapid and continuous reaction. Some oxide was formed as low as 265° . The decomposition was accompanied by marked textural changes of the solid. Surface areas of pure hydroxide as well as samples containing 1 atom % Li^+ , Zn^{+2} , Mg^{+2} , or Al^{+3} were measured after heating *in vacuo* for various times at temperatures from 150 to 500° . Al^{+3} -addition inhibited and Li^+ -addition enhanced oxide sintering up to 400° , through the destruction or creation of oxygen vacancies. At 450 and 500° both Al^{+3} and Li^+ additions increased sintering, suggesting that a cation vacancy mechanism became dominant.

During a study of the surface properties of CdO , it became necessary to prepare well-defined CdO samples by various means, including the thermal decomposition of the hydroxide. Although some work has been reported on the isobaric and isothermal dehydration of cadmium hydroxide,^{1,2} the information available was incomplete. Additional work was required and, consequently, the thermal decomposition of doped and undoped cadmium hydroxides was studied.

Experimental Details

Cadmium hydroxide was precipitated from the nitrate with ammonia,³ thoroughly washed and dried at 100° in air. A portion of the powder was mixed with enough LiOH , $\text{Zn}(\text{NO}_3)_2$, $\text{Mg}(\text{NO}_3)_2$, or $\text{Al}(\text{NO}_3)_3$ solution to yield a stiff paste, which was dried at 110° . The amounts of solutions and their concentrations were sufficient to result in hydroxide samples that, when converted to CdO , would contain 1 atom % of foreign cations. Differential thermal analyses (d.t.a.) were made at linear heating rates of $10^\circ/\text{min.}$, using Pt-10% Pt-Rh thermocouples. A slowly moving stream of purified nitrogen passed over the nickel detector block. Thermogravimetric analysis (t.g.a.) was made in air with a modified Ainsworth automatic recording balance, at linear rates of $4.6^\circ/\text{min.}$ from room temperature to 500° . Isothermal weight loss (i.w.l.) was measured in air with a modified analytical balance. Nitrogen adsorption isotherms and B.E.T. surface

areas⁴ were obtained with an apparatus of conventional design.⁵ The initial degassing of each sample was carried out overnight at room temperature because of the instability of the hydroxide. Surface areas were then measured for a sequence of heat treatments of various durations *in vacuo* at each temperature. The surface areas, each calculated from data at six relative pressures, are given in $\text{m}^2/\text{g.}$ of starting material.

Experiments and Results

D.t.a. Experiments. These experiments are described in somewhat greater detail than would normally be warranted, because electrical disturbances of the instrument brought about by CdO can be used to deduce information about the extent of the decomposition. In studying the hydroxide-oxide transformation, it seemed reasonable to use CdO as a reference substance. A sample of Baker Company C.P. material which had been heated in air to 300° for 2 hr., and which

(1) G. F. Hüttig and R. Mytyzek, *Z. anorg. allgem. Chem.*, **190**, 353 (1930).

(2) G. F. Hüttig, "Hydroxyde und Oxyhydrate," R. Fricke and G. F. Hüttig, Ed., Akademische Verlagsgesellschaft m.b.H., Leipzig, 1937, p. 413 ff.

(3) A. Cimino and M. Marezio, *J. Phys. Chem. Solids*, **17**, 57 (1960).

(4) S. Brunauer, P. H. Emmett, and E. Teller, *J. Am. Chem. Soc.*, **60**, 309 (1938).

(5) P. Faeth, "Adsorption and Vacuum Technique." Report No. 66100-Z-X, University of Michigan, 1962.

was the material it had been intended to use as reference, was subjected to d.t.a. using a γ -alumina reference. Near 200° a voltage indicating an endothermic process was produced that rapidly increased with increasing temperature. Cadmium hydroxide was examined in another experiment using alumina as the reference; in addition to endothermic peaks of dehydration processes, a large and increasingly endothermic signal began near 400° . On holding the temperature constant at 600° for 107 min., the signal remained at a constant value, then progressively became smaller as the temperature was decreased, and vanished near 350° . Figure 1 shows the results of another experiment in which the positions of hydroxide and alumina were reversed. The decomposition processes appeared as exothermic peaks. Near 265° the signal indicated an endothermic process. After keeping the temperature constant near 300° for 30 min., the temperature was decreased, and the signal declined.

The results of these and similar experiments suggest that the large endothermic signal appearing in the presence of the oxide was an artifact produced by electrical "leakage" between thermocouples and the detector block permitted by the relatively high electrical conductivity of CdO. More important is the deduction that CdO was formed at temperatures in the vicinity of 265° . This is in agreement with the observation that the white hydroxide turned brown within a few minutes at 300° .

Figure 2 shows the details of typical d.t.a. curves. All of the curves pertain to the Mg-doped sample, and were obtained under different conditions of packing of the sample into the heater block. The peak near 110° is ascribed to the desorption of water. An alumina reference was used with these and all other samples because of the electrical disturbance produced by a CdO reference substance. There were no significant differences in the d.t.a. curves ascribable to the effects of doping. The data are summarized in Table I.

T.g.a. Experiments. Each of the samples was subjected to t.g.a. with reproducible results. The doping of the hydroxide was without effect. There was no increase in sample weight on cooling the samples from 500° to room temperature in air, suggesting that oxygen sorption was negligible. The d.t.a. peak of Figure 2 near 260° split into peaks centering at 255 and 275° , and the shoulder near 325° appeared as weak shoulders centering near 230 , 260 , and 300° of a large shoulder of the t.g.a. curve. The data are summarized in Table I.

I.w.l. Experiments. A fresh sample was used at each temperature. With the exception of the plot of the Li-doped sample, marked Cd(OH)₂/Li, all plots of Figure 3 are for the decomposition of the undoped hydroxide.

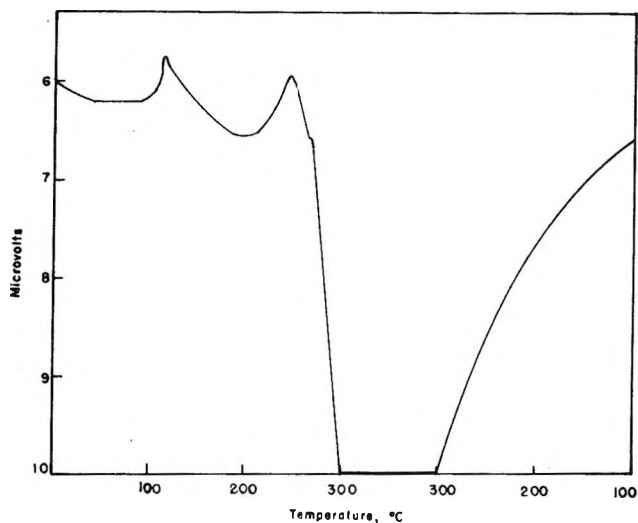


Figure 1. D.t.a. of Al_2O_3 vs. cadmium hydroxide. The alumina reference material was placed in the position normally used as sample position, the cadmium hydroxide being in the reference position of the detector block of the d.t.a. instrument.

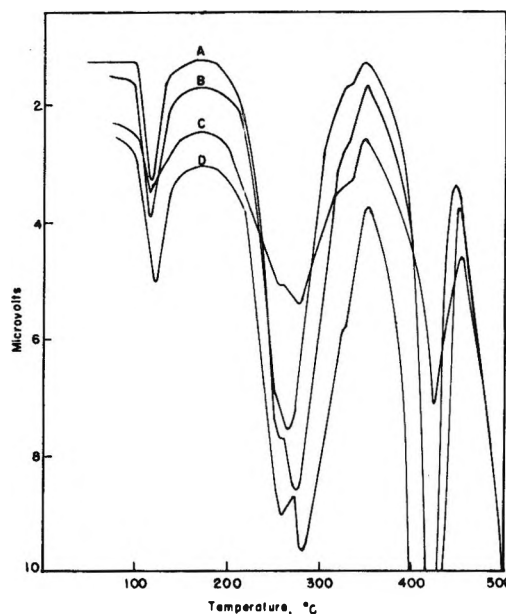


Figure 2. D.t.a. curves of cadmium hydroxide.

The following observations are noteworthy: (a) at and above 300° , a weight loss of about 21% occurred, indicated with arrow P; (b) decomposition at 300 and 350° , although much slower, was as effective as decomposition at 750° ; (c) there was a change in slopes after about an 8% weight loss, indicated with arrow Y; (d) there was a pronounced arrest in some plots after about 12% weight loss, indicated with arrow Z. The various plots suggest that the decomposition

Table I

Process	Temp., °C.						Composition at end of process	Process
	Initial	T.g.a. Center	Final	Initial	D.t.a. Center	Final		
I	25	...	190	...	110	170	CdO·1.65H ₂ O	Desorption
II	190	230	240	170	255		CdO·1.38H ₂ O } CdO·1.03H ₂ O }	Dehydration
III	240	260	270		275			
IV	270	300	340		325	350	CdO·0.76H ₂ O } CdO _{0.80} }	Dehydration and deoxygenation
V	370	410	430	350	420	450		

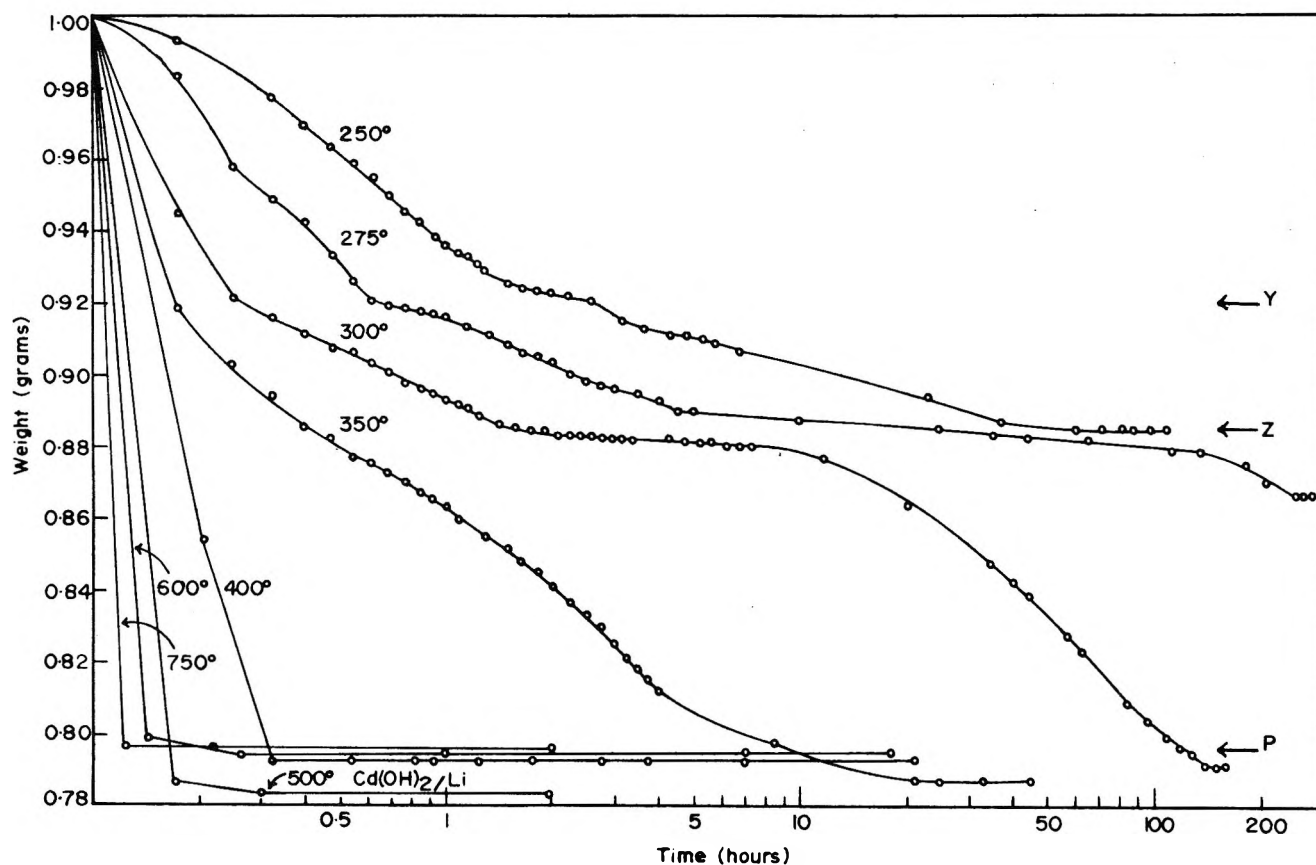


Figure 3. Isothermal weight loss of cadmium hydroxide.

at and above 350° was continuous, the various processes indicated by d.t.a. and t.g.a. experiments not being clearly distinguishable. Sequential decomposition is indicated at and below 300°.

Product Compositions. The interpretation of t.g.a. and i.w.l. curves was based on the final weights of the samples, in order to avoid errors in initial sample weights caused by fortuitous water loss or gain. To permit this, and also to check on the completeness of the decomposition, 11 samples of end decomposition products of pure and doped samples obtained at temperature from 350 to 750° were analyzed. Cadmium

was estimated by the method of Fernando and Freiser.⁶ As the dissociation pressure of CdO is small⁷ and the formation of cadmium mirrors was never observed, the empirical formulas of the final decomposition products were calculated on the assumption that the samples consisted only of cadmium and oxygen and that loss of water and oxygen accounted for the observed weight decreases. This resulted in the formula

(6) A. Fernando and H. Freiser in "Treatise on Analytical Chemistry," I. M. Kolthoff and P. J. Elving, Ed., Part II, Vol. III, Interscience Publishers, Inc., New York, N. Y., 1961, p. 199.

(7) I. G. F. Gilbert and J. P. Kitchener, *J. Chem. Soc.*, 3919 (1956).

$\text{CdO}_{0.80 \pm 0.03}$. There was no correlation between decomposition temperatures or coping and the small variation in formula, and consequently the average formula was used to compute the compositions given in Table I. If the end product at P in Figure 3 was taken as $\text{CdO}_{0.8}$, then at points corresponding to Y of that figure a product $\text{CdO} \cdot \text{H}_2\text{O}$ was formed. At points corresponding to Z, the product had the approximate composition $\text{CdO} \cdot 0.6\text{H}_2\text{O}$. Process I, indicated by an endothermic peak near 110° in d.t.a. curves and by a plateau in t.g.a. curves, is considered to be a loss of adsorbed water. Processes II, III, and IV are taken as dehydration steps. In view of the rapidity of the decomposition and the continuous weight loss indicated by the i.w.l. curves, it is probable that the compositions of intermediate products indicated in Table I are subject to some error. Also, the production of brown coloration at 300° , the continuous i.w.l. curves, and the electrical disturbance of the d.t.a. apparatus suggest that some oxide is produced near 265° and that some loss of oxygen occurs at stages of decomposition very far from completion.

Nitrogen Adsorption. The surface areas of pure and doped samples are shown by the plots of Figures 4 to 8. Some nitrogen adsorption-desorption isotherms at liquid nitrogen temperature were made with undoped samples after heating *in vacuo* and are shown in Figure 9. The adsorption-desorption cycles shown there as plots A, B, and C were made in sequence with one sample. A second sample was used for plot D.

The color changes that occurred during such heat treatments are of interest. The original hydroxide was a white powder and became yellowish after heating at 150° for 9 hr., suggesting that a small amount of decomposition had occurred. At 200° , however, the sample turned brown after about 1 hr., suggesting that substantially more decomposition had occurred than at 150° . At 300° the sample was within the furnace for 15 min. and emerged totally brown.

Discussion

The Decomposition Process. The present observations agree, in general, with those of Hüttig and Mytzyk,^{1,2} who studied the isobaric dehydration of cadmium hydroxides. Their samples, ranging in composition from $\text{CdO} \cdot 1.041\text{H}_2\text{O}$ to $\text{CdO} \cdot 2.207\text{H}_2\text{O}$, were stated to lose water continuously and irreversibly without a change of phase until $\text{CdO} \cdot \text{H}_2\text{O}$ was formed. A second phase, termed "hydro-oxide," of approximate composition $\text{CdO} \cdot 0.4\text{H}_2\text{O}$ was then formed, which could undergo further dehydration. On heating a cadmium hydroxide sample with a Teclu burner, they obtained a material of composition $\text{CdO}_{0.87}$, not inconsistent with

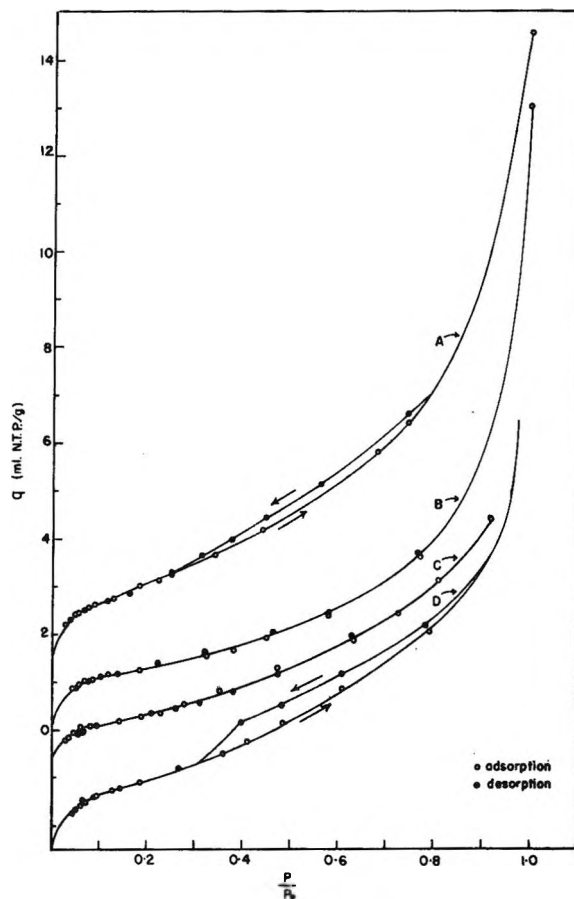


Figure 4. Nitrogen adsorption-desorption isotherms. The direction of the arrows indicates the order in which the various points were obtained: A, after degassing overnight at room temperature; B, after heating at 300° for 30 min.; C, after heating at 300° for 12 hr. displaced by -1 ml.; D, after heating at 500° for 1 hr., displaced by -2.5 ml.

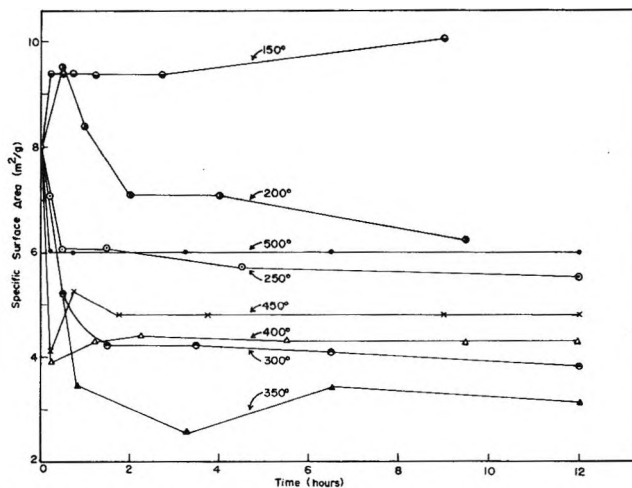
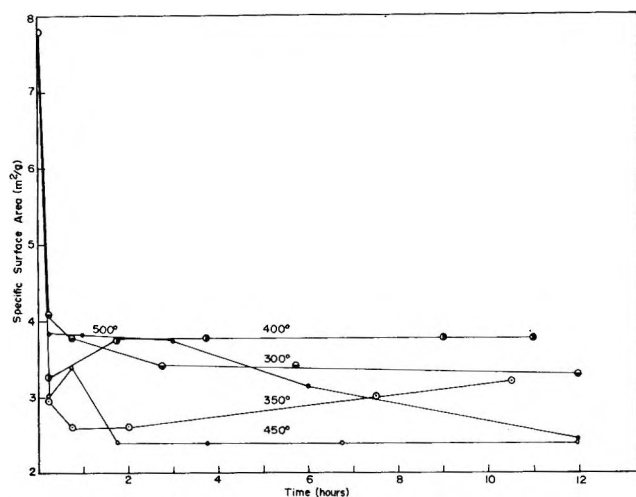
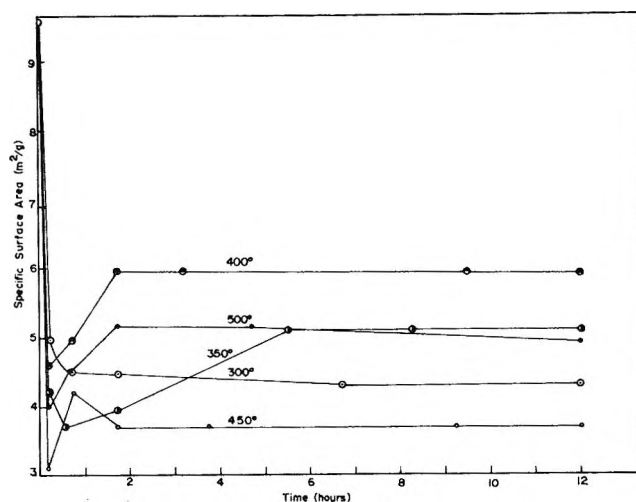
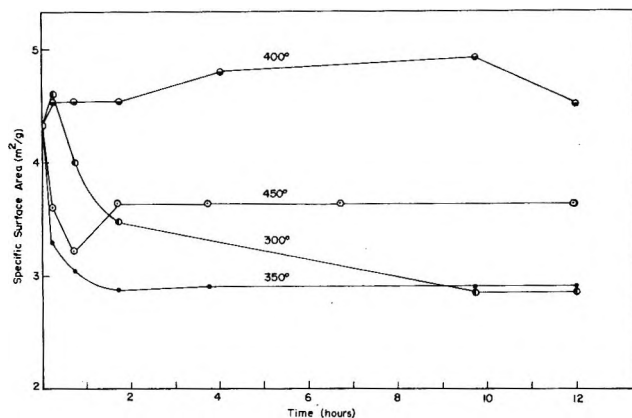
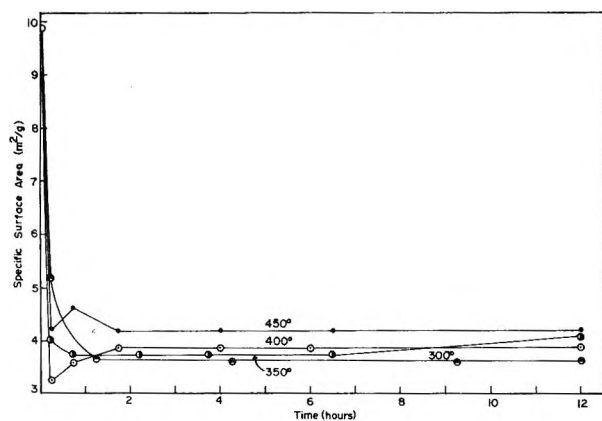


Figure 5. Surface area isotherms of cadmium hydroxide.

that reported presently. These observations are borne out by the continuous dehydration shown by the

Figure 6. Surface area isotherms of $\text{Cd}(\text{OH})_2\text{-Li}^+$.Figure 9. Surface area isotherms of $\text{Cd}(\text{OH})_2\text{-Al}^{+3}$.Figure 7. Surface area isotherms of $\text{Cd}(\text{OH})_2\text{-Mg}^{+2}$.Figure 8. Surface area isotherms of $\text{Cd}(\text{OH})_2\text{-Zn}^{+2}$.

i.w.l. experiments. The points Z, corresponding to a composition $\text{CdO}\cdot 0.6\text{H}_2\text{O}$, as well as process IV of d.t.a. and t.g.a. experiments, corresponding to a for-

mula $\text{CdO}\cdot 0.76\text{H}_2\text{O}$, can be taken as being reasonably close in composition to the hydro-oxide of Hüttig and Mytyzek. That the dehydration is not, in reality, continuous but occurs in four rather than two stages is shown by the present experiments. The precise nature of the structural changes occurring in the solid during the dehydration is not known and, in the absence of supporting data such as X-ray diffraction, speculation on the changes is fruitless. That considerable textural changes of the solid occur, however, is indicated by the changes in surface areas and in nitrogen absorption-desorption isotherms.

The surface areas of pure hydroxide increased by almost 20% on heating for 15 or 30 min. at 150 or 200°, respectively. Although some decomposition occurred at 150°, it is more plausible to ascribe this increase to an opening of a previously blocked pore system than to a generation of new surface through decomposition because the amount of decomposition occurring in 15 min. was small. This suggests that the overnight degassing at room temperature was incomplete, and that the untreated hydroxide had a system of small pores. Presumably, water molecules blocked the pore system and were desorbed above room temperature. This is in agreement with the existence of a system of cylindrical or ink bottle-shaped pores than can be deduced from the hysteresis⁸ and from the smooth closing of the hysteresis loop of plot A of Figure 9. The curves of Figure 4 of areas at 200, 250, 300, and particularly 350° show that rapid declines in areas occurred. This, as well as the disappearance of hysteresis and decline in area shown by plots B and C of Figure 9, suggests

(8) S. Brunauer, "Physical Adsorption of Gases and Vapors," Oxford University Press, Oxford, 1944.

that the original structure was subject to drastic change, the system of small pores and pore openings being destroyed or converted to one having relatively large pores. Increases in area occur at higher temperatures, shown by the 350 to 450° plots and in Figure 9 by plot D. The reappearance of a hysteresis loop in the latter indicates the reformation of a network of fine pores. Similar information can be derived from Figures 5 to 8, and also more clearly from isochrones or plots of surface area as function of temperature at constant heating times. The various decomposition processes cause minima in surface areas near 350 and 450° and a maximum near 400°. This is shown schematically by the generalized isochrone in part A of Figure 10.

The various data suggest that several general trends occur. (a) There was a rapid decline in surface area on heating to 300°, ascribable to the destruction of an original system of small pores. There was little change at 300° after this had occurred. (b) A new pore system began to form at 350°, but the new system also was subject to slow change. (c) The degree of porosity of the second system depended on the velocity of formulation of the pores. (d) The new pore system, if formed rapidly, was relatively stable. These data, in conjunction with those derived from d.t.a., t.g.a., and i.w.l., suggest four general processes: (1) loss of water with attendant destruction of the texture of the hydroxide; (2) formation of CdO, attended by increase in area; (3) sintering of CdO; and (4) deoxygenation of cadmium oxide. These are indicated schematically in part B of Figure 8, and result in the composite C.

The surface area and stability of the solid were, in general, greater the higher the temperature of decomposition. This may be connected with the change in crystal structure attending the hydroxide-oxide conversion. Cadmium hydroxide forms a layer structure⁹ in which every Cd is surrounded by 6OH. Every OH forms three bonds to Cd atoms in its layer and is in contact with 3OH of the adjacent layer. The characteristic feature of such a layer structure is unsymmetrical environment of the OH groups, which have their Cd neighbors all to one side and on the other side are in contact only with OH groups, in marked contrast to the rock salt structure of CdO. Two over-all steps are involved in the rearrangement from layer to rock salt structure: dehydration, whereby H₂O is lost, O²⁻ is formed, and OH vacancies are made in the anion sublattice; and rearrangement, whereby the depleted layer lattice collapses to form the rock salt lattice. In view of the larger surface areas found with increasing temperature, it is not implausible to suggest that this effect was in part brought about by a reten-

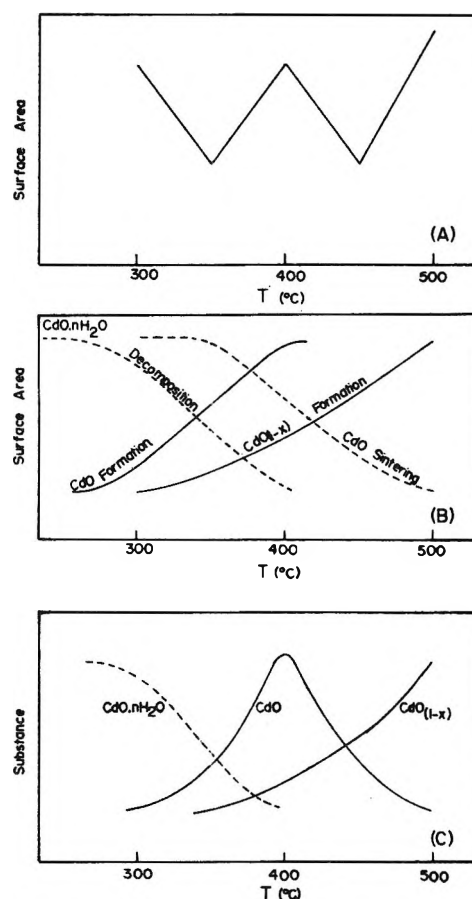


Figure 10. Schematic decomposition mechanism.

tion of the gross structure of the hydroxide crystallites by the newly formed oxide. Although local rearrangement could occur rapidly over regions of a few unit cells, the densification resulting from the diffusion and rearrangement of O²⁻ and Cd²⁺ ions attending the recrystallization of an entire crystallite could lag beyond the dehydration. The surface area of the original material could then be retained or increased at high decomposition rates.

The Effects of Doping. It is recognized that the foreign cations could not be distributed throughout the host lattice but were, initially, at least, on the surface of the hydroxide crystallites. Yet several effects of doping were discernible, appreciable changes in surface areas occurring even at low temperatures. As the "sintering curves" reflect the summation of the changes occurring in the solid, some attempt must be made to separate the effects of the two major over-all processes, *i.e.*, the hydroxide-oxide conversion, and the oxide sintering and deoxygenation. This can be

(9) G. Natta, *Gazz. chim. ital.*, **58**, 344 (1928); *Atti Accad. Lincei*, (6) **2**, 495 (1925).

done by considering relative surface area, *i.e.*, the actual surface area measured after a heat treatment divided by the surface area of the unheated sample. Table II summarizes the sintering data, using the simplified symbolism indicated. In each vertical column the samples are arranged in decreasing order of surface area, *e.g.*, at 300° the highest and lowest actual surface areas are given by E and C, respectively.

Table II: Actual and Relative Surface Areas after 12 Hr.^a

Temp., °C.				
300	350	400	450	500
E c	E c	E c	A c	C* c
A e	D e	C e	D a	A a
D a	A a	A a	E d	E d
B b	C b	D b	C e	D* e
C d	D d	B d	B b	B b

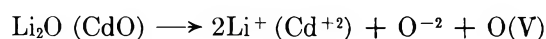
^a a, A = Cd(OH)₂; b, B = Cd(OH)₂-Li⁺; c, C = Cd(OH)₂-Mg²⁺; d, D = Cd(OH)₂-Zn²⁺; e, E = Cd(OH)₂-Al³⁺; C*: 12.5 m.²/g; D*: 4.9 m.²/g. Capital letters indicate the actual areas, lower case letters the relative surface areas.

There is little regularity in the order of actual surface areas, implying that doping had a random effect, but the order of relative areas is more consistent. Also, there appears to be a change in order in going from 400 to 450°. Reference to the postulated mechanism schematically shown in Figure 10 shows that this region is near that at which the hydroxide-oxide conversion is complete and also near the maximum of the range of existence of stoichiometric cadmium oxide. Although it thus seems possible to separate the effects of doping on the two major processes, only the sintering of the oxide will be considered because no supporting data such as electrical conductivities are available for the hydroxide.

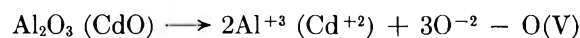
Haul and Just¹⁰ and Dümbgen¹¹ studied the disorder and oxygen transport in CdO by measuring the O¹⁶-O¹⁸ exchange between gaseous oxygen and CdO crystals from 630 to 855°. They found that Li⁺ addition resulted in a marked increase in the diffusion coefficients of oxygen in the oxide lattice, while In³⁺ addition had the reverse effect. The doping effects and the increase of diffusion coefficients with decreasing oxygen pressure furnished strong evidence for a transport mechanism involving vacancies in the anion sublattice. This is in agreement with the results of Baumbach and Wagner,¹² who found a decrease in the electrical conductivity of CdO with increasing oxygen pressure, and does not conflict with the results of Engell's study¹³ of doping on CdO electrode potentials. Cimino and Marezio³

studied the effect of Ag⁺ and In³⁺ doping on the lattice parameter of CdO and explained the results in terms of interstitial metal. However, as pointed out by Haul and Just, Cimino and Marezio's results are equally well in agreement with the concept of oxygen vacancies. Acceptance of the oxygen vacancy mechanism suggests that vacancies are also involved in the sintering of cadmium oxide.

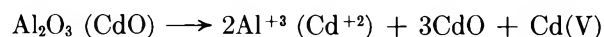
The various sintering data suggest that up to 400° the oxygen vacancy mechanism could account for the increased loss of surface area of the Li⁺-doped samples, Li⁺ incorporation causing an increase in oxygen vacancies, O(V)



and the decreased loss of area of the Al³⁺-doped samples through the destruction of vacancies



At 450 and 500°, however, the Al³⁺-doped samples exhibited smaller surface areas than undoped samples, suggesting that the effect of Al₂O₃ addition had brought about an increased rate of material transport. This does not necessarily mean that the oxygen vacancy mechanism ceased to operate, but merely suggests that that mechanism was no longer the dominant one above about 400°. An additional mechanism could become operative or dominant



where Cd(V) symbolizes a cadmium vacancy. This is based on the premise that the incorporation of 2Al³⁺ would result in the displacement of 3Cd²⁺ with the creation of one Cd(V). The postulated cation vacancy mechanism does not conflict with the anion vacancy or with changes of electrical conductivity of the solid. The effects of cation vacancies on the lattice parameters cannot be assessed.³

An adequate explanation for the effects of Zn²⁺ and Mg²⁺ additions is not at hand. In terms of a substitution mechanism, the presence of Zn²⁺ or Mg²⁺ at Cd²⁺ lattice positions should be without effect. The fact that large sintering effects have been found, however, suggests that the incorporation of the homovalent impurities brings about significant changes in the elec-

(10) R. Haul and D. Just, *J. Appl. Phys.*, **33**, 487 (1962).

(11) R. Haul, D. Just, and G. Dümbgen, "Reactivity of Solids," Proceedings of the 4th International Symposium on Reactivity in the Solid State, J. H. deBoer, Ed., Elsevier Publishing Co., New York, N. Y., 1961, p. 65 ff.

(12) H. H. Baumbach and C. Wagner, *Z. physik. Chem.*, **B22**, 199 (1933).

(13) H. J. Engell, *Z. Elektrochem.*, **60**, 905 (1956).

tronic nature of the solid which then make themselves felt as changes in rates of surface and bulk diffusion.

Acknowledgment. Support of this work by the Government of the United Arab Republic by means of a Fellowship for A. M. K., the Petroleum Research

Fund of the American Chemical Society, and the Research Council of Rutgers, The State University, is gratefully acknowledged. We are also grateful to the Phillips Minerals and Chemicals Company, Metuchen, N. J., for making the d.t.a. experiments possible.

The Catalytic Vapor Phase Oxidation of *o*-Methylbenzyl Alcohol

by Theodor Vrbaški and Walter K. Mathews

Sinclair Research, Inc., Harvey, Illinois (Received August 3, 1964)

A study was made of the oxidation of *o*-methylbenzyl alcohol over fused vanadium oxide catalyst from 280 to 460° in a flow system. The reaction course consists of four parallel routes: (1) the formation of phthalic anhydride by way of *o*-tolualdehyde, *o*-toluic acid, and phthalide as intermediates; (2) the simultaneous direct oxidation to phthalic anhydride; (3) the formation of carbon oxides by way of maleic anhydride; (4) the direct oxidation to carbon oxides. A minor portion of both maleic anhydride and carbon oxides is formed from phthalic anhydride and its precursors. The activation energy for the over-all reaction is 20.0 kcal/mole in the range from 300 to 350°, and the order of reaction with respect to the concentration of *o*-methylbenzyl alcohol is 0.48. The oxidation rate shows a square root dependence of the oxygen concentration below 0.2 atm. Both the reaction order and the activation energy for the formation of *o*-tolualdehyde were also determined.

Introduction

The vapor phase oxidation of *o*-xylene has gained considerable importance in the past decade as a commercial method for producing phthalic anhydride. The published literature,¹⁻⁷ however, is scanty and deals primarily with obtaining high yields. About 70 mole % of phthalic anhydride is attainable from *o*-xylene, whereas yields in the naphthalene oxidation are 85 to 90 mole %.^{8,9}

This discrepancy combined with the fact that about 85 mole % of *o*-toluic acid is converted to phthalic anhydride under conditions similar to those used in the *o*-xylene oxidation¹⁰ tends to indicate that in the *o*-xylene oxidation different branching reactions in the intermediate steps are taking place. Such reactions could be, for instance, decarbonylation of *o*-tolualdehyde and de-

hydrogenation of *o*-methylbenzyl alcohol followed by decarbonylation. Both of these reactions would lead, *via* toluene and benzoic acid, eventually to additional formation of carbon oxides. *o*-Methylbenzyl alcohol is

- (1) W. G. Parks and C. E. Allard, *Ind. Eng. Chem.*, **31**, 1162 (1939).
- (2) I. B. Gulati and S. K. Bhattacharyya, *J. Sci. Ind. Res. (India)*, **12B**, 450 (1953).
- (3) G. L. Simard, J. F. Steger, R. J. Arnott, and L. A. Siegel, *Ind. Eng. Chem.*, **47**, 1424 (1955).
- (4) S. K. Bhattacharyya and I. B. Gulati, *ibid.*, **50**, 1719 (1958).
- (5) G. Ibing, *Brennstoff-Chem.*, **42**, 357 (1961).
- (6) T. P. Forbath, *Chem. Eng.*, **69**, No. 19, 98 (1962).
- (7) S. K. Bhattacharyya and R. Krishnamurthy, *J. Appl. Chem.*, **13**, 547 (1963).
- (8) A. B. Welty and W. F. Rollman, U. S. Patent 2,489,346 (1949).
- (9) W. F. Rollman, U. S. Patent 2,489,347 (1949).
- (10) C. E. Morrell and L. K. Beach, U. S. Patent 2,443,832 (1948).

not found as a product of oxidation under conditions used in the oxidation of *o*-xylene to phthalic anhydride. Benzyl alcohol, however, was identified among the products of vapor phase oxidation of toluene at higher pressure.^{11,12} Finally, the formation of phthalide in the oxidation of *o*-toluic acid suggests that the oxidation of the methyl group proceeds by way of the corresponding alcohol.^{10,11,13}

Data on the reaction kinetics of the catalytic oxidation of *o*-xylene to phthalic anhydride are few with no firm agreement on the intermediates formed and reaction mechanism involved.^{11,14,15} Kinetic data on the catalytic oxidation of potential intermediates are completely lacking.

Clark, Serreze, Simard, and Berets¹⁴ reported that, in the presence of a silicon carbide supported vanadium catalyst, *o*-xylene is simultaneously oxidized by at least two mechanisms, of which one involves zero order kinetics with respect to the xylene and the other possibly entails first-order functionality. Maleic anhydride, carbon oxides, and part of the phthalic anhydride are formed by the first mechanism directly from *o*-xylene, whereas *o*-tolualdehyde and part of the phthalic anhydride (from *o*-tolualdehyde) are formed by the second. The rates of all reactions were dependent on the square root of the oxygen pressure below 0.2 atm.

Novella and Benloch¹⁵ measured the temperature and concentration effects on the oxidation of *o*-xylene over a vanadium oxide-potassium sulfate-silica gel catalyst in a semifluidized system and postulated a parallel consecutive oxidation mechanism similar to that proposed by Clark, *et al.*¹⁴

A basic study of vanadium oxide catalyzed oxidation of *o*-methylbenzyl alcohol and *o*-tolualdehyde, respectively, is of interest both for improving the existing art of phthalic anhydride manufacture and for advancing the general knowledge of heterogeneous catalysis. This work was undertaken to shed light on the reaction kinetics and mechanism which govern the formation of phthalic anhydride. It is also a contribution to the better understanding of oxidation processes which take place on the catalyst surface. The present study is the first contribution of a larger program directed toward the clarification of both the mechanism and kinetics of *o*-xylene oxidation over vanadium oxide catalyst.

Experimental

Apparatus. The all-glass flow unit used in this study consisted of a flow metering and preheating section, evaporator, gas carburetor, reactor, and product-collecting section. The gas input flow rates of pre-purified nitrogen and oxygen were measured by three capillary flow meters. Addition of the *o*-methylbenzyl

alcohol to the system was performed by saturation of the nitrogen flow with the alcohol vapors in the evaporator at a fixed temperature ($\pm 0.1^\circ$). After uniting the three preheated gas flows (N_2 + feed, O_2 , and secondary N_2) in a mixing bulb, the combined stream was passed through capillary tubing to a reactor which consisted of a preheat section and a reaction chamber. The preheat section was 1-mm. capillary tubing 20 cm. long. This was sufficient to heat the gas mixture from about 150° to the reaction temperature. The reaction chamber was of an annular design (11.3-mm. i.d.) with a central thermowell (6.0-mm. o.d.) which reached from the top to about 3 mm. above the bottom of the unit. The annular space between the thermowell and the reactor wall had a width of one diameter of the catalyst pellet. Four such reactors of identical design but different lengths were used in most of the experiments. Their volumes were 3.0, 4.2, 5.1, and 8.4 ml. In a limited number of runs at very high volume hourly space velocities, three additional reactor volumes of 0.8, 1.6, and 2.3 ml., respectively, were used. In this manner, it was possible to keep the evaporation rate of *o*-methylbenzyl alcohol within a narrow range (6.35 to 9.85×10^{-4} mole/hr.) even at widely different operating conditions. As a result, a fairly comparable temperature gradient in the catalyst bed was obtained in all the experiments. The temperature was measured by three chromel-alumel thermocouples in the lower, middle, and upper sections of the catalyst bed. The reactor was immersed in an electrically heated and stirred bath of Du Pont low-melting, heat-treating salt. The temperature was controlled to $\pm 0.5^\circ$.

Although isothermal conditions were not entirely attained in the catalyst bed, the temperature gradients were small. An average temperature increase of 1° above that in the bath was observed in experiments with *o*-methylbenzyl alcohol lean gas mixtures and also with rich gas mixtures at lower temperatures. In runs with highest severity (460° and 1.857×10^{-4} mole of *o*-methylbenzyl alcohol/l.) a maximum increase of 4° was recorded.

(11) I. E. Lavine, "The Chemistry of Petroleum Hydrocarbons," Vol. 3, Reinhold Publishing Corp., New York, N. Y., 1955, p. 1.

(12) W. G. Parks and J. Katz, *Ind. Eng. Chem.*, **28**, 319 (1936).

(13) W. R. Edwards and R. D. Wesselhoft, U. S. Patent 3,128,284 (1964).

(14) H. Clark, G. C. Serreze, C. L. Simard, and D. J. Berets, unpublished results of the American Cyanamid Co. presented at the Gordon Research Conference on Catalysis, June 1956. See J. K. Dixon and J. E. Longfield, "Hydrocarbon Oxidation in Catalysis," Vol. VII, P. H. Emmett, Ed., Reinhold Publishing Corp., New York, N. Y., 1960, p. 183.

(15) E. C. Novella and A. E. Benloch, *Anales Real Soc. Españ. Fis. Quim.* (Madrid), **B58**, 291 (1962).

The product-collecting section consisted of a detachable air-Dry Ice-glass condenser of special design, a Dry Ice trap, and scrubbers. The gas leaving the system was dried and then continuously analyzed for carbon oxides in a programmed temperature gas chromatograph equipped with a thermal conductivity detector and using a built-in 5A molecular sieve column. Finally, the gas was passed through a calibrated, wet test meter.

Materials. The *o*-methylbenzyl alcohol was prepared by the method of Colson.¹⁶ α -Bromo-*o*-xylene (Eastman Kodak) was hydrolyzed with a 0.5% aqueous solution of sodium hydroxide at reflux temperature for 72 hr. The crude *o*-methylbenzyl alcohol was salted out at room temperature, washed with a saturated solution of sodium bisulfite, and dried over sodium sulfate. The *o*-methylbenzyl alcohol obtained in this manner was 99% pure. Several distillations of the yellow oil at a pressure of 5–7 mm. and 90° gave a bromine-free, 99.9% pure *o*-methylbenzyl alcohol, m.p. 32°, n_D^{20} 1.5586, and ultraviolet adsorption maxima in ethyl alcohol at 2623 and 2715 Å. ($a = 2.02$ and 1.46, respectively). The purity of the *o*-methylbenzyl alcohol was established both by mass spectrometric and gas-liquid chromatographic analyses.

The oxygen used was 99.9% pure and was dried over anhydrous calcium chloride before use. The prepurified nitrogen was passed through a calcium chloride column and a Deoxo unit before use.

Catalyst. Fused vanadium pentoxide (C.P. grade, 99.9% pure) was obtained from the Vanadium Corp. of America. It had a surface area of about 2 m.²/g.¹⁷ By using this catalyst, with practically no interior surface, the harmful effect of internal diffusion was greatly minimized. Various charges of catalyst, depending on the volume of the reactor employed, were used. The void volume of the catalyst bed, determined as the volume of water which could be contained within a measured volume of catalyst, was 0.6 ml./ml. of catalyst bed.

Analytical Procedure. Total acids were determined in aliquots of solution of products in tetrahydrofuran by titration with aqueous sodium hydroxide. Maleic anhydride was determined by means of high temperature mass spectrometry and the volumetric method of Lange and Kline.¹⁸

o-Toluic acid was determined by high-temperature mass spectrometry, and per-*o*-toluic acid by iodometric titration. The identity of the latter was confirmed by infrared spectroscopy. Relative proportions of phthalic anhydride, phthalide, *o*-tolualdehyde, and unreacted *o*-methylbenzyl alcohol in the product were determined by both high-temperature mass spectrometry and gas-

liquid chromatography. These proportions, together with the values for total acidity and maleic anhydride, were used to calculate actual concentrations of products. The gas-liquid chromatograph was a high-temperature unit with a filament detector and a 0.635 cm. i.d. \times 3.04 m. stainless steel column packed with 15% bis(phenoxyphenoxyphenyl) ether on 60–80 mesh Chromosorb W. The unit was operated at 30 p.s.i. of helium and 175°.

In addition to the continuous determination of carbon oxide and carbon dioxide in the effluent gas during the experiment, gas samples were also analyzed by low mass spectrometry for carbon oxides, oxygen, and nitrogen. The concentration of carbon oxides was adjusted for the amount formed concurrently with maleic anhydride. The amount of *o*-methylbenzyl alcohol introduced into the system was determined from the difference in weight of the evaporator prior to and after the experiment. The carbon balance varied between 97 and 102% in all runs.

Experimental Procedure. The concentrations of *o*-methylbenzyl alcohol in the gas mixture entering the reactor were 0.62, 0.93, 1.24, and 1.86×10^{-4} mole/l., respectively. The gas mixture of desired composition was passed over the catalyst for 1 hr. at desired experimental conditions prior to the main run. After this period, steady-state conditions in the system were attained. Quantitative collection of the products was started by connecting the product-collecting section to the system and terminated by disconnecting it. The total length of the experiment varied from 3 to 4 hr. Three gas samples of the effluent gas were collected during the main experiment. Contact times varied from 0.075 to 0.6 sec. They were calculated from the void space of the catalyst bed and the feed rate of the reaction mixture corrected to the temperature and pressure in the reaction chamber. The mass velocity calculated with respect to the cross section of the empty reactor varied from 4 to 11×10^{-4} g. cm.⁻² sec.⁻¹.

In order to determine the mass transfer effect on the product distribution, a few experiments were carried out in a specially designed reactor at a mass velocity of 500×10^{-4} g. cm.⁻² sec.⁻¹ but at otherwise unchanged conditions. Since identical results were obtained it was concluded that mass transfer effects due to the reactor geometry were not significant.

Results

In order to determine the extent to which the homogeneous gas phase oxidation and also reactions on the

(16) A. Colson, *Ann. chim. phys.*, **6**, 114 (1885).

(17) M. M. Marisic, *J. Am. Chem. Soc.*, **62**, 2312 (1940).

(18) N. A. Lange and H. Kline, *ibid.*, **44**, 2709 (1922).

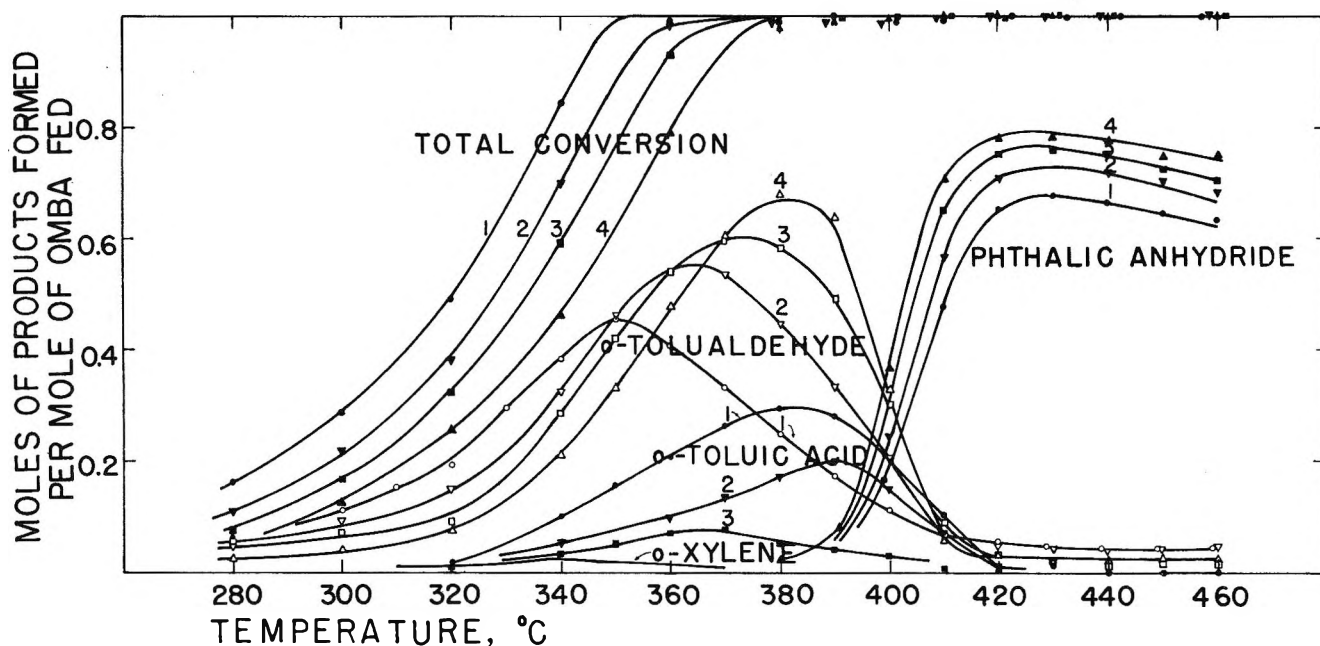


Figure 1. The oxidation of *o*-methylbenzyl alcohol (OMBA) over vanadia catalyst. Average oxygen concentration 9.3×10^{-3} mole/l. Contact time 0.6 sec. Initial OMBA concentrations: (1) 0.62; (2) 0.93; (3) 1.24; (4) 1.86×10^{-4} mole/l.

reactor wall participate in the catalytic reaction, a non-catalytic run was carried out under the most severe conditions of catalytic experiments, *i.e.*, 450° and 0.6-sec. contact time. Ninety-eight mole per cent of *o*-methylbenzyl alcohol was recovered unchanged. The remainder consisted of 1.4% *o*-tolualdehyde, 0.2% *o*-formylbenzyl alcohol, and 0.1% each of per-*o*-toluic acid, *o*-toluic acid, *o*-xylene, and maleic anhydride. Since the contribution of the above reactions was almost negligible, no correction of the measured catalytic rates was made.

In the catalytic oxidation the isolable products are *o*-tolualdehyde, per-*o*-toluic acid, *o*-toluic acid, *o*-xylene, phthalide, phthalic anhydride, maleic anhydride, carbon oxides, and traces of *o*-formylbenzyl alcohol.

In Figures 1 to 4 data for the formation of individual products are plotted as a function of temperature for each of the four initial concentrations of *o*-methylbenzyl alcohol at a contact time of 0.6 sec. In Figure 1 the plot of the total conversion of *o*-methylbenzyl alcohol is also shown. The type of products formed depends on the temperature used, and their rates of formation vary with the initial concentration of *o*-methylbenzyl alcohol in the gas mixture.

Below 390° *o*-tolualdehyde is the principal product, and *o*-toluic acid, phthalide, and carbon oxides are the main by-products. The concentration of carbon oxides is expressed as moles of *o*-methylbenzyl alcohol required for the formation of carbon oxides per mole of *o*-meth-

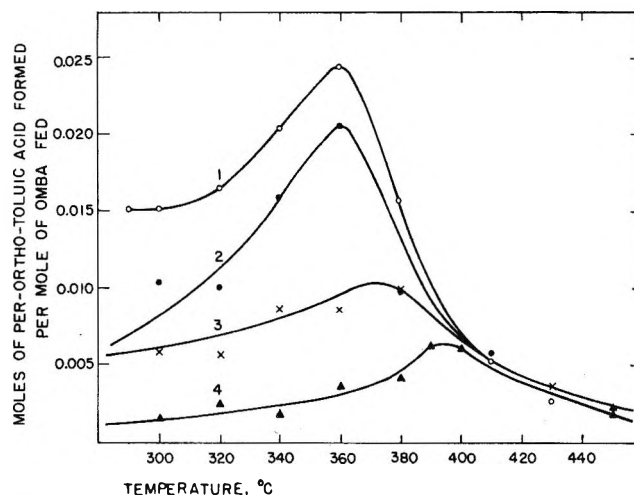


Figure 2. The formation of per-*o*-toluic acid over vanadia catalyst. Average oxygen concentration 9.3×10^{-3} mole/l. Contact time 0.6 sec. Initial OMBA concentrations: (1) 0.62; (2) 0.93; (3) 1.24; (4) 1.86×10^{-4} mole/l.

ylbenzyl alcohol employed. In these values account was taken for the carbon oxides formed concurrently with maleic anhydride. At temperatures at which complete conversion of *o*-methylbenzyl alcohol is obtained, the formation of *o*-tolualdehyde and that of carbon oxides reach maximum points which vary with the composition of the gas mixture used.

Above 380° phthalic anhydride begins to form, and it becomes the principal product at about 425°. It is

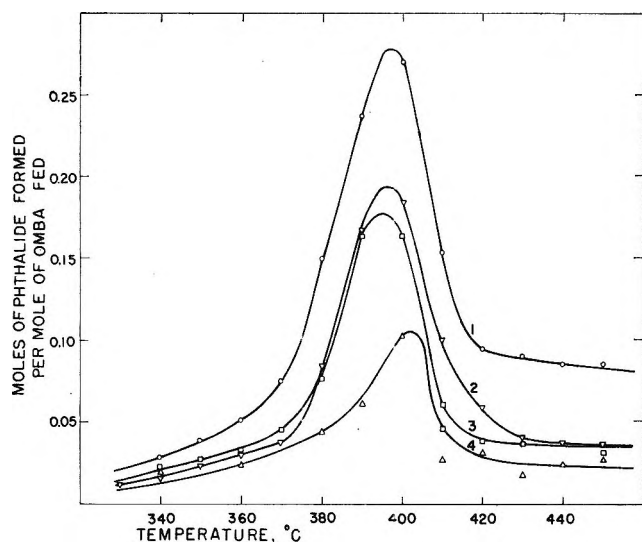


Figure 3. The formation of phthalide from *o*-methylbenzyl alcohol (OMBA) over vanadia catalyst. Average oxygen concentration 9.3×10^{-3} mole/l. Contact time 0.6 sec. The initial OMBA concentrations: (1) 0.62; (2) 0.93; (3) 1.24; (4) 1.86×10^{-4} mole/l.

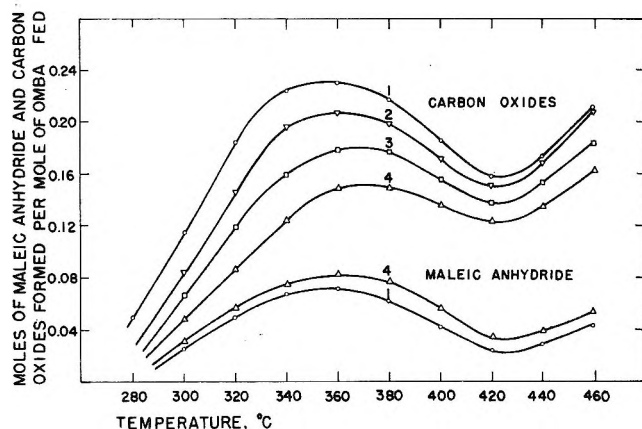


Figure 4. The formation of maleic anhydride and carbon oxides, respectively, from *o*-methylbenzyl alcohol (OMBA) over vanadia catalyst. Average oxygen concentration 9.3×10^{-3} mole/l. Contact time 0.6 sec. The initial OMBA concentrations: (1) 0.62; (3) 0.93; (3) 1.24; (4) 1.86×10^{-4} mole/l. In the values for carbon oxides account was taken for the amount formed concurrently with maleic anhydride.

accompanied by carbon oxides and maleic anhydride as the main by-products. Its formation goes through a maximum at temperatures between 420 and 430°, depending upon the concentration of *o*-methylbenzyl alcohol in the reaction mixture employed. The formations of *per-o*-toluic acid (Figure 2), *o*-toluic acid (Figure 1), and phthalide (Figure 3) exhibit similar behavior with rising temperature.

The formation of both carbon oxides and maleic anhydride (Figure 4) go through maxima at temperatures

where the over-all conversion of *o*-methylbenzyl alcohol has become unity. With rising temperature, the concentrations of carbon oxides and maleic anhydride decrease and proceed through minima at about 425°, which is the temperature of maximum formation of phthalic anhydride. At temperatures higher than 425°, the concentrations of these products increase, mainly because of the oxidation of phthalic anhydride.

Concerning the formation of phthalic anhydride two possible paths are considered. (1) Phthalic anhydride is formed by a consecutive route in which *o*-toluic aldehyde, *o*-toluic acid, and phthalide are intermediates, and (2) phthalic anhydride is formed directly from *o*-methylbenzyl alcohol by a process parallel to (1).

With regard to point (1) two additional series of experiments at 400 and 430° were carried out in which the contact time was varied while the concentrations of reactants were kept constant. At 400° (Figure 5) the concentration of phthalide increased with increasing contact time while a decrease of the concentrations of *o*-toluic aldehyde and *o*-toluic acid occurred. This indicates that a reaction leading to the formation of phthalide from *o*-toluic aldehyde and *o*-toluic acid is involved. The fact that *per-o*-toluic acid was found among the reaction products under these conditions suggests that *o*-toluic acid is also an intermediate.

At 430° (Figure 6) the concentration of phthalic anhydride increased at longer contact times while an almost linear decrease of the concentrations of *o*-toluic aldehyde, *o*-toluic acid, and phthalide occurred. This indicates that phthalic anhydride is formed at least in part from phthalide under these conditions.

Unpublished results, to be reported at a later date, show that the oxidation of *o*-toluic aldehyde, *o*-toluic acid, and phthalide, respectively, gives, under similar conditions, a product distribution and yields comparable to those obtained from *o*-methylbenzyl alcohol. Thus, about 82 mole % of phthalic anhydride is formed from *o*-toluic acid at more severe conditions, and about 55 mole % of phthalide is formed at milder conditions, with no *o*-phthalaldehydic acid present in the reaction product in either case.

It is therefore concluded that phthalic anhydride is formed at least in part from *o*-methylbenzyl alcohol by a consecutive series of reactions in which *o*-toluic aldehyde, *o*-toluic acid, and phthalide are intermediates.

The formation of small amounts of *o*-xylene at 340° can be explained by a disproportionation reaction of two molecules of *o*-methylbenzyl alcohol. In addition, only trace amounts of *o*-formylbenzyl alcohol were occasionally formed. It is the authors' opinion that both *o*-xylene and *o*-formylbenzyl alcohol have no significance in the formation of phthalic anhydride.

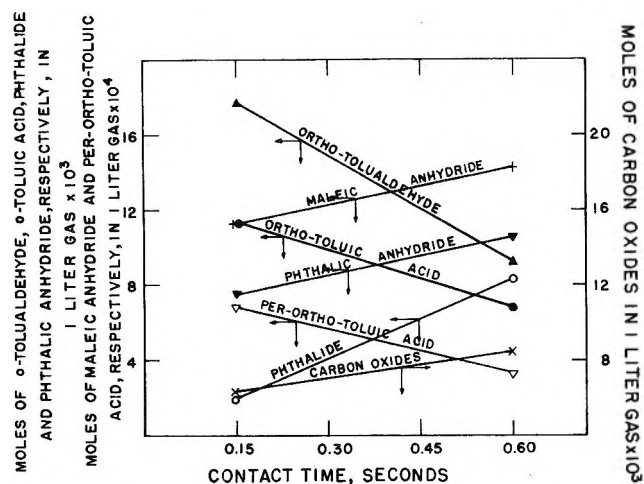


Figure 5. Variation with contact time of the concentration of *o*-tolualdehyde, *o*-toluic acid, per-*o*-toluic acid, phthalide, maleic anhydride, phthalic anhydride, and carbon oxides in the gas leaving the catalyst bed. In the values for carbon oxides account was taken for the amount formed concurrently with maleic anhydride. Initial OMBA concentration 0.93×10^{-4} mole/l. Oxygen concentration 9.3×10^{-3} mole/l. Temperature 400° .

With regard to point (2) the phthalic anhydride is also formed by a second simultaneous process directly from *o*-methylbenzyl alcohol; the total yields of phthalic anhydride and its precursors were found to be higher at the temperature where good yields of phthalic anhydride were obtained than the sum of yields of intermediates observed at a lower temperature but still at a total conversion of *o*-methylbenzyl alcohol. Using data in Figures 1, 2, and 3, the sum of yields of intermediates formed at 360° was found to vary from 0.70 to 0.77 mole/mole, depending on the *o*-methylbenzyl alcohol concentration in the gas mixtures used, whereas the corresponding values for phthalic anhydride and precursors at 425° were 0.82 and 0.84 mole/mole, respectively. The difference, therefore, varies from 7 to 12 mole %.

The fact that no toluene, bitolyl, or benzoic acid were found among the oxidation products ruled out the possibility that competitive degradation reactions occurred, especially at lower temperatures where *o*-tolualdehyde is in the highest concentration. These reactions, representing an alternate interpretation of the data, were believed (probably) to take place with lower activation energies than the sequential process and to become substantially less important at the higher temperatures.

It is noted that the catalytic vapor phase oxidation of *o*-tolualdehyde at a temperature of 380° but under otherwise similar conditions gave, in addition to a few per cent of *o*-toluic acid and phthalic anhydride, only

about 2 mole % of carbon oxides. No trace of toluene, bitolyl, and benzoic acid was found among the products. Furthermore, in a homogenous gas phase oxidation only a 6 mole % conversion of *o*-tolualdehyde was observed at 450° . The main product was per-*o*-toluic acid. A small quantity of *o*-toluic acid and trace amounts of maleic anhydride and carbon oxides were also formed.

The degradation reactions of *o*-tolualdehyde, probably by way of a free-radical mechanism, were found to become significant in the catalytic process at contact times higher than 8 sec. under otherwise comparable conditions.

It was therefore concluded that a portion of phthalic anhydride, corresponding approximately to the difference in concentrations previously mentioned, was formed by a simultaneous reaction directly from *o*-methylbenzyl alcohol. Taking into account that, in the consecutive route, part of the phthalic anhydride precursors is oxidized away to maleic anhydride and carbon oxides, this portion can be higher.

With regard to the formation of carbon oxides and maleic anhydride two alternatives were considered. (1) Carbon oxides are formed by a consecutive reaction in which maleic anhydride is an intermediate, and (2) carbon oxides and maleic anhydride are formed by two simultaneous reactions.

If maleic anhydride is an intermediate in the formation of carbon oxides, the ratio of moles of carbon oxides to moles of maleic anhydride formed should increase with an increase in contact time. If two simultaneous reactions are taking place, one leading to maleic anhydride and the other to carbon oxides, the mole ratio should remain constant unless the two reactions are of different order. It is the authors' opinion that a great difference in orders is unlikely since the over-all order of formation of both maleic anhydride and carbon oxides was found to be 0.54.

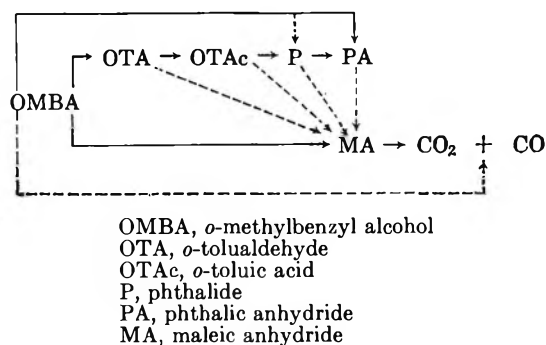
An almost linear increase of the mole ratio from 1.6 to 2.4 for an increase in the contact time from 0.3 to 0.6 was observed at 340° for reaction mixtures containing 0.93×10^{-4} mole of *o*-methylbenzyl alcohol and 9.3×10^{-3} mole of oxygen/l. of gas. At 430° , however, (Figure 6) this ratio increases only from 3.74 to 3.85 for an increase in the contact time from 0.15 to 0.60 sec. It is noted that the curves for carbon oxides and those for maleic anhydride in Figure 4 bear great resemblance through the temperature range studied, indicating an intrinsic relationship in the nature of their formation.

The rather unexpected decrease in concentrations of carbon oxides and maleic anhydride between about 360 and 425° (Figure 4) tends to indicate that a change in the rates of the competing reactions involved in the

formation of carbon oxides, on one side, and of phthalic anhydride, on the other side, is taking place. Normally, one would expect the concentration of carbon oxides to increase gradually or at least to remain constant as the temperature is increasing after all the *o*-methylbenzyl alcohol has been converted. Similar observation of increased formation of carbon oxides below the temperature of incipient formation of phthalic anhydride was observed in the oxidation of *o*-xylene and *o*-tolualdehyde, respectively.

It was concluded that, at lower temperatures and partial conversions of *o*-methylbenzyl alcohol, the carbon oxides are predominantly formed from *o*-methylbenzyl alcohol by a consecutive reaction in which maleic anhydride is the intermediate. At higher temperatures, such as 430°, the direct oxidation to carbon oxides appears to become competitive with the postulated consecutive route. Portions of both carbon oxides and maleic anhydride are also formed from the intermediates.

The data in Figures 1 to 6 therefore appear to be consistent and can be represented by the reaction scheme



It is noted that the ratio of the moles of carbon monoxide to carbon dioxide in the gas leaving the reactor increased about three times as the temperature was changed from 320 to 460° at constant gas composition and contact time. The ratio increased about two times as the concentration of *o*-methylbenzyl alcohol was increased from 0.6 to 1.8×10^{-4} mole/l. at otherwise unchanged conditions.

In Figure 7 the over-all reaction rate of *o*-methylbenzyl alcohol is plotted against the average of initial concentration of *o*-methylbenzyl alcohol in the reaction mixture. A series of rate isotherms is, thus, obtained. The conversion rate is dependent upon the *o*-methylbenzyl alcohol concentration at low values of the alcohol concentration and at higher temperatures. At higher concentrations and at lower temperatures the rate tends to become independent of the alcohol concentration.

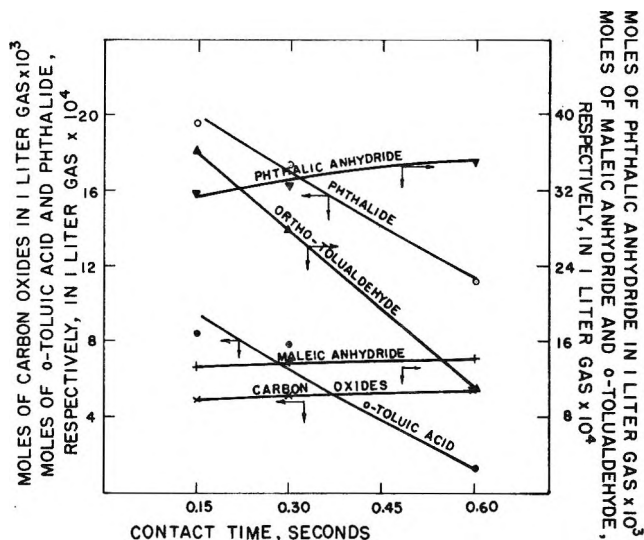


Figure 6. Variation with contact time of the concentration of *o*-tolualdehyde, *o*-toluic acid, phthalide, maleic anhydride, carbon oxides, and phthalic anhydride in the gas leaving the catalyst bed. In the values for carbon oxides account was taken for the amount formed concurrently with maleic anhydride. Initial OMBA concentration 1.86×10^{-4} mole/l. Oxygen concentration 9.3×10^{-3} mole/l. Temperature 430°.

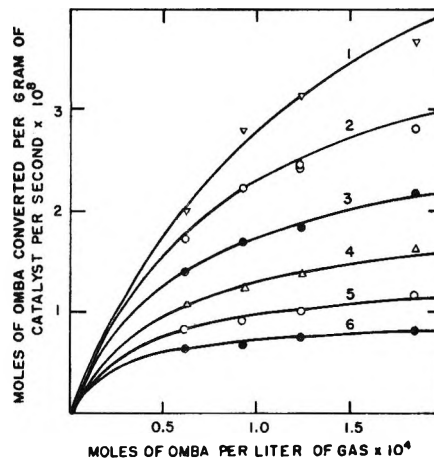


Figure 7. Rate of oxidation of *o*-methylbenzyl alcohol (OMBA) as a function of the initial concentration of OMBA. Average oxygen concentration 9.3×10^{-3} mole/l. Temperatures: (1) 350°; (2) 340°; (3) 330°; (4) 320°; (5) 310°; (6) 300°.

The apparent order of reaction, amounting to 0.48, was determined from the slopes of the lines in a plot where logarithms of the reaction rates were plotted against logarithms of the initial concentrations of *o*-methylbenzyl alcohol in the gas mixture. The logarithms of the averaged specific rate constants calculated by using this reaction order show a linear functionality of reciprocal absolute temperature (Figure 8). Thus

$$\ln k_1 = 3.28 - \frac{20,000}{RT} \quad (1)$$

The average activation energy for the over-all conversion of methylbenzyl alcohol in the temperature range studied is 20.0 kcal./mole.

The variation of the k_1 values with the initial concentration of *o*-methylbenzyl alcohol at three different temperatures is given in Table I.

Table I: Variation of the Over-All Specific Rate Constant k_1 with the Initial Concentration of *o*-Methylbenzyl Alcohol in the Gas Mixture at Various Temperatures

$C \times 10^3$, mole/l.	$k_1 \times 10^7$, l./g./sec.		
	320°	330°	340°
6	15.1	19.1	21.9
8	15.1	19.5	23.1
10	14.9	19.6	23.7
12	14.6	19.5	24.2
14	14.3	19.3	24.3
16	14.0	19.0	24.3
18	13.6	18.7	24.2
Av.	14.5	19.2	23.7

The rate isotherms for the formation of *o*-tolualdehyde are plotted in Figure 9. It is seen that the rate of formation is more dependent on the *o*-methylbenzyl alcohol concentration at higher temperatures and also on lower values of the alcohol concentration. At higher concentrations and lower temperatures the rate tends to become independent of the alcohol concentration.

The order of reaction, amounting to 0.37, was determined from the rate isotherms in Figure 9 in a manner similar to that described for the over-all reaction rate of *o*-methylbenzyl alcohol. The Arrhenius plot of the calculated specific rate constants, k_2 , is a straight line (Figure 8) which can be represented by the equation

$$\ln k_2 = 10.02 - \frac{30,400}{RT} \quad (2)$$

and the activation energy for the formation of *o*-tolualdehyde is 30.4 kcal./mole. The variation of the k_2 values with the initial concentration of *o*-methylbenzyl alcohol in the gas mixture is shown in Table II.

The dependence of the over-all reaction rate on the oxygen concentration was determined at constant initial concentration of *o*-methylbenzyl alcohol, constant contact time, and a temperature of 330°. The straight line in Figure 10 shows that the oxidation rate changes proportionally with the square root of the oxygen concentration in the concentration range studied. The re-

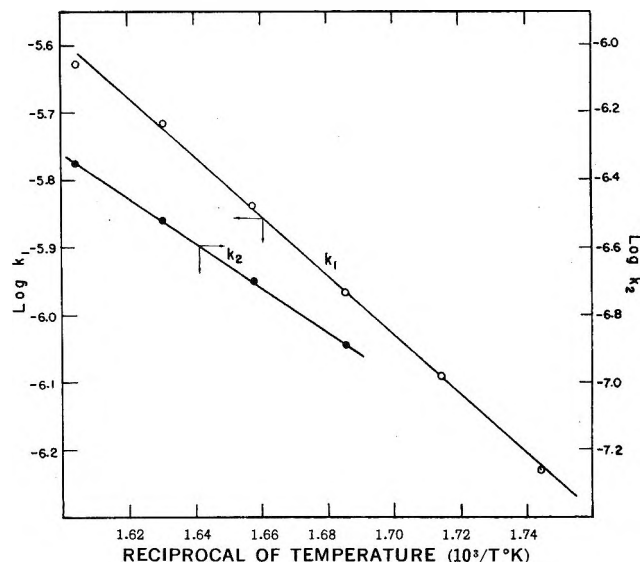


Figure 8. Arrhenius plot of (1) the over-all conversion of *o*-methylbenzyl alcohol (k_1) from 300 to 350° and (2) the formation of *o*-tolualdehyde (k_2) from 320 to 350°.

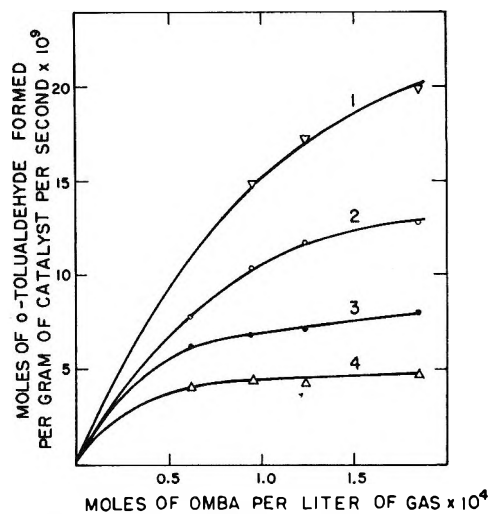


Figure 9. Rate of formation of *o*-tolualdehyde as a function of the initial concentration of *o*-methylbenzyl alcohol. Average oxygen concentration 9.3×10^{-3} mole/l. Temperatures: (1) 350°; (2) 340°; (3) 330°; (4) 320°.

production of data in experiments with oxygen-lean reaction mixtures was found to be somewhat difficult because of the increased instability of the catalyst under the conditions employed. Gas mixtures containing oxygen (less than 32.0×10^{-4} mole/l.) rapidly deactivated the catalyst by reducing it to a lower oxide which then promoted abundant formation of carbon oxides. Its original activity, however, was restored by simply flowing air over it for a few hours at a temperature of 450°. A similar observation was made by Simard, *et al.*,³ and

Table II: Variation of the Specific Rate Constant k_2 with the Initial Concentration of *o*-Methylbenzyl Alcohol in the Gas Mixture at 330 and 340°

$C \times 10^5$, mole/l.	$k_2 \times 10^7$, l./g./sec.	
	330°	340°
6	2.2	2.7
8	2.1	3.0
10	2.1	3.1
12	2.0	3.2
14	2.0	3.2
16	1.9	3.1
18	1.9	3.1
Av.	2.0	3.1

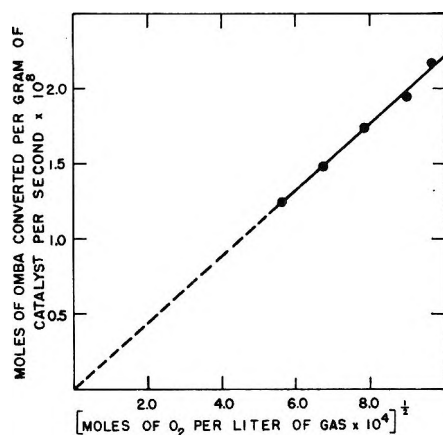


Figure 10. Rate of oxidation of *o*-methylbenzyl alcohol (OMBA) as a function of the square root of the initial concentration of oxygen in the reaction mixture. Average OMBA concentration 1.86×10^{-4} mole/l. Contact time 0.6 sec. and temperature 330°.

Hughes and Adams¹⁹ in the oxidation of *o*-xylene and phthalic anhydride, respectively.

The over-all oxidation rate data for *o*-methylbenzyl alcohol were also correlated by an expression based on the Hinshelwood model²⁰ and also on that developed by Hughes and Adams¹⁹ for unimolecular surface reactions. These results will be reported in a separate paper.

Discussion

To interpret the postulated parallel oxidation scheme in terms of reactions which occur on the catalyst surface in the light of solid-state properties of vanadium oxide, it is assumed that in the initial step the chemisorbed *o*-methylbenzyl alcohol molecule donates electrons to the catalyst and forms an intermediate positive ion. The work of Clark, Serreze, Simard, and Berets¹⁴ and Berets and Clark²¹ on the oxidation of *o*-xylene largely eliminates the possibility that free radi-

cals are participating either on the catalyst surface or in the gas phase in the oxidation process. However, the presence of per-*o*-toluic acid in the oxidation product of *o*-methylbenzyl alcohol suggests that the formation of *o*-toluic acid may occur at least in part by way of free radicals.

The chemisorption of the *o*-methylbenzyl alcohol on the catalyst surface can be visualized as taking place by way of (1) the aromatic nucleus, (2) the carbinol group, (3) the methyl group, and (4) both the carbinol and methyl groups. The available data suggest that, at milder conditions, chemisorption of type (1) and (2) occurs whereas, at more severe conditions, chemisorption of type (4) becomes competitive with (1) and (2). Thus, at milder conditions both the carbinol group and the aromatic nucleus of the molecule compete for the sites on the catalyst surface. The chemisorption of the former is expected to be more favored. This appears reasonable because of the polar character of the carbinol group.

The assumption that intermediate positive ions of *o*-methylbenzyl alcohol are formed on the catalyst surface is supported by the fact that chemisorbed *o*-xylene on vanadium oxide was found to donate electrons to the catalyst, even at temperatures below those where catalytic oxidation was first detected.²¹ The appearance of positively charged naphthalene ions was also detected on the catalyst surface when naphthalene was adsorbed on the oxidic semiconductors.²² Finally, benzyl halides, which may be considered as compounds related to *o*-methylbenzyl alcohol, are known to be prone to form intermediate carbonium ions stabilized by resonance. In the present instance the resonance would involve establishment of positive centers at the *ortho* and *para* positions in the nucleus as well as in the side chains. The hydroxyl radical formed would be instantaneously consumed by the oxygen on the catalyst surface. A similar series of ions can be visualized if the donation of the electron proceeds either from the methyl group with the abstraction of a hydrogen atom or from the aromatic nucleus by way of the π -electrons with no abstraction of a hydrogen atom.

If one assumes that the positive centers once formed remain localized at the part of the molecule adsorbed on the surface, the point of attack of oxygen becomes apparent. Thus, the *o*-methylbenzyl alcohol molecule chemisorbed by way of the carbinol group forms *o*-

(19) F. M. Hughes and R. T. Adams, *J. Phys. Chem.*, **64**, 781 (1960).

(20) C. N. Hinshelwood, "The Kinetics of Chemical Change," The Clarendon Press, Oxford, 1940, p. 207.

(21) D. J. Berets and H. Clark, *Advan. Catalysis*, **9**, 204 (1957).

(22) I. I. Rooney and R. C. Pink, *Proc. Chem. Soc.*, 70 (1961).

tolualdehyde upon oxidation whereas the oxidation of the nucleus-adsorbed molecule proceeds by way of ring rupture to maleic anhydride and carbon oxides. Single methyl group chemisorption appears to occur to a limited extent under these conditions, for only trace amounts of *o*-formylbenzyl alcohol were found among the products.

In the case of *o*-xylene the same type of ions with positive centers localized in the methyl substituent as well as in the nucleus are expected to form on the catalyst surface. However, the relative concentration of the latter is expected to be higher than it is in the oxidation of *o*-methylbenzyl alcohol, owing to the increased adsorption rate of the xylene molecule by way of the nucleus. This results from the lack of polarity in the side chains of the *o*-xylene molecule. It is, therefore, concluded that *o*-xylene is more susceptible than *o*-methylbenzyl alcohol to the nucleus type oxidation, which leads to the formation of carbon oxides.

At more severe conditions additional chemisorption by way of the methyl group of the *o*-methylbenzyl alcohol molecule, which is already chemisorbed by way of the carbinol group, becomes significant. This adsorption may occur, depending on the conditions employed, either simultaneously with that of the carbinol group or subsequently, *i.e.*, after the *o*-methylbenzyl alcohol has been oxidized to *o*-tolualdehyde or *o*-toluic acid. In either case a decrease in the rate of formation of carbon oxides in favor of phthalic anhydride would be expected. Experimental results confirmed this assumption.

The observed square root dependence of the oxygen concentration in the catalytic oxidation of *o*-methylbenzyl alcohol suggests that the adsorption of oxygen on the vanadium oxide is dissociative. Clark, Serreze, Simard, and Berets¹⁴ observed a square root dependence of the oxygen concentration in the oxidation of *o*-xylene and concluded that the chemisorption of oxygen followed by formation of an oxygen ion on the catalyst surface is the probable rate-controlling step.

Since *o*-tolualdehyde, *o*-toluic acid, and phthalide give, upon oxidation, product distributions comparable to that obtained from *o*-methylbenzyl alcohol, it is apparent that none of these compounds acts as a branch intermediate in the formation of phthalic anhydride.

In an attempt to shed light on the role of the oxygen of the vanadium pentoxide lattice in the oxidation process, an experiment was carried out in which a gas mixture of 0.4 mole % of *o*-methylbenzyl alcohol in pre-purified nitrogen was passed over vanadium pentoxide (8–10 mesh) under conditions at which normally good

yields of phthalic anhydride were obtained if air was used instead of nitrogen, *i.e.*, 420° and 0.6-sec. contact time. The normal product distribution was observed only at the very beginning, *i.e.*, in the first minute or two of the experiment. After 5 min. the formation of carbon oxides increased to 40 mole % with respect to the *o*-methylbenzyl alcohol introduced. It then passed through a maximum of 63 mole % after 40 min. and gradually decreased to 8 mole % after 6 hr. At this point the catalyst was almost completely reduced to V₂O₄, and only *o*-methylbenzyl alcohol was recovered.

Under these conditions, when the feed rate of *o*-methylbenzyl alcohol was 94.3 mg./hr. and the ratio of moles of oxygen consumed to moles of *o*-methylbenzyl alcohol converted was 4.53 as determined from the product distribution in the oxidation run, the rate of oxygen uptake was 3.55×10^{19} oxygen molecules/min.

Aebi²³ found that the O–O distance was essentially the same in V₂O₅ and V₂O_{4.34} and that the O–O distance along the octahedron edges of V₂O_{4.34} was 2.7 to 3.3 Å. Assuming all the oxygen atoms on the surface to be about 3 Å. apart, the vanadium oxide catalyst bed (4 g.) with a 2 m.²/g. surface area would have approximately 8.9×10^{19} oxygen sites. This suggests that, in the initial period of 2 min. when normal yields of phthalic anhydride were obtained, only about 1.5 to 2 layers of lattice oxygens in the surface region of the catalyst participated in the reaction.

The mechanism which emerges for the phthalic anhydride formation is that the adsorbed *o*-methylbenzyl alcohol in the form of an ion undergoes oxidation principally by oxygen ions which are either incorporated in a few surface layers of vanadium oxide or only loosely chemisorbed on the surface. Allen²⁴ came to a similar conclusion by using data reported in the literature^{21,25,26} on the solid state properties of vanadium oxide. The slow step appeared to be the rate of diffusion of oxygen ions through the surface layers of the catalyst.

Acknowledgment. The authors wish to acknowledge the assistance of Messrs. G. W. Cleary, D. C. Ford, and E. C. Lounsbury, who performed the mass spectrometric, gas-liquid chromatographic, and volumetric analyses.

(23) F. Aebi, *Helv. Chim. Acta*, **31**, 8 (1948).

(24) J. A. Allen, *Chem. Ind.* (London), 1225 (1963).

(25) L. A. Kasatkina, G. K. Boreskov, Z. I. Krylova, and V. V. Popovskii, *Izv. Vysshikh Uchebn. Zavedenii, Khim. i Khim. Tekhnol.*, **1**, 12 (1958).

(26) L. Ya. Margolis and E. Plyshevskaya, *Izv. Akad. Nauk SSSR, Otd. Khim. Nauk*, 415 (1952).

Fast Reactions Involving Hydrogen Bonding in 2,2-Disubstituted Malonic Acids

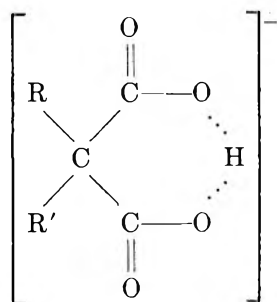
by Melvin H. Miles, Edward M. Eyring, William W. Epstein, and Richard E. Ostlund¹

Department of Chemistry, University of Utah, Salt Lake City, Utah (Received August 5, 1964)

Rate constants have been obtained by the temperature-jump method for acid-base reactions of 2,2-disubstituted malonic acids in aqueous solution. Differences of rate constants for a given reaction have been correlated with the effects substituent groups have on the intramolecular hydrogen bond. Activation energies, enthalpies, and entropies have been calculated which indicate that the substituent effect is primarily steric in nature. The acid dissociation constants for these substances were determined by potentiometric titrations at 0.1 *M* ionic strength and 25°.

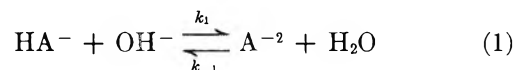
Introduction

The hydrogen bond is particularly well suited to play a role in reactions at or near room temperature because of its small bond energy (2 to 10 kcal./mole). This study of a series of substituted malonic acids shows the significant effect of slightly altering the nature of the substituents R and R' on the strength of the intramolecular hydrogen bond in a series of dicarboxylic acid monoanions.



The substituted malonic acids studied were diethyl-, ethylphenyl-, ethyl-*n*-butyl-, ethylisoamyl-, di-*n*-propyl-, di-*n*-butyl-, di-*n*-heptyl-, ethylisopropyl-, and diisopropylmalonic acids.

Since in the temperature-jump relaxation method the reaction cannot be identified by isolation of product, it was necessary to find other experimental evidence to establish which equilibrium was being perturbed. The results definitely favor the equilibrium



over the other possibilities for the chosen concentrations where $\text{pH} \geq 8.3$. Thus the rate constants k_1 and k_{-1} can be calculated from the relation²

$$\frac{1}{\tau} = k_1 \{ [\text{HA}^-] + [\text{OH}^-] \} + k_{-1} \{ [\text{A}^{2-}] + [\text{H}_2\text{O}] \} \quad (1a)$$

and

$$\frac{k_1}{k_{-1}} = K_{\text{eq}} \quad (1b)$$

Further experiments also showed that, under the chosen conditions, the indicator equilibrium had very little effect on the equilibrium in (1), contrary to the large effect predicted by theoretical correction factors.

Experimental

Synthesis. All except the diisopropylmalonic acid were routinely prepared by basic hydrolysis of readily available substituted malonic acid esters. The diisopropylmalonic acid was prepared by a slight modification of Marshall's procedure.³ The synthesized sub-

(1) National Science Foundation Undergraduate Research Participant.

(2) M. Eigen and L. DeMaeyer, "Technique of Organic Chemistry," Vol. VIII, Part II, 2nd Ed., Interscience Publishers, Inc., New York, N. Y., 1963, pp. 901-903.

stituted malonic acids were purified by recrystallizations from organic solvents, and all were found to have the physical properties previously reported in the literature.

Potentiometric Titrations. The ionization constants of the various disubstituted malonic acids were determined by means of the standard procedure described by Albert and Serjeant.⁴ Solutions 0.0100 *M* at three-fourths neutralization of the acid were titrated with 0.1020 *N* carbonate-free KOH in 0.100 *M* KCl. The titrations were carried out under a nitrogen atmosphere with a water bath maintaining the temperature at $25 \pm 0.1^\circ$. The base was added in 0.50-ml. portions to give the results as a set of eight points. The results of these titrations are shown in Table I. Similar titrations were made in 0.079 *M* NaClO₄·H₂O to obtain the *pK* values at mean ionic strength of 0.10, corresponding to the temperature-jump experiments. These *pK* values were approximately 0.03 larger than those of Table I.

Table I: Potentiometrically Determined Acid Dissociation Constants at 25° in 0.10 *M* KCl

Compound	<i>pK</i> ₁ ^M	<i>pK</i> ₂ ^M	<i>K</i> ₁ / <i>K</i> ₂
Malonic acid	2.85 (lit.) ^a	5.70 (lit.) ^a	700
Diethylmalonic acid	2.15	7.05	80,000
Ethyl- <i>n</i> -butylmalonic acid	2.15	7.25	130,000
Ethylisoamylmalonic acid	2.15	7.31	145,000
Di- <i>n</i> -propylmalonic acid	2.15	7.34	155,000
Ethylphenylmalonic acid	1.9	7.12	160,000
Di- <i>n</i> -butylmalonic acid	Insoluble	7.36	...
Di- <i>n</i> -heptylmalonic acid	Insoluble	7.45	...
Ethylisopropylmalonic acid	2.03	8.10	1,170,000
Diisopropylmalonic acid	2.18	8.60	2,630,000

^a See ref. 15.

These titrations and subsequent pH measurements were made with the radiometer Type TTT1 titrator equipped with a PHA630T scale expander calibrated in 0.01 pH units. The scale expander was standardized and adjusted with the Type PHN2 calibrator. A radiometer Type G202C glass electrode was used in conjunction with the Type K4312 calomel electrode.

Temperature Jump. A number of complete descriptions of the conventional Joule heating type, temperature-jump apparatus are available.⁵⁻⁸ Our equipment has been modified after the manner of Hammes and Steinfeld⁹ for single-beam operation.

The solutions studied were prepared by carefully weighing the required amount of the substituted malonic acid, adding NaClO₄·H₂O to adjust the ionic strength, introducing a measured amount of indicator,

diluting to the desired volume, and finally carefully adjusting the pH to the desired value. For low concentrations and high pH values, the change in pH due to CO₂ absorption becomes a serious problem; therefore, the pH was measured immediately before and after each temperature-jump experiment. All solutions were prepared with distilled, demineralized water, freshly boiled to reduce cavitation due to dissolved gases.

The main acid-base indicators used in this study were cresol red (*o*-cresolsulfonphthalein) and phenolphthalein. Relaxation curves observed on the Tektronix 545A oscilloscope screen were recorded with a Polaroid oscilloscope camera (Tektronix C-12). Duplicate solutions, where no malonic acid compound was added, gave no observable relaxation in the time region of interest, thus definitely relating the observed relaxation to the malonic acid component of the solutions. Temperature-jump experimental results are shown in Table II.

Results and Treatment of Data

Ionization Constants. The ionization constants of the malonic acid compounds, given in Table I, are actually "mixed constants"¹⁰ of the form $K_a^M = a_{H^+}[A^-]/[HA]$ since the pH is essentially a measurement of a_{H^+} , the hydrogen ion activity.^{11,12} Appropriate activity corrections are needed to convert the constants to either concentration or thermodynamic ionization constants,¹³ but the apparent ionization constants are most convenient for temperature-jump measurements. The ratio of *K*₁/*K*₂ is believed to be related to the effectiveness of the 2,2-substituent groups in strengthening the intramolecular hydrogen bond.¹⁴ The *pK*_a values given in Table I represent the average value of a set of eight titration points. The usual scatter was about 0.03 of a *pK* unit for a set, and no set showed a scatter greater than 0.06

(3) F. C. B. Marshall, *J. Chem. Soc.*, 2754 (1930).

(4) A. Albert and E. P. Serjeant, "Ionization Constants of Acids and Bases," Methuen and Co., Ltd., London, 1962, pp. 16-42.

(5) G. Czerlinski and M. Eigen, *Z. Elektrochem.*, **63**, 652 (1959).

(6) See ref. 2, pp. 969-981.

(7) G. G. Hammes and P. Fasella, *J. Am. Chem. Soc.*, **84**, 4644 (1962).

(8) H. Eyring and E. M. Eyring, "Modern Chemical Kinetics," Reinhold Publishing Corp., New York, N. Y., 1963, pp. 96-102.

(9) G. G. Hammes and J. I. Steinfeld, *J. Am. Chem. Soc.*, **84**, 4639 (1962).

(10) Reference 4, p. 57.

(11) Reference 4, pp. 57, 168-169.

(12) R. G. Bates, "Treatise on Analytical Chemistry," Vol. I, Part 1, Interscience Encyclopedia, Inc., New York, N. Y., 1959, p. 368.

(13) H. A. Laitinen, "Chemical Analysis," McGraw-Hill Book Co., New York, N. Y., 1960, pp. 5-21.

(14) D. H. McDaniel and H. C. Brown, *Science*, **118**, 370 (1953).

Table II: Relaxation Spectra of Malonic Acids in 0.1 M Ionic Strength Aqueous Solution and Calculated Rate Constants for the Reaction $\text{HA}^- + \text{OH}^- \xrightarrow{k_1} \text{A}^{2-} + \text{H}_2\text{O}$

$C_{\text{H}_2\text{A}},^a$ $10^{-4} M$	$T_i,^b$ °C.	pH ^c	$\tau,^d$ $\mu\text{sec.}$	$C_{\text{HIIn}},^e$ $10^{-5} M$	$k_1,^f$ 10^7 $M^{-1} \text{sec.}^{-1}$	$C_{\text{H}_2\text{A}},^a$ $10^{-4} M$	$T_i,^b$ °C.	pH ^c	$\tau,^d$ $\mu\text{sec.}$	$C_{\text{HIIn}},^e$ $10^{-5} M$	$k_1,^f$ 10^7 $M^{-1} \text{sec.}^{-1}$
2,2-Diethylmalonic acid						Ethylphenylmalonic acid					
5.0	3	8.70	405	2.3	19	5.0	3	8.60	521	2.0	9.5
3.38	3	8.40	390	2.5	16	3.0	3	8.50	640	2.0	10
3.38	3	8.51	352	2.5	22	4.0	3	8.50	610	4	8.5
4.5	4.5	8.50	360	4	17	5.0	16	8.70	344	2.0	14
3.0	16	8.65	221	2	34	3.0	16	8.50	364	2.0	15
2.0	16	8.30	272	...	27	4.0	16	8.50	370	4	12
5.0	16	8.70	205	2.3	28	2.5	16	8.38	400	2.0	15
4.5	16	8.55	240	4	22						
Ethylisoamylmalonic acid						Di-n-propylmalonic acid					
2.0	3	8.35	576	2	9.8	4.0	3	8.50	462	2.5	8.2
3.0	3	8.52	549	2.5	9.9	3.0	4	8.35	430	2.0	8.5
4.0	3	8.61	461	2.0	10	3.0	3	8.44	522	2.0	8.3
2.0	16	8.30	273	2	17	3.5	3	8.37	465	1.5	7.1
3.0	16	8.70	305	1.5	18	3.5	3	8.50	523	1.5	8.1
2.0	16	8.30	293	2	16	3.5	3	8.60	562	1.5	9.1
3.0	16	8.52	316	2.5	15	4.0	14	8.60	354	2.5	11
4.0	16	8.61	292	2.0	14	5.1	16	8.44	226	2.0	11
3.0	16	8.42	293	2	14	3.0	16	8.46	312	2.0	13
3.0	16	8.90	310	2	18	3.5	16	8.33	230	1.5	12
Ethylisopropylmalonic acid						Diisopropylmalonic acid					
2.0	3	8.30	553	2	2.6	2.0	5	8.30	417	2.0	1.8
4.0	3	8.60	490	2.7	2.4	3.0	4	9.3	601	2	2.7
3.34	3	8.40	405	2.5	2.5	4.0	3	8.61	194	2.7	2.6
3.34	3	8.60	464	2.5	3.1	3.19	3	9.52	755	2	2.7
5.41	3	9.35	629	4	4.7	3.08	3	8.80	453	4	1.9
3.0	3	8.30	383	3.0	2.5	3.0	3	9.30	654	2	2.7
3.0	3	8.69	464	1.7	3.3	6.5	3	9.55	588	3	2.2
2.0	6	8.20	411	2.0	3.0	2.0	16	8.30	194	2.0	3.7
2.0	16	8.20	181	2.0	6.5	3.0	16	9.50	287	2	4.5
5.0	16	9.50	288	2	5.9	3.19	16	9.54	321	2	4.0
4.0	16	8.80	283	1.5	5.2	3.08	16	8.70	214	4	3.2
2.0	16	8.30	249	2	5.4	3.0	16	9.7	156	2	7.4
4.0	16	8.60	203	2.7	5.4	6.5	16	9.6	228	3	4.0
5.41	16	9.40	296	4	6.3						
3.0	16	8.38	256	3	4.0						
3.0	16	8.68	323	1.7	4.9						

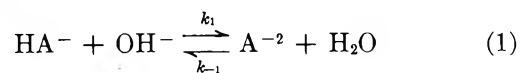
^a Total malonic acid concentration. ^b Solution temperature immediately before the temperature jump. ^c pH measured 10° above T_i . ^d Experimental relaxation time. ^e Total indicator concentration. ^f Rate constant calculated from eq. 1a.

of a pK unit. Several determinations at 12° showed that the pK values varied only slightly with temperature, with $\text{pK}_2(12^\circ) = \text{pK}_2(25^\circ) - 0.03$. This is about the same effect as has been found for malonic acid¹⁵ and other carboxylic acids.¹⁶

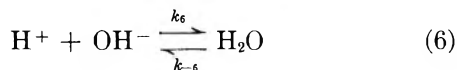
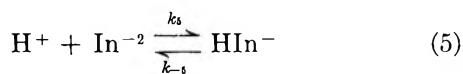
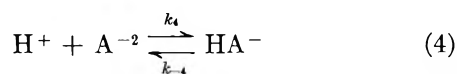
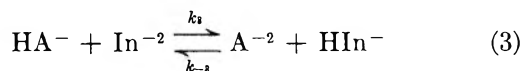
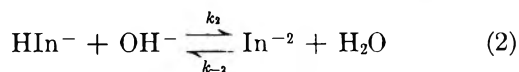
Several values located in the literature compared favorably with the pK values given in Table I.^{17,18}

Equilibrium Identification. Before interpreting rate data, one must first establish that the reaction under study is properly identified. This often presents a problem in temperature-jump studies, for a variety of equilibria may exist in the solution. For example, in this study with $\text{pH} \geq 7$, we have the following equilibria

to consider, of which only three are thermodynamically independent¹⁹



- (15) S. N. Das and D. J. G. Ives, *Proc. Chem. Soc.*, 375 (1951).
 (16) S. Bruckenstein and I. M. Kolthoff, "Treatise on Analytical Chemistry," Vol. I, Interscience Encyclopedia, Inc., New York, N. Y., 1959, p. 435.
 (17) M. Levy and J. P. Magoulas, *J. Am. Chem. Soc.*, **84**, 1345 (1962).
 (18) R. Gane and C. K. Ingold, *J. Chem. Soc.*, 2153 (1931).
 (19) G. W. Castellan, *Ber. Bunsenges. Physik. Chem.*, **67**, 905 (1963).



The rate of reaction 6 is much faster than the rates of the other reactions and is not observable with our temperature-jump apparatus; thus, it can be neglected. Reactions 4 and 5 may also be neglected outside the acid region. For $\text{pH} \sim 7$ the observed relaxation is due principally to equilibrium 3,²⁰ while for more basic solutions the observed effect can be attributed mainly to reaction 1 if an indicator system is chosen which responds much faster to the pH increase than does the system under investigation. Cresol red and phenolphthalein have been found to satisfy this requirement.²¹

The above assumptions can be demonstrated experimentally by considering the following expressions for the relaxation times

$$\frac{1}{\tau} = k_1 \left\{ [\text{HA}^-] + [\text{OH}^-] + \frac{K_w}{K_2} \right\}$$

where $K_2 = \frac{[\text{H}^+][\text{A}^{-2}]}{[\text{HA}^-]} \quad (7)$

$$\frac{1}{\tau} = k_2 \left\{ [\text{HIn}^-] + [\text{OH}^-] + \frac{K_w}{K_{\text{HIn}}} \right\}$$

where $K_{\text{HIn}} = \frac{[\text{H}^+][\text{In}^-]}{[\text{HIn}]} \quad (8)$

$$\frac{1}{\tau} = k_3 \left\{ K([\text{HA}^-] + [\text{In}^{-2}]) + [\text{A}^{-2}] + [\text{HIn}^-] \right\}$$

where $K = \frac{K_2}{K_{\text{HIn}}} \quad (9)$

$$\frac{1}{\tau} = k_4 \left\{ [\text{A}^{-2}] + [\text{H}^+] + K_2 \right\} \quad (10)$$

The equilibrium most nearly related to the observed relaxation time can be distinguished by the manner in which $1/\tau$ varies with changing concentration of the species in the above expressions. This is most clearly shown by plotting $1/\tau k_i$ vs. pH for fixed total acid and indicator concentrations. The calculated curve can then be compared with the experimental value of

$1/\tau k_i$ where τ is assumed to depend solely on equilibrium i . For the pH regions where the relaxation time τ is related entirely to a particular equilibrium, the theoretical and experimental points will coincide. The results for the ethylisoamylmalonic acid-cresol red system at 25° are shown in Figures 1 and 2. Since k_4 could not be obtained experimentally, a value was chosen such that one point fit the calculated curve. The results clearly show that reactions 4 and 5 can be ruled out for $\text{pH} \geq 7$. Figure 2 shows that, for $\text{pH} \sim 7$, τ is determined by reaction 3, and, for $\text{pH} \geq 8.3$, τ is determined by reaction 1. For $7.5 < \text{pH} < 8.3$, reactions 1, 2, and 3 must all be considered collectively.

The kinetic salt effect is also useful in identifying the reaction under study. A combination of the Brønsted-Bjerrum equation with the Debye-Hückel equation yields the following relationship between the rate constant and the ionic strength μ of the solution at 25°^{22,23}

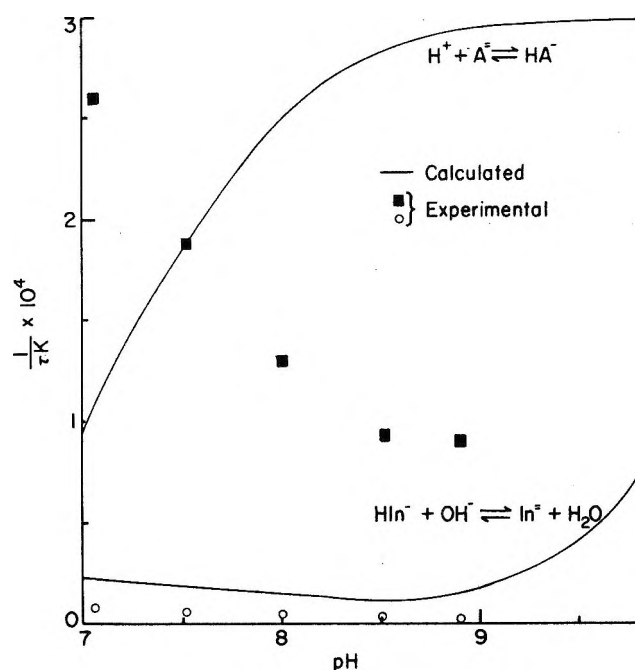


Figure 1. Plot of $(\tau k)^{-1}$ vs. pH for reactions 2 and 4 for the ethylisoamylmalonic acid-cresol red system where $C^{\text{H}_2\text{A}} = 3.00 \times 10^{-4} M$ and $C^{\text{HIn}} = 0.20 \times 10^{-4} M$; 25°.

(20) M. Eigen, *Angew. Chem.*, 75, 489 (1963).

(21) M. Eigen, W. Kruse, G. Maass, and L. DeMaeyer, "Progress in Reaction Kinetics," Vol. 2, G. Porter, Ed., Pergamon Press, Ltd., Oxford, England, 1964, p. 315.

(22) S. Glasstone, K. Laidler, and H. Eyring, "The Theory of Rate Processes," McGraw-Hill Book Co., Inc., New York, N. Y., 1941, pp. 427, 430.

(23) R. Livingston, "Technique of Organic Chemistry," Vol. VIII, Part 1, 2nd Ed., Interscience Publishers, Inc., New York, N. Y., 1963, pp. 43-45.

$$\log k = \log k_0 + 1.02Z_A Z_B \sqrt{\mu} \quad (11)$$

For reactions 1 through 6, $Z_A Z_B = +1, +1, +2, -2, -2,$ and $+1,$ respectively. For ethylisoamylmalonic acid, the best agreement with theory is obtained by assuming that τ is determined by reaction 1 for data at $\text{pH} > 8.3.$

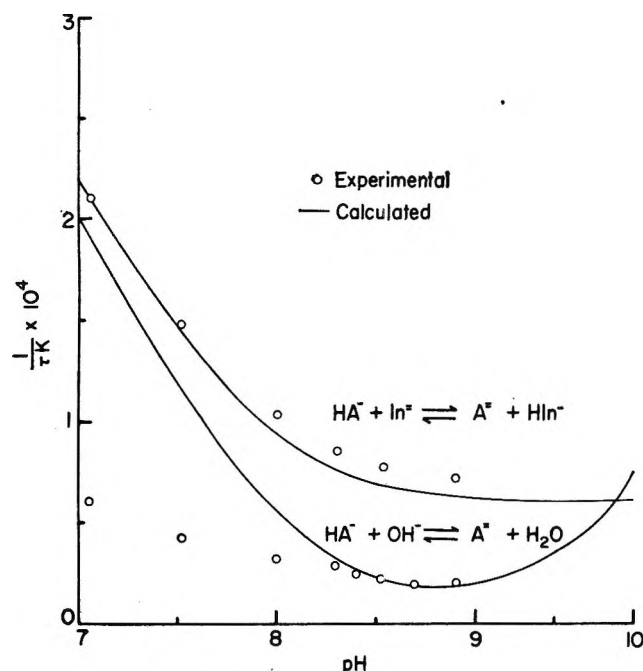
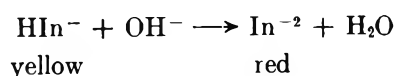


Figure 2. Plot of $(\tau k)^{-1}$ vs. pH for reactions 1 and 3 for the ethylisoamylmalonic acid-cresol red system where $C^0_{\text{H}_2\text{A}} = 3.00 \times 10^{-4} \text{ M}$ and $C^0_{\text{HIn}} = 0.20 \times 10^{-4} \text{ M}; 25^\circ.$

Indicator Correction. Considering once again equilibrium 1 and absorbing $[\text{H}_2\text{O}]$ into $K_{\text{eq}},$ we obtain the expression

$$K_{\text{eq}} = \frac{[\text{HA}^-][\text{OH}^-]}{[\text{A}^{2-}]} = \frac{K_w}{K_2} \quad (12)$$

where K_2 is insensitive to temperature change but where K_w changes significantly with temperature, increasing from $10^{-14.35}$ at 15° to $10^{-14.00}$ at $25^\circ.$ Thus, the net effect of the temperature jump is a perturbation of equilibrium 1 to the left. This perturbation is followed by the color change of the coupled indicator reaction going to the right. For cresol red we have



which results in decreasing light intensity being transmitted at $580 \text{ m}\mu.$ The question now arises as to what effect the coupled indicator reaction has on the ob-

served reaction. A correction factor previously given²⁴ is calculated from the conservation equations

$$\delta\text{HA}^- + \delta\text{A}^{2-} = 0 \quad (13)$$

$$\delta\text{HIn}^- + \delta\text{In}^{2-} = 0 \quad (14)$$

$$\delta\text{OH}^- - \delta\text{HA}^- - \delta\text{HIn}^- = 0 \quad (15)$$

with the assumption that only equilibria 1 and 2 require consideration. Solving (15) for $\delta\text{OH}^-,$ we obtain

$$\delta\text{OH}^- = \frac{\delta\text{HA}^-}{1 + \frac{\delta\text{In}^{2-}}{\delta\text{OH}^-}} = \frac{\delta\text{HA}^-}{1 + \alpha} \quad (16)$$

where $\alpha = \delta\text{In}^{2-}/\delta\text{OH}^-.$ This leads us to the rate expression³

$$\frac{-d\delta\text{HA}^-}{dt} = \left[k_1 \left(\frac{[\text{HA}^-]}{1 + \alpha} + [\text{OH}^-] \right) + k_{-1} \right] \delta\text{HA}^- \quad (17)$$

Thus the corrected expression for the relaxation time becomes

$$\frac{1}{\tau} = k_1 \left(\frac{[\text{HA}^-]}{1 + \alpha} + [\text{OH}^-] \right) + k_{-1} \quad (18)$$

By assuming that reaction 2 is already in an equilibrium state as reaction 1 approaches equilibrium, α can be calculated from the expression

$$K_{\text{In}} = \frac{[\text{HIn}^-][\text{OH}^-]}{[\text{In}^{2-}]} = \frac{K_w}{K_{\text{HIn}}} \quad (19)$$

where $K_{\text{HIn}} = [\text{H}^+][\text{In}^{2-}]/[\text{HIn}^-].$ Thus

$$K_{\text{In}}\delta\text{In}^{2-} = [\text{HIn}^-]\delta\text{OH}^- + [\text{OH}^-]\delta\text{HIn}^-$$

or

$$\frac{\delta\text{In}^{2-}}{\delta\text{OH}^-} = \alpha = \frac{[\text{HIn}^-]}{K_{\text{In}} + [\text{OH}^-]} \quad (20)$$

Thus, if the assumptions made are valid, the expression for the relaxation time corrected for the presence of indicator is

$$\frac{1}{\tau} = k_1 \left[\frac{[\text{HA}^-]}{1 + \frac{[\text{HIn}^-]}{K_{\text{In}} + [\text{OH}^-]}} + [\text{OH}^-] + \frac{K_w}{K_2} \right] \quad (21)$$

The experimental verification of the indicator correction factor of eq. 21 fails, as is evident from Table III. The precision of the uncorrected k_1 values for ethylisoamylmalonic acid is much better than that of the k_1 values obtained using the correction factor. This in-

(24) M. Eigen and W. Kruse, *Z. Naturforsch.*, **18b**, 857 (1963).

Table III: Comparison of the Corrected and Uncorrected k_1 Values for Ethylisobutyramalic Acid Showing the Greater Precision Where the Indicator Correction Is Not Applied^a

pH	$C_{H_2A}^b$	$C_{HI_n}^c$	$k_1,^d M^{-1}$ sec. ⁻¹ un- corrected	$k_1,^e M^{-1}$ sec. ⁻¹ corrected	$(1 + \alpha)^f$
8.00	2.0×10^{-4}	0.2×10^{-40}	1.5×10^8	6.7×10^8	5.4
8.30	3.0×10^{-4}	0.6×10^{-4h}	1.3×10^8	6.1×10^8	7.6
8.42	3.0×10^{-4}	0.2×10^{-4h}	1.4×10^8	2.9×10^8	2.6
8.60	4.0×10^{-4}	0.2×10^{-4h}	1.4×10^8	2.1×10^8	1.9
8.70	3.0×10^{-4}	0.15×10^{-4h}	1.8×10^8	2.3×10^8	1.5
8.80	10.0×10^{-4}	0.2×10^{-4h}	1.6×10^8	2.1×10^8	1.5

^a $pK_{HI_n} = 8.20$ for cresol red and 7.90 for phenol red; 25° ; $\mu = 0.1$. ^b Total ethylisobutyramalic acid concentration, mole/l. ^c Total indicator concentration, mole/l. ^d Calculated from eq. 1a. ^e Calculated from eq. 10. ^f α is the correction factor of eq. 9. ^g Phenol red. ^h Cresol red.

icates that the true indicator correction required is small and can be neglected in comparison to random errors inherent in the temperature-jump method (see Table VII). The failure of the correction factor in eq. 21 is probably due principally to the assumption that only reaction 2 need be considered in calculating $\ln^{-2}/\delta OH^-$. Other equilibria are present such as the proton exchange reaction, $HA^- + \ln^{-2} \rightleftharpoons HI_n^- + A^{-2}$. The neglect of these reactions in calculating α is not justified. A more exact treatment including the proton exchange reaction has been given^{19,20} which leads to

$$\frac{1}{\tau_{I,II}} = -\frac{S}{2} \left(1 \pm \sqrt{1 - \frac{4P}{S^2}} \right) \quad (22)$$

where

$$S = a_{11} + a_{22} \quad (23)$$

$$P = a_{11}a_{22} - a_{12}a_{21}$$

and

$$\begin{aligned} a_{11} &= -\{k_3(C_{HA^-} + C_{In^{-2}}) + k_{-3}(C_{A^{-2}} + C_{HI_n^-}) + \\ &\quad k_{-2} + k_2C_{OH^-}\} \\ a_{22} &= -\{k_2C_{HI_n^-} + k_{-1} + k_1(C_{OH^-} + C_{HA^-})\} \\ a_{12} &= -\{k_3C_{In^{-2}} + k_{-3}C_{HI_n^-} - k_2C_{HI_n^-}\} \\ a_{21} &= -\{k_{-1} + k_1C_{OH^-} - k_{-2} - k_2C_{OH^-}\} \end{aligned} \quad (24)$$

The values for k_3 , k_{-3} , k_2 , and k_{-2} can be determined experimentally and are given in Table IV. Also, $k_{-1} = K_w k_1 / K_2^M (0.83) [H_2O]$; thus, only one unknown (k_1) is left to solve for in eq. 22. Since the additional rate constants are not known exactly, the use of eq. 22 introduces other sources of error, but the several values calculated for k_1 from eq. 22 agree better with those cal-

culated from the simple uncorrected expression 7 than with values of k_1 calculated from eq. 21. This supports the assumption that, for the chosen experimental conditions, the indicator reactions can be neglected.

Kinetic Data. The measured τ characteristic of the perturbed equilibrium is a function of both the forward and back rate constant; hence, both k_f and k_{-f} have been determined from the experiments. As seen in Figure 3, τ changes greatly with temperature resulting in a large change in k_f . Thus, the energy of activation and ΔH^* , ΔS^* , and ΔF^* were calculated from the Arrhenius equation

$$k = A e^{-E_a/RT} \quad (25)$$

and from the Eyring rate equation²⁵

$$k = \frac{kT F^*}{h F_A F_B \dots} e^{-E_0/RT} = \frac{kT}{h} e^{-\Delta H^*/RT} e^{\Delta S^*/R} \quad (26)$$

Measurements were made at various concentrations and pH values. The results of the kinetic study of the forward reaction (k_1) are given in Table V, and the results for the reverse reaction (k_{-1}) are found in Table VI. The reported rate constant for each acid is the arithmetic mean of not less than three determinations, and the activation energies, enthalpies, and entropies are the values calculated assuming that the sample means are the true values of the rate constants. A statistical treatment of the errors is given in Table VII for the forward reaction. It was found that the sample standard deviation²⁶ between individual measurements was about 10% of the mean value, which is largely due to random errors inherent in the temperature-jump method. By taking n observations, the random errors present can be reduced by the factor²⁷ $1/\sqrt{n}$; thus, in Table VII s_m gives the probable error of the mean. Also, $\Delta \bar{k}_1$ gives the 95% confidence limits for the mean as calculated from the "student" t .²⁸ The probable errors in the activation energies and entropies can be calculated from the general expression^{29,30}

$$s_x^2 = \left(\frac{\partial X}{\partial x_1} \right)^2 s_{x_1}^2 + \left(\frac{\partial X}{\partial x_2} \right)^2 s_{x_2}^2 + \dots \quad (27)$$

and are given in Table VII. Since the rate constants

(25) Reference 22, pp. 189-199.

(26) Reference 13, p. 541.

(27) E. B. Wilson, Jr., "An Introduction to Scientific Research," McGraw-Hill Book Co., Inc., New York, N. Y., 1952, pp. 252-254.

(28) C. A. Bennett and N. L. Franklin, "Statistical Analysis in Chemistry and the Chemical Industry," John Wiley and Sons, Inc., New York, N. Y., 1954, pp. 28, 29, and 105-108.

(29) O. L. Davies, "Statistical Methods in Research and Production," 2nd Ed., Oliver and Boyd, Ltd., Edinburgh and London, 1949, p. 46.

(30) S. W. Benson, "The Foundations of Chemical Kinetics," McGraw-Hill Book Co., Inc., New York, N. Y., 1960, p. 91.

Table IV: Experimental Rate Constants at 25° and $\mu = 0.1$

Substance	Rate constants	
Cresol red	$k_2 = 6 \times 10^9 M^{-1} \text{sec.}^{-1}$	$k_{-2} = 2 \times 10^2 M^{-1} \text{sec.}^{-1}$
Ethylisoamylmalonic acid	$k_3 = 4.5 \times 10^7 M^{-1} \text{sec.}^{-1}$	$k_{-3} = 0.60 \times 10^7 M^{-1} \text{sec.}^{-1}$
Ethylisopropylmalonic acid	$k_3 = 2.2 \times 10^7 M^{-1} \text{sec.}^{-1}$	$k_{-3} = 1.5 \times 10^7 M^{-1} \text{sec.}^{-1}$

Table V: Kinetic Data for Reaction $\text{HA}^- + \text{OH}^- \xrightarrow{k_1} \text{A}^{2-} + \text{H}_2\text{O}$ in 0.10 M NaClO_4^a

Malonic acid	$k_1, M^{-1} \text{sec.}^{-1}$ (25°)	$k_1, M^{-1} \text{sec.}^{-1}$ (12°)	$E_a, \text{kcal./mole}$	$\Delta F^*, \text{kcal./mole}$	$\Delta H^*, \text{kcal./mole}$	$\Delta S^*, \text{cal./mole/deg.}$
Diethyl	28×10^7	19×10^7	5	6	4.5	-5
Ethyl- <i>n</i> -butyl	16×10^7	10×10^7	6	6.5	5.5	-3
Ethylisoamyl	16×10^7	10×10^7	6	6.5	5.5	-3
Ethylphenyl	14×10^7	9×10^7	6	6.5	5	-4
Di- <i>n</i> -butyl	14×10^7	9×10^7	6	6.5	5	-4
Di- <i>n</i> -heptyl	14×10^7	9×10^7	6	6.5	5	-4
Di- <i>n</i> -propyl	13×10^7	8×10^7	6.5	6.5	6	-1
Ethylisopropyl	5.5×10^7	3.0×10^7	7.5	7	7	0
Diisopropyl	4.5×10^7	2.4×10^7	8	7	7.5	+2

^a Values for ΔF^* , ΔH^* , and ΔS^* are for 25°.

Table VI: Kinetic Data for Reaction $\text{A}^{2-} + \text{H}_2\text{O} \xrightarrow{k_{-1}} \text{HA}^- + \text{OH}^-$ in 0.10 M NaClO_4^a

Malonic acid	$k_{-1}, M^{-1} \text{sec.}^{-1}$ (25°)	$k_{-1}, M^{-1} \text{sec.}^{-1}$ (12°)	$E_a, \text{kcal./mole}$	$\Delta F^*, \text{kcal./mole}$	$\Delta H^*, \text{kcal./mole}$	$\Delta S^*, \text{cal./mole/deg.}$
Ethylphenyl	0.43	0.10	19	18	18.5	+2
Diethyl	0.73	0.17	19	17.5	18.5	+3
Ethyl- <i>n</i> -butyl	0.71	0.15	20	17.5	19.5	+6
Ethylisoamyl	0.71	0.15	20	17.5	19.5	+6
Di- <i>n</i> -butyl	0.71	0.15	20	17.5	19.5	+6
Di- <i>n</i> -heptyl	0.86	0.19	20	17.5	19.5	+6
Di- <i>n</i> -propyl	0.63	0.13	20	17.5	19.5	+6
Ethylisopropyl	1.3	0.25	21.5	17.5	21	+12
Diisopropyl	3.9	0.72	22	16.5	21.5	+16

^a Values for ΔF^* , ΔH^* , and ΔS^* are for 25°.

for the reverse reaction were calculated from the expression $k_{-1} = K_w k_1 / K_2^M (0.83) [\text{H}_2\text{O}]$, k_{-1} contains the same percentage of error as found for k_1 . The probable errors in the activation energies and entropies for the reverse reaction (Table VI) are, on the average, $s(E_a) \sim 1.5 \text{ kcal./mole}$ and $s(\Delta S^*) \sim 5 \text{ cal./mole/deg.}$, or essentially the same as for the forward reaction.

If the results based on the mean values (Tables V and VI) are assumed correct, then a comparison of the activation enthalpies and entropies suggests that both the forward and reverse reactions belong to the extensive category for which the changes in rate within the series

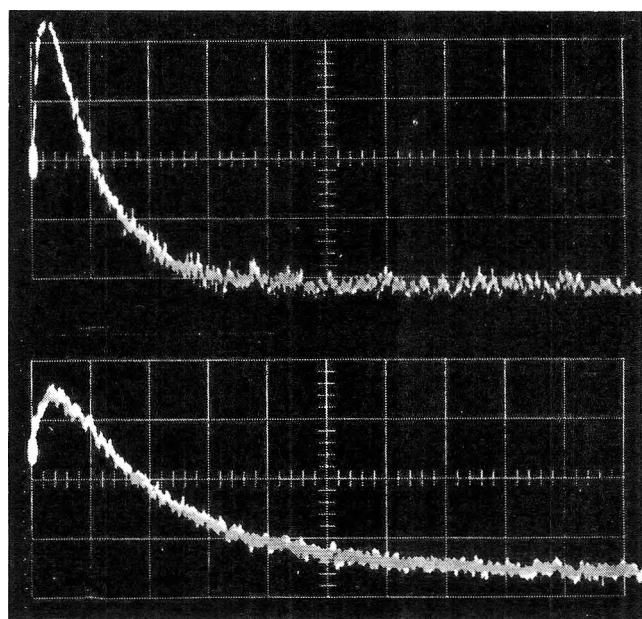


Figure 3. Top: experimental relaxation curve at 25° for ethylisopropylmalonic acid with $C^0_{\text{H}_2\text{A}} = 2.0 \times 10^{-4} M$; pH 8.2 and 0.1 M ionic strength. Bottom: experimental curve for same system at 12°. The ordinate of both is in arbitrary units proportional to the absorbance at $\lambda = 580 \text{ m}\mu$; the scale of the horizontal time axis is 0.2 msec./major division.

are due to parallel variations in ΔH^* and ΔS^* . For such reaction series, the slope of the linear plot of ΔH^* vs. ΔS^* is the isokinetic temperature—the absolute

Table VII: Statistical Treatment of the Random Errors Present in the Data for the Reaction⁷ $\text{HA}^- + \text{OH}^- \xrightarrow{k_1} \text{A}^{-2} + \text{H}_2\text{O}$

Malonic acid	$\bar{k}_1,^a M^{-1} \text{sec.}^{-1}$ (25°)	$\Delta\bar{k}_1^b \times 10^7$ (95%)	$s_m^c \times 10^7$	$\bar{k}_1,^a M^{-1} \text{sec.}^{-1}$ (12°)	$\Delta\bar{k}_1^b \times 10^7$ (95%)	$s_m^c \times 10^7$	$s(E_a), \text{kcal./mole}^d$	$s(\Delta S^\ddagger), \text{cal./mole/deg.}^e$
Diethyl	27.8×10^7	± 7.3	2.3	18.5×10^7	± 4.1	1.3	1.3	5
Ethylisoamyl	16.0×10^7	± 1.5	0.6	9.9×10^7	± 0.3	0.1	0.6	2
Ethylphenyl	14.0×10^7	± 2.2	0.7	9.3×10^7	± 1.9	0.4	1.1	4
Di- <i>n</i> -propyl	12.7×10^7	± 2.0	0.8	8.2×10^7	± 0.7	0.3	1.1	4
Ethylisopropyl	5.5×10^7	± 0.6	0.3	3.0×10^7	± 0.8	0.3	1.4	5
Diisopropyl	4.5×10^7	± 1.6	0.6	2.4×10^7	± 0.3	0.2	1.8	6

^a Arithmetic mean of the experimental rate constants. ^b Confidence limit of 95% for the mean rate constant. ^c Sample standard deviation of the mean rate constant. ^d Probable error in the activation energy. ^e Probable error in the activation entropy.

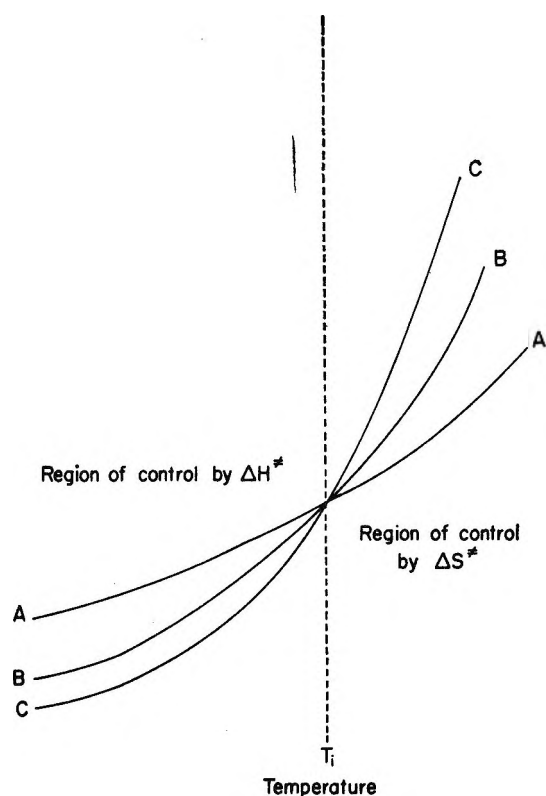


Figure 4. Illustration of inversion of relative rates at the isokinetic temperature T_i .

temperature at which the rate constants of the series become identical and the relative reactivity undergoes an inversion (Figure 4).³¹ This illustrates the danger in drawing conclusions from rate data for a reaction series measured at only one temperature.

Figure 5 suggests that the experimental temperature for the forward reaction is below the isokinetic temperature; hence, we have the familiar case where the kinetic data are measured in the "region of control by ΔH^\ddagger "; i.e., the reaction of lowest activation energy has the highest specific rate. From Figure 6 it appears that the

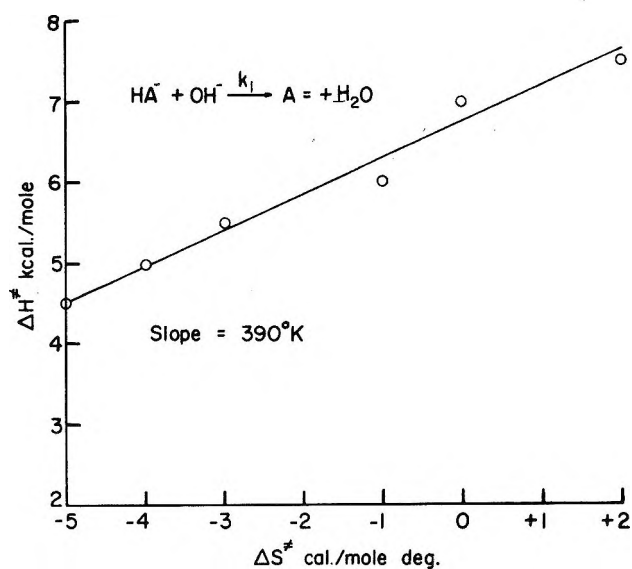


Figure 5. Enthalpy-entropy plot giving isokinetic temperature as 390°K. for $\text{HA}^- + \text{OH}^- \xrightarrow{k_1} \text{A}^{-2} + \text{H}_2\text{O}$ reaction.

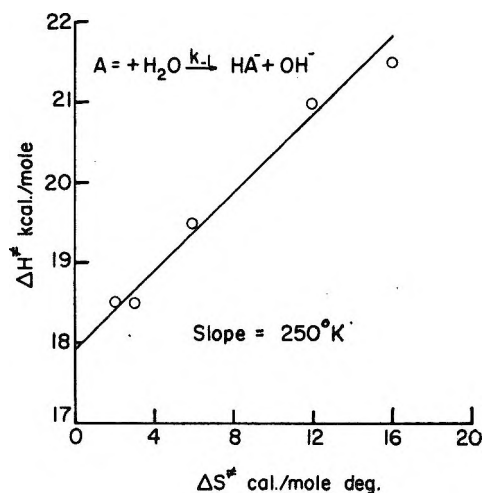
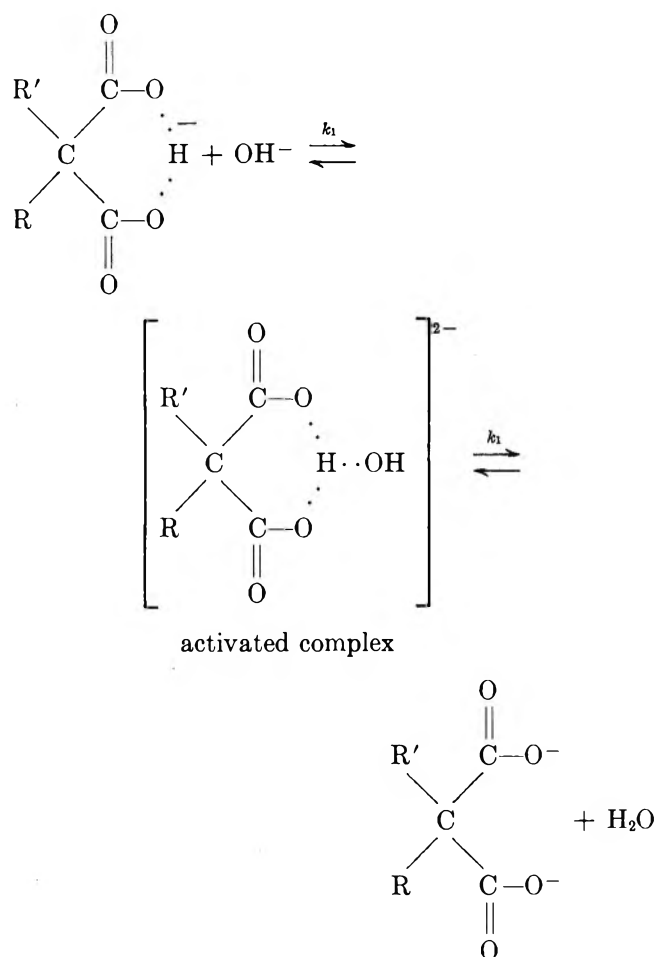


Figure 6. Enthalpy-entropy plot giving isokinetic temperature as 250°K. for $\text{A}^{-2} + \text{H}_2\text{O} \xrightarrow{k_{-1}} \text{HA}^- + \text{OH}^-$ reaction.

experimental temperature for the reverse reaction is above the isokinetic temperature; hence, we have the less familiar case where the kinetic data are measured in the "region of control by ΔS^* ." Control by ΔS^* is often encountered where the solvent is influencing the reaction rates, which is certainly the case for the reverse reaction.

Interpretations and Conclusions

The results in Tables V and VI may be interpreted by the mechanism



For the forward reaction, going to the activated complex involves seriously weakening the intramolecular hydrogen bond which primarily determines the activation energy. Thus, the compounds in Table V are arranged in the order of increasing strength of the hydrogen bond, for the stronger the H bond, the slower the reaction rate and the greater the activation energy. Not unexpectedly, the order is nearly the same as that of Table I based on acid dissociation constants. No explanation can be given for the position in Table V of di-*n*-propyl, except that it differs from di-*n*-butyl by an

amount smaller than the sample standard deviation of the mean. Ethylphenylmalonic acid does not properly belong in this series since the electron donor-acceptor effect of a benzene ring is opposite to that of an alkyl group. From a purely steric point of view, ethylphenylmalonic acid most closely resembles ethylisopropylmalonic acid in this series. The difference of 1.5 kcal./mole in the activation energies for the reaction $\text{HA}^- + \text{OH}^- \rightarrow \text{A}^{2-} + \text{H}_2\text{O}$ (see Table V) for these two acids can be attributed to the strong electron-withdrawing effect of the benzene ring which slightly weakens the intramolecular hydrogen bond. It appears likely from these observations that the primary effect of the alkyl substituents is steric in nature, and the small electronic variations of the alkyl groups are of less importance. For alkyl groups larger than ethyl the length of the chain seems to have little effect, and neither does branching on a remote carbon atom. However, branching on the carbon atom attached to the parent molecule is highly effective in "closing the jaws" to form a stronger intramolecular hydrogen bond.

In evaluating the results of Table VI for the reverse reaction, it should be recalled that this reaction was studied in the region of control by ΔS^* where the solvent is influencing the reaction rate. Thus the positive values obtained for ΔS^* may be attributed to the "melting" of solvent water molecules "frozen" about the A^{2-} ion. The increase in mobility of the surrounding water molecules in going to the activated complex contributes roughly 5 e.u./mole to ΔS^* , *i.e.*

$$\Delta S_{\text{fusion}} = \frac{\Delta H_{\text{fusion}}}{T} = \frac{1440 \text{ cal./mole}}{273 \text{ deg.}} \approx 5 \frac{\text{cal.}}{\text{mole deg.}}$$

The delocalization of charge in the activated complex renders it less effective than the dianion in immobilizing solvent molecules, thus the positive values of ΔS^* . In principle this explanation could be made more quantitative by combining alternative forms of the Eyring rate equation 15 to obtain

$$\Delta S^* = \frac{d(RT \ln K^*)}{dT} \quad (28)$$

However, writing a quotient of partition functions for K^* is difficult when solvent molecules are included.

The position of the di-*n*-heptyl acid in Tables V and VI indicates that doubling back of long alkyl chains is less effective than branching on the carbon atom adjacent to the parent molecule in strengthening the hydrogen bond. The position of ethylphenyl in Table

(31) J. F. Bunnett, "Technique of Organic Chemistry," Vol. VIII, Part 1, 2nd Ed., Interscience Publishers, Inc., New York, N. Y., 1963, pp. 204-210.

VI is probably due, once again, to the electron-withdrawing effect of the benzene ring.

While we can estimate from Table VI the number of water molecules that must be "melted" away from the dianion in the formation of an intramolecular hydrogen bond, we cannot shed more light on the interesting speculations of Chapman, *et al.*,³² regarding the number of water molecules remaining in the hydration spheres of this hydrogen bond once it is formed.

Summary

Intramolecular hydrogen bonding in various disubstituted malonic acids was studied by potentiometric titrations and by temperature-jump investigations of the reaction $\text{HA}^- + \text{OH}^- \rightleftharpoons \text{A}^{2-} + \text{H}_2\text{O}$. The results of both methods support the conclusion that the degree of hydrogen bonding is increased as branching close to the parent molecule is increased; *i.e.*, the principal effect is of a steric nature. The activation energy for the for-

ward reaction is about that expected for disrupting a hydrogen bond. The reverse reaction appears to be governed by a positive entropy of activation which can be attributed to the melting of solvent molecules in going to the activated state.

Acknowledgment. The authors wish to thank John L. Haslam and Gale A. Christiansen for their aid in preparing several of the compounds and Dean Henry Eyring for helpful discussions regarding the interpretation of the rate data. We also wish to acknowledge financial support from the University of Utah Research Fund, the National Institute of Arthritis and Metabolic Diseases (Grant AM-06231), and the Petroleum Research Fund of the American Chemical Society (Grant PRF 1515-A3).

(32) D. Chapman, D. R. Lloyd, and R. H. Prince, *J. Chem. Soc.*, 550 (1964).

Cleavage Reactions in Cross-Linked Urethane Elastomers

by A. V. Tobolsky, V. Johnson, and W. J. MacKnight

Department of Chemistry, Princeton University, Princeton, New Jersey (Received August 17, 1964)

A study of network cleavage in a cross-linked polyurethane elastomer was made using the technique of stress relaxation. It was found that the data could be well represented by a sum of two exponential decay terms, and a theoretical explanation for this is presented. Stress relaxation in the polyurethane sample investigated is discussed in terms of the reversible cleavage of various linkages formed by isocyanate reactions. It is possible to identify two different decay processes and to obtain activation energies for these processes. These are identified with cleavage of two different linkages. It is not possible, at present, to give a certain chemical identification of the linkages responsible for stress decay.

Introduction

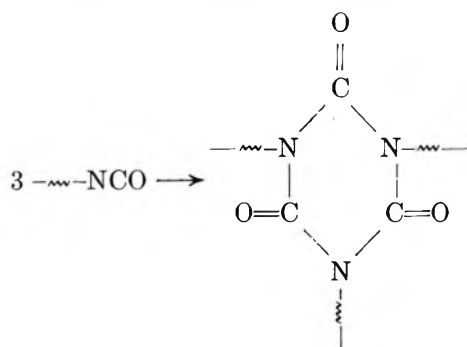
The polyurethanes are an important class of polymers which continue to find ever-widening applications in various fields. The building blocks of the polymer are primarily linked by urethane linkages; however, these may occasionally be replaced by other linkages. There are a large number of ways of preparing polyurethane

elastomers.¹ Very commonly a low molecular weight polyester or polyether with hydroxyl terminals is treated with an excess of diisocyanate. This leads to an isocyanate-terminated, liquid "prepolymer." The pre-

(1) J. H. Saunders and K. C. Frisch, "Polyurethanes: Chemistry and Technology, Part I. Chemistry," Vol. XVI in the series "High Polymers," John Wiley and Sons, Inc., New York, N. Y., 1962.

polymer is in some cases treated with a diol containing unsaturation in order to produce a "linear" polymer and yet allow for a subsequent vulcanization. Triols or higher polyols are often used to introduce cross linking directly. The isocyanate group is capable of reacting with essentially any functional group containing an active hydrogen, and it can also react with itself. In the case of the polyurethanes obtained by reaction with triol, it would be expected that, in addition to the urethane linkage, allophanate and "trimer linkage" may be present from side reactions.

The urethane linkage results from the reaction of an isocyanate and an alcohol; the allophanate, from an isocyanate and a urethane; the "trimer linkage," from reaction of three isocyanate groups as



If traces of water are accidentally present at any stage of the reaction, disubstituted urea linkages and biuret linkages are also formed.

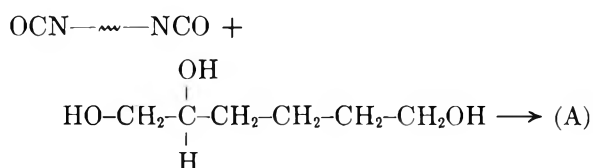
The polyurethanes are a remarkable class of elastomers in that they undergo stress relaxation or flow at elevated temperatures even though cross linked. This behavior is similar to that observed in the polysulfide and silicone rubbers. The term "chemical stress relaxation" or "chemical flow" is used to describe this phenomenon which is due to bond cleavage and re-formation.

The chemical stress relaxation of polyurethane elastomers was first studied by Offenbach and Tobolsky.² It was established that stress relaxation in the cross-linked elastomers occurs by scission of weak linkages formed by the reaction of the isocyanate group and other active hydrogen groups present in the cure mixture of prepolymer and polyol. Further work by Colodny and Tobolsky³ established that the disubstituted urea and biuret linkages are the weakest linkages normally present in the polyurethanes when water is purposely or accidentally present during cure.

It is the purpose of the present paper to show that stress relaxation in a particular sample of cross-linked polyurethane elastomer could be well represented by a sum of two exponential decay terms and to discuss the theoretical basis for this phenomenon.

Experimental

The cross-linked urethane elastomer (A) used in this study was kindly donated by the American Cyanamid Co. It was prepared from an isocyanate-terminated polyester prepolymer (Cyanoprene 4590) and 1,2,6-hexanetriol. A tertiary amine (dodecyldimethylamine) designated Armeen DM12D was used as a catalyst. The mixture was cured at 100° for 16 hr. Schematically



Stress relaxation studies were carried out on a relaxation balance.⁴ Purified nitrogen was kept streaming at slight overpressure through the thermostatic oven which contained the sample. Scission due to molecular oxygen was negligible under these conditions.² This was confirmed by "intermittent stress measurements."⁴ The intermittent modulus remained unchanged with time, showing that the bonds being cleaved were regenerating. A constant "intermittent modulus" is practically never observed under conditions of cleavage by molecular oxygen.

Results and Discussion

If there are exactly m identical linkages per network chain susceptible to cleavage or interchange, the expression for relative stress is obtained⁵

$$f(t)/f(0) = \exp(-kmt) \quad (1)$$

where $f(t)$ is the stress on the network at time t , $f(0)$ is the initial stress, k is the specific (first-order) rate constant for cleavage or interchange, and m is the number of bonds per network chain susceptible to cleavage or interchange. This simple exponential decay of stress was found to apply very well to the polysulfide rubbers^{6,7} although use of two exponential decay terms gives a slightly better fit to the data.^{8,9}

- (2) J. A. Offenbach and A. V. Tobolsky, *J. Colloid Sci.*, **11**, (1956).
- (3) P. C. Colodny and A. V. Tobolsky, *J. Am. Chem. Soc.*, **79**, 4320 (1957).
- (4) A. V. Tobolsky, "Properties and Structure of Polymers," John Wiley and Sons, Inc., New York, N. Y., 1960, Chapter V, p. 143.
- (5) A. V. Tobolsky, *ibid.*, Chapter IV, p. 12.
- (6) A. V. Tobolsky, R. B. Beevers, and G. D. T. Owen, *J. Colloid Sci.*, **18**, 395 (1963).
- (7) A. V. Tobolsky, *Polymer Letters*, **2**, 637 (1964).
- (8) R. B. Beevers, *J. Colloid Sci.*, **19**, 40 (1964).
- (9) A. V. Tobolsky, *Polymer Letters*, **B2**, 823 (1964).

Stress decay in the polyurethanes was also originally discussed on the basis of simple exponential decay.^{2,3} Equation 1 may be cast into the form

$$f(t)/f(0) = \exp(-t/\tau_{ch}) \quad (2)$$

where $\tau_{ch} = 1/km$. τ_{ch} may be measured as the time at which $f(t)/f(0) = 1/e$.

A more searching examination of the data shows that stress relaxation in the polyurethanes is more closely approximated by a sum of two exponentials rather than by a single exponential. The empirical expression for stress decay becomes (see Acknowledgment)

$$f(t)/f(0) = A \exp(-t/\tau_1) + B \exp(-t/\tau_2) \quad (3)$$

with $A + B = 1$ and $\tau_2 > \tau_1$.

If a plot of $\ln f(t)/f(0)$ is made as a function of linear time, the curve should become a straight line at long times with a slope of $-1/\tau_2$. If this line is extrapolated back to the ordinate, B is obtained. Also, a plot of $\ln (f(t)/f(0) - B e^{-t/\tau_2})$ as a function of time should be a straight line with slope $-1/\tau_1$ and intercept A . This method is mathematically the same as procedure X.¹⁰ It was found that the stress decay of sample (A) could be extremely well represented by this procedure. Only two exponential decay terms were required. For example, Figure 1 is a procedure X plot for (A) at 160°.

Experimentally, then, A , B , τ_1 , and τ_2 are accessible from stress relaxation data. These are tabulated in Table I. A plot of $\ln \tau_1$ or τ_2 as a function of $1/T$ should be a straight line, the activation energy for the

associated decay process being determinable from the slope. Figure 2 shows that τ_1 and τ_2 both fit the Arrhenius relation very well for (A). The activation energy for τ_2 is 42 ± 2 kcal. mole⁻¹, and for τ_1 , 37 ± 3 kcal. mole⁻¹.

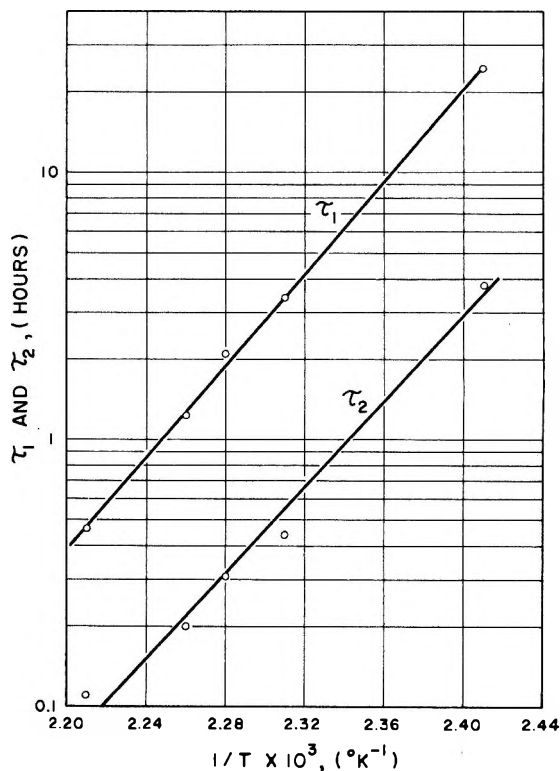


Figure 2. $\log \tau_1$ and τ_2 vs. $1/T$ for (A).

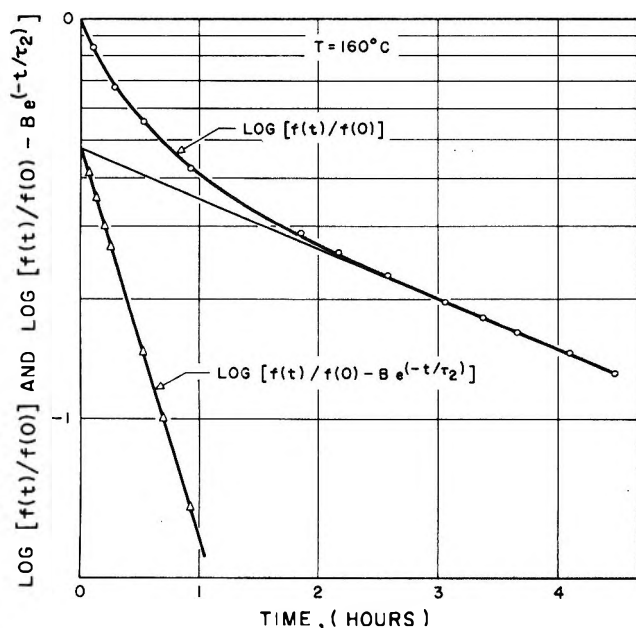


Figure 1. Procedure X for (A) at 160°.

Theory

The relaxation of stress represented by a sum of exponentials has been recently discussed theoretically in the following manner.⁹ It is assumed that the cleavable linkages divide into two types—strong and weak.

Consider a network with exactly m cleavable bonds per network chain. A fraction α of these bonds is weak linkages. Let the network chains be classified as N_{nul} , N_1 , N_2 , ..., N_m chains per cc. containing 0, 1, 2, 3, ..., m weak linkages. The total number of network chains per cc. is N_0 . From the binomial theorem

$$N_{nul} = N_0(1 - \alpha)^m$$

$$N_1 = N_0 m(1 - \alpha)^{m-1} \alpha$$

(10) A. V. Tobolsky and K. Murakami, *J. Polymer Sci.*, **40**, 433 (1959).

$$\begin{aligned}
 N_2 &= N_0 m \frac{(m-1)}{2} (1-\alpha)^{m-2} \alpha^2 & (4) \\
 &\dots \dots \dots \\
 N_m &= N_0 \alpha^m
 \end{aligned}$$

Restricting attention to N_{uni} and N_1 only, the theoretical equation for stress decay becomes

$$\frac{f(t)}{f(0)} = m(1-\alpha)^{m-1} \alpha \exp[(-k)(m-1)t + k_w t] + (1-\alpha)^m \exp(-kmt) \quad (5)$$

where k represents the specific rate constant for cleavage of the "strong" linkage and k_w represents the specific rate constant for cleavage of the "weak" linkage.

Comparing (5) with (3)

$$\begin{aligned}
 A &= m(1-\alpha)^{m-1} \alpha \\
 B &= (1-\alpha)^m \\
 1/\tau_1 &= k(m-1) + k_w \\
 1/\tau_2 &= km & (6)
 \end{aligned}$$

A , B , τ_1 , and τ_2 are determinable experimentally as already discussed. It remains to determine m , the number of cleavable linkages per network chain.

Inasmuch as the polyester and polyether chain backbones are very strong (and resistant to oxidative cleavage under our conditions),² the network linkages of interest are the urethane, allophanate, and perhaps the "trimer linkage." The rigorous exclusion of water during the preparation of sample (A) and the magnitude of τ_1 and τ_2 compared with previous data³ permit us to eliminate disubstituted urea and biuret linkages. It is probable that the trimer linkage is quite strong, and the allophanate linkage is weaker than the urethane (ref. 1, p. 328).

In principle, the possible number of distinct cleavable linkages in sample (A) is even greater than three since the urethane linkages formed from primary and secondary hydroxyls are different.¹¹ Different types of steric hindrance could also produce nonequivalent urethane linkages.

It is quite possible to generalize the theory to consider three or more types of cleavable linkages rather than just two. The theoretical treatment would invoke the multinomial theorem rather than the binomial theorem.

At present the experimental results are not extensive enough to warrant such a refinement. Equations 3 and 5 seem to fit the experimental data very well. However, we have somewhat of a problem with m because we cannot identify the two linkages being

cleaved with certainty at the present time. In order to identify these linkages a great deal of chemical work is required. Networks have to be prepared in which one could be sure that either the urethane or the allophanate or the trimer linkage was definitely absent, as well as the disubstituted urea and biuret. In addition, one would wish to be sure that all urethane linkages were equivalent. Such work is under way now and is very painstaking and time consuming.

Determination of the Value of m . If NCO-terminated prepolymer could be made to react quantitatively with an equivalent amount of triol, a network would be formed for which the only NCO-based linkages would be urethane linkages. In this case m is exactly 4 for each network chain. If there were two different types of urethane linkages, m would still be 4, and eq. 6 would hold exactly. This may be what is happening in sample (A).

On the other hand, if the NCO prepolymer were heated in the complete absence of triol or other curing agent, a gel would be formed based on allophanate and trimer linkages. If only allophanate formed, m would be 2.

Suppose sample (A) contained one type of urethane and one type of allophanate linkage (excluding trimer for the sake of argument), then m would not be the same in all chains but would have some average value \bar{m} between 2 and 4. Equations 4 still hold quite well even if m is an average value rather than the same in all network chains,⁷ but how could we obtain \bar{m} ?

Suppose α were the fraction of weak linkages, namely allophanate linkages. Then the following equation would hold

$$\bar{m} = 4(1-\alpha) + 2\alpha = 4 - 2\alpha \quad (7)$$

On the other hand, from eq. 6

$$B = (1-\alpha)^{\bar{m}} = (1-\alpha)^{4-2\alpha} \quad (8)$$

In other words, if the two linkages in question were a urethane linkage and an allophanate linkage, α could be determined from eq. 8 and the experimental value of B . From α , \bar{m} could be obtained from eq. 7. Then eq. 6 could be used to obtain k and k_w from τ_1 , τ_2 , and \bar{m} .

A graphical solution of α from the experimental value of B , according to eq. 8, is shown in Figure 3.

At this stage our ability to analyze the problem from a mathematical point of view is ahead of our ability to control the structure of the polyurethane networks. However, the interpretation of stress relaxation data

(11) T. L. Davis and J. M. Farnum, *J. Am. Chem. Soc.*, **56**, 883 (1934).

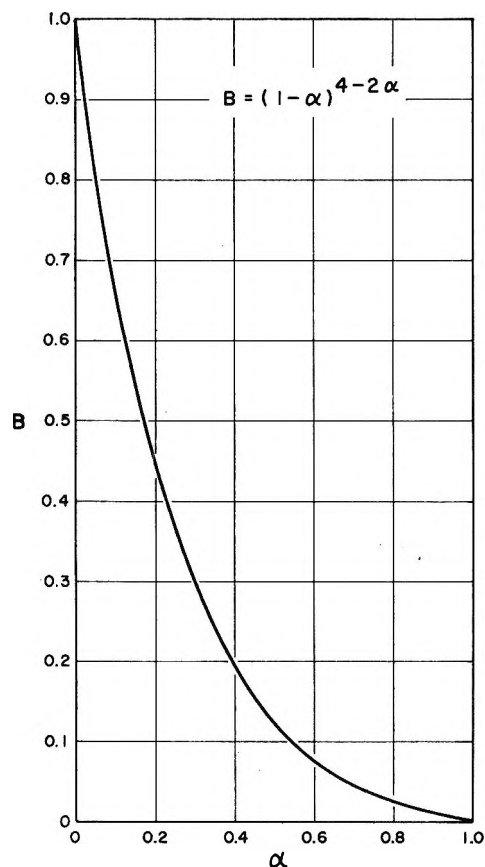


Figure 3. Plot of the relationship $B = (1 - \alpha)^{4-2\alpha}$.

for polyurethane networks prepared under very careful and well-defined conditions will be a very valuable conjunctive method for elucidation of the network structure.

The analysis presented in the present paper is more searching than the use of a single exponential decay term, which characterized earlier work in this field.^{2,3,12} Many of the previous conclusions are still valid, but it is quite possible that the role of allophanate and trimer linkages was overlooked.

The question arises as to whether a simple exponential decay as assumed here would occur even if only one type of linkage were susceptible to cleavage. Several theoretical discussions of this have been given,^{7,13,14} and the viewpoints vary to some extent. One author writes,¹³ "a partial analysis of randomization through interchange of chain bonds suggests that stress relaxation brought about by such processes should proceed by simple exponential decay." This is also the theoretical viewpoint taken in this paper and in previous papers emanating from this laboratory.⁷ The final proof has to be an experimental one, which is the attitude we have previously adopted.⁷

Table I

T , °C.	τ_1 , hr.	τ_2 , hr.	A	B
140	4.0	29	0.470	0.480
160	0.44	3.40	0.490	0.480
165	0.31	2.09	0.470	0.484
170	0.20	1.22	0.470	0.470

Acknowledgment. We are grateful to Drs. G. Mino, A. Singh, and L. Weissbein, who pointed out to us that chemical stress relaxation data for polyurethanes are better fitted by two relaxation times than by one. A preliminary report of their work has appeared¹⁵ and a complete paper has been submitted to the Journal of Polymer Science.

(12) A. V. Tobolsky and E. Peterson, *J. Phys. Chem.*, **67**, 930 (1963).

(13) P. J. Flory, *Trans. Faraday Soc.*, **56**, 722 (1960). See especially p. 743.

(14) J. Scanlan, *ibid.*, **57**, 839 (1961).

(15) A. Singh and L. Weissbein, Abstracts, 148th National Meeting of the American Chemical Society, Chicago, Ill., Sept. 1964, p. 14X.

The Shapes and Close-Pack Areas of Oriented Long-Chain Dipoles at the Water-Octane Interface

by Joseph J. Jasper and Robert D. Van Dell

Department of Chemistry, Wayne State University, Detroit, Michigan (Received August 17, 1964)

A vertical-pull filmometer with a sensitivity of ± 0.01 dyne was used to measure the interfacial surface pressures produced by soluble monolayers of eight normal alcohols which formed spontaneously at the *n*-octane-water interface as the result of positive adsorption from the *n*-octane phase. The pressures and other directly measured quantities are applied in the determination of a number of properties of the microscopic state of the monolayers. A number of equations are developed and from their plots (presented in two figures) the close-pack areas of the oriented dipoles, thickness of the monolayer, desorption energies, and the Szyszkowski constant, *a*, specific for each alcohol, are evaluated. The curves and the magnitudes of these quantities are analyzed and conclusions drawn concerning the structure of the monolayers.

A large body of data has been accumulated over the years with respect to insoluble monolayers on aqueous substrates as a consequence of pioneering studies of Rayleigh,¹ and in later years by Adam,² Langmuir,³ Harkins,⁴ and many others. These numerous and extensive investigations have led to a broad knowledge of the structures, states, and thermodynamic properties of a large number and variety of monolayers which were established at air-water interfaces. This knowledge has in turn enabled the formulation of important generalizations with respect to monolayers which have been very useful in surface chemistry.

Relatively little knowledge is presently available concerning the properties of insoluble monolayers of two-phase liquid systems. Although some studies of such monolayers have been reported,⁵ little experimental work appears to have been carried out in this direction, since the film-forming component of the system must be insoluble in both liquid phases but must possess a certain optimum work of adhesion with one of liquids and a relatively small work of cohesion.⁶

The primary concern of most monolayer studies reported in the literature is the identification and general properties of two-dimensional states of aggregation. Little consideration has been given, however, to the possible microscopic state of monolayers with respect to the exact structural arrangements, close-pack

areas of the oriented molecules in the interfacial region, and modes of orientation. It seemed reasonable to the authors that the most satisfactory approach to the study of the microscopic state of interfacial monolayers is through the appropriate equation of state. The present study is concerned with a series of octane-soluble dipoles which form a monolayer by positive adsorption chiefly from the organic phase in the water-octane interface. The equations applicable to the interfacial monolayers under consideration will be developed in a later section.

Experimental

Purification of the Compounds. The compounds selected for the monolayer component of the systems were 1-pentanol, 1-heptanol, 1-octanol, 1-nonanol, 1-decanol, 1-undecanol, 1-dodecanol, and 1-tetradecanol. This series represents a water-solubility gradation from

- (1) Lord Rayleigh, *Phil. Mag.*, **48**, 337 (1899).
- (2) N. K. Adam, "The Physics and Chemistry of Surfaces," 3rd Ed., Oxford University Press, London, 1941, Chapter 2.
- (3) I. Langmuir, *J. Am. Chem. Soc.*, **39**, 1848 (1917).
- (4) W. D. Harkins, "The Physical Chemistry of Surface Films," Reinhold Publishing Corp., New York, N. Y., 1952, Chapter 2.
- (5) F. A. Askew and J. F. Danielli, *Proc. Roy. Soc. (London)*, **A155**, 695 (1936); *Trans. Faraday Soc.*, **36**, 785 (1940).
- (6) N. K. Adam, "The Physics and Chemistry of Surfaces," 3rd Ed., Oxford University Press, London, 1941, p. 99.

slightly (but appreciable) to completely insoluble, which made it possible to compare the desorption energy of a soluble compound with those of the insoluble compounds.

The best quality of Matheson Coleman and Bell alcohols were obtained. These were fractionated in the usual manner and the middle third was selected for use. Vapor-phase chromatographic analysis indicated no significant impurities in the 1-pentanol, 1-heptanol, 1-octanol, and 1-tetradecanol. The 1-nonanol and 1-dodecanol tested 3% impurities, and the 1-decanol and 1-undecanol less than 1% impurities. The v.p.c. curves led to the conclusion that the impurities were isomeric alcohols and this was confirmed by infrared analysis. Such impurities, however, would have but negligible influence on the properties of the monolayers. Refractive indices of these compounds differed no more than one part in the fourth decimal from those of the critical tables. Pure grade *n*-octane (99 mole %) was obtained from Phillips Petroleum Co. and treated with lithium aluminum hydride. This was distilled and the distillate passed through a column of chromatographic quality adsorption alumina and silica gel. This was redistilled and the distillate examined by infrared spectroscopy, v.p.c., and refraction index. No impurities were detected.

It was essential that water of the highest possible purity be available. Doubly distilled water was first passed through a Barnstead block tin conductivity still and then redistilled in an all-quartz double chamber Heracus-Quarzschnmelze still. The water thus produced had a conductivity of 10^{-6} mho and was free of organic impurities.

Description of Apparatus. The interfacial surface pressures were measured with a modified form of the Wilhelmy balance adapted for use as a vertical-pull filmometer. The force of the vertical pull on the pendant slide was measured by an Ainsworth TCY semimicro keyboard balance. Complete details of instrumentation procedure and more important sources of error for a similar study have been described in a previous report.⁷ Some modifications, however, deserve mention. Many preliminary tests showed that the pendant slide is the most critical part of the apparatus and must be prepared with great care for operation. The present investigation required that the pendant slide be chemically inert, insoluble in all liquid phases, form a very small contact angle with the organic liquid, and a large one with water. DuPont Teflon (FEP) was found to meet these requirements very satisfactorily and, in addition, was practically impervious to the alcohols which constituted the monolayers. In contrast to the Teflon (TFE) used in

an earlier study, no polishing was necessary to remove the last traces of the alcohols adsorbed from the monolayer. The slide was constructed from a thin sheet of Teflon (FEP) with a perimeter of 3.48 cm. Use of a thin slide not only reduces its weight but also decreases the buoyancy damping effect with negligible change in the perimeter. Since it is of fundamental importance that the surface of the Teflon remain free from contaminants, the initial cleaning process and all subsequent ones between measurements were carried out in a series of boiling acids.

Experimental Procedure. The initial stage of the experimental procedure was to prepare the two-phase liquid systems. Seventy ml. of the purified *n*-octane and 90 ml. of water were mixed in a Pyrex bottle fitted with a Teflon seal. The bottle and contents were suspended in the thermostat bath for at least 5 hr. prior to their use in order that the two liquids become mutually saturated. This also provided the necessary time for any residual contaminants to diffuse into the interfacial region and become adsorbed. The bottle and contents were then carefully removed from the water bath without disturbing the interfacial region. Exactly 50 ml. of the organic liquid and 75 ml. of water were pipetted from the center of their respective bulk phases (again exercising every precaution not to disturb the interface) and placed in the pressure-measuring cell. To ensure a zero contact angle with octane, the slide was refluxed in pure octane for a half-hour period. The pendant slide was next attached to a fine gold chain suspended from the left arm of the chainomatic balance and then inserted through the interfacial region with a depth of immersion of about one-half of its length.

Balance readings were made on the interface during the first half-hour to test the constancy of the initial weight. The alcohols were introduced into the organic phase with the aid of a Starrett micrometer syringe calibrated to deliver liquid volumes up to 0.25 ml. with a precision of 0.0001 ml.

The operation involved the addition of exact measured quantities of the alcohols from the micrometer syringe into the octane phase just above the interface. After each addition, weighings were made until equilibrium was attained. During the weighings, care was taken to prevent the balance beam from swinging, in order that the pendant slide remain at the same depth of immersion throughout a given experiment. This minimizes the buoyancy effect, but, more important, it compensates for slight variations in the contact angle during the vertical motions of the slide.⁸ This proce-

(7) J. J. Jasper and B. L. Houseman, *J. Phys. Chem.*, **67**, 1548 (1963).

(8) D. F. Cheesman, *Biochem. J.*, **50**, 667 (1952).

dure requires a prior estimation of the weight increment Δw which must be added to the weight pan before the balance arm is released. This technique increased the sensitivity from ± 0.05 to ± 0.01 dyne. The bulk concentrations of the alcohols, C , are calculated by applying the appropriate data to eq. 1, in which D represents the density of the alcohol, v the volume delivered from

$$C = \frac{Dv}{VM} \quad (1)$$

the micrometer syringe, V the volume of the octane phase, and M the molecular weight of the alcohol. The values of C did not in any case exceed 0.0022 volume m . The interfacial surface pressure measurements were made at 25° and at this temperature and small concentrations studied, weight equilibrium was not attained in some cases for 72 hr. This seemed to imply that the desorption mechanism was very slow. Since the system could not be agitated, the interfacial region was subjected to infrared radiation to hasten desorption and, therefore, equilibrium. Although this procedure usually did speed up desorption, the system would still require 48 hr. to reach equilibrium. Whenever a measurement appeared to be excessively time-consuming, it was invalidated and a new one initiated.

The two-dimensional surface pressure P^s is a measure of the difference in the surface tension of the pure surface and that of the film-covered surface.⁹ If it is assumed that the surface pressure relation can be applied to the interfacial region, it may be written as

$$P_i^s = \gamma_i - \gamma_f \quad (2)$$

in which P_i^s represents the lateral pressure exerted by the interfacial monolayer, γ_i , the interfacial free surface energy, and γ_f , the interfacial free surface energy of the monolayer-covered interface. It is clear, therefore, that

$$P_i^s = -\Delta\gamma_i \quad (3)$$

Since the Teflon pendant slide was wet by the less dense octane only, the following equation was applied to convert differences in balance readings in dynes/cm.

$$\Delta\gamma_i = P_i^s = -\Delta Wg/p \quad (4)$$

where ΔW is the weight increment, g the gravitational factor, and p the perimeter of the slide. The sign of ΔW is dependent upon the wetting properties of the slide, negative if the slide is hydrophobic, and positive if hydrophilic.

Theoretical Discussion

The Szyszkowski equation was first applied to soluble monolayers formed at air-water interfaces in

1908,¹⁰ and at oil-water interfaces in 1958.^{11,12} The equation is written as

$$P^s = \frac{kT}{A_0} \ln \left(1 + \frac{C}{a} \right) \quad (5)$$

in which C is the bulk concentration, A_0 the close-pack area of the monolayer molecules, k the Boltzmann constant, T the absolute temperature, and a is a constant to be evaluated in following paragraphs. If the following form of the Gibbs surface excess equation¹³

$$\frac{1}{A} = \frac{C}{kT} \frac{dP^s}{dC} \quad (6)$$

is applied to eq. 5, the resulting relation obtained

$$\frac{1}{A} = \frac{1}{A_0} \left[\frac{C/a}{1 + C/a} \right] \quad (7)$$

is the Langmuir adsorption equation, in which $(1/A)$ represents the area occupied by 1 mole of the monolayer material. In the present systems, the alcohols are insoluble in the aqueous phase and the area chiefly occupied by these compounds is very probably in the octane side of the transitional region.¹⁴

When eq. 5 and 7 are combined, the equation of state for such monolayers is obtained. This is shown in

$$P_i^s = \frac{kT}{A_0} \ln \left(\frac{A}{A - A_0} \right) \quad (8)$$

This relation assumes that the molecules are adsorbed at fixed sites and that the monolayer is not mobile.¹⁵ This assumption, however, is not completely valid for two-phase liquid interfaces.

For low bulk concentrations, the Szyszkowski equation may be further simplified by rearranging to give

$$\frac{a}{a + C} = \exp \left[-\frac{P^s A_0}{kT} \right] \quad (9)$$

and expanding the exponential to include the first two terms only.

$$\frac{P^s}{C} = \frac{kT}{A_0 a} - \frac{P^s}{a} \quad (10)$$

(9) See ref. 4, p. 121.

(10) B. Szyszkowski, *Z. physik. Chem.*, **64**, 385 (1908).

(11) J. T. Davies, *Proc. Roy. Soc. (London)*, **A245**, 417, 429 (1958).

(12) H. P. Kling and E. Large, *Proc. 2nd Intern. Congr. Surface Activity*, **1**, 295 (1957).

(13) W. Gibbs, "Collected Works," Vol. I, Yale University Press, New Haven, Conn., 1948, p. 219.

(14) N. K. Adam and E. A. Guggenheim, *Proc. Roy. Soc. (London)*, **A139**, 218 (1933).

(15) D. A. Haydon and F. H. Taylor, *Phil. Trans.*, **252**, 225 (1960).

Equation 10 may also be obtained if it is assumed that the interfacial monolayer obeys the ideal two-dimensional gas law equation of Traube, $P^s A = kT$, and by substituting the Langmuir isotherm (eq. 7) for A . Equation 10, therefore, predicts that a plot of P^s/C vs. P^s should be linear with a negative slope for low-bulk concentrations. Under these conditions, the intercept is $(kT/A_0 a)$ and the slope is $(1/a)$.

To evaluate the constant a , it is necessary to examine the limiting adsorption isotherm (where $C = 0$) proposed by Davies and Rideal.¹⁶

$$1/A = (dCN/1000) \exp(\lambda/RT) \quad (11)$$

where d and N represent, respectively, the thickness of the monolayer and Avogadro's constant, λ , whose significance is discussed below, is the desorption energy per mole of film material. If C is very small, approaching zero, eq. 7 reduces to

$$1/A = C/Aa \quad (12)$$

Substitution of eq. 11 into eq. 12 and solving for a gives

$$a = \frac{1000}{NdA_0} \exp(-\lambda/RT) \quad (13)$$

λ depends on the type and number of groups anchored in the interfacial region as predicted by Traube's rule.¹⁷ For long-chain dipoles, such as normal acids, alcohols, etc., this rule is given by the equation

$$\lambda = \lambda_e + nw \quad (14)$$

where λ_e is the desorption energy of the hydrophilic end group ($-\text{CH}_3$, $-\text{COOH}$, $-\text{NO}_2$, $-\text{NH}_2$, etc.), n the number of $-\text{CH}_2-$ groups, and w the energy of desorption per $-\text{CH}_2-$ group. For dipoles oriented vertically to the interface, $\lambda = \lambda_e$. Normally, curves are obtained by plotting $\Delta W/v$ vs. ΔW . The resulting curve is linear with a negative slope in the low concentration range. The slope and intercept enable the calculation of a , A_0 , and d . Substitution of eq. 1 and 4 into eq. 10 gives the following relation expressed in terms of $\Delta W/v$

$$\frac{\Delta W}{v} = \frac{kTDp}{aA_0VgM} - \frac{D\Delta W}{aVM} \quad (15)$$

in which the first term on the right represents the intercept (I) and the quantity (D/aVM) the slope (S). From these relations, the following are obtained

$$a = D/SVM \quad (16)$$

$$A_0 = \frac{kTpS}{gI} \quad (17)$$

and finally

$$A = \frac{kTp}{gI} \left[\frac{1 + Sv}{v} \right] \quad (18)$$

When $\Delta W/v$ is plotted as a function of ΔW , linear curves are obtained for the series of alcohols as predicted by eq. 15. These are shown in Figure 1. The slopes all have nearly the same value of 5.00.

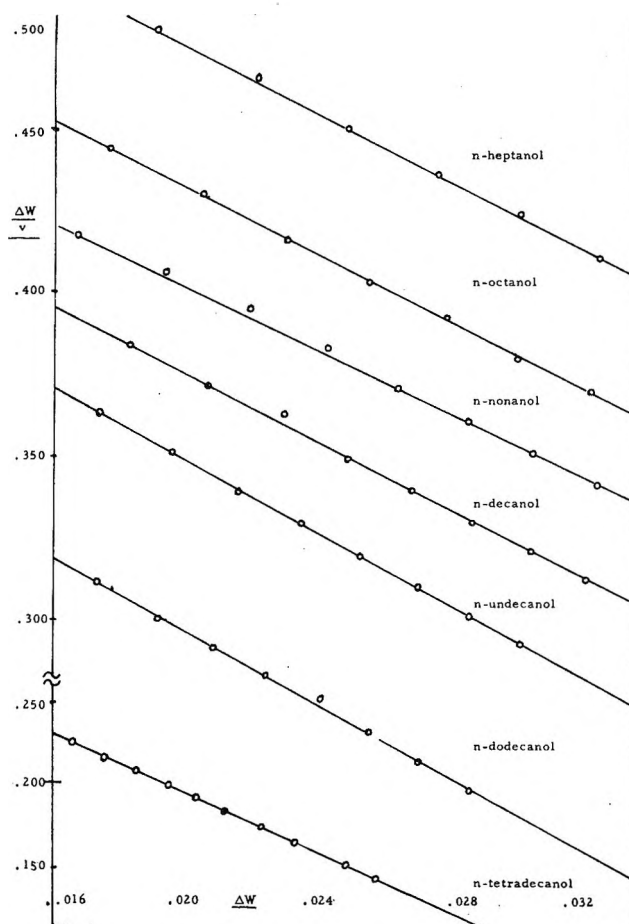


Figure 1. Variation of weight increment per unit volume of film material delivered with weight increment.

The curve for 1-pentanol is not included in Figure 1. The values of a , A_0 , and d are tabulated in Table I. It was found that A_0 varies with the fourth power of n and is shown in Figure 2.

It appears evident from values of A_0 that the alcohol molecules must be oriented perpendicularly in the interface as previously predicted.^{18,19} It seems reasonable

(16) J. T. Davies and E. K. Rideal, "Interfacial Phenomena," Academic Press, New York, N. Y., 1961, p. 155.

(17) I. Traube, *Liebigs Ann.*, **265**, 27 (1891).

(18) E. Hutchinson, *J. Colloid Sci.*, **3**, 413 (1948).

(19) A. F. H. Ward and L. Tordai, *Rec. trav. chim.*, **71**, 396 (1952).

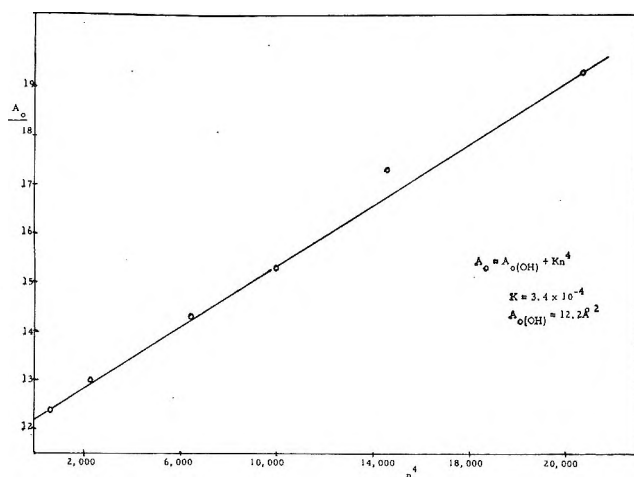


Figure 2. Close-pack area as a function of the fourth power of the number of carbons.

Table I: The Szyszkowski Constant, a , Close-Pack Values, A_0 , and Monolayer Thickness, d , for the Eight Alcohols

Dipole	a , mole ⁻¹	A_0 , Å ²	d , Å
1-Pentanol	0.0372	12.4	9.56
1-Heptanol	0.0284	13.0	12.2
1-Octanol	0.0254	13.7	12.8
1-Nonanol	0.0230	14.35	13.4
1-Decanol	0.0210	15.4	14.0
1-Undecanol	0.0193	17.3	13.2
1-Dodecanol	0.0179	19.3	12.9
1-Tetradecanol	0.0150	24.7	12.0

to assume, therefore, that the hydrophilic hydroxyl group is in the dimeric interface, and, consequently, the only group desorbed. This suggests that the desorption energy for all of the dipoles should be identical regardless of the chain length. To calculate the desorption energy λ for the -OH group, the values of A_0 , a , and d must be known for this group.

A_0 was obtained by extrapolating the curve of Figure 2 to the ordinate, which gives a value of 12.2 Å². Although this value is slightly larger than expected from bond-length calculations, it is possible that this may be due to the mobility of the monolayer molecules. To calculate the value of d , it is first necessary to postulate a shape for the volume occupied by the -OH group. Since this group possesses a degree of free rotation about the C-O bond, it was postulated that the effective volume would be cylindrical with a cross-sectional area equal to that of A_0 , and a length d equal to the

radius of the cylinder. The value of a was calculated from eq. 16 by applying the density D which was obtained by extrapolating the density vs. chain-length curves for normal alcohols to the density ordinate. From this, the density of the -OH group attached to the hydrocarbon chain was found to be 0.798 at 25°. With the aid of this model a value of 3.471 kcal./mole was obtained for λ from eq. 13. This value was then used in conjunction with the appropriate values of A_0 and a in eq. 13 to calculate the thickness d of the monolayer for each of the alcohols.

From examination of Table I, it is seen that there is a definite increase in the area occupied by a -CH₂- group with increasing chain length. This suggests that the chain is no longer oriented vertically but is folding over on itself to an increasing degree as the chain length increases. This may be the result of steric flexibility with chain length, increasing the probability of rotation along an axis parallel to the chain.

Chain interaction is ruled out because of the penetration of the octane molecules between those of the monolayer alcohols.²⁰ If this is the case, calculations should show a decrease in the monolayer thickness per -CH₂- group with increasing chain length. This tendency is clearly evident in Table I. Following 1-decanol, there is a slight but definite folding of the chain, which starts to level off with 1-tetradecanol.

The 1-pentanol, which had a slope of 3.12, was not included in Figure 1. The unexpected variation in the slope of this compound from that of the others was first considered to be the consequence of evaporation of the octane component of the system during the measurement. This would increase the bulk concentration with a resultant increase in the amount of monolayer adsorbed in the interface. Since the intercept is 0.392, a value much lower than would be expected, this cannot be the case, for evaporation should increase the intercept to a value greater than expected. The value of A_0 , however, is 12.4 Å². It is quite possible that the variation of the slope from that of the other alcohols may be due to some degree of solubility of 1-pentanol in the aqueous layer. The desorption energy for this compound into the octane phase is 3.203 kcal./mole, while that of the other alcohols is 3.471 kcal./mole.

(20) See ref. 16, p. 158.

Proton Magnetic Resonance Studies of Ten Diolefins^{1a}

by David F. Koster^{1b} and Alfred Danti

Department of Chemistry, Texas A. & M. University, College Station, Texas (Received August 20, 1964)

The proton magnetic resonance spectra of ten diolefins, with six to eight interacting spins and more complicated than any studied heretofore, have been measured with care and the complete theoretical spectra calculated for four of them. Chemical shifts and coupling constants are tabulated as completely as possible. The ten compounds are 1,2-butadiene, 1,2-pentadiene, 3-methyl-1,2-butadiene, 2,3-pentadiene, 2-methyl-1,3-butadiene, 2,3-dimethyl-1,3-butadiene, 1,*cis*-3-pentadiene, 1,*trans*-3-pentadiene, 1,4-pentadiene, and 1,5-hexadiene. Symmetry factoring of the energy levels was used in a number of instances and in some cases the molecule was broken up into lesser interacting parts before running the entire eight-spin problem. An interesting additive effect of substituents in reducing both the four-bond and five-bond *coupling constants* in allenic systems has been found. A noticeable coupling through six bonds was evident in two of the conjugated compounds.

Introduction

The proton magnetic resonance spectra of several compounds containing cumulative and conjugated double bonds have been analyzed previously.²⁻⁷ In most of these cases only three to five interacting protons were involved. In this study, more complicated members containing six to eight interacting protons have been examined. Where there were no more than eight interacting nuclei and the spectrum was well resolved, the theoretical spectrum was calculated completely using the computer program of Reilly and Swalen.⁸ In the allenic type systems, an additive effect on the four- and five-bond coupling constants appears to exist.

Experimental

The eight compounds listed in Tables I and II, along with 1,4-pentadiene (IX) and 1,5-hexadiene (X), were examined. The Roman numerals appearing beneath the semistructural formulas in Tables I and II will be used when referring to these compounds. All samples were extremely pure API Research samples available on loan from the API Research Projects 44 and 58B.⁹ Spectra were obtained on the pure liquids and 50% and 10% solutions (by volume) in CCl₄. Results reported for I through IV are for the pure liquid, the remainder being for the 50% solutions. For these hydrocarbons, spectra at different concentrations were very much alike. Spectra on which detailed

calculations were performed were run three times and peak positions averaged. A trace of tetramethylsilane was used as an internal reference.

Improved resolution was obtained by degassing the samples by the freeze-thaw technique at liquid nitrogen temperature and sealing them under vacuum in precision Varian A-60 tubes. Spectra of all of the compounds were recorded on a Varian Model A-60 spectrometer and for two of the compounds spectra were also obtained at 100 Mc. through the courtesy of Varian Associates. Sample temperature was approximately 37°. Line positions measured from TMS as

(1) (a) The studies were supported by The Robert A. Welch Foundation, Houston, Texas. Support for one summer for the Predoctoral Fellow was received from the American Petroleum Institute Research Project 44. (b) Predoctoral Fellow of The Robert A. Welch Foundation.

(2) E. B. Whipple, J. H. Goldstein, and W. E. Stewart, *J. Am. Chem. Soc.*, **81**, 4761 (1959).

(3) E. B. Whipple, J. H. Goldstein, and L. Mandell, *J. Chem. Phys.*, **30**, 1109 (1959).

(4) E. I. Snyder and J. D. Roberts, *J. Am. Chem. Soc.*, **84**, 1582 (1962).

(5) S. L. Manatt and D. D. Elleman, *ibid.*, **84**, 1579 (1962).

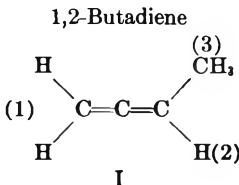
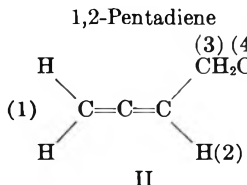
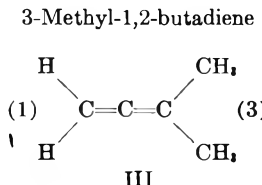
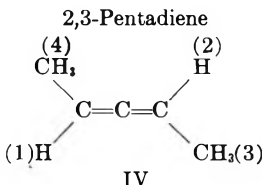
(6) J. A. Elvidge and L. M. Jackman, *Proc. Chem. Soc.*, 89 (1959).

(7) E. O. Bishop and J. I. Musher, *Mol. Phys.*, **6**, 621 (1963).

(8) C. A. Reilly and J. D. Swalen, *J. Chem. Phys.*, **37**, 21 (1962).

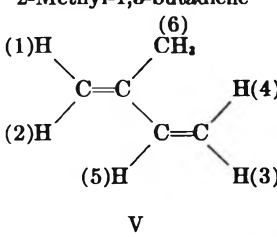
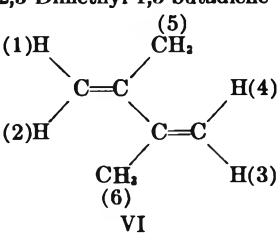
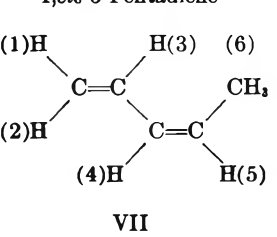
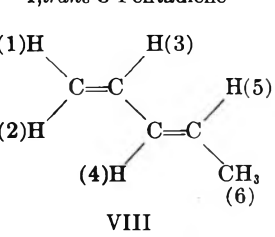
(9) American Petroleum Institute Research Project 44, Chemical Thermodynamic Properties Center, Department of Chemistry, Texas A. & M. University, College Station, Texas, and API Research Project 58B, Petroleum Research Laboratory, Department of Chemistry, Carnegie Institute of Technology, Pittsburgh 13, Pa.

Table I: Chemical Shifts and Coupling Constants for Alkyl Allenes^a

	1,2-Butadiene I	1,2-Pentadiene II	3-Methyl-1,2-butadiene III	2,3-Pentadiene IV
				
	δ, p.p.m.			
1	4.498	4.547	4.402	4.890
2	4.943	5.034
3	1.587	1.951	1.620	1.563
4	...	0.993
	J, c.p.s.			
12	-6.67	-6.77	...	-6.35
13	3.45	3.50	3.15 ^b	3.20
23	7.10	6.23	...	6.80
34	...	7.51

^a Except for III, where a first-order spectrum yields to immediate interpretation, data were obtained by calculation of the theoretical spectra. All data refer to the pure liquid. ^b Snyder and Roberts⁴ report a value of 3.03 ± 0.06 c.p.s.

Table II: Chemical Shifts and Coupling Constants in Conjugated Dienes^a

	2-Methyl-1,3-butadiene V	2,3-Dimethyl-1,3-butadiene VI	1,cis-3-Pentadiene VII	1,trans-3-Pentadiene VIII
				
	δ, p.p.m.			
1	4.87 ± 0.05	4.86 ± 0.05	4.99 ± 0.10	4.83 ± 0.10
2	4.87 ± 0.05	4.96 ± 0.05	5.07 ± 0.10	4.92 ± 0.10
3	4.94 ± 0.05	...	6.58 ± 0.05	?
4	5.05 ± 0.05	...	5.92 ± 0.05	?
5	6.35 ± 0.05	...	5.41 ± 0.05	?
6	1.79 ± 0.03	1.86 ± 0.03	1.70 ± 0.03	1.72 ± 0.03
	J, c.p.s.			
12		2.2		
13			10.5	
14	~0.6			
16	1.2	1.0	~0.6(?)	
23			16.6	
24	~0.6			
26	1.2			~0.6(?)
34	1.5		10.5	
35	10.5			
45	17.4		11.0	
46			1.5	
56			6.8	5.8

^a These data were obtained from first-order interpretation of the spectra and refer to samples diluted to 50% by volume with CCl₄.

zero are accurate to within ± 0.3 cycle. Differences in peak positions could be measured to ± 0.05 c.p.s. on expanded scans. Calibration of the chart for linearity was checked against CHCl_3 and *p*-anisaldehyde.¹⁰ Calculations were performed on the IBM 709 computer of the Data Processing Center at Texas A. & M. University.

The spectra in full have been contributed to the "Catalog of NMR Spectra" of the API Research Project 44 and may be found there.¹¹ The calculated spectra are also shown. Where two calculated spectra appear, the bottom one with fewer lines pertains to an initial calculation with certain lesser interacting protons left out. The upper calculated spectrum then refers to the full eight-spin problem.

Interpretation of the Spectra. Where the spectra were sufficiently resolved, the theoretical spectrum was calculated. This was the case for I, II, IV, and IX. Case III gives a first-order spectrum and the values given in Table I came directly from our experimental measurements. The remaining spectra were analyzed by first-order interpretation to give approximate chemical shifts and coupling constants for most of the protons.

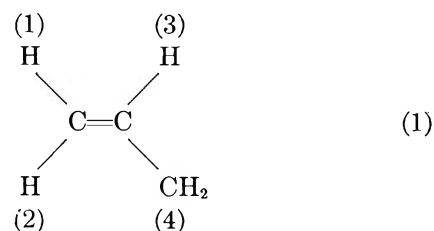
The general procedure for arriving at the calculated spectrum can be illustrated for I. Because the allenic structure is D_{2d} , one would expect the methyl proton resonance to be approximately two triplets. The high-field quintet that is obtained can be explained as two overlapping triplets. To give such a symmetrical quintet, J_{23} must be very close to twice J_{13} , J_{13} being very nearly equal to the spacing of the lines in the quintet. From approximate values of the chemical shifts and J_{12} , a calculated spectrum closely resembling the experimental was obtained. The calculated transitions were then assigned observed frequencies, the assignment being facilitated by symmetry factoring the energy levels.^{12,13}

The assigned transitions between these levels, when put into an energy level program (NMREN2),⁸ gave a set of experimental energy levels. Iteration on these energy levels gave the calculated spectrum and the final set of chemical shifts and coupling constants used to calculate it. (See Table I.) All coupling constants of the allenic compounds were assumed to be positive except the four-bond J_{12} constant which has been shown to be of opposite sign.^{4,5} However, it was found that a change of sign here did not affect the calculated spectrum noticeably.

Due to the large number of transitions and length of computer time, it was desirable to simplify the compounds containing eight protons. In the case of II, the previously mentioned procedure was followed

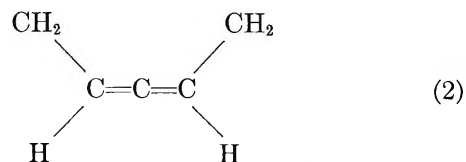
by ignoring the methyl protons, which are only coupled to the methylene protons. This gave all the coupling constants except J_{34} . The complete spectrum was then calculated including the methyl protons. For II, one obtains 256 energy levels that can be symmetry factored into eight groups, four of which are doubly degenerate; 869 transitions were assigned and the complete calculated spectrum with one iteration ran 198 min. on the IBM 709.

Similarly, IX (1,4-pentadiene) was first treated as



to obtain a good fit to the vinyl part of the spectrum. The final spectrum with all eight protons was then calculated. The agreement was good and no iterations were performed to arrive at the final spectrum. The results are given in a later discussion of this compound.

The spectrum of IV caused some difficulties in that there is no easy way to treat it without considering all eight protons ($A_3A_3^*XX^*$). A fairly good fit for the methyl proton resonance was obtained by removing one proton from each methyl and treating it as



This allows coupling constants to be determined with fair accuracy. The final calculated spectrum including all eight protons was then calculated. The fit was good and no iterations were performed.

Results and Discussion

In discussing the compounds studied, it will be convenient to separate them into three groups; those containing cumulative, conjugated, and isolated double bonds.

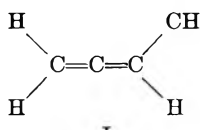
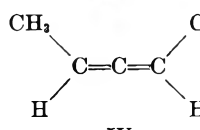
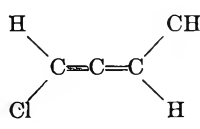
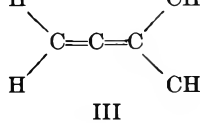
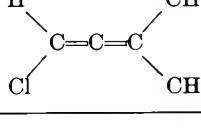
(10) Accurate measurements on *p*-anisaldehyde made available by N. F. Chamberlain, Humble Oil and Refining Co., Baytown, Texas.

(11) "Catalogs of NMR Spectra," American Petroleum Institute Research Project 44, Chemical Thermodynamic Properties Center, Department of Chemistry, Texas A. & M. University, College Station, Texas, B. J. Zwolinski, Director; Serial No. 465-475.

(12) H. M. McConnell, A. D. McLean, and C. A. Reilly, *J. Chem. Phys.*, **23**, 1152 (1955).

(13) E. B. Wilson, Jr., *ibid.*, **27**, 60 (1957).

Table III: Experimental and Predicted Coupling Constants in Allenic Systems

Compound	Ref.	Four-bond J_{HH} coupling		Five-bond J_{H,CH_3} coupling	
		Exptl.	Predicted	Exptl.	Predicted
 I	This work	6.67 ± 0.05		3.45 ± 0.05	(No entry, parent molecule)
 IV	This work	6.35 ± 0.10	6.34	3.20 ± 0.10	3.12
 II	4	5.80 ± 0.10	5.77	2.40 ± 0.10	2.22
 III	This work			3.15 ± 0.05	3.12
 V	4			2.14 ± 0.10	2.22

Cumulative Double Bonds. Several previous studies²⁻⁵ on compounds containing the allenic structure have all shown two distinct characteristics; a shift to high field of the allenic proton resonance relative to a vinyl proton, and relatively large four- and five-bond couplings between protons separated by this π -electronic structure. Both effects have been treated theoretically.^{14,15} Very good predictions on the magnitude of the coupling constants (including relative sign) have been made.¹⁴

The chemical shifts and coupling constants for I, II, III, and IV are summarized in Table I. Utilizing these data, along with coupling constants reported for other substituted allenes,²⁻⁴ it appears that an additive effect exists in the four-bond J_{HH} and five-bond J_{H,CH_3} coupling constants.

If allene, with the four-bond J_{HH} equal to 7.0 cycles,² is considered the parent compound, the effect of substituting one proton in allene by Cl, Br, I, CH₃, or a CH₂CH₃ group is found to be a decrease in the four-bond J_{HH} coupling constant by 0.9, 0.7, 0.7, 0.33, and 0.23 cycle, respectively. If each substituent has an additive (or subtractive) effect, a Cl and a CH₃ on the allenic structure might be expected to reduce J_{HH} by 1.23 cycles, a Cl and Br to reduce it by 1.6 cycles,

etc. Unfortunately, only a few of these compounds are available to check this. As shown in Table III, those that are known do check very closely.

It was thought that this same additive effect might also exist in the five-bond J_{H,CH_3} coupling, and it is here that some strength is added to the argument. If now I is considered the parent compound, and the five-bond J_{H,CH_3} coupling is examined in substituted compounds, it is found that the Cl and CH₃ groups have about the same effect here as on the J_{HH} four-bond coupling. The predicted and known four- and five-bond coupling constants are summarized in Table III.

A reasonable explanation of this appears available. Theoretical calculations¹⁴ of these long-range couplings involve a σ - and π -electronic term, the σ -term making only a small contribution. It is evidently the π -electronic structure that allows this relatively large coupling, and these mobile electrons are easily affected by substituents. It is not readily apparent why Cl and CH₃ should both reduce the magnitude of this long-range coupling.

(14) M. Karplus, *J. Am. Chem. Soc.*, **82**, 4431 (1960).

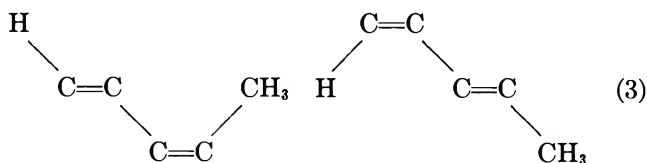
(15) J. A. Pople, *J. Chem. Phys.*, **24**, 1111 (1956).

Correlations of proton coupling with substituent have been made for substituted ethanes.¹⁶⁻¹⁸ These have been of the form, $J = A - B\Sigma E$, where A and B are constants and E is the electronegativity of the substituent(s) based on Huggins electronegativities. One might hope to find a similar correlation for allenic systems, if enough compounds of the type $\text{XHC}=\text{C}=\text{CHY}$ were available. However, from the standpoint of electronegativities, this does not appear too promising for the limited number of compounds for which data are now available. Information cited previously shows that bromoallene and iodoallene have the same coupling. The effect of substituents on the one-bond $^{13}\text{C}-\text{H}$ coupling has also been studied extensively.¹⁹⁻²¹

Conjugated Double Bonds. Previous studies on substituted 1,3-butadienes have been reported.^{6,7} A relatively small *trans*-vinyl coupling and a large 2,3-coupling (protons on carbons 2 and 3 of 1,3-butadiene) were reported for the *trans-trans*-muconic ester.⁶ Recent calculations⁷ on the *trans-trans*-muconic acid are more consistent and it has been suggested that several J 's may have been interchanged in the ester. Approximate coupling constants obtained in this study are in agreement with the latter authors.⁷

The spectra of V, VI, VII, and VIII were analyzed by inspection where possible. The 100-Mc. spectrum of VII²² greatly facilitated the assignment of the overlapping lines. The large number of overlapping resonances discouraged any detailed calculation. Our results are summarized in Table II. The lack of information on VIII is due to its extremely complex spectrum. The resonances of protons 3, 4, and 5 cannot be distinguished from an array of lines from ~ 333 to 385 cycles. Approximate coupling constants for V have been reported elsewhere.²³

It is interesting to note that there appears to be a detectable six-bond coupling between either proton(s) 1 and (or) 2 and the methyl protons in VII and VIII. Inspection of the resonance lines of protons 1 and 2 in VII and VIII suggests that it is the proton *cis* to the methyl group that is more strongly coupled, *i.e.*



The vinyl resonance of VI showed two broad lines. The line at higher field was assigned to proton 1 as is the case in VII and VIII. Attempts to analyze the spectrum of 1,3-butadiene (not listed in any of the

Tables and not mentioned heretofore) at 60 and 100 Mc.²² proved fruitless.

Isolated Double Bonds. Only two compounds were studied in this group, IX and X. The spectrum of IX (1,4-pentadiene) was analyzed as described earlier (eq. 1), with the following values of J and chemical shifts giving a good calculated spectrum

$$\begin{aligned} \delta_1 &= 4.920 \text{ (p.p.m.)} & \delta_2 &= 4.950 & \delta_3 &= 5.710 & \delta_4 &= 2.723 \\ J_{12} &= 2.20 & J_{13} &= 10.3 & J_{14} &= -1.50 & J_{23} &= 16.9 \\ & & & & J_{24} &= -1.30 & J_{34} &= 6.30 \end{aligned}$$

The negative sign given to J_{14} and J_{24} is on the basis of earlier work.^{6,24-27}

One would expect that the inclusion of one more methylene group between the two vinyl groups would have very little effect on the vinyl proton resonance. This is not the case in going from IX to X (1,5-hexadiene). The twelve lines expected for X are clearly evident, but they are superimposed on a much more complex group of lines. Likewise, the remaining terminal vinyl and methylene proton spectrum in X is not clearly resolved as in IX. At present, this cannot be easily explained, but it may be that the non-terminal vinyl protons in X are also coupled to the methylene protons in the position β to them. This would require a coupling through four single bonds.

Acknowledgments. We are grateful to The Robert A. Welch Foundation, Houston, Texas, for support of these studies. The API Research Project 44 also contributed support for one summer. We express thanks to the Data Processing Center of Texas A. & M. University for computer calculations. We acknowledge the help from F. S. Mortimer, C. A. Reilly, and J. D. Swalen of Shell Development, Emeryville, Calif.,

(16) R. C. Glick and A. A. Bothner-By, *J. Chem. Phys.*, **25**, 362 (1956).

(17) C. N. Banwell and N. Sheppard, *Discussions Faraday Soc.*, **34**, 115 (1962).

(18) R. J. Abraham and K. G. R. Pachler, *Mol. Phys.*, **7**, 165 (1963).

(19) H. S. Gutowsky and C. S. Juan, *J. Am. Chem. Soc.*, **84**, 306 (1962).

(20) C. Juan and H. S. Gutowsky, *J. Chem. Phys.*, **37**, 2198 (1962).

(21) A. W. Douglas, *ibid.*, **40**, 2413 (1964).

(22) Spectrum obtained by Varian Associates on a 100-Mc. instrument. Courtesy of James Shoolery and Norman Bhacca.

(23) J. A. Pople, W. G. Schneider, and H. J. Bernstein, "High-Resolution Nuclear Magnetic Resonance," McGraw-Hill Book Co., Inc., New York, N. Y., 1959, pp. 244, 245.

(24) S. Alexander, *J. Chem. Phys.*, **28**, 358 (1958).

(25) F. S. Mortimer, *J. Mol. Spectry.*, **3**, 335 (1959).

(26) A. D. Cohen and N. Sheppard, *Proc. Roy. Soc. (London)*, **A252**, 488 (1959).

(27) C. N. Banwell, A. D. Cohen, N. Sheppard, and J. J. Turner, *Proc. Chem. Soc.*, 266 (1959).

in making available the complete computer programs and the guidance which they gave. We acknowledge discussions with Dr. R. M. Hedges and the encourage-

ment of Dr. B. J. Zwolinski. The research samples were made available through the API Research Projects 44 and 58B.

Generation of Catalytic Activity in Silica Gel by Ionizing Radiation

by C. Barter and C. D. Wagner

Shell Development Company, Emeryville, California (Received August 20, 1964)

In a previous paper it was reported that acid centers are generated in silica gel by the action of ionizing radiation, *in vacuo*. These centers persist in the gel, in the absence of radiation, but are thermally sensitive. At 25° they disappear with a half-time of a few hours, as shown by the loss of acid titer and activity for isobutylene polymerization. Further study of irradiated silica gel has disclosed that radiation generates at least two other types of chemically active centers. These are stable at more elevated temperatures and are active for butene interconversions and for the conversion of cyclopropane to propylene.

Introduction

That irradiation of silica gel with X-rays results in surface changes other than the generation of acid centers has been suggested by spectroscopic evidence.¹ Following butylamine neutralization of the gel or thermal decay of its generated acid centers, the absorption spectrum of adsorbed *p*-dimethylaminoazobenzene is not at all characteristic of this indicator in its neutral form, in solution or adsorbed on unirradiated gel. The surface changes responsible for the altered spectrum are reversible; they may be due to atomic displacements, for the heating of irradiated silica gel at 500° for 10 hr. prior to adsorption of the indicator results in an absorption spectrum identical with that obtained with unirradiated gel.

The active centers studied in this work may be similar to those observed by Mikovsky and Weisz² as a result of neutron irradiation (10^{20} n.v.t.) of silica gel; they attributed the centers to atomic displacement.

Experimental

Davison 950 silica gel, 60–200 mesh, surface area 625 m.²/g., aluminum content <0.01%, was baked at 520° in air for several days, evacuated in a glass vessel

at 520° under high vacuum for 16 hr., and irradiated in its sealed container with bremsstrahlung from a 3-Mev. electron beam impinging on a gold target. The detailed procedure has been described previously.¹ The butenes used were Phillips research grade and contained less than 0.5% impurities (isomers). The cyclopropane contained about 0.5% propylene.

After the gel was irradiated, it was stored at –196° until it was used; this storage period varied from 1 to 18 hr. The 22-ml. vessel, shown in Figure 1, was connected to the vacuum system at B, the seal at C was broken, and the hydrocarbon was condensed into it at –196°. With its contents held at –196°, the tube was sealed under vacuum at D. Then space F was evacuated *via* a hypodermic needle through the silicone rubber plug E, the contents of A was warmed to about –10°, and seal G was broken by a solid needle inserted through E. At reasonable intervals, samples of 0.3% of the charge were removed from E by a hypodermic needle for gas chromatographic analysis.

The column used was a 5-mm. i.d. × 7-m. column,

- (1) C. Barter and C. D. Wagner, *J. Phys. Chem.*, **68**, 2381 (1964).
- (2) R. J. Mikovsky and P. B. Weisz, *J. Catalysis*, **1**, 345 (1962).

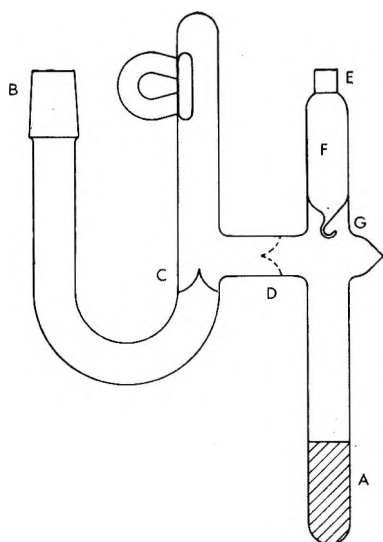


Figure 1. Gel irradiation apparatus.

filled with silicone on firebrick. This column, run at 50° with a helium flow rate of 75 cc./min., gave completely resolved peaks for the components analyzed. Since mole fractions of the components were found to be proportional to the peak heights, the latter were used in the analysis.

At the selected reaction temperature, 80° , the activity of the catalyst declined during the reaction. This was shown by the diminution of the apparent rate constant for the reaction, whether it was calculated as either first or second order in reactant partial pressure. Activity of the catalyst at zero time was used as the measure of catalyst activity. It was determined for the butene system in the following way. The product partial pressure was first plotted against reaction time. Values of the slope, dP/dt , were obtained graphically, and quantities, $dP/dt \times 1/R$ (R = reactant partial pressure), were plotted against time. The apparent first-order rate constants so derived at various reaction times decreased markedly as the reaction proceeded to half the initial value in 50–150 min.; the derived curve was extrapolated to zero time to give the apparent first-order rate constant for fresh, irradiated catalyst. In the cyclopropane system, the activity of the catalyst decreased very rapidly with time, sometimes by two orders of magnitude in 1 hr. This made the preceding procedure unreliable. Rough estimates of initial activity were made by estimating the initial slope of the curve of product concentration vs. time, as shown in Figure 2.

Results

In pilot experiments, portions of gel were irradiated at -196° to doses of 5 Mrads, stored for 1 hr. at

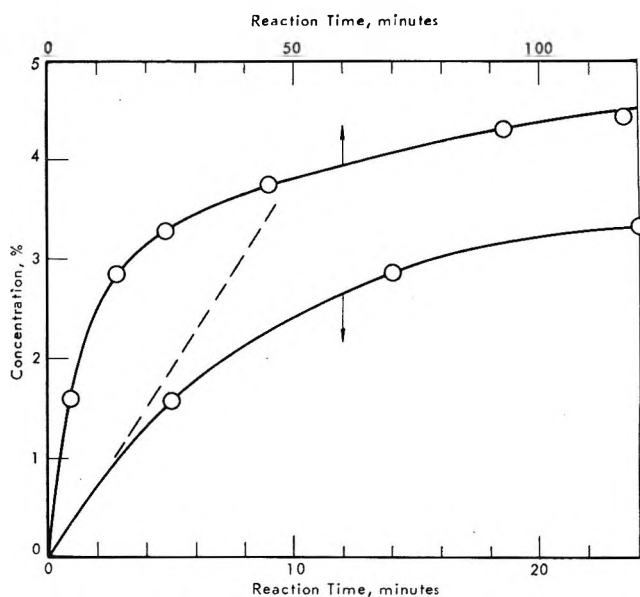


Figure 2. Propylene formation from cyclopropane over irradiated silica gel.

various elevated temperatures, and then tested for catalytic activity by using *cis*-2-butene or cyclopropane at 80° . It was found that storage of irradiated gel *in vacuo* at 100° had an adverse effect upon the activity for cyclopropane isomerization but not for butene isomerization. Storage at 200° caused the activity for cyclopropane isomerization to decrease still more, but the activity for butene isomerization was not affected until the gel was heated above 400° . Experiments were then performed with storage at 100, 200, and 420° in order to follow the decay of these activities. Other experiments under various irradiation and storage conditions were performed to obtain information about the activation energy for decay of the active centers and information on the effect of the irradiation temperature on the generation of activity. The data are given in Table I. The activities for butene and cyclopropane isomerization are believed reliable to $\pm 25\%$.

Discussion

Reduction in Activity during the Test Reaction. It was stated above that treatment of the butene isomerization reaction as either first or second order in hydrocarbon reactant partial pressure yielded a significant decrease in rate constant with time of reaction. This effect is not due to nonlinearity in the adsorption isotherm since this cause could only be significant for *cis*-2-butene, and, in this case, the adsorption isotherm was determined and found to be nearly linear over the range of interest. The decrease, also, cannot be attributed to the fact that the reaction is reversible; with

cis-2-butene this has only a small effect over the conversion range studied. A third possibility, thermal decay, cannot be responsible because storage of the irradiated gel at 80° for extended periods resulted in no change in its initial activity. The decrease in

the initial activity of the catalyst may have been derived from generated acid centers which early became ineffective through decay and coking.

Activation Energy for Decay. It seemed of particular interest to obtain information on the temperature dependence of decay of sites active for butene interconversions since these sites are so thermally stable. Data from Table I show that at 420° the decay fits a first-order rate curve reasonably well. An attempt was made to determine the decay activation energy by performing experiments with irradiated gel heated to 420, 448, and 481° for 1 hr., assuming the decay to be first order in each case. Arrhenius plots of decay constants corresponding to the preceding temperatures were not perfectly linear, but the general slopes corresponded to activation energies of the order of 15 kcal./mole.

Of particular interest is the relative rate of decay of sites active for isomerization of *cis*-2-butene to 1-butene and to *trans*-2-butene. Without decay, conversion to *trans*-2-butene was slightly faster than to 1-butene by about 20%. Heat treatment caused a greater decay in sites responsible for conversion to *trans*-2-butene so that heating above 400° for at least 1 hr. reversed the relative rates. It is concluded that at least two kinds of catalytic sites must be present.

Sites for cyclopropane isomerization behaved quite differently. There appeared to be at least two of them with differing degrees of thermal stability. A rapid deactivation of the gel to about one-fourth its initial value was observed as a result of heating for 1 hr. at 100 or 200°. Further heating at these temperatures had little effect on gel activity although a lower level was attained by heating for 1 hr. at 300°. The rapid, initial deactivation of the gel might be explainable if part of the activity is due to radiation-induced centers of the type which polymerize isobutylene.¹ Significantly, such centers would not have been effective for isomerization of the butenes.

Effect of Irradiation Temperature. With regard to the activity for the isomerization of *cis*-2-butene, the temperature of irradiation was of little effect, within experimental error, although there appeared to be a trend toward higher activities at higher irradiation temperatures (Figure 3). In the case of cyclopropane isomerization, however, there was a large, adverse effect of temperature in the range -196 to 25°. In this region the decrease in induced activity was about equal to the rapid, initial decrease in catalytic activity found as a result of post-irradiation heating.

Table I: Catalytic Activity of Irradiated Silica Gel^a

Irradiation temp., °C.	Post-irradiation heating of gel Time, hr.	Temp. °C.	Activity, ^b min. ⁻¹ × 10 ⁴	
			To <i>trans</i> - 2-butene	To 1-butene
<i>cis</i> -2-Butene				
Blank, unirradiated				
-196		-196	62, 95, 105 87 ± 23 (av.)	49, 58, 79 62 ± 15 (av.)
-196	1	373	75	69
-196	1	420	19	25
-196	2	420	12	20
-196	4	420	1.3	2.5
-196	1	448	9.3	19
-196	1	481	4.5	4.5
-130			67	64
25			48, 63	42, 60
100			86	70
200			52	47
300			79, 138	79, 123
Cyclopropane				
Blank, unirradiated				
-196			To propylene 0.2	
-196	1	100	85	
-196	2	100	20	
-196	4	100	26	
-196	1	200	29	
-196	1	200	13	
-196	2	200	20	
-196	4	200	17	
-196	1	300	10	
-130			34	
25			26	
200			23	
300			2, 5	

^a Gel, 3 g.; dose, 5 Mrads in 1 hr.; test reaction temperature, 80°; test hydrocarbon, ca. 1 mmole. ^b Expressed as an apparent first-order rate constant at the start of the test reaction. Values for irradiated samples corrected for blank.

activity must be attributed to some reaction of the hydrocarbon with the catalyst. Since a trace of C₃ hydrocarbon was observed in the reaction of *cis*-2-butene, it seems likely that a small amount of polymerization and cracking occurs, and that the products gradually cover or inactivate the sites.

In the case of cyclopropane isomerization, the very rapid, initial decrease in catalyst activity, once again, may have been due to catalyst poisoning.³ A part of

(3) R. M. Roberts, *J. Phys. Chem.*, **63**, 1400 (1959), observed a small decrease in the catalytic activity of certain solids with time and an increase in the activity of others.

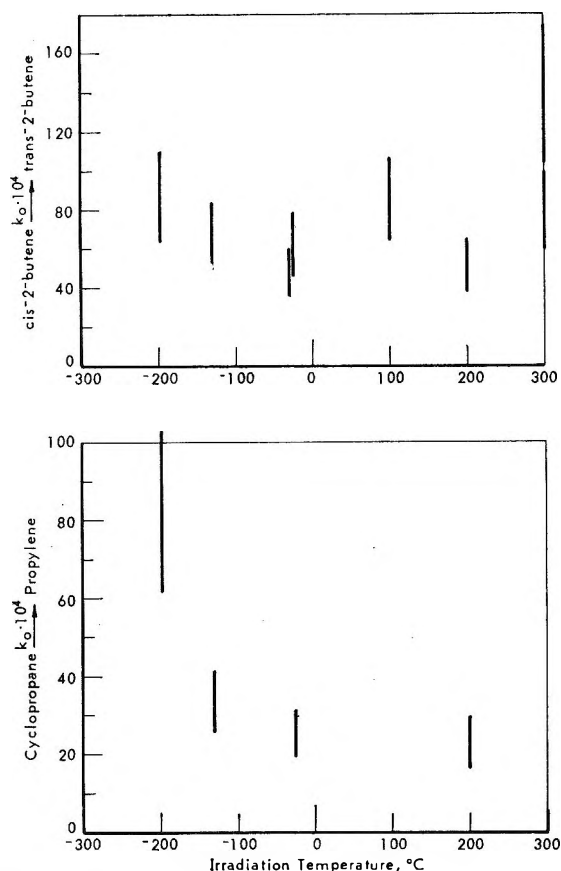


Figure 3. Effect of temperature of irradiation on generated catalytic activity: silica gel.

Above 200° there appeared to be a second region in which the temperature of irradiation had an adverse effect on catalytic activity.

Nature of the Catalytic Sites. The catalytic sites generated by light particle radiation in silica gel are the first sites reported that are chemically active and yet are thermally stable. The thermal stability demonstrates that they are not the acid sites, previously discovered, which anneal with half-times of the order of 1 hr. at 100°. Moreover, the magnitude of the activation energy for decay of the sites responsible for butene interconversions, *ca.* 15 kcal./mole, seems large for electron displacements (the activation energy for decay of the acid sites was only 2 kcal./mole). The foregoing and the fact that enhancement of activity for

butene isomerization resulted when irradiation was performed on heated gel (300°) lead to the belief that atomic displacements are responsible for activity. Durup and Platzman⁴ have described a mechanism for production of atomic displacements by the high-energy electrons which are produced in the process of irradiation with X-rays. In general, the incidence of ionization in an irradiated solid may give rise to potentials sufficient to cause atomic displacement. A special example is primary ionization involving a K electron, followed by a rapid Auger cascade, and resulting in new electric fields in a small volume that can displace atoms.

Mikovsky and Weisz² irradiated silica gel with reactor radiation to an integrated neutron flux of 10²⁰ n.v.t., corresponding to an energy deposition of the order of 2 × 10⁹ rads.⁵ At this very high dose they obtained a 50-fold increase in catalytic activity for butene isomerization at 370°. In their studies they found no effect of heating at 540° for an undisclosed time. This fact, plus the 10% reduction in surface area resulting from the high-dose, heavy-particle irradiation, led to the conclusion that atomic dislocations were responsible for catalytic activity. The extent of disordering was believed to amount to several per cent.

Since both butene⁶ and cyclopropane² isomerizations are catalyzed by acidic sites, it might be assumed that the generated sites here are acidic also. However, if they are strongly acidic, they must be present in amounts less than 0.2 μmole/g., undetectable by spectroscopy applied to adsorbed butter yellow. They might, however, have an acid strength insufficient to convert butter yellow to the acid form. Experiments with butter yellow did disclose that thermally stable sites were generated which changed the spectrum of adsorbed butter yellow, although not to the acid form.

(4) J. Durup and R. L. Platzman, *Discussions Faraday Soc.*, **31**, 156 (1961).

(5) A. Charlesby, *At. Eng. Technol.*, **5**, 12 (1954), determined that an integrated reactor flux of 10¹⁷ n.v.t. delivered a dose of about 5 × 10⁷ rads to an organic system. A system composed of silicon and oxygen should absorb about one-twentieth as much energy from fast neutrons as a hydrocarbon system. The above conversion to dose was made on this basis.

(6) D. M. Brouwer, *J. Catalysis*, **1**, 22 (1962).

Analytical Expressions for the Zero Pressure Thermodynamic Properties of Nitrogen Gas Including Corrections for the Latest Values of the Atomic Constants and the New Carbon-12 Atomic Weight Scale

by Robert E. Barieau

Helium Research Center, Bureau of Mines, U. S. Department of the Interior, Amarillo, Texas
(Received August 20, 1964)

Between 100 and 1000°R. (55–550°K.) the tabulated values of Goff and Gratch for the zero pressure thermodynamic properties of nitrogen gas may be represented with complete tabulated accuracy by

$$C_p \text{ (cal./mole } ^\circ\text{K.)} = 6.9550789 + 8.0448 \times 10^{-6}T + \frac{0.3786}{T^2} + 2.006387 \frac{u^2 e^u}{(e^u - 1)^2}$$

$$H - H^\circ_0 \text{ (cal./mole)} = -1.90405 - \frac{0.3786}{T} + 6.9550789T + 4.0224 \times 10^{-6}T^2 + 2.006387T \frac{u}{e^u - 1}$$

$$[S + R \ln P_{\text{atm}}]_{P=0} \text{ (cal./mole } ^\circ\text{K.)} = 6.1295822 + 6.9550789 \ln T + 8.0448 \times 10^{-6}T - \frac{0.1893}{T^2} + 2.006387 \left[\frac{u}{e^u - 1} - \ln(1 - e^{-u}) \right]$$

with T in °K. and $u = 3353.4061/T$. The preceding equations include corrections for the latest values of the atomic constants and also for the new carbon-12 atomic weight scale. Equations are also given for these properties expressed in B.t.u./lb. mole °R. as a function of degrees Rankine and in joules/g. mole °K. as a function of degrees Kelvin.

The latest values of the zero pressure thermodynamic properties of nitrogen were calculated by Goff and Gratch¹ from spectroscopic data.

We have discovered that the values tabulated by Goff and Gratch may be represented from 100 to 1000°R. by relatively simple analytical expressions. These expressions are

$$C_p = 6.95033885 + 4.4673 \times 10^{-6}T + \frac{1.225}{T^2} + 2.005020 \frac{u^2 e^u}{(e^u - 1)^2} \quad (1)$$

$$\frac{H - H^\circ_0}{T} = 6.95033885 + 2.23365 \times 10^{-6}T - \frac{3.424208}{T} - \frac{1.225}{T^2} + 2.005020 \frac{u}{e^u - 1} \quad (2)$$

$$[S + R \ln P]_{P=0} = 2.0415356 + 6.95033885 \ln T + 4.4673 \times 10^{-6}T - \frac{0.6125}{T^2} + 2.005020 \left[\frac{u}{e^u - 1} - \ln(1 - e^{-u}) \right] \quad (3)$$

where

$$u = \frac{6034.8119}{T} \quad (4)$$

In eq. 1-4, T is in $^{\circ}\text{R}.$; C_p , $(H - H^{\circ}_0)/T$, and $[S + R \ln P]_{P=0}$ are in B.t.u./lb. mole $^{\circ}\text{R}.$; and P is in international atmospheres.

Goff and Gratch tabulated their values to five decimal places. All calculated values of C_p , from eq. 1, between 100 and $950^{\circ}\text{R}.$, differ by less than one unit in the fifth decimal place (sixth significant figure) from the tabulated values. However, if the values from eq. 1 are rounded to the sixth significant figure, then eight out of forty of the calculated values differ from the tabulated value by one unit in the sixth significant figure. In the case of eq. 2, one out of forty-two of the rounded, calculated values differ by one unit in the sixth significant figure from the tabulated value. In the case of eq. 3, five out of forty-one of the rounded, calculated values differ by one unit in the seventh significant figure from the tabulated value. All other rounded, calculated values are identical with the tabulated values.

With such good analytical expressions, it was decided to make corrections for the latest values of the atomic constants and for the new carbon-12 atomic weight scale. This was done in the following way.

Equations 1-3 were divided by the value of R , the gas constant, used by Goff and Gratch. They state $R = 1.98581$ B.t.u./lb. mole $^{\circ}\text{R}.$, but in a companion paper Goff, *et al.*, give $R = 1.98581_{11} \pm 0.00018$ and tabulate the heat capacity of helium as 4.964528 B.t.u./lb. mole $^{\circ}\text{R}.$ With $C_p/R = 5/2$ for helium, we calculate $R = 1.9858112$. If we use $R = 1.9858111$, we calculate for helium $C_p = 4.964528$, which is identical with their tabulated value. If we use $R = 1.98581$, we obtain $C_p(\text{He}) = 4.964525$. Evidently, in their machine calculations, Goff and Gratch used $R = 1.9858111$ B.t.u./lb. mole $^{\circ}\text{R}.$

We first, therefore, divided eq. 1-3 by $R = 1.9858111$ and obtained

$$\frac{C_p}{R} = 3.5 + 2.2496 \times 10^{-6}T + \frac{0.617}{T^2} + 1.009673 \frac{u^2 e^u}{(e^u - 1)^2} \quad (5)$$

$$\frac{H - H^{\circ}_0}{RT} = 3.5 + 1.1248 \times 10^{-6}T - \frac{1.724337}{T} - \frac{0.617}{T^2} + 1.009673 \frac{u}{e^u - 1} \quad (6)$$

$$\left[\frac{S}{R} + \ln P \right]_{P=0} = 1.02806135 + 3.5 \ln T + 2.2496 \times 10^{-6}T - \frac{0.3085}{T^2} + 1.009673 \left[\frac{u}{e^u - 1} - \ln(1 - e^{-u}) \right] \quad (7)$$

where $u = 6034.8119/T$. The left-hand sides of eq. 5-7 are dimensionless and are independent of the value of the atomic constants. On the right-hand side, T must be expressed in $^{\circ}\text{R}.$ In the case of C_p/R and $(H - H^{\circ}_0)/RT$, 3.5 represents the translational contribution to these functions. The remaining parts of eq. 5 and 6 represent the internal energy state contributions to these functions. These all involve quantities of the form

$$\sum p_i \exp\left(-\frac{hc\epsilon_i}{kT}\right)$$

where ϵ_i represents an energy level expressed in cm^{-1} . We assume that ϵ_i is determined independent of the atomic constants. Then, if C_p/R were tabulated as a function of kT/hc , we would have a table completely independent of the atomic constants. This means that, in eq. 5 and 6, instead of expressing C_p/R and $(H - H^{\circ}_0)/RT$ as functions of T , if we expressed them as functions of kT/hc , we would have expressions completely independent of the atomic constants. Then, for any two sets of atomic constants $kT/hc = k'T'/h'c'$ or $T = (k'hc/kh'c')T'$, where k' , h' , and c' represent new values, and k , h , and c represent old values of the atomic constants.

Goff and Gratch used the atomic constant values given by Birge.^{3,4} These are $h = 6.6242 \times 10^{-27}$ erg sec., $k = 1.380474 \times 10^{-16}$ erg/ $^{\circ}\text{K}.$, $c = 2.99776 \times 10^{10}$ cm./sec., $0^{\circ}\text{C} = 273.16^{\circ}\text{K}.$, 1 atm. = 1.013246×10^6 dynes/cm.², $N_0 = 6.02283 \times 10^{23}$ /mole (chemical scale), mol. wt. of $\text{O}_2 = 32$ (chemical scale).

The latest values for the atomic constants, as recommended by the National Research Council Committee on Fundamental Constants,⁵ are $h' = 6.6256 \times 10^{-27}$ erg sec., $k' = 1.38054 \times 10^{-16}$ erg/ $^{\circ}\text{K}.$, $c' = 2.997925 \times 10^{10}$ cm./sec., $0^{\circ}\text{C} = 273.15^{\circ}\text{K}.$, $N'_0 = 6.02252 \times 10^{23}$ /mole (C^{12} scale), mol. wt. of $\text{C}^{12} = 12$.

(1) J. A. Goff and S. Gratch, *Trans. ASME*, **72**, 741 (1950).

(2) J. A. Goff, S. Gratch, and S. W. Van Voorhis, *ibid.*, **72**, 725 (1950).

(3) R. T. Birge, *Rept. Progr. Phys.*, **8**, 90 (1942).

(4) R. T. Birge, *Rev. Mod. Phys.*, **13**, 233 (1941).

(5) A. G. McNish, Chairman, Report of the National Research Council Committee on Fundamental Constants, April 26, 1963.

Then

$$T = \frac{1.38054}{1.380474} \times \frac{6.6242}{6.6256} \times \frac{2.99776}{2.997925} T'$$

or

$$T = 0.99978147T' \quad (8)$$

Substituting this value of T in eq. 5 and 6 we have

$$\frac{C_p}{R} = 3.5 + 2.2491 \times 10^{-6}T' + \frac{0.617}{(T')^2} + 1.009673 \frac{u^2 e^u}{(e^u - 1)^2} \quad (9)$$

$$\frac{H - H^c_0}{RT'} = 3.5 + 1.12455 \times 10^{-6}T' - \frac{1.724714}{T'} - \frac{0.617}{(T')^2} + 1.009673 \frac{u}{e^u - 1} \quad (10)$$

with T' in $^{\circ}\text{R.}$ and $u = 6036.1310/T'$.

The translational contribution to S/R is given by

$$\frac{S}{R} = \frac{5}{2} + \frac{3}{2} \ln 2\pi + \ln \frac{(kT)^{5/2} M^{3/2}}{h^3 (N_0)^{3/2} P} \quad (11)$$

with k in $\text{erg}/^{\circ}\text{K.}$, h in erg sec. , T in $^{\circ}\text{K.}$, and P in dynes/cm.^2 . If we wish an expression with the temperature in $^{\circ}\text{R.}$, we must replace T in $^{\circ}\text{K.}$ by T in $^{\circ}\text{R.}/1.8$, and, if we wish to express the pressure in atm. , we must replace P by $P_{\text{atm}} \times L$, where L is the number of dynes/cm.^2 in 1 atm. Then we have for the translational contribution

$$\left[\frac{S}{R} + \ln P_{\text{atm}} \right]_{P=0} = \frac{5}{2} + \frac{3}{2} \ln 2\pi + \ln \frac{(kT)^{5/2} M^{3/2}}{h^3 (N_0)^{3/2} (1.8)^{3/2} L} \quad (12)$$

In eq. 12, P is in atm. , k is in $\text{erg}/^{\circ}\text{K.}$, T is in $^{\circ}\text{R.}$, h is in erg sec. , and L is in $\text{dynes/cm.}^2 \text{ atm.}$ To change from one set of atomic constants to another, we set

$$\frac{(kT)^{5/2} M^{3/2}}{h^3 (N_0)^{3/2} L} = \frac{(k'T')^{5/2} (M')^{3/2}}{(h')^3 (N'_0)^{3/2} L'}$$

with the primed and unprimed values being the new and old values of the atomic constants, respectively. Then

$$\frac{5}{2} \ln T = \frac{5}{2} \ln \frac{k'}{k} + \frac{5}{2} \ln T' + \frac{3}{2} \ln \frac{M'}{M} - 3 \ln \frac{h'}{h} - \frac{3}{2} \ln \frac{N'_0}{N_0} - \ln \frac{L'}{L} \quad (13)$$

We find that $\frac{5}{2} \ln k'/k = 0.000119521$, $-3 \ln h'/h = -0.000633972$, and $-\frac{3}{2} \ln N'_0/N_0 = 0.000077208$.

Goff and Gratch used $L = 1.013246 \times 10^6 \text{ dynes/cm.}^2 \text{ atm.}$, while the latest value is $L' = 1.013250 \times 10^6 \text{ dynes/cm.}^2 \text{ atm.}$, so that $-\ln L'/L = -0.000003948$.

Goff and Gratch tabulated values for the pure isotope N^{14} and took for the molecular weight of N^{14}_2 on the chemical scale a value of the molecular weight, M , of $\text{N}^{14}_2 = 28.00744$ (chemical scale).

Everling, Konig, Mattauch, and Wapstra⁶ give the atomic weight of $\text{N}^{14} = 14.00307438 \pm 0.00000017$ ($\text{C}^{12} = 12.0$). Then the molecular weight, M' , of $\text{N}^{14}_2 = 28.00614876$, and $\frac{3}{2} \ln M'/M = -0.000069157$.

Substituting in eq. 13, we have

$$\frac{5}{2} \ln T = -0.00051035 + \frac{5}{2} \ln T' \quad (14)$$

Equation 14, when substituted into eq. 7, will correct the translational contribution for the change in atomic constants. The remaining temperature-dependent part, namely

$$\ln T + 2.24960 \times 10^{-6}T - \frac{0.30849}{T^2} + 1.0096730 \left[\frac{u}{e^u - 1} - \ln(1 - e^{-u}) \right]$$

is the internal contribution to S/R , and this is a function of kT/hc , so we substitute

$$T = \frac{k'hc}{kh'c'} T' = 0.99978147T'$$

and

$$\ln T = \ln \frac{k'}{k} - \ln \frac{h'}{h} - \ln \frac{c'}{c} + \ln T'$$

$$\ln T = -0.00021855 + \ln T'$$

Substituting for both the translational and internal contributions to S/R , we have, finally

$$\left[\frac{S}{R} + \ln P \right]_{P=0} = 1.02733245 + 3.5 \ln T' + 2.2491 \times 10^{-6}T' - \frac{0.3085}{(T')^2} + 1.009673 \left[\frac{u}{e^u - 1} - \ln(1 - e^{-u}) \right] \quad (15)$$

In eq. 15, $u = 6036.1310/T'$; P is in international atmospheres, and T' is in $^{\circ}\text{R.}$

The latest report⁵ of the National Research Council Committee on Fundamental Constants indicates that the I.T. calorie is defined as 4.1868×10^7 ergs and also gives $R = 8.3143 \times 10^7$ ergs/ $^{\circ}\text{K. g. mole.}$ Thus

(6) F. Everling, L. A. Konig, J. H. E. Mattauch, and A. H. Wapstra, *Nucl. Phys.*, **18**, 529 (1960).

$$R = \frac{8.3143 \times 10^7}{4.1868 \times 10^7} = 1.9858364 \text{ I.T. cal./}^\circ\text{K. g. mole}$$

and if we define the B.t.u. so that 1 B.t.u./lb. $^\circ\text{R.} = 1 \text{ I.T. cal./g. }^\circ\text{K.}$ and $1^\circ\text{K.} = 1.8^\circ\text{R.}$, then $R = 1.9858364 \text{ B.t.u./}^\circ\text{R. lb. mole.}$

We may now express eq. 9, 10, and 15 in engineering units by multiplying by R . The results are

$$C_p \text{ (B.t.u./lb. mole }^\circ\text{R.)} = 6.9504274 + 4.4664 \times 10^{-6}T + \frac{1.226}{T^2} + 2.005045 \frac{u^2 e^u}{(e^u - 1)^2} \quad (16)$$

$$\frac{H - H^\circ_0}{T} \text{ (B.t.u./lb. mole }^\circ\text{R.)} = 6.9504274 + 2.2332 \times 10^{-6}T - \frac{3.425000}{T} - \frac{1.226}{T^2} + 2.005045 \frac{u}{e^u - 1} \quad (17)$$

$$[S + R \ln P]_{P=0} \text{ (B.t.u./lb. mole }^\circ\text{R.)} = 2.0401142 + 6.9504274 \ln T + 4.4664 \times 10^{-6}T - \frac{0.613}{T^2} + 2.005045 \left[\frac{u}{e^u - 1} - \ln(1 - e^{-u}) \right] \quad (18)$$

where $u = 6036.1310/T$ and T is in $^\circ\text{R.}$ in eq. 16–18.

We may express eq. 9, 10, and 15 in $^\circ\text{K.}$ by replacing T' with $1.8T$. The results are

$$\frac{C_p}{R} = 3.5 + 4.0484 \times 10^{-6}T + \frac{0.1905}{T^2} + 1.009673 \frac{u^2 e^u}{(e^u - 1)^2} \quad (19)$$

$$\frac{H - H^\circ_0}{RT} = 3.5 + 2.0242 \times 10^{-6}T - \frac{0.958174}{T} - \frac{0.1905}{T^2} + 1.009673 \frac{u}{e^u - 1} \quad (20)$$

$$\left[\frac{S}{R} + \ln P \right]_{P=0} = 3.0845858 + 3.5 \ln T + 4.0484 \times 10^{-6}T - \frac{0.09525}{T^2} + 1.009673 \left[\frac{u}{e^u - 1} - \ln(1 - e^{-u}) \right] \quad (21)$$

where $u = 3353.4061/T$, and in eq. 19–21 the temperature is in $^\circ\text{K.}$

If we wish to express the thermodynamic properties in joules, we multiply by $R = 8.3143 \text{ joules/mole }^\circ\text{K.}$, while, if we wish to express the thermodynamic properties in thermochemical calories, where a thermochemical

calorie is defined as 4.1840 joules, we must multiply by $R = 8.3143/4.1840 = 1.9871654 \text{ cal./mole }^\circ\text{K.}$ The results are

$$C_p \text{ (cal./mole }^\circ\text{K.)} = 6.9550789 + 8.0448 \times 10^{-6}T + \frac{0.3786}{T^2} + 2.006387 \frac{u^2 e^u}{(e^u - 1)^2} \quad (22)$$

$$C_p \text{ (joules/mole }^\circ\text{K.)} = 29.100050 + 33.660 \times 10^{-6}T + \frac{1.584}{T^2} + 8.394724 \frac{u^2 e^u}{(e^u - 1)^2} \quad (23)$$

$$\frac{H - H^\circ_0}{T} \text{ (cal./mole }^\circ\text{K.)} = 6.9550789 + 4.0224 \times 10^{-6}T - \frac{1.90405}{T} - \frac{0.3786}{T^2} + 2.006387 \frac{u}{e^u - 1} \quad (24)$$

$$\frac{H - H^\circ_0}{T} \text{ (joules/mole }^\circ\text{K.)} = 29.100050 + 16.830 \times 10^{-6}T - \frac{7.96655}{T} - \frac{1.584}{T^2} + 8.394724 \frac{u}{e^u - 1} \quad (25)$$

$$[S + R \ln P]_{P=0} \text{ (cal./mole }^\circ\text{K.)} = 6.1295822 + 6.9550789 \ln T + 8.0448 \times 10^{-6}T - \frac{0.1893}{T^2} + 2.006387 \left[\frac{u}{e^u - 1} - \ln(1 - e^{-u}) \right] \quad (26)$$

$$[S + R \ln P]_{P=0} \text{ (joules/mole }^\circ\text{K.)} = 25.646172 + 29.100050 \ln T + 33.660 \times 10^{-6}T - \frac{0.792}{T^2} + 8.394724 \left[\frac{u}{e^u - 1} - \ln(1 - e^{-u}) \right] \quad (27)$$

where, in eq. 22–27, $u = 3353.4061/T$, and T is expressed in $^\circ\text{K.}$

Equations 16–18 and 22–27 are for the species N^{14}_2 . Regarding the thermodynamic properties of the normal isotopic mixture of nitrogen (N_2), Goff and Gratch¹ say: "Its enthalpy and isobaric specific heat are almost identical with those of the most abundant isotope N^{14}_2 ; its reduced entropy $[S + R \ln P]$ exceeds that of N^{14}_2 by about 0.00078 B.t.u./mole $^\circ\text{R.}$ because it contains some isotopes of higher molecular weight M than that of N^{14}_2 , by about 0.0102 B.t.u./mole $^\circ\text{R.}$ because the statistical weights p_i of $\text{N}^{14}\text{-N}^{15}$ differ from those of

N^{14}_2 , and by a mixing entropy of about 0.086 B.t.u./mole °R.”

In making the calculations for the corrections to be applied to obtain the thermodynamic properties of the naturally occurring isotopic mixture, it was assumed that the entropy of pure $N^{14}-N^{15}$ exceeds that of $N^{14}-N^{14}$ by

$$^{3/2}R \ln \frac{M_{14-15}}{M_{14-14}} + R \ln 2$$

and that the entropy of pure $N^{15}-N^{15}$ exceeds that of $N^{14}-N^{14}$ by

$$^{3/2}R \ln \frac{M_{15-15}}{M_{14-14}}$$

where M_{14-15} is the molecular weight of $N^{14}-N^{15}$, M_{15-15} is the molecular weight of $N^{15}-N^{15}$, and M_{14-14} is the molecular weight of $N^{14}-N^{14}$. The correction is then given by

$$S_{N_2} - S_{N^{14}_2} = ^{3/2}R y_2 \ln \frac{M_{14-15}}{M_{14-14}} + R y_2 \ln 2 + ^{3/2}R y_3 \ln \frac{M_{15-15}}{M_{14-14}} - R y_1 \ln y_1 - R y_2 \ln y_2 - R y_3 \ln y_3$$

where y_1 is the mole fraction of $N^{14}-N^{14}$, y_2 is the mole fraction of $N^{14}-N^{15}$, and y_3 is the mole fraction of $N^{15}-N^{15}$.

In calculating the mole fraction from the atomic abundance, it was assumed that, for the reaction, $N^{14}_2 + N^{15}_2 = 2(N^{14}-N^{15})$, the equilibrium constant $K = y_2^2/y_1 y_3 = 4$. If the relative abundance of the isotopes is given by N^{14}/N^{15} , then

$$y_1 = \frac{(N^{14}/N^{15})^2}{(N^{14}/N^{15} + 1)^2}$$

$$y_2 = \frac{2(N^{14}/N^{15})}{(N^{14}/N^{15} + 1)^2}$$

$$y_3 = \frac{1}{(N^{14}/N^{15} + 1)^2}$$

Using the relative abundance $N^{14}/N^{15} = 272.0 \pm 0.3$, as determined for atmospheric nitrogen by Junk and Svec,⁷ and the atomic weights of N^{14} and N^{15} given as 14.00307438 and 15.0001081, respectively, by Everling, König, Mattauch, and Wapstra,⁶ we find $M_{14-14} = 28.00614876$, $M_{14-15} = 29.00318248$, $M_{15-15} = 30.0002162$, and $y_1 = 0.9926874 \pm 0.0000081$, $y_2 = 0.0072992 \pm 0.0000080$, $y_3 = 0.000013418 \pm 0.000000030$.

Thus, we calculate that the reduced entropy of the naturally occurring mixture exceeds that of N^{14}_2 by 0.000763 B.t.u./lb. mole °R. owing to the molecular weight of heavier isotopes, by 0.010047 B.t.u./lb. mole °R. because the statistical weights p_i of $N^{14}-N^{15}$ differ from those of N^{14}_2 , and by 0.086082 B.t.u./lb. mole °R. owing to a mixing entropy. The total excess is, thus, 0.096892 B.t.u./lb. mole °R. This number should be added to eq. 18 to obtain the reduced entropy of the naturally occurring isotopic mixture. The corresponding numbers for eq. 26 and 27 are 0.096957 cal./mole °K. and 0.40567 joules/mole °K.

The Helium Research Center is presently calculating the zero pressure thermodynamic properties of nitrogen at even temperature intervals, both in degrees Rankine and in degrees Kelvin.

(7) G. Junk and H. J. Svec, *Geochim. Cosmochim. Acta*, **14**, 234 (1958).

The Wien Effect in Uranyl Ion Solutions. I. Uranyl Nitrate and Perchlorate from 5 to 65°. Negative Wien Effects¹

by Joseph F. Spinnler and Andrew Patterson, Jr.

Contribution No. 1706 from the Sterling Chemistry Laboratory, Yale University, New Haven, Connecticut
(Received August 24, 1964)

Experimental data on aqueous solutions of uranyl nitrate and uranyl perchlorate are presented for the temperatures 5, 15, 25, 50, and 65°. Plots of the pH vs. log of concentration, of the equivalent conductance vs. square root of concentration, and of the high-field conductance as a function of field are presented. The range of concentration studied lies between 10^{-6} and 10^{-3} M. The high-field conductance results are unprecedented, since under most circumstances application of the field decreases the conductance of the solutions, a phenomenon not heretofore observed with any other electrolytes.

Prompted by the unexpected observation of a decrease in the conductance of a solution of uranyl nitrate under the influence of a high electrical field,² we have studied the pH and low- and high-field conductance of a series of uranyl salts, including the fluoride,^{3a} sulfate,^{3b} nitrate, and perchlorate as a function of concentration and temperature. In this paper are presented the results of measurements of the pH and conductance as a function of field for dilute aqueous solutions of uranyl nitrate and perchlorate over a temperature range from 5 to 65°. In connection with this study we have computed the theoretical high-field conductances of these solutions using the theory of Onsager and Kim as programmed for machine computation.⁴

Extensive investigations have been made of the hydrolysis of the uranyl ion in the solutions of its various salts,⁵⁻¹⁹ to which reference will be made in the Discussion. Of particular interest are the results of Baes and Meyer,¹⁹ who have made acidity measurements on uranyl nitrate at elevated temperatures up to 148°. They find a rapid increase of hydrolysis with increasing temperature and an increasing proportion of the monomeric hydrolysis product, UO_2OH^+ , as predicted by Kraus⁶ and confirmed by the work of Hearne and White.¹⁵

The conductance of uranyl salts in solution has been investigated by numerous workers as well, but for the present purpose the measurements of Brown,

Bunger, Marshall, and Secoy²⁰ and of West and Jones²¹ are relevant. The measurements of Brown, *et al.*, were made at sufficiently low concentrations

- (1) This paper is taken in part from a dissertation submitted by J. F. Spinnler to the Graduate School, Yale University, in partial fulfillment of the requirements for the degree of Doctor of Philosophy, May 1961. For those who are interested, a limited number of copies of this dissertation are on hand and one can be provided on request.
- (2) F. E. Bailey, J. F. Spinnler, and A. Patterson, Jr., *J. Am. Chem. Soc.*, **83**, 1761 (1961).
- (3) (a) J. F. Spinnler and A. Patterson, Jr., *J. Phys. Chem.*, **69**, 508 (1965); (b) *ibid.*, **69**, 513 (1965).
- (4) H. Freitag and A. Patterson, Jr., *J. Electrochem. Soc.*, **108**, 529 (1961).
- (5) J. Bjerrum, G. Schwarzenbach, and L. Sillén, "Stability Constants; Part II, Inorganic Ligands," The Chemical Society, London, 1958, p. 9.
- (6) K. A. Kraus, *Proc. Intern. Conf. Peaceful Uses At. Energy, Geneva*, **7**, 245 (1956).
- (7) J. Sutton, *J. Chem. Soc.*, S275, S57 (1949).
- (8) J. Sutton, National Research Council of Canada, Atomic Energy Project Report CRC 325 (1947).
- (9) S. Ahrland, *Acta Chem. Scand.*, **3**, 374 (1949); **5**, 1151, 1271 (1951); **8**, 1907 (1954).
- (10) B. Singh and G. Ahmad, *J. Chem. Phys.*, **34**, 351 (1937).
- (11) L. G. Longworth and D. A. MacInnes, USAEC Report MDDC 911 (1947).
- (12) H. Guiter, *Bull. soc. chim. France*, **64** (1947).
- (13) J. Faucherre, *Compt. rend.*, **227**, 200 (1948).
- (14) R. H. Betts and R. K. Michels, *J. Chem. Soc.*, S286, S58 (1949).
- (15) J. A. Hearne and A. G. White, *ibid.*, 3168 (1957).
- (16) J. Sutton, *Nature*, **169**, 235 (1952).
- (17) H. W. Crandall, USAEC Report MDDC 1294 (1947).

and with adequate precision for determination of the limiting equivalent or ionic conductances, but the nitrate and perchlorate salts were not studied. Reference 21 gives data for uranyl nitrate at 35, 50, and 65°, temperatures used in this work, but for concentrations higher than those of interest to us. Data for uranyl perchlorate are not available.

Experimental

The experimental procedure was essentially that of Gledhill and Patterson.²² Two circuit changes contribute to increased precision of measurement, which is much to be desired, since the size of the effects observed is small: a vernier control of high voltage was provided, and small variable capacitors were shunted across the two primary windings of the bridge pulse transformer to compensate for small differences in the capacitance in the transformer. The precision of measurement on one solution at a given session of measurement was within 0.02 unit (absolute per cent) in $\Delta\Lambda/\Lambda(0)$; deviations of less than 0.05 unit were obtained in successive investigations at different times on the same solution. The principal limitation on the precision of measurement is drift in the resistance of the solutions. These drifts are not the result of inadequate temperature control, this being held to within 0.002° at all temperatures reported, but rather appear to be the result of passing high power pulses through the cells. The low-field conductances are measured to 0.1 ohm, but owing to these conductance drifts are not known to better than 0.05% during the entire course of an experiment.

The uranyl nitrate was a sample provided some years ago by the Atomic Energy Commission for conductance measurements. The uranyl perchlorate was purchased from the A. O. Mackay Co. Each salt was recrystallized from conductivity water and air-dried. The air-dry salts were added directly to the conductance cells until the desired cell resistance was obtained. The concentrations of the solutions whose Wien effects are reported were determined from the measured low-field conductances and interpolation from specific conductance-concentration graphs prepared in conjunction with the pH measurements referred to below. The concentrations are known to within 1 part in 500. This procedure, which leaves something to be desired in terms of precision, was chosen to avoid exposure of the cell contents to the atmosphere. The conductances reported in this paper were measured principally to aid in this determination of concentration and were made to four-figure precision only.

For the pH measurements, stock solutions of uranyl salts were prepared from the air-dry salts and conductivity water. The concentration was determined by the method of Frere,²³ in which uranyl ion is precipitated with 8-hydroxyquinoline in an acetate buffer. The analyzed stock solution was added to a conductance cell containing conductance water through a microburet whose tip projected into the upper part of the cell through a special cap which allowed passage of a constant stream of purified nitrogen through the upper part of the cell. The concentration of the solution was determined from the amount of stock solution added to the previously weighed conductivity water. Samples for the pH determination were withdrawn from the cell through the special cap after attainment of a stable conductance, indicating that the solution was thoroughly mixed. The low-field conductance was measured on the differential pulse transformer (DPT) bridge to within 0.1 ohm and recorded for later use as noted in the preceding paragraph. The pH measurements were made with a Pye Catalog No. 11085 pH meter. The electrode compartment was suspended in the thermostat oil bath together with the conductance cells. The meter was calibrated against a suitable reference buffer solution at each temperature. All parts of the apparatus and the solutions were allowed to reach temperature equilibrium before a measurement was made. The pH electrodes were rinsed in a 100-ml. sample of solution withdrawn from the conductance cell and the pH measured on a separate sample taken from the cell shortly before use. The pH electrode compartment was kept under an atmosphere of purified nitrogen. The contents of the conductance and pH cells were magnetically stirred except while the pH measurement was actually being made. Additional stock solution was then added to the conductance cell and the measurement continued at a higher concentration. The precision of measurement is 0.01 pH unit; the probable accuracy is estimated to be within 0.05 unit at 25° and below, and 0.1 unit at 35° and above.

Stock solutions of the reference electrolytes were prepared and analyzed in accord with appropriate analytical and conductance techniques. The reference

(18) N. P. Komar and Z. A. Tretyak, *Zh. Analit. Khim.*, **10**, 236 (1955).

(19) C. F. Baes and N. J. Meyer, ORNL Reactor Chemistry Division Annual Progress Report, Mar. 1961.

(20) R. D. Brown, W. B. Bunger, W. I. Marshall, and C. H. Secoy, *J. Am. Chem. Soc.*, **76**, 1532, 1580 (1954).

(21) A. P. West and H. C. Jones, *Am. Chem. J.*, **44**, 508 (1913).

(22) J. A. Gledhill and A. Patterson, Jr., *J. Phys. Chem.*, **56**, 999 (1952).

(23) F. J. Frere, *J. Am. Chem. Soc.*, **55**, 4362 (1933).

electrolytes were prepared directly in the conductance cells by adding measured volumes of the stock solutions to known weights of conductivity water. In most measurements, the reference electrolytes for the uranyl salt solutions were salt-acid mixtures; these were prepared by adding hydrochloric or nitric acid first and adjusting the pH to within 0.1 pH unit of that of the uranyl salt solution under study, followed by the addition of potassium chloride or potassium nitrate to establish the desired cell resistance. These reference electrolytes have been found to remain remarkably stable in conductance over extended periods of time in spite of the brutal electrical treatment they receive, and to obviate experimental difficulties due to differing polarization in the unknown and reference electrolytes. Because it is necessary to know some details of the behavior of these reference electrolytes in order to compute the Wien effects of these mixtures and of the uranyl salts, we have studied the high-field conductance of these acid-salt mixtures and report these results separately.²⁴

The cell constants of the conductivity cells were determined using 0.01 demal solutions of recrystallized potassium chloride according to the method of Jones and Bradshaw.²⁵

Results

The observed pH values are plotted *vs.* $\log c$ in Figures 1 through 3 for the temperatures 5, 15, 25, 35, 50, and 65°. All remaining data are presented for the same temperatures. The equivalent conductances, Λ , are plotted *vs.* $c^{1/2}$ in Figures 4 and 5. The high-field conductance quotients are plotted in Figures 6 and 7. In Figure 8, curves are plotted for the temperatures 15 and 50° with $\Delta\Lambda/\Lambda(0)$ data at two different concentrations of uranyl nitrate represented at each temperature. In Figure 9 is shown the effect on the high-field conductance quotients at 15 and 65° of adding small amounts of nitric acid to uranyl nitrate solutions. In Figure 10 are shown theoretical calculations of the high-field conductance quotient using two different models for the hydrolysis reactions.

Discussion

In each of the plots just listed there appear distinctive differences between the behavior of uranyl nitrate and perchlorate solutions, both as a function of concentration and of temperature.

Within the accuracy claimed for the pH data, uranyl perchlorate solutions exhibit a straight-line dependence of pH on log concentration, while uranyl nitrate exhibits an inflection point (in the range of concentration studied) at 5 and 15° which disappears at higher tem-

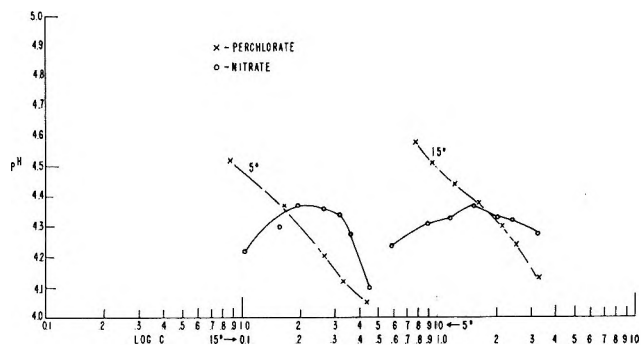


Figure 1. Observed pH values for uranyl nitrate (O) and perchlorate (X) solutions. The pH values are plotted *vs.* $\log c$ for temperatures of 5 and 15°. The log scales on the abscissa are shifted to the left (5°) and to the right (15°) so the curves will not overlap.

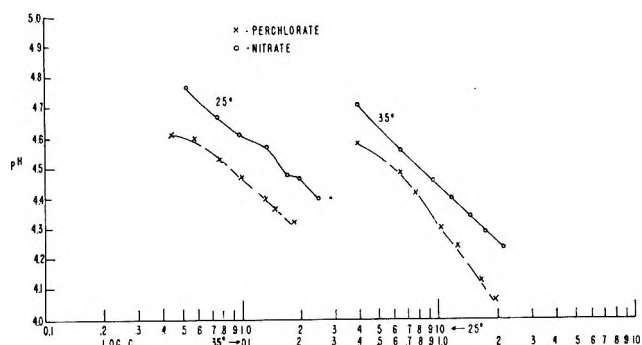


Figure 2. Observed pH values for uranyl nitrate (O) and perchlorate (X) solutions. The pH values are plotted *vs.* $\log c$ for temperatures of 25 and 35°. See Figure 1.

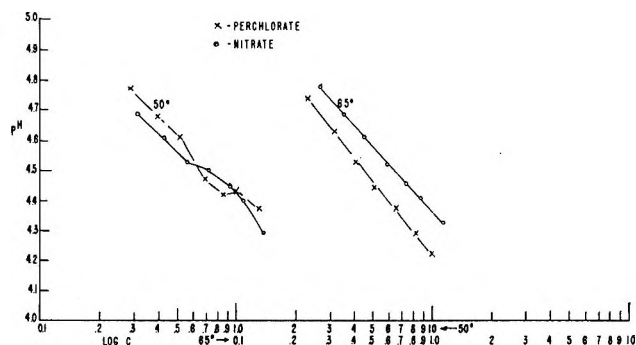


Figure 3. Observed pH values for uranyl nitrate (O) and perchlorate (X) solutions. The pH values are plotted *vs.* $\log c$ for temperatures of 50 and 65°. See Figure 1.

peratures. With some exceptions displayed in the graphs themselves, the pH of the perchlorate solutions

(24) J. F. Spinnler and A. Patterson, Jr., *J. Phys. Chem.*, **69**, 658 (1965).

(25) G. Jones and B. C. Bradshaw, *J. Am. Chem. Soc.*, **55**, 1780 (1933).

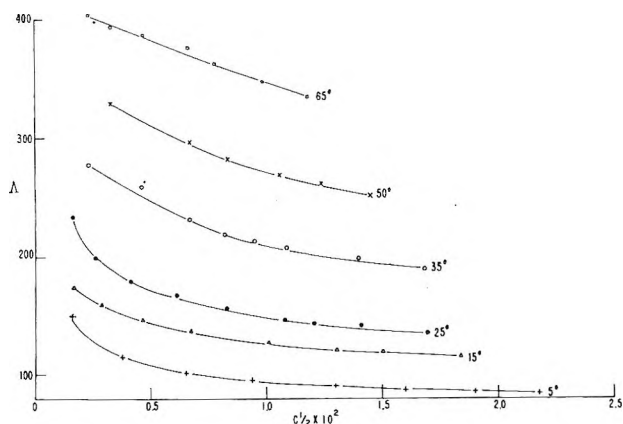


Figure 4. The equivalent conductances of solutions of uranyl nitrate are plotted vs. $c^{1/2}$ for a range of temperatures.

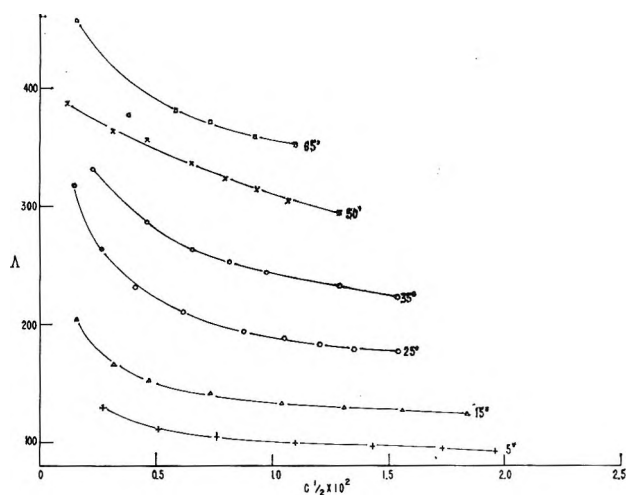


Figure 5. The equivalent conductances of solutions of uranyl perchlorate are plotted vs. $c^{1/2}$ for a range of temperatures.

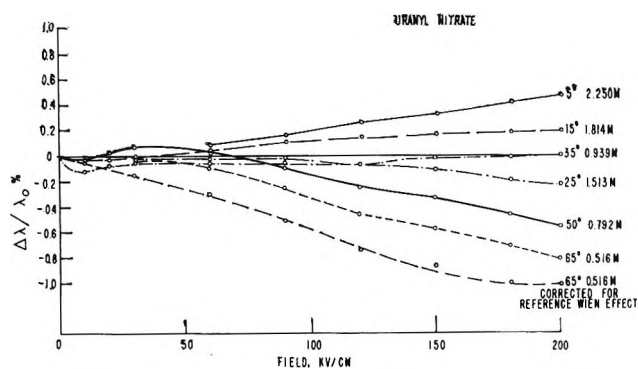


Figure 6. The high-field conductance quotients of solutions of uranyl nitrate are plotted as a function of field for a range of temperatures and concentrations. All concentrations given are to be multiplied by 10^{-4} . The lowest curve (long dashes) is derived from the curve immediately above (short dashes) by subtracting the high-field conductance quotient of the reference electrolyte.

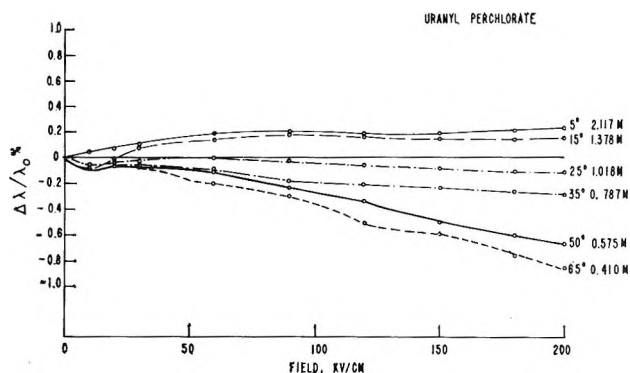


Figure 7. The high-field conductance quotients of solutions of uranyl perchlorate are plotted as a function of field for a range of temperatures and concentrations. All concentrations given are to be multiplied by 10^{-4} .

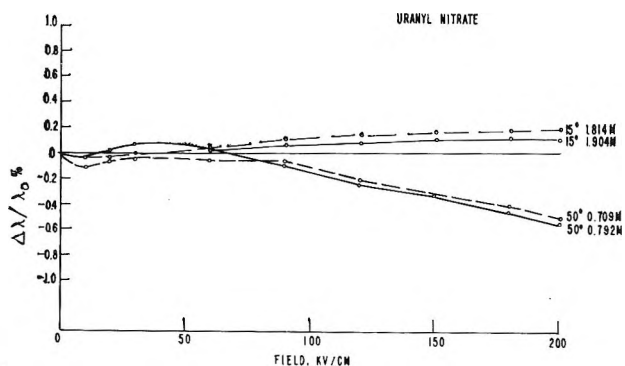


Figure 8. Effect of concentration on the high-field conductance quotient of uranyl nitrate: data are given at two concentrations at each of two temperatures, 15 and 50°. All concentrations given are to be multiplied by 10^{-4} .

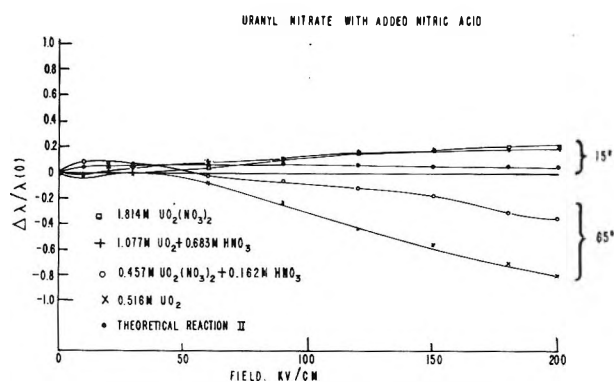


Figure 9. Effect of added nitric acid on the high-field conductance quotient of uranyl nitrate. Data are given for two temperatures, 15 and 65°. All concentrations given are to be multiplied by 10^{-4} .

is lower, suggesting that hydrolysis is more extensive in these solutions. (See Figures 1, 2, and 3.)

The conductance curves for the two electrolytes

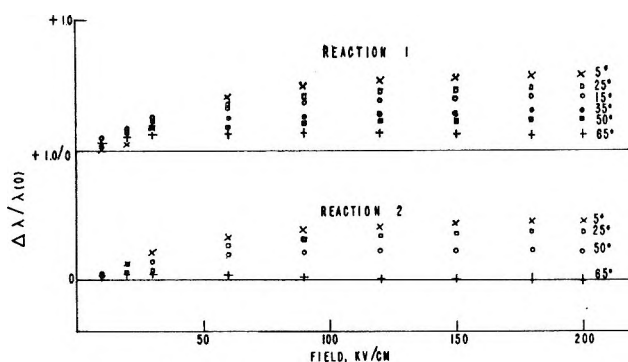


Figure 10. Theoretical calculations of the high-field conductance quotient of uranyl nitrate using two hydrolysis models; reaction 1 refers to eq. 1 (text) and reaction 2 to eq. 2. The concentrations used are those given in Figure 6 and corrections for the behavior of the reference electrolyte are included; *i.e.*, the curves are relative to the same reference electrolyte employed in obtaining the experimental data of Figure 6.

are similar, but in every case the conductance of the nitrate salt is lower than that of the perchlorate salt. There is also a noticeable difference between the temperature-concentration data in the two sets of curves, the most significant one being the appreciably lower conductance of the nitrate salt at 25°. The nitrate data at 5, 15, and 25° are crowded together in a way quite dissimilar to the perchlorate data. As a result, the equivalent conductances of the two salts are more nearly similar at 5 and 65°, and least similar at 25°. It is of interest that the equivalent conductance of the nitrate ion is slightly higher than that of perchlorate ion and that the conductances of the two anions closely parallel each other as a function of temperature, while in these data the conductance of the nitrate salt is in every case lower than that of the perchlorate salt. This observation, coupled with the lower pH of the uranyl perchlorate salts mentioned in the preceding paragraph, leads one to conclude that the nitrate and uranyl ions are associated to a significant degree and that the extent and variation of this association with temperature appear to be the most significant at the lower temperatures. (See Figures 4 and 5.)

The high-field conductance curves are distinctly unusual. In contrast with the typical curves shown in ref. 4, both uranyl nitrate and perchlorate high-field conductance quotients first exhibit an increase of conductance at lower temperatures and fields and a decrease in conductance at the higher temperatures and fields. These conductance changes, which one may appropriately denote negative Wien effects, are quite real and easily reproducible within the precision

of measurements claimed in previous paragraphs. It must also be kept in mind that the curves plotted are for the conductance changes relative to those of a reference electrolyte, in these measurements always a salt-acid mixture to minimize polarization differentials between the solutions being compared. Since the reference electrolytes always exhibit positive Wien effects, the absolute Wien effect of the electrolyte under study will be shifted by an amount equal to the absolute Wien effect of the reference electrolyte, with appropriate regard to algebraic sign. The computation of the Wien effects of these salt-acid mixtures is discussed in another paper.²⁴ For comparison with the relative measurements, the 65° data for uranyl nitrate are corrected for the reference electrolyte Wien effect and replotted as the lowest curve in Figure 6. This correction removes the inflection in the curve at low fields, which results from the sharp rise in reference electrolyte Wien effect toward an approximately constant value above fields of 50 kv./cm., and moves the curve downward to produce a larger absolute negative Wien effect. (See Figures 6 and 7.)

These data are taken at what is essentially constant specific conductance so the concentrations tend toward lower values at the higher temperatures. The curves for the perchlorate salt show a consistent downward trend, corresponding to an increasing negative Wien effect, with increasing temperature. The curves for the nitrate salt are similar, except that at the higher fields the 25 and 35° curves cross each other and are inverted in order. To indicate the effect of concentration on the magnitude of the high-field conductance quotient, data for two different concentrations have been plotted for the temperatures 15 and 50°; the concentrations of uranyl nitrate involved differ by the ratios 1.904/1.814 at 15° and 0.792/0.709 at 50°. In each case, the higher the concentration, the lower is the conductance quotient. The inversion in the uranyl nitrate 25 and 35° curves cannot be accounted for as an effect of concentration, since the magnitude of the effect of concentration difference is insufficient to account for the difference in high-field conductance quotients observed. It will be recalled that the nitrate conductance curves were oddly spaced, with the greatest difference occurring at 25°, so the high-field conductance results reflect also the competition between uranyl and nitrate ion association and hydrolysis of the uranyl ion, the pattern of which changes with increasing temperature. (See Figure 8.)

In itself, the observation of a smaller Wien effect in a more concentrated solution is abnormal. Curves for potassium chloride (Figure 1, ref. 4) show increased conductance quotients at increased concentrations.

Calculations made on a presumably normal 2-1 electrolyte, calcium chloride, show the same trend; these calculations agree satisfactorily with experimental measurements.

Since uranyl nitrate solutions are significantly hydrolyzed, and in anticipation of the probable role of hydrogen ion in the Wien effect results, measurements were made in which solutions of nitric acid were added to those of uranyl nitrate and the Wien effects of the mixtures observed, at the temperatures 15 and 65°. (See Figure 9.) It is not immediately clear how correctly to interpret these results; we shall discuss them further below in connection with the negative Wien effect phenomenon.

To perform theoretical calculations of the high-field conductance quotients, it is necessary to have the limiting equivalent conductances and, ultimately, the limiting ionic conductances of the ions involved. To obtain these from the available data, we have resorted to the use of the method of Kraus and Bray²⁶ and have employed Walden's rule²⁷ to obtain the values desired. Since the method of Kraus and Bray involves extrapolation to zero concentration and is an approximation technique, it is assumed that the values obtained with its use are known to be no better than 10%. The effect of such an error on the theoretical Wien effect calculations is not serious, however, as will be pointed out. The limiting ionic conductances of the well-studied ions are known to much higher degrees of precision. The data we have used for the limiting ionic conductances of ions such as H⁺, NO₃⁻, and ClO₄⁻ as a function of temperature were taken from Harned and Owen,²⁸ Robinson and Stokes,²⁹ and other authors.^{20,30,31} Limiting equivalent conductances of uranyl nitrate were taken from ref. 21; since no data were available for uranyl perchlorate, other than the data we have presented here which indicate essential similarities between the behavior of the two salts, the behavior of the cations (UO₂⁺², H⁺) in these solutions was assumed to be the same as in the nitrate solutions. Following the procedure outlined in ref. 24, we have then calculated a combined valence and a combined limiting conductance for the cations in the mixture. This procedure overlooks any possible mixture effects or specific interactions. It is convenient to proceed in this way since it is unnecessary to know the limiting ionic conductance of the uranyl ion itself along with the individual conductances of the hydrolysis products, all of which are uncertain or unknown. Moreover, it is simple to determine Λ_0^+ by subtracting from the limiting equivalent conductance of the total solution the limiting ionic conductance of the anion, while the

net z^+ is determined from the total concentration and pH measurements.

We have assumed that either of two reactions



or



is responsible for the hydrolysis and the observed pH of the hydrolyzed solution and computed the combined valence accordingly in the absence of an applied field. This entire procedure allows one to compute a Wien effect for a mixture of ions, but it does not take into account any kind of ionic or other interactions under the influence of field beyond those which we might term the classical Onsager³² and Onsager-Kim³³ types for weak and strong electrolytes.

Theoretical calculations are plotted assuming both reactions 1 and 2 as the hydrolysis equilibrium, and using conductance data for uranyl nitrate. Similar results are obtained for uranyl perchlorate, so these calculations are not reproduced here; however, the uranyl perchlorate calculations are perfectly regular, and any inversions or other unusual features found in the uranyl nitrate results are absent. In each case the conductance quotient obtained using reaction 2 is lower than when reaction 1 is assumed for the hydrolysis equilibrium. The quotients decrease with increasing temperature. The 25 and 15° curves are inverted in order when reaction 1 is employed; calculations were made only at 5, 25, 50, and 65° for reaction 2. At 65°, reaction 2 gives an apparent negative Wien effect; this is in reality due to the slower approach of the reference electrolyte Wien effect to its maximum value than that of the uranyl nitrate. (See Figure 10.) The differences between the calculated and observed values of the conductance quotient exceed those which can be attributed to experimental error, the choice of limiting conductances, errors in extrapolations or interpolations employed, or erroneous assumptions of the equilibrium status of the solutions at low fields.

(26) C. A. Kraus and W. C. Bray, *J. Am. Chem. Soc.*, **35**, 1315 (1913).

(27) P. Walden, *Z. physik. Chem.*, **55**, 207, 246 (1906).

(28) H. S. Harned and B. B. Owen, "The Physical Chemistry of Electrolytic Solutions," American Chemical Society Monograph Series, 3rd Ed., Reinhold Publishing Corp., New York, N. Y., 1958.

(29) R. A. Robinson and R. H. Stokes, "Electrolyte Solutions," Butterworths Scientific Publications, London, 1959.

(30) A. N. Campbell and E. Bock, *Can. J. Chem.*, **36**, 330 (1958).

(31) J. Johnston, *J. Am. Chem. Soc.*, **31**, 1010 (1909).

(32) L. Onsager, *J. Chem. Phys.*, **2**, 599 (1934).

(33) L. Onsager and S. K. Kim, *J. Phys. Chem.*, **61**, 198 (1957).

Keeping in mind as an example that the experimental conductance quotient of uranyl nitrate at 65° is -0.80% while the calculated value is 0.12%, we may estimate the influence of the factors just noted. An error in pH determination gives rise to an error in the computed valence factor fed into the computation. Comparing the results of the calculation at 25° using the two different hydrolysis reactions, we find that a difference in the valence factor of $(1.82 - 1.67) = 0.15$ unit gives rise to a change in the conductance quotient of 0.123 unit at 200 kv./cm. and corresponds to a change in hydrogen ion concentration of 0.27×10^{-4} mole/l. Since the pH can be determined at this temperature with sufficient accuracy that the hydrogen ion concentration is known within 0.05×10^{-4} mole/l., an error in pH or in the valence factor is not sufficient to account for the discrepancy between the experimental and calculated results. Using data for the 15° run where nitric acid has been added to the uranyl nitrate solution (Figure 9), there is a decrease of 0.19 in the cationic valence, a concentration change of 0.312×10^{-4} mole/l., an increase of 33 ohm⁻¹ cm.² equiv.⁻¹ in the cationic limiting ionic conductance, and a resulting decrease of 0.164 unit in $\Delta\Lambda/\Lambda(0)$ in the theoretical computation made with these data. The corresponding experimental change in $\Delta\Lambda/\Lambda(0)$ was 0.01 unit. Variations in the majority of the quantities used in the calculation are considerably less important than is the valence factor.

It thus appears that the processes in solution under the influence of high fields are sufficiently complex that they are not accounted for by the theoretical approach which we have used.

It can be concluded that both uranyl nitrate and perchlorate are nearly completely dissociated over the temperature and concentration ranges covered, for otherwise the small Wien effects at lower temperatures and the negative Wien effects at higher temperatures would be overshadowed by the effect of field on association reactions giving rise to large positive Wien effects. The importance of association will be noted in papers describing measurements on uranyl fluoride^{3a} and uranyl sulfate.^{3b} In spite of the observation just made, there is involvement between the nitrate ion and the uranyl ion or its hydrolysis products, since the low- and high-field conductances and the pH measurements are distinctively different from those on the presumably unassociated uranyl perchlorate, and since the specific conductance of the uranyl nitrate is lower than that of uranyl perchlorate in spite of the fact that the nitrate ion has a higher ionic conductance than does perchlorate ion.

It also appears that the limiting conductance of the

uranyl ion in solutions of these two compounds is abnormally high. At 65° more than half the uranyl ions are in hydrolyzed form with UO_2OH^+ predominating.¹⁹ Using our conductance data for uranyl nitrate at the same temperature and making a hydrolysis correction by the method of Owen and Gurry³⁴ assuming hydrolysis equilibrium (2), we find that the ionic conductance due to uranyl ion or the various possible types of uranyl complexes is approximately 320 ohm⁻¹ cm.² equiv.⁻¹. For comparison, at this temperature the limiting ionic conductance of potassium ion is 135 and that of calcium ion is 240. Thus the limiting ionic conductance observed is decidedly higher than that of a typical univalent ion, an ordinary divalent ion, or a combination of the two. It is the consensus of the references cited (ref. 5-19) that mono- and divalent cations are the principal types involved in any of the proposed hydrolysis schemes; although nonionic and anionic species have been proposed by Sutton, these are not to be expected in the range of concentration involved here. One is thus led to suspect some unusual conduction mechanism at low fields, possibly operating through an oxygen bridging mechanism as proposed by Longworth.¹¹

To explain the unusual conductance behavior and the lack of agreement with theoretical calculations at high fields, an influence of field upon the conduction mechanism must be invoked. Two possibilities are suggested by the observations of the previous paragraphs. If some bridging process is responsible for the abnormal conductance at low fields, orientation times for the conducting uranyl species at high fields may be long compared to the pulse lengths involved. A decrease in conductance might result from a failure of the ordinary conduction mechanism within the period of the high-field pulse, corresponding to a bulk polarization. It must be pointed out that there was no evidence of a relaxation process operating in the range of 4- μ sec. time intervals, so any time-dependent conduction mechanism must either respond in times shorter than 0.5 μ sec., the shortest time we can conveniently observe, in which case it would not be responsible for the experimental results, or require times larger than 10 μ sec., which we cannot observe at higher fields where the phenomenon becomes significant. For this reason, and since the solutions are appreciably hydrolyzed into hydrogen ions and polymeric uranium species, we prefer the explanation that the applied field causes increased collisions between the fast-moving hydrogen ions and the slower uranyl complexes, reversing the

(34) B. B. Owen and R. W. Gurry, *J. Am. Chem. Soc.*, **60**, 3074 (1938).

hydrolysis equilibria (*e.g.*, eq. 1 or 2). In either case—change of conduction mechanism or reversal of hydrolysis equilibria—the number of ions available for conduction decreases and the conductance decreases with increasing field.

The experimental data adduced are not adequate to answer which of these processes is operating. Additional confidence would be lent to the second suggestion if a model compound could be found which showed similar abnormal high-field conductance but had more nearly normal low-field conductance behavior. In search for such a compound we have examined a number of aquo complex compounds, including aquopentamminecobalt(III) perchlorate, the several chromium(III) aquo complexes, and the formally similar titanyle, vanadyle, and related compounds. None has been found to behave peculiarly in any way so far as they have been studied. We have not yet studied neptunium(VI) compounds, although we have hopes of so doing.

As another approach, we have made three kinds of additions of reagents to the uranyl nitrate solutions, utilizing nitric acid, potassium nitrate, and potassium hydroxide. Addition of the first and third is an obvious way to change the pH, while addition of nitrate ion is a way to examine the significance of nitrate-uranyl ion complexing on the high-field conductance results. When it became apparent that the effects of adding hydroxyl and nitrate ion were much less significant than that of adding hydrogen ion, these experiments were not carried out in as much detail as would otherwise have been appropriate.

The addition of hydroxide changed the shape of the high-field conductance curves, putting a dip in the middle and raising the low- and high-field ends of the curve above that of uranyl ion alone. The only experiments were done at 25°; it was found that stable solutions could be prepared with appreciably higher pH than that of the hydrolyzed uranyl ion, but if the increase of pH went much further than about 0.4 pH unit, the solutions were prone to precipitate when the high-field measurements were made, although they would remain stable if no such measurements were performed. The net effect of the addition of such small amounts of hydroxide (0.5×10^{-4} *M* final concentration) was to lower the high-field conductance curve in the direction of a greater negative Wien effect at the given temperature.

The effect of addition of nitrate was much smaller, not much larger than the precision of measurement in the case of an addition of nitrate to yield a 0.635×10^{-4} *M* concentration of potassium nitrate. With twice this concentration, 1.210×10^{-4} *M*, the general

result was to raise the high-field conductance quotient above that of uranyl ion at lower fields, below 100 kv./cm., and to lower it slightly below the salt alone at higher fields, above 175 kv./cm. In the absence of more extensive measurements on mixed electrolyte solutions than ref. 24, it is not possible to interpret this result meaningfully, except to say that the addition of nitrate ion should increase the uranyl nitrate ion association, and that if this occurred a larger field effect would be expected, which is what is observed. On the other hand, potassium nitrate will exhibit a normal Wien effect, and the result is not distinguishable from the expected change from this source.

The addition of nitric acid was studied at two temperatures, 15 and 65°. As will be seen in Figure 9, adding acid has a very small effect at 15°; below 150 kv./cm. it is to raise the conductance quotient slightly above that of the uranyl ion alone; above 150 kv./cm. the trend is reversed ever so slightly, but consistently. The concentration of acid added was 0.683 *M*. At 65°, in contrast, at all fields the conductance quotient of the mixture lies above that of the salt alone although the concentration of acid is 4.2-fold smaller. In these experiments, two phenomena might confuse the results: the effect of the nitrate ion in complexing the uranyl ion, and the uncertain conductance results to be expected from a mixture of ions of different valence type. By conducting the experiments at two temperatures these concerns are essentially cancelled out. The concentration of the nitric acid is much larger at the lower temperature, while there the effects of the addition are negligible, 0.01 unit at 200 kv./cm. At the higher temperature, the effects are large, 0.45 unit at the same field. The latter effect is 45 times as large as the former, and the direction of the change is to reduce the observed negative Wien effect. We have calculated the effect on the conductance quotient of adding the nitric acid if the results were only those to be expected from normal ionic interactions. The calculated effect on the conductance at 65° of adding the nitric acid, compared to the uranyl ion solution alone, is 0.011 unit for reaction 1 or 0.064 unit for reaction 2. The experimental effect, 0.45 unit, is so much larger that it can be ascribed only to the influence of the hydrogen ion on the hydrolysis equilibrium. It will be recalled that the results of other studies^{6,15,19} indicate the increased production of UO_2OH^+ at the higher temperatures; thus, at 65° with an initial UO_2^{+2} concentration of 0.516×10^{-4} *M* employed, the H^+ concentration is 0.263×10^{-4} *M*, indicating that half of the uranyl ion is hydrolyzed.

The observation that the addition of base increases the negative Wien effect while the addition of acid

markedly reduces the negative Wien effect indicates a clear effect of the change of pH on the hydrolysis equilibrium, for example, eq. 2. Addition of base favors an increase in the concentration of UO_2OH^+ while addition of acid decreases it. These changes have been observed to accompany an increase (not large) and a decrease (large) in the negative Wien effect. The conclusion seems inescapable that the effect of field is on the involvement between hydrogen

ion and the uranyl complex, presumably UO_2OH^+ , since it is the predominant species present at 65° not present at 15° .

Acknowledgment. This publication was supported by the Atomic Energy Commission, in part under Contract AT(30-1)-1375 and in part under Contract AT(30-1)-2890. An equipment loan contract with the Office of Naval Research supplied much of the equipment used.

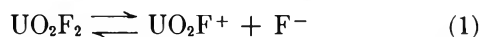
The Wien Effect in Uranyl Ion Solutions. II. Uranyl Fluoride from 5 to 65°

by Joseph F. Spinnler and Andrew Patterson, Jr.

Contribution No. 1756 from the Sterling Chemistry Laboratory, Yale University, New Haven, Connecticut (Received August 24, 1964)

Experimental measurements of the pH and the low- and high-field conductances of solutions of uranyl fluoride over the temperature range 5 through 65° are presented as a function of concentration. The salt exhibits a number of unusual properties. In keeping with the findings of earlier investigators, its behavior at low fields is that of a highly associated electrolyte. At high fields, however, it behaves like a relatively strong electrolyte. The pH values lie above those of other uranyl salts examined in the same range of temperature and concentration. The high-field conductance quotients vary only slightly with increasing temperature.

As part of a study of the associative behavior of uranyl ion in solution,^{1,2} we have measured the low- and high-field conductances and the pH of a series of solutions of uranyl fluoride over a range of concentration and temperatures. The conductance measurements of Brown, *et al.*,³ indicate that uranyl fluoride is a very weak electrolyte. These authors obtained values for a dissociation constant of 4.63 to 4.85×10^{-5} in the concentration range 10^{-4} to 10^{-2} *N*, assuming the dissociation reaction is represented by



The authors point out that the dissociation is more complex than represented by eq. 1 and that the constancy of the *K* values over this range of concentra-

tion may be largely fortuitous. Johnson, Kraus, and Young⁴ commented that it is unlikely that any significant concentration of fluoride ion can occur since the solutions of uranyl fluoride are acidic to a degree incompatible with the source of hydrogen ion being the ionization of hydrofluoric acid alone. Rather, they prefer the reaction



(1) J. F. Spinnler and A. Patterson, Jr., *J. Phys. Chem.*, **69**, 500 (1965).

(2) J. F. Spinnler and A. Patterson, Jr., *ibid.*, **69**, 513 (1965).

(3) R. D. Brown, W. B. Bunger, W. L. Marshall, and C. H. Secoy, *J. Am. Chem. Soc.*, **76**, 1580 (1954).

(4) J. S. Johnson, K. A. Kraus, and T. F. Young, *ibid.*, **76**, 1436 (1954).

as the hydrolysis equilibrium. These same authors present evidence from ultracentrifugation measurements that uranyl fluoride is dimerized in solution. All of these observations are useful in interpreting the results of the present paper which reveal uranyl fluoride to be an even more curious electrolyte than heretofore observed.

Experimental

The experimental procedure was essentially the same as described previously in ref. 1. The sample of uranyl fluoride was taken from the same lot used by the authors of ref. 3 and was provided by them through the courtesy of Prof. H. S. Harned. Since it was originally prepared for conductance measurements, it was not treated further before use.

Results

In Figure 1 are plotted the pH measurements as a function of $\log c$. Measurements of specific conductance as a function of the square root of the concentration and temperature are given in Figure 2. In Figure 3 are shown the experimental high-field conductance results, which may be compared with a variety of computations of theoretical conductance quotients in Figure 5. In Figure 4 is shown the effect of changing concentration on the results at 25 and 35°. All measurements have been performed over the range 5 to 65°.

Discussion

The pH data of Brown, *et al.*,³ are reported only for 25°. Their results lie close to ours; but not within our claimed accuracy of 0.05 pH unit. Their data are smoother, while ours cross theirs at several points. The pH values of uranyl fluoride solutions lie above those of the other uranyl salts examined.

The remaining experimental results exhibit a number of unusual features. The low-field conductance of uranyl fluoride solutions is appreciably smaller than that of other uranyl ion solutions, as may be highlighted by comparing Figure 2 with Figures 4 and 5 of ref. 1, and with Figure 2 of ref. 2. Thus, for a similar specific conductance of $L = 5.00 \times 10^{-5}$, a concentration of $1.33 \times 10^{-4} M$ of uranyl perchlorate is required, while for uranyl fluoride the concentration must be $16.8 \times 10^{-4} M$, 12-fold larger. If the statement is put in terms of equivalent conductances, the Λ vs. $c^{1/2}$ curve intersect those for uranyl perchlorate only when solutions of uranyl fluoride are in extreme dilution and at high temperature and the uranyl perchlorate is similarly dilute, in keeping with the conclusion that uranyl fluoride is a very weak electrolyte.

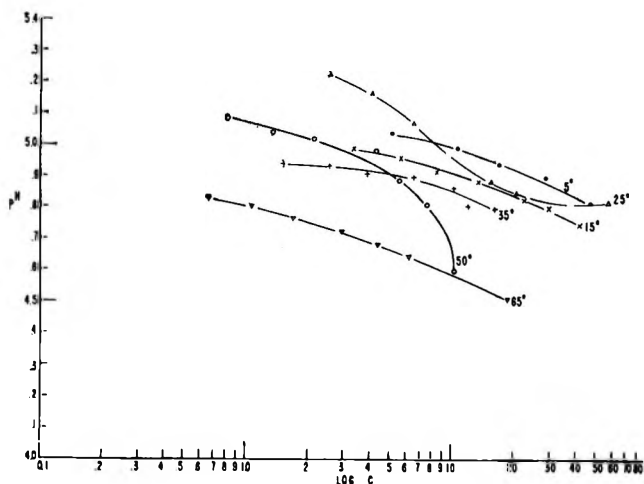


Figure 1. The pH of solutions of uranyl fluoride plotted as a function of log concentration, moles/l.

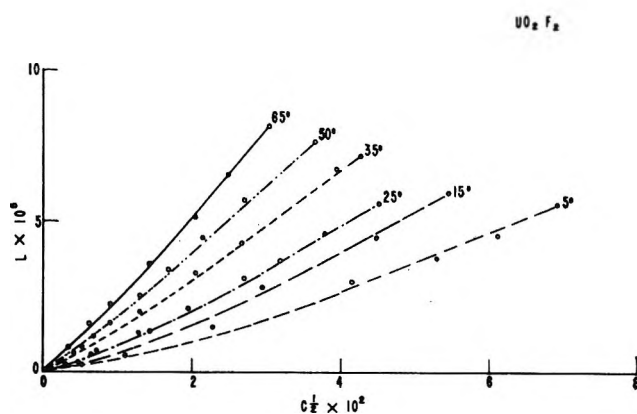


Figure 2. The specific conductance of solutions of uranyl fluoride plotted as a function of $c^{1/2}$. The concentration is specified in moles of the salt/l.

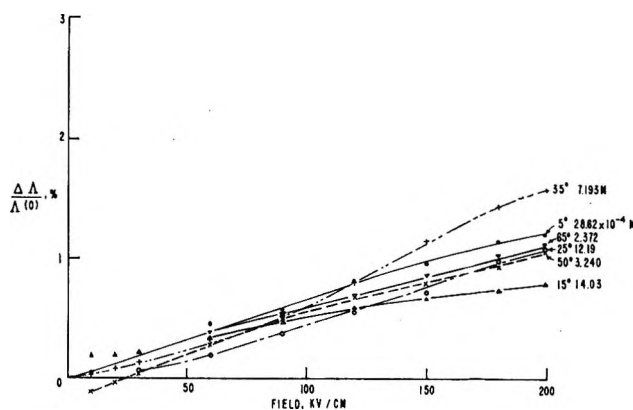


Figure 3. The high-field conductance quotients, $\Delta\Lambda/\Lambda(0)$, per cent, for solutions of uranyl fluoride as a function of field in kv./cm. The concentrations specified are all in moles/l. $\times 10^{-4}$.

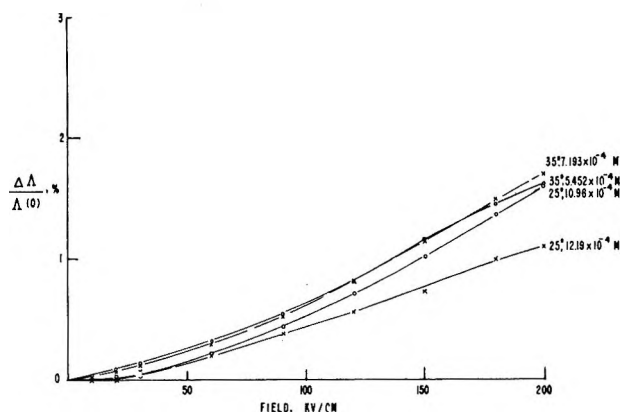


Figure 4. Plots of the high-field conductance quotient, $\Delta\Lambda/\Lambda(0)$, per cent, plotted as a function of field in kv./cm. for solutions of uranyl fluoride to show the effect on the results of changing the concentration at 25 and 35°.

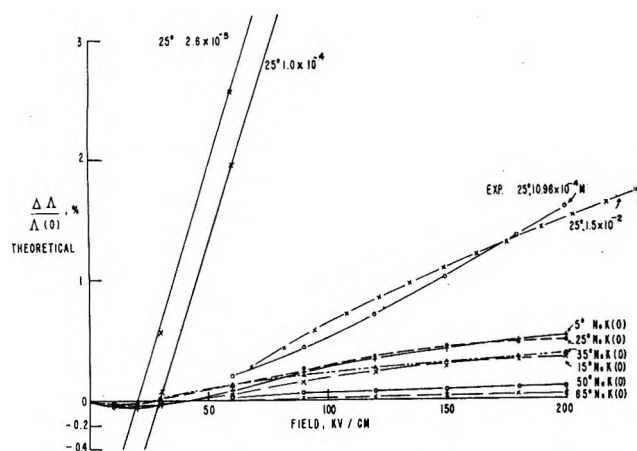


Figure 5. Plots of theoretical calculations of the high-field conductance quotient $\Delta\Lambda/\Lambda(0)$, per cent, for solutions of uranyl fluoride assuming the reaction products are univalent. See text. The curves in the lower sector are computed assuming no association constant and are intended to show the trend of the computations as a function of temperature. The central curve marked EXP. 25° denoted with \circ duplicates the experimental data at 25° found in Figures 3 and 4. The curve lying close by, denoted with \times , represents a calculation for a solution of the concentration and temperature specified and assuming an equilibrium constant of 1.5×10^{-2} . In the upper left side of the plot are found two curves computed for dissociation constants of 1.0×10^{-4} and 2.6×10^{-5} .

On the other hand, the high-field conductance results correspond to the behavior of a relatively strong or unassociated electrolyte, quite in contrast with what would be expected from an electrolyte with a dissociation constant of 4×10^{-5} such as reported in ref. 3 or from the apparent evidence of lack of dissociation indicated by the small low-field conductance.

An additional unusual feature of the results is the narrow range within which the high-field conductance quotient varies as a function of temperature. The range is narrower than that observed in the cases of uranyl nitrate, perchlorate, and sulfate, as well as in the cases of other normal electrolytes thus far examined by us.

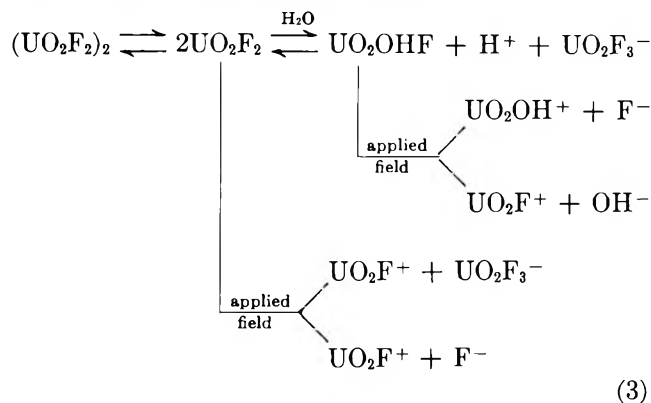
Finally, there is a large concentration differential, compared to the other uranyl ion solutions, to achieve the same specific conductance at two extremes of temperature. For example, to yield a value of $L = 5.00 \times 10^{-5}$ at 5° required a concentration of uranyl fluoride of $28.6 \times 10^{-4} M$, while at 65° the concentration was $2.32 \times 10^{-4} M$. With a solution of uranyl nitrate, the comparable data are 2.2×10^{-4} and $0.50 \times 10^{-4} M$. The ratios of the two concentrations are, respectively, 12.3- and 4.4-fold. If this same statement is converted into equivalent conductance terms, then it is impossible to choose an overlapping range of equivalent conductances for the two salts, which re-emphasizes the degree to which the fluoride behaves as a very weak electrolyte. In Figure 2 we have plotted specific conductance instead of equivalent conductance for the reason that to plot equivalent conductance commits us to some choice of number and valence type of ions. Such a commitment is not supportable by the complex results discussed below, and it seemed wiser not to mislead the reader. We have, of course, graphed the equivalent conductance and carried through the usual conductance calculations based on the assumption that UO_2F_2 dissociates into the expected ions. In further agreement with the observation of Brown, *et al.*,³ the plots of $\Lambda\eta$ vs. $c^{1/2}$ with temperature as parameter cluster very closely together, indicative of very little influence of temperature upon the equilibria in the system.

To perform necessary high-field conductance calculations to throw some light on these curious deviations from expected behavior, we have used the data of Brown, *et al.*,³ and applied the procedure of Kraus and Bray⁵ to obtain a value of the limiting equivalent conductance. It is assumed that the value is known to no better than 10%. To obtain the values of limiting ionic conductance and equivalent conductance at temperatures other than those for which data are available, Walden's rule⁶ has been employed. Only one value of the limiting ionic conductance of fluoride ion is available from the literature.³ Values at other temperatures were obtained by drawing a curve of suitable shape, guided by the actual data for other

(5) C. A. Kraus and W. C. Bray, *J. Am. Chem. Soc.*, **35**, 1315 (1913).

(6) P. Walden, *Z. physik. Chem.*, **55**, 207, 246 (1906).

anions, through this datum. The probable accuracy is 10%. Fortunately, as has been shown in ref. 1, these data are not critical in determining the theoretical result, for which the assumed fractional cationic valence factor, z^+ , is much more significant. In this case, we postulate the following set of possible equilibria, based on the suggestions of the authors of ref. 3 and 4.



Since all the hydrolytic products or products of dissociation by the applied field are univalent, z^+ remains unity, and the influence of valence factors vanishes in the Onsager-Kim theory (see ref. 1).

Performing the theoretical calculations with the data obtained as just described, and following essentially the procedure of Freitag and Patterson,⁷ one obtains results such as those depicted in Figure 5. The results conform to what one would conclude from inspection of Figure 4, namely, that the solute behaves as a relatively strong electrolyte. Thus, in Figure 5, which includes theoretical calculations of the high-field conductance based on the assumption of a field effect on the monomer UO_2F_2 or on the hydrolysis product UO_2OHF , the best fit of experimental data is obtained with an assumed $K(0)$ of 1.5×10^{-2} . A dissociation constant of unity yields values of the conductance quotient only slightly larger than if the association is ignored; examples of the latter assumption are shown in the lower portion of Figure 5, while at the upper left are shown curves resulting when $K(0)$ values in the order of 10^{-4} and 10^{-5} are used. The maximum change in the computed conductance quotient occurs when $K(0)$ lies between 10^{-2} and 10^{-4} .

There are several possible interpretations of these data, among which the data themselves offer no unique choice. The pH values of the solutions are relatively high, lying at all concentrations of solute above those for the other uranyl salts studied in this group of investigations. At a concentration of 1.00×10^{-3} in solute, the pH is just 5.0, indicating that only a small fraction (about 1%, depending on the hydrolysis reaction chosen) is hydrolyzed. If the equilibrium con-

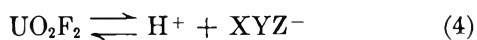
stant governing the hydrolysis were 1.5×10^{-2} , then the fraction hydrolyzed should be 50% or higher, depending on the detailed stoichiometry of the hydrolysis reaction. Both these estimates have assumed no dimerization of the solute. The field effect observed with the uranyl fluoride solute is characteristic of a weak electrolyte with linear dependence of the conductance quotient on increasing field rather than the characteristic ionic field dependence expected of univalent ions such as those resulting from hydrolysis reaction 2.

As one possible interpretation, one may conclude that uranyl fluoride is appreciably dimerized even at these low concentrations, in order to account for the relatively small concentration of monomer permitted if the hydrolysis reaction is governed by a constant as large as 1.5×10^{-2} . If the hydrogen ion concentration is a unique indication of the degree of hydrolysis, if the hydrolysis constant is 1.5×10^{-2} , and if reaction 2 is assumed, then the concentration of monomer consistent with pH 5 is $2.0258 \times 10^{-5} M$, and the dimerization constant must be in the order of 5×10^7 to have a sufficient amount of the solute in dimerized form. The authors of ref. 4 found a dimerization constant of 3; thus, the suggested set of values does not accord well with other experimental work on these solutions.

As a second possibility, one may undertake to use the equilibrium constant value 4.7×10^{-5} , a numerical value found in ref. 3 for the assumed ionization reaction 1, as the hydrolysis equilibrium constant. Proceeding as before, then, a monomer concentration of $2.461 \times 10^{-5} M$ is required, yielding a dimerization constant of the order of 3.8×10^5 . Not only is the dimerization constant still unreasonably large, but the very small change in monomer concentration with so large a change of equilibrium constant seems unreasonable as well. This is the mathematical consequence of assuming reaction 2, in which three products are formed, with the result that in the numerator of the expression to be solved the value $(1.00 \times 10^{-5})^3$ appears, and in the denominator $(x - 2.00 \times 10^{-5})^2$. The factor 2.00×10^{-5} far outweighs all other arithmetic portions of the expression, demanding a large number of significant figures and giving rise to the absurd mathematical result. One is perhaps then justified in assuming a hydrolysis reaction yielding two products in order to obtain a formulation which can be handled arithmetically.

If such a reaction is assumed for hydrolysis, for example

(7) H. Freitag and A. Patterson, Jr., *J. Electrochem. Soc.*, **108**, 529 (1961).



making no commitment to what are the products except that there are two, then by a process of approximation it is found that a consistent set of values is obtained with a hydrolysis constant of 1.1×10^{-4} and a dimerization constant of 9. There are, of course, many other possible solutions, but this selection puts the dimerization constant in the range found by the authors of ref. 4. The required hydrolysis constant lies between the extreme values of equilibrium constants, 4.7×10^{-5} and 1.5×10^{-2} , which apply to undefined equilibria investigated by low- and high-field conductance methods in ref. 3 and this paper.

On the other hand, it is quite possible that some specific interactions account both for the low- and high-field results, more especially the latter, so the preceding interpretation does not apply. The unusual results obtained with uranyl perchlorate and nitrate, ref. 1, lend credence to such a view. In those cases, presumably normal and unassociated electrolytes yield high-field conductance results which are unprecedented.

The suggestion leads us to the most attractive interpretation, in which one accepts a dimerization constant of the order of magnitude found in ref. 4 coupled with a hydrolytic reaction of small extent, indicated by the relatively high pH, producing two ions and governed by a small equilibrium constant in the vicinity of 10^{-4} , and explains the low conductivity at low fields as the result of the nonionization of UO_2F_2 and the low mobility of the large ion UO_2F_3^- and the nonconducting UO_2OHF produced by hydrolysis.

At high fields, the behavior observed (linear dependence of the conductance quotient on field) indicates a low concentration of ions and small interionic attractions, entirely consistent with the assumptions just advanced. If the concentration of ions were high, then the field effect would be typical of a strong electrolyte, with an abrupt rise of conductance quotient in the field region below 50 kv./cm. If the electrolytic species present were as highly associated as just assumed, then the field effect should be large, which is not the case. A small apparent increase of conductance with applied field can then arise only by cancellation of the expected conductance increase by some field-induced effect which lowers the number of ions available to conduct. Uranyl nitrate and perchlorate are examples of this situation. As was the case with these just-mentioned electrolytes, we have observed in this study of uranyl fluoride no time-dependent field effects which suggest relaxation phenomena in the 1-10- μ sec. range of pulse lengths. Uranyl fluoride thus appears to combine all the characteristics of a

weak electrolyte at low fields with those of a relatively strong electrolyte at high fields. The behavior of uranyl sulfate does not resemble that of any of these three salts.

Bailey and Patterson have studied two salts whose behavior might be formally similar to that of uranyl fluoride, since they are both 2-1 electrolytes, mercuric and cadmium chlorides.^{8,9} The high-field conductance of cadmium chloride at $1.7 \times 10^{-4} M$ and 25° lies quite close to that of uranyl fluoride; the concentration of uranyl fluoride is 10-fold greater to yield the same approximate specific conductance, and the shapes of the curves are quite different. That of cadmium chloride is curved and characteristic of "strong" electrolyte, although a dissociation constant of 0.011 has been attributed to the reaction



it being assumed the ionization of the salt into the CdCl^+ ions is complete. The shape of the curve is thus consistent with a well-developed ionic atmosphere and the magnitude of the field effect is consistent with the $K(0)$ of 1.1×10^{-2} . The results for mercuric chloride are entirely different. The low-field equivalent conductance of solutions of mercuric chloride is less than one-tenth as large at an identical concentration, e.g., $4.0 \times 10^{-3} N$. The high-field conductance quotient is much larger, and it was found that the conductance changed during the pulse. Whether this was a result of relaxation phenomena, which were being sought in the investigation, or polarization is not apparent from the data. Thus, the behavior of mercuric chloride is in no way comparable to that of uranyl fluoride.

We are forced to accept the conclusion that uranyl fluoride is subject to specific interactions of several kinds. At low fields, the conductance behavior is a result of a succession of equilibria producing ions whose identity undoubtedly changes with change in temperature. The apparent constancy of ionization is probably due to the interplay of a combination of these equilibria. At high fields, there are ample species upon which the field may exert an ionizing influence, but it is also possible that the hydrolysis reaction may be reversed by the field owing to collisions of the hydrogen ion with the other two species postulated in reaction 3, thus partly negating the effect of the field. Since the change of temperature at low fields causes an increase in the concentration of dimer, according

(8) F. E. Bailey and A. Patterson, Jr., *J. Am. Chem. Soc.*, **74**, 5759 (1952).

(9) F. E. Bailey and A. Patterson, Jr., *ibid.*, **75**, 1471 (1953).

to ref. 4, and little change of ionization according to ref. 3, it is perhaps not remarkable that the high-field quotients are but little changed over the same range of temperature.

Acknowledgment. The support of the Office of Naval Research through an equipment loan contract and of the Atomic Energy Commission through Contract AT(30-1)-2890 is gratefully acknowledged.

The Wien Effect in Uranyl Ion Solutions. III. Uranyl Sulfate from 5 to 65°

by Joseph F. Spinnler and Andrew Patterson, Jr.

Contribution No. 1765 from the Sterling Chemistry Laboratory, Yale University, New Haven, Connecticut (Received August 24, 1964)

The low-field conductance, pH, and high-field conductance of solutions of uranyl sulfate have been determined over a range of concentrations and temperatures from 5 through 65°. Uranyl sulfate is found to be an associated electrolyte, although disagreement between low-field conductance and ligand displacement determinations of the dissociation constant and ambiguities in the high-field conductance results make it impossible to place the dissociation constant precisely. The present results are consistent with the conclusion of low-field conductance measurements that the association of the electrolyte increases with increasing temperature.

We have measured the low- and high-field conductances and the pH of a series of solutions of uranyl sulfate over a range of concentrations and temperatures from 5 to 65°. In a previous paper, we have reviewed the current understanding of the ionic species which are thought likely to be present in the partially hydrolyzed solutions of uranyl nitrate and perchlorate.¹ In contrast with these electrolytes, uranyl sulfate is appreciably associated, as shown by the measurements of conductance over a wide range of concentration and temperature made by Brown, Bunger, Marshall, and Secoy,² and by the ligand displacement measurements of Ahrland.³ The high-field conductance measurements are thus of interest to compare with those on the two relatively unassociated electrolytes of ref. 1.

Experimental

The experimental procedure was essentially the same as described in ref. 1. The sample of uranyl sulfate is taken from the same lot as that used by the authors of ref. 2, and was kindly provided by them through

the good offices of Prof. H. S. Harned. Since it was originally prepared for conductance measurements, it was not further treated before use.

Results

Plots of the pH of the solutions *vs.* $\log c$ are given in Figure 1. The equivalent conductances of the solute employed are shown in Figure 2. Plots of the high-field conductance quotients measured are given in Figure 3. Figure 4 shows the effects on the high-field conductance quotient of changing the concentration of the solution at two temperatures, 25 and 35°.

Discussion

The experimental evidence from measurements of conductance at low fields is that uranyl sulfate is an associated electrolyte. The conductance measure-

(1) J. F. Spinnler and A. Patterson, *J. Phys. Chem.*, **69**, 500 (1965).

(2) R. D. Brown, W. B. Bunger, W. L. Marshall, and C. H. Secoy, *J. Am. Chem. Soc.*, **76**, 1532 (1954).

(3) S. Ahrland, *Acta Chem. Scand.*, **8**, 1907 (1954).

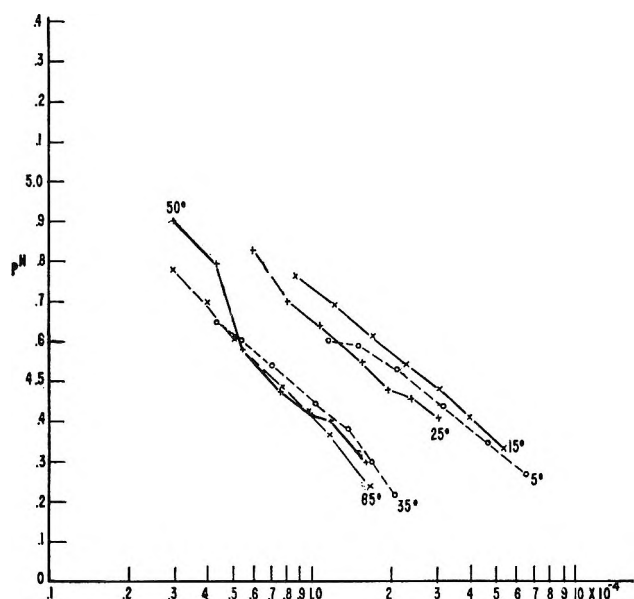


Figure 1. Plots of the pH of solutions of uranyl sulfate vs. $\log c$, moles/l., as a function of temperature.

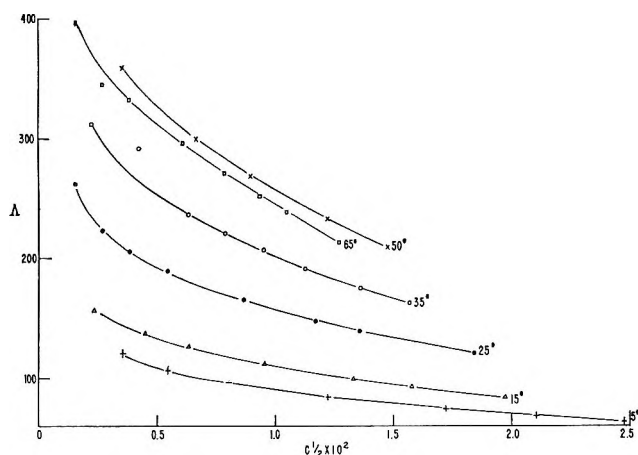


Figure 2. Plots of the equivalent conductance of solutions of uranyl sulfate vs. $c^{1/2}$, moles/l., as a function of temperature.

ments of Brown, *et al.*,² when plotted against $c^{1/2}$ approach the conductance axis asymptotically; the average dissociation constant at 25° determined by these workers after making correction for hydrogen and other expected ions present in the hydrolyzed mixture is 5.9×10^{-4} . These authors comment that the significance of a dissociation constant of an associated higher valence type electrolyte determined by low-field conductance measurements is questionable for lack of a completely dissociated 2-2 electrolyte with which to compare it. It is their opinion that greater credence should be given to Ahrlund's result,

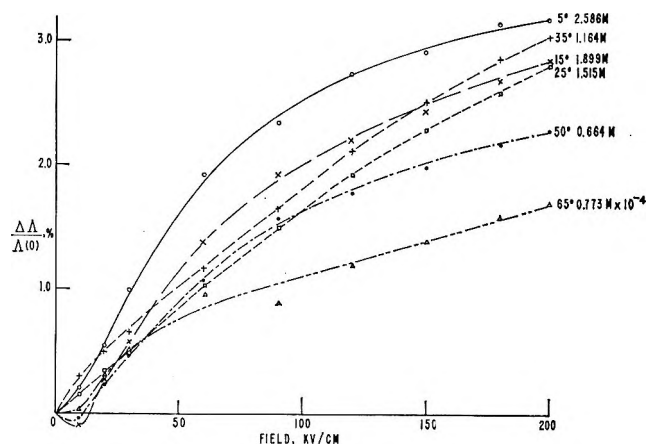


Figure 3. Plots of the high-field conductance quotient, $\Delta\Lambda/\Lambda(0)$, per cent, as a function of applied field in kv./cm. for different temperatures and concentrations. All concentrations are to be read as moles/l. $\times 10^{-4}$. The concentrations correspond approximately to the same specific conductance for each determination.

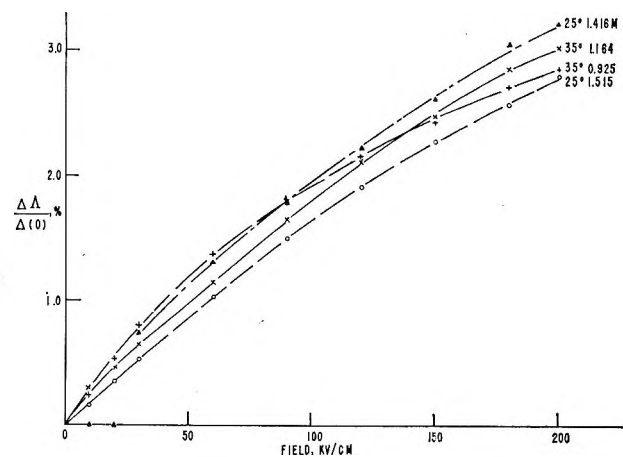


Figure 4. Plots of high-field conductance quotient vs. field to show the effect of changing concentration at two temperatures, 25 and 35°.

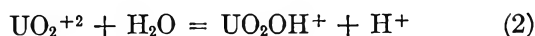
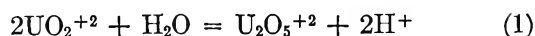
0.02, because of inherent weaknesses in conductometric methods. Magnesium sulfate is another example of a 2-2 valence type associated electrolyte, for which low-field conductance measurements yield a dissociation constant of 6.3×10^{-3} . Bailey and Patterson⁴ have shown that it is possible to combine the theories for weak and strong electrolyte high-field conductance in such a way as to permit computation of high-field conductance quotients agreeing satisfactorily with the experimental values obtained on magnesium sulfate, and Freitag and Patterson⁵ have

(4) F. E. Bailey and A. Patterson, Jr., *J. Am. Chem. Soc.*, **74**, 4428 (1952).

refined this calculation considerably. The excellent agreement between experimental and theoretical high-field conductance results obtained by them for magnesium, zinc, and copper sulfates⁵ lends considerable support to the idea of ion pairs in such associated electrolytes and to the physical significance of the dissociation constant in predicting other solution properties. It is thus a disappointment to find the experimental high-field conductance measurements of uranyl and magnesium sulfates in some ways quite similar and in other ways not: at 25° for solutions of similar concentration, $1.4 \times 10^{-4} M$, the conductance quotient is similar, 3.2%. The data on magnesium sulfate show quite a small variation with change in temperature from 5 to 55° in contrast to those of uranyl sulfate where the change is one unit in $\Delta\Delta/\Delta(0)$ over the same range. In view of the success of Freitag and Patterson,⁵ one would be led to assume the two electrolytes had similar association constants, which is quite in disagreement with the data quoted above. The high-field results are not consistent with the view that uranyl sulfate is associated to a degree that the equilibrium constant should be as small as 6×10^{-4} . Magnesium sulfate, for which such satisfactory high-field conductance calculations can be performed, has a dissociation constant of 6.3×10^{-3} , ten times larger, but the high-field conductances are similar. The first ionization constant of carbonic acid is of the order of magnitude of 10^{-4} , and the results⁶ are entirely in contrast with those obtained on uranyl sulfate, though it should be kept in mind that the valence types in the two electrolytes may be different.

Referring to Figure 3, we observe that the shapes of the high-field conductance curves are typical of those of "strong" electrolytes, in contrast with the results on uranyl fluoride,⁷ in which a linear increase of conductance quotient was found. This latter indicates small ion-atmosphere effects, while the shape of the curves in Figure 3 are typical of significant ionic field influences. That the curves dip below the origin at low fields is neither experimental error nor evidence of negative Wien effects¹; it is more probably due to the different rate of change of the ionic field effect in the uranyl sulfate and reference electrolyte solutions.

To perform high-field conductance theoretical calculations on uranyl sulfate for comparison with the experimental results, we have assumed, as in ref. 1, that two principal hydrolysis reactions are possible



We have made no attempt to deal with mixtures of

these two reactions, but have computed mixed valences and limiting ionic conductances for the combined cations⁸ and have employed these in the theoretical calculations. Further, the calculations have been made ignoring association; this is forced upon us by the fact that the mathematical development of the combined theories embodying association correction⁵ will admit calculations only on symmetrical electrolytes, although any valence type, including fractional valence types, can be accommodated so long as association is not involved. In spite of this limitation, the results are of considerable interest, as may be seen from inspection of Figure 5. At 5, 25, and 65°, the results of calculations assuming both reactions 1 and 2 are shown. At the other temperatures, only reaction 1 is shown. Considering for the moment only reaction 1, the theoretical calculation reproduces the experimental results quite closely at 5°, within 0.1 unit; this widens at 25°, and at 65° the disparity is 0.51 unit at 200 kv./cm. Reaction 2 is in every case a poorer compromise.

The validity of these theoretical calculations may be examined by making calculations in which only one parameter is varied. As in ref. 1, the concentration, limiting combined ionic conductance, and valence factor are the important variables. Using data of the

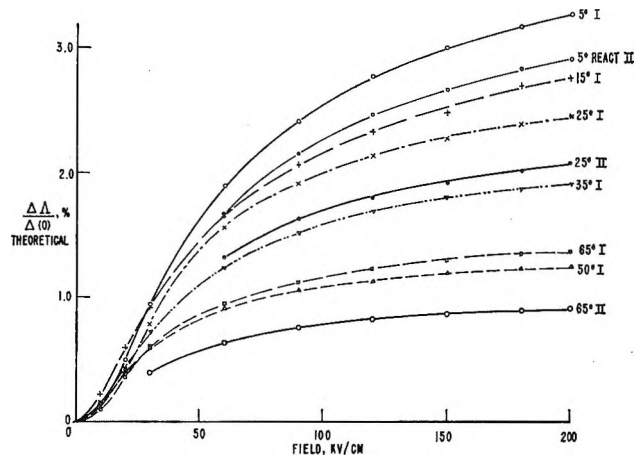


Figure 5. Plots of theoretically computed high-field conductance quotients vs. field as a function of temperature and for two choices of hydrolysis reaction of uranyl sulfate; see text.

(5) H. Freitag and A. Patterson, Jr., *J. Electrochem. Soc.*, **108**, 529 (1961).

(6) D. Berg and A. Patterson, Jr., *J. Am. Chem. Soc.*, **75**, 5197 (1953); K. F. Wissbrun and A. Patterson, Jr., *J. Phys. Chem.*, **58**, 693 (1954).

(7) J. F. Spinnler and A. Patterson, Jr., *ibid.*, **69**, 508 (1965).

(8) J. F. Spinnler and A. Patterson, Jr., *ibid.*, **69**, 658 (1965).

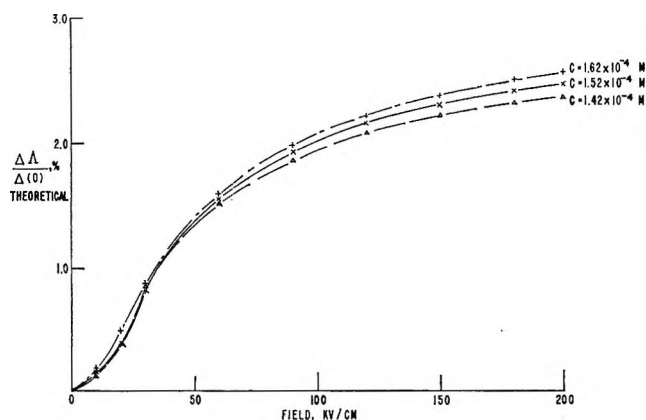


Figure 6. Plots of theoretically computed high-field conductance quotients vs. field to show effect of varying the concentration as a parameter. The data used, aside from the concentration variable, pertain to the experimental determination on a solution of uranyl sulfate at 25° found in Figures 3 and 4.

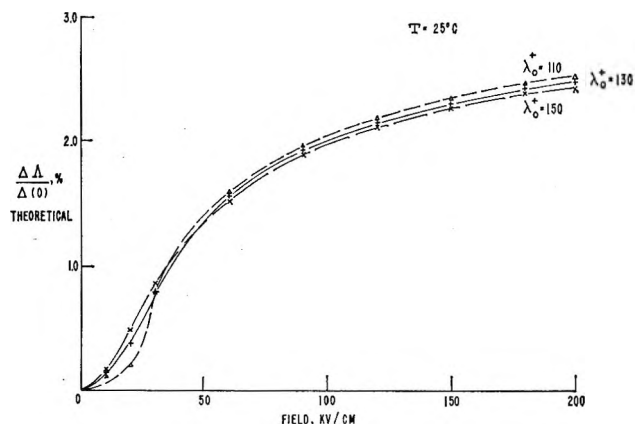


Figure 7. Plots of theoretically computed high-field conductance quotients vs. field to show effects of varying the limiting ionic conductance of the cation. As in Figure 6, the data used, except for the ionic conductance variable, pertain to the same experimental determination at 25° found in Figures 3, 4, and 6.

experimental determination found in Figures 3 and 4, concentration $1.515 \times 10^{-4} M$, and temperature 25°, in Figure 6 is shown the effect of changing the concentration, and in Figure 7 the effect of varying Λ_0^+ over quite a wide range in the calculation. A variation of 10% in the concentration results in a difference of approximately 0.1 in $\Delta\Lambda/\Delta(0)$ while a variation of 15% in the limiting ionic conductance results in a difference of less than 0.05 in the same quantity. Since the concentration is known with much higher accuracy and since the limiting ionic conductance is estimated to be known within 15%, these influences are of lesser importance, leaving the valence factor, z^+ , which in these measurements depends upon the pH measurements and on the assumption of a given hydrolysis reaction, as the determining factor in the precision of the theoretical calculation. In Figure 5, the two curves denoted 25° I and 25° II differ only in the z^+ employed, the values being 1.83 and 1.69, respectively. It can be seen that a decrease in z^+ of 0.14 results in a diminution of the high-field conductance quotient by 0.39% at 200 kv./cm., corresponding to a hydrogen ion concentration change of 0.003×10^{-4} mole/l. The pH measurements are made to 0.01 pH unit, corresponding to a variance of 0.007×10^{-4} mole/l. The importance of the valence factor and consequently of the pH determination is thus emphasized, and it is clear that theoretical results agreeing within 0.2% with the experimental high-field measurements are in good agreement by this criterion. Calculations at lower fields or with a smaller conductance quotient, as with uranyl perchlorate and nitrate, will be less seriously affected by errors in the hydrogen ion

determination, and agreement at the lower temperatures, at which the pH measurements are more precise, should be better, as observed.

However, the gradual and increasing divergence between the experimental and theoretical results at higher temperatures suggests, as is known to be the case with unassociated uranyl salts, that the hydrolysis pattern is changing, the valence factors applicable to the theoretical calculation changing at the same time, so that no one arbitrary choice of hydrolysis reaction, *e.g.*, reactions 1 or 2, will be applicable. A comment in ref. 2 is also pertinent; there it is noted that plots of $(\Delta\eta)_t^\circ/(\Delta\eta)_0^\circ$ over the wide temperature range studied yield curves with negative slope, indicative that fewer ions are present to carry the current at higher temperatures, and that accordingly there is an increase in association with increasing temperature. Inclusion of a dissociation constant would improve the agreement at higher temperatures where the experimental results lie above the present theoretical calculations. The calculation has been performed for uranyl fluoride⁶ in which case the expected hydrolysis products are all univalent and the salt itself sufficiently associated that it is reasonable to consider the ionic environment made up of symmetrical valence types. Although this cannot be done for uranyl sulfate, our results at 5 and 15° indicate that the degree of association is small, and that at 25° Ahrlund's value of 0.02 cannot be in error by so much as a factor of ten. It does seem quite clear that the low-field conductance-derived equilibrium constant result of Brown, *et al.*,² while entirely representative of the results of their careful measurements, is the consequence of

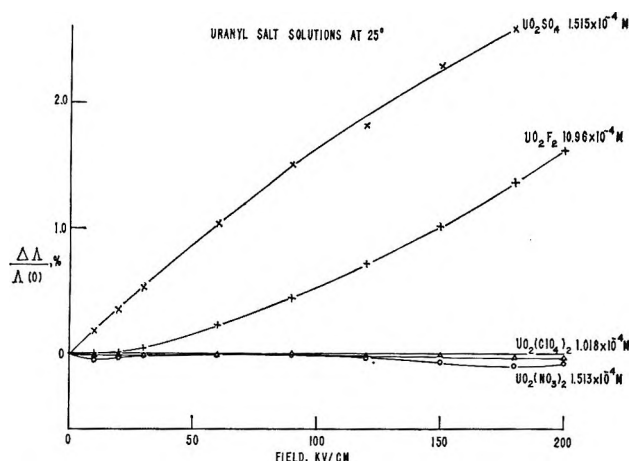


Figure 8. Plots of experimental high-field conductance quotient determination *vs.* field on solutions of uranyl perchlorate and nitrate, ref. 1, uranyl fluoride, ref. 7, and uranyl sulfate, this paper. The concentrations specified correspond roughly to constant specific conductance of the solutions.

complexities of ionic interaction and association which we do not presently understand.

In view of the decidedly unusual behavior of the other uranyl salts studied in this series of investigations, it is of interest to compare the results and to temper the conclusions reached in the previous paragraph in light of this comparison. The results for 25° and essentially constant specific conductance of the solutions have been brought together in Figure 8. The behavior of uranyl nitrate, perchlorate, and fluoride has been explained in terms of specific interactions under the influence of high fields, in which the hydrolysis equilibria are reversed and the conductance

quotient decreased below the value which would have been expected for a similar valence-type electrolyte. It is thus puzzling to understand why uranyl sulfate should be immune to these effects, if indeed this is the case. Thus, it is quite possible that the postulations of the preceding paragraph are in error, that uranyl sulfate is indeed as weak an electrolyte as a dissociation constant of 6×10^{-4} would indicate, and that the high-field conductance results are the consequence of specific interactions which are simply different in magnitude from those observed in the other uranyl salts. The principal basis in the present investigation for not coming to such a conclusion is the shape of the high-field conductance quotient *vs.* field curves. As noted earlier, the uranyl sulfate curves are indicative of an appreciable ionic atmosphere; the uranyl fluoride curves are not. Because of the orderly behavior of magnesium, zinc, and copper sulfates⁵ on the one hand, and the unusual behavior of uranyl nitrate, perchlorate, and fluoride^{1,6} on the other, one is forced to conclude that uranyl sulfate is an associated electrolyte with an association constant in the range determined by Ahrlund rather than that indicated by low-field conductance results, but that at high fields there is every possibility that specific interactions cause the results to deviate from what would be expected of an ordinary, well-behaved, hydrolyzed, 2-2 electrolyte.

Acknowledgment. This work was supported by the Atomic Energy Commission, in part under Contract AT (30-1)-1375 and in part under AT (30-1)-2890. An equipment loan contract with the Office of Naval Research has made available many of the high-field conductance bridge components.

Viscosity and Self-Diffusion of Liquid Thallium

from Its Melting Point to About 1300°K.

by J. A. Cahill and A. V. Grosse

The Research Institute of Temple University, Philadelphia, Pennsylvania (Received August 27, 1964)

The viscosity (η) of liquid thallium was measured by the oscillating crucible method between its melting point (577°K.) and about 1300°K. The values of η at the melting point and at 1000°K. were 2.65 and 1.05 cp., respectively. Self-diffusion, at the same temperatures, was calculated using the Frenkel theory to equal 0.16×10^{-4} and 0.80×10^{-4} cm.²/sec., respectively. The experimental activation energy for viscosity, H_η , equals 2500 cal./g.-atom; an empirical relationship between H_η and the melting point gives the value 2270 cal./g.-atom.

Neither the viscosity nor the self-diffusion of liquid thallium has been measured so far as we could ascertain. In view of its low melting point, the experimental determination of the viscosity should be rather simple. It affords an opportunity to check the empirical relationship¹⁻³ between the melting point and the activation energy of viscosity. It also would complete the subgroup IIIb of the periodic system, since both the viscosity and self-diffusion of gallium and indium have been measured.

Experimental

The viscosity was measured by the oscillating crucible method as described first by Andrade⁴ and later, among others, by Yao and Kondic,⁵ and reviewed by Bockris.⁶ A general treatment of this method, including a discussion of the experimental techniques required for precise measurements, has been published by Thresh.⁷ The apparatus used was similar to the one described by Thiele⁸ and consisted of a graphite crucible (5 cm. o.d. \times 3.5 cm. i.d. \times 9 cm. deep) suspended in a *bifilar* arrangement by a 0.018-mm. tungsten wire. It was calibrated with several liquids and checked with mercury. The relationship between the logarithmic decrements, $\lambda - \lambda_0$ (sec.⁻¹), and period of oscillation, T (sec.), of the system and the properties of the liquid is

$$(\lambda - \lambda_0) = c \frac{D_{m.p.}}{D_T} (\eta D_T T)^{1/2} \quad (1)$$

where the constant $c = 4.02 \times 10^{-4}$ cm.²/sec. g., $D_{m.p.}$ and D_T = density at the melting point and T° K., respectively, and η = viscosity in poises.

The amount of thallium used in this determination was ≈ 350 g. or ≈ 30 cc. The density values determined by Schneider, Stauffer, and Heymer⁹ from the melting point to 920°K. were selected and may be expressed by the equation

$$D \text{ (g./cc.)} = 12.16 - 15.21 \times 10^{-4} T \text{ }^\circ\text{K.} \quad (2)$$

Accordingly, the density varies from 11.29 g./cc. at the melting point (577°K.) to 10.64 g./cc. at 1000°K. These data were preferred to the data given in the "Liquid Metals Handbook,"¹⁰ which cover only a 30° temperature range.

(1) A. V. Grosse, *J. Inorg. Nucl. Chem.*, **23**, 333 (1961).

(2) A. V. Grosse, *ibid.*, **25**, 317 (1963).

(3) A. V. Grosse, *Science*, **140**, 788 (1963).

(4) E. N. da C. Andrade and Y. S. Chiong, *Proc. Phys. Soc. (London)*, **48**, 247 (1936).

(5) T. P. Yao and V. Kondic, *J. Inst. Metals*, **81**, 17 (1952).

(6) J. O'M. Bockris, J. L. White, and J. D. Mackenzie, "Physico-Chemical Measurements at High Temperatures," Academic Press, New York, N. Y., 1959, p. 325.

(7) H. R. Thresh, *Am. Soc. Metals, Trans. Quart.*, **55**, 790 (1962).

(8) M. Thiele, Doctorate Dissertation, Technical University of Berlin, 1956.

(9) A. Schneider, A. Stauffer, and G. Heymer, *Naturwissenschaften*, **41**, 326 (1954).

(10) R. W. Lyons, Editor in Chief, "Liquid Metals Handbook," II Ed., Department of the Navy, Washington, D. C.; NAVEXOS P-42 (Rev.), June 1952.

The purity of the thallium was 99.99%. Maximum amounts of impurities were, in p.p.m.: Pb, 40; Fe, 10; Cu, 10; Cd, 5; Zn, 2; total of others, 20.

Since the thallium was contained in graphite at high temperatures, any oxide present was converted to metallic thallium. The solubility of graphite in liquid thallium was reported to be negligible near its melting point by Moissan.¹¹ We determined the solubility at 900°K. by exposing a graphite rod to 10 cc. of liquid thallium contained in a stainless steel tube under argon for 4.0 hr. After the experiment, the thallium absorbed in the graphite rod was extracted with dilute HNO₃. Upon complete extraction, the graphite rod was weighed and only 1.5 mg. of carbon or less was lost. Thus, the solubility at 900°K. is 0.03 atomic % carbon or less. The usual precautions were taken to avoid poisoning by thallium.

A total of nine determinations was made during the course of five runs and these data are shown in Table I.

Table I: Experimental Viscosity Data

Temperature		Viscosity, cp.
°K.	1000/°K.	
644	1.552	2.11
645	1.550	1.97
661	1.513	2.04
665	1.503	2.03
672	1.488	2.26
787	1.270	1.62
928	1.077	1.03
1278	0.7824	0.78
1279	0.7818	0.72
1283	0.7794	0.71

Uncertainties in corrections for thermal expansion, inductive electrical effects, and ambient gas viscosity limit the accuracy of this determination to an error probability of ± 0.05 cp. at the melting point and ± 0.1 cp. at the boiling point.

Discussion of Viscosity Data

The best fit of the experimental points on a semilog plot is a straight line going through the points $\eta_{m.p.} = 2.65$ and $\eta_{1000^\circ K.} = 1.05$ cp. The equation of the straight line, in terms of Andrade's first equation (see ref. 1-3), is

$$\eta \text{ (poises)} = 2.983 \times 10^{-3} e^{2500/R^T} \quad (3)$$

where $R = 1.9865$ cal./g.-atom °K. and T is in °K. The experimental points and the straight line are illustrated in Figure 1.

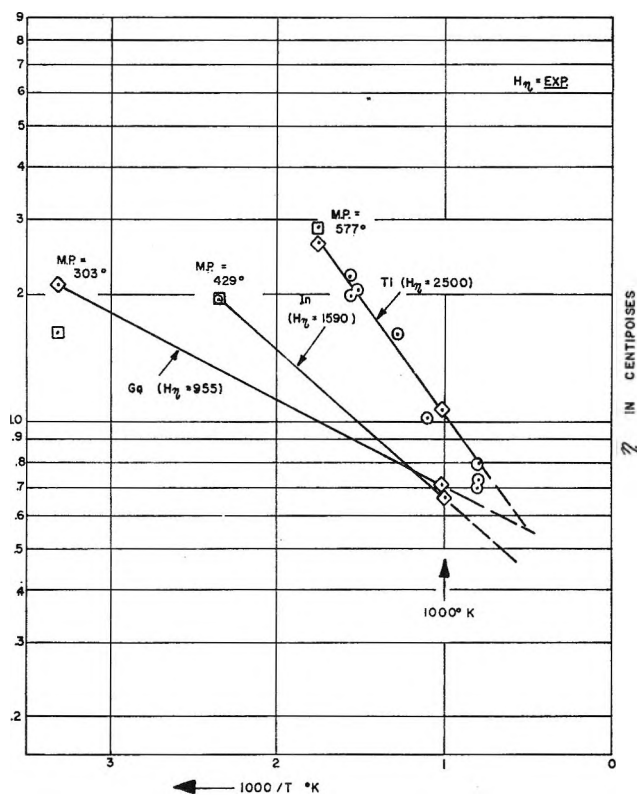


Figure 1. Plots of η vs. $1000/T$ for gallium, indium, and thallium.

It follows from the empirical relationship¹⁻³

$$H_\eta \text{ (cal./g.-atom)} = 0.431(T_{m.p.})^{1.348} \quad (4)$$

and for $T_{m.p.}$ of thallium = 577°K., that

$$H_\eta = 2270 \text{ cal./g.-atom} \quad (5)$$

This is in reasonable agreement with the experimental value of 2500 cal./g.-atom.

Now that data on thallium are available, it is appropriate to compare them with those of the other metals of subgroup IIIb of the periodic system, namely, gallium and indium.

The viscosity of gallium was measured by Spells¹² over the widest temperature range (30 to 1100°) of any metal, using the density measurements of Hoather¹³ over the same temperature range. Indium was investigated by Culpin.¹⁴ Their data were evaluated previously¹ and the constants of Andrade's first equation calculated; both metals are compared with thallium in Table II.

(11) H. Moissan, *Traité Chem. Minérale*, Paris, 2, 259 (1905).

(12) K. E. Spells, *Proc. Phys. Soc. (London)*, 48, 299 (1936).

(13) W. H. Hoather, *ibid.*, 48, 699 (1936).

(14) M. F. Culpin, *ibid.*, 20B, 1069 (1957).

Table II

Metal	$\eta_{\text{calcd.}}$, from Andrade's relationship at the melting point	M.p., °K.	—Constants of 1st Andrade equation—		Calcd. H_η , cal./g.-atom, from eq. 4	$\eta_{\text{exptl.}}$ at the m.p.	$\eta_{\text{exptl.}}$ at 1000°K.
			$a \times 10^3$	Exptl. H_η , cal./g.-atom			
Ga	1.63	303	4.359	955	954	2.04	0.71
In	1.96	429.3	3.020	1590	1525	1.94	0.67
Tl	2.86	577	2.983	2500	2270	2.65	1.05

The agreement between the experimental and the calculated H_η values for gallium and indium is very good. In line with increasing melting point in the sequence Ga \rightarrow In \rightarrow Tl, the slope of the viscosity increases so that at about 1000°K. indium's viscosity equals that of gallium and at temperatures above their normal boiling points thallium will be less viscous than indium. The behavior of these metals is illustrated in Figure 1; the three lines are based on the equations of Table II and the experimental values at the respective melting points and at 1000°K.

The viscosities at the melting point, as calculated from Andrade's well-known formula,⁴ are also shown as squares in Figure 1; the agreement, as can be seen, is good except for gallium, where the calculated value (1.63 cp.) is below the experimental one (2.04 cp.).

Discussion of Self-Diffusion Data

The experimental determination of self-diffusion of metals is much more difficult and less precise than that of viscosity; thus, the self-diffusion of only about eight metals has been measured^{15,16} as against about 30 for viscosity. Fortunately, the self-diffusion of gallium was measured by Nachtrieb¹⁷ and that of indium by Lodding¹⁸ and others.

It has been known for a long time that viscosity and self-diffusion are closely related by the Stokes-Einstein relationship equaling in its Eyring version, *i.e.*

$$\frac{\eta D}{T} = k/6\sigma \quad (6)$$

where k is the Boltzmann constant and σ the average distance between atoms or $(V_{\text{atom}}/N_{\text{Avog.}})^{1/3}$.

It was emphasized in a recent article¹⁹ that the self-diffusion properties of liquid metals follow directly from viscosity measurements, *provided* that both viscosity, η , in poises, and self-diffusion, D , in cm.²/sec., are expressed in a self-consistent manner, *i.e.*, that $\eta/T \times D$ equal the Stokes-Einstein relation. Applying one of the simplest theories of liquids, namely, Frenkel's kinetics theory,²⁰ it follows that

$$\eta = BT e^{-\gamma} e^{+E_{v.d.}/RT} \quad (7)$$

and

$$D = D_0 e^{\gamma} e^{-E_{v.d.}/RT} \quad (8)$$

where B , D_0 , and γ are constants, $E_{v.d.}$ is the activation energy for both viscosity and diffusion (cal./g.-atom), and R is the gas constant. It should be stressed

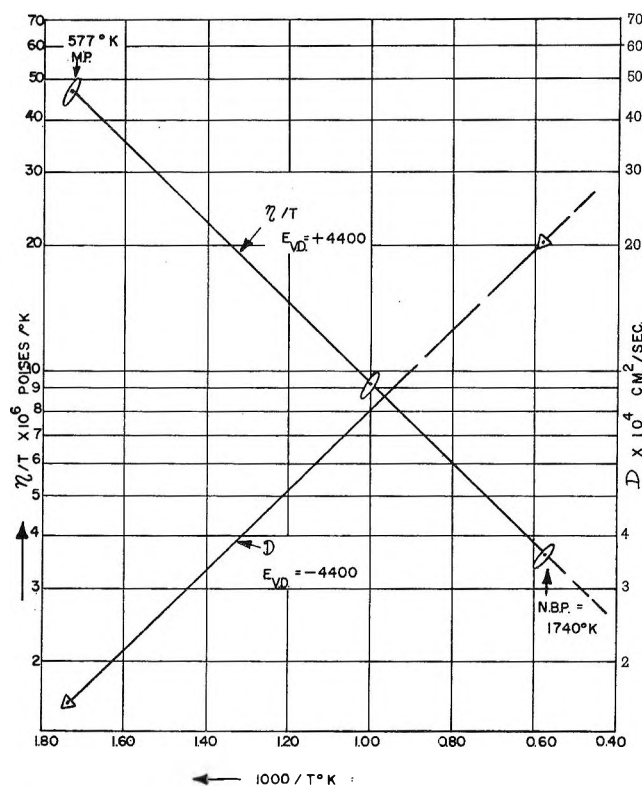


Figure 2. Viscosity (η/T) and self-diffusion of liquid thallium.

(15) H. J. Saxton and O. D. Sherby, *Trans. Am. Soc. Metals*, **55**, 826 (1962).

(16) H. J. Saxton and O. D. Sherby, Department of Materials Science Report No. 62-9, Oct. 19, 1962, Stanford University, Stanford, Calif.

(17) J. Petit and N. H. Nachtrieb, *J. Chem. Phys.*, **24**, 1027 (1956).

(18) A. Lodding, *Z. Naturforsch.*, **11a**, 200 (1956).

(19) A. V. Grosse, *Science*, **145**, 50 (1964).

(20) J. Frenkel, "Kinetic Theory of Liquids," Dover Publishing Co., Inc., New York, N. Y., 1955, pp. 31-36.

that $E_{v.d.}$ is different from Andrade's H_η . It follows further from Frenkel's theory that the constants B and D_0 can be calculated for any metal from the expressions

$$B = hN_{\text{Avog.}}/\theta_D V_{\text{atom}} \quad (9)$$

and

$$D_0 = (k/6HN_{\text{Avog.}}^{2/3})\theta_D V_{\text{atom}}^{2/3} \quad (10)$$

where h is Planck's constant and θ_D and V_{atom} are the Debye temperature in °K. and the liquid atomic volume of the metal (at the melting point), respectively. It was found²¹ that the two equations above correlate the experimental viscosity and diffusion data within experimental error for the eight metals for which self-diffusion data are available.^{15,16} Thus, there is every reason to expect that they will describe thallium as well. Therefore, let us convert the general equations to the specific case of thallium.

Since V_{atom} of thallium = 18.10 cm.³/g.-atom at its melting point while Debye's $\theta = 100^\circ$,²² it follows that the theoretical values for thallium are $B_{\text{theory}} = 2.205 \times 10^{-6}$ (poise) and $D_0 = 3.357 \times 10^{-4}$ (cm.²/sec.).

If we express our experimental results in terms of the Frenkel equation (7), we obtain the expression

$$\eta = 1.011 \times 10^{-6} T e^{+4400/RT} \quad (11)$$

We can adjust our experimental B value (1.011×10^{-6}) to B_{theory} above (2.205×10^{-6}) by means of the Frenkel factor, $e^{-\gamma}$; in our case, $e^{-\gamma} = 0.458$ or $\gamma = 0.78$. Thus eq. 11 now assumes the final form

$$\eta = 2.205 \times 10^{-6} e^{-0.78} T e^{+4400/RT} \quad (12)$$

This form lends itself readily to describe self-diffusion in terms of the general equation (8) by means of the calculated D_0 and the $E_{v.d.}$ together with the values of eq. 12, as

$$D = 3.357 \times 10^{-4} e^{+0.78} e^{-4400/RT} \quad (13)$$

Based on the above equation, the values for self-diffusion equal 0.16×10^{-4} at the melting point (577°K.), 0.80×10^{-4} at 1000°K., and 2.05×10^{-4} cm.²/sec at the normal boiling point.

On the semilog plot the straight lines for η/T and D vs. $1/T$ have the same slope of 4400 cal./g.-atom, but an opposite sign, as shown in Figure 2.

Acknowledgment. We gratefully acknowledge the financial support of the U. S. Atomic Energy Commission under Contract AT(30-1)2082.

(21) Reference 19 gives the data for sodium and zinc; a comparison of the other six metals, including gallium and indium, is in preparation.

(22) N. F. Mott and H. Jones, "The Theory of the Properties of Metals and Alloys," Dover Publishing Co., Inc., New York, N. Y., 1958, p. 14.

Chemical Reactions in Chromatographic Columns

by John M. Matsen, John W. Harding, and Ellington M. Magee

Contribution from the Central Basic Research Laboratory, Esso Research and Engineering Company, Linden, New Jersey (Received August 29, 1964)

Chemical reactions of the sort $A \rightleftharpoons B + C$ may be run by injecting pulses of A into a chromatographic column which catalyzes the reaction. Under such conditions, the products B and C will be separated from each other and the reaction should proceed to completion despite an unfavorable equilibrium constant. Experimental verification of such behavior was obtained from the dehydrogenation of cyclohexane to benzene in a column packed with a platinum-on-alumina catalyst. Under the most favorable conditions about 30% greater conversion was obtained in the chromatographic reactor than would result from allowing the same quantities of cyclohexane and carrier gas to reach a static equilibrium. An equilibrium reactor would need about four times as much diluent or carrier gas as the chromatographic one to reach the same degree of conversion.

Introduction

The techniques of gas chromatography have proved to be valuable tools in the field of catalysis. The most obvious and widespread applications have been analytical. The microreactor technique developed by Kokes, *et al.*,¹ is an analytical refinement which minimizes the problems of handling minute samples and detecting low conversions. Preparative chromatography has been invaluable in the purification of reactants. Less conventional has been the application of chromatography to the measurement of adsorption isotherms and heats of adsorption for cases where adsorption-desorption rates are fast.

A fourth field, in which chromatography and catalysis are much more closely intertwined, has recently been subjected to study. This is the case where a catalytic reaction occurs in a pulse of reactant traveling through a chromatographic column. Bassett and Habgood² studied the irreversible isomerization of cyclopropane to propylene in a chromatographic column and were able to obtain rate constants for the reaction. Klinkenberg³ made a theoretical study of the reversible reaction $A \rightleftharpoons B$ occurring on a chromatographic column and calculated the shape and retention time of the eluted peak. Keller and Giddings⁴ have analyzed similar cases in which the reaction rate is slow.

More interesting from an application viewpoint is the reversible reaction $A \rightleftharpoons B + C$ with a very low equi-

librium constant. In a chromatographic column the products B and C will be separated from each other so that they cannot re-react, and the reaction may proceed to completion despite the low equilibrium constant. This is a potentially attractive mode of operation for such equilibrium-limited reactions. The possibility has been recognized in patents by Dinwiddie⁵ and Magee,⁶ and Magee⁷ subsequently presented a mathematical analysis of such a reactor.

Roginskii, *et al.*,⁸ proposed chromatographic reaction independently. The same school studied the dehydrogenation of cyclohexane pulses under irreversible⁹ and reversible¹⁰ conditions. A mathematical treatment was presented in ref. 10 for simple irreversible reactions. Their experimental data were analyzed according to

(1) R. J. Kokes, H. Tobin, and P. H. Emmett, *J. Am. Chem. Soc.*, **77**, 5860 (1955).

(2) D. W. Bassett and H. W. Habgood, *J. Phys. Chem.*, **64**, 769 (1960).

(3) A. Klinkenberg, *Chem. Eng. Sci.*, **15**, 255 (1961).

(4) R. A. Keller and J. C. Giddings, *J. Chromatog.*, **3**, 205 (1960).

(5) J. A. Dinwiddie, U. S. Patent 2,976,132 (1961).

(6) E. M. Magee, Canadian Patent 631,882 (1961).

(7) E. M. Magee, *Ind. Eng. Chem. Fundamentals*, **2**, 32 (1963).

(8) S. Z. Roginskii, M. I. Yanovskii, and G. A. Gaziev, *Dokl. Akad. Nauk SSSR*, **140**, 1125 (1961).

(9) G. A. Gaziev, O. V. Krylov, S. Z. Roginskii, G. V. Samsonov, E. S. Fokina, and M. I. Yanovskii, *ibid.*, **140**, 863 (1961).

(10) S. Z. Roginskii, M. I. Yanovskii, and G. A. Gaziev, *Kinetika i Kataliz*, **3**, 529 (1962).

this treatment, but examination of their results indicates that the model was inapplicable to that experiment. This same treatment was extended to more complex cases¹¹ and seems far more pertinent to kinetic measurements than to chromatographic reactions.

Recently,¹² the mathematical model of Magee⁷ was related qualitatively to experimental data from this laboratory, although conditions of stoichiometry and elution velocity would not allow quantitative comparison. Thus the complex theoretical problem of the chromatographic reactor has not yet been solved completely.

It is felt that chromatographic reaction can be advantageous only under a well-defined and limited set of conditions.

1. The equilibrium constant for the reaction must be small.

2. Reaction rates should be high enough so that separation of products rather than rate of reaction limits the extent of reaction.

3. At least two products must be formed which are chromatographically separated in the reactor.

4. Reactants must not be separated in the reactor. For all practical purposes this limits one to a single reactant, or to two reactants where one also serves as the carrier gas.

Equilibrium Comparison

Chromatographic operation of a reaction is rather complicated, and the question naturally arises as to whether this method in practice has any advantages over a conventional equilibrium reactor. The problem lies in picking a meaningful basis of comparison, since in the present case the presence of carrier gas affects conversion not only by separating the products but also by diluting the reaction mixture.

Comparison was finally made on the following basis. The chromatographic reactor was repetitively pulsed with reactant at evenly spaced intervals. Effluent product was collected over an integral number of cycles and analyzed in order to obtain the experimental conversion. The corresponding "equilibrium" conversion was that which would result from allowing the amounts of reactant and carrier gas associated with a single pulse cycle to reach equilibrium in a static system. The ratio of carrier gas to cyclohexane was calculated in the present case from the equation

$$N = 4.43 \frac{Ft}{S}$$

where N = moles of carrier gas/mole of cyclohexane, F = carrier gas flow rate in cc./min. at 25° and 1 atm. pressure, t = time between pulses in min., and S =

cyclohexane sample size in μ l. at 25°. Total pressure was taken as 1 atm. despite the fact that it was higher than this except at the reactor outlet. This is a rather stringent basis of comparison but it seems to be the only one justified in the present case. For given average flow rates of reactant and carrier gas this will tell whether chromatographic operation gives an advantage in conversion over conventional equilibrium operation.

The problem of dilution does not exist for reactions in which the number of moles of reactants and products are equal. Any increase in conversion above equilibrium (which is here independent of dilution) would be due to chromatographic separation. One such reaction, $2\text{HD} \rightleftharpoons \text{H}_2 + \text{D}_2$, was examined in the present work on a reactor packed with palladium-coated asbestos. No quantitative data were obtained, but it appeared that the reaction was proceeding and that separation of the various reaction components did take place. Some earlier workers¹³ examined the chromatography of hydrogen-deuterium mixtures on palladium. It is interesting to note that some of their anomalous results may be explained in light of the present work by realizing that chemical reaction probably occurred on their column.

Experimental

The main reaction studied in the present work was the dehydrogenation of cyclohexane to benzene and hydrogen.



Fisher reagent grade cyclohexane was used without further purification. The catalyst, commercially available, consisted of 0.6% platinum on an alumina support, and the alumina served as the chromatographic adsorbent. It was ground to 40–60 mesh and activated by heating in a hydrogen atmosphere. Reactors consisted of lengths of 0.63-cm. stainless steel tubing packed with catalyst. Reactors were installed in place of the usual analytical column in an F and M Model 500 gas chromatograph, which was used without other modification.

Helium was used as the carrier gas. Cyclohexane was injected through a rubber septum at the column inlet. The thermal conductivity of the effluent gas was recorded potentiometrically. This trace will hereafter be called the product chromatogram, al-

(11) G. A. Gaziev, V. Ya. Filinovskii, and M. I. Yarovskii, *Kinetika i Kataliz*, **4**, 688 (1963).

(12) J. M. Matsen, J. W. Harding, and E. M. Magee, A.I.Ch.E. 56th Annual Meeting, Houston, Texas, Dec. 1953, Paper 19d.

(13) C. O. Thomas and H. A. Smith, *J. Phys. Chem.*, **63**, 427 (1959).

though it is not a chromatogram in the conventional sense of the word. Product samples were trapped from the effluent stream at -78° and were analyzed on a 2-m. Perkin-Elmer "R" column.

Results

During the first few pulses of cyclohexane over a fresh catalyst, the product chromatogram changed

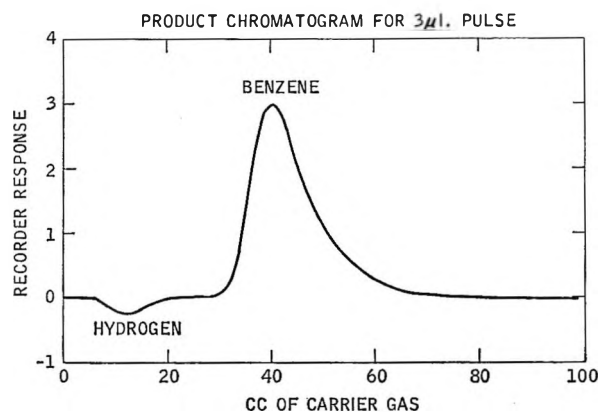


Figure 1. Product chromatogram for 3- μ l. pulse.

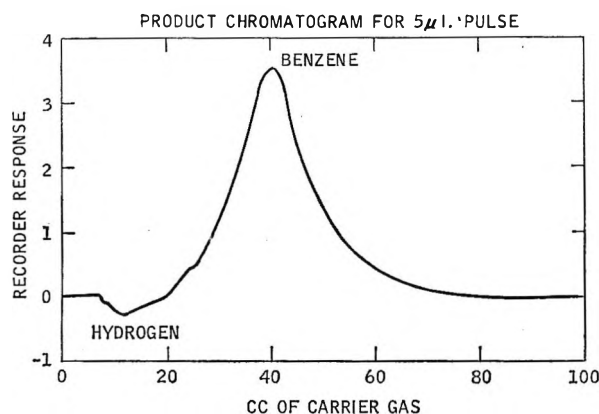


Figure 2. Product chromatogram for 5- μ l. pulse.

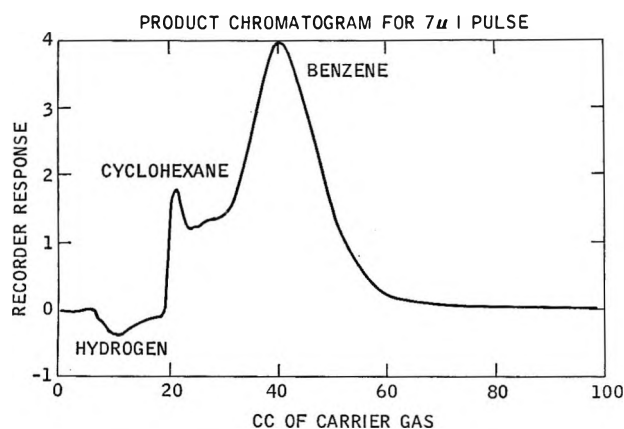


Figure 3. Product chromatogram for 7- μ l. pulse.

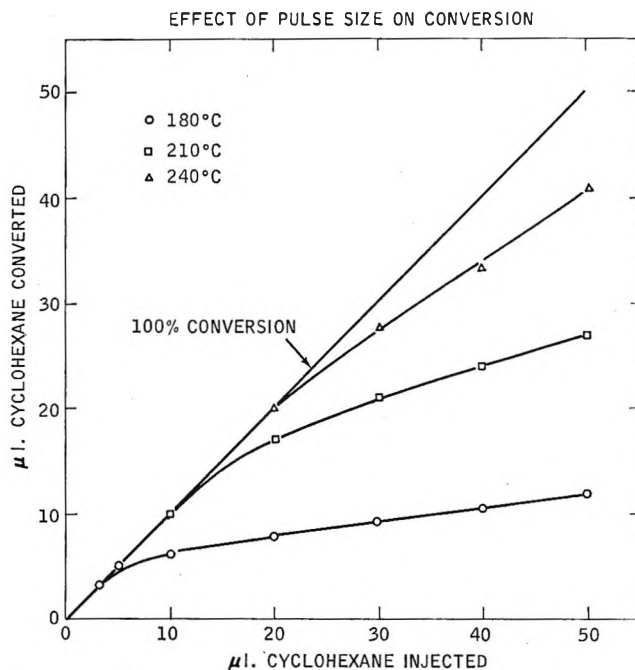


Figure 4. Effect of pulse size on conversion.

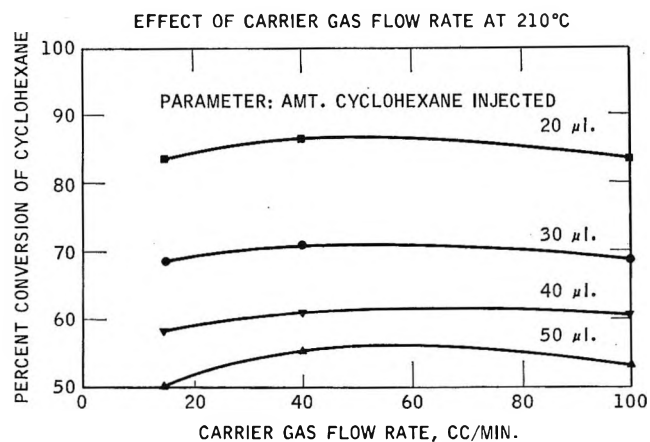


Figure 5. Effect of carrier gas flow rate at 210 $^{\circ}$.

considerably. This corresponded to coking of part of the catalyst surface. Any analysis of products during this period would be almost meaningless without knowledge of the coking process. After perhaps five or ten pulses, the reactor reached a steady state and there was little further change in pulse chromatograms. Material balances showed that 96 to 98% of the reactant left the reactor once a "steady state" had been reached. In all cases only benzene and hydrogen appeared as products, and no cyclohexane or cyclohexadiene was detected.

Effect of Pulse Size. Typical product chromatograms of single cyclohexane pulses are shown in Figures 1, 2, and 3. These are for a reactor 50 cm. long packed

with 8 g. of catalyst operated at 180° with 10 cc./min. carrier gas flow. With a small sample (Figure 1) the hydrogen and benzene peaks are well separated and fairly sharp. As sample size is increased, these peaks tend to tail off toward each other (Figure 2). Such tailing is inherent in this mode of operation and is due to the fact that the products are produced in decreasing amounts as cyclohexane is consumed along the column. When large samples are introduced, a sharp peak of unreacted cyclohexane appears between hydrogen and benzene (Figure 3). This peak increases in height very rapidly as pulse size is increased.

The quantitative effect of pulse size is shown in Figure 4. At a given temperature a certain amount of cyclohexane can be almost entirely converted, but additional amounts are converted to a lesser, though essentially constant, extent.

Effect of Flow Rate. Figure 5 shows the slight effect of carrier gas flow rate on conversion. This independence of conversion on residence time indicates that adsorption, reaction, and desorption were fast under the conditions studied and that the extent of reaction was equilibrium limited. Since conversion was virtually independent of residence time, the Roginskii model¹⁰ (which assumes that products are separated instantaneously and that forward reaction rate limits conversion) would be clearly incorrect in the present case.

The very slight effects of flow rates are explained as follows: at high flow rates conversion begins to drop off a bit because of kinetic effects. At low flow rates slightly less carrier gas is used in eluting the products, and this means less dilution of the reacting mixture by carrier gas and hence lower conversion due to equilibrium limitations.

Effect of Reactor Length. Examples cited thus far have been for reactors 50 cm. long packed with 8 g. of catalyst. When columns of different length were tried, it was found that the significant variable was the ratio of pulse size to column length (and hence weight of catalyst). Thus, the same conversions would result from pulsing 10 μ l. of cyclohexane into a 50-cm. column and 20 μ l. into a 100-cm. column. This effect is not expected on the basis of behavior in tubular flow reactors or in ordinary chromatographic columns. Its explanation awaits the solution of a realistic mathematical model of the reactor.

Repetitive-Pulse Experiments. Thus far only results of single-pulse experiments have been described. When repetitive pulsing is used, the additional variable of pulse frequency enters the picture. At very low frequencies, conversions are the same as for single pulses. For a given pulse size this represents the maximum conversion. This is wasteful of time and

carrier gas, however, and equal or greater conversions could be obtained in an equilibrium system diluted with that amount of carrier gas. Conversion drops off only slightly as frequency is increased, until pulsing is so rapid that the hydrogen peak from a fresh pulse comes soon enough to pass through part of the benzene peak from the previous pulse. When this happens the hydrogen and benzene recombine, and a new cyclohexane peak appears in the product chromatogram where the hydrogen peak had previously been. From this point on conversion decreases steadily as frequency increases.

Column Treatment. In the case of ideal chromatography, adsorption isotherms are linear, and peaks are sharp and show little tendency to tail off slowly. The isotherm for benzene adsorbed on fresh alumina is very nonlinear, however, causing the benzene peak to tail off slowly. Under such conditions the reactor could be pulsed only infrequently, and conversions were no better than for a continuous reactor operating at the same average dilution of cyclohexane by carrier gas. Data reported to this point are for such a case. Several adsorbents besides alumina were tried without success in an attempt to overcome this. Finally, an alumina was used which had been treated with a solution of 10% KOH in methanol. The treatment neutralized the very strongly acidic sites which give rise to the nonlinear isotherm. This reduced retention volume and adsorbent capacity and lessened the benzene tailing, as is shown in Figure 6.

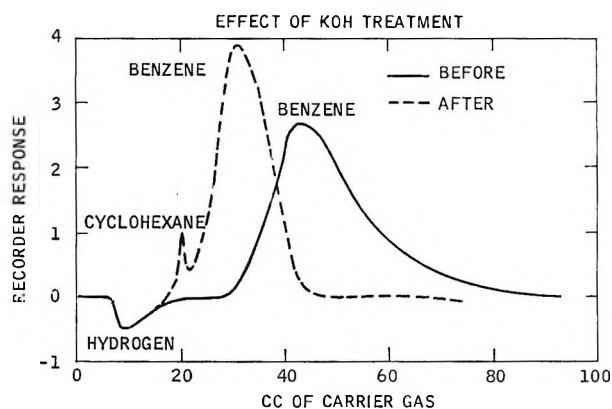


Figure 6. Effect of KOH treatment on chromatogram.

The treated alumina gave slightly less reproducible results than did the untreated alumina. Small but noticeable differences between successive product chromatograms were noted, although these changes showed no apparent trend after the first few pulses on a freshly activated column. On a long-term basis,

dependent more on time than on amount of cyclohexane injected, the treated alumina showed a greater tendency to become deactivated. The platinum-on-alumina catalyst used in the remainder of the work reported here was treated in this manner.

Comparison to Equilibrium. Quantitative results at three temperatures are shown in Figures 7, 8, and 9. Equilibrium constants were obtained from the data of Rossini.¹⁴ The "theoretical" equilibrium curve depends only on temperature and the extent of dilution of reactant by carrier gas. Additional parameters would be necessary for accurate representation of precise experimental data, and the experimental points therefore do not fall on a single curve. From Figure 9 it is seen that carrier gas flow rate has a noticeable effect when conversions are plotted in this manner. The amount of carrier gas needed to elute a peak at a high flow rate is somewhat greater, partly because adsorption-desorption rates are finite, and partly because gas at the column inlet is at higher pressure so that more moles are needed for a given amount of elution. This

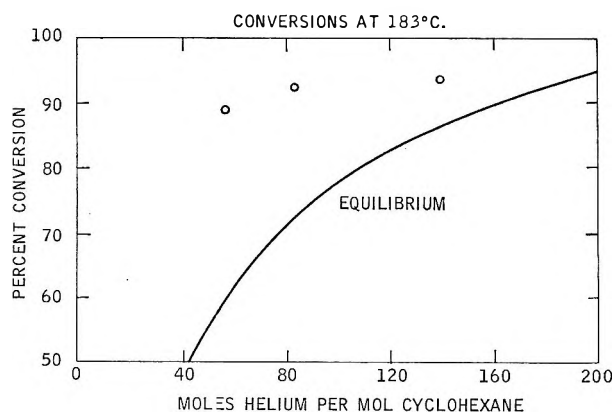


Figure 7. Repetitive-pulse conversions at 183°; equilibrium constant = 4.0×10^{-5} .

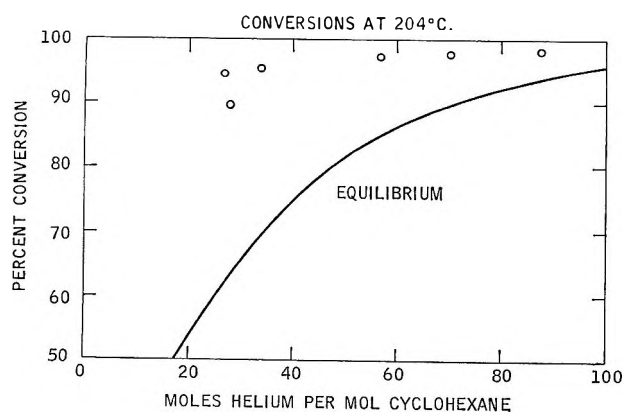


Figure 8. Repetitive-pulse conversions at 204°; equilibrium constant = 4.2×10^{-4} .

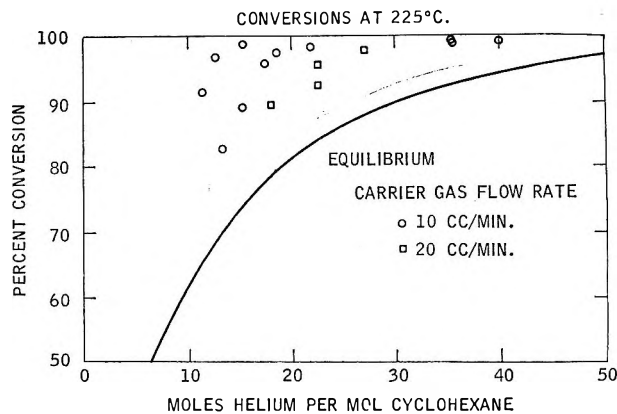


Figure 9. Repetitive-pulse conversions at 225°; equilibrium constant = 4.8×10^{-3} .

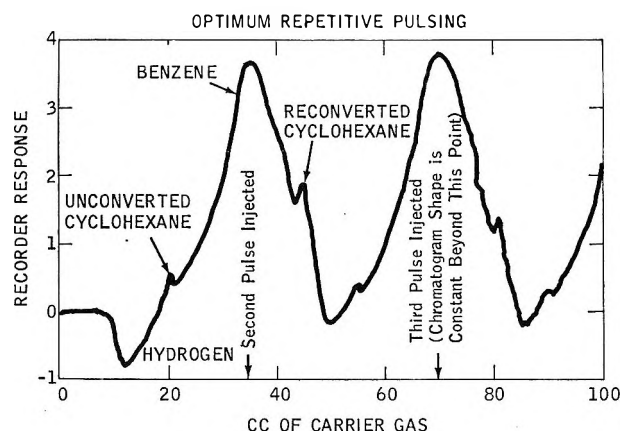


Figure 10. Optimum repetitive pulsing: temperature 225°; carrier gas flow rate 10 cc./min.; pulse size 12 μ l.; time between pulses 3.5 min.; 8 g. of catalyst in 50 cm. long reactor; conversion 96.4%

effect of flow rate is not seen in single-pulse experiments because correlation in that case is not made as a function of amount of carrier gas used.

Optimum Operation. The greatest improvement of experimental conversion above theoretical is about 30%. Three or four times as much carrier gas would be needed as diluent in a static system to attain the same conversion as in an optimum-pulsed case. The optimum mode of operation was to use a sample pulse as large as possible without allowing a peak of unconverted cyclohexane to appear and to pulse as frequently as possible while still keeping a peak of reconverted cyclohexane from appearing in the product chromatogram. This optimum mode of operation is shown in Figure 10.

(14) F. D. Rossini, "Selected Values of Physical and Thermodynamic Properties of Hydrocarbons and Related Compounds," Carnegie Press, Pittsburgh, Pa., 1953.

Discussion

It has been demonstrated that reactions can be conducted in chromatographic columns so that products can be separated during the course of reaction. Higher conversions can result from this type of operation than in a conventional equilibrium reactor. The improvement above equilibrium is modest as yet but certainly can be improved. Ultimate performance cannot be estimated until a solution is obtained for a realistic mathematical model.

In some cases, the fact that products are separated in the reaction step may prove to be a desirable feature quite apart from conversion considerations, since a separate separation step is unnecessary.

Any factors which would tend to cause peak spreading in ordinary chromatography will adversely affect the conversions in a chromatographic reactor. Some such factors are increase in packing size, increase in column diameter, and increase in carrier gas flow rate. These are potential trouble spots in scaling up a laboratory reactor to a large-scale process.

Nuclear Magnetic Resonance Studies of Boron Trifluoride Addition Compounds.

III. Rates and Mechanism for the Exchange of Boron Trifluoride

between Ethyl Ether-Boron Trifluoride and Tetrahydrofuran-Boron Trifluoride and between Ethyl Ether-Boron Trifluoride and Ethyl Sulfide-Boron Trifluoride¹

by A. C. Rutenberg and A. A. Palko

Chemistry Division, Oak Ridge National Laboratory, Oak Ridge, Tennessee 37831 (Received August 29, 1964)

Kinetic data for the exchange of BF_3 between $(\text{C}_2\text{H}_5)_2\text{O}\cdot\text{BF}_3$ and $\text{THF}\cdot\text{BF}_3$ and between $(\text{C}_2\text{H}_5)_2\text{O}\cdot\text{BF}_3$ and $(\text{C}_2\text{H}_5)_2\text{S}\cdot\text{BF}_3$ were obtained from ^{19}F n.m.r. spectra of mixtures of $(\text{C}_2\text{H}_5)_2\text{O}$, BF_3 , and THF or $(\text{C}_2\text{H}_5)_2\text{S}$. Both pairs of addition compounds followed the rate law, $R = k_1[\text{L}'\cdot\text{BF}_3][\text{L}\cdot\text{BF}_3] + k_2[\text{L}'\cdot\text{BF}_3][\text{L}] + k_3[\text{L}]/[\text{L}\cdot\text{BF}_3]$, in which R is the rate of BF_3 exchange between two BF_3 addition compounds, molecule L' forming the stronger BF_3 addition compound. Rate constants and activation energies were calculated and compared to previously measured systems.

Boron trifluoride forms stable 1:1 molecular addition compounds with many ethers and thioethers. In systems containing BF_3 and more than one ether or thioether, the BF_3 exchange between the different species is usually very rapid. The strong ^{19}F resonance and the large chemical shifts between the different BF_3 addition compounds permit study of these rapid exchanges by the n.m.r. technique. The exchanges of

$(\text{C}_2\text{H}_5)_2\text{O}\cdot\text{BF}_3$ with $(\text{CH}_3)_2\text{O}\cdot\text{BF}_3$ and $\text{C}_6\text{H}_5\text{OCH}_3\cdot\text{BF}_3$ were reported in earlier papers.^{2,3} It was of interest to

(1) Research sponsored by the U. S. Atomic Energy Commission under contract with the Union Carbide Corp.

(2) A. C. Rutenberg, A. A. Palko, and J. S. Drury, *J. Am. Chem. Soc.*, **85**, 2702 (1963).

(3) A. C. Rutenberg, A. A. Palko, and J. S. Drury, *J. Phys. Chem.*, **68**, 976 (1964).

study the exchange reactions of $(C_2H_5)_2O \cdot BF_3$ with both an addition compound significantly stronger than $(C_2H_5)_2O \cdot BF_3$ and with a compound weaker than $C_6H_5OCH_3 \cdot BF_3$. These requirements and the additional restriction that the rates of exchange occur in a range suitable for n.m.r. measurements were met by the $THF \cdot BF_3$ and $(C_2H_5)_2S \cdot BF_3$ addition compounds.

Experimental

The ten mixtures of $THF-(C_2H_5)_2O$ and BF_3 and five mixtures of $(C_2H_5)_2S-(C_2H_5)_2O$ and BF_3 used in this study were prepared from purified chemicals using high vacuum techniques. The n.m.r. measurements of the ^{19}F resonance were obtained using a Varian Associates high resolution spectrometer operating at 56.445 Mc. The experimental techniques were described in a previous paper.² The mean lifetime (τ) of an organic-boron trifluoride species was studied as a function of temperature and composition.

Results

The simple spectra obtained consisted at low temperatures of a pair of peaks, which, as the temperature was raised, broadened, merged, and coalesced to a single peak which narrowed with further increase in temperature. The τ -values were calculated⁴ from n.m.r. measurements of line widths and peak separations over as large a temperature range as the sample would permit. Only line width data from the portion of the temperature range for which the relaxation contribution to the line width was negligible were used. The values for the separation between the two peaks in the absence of exchange, used in the calculation of τ at the higher temperatures, were obtained from extrapolation of low-temperature measurements. The rate of exchange (R) of a BF_3 addition compound of concentration $[A]$ with another of concentration $[B]$ can be obtained from the concentration of either addition compound and its mean lifetime. $R = [A]/\tau_A$ or $[B]/\tau_B$.

Compositions, mean lifetimes (τ), rates of exchange (R), and activation energies ($\Delta E'$) of organic-boron trifluoride species are presented in Tables I and II. Table I contains data on ten mixtures of THF , $(C_2H_5)_2O$, and BF_3 , and Table II contains analogous data for five mixtures of $(C_2H_5)_2S$, $(C_2H_5)_2O$, and BF_3 . The mean lifetimes were plotted as a function of reciprocal temperature for the mixtures described in Tables I and II. The resulting least-squares straight lines are shown in Figures 1 and 2. $\Delta E'$ represents an average activation energy for the various paths contributing to the exchange. $\Delta E' = 2.303R \times$ (line slope, Figure 1 or 2).

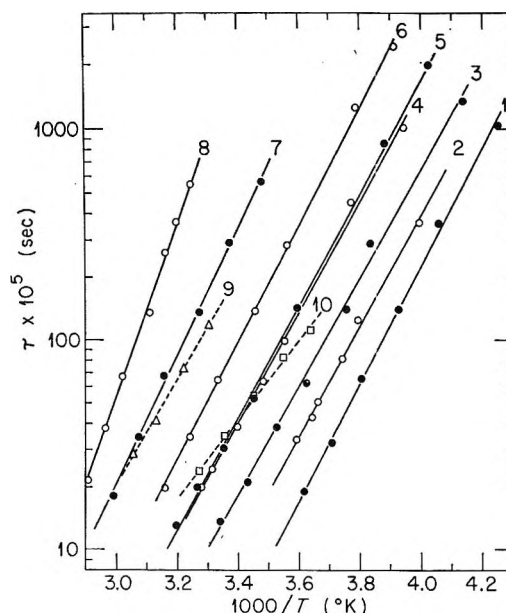


Figure 1. Temperature dependence of τ for ten mixtures of THF , $(C_2H_5)_2O$, and BF_3 . Compositions of mixtures are given in Table I.

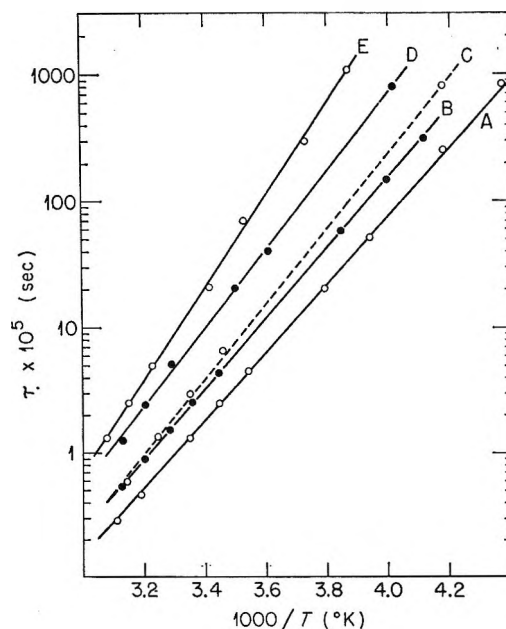


Figure 2. Temperature dependence of τ for five mixtures of $(C_2H_5)_2S$, $(C_2H_5)_2O$, and BF_3 . Compositions of mixtures are given in Table II.

For convenience in referring to the different types of mixtures composed of $(C_2H_5)_2O$, BF_3 , and a third ether or thioether, the mixture will bear the name of the

(4) J. A. Pople, W. G. Schneider, and H. J. Bernstein, "High-Resolution Nuclear Magnetic Resonance," McGraw-Hill Book Co., Inc., New York, N. Y., 1959, Chapter 10.

Table I: Characteristics of Ten $C_4H_8O-(C_2H_5)_2O-BF_3$ Mixtures at 25°

	$C_4H_8O \cdot BF_3$, moles/l.	$(C_2H_5)_2O \cdot BF_3$, moles/l.	$(C_2H_5)_2O$, moles/l.	$\tau \times 10^5$, sec.	$R \times 10^{-4}$, moles l. ⁻¹ sec. ⁻¹	$\Delta E'$, kcal. mole ⁻¹	95% confidence limit on $\Delta E'$
1	0.75	0.75	8.15	3.48	10.7	12.8	0.8
2	1.91	1.01	6.71	7.88	8.36	12.0	1.2
3	1.39	1.78	6.25	13.8	5.62	11.8	0.9
4	1.51	3.06	4.50	30.7	3.30	12.1	0.8
5	2.32	2.42	4.51	31.8	3.72	12.3	0.5
6	3.28	3.27	2.43	72.1	2.27	12.9	0.5
7	3.95	3.95	0.81	246	0.802	14.0	0.9
8	4.32	4.13	0.19	1590	0.133	19.2	1.1
9	4.26	4.26	0.00 ^a	157	1.36	11.5	1.0
10	4.22	4.21	0.00 ^b	34.1	6.18	8.6	0.7

^a Sample contains trace of uncomplexed BF_3 . ^b Sample contains $\sim 0.2 M$ uncomplexed BF_3 .

Table II: Characteristics of Five $(C_2H_5)_2S-(C_2H_5)_2O-BF_3$ Mixtures at 25°

	$(C_2H_5)_2S \cdot BF_3$, moles/l.	$(C_2H_5)_2O \cdot BF_3$, moles/l.	$(C_2H_5)_2S$, moles/l.	$\tau \times 10^5$, sec.	$R \times 10^{-4}$, moles l. ⁻¹ sec. ⁻¹	$\Delta E'$, kcal. mole ⁻¹	95% confidence limit on $\Delta E'$
A	1.36	1.41	5.98	1.34	51.7	12.5	0.6
B	2.31	1.18	5.15	2.38	33.5	12.8	0.2
C	1.85	2.90	3.73	2.80	40.4	13.8	0.6
D	3.18	3.18	1.53	7.01	22.7	14.2	0.7
E	3.74	3.74	0.13	13.8	13.55	16.7	0.7

third component. The expression, anisole system, will, thus, refer to mixtures of anisole, $(C_2H_5)_2O$, and BF_3 .

The study of the THF system included kinetic measurements on two mixtures (9 and 10) which contained small quantities of BF_3 in excess of the amount required to complex all the THF and $(C_2H_5)_2O$. The presence of uncomplexed BF_3 produced an increase in rate accompanied by a decrease in activation energy. The free BF_3 provided a low activation energy route for the exchange between the two complexes. The exchange between BF_3 and $THF \cdot BF_3$ in toluene solution was studied by Brownstein,⁵ *et al.*, who measured an activation energy of 4.6 kcal. mole⁻¹. No detailed study of free BF_3 dependence was attempted in the present work since the small free BF_3 concentrations were not known accurately, and larger BF_3 concentrations would result in high pressures in the glass sample tubes. All further discussion of the THF system will be limited to mixtures 1-8 which contained no free BF_3 .

If the kinetic data for the THF and $(C_2H_5)_2S$ systems are compared to similar data for the anisole system,³ some qualitative differences are apparent. The rates of exchange in the present study continue to increase as the concentrations of the BF_3 addition compounds

decrease, while in the anisole system the exchange rate goes through a maximum and then decreases as the addition compound concentrations are further reduced.

The addition of a third term to an expression analogous to that used for the anisole system rate law gave

Table III: Rate Constants^a for BF_3 Exchange between $(C_2H_5)_2O \cdot BF_3$ and $THF \cdot BF_3$ and between $(C_2H_5)_2O \cdot BF_3$ and $(C_2H_5)_2S \cdot BF_3$

	k_1 , l. mole ⁻¹ sec. ⁻¹	k_2 , l. mole ⁻¹ sec. ⁻¹	k_3 , moles l. ⁻¹ sec. ⁻¹
THF system			
25°	<7	236 ± 140	882 ± 104
0°	<0.4	41 ± 33	117 ± 25
ΔE , kcal. mole ⁻¹	~19	11.4	13.0
$(C_2H_5)_2S$ system			
25°	878 ± 13	2058 ± 70	7580 ± 1250
0°	60 ± 5	268 ± 29	1085 ± 530
ΔE , kcal. mole ⁻¹	17.4	13.2	12.6

^a Confidence limits all at 95% level.

(5) S. Brownstein, A. M. Eastham, and G. A. Latremouille, *J. Phys. Chem.*, **67**, 1028 (1963).

Table IV: Reactions of $(C_2H_5)_2O \cdot BF_3$

Reaction	k at 25°, l. mole ⁻¹ sec. ⁻¹	ΔE , kcal. mole ⁻¹
$(C_2H_5)_2O \cdot BF_3 + (C_2H_5)_2S \cdot BF_3 \longrightarrow (C_2H_5)_2O \cdot BF_3 + (C_2H_5)_2S \cdot BF_3$	878	17.4
$(C_2H_5)_2O \cdot BF_3 + C_6H_5OCH_3 \cdot BF_3 \longrightarrow (C_2H_5)_2O \cdot BF_3 + C_6H_5OCH_3 \cdot BF_3$	353	16.3
$(C_2H_5)_2O \cdot BF_3 + (CH_3)_2O \cdot BF_3 \longrightarrow (C_2H_5)_2O \cdot BF_3 + (CH_3)_2O \cdot BF_3$	~200 ^a	~16.1 ^a
$(C_2H_5)_2O \cdot BF_3 + THF \cdot BF_3 \longrightarrow (C_2H_5)_2O \cdot BF_3 + THF \cdot BF_3$	<7 ^a	~19.2 ^a
$(C_2H_5)_2O \cdot BF_3 + C_6H_5OCH_3 \longrightarrow (C_2H_5)_2O + C_6H_5OCH_3 \cdot BF_3$	798	10.6
$(C_2H_5)_2O \cdot BF_3 + (C_2H_5)_2S \longrightarrow (C_2H_5)_2O + (C_2H_5)_2S \cdot BF_3$	2058	13.2
$(C_2H_5)_2O \cdot BF_3 + THF \longrightarrow (C_2H_5)_2O + THF \cdot BF_3$	>10 ^{6b}	

^a Based on measurements of a single mixture. ^b Estimated from measured rate of reverse reaction and lower limit for K_{eq} .

eq. 1, which is consistent with the data of Tables I and II.

$$R = k_1[L' \cdot BF_3][L \cdot BF_3] + k_2[L' \cdot BF_3][L] + k_3[L]/[L \cdot BF_3] \quad (1)$$

Molecule L' forms a stronger BF_3 addition compound than L .

The difference in rate law between the anisole system and the THF and $(C_2H_5)_2S$ systems merits some discussion. There was no *a priori* reason to expect the systems to behave differently. We shall attempt to explain the experimental data, assuming the same mechanisms occur in all three systems. The first term of eq. 1 represents the exchange of BF_3 between two different addition compounds, and the remainder of the equation, $[L](k_2[L' \cdot BF_3] + k_3/[L \cdot BF_3])$, is associated with the transfer of BF_3 from the more stable $L' \cdot BF_3$ to a free L to give $L \cdot BF_3$. The $k_3/[L \cdot BF_3]$ term is interpreted to result from competition with the BF_3 transfer from one L molecule to another. If an $L' \cdot BF_3$ compound is near a free L molecule and a BF_3 is transferred to that L molecule from a nearby $L \cdot BF_3$, the $L' \cdot BF_3$ compound is prevented from transferring its BF_3 . In the anisole, $(C_2H_5)_2S$, and THF systems, L is anisole, $(C_2H_5)_2S$, and $(C_2H_5)_2O$, respectively. If the BF_3 transfer between the anisole addition compound and anisole is much slower than the corresponding transfers involving $(C_2H_5)_2S$ or $(C_2H_5)_2O$, which might be expected from steric considerations, the anisole system could have a k_3 term in its rate law too small to contribute measurably to the exchange rate. In the ¹⁹F n.m.r. studies, only the exchange of BF_3 between different environments is observable. The previous hypothesis could in principle be tested by proton n.m.r. spectroscopy, but the more complex spectra combined with smaller chemical shifts would limit the usefulness of this approach.

Table III gives rate constants and activation

energies calculated using eq. 1. The three rate constants for the $(C_2H_5)_2S$ system were calculated from the rates of exchange and concentrations of the five mixtures using the least-squares method. In the THF system k_1 was small, and an upper limit for k_1 was estimated from the data on mixture 8, which contained little free $(C_2H_5)_2O$. The k_2 and k_3 values were calculated from a least-squares treatment of the data on mixtures 1-6, neglecting the k_1 contribution.

The reactions of $(C_2H_5)_2O \cdot BF_3$, for which rate constants were measured, are summarized in Table IV. The data are based on the previously discussed rate laws. Although the rate laws presented fit the data better than other simple expressions tested, their validity has not been otherwise proven. The data of Table IV indicate the more stable the BF_3 addition compound reacting with $C_2H_5O \cdot BF_3$, the slower the BF_3 exchange. The activation energies for the exchange of BF_3 between pairs of addition compounds (Table IV, reactions 1-4) were larger than the heats of dissociation of the addition compounds involved. The reported heats of dissociation of the BF_3 addition compounds of THF,⁶ $(CH_3)_2O$,⁷ $(C_2H_5)_2O$,⁷ $C_6H_5OCH_3$,⁸ and $(C_2H_5)_2S$ ⁹ are 16.80, 13.65, 11.93, 12.3, and ~9.6 kcal. mole⁻¹, respectively. Comparing the reactions of $C_6H_5OCH_3$ and $(C_2H_5)_2S$ with $(C_2H_5)_2O \cdot BF_3$, the anisole reaction has an activation energy less than the heat of dissociation of $(C_2H_5)_2O \cdot BF_3$ while the opposite is true of the $(C_2H_5)_2S$ reaction. The anisole reaction could, therefore, proceed only by a displacement mechanism while the reaction of $(C_2H_5)_2S$ with $(C_2H_5)_2O \cdot BF_3$ could involve a dissociation step.

(6) D. E. McLaughlin, M. Tamres, and S. Searles, Jr., *J. Am. Chem. Soc.*, **82**, 5621 (1960).

(7) D. E. McLaughlin and M. Tamres, *ibid.*, **82**, 5618 (1960).

(8) A. A. Palko, R. M. Healy, and L. Landau, *J. Chem. Phys.*, **28**, 214 (1958).

(9) A. A. Palko and J. S. Drury, *ibid.*, **40**, 278 (1964).

Table V gives ^{19}F chemical shifts relative to $(\text{C}_2\text{H}_5)_2\text{O}\cdot\text{BF}_3 \equiv 0$ for the addition compounds studied. The numbers are average values measured at -30 to -50° . Although the chemical shifts vary with composition and temperature, even if the extreme values were used, the order of the compounds would not be changed. With the exception of $\text{THF}\cdot\text{BF}_3$ in which the cyclic nature of the compound reduces the shielding, the order follows the strength of the addition compounds.

The n.m.r. kinetic studies of mixtures of $(\text{C}_2\text{H}_5)_2\text{O}$, BF_3 , and three ethers and $(\text{C}_2\text{H}_5)_2\text{S}$ in which the organic-boron trifluoride ratios are greater than 1 are in accord with a two-path BF_3 exchange mechanism. The direct exchange between two addition compounds is a

Table V: ^{19}F Chemical Shifts^a of BF_3 Addition Compounds

Compound	Chemical shift, p.p.m.
$(\text{CH}_3)_2\text{O}\cdot\text{BF}_3$	+5.3
$\text{THF}\cdot\text{BF}_3$	+2.7
$(\text{C}_2\text{H}_5)_2\text{O}\cdot\text{BF}_3$	0.0
$\text{C}_6\text{H}_5\text{OCH}_3\cdot\text{BF}_3$	-1.3
$(\text{C}_2\text{H}_5)_2\text{S}\cdot\text{BF}_3$	-19.5

^a + shifts are upfield (greater shielding).

slower process of higher activation energy than the path involving BF_3 transfer to a free ether.

Ion Exchange on the Mineral Clinoptilolite

by Darryl G. Howery¹ and Henry C. Thomas

Department of Chemistry, University of North Carolina, Chapel Hill, North Carolina (Received August 31, 1964)

Cation-exchange equilibria on the zeolitic mineral clinoptilolite have been investigated for the pairs of ions Na^+-Cs^+ , $\text{Na}^+-\text{NH}_4^+$, and $\text{NH}_4^+-\text{Cs}^+$ at 30 and 70° using column techniques with radioactive tracers. The standard values of ΔF and ΔH are shown to obey the triangle rule with discrepancies of only about 0.1 kcal./mole. The system is discussed in terms of the excess thermodynamic functions.

The cation-exchange properties of the zeolitic mineral clinoptilolite have been the subject of several recent investigations.^{2,3} The individuality of the mineral has been established by Mumpton.⁴ It is considered to be an altered pyroclastic. Further alteration results in its conversion to the clay mineral hectorite. Clinoptilolite is being used quite extensively as a selective sorbent for certain radionuclides⁵; its behavior as an ion exchanger is of considerable interest for both practical and theoretical reasons. We here give an account of the equilibria reached by this material with solutions of the chlorides of sodium, ammonium, and cesium, in pairs. The measurements have been made at two

temperatures, so that a fairly complete thermodynamic treatment can be given.

(1) This paper is based on the dissertation submitted by D. G. Howery to the faculty of the University of North Carolina in partial fulfillment of the requirements for the degree of Doctor of Philosophy. The work was supported by the U. S. Atomic Energy Commission under Contract No. AT-(40-1)-2130.

(2) L. L. Ames, Jr., *Am. Mineralogist*, **45**, 689 (1960); **46**, 1120 (1961); **47**, 1067, 1310, 1317 (1962).

(3) G. R. Frysinger, *Nature*, **194**, 351 (1962).

(4) F. A. Mumpton, *Am. Mineralogist*, **45**, 351 (1960).

(5) D. K. Jamison, *et al.*, Ed., "The Use of Inorganic Exchange Materials for Radioactive Waste Treatment," U. S. Atomic Energy Commission, TID-7644 (1963).

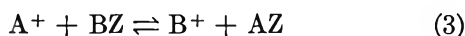
The complexities of ion exchange between solutions and silicate minerals of open structure⁶ are so varied that little is to be gained by attempting more than a formal thermodynamic treatment of the data, such as that given by Gaines and Thomas.⁷ This treatment implies that the free energy function of the solid exchanger will be simplest if compositions are given as equivalent fractions when ions of different charge types are involved. Thus the chemical potential associated with the ion A in a zeolite combination with ion B, (A,B)Z, is written

$$\mu_A^s = \mu_A^{os}(T) + RT \ln N_A f_A \quad (1)$$

where N_A is the equivalent fraction of A in (A,B). For the solution we write as usual

$$\mu_A^l = \mu_A^{ol} + RT \ln m_A \gamma_A \quad (2)$$

The condition for equilibrium in the exchange reaction, written here for singly charged ions



gives the usual equilibrium constant expression

$$K_B^A = \frac{(m_B \gamma_B)(N_A f_A)}{(m_A \gamma_A)(N_B f_B)} = \bar{K}_{cB} \frac{f_A}{f_B} \quad (4)$$

The evaluation of the thermodynamic equilibrium constant and of the solid phase activity coefficients results from an appropriate integration of the Gibbs–Duhem equation for the solid phase. In general this requires a knowledge of solvent uptake and solvent activity as well as of the co-ion concentration in the exchanger phase. The activity coefficients f_A, f_B are made definite by some convenient, arbitrary, selection of standard states for the solid, which also fixes the meaning of K_B^A and of the standard free energy. We take the standard states as the pure monoion solids and the usual solute standard states for the solution. Since it has been shown that clinoptilolite sorbs no anion and since we confine our attention to solutions sufficiently dilute so that the water activity changes inappreciably with composition, the Gibbs–Duhem equation together with eq. 4 gives the following rules for computing the activity coefficients and the value of K_B^A

$$\ln f_A = -N_B \ln K_{cB}^A + \int_0^{N_B} \ln K_{cB}^A dN_B \quad (5)$$

$$\ln f_B = N_A \ln K_{cB}^A - \int_{N_B}^1 \ln K_{cB}^A dN_B \quad (6)$$

$$\ln K_B^A = \int_0^1 \ln K_{cB}^A dN_B \quad (7)$$

For brevity, we refer to the stoichiometric equilibrium

quotient multiplied by the activity coefficient ratio for the solution phase as the *rational equilibrium quotient*, K_c .

Most of the interesting detail of the behavior of the exchanger is reflected in the activity coefficients; we may use them to calculate the various excess thermodynamic functions. For this purpose, when ions of different charges are to be considered, we must broaden somewhat the usual definition on the basis of which the excess quantities are calculated. We define an ideal mixed solid as one in which the free energy with respect to appropriate amounts of pure monoion solids, n_A and n_B moles, is given in terms of the equivalent fractions N_A, N_B

$$\frac{\Delta F^{id}}{RT} = n_A \ln N_A + n_B \ln N_B \quad (8)$$

It is to be noted that while the excess free energy of such a solid is certainly zero

$$\Delta F_m^X = \Delta F_m - \Delta F_m^{id}$$

the solid phase activity coefficients are not equal to unity unless the exchanging ions have like charge. Thus for A^+ competing with B^{+2} , we have

$$N_A = n_A/(n_A + 2n_B); N_B = 2n_B/(n_A + 2n_B)$$

and

$$\ln f_A = N_B/2; \ln f_B = -N_A$$

but

$$\Delta F^X = RT(n_A \ln f_A + n_B \ln f_B)$$

is identically zero for our ideal solid.

The temperature coefficients of the activity coefficients at fixed solid composition lead directly to the heat of mixing

$$\Delta H^X = \Delta H = -RT^2 \left\{ n_A \left(\frac{\partial \ln f_A}{\partial T} \right)_{P,N} + n_B \left(\frac{\partial \ln f_B}{\partial T} \right)_{P,N} \right\} \quad (9)$$

and hence to the excess entropy of the solid

$$T \Delta S_m^X = \Delta H_m - \Delta F_m^X \quad (10)$$

If complete exchange studies on three ions, A^+, B^+, C^+ , in pairs are made, the self-consistency of the work can be assessed by the "triangle rule" applied to the standard free energies and enthalpies of the exchange

(6) An excellent account of these, with many references to the original literature, is given in F. Helfferich, "Ion Exchange," McGraw-Hill Book Co., Inc., New York, N. Y., 1962, pp. 185–193.

(7) G. L. Gaines and H. C. Thomas, *J. Chem. Phys.*, **21**, 714 (1953).

reactions. In terms of the equilibrium constants we must have

$$K_B^A \times K_C^B = K_C^A \quad (11)$$

Experimental

The equilibrium column method was used to determine the ionic uptake of the mineral. In this procedure the exchanger is brought to equilibrium by extended treatment with a solution of given composition carrying an isotopic tracer for one (or possibly more) of the ions present. The uptake of the mineral for the traced ion is determined by exhaustive elution with any convenient "dead" solution. The method depends on a knowledge of the free volume of the column, which is simply determined from its increase in weight on filling. This procedure amounts to a definition of the free volume and is satisfactory for reasonably high uptake by the mineral. Great care is necessary in the near trace regions of composition, when the measured uptake must be given by the difference of two nearly equal numbers.

The sample of mineral used in these studies was kindly given to us by the Geochemical and Geophysical Research Unit, Hanford Laboratories Operation (Richland, Wash.). Because of variability in the composition of the mineral, we have carried out all of our experiments on this single sample. We are indebted to Dr. Peter A. Howell of the Tonawanda Laboratories of the Linde Company for optical and X-ray examination of this material. He has concluded that the major crystalline component is clinoptilolite with about 10% montmorillonite and quartz. A considerable quantity was crushed and sieved, the 30–140 mesh material being retained. This sample was exhaustively eluted, over an extended period of time, with 1 *N* NaCl until no trace of calcium or magnesium could be detected in the washings. This "sodium-based" zeolite was then freed of fines by swirling and decanting with water. After air-drying, the 30–80 mesh fraction was stored in a tightly stoppered bottle. Samples of this material were decomposed with HF–H₂SO₄ and, after evaporation, taken up in dilute HCl. The solution from 0.1 g. of zeolite was shown to contain less calcium than corresponds to 0.01% in the sample. We have used this very time-consuming method for freeing the mineral of calcite because acid treatment has been shown to attack the aluminosilicate network and we wished to examine the mineral in as nearly its natural form as possible. Our results therefore cannot be expected to agree exactly with data obtained by others, *e.g.*, Ames,² who have used acid-treated material.

Temperature control in the ion-exchange columns was maintained by pumping water from a thermostat through preheater jackets on the input lines just above

the columns and through jackets around the columns themselves. Previous experience with the equipment has shown that temperatures in the ion-exchanger bed are accurate to $\pm 0.1^\circ$ at 30° and to $\pm 0.5^\circ$ at 70° .

Due to the long periods necessary to reach equilibrium, several experimental factors were varied according to the relative concentrations of the input solutions. The various experimental conditions are summarized in Table I. It seems most probable that in some of the earlier work³ equilibrium was in many cases not reached.

Table I: Experimental Conditions

	$c_A \approx c_B$	$c_A \gg c_B$ or $c_B \gg c_A$
Weight of zeolite	0.5 g.	0.05 g.
Saturation time	1 day	7 days
Saturation volume	0.7 l.	3.8 l.
Flow rate	0.6 ml./min.	
Elution time	1.5 days	
Elution volume	0.5 l.	
Eluent	0.3 <i>N</i> NaCl	
Column dimensions	8 × 0.85 cm.	

Measurements of radioactivity were made on a single-channel γ -ray scintillation spectrometer using the usual NaI(Tl) crystal. Samples for counting were 4-ml. portions of the solutions carefully pipetted into uniform plastic tubes. Each determination was based on three independent samples for each of which 50,000–90,000 counts were taken. To check for complete elution, material from the columns was dried and counted directly. No significant "fixation" was detected with any of the ions here reported.

Carrier-free Cs¹³⁴ and Na²² were used as tracers. All solutions of the salts were prepared by weight from analytical grade reagents, using the manufacturer's assay. Our cesium chloride was the "optical grade" stated by A. D. Mackay, Inc., to be 99.9+ % pure.

The pH of all solutions used was in the range of 5.2 \pm 0.2.

Results

The cation-exchange capacities (c.e.c.), based on four determinations for each ion, are, for Na⁺, 2.046 \pm 0.017 mequiv./g., and, for Cs⁺, 2.039 \pm 0.011 mequiv./g. The c.e.c. for NH₄⁺ is inferred to be the same from an experiment in which a sodium zeolite lost 1.97 mequiv./g. when treated with 0.02 *N* NH₄Cl. Elution chromatograms demonstrated that the selectivity sequence is Cs > NH₄ >> Na.

When a sodium-based column is treated with solutions containing $\text{Na}^{+*}\text{-Cs}^{+}$ or $\text{Na}^{+*}\text{-NH}_4^{+}$, the activity of the effluent first approaches then exceeds the activity of the influent. After a period depending on the relative input concentration, the activity of the effluent finally levels off at the influent value. These chromatographic "humps" indicated the need for the very long saturation times mentioned earlier.

The uptake of the NH_4^{+} ion in mixtures has been obtained only by difference. Determinations in the $\text{Na}^{+}\text{-Cs}^{+}$ system reveal that, although the c.e.c. values for Na^{+} and Cs^{+} separately are identical within experimental error, the total uptake in the mixed systems is always less. This is demonstrated in Table II, where independently measured uptakes for the two ions are given together with their sums, which we would expect to be the same as the single-ion c.e.c.

Table II: Total Uptake in the Na-Cs System at 30° and $c_0 = 0.02 N$

$c(\text{Cs})/c_0$	q_{Na}	q_{Cs}	q_0
0.00	2.05	..	2.05
.05	0.57	1.32	1.89
.10	.45	1.46	1.91
.50	.14	1.74	1.88
.75	.099	1.88	1.98
.90	.07	1.99	2.06
.95	.04	2.02	2.06
1.00	..	2.04	2.04

That this effect is not due to some hysteresis appears to be proven by an experiment in which a column previously used in a determination at $c(\text{Cs})/c_0 = 0.5$ was switched to a solution at $c/c_0 = 0.1$. The cesium uptake at $c/c_0 = 0.1$ was found to be 1.455 mequiv./g. A fresh (sodium-based) column equilibrated directly at $c/c_0 = 0.1$ gave the nearly identical uptake, 1.457 mequiv./g. Furthermore, when a tagged sodium column was eluted with an untagged Cs-Na solution at $c/c_0 = 0.1$, no residual activity was left on the column, implying that all the sites are equally available to both cesium and sodium. It appears to be highly improbable that the variation of the total uptake with solution composition could be due to a large and variable sorption of negative ion. Direct experiment with solutions containing radioactive bromide shows that the zeolite either selectively sorbs water from these solutions or that the anion is repelled from the surfaces of the mineral. In addition we have found identical sodium capacities for both chloride and bromide solutions on two different samples of clinoptilolite. We are at a loss to explain the apparently variable

capacity with the mixed solutions. It can, however, be demonstrated by direct calculation that the uncertainty in the c.e.c. of the clinoptilolite produces a generally negligible effect in the computed values of the thermodynamic functions descriptive of the system.

We express concentrations and uptakes in terms of the selectively sorbed component; *e.g.*, if the sorption of A is favored, with uptake q_A

$$N_A = q_A/(q_A + q_B) = q/q_0 = 1 - N_B \quad (12)$$

The solutions used were at a total concentration of 0.02 N throughout, so that we identify the molality and molarity of the ions. For reaction 3 in which it is supposed that AZ is favored

$$K_{cB}^A = \frac{q(c_0 - c)}{c(q_0 - q)} \quad (13)$$

In the sodium-cesium system, for which the total uptake data are available, an attempt has been made to make the computations somewhat more self-consistent by using the appropriate total uptake value. For the sodium-ammonium and ammonium-cesium cases the single-ion c.e.c. has been used. In the sodium-cesium case, standard free energies calculated for $q_0 = 1.90$ and for $q_0 = 2.04$ mequiv./g. differ by only 125 cal. (in 2400 cal.).

From large scale plots, values of $\ln K_c$ were read from which all the computations of the thermodynamic quantities have been made. The standard values of these are given in Table III. Application of the triangle rule to these results demonstrates the self-consistency of the data. As is seen in Table III, the disagreement between the observed and calculated values of ΔF° is no more than might be expected from experimental uncertainty. That the agreement for the enthalpies is equally good must be somewhat fortuitous; the temperature derivative of a free energy is a notoriously unreliable quantity.

Table III: Standard Values of the Thermodynamic Functions at 30° (cal./mole)

	Cs-Na	NH ₄ -Na	Cs-NH ₄
ΔF°	-2420	-1290	-1020
ΔH°	-2700	-880	-1680
$T\Delta S^\circ$	-280	+410	-660
$\Delta F^\circ(\text{NH}_4\text{-Na}) + \Delta F^\circ(\text{Cs-NH}_4) = -2310, \Delta = 110 \text{ cal./mole}$			
$\Delta H^\circ(\text{NH}_4\text{-Na}) + \Delta H^\circ(\text{Cs-NH}_4) = -2560, \Delta = 140 \text{ cal./mole}$			

Deviations from ideality in the exchanger phase appear at once in the nonconstant values of K_c and are reflected in the activity coefficients. These for an ideal

Table IV: Excess Thermodynamic Quantities at 30°

$N_{\text{Cs}, \text{NH}_4}$	$\text{Cs}^+ - \text{Na}^+$			$\text{NH}_4^+ - \text{Na}^+$			$\text{Cs}^+ - \text{NH}_4^+$		
	$-\Delta F_m^x$	$-\Delta H_m^x$	ΔS_m^x	$-\Delta F_m^x$	$-\Delta H_m^x$	ΔS_m^x	$-\Delta F_m^x$	$-\Delta H_m^x$	ΔS_m^x
0.00	0	0	0.0	0	0	0	0	0	0.0
.02	13	18	.0	16	18	0	18	37	-0.1
.05	29	23	.0	37	23	0	44	68	-0.1
.10	54	27	.1	66	46	0.1	83	114	-0.1
.30	130	18	.4	137	278	-0.5	209	242	-0.1
.50	182	-5	.6	164	383	-0.7	274	160	.4
.70	181	-187	1.2	156	41	.4	240	-333	1.9
.90	102	41	0.2	83	-142	.7	92	-142	0.8
.95	63	55	.0	58	-96	.5	46	-68	.4
.98	33	-9	.1	21	-46	.2	19	-27	.2
1.00	0	0	0	0	0	0	0	0	0

solid and equi-charge exchanges should have the constant value unity. A numerical summary of the non-ideal behavior of clinoptilolite is given in Table IV in terms of the excess quantities for the imaginary molecular mixing at 30° of appropriate amounts of the monocation solids.

Discussion

Qualitatively, all three systems here examined exhibit similar behavior: the values of the K_c 's steadily decrease from the high value characteristic of the trace region for the selectively sorbed component to a lower value at the other extreme of composition. All the evidence at low proportion of either component points to definite limiting values of K_c , *i.e.*, to Henry's law behavior. This is most clearly seen at the low cesium end of the cesium-sodium isotherm, where the data are most abundant. The situation at the cesium-rich end of the isotherm is less satisfactory. For purely experimental reasons it is most difficult to obtain reproducible data in this region. It is also possible that an unobserved competition between cesium and hydrogen ion may here affect the results to some extent.

The main features, but certainly not the details, of these results can be accounted for by either of two oversimplifications. We might suppose that the sites are all alike and that the difference of the binding energies of a pair of ions for a site is influenced only by the population of neighboring sites. For simplicity, we suppose that the entropy of an aggregate of loaded sites is given by the ideal mixing law. We thus assume that the sites are equally accessible to all ions and attempt to represent the solid as an analog of a regular solution. On this basis we have first approximation activity coefficients, for ions of like charge, of the forms

$$\ln f_A = \frac{w}{RT} N_B^2; \quad \ln f_B = \frac{w}{RT} N_A^2 \quad (14)$$

These lead to a linear variation of $\ln K_{cB}^A$ with solid composition and to the well-known expression for the excess free energy of mixing

$$\Delta F_m^x = w N_A N_B \quad (15)$$

There result the parabolic plots for ΔF_m^x and ΔH_m vs. N_B , and if w is independent of the temperature, to a zero excess entropy. Inspection of Table IV shows that our systems indeed exhibit many of these characteristics. Since our values of ΔH_m are very sensitive to experimental error, we might with some justice disregard the irregularities that appear in these quantities or ascribe them perhaps more reasonably to an insufficiently elaborate form for the activity coefficients, this latter being called for by the complex nature of $\ln K_c$. Such qualitative agreement is an insufficient basis on which to draw conclusions as to the nature of the exchanger, as can be demonstrated by showing similar agreement with an entirely different model.

Let us make an alternative extreme supposition and assume that the sites are so widely separated that interactions between them may be entirely neglected but that the binding energies vary from site to site. To get the simplest results, we suppose that the sites are distributed uniformly over a definite total energy range and that in any small range of energy there are the same number of sites and that in this group the entropy of mixing is approximately ideal. As is shown in the Appendix, this supposition produces in first approximation the following expression for the rational equilibrium quotient as a function of exchanger composition, y . (Here y is a mole fraction; the formula does not hold for unequal charge types.)

$$K_c = \frac{y}{1-y} \frac{K_2^{1-y} - K_1^{1-y}}{K_1^{-y} - K_2^{-y}} \quad (16)$$

The quantities K_2 and K_1 are determined by the limit-

ing values of K_c at $y = 0$ and $y = 1$. The supposition as to the nature of the sites and their distribution in energy in effect predicts the whole course of K_c in terms of the extreme sorption energies. The prediction is very rough when applied to clinoptilolite. As can be most easily seen by a numerical example for a special case, expression 16 for K_c gives a plot of $\ln K_c$ vs. y scarcely distinguishable from the straight line between the intercepts at $y = 0$ and $y = 1$. Thus two extreme suppositions as to the nature of the exchanger predict nearly identical results for those thermodynamic functions immediately derivable from equilibrium data obtained at a single temperature. We can suggest no model which gives a convincing picture of the true nature of the exchange process in the zeolite mineral. Since we are in any case dealing with a somewhat heterogeneous material, better than rough agreement with any one model is not to be expected. It would be of interest to examine similarly highly purified natural or synthetic zeolites from the points of view here indicated.

Appendix

It is possible to give a nearly complete account of the experimental results to be expected when exchange sorption of a pair of ions of like charge takes place on a surface of varying site energy if we suppose that the distribution of energy is linear between a lowest and a highest value and that there are no interactions between sites. That is, we suppose that between definite limits for any given range of energy there are to be found the same number of sites regardless of the value of the energy. At first sight, such a distribution seems highly artificial, but if one admits an upper and a lower bound for the energy, any continuous distribution could be imagined as pieced together out of linear segments. Thus an exchanger with a complex distribution of energies of sorption could be considered to be a heterogeneous material, each part of which is in equilibrium with every other part through the medium of the common solution with each part obeying a linear distribution law.

The above ideas can be put into the following mathematical form: for a group of noninteracting sites all of the same energy, we have

$$\ln K_c = \ln \frac{y}{1-y} \frac{1-x}{x} = - \int \frac{\bar{L}_2 - \bar{L}_1}{RT^2} dT \quad (\text{A1})$$

where we write y for the fraction of species 1 on the surface and x for its fraction in solution. Here

$$\bar{L}_1 = \bar{H}_1 - \bar{H}_1^\circ \quad (\text{A2})$$

is the partial enthalpy of species 1 on the surface with respect to its standard enthalpy in solution. Thus

$\bar{L}_2 - \bar{L}_1$ is the enthalpy of exchange at compositions x, y .

We have already supposed that these enthalpies are independent of composition; let us in addition suppose that they are independent of temperature. We can then write

$$\ln \frac{y}{1-y} \frac{1-x}{x} = \frac{\Delta L}{RT} \quad (\text{A3})$$

Now according to the above simplification of the nature of the surface, we suppose that we have for a surface of N_0 sites

$$\Delta L = \frac{\Delta L_{\max} - \Delta L_{\min}}{N_0} N + \Delta L_{\min}$$

or, more simply, for $0 < \xi = N/N_0 < 1$

$$\frac{\Delta L}{RT} = A\xi + B \quad (\text{A4})$$

where the meanings of A and B are apparent. We note that for a group of sites of highest and lowest energies

$$K_2 = \exp \frac{\Delta L_{\max}}{RT}$$

$$K_1 = \exp \frac{\Delta L_{\min}}{RT}$$

It is to be pointed out that K_1, K_2 are *not* values of K_c for the entire surface.

Now if there are dn_1 ions on the group of sites dN with energy $A\xi + B$, we have

$$\frac{dn_1}{dN - dn_1} \frac{1-x}{x} = e^{A\xi+B}$$

$$\left(\frac{d\xi}{dy} - 1 \right) \frac{x}{1-x} = e^{-A\xi-B} \quad (\text{A5})$$

We find y for the entire surface from this expression after integrating over ξ from 0 to 1, remembering that all groups of sites are in equilibrium with the same solution in which the fraction of ion 1 is x

$$y = \int_0^1 \frac{d\xi}{1 + \frac{1-x}{x} e^{-A\xi-B}}$$

Because of our simple assumption as to the nature of the distribution of sites, we have here an expression which is easily evaluated. The result is the equation for the sorption isotherm of our surface

$$y = 1 - \frac{RT}{\Delta L_{\max} - \Delta L_{\min}} \ln \frac{1 + \frac{1-x}{x} e^{-\Delta L_{\min}/RT}}{1 + \frac{1-x}{x} e^{-\Delta L_{\max}/RT}}$$

$$y = 1 - \frac{1}{\ln \frac{K_2}{K_1}} \ln \frac{1 + \frac{1-x}{x} \frac{1}{K_1}}{1 + \frac{1-x}{x} \frac{1}{K_2}} \quad (\text{A6})$$

We may deduce at once some of the properties of K_o for this surface. Thus

$$\lim_{x,y \rightarrow 0} \frac{y}{x} = \lim_{x \rightarrow 0} K_o = \frac{K_2 - K_1}{\ln \frac{K_2}{K_1}} \quad (\text{A7})$$

and

$$\lim_{x,y \rightarrow 1} \frac{1-x}{1-y} = \lim_{x \rightarrow 1} K_o = \frac{K_1 K_2 \ln \frac{K_2}{K_1}}{K_2 - K_1} \quad (\text{A8})$$

It is thus seen that the intercepts of a $\ln K_o$ vs. y plot are indeed related to the limiting energies of sorption, but in no very simple fashion.

Because of the assumed variation of the exchange energy, it is seen at once that the average exchange energy is

$$\int_0^1 \Delta L d\xi = \frac{1}{2} (\Delta L_{\max} + \Delta L_{\min}) \quad (\text{A9})$$

which corresponds to an average free energy of exchange given by

$$\int_0^1 \ln K_o dy = \ln \sqrt{K_2 K_1}$$

This is also the standard free energy for the surface. It is of some interest to verify that we indeed get this value by the usual thermodynamic computation from $\ln K_o$ as deduced from the isotherm.

Starting by solving the expression for the isotherm for $(1-x)/x$, we find for K_o expressed as a function of y

$$\ln K_o = \ln \frac{y}{1-y} \frac{K_2^{1-y} - K_1^{1-y}}{K_1^{-y} - K_2^{-y}} \quad (\text{A10})$$

A direct integration of this expression has not been accomplished, but we can obtain the required result, as well as some illumination about the shape of the $\ln K_o$ vs. y curve, by putting the expression in the form

$$\ln K_o = \ln \frac{y}{1-y} + \ln \sqrt{K_1 K_2} + \ln \frac{\sqrt{\frac{K_1}{K_2}} \left(\frac{K_2}{K_1} \right)^{1-y} - 1}{1 - \left(\frac{K_2}{K_1} \right)^{-y}} \quad (\text{A11})$$

Examination of this expression shows that if $y \rightarrow 1-y$, the first and third terms simply change sign. Thus, the integral of these terms with respect to y over the whole range gives zero, and we verify that

$$\int_0^1 \ln K_o dy = \frac{1}{2} \ln K_1 K_2 \quad (\text{A12})$$

Vacuum Ultraviolet Photochemistry. VIII. Propylene

by D. A. Becker, H. Okabe, and J. R. McNesby

National Bureau of Standards, Washington, D. C. 20234 (Received September 5, 1964)

The direct photolysis of propylene was carried out below (at 1470 Å.) and above (at 1236 Å.) the ionization potential. Major products were acetylene, ethylene, hydrogen, methane, ethane, propane, propyne, allene, isobutane, and C₄-unsaturated hydrocarbons. No appreciable energy dependence was observed in the distribution of products. Isotopic analysis of photolytic products, hydrogen, methane, ethane, and ethylene, from the mixture of C₃H₆-C₃D₆ and from CH₃CHCD₂, was made to obtain information on the reaction mechanism. The isotopic composition of the ethylene product, which must at least partially be produced at 1236 Å. from the ion-molecule reaction, C₃H₆⁺ + C₃H₆ → C₄H₈⁺ + C₂H₄, was not sufficiently well defined to confirm the occurrence of this reaction. The following primary processes reasonably explain the isotopic distribution of products: C₃H₆ → CH₃ + H + C₂H₂; C₃H₆ → CH₄ + C₂H₂; C₃H₆ → H₂ + C₃H₄; C₃H₆ → H + C₃H₅; C₃H₆ → CH₂ + C₂H₄; and C₃H₆ → CH₃ + C₂H₃.

Introduction

Since the ionization potential of propylene is 9.7 e.v.,^{1,2} it is possible to study its photochemistry above and below the ionization potential with xenon (mainly 1470 Å., 8.4 e.v.) and krypton (mainly 1236 Å., 10.0 e.v.) resonance lamps. Thus, it is of interest to examine the product distribution with these light sources. Isotopic analysis of products might reveal that certain of them are formed from ion-molecule reactions. Since photons of an energy of 10.0 e.v. produce only the parent ion,³ the interpretation of the results should be simplified. In this work, attempts were made to clarify the energy dependencies of the reaction mechanisms.

Experimental

The light sources were gettered xenon and krypton resonance lamps of high chromatic purity.⁴ A lithium fluoride window was sealed to the Pyrex body of the reaction vessel with Apiezon W wax. The lamps were external to the reaction vessel and a 1-mm. space between the lamp window and reaction vessel window was flushed with nitrogen to prevent atmospheric absorption. In order to distribute the reaction products throughout the reaction vessel so as to prevent their own photolysis, a circulating pump, similar to that described by Watson,⁵ was employed. Figure 1 is a schematic representation of the apparatus.

The volume of the sampling chamber, A, is only about 1% of the volume containing the reacting gas. In order to sample the reaction mixture during photolysis, valve B is opened, allowing the mixture to expand into the evacuated sampling chamber, A. After closing valve B, the sample is taken by inserting a 1-cc. gas-tight hypodermic syringe, which had been flushed with helium, into A through a self-sealing rubber septum, C. This technique allows analysis to be made as a function of time or per cent decomposition. Gas chromatographic calibrations (squalane) were done on all major products and it was found that peak areas (peak height × peak width at the half-height) were proportional to the amounts of products. Flame ionization detection was used throughout the work.

Materials. Phillips research grade propylene and Merck C₃D₆ and CH₃CH=CD₂ were purified by gas chromatography on a silica gel column. After this treatment, the only detectable impurity in the propylene was 0.02% *n*-butane.

By mass spectrometry, it was found that 3.3% propylene-*d*₅ was present as an impurity in propylene-*d*₆.

- (1) K. Watanabe, *J. Chem. Phys.*, **26**, 542 (1957).
- (2) J. A. R. Samson, F. F. Marmo, and K. Watanabe, *ibid.*, **36**, 783 (1962).
- (3) B. Steiner, C. F. Giese, and M. G. Inghram, *ibid.*, **34**, 189 (1961).
- (4) H. Okabe, *J. Opt. Soc. Am.*, **54**, 478 (1964).
- (5) J. S. Watson, *Can. J. Technol.*, **34**, 373 (1956).

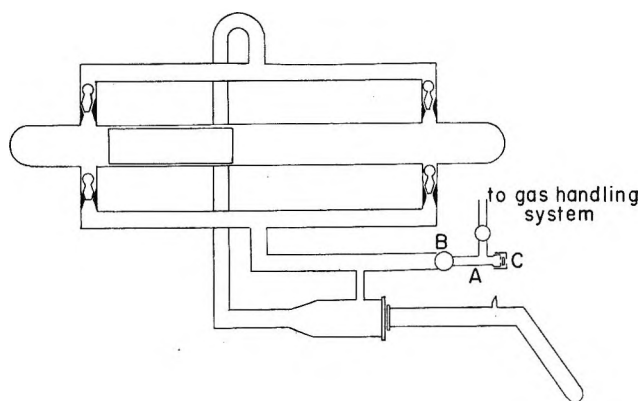
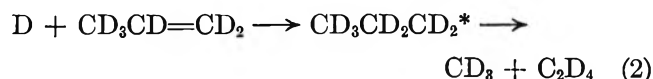
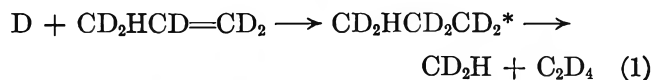


Figure 1. Schematic representation of the photolysis apparatus.

It is more difficult to detect a propylene- d_4 impurity. The number of CD_2H groups in the nominal propylene- d_6 was determined by near-ultraviolet photolysis of D_2S in its presence. The D atoms sometimes add nonterminally to propylene and the excited n -propyl (but not isopropyl) decomposes to give CD_2H and CD_3 approximately in the ratio of CD_2H groups: CD_3 groups.⁶ The abstraction of D from D_2S by methyl is



a fast reaction and the relative abundance of CD_2H and CD_3 radicals and, therefore, of CD_2H and CD_3 groups is given by the reaction product ratio CD_3H/CD_4 . It was found that 5.5% of the methyl groups are CD_2H and 94.5% are CD_3 . Mass spectrometer analysis reveals 3.3% propylene- d_5 in the propylene- d_6 . It was not possible to assess the integrity of $CH_3CH_2=CD_2$.

Results

Some preliminary photolyses at 1470 and 1236 Å. were done in a static, noncirculating system. In these experiments the total number of moles of hydrogen and methane produced were determined absolutely by means of a Toepler pump-gas buret assembly and the relative amounts of these by mass spectrometry. The relationship between the amounts of methane and other hydrocarbons formed was determined by gas chromatography. It was found that at 1470 Å., $H_2/CH_4 = 2.2$ and, at 1236 Å., $H_2/CH_4 = 3.8$. Further, the H_2/C_2H_2 ratios were 0.20 and 0.42 at 1470 and 1236 Å., respectively. While the product analyses for these experiments were only in fair agreement with those obtained in the more reliable circulating system, they

provided a material balance measurement which is an indication of the reliability of the analytical method. Hydrogen and methane were not determined in experiments done with the circulating pump. The material balance in the static system experiments is indicated by the cumulative formula of the reaction products of $C_3H_{5.7}$ and $C_3H_{6.1}$ at 1470 and 1236 Å., respectively.

There is the possibility that, even at conversions of less than 1%, the photolysis of primary reaction products can contribute in an important way to the observed chemistry. Such a situation can arise if reaction products accumulate near the window of the reaction vessel and if they have very much higher absorption coefficients than the parent molecule. Table I shows that the absorption coefficients of two of the most important products are smaller than those of the parent and therefore it is unlikely that secondary photolysis is important. In the static system, measurable amounts of higher hydrocarbons were formed while none were produced in the circulating system.

Table I: Absorption Coefficients of Propylene and Some Important Reaction Products

	1470 Å.	1236 Å.
Propylene ^b	530	1000
Ethylene ^c	400	~600
Acetylene ^d	~530	~200

^a Definition of ϵ : $I/I_0 = \exp(-\epsilon P_{atm} x_{cm})$. ^b See ref. 2 in text. ^c M. Zelkoff and K. Watanabe, *J. Opt. Soc. Am.*, **43**, 756 (1953). ^d T. Nakayama and K. Watanabe, *J. Chem. Phys.*, **40**, 558 (1964).

In order to learn if the reaction products are involved in the reaction to a significant extent, product analyses, as a function of conversion, were performed. The observed rate of formation of a reaction product, which is itself being consumed in proportion to its rate of accumulation, cannot be independent of the per cent decomposition of the parent. The slopes of the curves in Figure 2 represent the rates of formation of ethylene. The lack of dependence of the rate on the per cent decomposition at either 1470 or 1236 Å. shows that secondary reactions of ethylene are not involved. Similarly, Figures 3 and 4 show that acetylene, allene, ethane, and isobutane are primary products whose rates of formation are independent of conversion at both wave lengths. The analyses for hydrocarbon products other

(6) T. Yokota and B. deB. Darwent, unpublished results.

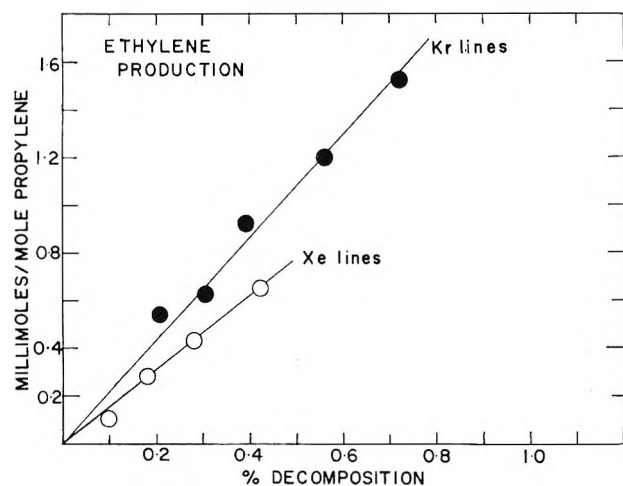


Figure 2. Dependence of ethylene production on per cent decomposition.

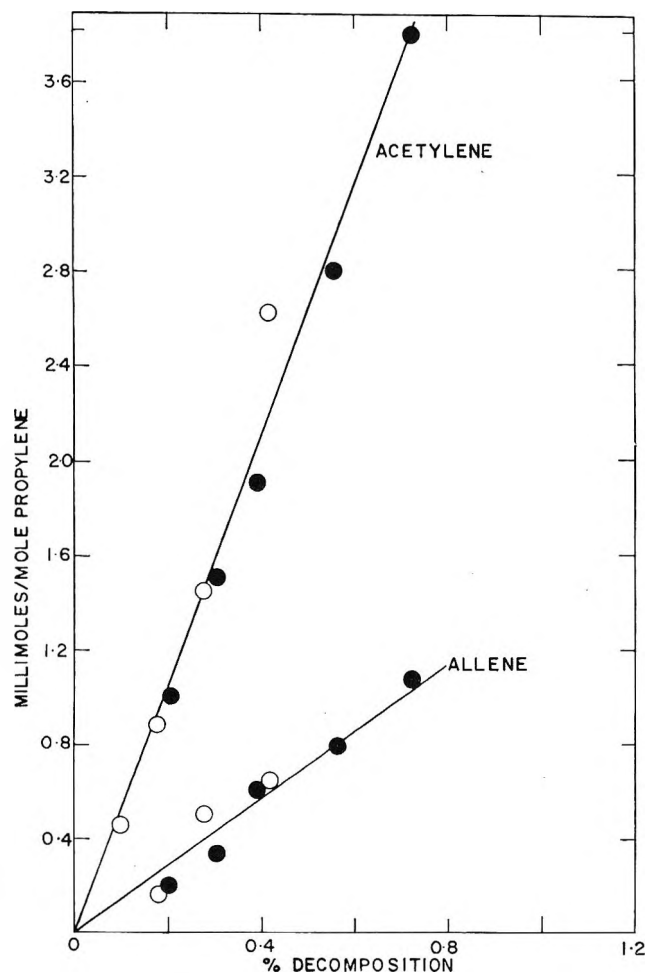


Figure 3. Dependence of acetylene and allene production on per cent decomposition: O, xenon lines; ●, krypton lines.

than CH_4 for photolysis at low conversion ($\sim 0.2\%$) are presented in Table II.

Table II: Percentage Composition of Products in Propylene Photolysis^a at 0.2% Conversion

	$\lambda, \text{\AA}$	
	1470	1236
Hydrogen	(7.6) ^b	(14.7) ^t
Methane	(3.4) ^b	(3.8) ^t
Acetylene	38.0	34.9
Ethylene	12.2	18.2
Ethane	7.4	4.1
Allene	7.4	6.8
Isobutane	11.4	8.6
Isobutene + butene-1	3.5	4.8
<i>trans</i> -Butene-2	7.2	4.1
<i>cis</i> -Butene-2	1.9	0.0

^a Propylene pressure at 10 mm. ^b These figures are from separate experiments which showed that, at 1470 \AA , $\text{H}_2/\text{CH}_4 = 2.2$ and $\text{H}_2/\text{C}_2\text{H}_2 = 0.20$; at 1236 \AA , $\text{H}_2/\text{CH}_4 = 3.8$ and $\text{H}_2/\text{C}_2\text{H}_2 = 0.42$. Experiments with a different chromatographic column revealed propyne and propane each approximately equal to allene.

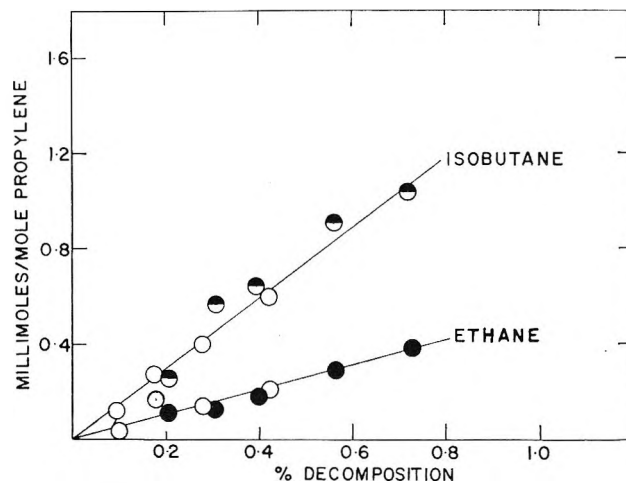


Figure 4. Dependence of isobutane and ethane on per cent decomposition: O, xenon lines; ● and ○, krypton lines.

Photolysis of Labeled Propylenes. The analysis of the ethane fraction from the photolysis of $\text{C}_3\text{H}_6 + \text{C}_3\text{D}_6$ at both 1470 and 1236 \AA . was not done with great

Table III: Photolysis of 1:1 Mixture^a of $\text{C}_3\text{H}_6 + \text{C}_3\text{D}_6$

$\lambda, \text{\AA}$	Isotopic analysis of ethane and ethylene (percentages)				$(\text{C}_2\text{D}_2\text{H}/\text{C}_2\text{D}_4)\text{cor.}$
	C_2D_6	$\text{C}_2\text{D}_5\text{H}$	$\text{C}_2\text{D}_4\text{H}_2$	$\text{C}_2\text{D}_3\text{H}_3$	
1470 (1295)	25	16	2	57	0.88 ^b
1236 (1165)	22	19	5	54	0.60

^a Total pressure at 10 mm. ^b The ratio is unchanged by the addition of 15% NO.

Table IV: Photolysis of Propylene^a

	λ , Å.	Isotopic analysis of hydrogen and methane, %							
		H ₂	HD	D ₂	CH ₄	CH ₃ D	CH ₂ D ₂	CD ₃ H	CD ₄
1:1 Propylene:propylene- <i>d</i> ₆	1470	57	11 ^b	32	44	8	(15) ^c	8 ^a	25
1:1 Propylene:propylene- <i>d</i> ₆ + 15% NO	1470	62	3 ^b	34	49	~0	(8) ^c	0 ^a	43
CH ₃ CH=CD ₂	1470	64	27	8	38	23	(34) ^c	5	0
1:1 Propylene:propylene- <i>d</i> ₆	1236	59	18	23	40	12	(8) ^c	13	27

^a Total pressure at 10 mm. ^b Corrected for blank experiment with nominal C₃D₆. ^c These values are uncertain due to the inability of the mass spectrometer to distinguish between the small amounts of CH₂D₂ and background H₂O.

precision because of the uncertainty of the cracking patterns and the interference of air at masses 28 and 32. However, it was possible to analyze the ethanes having at least three deuterium atoms using the cracking patterns of Bell and Kistiakowsky.⁷ The results are given in Table III. Included are the ratios C₂D₃H/C₂D₄ after correction for C₂D₃H obtained in the photolysis of the nominal C₃D₆. These results show that an important source of ethylene is molecular elimination. Nevertheless, substantial mixing is evident in the ethylenes, and abstraction of H and D by the vinyl radical, which is not scavenged by NO, is undoubtedly involved. Acetylene produced in the photolysis of C₃H₆ + C₃D₆ in the presence and absence of NO is more than 90% unmixed.

Discussion

I. Photolysis at the Xenon Lines. A. Molecular Elimination of Hydrogen and Allene Formation. Table IV shows that the hydrogen produced in the photolysis of mixtures of propylene and propylene-*d*₆ is nearly 90% H₂ and D₂, which indicates that molecular elimination is an important process. A small amount of atomic hydrogen is produced which is eliminated almost entirely in the presence of NO. Since nearly two-thirds of the hydrogen in the photolysis of CH₃CH=CD₂ is H₂, it is certain that the methyl group is involved in the elimination of H₂. There are two possible mechanisms

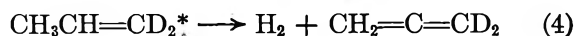
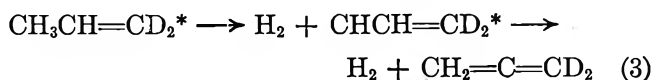


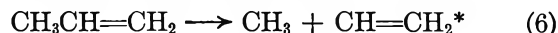
Table II shows that the allene is approximately equal to the hydrogen.

B. Acetylene Formation. The fact that (Table II) hydrogen and allene are not the major products indicates that modes of decomposition of the excited state, other than molecular hydrogen elimination, are predominant. The possibility that the excited states of cyclopropane and propylene decompose through intermediates of similar configuration is entirely discounted be-

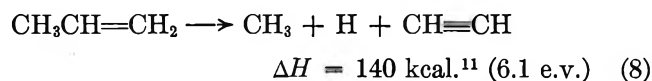
cause ethylene is overwhelmingly the major hydrocarbon product in cyclopropane photolysis at 1470 Å,⁸ while acetylene dominates the products of propylene photolysis. Since the amount of acetylene produced is so much greater than that of methane, the molecular elimination of methane, while it is a major source of methane, is only a minor source of acetylene.



As is the case in the photolysis of ethylene,^{9,10} the rapid, consecutive rupture of two bonds is probably responsible for the production of acetylene.

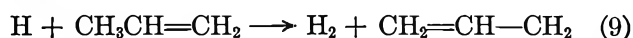


The sum of the sequence (6), (7) is



Thus, the energy of the 1470-Å. photon (8.4 e.v.) is more than enough to cause reactions 6 and 7 to occur.

C. H Atom Formation. From the observation recorded in Table IV that HD is produced, to some extent, in the photolysis of C₂H₆ + C₃D₆, it is obvious that H atoms are not totally scavenged by propylene as they are by ethylene in ethylene photolysis. Rather, there is some contribution to H atom disappearance made by the abstraction reaction



It is evident (Table IV) that NO scavenges most of the H atoms that would otherwise abstract H from propyl-

(7) J. A. Bell and G. B. Kistiakowsky, *J. Am. Chem. Soc.*, **84**, 3417 (1962).

(8) C. L. Currie, H. Okabe, and J. R. McNesby, *J. Phys. Chem.*, **67**, 1494 (1963).

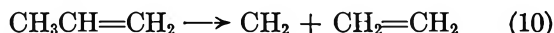
(9) M. Sauer and L. M. Dorfman, *J. Chem. Phys.*, **35**, 497 (1961).

(10) H. Okabe and J. R. McNesby, *ibid.*, **36**, 601 (1962).

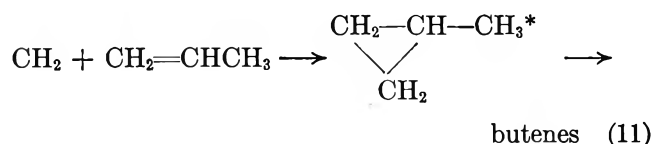
(11) The heat of formation of CH₃ is 32.6 kcal. (ref. 7) and the heat of formation of propylene is -1.9 kcal. ("Handbook of Chemistry and Physics"). Other data from National Bureau of Standards Circular 500, U. S. Government Printing Office, Washington, D. C.

ene. It is possible that H atoms associate rather than abstract to form H_2 .

D. Ethylene and Butene Formation. The fact that $C_2D_4 > C_2D_3H$ in the photolysis of a mixture of C_3H_6 and C_3D_6 (Table III) shows that, in the photolysis of propylene, ethylene is formed partially by a molecular elimination reaction.



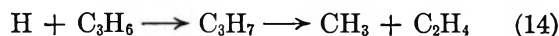
The CH_2 species released in the ethylene elimination may be expected to react with propylene and this reaction accounts for the appearance of the various butenes.¹²



The question of whether methylcyclopropane is formed has not been resolved because of analytical difficulties. The observation that a substantial amount of isotopic mixing occurs in the ethylene formation at 1470 Å suggests that, in addition to the molecular elimination of ethylene, vinyl radicals, which are not scavenged by NO, are involved in ethylene formation.

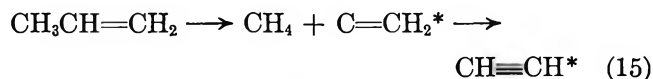


It is also possible to form ethylene from the reaction

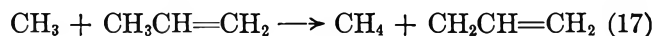


E. Ethane Formation. Judging by the dominance of CH_3CD_3 in the ethanes resulting from the photolysis of $C_3H_6 + C_3D_6$ (Table III), ethane formation is largely attributed to association of methyl radicals. The appearance of appreciable amounts of C_2D_5H is not easily understood but it may involve atomic cracking reactions of propyl and isopropyl radicals. However, with the information at hand, further comment on the mechanism of C_2D_5H formation is purely speculative.

F. Methane and Isobutane Formation. According to Table IV, the methane produced in the photolysis of $C_3H_6 + C_3D_6$ is mainly CH_4 and CD_4 and, in the presence of a scavenger, NO, it is almost entirely CH_4 and CD_4 . The photolysis of $CH_3CH=CD_2$ gives CH_4 and CH_3D . The mechanisms of molecular elimination of methane are, therefore

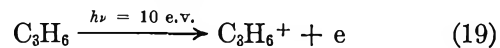


In the absence of NO, the methanes show some isotopic mixing and the abstraction or association reaction is responsible for this observation.



Isobutane undoubtedly comes from the addition of H atoms to propylene followed by association of the isopropyl radicals so formed with methyl radicals.

II. Photolysis at the Krypton Lines. The ionization efficiency of propylene at 1236 Å, measured by Samson, Marmo, and Watanabe,² is 0.32 and only the parent ion, $C_3H_6^+$, is formed at this wave length.³ The only significant ion-molecule reaction to be expected at this wave length is the condensation reaction



which has a large reaction cross section of 74×10^{-16} cm.².^{13,14} If a mixture of $C_3H_6-C_3D_6$ is photolyzed at 1236 Å, a large isotopic mixing in the ethylene would be expected to occur from this reaction. Therefore, if there were no isotopic mixing in ethylene at 1470 Å, where no ions are formed, and a large amount of mixing at 1236 Å, this would suggest the occurrence of reaction 20. Unfortunately, for the purpose of the projected experiment, isotopic mixing in ethylene is appreciable at 1470 Å even in the presence of 15% NO. In addition, a large air background, at masses 28 and 32, made it practically impossible to measure an accurate isotopic distribution of ethylene. This and other ion-molecule reactions or neutralization reactions involving $C_3H_6^+$, $C_4H_8^+$, etc., appear to have an insignificant effect upon the distribution of products.

Acknowledgment. This research was supported by the U. S. Atomic Energy Commission.

(12) J. N. Butler and G. B. Kistiakowsky, *J. Am. Chem. Soc.*, **82**, 759 (1960).

(13) D. O. Schissler and D. P. Stevenson, *J. Chem. Phys.*, **24**, 926 (1956).

(14) D. P. Stevenson, *J. Phys. Chem.*, **61**, 1453 (1957).

Tetrapropylammonium Bromide: Ion Size Parameters in Solution and in the Solid State

by H. K. Bodenseh¹ and J. B. Ramsey

*Department of Chemistry, University of California at Los Angeles, Los Angeles, California
(Received September 5, 1964)*

The association constants at 25° of tetra-*n*-propylammonium bromide in CH₃COCH₃ ($D = 20.7$) and CH₃CHCl₂ ($D = 10.03$) have been determined. It is shown that these two K_A values along with those obtained by others in four other solvents conform to a straight-line relation between $\ln K_A$ and $1/D$. The a parameter of this salt determined from the slope of this straight line ($a = \epsilon^2/kT \times \text{slope}$) is found to be $\sim 17\%$ less than the N-Br distance in its crystal. A probable reason for expecting such a difference is given.

From a thermodynamic consideration of a stepwise process for bringing about the change from an associated ion pair of a uni-univalent salt (in which the interionic distance has been called the "contact distance" and designated the a parameter) to the two free ions with interionic distances sufficiently large to permit the intervention of solvent molecules, the equation

$$\ln K_A = \ln K_A^0 + \epsilon^2/aDkT \quad (1)$$

can be obtained.² K_A is the association constant, K_A^0 is the association constant of the two uncharged ions, D is the dielectric constant of the solvent at temperature T , and ϵ and k are the electronic charge and the Boltzmann constant, respectively.

Since 1956, Fuoss and collaborators³ have determined the effect of varying the dielectric constant of the solvent of a number of uni-univalent salts by use of a series of mixtures of two solvents which in their pure state differ appreciably in dielectric constant. Their results show that in general the linearity between $\ln K_A$ and $1/D$ does exist over a limited range of composition of the solvent mixtures, namely for those mixtures which have the greater D values. Recent results obtained in this laboratory⁴ provide substantial evidence for the conclusion that the deviations from linearity found by these investigators³ in solvent mixture having D values in the lower range are to be expected and also that these deviations may be interpreted in a way which is consistent with the requirement of eq. 1 that $\ln K_A$ vary linearly with $1/D$ if D

are considered to be the effective dielectric constants of these mixtures, not their macroscopic (measured) values.

Direct substantiation of the requirement, namely that $\ln K_A$ vary linearly with $1/D$, has been given² by the results obtained with tetrabutylammonium perchlorate in a series of one-component, monomolecular solvents with D values ranging from 8.78 to 25.2 at 25°. No deviation from linearity was observed over this entire range.

The values of the a parameter of numerous uni-univalent salts to which eq. 1 is applicable have been derived from the slope ($=\epsilon^2/akT$) of the straight line obtained on plotting $\ln K_A$ vs. $1/D$. In general, the values of a so obtained are in reasonable agreement with qualitative estimates of the sums of the ionic radii of the two ions of the salt. Greater confidence in the physical interpretation of the a parameter should be provided if it were found that the value of the a parameter so obtained, relative to the minimum center-to-center distance between cation and anion in the crystalline salt, conforms with that to be expected

(1) Postdoctoral Fellow at the University of California at Los Angeles, 1961-1962.

(2) H. Y. Inami, H. K. Bodenseh, and J. B. Ramsey, *J. Am. Chem. Soc.*, **83**, 4745 (1961); for the approximate form of this equation, see J. T. Denison and J. B. Ramsey, *ibid.*, **77**, 2615 (1955).

(3) References to the publication of several of these investigations have been given elsewhere.²

(4) H. K. Bodenseh and J. B. Ramsey, *J. Phys. Chem.*, **67**, 140 (1963).

from other considerations. As yet a comparison of these two values has not been reported.

So far as is known to the authors, the crystal structure of but one salt of the type commonly used in the determination of K_A values in solvents with relatively low dielectric constants (less than ~ 40 at 25°) has been established. This salt is tetra-*n*-propylammonium bromide, the crystal structure of which was determined by Zalkin⁵ in 1957.

Conductometric determinations of the K_A values of this salt in six one-component solvents have been reported (references given later). The D values of these solvents cover the range 19 to 37.8. In order to obtain with greater certainty the most probable straight line depicting the variation $\ln K_A$ of this salt with $1/D$, its K_A values in the two solvents acetone ($D_{25^\circ} = 20.70$) and ethylidene chloride ($D_{25^\circ} = 10.03$) have been determined. It is shown that the K_A values found in these two solvents along with four of the six K_A values obtained by others in other solvents give unequivocally a straight-line relation between $\ln K_A$ and $1/D$. The value of the a parameter of this salt derived from the slope of this straight line is found to be $\sim 17\%$ less than the minimum center-to-center distance between the $(n\text{-C}_3\text{H}_7)_4\text{N}^+$ ion and the Br^- in its crystal. A probable reason for this difference is suggested.

Experimental

The salt, tetra-*n*-propylammonium bromide, $(n\text{-C}_3\text{H}_7)_4\text{NBr}$, was prepared by the interaction of tri-*n*-propylamine and *n*-propyl bromide in absolute alcohol. Exactly 30 ml. of $(n\text{-C}_3\text{H}_7)_3\text{N}$ and 30 ml. of $n\text{-C}_3\text{H}_7\text{Br}$ (mole ratio of the bromide to the amine $\approx 2:1$) were added to 150 ml. of absolute ethanol and the mixture was refluxed for 24 hr. at atmospheric pressure in the absence of moisture of the air. During refluxing, the boiling point rose from 71 to 74° . Two-thirds of the solvent was then removed by evaporation after which the salt was precipitated by the addition of ether. After filtering and washing with ice-cooled ether, the salt was recrystallized twice from an ethyl acetate-ethanol mixture and dried for 18 hr. at 100° *in vacuo*. Its melting point (252°) agreed with that reported by Sugden and Wilkins.⁶ *Anal.* Calcd. for $(n\text{-C}_3\text{H}_7)_4\text{NBr}$: C, 54.13; H, 10.60. Found: C, 54.24; H, 10.35.

Treatment and Properties of Solvents. The ethylidene chloride (Eastman White Label) was fractionally distilled and stored as previously described.² Its boiling point at atmospheric pressure was $57.0\text{--}57.1^\circ$. Its specific conductance at 25° did not exceed 2.4×10^{-9} ohm⁻¹ cm.⁻¹. The value of its dielectric con-

stant determined by the bridge method previously described⁴ was found to be 10.03 (~ 0.1 unit greater than that obtained earlier² by the heterodyne beat, substitution method). Its density and viscosity at 25° , 1.168 g./ml. and 4.55 millipoises, were those previously accepted by Denison and Ramsey² from reliable sources.

The acetone (Baker's Analyzed Reagent) was merely dried thoroughly with Davison silica gel and stored in contact with this desiccant. Its specific conductance at 25° did not exceed 1.06×10^{-7} ohm⁻¹ cm.⁻¹. The values of its viscosity and density (each at 25°) used in this investigation were those determined by Reynolds and Kraus,⁷ namely 3.04 mpoises and 0.7845 g./ml., respectively. Its D value, 20.7, is that given by Maryott and Smith.⁸

Conductance Measurements. The Shedlovsky⁹ alternating current bridge, with the modifications previously described,² was used. The conductance cell of the Kraus erlenmeyer type¹⁰ had a cell constant equal to 0.1473 cm.⁻¹. The procedure followed in preparing the initial solution and making successive dilutions has been described.²

Results

The graphical method based on the equation developed by Shedlovsky¹¹ was used to determine the K_A value of the salt $(n\text{-C}_3\text{H}_7)_4\text{NBr}$ in each of the solvents, acetone and ethylidene chloride. By use of the IBM 7090 computer as done previously,⁴ it was found that the maximum probable error in each of the K_A values so obtained was less than 1%.

In Table I are given the values of the constants pertinent to this investigation.

In each of the investigations reported by Sears and co-workers, the dissociation constant ($= 1/K_A$) was determined by use of the Shedlovsky¹¹ equation. Gutvang and Utvary (footnote *d*, Table I) made similar use of the Fuoss¹² equation.

The plot of the values of $\log K_A$ vs. those of $100/D$, given in Table I, is shown in Figure 1. It was evident that the points 5 and 7 for benzoyl bromide and dimethylformamide, respectively, deviated quite noticeably from a straight line which would represent quite

(5) A. Zalkin, *Acta Cryst.*, **10**, 557 (1957).

(6) S. Sugden and H. Wilkins, *J. Chem. Soc.*, 1297 (1929).

(7) M. B. Reynolds and C. A. Kraus, *J. Am. Chem. Soc.*, **70**, 1709 (1948).

(8) A. A. Maryott and E. R. Smith, National Bureau of Standards Circular 514, U. S. Government Printing Office, Washington, D. C., 1951.

(9) T. Shedlovsky, *J. Am. Chem. Soc.*, **52**, 1793 (1930).

(10) R. M. Fuoss and C. A. Kraus, *ibid.*, **55**, 1019 (1933).

(11) T. Shedlovsky, *J. Franklin Inst.*, **220**, 739 (1938).

(12) R. M. Fuoss, *J. Am. Chem. Soc.*, **57**, 488 (1935).

Table I: Constants for $(n\text{-C}_3\text{H}_7)_4\text{NBr}$ in Various Solvents at 25°

Solvent	D	$100/D$	K_A	$\log K_A$
(1) $\text{CH}_3\text{CHCl}_2^a$	10.03	9.97	5.38×10^5	5.73
(2) $\text{CH}_3\text{CHOHCH}_3^b$	19.1	5.24	1.00×10^3	3.00
(3) $\text{CH}_3\text{CH}_2\text{CH}_2\text{OH}^c$	20.4	4.90	3.85×10^2	2.59
(4) $\text{CH}_3\text{COCH}_3^a$	20.7 ₀	4.83	3.32×10^2	2.52
(5) $\text{C}_6\text{H}_5\text{COBr}^d$	20.74	4.82	2.09×10^2	2.32
(6) $\text{CH}_3\text{CH}_2\text{CON}(\text{CH}_3)_2^e$	33.1	3.02	0.417×10^2	1.62
(7) $\text{HCON}(\text{CH}_3)_2^f$	36.7	2.72	0.123×10^2	1.09
(8) $\text{CH}_3\text{CON}(\text{CH}_3)_2^g$	37.8	2.65	0.200×10^2	1.30

^a This investigation. ^b H. M. Smiley and P. G. Sears, *Trans. Kentucky Acad. Sci.*, **18**, 40 (1957). ^c T. A. Gover and P. G. Sears, *J. Phys. Chem.*, **60**, 330 (1956). ^d V. Gutmann and K. Utvary, *Monatsh. Chem.*, **89**, 731 (1958). ^e E. D. Wilhoit and P. G. Sears, *Trans. Kentucky Acad. Sci.*, **17**, 123 (1956). ^f P. G. Sears, E. D. Wilhoit, and L. R. Dawson, *J. Phys. Chem.*, **59**, 373 (1955). ^g E. R. Lester, T. A. Gover, and P. G. Sears, *ibid.*, **60**, 1076 (1956).

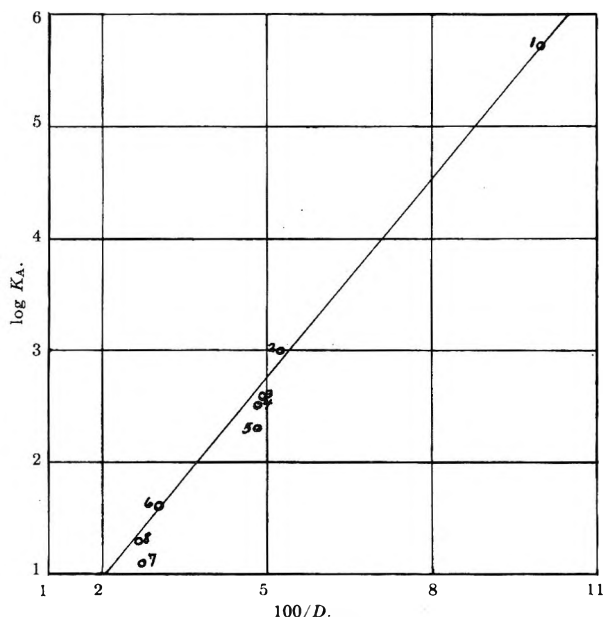


Figure 1. Dependence of the association constant of $(n\text{-C}_3\text{H}_7)_4\text{NBr}$ on the macroscopic dielectric constant of the solvent. Point numbers correspond to those given to the solvents in Table I.

satisfactorily the arrangement of the other six points. These two points were therefore not included in obtaining the straight line shown in Figure 1 which was established by the method of least squares. From the slope (0.592) of this line the value of the a parameter of $(n\text{-C}_3\text{H}_7)_4\text{NBr}$ ($a = \epsilon^2/230.3kT \times \text{slope}$) is determined and found to be 4.11×10^{-8} cm.

From the results of his X-ray analysis, Zalkin⁵ showed that $(n\text{-C}_3\text{H}_7)_4\text{NBr}$ crystallizes in the tetrag-

onal space group $I\bar{4}$ having the cell constants $a = 8.24 \pm 0.01 \text{ \AA}$. and $c = 10.92 \pm 0.01 \text{ \AA}$., with two molecules per unit cell. The ions pack in the cubic zinc sulfide type arrangement with each Br^- surrounded by a tetrahedron of $(n\text{-C}_3\text{H}_7)_4\text{N}^+$ ions and with each $(n\text{-C}_3\text{H}_7)_4\text{N}^+$ by a tetrahedron of Br^- ions. The distances between the Br^- at 0,0,0 and N at $1/2, 0, 1/4$, along the three-coordinate axis are therefore, $\Delta x = (1/2)a = 4.12 \text{ \AA}$., $\Delta y = 0$, and $\Delta z = (1/4)c = 2.73 \text{ \AA}$. It follows that

$$\text{N-Br distance} = \sqrt{(4.12)^2 + (2.73)^2} = 4.94 \text{ \AA}.$$

It is seen that the mean distance between the centers of the oppositely charged ions of this salt in associated ion pairs, 4.11 \AA ., as derived above (*viz.*, its a parameter) in the six nonaqueous solvents considered is 16.8% less than the N-Br distance, 4.94 \AA ., in its crystal.

Discussion

That the value of the a parameter of a salt in solution should be appreciably less than the minimum center-to-center distance between its oppositely charged ions in the crystalline state is corroborated by the results derived from the electron diffraction patterns¹³ and the microwave spectra¹⁴ given by the vapors of the halides of sodium, potassium, rubidium, and cesium. The values derived for the interatomic (*i.e.*, interionic) distances (designated the r_e values) in the molecules (*i.e.*, the associated ion pairs) of these halides in the vapor state were found in each of these investigations to be from ~ 10 to $\sim 17\%$ less than corresponding minimum distances in the respective crystals. Also, from the microwave spectra of the vapors of the chlorides, bromides, and iodides of monovalent thallium, indium, and gallium, Barrett and Mandel¹⁵ derived r_e values which were from 21 to 25% less than the corresponding crystallographic distances.

Since each ion in an associated ion pair whether in solution or in the vapor state is bonded or coordinated (electrostatically if the only force stabilizing the ion pair is coulombic) with only one ion of opposite charge, it seems reasonable to expect from results of the investigations referred to above that the distance between the ions in an associated ion pair of a salt in solution (namely its a parameter) will be appreciably less than the distance between each ion and its equidistant nearest neighbors of opposite charge in its crystal.

(13) L. R. Maxwell, S. B. Hendricks, and V. M. Mosley, *Phys. Rev.*, **52**, 968 (1937).

(14) A. Honig, M. Mandel, M. L. Stretch, and C. H. Townes, *ibid.*, **96**, 629 (1954).

(15) A. H. Barrett and M. Mandel, *ibid.*, **109**, 1572 (1958).

This expectation conforms with the well-known fact that the smaller the number of nearest neighbors of opposite charge coordinated or associated with any ion in a certain salt in the crystalline state, the smaller will be the minimum distance between the oppositely charged ions of this salt.

From these considerations it may be concluded that the value of the a parameter of a salt in solution however it may be derived from its K_A values, obtained from conductance measurements, should be appreciably less than the corresponding minimum distance between its oppositely charged ions in its crystal. The fact that the value of the a parameter obtained for $(n\text{-C}_3\text{H}_7)_4\text{NBr}$ in a series of one-component monomolecular solvents is appreciably less (approximately

17% less) than the N-Br distance in its crystal gives some credence to the method used in deriving its value, namely from the slope of the straight line which represents the relation between its $\log K_A$ values and those of $1/D$. It may be noted that this conclusion regarding the relative magnitude of the a parameter to that of the crystallographic distance may not be valid for a salt if the solvent molecules form such a stable complex with either of its ions that these complexing solvent molecules remain an integral part of that ion in the presence of oppositely charged ions.

Acknowledgment. We wish to thank Dr. J. D. McCullough for helpful suggestions and particularly for his aid in the interpretation of crystallographic data.

The Role of Copper(I) in the Kinetics of Hydrogen

Reduction of Aqueous Cupric Sulfate Solutions

by E. A. von Hahn and E. Peters*

Department of Metallurgy, The University of British Columbia, Vancouver, Canada (Received September 10, 1964)

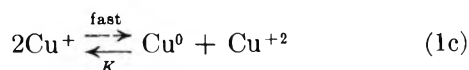
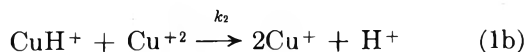
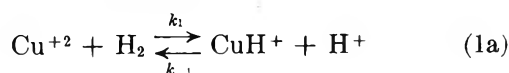
The kinetics and mechanism of the autocatalytic effect of cuprous ions in the hydrogen reduction of aqueous cupric sulfate solutions have been investigated at elevated temperatures and pressures. The reduction rates as measured by the appearance of the cuprous species were found to depend on the Cu^{I} and Cu^{II} concentrations and to be consistent with the rate equation

$$-\frac{d[\text{H}_2]}{dt} = \frac{k_1[\text{Cu}^{\text{II}}]^2[\text{H}_2]}{\frac{k_{-1}}{k_2}[\text{H}^+] + [\text{Cu}^{\text{II}}]} + \frac{k_3[\text{Cu}^{\text{I}}][\text{Cu}^{\text{II}}]^2[\text{H}_2]}{\left(\frac{k_{-1}}{k_2}[\text{H}^+] + [\text{Cu}^{\text{II}}]\right)\left(\frac{k_{-3}}{k_4}[\text{H}^+] + [\text{Cu}^{\text{II}}]\right)}$$

Values of the rate constants and ratios obtained at 160° are $k_1 = 3.2 \times 10^{-3} \text{ M}^{-1} \text{ sec.}^{-1}$, $k_3 = 6.4 \times 10^{-2} \text{ M}^{-1} \text{ sec.}^{-1}$, $k_{-1}/k_2 = 0.13$, and $k_{-3}/k_4 = 0.45$. Activation energies and entropies estimated for k_1 and k_3 are $E_1 = 22.4 \text{ kcal./mole}$, $\Delta S_1^* = -21 \text{ e.u.}$, $E_3 = 15.3 \text{ kcal./mole}$, and $\Delta S_3^* = -31 \text{ e.u.}$

Introduction

Extensive studies have been made in recent years on the kinetics of the homogeneous reduction of aqueous metal ions by hydrogen at elevated temperatures and pressures.¹ In particular, the reduction of the cupric salts and the catalytic activity of Cu^{I} toward H_2 have been investigated in considerable detail, especially in perchlorate and sulfate solutions.¹⁻⁶ It was shown⁶ that in perchlorate solutions the mechanism of this reaction can be represented by the set of equations



Subsequent experimental work^{2,7} revealed, further, that cuprous ions also exhibit moderate catalytic activity toward hydrogen in the perchlorate system, in addition to this mechanism, and up to 20% of the total reduction rates could be attributed to this effect. The cuprous species acted, thus, as a homogeneous

catalyst in the reduction of cupric ions. The mechanism of this effect, however, was not resolved since it was observable only if the rates were corrected for a perchlorate decomposition reaction.

Also, a considerable cuprous effect had been observed earlier in sulfate solutions³ although the kinetics of this effect were not completely resolved.

In view of the preceding it was decided to make a reinvestigation of the cuprous activity toward hydrogen. This study was conducted in sulfate solutions (a) because of the greater cuprous effect and (b) because

* To whom reprint requests should be addressed.

(1) (a) J. Halpern, *Advan. Catalysis*, 11, 301 (1959); (b) *J. Phys. Chem.*, 63, 398 (1959).

(2) E. Peters and E. A. von Hahn in "Unit Processes in Hydrometallurgy, Part II: Pressure Leaching and Reduction," M. E. Wadsworth and F. T. Davis, Ed., Gordon and Breach Science Publishers, Inc., New York, N. Y., in press.

(3) W. J. Dunning and P. E. Potter, *Proc. Chem. Soc.*, 244 (1960).

(4) J. Halpern, E. R. Macgregor, and E. Peters, *J. Phys. Chem.*, 60, 1455 (1956).

(5) E. A. Hahn and E. Peters, *Can. J. Chem.*, 39, 162 (1961).

(6) E. R. Macgregor and J. Halpern, *Trans. AIME*, 212, 244 (1958).

(7) E. A. Hahn, Ph.D. Thesis, The University of British Columbia, 1963.

of the greater stability of sulfate ions toward reduction by cuprous ions as compared to that of ClO_4^- .

For this purpose accurate measurements of the cuprous concentration in solution at experimental temperatures were required. For obtaining such measurements, disproportionation of Cu^{I} during sampling, owing to rapid cooling of the solutions, had to be prevented. This was achieved by utilizing a pressure-sampling technique developed in earlier studies of the perchlorate system.²

Experimental

Materials. All chemicals were of reagent grade, and distilled water was used throughout. Cupric sulfate stock solutions were prepared by dissolving CuO in sulfuric acid and diluting to the desired concentration. Nitrogen or helium and hydrogen were obtained from Canadian Liquid Air Co. and used without further purification.

Apparatus and Procedure. The experimental apparatus, procedure, and sampling technique have been described in detail.^{2,7} The autoclave used in these experiments was a 2-l. vessel manufactured by the Parr Instrument Co., with a capability of 1000 p.s.i.g. working pressure at 300° . All parts in contact with the experimental solutions were made of titanium. To follow the course of copper reduction, liquid samples were taken periodically, and the Cu^{I} concentration was determined. For obtaining the high temperature concentrations of these ions, a special sampling system was designed which included a pressurized sampling flask and a pressure "buret." These vessels were connected with each other and to the autoclave sampling valve with 0.16-cm. o.d. titanium tubing *via* a "tee." The hot solution samples flowing into the pressurized sampling flasks were oxidized with a measured amount of dichromate solution introduced into the sample stream from the pressure buret. Premature cooling of the solutions and disproportionation of cuprous ions was, thus, effectively prevented.

Analyses. The excess unreacted dichromate in the samples was determined with a Beckman DU spectrophotometer at $350\text{ m}\mu$, and, from the results, the cuprous concentrations were calculated by difference. The total amount of dissolved copper was determined electrolytically or by titration with EDTA. Total sulfate was determined as BaSO_4 .

Results and Discussion

The reduction of cupric sulfate by hydrogen and the catalytic effect of cuprous ions are illustrated in Figure 1 with a series of rate curves in the form of $[\text{Cu}^{\text{I}}]$ vs. time plots. These curves show an increase of rates

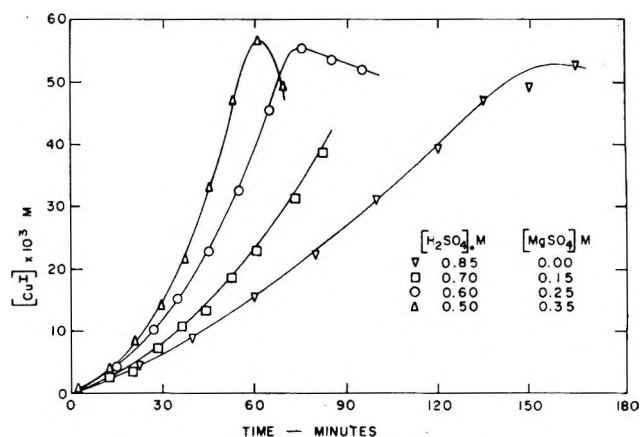
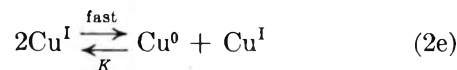
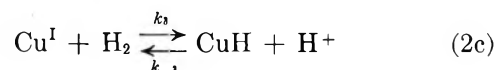
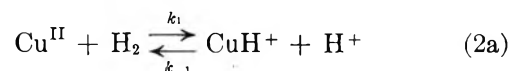


Figure 1. Rate curves as a function of sulfuric acid concentration; $0.15\text{ M } [\text{CuSO}_4]_0$, 5 atm. H_2 , 160° .

along a considerable portion of their length, despite the accompanying decrease in $[\text{Cu}^{\text{II}}]$, which indicates that the enhancing effect of Cu^{I} is large. It is further evident that both the initial rates and the catalytic effect of cuprous ions are lowered by raising the initial acid levels in solution.

Rates measured at several $[\text{Cu}^{\text{I}}]$ levels along the ascending portions of the curves are shown plotted against $[\text{Cu}^{\text{I}}]$ in Figure 2. The linearity of these plots suggests a first-order effect of the cuprous species. The intercepts obtained by extrapolating these curves to zero $[\text{Cu}^{\text{I}}]$ correspond to the reduction rates due to the activation of hydrogen by cupric ions alone. Also evident in Figure 2 is the adverse effect of acidity on both the cuprous- and cupric-activated reduction rates, as seen from the decreased slopes and intercepts with increased initial sulfuric acid concentration.

The most probable mechanism to describe the kinetic results is



where Cu^{II} and Cu^{I} are the sums of the aquo complexes and any possible sulfate complexes of these ions. The two-term rate law derived by a steady-state approximation in both of the reactive intermediates CuH^+ and CuH has the form shown in eq. 3.

$$\begin{aligned}
 -\frac{d[\text{H}_2]}{dt} &= \frac{k_1[\text{Cu}^{\text{II}}]^2[\text{H}_2]}{\frac{k_{-1}}{k_2}[\text{H}^+] + [\text{Cu}^{\text{II}}]} + \\
 &\quad \frac{k_3[\text{Cu}^{\text{I}}][\text{Cu}^{\text{II}}]^2[\text{H}_2]}{\left(\frac{k_{-1}}{k_2}[\text{H}^+] + [\text{Cu}^{\text{II}}]\right)\left(\frac{k_{-3}}{k_4}[\text{H}^+] + [\text{Cu}^{\text{I}}]\right)} \\
 &= R_{\text{Cu}^{\text{II}}} + R_{\text{Cu}^{\text{I}}} \quad (3)
 \end{aligned}$$

The present mechanism (eq. 2) had been proposed earlier by Dunning and Potter,³ and they had verified the first term of the rate law (eq. 3). However, their second cuprous-dependent term was linear in both $[\text{Cu}^{\text{II}}]$ and $[\text{H}^+]$ in the denominator, rather than the quadratic form shown here.

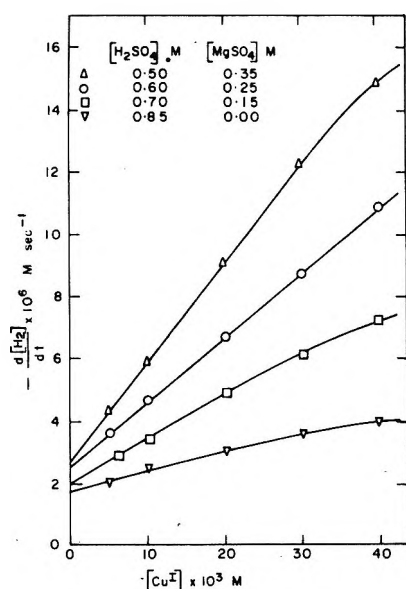


Figure 2. Plots of rate vs. $[\text{Cu}^{\text{I}}]$ as a function of acidity; 0.15 M $[\text{CuSO}_4]_0$, 5 atm. H_2 , 160°.

The expression for $R_{\text{Cu}^{\text{II}}}$ in eq. 3 corresponds to the rate values obtained from the intercepts, I , of the plots in Figure 2 since $R_{\text{Cu}^{\text{I}}}$, the cuprous dependent term, vanishes there. By inverting and rearranging $R_{\text{Cu}^{\text{II}}}$, one obtains

$$\begin{aligned}
 \frac{1}{R_{\text{Cu}^{\text{II}}}} &= \frac{1}{-d[\text{H}_2]/dt} = I^{-1} = \\
 &\quad \frac{\frac{k_{-1}}{k_2}[\text{H}^+]}{k_1[\text{Cu}^{\text{II}}]^2[\text{H}_2]} + \frac{1}{k_1[\text{Cu}^{\text{I}}][\text{H}_2]} \quad (4)
 \end{aligned}$$

which is a linear equation of I^{-1} in $[\text{H}^+]$. A linear plot of this form is depicted in Figure 3 for the inverse values

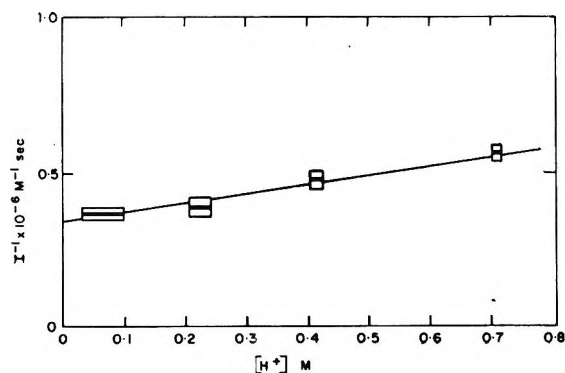


Figure 3. Plot of I^{-1} vs. $[\text{H}^+]$.

of the intercepts from Figure 2. Values of k_1 and k_{-1}/k_2 were calculated from the intercept and slope, respectively, of this plot with the appropriate expressions in eq. 4 and using H_2 solubilities for pure water⁸; they are $k_1 = (3.2 \pm 10\%) \times 10^{-3} \text{ M}^{-1} \text{ sec}^{-1}$ and $k_{-1}/k_2 = 0.13 \pm 30\%$.

The rate constant k_3 for the reaction of hydrogen with Cu^{I} and the ratio k_{-3}/k_4 can be evaluated from the initial slopes of the rate vs. $[\text{Cu}^{\text{I}}]$ plots in Figure 2 as follows. The slopes of these plots are equivalent to the equation

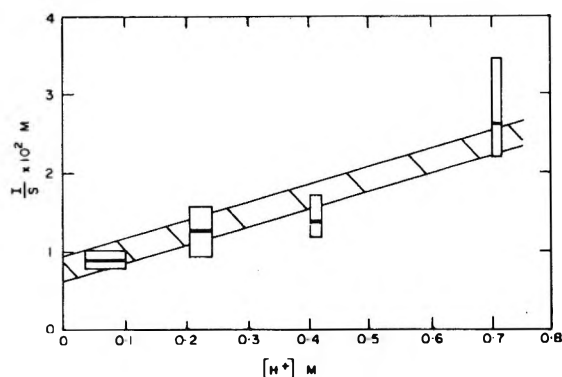
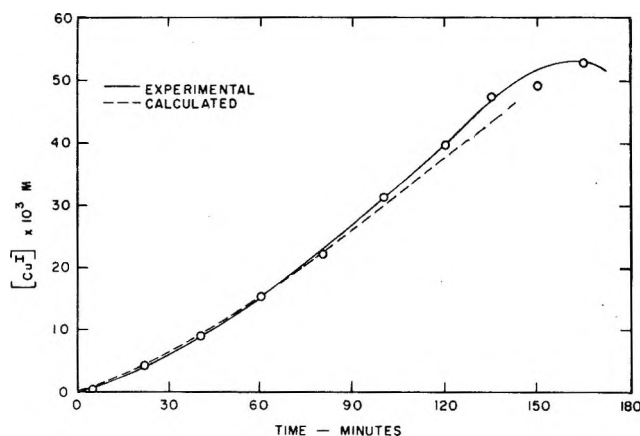
$$S = \frac{k_3[\text{Cu}^{\text{II}}]^2[\text{H}_2]}{\left(\frac{k_{-1}}{k_2}[\text{H}^+] + [\text{Cu}^{\text{II}}]\right)\left(\frac{k_{-3}}{k_4}[\text{H}^+] + [\text{Cu}^{\text{I}}]\right)} \quad (5)$$

where S is obtained on dividing $R_{\text{Cu}^{\text{I}}}$ by $[\text{Cu}^{\text{I}}]$. When S is divided into I (i.e., the first term in eq. 3), one obtains

$$\frac{I}{S} = \frac{k_1}{k_3} \times \frac{k_{-3}}{k_4}[\text{H}^+] + \frac{k_1}{k_3}[\text{Cu}^{\text{II}}] \quad (6)$$

which is a linear equation of I/S in $[\text{H}^+]$. Ratios of I/S for each experiment were calculated from the values of I and S measured from the intercepts and initial slopes, respectively, of the plots in Figure 2. They are shown plotted against $[\text{H}^+]$ in Figure 4. This plot is reasonably linear, despite the uncertainties introduced by the involved treatment of the experimental data. A value of $k_3 = (6.4 \pm 25\%) \times 10^{-2} \text{ M}^{-1} \text{ sec}^{-1}$ was calculated from the intercept of this plot, with the appropriate expression in eq. 6 and the earlier obtained value of k_1 . Similarly, a value of $k_{-3}/k_4 = 0.45 \pm 40\%$ was obtained from the slope of this plot. It is evident that k_3 is considerably larger than k_1 which reflects the high catalytic effect of the cuprous ions.

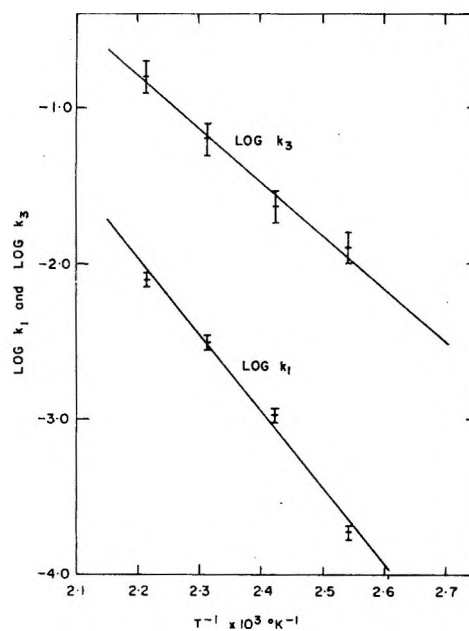
(8) R. T. MacAndrew, Ph.D. Thesis, The University of British Columbia, 1962.

Figure 4. Plot of I/S vs. $[H^+]$.Figure 5. Comparison of experimental and calculated rate curves; $0.15 M [CuSO_4]_0$, $0.85 M [H_2SO_4]_0$, 5 atm. H_2 , 160° .

The validity of the copper sulfate reduction mechanism given in eq. 2 was checked by a graphical integration of the rate law, eq. 3, using the rate constants and ratios obtained previously and the experimental conditions for one test. Figure 5 depicts both the experimental and integrated rate curves. The agreement between the two curves can be considered good, despite the uncertainties in the rate constants and ratios. Sources of these uncertainties are discussed below.

The activation energies and entropies for the hydrogen activation reactions involving Cu^{II} and Cu^I (eq. 2a and 2c) were obtained from Arrhenius plots of k_1 and k_3 (Figure 6). They are listed in Table I together with values by earlier workers. The agreement is reasonably good, despite the approximations used in calculating k_1 and k_3 at temperatures other than 160° (see below). The low value of 9.3 kcal. for E_3 is probably in error since it was obtained from the same experimental work as that of 15.9 kcal.

Values of k_1 and k_3 were estimated for 120, 140, and

Figure 6. Plots of $\log k_1$ and $\log k_3$ vs. T^{-1} .

180° by performing a single experiment at each of these temperatures under the following initial conditions: $0.15 M [CuSO_4]$, $0.70 M [H_2SO_4]$, $0.15 M [MgSO_4]$, and 5 atm. H_2 . Rate measurements from each test were plotted vs. $[Cu^I]$ in the same manner as shown in Figure 2. k_1 and k_3 were then calculated, respectively, from the intercepts and initial slopes of these plots with the first term of eq. 3, eq. 5, H_2 solubilities for pure water, $k_{-1}/k_2 = 0.13$, and $k_{-3}/k_4 = 0.45$. In these calculations it was assumed that both k_{-1}/k_2 and k_{-3}/k_4 did not change with temperature.⁹ Values of the rate constants for each temperature are listed in Table II.

The rate law and mechanism of this study were established from measurements along the initial sections of the rate curves in Figure 1 before disproportionation of cuprous ions had begun. However, the rate law is also valid after disproportionation since metallic copper was shown to have no catalytic effect on the activation of dissolved hydrogen.^{3,8} For it to have general applicability, the cupric and hydrogen ion concentrations must be given by $[Cu^{II}] = [Cu^{II}]_0 - [Cu^I] + Cu^0$ and $[H^+] = [H^+]_0 + [Cu^I] + 2Cu^0$. Before disproportionation $Cu^0 = 0$, and after disproportionation $Cu^0 = [Cu^{II}]_0 - [Cu^{II}] - [Cu^I]$, where $[Cu^{II}] = K[Cu^I]^2$, and K is the equilibrium constant for eq. 2e. The applicability of the rate law

(9) This assumption is based on an observation in the perchlorate system, where it was found that k_{-1}/k_2 remained nearly constant between 120 and 200° in the Cu^{+2} -catalyzed hydrogen reduction of dichromate.⁶

Table I: Summary of Activation Energies and Entropies

System	E_1 , kcal./mole	ΔS_1^* , e.u.	E_2 , kcal./mole	ΔS_2^* , e.u.	Source
Sulfate	22.4 ± 2.2	-21 ± 5	15.3 ± 1.4	-31 ± 3	This work
Sulfate	24	...	9.3	...	Ref. 3
Sulfate	23.5	-10.4	15.9	-34.5	Ref. a
Perchlorate	25.8 ± 1.7	-12.1 ± 4.5	Ref. 5

^a P. E. Potter, Ph.D. Thesis, The University of Bristol, 1958.

Table II: Values of k_1 and k_3 at Different Temperatures

Temp., °C.	k_1 , ^a $M^{-1} \text{sec.}^{-1}$	k_3 , ^a $M^{-1} \text{sec.}^{-1}$	$[\text{H}_2]$, M at 5 atm. ⁸
120	1.9×10^{-4}	1.3×10^{-2}	4.50×10^{-3}
140	1.1×10^{-3}	2.4×10^{-2}	5.13×10^{-3}
160	3.2×10^{-3}	6.4×10^{-2}	5.90×10^{-3}
180	7.8×10^{-3}	16.2×10^{-2}	6.80×10^{-3}

^a Estimated accuracy for k_1 is $\pm 10\%$; for k_3 , $\pm 25\%$ at each temperature.

in the presence of metallic copper was not verified in the present work. However, in the reduction of cupric perchlorate a similar rate law was shown to be valid in the presence of Cu^0 although the small cuprous effect on rates in that system was disregarded.⁷ In perchlorate solutions² $K = 26 M^{-1}$ at 160° .

One difficulty in evaluating the rate constants and ratios is the uncertainty of the correct hydrogen ion concentration in the experimental solutions at 160° , because of the lack of knowledge of the bisulfate dissociation constant K_b (or rather the concentration quotient) at the high experimental temperatures. In this work K_b was assumed to have a value in the range of 10^{-3} to $10^{-2} M$ at 160° ,¹⁰⁻¹² and the possible spread in the hydrogen ion concentration at each acid level was calculated on that basis. This spread, shown in Figures 3 and 4, is in part responsible for the uncertainties in the values of the rate constants and ratios.

The effect on the hydrogen ion concentration of complexing of free SO_4^{-2} with cupric and/or cuprous ions had to be disregarded since no information exists on the stability constants of these complexes at 160° , and the complex concentrations are also not known. It is clear, however, that $[\text{H}^+]$ would be increased by complexing of this kind. By inspection of Figures 3 and 4 it becomes evident that this increase would cause a lowering of the intercepts and an increase in the slopes of the linear plots since the relative increase in $[\text{H}^+]$ would be greatest at the lower acid levels. The result of this effect would be that the values of both rate constants and ratios would become larger.

The values of $k_1 = 3.2 \times 10^{-3} M^{-1} \text{sec.}^{-1}$ and $k_{-1}/k_2 = 0.13$ are smaller than those obtained in the Cu^{+2} -catalyzed reduction of dichromate in perchlorate solutions⁵ ($k_1 = 5.4 \times 10^{-3} M^{-1} \text{sec.}^{-1}$, $k_{-1}/k_2 = 0.4$). This is due partly to the uncertainty in $[\text{H}^+]$ for the reasons mentioned previously and partly to the use of hydrogen solubilities in pure water⁸ in calculating k_1 since no solubility data are available for these solutions at 160° . Both sulfate and perchlorate salts in solution will lower the hydrogen solubility, but this effect is greater in the sulfate solutions of the present work because of their higher ionic strength relative to that of the earlier work.⁵

The experimental evidence of this study indicates that the activation of hydrogen by both cupric and cuprous ions takes place by heterolytic splitting of the H_2 molecule resulting in the formation of copper hydrides (CuH^+ and CuH) and the simultaneous release of a proton in the activation step. The formation of CuH^+ in this activation reaction was shown to be energetically probable.¹³ CuH has been prepared in the solid state,¹⁴ and thermochemical data of the gaseous species have been published.¹⁵ Its formation in aqueous solutions in the H_2 activation reaction was also

(10) This estimate for K_b is based on the fact that its value decreases considerably with increasing temperature. For example, extrapolation of a linear plot of $\log K_b$ vs. temperature from published figures¹¹ between 5° ($K_b = 1.80 \times 10^{-2} M$) and 55° ($K_b = 4.1 \times 10^{-3} M$) gives a value of $K_b = 2 \times 10^{-4} M$ at 160° . These are values for solutions at infinite dilution and therefore are not applicable to the present experimental solutions because K_b increases markedly with ionic strength. Thus, a value of $K_b = 0.48 M$ was estimated from published data¹² for a $1.0 M \text{H}_2\text{SO}_4$ solution at 25° . If the above extrapolation to high temperatures is used for this figure, then, at 160° , $K_b = 9 \times 10^{-3} M$, which is within the specified range of the present work.

(11) R. W. Gurney, "Ionic Processes in Solution," Dover Publications, Inc., New York, N. Y., 1962, p. 121.

(12) C. J. Brubaker, *J. Chem. Educ.*, **34**, 325 (1957).

(13) E. Peters, Ph.D. Thesis, The University of British Columbia, 1956.

(14) H. J. Emeléus and J. S. Anderson, "Modern Aspects of Inorganic Chemistry," 3rd Ed., Routledge and Kegan Paul, Ltd., London, 1960, p. 415.

(15) (a) W. M. Latimer, "Oxidation Potentials," 2nd Ed., Prentice-Hall, Inc., Englewood Cliffs, N. J., 1952, p. 184; (b) F. D. Rossini, D. D. Wagman, W. H. Evans, S. Levine, and I. Jaffe, National Bureau of Standards Circular 500, U. S. Government Printing Office, Washington, D. C., 1952, p. 208.

shown to be probable on energetic grounds.⁷ The formation of other aqueous metal hydrides in the activation of hydrogen has been reviewed in the literature.¹

CuH is analogous to AgH which has been proposed to account, in part, for the kinetics of hydrogen activation by aqueous Ag⁺.¹⁶ The mechanism of activation by silver ions in aqueous perchlorate solutions involves both homolytic and heterolytic splitting of the H₂ molecule. The latter path predominates at higher temperatures (100 to 120°) and in dilute silver solutions (~0.01 M) whereas the former, being a termolecular reaction, is prevalent in the range of 30 to 70° at higher concentrations of Ag⁺ (~0.1 M). In view of this, it is plausible that cuprous ions also activate H₂ by homolytic splitting in aqueous systems, but this reaction never becomes important because at high temperatures it is masked by the heterolytic path, and at low temperatures the cuprous ions disproportionate to such an extent in acid solutions that concentrations high enough to permit observation of any activity cannot be obtained. The homolytic activation path occurs in quinoline solutions in the Cu^I-catalyzed hydrogen reduction of cupric acetate,¹⁷ and the activation step of this reaction, which was studied between 25 and 100°, is $2\text{Cu}^{\text{I}} + \text{H}_2 = 2\text{Cu}^{\text{I}}\cdot\text{H}$. The same reaction should also be observable in aqueous solutions in this temperature range if Cu^I is stabilized by complexing.

The activation energies and entropies for the heterolytic H₂ splitting mechanism by cuprous and silver ions are markedly different although both have the same charge and outer electron configuration. They are, for Cu^I, $E_a = 31$ kcal./mole and $\Delta S^* = -31$ e.u. (Table I); for Ag⁺,^{1b} $E_a = 24$ kcal./mole and $\Delta S^* = -10$ e.u. The lower values of E_a and ΔS^* for Cu^I as

compared to Ag⁺ are an indication that the heat of formation, ΔH° , and the partial molar entropy, S° , of the activated complex, Cu^I...H₂, are lower than those of the complex Ag⁺...H₂. This is in line with the published values of ΔH° and S° for the cuprous and silver ions.¹⁵ It suggests that water molecules are solvated to a greater extent by Cu^I...H₂ than by Ag⁺...H₂, which would be expected because the charge density of Cu^I, owing to its smaller ionic radius, is greater than that of Ag⁺.

The mechanism and rate law given in this paper for the hydrogen reduction of cupric sulfate are probably also valid for the perchlorate system. To resolve this question, further work is necessary in which the effect on reduction rates of perchlorate decomposition due to reaction with Cu^I is measured.

Conclusions

The rate of reduction of aqueous cupric sulfate by hydrogen depends, in part, on a strong first-order catalytic effect of cuprous ions. In this reaction the activation of hydrogen by both the cupric and cuprous ions occurs by heterolytic splitting of the H₂ molecule. Rate constants, calculated for the activation steps, using a two-term rate law, show Cu^I to be about 20 times more active toward H₂ than Cu^{II}.

Acknowledgment. Support of this work by a grant from the National Research Council of Canada and by a National Research Council Studentship to E. A. v. H. is gratefully acknowledged.

(16) A. H. Webster and J. Halpern, *J. Phys. Chem.*, **61**, 1239, 1245 (1957).

(17) W. K. Wilmarth and M. K. Barsh, *J. Am. Chem. Soc.*, **78**, 1305 (1956).

The Hydration of Tricalcium Silicate

by S. A. Greenberg¹ and T. N. Chang

Portland Cement Association, Skokie, Illinois (Received September 11, 1964)

In this investigation of the hydration of tricalcium silicate, the solutions were analyzed as a function of time for the concentrations of calcium and silicic acid. The electrical conductivities and pH values were also measured. The compositions of the solutions were examined as functions of the concentration of the tricalcium silicate and stirring speed. The rates of formation of hydrated calcium silicate from solutions of monosilicic acid and calcium ions were followed by light-scattering measurements. In the latter experiments the rate was examined as a function of the concentrations of reactants and of the pH values of the aqueous phases. The results substantiated the solution theory for hydration. The ions in crystalline tricalcium silicate, Ca^{+2} , O^{-2} , and SiO_4^{-4} , hydrolyzed during the solution reactions. When the concentrations of calcium and $\text{H}_2\text{SiO}_4^{-2}$ ions in solution are high, crystallization of hydrated calcium silicates occurs with the surfaces of the tricalcium silicate acting as nuclei. After the reactant surfaces are covered with hydration product, the reaction rate decreases. The light-scattering experiments indicate that the solution reaction proceeds by the combination of calcium and $\text{H}_2\text{SiO}_4^{-2}$ ions.

Introduction

The substances tricalcium silicate ($3\text{CaO}\cdot\text{SiO}_2$) and β -dicalcium silicate ($2\text{CaO}\cdot\text{SiO}_2$) are considered the most important constituents of portland cement. These constituents contribute to the formation of a hydrated calcium silicate gel which gives concrete its strength. Because it is important for the users of cement to control the rates of hydration and setting, it is necessary to know more about the mechanisms of hydration and gel formation for these constituents of cement. In this paper the mechanism of hydration of tricalcium silicate is discussed.

Le Chatelier^{2a} in the last century proposed that the hydrated calcium silicate and calcium hydroxide products precipitated from the supersaturated solutions produced by tricalcium silicate. It is now believed by many investigators that the hydrated calcium silicates immediately cover the surfaces of the unreacted tricalcium silicate particles.^{2b} After this surface layer is deposited, the reaction rate decreases and becomes dependent upon the rates of diffusion of the reactive species through this layer. Some Russian investigators³ follow the theory of Baikov,⁴ who proposed that, after an amorphous gel of hydrated calcium silicate forms, the particles in the gel crystallize.

Graham, Spinks, and Thorvaldson⁵ have conducted an extensive investigation of the hydration of tricalcium silicate. Efforts are being made^{2b} to write quantitative expressions for the kinetics of this heterogeneous reaction. The present study will provide some of the information necessary for a quantitative approach.

In the present study, samples of pure tricalcium silicate were stirred with water, and the compositions of the solutions were examined as a function of time by (1) calcium ion determinations, (2) analyses for silicic acid contents, (3) pH determinations, and (4) measurements of the electrical conductivities of the solutions. Solutions of monosilicic acid and calcium ions were mixed, and the rates of crystallization of the calcium silicate

(1) Merchrolab, Inc., Mountain View, Calif.

(2) (a) H. Le Chatelier, "Experimental Researches on the Constitution of Hydraulic Mortars," translated by J. L. Mack, McGraw-Hill Publishing Co., New York, N. Y., 1905; (b) for review see S. Brunauer and S. A. Greenberg, "Proceedings of the 4th International Symposium on the Chemistry of Cements," Washington, D. C., 1960.

(3) P. A. Reh binder, "Reports of Symposium on the Chemistry of Cements," P. P. Budnikov, *et al.*, Ed., State Publication of the Literature on Structural Materials, Moscow, 1956, pp. 125-137.

(4) M. Baikov, *Compt. rend.*, **182**, 128 (1926).

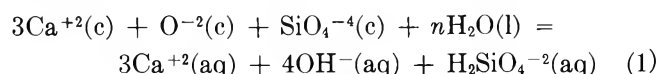
(5) W. A. G. Graham, J. W. T. Spinks, and T. Thorvaldson, *Can. J. Chem.*, **32**, 129 (1954).

product were followed by light-scattering measurements.

Theoretical

Before discussing the results of this investigation, it would be profitable to list the processes involved in a solution mechanism for the hydration of tricalcium silicate: (1) solution of the solid; (2) reaction of calcium ions, hydroxyl ions, silicic acid, and water in solution; (3) formation of nuclei of hydrated calcium silicate and calcium hydroxide crystals; (4) growth of the nuclei; (5) flocculation and precipitation.

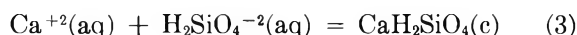
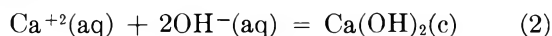
The crystals of tricalcium silicate contain calcium (Ca^{+2}), oxygen (O^{-2}), and silicate (SiO_4^{-4}) ions.⁶ During the solution reactions these ions will hydrate.



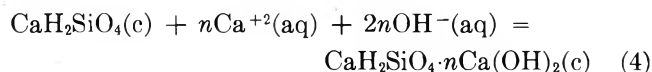
The $\text{H}_2\text{SiO}_4^{-2}(\text{aq})$ ions will hydrolyze to $\text{H}_3\text{SiO}_4^{-}(\text{aq})$ and $\text{H}_4\text{SiO}_4(\text{aq})$ species as a function of the dissociation constants of silicic acid H_4SiO_4 , the concentrations of silicic acid, and the pH of the solutions.⁷

Very little is known about the formation of hydrated calcium silicates or calcium hydroxide from solutions. These reactions fall into the general class known as hydrothermal. Hydrothermal reactions are those which proceed in the presence of liquid water and which have rates that increase with temperature. Morey and Ingerson⁸ proposed in 1934 that hydrothermal reactions were those in which products crystallized from aqueous solutions. Hydrated calcium silicates have been reported^{2b} to precipitate from solutions of sodium silicate and calcium salts.

When the concentrations of the calcium, silicate, and hydroxyl ions exceed the solubility products of hydrated calcium silicate and calcium hydroxide, these products will tend to precipitate.⁹ Reactions 2 and 3 will occur.



Additional calcium hydroxide may enter the hydrated calcium silicate structure by the reaction



The solubility product for hydrated calcium silicate

$$K_{\text{sp}_1} = a_{\text{Ca}^{+2}} a_{\text{H}_2\text{SiO}_4^{-2}} \quad (5)$$

(a refers to the activity of each ion) is 10^{-7} ($\text{p}K_{\text{sp}_1} = -\log K_{\text{sp}_1} = 7$). At 30° the activity solubility product for calcium hydroxide

$$K_{\text{sp}_2} = a_{\text{Ca}^{+2}} a_{\text{OH}^{-2}} \quad (6)$$

is 8.25×10^{-6} ($\text{p}K_{\text{sp}_2} = 5.08$).¹⁰ Therefore, solutions with $\text{p}K_{\text{sp}_1}$ and $\text{p}K_{\text{sp}_2}$ values less than 7 and 5.08 are supersaturated with hydrated calcium silicate or calcium hydroxide, respectively. Those solutions which exhibit $\text{p}K_{\text{sp}}$ values greater than the equilibrium values are unsaturated.

Experimental

Materials. A sample of pure tricalcium silicate with a surface area of 4400 cm^2/g . was kindly supplied by Dr. D. Kantro and Mr. C. Weise of this laboratory. This sample has been described.¹¹ The sample contained 0.75% free calcium oxide. Evidence for only a trace of dicalcium silicate was noted in the X-ray pattern. Solutions of calcium hydroxide, calcium nitrate, and sodium silicate were prepared from Baker A.R. grade chemicals. Mallinckrodt standard luminescent grade silica gel was shaken with distilled, boiled water to prepare solutions of monosilicic acid.

Equipment. A Leeds and Northrup pH meter, a glass measuring electrode, and a calomel reference electrode were used for obtaining the pH values of the solutions. For measuring the electrical resistances of the solutions, an Industrial Instruments Co. bridge, Model R. C., and a dip conductivity cell with a constant of 2 were employed. The Brice-Phoenix spectrophotometer¹² was used for the 135, 90, and 45° scattering measurements. The scattering was performed with 4360-Å light. The solutions were filtered through Millipore HA filters, size 0.45 μ (Millipore Filter Corp., Bedford, Mass.). It is possible to make water almost dust-free by this procedure.

Procedures A. Reactions of Soluble Species. Solutions of monosilicic acid or sodium silicate were mixed with solutions of calcium hydroxide or nitrate or mixtures of the latter solutions and placed in a 40×40 mm. semioctagonal, light-scattering cell. Light-scattering measurements were made as a function of time.

B. Hydration of Tricalcium Silicate. Solutions were placed in a three-necked flask with a stirrer in one neck; a thermometer, conductivity cell, or tube to withdraw samples could be inserted in the other two

(6) J. D. Bernal, J. W. Jeffery, and H. F. W. Taylor, *Mag. Concrete Res.*, **11**, 49 (1952).

(7) S. A. Greenberg, *J. Am. Chem. Soc.*, **80**, 6508 (1958).

(8) G. W. Morey and E. Ingerson, *Econ. Geol.*, **32**, 607 (1937).

(9) S. A. Greenberg, T. N. Chang, and E. Anderson, *J. Phys. Chem.*, **64**, 1151 (1960).

(10) S. A. Greenberg and L. E. Copeland, *ibid.*, **64**, 1057 (1960).

(11) D. L. Kantro, S. Brunauer, and C. H. Weise, *Advances in Chemistry Series*, No. 33, American Chemical Society, Washington, D. C., 1961, p. 199.

(12) B. A. Brice, M. Halwer, and R. Speiser, *J. Opt. Soc. Am.*, **40**, 768 (1950).

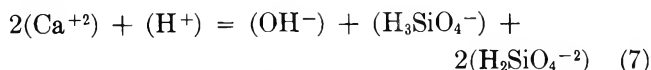
necks. The flasks were placed in a constant temperature bath at $30 \pm 0.02^\circ$. The samples were stirred at moderate speeds, and at various reaction times portions of the solutions were withdrawn and filtered through a fine, sintered glass filter in the absence of carbon dioxide. Analyses were made immediately to avoid the possibility of precipitation from the super-saturated solutions.

Efforts were made to exclude carbon dioxide by making seals in the equipment airtight and by passing nitrogen through the solutions. However, these extra precautions were found to be unnecessary.

Analyses of Solutions. The calcium concentrations were determined by a versene titration with Eriochrome Black T as indicator.¹³ The molybdenum blue method¹⁴ was employed for the determination of soluble monosilicic acid, H_4SiO_4 . The pH and electrical resistance values of the solutions were also measured.

Evaluation of the Solubility Products. It is possible to evaluate the activities of the calcium, hydroxyl, and $\text{H}_2\text{SiO}_4^{-2}$ ions from a knowledge of the concentrations of calcium ions and silicic acid, the pH values of the solutions, the Debye-Hückel theory,¹⁵ the dissociation constants of silicic acid,⁷ and the constants for water.

It is convenient to keep in mind two equations when examining the compositions of solutions of hydrated calcium silicates. One is the electroneutrality equation



where the quantities in parentheses are the concentrations in moles/l. The hydrogen ion concentration is negligible in the basic solutions and can be neglected. The second equation relates the total concentration of silicic acid in solution to the concentration of each species



It is assumed that all silicic acid in solution is monomeric. The amount of monomeric silicic acid in solution can be detected in the presence of colloidal silicic acid in solution.¹⁴

The first and second dissociation constants for silicic acid, H_4SiO_4 , may be expressed by the equations

$$K_1 = \frac{a_{\text{H}^+}(\text{H}_3\text{SiO}_4^-)f_{\text{H}_3\text{SiO}_4^-}}{(\text{H}_4\text{SiO}_4)f_{\text{H}_4\text{SiO}_4}} \quad (9)$$

$$K_2 = \frac{a_{\text{H}^+}(\text{H}_2\text{SiO}_4^{-2})f_{\text{H}_2\text{SiO}_4^{-2}}}{(\text{H}_3\text{SiO}_4^-)f_{\text{H}_3\text{SiO}_4^-}} \quad (10)$$

where the activity a is the product of the concentration and activity coefficient, f , of each species, and the

quantities in parentheses are the concentrations in moles/l. Since H_4SiO_4 is not ionic, the activity coefficient of this species may be assumed to be unity.¹⁶⁻¹⁸ The negative logarithms of the ionization constants for silicic acid, $\text{p}K_1$ and $\text{p}K_2$, are 9.7 and 11.7 at 30° , respectively.⁷

From the experimental data and solution theory the activities of the hydroxyl, calcium, and silicate ions were evaluated.

Results

Solution Reactions. The dependence of reaction rate on calcium concentration was examined first. Solutions of sodium silicate, 0.004 M in monosilicic acid, were mixed with equal volumes of calcium nitrate solutions. In the three experiments, the final concentrations were 0.002 M in monosilicic acid and 0.0001, 0.0003, and 0.0005 M in calcium ions. The pH values of the solutions were 12 ± 0.1 . The light scattered from the solutions was measured at 135, 90, and 45° as a function of reaction time. The 90° scattering results are shown graphically in Figure 1. It may be noted that the rate of change of scattering increases markedly with calcium concentration. The dissymmetries, $Z = i_{45}/i_{135}$, for values greater than 1.2 were corrected for reflection of the primary beam at the exit window of the cell.¹⁹ The dissymmetries of these solutions were in the range 6 ± 1 , and no correlation between the amount of reaction and reaction time was evident.

The rates of reaction were measured also as functions of pH. Solutions of monosilicic acid were mixed with solutions of calcium hydroxide or mixtures of calcium hydroxide and calcium nitrate. The concentrations of monosilicic acid and calcium ions were 0.001 and 0.005 M , respectively. Solutions B, C, and D exhibited pH values of 11.9, 11.7, and 11.4, respectively. To obtain a solution with a higher pH value, a solution of sodium silicate was mixed with a saturated solution of calcium hydroxide. This solution (A) exhibited a pH value of 12. Figure 2 demonstrates the scattering at 90° of these solutions as a function of reaction time.

(13) H. H. Willard, N. H. Furman, and C. E. Bricker, "Elements of Quantitative Analysis," 4th Ed., D. Van Nostrand Co., Inc., Princeton, N. J., 1956, p. 138.

(14) W. E. Bunting, *Ind. Eng. Chem., Anal. Ed.*, **16**, 612 (1944).

(15) P. Debye and E. Hückel, *Physik. Z.*, **24**, 185, 305 (1923).

(16) S. A. Greenberg and E. P. Price, *J. Phys. Chem.*, **61**, 1539 (1957).

(17) R. G. Bates, "Electrometric pH Determinations," John Wiley and Sons, Inc., New York, N. Y., 1954.

(18) H. S. Harned and B. B. Owen, "The Physical Chemistry of Electrolytic Solutions," 2nd Ed., Reinhold Publishing Corp., New York, N. Y., 1950, Chapter 15.

(19) R. Moore, *J. Polymer Sci.*, **10**, 551 (1953).

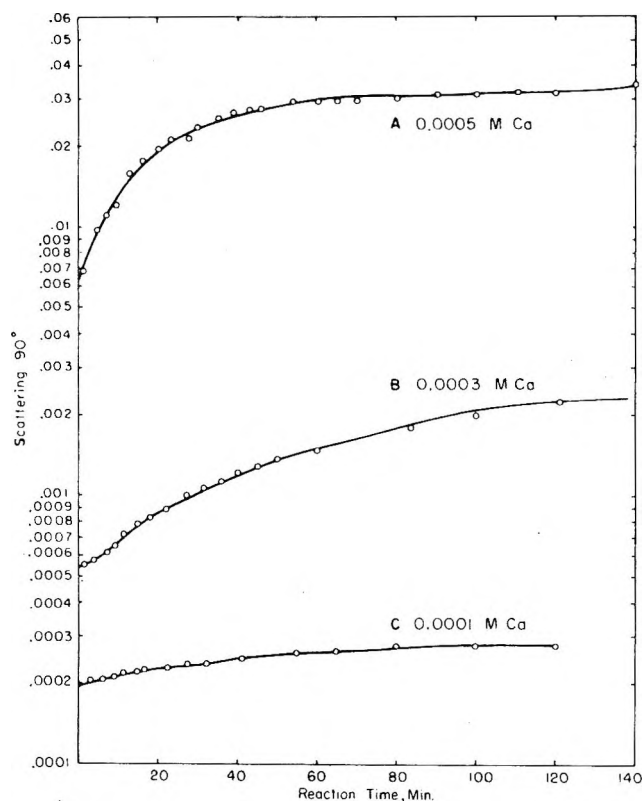


Figure 1. The dependence of the rate of reaction of calcium ions and monosilicic acid in solution on the calcium concentration.

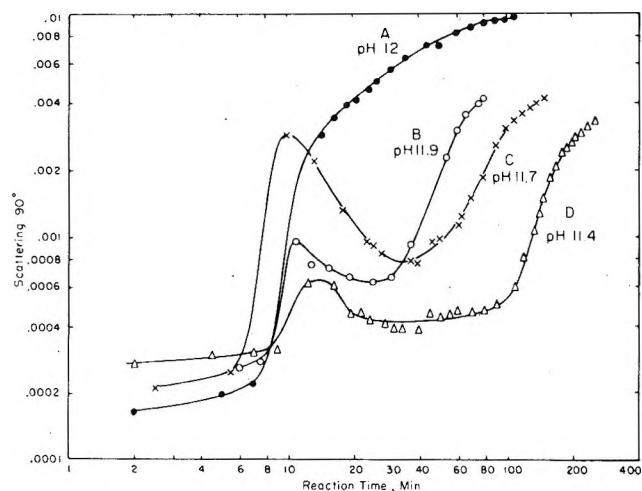


Figure 2. The rate of formation of hydrated calcium silicate from soluble calcium ions and monosilicic acid as a function of pH.

Solutions with the same silicic acid and calcium ion concentrations at pH values lower than 11.4 did not exhibit any turbidity in 24 hr. It may be seen in Figure 2 that the 90° scattering curves for solutions B,

C, and D rise to a peak at 10 to 13 min. Solution A with a pH of 12 did not exhibit this peak. After 30 min. of reaction time, it may be noted that the rate of increase of 90° scattering is a function of pH.

The dissymmetry values of the solutions A to D varied considerably with reaction time. Peaks in the dissymmetry between 9.6 and 16.0 were observed at 10 to 13 min. of reaction time. Solution C exhibited a second peak of 12.2 at 50 min. of reaction time. After 200 min. of reaction time the dissymmetries of the solutions A–D decreased to 4.

The peaks in the 90° scattering–reaction time curves (Figure 2) and in the dissymmetry may be attributed partially to the changes in size of the growing particles, to the anisotropy of hydrated calcium silicate particles, and to flocculation.

The reaction times necessary to form turbid solutions were observed. At pH 12.2, 11.9, 11.7, and 11.4 the times were 3 min., 1, 3, and 20 hr., respectively.

Hydration of Tricalcium Silicate. The compositions of solutions containing 0.25, 1.25, and 5.0 g. of tricalcium silicate/l. of water were determined as a function of time. In Tables I–III and Figures 3–5 the results are given. In the tables the following quantities are listed in order: (1) reaction time, (2) and (3) concentrations of calcium and silicic acid, (4) the mole ratio CaO:SiO₂ in solution, (5) pH, (6) pK_{sp1} for hydrated calcium silicate, and (7) pK_{sp2} for calcium hydroxide.

Table I: The Compositions of Solutions at 30° for 0.25 g. of $3\text{CaO}\cdot\text{SiO}_2/\text{l.}$

Reaction time, min.	(Ca) _t × 10 ³ , moles/l.	(SiO ₂) _t × 10 ⁴ , moles/l.	CaO:SiO ₂ in soln.	pH	pK_{sp1}	pK_{sp2}
2	2.11	6.42	3.28	11.50	6.51	7.48
5	2.67	8.17	3.26	11.53	6.31	7.33
10	2.95	9.00	3.28	11.57	6.22	7.22
15	3.02	9.33	3.23	11.59	6.18	7.17
30	3.09	9.75	3.17	11.65	6.10	7.04
42	3.24	9.75	3.32	11.60	6.14	7.12
52	3.05	9.92	3.07	11.60	6.15	7.15
62	3.22	8.33	3.86	11.69	6.16	6.95
80	3.14	10.83	2.90	11.69	6.06	6.95
100	3.05	8.92	3.42	11.60	6.20	7.15
124	3.30	10.10	3.27	11.59	6.12	7.14
150	3.14	10.00	3.14	11.65	6.11	7.03
185	3.08	10.25	3.00	11.60	6.13	7.14
223	3.14	10.17	3.09	11.65	6.10	7.03
260	3.10	10.17	3.05	11.60	6.13	7.14
21 hr.	2.95	6.33	4.66	11.60	6.35	7.26

When 0.25 g. of tricalcium silicate was placed in 1 l. of water and stirred at a moderate speed, the suspension

Table II: The Compositions of Solutions at 30° for 1.25 g. of 3CaO·SiO₂/l.

Reaction time, min.	(Ca) _t × 10 ³ , moles/l.	(SiO ₂) _t × 10 ⁴ , moles/l.	CaO:SiO ₂ in soln.	pH	pK _{sp1}	pK _{sp2}
2.5	3.85	11.9	3.23	11.80	5.91	6.66
7	4.00	11.6	3.46	11.80	5.91	6.65
18	3.94	11.4	3.41	11.85	5.90	6.55
35	4.26	19.1	2.23	11.93	5.63	6.37
60	4.68	5.43	8.62	12.00	6.13	6.19
94	5.01	5.93	8.45	12.10	6.05	5.97
120	4.90	2.88	17.0	12.07	6.38	6.04
180	5.23	1.80	29.0	11.90	6.61	6.35
285	5.23	1.37	38.2	12.07	6.68	6.01
20 hr.	5.55	0.766	72.5	12.10	6.91	5.93

Table III: The Compositions of Solutions at 30° for 5 g. of 3CaO·SiO₂/l.

Reaction time, min.	(Ca) _t × 10 ³ , moles/l.	(SiO ₂) _t × 10 ⁴ , moles/l.	CaO:SiO ₂ in soln.	pH	pK _{sp1}	pK _{sp2}
3.5	4.72	10.5	4.48	11.86	5.88	6.47
8	5.02	9.47	5.30	11.92	5.89	6.33
15	5.22	8.10	6.44	12.00	5.92	6.15
25	6.89	5.83	11.8	12.10	5.97	5.86
30	7.18	4.53	15.9	12.20	6.05	5.64
35	7.14	3.90	18.3	12.28	6.11	5.48
40	7.78	2.93	26.6	12.30	6.21	5.41
50	7.87	2.03	38.8	12.45	6.35	5.11
60	8.37	2.77	30.2	12.40	6.20	5.19
70	8.61	1.33	64.7	12.42	6.51	5.14
80	8.86	1.17	75.7	12.60	6.55	4.77
95	9.45	1.00	94.5	12.52	6.61	4.91
110	9.74	1.05	92.8	12.55	6.58	4.84
130	10.3	0.783	132	12.66	6.68	4.60
160	10.3	0.767	134	12.64	6.69	4.64
200	11.0	0.667	165	12.76	6.73	4.38

became clear in 20 min. Only in the case of the 0.25-g. sample was solution complete.

A. pH Values of Solutions. The pH values of the solution containing 0.25 g. of tricalcium silicate/l. remained almost constant and changed from only 11.50 to 11.60 in 21 hr. (Table I, column 5). Table II shows that with 1.25 g. of solids/l. the pH values rise smoothly from 11.80 to 12.10 in 94 min. After 20 hr. the pH was 12.10. An increase in the pH values of the 5-g./l. mixture from 11.86 to 12.76 may be noted in Table III. A saturated solution of calcium hydroxide at 30° was reported by Bates, *et al.*,²⁰ to exhibit a pH value of 12.29.

B. Calcium Concentrations. It may be seen in

Table I, column 2, that the calcium concentration of the 0.25-g./l. solution increased in 30 min. from 2.11×10^{-3} to 3.09×10^{-3} mole/l. The data in Table II show that the calcium concentration of the 1.25-g./l. solution rose to 5.23×10^{-3} mole/l. in 180 min. The calcium concentration of the 5-g./l. solution is shown in Table III to increase gradually from 4.72×10^{-3} to 11.0×10^{-3} mole/l. in 200 min.

C. Silicic Acid Concentrations. The 0.25-g./l. solution showed a smooth, rapid increase in concentration (Figure 3; Table I, column 3) to about 9×10^{-4} mole/l. in 10 to 15 min. Figure 3 demonstrates the

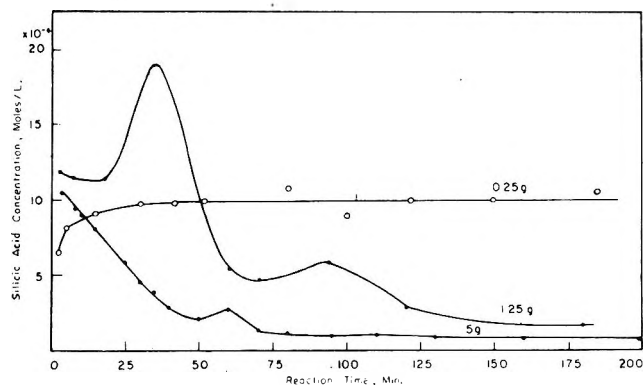


Figure 3. The silicic acid concentrations as a function of reaction time.

fluctuations in the concentration of the silicic acid in the 1.25-g./l. solution. This experiment was repeated to check the reproducibility of the fluctuations in the silicic acid concentration. Maxima may be seen in this curve at 35 and 94 min. However, after 35 min. the concentration gradually decreased to 0.766×10^{-4} mole/l. at 20 hr. (Table II). The curve in Figure 3 shows a slow decrease in concentration of the 5-g./l. solution from 10.5×10^{-4} to 0.667×10^{-4} mole/l. in 200 min. (Table III). A small peak at 60 min. may be noted.

D. Mole Ratio CaO:SiO₂. The mole ratio of the 0.25-g./l. solution was approximately 3:1 (Table I, column 4) over 260 min. of reaction time. After 21 hr. the ratio rose to 4.66. This indicates that the solid dissolves completely, and only sometime between 260 min. and 21 hr. does a hydrate product form. If all the sample had dissolved, the theoretical concentrations would have been 3.3×10^{-3} mole of calcium/l. and 1.1×10^{-3} mole of monosilicic acid/l. The solutions were found to contain maximum concentrations of $3.3 \times$

(20) R. G. Bates, V. E. Bower, and E. R. Smith, *J. Res. Natl. Bur. Std.*, **56**, 305 (1956).

10^{-3} mole of calcium/l. and 1.08×10^{-3} mole/l. of silicic acid. The differences between the experimental and theoretical values may be attributed to errors in the analysis or to the deviation of the tricalcium silicate from the theoretical composition.

The CaO:SiO₂ mole ratios of the 1.25-g./l. solution are listed as a function of time in Table II. It may be seen that the ratio increases from 3.23 to 72.5 in 20 hr. From a knowledge of the solution composition and the quantity of tricalcium silicate added to the water, it is possible to calculate the mole ratio of CaO:SiO₂ in the solids. Initially, the solids exhibited a ratio of 3:1, but, as the reaction proceeded, the ratio dropped to 2:1 in 20 hr. Presumably, under these conditions at complete reaction the ratio would be lower than 2:1.

An increase in the CaO:SiO₂ ratio of the 5-g./l. solution to 165 in 200 min. may be seen in the data listed in Table III.

E. Silicate Solubility Products. The pK_{sp1} values of the 0.25-g./l. solution are given in Figure 4 and Table I, column 6. The product is an indication of the degree of saturation of the solution. The equilibrium pK_{sp1} value is 7.0 ± 0.1 for a silicate formed from calcium oxide, silica gel, and water.⁹ A line corresponding to this value is drawn in Figure 4. Values of pK_{sp1} lower than 7.0 indicate a supersaturated solution. The pK_1 values of the 0.25-g./l. solution may be seen to decrease to 6.22 in 10 min., after which the value remained almost constant for 260 min. After 21 hr., the value increased to 6.35.

In Figure 4 and Table II the pK_{sp1} values for the 1.25-g./l. solution may be seen to rise from 5.91 to 6.91 in 20 hr. The pK_{sp1} values of the 5-g./l. solution decreased from 5.88 to 6.73 in 200 min. (Table III, Figure 4).

F. Calcium Hydroxide Solubility Products. In Figure 5 and Table I, column 7, the pK_{sp2} values for calcium hydroxide of the 0.25-g./l. solution may be seen to remain essentially constant at about 7.1 after 10 min. The 7.1 value demonstrates that this solution is unsaturated with respect to calcium hydroxide solid, which exhibits a pK_{sp2} of 5.08.¹⁰ It may be observed in Table II that the pK_{sp2} values of the 1.25-g./l. solution decrease from 6.66 to 6.04 in 2 hr. However, the pK_{sp2} values do not decrease below the equilibrium value even in 20 hr. The pK_{sp2} data in Table III of the 5-g./l. solution show a decrease from 6.47 to 4.38 in 200 min. At about 70 min. the pK_{sp2} value is below the equilibrium value, which demonstrates that the solution is supersaturated with respect to calcium hydroxide.

It is interesting to note that the fraction of tricalcium

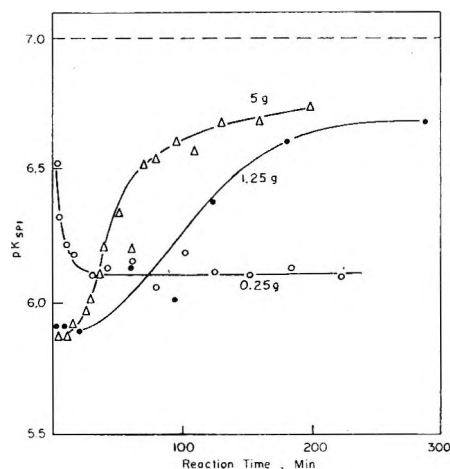


Figure 4. The pK_{sp2} values for hydrated calcium silicate as a function of time.

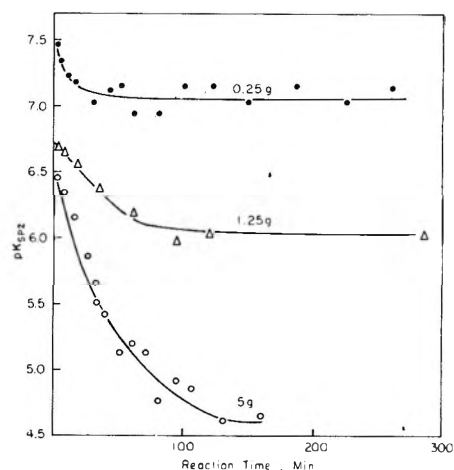


Figure 5. The change with reaction time in pK_{sp2} values for calcium hydroxide.

silicate that dissolved in 3 min. decreased with weight of sample per liter of solution in the range 0.25 to 5 g. In the range 0.25 to 5 g. of sample per liter, the fraction dissolved was reduced from 64 to 7%. The fraction dissolved is defined as the ratio in moles of the calcium in solution at 3 min. to the moles of calcium in the original tricalcium silicate sample.

The Paste Experiment. The trend shown in Figure 4 that the rate at which the solution becomes saturated with respect to hydrated calcium silicate increases with the amount of tricalcium silicate was tested again. A paste with a 0.7:1 water-tricalcium silicate ratio by weight was examined. To 70 ml. of water at 15.5°, 100 g. of tricalcium silicate was added in 15 sec. with mild agitation. For 45 sec. the paste was vigorously agitated in a Waring Blender which brought the tempera-

ture to 25.5°. After 1.75 min. the aqueous phase was separated from the solids on a porous glass filter.

The solution was immediately analyzed. A pH value of 12.8, a calcium concentration of 0.032 mole/l., and a silicic acid concentration of 0.667×10^{-4} mole/l. were found. The K_{sp1} value corresponding to this solution is 1.1×10^{-7} ($pK_{sp1} = 6.96$), which is within experimental error the equilibrium value for hydrated calcium silicate. Therefore, we may conclude that the saturation concentration was reached within 2.75 min.

The Electrical Resistance Measurements. The electrical conductivities of stirred suspensions of tricalcium silicate in water were measured. The concentrations were varied between 0.20 and 1.25 g./l. of tricalcium silicate. In Figure 6 the results are shown. The specific resistance of each solution may be seen to fall with time and then level off. In each curve a plateau appears for a few minutes between 10 and 20 min. It is interesting to note that the curves for 0.5- and 1.25-g. samples level off at the same resistance. This behavior demonstrates that, when more than 0.5 g. of sample/l. is added, the silicate does not dissolve completely. Even the 0.5-g. sample may not have dissolved completely.

A comparison of the specific resistances of tricalcium silicate solutions after 140 min. of hydration (Figure 7) with those of calcium hydroxide solutions having the same concentration of calcium illustrates several things. The resistances of the calcium hydroxide solutions are

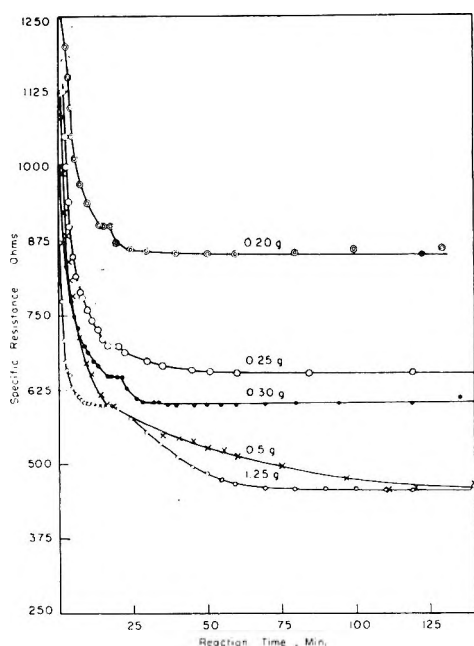


Figure 6. The change in specific resistance as a function of time.

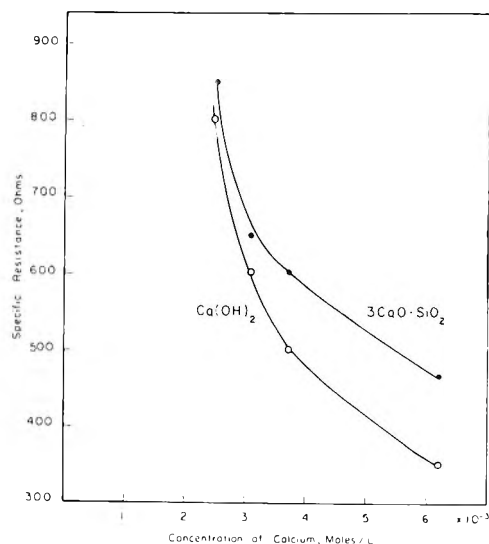


Figure 7. The specific resistances of tricalcium silicate and calcium hydroxide solutions of the same total calcium ion content.

lower than those for the silicate solutions. The calcium hydroxide solutions contain calcium and hydroxyl ions whereas the tricalcium silicate solutions consist of calcium, hydroxyl, $H_2SiO_4^{-2}$, and $H_3SiO_4^{-}$ ions. Since the ion conductance of hydroxyl ions at 25° is $198.5 \text{ ohm}^{-1} \text{ cm.}^2$ compared with the $35 \text{ ohm}^{-1} \text{ cm.}^2$ for the ion conductance of $H_2SiO_4^{-2}$,⁷ the silicate solutions should show higher resistances than the calcium hydroxide solutions. This is actually the case, but it was found, also, that the differences in resistances as shown in Figure 7 increased with the amount of tricalcium silicate added to water. This would indicate that complete solution does not occur with concentrations of solids greater than about 0.5 g./l. since, otherwise, the curves in Figure 7 would be approximately parallel.

The Effect of Stirring on Rate. This effect was examined in order to obtain some information on the mechanism of solution of tricalcium silicate. To 1 l. of water, a 0.25-g. sample was added. It will be recalled that this sample will dissolve completely if the mixture is stirred. The curves in Figure 8 demonstrate the results. Curve 1 illustrates the resistance vs. time relationship for no stirring, except for an initial 0.5-min. mixing. Curves 2 and 3 show the effects of increased stirring speed. It will be noted that the rates of solution or slopes of the curves increase with stirring speed. It is also apparent that the resistance values at which the curves level off decrease with an increase in stirring speed. It may be concluded that, unless the dissolving species are removed from the surface, crystallization of the product will proceed there.

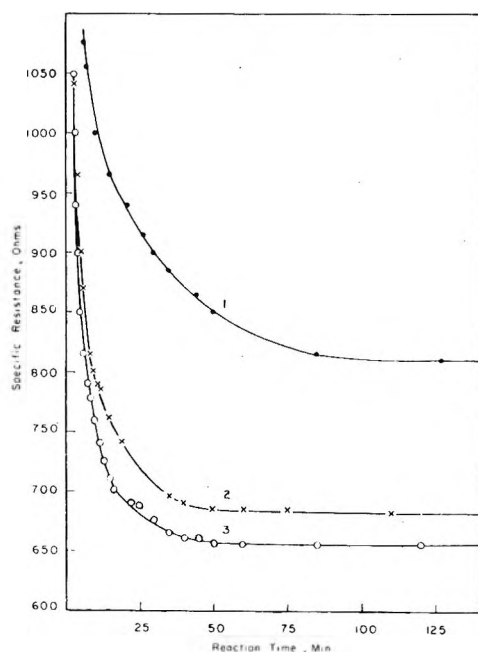


Figure 8. The effect of stirring speed on the rate of hydration.

X-Ray Measurement. Samples of 1.25 g. of tricalcium silicate in 1 l. of water at 30° were stirred at a fast rate. After 100 and 200 min., 500-ml. portions of the solutions were removed and filtered in a carbon dioxide-free box. The solid residues were vacuum dried for 2 weeks. Then X-ray patterns of the sample were made. The patterns showed strong lines for tricalcium silicate, a trace of dicalcium silicate, and evidence for the presence of hydrated calcium silicate. No evidence for calcium carbonate was detected.

Discussion

Mechanism of Reaction. The experiments show that it is possible to dissolve small amounts of tricalcium silicate completely in water. Therefore, the hydration of the ions in tricalcium silicate shown in eq. 1 can go to completion under the proper conditions. On the other hand, the results also illustrate that, if the calcium and silicic acid species are not diluted by being immediately carried into the solution by agitation of the suspension, these species may combine on the surfaces of the particles to form hydrated calcium silicates. Therefore, the surface of the tricalcium silicate serves as a site for nucleation and growth.

The rate at which the solution approaches equilibrium, with respect to the hydrated calcium silicate product, increases with the weight or surface area of calcium silicate (Figure 4) until it is almost instantaneous with concentrated suspensions. The rate of nucleation is, apparently, relatively slow in the case of

the 0.25-g. sample which dissolves completely. The solution with this amount of sample begins to reach equilibrium with respect to hydrated calcium silicate in about 20 hr.

Even after 200 min., the 5-g./l. solution was supersaturated with respect to calcium hydroxide. It has been fairly well established that supersaturated solutions of calcium hydroxide are relatively stable.²⁰ Therefore, it may be concluded from these experiments that calcium hydroxide crystals are slow to form under these conditions.

After the initial rapid reaction of the surface of tricalcium silicate with water, further reaction in concentrated mixtures proceeds from a solution which is only slightly supersaturated with respect to the hydrated calcium silicate product but highly supersaturated with respect to calcium hydroxide. This, of course, demonstrates that the rate of crystallization of the hydrated silicate product from solution is much faster than the rate of hydration after the initial surface reaction.

The changes in silicic acid concentration with time (Figure 3) demonstrate, also, the processes of reaction. In the case of the 0.25-g. sample, no precipitation occurs initially. Consequently, the concentration increases steadily with time. The concentration in the 5-g./l. solution shows only a decrease with time, with the exception of a small maximum at 60 min. On the other hand, the concentration for the 1.25-g. sample first builds up and then drops sharply. Therefore, one may conclude that, in the presence of sufficient reactant (5-g. sample), crystallization of the product proceeds immediately. However, at intermediate concentrations (1.25-g. sample) some time (40 min.) elapses before the silicic acid concentration is sufficient to cause rapid crystallization. Similar results were found for the solution reaction in the silica-calcium hydroxide solution system.⁹

The rate of formation of hydrated calcium silicate from solutions of monosilicic acid and calcium ions was shown in this investigation to be a function of pH and calcium concentration. It may be assumed that the reaction proceeds through the combination of calcium and silicate ($\text{H}_2\text{SiO}_4^{-2}$) ions (eq. 3). This is based on the knowledge that, as the pH of the medium increases, the relative amount of completely dissociated silicic acid species increases.⁷ Therefore, the increase in rate of reaction with pH may be attributed to the increase in concentration of $\text{H}_2\text{SiO}_4^{-2}$ with pH. It has also been demonstrated in other studies that the hydrated calcium silicates may be represented by the formula CaH_2SiO_4 and that calcium hydroxide may dissolve in this substance.⁹

Kinetics of Solution. Since 0.25 g. of tricalcium silicate dissolves completely in 1 l. of water, it is possible to study the kinetics of solution by means of electrical resistance measurements. As a first approximation, the tricalcium silicate crystals were assumed to be approximately spherical and isotropic. The rate of solution was not found to be proportional to the surface area alone. The data also did not fit the assumption that solution and precipitation were proceeding simultaneously

$$-\frac{d(C_3S)}{dt} = k_1S - k_2(C_3S)_dS \quad (11)$$

where (C_3S) is the concentration of unreacted tricalcium silicate, $(C_3S)_d$ is the concentration of dissolved tricalcium silicate, S is the surface area, which is proportional to $(C_3S)^{2/3}$, and k_1 and k_2 are the constants for solution and precipitation, respectively.

If the rate of hydration of the surface of $3CaO \cdot SiO_2$ is very fast and the hydrated species form on the sur-

face, then the rate of solution is controlled by the rate of diffusion of the ions into solution according to the Nernst-Brunner treatment²¹

$$-\frac{d(C_3S)}{dt} = kS [(C_3S)_s - (C_3S)_d] \quad (12)$$

where k is the rate constant, S is the surface area of the tricalcium silicate, and (C_3S) , $(C_3S)_s$, and $(C_3S)_d$ are the concentrations in moles/l. of undissolved C_3S , of dissolved C_3S at the surface, and of dissolved C_3S in bulk solution, respectively. The constant k is a function of the diffusion constants of the ions. However, it was not possible to fit the data to eq. 12.

Acknowledgments. The authors wish to thank Dr. Stephen Brunauer for his careful reading of the manuscript and his many helpful suggestions. Thanks are also due to Dr. Paul Seligmann for his solution of the differential equation (eq. 12).

(21) For discussion see C. V. King, *Trans. N. Y. Acad. Sci.*, **10**, 262 (1948).

The Use of Large Anodic Galvanostatic Transients to Evaluate the Maximum Adsorption on Platinum from Formic Acid Solutions

by S. B. Brummer

Tyco Laboratories, Inc., Waltham, Massachusetts (Received September 11, 1964)

The adsorption on smooth Pt from HCOOH solutions in 1 N HClO₄ at 40° has been studied with anodic and cathodic galvanostatic transients. During the application of a large anodic current, i_a , three processes contribute to the charge passed, Q_a . These are (I) oxidation of adsorbate, (II) oxidation of a species in solution, and (III) surface oxidation of the electrode. By applying a cathodic current, i_c , at various times during the anodic transient, it is possible to measure III directly and, from the charge passed in deposition of H atoms prior to H₂ evolution, one can follow changes in the concentration of adsorbed HCOOH. By varying i_a , one can assess the effect of II. It is found that the contributions of processes I, II, and III can be effectively separated. The maximum adsorption from HCOOH solutions of a species which poisons the low potential oxidation of the HCOOH requires 310 $\mu\text{coulombs/real cm.}^2$ of electrode for its oxidation. This value is too large to correspond to adsorbed HCOOH itself ($\sim 230 \mu\text{coulombs/cm.}^2$). The oxidation involves two electrons per surface site. The maximum coverage of the electrode with this species is $\sim 73\%$. This maximum coverage is found below ~ 0.35 v. (*vs.* H₂/H⁺ in the same solution) in the concentration range investigated, 10⁻³ to 1 M. Adsorption declines as the potential increases and is essentially zero at 0.70 v. Surface oxidation, during the anodic transient, is considerably retarded even when the electrode is extensively free of the adsorbate. This effect is greatest at small current densities (~ 10 ma./cm.²). Some studies have also been made of the adsorption kinetics in the low potential region (below 0.2 v.).

Introduction

The anodic oxidation of HCOOH is currently of interest as a model system for organic anode materials in fuel cells. In a previous publication¹ an investigation was made of current potential curves for the reaction on Pt in dilute HClO₄ solutions. In addition, anodic and cathodic transients were used to examine the adsorption behavior of the system. It was found that, especially at low potentials, a material is slowly adsorbed which poisons the oxidation of HCOOH. Evidence that the oxidation is poisoned by some adsorbed species has also been shown by the work of Buck and Griffith,² Slott,³ Rhodes and Steigelmann,⁴ and Giner.⁵

Slott and Rhodes and Steigelmann suggested that this poisoning agent is CO formed from the catalytic decomposition of HCOOH on the electrode. The evi-

dence presented by Rhodes and Steigelmann is (a) that during an anodic linear potential sweep, a current peak is observed in HCOOH solution which is similar to that found in CO-saturated solutions and (b) that the charge passed in the region of this peak is the same in HCOOH as in CO-saturated solutions. However, it should be pointed out that (a) the electrode oxidizes in the vicinity of the current peaks, and material not

(1) S. B. Brummer and A. C. Makrides, *J. Phys. Chem.*, **68**, 1448 (1964).

(2) R. P. Buck and L. R. Griffith, *J. Electrochem. Soc.*, **109**, 1005 (1962).

(3) R. Slott, Doctor of Science Thesis, Massachusetts Institute of Technology, Jan. 1963.

(4) D. R. Rhodes and E. F. Steigelmann, Extended Abstract 213, Theoretical Division, Electrochemical Society Meeting, Toronto, May 1964; *J. Electrochem. Soc.* **112**, 16 (1965).

(5) J. Giner, *Electrochim. Acta*, **9**, 63 (1964).

previously desorbed from Pt is invariably desorbed in this potential region; (b) the area under the peak, a little more than $100 \mu\text{coulombs/cm}^2$, is much too low to correspond to the approximate monolayer coverage of a species from HCOOH which is thought to be present^{1,6,7} or to the coverage of CO found on Pt.⁸⁻¹⁰ Therefore, the coincidence of the area under the peaks is by no means conclusive, particularly as Rhodes and Steigelmann⁴ were compelled to use an arbitrary upper potential at which to terminate their integration of charge under the current peak to avoid too much overlap with the oxidation of the electrode and with oxidation of material from the solution. Gilman,¹¹ also, has suggested that the evidence of Rhodes and Steigelmann may not be conclusive. He has pointed out that CO oxidation on Pt proceeds through a "reactant pair" mechanism,⁸ *i.e.*, a mechanism involving the juxtaposition of adsorbed CO and adsorbed oxidant; this mechanism is probably not unique to CO and may not depend on the exact chemistry of the adsorbate.

Giner⁵ has found a qualitative similarity between the material which poisons CH_3OH and HCOOH oxidation on Pt and the species he obtained on Pt under CO_2 stirring,¹² which he calls "reduced CO_2 ." He did not show that the HCOOH poison is entirely or only reduced CO_2 , nor did he show whether the latter is the same as adsorbed CO.

The resolution of the various possibilities for the identity of the poison depends, in part, on the availability of good quantitative measurements of the maximum adsorption from HCOOH solutions. To date, two attempts have been made to examine this maximum adsorption,¹⁷ and, as will become apparent from the present work, neither was completely successful.

Breiter⁷ has used both anodic and cathodic galvanostatic transients on Pt electrodes which were slowly cycled between hydrogen and oxygen evolution. The cathodic transients, which measured the amount of H which is plated onto the electrode from solution (see below), give the relative coverage of the HCOOH, θ_{HCOOH} ; the anodic transient can give the maximum HCOOH coverage in absolute terms.

A typical anodic galvanostatic transient as found by Breiter⁷ and Brummer and Makrides¹ is shown in Figure 1. Breiter suggested that plateau BC probably corresponds to the oxidation of adsorbed HCOOH. Since, however, this plateau is indistinct, he suggested that a better estimate for $Q_{\text{HCOOH}}^{\text{max}}$ (the charge/cm² corresponding to the oxidation of adsorbed HCOOH) could be obtained by using the charge in region BD and subtracting from it the charge found in the absence of HCOOH. This assumes (a) that the extent of oxidation of the surface during the (fast) anodic transient

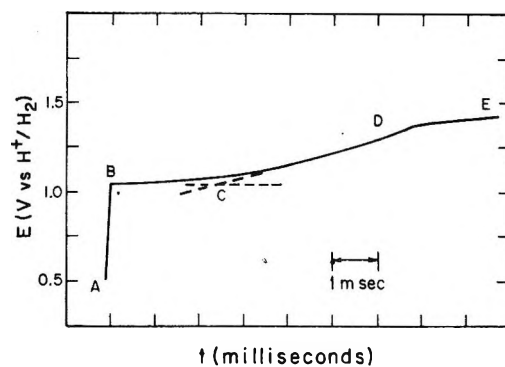


Figure 1. Typical anodic galvanostatic, potential-time trace taken in 1 M HCOOH solution, 2 min. after anodic cleaning of the electrode, with 50 ma./cm^2 .

is the same in the presence as in the absence of HCOOH, (b) that double-layer charging is the same in each case, (c) that all HCOOH on the surface is oxidized, and (d) that the contribution from oxidation of HCOOH, diffusing up to the electrode during the transient, is negligible.

The evidence presented by Breiter for (a) is that, at 1.6 v. during the *slow* anodic potential sweep, the O coverage of the electrode is "nearly the same" in the absence or presence of HCOOH. It was pointed out previously¹ that one may not confidently assume from this observation that the electrode oxidation is the same during the *fast* anodic galvanostatic transient. The effect of (b) was shown to be small; (c) was not taken into account, and (d) was justified from the fact that varying the anodic current density apparently led to no change in $Q_{\text{HCOOH}}^{\text{max}}$. In this way, Breiter found that the maximum coverage from HCOOH solutions, during the *slow* potential cycling, is $260 \mu\text{coulombs/cm}^2$ of real surface (a definition of a "real" cm² is given later).

Brummer and Makrides¹ estimated $Q_{\text{HCOOH}}^{\text{max}}$ directly from Q_{BC} . They assumed that during BC surface oxidation and double-layer charging are negligible, arguing that the adsorbed species probably has to be largely removed before surface oxidation can commence and that the potential increase during BC is so

(6) C. W. Fleischmann, G. K. Johnson, and A. T. Kuhn, *J. Electrochem. Soc.*, **111**, 602 (1964).

(7) M. W. Breiter, *Electrochim. Acta*, **8**, 447, 457 (1963).

(8) S. Gilman, *J. Phys. Chem.*, **66**, 2657 (1962); **67**, 78 (1963); **68**, 70 (1964).

(9) T. B. Warner and S. Schuldiner, Extended Abstract 209, Theoretical Division, E.C.S. meeting in Toronto, May 1964; *cf.* Naval Research Lab. Report 6058, U.S.N.R.L., Washington, D. C., April 1964. See also *J. Electrochem. Soc.*, **111**, 992 (1964).

(10) S. B. Brummer and J. I. Ford, to be published.

(11) S. Gilman, discussion or ref. 4 at E.C.S. meeting.

(12) J. Giner, *Electrochim. Acta*, **8**, 857 (1963).

small that $Q_{\text{double layer}}$ may be ignored. Possibility (c), above, was ignored and condition (d), above, was assumed unimportant from the approximate independence of Q_{BC} on the anodic current density. They found that $Q_{\text{HCOOH}}^{\text{max}}$ is $210 \mu\text{coulombs/cm}^2$. Brummer and Makrides and Breiter *substantiated* their results for $Q_{\text{HCOOH}}^{\text{max}}$ by obtaining good agreement between θ_{HCOOH} values calculated from it and those obtained from cathodic charging. The values for $Q_{\text{HCOOH}}^{\text{max}}$ were also fairly close to the value expected for close-packed HCOOH adsorption ($230 \mu\text{coulombs/cm}^2$). However, it is not likely that HCOOH itself is the adsorbed species,¹ for, as has been indicated above, the adsorbed species poisons the HCOOH oxidation. (This is not to discount a "reactant-pair" mechanism, as suggested by Gilman⁸ for CO oxidation.)

The purpose of the present study is to provide the quantitative information required to discuss the nature of the adsorbed species. The point of departure of this investigation was that all of the above assumptions about the anodic transient can be tested. Thus, by applying a large cathodic current sometime during the anodic transient, it should be possible to measure Q_0 (the charge/cm.² corresponding to the reduction of surface oxidized in the preceding anodic transient). Also, by measuring θ_{H} (the ratio of the amount of hydrogen which can be plated onto the electrode to the maximum amount which is determined in the absence of HCOOH), one can estimate the fraction of the surface which has been bared of adsorbed HCOOH during the anodic transient. (For justification of this procedure, see below.)

Experimental

The main experimental technique is illustrated in Figure 2. The electrode was cleaned with a short (~ 1 sec.) anodic galvanostatic pulse ($20\text{--}100 \text{ ma./cm}^2$) and then put under potentiostatic control (Wenking fast-rise potentiostat) at the potential of interest for a time long enough (2 min.) to allow steady-state adsorption.¹ The solution was not stirred. Then (at D) an anodic current, i_a , was applied, and a short time later (F) a cathodic current, i_c , was applied. The potential-time sequence from D to J was recorded on an oscilloscope (Tektronix Type 535A with Type L plug-in). The method of estimating the anodic charge, Q_a , and Q_0 and Q_{H} is indicated in the figure.

Unless otherwise stated, all experiments were carried out in 1 N HClO_4 at 40° with a smooth platinum electrode. Water for making up the solutions was triple distilled (once from alkaline KMnO_4); the reagents were Baker Analyzed grade. N_2 and H_2 gases were "pre-purified" grade and were passed through several cold

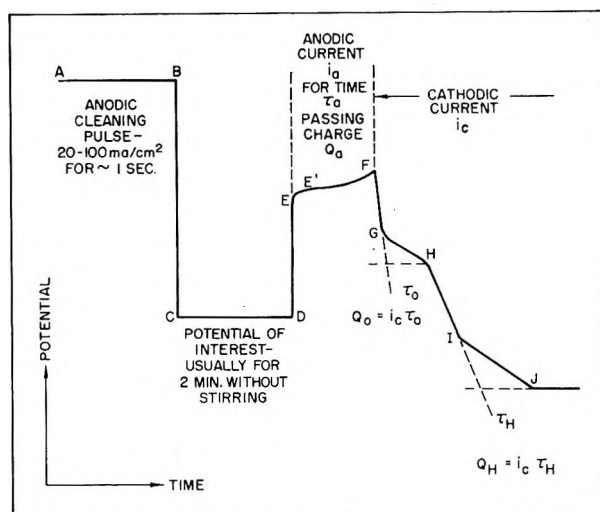


Figure 2. Potential-time sequence used to clean the electrode and to make the measurements.

traps, packed with glass beads, and surrounded with liquid N_2 , before being bubbled first through a pre-saturator containing the test solution and then through the cell. The cell has been described previously.¹ The working electrode was "thermocouple grade" Pt wire which was sealed into glass so as to expose about 0.6 cm^2 of geometric area. Prior to use, both cell and working electrode were washed in H_2SO_4 cleaning mixture and then thoroughly washed with hot, triple distilled water and with the test solution. Solutions were extensively pre-electrolyzed on a separate Pt electrode before carrying out experiments although there was no evidence that this pre-electrolysis affected the results. Potentials were measured (and are reported) against the reversible hydrogen electrode in the same solution (r.h.e.).

Constant current was applied by switching the counter electrode line from the potentiostat to a current source with a Hg-wetted relay (Clare, Type HG 1002). For the simple application of a constant current, the circuit consisted of a 45-v. battery and a bank of resistors. For the application of the sequence shown in Figure 2, a special circuit was developed. This will be described more fully elsewhere,¹³ but its general features are as follows. The circuit consisted of two zener diode-controlled, transistor constant-current sources. The first current, i_a , was applied on the closing of the previously mentioned relay. The second circuit, which was held off with a silicon-controlled rectifier, was applied a short time later (from $200 \mu\text{sec.}$ to 2 sec.) in such a way as to overpower the first circuit. The time delay was controlled with a slightly modified

(13) R. Dobkin and S. B. Brummer, to be published.

Tektronix pulse generator (Type 161) which was started by the closing of the relay. Currents were measured with a Greibach ammeter (Model 510) with a precision of 0.5%.

Unless otherwise stated, the measurements are given on the basis of "real cm.²." There is no unambiguous way to estimate the real area of a Pt electrode, and the best way to do so is still in dispute. Thus, Gottlieb¹⁴ has used both the double-layer capacity, which he assumed to be 24 $\mu\text{f./true cm.}^2$, and the potentiostatic oxidation results of Laitinen and Enke.¹⁵ The latter results themselves cannot be unambiguously related to true surface area. Schuldiner and Roe¹⁶ have asserted that the most satisfactory way to estimate the true area is through the assumption that the linear region from ~ 0.9 to 1.8 v., during an anodic galvanostatic transient, prior to O₂ evolution, Q_{O}^{AN} , corresponds to a monolayer of chemisorbed O atoms. The present author has found that using wire electrodes (Schuldiner and Roe¹⁶ used beads) and using a technique whereby considerable O₂ evolution occurs while making the anodic transient measurements tends to roughen the electrode. In addition, under these circumstances, some dependence on the current density (albeit these were usually lower than those employed by Schuldiner and Roe) was found.

Yet another method of estimating the surface area is to assume that there is a monolayer of H atoms, *i.e.*, one atom per surface Pt atom at the reversible H₂ potential. There can be little doubt that this is approximately true (see for example Breiter, *et al.*,¹⁷ and for a more recent discussion Frumkin¹⁸). The predominant face on polycrystalline Pt is the (100) plane, and this would correspond to 1.3×10^{15} atoms/cm.² or 210 $\mu\text{coulombs/cm.}^2$ for a monolayer of H. The work of Breiter, Knorr, and Völkl¹⁹ suggests that $2Q_{\text{H}}^{\text{max}}/Q_{\text{O}}^{\text{AN}}$ is close to 1, and this would suggest, unless it were mere coincidence, that *both* the oxygen and the hydrogen layers are close to monolayers.

The measurement of Q_{O}^{AN} is, as has been indicated above, not completely satisfactory. The anodic measurement of $Q_{\text{H}}^{\text{max}}$, also, is not satisfactory for use as a routine measure of surface area since allowance has to be made for the molecular F₂ which is generated at the reversible potential; recent measurements by Gilman²⁰ suggest that this cannot be done unambiguously. It was preferred, then, to estimate the area by measuring $Q_{\text{H}}^{\text{max}}$ cathodically, *i.e.*, plating the H layer onto the electrode with a large constant current, starting from a potential where the electrode is bare. To ensure that the surface was clean, the measurement was done while the electrode was slowly cycled at 0.1 c.p.s., without stirring, between 0.25 and 1.25 v., the

measurement being taken from 0.6 v. on the anodic sweep.

$Q_{\text{H}}^{\text{max}}$, as determined in this way, is reproducible and does not vary with the measuring current, in the range investigated, 1–300 ma./cm.². It is not certain that $Q_{\text{H}}^{\text{max}}$ measured in this way is, in fact, the same as $Q_{\text{H}}^{\text{max}}$ measured anodically; see, for example, ref. 20. However, the reversibility observed in slow triangular sweeps,²¹ and the independence of $Q_{\text{H}}^{\text{max}}$ on the rate of deposition, in the range used, suggests that this is a fairly good estimate. Thus, the area of the electrode is based on the $Q_{\text{H}}^{\text{max}}$ value measured at 40° in 1 N HClO₄, on the assumption that $Q_{\text{H}}^{\text{max}}$ is 210 $\mu\text{coulombs/real cm.}^2$.

As has been indicated, Q_{H} was also measured in the presence of HCOOH, and the assumption was made that $\theta_{\text{H}}^{\text{obsd}} (= Q_{\text{H}}^{\text{obsd}}/Q_{\text{H}}^{\text{max}})$ is a measure of the cleanness of the surface at the time of the measurement. This technique has recently been used for HCOOH adsorption,^{1,6,7} for CH₃OH adsorption,²² and for CO adsorption.⁸ It seems to have been used originally by Oikawa and Mukaibo²³ to study the adsorption of CH₃COOH and by Franklin and Sothorn²⁴ for the adsorption of nitriles.

The $\theta_{\text{H}}^{\text{obsd}}$ values could be in error for one or more of the following reasons. (a) Some of the more loosely adsorbed HCOOH could be desorbed during the measurement of Q_{H} , particularly as H has a very high affinity for Pt. (b) Some HCOOH which had been displaced at the higher potentials could readsorb during the measurement of Q_{H} . (c) HCOOH or one of its oxidation products could be reduced during the measurement of Q_{H} . Regarding (a), if the HCOOH were desorbed during the cathodic pulse, one might expect to see discontinuities in the range of $\theta_{\text{H}}^{\text{obsd}}$ independent

(14) M. H. Gottlieb, *J. Electrochem. Soc.*, **111**, 465 (1964).

(15) H. A. Laitinen and C. G. Enke, *ibid.*, **107**, 773 (1959).

(16) S. Schuldiner and R. M. Roe, *ibid.*, **110**, 332 (1963).

(17) M. W. Breiter, H. Kammermaier, and C. A. Knorr, *Z. Elektrochem.*, **60**, 37, 119 (1956); M. W. Breiter, "Transactions of the Symposium on Electrode Processes," John Wiley and Sons, Inc., New York, N. Y., 1961.

(18) A. N. Frumkin, "Advances in Electrochemistry and Electrochemical Engineering," Vol. 3, John Wiley and Sons, Inc., New York, N. Y., 1963.

(19) M. W. Breiter, C. A. Knorr, and W. Völkl, *Z. Elektrochem.*, **59**, 681 (1955).

(20) S. Gilman, Interim Report No. 8 on Contract DA 44-009-ENG-4909, Dec. 1963; see also *J. Electroanal. Chem.*, **7**, 382 (1964).

(21) M. W. Breiter, *Ann. N. Y. Acad. Sci.*, **101**, 709 (1963).

(22) M. W. Breiter and S. Gilman, *J. Electrochem. Soc.*, **109**, 622 (1961).

(23) M. Oikawa and T. Mukaibo, *J. Electrochem. Soc. Japan, Overseas Ed.*, **20**, 568 (1952).

(24) T. C. Franklin and R. D. Sothorn, *J. Phys. Chem.*, **58**, 951 (1954).

of the initial state of the electrode. Specifically, θ_H^{obsd} might tend to unity. In fact (see below), a continuous range of θ_H was observed from ~ 0.2 to 1. With respect to (b), HCOOH is apparently re-adsorbed during the cathodic transient if the time of measurement is long (see below for discussion). Thus, all the measurements of Q_H were taken with large current densities (short times), usually ~ 80 ma./cm.². Con-

cerning (c), there is no evidence for HCOOH reduction, and reduction of the oxidation product, CO₂, is too slow to be relevant here.¹² To justify this point, we may note that in HCOOH solutions the maximum value of θ_H found was just 1. Occasionally, values of θ_H slightly greater than 1 were found, but these were never outside the range of the repeatability of the experiments.

A glossary of symbols is given in Table I.

Table I: Glossary of Important Symbols

i_a	Anodic current density applied to electrode (see Figure 2)
i_c	Cathodic current density applied to electrode, some time after application of i_a (see Figure 2)
Q	Charge (density) passed during process subscripted and superscripted
Q_a	Charge passed during anodic transient (i_a) for time τ_a
$(Q_a)\theta_{H \rightarrow 1}$	Charge passed during anodic transient corresponding to complete cleaning of the electrode
Q_{BC}	Charge passed during region BC of Figure 1
Q_{BD}	Charge passed during region BD of Figure 1
$Q_{\text{double layer}}$	Charge passed during anodic transient used in charging the double layer
Q_H or Q_H^{obsd}	Charge passed, galvanostatically, in presence of HCOOH, in depositing H atoms on the Pt electrode, anodically or cathodically, but usually cathodically
Q_H^{max}	Charge passed galvanostatically in 1 N HClO ₄ , in absence of HCOOH, in depositing H atoms on the Pt electrode anodically or cathodically, but usually cathodically
$Q_{\text{HCOOH}}^{\text{max}}$	Charge corresponding to oxidation of the maximum adsorption of HCOOH
Q_O	Charge for the reduction of surface oxidized during an anodic transient (see Figure 2)
Q_O^{AN}	Charge passed during an anodic galvanostatic transient corresponding to surface oxidation. Also, total charge passed in this way before O ₂ evolution
$Q_O^{\text{I-BD}}$ or Q_O^{BD}	Q_O for the time BD in Figure 1
Q_{soln}	Charge for oxidation from solution, during the anodic transient
Γ_{HCOOH}	Surface concentration of HCOOH (less than maximum)
$\Gamma_{\text{HCOOH}}^{\text{max}}$	Maximum surface concentration of HCOOH, equivalent to $Q_{\text{HCOOH}}^{\text{max}}$ if expressed as $\mu\text{coulombs/cm.}^2$
θ_H or θ_H^{obsd}	Q_H/Q_H^{max}
$(\theta_H)_{Q_a \rightarrow 0}$	Value of θ_H when Q_a tends to zero, i.e., the initial condition of the electrode, as obtained from the θ_H - Q_a plots
θ_{bare}	Average fraction of surface bare during a given transient; defined in eq. 5
τ	Time
τ_a	Time elapsed during anodic transient
τ_{BD}	τ for time BD in Figure 1
τ_H	Time elapsed during measurement of Q_H

Results and Discussion

General Features of the Anodic Transients. In Figure 3, the variation of θ_H and Q_O is shown during the progress of two different anodic galvanostatic pulses. The measurements were taken in 1 M HCOOH solution from 0.3 v., 2 min. after a cleaning pulse; similar results are obtained with other concentrations and starting potentials. The usual starting potential of 0.3 v. falls in the range where HCOOH adsorption is independent of potential and at a maximum.¹ The general features of the potential dependence of the adsorption previously reported¹ were substantiated in the present work. With starting potentials lower than ~ 0.3 V., it is not possible to compare results obtained from anodic transients with those from direct

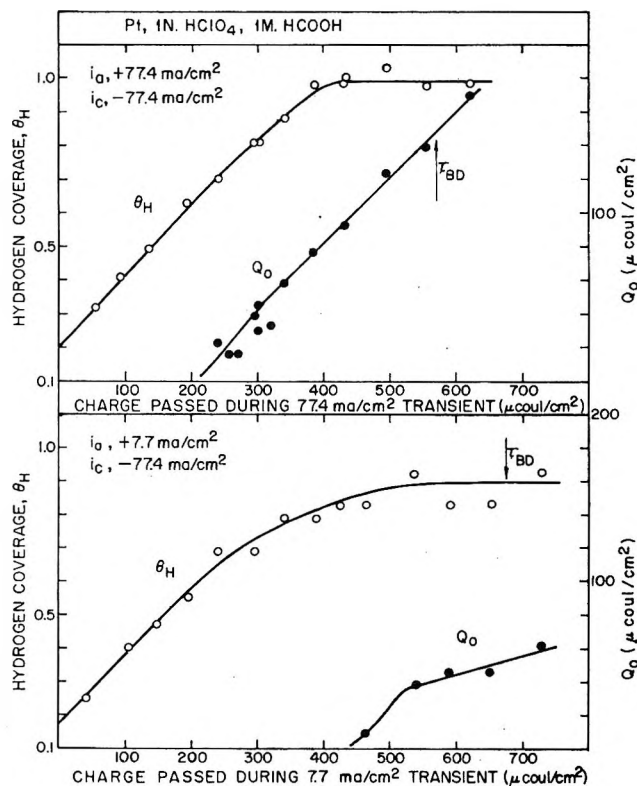


Figure 3. General behavior of θ_H and Q_O with Q_a in 1 M HCOOH. The measurements were taken from 0.3 v., 2 min. after a cleaning pulse.

cathodic charging (see later). We see that both θ_H and Q_O increase during the progress of the anodic transient. θ_H appears to increase essentially linearly at first, then less rapidly with increase of Q_a , and finally comes to a limiting value close to unity. This indicates that the anodic pulse is effective in removing (what for the present we will call) "adsorbed HCOOH." Because the lower current density was not quite as effective in cleaning the surface, the cleaning pulse was never less than 20 ma./cm.². We see from Figure 3 that the oxidation of the surface is retarded particularly at lower current densities. It is interesting that, at the lower current density shown, the surface does not oxidize even though the θ_H values suggest that it is almost clean of adsorbate and the potential is sufficiently high (*cf.* Figure 1).

The indication of the "transition time," τ_{BD} , refers to the time BD in Figure 1. It is interesting that Q_O does not show any change corresponding to this time—nor is its value at τ_{BD} anything like that of a monolayer. In the range studied, 0.01–1 M, τ_{BD} depends on the current density. In addition, section DE is not flat at higher current densities, and a second inflection, followed by a flat region, is found at the highest current densities, particularly in concentrated solutions. Also an overshoot (*cf.* ref. 2) is found at the lowest current densities. Since the over-all description of the anodic transients is rather complex, we will concentrate on the initial region, in particular on the region BC in Figure 1.

The Variation of θ_H with Q_a and the Maximum Adsorption from HCOOH Solutions. In Figure 4, we take a closer and more detailed look at the variation of θ_H with Q_a in a 1 M HCOOH solution. Measurements were taken over a range of currents (~ 8 to 90 ma./cm.²) to try to separate any contribution from the oxidation of species which diffuse to the electrode during the anodic transient. It was not possible in 1 M solution to work at less than about 8 ma./cm.² as the potential tends to oscillate under galvanostatic conditions. Measurements were not made above ~ 90 ma./cm.² since the oxidation of the surface then obtrudes more into the low Q_a region. For low values of Q_a (~ 30 – 100 μ coulombs/cm.²), all the points fall, more or less, on a common line, but, as Q_a increases, the lower current densities are no longer effective in increasing θ_H , *i.e.*, in cleaning the surface, and the θ_H – Q_a lines tail off from the main line. The line in Figure 4 has been put through the highest current density points. The line has been dotted, at the top end, from the point where electrode oxidation becomes appreciable to $\theta_H = 1$. Then, assuming both of the extrapolations to the axes indicated by the broken lines, we find

$$(\theta_H)_{Q_a \rightarrow 0} = 0.205 \quad (1)$$

$$(Q_a)_{\theta_H \rightarrow 1} = 370 \text{ } \mu\text{coulombs/cm.}^2 \quad (2)$$

and

$$\frac{dQ_a}{d\theta_H} = 2.21 \quad (3)$$

The various current densities overlap fairly well at low and intermediate values of Q_a (short times) and less so at longer times (*viz.*, with low values of i_a). It may be that for the shorter times the sole process which consumes Q_a is oxidation of adsorbed material, and at longer times (but before electrode oxidation becomes appreciable) we have some contributions to Q_a from diffusional processes. There are a number of ways of treating the simultaneous contributions of adsorption and diffusion to a chronopotentiometric wave.²⁵ None of these is applicable in the present case since the variation with current density shown in Figure 4 is much less than would be found if this process were limited by diffusion of the HCOOH. The supply of other species (*e.g.*, HCOO⁻, (HCOOH)₂, (HCOOH)₂ single anion) would presumably also be limited by the

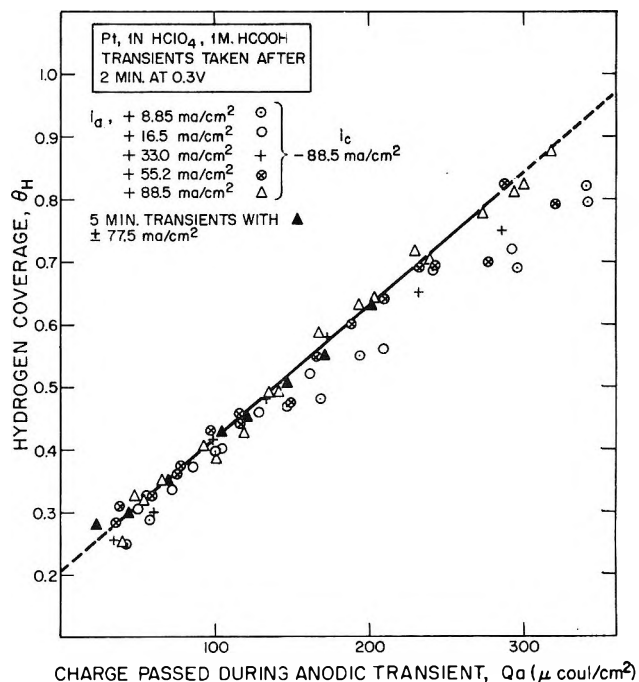


Figure 4. Variation of θ_H with Q_a in 1 M HCOOH. The measurements were usually taken from 0.3 v., 2 min. after cleaning pulse. Also shown are measurements taken 5 min. after the cleaning pulse. The line has been drawn through the high current density points.

(25) See, for example, H. A. Laitinen and L. M. Chambers, *Anal. Chem.*, **36**, 5 (1964).

supply of the HCOOH itself. If we assume, then, that HCOOH from solution will oxidize on the bared surface according to

$$Q_{\text{soln}} = k\tau_a\bar{\theta}_{\text{bare}} \quad (4)$$

where Q_{soln} is the charge supported by this oxidation from solution during the time of the anodic transient τ_a , and $\bar{\theta}_{\text{bare}}$ is the average fraction of the surface which is bare during this time, and if $\bar{\theta}_{\text{bare}}$ is estimated using

$$\bar{\theta}_{\text{bare}} = \frac{1}{2}(\theta_{\text{H}}^{t=0} + \theta_{\text{H}}^{t=\tau_a}) \quad (5)$$

Then k is 4.5 ma./cm.², and the data for the different current densities overlap in the manner shown in Figure 5. Again, assuming that we can extrapolate, as indicated by the dotted regions of the line in Figure 5, we obtain

$$(Q_{\text{H}})_{Q_a \rightarrow 0} = 0.205 \quad (6)$$

$$(Q_a - Q_{\text{soln}})_{\theta_{\text{H}} \rightarrow 1} = 356 \mu\text{coulombs/cm.}^2 \quad (7)$$

and

$$\frac{d(Q_a - Q_{\text{soln}})}{dQ_{\text{H}}} = 2.13 \quad (8)$$

All the current densities now overlap, and, if the extrapolations are valid, it can be assumed that the values given in (6), (7), and (8) refer to the adsorbed film alone. No allowance has been made for charging of the double layer.

If we consider measurements taken with a 0.1 M HCOOH solution (Figure 6), we see that, even without correction for Q_{soln} , the overlap between the different current densities is good. This implies that almost all of Q_a is used in oxidizing the adsorbate, and very little is used in any other process. In this case, there is no surface oxidation until $Q_a \geq 300 \mu\text{coulombs/cm.}^2$. Then, extrapolating as indicated, we find

$$(\theta_{\text{H}})_{Q_a \rightarrow 0} = 0.235 \quad (9)$$

$$(Q_a)_{\theta_{\text{H}} \rightarrow 1} = 331 \mu\text{coulombs/cm.}^2 \quad (10)$$

and

$$\frac{dQ_a}{dQ_{\text{E}}} = 2.03 \quad (11)$$

If we correct these values using eq. 5 and assuming k to be about 1 ma./cm.² (which gives the best overlap), we find

$$(Q_a)_{\theta_{\text{H}} \rightarrow 1} = 327 \mu\text{coulombs/cm.}^2 \quad (12)$$

and

$$\frac{dQ_a}{dQ_{\text{H}}} = 2.01 \quad (13)$$

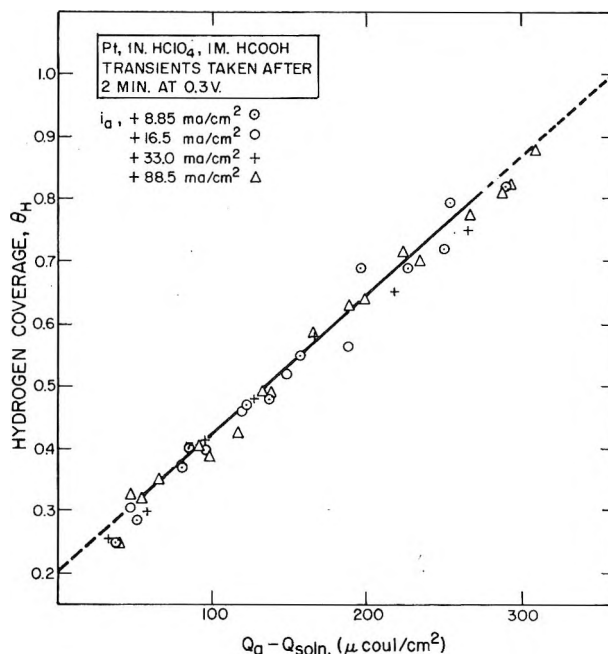


Figure 5. Variations of θ_{H} with Q_a . The latter is corrected for contributions from oxidation from solution species by means of eq. 4 and 5.

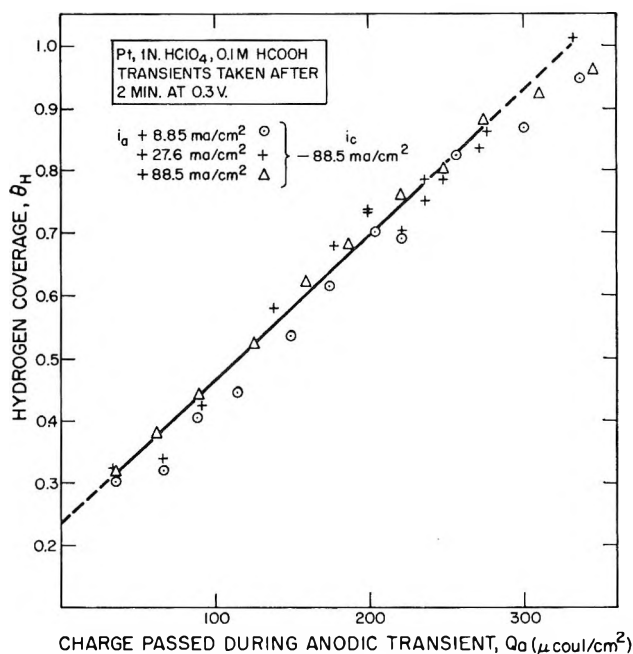


Figure 6. Variation of θ_{H} with Q_a in 0.1 M HCOOH. The measurements were taken from 0.3 v., 2 min. after cleaning pulse.

Since these results differ from those in eq. 9–11 by less than the experimental uncertainty, we will pay most attention to the more directly observed results in (9), (10), and (11).

The value of $(Q_a)_{\theta_H \rightarrow 1}$ depends on the validity of the extrapolations which have been dotted in Figures 4-6. The upper extrapolation, *i.e.*, to the value of Q_a when $\theta_H = 1$, is almost certainly accurate. To justify this, we note that in Figure 6, if Q_0 and Q_{soln} are subtracted from the Q_a values, the extrapolation which is present as only ~ 0.1 in θ_H essentially disappears. At the lower end of the line, it should not theoretically be necessary to extrapolate since the measurements themselves can be extended right into this region. In practice, the initial shape of region EF in Figure 2 allows considerable uncertainty when Q_a is less than $\sim 30 \mu\text{coulombs/cm}^2$. For the 1 M HCOOH solution, the situation is even more uncertain as the potential arrests only gradually (E), eventually becoming more or less flat (E'). This directly introduces an uncertainty as to whether to measure Q_a from E or E'. This uncertainty itself is $\sim 35 \mu\text{coulombs/cm}^2$.

In order to check the lower extrapolation, one can adsorb the HCOOH from the various solutions for 2 min. as before and measure θ_H directly without anodic charging. In this case, one observes a value between 0.26 and 0.28, independent of concentration, in the measured range of 10^{-3} to 1 M (Figure 7), whereas the extrapolated values are invariably lower than this (*cf.* eq. 1, 6, and 9). We can explain this difference by assuming that the first part of Q_a does not go to the oxidation of adsorbed material. Alternatively, we could postulate that the first part of Q_a oxidizes material that is so weakly adsorbed that it is desorbed during the direct measurement of θ_H . It seems reasonable to make the former assumption since, if the latter were true, the values of $(\theta_H)_{Q_a \rightarrow 1}$ in eq. 1 and 9 would presumably be the same. Then, if we make the first assumption, $(Q_a)_{\theta_H \rightarrow 1}$ is reduced by about $20 \mu\text{coulombs/cm}^2$ for the 0.1 M solution (Figure 6), and the charge required to remove the adsorbed layer, $Q_{\text{HCOOH}}^{\text{max}}$, is about $310 \mu\text{coulombs/cm}^2$. For the 1 M solution, we obtain $320 \mu\text{coulombs/cm}^2$. These values agree within the precision of the experiments.²⁶

We may be certain that these values represent the maximum adsorption on Pt from HCOOH solutions for the following reasons: (1) 2-min. and 5-min. results at 0.3 v., from 1 M HCOOH solution, are indistinguishable (Figure 4). (2) Results at 0.2 v. are indistinguishable from those at 0.3 v. Thus, the adsorption does not increase, as the potential is lowered, to values greater than at 0.3 v. Above 0.35 v., the adsorption declines (Figure 7). (3) Cathodic charging (Figure 7) showed the same value ($\sim 10\%$ precision) over a wide concentration range at 0.3 v., so the surface is already saturated with quite dilute solution.

The fact that the Q_a - θ_H lines are essentially straight

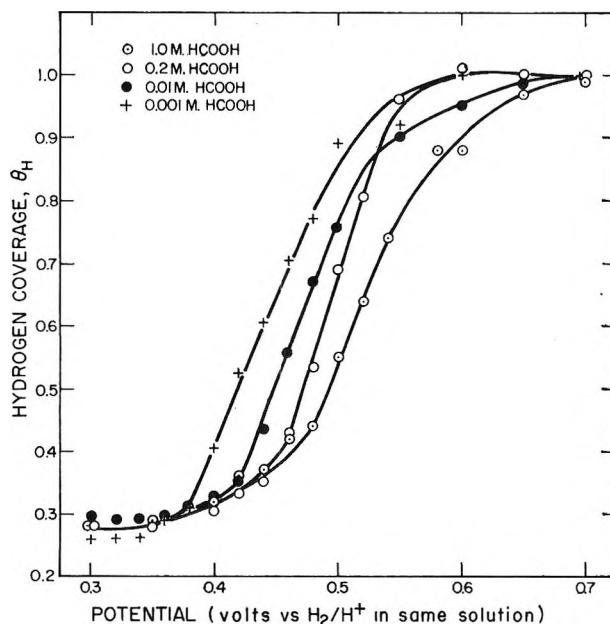


Figure 7. Variation of θ_H with electrode potential in HCOOH solutions. The measurements were taken 2 min. after cleaning pulse, usually with 50-ma./cm.² pulses.

over the whole range of θ_H means that the adsorbed species is homogeneous. At least, it is homogeneous in the sense that its oxidation involves the same number of electrons per unit over the whole range of electrode coverage. Since the maximum value of Q_H closely corresponds to a monolayer^{17,18} of H atoms and these each release one electron in their oxidation, the ratio dQ_a/dQ_H is the number of electrons required for each site which is oxidized free from adsorbate. We see that this number is 2. This is the value which one would expect for adsorbed CO, and, indeed, the value reported for $Q_{\text{HCOOH}}^{\text{max}}$ is close to that reported previously for CO.^{1,8} However, other experiments by the present author¹⁰ and by Warner and Schuldiner⁹ suggest that this is too low a value for the maximum adsorption of CO. Subsequently,¹⁰ a detailed comparison of the oxidation kinetics of the film adsorbed from HCOOH solutions with that adsorbed in CO saturated solutions will be made. The value of $310 \mu\text{coulombs/cm}^2$ is, however, too high to correspond to the maximum adsorption of HCOOH. The area of the HCOOH molecule is 14 \AA^2 ,²⁷ and the maximum (two-electron oxidation) to which this would correspond is $\sim 230 \mu\text{coulombs/cm}^2$.²⁷

(26) These values should be corrected for double-layer charging. The extent of this correction is difficult to estimate, but it can be shown to be about $25 \mu\text{coulombs/cm}^2$ (ref. 10) with an uncertainty of $\pm 10 \mu\text{coulombs/cm}^2$.

(27) B. E. Conway and M. Dzieciuch, *Can. J. Chem.*, **41**, 21, 38, 55 (1963).

Adsorption from HCOOH Solutions As a Function of Potential and Concentration. From the boundary conditions that $\theta_H = 1$ when $\theta_{\text{HCOOH}} = 0$ and $\theta_H = 0.27$ when θ_{HCOOH} has its maximum value (Figure 7) and also from the assumption that θ_H and θ_{HCOOH} are linearly related, which is clearly demonstrated by Figure 6 but is in disagreement with the results of Breiter,⁷ we can derive the surface concentration of HCOOH, Γ_{HCOOH} , relative to its maximum value, $\Gamma_{\text{HCOOH}}^{\text{max}}$, according to

$$\theta_{\text{HCOOH}} = \frac{\Gamma_{\text{HCOOH}}}{\Gamma_{\text{HCOOH}}^{\text{max}}} = 1.37(1 - \theta_H) \quad (14)$$

Values calculated in this way are shown in Figure 8.

We see that θ_{HCOOH} is unity (assumed) at high concentrations and low potentials and decreases as the potential is raised and the bulk concentration is lowered. The effect of lower concentration is to lower the potential at which adsorption becomes less than the maximum. However, the adsorption is strong, and the maximum is observed at low potentials even in $10^{-3} M$ HCOOH solution. If the adsorbate is formed from decomposition of HCOOH on the electrode, then, in

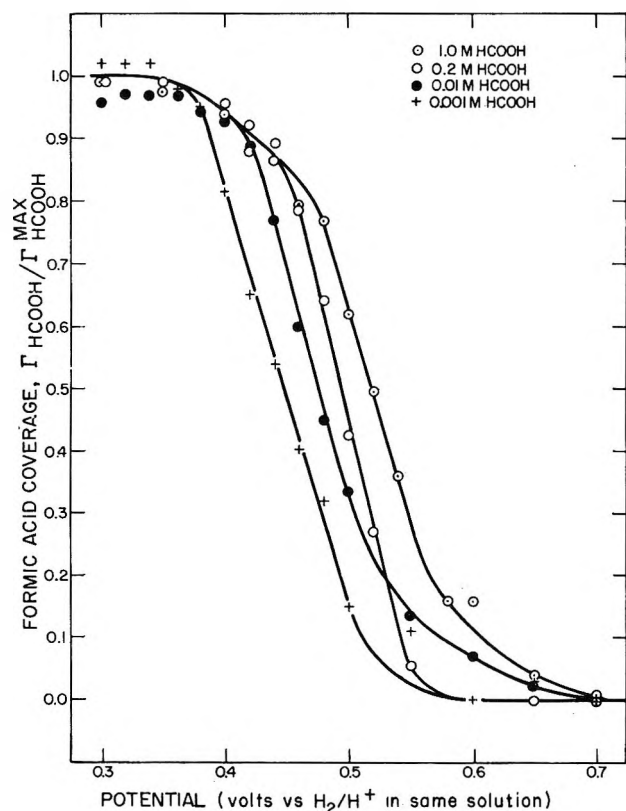


Figure 8. Variation of θ_{HCOOH} with electrode potential. Results were computed from the data shown in Figure 7 by means of eq. 14.

the more dilute solutions—where the kinetics of adsorption, *i.e.*, decomposition, would be slower—it is possible that some of the values of θ_{HCOOH} , as measured at 2 min., are too low. This has been discussed previously.¹

The fact that the adsorption of an oxidizable species from HCOOH solutions declines essentially to zero as the potential is raised clearly rules out those mechanisms which would account for the activation-limited current,¹ which is observed in the potential region when θ_{HCOOH} declines from unity, in terms of the limiting high coverage with an intermediate, *e.g.*, HCOO', whose nonelectrochemical breakdown is the rate-limiting step, *viz.*, ref. 27.

Readsorption of HCOOH during Measurement of θ_H . One of the assumptions made in using θ_H as a measure of the bare surface at the point of the current reversal (F in Figure 2) is that no HCOOH readsorbs on the electrode during the measurement. This was tested in the following way. The electrode was cleaned and polarized at a convenient potential for 2 min. without stirring, and then θ_H was measured with a range of currents so as to vary τ_H , the time of measurement of Q_H . The results are shown in Figure 9. We see that in a 1 M HCOOH solution the initial rate

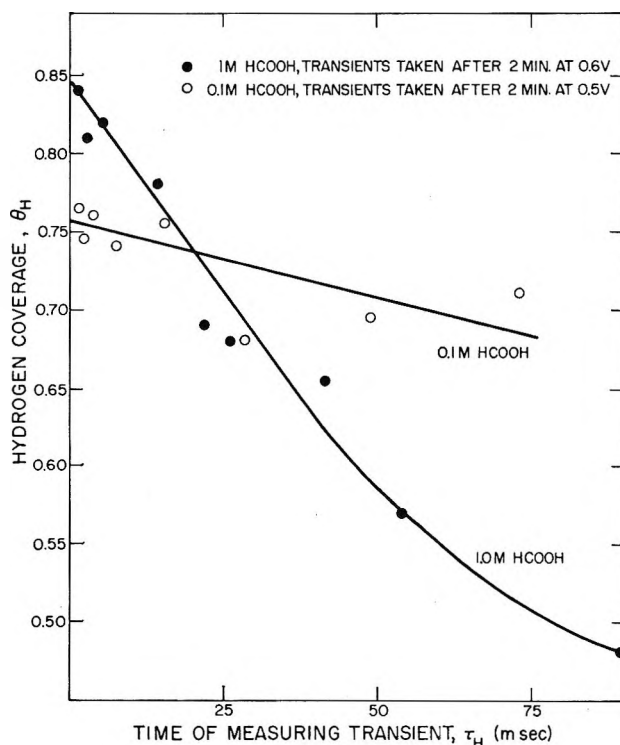


Figure 9. Variation of θ_H with the time of measurement of Q_H , τ_H . These values of τ_H were not corrected for double-layer charging (*cf.* Figure 2) as the actual time elapsed during the measurement is significant here.

of readsorption, standardized to unit bare surface, is ~ 0.006 of a monolayer of $\theta_{\text{H}}/\text{cm}^2$ of bare surface/msec. In a $0.1 M$ HCOOH solution, the initial rate is ~ 0.0011 of a monolayer of $\theta_{\text{H}}/\text{cm}^2$ of bare surface/msec. This means that in $1 M$ HCOOH the observed value of θ_{H} in the vicinity of $\theta_{\text{H}} = 1$ is lower than its true value by $\sim 2.5\%$; thus, the value for $(Q_{\text{a}})_{\theta_{\text{H}} \rightarrow 1}$ given in eq. 7 should probably be reduced by $\sim 2.5\%$, *i.e.*, to $347 \mu\text{coulombs}/\text{cm}^2$. This adjusts the corrected value for $Q_{\text{HCOOH}}^{\text{max}}$ in $1 M$ HCOOH to $312 \mu\text{coulombs}/\text{cm}^2$ ($347 - 35$). Similarly, the value in a $0.1 M$ solution would be reduced to $308 \mu\text{coulombs}/\text{cm}^2$.

The net rate of adsorption (or decomposition) of HCOOH shown in Figure 9 appears to be much higher than the adsorption rates reported earlier.¹ However, those measurements refer to potentials higher than those of Figure 9, which are in the H-adsorption region. It was shown previously that the net rate of adsorption increases as the potential is lowered, and, thus, there is no significant conflict. The slow adsorption rates determined previously at the higher potentials are the main reason why Breiter's θ_{HCOOH} potential curves, which were made during a slow triangular sweep, do not agree with those shown in Figure 8.

Summary and Conclusions

It appears, then, that, using the anodic charging method coupled with current reversal, we can obtain important information on the species adsorbed from HCOOH solutions, as follows. (1) Two electrons are involved, during the anodic transient, to expose each Pt atom. With the double-layer correction, this would be reduced to about 1.9. (2) $Q_{\text{HCOOH}}^{\text{max}}$, the maximum

adsorption from HCOOH solutions, has a value of $310 \mu\text{coulombs}/\text{cm}^2$. With the double-layer correction, this would be reduced to about $285 \mu\text{coulombs}/\text{cm}^2$. (3) When the surface has its maximum adsorbed film, it is about 73% covered. This follows from direct cathodic charging and assumes that all of the sites are available for the adsorption of HCOOH or H atoms. (4) During the removal of the film by anodization, the oxidation of the electrode is impeded (*cf.* Figures 1 and 3). This is so even on surfaces which are substantially free from adsorbate. At large current densities the oxidation of the adsorbed film and of the electrode tend to overlap. (5) HCOOH (or its decomposition product) readsorbs relatively quickly at low potentials. (6) Adsorption from HCOOH solutions declines at potentials much in excess of 0.3 v. , particularly in more dilute solutions.

The evidence presented above does not prove whether the adsorbed film is or is not CO or "reduced CO_2 ." However, the method used here appears to yield a reliable quantitative description of the adsorbed film, and, from this description, it is clear that the adsorbed film is unlikely to be HCOOH itself. In further work,¹⁰ a direct comparison will be made of the properties of this adsorbed film with those of adsorbed CO.

Acknowledgments. The author wishes to thank Miss J. I. Ford for her skillful assistance with the experimental part of this work and also wishes to acknowledge support by the Office of Naval Research under Contract Nonr-3765(00). This work was presented in part at the 126th Meeting of the Electrochemical Society in Washington, D. C.

Ionic Reactions in Gaseous Acetylene¹

by M. S. B. Munson

Humble Oil and Refining Company, Research and Development, Baytown, Texas (Received September 21, 1964)

Mass spectrometric studies of ionic reactions in acetylene have been made which gave rate constants of 0.9 and 1.3×10^{-9} cc./molecule-sec. for reaction of $C_2H_2^+$ and C_2H^+ . Consecutive ionic reactions were observed giving ionic species up to C_{12} and perhaps C_{14} . $C_4H_4^+$ was observed as a third-order product ion with no indications of chemi-ionization reactions being involved in its formation. No appreciable concentration of $C_6H_6^+$ ions was observed. Product ions were observed which were apparently formed by reaction of excited states of the acetylene ion. Analogous reactions were observed in C_2D_2 and the rate constant for reaction of $C_2D_2^+$ was within experimental error the same as the rate constant for reaction of $C_2H_2^+$.

Introduction

The radiation chemistry of acetylene has been studied for many years; the major products are benzene and an uncharacterized polymer, called "cuprene."^{2a} At various stages in the history of these studies the reactive intermediates have been considered as radicals or ions and it appears that both may be important.^{2b} Recently, work has been done in these laboratories on the radiation chemistry of acetylene³ which made it seem worthwhile to continue the studies of ionic reactions in gases with experiments on acetylene with the mass spectrometer available at Humble at pressures as high as possible.

Mass spectrometric studies of ionic reactions in acetylene have been made which gave values of rate constants for the formation of some second-order product ions.⁴⁻⁶ In work on the bombardment of C_2H_2 with positive ions, second-order products ions were also observed.⁷ Experiments have been made with acetylene in a mass spectrometer at a pressure of about 100 μ which showed the presence of some higher-order products,^{8,9} but no kinetic data were reported.

Experimental

The mass spectrometer was that described by Field¹⁰ and was used with a Faraday cup or an electron multiplier as an ion detector. Appearance potentials were determined by the modification of the retarding potential difference technique¹¹ which has been discussed previously with regard to operation at high

pressures.¹² The source pressure was determined in the previously described manner.¹²

The source temperature was varied between 130 and 220° in different experiments and was maintained constant within a few degrees during each experiment. The residual source pressure was about 1×10^{-6} mm. The electron current was several hundredths to a few tenths of a microampere (μ a.) using the electron multiplier as the ion detector and larger electron currents were used in the experiments with low electron voltage to increase the observed ion current. When the Faraday cup was used, electron currents of about 1 μ a. were used. Pressure studies were made with

(1) Supported in part by Project SQUID under Contract Nonr-3623 (S-18).

(2) (a) S. C. Lind, "The Radiation Chemistry of Gases," Reinhold Publishing Corp., New York, N. Y., 1961; (b) L. M. Dorfman and A. C. Wahl, *Radiation Res.*, **10**, 680 (1959).

(3) F. H. Field, *J. Phys. Chem.*, **68**, 1039 (1964).

(4) F. H. Field, J. L. Franklin, and F. W. Lampe, *J. Am. Chem. Soc.*, **79**, 2665 (1957).

(5) R. Barker, W. H. Hamill, and R. R. Williams, Jr., *J. Phys. Chem.*, **63**, 825 (1959).

(6) R. Fuchs, *Z. Naturforsch.*, **16a**, 1026 (1961).

(7) E. Lindholm, I. Szabo, and P. Wilmenius, *Arkiv Fysik*, **25**, 417 (1963).

(8) P. S. Rudolph and C. E. Melton, *J. Phys. Chem.*, **63**, 916 (1959).

(9) A. Bloch in "Advances in Mass Spectrometry, II," R. M. Elliot, Ed., Pergamon Press, New York, N. Y., 1963, p. 48.

(10) F. H. Field, *J. Am. Chem. Soc.*, **83**, 1523 (1961).

(11) R. E. Fox, W. M. Hickam, D. J. Grove, and T. Kjeldaas, Jr., *Rev. Sci. Instr.*, **26**, 1101 (1955).

(12) M. S. B. Munson, J. L. Franklin, and F. H. Field, *J. Phys. Chem.*, **67**, 1542 (1963).

ionizing electrons of nominal energy of 10–50 v. in the presence of repeller voltages of 2.5 or 5 v.

The acetylene was obtained from the Matheson Co. and was purified by passing through two traps kept in a slurry of CO₂ and acetone and then frozen and sublimed twice with liquid nitrogen, discarding the first and last fractions from each sublimation. Acetone, air, and water were the only observed impurities in concentrations of the order of 0.01%. C₂D₂ was obtained from Merck & Company of Canada and contained only a few per cent of C₂DH and was used without further purification. D₂O was allowed to flow through the vacuum manifold, gas reservoir, and mass spectrometer for several hours before the experiments with C₂D₂ were performed.

Results

In the primary mass spectrum of acetylene at low pressures these data confirm the previous reports of the formation of CH₂⁺ as a rearrangement ion and the presence of C₂H₂⁺² and C₂H⁺².^{13,14} These data indicate that C₂H₂⁺² is about 40% of the total intensity at mass 13 in acceptable agreement with the other values of 75%¹³ and 43%.¹⁴ A(CH₂⁺) and A(13) were determined as 21.1 ± 0.1 v. and 21.8 ± 0.2 v., respectively, the latter in good agreement with earlier work.¹⁵ From the heats of formation of CH₂⁺,¹⁶ C,¹⁷ and CH,¹⁸ and the spectroscopic ionization potential of CH,¹⁶ one may calculate that appreciable excess kinetic energy is involved in these decompositions.

A kinetic analysis of the sequence of second-order reactions involved has been given previously.¹⁹ With the assumption that the observed ion current is proportional to the ion concentration with the same proportionality constant for all ions and that the fragmentation pattern for decomposition of the initially excited C₂H₂⁺ is independent of pressure, then for primary ions, since (C₂H₂) ≫ (C₂H₂⁺)

$$\ln(I_i/\Sigma I_i) = \ln A_i - k_i(C_2H_2)t_i \quad (1)$$

for which (P_i⁺)₀, the initial concentration of P_i⁺, is A_iΣI_i; t_i = (2dM_i/eFS)^{1/2}, in which d is the ion path in the source, M_i is the mass of P_i⁺, e is the electronic charge, FS is the repeller field strength in the source; and k_i is the rate constant for reaction of P_i⁺ with acetylene. From the slopes of plots of the logarithms of relative intensity against source pressure one can obtain rate constants for reaction of the primary ions.

Using an electron multiplier as the ion collector, the rate constant for the reaction of C₂H₂⁺ with acetylene, k_{C₂H₂⁺}, was determined as 1.03 ± 0.07 × 10⁻⁹ cc./molecule-sec. (since kt = Qd, Q = 48 × 10⁻¹⁶ cm.²

at FS = 12.5 v./cm.). This value is the average of rate constants determined from experiments at temperatures from 130 to 220°, with nominal energy of the ionizing electrons of 9–50 v., and at repeller field strengths of 6.3 and 12.5 v./cm. (corresponding to final ion energies of 1.3 and 2.5 v.). None of these parameters had any significant effect on the rate constant. The activation energy for this reaction must be less than 1.5 kcal./mole, if one assumes that a 40% increase in rate constant between 130 and 220° could have been detected unequivocally if it had occurred.

From experiments with 50-v. electrons, k_{CH⁺} is 1.6 ± 0.2 × 10⁻⁹ cc./molecule-sec. (Q = 72 × 10⁻¹⁶ cm.² at FS = 12.5 v./cm.) and k_{C₂⁺} is 1.7 ± 0.2 × 10⁻⁹ cc./molecule-sec. (Q = 75 × 10⁻¹⁶ cm.² at FS = 12.5 v./cm.). Plots of log(I₁₃/ΣI_i) against source pressure gave reasonable straight lines from which a "rate constant" of 2 × 10⁻⁹ cc./molecule-sec. could be estimated. The residence time of CH⁺ and C₂H₂⁺² would be the same, but since mass 13 probably consists of roughly equal amounts of CH⁺ and C₂H₂⁺² and the CH⁺ is formed with excess kinetic energy, this number should not be considered as other than an indication that these ions react rapidly. From data of rate constants for reaction of CH⁺ with D₂, CH₄, and C₂H₆ for which the rate constants vary approximately as the polarizability of the neutral,²⁰ a value of about 2 × 10⁻⁹ cc./molecule-sec. would be expected for k_{CH⁺} in acetylene.

Appearance potentials of product ions are shown Table I. Appearance potentials of some product ions were determined in C₂D₂ because of interferences from carbon isotopes. Agreement with earlier data for the major ions is good. No major secondary ion was observed of appearance potential corresponding to C₂H⁺ (the concentration of C₁H⁺ was small compared to that of C₂H⁺), but the C₂H⁺ reacted rapidly with acetylene. The ratio I₅₀/I₅₁ increased with increasing electron energy so that in addition to

(13) C. E. Melton, M. M. Bretscher, and R. Baldock, *J. Chem. Phys.*, **26**, 1302 (1957).

(14) F. L. Mohler, V. H. Eibeler, L. Williamson, and H. Dean, *J. Res. Natl. Bur. Std.*, **48**, 188 (1952).

(15) J. T. Tate, P. T. Smith, and A. L. Vaughn, *Phys. Rev.*, **48**, 525 (1935).

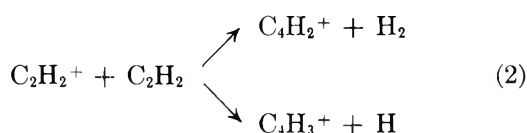
(16) F. H. Field and J. L. Franklin, "Electron Impact Phenomena," Academic Press, New York, N. Y., 1957.

(17) L. Brewer and A. W. Searcy, *Ann. Rev. Phys. Chem.*, **7**, 271 (1956).

(18) R. G. Brewer and F. L. Kester, *J. Chem. Phys.*, **40**, 812 (1964).

(19) F. W. Lampe, J. L. Franklin, and F. H. Field, "Progress in Reaction Kinetics," Vol. 1, Pergamon Press, Oxford, 1961, pp. 73–79.

(20) M. S. B. Munson, J. L. Franklin, and F. H. Field, *J. Phys. Chem.*, **68**, 3098 (1964).



C_4H_2^+ is produced by another reactions as well, probably



From experiments bombarding C_2H_2 with positive ions, it has been suggested that C_4H_3^+ comes from a low

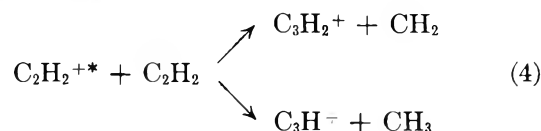
Table I: Product Ions in Acetylene

Ion	AP, e.v.	Lowest energy precursor	Order
C_4H_3^+	11.3 ± 0.1	C_3H_2^+	Second
C_4H_2^+	11.5 ± 0.1	C_2H_2^+	Second
C_3H^+	15.6 ± 0.1	$\text{C}_2\text{H}_2^{*+}$	Second
C_3H_2^+	15.5 ± 0.1	$\text{C}_2\text{H}_2^{*+}$	Second
C_4H^+	17.4 ± 0.4	C_2H^+	Second
C_2D_3^+	12.5-13	$\text{C}_2\text{D}_2^{*+}$	Second
C_3H_3^+	11.6 ± 0.1	C_2H_2^+	Third
C_4D_4^+	11.4 ± 0.1	C_2D_2^+	Third
C_6H_3^+	11.4 ± 0.1	C_2H_2^+	Third
C_6H_2^+	Low	Probably C_2H_2^+	Third
C_6H_1^+	Low	Probably C_2H_2^+	Third
C_6H_4^+	11.4 ± 0.1	C_4H_2^+	Fourth
C_6H_5^+	11.3 ± 0.1	C_4H_3^+	Fourth
C_8H_6^+	Low	Probably C_2H_2^+	Sixth (?)
C_3H_7^+	Low	Probably C_2H_2^+	Sixth (?)

energy state (probably the ground state) and that C_4H_2^+ comes from a state around 15.5 v.⁷ However, in the present experiments appreciable concentrations of C_4H_2^+ were observed at electron energies below 15 v. I_{50}/I_{51} was 0.44 ± 0.04 for electrons with nominal energy up to 15 v. and then increased with increasing electron energy to 0.85 ± 0.10 for 50-v. electrons. The values at low voltage compare reasonably well with the ratio 0.61 ± 0.05 obtained by Rudolph and Melton with their α -particle spectrometer for which C_2H_2^+ was the only primary ion.⁸ The ratio at 50 v. compares well with the other values of this ratio determined with 70-v. electrons.⁴⁻⁶ Recent measurements have been reported on appearance potentials of ions in acetylene²¹ which indicate a sharp break at about 17.0 v. in the ionization efficiency curves of C_4H_3^+ and C_2H_2^+ but not C_4H_2^+ , which is interpreted in terms of reaction of $\text{C}_2\text{H}_2^{*+}$ to give C_4H_3^+ and not C_4H_2^+ . This observation is at variance with these data for which C_4H_2^+ is formed by the higher energy species.

Other second-order product ions were detected in

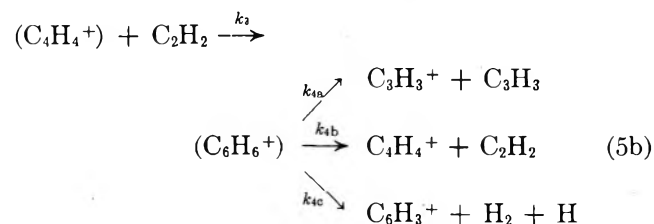
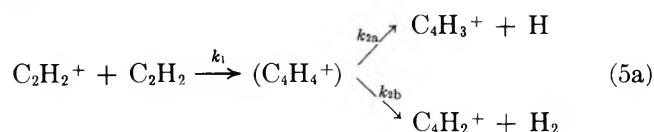
small concentrations: C_2H_3^+ , C_3H^+ , C_3H_2^+ , and C_4H^+ . The relative concentration of these ions passed through a maximum with increasing pressure; hence, they all react rapidly with acetylene, k of the order of 10^{-10} cc./molecule-sec. The appearance potentials suggest that these ions are formed to some extent from reaction of excited acetylene ions



Both reactions were exothermic for an excited state of this energy. The 15.5-v. state of acetylene corresponds to the suggested state of Lindholm and co-workers⁷ and is perhaps indicated by the data of Collin,²² although he did not interpret his data in this fashion. The previous studies gave appearance potentials of 20-22 v. for these ions, corresponding to CH^+ as a primary ion. It is very probable that higher energy processes other than the reaction of $\text{C}_2\text{H}_2^{*+}$ are also involved and the lower appearance potentials in this paper are merely the consequence of a higher sensitivity which enables the lower energy processes to be seen.

In C_2D_2 , $A(\text{C}_2\text{D}_3^+)$ was determined as 12.5-13 v. The shape of the plot of ion current against electron energy indicated that the ion is formed by more than one process. The vinyl ion can be formed exothermally from a second-order reaction of an excited acetylene ion of about 13 v. energy and Collin²² reports an excited ionic state at 13.0-13.2 v.

Two other product ions were observed which could be second order based on their stoichiometry, C_3H_3^+ and C_4H_4^+ . These two ions, however, were actually third-order ions. No evidence was found for a chemionization reaction leading to the formation of C_4H_4^+ or C_4D_4^+ . These ions can be formed exothermally by a reaction of the $(\text{C}_2\text{H}_2 \cdot \text{C}_2\text{H}_2^+)$ complex ion



(21) C. E. Melton and W. H. Hamill, *J. Chem. Phys.*, **41**, 1469 (1964).

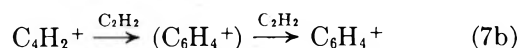
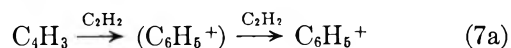
(22) J. E. Collin, *Bull. soc. chim. Belges*, **71**, 15 (1962).

If the second-order product ions, $C_4H_3^+$ and $C_4H_2^+$, do not undergo appreciable reaction then,¹⁹ for example

$$(C_3H_3^+)/ (C_4H_3^+) = (k_{4a}/\Sigma k_{4i})(k_3/k_{2a})(C_2H_2) \quad (6)$$

At pressures up to about 100 μ there is no evidence for appreciable reaction of $C_4H_3^+$ and a plot of I_{39}/I_{51} is linear in acetylene pressure. $C_6H_3^+$ is included in reaction 5b since it exhibits the same pressure behavior as $C_3H_3^+$ and $C_4H_4^+$. k_3/k_{2a} is approximately 2×10^{-17} cc./molecule. Unfortunately, there is no way at present of establishing the values of k_{2a} and k_3 separately. k_{2a} cannot be as low as 10^6 sec.⁻¹ because no $C_4H_4^+$ was observed as a second-order ion nor were any spontaneous decompositions of $C_4H_4^+$ to $C_4H_3^+$ observed as "metastable ions" in the mass spectrum. $(I_{39} + I_{52} + I_{75})/\Sigma I_i$, the sum of relative concentrations of the third-order products from reaction 5b, never amounts to more than a few per cent of the total ionization, although the concentration of the fourth-order ions becomes much greater than this. The low value for the relative concentration of third-order ions suggests that $(k_{2a} + k_{2b})$ is large and that the complex ($C_4H_4^+$) disappears predominantly by dissociation.

The ions, $C_6H_4^+$ and $C_6H_5^+$, are the major higher-order ions at these pressures. At about 300 μ , the sum $I_{76} + I_{77}$ was about 30% of the total ionization ($EV = 50$ v. and $FS = 12.5$ v./cm.); the processes forming these ions are therefore very rapid. The ratio I_{77}/I_{76} increases with increasing pressure, so that the two ions cannot be formed from dissociation of the same complex. Although their stoichiometry requires only three acetylene molecules, the pressure dependence is fourth order; that is, $C_6H_5^+/C_4H_3^+$ increases approximately with the square of the acetylene pressure. These results are best explained by



The complex formed by combination of the ion with a molecule should not be stable since it is 60–70 kcal./mole above the ground state of the ion. The dissociation of the ($C_6H_5^+$) complex to $C_6H_4^+$ or $C_6H_3^+$ is endothermic.

No significant concentration of $C_6H_6^+$ was observed as a product ion at these pressures, although there was generally a slightly greater ion current at mass 78 than could be accounted for from ¹³C isotopes ($\approx 0.1\%$ of the total ionization).

$C_5H_2^+$ and $C_5H_3^+$ were observed as third-order ions, maximum concentration about 1% of the total ioniza-

tion. The ions were formed from low energy processes, probably from $C_2H_2^+$ or one of its product ions. Very small concentrations of $C_7H_3^+$ ($m/e = 87$) were also observed, but in general the higher products contained an even number of carbon atoms.

Ions of $m/e = 100$ through 104 were observed which probably came from more than one source since the ratios of ion currents varied with electron voltage at constant pressure. They were formed partly from $C_2H_2^+$ since these ions were found in the low voltage experiments when $C_2H_2^+$ was the only primary ion. The most abundant of these ions were 102, $C_8H_6^+$, and 103, $C_8H_7^+$, perhaps formed by sixth-order processes since I_{102}/I_{76} increased approximately with the square of the acetylene pressure.

Very small amounts of C_9 species were found; the most abundant was at $m/e = 114$, $C_9H_6^+$. Larger concentrations of C_{10} ionic species were present up to 129, $C_{10}H_9^+$. Very small amounts of C_{12} ions were observed, and it is possible that the trace concentrations of ions at $m/e = 180$ ($C_{14}H_{12}^+$) were products of ionic reactions.

Typical data for relative concentrations of ions in acetylene are shown in Figures 1 and 2. The curve for $C_2H_2^+$ was calculated using the average value of the rate constants. The dashed curves for $C_4H_3^+$ and $C_4H_2^+$ are calculated assuming that $C_2H_2^+$ reacts to give only these two ions in the ratio $C_4H_2^+/C_4H_3^+ = 0.44$ and that these ions do not undergo further reaction. The deviations of the experimental data from this curve show the extent of higher order reactions. The sequential reactions, $C_2H_2^+ \rightarrow C_4H_3^+ \rightarrow C_6H_5^+$ are readily apparent in Figure 1. The higher order of reaction for formation of $C_6H_4^+$ than $C_3H_3^+$ or $C_4H_4^+$ and the large ratio of fourth- to third-order products are apparent in Figure 2.

Some experiments were done with a Faraday cup as an ion detector. The general pattern of results was the same with the two types of detectors; however, there was a difference in rate constants. $k_{C_2H_2^+}$, using the Faraday cup as an ion detector, was $0.66 \pm 0.12 \times 10^{-9}$ cc./molecule-sec. (to be compared with 1.03×10^{-9} using the electron multiplier). This difference in rate constants is not the result of discrimination in the multiplier for ions of different masses since a comparison of ion currents between the Faraday cup and the electron multiplier for primary fragment ions of masses 27 to 84 indicated a decrease in sensitivity of less than 20% over this threefold mass range. These effects would produce a change in rate constant within experimental error and in the wrong direction. It was suggested by one of the reviewers that saturation at high ion currents could be the cause of this difference.

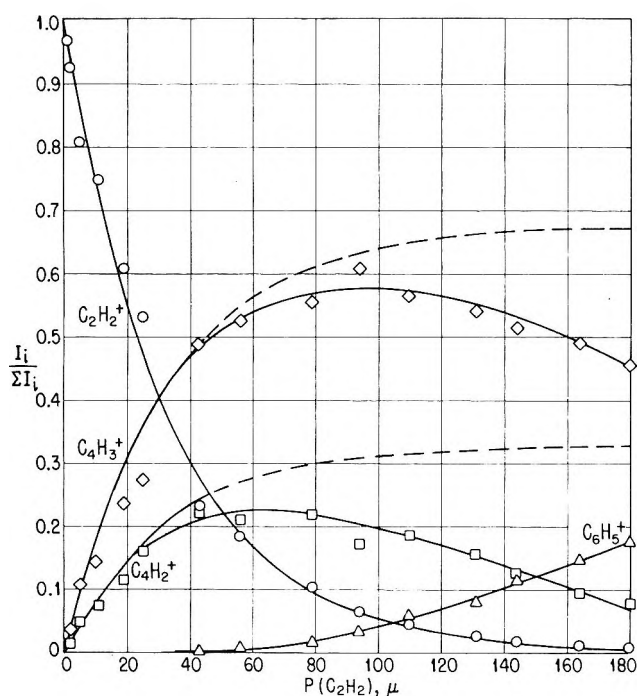


Figure 1. Relative concentrations of ions in C_2H_2 : $EV = 11$ v.; $FS = 6.3$ v./cm.

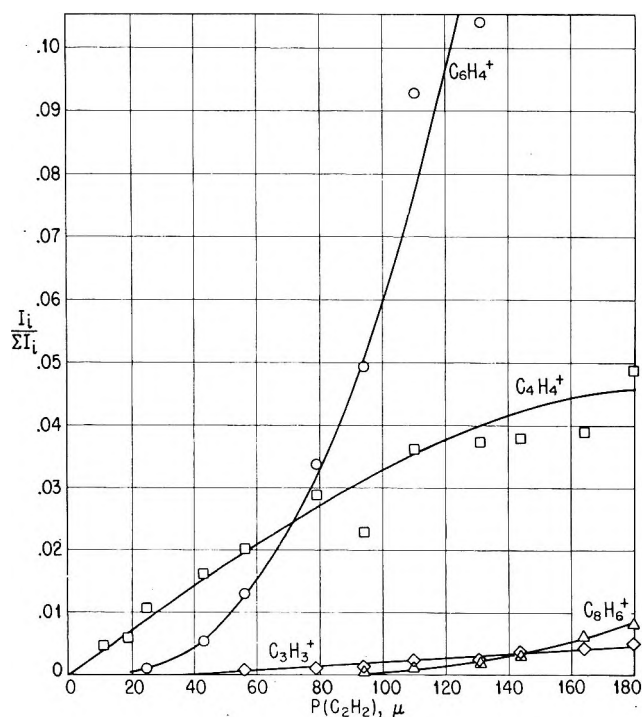


Figure 2. Relative concentrations of ions in C_2H_2 : $EV = 11$ v.; $FS = 6.3$ v./cm.

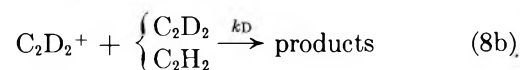
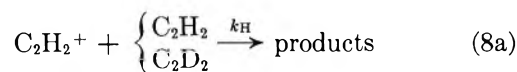
There is appreciably more scatter in the experimental data and the plots of $\log(I_{26}/\Sigma I_i)$ vs. $P(C_2H_2)$ are not linear over as wide a pressure range (with upward

curvature) for the experiments using the Faraday cup compared with those using the electron multiplier. In previous work it has been observed that high electron currents (necessary in this case to allow detection of ions with reasonable accuracy) gave lower rate constants at high pressures than those obtained from experiments with a smaller extent of ionization. It is likely that the results with the Faraday cup are somewhat low. The differences in experimental conditions were not great and a personal preference for one set of data does not seem sufficient reason for discarding the other. These two values should be considered as extremes and the average of 0.85×10^{-9} cc./molecule-sec. (with a probable accuracy of $\pm 0.20 \times 10^{-9}$) should be taken as the "best" value.

$k_{C_2H^+}$ from the experiments with the Faraday cup was $1.0 \pm 0.2 \times 10^{-9}$ cc./molecule-sec. (to be compared with $1.6 \pm 0.2 \times 10^{-9}$ using the electron multiplier). The average of these two values, $1.3 \pm 0.3 \times 10^{-9}$ cc./molecule-sec. should be taken as the "best" value of these data.

Experiments were performed with C_2D_2 to obtain appearance potentials of $C_2D_3^+$ and $C_4D_4^+$. Pressure studies showed no evidence for chemi-ionization reactions in the formation of $C_4D_4^+$, which was a third-order ion from $C_2D_2^+$. These experiments also confirmed the observation that $C_2H_3^+$ was a second-order product ion. The assignment of the higher mass ions in C_2H_2 was confirmed by the experiments with C_2D_2 .

Studies were made on C_2D_2 and mixtures of C_2H_2 and C_2D_2 to see if an isotope effect were observable for these reactions, but essentially none was observed. $k_{C_2D_2^+}$ was $0.53 \pm 0.05 \times 10^{-9}$ cc./molecule-sec. with the Faraday cup and $0.98 \pm 0.07 \times 10^{-9}$ cc./molecule-sec. with the electron multiplier, for reaction with C_2D_2 . These values are perhaps lower than the values for the rate constant for reaction of $C_2H_2^+$ but any difference in rate constants is within the experimental precision of the two numbers. A pressure study was made on a mixture (about 1:1) of C_2H_2 and C_2D_2 . Since the reactions

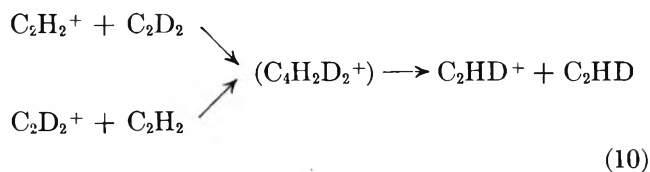


both occur in this mixture, from eq. 9

$$\ln \frac{(C_2H_2^+)}{(C_2D_2^+)} + \ln \frac{(C_2H_2^+)_0}{(C_2D_2^+)_0} = (k_H - k_D)[(C_2H_2) + (C_2D_2)]t \quad (9)$$

(neglecting the 2% difference between t_{26} and t_{28}) one may calculate the difference in rate constants for $C_2H_2^+$ and $C_2D_2^+$. ($k_H - k_D$) was $0.00 \pm 0.06 \times 10^{-9}$ cc./molecule-sec.; that is, within experimental error there is no isotope effect. The total rate constant for disappearance of $C_2H_2^+$ or $C_2D_2^+$ in the mixture was the same as the rate constant for reaction in C_2H_2 or C_2D_2 , respectively.

An interesting question arises about the decomposition of the $C_4H_4^+$ complex. For mixtures of C_2D_2 and C_2H_2 all of the possible $C_4H_nD_{3-n}^+$ and $C_4H_nD_{2-n}^+$ species are observed, but the overlapping of the two species prevents any statement about the preferential modes of decomposition, if any, of the complex. If there is appreciable reversible decomposition of the complex, then one would expect



as well as decomposition of $C_2H_2^+$ or $C_2D_2^+$. It was possible to reduce the energy of the ionizing electrons low enough to eliminate practically all of the $C_2H_3^+$. There was a small concentration of C_2HD present in the C_2D_2 which gave mass 27. The ratio $C_2HD^+/C_2D_2^+$ was small, about 0.03 and independent of pressure, so that essentially no C_2HD^+ was formed. An estimate can be made that less than 5% of the $(C_4H_2D_2^+)$ complexes dissociate according to reaction 10.

Conclusions

Table II gives a summary of the available data for rate constants or cross sections for reactions of $C_2H_2^+$ with acetylene. The earlier results were determined from the formation of $C_4H_3^+$ and $C_4H_2^+$ with electrons of about 70 v. energy and are necessarily slightly large since part of the $C_4H_2^+$ is formed from C_2H^+ . The pressure measurements are the critical problem, however. The values of Fuchs⁶ are notably higher than the others but since he considers the absolute value of his pressure calibrations as correct to within about a factor of two, this disagreement is not surprising. There is no marked variation in rate constant over the range of ion energies given in this table. The value of $k_{C_2H_2^+}$ of $8.5 \pm 2.0 \times 10^{-10}$ cc./molecule-sec. appears to be a good choice for the absolute value of the rate constant. This number is not as well established as the values for $k_{CH_4^+}$ and $k_{CH_3^+}$ in methane,²³ but the agreement is satisfactory.

No comparison can be made for $k_{C_2H^+}$ since the other experiments reported no values for this rate constant.

Table II: Comparison of Rate Constants Obtained by Different Workers for Reaction of $C_2H_2^+$ with C_2H_2

$F.S.$, v./cm.	E_{max} , v.	$k_{C_2H_2^+} \times 10^{-10}$, cc./molecule-sec.	$QC_2H_2^+ \times 10^{-16}$ cm. ²
2	0.10	4.9	68 ^a
6	0.30	8.1	90
8	0.40	8.7	87
10	0.50	8.2	77
20	1.0	5.9	41
0.74	0.1	25	568 ^b
7.4	1.0	12	85
37	5.0	13	44
6.6	0.66	22	172 ^c
13.3	1.33	20	97
20.0	2.00	17	66
12.5	2.5	8.5 ± 2.0	40 ^d

^a See ref. 4. ^b See ref. 5. ^c See ref. 6. ^d These data.

The earlier values for the other rate constants were based on the formation of relatively low intensity secondary ions and there is some doubt about the assignments of the product and reactant ions. Field, Franklin, and Lampe⁴ report $k_{C_2^+}$ as about 7×10^{-10} cc./molecule-sec. based on the formation of C_4H^+ . Considering the probable complications in mechanisms, one should consider this value as acceptably close to the present value of 17×10^{-10} cc./molecule-sec.

The general pattern of reactivity in this paper confirms that indicated by Rudolph and Melton⁸ and it was possible to establish a more detailed mechanism than they were able to do. In particular: $C_2H_3^+$ is formed by a second-order reaction of excited $C_2H_2^+$ (ruling out reaction of $C_4H_3^+$), $C_4H_4^+$ is a third-order ion from $C_2H_2^+$ (one would certainly expect the second-order ($C_4H_4^+$) complex to be unstable), and the formation of $C_6H_4^+$ and $C_6H_5^-$ from $C_4H_2^+$ and $C_4H_3^+$ is not a direct ion-molecule association, but requires a third body for stabilization. In addition, even higher-order product ions of the polymerization reactions are reported in this paper.

No evidence was found for chemi-ionization reactions in acetylene as has been reported for the formation of $C_4H_2^+$ and $C_4H_3^+$ in photochemical experiments²⁴ and it is very difficult to understand why photoexcitation should show this but not excitation by electron impact. The formation of these products from acetyl-

(23) F. H. Field, J. L. Franklin, and M. S. B. Munson, *J. Am. Chem. Soc.*, **85**, 3575 (1963).

(24) I. Koyano, I. Tanaka, and I. Omura, *J. Chem. Phys.*, **40**, 2734 (1964).

ene excited to 10.2 v. is endothermic unless the heats of formation of $C_4H_2^+$ and $C_4H_3^+$ are much lower than the presently accepted values.

The observation that $C_2H_3^+$, and C_3H^+ , and $C_3H_2^+$ may be formed by reaction of excited ions is further evidence that reactions of excited ions may be more common than has been considered in the past. No evidence was observed for different reactivities of excited states of acetylene; however, unless the rate constants were greatly different and the relative concentrations of two states were about the same, one would not expect to be able to observe this phenomenon. The curves for the disappearance of mass 13, CH^+ and $C_2H_2^{+2}$, indicate that the doubly charged ions react rapidly, but quantitative data are not available.

The failure to observe $C_6H_6^+$ as an important product ion militates against benzene being formed by a purely ionic process. The heat of reaction of



is not known with sufficient certainty to say anything about the permissibility of this reaction. Neutralization and hydrogen abstraction at the wall or in the gas phase could produce benzene. However, the gas phase abstraction of hydrogen from acetylene by phenyl radicals is probably endothermic and would not compete effectively with addition.

On the other hand, the rapid ionic polymerization can account for the disappearance of some of the acetylene and the formation of high molecular weight polymer. After the initial loss of H or H_2 in this process (to give $C_4H_3^+$ and $C_4H_2^+$) the reactions seem to involve only addition. This addition is stabilized by collision for small aggregates, but for high molecular weight polymers one expects that "sticky" ion-molecule collisions would occur. Little hydrogen would be produced by this mechanism and little hydrogen is observed in the early stages of reaction.^{2a} The major primary ions in any radiolysis of C_2H_2 should be $C_2H_2^+$ and to a lesser extent C_2H^+ , both of which will fall into this polymerization sequence. Remarkably little is known about the polymeric material ("cuprene") or any differences which might occur from different methods of formation. If one takes the temperature coefficient for $G(-C_2H_2)$ from Field³ in the radiation of acetylene with 2-Mev. electrons and calculates an activation energy, a value of 1.5 kcal./mole is obtained. This rather small temperature coefficient does not seem

to be incompatible with a complicated, predominantly ionic reaction mechanism.

The confusion about the formation of benzene in radiolysis of acetylene to essentially complete reaction may be helped by observations made on ionic reactions in benzene. In a brief and qualitative pressure study of benzene in the mass spectrometer it was observed that $C_2H_2^+$ fragment ions from benzene reacted rapidly with benzene but that $C_6H_6^+$ ions were relatively inert. Many ions of mass greater than 78 were observed so that ion-molecule reactions giving higher molecular weight product ions are probable in addition to charge transfer reactions established by Rudolph and Melton.²⁵ One would expect that the higher molecular weight ions might also react with acetylene in a manner analogous to the ionic polymerization reactions in acetylene and the inhibition of acetylene radiolysis by benzene should be less than 100% efficient. Also, the benzene may be removed by reaction with acetylene ions although benzene is relatively unreactive with itself under radiation.

It is of interest to consider previous work from this laboratory about reactions of acetylene and oxygen in terms of effects on acetylene radiolysis.²⁶ Reactions of O_2^+ with C_2H_2 to give oxygenated product ions were very slow, of the order of 10^{-11} cc./molecule-sec. and no evidence was observed for reactions of $C_2H_2^+$ with O_2 . Consequently, it seems reasonable that ionic polymerization of acetylene should occur readily in the presence of oxygen although termination could easily occur at different stages to give different polymers. According to Lind,^{2a} a polymer containing very little oxygen is produced in radiolysis of oxygen-acetylene mixtures. No mention was made of any benzene being observed under these conditions. Since no CO_2^+ and very little CO^+ were observed, it seems likely that the oxidation of C_2H_2 to CO_2 and CO occurs through a predominantly radical process.

Acknowledgments. The author is very grateful to Mr. W. C. Gieger for performing these experiments in his usual enthusiastic and competent manner as well as for his help with many of the calculations, and to J. L. Franklin for his helpful discussion.

(25) P. S. Rudolph and C. E. Melton, *J. Chem. Phys.*, **32**, 586 (1960).

(26) J. L. Franklin and M. S. B. Munson, "Xth International Combustion Symposium," Cambridge, England, Aug 1964.

The Nuclear Magnetic Resonance Spectra of Some 1,4-Diheterocyclohexanes

by William B. Smith and Ben A. Shoulders

Department of Chemistry, Texas Christian University, Fort Worth, Texas (Received September 16, 1964)

The n.m.r. spectra of morpholine, N-methylmorpholine, N-phenylmorpholine, and thioxane have been analyzed, and the pertinent chemical shifts and coupling constants have been determined. The spectra are all of the A_2B_2 type. The C^{13} -H spectrum of dioxane has also been re-examined.

Introduction

The utility of the Karplus equation for determining the relationship between the dihedral angle of C-H bonds on adjacent carbons and vicinal proton coupling constants is now well established.^{1,2} However, it is well known that factors other than the dihedral angle may play a role, as well, in determining the exact values of vicinal coupling constants.¹³ Perhaps the most significant other effect is that of the electronegativity of substituent groups.

A number of studies have established that for certain specific systems there is a linear decrease in vicinal coupling constants with increasing substituent electronegativity. Among these, mention should be made of measurements on rigid systems made by Williamson³ and by Laszlo and Schleyer.⁴ Recently, Abraham and Pachler⁵ have made determinations on a number of di-substituted ethanes. On the basis of the average coupling constants in 103 differently substituted ethanes, they derived the relation, $J_{av} = 17.97 - 0.796 \sum E$, where E is the Huggins electronegativity for the six atoms joined to the C-C fragment.

Recently, Huitric, *et al.*,⁶ have determined the axial-axial and axial-equatorial coupling constants for a series of partially deuterated *cis*- and *trans*-1-substituted-2-arylcyclohexanes. In contrast to the results above, they found no simple correlation between the electronegativity of the substituents and the various vicinal coupling constants.

The 1,4-diheterocyclohexanes offer an interesting system related to the studies of both Abraham and Pachler⁵ and Huitric, *et al.*⁶ We have determined the chemical shifts and coupling constants for a series of these compounds, and the results are reported below.

Experimental

The compounds, with one exception, used in this study were all commercially available substances. Their n.m.r. spectra were those of pure compounds and were consistent with the expected structures. Dimethylmorpholinium iodide was prepared by treating a sample of morpholine in benzene with an excess of methyl iodide. An exothermic reaction occurred, and the precipitated salt was collected and recrystallized from absolute ethanol, m.p. 244-246°; reported⁷ m.p. 246°.

The spectra were determined on a Varian A-60 spectrometer equipped with a variable temperature probe assembly. The frequency was calibrated against chloroform, and chemical shifts were read directly from the charts. The operating temperature of the probe was around 43°. Resolution checks on the instrument indicated 0.3 c.p.s. or slightly better.

Solutions of morpholine, N-methylmorpholine, N-phenylmorpholine, and thioxane in both carbon tetrachloride and benzene were outgassed before each determination. Tetramethylsilane was used as an internal standard. The only effect of the solvent change was a

(1) (a) M. Karplus, *J. Chem. Phys.*, **30**, 11 (1959); (b) *J. Am. Chem. Soc.*, **85**, 2870 (1963).

(2) For a general discussion and some applications see L. M. Jackman, "Applications of Nuclear Magnetic Resonance Spectroscopy in Organic Chemistry," Pergamon Press, New York, N. Y., 1959, Chapter 6; also, C. N. Banwell and N. Sheppard, *Discussions Faraday Soc.*, **34**, 115 (1962).

(3) K. L. Williamson, *J. Am. Chem. Soc.*, **85**, 516 (1963).

(4) P. Laszlo and P. von R. Schleyer, *ibid.*, **85**, 2709 (1963).

(5) R. J. Abraham and K. G. R. Pachler, *Mol. Phys.*, **7**, 165 (1963-1964).

(6) A. C. Huitric, J. B. Carr, W. F. Trager, and B. J. Nist, *Tetrahedron*, **19**, 2145 (1963).

(7) L. Knorr, *Ann.*, **301**, 13 (1898).

slight variation in the chemical shift of the ring methylene groups. Since the amines slowly reacted with carbon tetrachloride, the coupling constants were determined only for the benzene solutions. All determinations are reported on the average values taken from five or six spectral determinations.

The spectrum of N-phenylmorpholine was determined in carbon disulfide at 0 and -70° and on the pure liquid melt up to 180° . The only observed change in the spectrum was a slight broadening of lines at -70° . Since the tetramethylsilane line was also broadened at this temperature, it was assumed that this was an instrumental effect.

The methylene ring spectra in each case consisted of two multiplet bands symmetrical about the midpoint. A detailed display of the upfield multiplet of morpholine is given in Figure 1. The chemical shifts (τ) taken from the midpoint of each multiplet in carbon tetrachloride are shown in Table I.

Table I

	OCH ₂	XCH ₂
Morpholine ^a	6.45	7.27
N-Methylmorpholine	6.38	7.68
N-Phenylmorpholine	6.28	7.03
Thioxane	6.12	7.43
Dioxane	6.30	

^a The spectrum of morpholine is given in the "Varian Spectra Catalog," Varian Associates, Palo Alto, Calif., No. 83.

The structure of the morpholine methylene bands remain the same for the pure liquid, in carbon tetrachloride, in benzene, and in deuterium oxide. The usual upfield shift of the N-H is observed on dilution with the nonaqueous solvents indicating that morpholine is hydrogen bonded.

Addition of hydrochloric acid in portions to morpholine in D₂O first causes the upfield multiplet to be badly washed out and to reduce slightly the chemical shift between the methylene groups. In concentrated acid, the upfield band was broad, but seven perceptible humps appeared on the envelope. The downfield multiplet was broadened. However, the major structural features remained intact. The value of *N* (as defined below) was readily ascertained from the downfield multiplet. The internal chemical shift was estimated from the midpoints of each multiplet.

The solution of dimethylmorpholinium iodide in D₂O also gave two multiplets for the ring methylenes. In this case, the downfield multiplet was badly washed

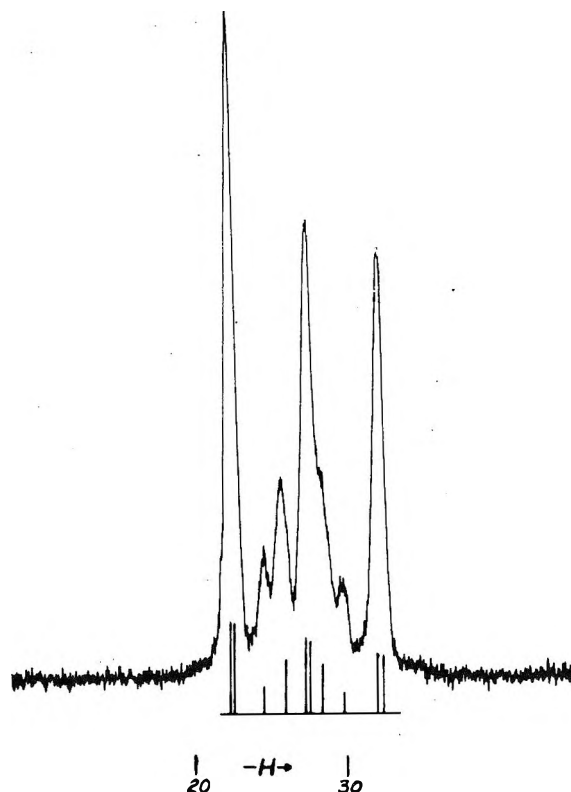


Figure 1. The N-methylene multiplet of morpholine determined in benzene solution at 60 Mc. This is the upfield half of an A₂B₂ spectrum. Frequencies are in c.p.s. from the band center. The line assignments from left to right are 4, 3, 12, 11, 8, 5, 10, 9, 2, and 1.

out with eight peaks on the envelope. While the upfield multiplet was slightly broadened, the features of the morpholine structure were quite evident again allowing an evaluation of *N*. The chemical shift difference was estimated as above.

The methylene multiplet structures for N-phenylmorpholine, N-methylmorpholine, and thioxane were all very similar to that of morpholine (Figure 1). The major alteration in the first two cases was due to lines 9-10 and 11-12 which merged into two somewhat broadened bands. The positions of these lines were estimated from the amount of broadening. In thioxane, line 12 appeared as a distinct shoulder on band 3-4, and line 9 appeared similarly on the downfield edge of band 1-2. Neither was resolved to the base line, and this was taken into account in estimating their frequencies.

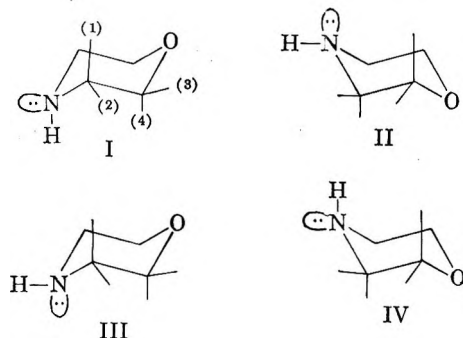
The C¹³-H spectrum of dioxane has been determined previously.⁸ The determination was repeated here on

(8) A. D. Cohen, N. Sheppard, and J. J. Turner, *Proc. Chem. Soc.*, 118 (1958).

the pure liquid. The results are reported in Table II, where it may be seen that a slight difference from the reported coupling constants was found.

Results and Discussion

1,4-Diheterocyclohexanes, such as those encountered in this study, most reasonably consist of rapidly equilibrating chair forms, for certainly the number of non-bonding hydrogen interactions are less than for cyclohexane itself. Given this statement, the following forms for morpholine may be considered.



In addition to the chair-chair interconversion, one must also take into account the rapid inversion of the nitrogen and the exchange of the mobile hydrogen on the nitrogen. This latter factor must also be rapid; otherwise, coupling of the N-H with the nitrogen methylenes would have been observed.

Reeves and Stromme⁹ have concluded from the n.m.r. spectrum of N,N'-dimethylpiperazine that chair-chair interconversion is rapid at room temperature. From a consideration of the change in the spectrum as the temperature is lowered, they concluded that the interconversion is relatively slow at -40° and that the two methyl groups most likely remain in equatorial positions owing to the rapid nitrogen inversion process.

The symmetrical spectrum of morpholine could arise either through a rapid equilibrium of I with IV or II with III, or through a rapid equilibrium among I, II, III, and IV. Aroney and LeFevre¹⁰ have concluded on the basis of dipole moment measurements that the hydrogen on the morpholine nitrogen remains in an axial position (*i.e.*, I \rightleftharpoons IV).^{11,11a} It is evident from the results reported here that the n.m.r. spectrum of morpholine offers no opportunity for a decision on this matter and that, as far as n.m.r. is concerned, all that can be said is that morpholine is a rapid equilibrium of interconverting chair forms in which the respective methylene hydrogens experience the same chemical shift. Reasonably, N-methylmorpholine and N-phenylmorpholine are rapidly interconverting chairs in which the N-substituent is always equatorial owing to

the rapid nitrogen inversion process. It follows also that thioxane and dioxane are rapidly interconverting chairs at room temperature.

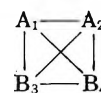
The spectra of the preceding compounds were analyzed as examples of typical A_2B_2 systems.^{12,13} The pertinent relations for interpreting the spectra are

$$N = J_{13} + J_{14} \quad J_{13} = J_{24}$$

$$L = J_{13} - J_{14} \quad J_{14} = J_{23}$$

$$K = J_{12} + J_{34}$$

$$M = J_{12} - J_{34}$$



where the numbers are for the hydrogens given in the preceding structures for morpholine. For rapidly equilibrating chair structures $J_{14} = (J_{aa} + J_{ee})/2$, $J_{13} = J_{ae}$, and J_{12} and J_{34} are the appropriate geminal coupling constants. The usual sum and difference relations for line frequencies may be used to determine N , L , M , and the internal chemical shift, Δ_{AB} .^{12,13} Assuming that J_{ae} equals J_{ee} , one may then calculate J_{aa} , J_{ae} , and the difference between the geminal coupling constants.

Initially, the line assignments for morpholine were made with the aid of reasonable values of Δ_{AB} , the appropriate J values, and the assumption that the spectrum approximated an A_2X_2 situation. Subsequent calculations of the exact A_2B_2 spectrum were made with the aid of the Freqint A 1620 computer program. Under the conditions encountered here, the value of K cannot be approximated from the experimental spectrum which, in fact, is quite insensitive to the exact value of K .^{5,14} For the purposes of the calculation, it was assumed that J_{12} was -13.2 c.p.s.⁹ The values for the coupling constants and Δ_{AB} for the compounds studied here are given in Table II.

(9) L. W. Reeves and K. D. Stromme, *J. Chem. Phys.*, **34**, 1711 (1961).

(10) M. Aroney and R. J. W. LeFevre, *J. Chem. Soc.*, 3002 (1958).

(11) A referee has pointed out that N. Allinger has recently presented evidence against this postulation (144th National Meeting of the American Chemical Society, Los Angeles, Calif., April 1963). Unfortunately, the abstract does not present this evidence.

(11a) NOTE ADDED IN PROOF. For the evidence on this point, see N. L. Allinger, J. G. D. Carpenter, and F. M. Karkowski, *Tetrahedron Letters*, **45**, 3345 (1964).

(12) (a) J. A. Pople, W. G. Schneider, and H. J. Bernstein, *Can. J. Chem.*, **35**, 1060 (1957); (b) "High Resolution Nuclear Magnetic Resonance," McGraw-Hill Book Co., Inc., New York, N. Y., 1959.

(13) D. M. Grant, R. C. Hirst, and H. S. Gutowsky, *J. Chem. Phys.*, **38**, 470 (1963).

(14) R. C. Hirst and D. M. Grant, *ibid.*, **40**, 1090 (1964).

Table II: Coupling Constants and Chemical Shifts of Some 1,4-Diheterocyclohexanes^a

Compound	<i>N</i>	<i>J_{aa}</i>	<i>J_{ae}</i>	Δ_{AB}	ΔJ_{gem}
Thioxane	10.0	12.05	2.65	83.60	1.97
Morpholine	9.7	10.28	3.04	54.24	1.45
N-Methylmorpholine	9.7	10.25	3.05	87.57	0.16
N-Phenylmorpholine	9.9	9.66	3.38	48.50	0.60
Morpholinium ion	9.9	39.5	...
N,N-Dimethylmorpho- linium iodide	9.7	33	...
Dioxane	9.3	10.2	2.8	...	0.00
Karplus values	7.2	9.2	1.7

^a All determinations were made in benzene solution, except the two ionic compounds, which were run in D₂O. All values are in c.p.s.

For the series, thioxane, morpholine, and dioxane, there is a marked decrease in *N*, a form of averaged *J_{aa}* and *J_{ae}*, with increasing electronegativity of the heteroatom substituents.¹⁵ The relation is not linear in the most exact sense. However, the fit would probably be no worse than that observed for several series of compounds by Abraham and Pachler.⁵ These authors observed that as the percentage of *trans* rotomer increased in their series of 1,2-disubstituted ethanes, there was a departure from linearity with the electronegativity relationship. The factor responsible for this deviation has not yet been ascertained.

One point of interest brought out by the data in Table II is the fact that the decrease in *N* in the preceding series is not due to a monotonic decrease in *J_{aa}* and *J_{ae}*. The linear relationship between the average vicinal coupling constants and the electronegativity of the substituents is obviously influenced in some subtle fashion by effects other than the electronegativity of the substituents.

The values of *N* and Δ_{AB} in Table II for the series morpholine, N-methylmorpholine, N-phenylmorpholine, morpholinium ion, and dimethylmorpholinium ion offer an interesting commentary on the question of group electronegativities *vs.* atom electronegativities in considerations of vicinal coupling constant effects. Presumably, the value of Δ_{AB} reflects the group electronegativity of the nitrogen moiety in the sense defined by Cavanaugh and Dailey.¹⁶ Williamson³ and Laszlo and Schleyer⁴ have found a relation between *J*

and *E_R* (the substituent electronegativity). Abraham and Pachler⁵ relied only on the Huggins atom electronegativity feeling that the anisotropy effects^{16,17} incorporated in the substituent electronegativities offered a fundamental point of objection to their use. Certainly, here the latter point of view would seem to be the more justified. Thus, Δ_{AB} varies over 160% between the dimethylmorpholinium ion and N-methylmorpholine while the value of *N* is unchanged. The enhanced inductive deshielding of the N-methylene in the quaternary salts compared to the N-methyl group is hardly surprising, but the lack of variation in the value of *N* again points to our inexact knowledge of how substituents influence vicinal coupling constants.

Finally, the spectra of the two quaternary nitrogen compounds deserve comment. In concentrated hydrochloric acid the exchange of the hydrogens on the morpholine nitrogen has been slowed, allowing the coupling of the N-H with the nitrogen methylene hydrogens to be observed. The system has now become an A₂B₂X₂ case, and the splittings of the O-methylene are broadened. However, the essential features of the morpholine O-methylene are still observable, and the value of *N* can be obtained. These observations parallel those of Grunwald, Loewenstein, and Meiboom¹⁸ on the spectrum of methylamine in acid. In dimethylmorpholinium iodide, the coupling is between the N¹⁴ nucleus and the O-methylene group. Since this splitting is imposed on the A₂B₂ multiplet structure of this group, the effect is to wash out the features of the band. The N-methylene band is somewhat broadened, but again a reliable value for *N* can be obtained. Similar couplings of N¹⁴ have been observed before.^{19,20}

Acknowledgment. We wish to express our gratitude to the Robert A. Welch Foundation for their generous support of this work.

(15) The sums of the heteroatom electronegativities: (O,S) 5.65; (O,N) 6.55; (O,O) 7.00 (M. L. Huggins, *J. Am. Chem. Soc.*, **75**, 4123 (1953)).

(16) J. R. Cavanaugh and B. P. Dailey, *J. Chem. Phys.*, **34**, 1099 (1961).

(17) See ref. 3, footnote 28.

(18) E. Grunwald, A. Loewenstein, and S. Meiboom, *J. Chem. Phys.*, **27**, 630 (1957).

(19) J. M. Anderson, J. D. Baldeschwieler, D. C. Dittmer, and W. D. Phillips, *ibid.*, **38**, 1260 (1963).

(20) M. Franck-Newmann and J. M. Lehn, *Mol. Phys.*, **7**, 197 (1963-1964).

The Kinetics of Calcium Formate Pyrolysis in Potassium Bromide Matrix¹

by K. O. Hartman and I. C. Hisatsune

Department of Chemistry, Whitmore Laboratory, The Pennsylvania State University, University Park, Pennsylvania 16802 (Received September 21, 1964)

The thermal decomposition of calcium formate dispersed in potassium bromide disks (infrared pellets) has been studied by observing the changes in optical densities with heating of several infrared absorption bands of the reactant formate and the product carbonate. The reaction was found to be first order in formate with a rate constant of k (sec.^{-1}) = $4.4 \times 10^{11} \exp[(-52,000 \pm 3000)/RT]$. Changing the matrix to potassium iodide, varying the initial formate concentration over a range of a factor of ten, or changing several conditions in the fabrication of the disks still gave the same kinetic results to within experimental errors. The deuterium isotope effect has also been measured.

Introduction

Quantitative kinetic studies of solid state chemical reactions have been conducted in the past largely by thermogravimetric method (t.g.a.) or by measuring the pressure of evolved gas as a function of time. In neither of these techniques can the concentrations of the reactant be determined directly nor can reaction intermediates be easily detected. Also, results from these techniques are often dependent on the particle size of the reacting phase.²

In this work we used an infrared spectroscopic method similar to that of Bent and Crawford^{3a} and Hisatsune and Suarez^{3b} to study the thermal decomposition of calcium formate in the solid state. The reactant was isolated in an inert matrix and quantitative kinetic results were obtained by directly following the concentrations of the reactant and the product.

The investigation of the calcium formate pyrolysis was chosen because this reaction appeared relatively free of complications and because some data such as the decomposition temperature⁴ and the product analysis⁵ were available. Also, the decomposition of mixtures of calcium formate and cupric formate⁶ and calcium palmitate⁷ have been reported. In the present work the stoichiometry, the reaction order, rate constants, and the activation energy were determined. Since a number of product and reactant infrared bands were followed, we were able to test our data for internal consistency. Results from thermogravimetric and differential thermal analyses were found to corroborate our results.⁸

Experimental

Chemicals. Calcium formate from Matheson Coleman and Bell (98.5%) was recrystallized from 20% ethanol. The crystals were transparent and most of them were light tan while some were colorless. The original powder had a light brown color.

Calcium formate-*d* was prepared from Fisher reagent grade calcium chloride and sodium formate-*d* (99%) of Merck Sharp and Dohme of Canada, Ltd. Approximately 0.1 g. of formate-*d* and 0.3 g. of calcium chloride were dissolved in 3 ml. of deionized water that had been distilled from a dilute KMnO_4 solution. Small colorless crystals precipitated, which were filtered and washed with 95% ethanol.

The matrix material was optical grade potassium bromide powder or potassium iodide crystal obtained

(1) Abstracted in part from a Ph.D. Thesis of K. O. Hartman.

(2) A. R. Carthew, *Am. Mineralogist*, **40**, 107 (1955).

(3) (a) H. A. Bent and B. Crawford, Jr., *J. Am. Chem. Soc.*, **79**, 1793 (1957); (b) I. C. Hisatsune and N. H. Suarez, *Inorg. Chem.*, **3**, 168 (1964).

(4) V. Zapletal, J. Jedlicka, and V. Ruzicka, *Chem. Listy*, **50**, 1409 (1956).

(5) (a) F. Fischer, A. Tropsch, and A. Schellenberg, *Ges. Abhandl. Kenntnis Kohle*, **6**, 330 (1921); (b) K. A. Hofmann and K. Schumpelt, *Ber. Chem. Ges.*, **49**, 303 (1916).

(6) V. Ruzicka and E. Kalařova, *Collection Czech. Chem. Commun.*, **27**, 429 (1962).

(7) H. Sakurai and Y. Okamoto, *Mem. Inst. Sci. Ind. Res. Osaka Univ.*, **17**, 209 (1960).

(8) F. W. Freeberg, Ph.D. thesis research in progress, Department of Chemistry, The Pennsylvania State University.

from Harshaw Chemical Co. The calcium carbonate was a Fisher reagent grade product.

Apparatus. The oven used for most of the work was a Tempco Model FA-1415M built by Thermolyne Co. In preliminary runs the oven temperature was only controlled from about ± 4 to $\pm 10^\circ$, but in subsequent runs a modification in the control unit allowed us to maintain constant temperature to within 0.8° . The oven could be operated up to about 900° . Oven temperatures were measured with a chromel-alumel thermocouple and a Minneapolis-Honeywell potentiometer (Rubicon Inst.) Model No. 2745.

The 13- and 15-mm. pellet dies, the mechanical grinder, and the hydraulic press that were used have been described previously.^{3b}

A Mettler semimicro balance Model S-6 was used to weigh samples for kinetic runs. Masses were read to 5×10^{-6} g. It was found by weighing an aluminum foil of 0.355 g. that the average deviation was 15×10^{-6} g. and that the maximum deviation was 50×10^{-6} g. These figures were determined by making 20 weighings over a period of 44 min. during which the room temperature varied between 25.0 and 25.5° . The balance zero was set before each weighing as was done when weighing samples for kinetic runs. A similar calibration carried out when room temperature varied from 21 to 25° indicated an average deviation of 50×10^{-6} g.

The spectra were recorded on a Perkin-Elmer Model 21 with a NaCl prism from 2 to 15μ or on a Perkin-Elmer Model 521 dual grating instrument from 2.5 to 40μ . The frequencies could be read from the grating instrument with a precision of 0.5 cm.^{-1} and the transmittance to 1%. Under the scanning conditions employed, the accuracy was of the order of 1.0 cm.^{-1} and 1% in transmittance.

Pellet Preparation. Initially, samples were prepared simply by weighing by difference the desired amount of calcium formate and potassium bromide. Since concentrations as low as 0.4 mg./g. , *i.e.*, 0.4 mg. of solute/g. of matrix salt, had to be prepared, a dilution method was used for later samples. A sample of calcium formate with a concentration of $20.63 \pm 0.06 \text{ mg./g.}$ was prepared, ground for 2 min., and heated for 1 hr. at 110° . Portions of this sample were weighed with additional potassium bromide. The concentrations of pellets prepared in this manner were known to 1%. The concentrations of calcium formate studied ranged from 0.4 to 4.0 mg./g.

The calcium formate and the alkali halide matrix were mixed by grinding them together in an agate vial and ball on a mechanical vibrator. The grinding time

was varied from 1 to 5 min. Some samples were mixed by hand grinding in an agate mortar.

After mixing, the powdered samples were evacuated for at least 3 min. in the pellet die before pressing. The pressing time was varied from 1 to 5 min., and the pressure from 5.84×10^4 to 17.5×10^4 p.s.i. Our pressed pellets were transparent and colorless or slightly cloudy. Typically, they weighed about 0.5 g.

Stoichiometry. The stoichiometry of the decomposition reaction was determined by using pellets containing known amounts of product, calcium carbonate, which were prepared by the dilution technique. From the spectra of these pellets a graph of absorbance of the 875 cm.^{-1} band *vs.* mg. of carbonate was constructed. The absorbance of the 875-cm.^{-1} band from the spectrum of a pellet in which the formate was completely decomposed was then read, corrected for pellet weight loss (see Kinetics section), and compared with the graph to determine the amount of carbonate produced.

The 875-cm.^{-1} band was used to determine the stoichiometry because it was an intense band and its band width in the product spectrum and in the reagent grade carbonate was approximately the same. Furthermore, it is a nondegenerate mode band⁹ which is less likely to be affected by the environmental differences.

Kinetics. The kinetic data were obtained in the following manner. The pellets were placed in the oven at a reaction temperature between 450 and 520° for the appropriate time period. They were then removed from the oven, cooled to room temperature, and the spectra were recorded. The pellets were usually cool to the touch within 30–40 sec. after removal from the oven. Such heating and quenching processes were repeated until the reaction was complete.

Besides simple observation of the change in the spectrum with heating, the following experiments were performed. After various heating times, the pellets were ground under atmospheres of nitrogen or oxygen. Others were ground under benzene. After such treatments the pellets were repressed and the spectra were again recorded. The effects of subsequent heating on these pellets were also investigated.

When a pellet was heated, it expanded, became opaque, and had to be re-pressed in order to restore transparency. This was done in early runs by breaking the pellet in half, placing the pieces in the die, and pressing at the usual pressure. This procedure led to inhomogeneities as evidenced by the change in optical density of solute bands with rotation of the pellet. With many re-pressings over the course of a long kinetic run,

(9) K. Nakamoto, "Infrared Spectra of Inorganic and Coordination Compounds," John Wiley and Sons, Inc., New York, N. Y., 1963, p. 92.

the optical density was observed to vary by as much as 30% with rotation of the pellet. Uniformly sanding off the pellets around the circumference so that they fitted the die eliminated this problem, and the optical density was independent of the orientation of the pellet in the spectrometer beam. With this method, however, 0.5 to 1.5% of the total weight of the pellet was lost with each re-pressing. The absorbances of the observed bands were corrected for this weight loss by multiplying the absorbance at time t by the initial weight of the pellet divided by the weight at time t . In early runs, the absorbance readings were corrected by following the decreasing thickness of the pellet with a micrometer. The thickness could not be determined with as much sensitivity as the weight, however. A weak band at 2170 cm^{-1} due to cyanate impurity^{3b} appeared in most of the heated pellets.

Results

Within the limits described in the Experimental section, variation of the pressure used to press the powder into pellets had no effect on the solute spectrum or on the decomposition rate. Increasing the grinding time, however, led to better dispersion of the solute in the matrix and, hence, to sharper absorption bands, but it did not cause a variation in the decomposition kinetics. It was found that grinding the powder while it was hot (approximately 90°) also gave better dispersion. Increments in grinding time beyond 3 min. had a negligible effect on the spectrum.

The following changes were observed in the spectrum of calcium formate with heating at high temperatures. The spectrum of the unheated pellet which consisted of crystallites of calcium formate embedded in potassium bromide matrix showed doublet structures in most of the formate bands. With short heating, the doublet structures of the calcium formate bands coalesced into singlets (Table I). The bands were still broad and remained so throughout the reaction. In some pellets the initial spectra did not show the doublet structure but showed instead the singlet bands, which were usually observed after heating. With continued heating, the intensities of the formate bands decreased until they finally disappeared. Another set of absorption bands, which were identified as those of calcium carbonate, appeared and grew with heating.

The observed frequencies of $\text{Ca}(\text{HCO}_2)_2$ and $\text{Ca}(\text{DCO}_2)_2$ in both potassium bromide and iodide matrices and their assignments are given in Table I. The frequencies are in good agreement with those reported by Harvey, *et al.*,¹⁰ except for the hydrogen out-of-plane bending mode which differs by 6 cm^{-1} for both

Table I: Observed Calcium Formate Frequencies (cm^{-1})

Mode ^a	Ca(HCO ₂) ₂				Ca(DCO ₂) ₂	
	Initial		Heated		Initial KBr only	Heated
	KBr	KI	KBr	KI		
$\nu(\text{C-H})$	2889 w 2862 w	2890 2865	2872 w	2875	2155	2143
$\nu_\alpha(\text{CO}_2)$	1580 vs	1585	1598 vs	1600	1590	1585
$\nu_\beta(\text{C-H})$	1397 s 1387 s	1400 1390	1378 s	1380	1029	1009
$\nu_\sigma(\text{CO}_2)$	1359 s 1348 s	1361 1351	1350 s	1354	1348	1340
$\nu_\omega(\text{C-H})$	1078 w 1068 w	1077 1066			909	
$\nu_\beta(\text{CO}_2)$	799 s 777 s	802 781	784 s	784	792	779

^a α = antisymmetric stretch; β = bending; σ = symmetric stretch; and ω = out-of-plane wagging.

doublet frequencies. The formate frequencies after heating are also listed in this table.

Table II gives a comparison of the frequencies of the reaction product and those of calcium carbonate in the calcite crystal structure dispersed in KBr matrix. All of the frequencies are in good agreement except for the antisymmetric stretch band at 1440 cm^{-1} , which is degenerate.

Table II: Observed Calcium Carbonate Frequencies, KBr Matrix (cm^{-1})

Assignment ^a	Decomposition product	Reagent salt
1087 (R) + 2 × 711	2500 w	2500
1087 (R) + 711	1790 m	1790
$\nu_\alpha(\text{CO})$	1440 vs	1420
ν_ω	875 s	874
	846 w	845
ν_β	711 m	710
$\nu(\text{Ca-O})$	310 m	308

^a See footnote of Table I. (R) = Raman active fundamental, see ref. 9.

Since formate samples prepared by the dilution technique had the most reliable concentrations, they were used to analyze the stoichiometry. In 19 runs, the ratio of moles of calcium formate to moles of calcium carbonate formed was found to be 0.96 ± 0.12 with a maximum deviation of 0.23. The ratio was independent of initial formate concentration which was

(10) K. B. Harvey, B. A. Morrow, and H. E. Shurvell, *Can. J. Chem.*, **41**, 1181 (1963).

varied by a factor of eight. The over-all reaction therefore is



Carbon monoxide trapped in the pellet was observed only twice in 40 runs. Its band was very weak and had the P- and R-branches at about 2150 and 2180 cm.^{-1} which were characteristic of a gas phase spectrum. It appeared after the initial heating in a kinetic run and then vanished after the next heating interval.

Other absorption bands observed during the course of the reaction were 2330 (w), 1630 (w), and 2655 (vw) cm.^{-1} . The 1630 and 2655 cm.^{-1} bands were due to formate ion isolated in the potassium bromide matrix. The 2330 cm.^{-1} band was due to carbon dioxide trapped in the matrix.^{3a}

No new bands were observed when a heated pellet was ground in oxygen or nitrogen and then repressed. In general, the absorbance of both the formate and carbonate increased regardless of whether oxygen or nitrogen was used. A new band at 662 cm.^{-1} was observed in the spectra of pellets that were ground under benzene and then re-pressed. This band was weak and disappeared upon heating the pellet at 100°.

By recording the spectrum at appropriate time intervals, optical density *vs.* heating time curves were constructed. These plots showed the continuous decrease of the formate concentration and the concomitant increase of the carbonate concentration.

Two methods were used to determine the order of the decomposition reaction. In the first method, the logarithm of $\Delta\text{O.D.}/\Delta t$ was plotted against the logarithm of O.D., where O.D. is the optical density of the reactant absorption band. Since the optical density is proportional to the concentration of the formate ion, the slope of this line is equal to the order of the reaction. Applying this treatment to the 784 cm.^{-1} formate band, we obtained a reaction order of 1.0 ± 0.1 in eight runs. Orders of 1.04 and 1.09 were found from a similar treatment on the 711 and 1440 cm.^{-1} carbonate absorption bands. The second method was simply plotting the logarithm of any formate band optical density against time and observing that this was a linear function of time for over 90% of the reaction.

To evaluate the rate constants, the logarithm of the optical density of a formate band or the logarithm of the carbonate optical density at the end of the reaction minus its value at time *t* was plotted against time. This was done for absorption bands which did not appreciably overlap with other bands. Such plots for different bands gave approximately the same slopes. The rate constants obtained from the various carbonate

Table III: Calcium Formate Decomposition Rate Constants ($10^{-3} \text{ min.}^{-1}$ units)

Temp., °C.	784 cm.^{-1} (HCO_2^-)	711 cm.^{-1} (CO_3^{2-})	875 cm.^{-1} (CO_3^{2-})
Potassium bromide matrix			
450 ± 1	5.1	4.9	5.4
450 ± 1	5.2	4.8	5.5
454 ± 6	6.0	12	15
454 ± 6	5.7	7.5	9.3
454 ± 6	6.7	6.9	7.0
456 ± 5	9.0	14	16
456 ± 5	8.7	11	15
480 ± 1	23	27	
490 ± 1	37	41	
490 ± 1	37	37	40
500 ± 4	48	47	
500 ± 4	49	44	49
500 ± 4	58	55	
505 ± 10	48	40	23
505 ± 10	62	57	52
505 ± 10	86	38	41
507 ± 1	82	91	88
515 ± 8	72	70	71
515 ± 8	72	72	71
518 ± 6	120	110	120
518 ± 6	98	100	110
Potassium iodide matrix			
491 ± 1	42	43	44
491 ± 1	40	41	39
Calcium formate-d in potassium bromide matrix			
468 ± 1	4.8	5.0	5.0
491 ± 1	19	19	23
509 ± 1	46	45	45

and formate bands are listed with the reaction temperatures in Table III. The scatter in some of the constants that should be the same was due to two things: poor temperature control and inhomogeneities introduced by breaking the pellets in the re-pressing process. With the elimination of these sources of error, the precision of the rate constants was improved to 10% uncertainty. The rate constants were observed to be independent of the concentration for the range studied which was from 0.4 to 4.0 mg./g.

The first-order rate constants for the decomposition of calcium formate in a potassium iodide matrix at 490° are also listed in Table III. They are within experimental error of those obtained in the potassium bromide matrix.

In Table IV the activation energies and frequency factors obtained from various absorption bands that were followed are summarized. The results from the 784 cm.^{-1} formate band are the most reliable since this band had sufficient intensity and did not overlap with

Table IV: Experimental Activation Energy and Frequency Factor

Frequency, cm.^{-1}	Activation energy, kcal./mole	Frequency factor, sec.^{-1}
Potassium bromide matrix		
784 (formate)	52.0 ± 3.0	4.4×10^{11}
1598 (formate)	49.0 ± 3.0	8.0×10^{10}
875 (carbonate)	50.0 ± 3.0	1.3×10^{11}
711 (carbonate)	51.5 ± 3.0	3.2×10^{11}
Potassium iodide matrix		
784 (formate)	$(52.0)^a$	4.0×10^{11}
Calcium formate- <i>d</i> in potassium bromide matrix		
779 (formate)	59.0 ± 3.0	1.5×10^{13}
Thermogravimetric analysis		
Undiluted $\text{Ca}(\text{HCO}_2)_2$	47 ± 6^b	
Undiluted $\text{Ca}(\text{HCO}_2)_2$	56 ± 6^c	6.0×10^{13}
$\text{Ca}(\text{HCO}_2)_2$ in KBr disk	56 ± 6^c	1.0×10^{13}
$\text{Ca}(\text{HCO}_2)_2$ in KBr disk	$(52)^c$	5.0×10^{11}

^a Activation energy from 784 cm.^{-1} band in KBr matrix.

^b Isothermal run. ^c Temperature programmed run. ^d Isothermal run, activation energy from 784 cm.^{-1} band in KBr matrix.

other absorption bands. The 3 kcal./mole error was calculated on the basis of 10% error in the experimental rate constants, and activation energies calculated from different calcium formate and calcium carbonate bands agreed within this estimated error.

The rate constants and activation energies determined by the thermogravimetric analysis⁸ are also listed in Table IV. The frequency factor for the isothermal run in KBr disk was calculated using the spectroscopically determined activation energy.

The pyrolysis of calcium formate-*d* was investigated at three temperatures and the observed rate constants are given in Table III. The activation energy was 59 ± 3 kcal./mole.

Discussion

We observed spectroscopically that two formate ions decomposed to form one carbonate ion. This stoichiometry was also confirmed by the thermogravimetric analysis.⁸ Although oxalate has been reported as a minor product,^{5b} we did not observe its characteristic infrared bands during our pyrolysis. The other products, hydrogen and carbon monoxide, would easily diffuse out of the matrix during the heating cycle and, in fact, our disks showed blistering after heating. There was also strong evidence that carbon monoxide, which was actually observed twice, disproportionated into carbon dioxide and carbon in the disks. Trapped carbon dioxide was observed in all pellets, and a gray or brown color developed in the disks with heating. Similar color changes have been reported also by pre-

vious investigators.^{5b} Samples run in the differential thermal analyzer under nitrogen atmosphere also had a gray color while those decomposed under oxygen atmosphere, where the carbon monoxide was completely oxidized to carbon dioxide, were white. Undoubtedly, the coloring of the pellets with heating is due to formation of dispersed carbon in the matrix. Such disproportionation of carbon monoxide has been observed by others in the solid state decomposition of oxalates.¹¹ Glasner and Steinberg¹² have measured the extent of disproportionation in rare earth oxalates under a variety of conditions and found as much as 70% reaction.

The broadness of the infrared bands throughout the reaction and the fact that calcite was the reaction product indicated that most of the calcium formate did not go into solid solution with the matrix salt. The sharp although weak bands at 1630 and 2655 cm.^{-1} showed, however, that a small amount of formate ions did go into the matrix. These bands have been identified as solid solution bands of formate ion in potassium bromide matrix on the basis of a parallel work in progress in this laboratory on the decomposition of sodium and potassium formate in potassium bromide matrix.

Since the calcium formate did not go into solid solution with the matrix to any significant extent, the matrix should not greatly affect the decomposition kinetics of calcium formate. Other experimental observations which support this view are as follows. In both potassium bromide and iodide matrices, the reaction rate constants were the same within experimental error. Arrhenius activation energies obtained from the thermogravimetric analysis on undiluted calcium formate are also in agreement with our spectroscopic values. The rate constants from the t.g.a., however, are higher than ours by a factor of about 30. These differences, we believe, are due to the fact that in the t.g.a. the oven temperature rather than the sample temperature was measured and that self-heating of the sample¹³ occurred during the decomposition. The differential thermal analysis of the undiluted calcium formate in oxygen atmosphere showed an exothermic peak due to CO oxidation and a large jump in the sample temperature.

Freeberg also followed the decomposition of calcium formate in KBr matrix by the t.g.a. method.⁸ An isothermal run at 472° on a pellet containing 10 mg. of calcium formate/g. of potassium bromide gave a rate

(11) E. L. Head and C. E. Holley, Jr., *J. Inorg. Nucl. Chem.*, **26**, 525 (1964).

(12) A. Glasner and M. Steinberg, *ibid.*, **22**, 39 (1961).

(13) A. E. Newkirk, *Anal. Chem.*, **32**, 1558 (1960).

constant of $25 \times 10^{-3} \text{ min.}^{-1}$ with an estimated error of about 30%. A temperature-programmed run on a similar pellet gave $56 \pm 6 \text{ kcal./mole}$ for the reaction activation energy. These results are in good agreement with the spectroscopic values of $18 \times 10^{-3} \text{ min.}^{-1}$ and $52 \pm 3 \text{ kcal./mole}$, respectively, for the rate constant at the same temperature and the activation energy. Interestingly, smoother thermogravimetric curves were obtained from decomposition studies with KBr disks compared to those from undiluted material.

The large difference between the rate constants for the decomposition of $\text{Ca}(\text{HCO}_2)_2$ and $\text{Ca}(\text{DCO}_2)_2$ suggests that we have a primary isotope effect with a C-H bond of the formate ion being broken in the transition state. The temperature dependence of the kinetic isotope effect can be estimated by considering the zero-point energy effect¹⁴

$$k_{\text{H}}/k_{\text{D}} = \exp[h\nu(\nu_{\text{H}} - \nu_{\text{D}})/2kT]$$

where ν is the C-H (C-D) bond stretching frequency in cm.^{-1} . Using the observed frequencies given in Table I, we have calculated the ratios of $k_{\text{H}}/k_{\text{D}}$, and these together with the observed ratios are listed in Table V.

Table V: Kinetic Isotope Effect

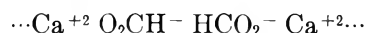
Temp., °K.	$k_{\text{H}}/k_{\text{D}}$	
	Obad.	Calcd.
782 \pm 1	1.87 \pm 0.35	1.95
764 \pm 1	2.00 \pm 0.40	1.97
741 \pm 1	2.75 \pm 0.55	2.02
Temperature dependence	$\exp[(+7000 \pm 6000)/RT]$	$\exp[+2000/RT]$

The temperature dependence of $k_{\text{H}}/k_{\text{D}}$ is also given in this table. The agreement between theory and experiment is reasonable in view of the approximate nature of the above equation.

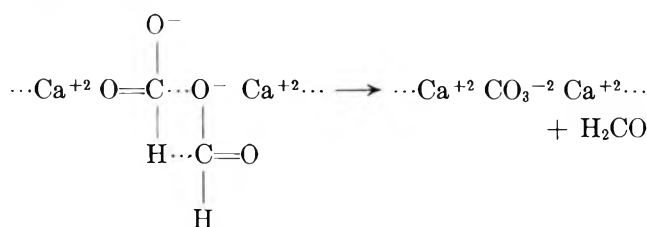
Ovenall and Whiffen¹⁵ have generated CO_2^- radical in sodium formate single crystals by γ -irradiation, and Brivati, *et al.*,¹⁶ have produced the same free radical in calcium formate in a similar manner. Since there was the possibility that the CO_2^- radical may have been generated thermally in our pellets, we have examined the e.p.r. spectra of several of the heated disks. However, no signal due to free radicals was observed. This negative result together with the fact that the observed activation energy is smaller than the formate C-H bond dissociation energy, which we estimate to be about 76 kcal./mole by analogy with formaldehyde,¹⁷ suggests that the reaction rate-determining step is not

a simple dissociation of the formate ion into a hydrogen atom and a CO_2^- free radical.

Some insight into the mechanism of the decomposition reaction of calcium formate can be gained by examining the crystal structure even though our spectral data show that the structure of this compound in heated pellets is not the same as the room temperature structure. The room temperature single crystal structure¹⁸ shows that there is an alternating chain illustrated schematically as follows.



The distance between the carbon atom of one formate ion and the closest oxygen atom of the next ion is 3.3 Å., and the distance between the carbon atoms of the two ions is 3.85 Å. Since the C-O distance in carbonate ion is 1.3 Å., the formate ions need only move by about 1 Å. toward each other and rotate slightly to form the following transition complex.



This complex can then break as shown above, into a carbonate ion, which is between two calcium ions, and formaldehyde, which immediately decomposes into hydrogen gas and carbon monoxide. Formaldehyde is known to decompose readily above about 150°.¹⁹ The distance between two calcium ions in room temperature structure of calcium formate is 6.7 Å., and this may be compared to a distance of 6.36 Å. in calcite. The mechanism described above is similar to one of the three decomposition mechanisms proposed earlier by Hofmann and Schumpelt.⁵

The energetics of the above reaction scheme can be estimated and compared with experimental quantities. From the standard heats of formation and available heat capacity data, we calculate that the over-all decomposition reaction is endothermic by 14 kcal./mole.

(14) L. Melander, "Isotope Effects on Reaction Rate," Ronald Press Co., New York, N. Y., 1962, p. 20.

(15) D. W. Ovenall and D. H. Whiffen, *Mol. Phys.*, **4**, 135 (1960).

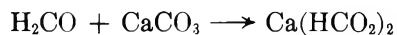
(16) J. A. Brivati, N. Keen, M. C. R. Symons, and P. A. Trevalian, *Proc. Chem. Soc.*, 66 (1961).

(17) T. L. Cottrell, "The Strengths of Chemical Bonds," 2nd Ed., Butterworth and Co., Ltd., London, 1958, p. 184.

(18) I. Nitta and K. Osaki, *X Sen* (Osaka Univ.), **5**, 47 (1948), cited in *Struct. Rept.*, **2**, 556 (1948).

(19) H. Newton and B. F. Dodge, *J. Am. Chem. Soc.*, **55**, 4747 (1933).

This value compares favorably with an experimental value of 15.5 ± 2 kcal./mole obtained by differential thermal analysis.⁸ From the experimental enthalpy of activation of 52 kcal./mole and the estimated enthalpy of decomposition of formaldehyde of +2.6 kcal./mole, we obtain an enthalpy of activation of 40.6 ± 3 kcal./mole for the reverse reaction



This value may be compared with 45 kcal./mole calculated from the Hirschfelder rule²⁰ in which the C-H bond energy in formaldehyde and the CO bond energy in the carbonate ion were taken, respectively, as 76 kcal./mole¹⁷ and 84 kcal./mole.²¹ The experimental entropy of activation for the over-all reaction is a small negative value (-7.1 ± 5 cal./deg.-mole), and this is also consistent with the above reaction scheme which involves a cyclic transition complex. Another evidence which suggests that formaldehyde may be involved in our reaction is the observation made by Toyoda.²² He has identified formaldehyde as one of the products of calcium formate pyrolysis carried out at reduced pressure.

Summary

The thermal decomposition of calcium formate has been studied in the solid state by observing the changes

in the infrared absorption bands of calcium formate dispersed in KBr matrix. The changes in concentrations of both the reactant and product were followed spectroscopically, and the reaction rate constants, activation energy, kinetic isotope effect, and stoichiometry were determined. Our spectroscopic kinetic results were found to be in good agreement with those from thermogravimetric analysis. Comparison of these data suggests that our spectroscopic method gave good experimental precision. Furthermore, our technique enables checks for internal consistency of the data and also affords opportunities of observing possible reaction intermediates. The present infrared pellet method should be of general utility in the study of solid state chemical reactions.

Acknowledgments. We are pleased to acknowledge the financial assistance from the National Science Foundation in the form of a research grant, NSF-G17346. We are indebted to F. E. Freeberg for the thermogravimetric and differential thermal analyses data.

(20) A. A. Frost and R. G. Pearson, "Kinetics and Mechanism," 2nd Ed., John Wiley and Sons, Inc., New York, N. Y., 1962, p. 107.

(21) L. Pauling, "The Nature of Chemical Bond," 3rd Ed., Cornell University Press, Ithaca, N. Y., 1960, p. 85.

(22) R. Toyoda, *Bull. Inst. Chem. Res. Kyoto Univ.*, **20**, 11 (1950).

The Dehydration of Ethanol on Aluminas of Various Specific Surface Areas

by William H. Wade, Shiichiro Teranishi, and Jack L. Durham

Department of Chemistry, The University of Texas, Austin 12, Texas (Received September 25, 1964)

Samples of alumina with surface areas from 2.72 to 221 m.²/g. were studied to compare their catalytic activities for the dehydration of ethanol. The individually adsorbed amounts of ethanol, ethyl ether, and water measured by gas chromatography indicated three adsorption modes of water and ethanol and at least two modes for ethyl ether. The order of adsorbed amounts of water, ethanol, and ethyl ether correlated with the order of heats of immersion of the aluminas in water, which was previously found to be directly proportional to particle size. On the other hand, the catalytic activities as a function of particle size exhibit a maximum, with both the lowest and highest area aluminas having minimal activity.

Introduction

Though many papers have been published¹⁻⁶ regarding the dehydration of ethanol on alumina, in general, the aim has referred to the mechanism on a fixed alumina, and the mechanisms sometimes conflict with each other. The generally accepted mechanism involves the bonding of ethanol by a surface-OEt linkage. Ether production is by interaction of two adjacent OEt groups and ethylene production by an internal degradation of individual OEt groups.

It has been shown in previous publications from this laboratory that there is a considerable decrease in the heat of immersion in water and methanol with increased specific area for alumina samples⁷ as well as for silica and titania.⁸ This variation of heat of immersion has been interpreted as a fundamental variation of surface amorphous character with particle size and is consistent with the entropies of adsorption calculated from the water and methanol adsorption isotherms for these samples.⁹

The aim of the present investigation is to determine the influence of alumina particle size on the adsorption behavior of ethanol, ethyl ether, ethylene, and water both separately and under simulated reaction conditions. This reaction was chosen for its relative simplicity, quantitateness, and applicability to previous studies. Gas-solid chromatography as a dynamic method is well suited to such studies of adsorption on catalytically active surfaces.¹⁰ By this technique the heat of adsorption and partition coefficients by the rele-

vant species under reaction conditions may also be determined.

Experimental

The B.E.T. surface areas were obtained from krypton adsorption isotherms and surface areas of all samples were independent of outgassing temperature above 120°. The crystalline modification was determined both by X-ray and infrared spectrometry.

The following three types of experimental measurements were performed.

(A) *Reaction Pattern Studies.* The equipment is diagrammed in Figure 1. The reaction products were separated on a Carbowax-400 column with helium as a carrier gas. Columns containing the various alumina catalysts were U-shaped capillary tubes of 40 cm. total length. A soap film flowmeter was used to monitor

(1) P. N. Peace and C. C. Yung, *J. Am. Chem. Soc.*, **46**, 390, 2397 (1924).

(2) W. S. Brey and K. A. Krieger, *ibid.*, **71**, 3637 (1949).

(3) K. V. Topchieva, K. Yun-Pin, and I. V. Smirnova, *Advan. Catalysis*, **9**, 799 (1957).

(4) J. B. Butt, H. Bliss, and C. A. Walker, *A.I.Ch.E. J.*, **8**, 42 (1962).

(5) J. E. Stauffer and W. L. Kranish, *Ind. Eng. Chem., Fundamentals*, **1**, 107 (1962).

(6) J. H. de Boer, *et al.*, *J. Catalysis*, **2**, 1 (1963).

(7) W. H. Wade and N. Hackerman, *J. Phys. Chem.*, **64**, 1196 (1960).

(8) W. H. Wade and N. Hackerman, *ibid.*, **66**, 1823 (1962).

(9) R. L. Every, W. H. Wade, and N. Hackerman, *ibid.*, **65**, 937 (1961).

(10) S. A. Greene and H. Pust, *ibid.*, **62**, 55 (1958).

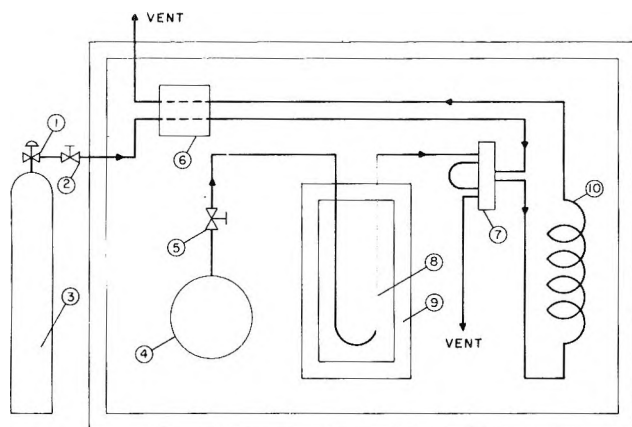


Figure 1. Diagram of equipment used for the dehydration of ethanol: 1, 2, and 5, metering valve; 3, helium tank; 4, ethanol bulb; 6, detector cell; 7, sampling valve; 8, catalyst tube; 9, dewar flask; and 10, Carbowax column.

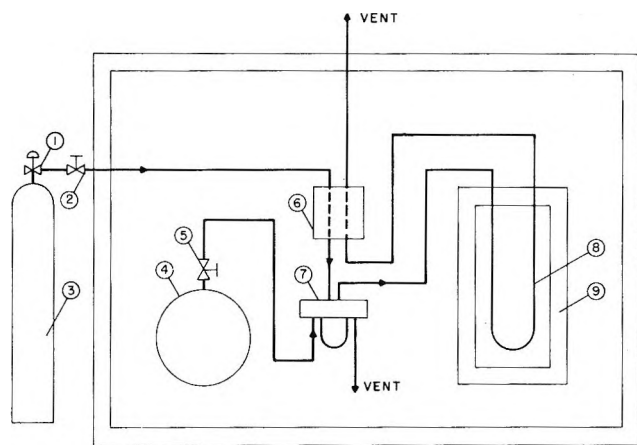


Figure 2. Diagram of equipment used for the measurement of adsorption amounts of ethanol, ethyl ether, and water. The numbers have the same meaning as in Figure 1, where sample bulb 4 contains either ethanol, ethyl ether, or water.

gas flow rates. The catalytic activity of each alumina sample was determined by measuring the rate of formation of ethyl ether and ethylene as a function of temperature and ethanol flow rate.

(B) *Studies of Adsorbed State for Individual Species.* The heats of adsorption and partition coefficients of pure water, ethanol, and ethyl ether on the four aluminas were also determined by gas chromatographic techniques by measuring the retention times on the four samples at temperatures below which measurable reaction occurs. The equipment is diagrammed in Figure 2. For each alumina sample, the reaction tube and sample were the same as previously used in the reaction pattern studies.

(C) *Studies of Adsorbed State under Reaction Conditions.* In a separate series of experiments, the heats of

adsorption of ethanol and ether were measured under simulated reaction conditions, *i.e.*, in the "working state." For the adsorption of ethanol in the reaction process, ethyl ether was the carrier gas, and reaction vapor in a delay coil was used as the reference gas. Analogously, for the adsorption of ether, ethanol was the carrier gas.² The retention times were measured as a function of catalyst temperature by injecting a small amount of either gaseous ethanol or ether into a steady vapor stream of the other preceding the alumina sample. The retention time was taken to be the time corresponding to the maximum deviation of the reaction vapor composition from the steady-state concentration.

All measurements were made with a Gow-Mac detector cell and power supply and a Moseley 1-mv. recorder. Sample volumes of 0.25 cc. were injected into the system with an Aerograph sampling valve. The detector cell, sampling valve, and, when used, the Carbowax-400 column were operated in an air bath at $100 \pm 1^\circ$.

Results

The four samples of alumina used in these studies are listed in Table I with their specific surface areas and crystalline modifications.

Table I: Alumina Samples

Sample	Manufacturer's designation	Area, m. ² /g.	Crystal mod.
A ^a	F-10	221	Amorphous
B ^b	Alucer MA	104	γ -Al ₂ O ₃
C ^b	Alon C	65	γ -Al ₂ O ₃
D ^c	Alucer MC	2.72	α -Al ₂ O ₃

^a Supplied by Aluminum Company of America. ^b Supplied by Gulton Industries, Inc. ^c Supplied by Godfrey L. Cabot, Inc.

The partition coefficients for water, ethanol, and ethyl ether normalized to unit area were calculated from eq. 1¹¹

$$\frac{V}{WRT\Sigma} = K \quad (1)$$

where W = weight of alumina in grams; R = gas constant, 6.236×10^6 mm. cc. deg.⁻¹ mole⁻¹; T = temperature of the flow meter (298°K.); V = corrected retention volume in cc.; K = partition coefficient between the adsorbed and gas phase; and Σ = specific surface area of alumina in m.²/g.

(11) S. Ogasawara and J. Cvjetanovic, *J. Catalysis*, 2, 45 (1963).

I. General Dehydration Behavior. In the dehydration of ethanol on alumina at low temperatures (220–280°) samples A, B, and C have ethyl ether and water as the main reaction products. Ethyl ether concentration initially increases as the reaction temperature increases and passes through a maximum. At high temperatures (290–340°) ethylene concentration increases and ethylene and water become the main products. This is the normal course of the reaction.

Typical isothermal curves that show the relationship between the mole per cent of ethyl ether and ethylene *vs.* the reciprocal flow rate of ethanol are shown in Figure 3. The rate of formation, r , of these species is calculated from

$$\begin{aligned} r_{(\text{C}_2\text{H}_5)_2\text{O}} &= [(\text{C}_2\text{H}_5)_2\text{O}]/(\Sigma/F) \\ r_{\text{C}_2\text{H}_4} &= [\text{C}_2\text{H}_4]/(\Sigma/F) \end{aligned} \quad (2)$$

where $r_{(\text{C}_2\text{H}_5)_2\text{O}}$ and $r_{\text{C}_2\text{H}_4}$ represent the rate of formation of ethyl ether and ethylene from ethanol in cc./mm.²-min.; $[(\text{C}_2\text{H}_5)_2\text{O}]$ and $[\text{C}_2\text{H}_4]$ are the mole fractions of $(\text{C}_2\text{H}_5)_2\text{O}$ and C_2H_4 in the exit gas stream; Σ is the total surface area of alumina in catalyst tube in m.²; and F is the flow rate of ethanol in cc./min.

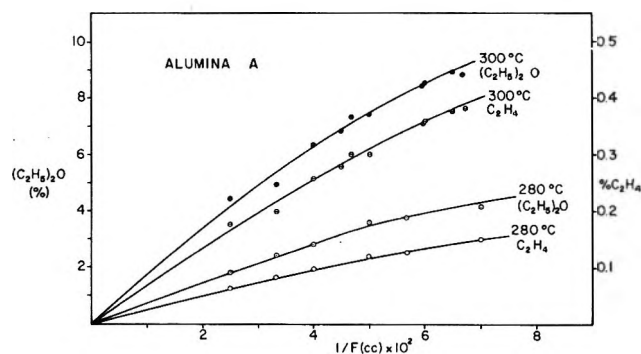


Figure 3. Rate of formation of ether (%) and ethylene (%) from ethanol on alumina *vs.* reciprocal of flow rate of ethanol.

The nonlinearity of the data of Figure 3 is indicative of a significant depletion of ethanol vapor at low flow rates. For this reason, the curves were extrapolated to $(1/F) = 0$ and these initial rates are given in Table II. Also, the corresponding values of the apparent activation energy are likewise tabulated. As can be seen in this table, the catalytic activities for the production of both ethylene and ethyl ether have the order: D, A, B, and C.

II. The Adsorption of Ethanol, Ethyl Ether, and Water on Alumina. A. *Ethanol.* Typical corrected retention times of ethanol for alumina A as a function of temperature are shown in Figure 4. Similar curves for all samples are distinguished by having two maxima

Table II: Catalytic Activities of Aluminas for the Dehydration of Ethanol

Sample	$\Delta E_{(\text{C}_2\text{H}_5)_2\text{O}}$, ^a kcal./mole	$\Delta E_{\text{C}_2\text{H}_4}$, ^b kcal./mole	$r_{(\text{C}_2\text{H}_5)_2\text{O}}$, ^c at 280°	$r_{\text{C}_2\text{H}_4}$, ^d at 320°	Temp. range, °C.
A	30.2	31.1	3.59×10^{-3}	7.31×10^{-4}	220–340
B	28.8	36.5	4.97×10^{-2}	3.14×10^{-2}	220–340
C	25.2	39.3	6.88×10^{-2}	9.03×10^{-2}	220–340
D	24.7	28.1	$(3.42 \times 10^{-6})^e$	0.74×10^{-4}	310–380

^a Apparent activation energy for the dehydration of ethanol to ethyl ether. ^b Apparent activation energy for the dehydration of ethanol to ethylene. ^c The initial rate of formation of ethyl ether from ethanol (cc./m.² min.). ^d The initial rate of formation of ethylene from ethanol (cc./m.² min.). ^e Extrapolated value.

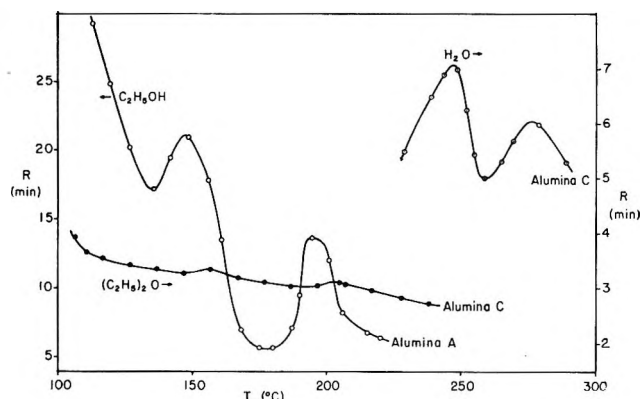


Figure 4. Adsorption behavior of ethanol, ethyl ether, and water on aluminas; typical curves of the retention time *vs.* temperature.

corresponding to three regions of differing adsorptive behavior: a low temperature region ($<140^\circ$), an intermediate temperature region ($140\text{--}210^\circ$), and a high temperature region ($>210^\circ$). Since the retention time is directly proportional to the steady-state adsorption amount of ethanol, the curve in Figure 4 for alumina C is, in essence, an adsorption isobar for ethanol. Isobar maxima are usually associated with transitions between different modes of adsorption. For n maxima there must be $(n + 1)$ adsorbed modes. In these studies, the low temperature mode is referred to as physical adsorption, the high temperature mode as chemisorption, and the intermediate mode as “weak” chemisorption.

The partition coefficients of ethanol calculated by eq. 1 are shown in Figure 5 as a function of temperature for all four catalysts. These coefficients must be average values because the adsorption isotherms are outside the Henry's law region as evidenced by the asymmetrical chromatographic peak shapes for ethanol and

reaction products. The heats of adsorption of ethanol calculated from Clausius-Clapeyron plots for each alumina sample are given in Table III. It is evident

Table III: Partition Coefficients, K' ($\mu\text{mole}/\text{m}^2 \text{ torr}$), and Heats of Adsorption, ΔH (kcal./mole), for Ethanol, Ethyl Ether, and Water on Alumina Samples

Sample	T. °C.	—C ₂ H ₅ OH—		—(C ₂ H ₅) ₂ O—		—H ₂ O—	
		K'	ΔH	K'	ΔH	K'	ΔH
A	200	1.27×10^{-2}	8.5	1.21×10^{-3}	8.3		
	280					1.05×10^{-2}	8.9
B	200	1.46×10^{-2}	8.3	1.01×10^{-2}	7.3		
	280					2.28×10^{-2}	8.6
C	200	2.70×10^{-2}	7.6	2.8×10^{-2}	7.1		
	280					4.52×10^{-2}	7.8
D	200	8.61×10^{-2}	7.5	6.26×10^{-2}	7.1		
	280					1.09×10^{-1}	7.6

from Figure 5 that the order of surface concentration of ethanol for the four aluminas at temperatures just less than those leading to measurable reaction is A, B, C, and D; *i.e.*, alumina D, has the greatest amount of adsorbed ethanol per unit surface area and alumina A has the least amount.

(B) *Ethyl Ether*. In the case of the adsorption of ethyl ether on alumina, the relationship between the retention time and temperature does not yield as pronounced maxima and minima as does ethanol as is seen in Figure 6. However, the ether partition coefficients on the four catalysts are in the same order as for ethanol. The heats of adsorption on each alumina sample are given in Table III.

(C) *H₂O*. The retention time of water as a function of temperature on alumina C is also shown in Figure 4. In this case, the temperature upper limit was extended to 300°. The high-temperature region was considered to be above 250°, but the low-temperature region is difficult to define because of excessive retention times. In the intermediate temperature region (200–270°), generally two peaks were found. The adsorbed amounts of water as a function of temperature are given in Figure 7. The heats of adsorption of water on each alumina are shown in Table III. The adsorption amounts of water at the same temperature (in the high-temperature region) are once again in increasing order: A, B, C, and D.

III. *Adsorption under Reaction Conditions*. The heats of adsorption and partition coefficients under simulated reaction conditions are listed in Table IV. By comparison of the relevant data of Tables III and IV, both similarities and differences are noted. The partition coefficients show a close parallelism for the two types of measurements. The extent of adsorption

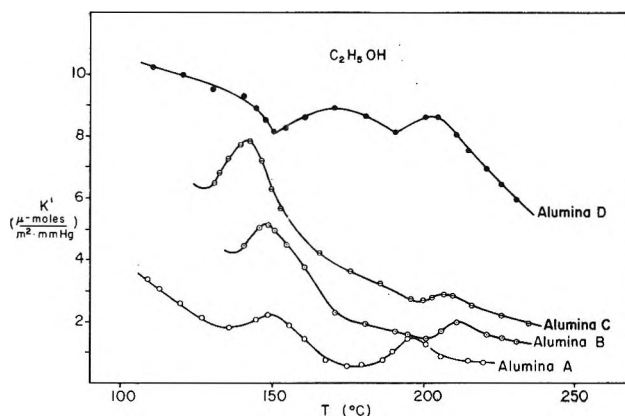


Figure 5. Adsorption amounts of ethanol on aluminas as a function of temperature.

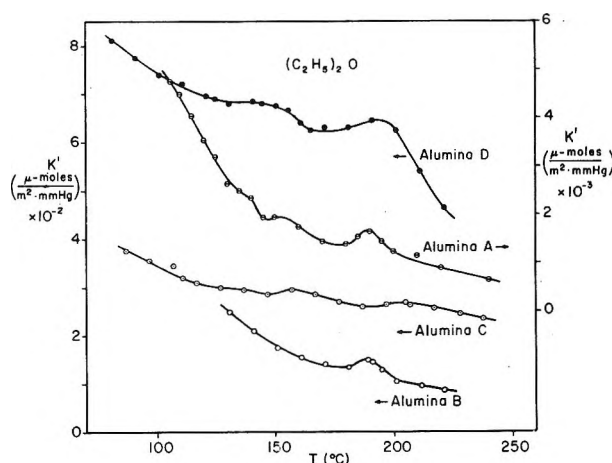


Figure 6. Adsorption amounts of ethyl ether on aluminas as a function of temperature.

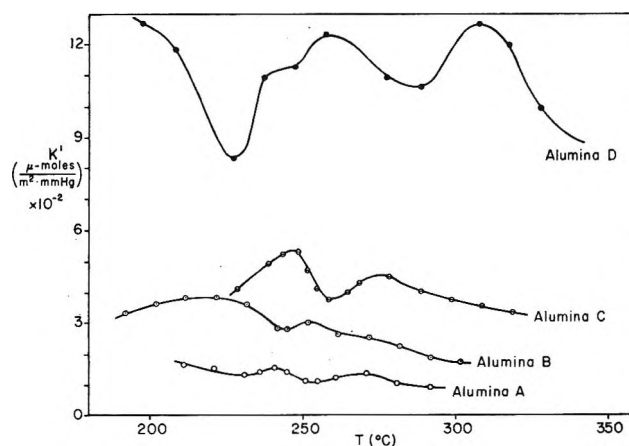


Figure 7. Adsorption amounts of water on aluminas as a function of temperature.

at high temperatures under reaction conditions is but slightly less than at low temperatures and the order

Table IV: Partition Coefficients, K' (mole/m.², torr), and Heats of Adsorption, ΔH (kcal./mole) for Ethanol and Ethyl Ether on Aluminas in the "Working State"

Sample	T. °C.	C ₂ H ₅ OH-		-(C ₂ H ₅) ₂ O-	
		K'	ΔH	K'	ΔH
A	270	3.33×10^{-3}	22.5		
	280	3.12×10^{-3}			
	286			1.57×10^{-3}	11.1
	296			1.53×10^{-3}	
B	270	1.07×10^{-2}	22.1	7.2×10^{-3}	17.6
	280	8.73×10^{-3}		5.9×10^{-3}	
C	270	2.23×10^{-2}	18.6	1.42×10^{-2}	14.6
	280	1.90×10^{-2}		1.23×10^{-2}	
D	310	8.9×10^{-2}	19.3	5.4×10^{-2}	10.1
	320	7.9×10^{-2}		5.2×10^{-2}	

among the four catalysts is the same as before. However, the calculated heats of adsorption are much higher and closer to what would be expected *a priori*. Once again the interpretation of this heat data is open to question as manifested in the asymmetry (tailing) and broadness of the chromatographic peaks.

Discussion

Two types of adsorption studies were made: (1) adsorption using helium as the carrier gas with the catalyst not in the "working state," and (2) adsorption of ether pulses using the other gas as the carrier gas.

In adsorption using helium as the carrier gas and the catalyst not in the "working state," the gas chromatographic experiments in which ethanol was adsorbed on alumina indicate at least three different adsorption modes for ethanol molecules. The exhibited relationships between retention time and temperature are directly related to the adsorption isobars of ethanol on alumina *via* eq. 1. The observation of isobar maxima in the intermediate temperature range (140–210°) must correspond to distinguishable intermediate adsorbed states such as adsorption on relatively monoenergetic sites. The shapes of the isobars observed in these experiments are surprisingly similar to the isobars of hydrogen adsorption on metals^{12,13} or metal oxide¹⁴ surfaces. For these systems, the same explanation is usually given: physical adsorption predominates at low temperatures, chemisorption at high temperatures, with a weak chemisorption at intermediate temperatures.

For ethyl ether adsorption on all the alumina samples, only one peak could be detected in the intermediate temperature region (120–200°) except perhaps for aluminas D and C, indicating the absence of any intermediate chemisorbed state. The one peak de-

tected corresponds to the transition from the physically adsorbed to the sole chemisorbed state.

There are three distinguishable adsorption modes for water as for ethanol since two peaks occur in the intermediate region (200–310°). The explanation of these transition must be similar to that offered for ethanol adsorption. This indicates that the bonding of both water and ethanol may be quite similar in nature.

The calculated partition coefficients for ethanol and ethyl ether in the "working state" are listed in Table IV. Although some differences are noted where the temperature regions overlap, the qualitative interrelationship of the four samples is the same. In particular, alumina D has the largest surface coverage by ethanol and ethyl ether even in the "working state" and shows little if any catalytic activity below 310°. The order of the adsorption amounts per unit surface area for ethanol, ethyl ether, and water at identical temperatures in the high temperature region is A, B, C, and D. It is interesting that this is the same order as the amounts of water and menthol adsorbed at room temperature on these same samples outgassed at 160°. Moreover the same qualitative variation is obtained for the room temperature heats and entropies of adsorption, namely, a decrease with decreasing particle size. The previous explanation of these latter two phenomena has required the postulation of a fundamental variation of surface amorphous character with particle size. This similarity of behavior noted in both the present and previous studies greatly adds to the internal consistency of these postulates. This indicates that the heats of chemisorption might be expected to have the same variation with particle size as the heats of immersion. This apparently is not true.

The foregoing results demonstrate that it would be dangerous to attempt to predict catalytic activities for this particular reaction. There is no correlation between the heats of immersion and the here measured heats of adsorption as related to particle size and no one-to-one correspondence between the heats of immersion and catalytic activity. For different reactions such a simple correlation might exist, *i.e.*, those where reactant but not product molecules compete for surface sites. That the opposite is true for the present study has been clearly demonstrated. Although the dehydration of ethanol is a particularly clean reaction in terms of absence of competing side

(12) A. F. Benton and T. A. White, *J. Am. Chem. Soc.*, **54**, 1820 (1932).

(13) H. S. Taylor, *Advan. Catalysis*, **1**, 1 (1948).

(14) H. S. Taylor and C. O. Strother, *J. Am. Chem. Soc.*, **56**, 586 (1934).

reactions, the alumina surfaces are highly covered with all the reactant and product species except ethylene. Catalyst D, the α -alumina, most clearly illustrates the problem. No catalytic activity is noted below 300° although ethanol surface coverage is extensive at these temperatures. Chemisorption thus must not be a sufficient requirement for catalytic activity. At those same temperatures water coverage is also high. One must then worry about competition between the two species, if not a third (ether), for favorable sites which in effect undermines any hope for correspondence between gross surface coverage and catalytic activity.

The disagreement between the chromatographic heats of chemisorption and the heats of immersion with regard to particle size variation may arise from a number of sources: (a) chemisorption energies are only a partial contribution to the immersionsal heat; (b) very likely the standard thermodynamic treatment requiring adsorption reversibility is inapplicable; (c) the chromatographic heats are average values.

Actually, the two sets of heat measurements are not necessarily in conflict. If all the samples are similar in the surface hydroxyl group character, the energies of chemisorption corresponding to the formation of Al-OR groups will likewise be similar. This would require the variation of heat of immersion with particle size to arise largely from electrostatic field dipole energy variation at supramonolayer coverages. Recent support for this hypothesis has been obtained.¹⁵

There are a few papers concerning the mechanism of the dehydration of ethanol which indicate that this reaction is catalyzed by a weak acid center on the surface. Krieger, *et al.*,² considered the carbonium ion as the intermediate species in the process of the dehydration of ethanol. In dehydration, usually weak acid sites on alumina are considered to be catalytically active centers. In a series of experiments which will more

appropriately be reported later, the surface acidities of these aluminas were estimated by a microcalorimetric method. The heats of immersion of these aluminas in butylamine-decane solutions, which is assumed to be a measure of surface acidity, correlates well with the catalytic activities here measured and will be the subject of a subsequent publication.

Summary

The adsorption amounts of ethanol, ethyl ether, and water on alumina measured by gas chromatography indicated three adsorption modes for water and ethanol and perhaps two modes for ethyl ether. For the adsorption of ethanol and water, physical adsorption predominates in the low-temperature region, and in the high-temperature region chemisorption predominates. A weak chemisorption occurs in the intermediate temperature region. In the adsorption of ethyl ether, a weak chemisorption or intermediate temperature region was not as clear.

The order of adsorbed amounts of water, ethanol, and ethyl ether was alumina D, C, B, and A, which corresponds to their order of heats of immersion of water and methanol. The catalytic activities of the aluminas for the dehydration of ethanol indicate that alumina D has the minimum activity although it has the largest adsorbed amount of ethanol. This fact correlates with the adsorption behavior of water on alumina and this low activity of alumina D is due to the poisoning effect of water.

Acknowledgment. The authors express appreciation to the Robert A. Welch Foundation for continued interest and support. Also, appreciation is expressed to Mr. James Gardner for his assistance in constructing the experimental apparatus.

(15) R. Venable, W. H. Wade, and M. Hackerman, to be published.

The Electronegativity of Noble Gases

by Bing-Man Fung

Contribution No. 3140 from the Division of Chemistry and Chemical Engineering, California Institute of Technology, Pasadena, California (Received September 29, 1964)

The electronegativity of xenon is evaluated from the Xe-F bond energy applying Pauling's new concept of the "transargononic bond." Values of electronegativity of other noble gases are calculated from their estimated covalent radii as well as by the Iczkowski-Margrave formula connecting the electronegativity with ionization potentials. The selected values of the electronegativity are 2.5-3.0, 4.4, 3.5, 3.0, 2.6, and 2.3-2.5 for helium, neon, argon, krypton, xenon, and radon, respectively. On the basis of the estimated electronegativity of neon, new noble gas compounds such as HNe^+ , CF_3Ne^+ , and BF_3Ne are predicted.

The concept of electronegativity was introduced by Pauling¹ and has been used extensively in relation to the chemical and physical properties of elements and compounds.² It is described as "the power of an atom in a molecule to attract electrons to itself."²

The values of electronegativity have been calculated for almost all elements in the periodic table by several different methods whose results are in good agreement with Pauling's values³⁻⁷; the electronegativity for noble gases was estimated very crudely with Mulliken's formula,³ taking the electron affinity of the noble gases to be zero.^{8,9} However, in view of the growing interest in noble gas compound,¹⁰ it is more desirable to investigate in greater detail other possible ways of calculating the electronegativity of noble gases in order to get better insight into their chemistry. We shall discuss three methods and then list the results of numerical calculations.

Bond Energy. Pauling^{1,2} defined the electronegativity x by

$$D(\text{A-B}) = [D(\text{A-A}) \times D(\text{B-B})]^{1/2} + 30(x_{\text{A}} - x_{\text{B}})^2 \quad (1a)$$

or

$$D(\text{A-B}) = 1/2[D(\text{A-A}) + D(\text{B-B})] + 23(x_{\text{A}} - x_{\text{B}})^2 \quad (1b)$$

where $D(\text{A-B})$ stands for the bond energy between two atoms A and B in kcal./mole, etc. These formulas can be applied only to normal covalent bonds, in which each

atom has the electronic configuration of noble gases. For compounds (*e.g.*, PCl_5 , P_2O_5 , etc.) to which valence bond structures of another kind are assigned, Pauling introduced the term "transargononic structure" to describe the electronic configurations beyond those of noble gases.¹¹ For example, the bond energy of the two "transargononic bonds" in PCl_5 is assigned the value of 40.1 kcal./mole from the reaction $\text{PCl}_3(\text{g}) + 2\text{Cl}(\text{g}) \rightarrow \text{PCl}_5(\text{g}) + 2 \times 40.1$ kcal./mole.

In Table I we list values¹²⁻¹⁴ of transargononic bond energy for several other types of bonds containing halogen atoms. The assignment of transargononic

- (1) L. Pauling, *J. Am. Chem. Soc.*, **54**, 3570 (1932).
- (2) L. Pauling, "The Nature of the Chemical Bond," 3rd Ed. Cornell University Press, Ithaca, N. Y., 1960, p. 88.
- (3) R. S. Mulliken, *J. Chem. Phys.*, **2**, 782 (1934); **3**, 573 (1935).
- (4) W. Gordy, *Phys. Rev.*, **69**, 604 (1946).
- (5) W. Gordy, *J. Chem. Phys.*, **14**, 305 (1946).
- (6) W. Gordy and W. J. O. Thomas, *ibid.*, **24**, 439 (1956).
- (7) R. P. Iczkowski and J. L. Margrave, *J. Am. Chem. Soc.*, **83**, 3547 (1961).
- (8) R. E. Rundle, *ibid.*, **85**, 113 (1963).
- (9) A. B. Neiding, *Russ. Chem. Rev.*, **32**, 224 (1963).
- (10) H. H. Hyman, Ed., "Noble-Gas Compounds," University of Chicago Press, Chicago, Ill., 1963.
- (11) L. Pauling in "The Law of Mass-Action, a Centenary Volume," Det Norske Videnskaps-Akademi i Oslo, Universitetsforlaget, Oslo, 1964.
- (12) F. D. Rossini, *et al.*, Ed., National Bureau of Standards Circular 500, U. S. Government Printing Office, Washington, D. C., 1952.
- (13) W. H. Evans, T. R. Munson, and D. D. Wagman, *J. Res. Natl. Bur. Std.*, **55**, 147 (1955).
- (14) R. K. Steunenberg, R. C. Vogel, and J. Fischer, *J. Am. Chem. Soc.*, **79**, 1320 (1957).

bonds in a compound is somewhat arbitrary¹¹; molecular symmetry and other factors of convenience are considered; *e.g.*, in Table I the reactions $S + 6F \rightarrow SF_6$, etc., rather than $SF_2 + 4F \rightarrow SF_6$, etc., are listed because of the equivalence of the six S-F bonds in the compound SF_6 .

Table I: Some Values of Transargononic Bond Energy of Bonds Containing Halogen Atoms^a

Bond	Reactions considered (all in gaseous state at 298°K.)	Trans-argononic bond energy, kcal./mole	Normal bond energy, kcal./mole		Difference between columns 4 and 3, kcal./mole
			Calcd. from (1b)	Exptl.	
P-Cl	$PCl_3 + 2Cl \rightarrow PCl_5$	40	73	76.3	33
P-Br	$PBr_3 + 2Br \rightarrow PBr_5$	35	60	64	25
Sb-Cl	$SbCl_3 + 2Cl \rightarrow SbCl_5$	39	72	74.3	33
S-F	$S + 6F \rightarrow SF_6$	71	96	..	25
Se-F	$Se + 6F \rightarrow SeF_6$	67	99	..	32
Te-F	$Te + 6F \rightarrow TeF_6$	79	118	..	39
Cl-F	$ClF + 2F \rightarrow ClF_3$	32	70	61	38
Br-F	$BrF + 2F \rightarrow BrF_3$	50	74	60	24
	$BrF + 4F \rightarrow BrF_5$	45	29
I-F	$IF + 4F \rightarrow IF_5$	62	88	67	26
	$IF + 6F \rightarrow IF_7$	53	35

^a Data taken from ref. 12-14.

As can be seen from Table I, the normal covalent bond energies calculated by Pauling's formula (1b) and the transargononic bond energies differ by a certain amount, which lies within 24 to 40 kcal./mole for bonds containing halogen atoms. If the value 30 kcal./mole is used as a correction term in (1b) for those bonds, the result will be quite satisfactory for the estimation of electronegativity, which is less sensitive to small variations in values of bond energy. Therefore, we obtain

$$D(A-X) + 30 = \frac{1}{2}[D(A-A) + D(X-X)] + 23(x_A - x_X)^2 \quad (2)$$

where A-X denotes a transargononic bond containing a halogen atom. Since the correction term 30 is only approximate, eq. 2 should not be applied to elements with values of electronegativity too close together or too far apart.

In evaluating the electronegativity of the noble gases we must also know the bond energy between two noble gas atoms. Though some noble gas diatomic cations^{15,16} and certain interactions in a diatomic xenon system¹⁷ were reported, no experimental evidence has

yet demonstrated the existence of noble gas molecules. The interaction between two noble gas atoms would not exceed the van der Waals interaction,¹⁸ which has a value of about 0.5 kcal./mole for noble gases. Therefore, the vaguely defined noble gas diatomic molecules^{17,18} cannot be regarded as containing real transargononic bonds, and, consequently, for noble gases the term $D(A-A)$ in (2) can be dropped compared with the normal covalent bond energy $D(X-X)$ of halogens. Thus, we can calculate the electronegativity of a noble gas from the bond energy of its halides by

$$D(A-X) + 30 = \frac{1}{2}D(X-X) + 23(x_A - x_X)^2 \quad (3)$$

Covalent Radii. Gordy⁴ proposed that the electronegativity of an element can be related to its effective nuclear charge and covalent radius by

$$x = 0.31 \left(\frac{n+1}{r} \right) + 0.50 \quad (4)$$

where n is the number of electrons in its valence shell and r is the covalent radius. Equation 4 can be applied to estimate the electronegativity of the noble gases if their covalent radii are known.

Ionization Potential and Electron Affinity. Mulliken's definition for the electronegativity of an element is given by³

$$x = \frac{I_1 + I_{-1}}{2} \quad (5)$$

where I_1 is the first ionization potential and I_{-1} the electron affinity of the element. Expressing these quantities in e.v. and bringing them to Pauling's scale, one obtains¹⁹

$$x = \frac{I_1 + I_{-1}}{5.56} \quad (6)$$

The ionization potentials of most elements including the noble gases are tabulated,²⁰ but the electron affinity values are known experimentally for only a few elements. Theoretical calculations of electron affinity have been proposed by several authors.^{3,7,19,21-26}

- (15) J. A. Hornbeck and J. P. Molnar, *Phys. Rev.*, **84**, 621 (1962).
- (16) H. T. Davis, S. A. Rice and L. Meyer, *J. Chem. Phys.*, **37**, 947 (1962).
- (17) H. C. Torrey, *Phys. Rev.*, **130**, 2306 (1963).
- (18) N. Bernardes and H. Primakoff, *J. Chem. Phys.*, **30**, 691 (1959).
- (19) H. O. Pritchard, *Chem. Rev.*, **52**, 529 (1953).
- (20) C. E. Moore, National Bureau of Standards Circular 467, U. S. Government Printing Office, Washington, D. C.
- (21) G. Gloker, *Phys. Rev.*, **46**, 111 (1934).
- (22) D. R. Bates, *Proc. Roy. Irish Acad.*, **51**, 151 (1947).
- (23) H. A. Skinner and H. O. Pritchard, *Trans. Faraday Soc.*, **49**, 1254 (1953).

Iczkowski and Margrave⁷ suggested that the total energy of electrons in an atom or ion with a net charge ($-N$) can be represented by

$$E(N) = aN + bN^2 + cN^3 + dN^4 \quad (7)$$

and the electronegativity expressed by

$$x = -\left(\frac{\partial E}{\partial N}\right)_{N=0} = -a \quad (8)$$

assuming the $E-N$ curve to be continuous at $N = 0$. From (7) we get the electronegativity by Mulliken (eq. 5)

$$x = -a - c \quad (9)$$

which differs from (8) by $-c$. The coefficients a , b , c , and d can be obtained by fitting experimental values of the ionization potentials (and electron affinity where available) into (7) and solving the resulting simultaneous equations; the results show that c is always much smaller than a and b ,⁷ hence, expressions 8 and 9 are not very different. Therefore, we can calculate the electronegativity of the noble gases without knowing their electron affinity.

Results of Calculation

Bond Energy. Detailed thermodynamic data are available for xenon tetrafluoride and xenon hexafluoride.¹⁰ The average bond energy taken from those works is 31.0 kcal./mole. Substituting this into (3) we get $x_{Xe} = 2.6$. If the correction term is allowed to vary from 24 to 40 kcal./mole, the value of x_{Xe} varies from 2.7 to 2.5, which is well within the error of such an approximation.

Though some krypton and radon compounds have been reported,^{10,27-29} no detailed data about their properties are available, obviously owing to the instability of the krypton compounds and the difficulty of handling the highly radioactive radon compounds. Bartlett³⁰ estimated the bond energy of krypton tetrafluoride to be ~ 18 kcal./mole; granted that this is a reasonable estimation, we have $x_{Kr} = 2.9$ from (3).

Covalent Radii. The Xe-F and the Xe-O bond distances in several xenon compounds have been measured.¹⁰ The average value for the Xe-F bond is 2.00 Å. in XeF₂ and 1.94 Å. in XeF₄. In comparing the bond lengths of halogen fluorides, Gillespie³¹ indicated that the "long" bonds in the members having a larger number of fluorine atoms usually represent the additivity of covalent radii better. For this reason the average value of 1.94 Å. for the Xe-F bond in XeF₄ is used to calculate the covalent radius of xenon. Taking the covalent radius of fluorine to be $r_F = 0.64$ Å.,² we have $r_{Xe} = 1.30$ Å. A similar value (1.31 Å.) was obtained

by Sanderson.³² Starting from this, we can deduce the covalent radii of other noble gases. Figure 1 shows the trends of univalent radii² and covalent radii³³ of atoms in the last four groups of the periodic table. Since the univalent radii of the noble gases have practically the same trend as those of the other groups, we may hope that their covalent radii behave in the same way. In Figure 1 the dotted line, which is drawn from the starting experimental value $r_{Xe} = 1.30$ Å., gives the following covalent radii of the noble gases (in units of Å.): Rn, 1.40-1.50; Xe, 1.30; Kr, 1.09; Ar, 0.94; Ne, 0.70; He, 0.40-0.60.

In estimating these values, Schomaker-Stevenson values for the covalent radii of the first-row elements³³ are used rather than those by Pauling² because we are going to apply (4) in which the values given by the former authors are to be used.⁴ For the sake of comparison, we list the values by Gillespie³¹ ($r_{Xe} = 1.30$ Å., $r_{Kr} = 1.11$ Å., and $r_{Ar} = 0.95$ Å.) which are quite close to ours.

From the values of covalent radii estimated in the above manner, we have deduced, as follows, the electronegativity of the noble gases according to (4): Rn, 2.3-2.5; Xe, 2.7; Kr, 3.0; Ar, 3.5; Ne, 4.5; He, 2.1-2.8.

Ionization Potential. From the values of the ionization potentials of the noble gases²⁰ we can calculate their electronegativity according to (7). The results of $-2a/5.5$, obtained from (8) after being brought to

Table II: Values of Electronegativity of Noble Gases Calculated by the Iczkowski-Margrave Formula

	Two terms	Three terms	Four terms
He	3.5
Ne	4.3	4.7	4.1
Ar	3.6	3.7	3.4
Kr	3.2	3.4	...
Xe	2.8	3.0	...
Rn

(24) J. L. Margrave, *J. Chem. Phys.*, **22**, 636 (1954); **22**, 1937 (1954).

(25) H. O. Pritchard and H. A. Skinner, *ibid.*, **22**, 1936 (1954).

(26) G. Klopman, *J. Am. Chem. Soc.*, **86**, 1463 (1964).

(27) D. R. MacKenzie, *Science*, **141**, 1171 (1963).

(28) A. V. Grosse, A. D. Kirshenbaum, A. G. Streng, and L. V. Streng, *ibid.*, **139**, 1047 (1963).

(29) C. L. Chernick, *ibid.*, **138**, 136 (1962).

(30) N. Bartlett, *Endeavour*, **23**, 3 (1964).

(31) R. J. Gillespie, ref. 10, p. 333.

(32) R. T. Sanderson, *Inorg. Chem.*, **2**, 660 (1963).

(33) V. Schomaker and D. D. Stevenson, *J. Am. Chem. Soc.*, **63**, 37 (1941).

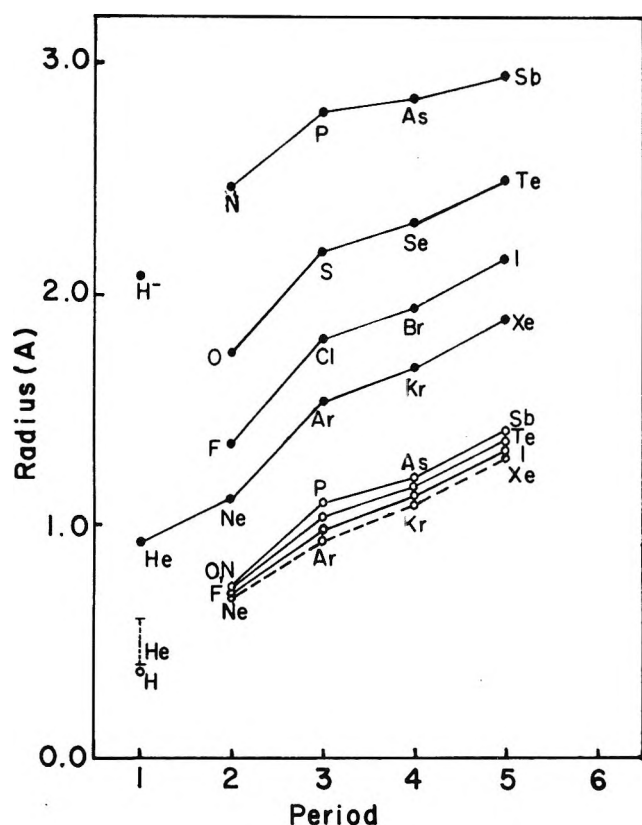


Figure 1. Covalent and univalent radii of elements of the last four groups in the periodic table: full points, univalent radii; empty points, covalent radii.

Pauling's scale, are shown in Table II. It should be noted here that (7) is, in general, less satisfactory for heavier atoms.⁷

Discussion

Since methods based on different experimental data (for xenon) and theoretical bases (for xenon and other noble gases) have given fair agreement on estimations of the electronegativity of the noble gases, it is natural for us to express confidence in these results. The selected values of the electronegativity of the noble gases are as follows: He, 2.5–3.0; Ne, 4.4; Ar, 3.5; Kr, 3.0; Xe, 2.6; Rn, 2.3–2.5.

Electronegativity is *not* a measurement of the reactivity of elements; therefore, there is no inconsistency between the large electronegativity values of the noble gases and their chemical inertness. On the other hand, based upon those values, we can explain certain experimental facts and make some speculations about other possible noble gas compounds.

In a compound containing transargononic bonds, those bonds are unlikely to be polarized in such a way that there is a net negative charge on the central atom; otherwise, the Coulombic repulsion between the "trans-

argononic electrons," *i.e.*, electrons in a configuration beyond noble gas structures, would be too large for stable bonding. Therefore, the stability of those compounds will depend upon the difference between the electronegativity of the central atom and the coordinated atoms, in addition to other factors such as molecular geometry.

From this argument, we can readily visualize the stability orders of some noble gas compounds (radon fluorides > xenon fluorides > krypton fluorides; xenon fluorides > xenon oxides) and the fact that, in photolysis, products of either the F–Xe–Ar system or the F–Kr–Ar system contain no argon fluorides while the fluorides of the other two elements are produced.¹⁰ Though the above discussion also rules out the possibility of formation of compounds with transargononic structure for the highly electronegative elements, neon and argon, it does not exclude the predicted compound HeF₂ discussed by Pimentel and Spratley.³⁴ Moreover, we may speculate on some possible neon and argon compounds not containing transargononic structure. For example, the cation HNe⁺ is likely to exist owing to the large electronegativity of neon. Comparing the series NH₃, H₂O, HF, Ne, and NH₄⁺, H₃O⁺, H₃F⁺, HNe⁺, we should expect the hydroneonium ion HNe⁺ to be a very strong acid and neon, an extremely weak base. The hydroneonium ion might not be very stable but should be detectable in the gaseous reaction products of neon and the strongest inorganic acids by spectroscopic and mass spectroscopic methods. If some strong organic acids are soluble in the nonpolar liquid neon, their electric conductivity should be substantially larger than that expected for nondissociated molecules because of the formation of ion pair and the rapid propagation of protons in the form of hydro-neonium ion in liquid neon. The hydroargonium ion HAr⁺ may also exist but would be less stable. In fact, Rank and co-workers³⁵ reported the complexes HCl–Ar and HCl–Xe in their analysis of the spectroscopic data of the gaseous systems of hydrogen chloride–noble gases.

Substituted fluorocarbons such as CF₃Ne⁺ and the compound of neon with boron trifluoride are also possible. Booth and Willson reported³⁶ the "compounds" ArBF₃, Ar(BF₃)₂, etc., from the thermal analysis of the argon–boron trifluoride system; those "compounds" are said to be unstable and dissociate above their

(34) G. C. Pimentel and R. D. Spratley, *J. Am. Chem. Soc.*, **85**, 826 (1963); *Science*, **143**, 674 (1964).

(35) D. H. Rank, P. Sitaram, W. A. Glickman, and T. A. Wiggins, *J. Chem. Phys.*, **39**, 2673 (1963).

(36) H. S. Booth and K. S. Willson, *J. Am. Chem. Soc.*, **57**, 2273, 2280 (1935).

melting points. The failure to find adducts of argon, krypton, and xenon to boron trifluoride at 20°K. was reported.¹⁰ We feel that neon may form a real compound with BF₃, which would have a heat of formation of about -440 kcal./mole. The compounds CF₃Ne⁺ and BF₃Ne are expected to be reasonably stable, though not quite comparable to their isoelectronic species CF₄ and BF₄⁻. The corresponding argon compounds would be at the margin of stability if they can form at all. Similar compounds of the other noble gases are unlikely.

In conclusion, we are looking forward to more accurate calculations of the electronegativity of noble gases in the hope of obtaining more valuable information and predictions with regard to this new and broad field of chemistry, the chemistry of noble gases.

Acknowledgments. The author is indebted to Professor Linus Pauling for his introduction of the concept of the transargononic bond and to Dr. Sunney I. Chan for his many valuable suggestions.

Sorption Rates Indicative of Structural Changes in Solid Polypeptides¹

by W. W. Brandt and R. S. Budrys

Department of Chemistry, Illinois Institute of Technology, Chicago, Illinois 60616 (Received September 30, 1964)

The sorption isotherms of H₂O on poly-L-leucine (PL) and poly-L-valine (PV) have been measured, as well as sorption rates of H₂O, CH₃OH, HCl, and CF₃COOH on PL and of H₂O and CF₃COOH on PV. In certain systems, the rates are found to furnish a sensitive indication of the onset of structural changes in the polymer. Several distinct processes occur in the system H₂O-PL; they are tentatively identified as the irreversible partial opening of helical segments and the reversible breakage and re-forming of intermolecular H bonds. A plot of the sorption isotherms, according to the Frenkel, Halsey, and Hill equation, reveals that structural changes which are too fast to be sorption rate controlling probably occur in certain other sorbate-polypeptide systems. In some of these systems, the apparent diffusion coefficients decrease with increasing sorbate concentrations, presumably owing to the simultaneous effect of these fast structural changes and the nonlinearity of the corresponding sorption isotherms.

Introduction

Earlier studies carried out in this laboratory² showed that sorption and desorption of trifluoroacetic acid (TFA) causes certain distinct structural changes in poly-L-valine (PV) and poly-L-leucine (PL), judging from X-ray diffraction patterns taken before and after the sorption experiments. The sorption isotherms obtained for PV shifted in a sequence of consecutive runs, and the rates of sorption increased with sorbate concentration. PL showed distinct but less pronounced

isotherm shifts. Barrer noted similar shifts and measured concentration-dependent diffusion coefficients for various H-bonding sorbates in ethyl cellulose.³

(1) (a) Abstracted in part from the work of R. S. Budrys to be submitted in partial fulfillment of the research requirement for the Ph.D. degree in the Department of Chemistry at Illinois Institute of Technology; (b) this work was supported by Public Health Service Grant A-4324.

(2) W. W. Brandt and R. S. Budrys, *J. Biol. Chem.*, **239**, 1442 (1964).

(3) R. M. Barrer, J. A. Barrie, and J. Slater, *J. Polymer Sci.*, **23**, 315, 331 (1957).

He ascribed these anomalies to structural changes of the polymer, even though he did not have independent evidence for such changes. Reyerson and Peterson⁴ reported sorption rate data for the system HCl-nylon which showed an initial fast uptake followed by a very slow release of sorbate, at constant vapor pressure. This is very similar to what has been found for the system TFA-PV mentioned previously.² Reyerson and Peterson also noted a marked improvement of the polymer state of order after the sorption experiments, but no mention was made of isotherm shifts and concentration-dependent diffusion coefficients.

By contrast, for the systems HCl-PL and HCl-PV the uptake did not go through a maximum during the early stages of the sorption process, and the isotherms did not shift in successive runs.⁴ The apparent diffusion coefficients derived from these measurements were constant or even slightly decreasing with increasing concentration. Thus, there was no direct evidence that HCl softens or swells the polypeptides PL and PV, in contrast to nylon, except, perhaps, the fact that PL became opaque during these experiments.

The present study deals largely with the sorption of H₂O on PL; it will be shown that, in this case, distinct structural changes occur during sorption and desorption. Rate data not only furnish a sensitive indication of the presence of these changes but also permit a rough estimate of their rates and of the sorbate pressure at which the structural effects become important. In addition, one can speculate on the nature of the processes in question, using X-ray diffraction patterns as additional evidence.

Experimental

The poly-L-leucine (PL) and poly-L-valine (PV) used in the present work originated from the same batches used and described previously.² The experimental techniques employed for the sorption and X-ray measurements were likewise outlined before.² PL was used as a cast film, 0.006 ± 0.001 cm. thick (H₂O and CH₃OH experiments) or 0.0017 ± 0.0007 cm. thick (TFA experiments²), as measured by a thickness gauge (Products Corp., Providence, R. I.). PV consisted of small grains 0.00024 ± 0.00005 cm. in diameter measured microscopically.

Results

Table I lists the sorbate pressures, the corresponding final uptakes, and the apparent diffusion coefficients computed from the initial, nearly linear portion of each individual rate curve using the previously mentioned sample dimensions. Three over-all runs were made on the system H₂O-PL at 0.57°; the first and third of

these consisted of a good number of individual steps. Several individual sorption and desorption rate curves are shown in Figures 1 and 2, respectively. Curves obtained at uptakes higher than those shown in Figures 1 and 2 were of normal shape, very much like the top and bottom curves of Figure 1 and the top curve of

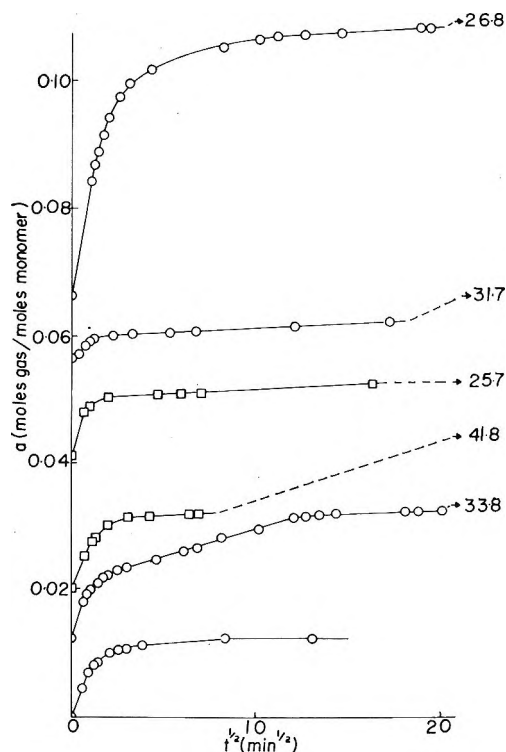


Figure 1. Sorption rates for H₂O on poly-L-leucine (PL) at 0.6°; uptake, a , against square root of time, $t^{1/2}$: O, first sequence of steps; Δ , second sequence of steps; \square , third sequence. Only selected steps of the over-all sequence are shown in each case for clarity. Numbers on right give the value of $t^{1/2}$ (min.)^{1/2} at which the last reading was taken if this reading is outside the time range of the abscissa. Arrows indicate the uptake at such values of $t^{1/2}$.

Figure 2. They are not presented in detail for this reason. An extended time range had to be covered to follow the slow changes of interest which are evident in Figures 1 and 2. Experiments of even longer duration (lower experimental temperatures) are very impractical, and, as a consequence, the initial fast changes which lead to the tabulated diffusion coefficients must be measured very quickly. The D values of Table I are, thus, not very precise, but they are quite satisfactory for the present purposes.

The sorption isotherms of the systems H₂O-PL,

(4) H. H. Reyerson and L. E. Peterson, *J. Phys. Chem.*, **60**, 1172 (1956).

Table I: Diffusion Coefficients, D , of Several Sorbates in Poly-L-leucine (PL) and Poly-L-valine (PV) and the Amounts of Sorbate Taken up, a , Prior to the Particular Sorption or Desorption Run

Sorption		Desorption	
a , moles of gas/ moles of monomer	$D \times 10^8$, cm. ² /sec.	a , moles of gas/ moles of monomer	$D \times 10^8$, cm. ² /sec.
H ₂ O on poly-L-leucine, 0.57°, first run			
0.000	5.4	0.166	3.6
0.012	3.3	0.151	3.6
0.066	2.0	0.131	4.3
0.128	1.2	0.112	4.1
0.157	0.4	0.100	7.2
		0.089	10.5
		0.072	0.11
H ₂ O on poly-L-leucine, second run			
0.000	4.3	0.092	4.8
		0.056	4.1
		0.038	4.1
H ₂ O on poly-L-leucine, third run			
0.000	0.9	0.169	3.6
0.045	6.9	0.155	3.5
0.052	3.7	0.128	2.4
0.074	3.1	0.100	4.3
0.098	2.2	0.079	3.1
0.122	2.5	0.061	1.3
0.145	0.9	0.053	3.0
		0.047	0.3
CH ₃ OH on poly-L-leucine, 1.0°			
0.000	2.3	0.489	0.8
0.027	2.7	0.410	0.9
0.084	2.6	0.313	1.4
0.124	2.4	0.254	1.7
0.154	1.7	0.194	2.3
0.192	1.6	0.146	3.3
0.230	1.5	0.101	4.2
0.269	0.8	0.079	5.9
0.315	0.8	0.060	3.7
0.364	0.3	0.048	0.5
HCl on poly-L-leucine, 0.57°, third run			
0.000	7.2	0.461	3.7
0.063	6.3	0.438	4.5
0.126	5.5	0.413	4.8
0.197	4.8	0.383	5.2
0.307	4.7	0.346	5.5
0.355	4.8	0.296	6.7
0.408	4.1	0.254	7.8
0.438	2.0	0.203	4.8
		0.148	3.0
CF ₃ COOH on poly-L-leucine, 59.5°			
0.000	0.7	0.487	2.5
0.185	1.4	0.468	1.3
0.254	1.7	0.416	1.0
0.325	2.2	0.381	1.0
0.405	2.3	0.335	0.1
0.460	1.7	0.309	0.8

Table I (Continued)

Sorption		Desorption	
a , moles of gas/ moles of monomer	$D \times 10^8$, cm. ² /sec.	a , moles of gas/ moles of monomer	$D \times 10^8$, cm. ² /sec.
CF ₃ COOH on poly-L-valine, 59.5°, first run			
0.000	0.02	0.613	0.2
0.256	0.19	0.553	0.16
0.366	0.10	0.484	0.17
0.429	0.11	0.354	0.26
0.495	0.26	0.311	0.21
CF ₂ COOH on poly-L-valine, 59.5°, second run			
0.000	0.23	0.584	0.17
0.279	0.33	0.522	0.23
0.372	0.26	0.462	0.23
0.443	0.19	0.382	0.19
0.493	0.15	0.327	0.28
0.540	0.13	0.287	0.37
		0.253	0.33
		0.231	0.77
HCl on poly-L-valine, 27.8°, second run			
0.000	0.19	0.395	0.124
0.126	0.061	0.357	0.078
0.153	0.050	0.338	0.091
0.196	0.050	0.279	0.057
0.251	0.055	0.243	0.038
0.363	0.050	0.290	0.052
		0.158	0.024

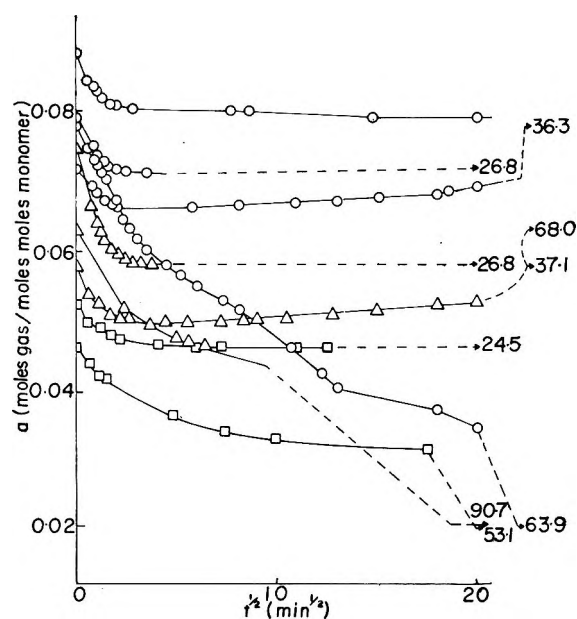


Figure 2. Desorption rates of H₂O from poly-L-leucine (PL) at 0.6°. For designations and details, see legend to Figure 1.

H₂O-PV, and CH₃OH-PL, as well as related information, are reported elsewhere.⁵

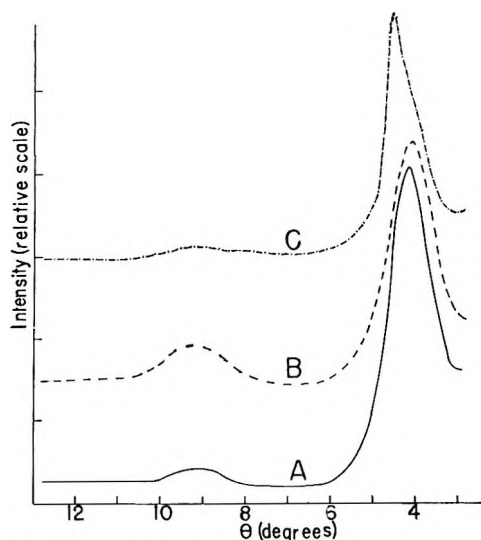


Figure 3. X-Ray diffraction patterns of poly-L-leucine: A, before sorption experiments; B, after H₂O sorption experiments; C, after TFA sorption experiments.

X-Ray diffraction patterns for the original PL, as well as for samples exposed to H₂O and TFA, respectively, are given in Figure 3. Upon exposure to H₂O, the α -helical spacing has increased from 10.55 to 10.91 Å, and the intensity of the peak has decreased; also, the very low and broad peak corresponding to an average spacing of about 4.7 Å. has become more pronounced. It appears that many of the helical segments are slightly expanded and that, at least, some have disappeared. By contrast, exposure of PL to TFA was found to lead to an improvement of the α -helical structure² of this polymer (see also curve C of Figure 3).

Discussion

Table I shows that the apparent initial diffusion coefficients of H₂O in PL decrease with increasing sorbate concentration over most of the pressure range covered. The first and last steps of each over-all run frequently involve very low initial sorption rates and will be ignored for the moment. Data for the system CH₃-OH-PL and the sorption runs (only) on HCl-PL show similar trends. These findings are surprising in view of the pronounced changes in the X-ray pattern of PL upon completion of the H₂O experiments (see curve B of Figure 3), which indicate that, at least, some softening of the polymer must have taken place during the sorption process. It is quite possible that swelling of the polymer structure is a rapid process compared to diffusion. In addition, the sorption isotherms are distinctly concave toward the abscissa over most of the pressure ranges covered.⁵ It is known that under these conditions the apparent diffusion coefficients

will decrease with increasing concentration,⁶ and, as a consequence, a moderate, positive concentration dependence of the true diffusion coefficients may simply be hidden. The two counteracting effects may well be of comparable strength in the HCl-PL and HCl-PV systems, thus causing the apparent diffusion coefficients to be nearly constant in these cases.

As a second feature, one notes that after the first, second, and third complete sorption-desorption runs at 0.57° some of the sorbate is tightly held by the polymer (Figure 3 and isotherm data⁵). This irreversible sorption process is designated a.

Next, it is obvious from Figures 1 and, especially, 2 that the first and last one or two steps of each sequence involve very slow but pronounced changes, even after $t \simeq 4$ min. or $t^{1/2} = 2$ (min.)^{1/2}, that is, in a time range when a "normal" sorption step is nearly completed (see top curves of figures). Presumably, this slow process starts at $t = 0$, and, thus, it is at least partly responsible for the very low initial slopes⁷ and the low apparent diffusion coefficients of the first and last steps in the second and third sequences. This slow process, designated b, presumably involves the breakage and re-formation of polymer-polymer H bonds and, thus, causes formation or destruction of sorption sites during sorption and desorption, respectively. Process b is reversible, or else the residual uptake after the first, second, and third complete series of experiments could not be the same.

Finally, a very slow process is observed in several desorption steps of the first, second, and third sequences which leads to an increase of uptake. This process must be reversible, for the same reason as process b.

On the basis of these findings and the changes in the X-ray diffraction patterns, one may assume that process a involves the "opening" of many helices and the destruction of some, while processes b and c are related to the reversible breakage and formation of the intermolecular H bonds during sorption and desorption, respectively. The present data, of course, do not show exactly what types of H bonds are involved, but, undoubtedly, structural changes of the polymer must be held responsible for the increase of uptake after a lowering of the sorbate pressure (process c).

Some additional information is available from a study of the shapes of the sorption isotherms. The

(5) Copies available from the American Documentation Institute, Auxiliary Publications Project, Library of Congress, Washington 25, D. C., Document No. 8130. Price \$1.75 for microfilm; \$2.50 for a photocopy.

(6) J. Crank, "The Mathematics of Diffusion," Clarendon Press, Oxford, 1957, pp. 122-124.

(7) See ref. 6, pp. 132-145.

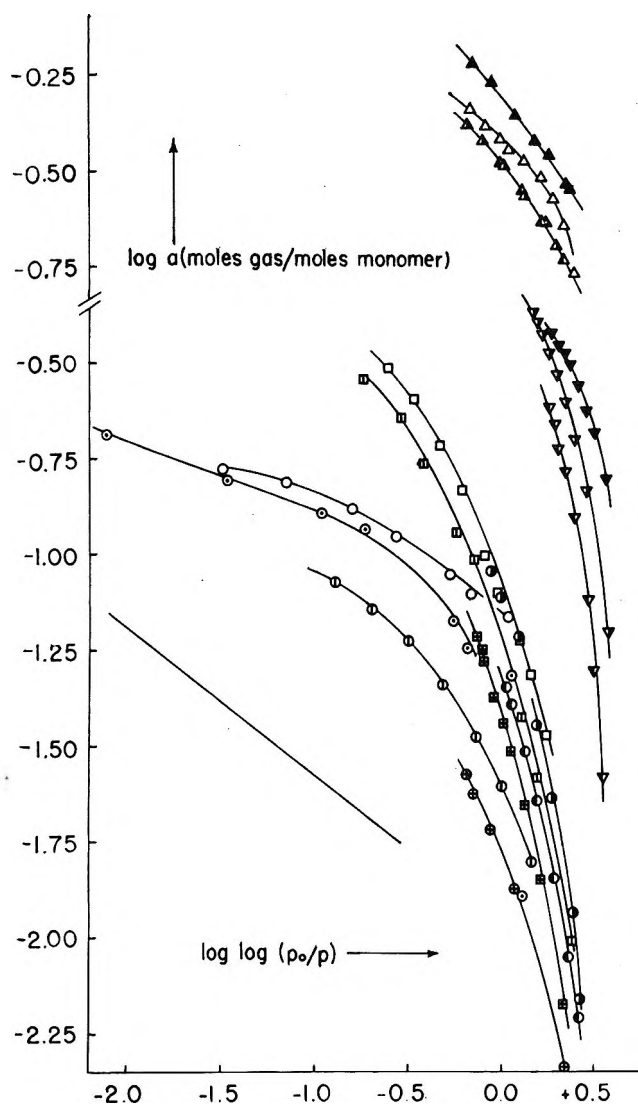


Figure 4. Desorption branches of the isotherms plotted according to the Frenkel, Halsey, and Hill equation. Poly-L-leucine isotherms: \oplus , H₂O, 60.1°; \odot , H₂O, 27.8°; \circ , H₂O, 0.6°; \boxplus , CH₃OH, 27.8°; \square , CH₃OH, 1.0°; ∇ , HCl, 27.8°; ∇ , HCl, 0.6°; Δ , TFA, 59.5°. Poly-L-valine isotherms: \bullet , H₂O, 75.2°; \circ , H₂O, 59.7°; ∇ , HCl, 27.8°; Δ , TFA, 59.5°; \blacktriangle , repeat run; \blacktriangle , TFA on "settled" polymer, 59.5°; \odot , sorption branch of isotherm for H₂O on poly-L-leucine at 0.6°. The unmarked line corresponds to the F.H.H. equation with $n = 2.5$.

structural changes discussed above are probably, in part, responsible for the deviations of the observed H₂O-PL isotherms⁵ from those predicted by the Brunauer, Emmett, and Teller (B.E.T.) theory.⁸ Monolayer uptakes, consequently, cannot be deter-

mined directly by B.E.T. analysis. On the other hand, one can estimate the uptake a , at which multilayers of sorbate are first formed in an indirect way from the Frenkel, Halsey, and Hill (F.H.H.) isotherm equation⁹ $\log(p_0/p) = k(a_m/a)^n$ or $\log \log(p_0/p) = \log k + n \log a_m - n \log a$.

Here k and n are constants, a_m is the monolayer coverage, and a is the uptake measured at the relative pressure p/p_0 . The constant n should be 3.0 if the simple derivation referred to above⁹ is to hold, but experimental data are frequently better fitted by $n = 2.5$,¹⁰ which corresponds to the slope of the undesignated line in Figure 4. The F.H.H. equation has been derived specifically for the multilayer region of sorption. The relative pressure, p/p_0 , at and above which the equation is followed, thus, should enable one to estimate the uptake at which the multilayer formation starts.

Isotherm data obtained in the present⁵ and previous studies² are plotted according to the F.H.H. equation in Figure 4. Only the H₂O isotherms at high relative sorbate pressures correspond to the expected multilayer sorption, in spite of the structural changes discussed previously. One may conclude, therefore, that in this particular case the sorption rates furnish, perhaps, the most sensitive indication of structural changes accompanying sorption. At the same time, it is quite possible that similar changes occurred in the CH₃OH-PL, HCl-PL, and HCl-PV systems and that rate anomalies were not detected because the over-all sorption process is controlled by the (relatively slow) diffusion step. This is in accord with the earlier interpretation of the inverted concentration dependence of the diffusion coefficients. Measurements on thinner films or smaller granules at lower temperatures would be necessary to bring the rates of structural change into the accessible experimental time range, but considerable overlap of the initial, fast sorption process and the slow changes discussed here will, in many cases, constitute a serious experimental limitation.

In summary, structural changes accompanying sorption can, in principle, be detected from isotherm data or from a detailed analysis of sorption rates. Separate processes can be distinguished, under optimum conditions, but the identification of these processes requires additional evidence.

(8) S. Brunauer, P. H. Emmett, and E. Teller, *J. Am. Chem. Soc.*, **60**, 309 (1938).

(9) E. H. Hill, *Advan. Catalysis*, **4**, 244 (1952).

(10) C. Pierce, *J. Phys. Chem.*, **64**, 1184 (1960).

Irregular Solutions of Iodine

by Kōzō Shinoda and Joel H. Hildebrand

Department of Chemistry, University of California, Berkeley, California (Received October 3, 1964)

The solubility of iodine at 25° has been determined in a series of solvents selected as tests of certain types of irregular behavior. Mole per cents of iodine at 25° are as follows: cyclopentane, 0.773; *cis*-decalin, 1.540; *trans*-decalin, 1.451; methylcyclohexane, 0.920; *trans*-1,2-dimethylcyclohexane, 0.937; toluene, 6.256; *m*-xylene, 8.201; methylene chloride, 1.524; *n*-hexadecane, 1.450. In the last two cases, measurements were made over a range of temperatures giving for $R(\partial \ln x_2 / \partial \ln T)$ 20.4 in CH₂Cl₂ and 20.65 in *n*-C₁₆H₃₄. Points for cyclopentane and the two decalins fall on a line for regular solutions in a plot of $\log x_2$ vs. $(\delta_2 - \delta_1)^2$, the solubility parameters. Solvents containing methyl groups diverge in the direction indicating that the well-known failure of many saturated hydrocarbons to agree with solubility parameter theory is attributable mainly to methyl groups, with solvent-solute attraction less than that of a geometric mean. These divergences do not involve irregular entropy. A solubility parameter for CH₂Cl₂ calculated from its energy of vaporization, $(\Delta E^v/v)^{1/2}$, is larger than the value calculated from its solvent power because of its dipole moment.

Hiraoka and Hildebrand¹ recently published a plot of the solubility of iodine as the logarithm of its mole fraction vs. the square of the difference between the solubility parameters of iodine and solvent. This constitutes a test of the equation²

$$RT \ln a_2^s = RT \ln x_2 + v_2 \phi_1^2 (\delta_2 - \delta_1)^2 \quad (1)$$

where a_2^s is the activity of solid iodine with respect to its supercooled liquid (0.256 at 25°), v_2 the molal volume of its supercooled liquid (58.5 cc.), x_2 the mole fraction of iodine at saturation, ϕ_1 the volume fraction of the solvent, δ_2 the solubility parameter of iodine (14.1), and δ_1 that of the solvent. The plot in ref. 1 showed points for violet solutions in 15 solvents that fall closely on the line of the equation, with x_2 values spread over a 300-fold range. Figure 1 in the present paper includes these points.

The original plot showed two groups of solutions whose points diverge from the line, one consisting of solutions in benzene, *p*-xylene, and mesitylene, the other, of solutions in *n*-heptane, 2,2-dimethylbutane, and 2,2,4-trimethylpentane, "isooctane." This research was undertaken, first, to add toluene and *m*-xylene to the first group, the electron donor-acceptor nature of which is now well known, but especially to

seek an explanation of the divergence of the second group although it is violet in color. It has not been at all clear whether this irregularity should be attributed to failure of the term in eq. 1 for entropy, $-R \ln x_2$, or to failure of the one for enthalpy, $v_2 \phi_1^2 (\delta_2 - \delta_1)^2$.

Experimental

Materials. Toluene, *m*-xylene, cyclopentane, and methylcyclohexane were Matheson Coleman and Bell Spectroquality reagents. Methylene dichloride was Eastman Organic Chemicals Spectrograde materials; *trans*-1,2-dimethylcyclohexane was Matheson Coleman and Bell Pure grade. These were fractionally distilled shortly before use. *n*-Hexadecane from Humphrey-Wilkinson was obtained through the kindness of Dr. Sawyer of Shell Development Co. It was passed through silica gel and distilled. Vapor phase chromatography showed about 2% of tetradecane and 4% of pentadecane but no other impurities. *cis*- and *trans*-decahydronaphthalene were K and K Laboratories, Inc., Pure grade materials. The apparatus and procedure were those in earlier studies.³

(1) H. Hiraoka and J. H. Hildebrand, *J. Phys. Chem.*, **67**, 916 (1963).

(2) J. H. Hildebrand and R. L. Scott, "Regular Solutions," Prentice-Hall, New York, N. Y., 1962, p. 102.

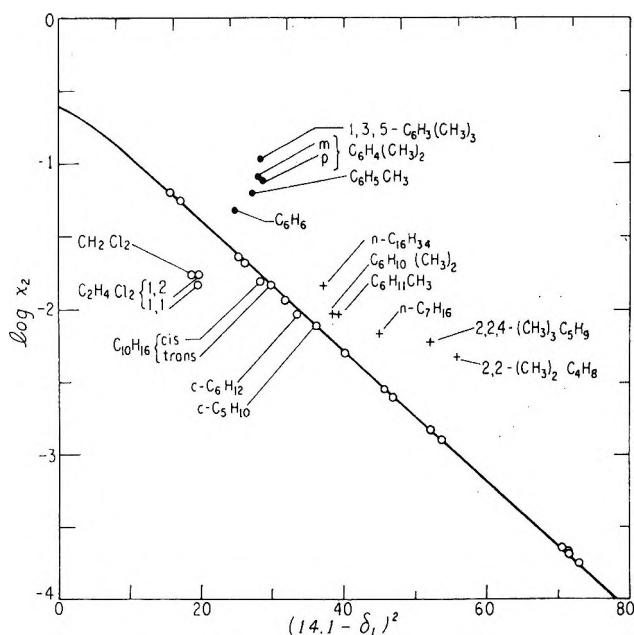


Figure 1. Irregular solubility of iodine in solvents whose molecules contain π -electrons, methyl groups, and dipoles. The solvents corresponding to the unlabeled open circle points may be identified, if desired, from Figure 1 in ref. 1.

Results

Table I gives the results for the solvents n - $C_{16}H_{34}$ and CH_2Cl_2 . These were determined over a range of temperature sufficient to give values for the temperature coefficient.

Table I: Solubility of Iodine in Mole %, $100x_2$

					$R \frac{d \ln x_2}{d \ln T}$
n - $C_{16}H_{34}$	$t, ^\circ C.$	18.91	20.47	25.06	30.05
	$100x_2$	1.167	1.233	1.450	1.722
CH_2Cl_2	$t, ^\circ C.$	15.01	19.90	25.00	
	$100x_2$	1.088	1.283	1.524	20.4

Table II: Solubility of Iodine at 25° , $100x_2$, and Solubility Parameter of Solvent, δ_1

Solvent	$100x_2$	δ_1
Cyclopentane	0.773	8.1
<i>cis</i> -Decalin	1.540	8.8
<i>trans</i> -Decalin	1.451	8.6
Methylcyclohexane	0.920	7.8
<i>trans</i> -1,2-Dimethylcyclohexane	0.937	7.9
Toluene	6.256	8.9
<i>m</i> -Xylene	8.201	8.8
Methylene chloride	1.524	9.8
<i>n</i> -Hexadecane	1.450	8.0

The solubility parameters of all but three liquids are from ref. 2, p. 171. The missing ones were calculated from boiling points by the empirical equation given in ref. 2, p. 168: $\Delta H_{298}^v = -2950 + 23.7T_b + 0.020T_b^2$. The figures are given in Table III.

Table III^a

	T_b	ΔH_{298}^v	v	δ
<i>cis</i> -Decalin	194.5	12,510	153.2	8.8
<i>trans</i> -Decalin	185.8	12,150	155.0	8.6
<i>trans</i> -1,2-Dimethylcyclohexane	123.2	9,585	145.3	7.9

^a Units: cal. and cc.

Seyer and Mann⁴ have published data for the vapor pressures of the decalins from room temperatures to boiling points, but the plot of $\log P$ vs. $1/T$ gives lines curving in ways that are incredible; therefore, we calculated from the boiling points.

Discussion

We invite attention, first, to the addition of toluene and *m*-xylene to the aromatic solvents heretofore used; see Figure 1. The solubility of iodine in benzene is larger than the regular solution value corresponding to its solubility parameter, 9.15, which is close to that of chloroform. Solubility increases in order in the series, benzene, toluene, the xylenes, and mesitylene, given in the order of increasing basic donor strength in decreasing ionization potential.

The more important results of this study concern the solubility of iodine in the group of saturated hydrocarbons—straight, branched chain, and cyclic. We were struck long ago by the fact that cyclohexane behaves normally, whereas *n*-heptane and isooctane do not. The magnitudes of solubility parameters that would conform to empirical solvent parameters for iodine exceed the values derived from their energies of vaporization, $(\Delta E_1^v/v_1)^{1/2}$, by 0.6 for *n*-heptane and 1.0 for isooctane.

We see in Figure 1 that three additional cyclic compounds, cyclopentane and *cis*- and *trans*-decahydronaphthalene, conform as does cyclohexane. On the other hand, *n*-hexadecane is off the regular line by about the same amount as *n*-heptane. Further, the departure from the line of the two branched paraffins is nearly double that of the two normal paraffins. These correlations suggest that it is the methyl groups that are responsible for the irregular behavior. We see

(3) D. N. Glew and J. H. Hildebrand, *J. Phys. Chem.*, **60**, 616 (1956).
 (4) W. F. Seyer and C. W. Mann, *J. Am. Chem. Soc.*, **67**, 328 (1945).

that the introduction of one or two methyl groups into cyclohexane makes them, likewise, poorer solvents for iodine (see Figure 1).

It remains to be determined whether the departures from the regular solution line in Figure 1 are to be attributed to entropy or to enthalpy. In order to reveal the entropy, we have added points for the new data to a plot of $R(\partial \ln x_2 / \partial \ln T)_{\text{sat}}$ vs. $-R \ln x_2$, a plot devised for this purpose by Hildebrand and Glew.⁵ This plot does not involve solubility parameters.

The entropy of solution at saturation is

$$\bar{S}_2 - S_2^s = R(\partial \ln x_2 / \partial \ln T)_{\text{sat}}(\partial \ln a_2 / \partial \ln x_2)_T \quad (2)$$

The factor, $(\partial \ln a_2 / \partial \ln x_2)_T$, which is "Henry's law" factor, is so nearly unity that it can be ignored without affecting the argument. Walkley and Hildebrand,⁶ by measuring the partial vapor pressure of iodine over its solutions, found it to be 0.86 in CS_2 and 0.98 in CCl_4 . It is necessarily still closer to unity in all solvents in which iodine is less soluble than in CCl_4 .

The fact that certain points which depart strongly from the normal line in Figure 1 fall on the line in Figure 2 has already been noted in the cases of solutions in *n*-heptane, isooctane, 2,2-dimethylbutane, and octamethylcyclotetrasiloxane. This indicates that any factor of a purely physical nature, such as expansion, which causes the entropy to depart from the ideal $-R \ln x_2$, is offset by a corresponding change in enthalpy, a relation pointed out long ago by Scatchard.⁷ This is not the case where departures are the result of chemical complexing, as seen by the points in Figure 2 for the aromatics. It is significant that an empirical increase in the solubility parameter of isooctane from 6.85, the value of $(\Delta E_1^v / v_1)^{1/2}$, to 7.85 would correct its solvent power for iodine and also its partial molal volume⁸ at high dilution in CCl_4 and CS_2 .

We must conclude, therefore, that solubility parameters do not give a correct measure of attractive forces between iodine and methyl groups. The term

$$(\delta_2 - \delta_1)^2 = \frac{\Delta E_1^v}{v_1} + \frac{\Delta E_2^v}{v_2} - 2 \left(\frac{\Delta E_1^v}{v_1} \times \frac{\Delta E_2^v}{v_2} \right)^{1/2}$$

is twice the difference between an arithmetic and a geometric mean. The geometric mean is clearly too large to represent accurately the attraction between molecules of iodine and those of a molecule containing methyl groups. Methylene groups clearly do not cause serious departures, as shown by the conformity of solutions in cyclopentane, cyclohexane, and the two decalins. The divergence begins with the introduction of methyl groups into cyclohexane.

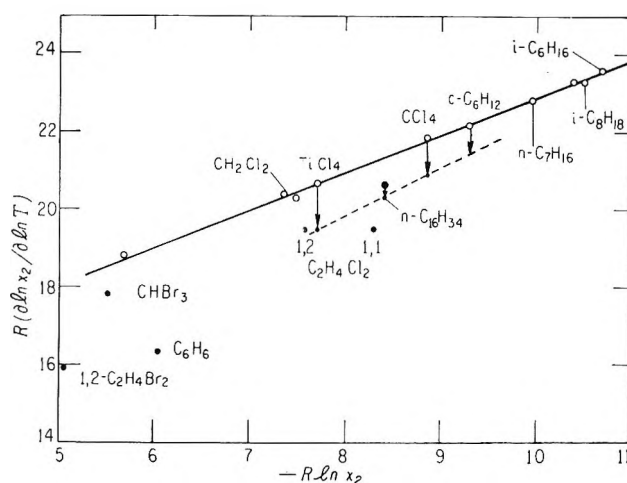


Figure 2. Plot for distinguishing between entropy and enthalpy as the cause of irregularity.

The point in Figure 2 for *n*- $\text{C}_{16}\text{H}_{34}$ falls below the line by 0.8 cal. deg.⁻¹, an amount that is almost trivial and which may be explained by relative departures from unity of the Henry's law factor, $(\partial \ln a_2 / \partial \ln x_2)_T$, in eq. 2. An expression for it may be obtained by differentiating eq. 1⁹ to give

$$\left(\frac{\partial \ln a_2}{\partial \ln x_2} \right)_T = 1 - 2 \frac{\phi_2}{x_1} \ln \frac{a_2}{x_2} \quad (3)$$

If this is applied to this solution and its near neighbors, we get the following values for this factor: TiCl_4 , 0.940; *n*- $\text{C}_{16}\text{H}_{34}$, 0.983; CCl_4 , 0.956; cyclo- C_6H_{12} , 0.967. With these corrections, the points for each solution fall on the same line, shown dotted in the figure.

The solution in CH_2Cl_2 is interesting in that it is the first one found to give a point below the line in Figure 1. This prompted us to plot points for 1,1- $\text{C}_2\text{H}_4\text{Cl}_2$ and 1,2- $\text{C}_2\text{H}_4\text{Cl}_2$, using the measurements by Benesi and Hildebrand¹⁰ made in 1948. They had not previously been included in this kind of plot because they complex weakly with iodine, as seen in the plot by Hildebrand and Glew and in the shift they cause in the wave length of the visible peak of iodine reported by Walkley, Glew, and Hildebrand.¹¹ Complexing alone would

(5) J. H. Hildebrand and D. N. Glew, *J. Phys. Chem.*, **60**, 618 (1956); see ref. 2, p. 120, Figure 3.

(6) J. Walkley and J. H. Hildebrand, *ibid.*, **63**, 1174 (1959).

(7) G. Scatchard, *Trans. Faraday Soc.*, **33**, 160 (1937).

(8) See ref. 2, pp. 110, 123.

(9) See ref. 5 and also K. Shirōda and J. H. Hildebrand, *J. Phys. Chem.*, **61**, 789 (1957).

(10) H. A. Benesi and J. H. Hildebrand, *J. Am. Chem. Soc.*, **70**, 3978 (1948).

(11) J. Walkley, D. N. Glew, and J. H. Hildebrand, *J. Chem. Phys.*, **33**, 621 (1960).

be expected to raise the points for these solutions above the line in Figure 1. The fact that instead they fall below, as does CH_2Cl_2 , would seem to be related to the considerable polarity of these three liquids, raising their energies of vaporization without correspondingly enhancing their solvent power for iodine. In other words, $(\Delta E_1^v/v_1)^{1/2}$ is too large for an effective solubility parameter. A comparison of the dielectric constants, ϵ , and the dipole moments, μ , of these anomalous solvents with those of conforming solvents, CHCl_3 and Cl_4 , is seen in Table IV.

Table IV: Dielectric Constants and Dipole Moments

	CCl_4	CHCl_3	CH_2Cl_2	$1,2\text{-C}_2\text{H}_4\text{Cl}_2$	$1,1\text{-C}_2\text{H}_4\text{Cl}_2$
ϵ	2.24	4.81	9.08	10.4	10.0
$10^{18}\mu$	0	1.02	1.54	1.20	2.06

Acknowledgment. This work was supported by the Atomic Energy Commission, for which we express our appreciation.

Studies of Ions and Ion Pairs in Tetrahydrofuran Solution.

Alkali Metal Salts of Tetraphenylboride

by D. N. Bhattacharyya, C. L. Lee, J. Smid, and M. Szwarc

Department of Chemistry, State University College of Forestry, Syracuse University, Syracuse, New York 13210
(Received September 29, 1964)

The conductance of tetraphenylborides of Li^+ , Na^+ , K^+ , Cs^+ , Bu_4N^+ , and $(\text{isoamyl})_3\text{BuN}^+$ in THF was investigated at 25° in the concentration range 10^{-6} to $2 \times 10^{-4} M$. Fuoss plots gave straight lines from which the limiting conductances and the ionic dissociation constants were calculated. The limiting conductances of the cations in THF were obtained by assuming $\Lambda_0^+((\text{isoamyl})_3\text{BuN}) = \Lambda_0^-(\text{BPh}_4)$. The lowest value of Λ_0^+ was obtained for Li^+ , showing the high degree of solvation of this intrinsically small ion, and the largest Λ_0 was found for Cs^+ , which apparently is not solvated. These findings corroborate with the data for K_{dis} . The Li^+ and Na^+ salts are the most dissociated, whereas K_{dis} of the Cs^+ salt is about one-fiftieth as large as that of Na^+ . In spite of their bulkiness, the tetraalkylammonium salts are less dissociated than the Na^+ or Li^+ salts, indicating lack of solvation of these ammonium ions.

Kinetic studies of anionic polymerization of styrene in tetrahydrofuran revealed that the free polystyryl ions $\sim\text{S}^-$, as well as the respective ion pairs, $\sim\text{S}^-\text{M}^+$, participate in the propagation.^{1,2} Further investigations of these problems required determination of the limiting conductance, Λ_0^+ , of alkali cations in tetrahydrofuran. To achieve this goal, we investigated the conductivities of alkali salts of tetraphenylboron in this solvent, and our results are reported here.

Preparation and Purification of Alkali Tetraphenylborides. The sodium salt, NaBPh_4 , was acquired from Fisher (99.7%) and it was recrystallized three times from aqueous acetone (3 parts of acetone by volume to 1 part of water). The absence of other alkalis in the

(1) D. N. Bhattacharyya, C. L. Lee, J. Smid, and M. Szwarc, *Polymer*, **5**, 54 (1964).

(2) H. Hostalka, R. V. Figini, and G. V. Schulz, *Makromol. Chem.*, **69**, 198 (1964).

purified salt was established by flame spectrophotometry.

The purified sodium salt served as a starting material for the preparation of the other salts. Thus, the potassium, rubidium, and cesium salts were obtained by treating dilute aqueous solutions of sodium tetraphenylboride with an equivalent amount of the respective chlorides.³ The relatively insoluble KBPh₄, RbBPh₄, and CsBPh₄ precipitated, and the filtered and washed crystals were then purified by repeated crystallization from aqueous acetone. Again, using flame spectrophotometry,⁴ it was established that their contamination by sodium tetraphenylboride was within 0.15–0.7%.

The lithium salt was prepared by adding a slight excess of a concentrated THF solution of LiCl to a concentrated THF solution of NaBPh₄. The relatively insoluble NaCl precipitated, the crystals were removed by centrifugation, and the lithium salt was recovered by evaporating the solvent. The salt was then redissolved in ethylene dichloride, excess LiCl was filtered off, and the LiBPh₄ was precipitated by addition of cyclohexane. This procedure was then repeated, and the final product was found to be free of sodium salt.

The tetrabutylammonium salt was prepared by treating sodium tetraphenylboride with an equivalent amount of tetrabutylammonium iodide in aqueous solution and recrystallizing thereafter the sparsely soluble ammonium salt from aqueous acetone.⁵ The product contained only 0.3% of NaBPh₄. The triisooamylbutylammonium salt of tetraphenylboron was prepared by following the procedure outlined by Coplan and Fuoss.⁶

All these salts were dried by heating them to about 50° under high vacuum for several days. It is essential to prevent prolonged contact between the prepared salt, or its solution, and oxygen. A contact with oxygen leads to the formation of some impurities, probably peroxides, which increase the conductivity of the investigated solution.

Tetrahydrofuran was refluxed overnight on sodium-potassium alloy and then fractionated. In some experiments the purified solvent was stirred again with sodium-potassium alloy to which benzophenone was added and then vacuum distilled. The same results were obtained with both solvent samples, indicating that our results are not affected by traces of water.

The solubility of the sodium and lithium salts in THF is very high, while the potassium, rubidium, and cesium salts are rather insoluble. The THF solutions of the sodium salt have absorption maxima at $\lambda = 266$ and 274 m μ , the respective extinction coefficients

being 3070 and 2220. The extinction coefficients of aqueous solutions were reported³ to be 3225 and 2100, respectively.

*Conductivity Measurements.*⁷ A Leeds and Northrup a.c. conductance bridge operating at 1000 c.p.s. was used for the conductivity studies. A General Radio Corp. tuned amplifier and a null detector coupled with an oscilloscope were used as a balance instrument. The bridge was sensitive to 1 part in 10⁶, and its basic features, as well as the measuring procedure, were fully described by Edelson and Fuoss.⁸

The thermostatic bath was maintained at $25 \pm 0.01^\circ$. An ordinary glass cell with platinum electrodes was used for most of the experiments; some were performed, however, in a vacuum cell. Since the same results were obtained in both cells it was superfluous to apply the high-vacuum technique for this study. The cell was calibrated with aqueous KCl solution, and its constant was found to be 0.1785.

In view of the low solubilities of the K and Cs salts in THF, their conductivities were determined in the 10⁻⁴ to 10⁻⁶ M range. The extremely low solubility of the Rb salt prevented any accurate measurements of its conductivity. The stock solutions were made by dissolving about 100 mg. of salt in 1 l. of THF at 25°. For highly diluted solutions it was necessary to use a calibrated 10⁵-ohm resistance parallel with the cell.

The conductivity of the pure solvent was extremely low, and therefore corrections had to be introduced only when determining the conductivities of the most diluted solutions.

Results

Our results are given in Table I. The following relation was derived by Fuoss⁹ for the conductivity of a system composed of ion pairs and their ions, in the absence of triple ions and higher aggregates, $F/\Lambda = 1/\Lambda_0 + (f^2c\Lambda/F)(K_{dis}\Lambda_0^2)^{-1}$.

The functional dependence of f and F on Λ , on the concentration of the salt, on the dielectric constant and viscosity of the solvent, and on the temperature is given

-
- (3) R. P. Pfau and L. C. Howick, *Anal. Chem.*, **28**, 1542 (1956).
 - (4) The analysis was kindly performed by Miss Divers from Solvay Division of Allied Chemicals in Syracuse, N. Y.
 - (5) F. Accascina, S. Petrucci, and R. M. Fuoss, *J. Am. Chem. Soc.*, **81**, 1301 (1959).
 - (6) M. A. Coplan and R. M. Fuoss, *J. Phys. Chem.*, **68**, 1177 (1964).
 - (7) In the early stage of our work, we used the conductivity bridge constructed by Dr. Henry Wirth of Syracuse University. It is a pleasure to thank him for his cooperation as well as for his technical advice.
 - (8) D. Edelson and R. M. Fuoss, *J. Chem. Educ.*, **27**, 610 (1950).
 - (9) F. Accascina and R. M. Fuoss, "Electrolytic Conductance," John Wiley and Sons, Inc., New York, N. Y., 1959.

Table I: Conductance of Tetraphenylboride Salts in Tetrahydrofuran at 25^oa

$C \times 10^6$		$C \times 10^5$		$C \times 10^4$		$C \times 10^3$	
M	Δ	M	Δ	M	Δ	M	Δ
(iso-amyl) ₃ BuN ⁺		Bu ₄ N ⁺		Li ⁺		Cs ⁺	
0.325	75.91	0.100	82.9	0.403	72.64	0.093	79.5
0.650	72.16	0.200	79.6	1.008	67.42	0.131	71.2
0.975	69.50	0.300	78.5	2.016	63.06	0.187	68.9
1.625	65.44	0.400	76.7	4.033	56.45	0.187	66.3
3.250	58.15	0.500	75.2	6.049	52.31	0.281	63.1
6.500	50.82	0.700	72.8	10.8	46.66	0.374	58.0
9.750	46.14	1.000	70.0			0.374	55.6
		2.000	63.1			0.468	50.1
		4.000	54.9			0.561	48.2
		6.92	47.8			0.602	48.4
K ⁺				Na ⁺			
0.040	90.0	8.00	46.6	0.197	84.7	0.748	42.8
0.100	85.5	9.89	43.4	0.394	82.9	1.000	41.3
0.200	84.3	19.80	35.5	0.403	83.2	1.122	37.2
0.300	81.8			0.591	81.2	1.309	34.9
0.400	80.3			0.788	79.6	1.496	32.7
0.600	77.6			0.806	80.5	1.683	32.1
0.800	73.7			0.985	77.3	1.870	31.0
1.00	70.5			1.050	77.5 (?)	2.000	29.6
2.00	63.3			1.970	72.4	4.000	22.1
4.00	54.1			2.010	74.0	8.00	17.0
8.00	45.0			3.94	65.8	20.00	11.2
				4.03	66.0		
				7.88	57.9		
				8.06	57.7		

^a Dielectric constant of THF, $D = 7.39$; density, $d = 0.880$; viscosity, $\eta = 0.00460$ poise.

in ref. 9. An IBM computer 1620^{II} was used for calculating these parameters.

The plots of F/Λ vs. $f^2c\Delta/F$ are shown in Figure 1. Their intercepts give $1/\Lambda_0$, and the reciprocals of their slopes yield $K_{dis}\Lambda_0^2$. In this way the data listed in Table II were obtained, and the least-square calculation shows them to be reliable within 2%, except those derived for the Cs salt, which are reliable within 4%.

Recent work of Coplan and Fuoss⁶ proved that in methanol the limiting conductances of (isoamyl)₃BuN⁺ ions and BPh₄⁻ ions are identical within 1%, while the limiting conductance of N⁺Bu₄ is about 8% higher than that of the tetraphenylboride ion. On this basis we assumed the equality of the limiting conductances of these two ions in THF, and, thus, we obtained the Λ_0^+ values given in Table II. The Λ_0^+ for Bu₄N⁺ appears to be about 10% higher than that of (isoamyl)₃BuN⁺, and this close agreement with Fuoss' data justifies our assumption.

Discussion

The plots shown in Figure 1 are based on the data obtained in the concentration range of 10^{-6} to 2×10^{-4}

Table II: Limiting Conductance and Equilibrium Constants of Dissociation of Tetraphenylborides in Tetrahydrofuran at 25^oa

Counterion	Λ_0	Λ_0^+	$K_{dis} \times 10^5$	$K_{dis} M^+ / K_{dis} Na^+$
Bu(isoamyl) ₃ N ⁺	80.6	40.3	6.04	0.709
Bu ₄ N ⁺	84.8	44.5	4.32	0.508
Li ⁺	76.9	36.6	7.96	0.935
Na ⁺	88.5	48.2	8.52	1.000
K ⁺	90.1	49.8	3.22	0.377
Cs ⁺	108.7	68.4	0.187	0.0219

^a Assumed $\Lambda_0^-(BPh_4^-) = \Lambda_0^+((isoamyl)_3BuN^+)$.

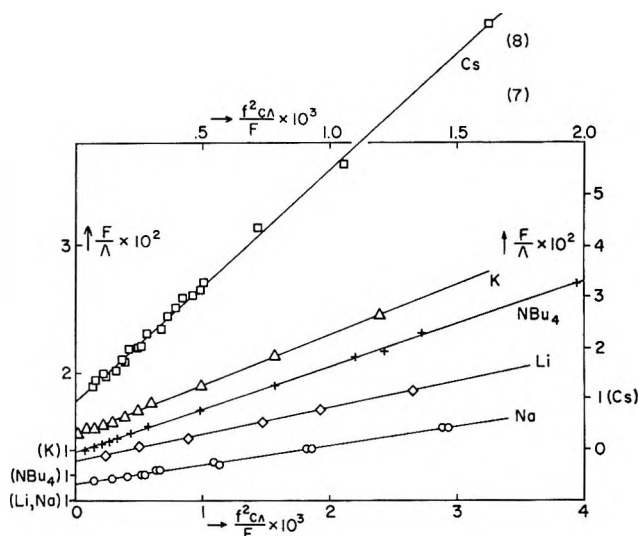


Figure 1. The Fuoss conductivity plot for tetraphenylboride salts of Li⁺, Na⁺, K⁺, Bu₄N⁺, and Cs⁺ in THF at 25^o. The scales of F/Λ and $f^2c\Delta/F$ for Na⁺, Bu₄N⁺, and K⁺ are given on the left side and on the bottom of the drawing, respectively. The values for F/Λ are shifted to avoid the overlap; thus, for each salt, $F/\Lambda = 1$ in the place denoted by (Li,Na) or (Bu₄N) or (K), respectively. The scales for the Cs⁺ salt are given on the right side and on the top of the drawing. For the salt of (isoamyl)₃BuN⁺ a similarly good straight line was obtained, the respective points lay close to the line of (Bu₄)N⁺.

M . At higher concentrations the points deviate from the linear relation, indicating formation of triple ions, most probably $(BPh_4^-)(cation^+)_2$.

The variations of Λ_0^+ shown in Table II seem to be significant. The lowest Λ_0^+ was found for Li⁺, indicating that this intrinsically small ion is highly solvated by THF.¹⁰ On the other hand, the intrinsically large Cs⁺ gives the largest Λ_0^+ , indicating its poor solvation. The solvation of Na⁺ and K⁺ must be

(10) By solvation we understand a specific interaction binding solvent molecules to an ion which comes over and above the general interaction given by Born's approximation.

substantial since the respective Λ_0^+ values are slightly larger than those found for the bulky tetraalkylammonium ions.

These findings corroborate with the observed dissociation constants. The extremely low value of $K_{\text{dis}} = 0.187 \times 10^{-5} M$ for $\text{Cs}^+, \text{BPh}_4^-$ results from the lack of solvation or only a slight solvation of Cs^+ , and therefore this ion pair is only about one-fiftieth as dissociated as $\text{Na}^+, \text{BPh}_4^-$. The slightly lower dissociation constant of $\text{Li}^+, \text{BPh}_4^-$, when compared with $\text{Na}^+, \text{BPh}_4^-$, indicates some penetration of the small Li^+ ion into BPh_4^- since, on the basis of Λ_0^+ data, the reverse would be anticipated (see, *e.g.*, the results of the following paper). The gradation in K_{dis} of the two ammonium salts reflects the increase of their bulkiness. Apparently, the ammonium ions are not solvated, and, therefore, in spite of their size, they are less dissociated than the Na^+ and Li^+ salts.

Finally, the behavior of the tetrabutylammonium salt of tetraphenylboride in various nonaqueous solvents is compared in Table III. The validity of Walden's rule is remarkable when we compare the solvents

Table III: Applicability of the Walden Rule for $\text{N}(\text{Bu})_4\text{B}(\text{Ph})_4$ at 25°

Solvent	ϵ	$\eta \times 10^{-3}$, poise	Λ_0	$\eta\Delta_0$	Ref.
THF	7.39	0.460	84.75	0.390	<i>a</i>
Ethylene dichloride	10.35	0.7834	49.77	0.390	<i>b</i>
$\text{CH}_3\text{CN}-\text{CCl}_4$	15.35	0.550	70.26	0.386	<i>c</i>
$\text{CH}_3\text{CN}-\text{dioxane}$	13.33	0.644	61.31	0.397	<i>d</i>
CH_3CN	35.99	0.344	119.60	0.411	<i>c</i>
CH_3OH	32.63	0.545	76.00	0.413	<i>e</i>

^a This work. ^b J. J. Zwol̄nik and R. M. Fuoss, *J. Phys. Chem.*, **68**, 903 (1964). ^c See ref. 4. ^d A. D'Aprano and R. M. Fuoss, *J. Phys. Chem.*, **67**, 1704 (1963). ^e R. W. Kunze and R. M. Fuoss, *ibid.*, **67**, 385 (1963).

having not too different dielectric constants. Thus, for ϵ varying from 7 to 15 and Λ_0 changing from 50 to 85, the product $\Lambda_0\eta$ remains constant within $\pm 1\%$.

Acknowledgments. We wish to acknowledge the support of this investigation by the National Science Foundation through Grant GP-1935.

Reactivities and Conductivities of Ions and Ion Pairs in Polymerization Processes

by D. N. Bhattacharyya, C. L. Lee, J. Smid, and M. Szwarc

Department of Chemistry, State University College of Forestry, Syracuse University, Syracuse, New York 13210
(Received September 29, 1964)

The apparent rate constants, k_p , of homopropagation of living polystyrene in THF (tetrahydrofuran) were shown to be linear with $1/[\text{living polymer}]^{1/2}$. The intercepts of such lines give k'_{S^-,M^+} , the propagation rate constants of ion pairs, $\sim S^-,M^+$; the slopes yield $k''_{S^-}(K_{S^-,M^+})^{1/2}$, k''_{S^-} being the propagation rate constant of free $\sim S^-$ ion and K_{S^-,M^+} the dissociation constant of an ion pair into free ions. By studying the inhibitory effect of alkali tetraphenylborides on the rate of polymerization, the values of k''_{S^-} and K_{S^-,M^+} could be separately determined. Thus, at 25°, $k''_{S^-} = 65,000$ l./mole sec., and the values of k'_{S^-,M^+} are 160 for Li^+ , 80 for Na^+ , ~ 60 for K^+ , ~ 50 for Rb^+ , and 22 for Cs^+ ion pairs, all given in units of l./mole sec. The free ion is therefore 400 times as reactive as the most reactive ion pair. Studies of conductivity led to an independent determination of K_{S^-,M^+} . The agreement between these two methods is most satisfactory with the exception of a two-ended $Cs^+, S^-\sim S^-, Cs^+$. In the latter system a new phenomenon takes place. Analysis of this phenomenon showed that an ion $\sim S^-\sim S^-, Cs^+$ cyclizes and forms a triple ion, S^-, Cs^+, S^- . For a $\overline{DP} \sim 25$, the equilibrium constant for cyclization was found to be ~ 5.5 , and the propagation rate constant of the triple ion was found to be 2000 l./mole sec.

Kinetic studies of anionic polymerization of styrene in tetrahydrofuran were reported by Geacintov, Smid, and Szwarc,¹ who investigated this fast reaction by a capillary flow technique. They concluded that the propagation kinetically behaves as a second-order reaction, *viz.*, $-d[S]/dt = k_p[\text{living ends}][S]$, where S denotes styrene and [living ends] the concentration of growing polystyrene. The latter remains constant in the course of each experiment since this type of polymerization proceeds without termination. Although k_p is constant and independent of styrene concentration in each individual run, variation of [living ends] leads to small changes in k_p , its value increasing with decreasing concentration of living polystyrene. Subsequent studies of other anionic homo- and copolymerizations in THF revealed a similar behavior,^{2,3} indicating that the variation of k_p is characteristic for anionic polymerizations in this solvent.

Two phenomena may account for this peculiarity. It is known⁴ that some living polymers, *e.g.*, $\sim S^-, Li^+$

in benzene, dimerize. The associated form is unreactive, whereas the ordinary nonassociated ion pairs grow, and in such systems the apparent k_p increases on dilution of living ends.

The dimerization of living polymers may be recognized easily. The viscosity of the associated polymer solution markedly decreases when the active terminal groups are destroyed by protonation, *e.g.*, on adding a drop of methanol.⁵ Such behavior is not observed in THF solutions of living polystyrene, indicating a lack of their association in this solvent.

Alternatively, the increase of k_p on dilution may arise

- (1) C. Geacintov, J. Smid, and M. Szwarc, *J. Am. Chem. Soc.*, **84**, 2508 (1962).
- (2) D. N. Bhattacharyya, C. L. Lee, J. Smid, and M. Szwarc, *ibid.*, **85**, 533 (1963).
- (3) M. Shima, D. N. Bhattacharyya, J. Smid, and M. Szwarc, *ibid.*, **85**, 1306 (1963).
- (4) D. J. Worsfold and S. Bywater, *Can. J. Chem.*, **38**, 1891 (1960).
- (5) H. Brody, D. H. Richards, and M. Szwarc, *Chem. Ind. (London)*, **45**, 1473 (1958).

from the ionic dissociation of living ion pairs, *viz.*, $\sim\text{S}^-\text{Na}^+ \rightleftharpoons \sim\text{S}^- + \text{Na}^+$, if a free $\sim\text{S}^-$ ion propagates faster than its ion pair. This explanation was erroneously rejected by Geacintov, *et al.*,¹ and it is instructive to consider their reasons.

The data of Geacintov, *et al.*,¹ covered a relatively narrow range of living end concentrations, namely from 10^{-3} to $2 \times 10^{-2} M$. Extrapolation to zero concentration led to k_p of 600–700 l./mole sec. Accepting this value as the propagation rate constant of the free $\sim\text{S}^-$, one can calculate the concentration of ions in the investigated solutions. For example, the experimental data led to an apparent ionic dissociation of 50% in a $10^{-3} M$ solution of $\sim\text{S}^-\text{Na}^+$, whereas the conductivity studies of Worsfold and Bywater⁶ indicated only $\sim 1\%$ dissociation.

Ionic dissociation of $\sim\text{S}^-\text{Na}^+$ should be depressed on adding NaClO_4 to its solution. Therefore, the addition of this salt should slow down the polymerization if the observed increase of k_p with dilution is due to ionic dissociation. Such an effect was not observed,¹ contradicting again the hypothesis of participation of free ions in the process.

The two negative results induced us to look for more exotic explanations,⁷ and these appeared attractive for a while. However, further consideration of the problem forced us to return to the concept of free ions and suggested that the evidence presented by Geacintov, *et al.*,¹ was not entirely convincing. The extrapolation to zero concentration of living ends could be unreliable since the data were limited to [living ends] $\geq 10^{-3} M$. The effect of sodium perchlorate could be negligible if its degree of dissociation in THF is minute. It was decided, therefore, to extend the kinetic studies to much lower concentrations and to investigate the conductivities of living polystyrene and of NaClO_4 in THF.

Experimental Technique of Kinetic Studies

The capillary flow technique, used in previous studies,^{1,2} is unreliable when investigating the polymerization at concentrations of living ends lower than $10^{-3} M$ because the destruction of living ends then becomes excessive. We developed, therefore, a static technique in which the progress of polymerization is followed spectrophotometrically by monitoring the absorption of styrene at $291.4 m\mu$. At this wave length the monomer has an absorption maximum, $\epsilon = 673$, and its optical density obeys Beer's law.

The apparatus used for kinetic studies is shown in Figure 1. It consists of a 2-l. flask, A, filled with specially purified nitrogen at atmospheric pressure. The flask is connected through a stopcock to two con-

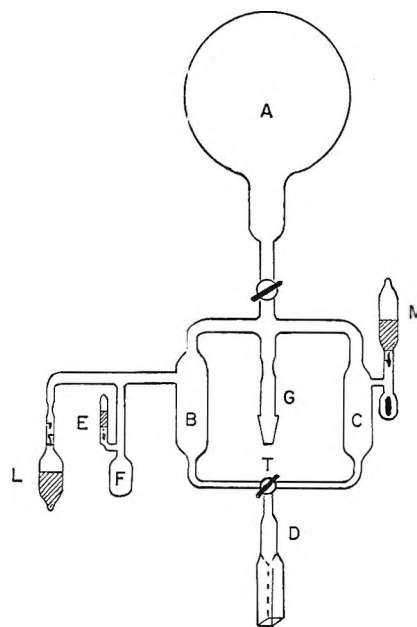


Figure 1. The apparatus used for kinetic studies of fast anionic polymerizations.

tainers, B and C. The latter are linked by a three-way Teflon stopcock, T, to an optical quartz cell, D. Three ampoules, M, L, and E, each equipped with a break-seal, are sealed to the unit. The first contains a THF solution of the monomer, while the second and third contain, respectively, a very dilute and a concentrated THF solution of living polystyrene.

The whole unit, with exception of flask A, is evacuated on a high-vacuum line, flamed, and thereafter sealed off. The break-seal on ampoule E is crushed, and, by tilting the unit, the containers and the optical cell are rinsed with the concentrated solution of living polystyrene. This procedure destroys traces of water and other impurities adsorbed on the inner walls of the apparatus. The unit is turned upside down, the concentrated solution is returned to ampoule F, and, by cooling the outside walls with a pad soaked with liquid nitrogen, the solvent from F is condensed on the inner walls. This "washing" removes all the living polymer from the unit and transfers it to F. Ampoule F is then sealed off at liquid nitrogen temperature.

The optical cell (optical path 1 cm.) is now inserted into a spectrophotometer equipped with a recorder. Through crushing the break-seals, the solutions of styrene and of living polystyrene are transferred to the appropriate containers, B and C, which are then pres-

(6) D. J. Worsfold and S. Bywater, *J. Chem. Soc.*, 5234 (1960).

(7) M. Szwarc and J. Smid, "Progress in Reaction Kinetics," Vol. II, Pergamon Press, Inc., New York, N. Y., 1964, pp. 243–246.

surized with the purified nitrogen while the optical cell remains evacuated. The monochromator is set at the required wave length ($291.4 \text{ m}\mu$), and the recorder is switched on. Quick opening of stopcock T lets both solutions rapidly into the evacuated optical cell, and the resulting turbulence efficiently mixes the reagents. The stopcock is then closed to prevent the diffusion of the reagents into the cell. In this device the concentration of the monomer is monitored in less than 1 sec. after the onset of polymerization, and reactions having half-lifetimes of about 3–4 sec. may easily be investigated. The concentration of living ends is determined spectrophotometrically at the end of the experiment, but not later than 10–20 sec. after the onset of the reaction, by turning the monochromator to $340 \text{ m}\mu$, *viz.*, the λ_{NM} of $\sim\text{S}^-\text{Na}^+$. The ratio of initial concentrations of the monomer to living ends was about 20:1.

In runs lasting more than 50 sec. the concentration of living polymers is determined during the experiment by turning the monochromator at regular intervals to $340 \text{ m}\mu$. This procedure is illustrated in Figure 2. Usually the concentration of living polymers remains constant during the whole course of polymerization; however, if it does not, the appropriate corrections are applied. It is important that [living ends] is determined *in* the polymerizing solution and not in the stock solution. This procedure eliminates any errors arising from accidental killing caused by the addition of monomer.

For very slow reactions—half-lifetime of about 2 min. or more—a simplified procedure is used. The apparatus is depicted in Figure 3 which is self-ex-

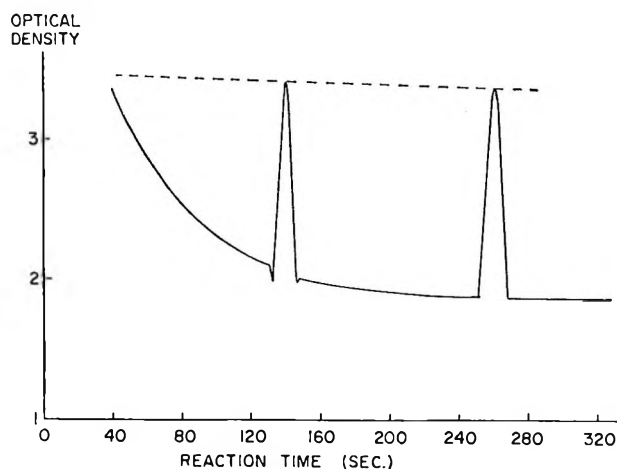


Figure 2. A typical recorder tracing of the optical density at $291.4 \text{ m}\mu$ (λ_{max} of styrene) as a function of time. The high peaks give the optical density at $340 \text{ m}\mu$ (λ_{max} of living polystyrene).

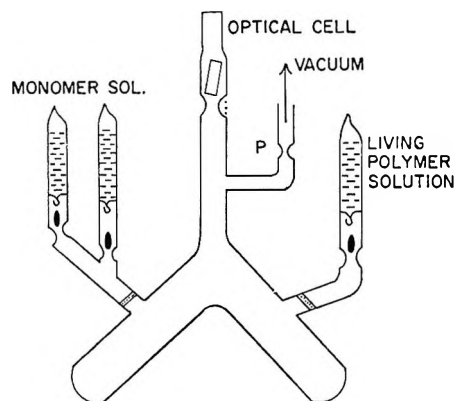


Figure 3. The apparatus used for kinetic studies of slower anionic polymerizations.

planatory. The solutions of the monomer⁸ and the polymer are sealed in the appropriate ampoules, and, through crushing the break-seals, they are admitted to the respective arms of a V-shaped reactor which previously was purged with a concentrated solution of living polymer. The contents are then vigorously shaken, the mixture poured into the attached optical cell by turning the unit upside down, the cell placed in the spectrophotometer, and the recorder switched on. This procedure takes about 15 sec.

The length of the optical cell used for such kinetic studies depends on the dilution; 1-cm. cells were used for higher concentrations, ($[\sim\text{S}^-\text{M}^+] \sim 10^{-4} \text{ M}$), whereas for diluted solutions (10^{-5} M or less) 5- or 10-cm. cells had to be employed. The initial concentration of styrene was usually 10 to 20 times that of the living ends.

The extremely diluted THF solutions of living polystyrene are relatively unstable, and $\sim\text{S}^-\text{Li}^+$ seems to be the least stable alkali salt of living polystyrene. Therefore, it is advisable to store a more concentrated solution in the respective ampoule; then, by crushing the break-seal and tilting the unit, a fraction of it may be transferred into the appropriate reservoir and diluted by distilling in the THF from the remaining concentrated solution. The dilution is accomplished a few minutes prior to the actual experiment.

The rate of decay of 10^{-5} M solutions of living polystyrene is about a few per cent per minute; the two-ended $\sim\text{S}^-\text{Cs}^+$ is, however, exceptionally stable. It appears that the decay is due to a reaction of the *free* $\sim\text{S}^-$ ions with THF leading to the formation of $\sim\text{S}(\text{CH}_2)_4\text{O}^-$.

The results are calculated by plotting $\{\log (\text{O.D.}_t -$

(8) It is more convenient to introduce into the ampoule a pure, undiluted monomer; this minimizes the extent of killing.

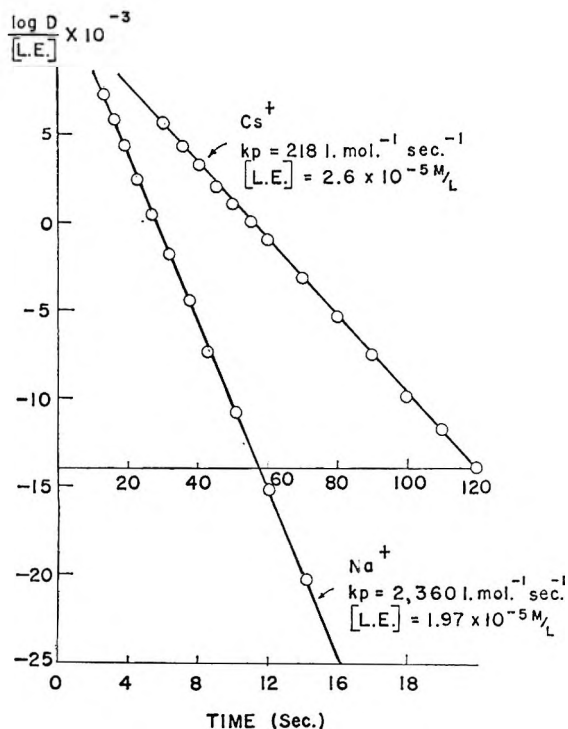


Figure 4. Plot of $\log(O.D.t - O.D.\infty) = \log D$ vs. time.

$O.D.\infty\} / [\text{living ends}]$ vs. time as shown in Figure 4. The term $O.D.\infty$ corrects for the absorption of living polystyrene at $291.4 \text{ m}\mu$. The plots remain linear even if the reaction is followed for 3 or 4 half-lifetimes of the process.

Preparation of Living Polymers. Living polystyrenes endowed with two growing ends and possessing Na^+ or K^+ counterions were prepared in a conventional way from living α -methylstyrene dimers or tetramers (see ref. 1 for further details). The \overline{DP} of the resulting polymer was usually between 20 and 25.

Living polystyrene with Li^+ counterion was prepared by treating ethyllithium recrystallized from benzene with an excess of styrene in THF. It was checked that *all* the ethyllithium reacted, and *none* was left in the solution. Notice that such polymers have only one living end per chain.

Polymers having Rb^+ or Cs^+ counterions were prepared by slowly adding a THF solution of styrene to the respective alkali metals. Cesium and rubidium were prepared by heating the respective chlorides with metallic calcium and distilling the liberated metal under high vacuum into the reaction flask.

It was found desirable to have a slight excess of cesium and to filter the solution 10–15 min. after the onset of the reaction when some free cesium is still present. A prolonged contact with the metal results

in a blue tint of the solution which eventually becomes black. Properly prepared solutions show only one fairly sharp absorption peak (for $\sim\text{S}^-\text{Cs}^+$, $\lambda_{\text{max}} 345 \text{ m}\mu$).

The living $\sim\text{S}^-\text{Cs}^+$ having only one growing end per chain was prepared by slowly adding a THF solution of styrene to the stirred solution of cumyl $^-\text{Cs}^+$. The resulting polymer of a $\overline{DP} \sim 25$ shows an absorption at $\lambda_{\text{max}} 341 \text{ m}\mu$. The slight difference in the absorption spectra of the two-ended and one-ended cesium polystyrenes may indicate the intramolecular association of the former polymer; *i.e.*, its structure may be $[\text{S}^-\text{Cs}^+\text{S}^-]_n\text{Cs}^+$. The problem of intramolec-

ular association of $\sim\text{S}^-\text{Cs}^+$ ends will be discussed at length in a later part of this paper.

A solution of cumyl $^-\text{Cs}^+$ is prepared by adding to a stirred dispersion of metallic cesium in THF a THF solution of methyl cumyl ether. The blue color of the Cs solution disappears instantly and, gradually, a yellow coloration appears which eventually turns to a deep red. As the reaction proceeds, cesium methoxide precipitates. The reaction is continued overnight; then the mixture is cooled to -80° to enhance the sedimentation of the precipitate, and after 2 hr. the clear solution is decanted through a glass sinter plate. The absorption spectrum of cumylcesium shows a maximum at $345 \text{ m}\mu$, and by titrating the solution, the extinction coefficient was determined to be $\sim 1.8 \times 10^4$. Conversion exceeds 90%, but a much longer exposure to the metal is not recommended since it leads to some side reactions which are manifested by the appearance of new absorption peaks.

Extinction Coefficients of Living Polymers. In the kinetic studies, as well as in studies of conductivities which will be described in a later part of this paper, we determined the concentration of living polymers from their optical densities. It was necessary, therefore, to determine accurately their extinction coefficients.

The following device, shown in Figure 5, was used for this purpose. Ampoule A, containing an aliquot of concentrated living polymer solution ($\sim 1-2 \times 10^{-2} M$), and ampoule F, having a small amount of dry and deaerated methyl iodide, are sealed to the left arm of the apparatus. This consists of an optical quartz cell, B, having a 2-mm. optical path, equipped with a 1.9-mm. spacer, C, a flask, D, with a calibrated narrow neck which serves to determine accurately the total volume of the solution, and a round-bottom flask, E, with a magnetic stirrer in which the titration of living polymers is accomplished. The apparatus is evacuated through the connected tube, flamed under high vacuum, and eventually sealed off at constriction P_1 . The break-seal on ampoule A is crushed, and the concen-

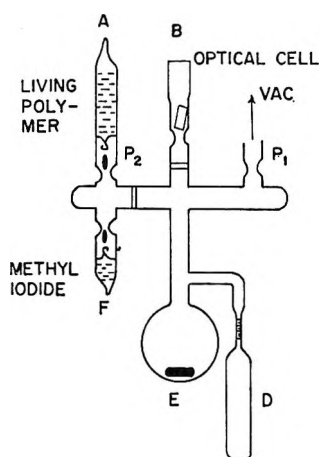


Figure 5. Apparatus used for determining extinction coefficients of living polymers.

trated solution of living polymers ($\sim 1-2 \times 10^{-2} M$) is introduced into E. Ampoule A is washed by chilling its walls with a pad soaked in liquid air, then the wash solution is frozen in E, and A is sealed off at constriction P_2 . By rinsing the apparatus with the living polymer solution all the impurities and any residual moisture adsorbed on the walls are removed. All the contents are then collected in E, and the remaining parts of the equipment are washed by chilling the walls and condensing the solvent. From E the liquid is quantitatively transferred into D and brought to the desired temperature; its volume is measured by determining the position of the meniscus in the narrow neck. The solution is then introduced into optical cell B; it is mixed well by being poured in and out a few times, and eventually its spectrum is recorded. Thence, it is again quantitatively transferred into E, chilled, and magnetically stirred. The break-seal on the methyl iodide ampoule, F, is crushed, and, as soon as the red color disappears, the distillation of methyl iodide is interrupted by chilling F. Flask E is then cut off; the solvent and the slight excess of methyl iodide are evaporated; the residue containing the killed polymer and sodium iodide is dissolved in distilled water and titrated for inorganic iodide, following a conventional analytical procedure. To secure complete solution of the salts in water, a small amount of benzene is added to dissolve any polymer. The titration of a concentrated solution of living polymer with methyl iodide is reliable although difficulties are encountered in titrating very dilute solutions.

The procedure may be improved by eliminating all the difficulties of analysis arising from the uncertainty in the end-point determination. Instead of ampoule F containing an excess of methyl iodide, a small am-

poule containing an exactly weighed amount of de-aerated water or other suitable protonating agent is attached to flask E. The amount of water should not be sufficient to destroy all the living ends, and, thus, after its contents are introduced into the flask, the optical density of the remaining polymer may be re-determined. The difference in optical densities, in conjunction with the known amount of the "killing" agent, gives the extinction coefficient. The values of the extinction coefficients determined in this laboratory are listed in Table I. The validity of Beer's law was

Table I: Decimal Extinction Coefficients of Salts of Living Polystyrene at 25°

Counterion	Solvent	λ_{\max} , m μ^a	$\epsilon \times 10^{-4}$
Li ⁺	THF	337 (338)	1.00
Li ⁺	Dioxane	336	1.02
Na ⁺	THF	342 (343)	1.20 (1.18)
Na ⁺	Dioxane	339	1.21
K ⁺	THF	343 (346)	1.20
K ⁺	Dioxane	340	1.21
Rb ⁺	THF	340	1.2 (?)
Rb ⁺	Dioxane	341	1.23
Cs ⁺ (two-ended)	THF	345	1.3 (?)
Cs ⁺ (one-ended)	THF	341	1.25
Cs ⁺ (two-ended)	Dioxane	342	1.24

^a The values in parentheses are those of S. Bywater, A. F. Johnson, and D. J. Worsfold, *Can. J. Chem.*, 42, 1255 (1964).

established by using a procedure similar to that described in the section dealing with the conductivity measurements.

Results

The results of the kinetic experiments are summarized in Tables II and III. The sodium salt of living polystyrene was most extensively studied, its apparent k_p values being determined for [living ends] ranging from 10^{-5} to $10^{-2} M$. The kinetics of polymerization of other salts, *viz.*, those of Li⁺, K⁺, Rb⁺, and Cs⁺, were studied at sufficiently low concentrations to establish unequivocally the functional dependence of the respective k_p values on [living ends].

Let us assume that ion pairs, $\sim S^-, M^+$, and free $\sim S^-$ ions participate in the propagation, their respective rate constants of growth being k'_{S^-, M^+} and k''_{S^-} . If fraction x of living polymers is dissociated into ions, then the observed k_p is given by the equation $k_p = (1 - x)k'_{S^-, M^+} + xk''_{S^-}$. For $x \leq 0.05$, the approximations $(1 - x) \approx 1$ and $x = (K_{S^-, M^+})^{1/2} / [\text{living ends}]^{1/2}$ are valid and, thus, $k_p \approx k'_{S^-, M^+} + k''_{S^-} (K_{S^-, M^+})^{1/2} / [\text{living ends}]^{1/2}$. In this equation

Table II: Concentration Dependence of k_p in Anionic Polymerization of Styrene in THF at 25°

Counterion	[LE] × 10 ⁶ M	k_p , l./mole sec.
Li ⁺ (one end per chain)	4.0	4900
	8.0	3520
	9.6	3380
	16.3	2830
	83.0	1440
Na ⁺ (two ends per chain)	1.97	5420
	6.22	3620
	7.33	3560
	11.0	2450
	16.5	2050
	100	900
	300	550
	490	538
	750	434
	1000	396
1810	315	
K ⁺ (two ends per chain)	3.21	2800
	4.75	2670
	6.86	2280
	11.9	1890
	190	484
Rb ⁺ (two ends per chain)	230	374
	2.30	2080
	4.37	1210
	13.0	711
	25.9	445

K_{S^-,M^+} denotes the dissociation constant of the relevant ion pair, $\sim S^-,M^+$. Hence, plots of k_p vs. $1/[living\ ends]^{1/2}$ should result in straight lines, and, indeed, such lines are shown in Figures 6 and 7, sup-

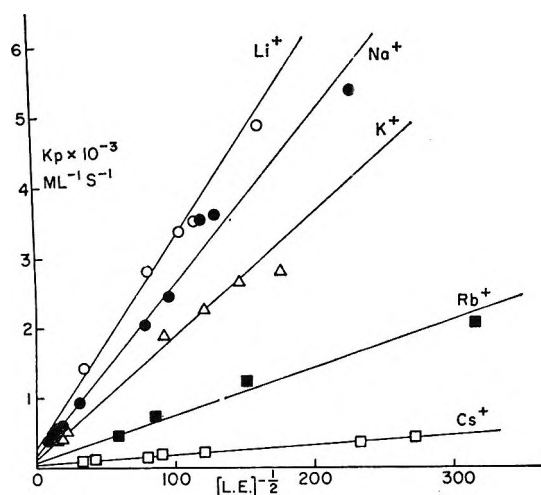


Figure 6. Plots of the apparent rate constants of propagation, k_p , of alkali salts of living polystyrene in THF vs. $1/[living\ polymers]^{1/2}$ at 25°: \circ , Li⁺; \bullet , Na⁺; Δ , K⁺; \blacksquare , Rb⁺; \square , Cs⁺ (two ends per chain).

Table III: Concentration Dependence of k_p in Anionic Polymerization of Styrene in THF at 25° with Cs⁺ Counterion. Comparison of One-Ended and Two-Ended Polymers

[LE] × 10 ⁶ M	k_p , l./mole sec.	k_p , l./mole sec.
Two ends per chain	$\overline{DP} \sim 20-25$	$\overline{DP} \sim 5000$
1.36	442	...
1.80	...	545
1.85	362	...
3.76	...	387
6.9	223	...
12.8	181	...
16.0	148	...
53.0	107	...
94.0	99	...
One end per chain	$(\overline{DP} \sim 20)$	
2.80	600	
3.04	568	
6.9	385	
31.0	169	
44.6	136	
116	108	

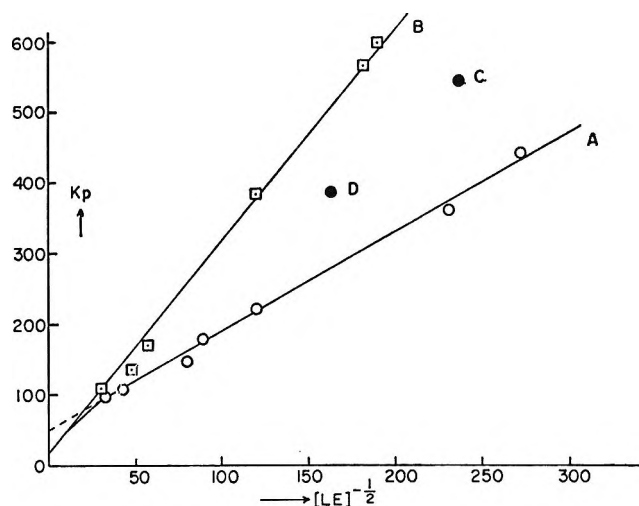


Figure 7. Plots of the apparent rate constants of propagation, k_p , of cesium salts of living polystyrene in THF vs. $1/[living\ polymers]^{1/2}$ at 25°: \square , Cs⁺, one end per chain; \circ , Cs⁺, two ends per chain, $\overline{DP} \sim 25$; \bullet , Cs⁺, two ends per chain, $\overline{DP} \sim 1000$.

porting, therefore, the proposed explanation for the variations of k_p . The slopes of these lines give $k''_s(K_{S^-,M^+})^{1/2}$, and their intercepts lead to k'_{S^-,M^+} . The experimental results are summarized in Table IV. These values differ slightly from those reported in our preliminary note.⁹

The decreasing slopes seem to signify a decrease in

(9) D. N. Bhattacharyya, C. L. Lee, J. Smid, and M. Szwarc, *Polymer*, 5, 54 (1964).

Table IV

Counterion	Li ⁺	Na ⁺	K ⁺	Rb ⁺	Cs ⁺ (two-ended)	Cs ⁺ (one-ended)
Slope = $k''_{S^-,M^+} (K_{S^-,M^+})^{1/2}$, l. ^{1/2} /mole ^{1/2} sec.	30.3	25.2	18.0	6.7	1.4	3.0
Intercept = k'_{S^-,M^+} , l./mole sec.	~250	~150	~100	~80	~50	25

the dissociation constants of the $\sim S^-,M^+$ salts, $\sim S^-,Li^+$ being the most dissociated in THF, whereas $\sim S^-,Cs^+$ is the least dissociated. Since the intercepts are very small, it is difficult to determine their exact values. Nevertheless, it is unquestionable that the $\sim S^-,Li^+$ ion pair is the most reactive, and the $\sim S^-,Cs^+$ the least. In a later part of this paper we shall describe a more accurate method for determining the propagation rate constants, k'_{S^-,M^+} , of these ion pairs.

Conductivities of Salts of Living Polystyrene in THF. The kinetic studies led us to the ratios of the dissociation constants of $\sim S^-,M^+$ ion pairs. To confirm the kinetic results and to determine the absolute propagation rate constant, k''_{S^-} , of the living polystyrene ions, the conductivities of $\sim S^-,M^+$ in THF had to be investigated.

Conductivities were determined in the apparatus shown in Figure 8. It consists of a sealed conductivity cell, H, and three optical cells, D, E, and F, having optical path lengths of 10, 1, and 0.2 cm., respectively, the last one being equipped with a 0.19-cm. spacer. Flask B contains a living polymer solution to be used for purging the apparatus and destroying all the residual impurities adsorbed on the walls. Ampoule A contains a fairly concentrated solution of the polymer to be investigated.

The apparatus is evacuated on a high-vacuum line, flamed, and sealed off at constriction P₁. The break-seal on ampoule B is crushed, and the whole unit is rinsed with the solution. The rinsing solution is then returned to B, and the unit is "washed" by condensing the solvent on the walls which are chilled in the usual way from outside. A desirable amount of the solvent is distilled from B to a graduated cylinder, C, and then B is sealed off at P₂.

The break-seal on A is then crushed, the sample to be investigated diluted with the solvent in C, and the optical density of the resulting solution determined in the appropriate optical cell. The solution is then transferred to conductivity cell H, and its resistance is measured. The optical density is redetermined, and thereafter about two-thirds of the solution is transferred to C. The solvent from C is distilled into the chilled ampoule G and used to dilute the residual solution left in H. The conductivity and the optical density of this solution are determined as described

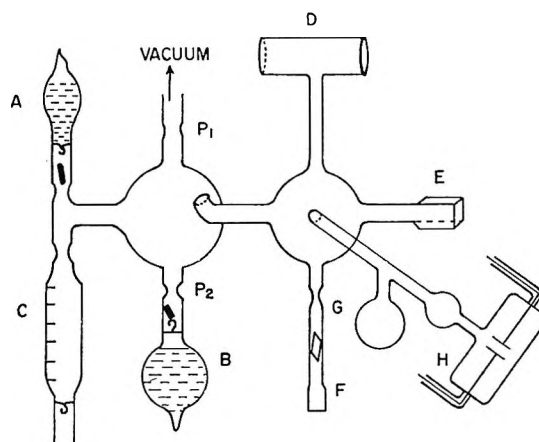


Figure 8. Apparatus for determining the conductivities of living polystyrene.

previously; thereafter, two-thirds is again transferred to C, and the remaining one-third is diluted by the above-described procedure. In this way the conductivities are determined for decreasing concentrations of living polymer, allowing us to calculate Λ as a function of [living polymer] down to about $10^{-5} M$.

The described method has a few advantages. (1) The products derived from impurities are removed from the system together with the purging solution, and, therefore, they do not contribute to the measured conductivity. Such a contribution might be appreciable at extremely low concentrations of living polymer. (2) No impurities are introduced on dilution, since the same solvent is used over and over again. (3) The destruction or "isomerization" of living polymers, which sometimes occurs in a highly dilute solution, is minimized since one proceeds from a more concentrated to a more dilute solution.

The conductivities of living polystyrene solutions were determined at 1-kc. frequency with a bridge described in the preceding paper.¹⁰ The conductivity cell had a volume of 60 cc. and a constant of 0.0801 cm.⁻¹ and was maintained at $25 \pm 0.02^\circ$. The experimental data are collected in Table V, the respective concentrations being determined a few minutes before and after measuring the conductivity, and, if the

(10) D. N. Bhattacharyya, C. L. Lee, J. Smid, and M. Szwarc, *J. Phys. Chem.*, **69**, 608 (1965).

Table V: Conductivity Data of Living Polystyrene in THF at 25°^a

Cation	$C \times 10^5 M$	Λ
Li ⁺ (one-ended)	310.0	0.460
	83.5	0.774
	40.3	1.18
	34.0	1.27
	19.6	1.52
	11.5	2.11
	8.1	2.27
	4.0	3.66
	2.1	5.31
	1.14	7.24
Na ⁺ (two-ended)	430	0.397
	400	0.416
	330	0.477
	26.0	1.50
K ⁺ (two-ended)	639	0.282
	332	0.355
	74.5	0.659
	10.3	1.76
	5.46	2.45
	2.04	3.71
Cs ⁺ (two-ended)	321.0	0.241
	144	0.318
	55.1	0.475
	28.3	0.659
	15.8	0.864
	5.92	1.36
Cs ⁺ (one-ended)	220	0.138
	116	0.173
	61.4	0.218
	31.8	0.282
	15.6	0.384
	7.04	0.531
NaClO ₄ ^b	3.23	0.766
	96	0.565
	394	0.331
	1510	0.242
	6050	0.274
	13340	0.417

^a Dielectric constant of THF = 7.39; density = 0.880 g./cm.³; viscosity, η = 0.00460 poise. ^b Notice the minimum in Λ indicating the formation of triple ions and probably a decrease in $[\text{Na}^+]$ at higher concentrations of sodium perchlorate.

concentrations varied during this time, the average value was taken for calculation (the maximum change was less than 2%). A reliable sample of living polymers shows only one fairly sharp absorption peak with a maximum at about 340 m μ . However, dilute solutions of the K and Rb salts, and, to a lesser extent, also of the Na salts, undergo spectral changes when left for a few hours at room temperature.¹¹ These changes are associated with an increase in the conductivity, indicating the formation of new ionic species which prob-

ably are more extensively dissociated than the $\sim\text{S}^-\text{M}^+$ ion pairs. A similar observation was reported earlier by Worsfold and Bywater.⁶

The degree of dissociation of alkali salts of living polystyrene in THF is substantially lower than that of the corresponding salts of tetraphenylborides. The results were calculated in terms of Fuoss relations (see the preceding paper¹⁰ for the details), and the respective plots are shown in Figure 9. The conductivities of the sodium salt were measured only for a few concentrations in order to compare our results with those reported by Worsfold and Bywater.⁶ The agreement was found to be most satisfactory.

The slopes of the lines shown in Figure 9 give us $1/\Lambda_0^2 K_{\text{S}^-\text{M}^+}$ and the results are collected in Table VI. Therefore, the dissociation constant $K_{\text{S}^-\text{M}^+}$

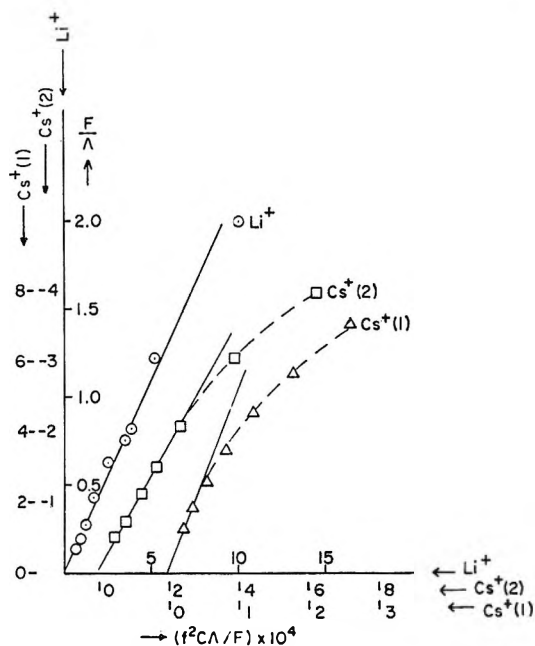


Figure 9. Fuoss plots of conductivity of living polystyrene: \circ , Li⁺; Δ , Cs⁺, one end per chain; \square , Cs⁺, two ends per chain, $\overline{DP} \sim 25$.

Table VI: Slopes of Fuoss Lines for the Alkali Salts of Living Polystyrene in THF at 25°

Counterion	Slope = $1/K_{\text{S}^-\text{M}^+} \Lambda_0^2$	Ref.
Li ⁺ (one-ended)	2.14×10^3	This report
Na ⁺ (two-ended)	1.74×10^3	Ref. 6
K ⁺ (two-ended)	3.52×10^3	This report
Cs ⁺ (two-ended)	9.0×10^3	This report
Cs ⁺ (one-ended)	53.0×10^3	This report

(11) G. Spach, M. Levy, and M. Szwarc, *J. Chem. Soc.*, 355 (1962).

for $\sim\text{S}^-\text{M}^+$ may be calculated if the limiting conductivities Λ_0 are known. In fact, the intercepts of the lines shown in Figure 9 give $1/\Lambda_0$, but unfortunately they are too small to allow any reliable determination.

The limiting conductivity $\Lambda_0 = \Lambda_0^+ + \Lambda_0^-$, where Λ_0^+ and Λ_0^- denote the limiting conductivities of the alkali cation and $\sim\text{S}^-$ anion. In the preceding paper¹⁰ we reported the Λ_0^+ values for Li^+ , Na^+ , K^+ , Rb^+ and Cs^+ ions in THF, as derived from the conductivity studies of the respective tetraphenylborides. Therefore, to complete our task, we have only to determine Λ_0^- for $\sim\text{S}^-$ ion. The following method was tried. Let us denote the slopes of the Fuoss lines for two living polystyrene salts, say of Li^+ and Cs^+ , by γ_1 and γ_2 . From the kinetic studies we find the slopes of the respective k_p values *vs.* $1/[\text{living polymer}]^{1/2}$ lines, which we denote by β_1 and β_2 , respectively. Since $(\gamma_1)^{1/2} = 1/(\Lambda_{0,\text{M}_1^+} + \Lambda_0^-)(K_{\text{S}^-\text{M}_1^+})^{1/2}$ and $\beta_1 = k''_{\text{S}^-\text{M}_1^+}/(K_{\text{S}^-\text{M}_1^+})^{1/2}$, with analogous expressions for γ_2 and β_2 , one finds $\Lambda_0^- = (\beta_1\gamma_1^{1/2}\Lambda_{0,\text{M}_1^+} - \beta_2\gamma_2^{1/2}\Lambda_{0,\text{M}_2^+})/(\beta_2\gamma_2^{1/2} - \beta_1\gamma_1^{1/2})$. Unfortunately, this approach is again experimentally unsatisfactory since the numerator represents a small difference of two large numbers.

Reactivities of Living Polystyrene Salts in the Presence of the Corresponding Alkali Tetraphenylborides. It was reported by Geacintov, *et al.*,¹ that the rate of anionic polymerization of living polystyrene (Na^+ counterion) was not affected by the addition of sodium perchlorate. On the other hand, our present work demonstrates that $\sim\text{S}^-\text{Na}^+$ ion pairs, as well as $\sim\text{S}^-$ free ions, participate in the propagation, and the presence of the latter is responsible for a considerable increase of the observed rate constant on dilution of the living polymer solution. It appears, therefore, that, in THF, NaClO_4 is dissociated to a lesser extent than $\sim\text{S}^-\text{Na}^+$, and indeed a few conductivity data, which are included in Table V, confirm this conclusion. Moreover, Geacintov, *et al.*,¹ used too high concentrations of NaClO_4 , causing dissociation by formation of triple ions (see footnote *b* in Table V). However, addition of the more easily dissociable $\text{Na}^+\text{BPh}_4^-$ to living polystyrene solution should have a pronounced retarding effect upon the rate of propagation, and, indeed, such an effect was reported in our preliminary note.⁹

The retarding effect of $\text{Na}^+(\text{BPh}_4)^-$ forms a basis of a method by which the dissociation constant of $\sim\text{S}^-\text{Na}^+$ may be determined. In a solution of $\sim\text{S}^-$, Na^+ containing an excess of the more dissociable $\text{Na}^+\text{BPh}_4^-$, nearly all Na^+ ions arise from the dissociation of the boride. Let us denote the ratio $[\text{Na}^+]/[\text{Na}^+\text{BPh}_4^-]_0$ by x , where $[\text{Na}^+\text{BPh}_4^-]_0$ denotes c , the total

concentration of the salt. The dissociation constant of $\text{Na}^+(\text{BPh}_4)^-$ is denoted by K_B , and that of $\sim\text{S}^-$, Na^+ , by $K_{\text{S}^-\text{Na}^+}$. Since $cx^2/(1-x) \approx K_B$, $xc = 1/2[(K_B^2 + 4K_{\text{BC}})^{1/2} - K_B]$. Now, $xc[\sim\text{S}^-]/[\text{living polymer}] = K_{\text{S}^-\text{Na}^+}$; hence, $[\sim\text{S}^-]/[\text{living polymer}] = K_{\text{S}^-\text{Na}^+}/xc$, and $k_p = k'_{\text{S}^-\text{Na}^+} + k''_{\text{S}^-}K_{\text{S}^-\text{Na}^+}/xc$.

We may determine, therefore, k_p for a series of solutions having variable amounts of $\text{Na}^+(\text{BPh}_4)^-$ and plot the observed k_p *vs.* $1/xc$. Such a plot is shown in Figure 10, the respective data being given in Table VII.

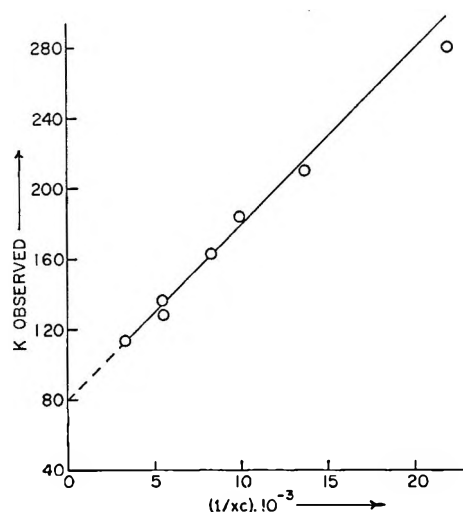


Figure 10. Plot of the apparent rate constant of $\sim\text{S}^-\text{Na}^+$ in the presence of $\text{Na}^+\text{BPh}_4^-$ *vs.* $1/xc$. $xc = [\text{Na}^+]$; $c = [\text{Na}^+\text{BPh}_4^-]$.

Table VII: Observed k_p of Propagation of $\sim\text{S}^-\text{Na}^+$ in the Presence of $\text{Na}^+\text{BPh}_4^-$ at 25° in THF ($k_{\text{Na}^+\text{B}^-} = 8.52 \times 10^{-5}$ mole/l.)

$[\sim\text{S}^-\text{Na}^+] \times 10^5 M$	$c = [\text{Na}^+\text{BPh}_4^-] \times 10^5 M$	k_p , l./mole sec.	$(1/xc)10^{-3}$
7.1	132.0	114	3.38
16.9	55.5	127	5.58
15.1	58.6	137	5.40
18.5	29.5	163	8.22
11.5	22.0	184	9.91
16.7	13.5	210	13.7 ^a
31.0	7.0	280	21.9 ^a

^a Even in these experiments 90% or more of the Na^+ ions come from the boride.

The intercept of the line gives $k'_{\text{S}^-\text{Na}^+} = 80$ l./mole sec., and its slope, $k''_{\text{S}^-}K_{\text{S}^-\text{Na}^+} = 9.8 \times 10^{-3}$ sec.⁻¹. Since the previous kinetic studies led to $k''_{\text{S}^-}(K_{\text{S}^-\text{Na}^+})^{1/2} = 25.2$ l.^{1/2}/mole^{1/2} sec., by combining these data we find $K_{\text{S}^-\text{Na}^+} = 1.52 \times 10^{-7} M$ and $k''_{\text{S}^-} = 65,000$ l./mole sec.

It should be added that the experiments described above have to be performed in highly diluted solutions. At higher concentrations of the salts the formation of triple ions is observed, and, consequently, the system then behaves differently than assumed.

Discussion

Let us summarize the results. By combining the kinetic data from the studies of the anionic polymerization of living $\sim\text{S}^-\text{Na}^+$ in the presence and absence of $\text{Na}^+(\text{BPh}_4)^-$ we derived the values for the propagation rate constants of the $\sim\text{S}^-\text{Na}^+$ ion pair ($k'_{\text{S}^-\text{Na}^+} = 80$ l./mole sec.) and for the free $\sim\text{S}^-$ ion ($k''_{\text{S}^-} = 65,000$ l./mole sec.). Moreover, the calculation also gives the dissociation constant of the $\sim\text{S}^-\text{Na}^+$ ion pair in THF, *viz.*, $K_{\text{S}^-\text{Na}^+} = 1.52 \times 10^{-7} M$.

It should be stressed that the values of $k'_{\text{S}^-\text{Na}^+}$ are given by the intercepts of lines obtained from each kinetic study. The results obtained in the absence of $\text{Na}^+(\text{BPh}_4)^-$ produce a steep line with a small intercept, and, therefore, the derived $k'_{\text{S}^-\text{Na}^+}$ is experimentally not too accurate. The other method, based on the effect of $\text{Na}^+(\text{BPh}_4)^-$ on the observed k_p , gives a much more reliable value for $k'_{\text{S}^-\text{Na}^+}$, and, hence, the latter is quoted above.

A few experiments were therefore performed with other salts of living polystyrene in the presence of the respective alkali borides, and these led to the values $k'_{\text{S}^-\text{Li}^+} = 160$ l./mole sec. and $k'_{\text{S}^-\text{Cs}^+}$ (one-ended) = 22 l./mole sec.

Having a reliable value for k''_{S^-} we may now calculate the dissociation constants of other $\sim\text{S}^-\text{M}^+$ ion pairs from the kinetic data derived from the experiments performed in the absence of borides. The results are collected in Table VIII. The same constants may also be derived from the conductivity data. Having independently determined $K_{\text{S}^-\text{Na}^+}$ and knowing the slope of the respective Fuoss line for $\sim\text{S}^-\text{Na}^+$, we calculate $\Lambda_0^- + \Lambda_{0,\text{Na}^+} = \{(\text{slope of the Fuoss line}) \cdot$

$K_{\text{S}^-\text{Na}^+}\}^{-1/2}$. The value for $\Lambda_{0,\text{Na}^+} = 48.2$ is given in the preceding paper,¹⁰ and therefore $\Lambda_0^- = 13.5$. This result agrees remarkably well with that previously reported by Worsfold and Bywater,⁶ namely $\Lambda_0^- = 14$. These investigators derived it by applying Stokes' law to the extrapolated data on long-chain electrolytes reported by Pickering and Kraus.¹² Since the values for other Λ_{0,M^+} have been determined,¹⁰ we may now calculate the respective $K_{\text{S}^-\text{M}^+}$ values from the corresponding Fuoss lines. These constants are also listed in Table VIII, and the agreement between both sets is most gratifying.

Inspection of Table VIII shows that the dissociation constants of $\sim\text{S}^-\text{M}^+$ ion pairs decrease along the series $\text{Li}^+ > \text{Na}^+ > \text{K}^+ > \text{Rb}^+ > \text{Cs}^+$ (one-ended). The problem of two-ended Cs^+ -living polystyrene will be dealt with later. In this respect the alkali salts of living polystyrene in THF closely resemble the alkali borides, and to stress this similarity we included in Table VIII the values of the ratio $K_{\text{Na}^+(\text{BPh}_4)^-}/K_{\text{M}^+(\text{BPh}_4)^-}$ for comparison with those of the ratio $K_{\text{S}^-\text{Na}^+}/K_{\text{S}^-\text{M}^+}$. The slight difference observed for the $\text{Li}^+(\text{BPh}_4)^-$ seems to arise from the penetration of the small Li^+ ion into the bulky $(\text{BPh}_4)^-$ ion (see ref. 10).

The similarity of the behavior of these two series of salts indicates that in THF the specific solvation of the small alkali ions is the main driving force leading to the dissociation of the relevant ion pairs. The small Li^+ ion is the most solvated as shown by its low mobility ($\Lambda_{0,\text{Li}^+} = 36.6$)—a striking observation in view of its short radius. The larger Na^+ ion is less solvated ($\Lambda_{0,\text{Na}^+} = 48.2$), and the large Cs^+ ion is probably not solvated (see the following paper)—its mobility being the highest ($\Lambda_{0,\text{Cs}^+} = 68.4$) for the investigated series.

For alkali ions the solvation energy exceeds the Coulombic interaction energy which binds the ions into ion pairs, and therefore in THF the dissociation of ion pairs is exothermic. This conclusion is confirmed by the preliminary studies of temperature dependence of the conductivity, indicating its increase with decreasing temperature. The solvation of ions decreases the entropy of the system—the gain in entropy arising from the dissociation of an ion pair into two free ions is nullified by the substantial loss caused by the immobilization of several solvent molecules around the ion.

The extremely high reactivity of the free $\sim\text{S}^-$ ion, which is 400 times as reactive as the most reactive ion pair, is most significant. It shows that the polystyryl

Table VIII: Dissociation Constants for Living Polystyrene-Alkali Ion Pairs in THF at 25°

Counterion	$K_{\text{S}^-\text{M}^+} \times 10^7 M$		$K_{\text{S}^-\text{Na}^+}$		$\frac{K_{\text{Na}^+(\text{BPh}_4)^-}}{K_{\text{M}^+(\text{BPh}_4)^-}}$
	From reactivity	From conductivity	React.	Cond.	
Li^+ (one-ended)	2.18	1.86	0.69	0.81	1.07
Na^+ (two-ended)	1.52	(1.52)	(1.00)		(1.00)
K^+ (two-ended)	0.77	0.71	1.96	2.14	2.65
Rb^+ (two-ended)	0.107	...	14.3
Cs^+ (one-ended)	0.021	0.028	72	54	45.6
Cs^+ (two-ended)	0.00465 ^a	0.165 ^a	324	9.35	45.6

^a Calculated on the assumption that this species dissociates into the free $\sim\text{S}^-$ ion.

(12) H. L. Pickering and C. A. Kraus, *J. Am. Chem. Soc.*, **71**, 3288 (1949).

anion is not strongly solvated in THF. Our knowledge of reactivities of free ions is very meager, and in fact it has not been certain at all whether a free ion is more reactive than its ion pair. For example, one of us pointed out¹³ that a higher reactivity of an ion pair could be anticipated if a push-pull mechanism operates.

The high reactivity of free $\sim\text{S}^-$ ions in THF has been confirmed by the independent work of Hostalka, Figini, and Schulz.¹⁴ Their polymerization studies of living sodium polystyrene, reported shortly after the appearance of our preliminary note,⁹ led to results very similar to ours. The slope of their line, giving k_p as a function of $[\text{living polymers}]^{-1/2}$, is $25 \text{ l.}^{1/2}/\text{mole}^{1/2} \text{ sec.}^{-1}$ as compared with our value of 25.2, and their intercept, $k'_{\text{S}^-, \text{Na}^+}$, is 175 l./mole sec. This value is higher than that reported here; *i.e.*, $k'_{\text{S}^-, \text{Na}^+} = 80 \text{ l./mole sec.}$, because in Schulz's work, as in our preliminary investigation,⁹ one experiences difficulties of extrapolation owing to the steepness of the line. In fact, the addition of $\text{Na}^+, (\text{BPh}_4)^-$ led to a decrease of k_p observed by Schulz's group,¹⁴ indicating that the true $k'_{\text{S}^-, \text{Na}^+}$ is lower than their intercept.

It should be stressed that at higher concentrations of $\text{Na}^+, (\text{BPh}_4)^-$ the observed k_p passes through a minimum and then increases. Apparently, the formation of $\text{Na}^+, (\text{BPh}_4)^-, \text{Na}^+$ triple ions decreases the concentration of Na^+ ions and, therefore, increases that of $\sim\text{S}^-$ ions.

In a recent note, Löhr and Schulz¹⁵ pointed out that the existence of two types of centers, each growing at a different rate, affects the molecular weight distribution of the resulting polymer, even if the exchange between the centers takes place. The effect depends, in fact, on the rate of exchange, and it was considered by our group in a paper dealing with dormant polymers.¹⁶ A mathematical treatment of such problems was reported by Szwarc and Hermans¹⁷ and by Figini.¹⁸

Löhr and Schulz¹⁵ utilized this phenomenon to calculate the rate constant of dissociation of living ion pairs into ions and arrived at a value of 80 sec.^{-1} .

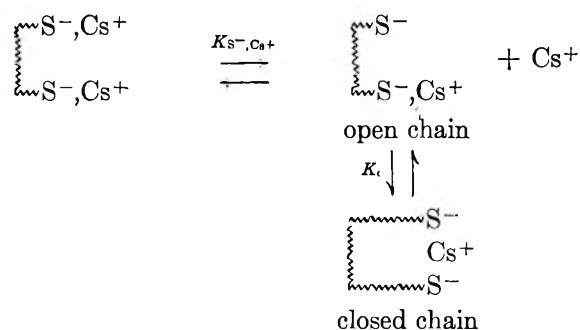
The Problem of Activation Energy of Anionic Polymerization. The participation of two types of centers in the anionic propagation in THF influences the temperature dependence of the over-all k_p . By changing the temperature one varies not only the individual k' and k'' , but also the fraction of free ions present in the solution. Since the dissociation of ion pairs is *exothermic*, the fraction of free ions *increases* on decreasing the temperature of polymerization. The ions are enormously more reactive than the ion pairs, and, hence, this effect *increases* the over-all k_p . It is not surprising, therefore, that Geacintov, *et al.*,¹ and Dainton, *et al.*,¹⁹ found an abnormally low "activation

energy" for such a polymerization (about 1 kcal./mole). In fact, it is possible to observe in such systems "negative" activation energies, and examples of such a behavior were found in our laboratory. The problem of activation energy for the propagation by free ions and by ion pairs will be discussed in a future paper.

The Problem of One-Ended and Two-Ended $\sim\text{S}^-, \text{Cs}^+$. Living polymers may be prepared with either one or both ends active, *e.g.*, $\text{X}\sim\text{S}^-, \text{Cs}^+$, referred to as a one-ended living polymer, and $\text{Cs}^+, \text{S}^-\sim\text{S}^-, \text{Cs}^+$, a two-ended polystyrene. As seen from Table VIII, the one-ended $\sim\text{S}^-, \text{Cs}^+$ behaves normally; namely, the calculations based on the reactivity or on the conductivity data lead virtually to the same dissociation constant, $K_{\text{S}^-, \text{Cs}^+}$. This is not the case with the two-ended polymer. The dissociation constant $K_{\text{S}^-, \text{Cs}^+}$ seems to be $4.6 \times 10^{-10} M$, if calculated from the reactivity data, and $1.65 \times 10^{-8} M$, if derived from the conductivity studies. The former is substantially lower, and the latter is much higher than the value obtained for the one-ended polymer, *viz.*, $K_{\text{S}^-, \text{Cs}^+} = 2.1\text{--}2.8 \times 10^{-9} M$.

Consideration of these discrepancies led us to conclude that the $\text{S}^-\sim\text{S}^-, \text{Cs}^+$ ions, which are formed on the dissociation of a two-ended polymer, associate with the ion pair located on the other end of the chain into a triple ion, $\text{S}^-, \text{Cs}^+, \text{S}^-$. In such a system one deals

with the following equilibria



where $K_{\text{S}^-, \text{Cs}^+}$ denotes the "ordinary" dissociation constant of the $\sim\text{S}^-, \text{Cs}^+$ ion pair into free ions, and K_c represents the equilibrium constant of the cyclization.

(13) M. Szwarc, *Makromol. Chem.*, **35A**, 123 (1960).

(14) H. Hostalka, R. V. Figini, and G. V. Schulz, *ibid.*, **71**, 198 (1964).

(15) G. Löhr and G. V. Schulz, *Makromol. Chem.*, **77**, 240 (1964).

(16) S. N. Khanna, M. Levy, and M. Szwarc, *Trans. Faraday Soc.*, **58**, 747 (1962).

(17) M. Szwarc and J. J. Hermans, *J. Polymer Sci. PB*, **2**, 815 (1964).

(18) R. V. Figini, *Makromol. Chem.*, **71**, 193 (1964).

(19) F. S. Dainton, D. M. Wiles, and A. N. Wright, *J. Polymer Sci.*, **45**, 111 (1960).

The former constant is known from the studies of the one-ended polymers; *viz.*, $K_{S^-,Cs^+} = 0.021$ or $0.028 \times 10^{-7} M$ (see Table VIII). The value of the latter constant depends on the length of the polymeric chain and on its flexibility.

Under our experimental conditions the concentration of *all* the ions is negligible when compared to the undissociated salt. Let us assume, therefore, that the concentration of Cs^+ ions is x , that of free $\sim S^-$ ions is y , and that of the triple ions S^-,Cs^+,S^- is z . The

concentration of the ion pairs, which is virtually equal to the total concentration of living ends, is denoted by c . The following equations have to be fulfilled:

$x = y + z$; $z/y = K_c$; $xy/c = K_{S^-,Cs^+}$. Hence, $y = \{(K_{S^-,Cs^+})/(1 + K_c)\}^{1/2}c^{1/2}$, $x = \{(K_{S^-,Cs^+})(1 + K_c)\}^{1/2}c^{1/2}$ and $z = K_c\{(K_{S^-,Cs^+})/(1 + K_c)\}^{1/2}c^{1/2}$. The fraction of ion pairs dissociated into the respective ions is, therefore, $f_{S^-} = \{(K_{S^-,Cs^+})/(1 + K_c)\}^{1/2}c^{-1/2}$, $f_{S^-,Cs^+,S^-} = K_c\{(K_{S^-,Cs^+})/(1 + K_c)\}^{1/2}c^{-1/2}$ and $f_{Cs^+} = \{(K_{S^-,Cs^+})(1 + K_c)\}^{1/2}c^{-1/2}$. Thus, the linear relations between the observed k_p and $c^{-1/2}$ and between $1/\Lambda$ and Λc are preserved, but the slopes of the respective lines now have a different meaning; namely, the slope of the reactivity line $\beta' = (k''_{S^-} + k^*K_c)\{(K_{S^-,Cs^+})/(1 + K_c)\}^{1/2}$, where k^* denotes the rate constant of propagation of the triple ion, and the slope of the Fuoss line $\gamma' = \{\Lambda_{Cs^+} + [K_c/(1 + K_c)]\Lambda_{S^-,Cs^+,S^-} + [1/(1 + K_c)]\Lambda_{S^-}\}^{-2}\{K_{S^-,Cs^+}(1 + K_c)\}^{-1}$. Let us assume for the first approximation that $k''_{S^-} \gg k^*K_c$, then $\beta' = k''_{S^-}\{(K_{S^-,Cs^+})/(1 + K_c)\}^{1/2}$; *i.e.*, β' is smaller by a factor of $(1 + K_c)^{1/2}$ than the β referring to the one-ended polymer. Thus, $1 + K_c \approx (\beta/\beta')^2 = (3/1.4)^2 = 4.6$. Now, the non-approximate equation is $1 + K_c = (\beta/\beta')^2[1 + (k^*/k''_{S^-})K_c]$, and it leads to a higher value of $1 + K_c$. For $k^* = 1000$ l./mole sec., *i.e.*, when a triple ion is 40–50 times as reactive as the ion pair, the correction term in the brackets amounts to 14%, and for $k^* = 3000$ l./mole sec. it increases to 75%. We may conclude, therefore, that the reactivity data lead to $K_c = 4.3$ for $k^* = 1000$ l./mole sec. and to $K_c = 7.0$ for $k^* = 3000$ l./mole sec.

To calculate K_c from the conductivity data,²⁰ we introduce the plausible assumption that $[K_c/(1 + K_c)]\Lambda_{S^-,Cs^+,S^-} + [1/(1 + K_c)]\Lambda_{S^-} = 10$ since $\Lambda_{S^-} = 13.5$ and $\Lambda_{S^-,Cs^+,S^-} < \Lambda_{S^-}$. Having $\Lambda_{Cs^+} = 68.4$,

we calculate the total $\Lambda_0' = 78.4$, and, hence, $\gamma' = 1/(78.4)^2 K_{S^-,Cs^+}(1 + K_c)$; therefore, $1 + K_c = (\gamma/\gamma')(\Lambda_0/\Lambda_0')^2 = (53.0/9.0)(81.9/78.4)^2 = 6.5$ (see Table VII for the pertinent data), and certainly it is not more than 7.3.

The agreement between these two methods of calculation of K_c is fair, and it indicates that K_c is most probably 5.5; the propagation rate constant of the triple S^-,Cs^+,S^- ion is then $k^* = 2200$ l./mole sec.

Thus, the triple ion is about 100 times as reactive as the $\sim S^-,Cs^+$ ion pair and about one-thirtieth as reactive as the free $\sim S^-$ ion. This seems to be reasonable.

It should be stressed that the *intermolecular* formation of triple ions is just noticeable in the conductivity of one-ended $\sim S^-,Cs^+$ at the concentration of $3 \times 10^{-4} M$ (see Figure 9). At this concentration the average distance between a $\sim S^-$ ion and a neighboring $\sim S^-,Cs^+$ ion pair is about 180 Å., whereas the distance between a $\sim S^-$ ion and the $\sim S^-,Cs^+$ ion pair located on the other end of the same chain ($\overline{DP} \sim 25$) is about 15 Å. Hence, the *intermolecular* association may be neglected when we deal with such low molecular weight polymers.

The effect described here should diminish for longer polymers. This is indeed the case. Two experiments were performed with a two-ended $\sim S^-,Cs^+$ living polymer having $\overline{DP} \sim 1000$. The respective k_p values of such polymers approximate the values observed for a one-ended $\sim S^-,Cs^+$, showing a substantial decrease of intramolecular association to triple ions (see Figure 7).

Finally, we should emphasize that the *intramolecular* association is not observed in sodium or potassium salts of living polystyrene (see Table VIII). Apparently the solvation of these ions prevents their association with the ion pairs.

Acknowledgment. We wish to thank Dr. J. Toelle for performing the experiments described in Table VII. We acknowledge the generous support of this study by the National Science Foundation and by the Quartermaster Corps.

(20) In deriving the equation for the conductivity, it is assumed that $S^-\sim S^-,Cs^+$ does not dissociate further.

Alternative Paths in Anionic Propagation of Ion Pairs.

Effect of Solvent and Counterion

by D. N. Bhattacharyya, J. Smid, and M. Szwarc

Department of Chemistry, State University College of Forestry, Syracuse University, Syracuse, New York 13210
(Received September 29, 1964)

Living polystyrene exists in dioxane entirely in the form of $\sim\text{S}^-\text{M}^+$ ion pairs; the presence of the free $\sim\text{S}^-$ ions could not be detected—a not surprising observation in view of the very low dielectric constant of this solvent. The propagation constant, k_p , is therefore independent of the living polymer concentration, and, in this respect, the dioxane solutions differ from the solutions in tetrahydrofuran (dielectric constant 7.4 as compared to 2.2 for dioxane). In that solvent an increase in the fraction of the highly reactive $\sim\text{S}^-$ ions, arising from dilution, leads to an increase in the observed k_p . The propagation constant depends on the nature of the counterion; at 25° in dioxane k_p is 0.9 for Li^+ , 3.5 for Na^+ , 19.8 for K^+ , 21.5 for Rb^+ , and 24.5 for Cs^+ , all in l./mole sec. In tetrahydrofuran the ion pairs grow faster, and the order of reactivity is reversed; thus, $k'_{\text{S}^-\text{M}^+}$ is 160 for Li^+ , 80 for Na^+ , about 50 for K^+ and Rb^+ , but again ~ 22 for Cs^+ . It seems that the partial solvation of the counterion in the transition state represents a major driving force of the polymerization in THF (tetrahydrofuran). Thus, the most strongly solvated Li^+ gives the most reactive ion pair; the poorly solvated Cs^+ produces the least reactive. In dioxane the solvent apparently does not help in separating the ions in the transition state, and therefore the reactivity of an ion pair is determined by the Coulombic binding energy of the pair. Hence, the small and strongly bonded Li^+ ion gives the least reactive ion pair, and the large Cs^+ yields the most reactive one. Since the reactivity of the $\sim\text{S}^-\text{Cs}^+$ ion pair is similar in both solvents, it appears that even in the transition state of propagation taking place in THF the Cs^+ is not specifically solvated.

Anionic polymerization of the sodium salt of living polystyrene in dioxane was investigated by Allen and his associates.^{1,2} They followed the progress of the reaction by a dilatometric technique and established the following facts.

(1) The bimolecular rate constant of propagation k_p is 4 ± 1 l./mole sec. at 25°, and its value is *independent* of the concentration of growing polymers, at least within the investigated range of [living polymer], *i.e.*, from 10^{-3} to 10^{-4} M.

(2) The activation energy of propagation is 9 ± 3 kcal./mole, and it corresponds to a "normal" frequency factor of about 10^8 l./mole sec. These findings contrast with those reported for the anionic polymerization of styrene in THF.³⁻⁵ In that solvent, k_p was found to be linear with $1/[\text{living polymer}]^{1/2}$ —

proving that ion pairs, $\sim\text{S}^-\text{M}^+$, as well as the free $\sim\text{S}^-$ ions, propagate the polymerization. The apparent activation energy appears to be exceptionally low^{6,7}—about 1 kcal./mole only. The last feature of the reaction arises from the exothermicity of the dis-

(1) G. Allen, G. Gee, and C. Stretch, *J. Polymer Sci.*, **48**, 189 (1960).

(2) C. Stretch and G. Allen, *Polymer*, **2**, 151 (1961).

(3) D. N. Bhattacharyya, C. L. Lee, J. Smid, and M. Szwarc, *Polymer*, **5**, 54 (1964).

(4) H. Hostalka, R. V. Figini, and G. V. Schulz, *Makromol. Chem.*, **71**, 198 (1964).

(5) D. N. Bhattacharyya, C. L. Lee, J. Smid, and M. Szwarc, *J. Phys. Chem.*, **69**, 612 (1965).

(6) F. S. Dainton, D. M. Wiles, and A. N. Wright, *J. Polymer Sci.*, **45**, 111 (1960).

(7) C. Geacintov, J. Smid, and M. Szwarc, *J. Am. Chem. Soc.*, **84**, 2508 (1962).

sociation of ion pairs into free ions; hence, the fraction of the highly reactive $\sim\text{S}^-$ ions increases at lower temperatures.

These differences of behavior prompted us to investigate the anionic polymerization of styrene in dioxane. Our results confirm Allen's findings and prove that the dissociation of ion pairs into free ions is not detectable in this solvent. This is not surprising since the dielectric constant of dioxane (2.2) is one-third as high as that of THF (7.4). Moreover, the propagation rate constants of ion pairs were found to increase with increasing size of the counterion, *viz.*, $\text{Li}^+ < \text{Na}^+ < \text{K}^+ \sim \text{Rb}^+ < \text{Cs}^+$. Since a reverse trend was observed in THF,^{3,5} one concludes that the factors which dominate the transition state of the propagation taking place in dioxane differ from those which govern the reaction in THF.

Experimental

Difficulties in preparing the α -methylstyrene dimer or tetramer initiators in dioxane solution prevented us from producing living polystyrene directly in this solvent. NP^- initiator (NP = naphthalene) was undesirable because of interference with the spectrophotometric determination of the monomer concentration. Consequently, the following method was developed.

The polymers are prepared in THF as described in ref. 4 and 7. After completing the polymerization, THF is distilled off on a high-vacuum line until a dark red, viscous residue is left. Rigorously purified dioxane is then distilled into the flask, and the resulting solution is slowly chilled while stirred. When the contents solidify, the flask is cooled for 10–15 min. with liquid nitrogen, the cooling bath is removed, and the polymer freeze-dried by pumping for 24 hr. The resulting dry, powdery polymer is redissolved in dioxane, and the whole procedure repeated at least once again. The absence of THF in the product is established by dissolving a fraction of the resulting polymer in benzene, killing it by a trace of water, and analyzing the solution for THF by v.p.c.

A properly prepared dioxane solution of living PS^- , Na^+ (PS = polystyrene) shows only one fairly sharp peak at $337 \text{ m}\mu$. However, sometimes a broad hump develops at around $400 \text{ m}\mu$, and, in such a case, the solution has to be rejected. Even a "good" solution is not too stable—after ~ 3 hr., the height of the $337 \text{ m}\mu$ peak in a $10^{-2} M$ solution decreases by 15–20%. Hence, the powdery polymer is kept in sealed ampoules in a deep freeze until needed, and a solution is prepared just before the start of an experiment.

Dioxane is purified by refluxing it on a Na–K alloy, followed by careful fractionation. After repeating

this procedure, the solvent is stirred with Na and 9-fluorenone under vacuum. The dioxane is then distilled from the green solution into the desired ampoules.

For no apparent reasons, some batches of dioxane catalyze the appearance of the $400\text{-m}\mu$ hump. Such batches are rejected, and a new batch of dioxane is then purchased and purified.

The kinetics of polymerization were investigated by monitoring the optical density of the solution at $291.4 \text{ m}\mu$ (an absorption maximum of styrene). The apparatus and the technique are described in the preceding paper.⁵

Results

In dioxane the propagation of living polystyrene is found to be a second-order reaction, the bimolecular rate constant, k_p , being independent of the monomer and living polymer concentrations. A typical conversion curve, giving $\log (\text{O.D.}_t - \text{O.D.}_\infty) / [\text{living polymer}]$ plotted *vs.* time, is shown in Figure 1. All

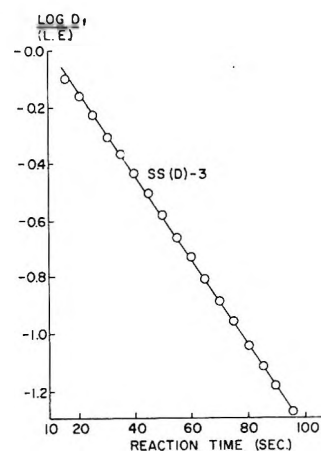


Figure 1.

the results are collected in Table I. For $\sim\text{S}^-$, Na^+ the constancy of k_p has been established over a 24-fold range of concentration from 0.5×10^{-3} to $12 \times 10^{-3} M$. A 10-fold change of concentration did not affect the k_p of $\sim\text{S}^-$, K^+ , $\sim\text{S}^-$, Rb^+ , and $\sim\text{S}^-$, Cs^+ . The instability of $\sim\text{S}^-$, Li^+ solutions prevented us from studying this system at higher dilution.

Discussion

The dielectric constant of dioxane (2.2) is substantially lower than that of tetrahydrofuran (7.4), and therefore the degree of dissociation of ion pairs should be much lower in the former solvent than in the latter. Indeed, no conductivity could be observed in dioxane

Table I: Homopolymerization of Living Polystyrene in Dioxane at 25°^a

Counterion	[Living polymer] × 10 ³ moles/l.	[S] ₀ × 10 ³ moles/l.	% conversion	k _p , l./mole sec.
Li ⁺ (one-ended)	2.5	40.0	10-90	0.96
Li ⁺ (one-ended)	2.2	115.0	10-70	0.92
Na ⁺ (two-ended)	0.50	7.5	28-68	3.24
Na ⁺ (two-ended)	3.02	63.5	15-55	3.42
Na ⁺ (two-ended)	4.95	89.5	20-73	3.42
Na ⁺ (two-ended)	9.36	93.8	44-89	3.30
Na ⁺ (two-ended)	12.0	41.6	76-97	3.80
K ⁺ (two-ended)	0.58	92.0		19.6
K ⁺ (two-ended)	5.9	40.0		20.0
Rb ⁺ (two-ended)	0.46	12.0		22.0
Rb ⁺ (two-ended)	4.6	58.0		21.0
Cs ⁺ (two-ended)	0.58	13.0		23.5
Cs ⁺ (two-ended)	6.5	95.0		25.5

^a These experiments were followed for time periods which varied from 17 to 1500 sec., depending on the value of the product, k_p[living polymer].

solutions of $\sim\text{S}^-\text{Na}^+$, indicating that the respective dissociation constants are less than 10⁻¹² mole/l. It is not surprising, therefore, that in dioxane the observed k_p is independent of [living polymer] since the contribution of free ions to the reactivity is below the limits of our detection, and the observed propagation is due entirely to the growth of ion pairs.

To focus the reader's attention on the different patterns of behavior of ion pairs in dioxane and in tetrahydrofuran we collected all the pertinent data in Table II. Its inspection shows that (1) the propagation rate constants of ion pairs are considerably larger in tetrahydrofuran than in dioxane; (2) the ion pairs dissociate relatively easily in tetrahydrofuran, but with great difficulty, if at all, in dioxane; (3) in tetrahydrofuran the most easily dissociable $\sim\text{S}^-\text{Li}^+$ ion pairs are the most reactive, whereas the least dissociable $\sim\text{S}^-\text{Cs}^+$ show the lowest reactivity. In dioxane, where the dissociation is undetectable, the order is reversed; $\sim\text{S}^-\text{Cs}^+$ is the most reactive, and $\sim\text{S}^-\text{Li}^+$ is the least.

Apparently, the partial solvation of the counterion in the transition state of the propagation in THF represents a major contribution to the driving force of the process, and the better the solvation, the faster the reaction. Hence, the small Li⁺ ion, which on dissociation becomes most solvated, as indicated by its low mobility (see the Λ₀⁺ values given in the last column of Table II), forms the most reactive ion pair. The poor specific solvation of the large Cs⁺ ion, demonstrated by its high

Table II: Comparison of Anionic Polymerization of Styrene in THF and in Dioxane at 25°

Counterion	k _{S⁻M⁺} (dioxane), l./mole sec.	k' _{S⁻M⁺} (THF), l./mole sec.	K _{S⁻M⁺} (THF), 10 ⁷ moles/l.,		Λ ₀ ⁺ (THF)
			React.	Cond.	
Li ⁺ (one-ended)	0.94	160	2.18	1.86	36.6
Na ⁺ (two-ended)	3.4	80	1.52	(1.52)	48.2
K ⁺ (two-ended)	19.8	~60-80	0.77	0.71	49.8
Rb ⁺ (two-ended)	21.5	~50-80	0.11
Cs ⁺ (one-ended)	..	22	0.021	0.028	68.4
Cs ⁺ (two-ended)	24.5	(47)	Forms triple ions		68.4

Λ₀⁺, results in the low reactivity of its ion pair, in spite of the weak Coulombic binding force.

The relatively poor solvation of the $\sim\text{S}^-\text{Na}^+$ ion pair in THF becomes evident from studies of the temperature dependence of its conductivity in this solvent (to be published). Hence, the partial separation of the counterion from the $\sim\text{S}^-$ anion, which takes place in the transition state of propagation, makes possible a specific solvation of the alkali ion by THF and contributes, therefore, to the driving force of the reaction.

The reactivities of ion pairs in THF go hand-in-hand with the respective dissociation constants (see Table III); although the relation between log K_{S⁻M⁺} and log k'_{S⁻M⁺} is not linear, the $\sim\text{S}^-\text{Cs}^+$ ion pair appears to be more reactive than would be anticipated on the basis of its dissociation constant. This may be due to the low degree of separation of the $\sim\text{S}^-\text{Cs}^+$ ion pair in the transition state.

Alternatively, the high reactivity of ion pairs in THF solution may be interpreted by the presence of two species: (a) less reactive contact ion pairs and (b) much more reactive solvent separated ion pairs. The study of fluorenyl salts in THF⁸ demonstrates that both species are present in this system, which makes the above suggestion quite plausible. Moreover, studies of temperature dependence (to be published) indicate a "negative" activation energy for the growth of ion pairs in THF. This may only be accounted for by the presence of two species (contact and solvent separated ion pairs), and on lowering the temperature the equilibrium shifts toward the more reactive species.

The low dielectric constant of dioxane makes the dissociation of ion pairs into free ions virtually impossible; hence, the lack of conductivity in this solvent is fully justified. However, one might argue that intrinsically this solvent solvates counterions well; e.g., two dioxane molecules may surround a cation placing four O atoms tetrahedrally around the positive

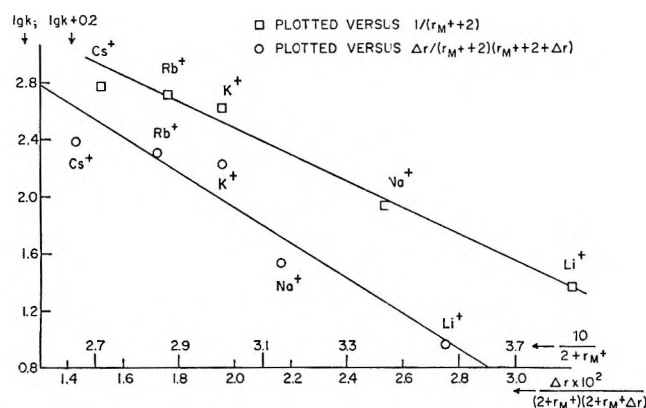


Figure 2.

center. Hence, the low reactivity of S^- -alkali $^+$ ion pairs in dioxane may be explained either by assuming equally good solvation of the counterion in the parent ion pair and in the transition state of its propagation, or by assuming a lack of specific solvation in the initial as well as in the transition state. It seems that the latter explanation is more correct and that dioxane is a poorer solvating agent than tetrahydrofuran. The evidence supporting the latter statement comes from the following two observations.

(1) Equal solvation of the initial and the transition state, as well as lack of specific solvation of both states, deprives the system of some driving force, and this accounts for the slower propagation in dioxane than in THF. The order of the reactivities of ion pairs should depend, therefore, on the Coulombic attraction between S^- and alkali $^+$ ions; the tighter the ion pair, the slower the process. Since the solvated Li^+ may be larger than the nonsolvated Cs^+ , the observed order of reactivities (see Table II) would appear strange, making implausible the assumption that the small cations are fully solvated in the initial and the transition states. However, if the cations are not solvated in either state, the observed order of reactivities is fully justified; *i.e.*, S^- - Li^+ should be the least reactive and S^- - Cs^+ the most.

(2) Studies of fluorenylsodium and fluorenyllithium solutions, performed in this laboratory,⁸ showed that these salts exist in THF as contact (intimate) ion pairs in equilibrium with the solvent-separated ion pairs. However, in dioxane, as well as in toluene, only the contact ions are observed. Hence, again we see that dioxane is a poorer solvating agent than THF.

The importance of Coulombic attraction is seen from Figure 2; a reasonably straight line results when $\log k_{\text{S}^-, \text{M}^+}$ is plotted against $1/(r_{\text{M}^+} + 2)$,⁹ r being the

radius of the bare cation. Such a linear relation implies that the free energy of activation of propagation involves a term proportional to the Coulombic binding energy—other terms being constant. This means $\Delta F^* = \text{const.} + \alpha e^2/(r_{\text{M}^+} + 2)D$, the proportionality factor, α , giving the fraction of binding energy lost in the transition state. Since the slope of the line seen in Figure 2 is $10^8 \alpha e^2/2.3DkT$, the value of α may be calculated from the experimental data. Taking a reasonable estimate, $D = 2$, we find $\alpha = 0.14$; *i.e.*, the S^- - M^+ bond is stretched in the transition state by about 14% of its original length.¹⁰

The linear relation discussed in the preceding paragraph implies $\alpha/(r_{\text{M}^+} + 2) = 1/(r_{\text{M}^+} + 2) - 1/(r_{\text{M}^+} + 2 + \Delta r) \approx \Delta r/(r_{\text{M}^+} + 2)^2$ or $\Delta r = \alpha(r_{\text{M}^+} + 2)$. Hence, the longer the bond, the larger its stretching in the transition state. This appears to be reasonable. The increase in the bond length results from the increasing bulkiness of the counterion, and this may introduce a steric hindrance which, in turn, demands a larger stretching of the bond in the transition state. However, one may argue that Δr should be approximately constant and independent of the bond length and the nature of the counterion. In such a case, the variable term in the free energy of activation acquires the form $e^2 \Delta r/(r_{\text{M}^+} + 2)(r_{\text{M}^+} + 2 + \Delta r)D$, and $\log k = \text{const.} + e^2 \Delta r/(r_{\text{M}^+} + 2)(r_{\text{M}^+} + 2 + \Delta r)DkT$. Therefore, we plotted also in Figure 2 $\log k$ vs. $\Delta r/(r_{\text{M}^+} + 2)(r_{\text{M}^+} + 2 + \Delta r)$, and, since the slope of such a line must be $10^8 e^2/2.3DkT$, this condition imposes a rather small value of 0.2 Å. for Δr . As seen from Figure 2, this relation provides a poorer fit of experimental points with the line than the $1/(r_{\text{M}^+} + 2)$ relation, and, to clearly reveal this fact, similar scales were chosen for both graphs. We conclude, therefore, that the stretching of the C^- - M^+ bond in the transition state increases with the cation size although the elongation may become less pronounced for the largest cations, thus, leading to the observed deviation of Rb^+ and Cs^+ from the linear relation. A similar reactivity of S^- - Cs^+ in dioxane and in THF indicates again that Cs^+ is poorly solvated even in THF.

Acknowledgment. We wish to acknowledge the financial support of these studies by the National Science Foundation.

(8) T. Hogen-Esch and J. Smid, 87, 669 (1965).

(9) Similar results are obtained if 1.5 or 2.5 is substituted for 2.

(10) The lowest possible value for D is 1. For $D = 1$, $\alpha = 0.07$, and the stretching of the bond in the transition state amounts to only 7%.

Electron Affinities of Aromatic Hydrocarbons in Tetrahydrofuran Solution

by J. Jagur-Grodzinski, M. Feld, S. L. Yang, and M. Szwarc

Department of Chemistry, State University College of Forestry, Syracuse University, Syracuse, New York 13210, and Donnan Laboratories, The University, Liverpool, England (Received November 12, 1964)

The relative electron affinities (= relative reduction potentials) of a series of aromatic hydrocarbons were determined in tetrahydrofuran (THF) solution. Two methods were employed: (1) potentiometric titration and (2) spectrophotometric studies of equilibria, $\text{aromatic}_1 + \text{aromatic}_2^- \rightleftharpoons \text{aromatic}_1^- + \text{aromatic}_2$. Potentiometric titration, originally developed by Hoijtink, was improved. The effect of various factors, not considered previously, was discussed, and special attention was paid to the fact that the radical ions exist essentially as ion pairs, and not as free ions. Hoijtink's treatment implicitly assumes a complete dissociation of ion pairs into ions. The final results show a good agreement between both methods. The results lead to the electrochemical series reported by Hoijtink, but numerically the potentials found in our study are substantially lower than those reported previously. The interesting case of tetraphenylethylene is discussed. In this compound the two-electron reduction potential (E_2) is *higher* than the first one (E_1). The reason for this reverse in the order of reduction potentials is suggested, and its effect on the potentiometric titration curve is elucidated.

Relative electron affinities of aromatic hydrocarbons were determined by Hoijtink, *et al.*,¹ who developed for this purpose a potentiometric technique. In the same year Paul, Lipkin, and Weissman² reported their spectrophotometric studies of the equilibria of electron-transfer processes, such as phenanthrene⁻ + naphthalene \rightleftharpoons phenanthrene + naphthalene⁻, from which they deduced the values of the relative electron affinities for the same series of hydrocarbons. Unfortunately, their data differed greatly from those reported by Hoijtink, thus raising the question of which method is reliable.

Both methods were used recently by our group to determine the relative electron affinities of pyrene, anthracene, and 9,10-dimethylanthracene³ in tetrahydrofuran (THF). Self-consistent results were obtained and these were confirmed by independent kinetic studies.³ However, since our reduction potentials somewhat differed from those published by Hoijtink,¹ we decided to reinvestigate the whole problem and to extend our studies to other aromatic hydrocarbons in order to ascertain the reliability of each method.

Experimental

Potentiometric Titrations. Hoijtink's apparatus and procedure were slightly modified. The unit used by us is shown in Figure 1, which is self-evident. The buret was terminated by a 2-mm. bore capillary, its lower tip being sealed and then punched with a needle to form six or seven tiny, parallel capillaries. This arrangement considerably slowed down the diffusion of the liquid from reactor R to the upper platinum wire electrode which was touching the sealed tip. The resistance of the unit, when filled with a 0.016 M THF solution of sodium biphenyl, was about 10 megohms.

The potential between electrodes was measured by a valve voltmeter⁴ which was described by Scroggie.⁵

(1) G. J. Hoijtink, E. De Boer, P. H. van der Meij, and W. P. Weijland, *Rec. trav. chim.*, **75**, 487 (1956).

(2) D. E. Paul, D. Lipkin, and S. I. Weissman, *J. Am. Chem. Soc.*, **78**, 116 (1956).

(3) D. Gill, J. Jagur-Grodzinski, and M. Szwarc, *Trans. Faraday Soc.*, **60**, 1424 (1964).

(4) We wish to thank Dr. A. Hickling of Liverpool University for providing us with this device and for his many valuable comments.

(5) M. G. Scroggie, *Wireless World*, **14** (1952).

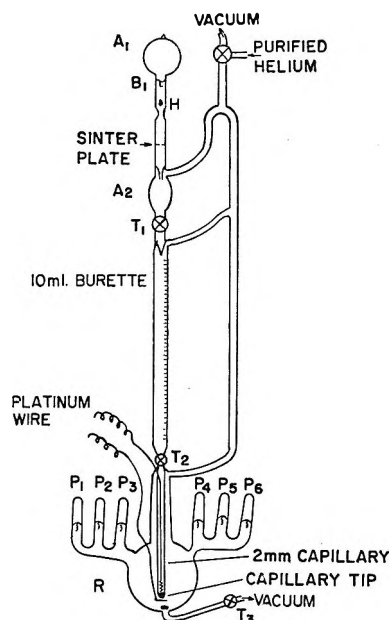


Figure 1. Apparatus used in the potentiometric titration of aromatic hydrocarbons.

In function it is essentially a very stable impedance converter by means of which an input d.c. voltage in a high resistance circuit is converted into an identical output d.c. voltage in a very low resistance circuit. The latter can be measured by any conventional voltmeter with a resistance exceeding 400 ohms. The current drawn from the source by the converter is less than 10^{-10} amp., and therefore its reading is reliable even if the resistance of the external circuit exceeds 100 megohms. To secure the maximum stability of the device, the input terminals are bridged by a 0.01- μ f. capacitor, and the negative input terminal is grounded through the case of the instrument. The voltmeter was calibrated, and the results seem to be reliable within 1%. For a low potential of about 0.04 v. the accuracy is about 0.002 v.

All the aromatic hydrocarbons used in this work were carefully crystallized and then sublimed under high vacuum. Their solutions were prepared on a high-vacuum line and sealed in small tubular ampoules equipped with break-seals. The purification of THF is described in ref. 6. The sodium biphenyl solution, used in the titration, was prepared by overnight reaction at room temperature of a 0.1 M solution of biphenyl in THF with a sodium mirror. The reaction proceeds to 16% conversion, and at this stage the system seems to reach its equilibrium. The concentration of sodium biphenyl was determined by titrating aliquots of the solution with HCl or with methyl iodide. Both methods gave concordant results. The prepared solution was

stored in an ampoule equipped with a break-seal, the latter eventually being sealed to the titration unit (ampoule A₁ in Figure 1).

The following procedure was used during the titration. After sealing ampoule A₁ containing the biphenyl-sodium biphenyl mixture (in 5:1 mole proportions) and the six P ampoules containing the investigated hydrocarbons, the whole unit was evacuated through the three-way stopcock T₀. Thereafter, by turning this stopcock, purified helium, bubbling through a sodium biphenyl solution, was admitted. The unit was again evacuated, the break-seal on ampoule A₁ crushed, and its contents quantitatively transferred into ampoule A₂. The whole unit was then repressurized with helium, and the titrating solution was introduced into the buret of 10-cc. capacity. About 10 cc. of the solution was introduced into reactor R, stirred magnetically, and eventually sucked out through stopcock T₃. Thus, the residual moisture adsorbed on the walls of the reactor was purged. Next, 10 cc. of solution were introduced into the reactor, and the potential was measured. It was found that in all the blank runs no potential difference was detected, indicating the absence of any polarization of the electrodes.

The second batch of sodium biphenyl solution was then sucked out, and one of the investigated solutions of the aromatic hydrocarbons was transferred into the reactor by crushing the appropriate break-seal. This was titrated by adding, under stirring, the sodium biphenyl solution in 0.5- or 1-cc. increments. About 1 sec. after each addition, the potential, which became constant, was read, and its value was plotted

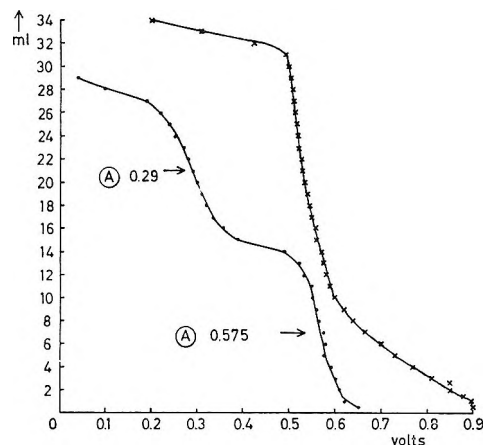


Figure 2. Potentiometric titration: X, tetraphenylethylene; ●, anthracene.

(6) J. Jagur, M. Levy, M. Feld, and M. Szwarc, *Trans. Faraday Soc.*, 58, 2168 (1962).

Table I: Reduction Potentials^a for Aromatic Hydrocarbons in THF Solution at 25°. Titrated by Biphenyl-Sodium Biphenyl Mixture in Molar Ratio 5:1; Concentration of Sodium Biphenyl, 0.016 M

Aromatic hydrocarbon	Expt. no.	Our reduction potentials		Hoijtink's reduction potentials ^b	
		E_1 , v.	E_2 , v.	E_1 , v.	E_2 , v.
Biphenyl	..	(0.0)	...	(0.0)	...
Naphthalene	10	0.066 ± 0.02 ^c	...	0.09	...
Triphenylene	5	0.113 ± 0.01	...	0.19	...
Phenanthrene	4	0.124 ± 0.005	...	0.17	...
Pyrene	4	0.505 ± 0.005	...	0.60	...
9,10-Dimethylanthracene	2	0.607 ± 0.005	0.34 ± 0.01
Anthracene	4	0.624 ± 0.005	0.33 ± 0.01	0.78 (in THF 0.74)	0.20 (in THF 0.40)
Perylene	3	0.917 ± 0.005	0.56 ± 0.01	1.09	0.46
Tetracene	3	1.025 ± 0.01	...	1.28 (in THF 1.28)	0.66 (in THF 0.82)

^a To all the observed potentials 0.04 v. was added to correct for the standard potential corresponding to a 1:1 mixture of biphenyl-sodium biphenyl. ^b Hoijtink's potentials were determined in dimethoxyethane solution and not in THF. He assumed also that the ratio biphenyl to sodium biphenyl is 1:1. This seems to be erroneous. ^c Corrected for the equilibrium $\text{biphenyl}^- + \text{naphthalene} \rightleftharpoons \text{biphenyl} + \text{naphthalene}^-$; *i.e.*, 80% more than 0.5 equivalent of B^- has to be added to give $N^-/N = 1$.

against the volume of the added liquid. Such plots are shown in Figures 2 and 3.

After completion of the titration, the contents of the reactor were sucked out, and the next sample of the aromatic hydrocarbon was introduced and titrated. This arrangement has a twofold advantage. (1) Three different aromatic hydrocarbons could be titrated in duplicates without exposing the electrodes to the air. (2) The same solution of sodium biphenyl was used for all these titrations. It is believed, therefore, that for such a series of experiments the differences in the reduction potentials should be very reliable. To ascertain the reliability of this setup, the experiments were staggered; *viz.*, any investigated hydrocarbon was retitrated after the others were investigated.

Results

The reproducibility in each series of titrations was better than ±0.005 v., and on repetition of the whole experiment the measured voltages were reproduced within ±0.01 v. In some experiments the duplicate titrations were performed with doubled concentrations of the investigated hydrocarbons—the results being unaltered by such a change of conditions.

The potential, measured at the stage of an experiment for which the ratio $H_y:H_y^- = 1$, is recorded in Table I as the respective relative reduction potential, E_1 , H_y and H_y^- denoting the concentrations of the investigated hydrocarbon and of its radical anion, respectively. In most titrations this stage is attained when the amount of the added biphenyl⁻ is equal to one-half of the titrated hydrocarbon, and, as seen in Figures 2 and 3, the relevant point is the center of the plateau of the respective experimental titration

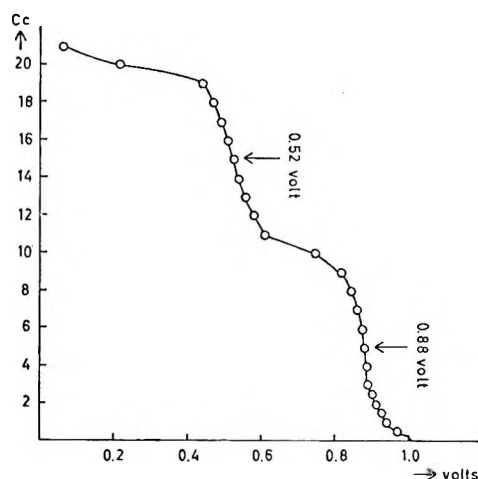


Figure 3. Potentiometric titration: perylene.

curve. However, in titration of naphthalene a correction is introduced to account for the equilibrium,⁷ $\text{biphenyl}^- + \text{naphthalene} \rightleftharpoons \text{naphthalene}^- + \text{biphenyl} \dots K$. Let us denote by B^- the amount of the biphenyl⁻ necessary to convert one-half of the, titrated naphthalene into naphthalene⁻; by N^- the amount of resulting naphthalene⁻, and by f , the ratio B/B^- in the original solution of biphenyl⁻. Then $(fB^- + N^-)/(B^- - N^-) = K$; and therefore $1 + x = B^-/N^- = (K + 1)/(K - f)$, where x is the required excess of B^- . In our titrations $f = 5$, and from the titration curves one calculates $K = 12.6$ and $x = 0.8$.

A further check for our data was provided by the titrations of some hydrocarbons with 1:1 solutions of

(7) Those corrections were not considered by Hoijtink.

naphthalene⁻-naphthalene or pyrene⁻-pyrene. The relevant results are collected in Table II. To evaluate the titration of terphenylene and phenanthrene with naphthalene⁻ solution, it was again necessary to introduce the relevant corrections. For terphenylene, $K = 3$ (a value derived from the spectrophotometric studies, see Table V), and since $f = 1$, one finds $x = 1.0$. For phenanthrene, $K = 10$ (derived from the data given in Table I), and therefore $x = 0.6$.

Table II: Reduction Potentials for the Aromatic Hydrocarbons in THF Solution at 25°

Aromatic hydrocarbon	E_1' v.	ΔE_1 from biphenyl-titration, v. ^a
Titrated by 0.0082 <i>N</i> solution of naphthalene ⁻ ($N^-/N = 1:1$)		
Triphenylene	0.062 ^b	0.047
Phenanthrene	0.075 ^b	0.058
Titrated by 0.0088 <i>N</i> solution of pyrene ⁻ ($\pi^-/\pi = 1:1$)		
Anthracene	0.090 0.081	0.119
9,10-Dimethylanthracene	0.075 0.070	0.102

^a ΔE_1 is derived from Table I by subtracting E of the hydrocarbon used in the standard solution (naphthalene or pyrene) from the E of the titrated hydrocarbon. ^b Corrected for the equilibrium between the titrating ion and the formed ion. This means that a 100% excess of naphthalene⁻ solution has to be used in titrating terphenylene and 60% in titrating phenanthrene.

No corrections are necessary in evaluating the results of the titration of anthracene and dimethylanthracene by the solution of pyrene⁻.

The agreement between the data given in Tables I and II is fair. The titrations with the solution of naphthalene⁻ led to reduction potentials for terphenylene and phenanthrene which are ~ 0.025 v. lower than those derived from the titrations with biphenyl⁻. The titrations of anthracene and dimethylanthracene with the solution of pyrene⁻ yielded results 0.03 v. higher than the titration with biphenyl⁻. Various factors may contribute to these small discrepancies, and in the following section some of them will be considered.

Some General Problems Concerned with the Potentiometric Titration of Aromatic Hydrocarbons. Most of the aromatic hydrocarbons may acquire either one electron, giving the respective radical anions, or two, being, thus, converted into dianions. Let us denote the relevant hydrocarbon by A and the products of its reduction by A⁻ and A⁻². The reductions are represented by the equations, $A + e \rightleftharpoons A^- \dots E_1^\circ$ and $A^- + e \rightleftharpoons A^{-2} \dots E_2^\circ$, where e denotes an electron and

E_1° and E_2° are the respective standard reduction potentials. Let us denote by x , y , and z the mole fractions of A, A⁻, and A⁻² in an equilibrated mixture, and by g the ratio of the added electron donor to the total amount of the titrated hydrocarbon. Of course, $x + y + z = 1$, and, if the electron transfer is quantitative, then $y + 2z = g$. The system is in equilibrium with respect to the disproportionation $A + A^{-2} \rightleftharpoons 2A^- \dots K_d$, and therefore $K_d = y^2/xz$. Hence, $y = \{K_d \pm [K_d^2 - K_d(K_d - 4)g(2 - g)]^{1/2}\}/(K_d - 4)$, $x = 1 - 1/2(g + y)$, and $z = 1/2(g - y)$.

For a large K_d and $g \ll 1$, $y = \{1 - [1 - (1 - 4/K_d)g(2 - g)]^{1/2}\}/(1 - 4/K_d) \approx g$; therefore $x \approx 1 - g$ and $z \approx 0$. For $2 - g \ll 1$, $y \approx 2 - g$, $x \approx 0$, and $z \approx g$. Of course, for $g = 1$, $y = 1$. These rather trivial results show that for a large K_d , $x/y = 1$ when $g = 1/2$, and $y/z = 1$ when $g = 3/2$. Hence, the potential measured at the stage of an experiment corresponding to $g = 1/2$ gives E_1 , and at $g = 3/2$ it gives E_2 , E_1 being larger than E_2 .

The situation may be less trivial when K_d is very small. In such a case $y = 1/2\{g(2 - g)K_d\}^{1/2}$, and therefore it is always very small; hence, $x \approx 1 - 1/2g$ and $z \approx 1/2g$. Thus, for a very small K_d , the potential E_1 is attained toward the end of titration when $x \approx 1 - 1/2g$ is equal to $y = 1/2\{g(2 - g)K_d\}^{1/2}$; i.e., $g = 2(1 + K_d)^{-1}$, and the potential E_2 is observed at the early stage of titration when $z \approx 1/2g$ is equal to $y = 1/2\{g(2 - g)K_d\}^{1/2}$ or $g = 2(1 + 1/K_d)^{-1}$. This means that $E_1 < E_2$, an obvious consequence of the smallness of K_d , and, as before, for $g = 1$, the potential is given by $1/2(E_1 + E_2)$.

Electron Affinity of Tetraphenylethylene. The less common situation, when $E_1 < E_2$, is exemplified by the behavior of tetraphenylethylene. The potentiometric titration curve of this hydrocarbon is seen in Figure 2. For $g = 1$, the potential is 0.55 v.

The peculiarity of tetraphenylethylene was briefly discussed by Szwarc.⁸ Steric strain forces the phenyl groups in *cis*-stilbene and in tetraphenylethylene to take positions nearly perpendicular to the C=C plane. Hence, the first acquired electron is not stabilized by the resonance of a diphenylmethyl group, because of the unfavorable geometry of the molecule, and, consequently, the respective reduction potential is low. On acquiring the second electron, the molecules of tetraphenylethylene lose the rigidity imposed by the C=C double bond, and the rotation around the C-C bond produces two planar Ph-C-Ph groups, lying in mutually perpendicular planes. Both electrons now

(8) M. Szwarc, *Proc. Roy. Soc. (London)*, **A279**, 260 (1964).

enjoy the stability arising from the resonance of the respective diphenylmethyl groups, and this leads to a high value of E_2 . Thus, it is easier to transfer two electrons to tetraphenylethylene than one. A similar situation should be encountered in *cis*-stilbene.

The Effect of Ionic Dissociation on the Results of Potentiometric Titrations. In his treatment of potentiometric titration of aromatic hydrocarbons, Hoiijtink implicitly assumed⁹ that the reduction products, hydrocarbon⁻ or hydrocarbon⁻², are present in the titrated solution as free ions. This certainly is not the case in a tetrahydrofuran solution, and probably also not in dimethoxyethane. Therefore, it is desirable to discuss the effect of incomplete dissociation of ion pairs on the results of potentiometric titration.

Let us denote by B_f^- and A_f^- the concentrations of the free ions derived from the salts of the relevant radical ions: biphenyl⁻,Na⁺ and aromatic⁻,Na⁺; by B^- and A^- we denote the concentrations of the respective ion pairs, and by K_B and K_A , their dissociation constants. The potential between the solution and the electrode is therefore $E_B' = E_{0,B} + 0.06 \log B/B_f^- = E_{0,B} + 0.06 \log B/B^- + 0.03 \log B^- - 0.03 \log K_B$ with a similar expression for E_A' . Hence, the correct relative reduction potential, E_1^* , is given by the equation $E_1^* = E_1 - 0.03 \log (K_B/K_A) - 0.03 \log (A^-/B^-)$, where E_1 is the measured potential given in Table I, and B^- and A^- denote the *total* concentrations of the respective radical ions in the standard diphenyl⁻ solution and in the titrated solution at the half-point of titration. The ratio A^-/B^- is usually 0.5. The dissociation constants of various radical ion salts will be reported later; they were found to be of the order of 10^{-6} M and do not differ by more than a factor of 10 or 20. Therefore, the corrections arising from the incomplete dissociation of ion pairs into free ions are never greater than 0.05 v. and frequently are substantially smaller. This conclusion is confirmed by the results given in Tables II and III. These corrections may be larger for E_2 .

The second reduction potential, E_2 , is measured when one-half of the titrated hydrocarbon is in the form $A^{-2},2Na^+$, the remaining being A^-,Na^+ . Let us denote by E_{0,A^-,Na^+} the standard reduction potential for the process $A^-,Na^+ + e \rightleftharpoons A^{-2},Na^+ \dots E_{0,A^-,Na^+}$, and by E_2' the potential between the electrode and the solution when the measured value is read. Hence, $E_2' = E_{0,A^-,Na^+} + 0.06 \log \{A^-,Na^+/A^{-2},Na^+\}$. Denoting by K_2 the dissociation constant of $A^{-2},2Na^+ \rightleftharpoons A^{-2},Na^+ + Na^+$, we find $E_2' = E_{0,A^-,Na^+} + 0.03 \log (C/2K_2)$, where C is the total concentration of the hydrocarbon in all its forms. This derivation implicitly assumes $K_2 > K_1$, where K_1 is the dissociation

Table III

Investigated pair ^a	Equilibrium	$\Delta E =$	$\Delta E = E_1 - E_2$	Hoiijtink
	constant	$(RT/23000)$	Ours	
	K^b	$\ln K$		
(1) Tetracene } (2) Perylene }	52	0.102	0.108	0.19
(1) Triphenylene } (2) Naphthalene }	3	0.029	0.047	0.10
(1) Anthracene } (2) Pyrene }	111	0.125	0.119 ^c	0.18
(1) 9,10-Dimethylanthracene } (2) Pyrene }	91	0.117	0.102	..

^a Using Hoiijtink's half-wave potentials, we obtain values for ΔE of the first pair 0.09 v., for the second 0.12 v., and for the third 0.12 v. The first and the last values agree with our reduction potentials; the middle one agrees with Hoiijtink's potentials. ^b $K = [\text{aromatic}_1^-][\text{aromatic}_2^-]/[\text{aromatic}_1^-][\text{aromatic}_2^-]$. ^c The reduction potential of anthracene is 0.03 v. lower than that given in ref. 3. This change results from the contribution of two more experiments.

tion constant of $A^-,Na^+ \rightleftharpoons A^- + Na^+$. The potential E_1' established for the 1:1 mixture of A and A^-,Na^+ is given by $E_1' = E_{0,A} + 0.03 \log (C/2K_1)$. The correct difference, ΔE^* , is $E_{0,A} - E_{0,A^-,Na^+} = \Delta E^* = E_1' - E_2' + 0.03 \log (K_1/K_2)$. Since $\Delta E = E_1 - E_2$ derived from Table I is identical with $E_1' - E_2'$, $\Delta E^* = \Delta E + 0.03 \log (K_1/K_2)$. The disproportionation equilibrium constant, K_d , of the process $A + A^{-2},2Na^+ \rightleftharpoons 2A^-,Na^+$ is given by the relation $0.06 \log K_d = E_{0,A} - E_{0,A^-,Na^+} + 0.06 \log (K_2/K_1)$, and therefore $0.06 \log K_d = E_1 - E_2 + 0.03 \log (K_2/K_1)$. Again, the correction in calculating K_d is not too large—probably less than 0.02 v.—and therefore $E_1 - E_2$ gives a good estimate of K_d .

Studies of Equilibria $\text{Aromatic}_1^- + \text{Aromatic}_2^- \rightleftharpoons \text{Aromatic}_1 + \text{Aromatic}_2^-$. A system suitable for equilibrium study should fulfill two conditions. (1) The difference in the respective reduction potentials should not exceed about 0.15 v., and (2) the spectra of the respective anions must not overlap too closely. The latter condition is obvious if a spectrophotometric technique is used in the study. The former condition implies that the relevant equilibrium constant should not exceed ~ 250 ; otherwise, an enormous excess of one of the hydrocarbons has to be used in order to determine reliably the concentration of the respective radical ions. This leads to technical difficulties and

(9) The derivation given in Hoiijtink's paper (ref. 1) treats the reduced species as free ions and not ion pairs. However, Hoiijtink pointed out in later papers (e.g., A. C. Aten, J. Dieleman, and G. J. Hoiijtink, *Discussions Faraday Soc.*, 29, 185 (1960)) that the aromatic radical ions are present in THF mainly as ion pairs.

introduces substantial experimental errors see, *e.g.*, ref. 2. Moreover, for such a pair, the observed spectrum may be complicated by the presence of the respective dianion and indeed this difficulty accounts for some strange results given in ref. 2.

Keeping in mind these restrictions, we decided to choose the following four pairs for our study: tetracene-perylene, triphenylene-naphthalene, pyrene-anthracene, and pyrene-9,10-dimethylanthracene. The equilibrium constants for the last two pairs were already reported in a previous communication from this laboratory,³ and, therefore, for these systems only the final results are given in Table III.

Spectrophotometric techniques require accurate knowledge of the relevant extinction coefficients. In preparation of a radical ion solution one may unintentionally destroy a fraction of the investigated ions, and then the calculated results are too low. Therefore, special precautions were taken in order to remove traces of water and other impurities from the solvent, from the investigated hydrocarbons, and from the walls of the reactors. Furthermore, we facilitated our task by working with relatively concentrated solutions, prepared in batches of about 100 ml., and by using an optical cell having a path of about 10^{-2} cm.

It is assumed that under these conditions the conversion of the aromatic hydrocarbon to the respective radical ions or dianions is quantitative. This was checked by titrating the resulting alkali solution, and in only two cases was the conversion found to deviate from 100%. In biphenyl solution (total $B = 0.1 M$) only 16–17% of biphenyl is converted into sodium biphenyl, indicating that the standard reduction potential of biphenyl in THF is 0.04 v. lower than that of metallic sodium with respect to Na^+ ions present in this solution.¹⁰ In the case of naphthalene the conversion seems to be 98–99%; the correction is therefore negligible. Notice that 99% conversion corresponds to a standard reduction potential of 0.078 v. for naphthalene with respect to biphenyl (assuming comparable concentrations of Na^+ in both solutions).

To test further the reliability of our extinction coefficients, the following method was developed. A standard solution of dry stearic acid was prepared in rigorously dried THF. Known aliquots (about 10 ml. each) of this solution were enclosed in ampoules equipped with a break-seal, and then such an ampoule was sealed to a flask linked to an optical cell containing a spacer. About 100 ml. of solution of the investigated radical ions was introduced into the flask and its optical density was determined. Thereafter, the breakseal was crushed, and the stearic acid solution was thoroughly mixed with the contents of the

flask. Its amount was chosen to be sufficient to destroy 0.5–0.75 of the radical ions. The optical density was then redetermined, and, thus, the extinction coefficient of the investigated radical ions was calculated. For solutions of sodium naphthalene, anthracene, pyrene, tetracene, and terphenylene, extinction coefficients determined in this way agreed with those based on a direct titration. The values needed in the studies of equilibria are given in Table IV, the respective spectra being shown in Figures 4 and 5.

Such a determination still may be slightly in error if a trace of moisture is present in the standard stearic

Table IV: Extinction Coefficients of Aromatic Radical Ions^a

Radical ion	λ , $m\mu$	ϵ , decimal scale	λ , $m\mu$	ϵ , decimal scale
Naphthalene ⁻	λ_{\max} (820)	2,460	λ (410)	3,600
Terphenylene ⁻	λ (820)	550	λ_{\max} (410)	13,200
Tetracene ⁻	λ_{\max} (711)	14,500	λ (577)	1,500
Perylene ⁻	λ_{\min} (711)	3,000	λ_{\max} (577)	59,000

^a Counterion, Na^+ ; solvent, THF at 25°. These wave lengths were used in the spectrophotometric analysis.

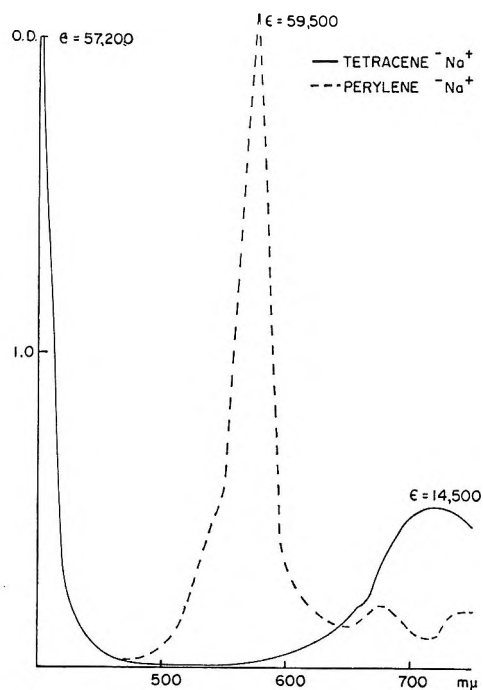


Figure 4.

(10) The concentration of free Na^+ can be determined if the dissociation constant of Na^+ ,biphenyl⁻ into free ions is known. In his paper (ref. 1) Hoihtink assumes a 100% dissociation of sodium biphenyl in dimethoxyethane.

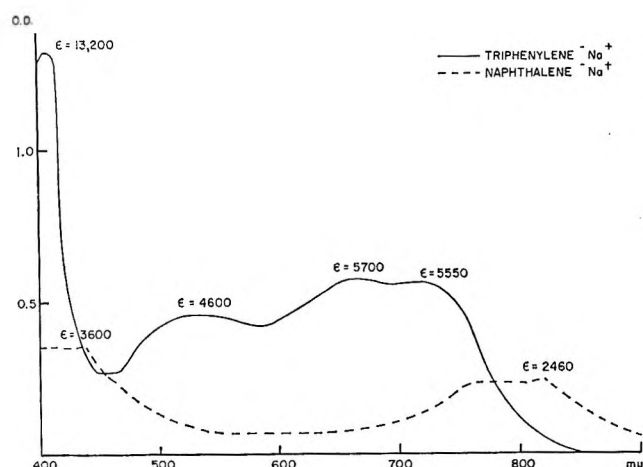


Figure 5.

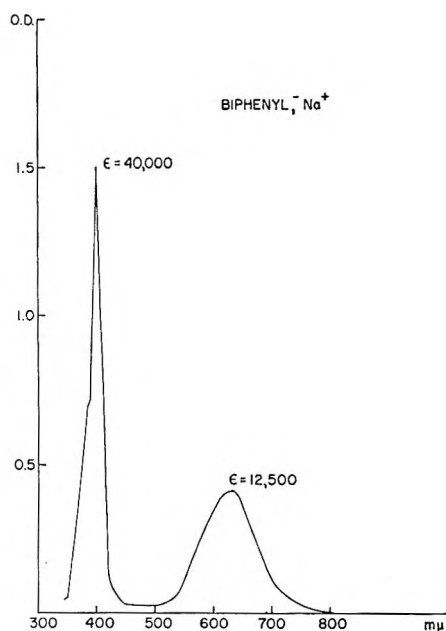


Figure 6.

acid solution. However, if all the extinction coefficients are determined in this way, such an error, if any, does not affect the equilibrium constant of the electron-transfer reaction. The method may fail if the resulting dihydro derivative reacts with the radical ions, and, in fact, this seems to happen in the perylene system. The absence of such disturbing reactions may be ascertained by scanning the visible spectrum of the radical ions before and after killing and ascertaining that no new peaks appear.

The extinction coefficients determined in this work are *higher* than those determined by Hoijtink.¹¹ In most cases the increase amounts to 10 or 20% only, although for sodium biphenyl our value is three times

higher than that derived from Hoijtink's paper. In recent papers of Hoijtink, the results were improved and the excellent agreement between data of our and his group is seen in Table V. The extinction coefficients reported by Paul, Lipkin, and Weissman² are usually even lower than those of Hoijtink, indicating more extensive "killing" of the radical ions.

Table V

	λ_{\max} , m μ		ϵ (decimal)		Ref.
	This work	Hoijtink	This work	Hoijtink	
Biphenyl	400	400	40,000	36,000	a
Naphthalene	820	821	2,460	3,170	b
Anthracene	720	725	10,000	9,650	b
Pyrene	491	483	49,500	51,500	b
Perylene	577	574	59,000	58,900	b
Tetracene	711	711	14,500	11,300	b
Terphenylene	410	406	13,200	14,300	c

^a K. H. J. Buschow, J. Dieleman, and G. J. Hoijtink, *Mol. Phys.*, **7**, 1 (1963). ^b G. J. Hoijtink and P. J. Zandstra, *ibid.*, **3**, 371 (1960). ^c G. J. Hoijtink, *ibid.*, **2**, 85 (1959). Notice that our values were determined in THF solution at 25°. Hoijtink's data were determined in methyl THF at -180° (ref. b). Data of ref. a are given for Li⁺ at 77°K. The agreement is more remarkable since the spectra refer to different temperatures. Our work indicates that the temperature (25° down to -80°) has hardly any effect on the value of ϵ or the shape of the curve. We were informed by Prof. Hoijtink that some numerical error vitiated the extinction coefficients given in the recent paper of K. H. J. Buschow and G. J. Hoijtink, *J. Chem. Phys.*, **40**, 2501 (1964).

The equilibria were investigated in all glass equipment, containing break-seals instead of stopcocks. Two optical cells with spacers were sealed to the unit to allow the determination of the optical density for each component solution. All the preparations were carried out on a high-vacuum line, and the unit was flamed while pumped out and then sealed off the line.

The equilibrium was established within less than 1 sec.,³ and the mixture was well shaken before its absorption spectrum was recorded. All the pertinent data are given in Table VI, and the absence of any side reactions is indicated by the good balances of the products (see Table VI).

Discussion

The average values of the equilibrium constants determined in the present study, as well as those taken from ref. 3, are collected in Table III. The third

(11) P. Balk, S. De Bruijn, and G. J. Hoijtink, *Rec. trav. chim.*, **76**, 907 (1957).

Table VI^a

perylene⁻ + tetracene \rightleftharpoons perylene + tetracene⁻
 $K = [\text{Pe}][\text{Tr}^-]/[\text{Pe}^-][\text{Tr}]$

[Pe ⁻] ₀	[Pe] ₀	[Tr ⁻] ₀	[Tr] ₀	[Pe ⁻] ₀	[Tr ⁻] ₀	[Tr] ₀ ^b	K
3.0	139	0.0	2.8	1.8	1.1	1.6	53.5
Checks: $\Sigma_0^- = 3.0$, $\Sigma_e^- = 2.9$; $\Sigma_0^{\text{Tr}} = 2.8$, $\Sigma_e^{\text{Tr}} = 2.7$							
19.7	73.5	0.0	11.0	10.7	9.3	1.5	48.0
Checks: $\Sigma_0^- = 19.7$, $\Sigma_e^- = 20.0$; $\Sigma_0^{\text{Tr}} = 11.0$, $\Sigma_e^{\text{Tr}} = 10.8$							
2.4	129	0.0	4.0	1.1	1.1	2.7	48.2
Checks: $\Sigma_0^- = 2.4$, $\Sigma_e^- = 2.2$; $\Sigma_0^{\text{Tr}} = 4.0$, $\Sigma_e^{\text{Tr}} = 3.8$							
0.0	234	3.5 + 2.5[Tr ⁻²]	0.0	5.1	3.4	2.6	58.9
Checks: $\Sigma_0^- = 8.5$, $\Sigma_e^- = 8.5$; $\Sigma_0^{\text{Tr}} = 6.0$, $\Sigma_e^{\text{Tr}} = 6.0$							

naphthalene⁻ + terphenylene \rightleftharpoons naphthalene + terphenylene⁻
 $K = [\text{N}][\text{T}^-]/[\text{N}^-][\text{T}]$

[N ⁻] ₀	[N] ₀	[T ⁻] ₀	[T] ₀	[N ⁻] ₀	[T ⁻] ₀	K	
0.0	1600	160	0.0	121	34	3.3	
Check: $\Sigma_0^- = 160$, $\Sigma_e^- = 155$							
0.0	154	29.2	0.0	19.5	8.5	2.8	
Check: $\Sigma_0^- = 29.2$, $\Sigma_e^- = 28.0$							
160	430	0	138	99	55	3.3	
Check: $\Sigma_0^- = 160$, $\Sigma_e^- = 154$							
0.0	970	97	0.0	77	19	2.8	
Check: $\Sigma_0^- = 97$, $\Sigma_e^- = 96$							

^a All the concentrations given in $M \times 10^{-4}$. $\epsilon_{\text{Tr}} = 8.2 \times 10^3$, $\epsilon_{\text{Tr}^-} = 10^3$; $\epsilon_{\text{Pe}} = 10^3$, $\epsilon_{\text{Pe}^-} = 22$. ^b Concentration of tetracene determined from the optical density at 472 m μ .

column of this table lists the differences in reduction potentials of the respective hydrocarbons calculated from the equilibrium constants. The directly determined differences of the reduction potentials, with respect to biphenyl⁻-biphenyl, are given in the next column, and in the last we give the ΔE values calculated from Hoijsink's data.¹²

The agreement between the two methods used in our studies is remarkably good. Hoijsink's data are in each case substantially higher, and not only his reduction potentials (see Table I) but also their differ-

ences are larger than ours. However, the order of electron affinities remains the same in both studies, triphenylene-phenanthrene being the only exception. These two hydrocarbons have nearly identical electron affinities, and therefore the change of order for this pair is insignificant.

Conclusions

The spectrophotometric method of determining the relative reduction potentials of aromatic hydrocarbons (= relative electron affinities in THF) is more direct and free of the complications encountered in potentiometric titrations. On the other hand, it is experimentally limited since only hydrocarbons having similar electron affinities may be compared. To span hydrocarbons of greatly different electron affinities, one has to investigate a sequence of intermediate equilibria, and this would lead to a substantial accumulation of errors. A direct comparison is most difficult and would lead to unreliable results, as shown, *e.g.*, in ref. 2 (the results of the equilibrium study between anthracene⁻ and naphthalene).

The potentiometric technique is most reliable when the differences in electron affinities are large since the corrections are then relatively small. It is most useful in determining the sequence of electron affinities of a large series of electron acceptors and this was achieved by Hoijsink.

Acknowledgments. This work was partially supported by the National Science Foundation. It was carried out in the Donnan Laboratories of Liverpool University and in the Chemistry Department of the State University College of Forestry at Syracuse, N. Y. M. S. wishes to thank Professor C. E. H. Bawn for hospitality during his stay at Liverpool University and The Royal Society for awarding him their Visiting Research Professorship.

(12) Hoijsink's titrations usually were carried out in dimethoxyethane. However, judging from a few of his experiments performed in THF, this change of solvent has only a small effect on the ΔE values.

The Conformation of the Pyranose Rings in Mono-, Di-, and Polysaccharides at High pH by Proton Magnetic Resonance Studies

by V. S. R. Rao and Joseph F. Foster

Department of Chemistry, Purdue University, Lafayette, Indiana (Received October 12, 1964)

Starch and amylose as well as many model sugars and sugar derivatives show pronounced alterations of their specific optical rotation on passing from neutral to alkaline solution. In the past, these effects have been attributed to modifications in ring conformation resulting from ionization of hydroxyl groups. By means of n.m.r. it is shown that the D-glucopyranose ring in all compounds examined exists in the C1 conformation in alkaline as well as in neutral aqueous solution. The changes in optical rotation of the free sugars D-glucopyranose and D-maltose are due to a shift of the anomeric equilibrium toward the β -form in alkali. The changes in rotation of methyl- β -maltoside and amylose are probably due to an increase in rotational freedom about the α -1,4-glucosidic bond in alkaline solution, although the possibility of some contribution from a helix-coil transition in the case of amylose cannot be ruled out. The n.m.r. spectra of methyl β -L-arabinopyranoside in neutral and alkaline solution are virtually identical. The known change in specific rotation in this case must be due to slight distortions in the ring caused by ionization of the axial hydroxyl group.

Optical rotation studies have played an important role in conformational studies of carbohydrates. Reeves and Blouin¹ studied a number of methylglycosides and observed that in some cases the specific optical rotation is lower in alkaline than in neutral solution. It was observed further that these "alkali-sensitive" glycosides have hydroxyl groups which would be in axial orientation in the assumed most stable C1 conformation. These changes in rotation in alkaline media were explained by assuming that axial ring hydroxyl groups have a tendency to assume an equatorial orientation on ionization. However, it was also noticed that some of the glycosides¹ having axial hydroxyl groups in the C1 conformation are alkali stable. In the case of di- and polysaccharides, the situation is more complex. Changes in optical rotation in alkaline media were observed for methyl β -maltoside,² sucrose,¹ and to a pronounced extent for amylose.² The glucose units in these compounds would not possess any axial hydroxyl groups in the C1 conformation. Hence, Reeves² proposed that some of the glucopyranose rings of both amylose and maltose exist in the B1 conformation (one axial OH) in neutral solution and shift to the

3B conformation on ionization of hydroxyl groups. On the other hand, Hollo, *et al.*,³ have observed a marked decrease in rotation in alkaline solutions for D-glucose and maltose as well as amylose and suggested that the changes in rotation are caused by a shift from the C1 to 3B conformation of the pyranose rings. The present authors⁴ earlier presented evidence that the D-glucopyranose units in these sugars exist exclusively in the C1 conformation in neutral solution. The specific explanation presented by Reeves is thus ruled out, but the transformation from C1 to 3B suggested by Hollo, *et al.*, remains a possibility. We have been most interested in this possibility in view of their suggestion that the C1 conformation would result in a natural tendency for amylose to exist in a helical configuration while the 3B conformation should lead to a flexible coil. Upon raising the pH of amylose solu-

(1) R. E. Reeves and F. A. Blouin, *J. Am. Chem. Soc.*, **79**, 2261 (1957).

(2) R. E. Reeves, *ibid.*, **76**, 4595 (1954).

(3) J. Hollo, J. Szejtli, and M. Toth, *Stärke*, **13**, 222 (1961).

(4) V. S. R. Rao and J. F. Foster, *J. Phys. Chem.*, **67**, 951 (1963).

Table I: Summary of N.m.r. Data

Sample	Solvent	Coupling const., $J_{H_1H_2}$, c.p.s.	Anomeric protons		Chemical shifts, τ -values					Methyl protons
			H_{1a}	H_{1b}	Other protons					
Methyl α -D-glucopyranoside	D_2O	...	5.2	..	6.18	6.37				6.55
	1 N KOD	2.6	5.14	..	6.13	6.36				6.50
Methyl β -D-glucopyranoside	D_2O	7.7	..	5.54	6.13	6.58				6.43
	1 N KOD	7.4	..	5.6	6.13	6.56				6.36
Methyl β -L-arabinopyranoside	D_2O	1.7	5.12	..	5.95	6.12	6.22			6.54
	2 N KOD	2.0	5.12	..	5.95	6.12	6.20			6.50
D-Glucose	D_2O	3.0	4.7		6.14	6.37	6.52			
		7.0		5.3						
	1.5 N KOD	...	4.62 (small)							
Sucrose	D_2O	6.7		5.2	6.12		6.55			
	2 N KOD	3.0	4.52		5.75	5.9	6.1	6.15	6.25	6.35
D-Maltose	D_2O	3.1	4.52		6.0	6.15	6.25	6.3	6.4	
		3.0	4.75							
		8.0		5.3	6.13	6.32				
	2 N KOD	2.8	4.58							
Amylose	2 N KOD	7.2		5.2	6.14	6.38				
		2.4	4.78							
		4.7			6.10	6.30				

tions, alterations in various hydrodynamic properties occur which can best be rationalized on the basis of a helix-coil transformation.⁵

In the present work, it is shown by means of n.m.r. that the C1 conformation in D-glucose and simple glucosides as well as in maltose and higher saccharides is stable toward alkali and that various structural modifications must be invoked to account for the changes in optical rotation in the various cases.

Experimental

The n.m.r. spectra were obtained on a precalibrated chart paper with a Varian A-60 proton magnetic resonance spectrometer. The position of τ 10 on this paper was checked with an external reference (tetramethylsilane in carbon tetrachloride). The impure water peak of D_2O in simple D_2O -sugar solutions was found to appear at τ 5.2. Optical rotation measurements were made with a Rudolph Model 220-80 spectropolarimeter equipped with a mercury-xenon source and rocking polarizer.

The methyl α -D-glucoside and methyl β -D-glucoside were kindly provided by Dr. N. K. Richtmeyer of the National Institutes of Health. The corn amylose was prepared by butanol fractionation of acid-modified corn starch and was kindly supplied by Dr. T. J. Schoch of the Corn Products Refining Co. The β -methyl L-arabinoside ("C" grade) was obtained from the California Corporation for Biochemical Research and was recrystallized once from 95% ethanol. The other chemicals employed were C.P. grade.

Results and Discussion

The n.m.r. data are summarized in Table I. In Table II are given differences in specific rotation between values measured in neutral and in alkaline solution. Reeves and Blouin¹ have classified the methyl D-glucosides as "alkali stable" and methyl β -L-arabinoside as "alkali sensitive" by optical rotation studies. From Table I it is evident that the coupling constant $J_{H_1H_2}$ indicates the protons at C₁ and C₂ of methyl α -D-glucoside to be in axial-equatorial orientation.

Table II: Difference in Specific Rotation $[\alpha]_D$ or $[\alpha]_{436}$ in Neutral Solution and in 1 N NaOH or KOH

Compound	Difference
Methyl α -D-glucoside	0.0
Methyl β -D-glucoside	-1.7
Methyl β -L-arabinoside	10.0
D-Glucose	27.0 ^a
D-Xylose	18.3 ^a
D-Ribose	13.0 ^a
D-Mannose	-9.8 ^a
D-Lyxose	-8.9 ^a
Sucrose	7.8
Maltose	42.5 ^a
Methyl β -maltoside	15.0
Amylose	40.0

^a The difference in specific rotation at 436 m μ .

(5) V. S. R. Rao and J. F. Foster, *Biopolymers*, 1, 527 (1963).

Similarly, the values of the coupling constants, 7.7 and 7.4 c.p.s., indicate that the protons at C₁ and C₂ of methyl β -D-glucoside are in axial-axial orientation, both in D₂O and in strong alkaline media. These results are consistent with the C1 conformation and in agreement with Reeves' interpretation that α - and β -methyl D-glucosides exist in the same conformation in both the solvents,^{1,6} *i.e.*, C1.

Reeves and Blouin¹ observed a decrease in optical rotation, $[\alpha]_D$, of about 10° for methyl β -L-arabinoside in 1 N NaOH as compared to neutral solution. These results were explained by assuming a shift in the ring conformation from C1 to B2. It is clear from Table I that the values of the chemical shifts are virtually the same in both the solvents, indicating no significant change in the ring conformation. The slight change in the coupling constant J_{H_1, H_2} is not significant enough to suggest any change in ring conformation. If there were any major changes in ring conformation, drastic changes in n.m.r. spectra would be expected. The values of the coupling constants J_{H_1, H_2} , 1.7 and 2.0 c.p.s., indicate that the protons at C₁ and C₂ are in equatorial-axial orientation and are consistent with the C1 conformation. These results are in disagreement with Reeves' suggestion. Methyl β -L-arabinoside has the C₄ hydroxyl group in axial orientation in the C1 conformation. Since the hydroxyl probably requires greater space on ionization (see below), the C₄ hydroxyl would come closer to the axial protons on the same side of the ring and thereby might cause a slight distortion in the ring. Such a small distortion might explain the observed changes in optical rotation and might not be detectable in the n.m.r. spectrum.

The optical rotations measured at different pH values for D-glucose are shown in Figure 1. Similar to amylose, D-glucose also shows a decrease in rotation above approximately pH 10.5.

The n.m.r. spectra of D-glucose in D₂O and in 1.5 N KOD solutions are shown in Figure 2. Significant changes in the spectra are noticeable. In alkaline solution (curve II) the peak at τ 4.7, which has been assigned to the anomeric proton of α -D-glucose, is nearly absent. The peak at τ 6.37,⁷ which has been attributed to the ring protons of α -glucose, is also missing. The coupling constant obtained from the peak splitting of the anomeric proton is virtually the same as that obtained for β -D-glucose (6.7 and 7.0 c.p.s.). In all respects this spectrum is similar to that of β -D-glucose in D₂O. This means that at high alkaline concentrations the equilibrium mixture of α - β -anomers of D-glucose shifts toward the β -anomer. Even in neutral solution the β -anomer of D-glucose predominates at equilibrium; presumably, it has all hydroxyls in equa-

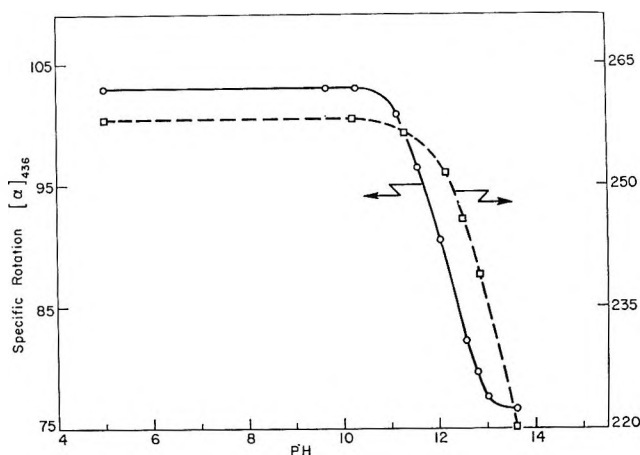


Figure 1. Dependence of specific optical rotation at 436 m μ on pH: \circ , D-glucose; \square , maltose.

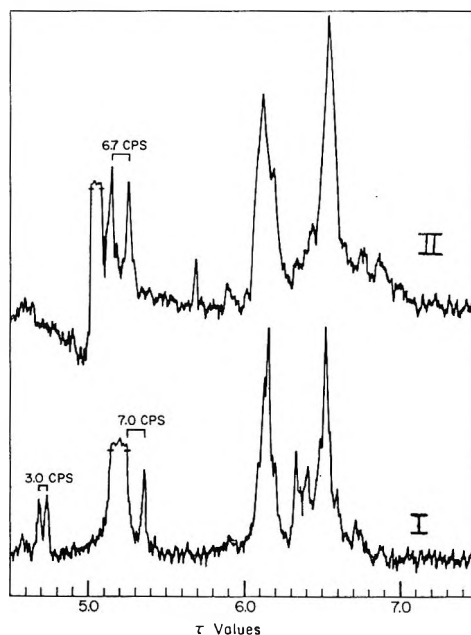


Figure 2. N.m.r. spectra of D-glucose: I, in D₂O; II, in 1.5 N KOD.

torial positions.⁸ The charged RO group would be more strongly solvated and have a greater effective volume than the neutral ROH groups. Hence, under ionizing conditions, there would be an enhanced destabilization of the α -form relative to the β -anomer. It appears certain that the observed decrease of the rotation of D-glucose with increasing pH above 10.5 is not due to a change in ring conformation but rather

(6) R. E. Reeves, *J. Am. Chem. Soc.*, **71**, 215 (1949).

(7) R. W. Lenz and J. P. Heeschen, *J. Polymer Sci.*, **51**, 247 (1961).

(8) R. E. Reeves, *J. Am. Chem. Soc.*, **72**, 1499 (1950).

to a shift in the equilibrium mixture toward the β -anomer.

Changes in optical rotation similar to that of D-glucose are observed for D-xylose and D-ribose. On the contrary, for D-mannose and D-lyxose it is observed that the specific rotation remains constant up to pH 10.5, but increases with further increase in pH. N.m.r. spectra on these latter two sugars, while of relatively poor quality, did show that the α -anomer increases in the equilibrium mixture in 1.5 N KOD solutions. It is known that the acetylated sugars of D-mannose and D-lyxose exist in the C1 conformation in neutral solution.⁹ In this conformation for β -D-mannose and β -D-lyxose, the oxygen atoms at C₁, C₂, and the ring oxygen come very close, which causes a particular instability. Hence, under ionizing conditions, even though the α -anomers of these compounds have one hydroxyl group more in axial orientation than the corresponding β -anomers, the equilibrium shifts toward the α -form. This further indicates that the rule that the anomer having more hydroxyl groups in the equatorial position will predominate in the equilibrium mixture is not completely general.

Sucrose is also found to exhibit a decrease in specific rotation $[\alpha]_D$ of about 10° in 1 N NaOH. It is known that the glucopyranose unit in sucrose exists in the C1 conformation in the crystalline state.¹⁰ Since it has all the hydroxyl groups in equatorial positions, there is no reason to expect that the observed changes in rotation are due to changes in ring conformation from C1 to some boat form. The n.m.r. data for sucrose are given in Table I. The peak at 4.5 is attributed to the anomeric proton of the glucopyranose unit. The value of the coupling constant $J_{H_1H_2}$, 3.0 c.p.s., obtained from the splitting of this peak, indicates the protons at C₁ and C₂ of the glucopyranose unit to be in equatorial-axial orientation, which is consistent with the C1 conformation. Minor changes in the n.m.r. spectrum at high field have been observed in alkaline media. In the absence of a complete analysis of the spectrum it is difficult to interpret such changes. However, the position and the magnitude of the dihedral splitting of the peak due to the anomeric proton of the glucopyranose unit are the same in both D₂O and in 1.5 N KOD, indicating that no change has taken place in the conformation of this unit. The possibility of some alteration in the conformation of the fructose ring cannot be ruled out.

Maltose also exhibits changes in specific rotation similar to D-glucose and amylose with increasing pH. In the spectrum of maltose in alkali (Table I) only two peaks corresponding to anomeric protons are observed, at τ 4.8 and 5.2, as compared to three, at τ 4.6, 4.7, and

5.3, in neutral solution. The peaks at τ 4.7 and 5.3 have been attributed⁴ to the anomeric proton of the reducing unit and the peak at τ 4.6 to the anomeric proton of the nonreducing unit. In alkali, the peak at τ 5.2 is enhanced in intensity, and the peak at τ 4.7 is missing, indicating that the reducing unit of maltose exists as the β -anomer, similar to the case of D-glucose. This is in agreement with the optical rotation data, since the value of $[\alpha]_{436}$ for D-maltose at pH 13.7 is about the same as that of β -maltose in neutral solution. The peak at τ 4.8 undoubtedly is due to the anomeric proton of the nonreducing unit of maltose and is slightly shifted to the high-field side. Such a change is not observed in the position of the anomeric proton of the glucopyranose unit of sucrose. This might be due to the fact that when glucose units are connected through an α -1,4 linkage, space conflict restricts somewhat the rotation about glucosidic bonds connecting the units. Such a steric hindrance to freedom of rotation might change on ionization of hydroxyls, which in turn might affect the shielding of the anomeric proton, causing a change in the chemical shift. The value of the coupling constant $J_{H_1H_2}$ obtained from the peak splitting of the anomeric proton of the nonreducing unit is 2.4 c.p.s. This indicates that the protons on C₁ and C₂ carbons of the nonreducing unit of maltose are in equatorial-axial or equatorial-equatorial orientation. The 3B conformation would demand an axial-axial orientation of these two protons with an expected coupling constant $J_{H_1H_2}$ of about 6-9 c.p.s. Some changes in the nature of the spectra would also be expected in the region τ 6-6.5, since the CH₂OH group would be in axial orientation in the 3B conformation. The magnitude of the coupling constant, the position of the peak due to the anomeric proton of the nonreducing unit of maltose, and the pattern of the spectra in the region τ 6-6.5 all indicate that the conformation of the nonreducing unit of maltose in alkali is the same as that in neutral solution,⁴ namely C1. Moreover, if the nonreducing unit of maltose is in the C1 conformation in neutral solution, there is no reason for the ring to change its conformation in alkali, since it does not have any axial hydroxyls to cause further instability on ionization. The present results show that the change in rotation with pH above 10.5 is due primarily to a shift in the α - β equilibrium toward the β -anomer. There may be a small additional contribution from an alteration of the geometry of the α -1,4-glucosidic bond, possibly an increase in rotational

(9) R. U. Lemieux, R. K. Kullnig, H. J. Bernstein, and W. G. Schneider, *J. Am. Chem. Soc.*, **79**, 1005 (1957).

(10) C. A. Beevers and W. Cochran, *Nature*, **157**, 872 (1946).

freedom. Probably this is the major contributing factor in the case of methyl- β -D-maltoside where the decrease is much smaller (15°).

Because of the poor solubility of amylose in D_2O , it has not been possible to obtain good n.m.r. spectra in neutral solution. Low molecular weight amylose was dissolved in 2 *N* KOD solution. The n.m.r. data obtained on such solutions are shown in Table I. The peaks are broad because of the high polymeric nature of the compound. The nature of the spectra and the approximate positions of these peaks are in agreement with those of α -D-glucose. The single peak on the low-field side (τ 4.7) also indicates that the glucopyranose units exist in a single conformation. The data are consistent with the X-ray result that all the glucopyranose units in alkali amylose exist in the single conformation, C1.¹¹ This result, together with the known alkali stability of the methyl glucosides, virtually eliminates the possibility that the decrease in specific rotation of amylose in alkali is due to any alteration in ring conformation. In this case, the decrease must result from a change in the polymer configura-

tion, for example a helix-coil transition, or possibly from an increase of rotational freedom about the glycosidic linkages. In this connection it is of interest that the observed decrease in specific rotation of methyl β -maltoside in alkali (15.0°) leads to the prediction of a change of 33° for an infinitely long amylose polymer assuming the effect to be due to a change in rotational freedom and to be the same in all α -1,4-glucosidic bonds. In other words, the observed change of 40° in the case of amylose can be almost completely accounted for on this basis without the need of invoking special effects in the polymer such as a helix-coil transition.

Acknowledgments. The authors wish to express their appreciation to the Corn Industries Research Foundation for financial support of this work, and to Drs. T. J. Schoch and N. K. Richtmeyer for furnishing some of the carbohydrate samples.

(11) F. R. Senti and L. P. Witnauer, *J. Am. Chem. Soc.*, **70**, 1438 (1948).

Dye-Sensitized Photopolymerization Processes.^{1a} I.

The Thionine-Nitrilotripropionamide-Acrylamide System^{1b}

by S. Chaberek, A. Shepp, and R. J. Allen

Technical Operations Research, Burlington, Massachusetts (Received September 12, 1964)

A reinvestigation of the anaerobic, thionine-sensitized photopolymerization of acrylamide reported earlier showed that this is indeed an amine-activated process, in which traces of nitrilotripropionamide present in the monomer served as the weak reducing agent. Experimental data on the rates of dye fading and of polymerization are in accord with a reaction mechanism in which the polymerization-initiating free radical is semithionine. Quantum yields of polymerization as high as 0.12 polymer molecules/photon were obtained.

Introduction

In 1962 we reported the thionine-sensitized photopolymerization of acrylamide² by a process differing from that described by Oster and co-workers^{3,4} in two respects; namely, neither oxygen nor weak reducing agents such as tertiary amines and amino acids were required for polymer formation. On the basis of data available at that time, we postulated a reaction mechanism in which the polymerization-initiating free radical was semithionine and possibly hydroxyl radical formed by an oxidation-reduction reaction between the light-excited dye and hydroxyl ion. Further work on this system, as part of a general program to develop rapid, dye-sensitized photopolymerization processes for photographic purposes, showed that our conclusions were untenable. The acrylamide used in the prior investigation contained traces of nitrilotripropionamide in amounts insufficient to be detected by elemental analysis but sufficient to function as a weak reducing agent for the light-excited dye to cause dye bleaching and polymerization. Our system, therefore, is an amine-activated one, similar in some respects to those described by Oster and co-workers^{3a,4} but different in that oxygen is not required for the process. However, since its quantum efficiency for polymerization was the highest reported to date, we considered it desirable to reinvestigate its reaction mechanism. The results of this study are summarized in this paper.

Experimental

The acrylamide used in this investigation was a pure sample obtained from the American Cyanamid Co.

Preliminary screening of this sample for anaerobic, thionine-sensitized photopolymerization showed no polymer formation in the absence of added activators and only a trace of dye bleaching over periods of 10 to 15 min.

A pure sample of nitrilotripropionamide (NTP) was obtained from the American Cyanamid Co.

Thionine was purified by two recrystallizations from water, followed by chromatography on alumina. Material purified in this way shows no impurities upon subsequent repetition of the chromatographic step. The absorption coefficient of this purified dye was found to be 6.2×10^4 l. cm.⁻¹ mole⁻¹ at 5980 Å.

The experimental procedures used in this study were substantially the same as those described previously.² The rate of dye bleaching, R_t , was calculated directly from spectrophotometric measurements. The polymerization rate, R_p , was determined by taking aliquots of the reaction solution at several time intervals, precipitating the polyacrylamide in methanol, filtering it, and drying the residue to constant weight. Polymer molecular weights were determined viscometrically.

(1) (a) These studies were performed under Contract No. AF33-(657)-8754, Reconnaissance Division, Aeronautical Systems Division, Wright-Patterson Air Force Base, Ohio; (b) presented in part at the Photochemistry Symposium, University of Rochester, Rochester, N. Y., March 27-29, 1963.

(2) A. Shepp, S. Chaberek, and R. MacNeil, *J. Phys. Chem.*, **66**, 2563 (1962).

(3) (a) G. Oster, *Nature*, **173**, 300 (1954); (b) *Phot. Eng.*, **4**, 173 (1953).

(4) G. K. Oster, G. Oster, and G. Prati, *J. Am. Chem. Soc.*, **79**, 595 (1957).

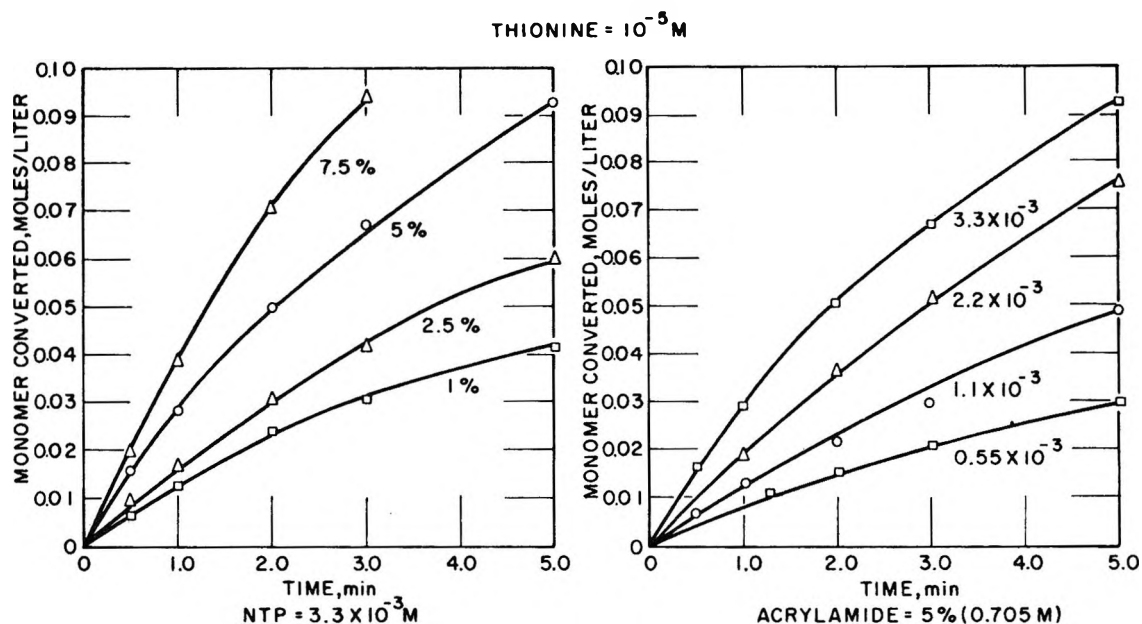


Figure 1. Polymerization data for the thionine-NTP-acrylamide system: a, monomer variation; b, NTP variation.

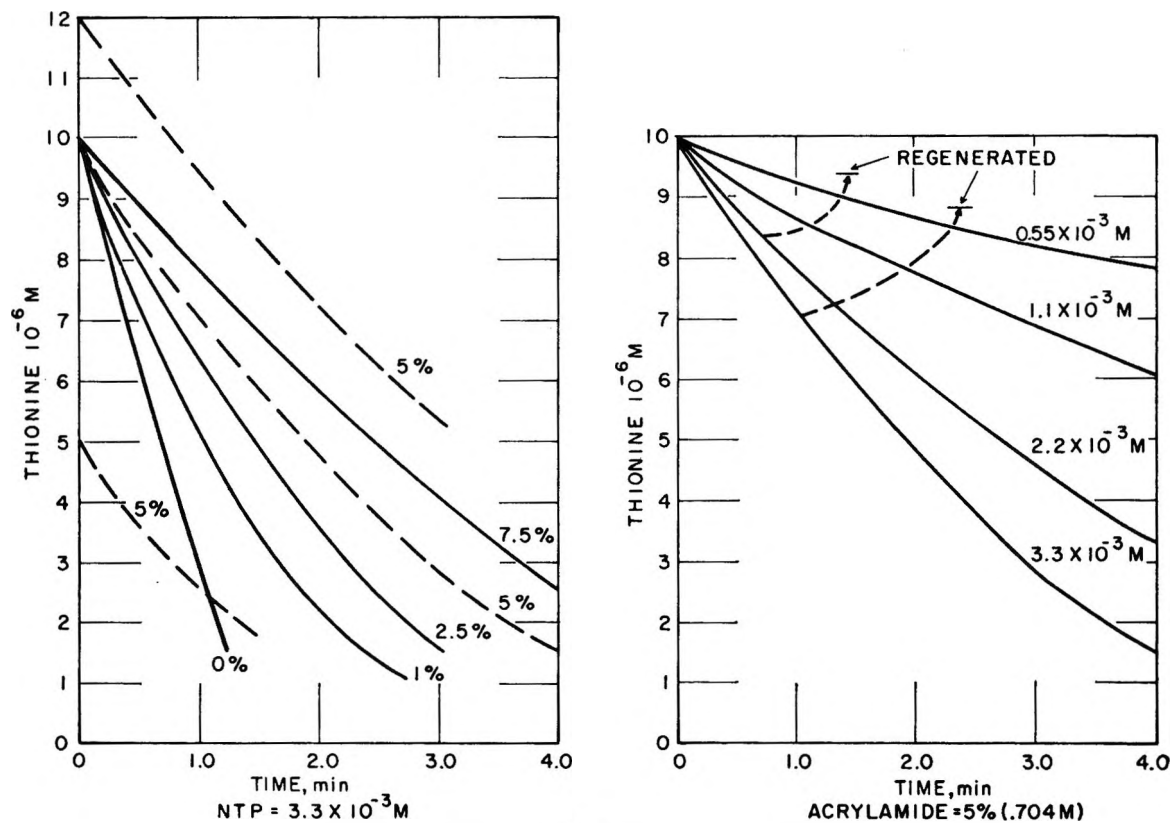


Figure 2. Thionine fading for the thionine-NTP-acrylamide system: a, monomer variation; b, NTP variation.

Results and Discussion

Dye Bleaching and Photopolymerization under Anaerobic Conditions. Figure 1 shows a set of photopolymerization data in which the thionine concentration is

$10^{-5} M$. In Figure 1a the NTP concentration was maintained at $3.3 \times 10^{-3} M$, and the monomer level was varied from 1 to 7.5% (0.141–1.054 M). It can be seen that, as the monomer is increased, the rate of

polymerization increases. Moreover, the rate is linear up to a reaction time of about 2 min., after which the rate falls off. This 2-min. reaction time corresponds to a conversion of about 10%. Figure 1a shows the rate of polymerization as a function of the concentration of the activator NTP with the monomer held constant at 5% (0.075 mole). Here, again, there is an increase in the rate of polymerization with the concentration of the activator.

Figure 2 summarizes the effects of NTP and monomer levels on the dye-bleaching reaction. Figure 2a shows that the maximum rate of dye fading is obtained in the absence of monomer and that R_t progressively decreases with an increase in the acrylamide concentration. This trend must be interpreted as a quenching of light-excited thionine by the monomer. Figure 2a also summarizes the effect of thionine concentration on photo bleaching. The dashed lines indicate the bleaching rates at three dye concentrations, 0.5×10^{-5} , 1.0×10^{-5} , and $1.2 \times 10^{-5} M$, at the same activator and monomer levels. The initial R_t values are independent of the thionine levels. Figure 2b shows the variation of R_t with NTP level. It is seen to increase with an increase in NTP.

Effect of Solution pH. Both the dye-bleaching and polymerization reactions are sensitive to solution pH. Table I summarizes the variation of R_t and R_p with solution acidity for anaerobic solutions containing $10^{-5} M$ thionine, $0.704 M$ acrylamide, and $3.3 \times 10^{-3} M$ NTP. It is seen that R_p increases in the pH range 5.55 to 7.6 and then falls off at higher pH levels; R_t appears to follow the same trend although it is not as well defined. We believe that the pH dependence in the range of 5.55 to 7.6 must be predominantly related to the acid-base properties of NTP and that the free base must be considerably more reactive than the protonated species. This is because, all other reaction parameters being equal, changes in the acidity alter only the relative proportions of these forms and not the total amount. Thus, if both species had the same reactivities and if hydrogen ions were not involved directly in the formation of free radicals, this initiator system would be insensitive to changes in solution pH. Let us compare, therefore, the R_t and R_p values in Table I with the percentage of free base, B, existing at equilibrium.⁵ At a pH of 5.55, NTP exists predominantly in the protonated form. As the pH is increased, the concentration of free base increases rapidly in the 6.61–7.90 interval and at higher alkalinities approaches more slowly toward 100% conversion. The R_p values parallel the increase in the amount of B. For example, a pH increase from 6.61 to 7.6 doubles the amount of free base, and R_p is about twice as great. The trend in

R_t is not as clear-cut although a large increase in reactivity is obtained by increasing the pH above 5.55. Both rates decrease, however, at pH levels exceeding 8.0. We believe that this loss of activity, so characteristic of thionine-containing systems, is the result of a change in the absorption characteristics of the dye. Absorption spectra show that the onset of spectral change begins at pH levels of about 8 to 9.

Table I: Effect of pH on the Anaerobic Thionine-NTP-Acrylamide System

pH	$R_t \times 10^4$, mole l. ⁻¹ sec. ⁻¹	$R_p \times 10^4$, mole l. ⁻¹ sec. ⁻¹	Free base (B), %
5.55	Very slow	None	6.2
6.61	8.33	3.0	43.1
7.62	8.33	5.9	88.6
7.90	8.33	5.4	93.6
8.50	6.94	4.5	98.3

Effect of Oxygen. Oxygen profoundly affects the behavior of the thionine-NTP-acrylamide systems in that it introduces an induction period prior to the onset of photopolymerization. In Figure 3 are plotted the degrees of dye bleaching and polymerization of solutions containing $10^{-5} M$ thionine, $3.3 \times 10^{-3} M$ NTP, and $0.704 M$ acrylamide at two oxygen levels. Also plotted are dashed curves showing the degrees of bleaching and polymerization of a similar system containing no oxygen. It is seen that the introduction of oxygen produces an induction period during which the dye is slowly bleached, but no polymer is produced. The initial bleaching rates decrease as the oxygen concentration increases. At the conclusion of the induction period, fading of thionine proceeds at a rate comparable to that of the anaerobic control, and polymer is formed. The relation between the length of the induction period and the oxygen level is apparent from Figure 3. The induction times were obtained both by extrapolating the polymerization curves to zero conversion and by determining the time corresponding to the intersection of the slopes of the two different dye-fading rates during and after the inhibition reaction. These data show conclusively that the length of the induction period is proportional to the amount of oxygen in the system and that the onset of polymerization coincides with the termination of the induction as measured by changes in the dye-bleaching rate.

(5) The equilibrium constant for the reaction $HB^+ \rightleftharpoons H^+ + B$ was calculated from potentiometric titration data at 25° in 0.1 M KCl and has a value of $10^{-6.73}$.

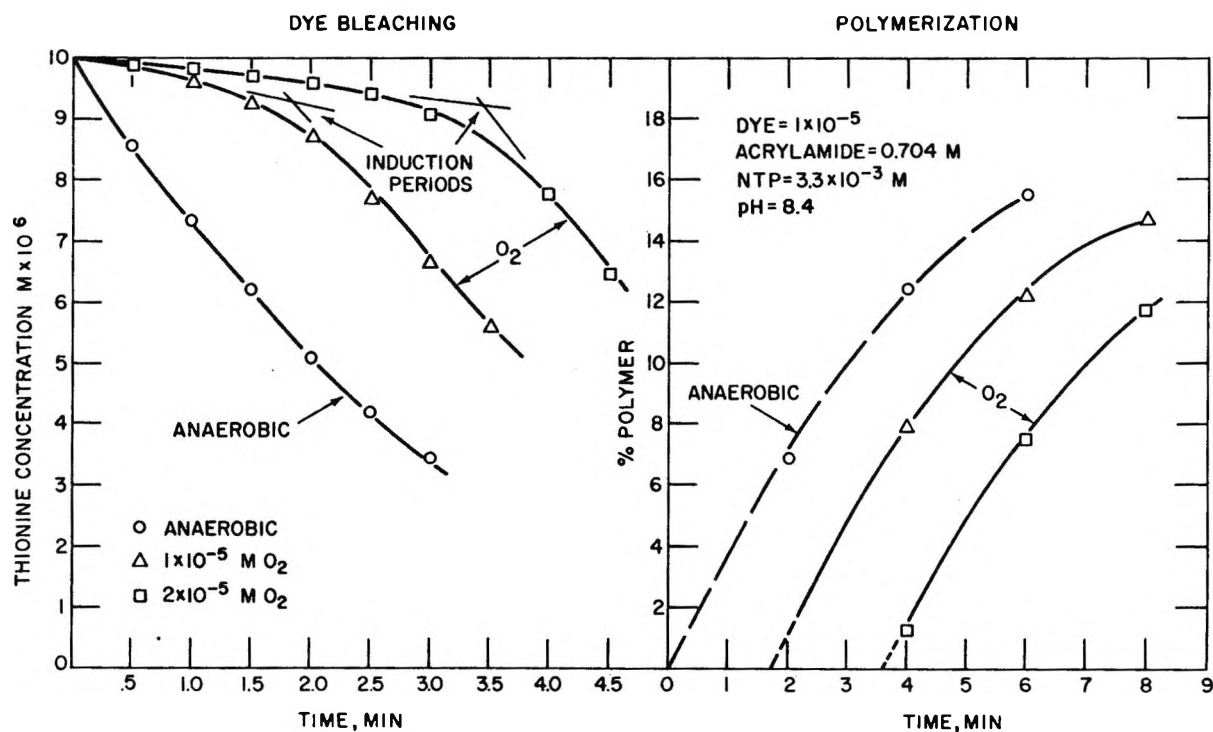
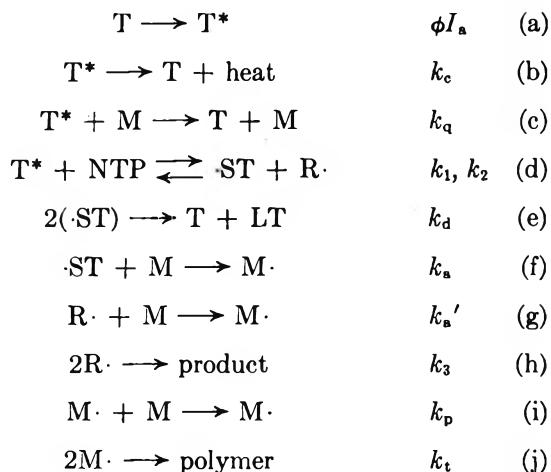


Figure 3. Effect of oxygen on the thionine-NTP-acrylamide system.

The Photopolymerization Mechanism. A photopolymerization mechanism consistent with the experimental data is represented by the sequence of reactions



In reaction a, T^* represents the triplet state of light-excited thionine, and ϕ is the efficiency of the formation of the triplet state when thionine has absorbed the quantity of light I_a . Reaction b represents the thermal deactivation of T^* to the ground state. The rate constant for this reaction has been measured by Hatchard and Parker⁶ to be $5 \times 10^4 \text{ sec}^{-1}$. Reaction c denotes the quenching of light-excited dye by the monomer M.

The reaction of excited thionine with NTP to form semithionine, $\cdot\text{ST}$, and a radical, $\text{R}\cdot$, is shown by (d). The exact structure of $\text{R}\cdot$ or its ultimate fate during the photoreaction is not known at this time. Reaction d shows both forward and backward reaction steps, denoted by rate constants k_1 and k_2 , respectively. As in most kinetic schemes of this sort, k_2 is probably comparable in magnitude to k_1 , but rapid removal of $\cdot\text{ST}$ and $\text{R}\cdot$ by other reactions suppresses this reversal reaction.

Reaction e is the dismutation reaction that forms thionine and leucothionine (LT). In our mechanism it is the only reaction by which LT is formed. Hatchard and Parker⁶ report k_d to be $2 \times 10^9 \text{ l. mole}^{-1} \text{ sec}^{-1}$.

Reaction f represents the initiation of polymerization by the reaction of $\cdot\text{ST}$ with the monomer to form the initiating radical $\text{M}\cdot$. The rate constant k_a for this reaction cannot be measured by ordinary vinyl polymerization because it cancels out in the mathematical analysis of the reaction. However, because of our measurements of the regeneration of LT, to be described later, we will be able to evaluate k_a . Reactions g and h are possible reactions of the photoproduct $\text{R}\cdot$ formed in reaction d. Reactions

(6) G. G. Hatchard and C. A. Parker, *Trans. Faraday Soc.*, 57, 1093 (1961).

i and j are the usual polymer propagation and polymer termination steps, respectively.

Verification of the Reaction Mechanism with Respect to R_f . The following three equations form the basis of the mathematical analysis of this reaction mechanism with respect to R_f

$$\frac{d(T^*)}{dt} = 0 = \phi I_a - [k_c + k_1(NTP) + k_d(M)](T^*) \quad (1)$$

$$\frac{d(\cdot ST)}{dt} = 0 = k_1(T^*)(NTP) - k_2(\cdot ST)(R\cdot) - 2k_d(\cdot ST)^2 - k_a(\cdot ST)(M) \quad (2)$$

$$R_f = \frac{-d(T)}{dt} = k_1(T^*)(NTP) - k_2(\cdot ST)(R\cdot) - k_d(\cdot ST)^2 \quad (3)$$

Combination of eq. 2 and 3 gives

$$R_f = k_a(\cdot ST)(M) + k_d(\cdot ST)^2 \quad (4)$$

This equation shows that R_f is made up of two terms: the first is $k_a(\cdot ST)(M)$, which represents the formation of polymer by reaction f; the second is $k_d(\cdot ST)^2$, which represents the formation of leucothionine by reaction e.

The solution of eq. 4 for $\cdot ST$ is complex; to simplify the solution, a series of thionine regeneration experiments was performed on typical anaerobic photopolymerization runs to determine which of the two terms was more important.

By cutting off the irradiation (thus terminating the reaction at 1- and 2-min. intervals) and then introducing oxygen, we could estimate how much of the dye fading resulted from the formation of leucothionine and how much resulted from the formation of polymer by semithionine radicals. The results of two regeneration experiments are shown in Figure 2b. In the first case, the reaction was stopped at 30 sec., oxygen was introduced, and the thionine concentration was increased from 0.8×10^{-5} to $0.94 \times 10^{-5} M$. In the second case, the reaction was stopped after 60 sec., and the same regeneration ratio was obtained. Approximately 60% of the faded dye was restored in both cases. We, therefore, concluded from this experiment that 60% of the fading of thionine results in formation of leucodye and the remaining 40% of fading results in formation of polymer. This is expressed by the equations

$$k_d(\cdot ST)^2 = 0.6R_f \quad (5a)$$

$$k_a(\cdot ST)(M) = 0.4R_f \quad (5b)$$

Therefore, to a first approximation, $k_d(\cdot ST)^2$ is the dominant term in eq. 4.

We must now solve eq. 2 for $\cdot ST$. Since this equation contains terms in both $\cdot ST$ and $(\cdot ST)^2$, an exact solution cannot be obtained simply, and an approximation must be made. Referring to eq. 5, we see that in eq. 2 we have $2k_d(\cdot ST)^2 = 1.2R_f$, while $k_a(\cdot ST)(M) = 0.4R_f$. Thus, we may neglect the latter term. Then, if we assume that $k_2(\cdot ST)(R\cdot)$ is less than $k_1(T^*)(NTP)$, eq. 2 becomes

$$2k_d(\cdot ST)^2 \doteq k_1(T^*)(NTP) \quad (6)$$

By putting eq. 6 into the dominant term of eq. 4, we obtain

$$R_f \doteq \frac{k_1(T^*)(NTP)}{2} \quad (7)$$

Finally, solution of eq. 1 for T^* and its substitution into eq. 7 gives

$$R_f = \frac{k_1(NTP)}{2} \left[\frac{\phi I_a}{k_c + k_1(NTP) + k_d(M)} \right] \quad (8)$$

For data analysis, eq. 8 is written in reciprocal forms

$$\frac{1}{R_f} = \frac{2[k_c + k_d(M)]}{\phi I_a k_1} \left[\frac{1}{(NTP)} \right] + \frac{2}{\phi I_a} \quad (8a)$$

$$\frac{1}{R_f} = \frac{2[k_c + k_1(NTP)]}{k_1(NTP)\phi I_a} + \frac{2k_d}{k_1(NTP)\phi I_a} (M) \quad (8b)$$

Thus, eq. 8a and 8b predict linear plots of $1/R_f$ vs. $1/(NTP)$ and (M) , respectively.

Figure 4 shows the plots of these equations, using the data of Figures 1 and 2. The plots of these equations are both linear and, within experimental error, have the same intercept.

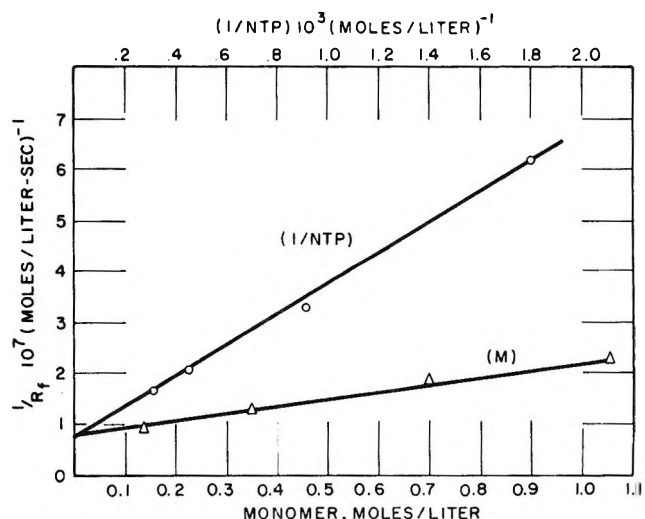


Figure 4. Confirmation of R_f dependence on NTP and acrylamide concentrations.

Verification of Reaction Mechanism with Respect to R_p . Let us now derive the expression for the rate of polymerization R_p . From reaction i it follows that

$$R_p = k_p(M)(M\cdot) \quad (9)$$

We must now obtain an expression for $M\cdot$, assuming a steady state in $M\cdot$. This, in turn, will require a steady-state assumption for $R\cdot$

$$\frac{d(M\cdot)}{dt} = 0 = k_a(\cdot ST)(M) + k_a'(R\cdot)(M) - 2k_t(M\cdot)^2 \quad (10)$$

$$\frac{d(R\cdot)}{dt} = 0 = k_1(T^*)(NTP) - k_2(R\cdot)(\cdot ST) - 2k_3(R\cdot)^2 - k_a'(R\cdot)(M) \quad (11)$$

There are no simple solutions for eq. 10 and 11 unless simplifying assumptions are made. In the case of $\cdot ST$, we know that $k_d(\cdot ST)^2$ is slightly greater than $k_a(\cdot ST)(M)$, and, by analogy, we expect $k_3(R\cdot)^2$ to be slightly greater than $k_a'(R\cdot)(M)$. Therefore, neglecting the term k_2 in eq. 11, we obtain

$$2k_3(R\cdot)^2 + k_a'(R\cdot)(M) = k_1(T^*)(NTP) \quad (12)$$

As a first approximation, let us assume that

$$k_a'(R\cdot)(M) \doteq k_1(T^*)(NTP) \quad (13)$$

Equation 10 then reduces to

$$2k_t(M\cdot)^2 \doteq k_1(T^*)(NTP) + k_a(\cdot ST)(M) = 2R_f \quad (14)$$

We believe that the functional dependence of eq. 14 is correct, but that the approximations involved make the coefficient of $2R_f$ incorrect. Using eq. 14 in eq. 9, we arrive at the final equation

$$R_p = k_p k_t^{-1/2} R_f^{1/2} (M) \quad (15)$$

Figure 5 shows a plot of R_p vs. $(M)\sqrt{R_f}$, using the

Table II: Rate Constant Data for Thionine-NTP-Acrylamide System

Rate constant ^a	Value of constant	Species	Steady-state ^b values
k_1	2.7×10^7	I_a	8×10^{-7}
k_a	1.7×10^6	T^*	9×10^{-12}
k_c	5×10^4	$\cdot ST$	4×10^{-9}
k_d	2.4×10^9
k_a	7.5
...
$k_p/\sqrt{k_t}$	2.5

^a All rate constants have the dimensions l. mole⁻¹ sec.⁻¹.

^b Values are computed for monomer = 0.704 M, NTP = 3.3×10^{-3} M, and for $\cdot ST$ and T^* at steady-state values.

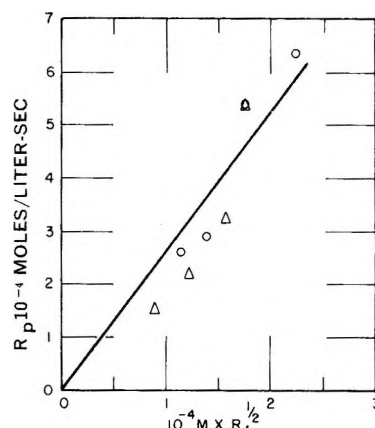


Figure 5. Confirmation of R_p dependence on monomer concentration.

data of Figures 1 and 2. A linear plot is obtained. However, the scatter of the data points is probably due to the approximations leading to eq. 12 through 15.

Evaluation of Rate Constants. Reaction rate constants and steady-state concentrations of the transient species were calculated from the slopes and intercepts of the data plots of Figures 4 and 5, using the following values⁷: $I_a = 8 \times 10^{-7}$ einstein l.⁻¹ sec.⁻¹; $k_c = 5 \times 10^4$ l. mole⁻¹ sec.⁻¹; $k_d = 2.4 \times 10^9$ l. mole⁻¹ sec.⁻¹. These data are summarized in Table II.

Table III: Quantum Yield Data

Acrylamide, M	1×10^{-6} M dye, 3.3×10^{-1} M NTP	ϕ_{th}	ϕ_p
0	0.15	0	0
0.350	...	0.023	0.023
0.490	0.10	0.027	0.027
0.704	0.077	0.047	0.047
1.060	0.055	0.057	0.057
NTP, M $\times 10^4$	1×10^{-5} M dye, 0.704 M monomer		
0.55	0.02	0.018	0.018
1.1	0.04	0.019	0.019
2.2	0.06	0.028	0.028
3.3	0.08	0.048	0.048

Quantum Yields. Experimental quantum yields for polymerization ϕ_p and for dye fading ϕ_{th} were calculated with the equations

$$\phi_p = \frac{R_p}{I_a} \times \frac{\text{monomer mol. wt.}}{\text{polymer mol. wt.}} \quad (16)$$

(7) Values for k_c and k_d are those determined by Hatchard and Parker, ref. 6.

$$\phi_{th} = \frac{R_t}{I_a} \quad (17)$$

Table III summarizes ϕ_p and ϕ_{th} values as a function of monomer and NTP levels. In these calculations the polymer molecular weight was taken as 10^6 . These

data show that ϕ_p increases with an increase in both monomer and NTP levels. However, ϕ_{th} increases with an augmentation of the NTP concentration but decreases with increasing monomer owing to dye quenching by reaction c. These quantum yields of 0.05 molecule/photon of light absorbed are the highest reported on a controlled, visible light-induced system.

Dye-Sensitized Photopolymerization Processes.^{1a} II. A Comparison of the Photoactivities of Thionine and Methylene Blue

by S. Chaberek^{1b} and R. J. Allen

Technical Operations Research, Burlington, Massachusetts (Received September 12, 1964)

The mathematical analysis of the experimental data on the anaerobic thionine- and methylene blue-TEA-acrylamide systems is consistent with the postulation that the polymerization-initiating radical is semithionine (or semi(methylene blue)) produced by the reaction of the light-excited dye with TEA. The predominant reactivity of TEA lies in its free base form, and the rate constant for this reaction is four to five times greater with thionine than with methylene blue. However, methylene blue is a better photosensitizer at pH levels exceeding 9. The presence of oxygen in these systems causes an induction period during which no polymer is formed, but the dyes are slowly bleached. The length of the induction period is proportional to the oxygen level. Systems containing methylene blue appear to be about twice as sensitive to oxygen content as those containing thionine. The quantum yields for polymerization for both dyes can be as high as 4 photons/polymer molecule and are the highest obtained to date with amine-containing systems.

Introduction

During studies of dye-sensitized free radical photopolymerization processes, it became desirable to increase the pH-operating range of photoinitiator systems. Most of our studies involved red-light-absorbing thionine. Although this dye has many attractive properties, it also has a disadvantage—namely, its photoinitiating efficiency at pH values exceeding 8.5 is greatly reduced. Exploratory experiments showed that the structurally similar phenothiazine dye, methylene blue, was apparently superior to thionine in this respect. However, the latter appeared to be more sen-

sitive to oxygen. In view of the differences in the behavior of these two closely related dyes, it was considered desirable to make a more quantitative assessment of their relative efficiencies. This paper summarizes studies on the photopolymerization of acrylamide by thionine- and methylene blue-triethanolamine (TEA) initiator systems.

(1) (a) This study was performed under Contract No. AF33(657)-11553, Photographic Branch, Reconnaissance Division, Air Force Avionics Laboratory, Wright-Patterson Air Force Base, Ohio; (b) to whom inquiries should be sent.

Experimental

The acrylamide used in this investigation was a pure sample obtained from the American Cyanamid Co. Preliminary screening of this sample for anaerobic thionine-sensitized photopolymerization showed no polymer formation in the absence of added activators and only a trace of dye bleaching over periods of 10 to 15 min.

Thionine and methylene blue were purified by three recrystallizations from water. The absorption coefficients were found to be 5.8×10^4 l. cm.⁻¹ mole⁻¹ for thionine (at 5980 Å.) and 6.4×10^4 l. cm.⁻¹ mole⁻¹ for methylene blue (at 6620 Å.).

Standard stock solutions of triethanolamine (TEA) were prepared gravimetrically from freshly distilled TEA.

The general experimental procedures used in this study were the same as those described previously.² The rate of dye bleaching, R_t , was calculated directly from spectrophotometric measurements. The polymerization rate, R_p , was determined by taking aliquots of the reaction solution at several time intervals, precipitating the polyacrylamide in methanol, filtering it, and drying the residue to constant weight. Polymer molecular weights were determined viscometrically.

Experimental Data on Dye Bleaching and Polymerization Rates as a Function of Reaction Parameters. The experimental approach in this study consisted of measuring the rates of dye bleaching R_t and of polymerization R_p as functions of reaction parameters, such as reactant concentrations, solution pH, and light intensity, and then calculating and comparing the quantum efficiencies of the two systems.

TEA Concentration. Rates of dye bleaching and polymerization were determined for systems containing 10^{-5} M methylene blue, 5% acrylamide, and varying concentrations of TEA between 4.0 and 80.0×10^{-3} M, at pH 8.55. These data, together with similar values for thionine-containing systems, are summarized in Table I. We see that, for both systems, R_t and R_p increase with an increase in the TEA level. Unfortunately, a direct, broad comparison of these systems under comparable conditions is not possible on the basis of the data of Table I. The limitation of the experimental procedure required our working at higher TEA levels in the methylene blue system. Only one set of experiments (at 3.75×10^{-3} M TEA for thionine and 4.0×10^{-3} M TEA for methylene blue) was done under essentially comparable conditions. A comparison shows that the R_t for thionine is about twice as great as that for methylene blue, and the R_p is only about 32% greater. These rate variations are discussed further in a later section of this paper.

Table I: Variation of R_t and R_p with TEA Concentration for the Thionine- and Methylene Blue-TEA-Acrylamide Systems^a

TEA, $M \times 10^4$	Thionine systems		Methylene blue systems	
	$R_t \times 10^8$, mole l. ⁻¹ sec. ⁻¹	$R_p \times 10^4$, mole l. ⁻¹ sec. ⁻¹	$R_t \times 10^8$, mole l. ⁻¹ sec. ⁻¹	$R_p \times 10^4$, mole l. ⁻¹ sec. ⁻¹
0.20	3.34	3.00
0.313	5.38	4.47
0.50	7.49	5.47
0.75	8.72	7.03
0.80	3.70	2.90
1.25	12.58	10.13
1.50	6.10	...
3.75	26.14	14.67
4.0	11.60	10.00
8.0	14.90	12.60
16.0	30.30	14.30
24.0	~35	15.80
40.0	~41	17.80
80.0	~56	18.40

^a All thionine systems contain 10^{-6} M dye and 0.704 M acrylamide at pH 8.55; all methylene blue systems contain 10^{-6} M dye and 0.704 M acrylamide at pH 8.60.

Monomer Concentration. Table II summarizes R_t and R_p data for systems in which the acrylamide concentration was varied between 0.141 and 1.056 M, with all other reaction parameters held constant. The polymerization rates for both dyes increase with an increase in monomer level. The dye-bleaching rate

Table II: Variation of R_t and R_p with Acrylamide Concentration for the Thionine- and Methylene Blue-TEA-Acrylamide Systems^a

Acrylamide, M	Thionine systems		Methylene blue systems	
	$R_t \times 10^8$, mole l. ⁻¹ sec. ⁻¹	$R_p \times 10^4$, mole l. ⁻¹ sec. ⁻¹	$R_t \times 10^8$, mole l. ⁻¹ sec. ⁻¹	$R_p \times 10^4$, mole l. ⁻¹ sec. ⁻¹
0.141	9.52	0.73	14.8	2.90
0.352	8.89	3.20	14.2	8.90
0.704	8.40	7.03	13.4	13.3
1.056	7.41	11.03	12.4	12.0

^a All thionine systems contain 10^{-5} M dye and 7.5×10^{-4} M TEA at pH 8.55; all methylene blue systems contain 10^{-5} M dye and 8×10^{-3} M TEA at pH 8.55.

varies inversely; however, the highest rate is obtained in the absence of monomer. Thus, this decrease in R_t with increasing monomer concentration must be

(2) A. Shepp, S. Chaberek, and R. MacNeil, *J. Phys. Chem.*, **66**, 2563 (1962).

interpreted as the quenching of the light-excited dye by acrylamide. A direct comparison of the relative magnitudes of R_t and R_p for the two dyes is not possible since the amount of TEA is about ten times greater in the systems containing methylene blue than in the ones containing thionine. Nevertheless, this tenfold difference in activator level results in only a two- to threefold increase in R_t and R_p . Thus, the rate constants for bleaching and polymerization must be greater for the thionine-sensitized systems than for the methylene blue ones.

Light Intensity. Calibrated neutral density filters were used to determine the effect of light intensity on R_t and R_p . Our experimental results are listed in Table III. The reaction rates for both dyes decrease with a decrease in light intensity.

Table III: Effect of I_a on R_t and R_p for the Thionine- and Methylene Blue-TEA-Acrylamide Systems^a

ND filter	Thionine systems		Methylene blue systems	
	$R_t \times 10^8$, mole l. ⁻¹ sec. ⁻¹	$R_p \times 10^4$, mole l. ⁻¹ sec. ⁻¹	$R_t \times 10^8$, mole l. ⁻¹ sec. ⁻¹	$R_p \times 10^4$, mole l. ⁻¹ sec. ⁻¹
None	27.8	13.6	17.2	12.7
0.28	16.2	10.8	7.9	7.5
0.45	10.4	8.7	4.4	5.9

^a All systems contain 10^{-5} M dye, 8×10^{-3} M TEA, and 0.704 M acrylamide at pH 8.55 and at $24 \pm 1^\circ$.

Dye Concentration. Dye-fading and polymerization rates were found to be independent of dye concentration over the range of 0.5 to 1.5×10^{-5} M, except for the dependence of the reactions on the light absorbed, I_a . As the dyes fade, I_a decreases, and, thus, the reaction rates decrease.

Solution pH. The magnitudes of R_t and R_p were determined as a function of solution pH for systems containing 10^{-5} M methylene blue, 8×10^{-3} M TEA, and 0.704 M acrylamide, and for those containing 10^{-5} M thionine, 7.5×10^{-4} M TEA, and 0.704 M acrylamide. The results are shown in Figure 1.

Since the amount of TEA differs in the two dye systems, let us consider the relative shapes of the plots in Figure 1 rather than their magnitudes. For the two dyes, both R_t and R_p increase with increasing pH in the range of 6.5 to about 8.2–8.5. At higher pH levels, the rates decrease markedly for the thionine systems, but for methylene blue they remain essentially constant to pH ~ 10 . Thus, the methylene blue is obviously superior to thionine in the alkaline pH range. We believe that this loss of activity so characteristic of

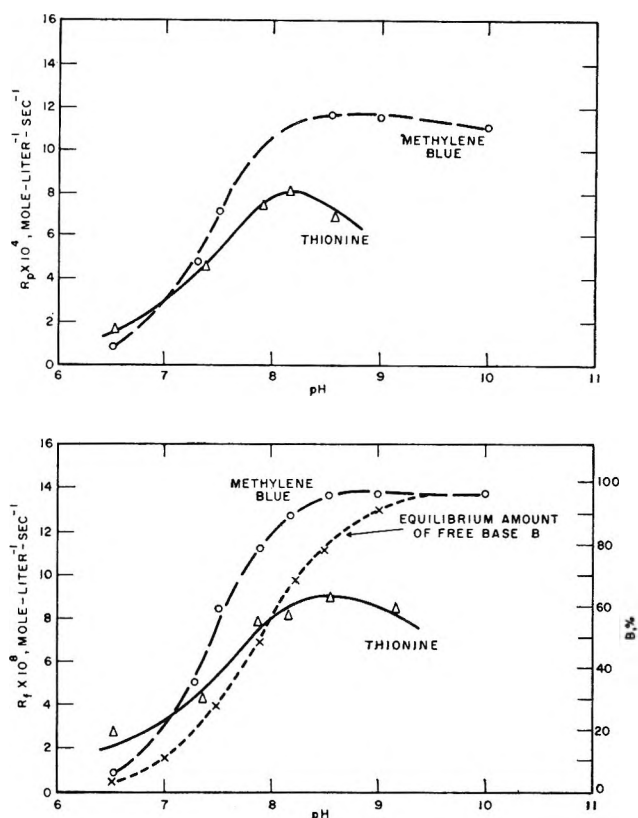
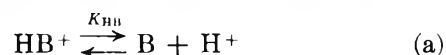


Figure 1. R_p and R_t as a function of solution pH: a, R_p vs. pH; b, R_t vs. pH.

thionine-containing systems is the result of a change in the absorption characteristics of the dye. Absorption spectra show that the onset of spectral change begins at pH levels of about 8 to 9 with thionine but at about 11 with methylene blue.

In the pH range of 6 to 8.5, the strong dependence of R_t and R_p on solution pH indicates that hydrogen ions are somehow involved in the process. We believe that this pH effect must be predominantly related to the acid-base properties of TEA as defined by



which governs the amount of free base, B, at equilibrium. The free base of TEA appears to be the most reactive species. A comparison of the shapes of the R_t curves with that denoting the pH variation in the percentage of B at equilibrium shown by the dashed curve in Figure 1 substantiates this postulation. The strikingly similar shapes of these curves show that the increase in R_t with pH closely parallels the increase in B.

Oxygen. Oxygen profoundly affects the behavior of the thionine- and methylene blue-TEA-acrylamide systems in that it introduces an induction period

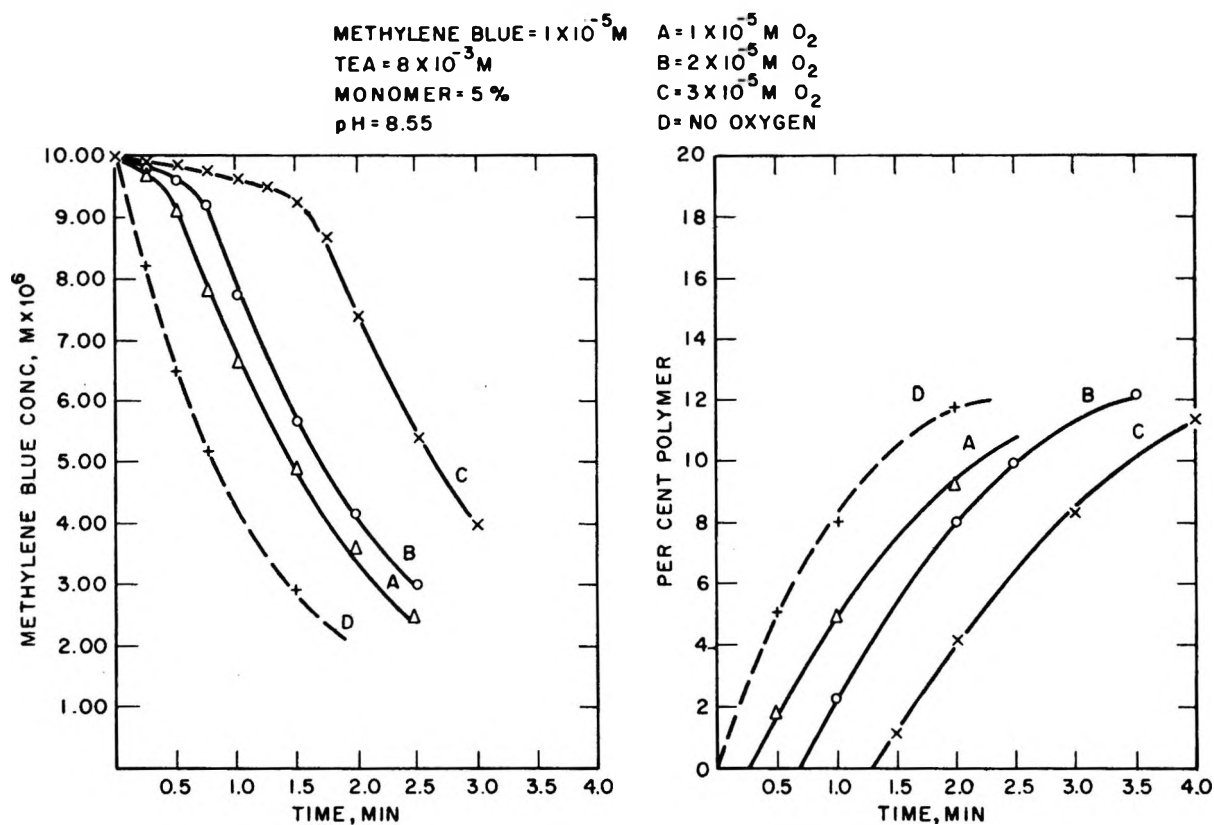


Figure 2. Effect of oxygen level on methylene blue-TEA-acrylamide systems: a, dye bleaching; b, polymerization.

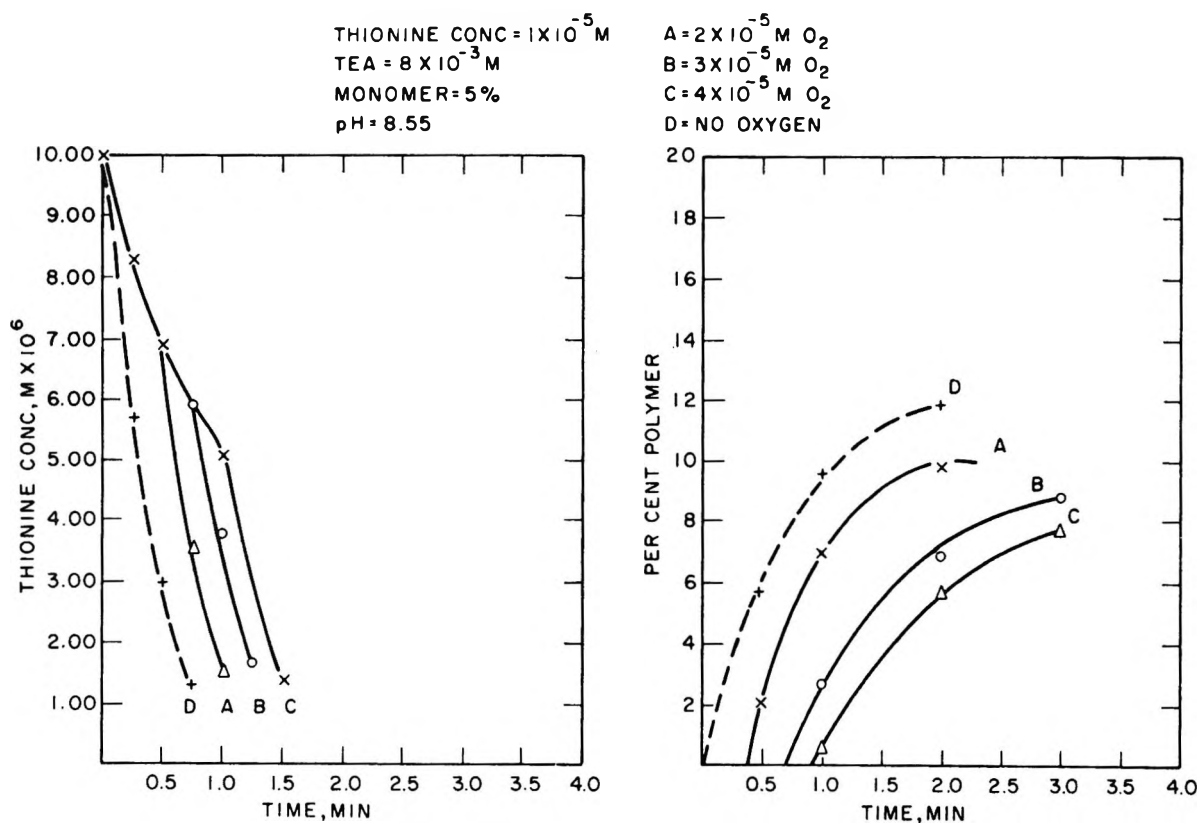


Figure 3. Effect of oxygen level at constant thionine-TEA-acrylamide: a, dye bleaching; b, polymerization.

prior to the onset of photopolymerization. Some implications of this inhibition phenomenon were explored as a function of oxygen and TEA levels.

Effect of Oxygen Concentration. In Figures 2 and 3 we have plotted the degrees of dye bleaching and of polymerization as functions of time for the thionine- and methylene blue-TEA-acrylamide systems. In the presence of varying amounts of oxygen, all systems contain $10^{-5} M$ dye, $8 \times 10^{-3} M$ TEA, and $0.704 M$ acrylamide at pH 8.55. Also plotted are dashed curves showing the degrees of bleaching and of polymerization of similar systems in the absence of oxygen. In Figure 2 we see that the introduction of oxygen produces an induction period during which the dye is slowly bleached, but no polyacrylamide is produced. The initial bleaching rates decrease as the oxygen concentration increases. At the conclusion of the induction period, fading of methylene blue proceeds at a rate comparable to that of the anaerobic control, and polymer is formed. Similar data for the thionine systems in Figure 3 show that these are qualitatively similar to the ones containing methylene blue. In this case, however, the bleaching rates during the induction period are much greater and are less sensitive to the oxygen level. The relations between the lengths of the induction periods and the oxygen level are shown in Figure 4. The induction times were obtained both by extrapolating the polymerization curves to zero conversion and by determining the time corresponding to the intersection of the slopes of the two different dye-fading rates during and after the inhibition reaction. These data show conclusively that the length of the induction period is proportionate to the amount of oxygen in the system and that the onset of polymerization coincides with the termination of the induction as measured by changes in the dye bleaching rate. In addition, the difference in the slopes of the plots, $\Delta t/\Delta O_2$, indicates a difference in the sensitivity to oxygen of these two dyes. The methylene blue plot has a slope approximately twice that of thionine; thus, the latter is about half as sensitive to oxygen. This lower sensitivity with thionine must be related to its higher fading rate during the induction period when the oxygen reacts with the light-excited dye.

Effect of TEA Concentration. In Figure 5 are plotted the degrees of thionine bleaching and polymerization of acrylamide at an oxygen level of $2 \times 10^{-5} M$ as a function of TEA concentration. The general shapes of the curves are similar to those of Figures 3 and 4. Most important, however, Figure 5 shows that the length of the inhibition period can be *markedly decreased* by increasing the concentration of TEA. For example, a 20-fold increase in the TEA level decreased

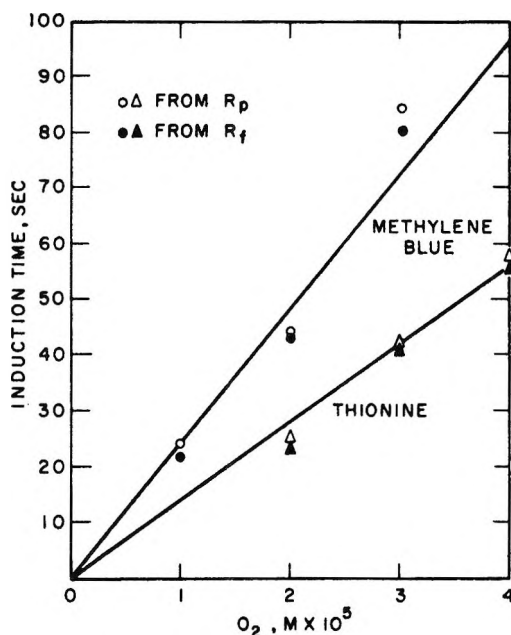
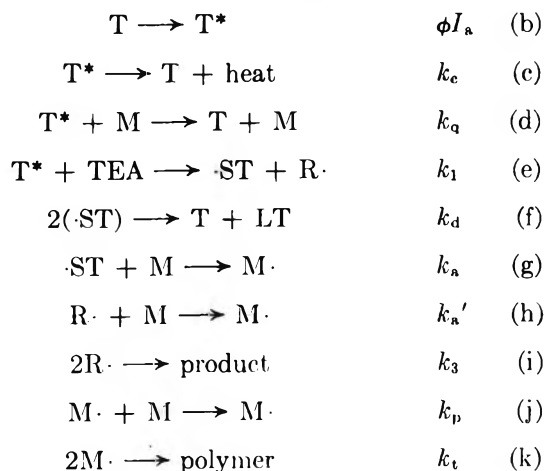


Figure 4. Effect of oxygen concentration on induction period for dye bleaching and photopolymerization.

the polymerization inhibition period by a factor of about 10. Similar results (not shown) were obtained with systems containing methylene blue. These data show, therefore, that the effect of oxygen may be decreased by increasing the concentration of components in the photoinitiator combination.

Polymerization Reaction Mechanism

The basic reaction mechanism for the methylene blue and thionine-TEA-acrylamide systems is identical with that described for thionine-nitrotripropionamide-acrylamide.³ It may be represented by the sequence of reactions



In reaction b, T^* represents the triplet state of light-excited thionine, and ϕ is the efficiency of the formation

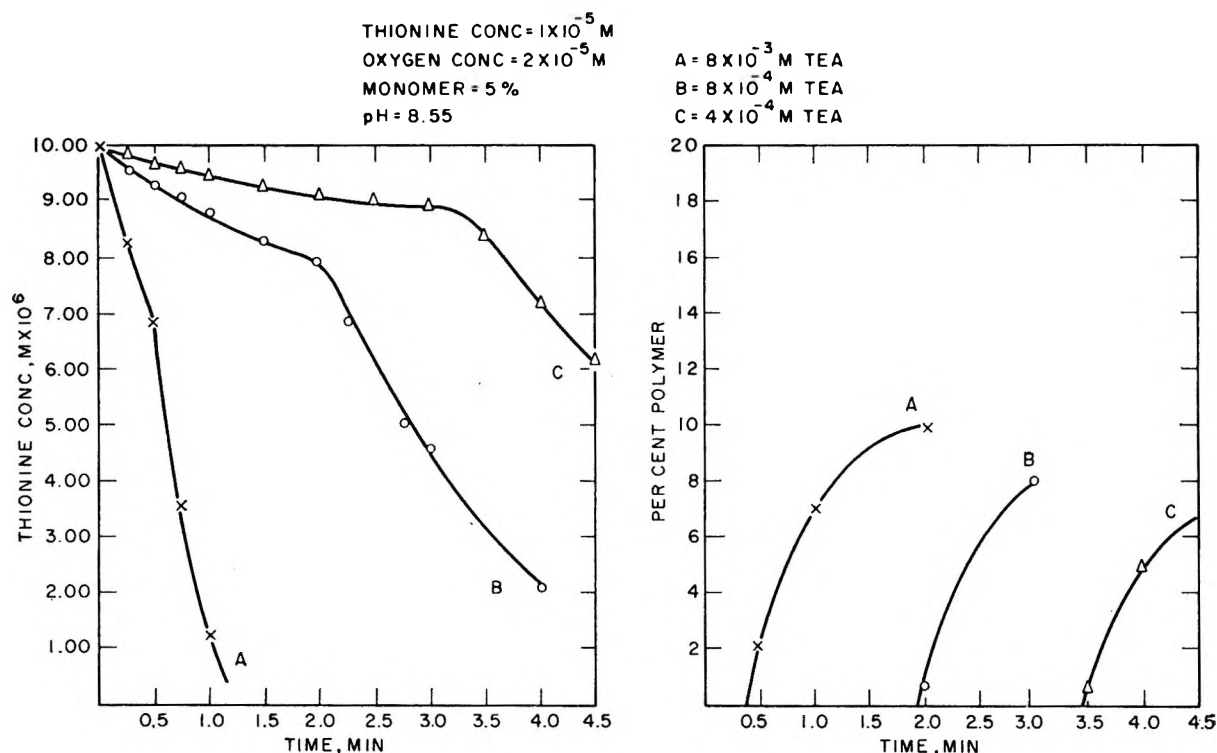


Figure 5. Effect of TEA concentration on aerobic thionine-TEA-acrylamide systems: a, dye bleaching; b, polymerization.

of the triplet state when thionine has absorbed the quantity of light I_a . Reaction c represents the thermal deactivation of T^* to the ground state. The rate constant for this reaction has been measured by Hatchard and Parker⁴ to be $5 \times 10^4 \text{ sec}^{-1}$. Reaction d denotes the quenching of light-excited dye by the monomer M. The reaction of excited thionine with TEA to form semithionine $\cdot ST$ and a radical $R\cdot$ is shown by (e). The exact structure of $R\cdot$ or its ultimate fate during the photoreaction is not known at this time. Reaction f is the dismutation reaction that forms thionine and leucothionine LT. In our mechanism it is the only reaction by which LT is formed. Hatchard and Parker⁴ report k_d to be $2 \times 10^9 \text{ l. mole}^{-1} \text{ sec}^{-1}$. Reaction g represents the initiation of polymerization by the reaction of $\cdot ST$ with the monomer to form the initiating radical $M\cdot$. Reactions h and i are possible reactions of the photo-product $R\cdot$ formed in reaction e. Reactions j and k are the usual polymer propagation and polymer termination steps, respectively.

Verification of the Reaction Mechanism for R_f . The basic relation between R_f and reaction parameters is expressed by eq. 1.⁵

$$R_f = \frac{k_1(\text{TEA})}{2} \left[\frac{\phi I_a}{k_c + k_1(\text{TEA}) + k_q(M)} \right] \quad (1)$$

For data analysis, eq. 1 is written in reciprocal forms

$$\frac{1}{R_f} = \frac{2[k_c + k_q(M)]}{\phi I_a k_1} \left[\frac{1}{(\text{TEA})} \right] + \frac{2}{\phi I_a} \quad (1a)$$

$$\frac{1}{R_f} = \frac{2[k_c + k_1(\text{TEA})]}{k_1(\text{TEA})\phi I_a} + \frac{2k_q}{k_1(\text{TEA})\phi I_a} (M) \quad (1b)$$

Equation 1a predicts a linear relation between $1/R_f$ and $1/(\text{TEA})$. Figure 6 shows plots of the data of Table I according to this relation. The adequate linear relations obtained for both dye systems substantiate that the postulation of similar reaction mechanisms is valid. The $1/R_f$ vs. $1/(\text{TEA})$ plots show further that, at the same TEA concentration, thionine containing systems bleach faster than the corresponding methylene blue containing ones ($1/R_f$ is smaller for thionine). In addition, the unequal slopes of these plots indicate that the rates of fading of these dyes differ in their sensitivities to activator concentration. Simple calculation of the slope ratios of the plots shows that R_f for thionine is about two and a half times more sensitive to the TEA level than is methylene blue.

(3) S. Chaberek, A. Shepp, and R. J. Allen, *J. Phys. Chem.*, **69**, 641 (1965).

(4) G. G. Hatchard and C. A. Parker, *Trans. Faraday Soc.*, **57**, 1093 (1961).

(5) For details of the derivation of the rate equations for R_f and R_p , see paper I of this series.³

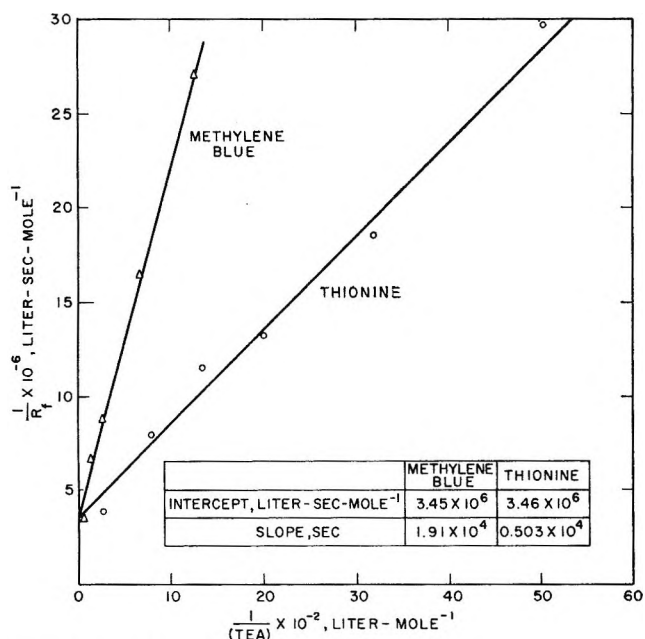


Figure 6. R_t dependence on TEA level.

Data plots such as those of Figure 6 provide a valuable method by which relative reactivities of systems may be assessed when the data cannot be gathered under exactly the same reactant concentrations or experimental conditions.

Equation 1b further predicts a linear relation between $1/R_t$ and (M) . Figure 7 shows that this linear relation holds for both systems. However, the greater sensitivity of R_t of monomer levels for the thionine-containing systems is apparent from the greater slope of

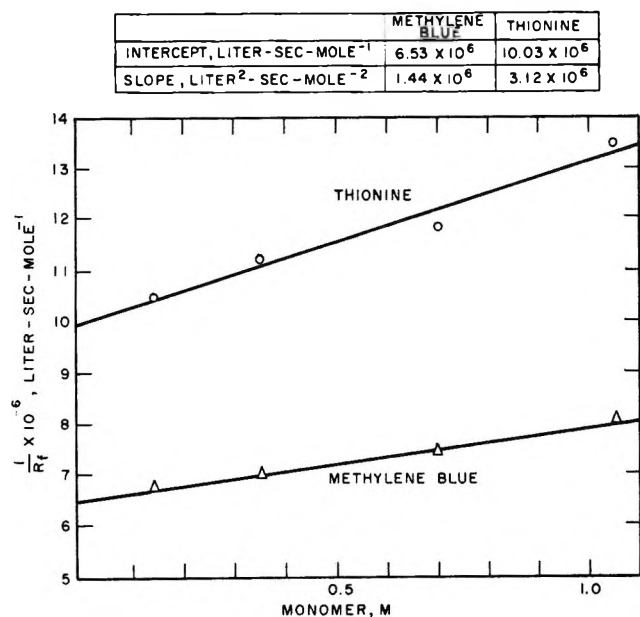


Figure 7. R_t dependence on monomer level.

the thionine plot (about twice the value of that for methylene blue containing systems).

Equation 1 shows that R_t should be directly proportional to I_a if all other reaction parameters are held constant. Figure 8 shows that the experimental results are in accord with prediction.

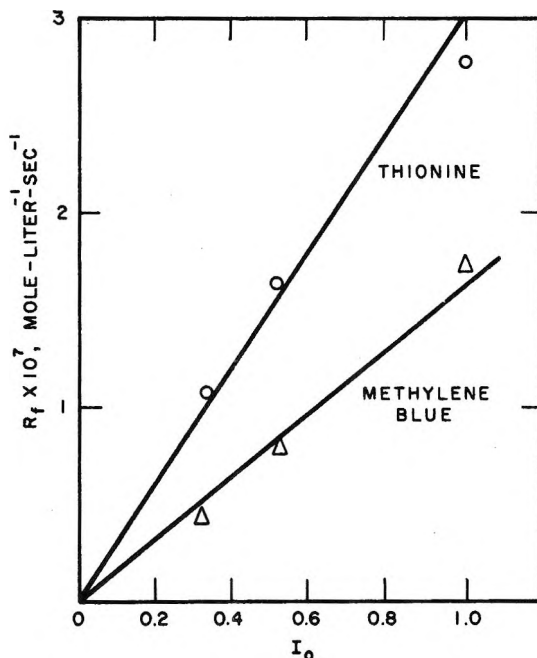


Figure 8. R_t dependence on light intensity.

Dependence on pH. Equations 1, 1a, and 1b do not indicate a pH dependence in their present form. To introduce a hydrogen ion concentration into the rate equation, let us substitute the following two reactions for reaction e



Thus, we have assigned separate reactivities to the protonated TEA, HB^+ , and to its free base, B . Solution of the rate equation gives the relation for R_t

$$R_t = \frac{k_{HB}(HB) + k_B(B)}{2} \times \left[\frac{\phi I_a}{k_c + k_q(M) + k_{HB}(HB) + k_B(B)} \right] \quad (2)$$

Elimination of (B) with the aid of

$$K_{HB} = \frac{(H^+)(B)}{(HB^+)} = 10^{-7.90} \quad (3)$$

and rearrangement of terms then gives finally

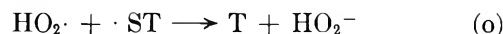
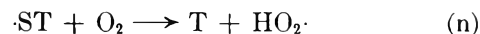
$$\frac{2R_t[k_c + k_q(M)]}{(\text{HB})(\phi I_a - 2R_t)} = \Phi = k_{\text{HB}} + \frac{k_{\text{B}}K_{\text{HB}}}{(\text{H}^+)} \quad (4)$$

Equation 4 shows that a plot of Φ vs. $1/\text{H}^+$ should be a straight line whose intercept is the rate constant k_{HB} and whose slope is related to k_{B} . All the terms in Φ either are known or may be calculated from available data. Figure 9 shows the excellent correspondence obtained between theory and experimental measurements. Moreover, the greater slope of the thionine plot indicates that the rate constant of B with this dye is considerably greater than that with methylene blue.

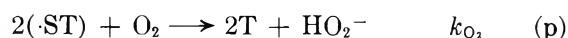
Effect of Oxygen. We have discussed qualitatively the effect of oxygen on these photopolymerization systems. A reaction mechanism must account for the following: (1) Slow dye bleaching occurs *without* polymer formation during the early stages of the reaction. (2) The rate of this initial dye bleaching increases with an increase in TEA concentration and with a decrease in oxygen level, all other reaction parameters remaining constant.

Basically, oxygen can affect the photopolymerization process in several ways. It can quench the light-excited dye by a reaction similar to (d), or it can react with free radicals (semithionine in our case)

required for the initiation of the polymerization reaction. Let us assume that the interaction of oxygen with $\cdot\text{ST}$ occurs by



The net reaction is then



Let us assume further that the rate constant k_{O_2} is much greater than the corresponding rate constant associated with the quenching of the light-excited dye so that reaction p denotes the primary way oxygen affects the photopolymerization process. If we now include reaction p in the general mechanism outlined by reactions b-k and solve the rate equation, we obtain the following relation between R_t and the oxygen content

$$R_t = \frac{k_1(\text{TEA})}{2} \left[\frac{\phi I_a}{k_c + k_q(M) + k_1(\text{TEA})} \right] \times \left[\frac{k_d}{k_d + k_{\text{O}_2}(\text{O}_2)} \right] \quad (5)$$

A comparison of eq. 5 with eq. 1 shows that the first two terms of (5) are identical with (1). Therefore, at constant levels of oxygen we would expect the same relation between R_t and TEA under aerobic and anaerobic conditions, that is, $1/R_t$ is a linear function of $1/(\text{TEA})$. This relation was checked on thionine-TEA-acrylamide-oxygen systems containing $10^{-5} M$ thionine, $0.704 M$ acrylamide, $2 \times 10^{-5} M$ O_2 , and varying amounts of TEA (pH 8.55). The results are shown in Figure 10. Although the data are indeed limited, it appears that the predicted relationship holds.

Similarly, eq. 5 may be readily rearranged to

$$\frac{1}{R_t} = A + B(\text{O}_2) \quad (6)$$

where A and B are constants.

Equation 6 predicts that $1/R_t$ should be a linear function of the oxygen concentration. This relation was checked with methylene blue systems containing $10^{-5} M$ dye, $0.704 M$ acrylamide, $8 \times 10^{-3} M$ TEA, and varying amounts of oxygen at pH 8.55. The results are shown in Figure 11. The linear relation obviously holds for this system.

Verification of the Reaction Mechanism for R_p . Solution of the rate equation with respect to R_p for the mechanism outlined above gives

$$R_p = k_p k_t^{-1/2} R_t^{1/2} (M) \quad (7)$$

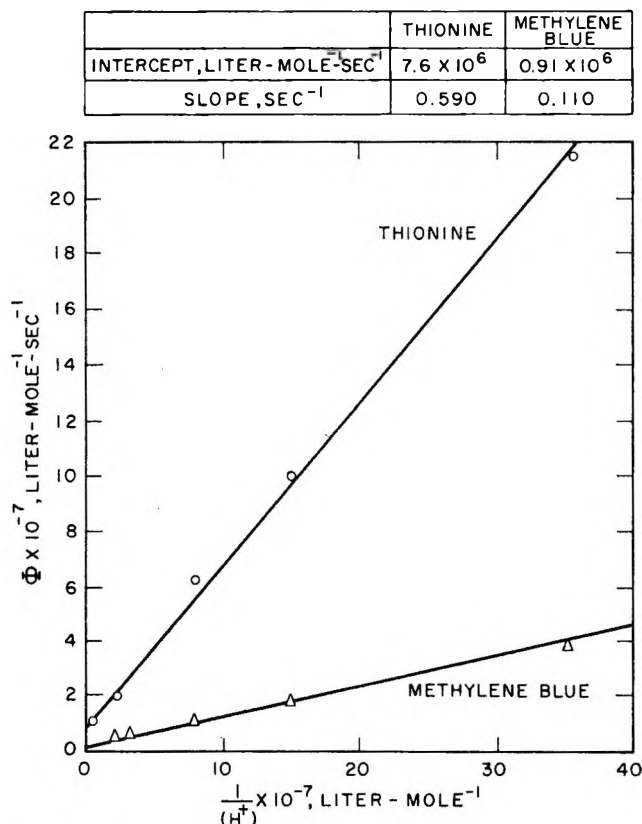


Figure 9. R_t dependence on pH.

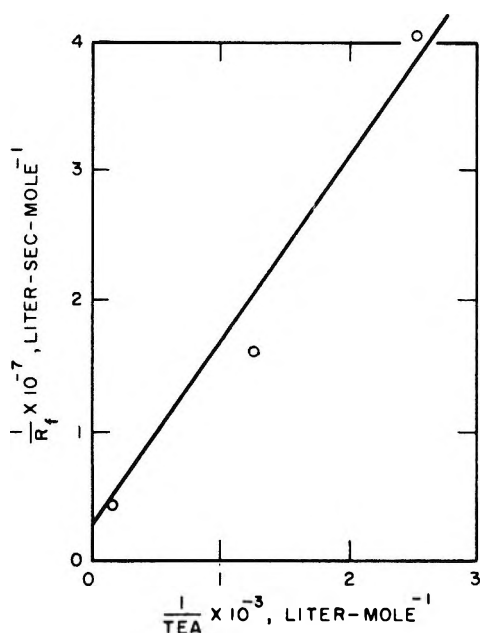


Figure 10. R_f dependence on TEA level in aerobic thionine-TEA-acrylamide systems.

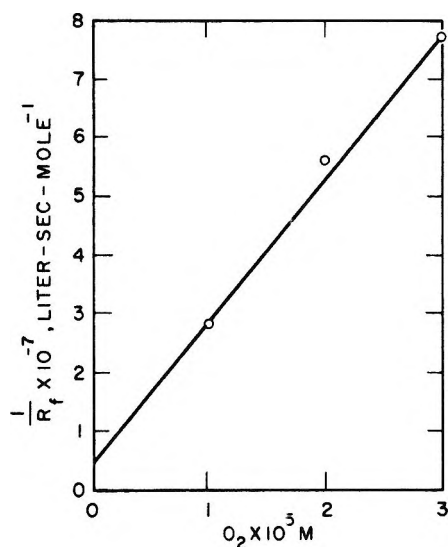


Figure 11. R_f dependence on oxygen level.

Figure 12 shows a plot of R_p vs. $(M)\sqrt{R_f}$, according to eq. 7 using the data of Tables I and II. A linear plot through the origin is obtained, but the scatter of the data points is probably due to the approximations made in deriving eq. 7.⁴ Note that the data for both thionine and methylene blue fit the same line equally well. Therefore, the magnitudes of $k_p k_t^{-1/2}$ are comparable for both systems.

Evaluation of Rate Constants. The data plots of Figures 6, 7, 9, and 12, together with the following values

Table IV: Rate Constants for the Thionine- and Methylene Blue-TEA-Acrylamide Systems

Rate constant	Thionine systems	Methylene blue systems
ϕ	0.72	0.72
k_{HB}	$\leq 7.6 \times 10^6$	$\leq 9.1 \times 10^6$
k_B		
From TEA dep. ^a	5.4×10^7	14.2×10^6
From monomer dep. ^a	4.1×10^7	8.2×10^6
From pH dep.	4.7×10^7	8.7×10^6
k_B , av.	4.7×10^7	8.4×10^6
k_a	2.4×10^4	2.3×10^4
$k_p k_t^{-1/2}$	3.9^b	3.9^b

^a k_B was calculated from the relation $k_B \approx k_1[(H^+)/K_{HB} + 1]$, where k_1 is the rate constant for reaction e. ^b In dimensions of $l.^{1/2} \text{ mole}^{-1/2} \text{ sec.}^{-1/2}$; all other constants in $l. \text{ mole}^{-1} \text{ sec.}^{-1}$.

Table V: Quantum Yield Data for the Thionine- and Methylene Blue-TEA-Acrylamide Systems^a

TEA, $M \times 10^4$	Thionine systems		Methylene blue systems	
	ϕ_f	ϕ_p	ϕ_f	ϕ_p
	10 ⁻⁵ M dye, 0.704 M acrylamide, pH 8.55		10 ⁻⁵ M dye, 0.704 M acrylamide, pH 8.55	
0.20	0.04	0.04
0.33	0.07	0.06
0.50	0.09	0.08
0.75	0.11	0.10
0.80	0.05	0.04
1.25	0.16	0.15
1.50	0.08	..
3.75	0.32	0.21
4.0	0.14	0.15
8.0	0.18	0.18
16.0	0.37	0.21
24.0	0.43	0.23
40.0	0.51	0.26
	10 ⁻⁵ M dye, 7 x 10 ⁻⁴ M TEA, pH 8.55		10 ⁻⁵ M dye, 8 x 10 ⁻³ M TEA, pH 8.55	
0.141	0.12	0.01	0.18	0.04
0.352	0.11	0.05	0.18	0.13
0.704	0.10	0.10	0.17	0.19
1.056	0.09	0.16	0.15	0.18
	10 ⁻⁵ M dye, 7 x 10 ⁻⁴ M TEA, 0.704 M acrylamide		10 ⁻⁵ M dye, 8 x 10 ⁻³ M TEA, 0.704 M acrylamide	
pH				
6.50	0.01	0.01
6.53	0.03	0.02
7.30	0.06	0.07
7.38	0.05	0.07
7.50	0.10	0.10
7.90	0.10	0.11	0.14	0.08
8.18	0.10	0.12	0.16	0.12
8.55	0.11	0.10	0.17	0.17
9.00	0.17	0.17
10.00	0.17	0.16

^a A molecular weight value of 6×10^6 was used in all cases.

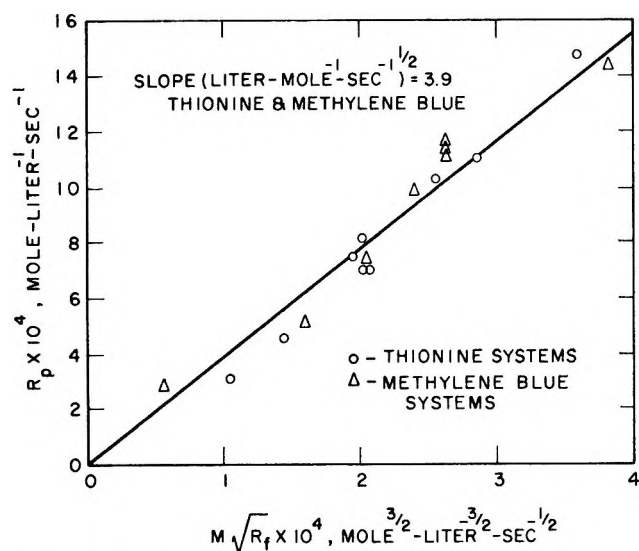


Figure 12. R_p dependence on monomer level.

for I_a and k_c , were used to evaluate the various rate constants: $I_a = 8 \times 10^{-7}$ einstein l.⁻¹ sec.⁻¹; $k_c = 5 \times 10^4$ l. mole⁻¹ sec.⁻¹. These values are summarized in Table IV. The data show both similarities and differences in the behavior of these dyes. They are similar in that the quenching constants k_q , the $k_p k_t^{-1/2}$ values, and the efficiencies of formation of the light-excited dyes are all comparable in magnitude. They are also similar because the primary reactivity of TEA lies in the free base B as opposed to the protonated base HB⁺. The magnitudes of k_{HB} listed in Table IV represent their maximum value, and, indeed,

they may be even smaller. The systems differ in that the rate k_B for thionine is about five times greater than that for methylene blue. Further studies are in progress to determine the reason for this difference in reactivity.

Quantum Efficiencies of the Dye-TEA-Acrylamide Systems. Experimental quantum yields for polymerization, ϕ_p , and for dye fading, ϕ_f , were calculated from eq. 8 and 9 and are summarized in Table V.

$$\phi_p = \frac{R_p}{I_a} \times \frac{\text{monomer mol. wt.}}{\text{polymer mol. wt.}} \quad (8)$$

$$\phi_f = \frac{R_f}{I_a} \quad (9)$$

The trends in ϕ_f and ϕ_p are the same for both dyes. Both yields increase with an increase in TEA level. An increase in monomer level also results in an increase in ϕ_p but in a decrease in ϕ_f owing to monomer quenching.

A detailed comparison of the quantum yields for thionine and methylene blue systems cannot be made because substantially higher TEA concentrations were required with the latter dye to obtain measurable R_f and R_p values. One set of measurements at TEA levels of 3.75 and 4.0×10^{-3} M show, however, that ϕ_f is about twice as great for thionine while the ϕ_p values are almost comparable for both dyes. In general, the data show conclusively that the quantum efficiency for photopolymerization can be as high as 4 photons/polymer molecule—the highest achieved to date with amine-initiator combinations.

NOTES

An Addition Complex between Carbohydrates and Dimethyl Sulfoxide as Revealed by Proton Magnetic Resonance

by V. S. R. Rao and Joseph F. Foster

Department of Chemistry, Purdue University, Lafayette, Indiana
(Received October 12, 1964)

In the course of a study of the optical rotatory dispersion behavior of carbohydrates, certain observations

led us to suspect that dimethyl sulfoxide (DMSO) might be forming a specific complex with certain sugars. We wish now to present evidence that this is indeed true and that the complex formation involves *cis* hydroxyls in axial-equatorial relationship.

In Table I are presented values of the specific rotation for several sugars at $436 \text{ m}\mu$ as determined in both water and in DMSO. It will be seen that for D-glucose and D-xylose, the rotations in DMSO are very much more positive than in water. It is well known that the α -anomers of these sugars have a more positive rotation

Table I: Comparison of Optical Rotations of Sugars in Water and in DMSO

Compound	—Specific rotation at 436 m μ —	
	Water	DMSO
D-Glucose	112	220
D-Xylose	37	178
D-Mannose	31	22
D-Ribose	-39	-27
α -Methyl D-glucose	306	327

than the β -anomers and that in aqueous solution the anomeric equilibrium favors the β -isomer. These results suggested the possibility that DMSO might favor the α -anomer due to complex formation. This is supported by the relatively trivial difference in specific rotation found in the case of methyl α -D-glucose. In the case of D-mannose, the difference in rotation in the two solvents is again small but is in the opposite direction. If anything, in this case DMSO might be stabilizing the β -anomer.

To throw more light on these questions, proton magnetic resonance studies were carried out on these sugars in deuterated DMSO. The n.m.r. spectra were determined in a Varian A-60 instrument and the results are summarized in Table II. Here are shown chemical shifts for the readily identifiable anomeric hydrogen atoms together with the corresponding coupling constants J_{12} obtained from the magnitude of the peak

splittings. It is clear from the table that the signal corresponding to the anomeric protons in the free sugars is shifted toward low field in DMSO. Secondly, only one type of anomeric proton is observed in each of the sugars D-glucose, D-xylose, and D-mannose, indicating that these sugars in DMSO exist in a single anomeric form. For D-glucose and D-xylose this is clearly the α -anomer. This is in agreement with the conclusion arrived at from the optical rotation measurements. From Table II it is also evident that the coupling constants J_{12} in DMSO are considerably higher than for the corresponding anomeric forms in D₂O. This indicates a significant decrease in the C₁H₁-C₂H₂ dihedral angle. Such a decrease in dihedral angle is reasonable if a complex is formed across the *cis* hydroxyl groups at C₁ and C₂ of α -D-glucose and α -D-xylose. Such significant changes in coupling constants are not observed for the methyl glucosides and sugar acetates, again in support of the thesis that the effects are due to complex formation with hydroxyl groups.

It has been shown recently that the oxygen atom in DMSO can form hydrogen bonds with two chloroform molecules.¹ It does not seem unreasonable to postulate a similar doubly hydrogen-bonded complex with two *cis* hydroxyl groups at C₁ and C₂. Such complex formation might easily cause a slight deformation of the ring with a decrease in the C₁H₁-C₂H₂ dihedral angle and an increase in the distance between the axial protons at C₂ and C₄. Comparatively little energy would be necessary for such a deformation. On the other hand, a similar deformation caused by complex formation across *trans*-situated hydroxyls would tend to push together the axial protons. Such a deformation is much less favorable. In general, complex formation across *trans* hydroxyls is sterically hindered.²

In the case of D-mannose also only one peak is observed in the low-field region in DMSO. While it cannot be stated positively that this corresponds to the β -anomeric form, inspection of models of D-mannose in the C₁ ring conformation shows that complex formation between DMSO and the C₁ and C₂ hydroxyls would be impossible in the α -form. It is therefore inferred that D-mannose is stabilized in the β -form by DMSO. Again, the increase in J_{12} is in agreement with a complex of this type with a slight distortion of the ring.

D-Ribose presents a more complex problem. The earlier optical rotation data have been interpreted by assuming that this sugar exists in equilibrium both in pyranose and furanose forms.^{3,4} On the other hand,

Table II: Summary of N.m.r. Data

Carbohydrate	Chemical shifts (τ -values) of anomeric pro- tons ^a				Coupling constant, $J_{H_1H_2}$, c.p.s.
	In D ₂ O	In DMSO	In D ₂ O or chloroform	In DMSO	
	D-Glucose	4.7 5.3	3.82	3.0 7.0	
D-Xylose	4.82 5.45	3.9	2.2 7.2	4.5	
D-Mannose	4.72 5.10	3.79	1.4 1.0	4.0	
D-Ribose ^b	4.73 4.95	3.70 3.90	Undefined 5.4	5.6 5.7	
Methyl α -D xylopyranoside	5.2	5.48	...	8.5	
Methyl β -D xylopyranoside	5.62	5.95	7.2	7.0	
α -D-Glucose pentaacetate	3.58	3.86	3.2	3.5	
β -D-Glucose pentaacetate	4.1	4.03	7.7	8.0	

^a The chemical shifts are measured relative to the internal standard tetramethylsilane (τ 10) in deuterated DMSO and chloroform and relative to the water impurity band in the case of D₂O (τ 5.2). ^b The data in D₂O are from ref. 5.

(1) A. L. McClellan, S. W. Nicksic, and J. C. Guffy, *J. Mol. Spectry.*, **11**, 340 (1963).

(2) S. J. Angyal and C. G. MacDonald, *J. Chem. Soc.*, 686 (1952).

from the n.m.r. data in D₂O, Lenz and Heeschen⁵ concluded that D-ribose exists as furanoside. If the later interpretation is correct, one should expect either one or two peaks in the low-field region, depending on whether D-ribose forms a complex similar to glucose and xylose. The observed three peaks at 3.7, 3.9, and 3.95 are compatible with the interpretation that D-ribose exists in equilibrium in both furanose and pyranose forms in DMSO.

Acknowledgment. We are indebted to the Corn Industries Research Foundation for financial support of this work.

(3) F. P. Phelps, H. S. Isbell, and W. Pigman, *J. Am. Chem. Soc.*, **56**, 747 (1934).

(4) R. W. Jeanloz and H. G. Fletcher, Jr., *Advan. Carbohydrate Chem.*, **6**, 135 (1951).

(5) R. W. Lenz and J. P. Heeschen, *J. Polymer Sci.*, **51**, 247 (1961).

The Wien Effect in Mixed Electrolyte Solutions. I. Reference Electrolytes

by Joseph F. Spinnler and Andrew Patterson, Jr.

Contribution No. 1766 from the Sterling Chemistry Laboratory, Yale University, New Haven, Connecticut (Received August 24, 1964)

In performing measurements of the high-field conductance of electrolytes, as is often the case with other electrolytic measurements, the presence of unavoidable impurities is a cause of concern. If the unwanted materials are ionized significantly or are subject to ionization by the applied field and if the ionic mobilities and valence type of the contaminants differ markedly from those of the solute being investigated, the results may be altered in some unexpected way by their presence. It makes little difference if these unavoidable impurities result from hydrolysis of the solute or are introduced from some other source; one would wish to calculate what effect they may have on the measurement.

A recent set of measurements on uranyl salts¹⁻³ has raised all these problems and suggested the need for an empirical study, since it is not yet possible to handle theoretically the computation of the behavior of mixtures of ions under high fields. In working with these solutions, all of which are appreciably hydrolyzed, we have found it convenient to use mixtures of acid and salt as the reference electrolyte, for example, hydrochloric acid and potassium chloride, and to adjust the pH of the reference electrolyte solution as closely as is

reasonable, or within 0.1 pH unit, to that of the uranyl salt under study. Without this being done, polarization in the uranyl salt solution makes conductance bridge balancing difficult or impossible, while if the acid-salt mixture is used as a reference electrolyte the difficulty is markedly diminished, and reproducible measurements become possible.

In order to understand the behavior of these reference electrolyte solutions, we have accordingly studied the relative Wien effects of mixtures of potassium nitrate and nitric acid *vs.* potassium chloride, of mixtures of the same electrolytes *vs.* potassium chloride-hydrochloric acid mixtures, and of potassium chloride-hydrochloric acid mixtures *vs.* hydrochloric acid. The concentrations have been chosen to resemble those used in the reference electrolyte solutions relative to which uranyl salts have been studied.

We have computed the theoretical Wien effects, as described in ref. 4, using two approximations; in one we simply consider the Wien effects of the two constituents to be additive; in the other, we calculate a combined valence and a combined limiting ionic conductance, in these cases that of the cation. On the reasonable assumption that these 1-1 electrolytes will behave normally and as closely in accord with theory as any available, the comparison of the theoretical results using the two methods of calculation with the experimental results may yield some guidance in how best to proceed with the theoretical computation for these and other solutions.¹ The amount of information which can be obtained in this way is limited in this particular study by the fact that the measurements are being made between solutions in which it is known in advance that polarization will occur and make bridge balancing difficult.

The experimental procedure has been described in ref. 1. In the rest of this paper we shall refer to method I as the assumption of additivity of the Wien effects

$$\Delta\Lambda/\Lambda(0)_{\text{total}} = \Delta\Lambda/\Lambda(0)_{\text{acid}} + \Delta\Lambda/\Lambda(0)_{\text{salt}} \quad (1)$$

and method II as the computation and use of combined valences and limiting ionic conductances for the appropriate ions in the theoretical calculation

$$(\Lambda_0^+)_{\text{total}} = N_i(\Lambda_0^+)_i + N_j(\Lambda_0^+)_j \quad (2)$$

$$|z^+|_{\text{total}} = N_i|z_i^+| + N_j|z_j^+| \quad (3)$$

(1) J. F. Spinnler and A. Patterson, Jr., *J. Phys. Chem.*, **69**, 500 (1965).

(2) J. F. Spinnler and A. Patterson, Jr., *ibid.*, **69**, 508 (1965).

(3) J. F. Spinnler and A. Patterson, Jr., *ibid.*, **69**, 513 (1965).

(4) H. Freitag and A. Patterson, Jr., *J. Electrochem. Soc.*, **108**, 529 (1961); also H. Freitag, Dissertation, Yale University, 1959.

It is realized that these equations are approximations, since they overlook mixture effects in which departures from the Kohlrausch principle of independent ionic mobilities appear when the electrolyte mixture contains ions of like sign but of very different mobilities. Thus the experimental results of Longworth⁵ show that in a potassium chloride-hydrochloric acid mixture the limiting ionic conductance of the hydrogen ion was approximately 3% less and that of the potassium ion 1.5% greater than the theoretical values calculated by Onsager and Fuoss⁶ for the mixture. No correction has been made for this effect in the theoretical calculations plotted in Figure 1, although this could be done. We expect to extend these measurements and calculations to other electrolytes, including higher valence types, and will then undertake to make such corrections. In the same calculations,¹ the limiting ionic conductances of the other ions involved are known with a considerably poorer degree of precision than those of the mixtures determined as in eq. 2, especially at temperatures other than 25°, in which cases this refinement is certainly not necessary.

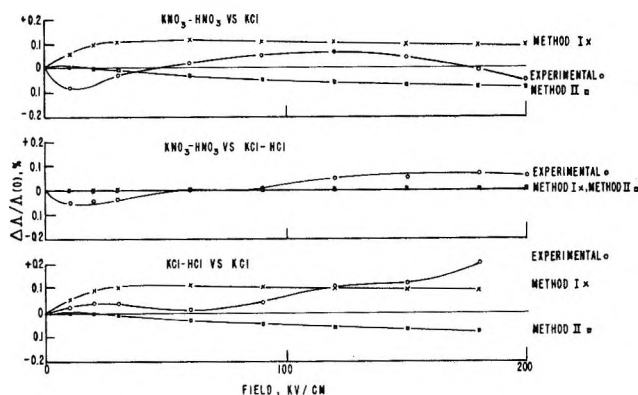


Figure 1. Plots of the experimental and theoretical high-field conductance quotients *vs.* field for three pairs of reference electrolyte solutions. At top, for a potassium nitrate-nitric acid mixture *vs.* potassium chloride, the concentrations were 1.830 , 0.488 , and $3.024 \times 10^{-4} M$, respectively. In the center, for a potassium nitrate-nitric acid mixture *vs.* a potassium chloride-hydrochloric acid mixture, the concentrations were, in order, 1.830 and 0.488 *vs.* 1.849 and $0.477 \times 10^{-4} M$. At the bottom, for a potassium chloride-hydrochloric acid mixture *vs.* potassium chloride, the concentrations were 1.849 and 0.477 *vs.* $3.028 \times 10^{-4} M$.

It can be seen from inspection of the curves of Figure 1 that both methods I and II agree to within 0.1 unit of $\Delta\Delta/\Lambda(0)$, %, with the experimental measurement. A higher experimental error is to be expected in the measurements of acid-salt mixtures against a salt because of concentration polarization, as noted

above. Nevertheless, the average difference in $\Delta\Delta/\Lambda(0)$ determinations at a given field strength with the same solutions was 0.02 unit. Consequently, the accuracy attained in these measurements of $\Delta\Delta/\Lambda(0)$ is estimated to be within 0.05 unit in the range of fields between 0 and 90 kv./cm., decreasing to 0.1 unit at 200 kv./cm.

It will be seen that the curve calculated for $\text{KNO}_3\text{-HNO}_3$ *vs.* KCl by method I rises rapidly, 0.1 unit in 15 kv./cm., and then remains constant, while that calculated by method II slowly decreases to -0.085 unit at 200 kv./cm. A similar situation exists in the calculation for KCl-HCl *vs.* KCl . The rapid increase followed by a flat portion for most of the range of fields calculated by method I is due to the absolute Wien effect of the acid in the mixture. At 6 kv./cm. its absolute Wien effect is approximately 0.03%, while that of the salt is about 0.016%. At 100 kv./cm., the absolute Wien effect of the acid is approximately 0.13%, while that of the salt is 0.31%. Thus the theoretical results predicted by method I are at first dependent on the acid constituent, in particular because of the large limiting ionic conductance of the hydrogen ion, and become more dependent on the salt at higher field strengths. It can be demonstrated¹ that an increase in the limiting ionic conductance of the cation results in a decrease in the magnitude of the Wien effect at high field strengths, other parameters being held constant.

The curves representing the theoretical results calculated by method II agree with the experimental results within 0.05 unit between 0 and 60 kv./cm. and within 0.05 unit at the higher field strengths in the $\text{KNO}_3\text{-HNO}_3$ *vs.* KCl case, but the agreement is considerably poorer with the KCl-HCl *vs.* KCl case, where experimentally there was much more trouble with polarization. Why this should be observed in the one case and not in the other is not known; the same conductance cells were not used, however, and this may have had some effect. In the case where the pH of the two cell solutions was balanced, both methods yield results in close agreement with the experimental values, and the experimental values are at least as accurate as the precision claimed previously: 0.02 $\Delta\Delta/\Lambda(0)$, %.

Thus, it appears that the effects of the hydrogen ion tend to be overcompensated for by method I and that any errors introduced by ignoring the mixture effect will be greatly magnified at the lower field strengths. At higher fields errors of this type are not so significant, but errors due to concentration polariza-

(5) L. G. Longworth, *J. Am. Chem. Soc.*, **52**, 1897 (1930).

(6) L. Onsager and R. M. Fuoss, *J. Phys. Chem.*, **36**, 2684 (1932).

zation become the major source of disagreement between the theoretical values and experiment. As a consequence of these facts, coupled with the agreement of the method II theoretical calculations and the experimental results at low fields where polarization effects were not troublesome, it is concluded that method II is the more satisfactory of the two.

We propose to continue this empirical investigation on mixtures of a variety of salts of different valence types where the difficulties from polarization forced upon us by necessity in the present investigation will be absent.

Acknowledgment. This work was supported under AEC Contract AT (30-1)-2890.

Charge-Transfer Complexes of Titanium Tetrachloride, Titanium Tetrabromide, and Vanadium Oxytrichloride with Aromatic Hydrocarbons

by C. Dijkgraaf

Central Laboratory, Staatsmijnen in Limburg, Geleen, The Netherlands (Received July 6, 1964)

From experimental observations it appears that the combination of aromatic hydrocarbons and TiCl_4 , TiBr_4 , and VOCl_3 , respectively, gives rise to broad absorption bands in the visible and/or the ultraviolet part of the spectrum. These absorption bands are not observed in the spectra of the relative partners. As a consequence, the bands must be caused by some complex formation. Investigations into the nature of the chemical bonding in these complexes lead to Mulliken's charge-transfer theory.¹

Observed Spectra

The spectra were run on a Beckman Type DK-2 spectrophotometer. Curve 1 of Figure 1 represents the spectrum of a solution of naphthalene in cyclohexane, whereas curve 2 corresponds to the spectrum of a solution of TiCl_4 in cyclohexane. The spectrum of a mixture of naphthalene and TiCl_4 is represented by curve 3 of Figure 1. It appears that new absorption bands arise. (Note that the spectra are drawn on different ordinates, so that no intensity conclusions can be drawn.) The spectra of a number of molecular compounds of aromatic hydrocarbons and TiCl_4 , TiBr_4 , and VOCl_3 were investigated. The wave numbers of maxi-

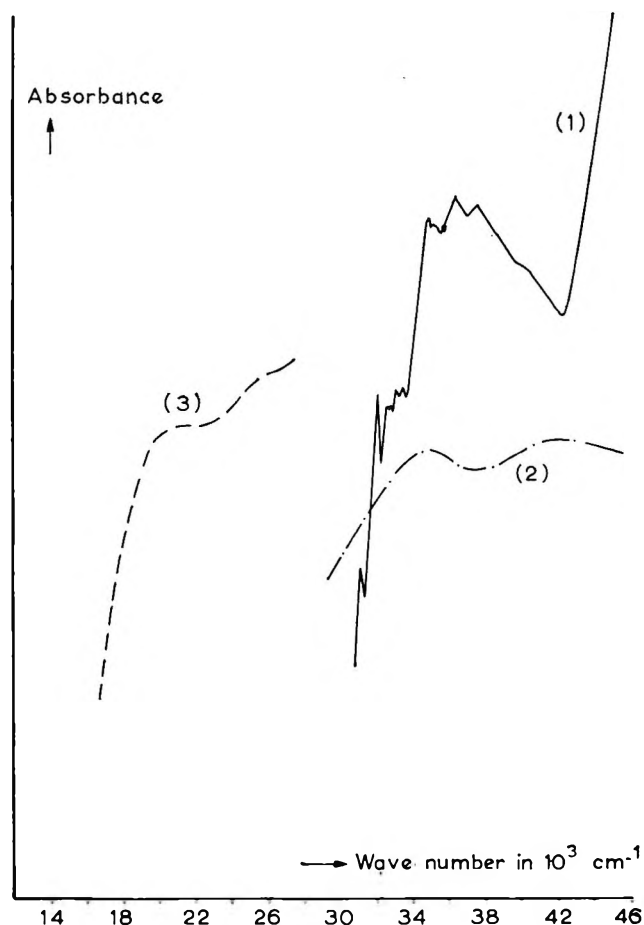


Figure 1.

mum absorption of the bands are summarized in Table I. The charge-transfer bands of VOCl_3 in combination with benzene, naphthalene, and phenanthrene agree with those already observed by Krauss and Gnatz.²

Discussion

In our opinion the observed absorption bands are caused by charge-transfer interaction between the halogen compounds of titanium and vanadium, on the one hand, and the aromatic hydrocarbons, on the other. As stated by Hastings, *et al.*,³ a relation of the following type exists in charge-transfer complexes

$$h\nu = I_D - E_A - E_C + \frac{2\beta^2}{I_D - E_A - E_C}$$

where $h\nu$ = energy of maximum absorption, I_D = ion-

(1) R. S. Mulliken, *J. Am. Chem. Soc.*, **72**, 600 (1950); **74**, 811 (1952); *J. Phys. Chem.*, **56**, 801 (1952); *Rec. trav. chim.*, **75**, 845 (1956).

(2) H. L. Krauss and G. Gnatz, *Ber.*, **95**, 1023 (1962).

(3) S. H. Hastings, J. L. Franklin, J. C. Schiller, and F. A. Matsen, *J. Am. Chem. Soc.*, **75**, 2000 (1953).

Table I: Wave Number (in 10^3 cm^{-1}) of Observed Maxima of Charge-Transfer Compounds

	TiCl ₄				TiBr ₄				VOCl ₃					
	CTB ₁	CTB ₂	$\Delta\sigma_{1-2}$	Solvent	CTB ₁	CTB ₂	$\Delta\sigma_{1-2}$	Solvent	CTB ₁	CTB ₂	CTB ₃	$\Delta\sigma_{1-2}$	$\Delta\sigma_{2-3}$	Solvent
Benzene	29.8			C ^a	27.0 ^b			C	23.8					C
Naphthalene	21.0	25.8	4.8	..	21.3			C	16.0					..
Anthracene	16.7	25.0 ^b	8.3	..	16.5	22.9 ^b	6.4	C	12.2					C
Phenanthrene	22.0			..	21.3			C	16.2					..
Chrysene	19.2	27.0 ^b	7.8	..	18.5			C	14.5					..
Pyrene	17.2	23.5	6.3	..	16.8			C	12.5	18.8		6.3		C
Perylene	14.5	21.0	6.5	..	14.2	19.2	5.0	C	8.0	15.2	20.4	7.2	12.4	C

^a C = cyclohexane. ^b Inaccurate value.

ization potential of the donor molecule, E_A = electron affinity of the acceptor molecule, E_C = Coulomb energy of the ions D^+ and A^- , and β = a constant. McConnell, *et al.*,⁴ give a linear relationship of the type $h\nu = aI_D + b$.

In Figure 2 the $h\nu$ values of maximum absorption of

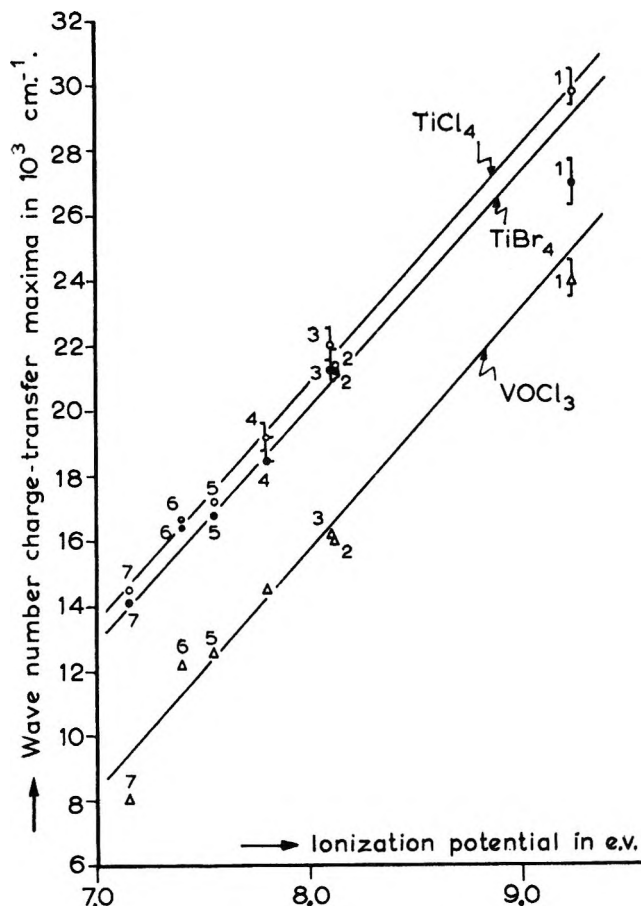


Figure 2. O, complexes with TiCl₄; ●, complexes with TiBr₄; Δ, complexes with VOCl₃. 1, benzene; 2, naphthalene; 3, phenanthrene; 4, chrysene; 5, pyrene; 6, anthracene; 7, perylene.

the longest wave length band observed in the complexes are plotted against the ionization potential of the aromatic hydrocarbons. The observed linear relationship strongly supports the charge-transfer character of the complexes.

In some charge-transfer complexes a number of charge-transfer bands have been observed. It appears that the differences $\Delta\sigma$ are independent of the acceptor molecules. So the reason for these additional bands will have to be found in the donor molecules. The $\Delta\sigma$ values observed by us agree reasonably well with a number of $\Delta\sigma$ values found by Briegleb, *et al.*,⁵ who measured the charge-transfer spectra of complexes of tetracyanoethylene and chloranil with aromatic hydrocarbons. In agreement with the interpretation of these authors we assign these additional absorption bands to transitions from the ground level of the complex to charge-transfer levels of which the D^+ ion is excited.

Acknowledgments. The author wishes to thank Mr. J. P. C. van Heel and Mr. J. P. G. Rousseau for their experimental assistance and Dr. C. Bokhoven for his stimulating remarks.

(4) H. McConnell, J. S. Ham, and J. R. Platt, *J. Chem. Phys.*, **21**, 66 (1953).

(5) G. Briegleb, J. Czekalla, and G. Reuss, *Z. physik. Chem. (Frankfurt)*, **30**, 316 (1961).

The Role of Silver Nitrate Ion Pairs in the Alkyl Halide-Silver Nitrate Reaction

by G. D. Parfitt, A. L. Smith, and A. G. Walton

Chemistry Department, University of Nottingham, Nottingham, England (Received July 27 1964)

In connection with some light scattering studies¹ on the precipitation of silver iodide from homogeneous

solution, using the reaction between silver nitrate and ethyl iodide in ethanol, an expression for the over-all kinetics of this reaction was assumed involving the degree of dissociation of the silver nitrate. This expression is now discussed further in the light of subsequent conductometric studies of silver nitrate in ethanol-water mixtures.

The kinetics of the reactions between alkyl halides and silver nitrate in a variety of solvents have been extensively studied since the papers of Donnan, Burke, and Potts, published between 1904 and 1910.²⁻⁴ A recent review of the literature is that of Melendez-Andreu.⁵

Kinetic data have usually been interpreted in terms of the stoichiometric concentrations of the reactants, leading to fractional over-all apparent orders between 2 and 3. The contribution of the alkyl halide to the over-all order has invariably been found close to unity, but attempts to separate the contributions of the Ag^+ and NO_3^- ions to the over-all order, again using stoichiometric concentrations, have led to a complicated picture. Many of the apparent anomalies are, however, resolved if quantitative allowance is made for ionic strength effects, association of silver nitrate to ion pairs, and the effect of reaction products.

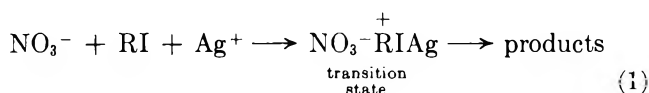
The suggestion that silver nitrate ion pairs may be involved in the reaction was, in effect, made in 1909 by Donnan,³ who postulated that in ethanol "undissociated silver nitrate molecules" may be the reacting species. Senter,⁶ however, found that the apparently similar reaction between silver nitrate and salts of brominated aliphatic carboxylic acids in aqueous solution was catalyzed by the solid silver bromide produced, and the ion pair mechanism was also strongly criticized by Hughes, Ingold, and Masterman,⁷ who suggested that heterogeneous catalysis was "diagnostic of the reaction between silver ions and alkyl halides." Although heterogeneous catalysis may be significant in aqueous and some other solutions, there is good evidence that, *e.g.*, in ethanol⁴ and acetonitrile,⁸ it is negligible. The autocatalytic effects observed in the reaction can, moreover, be explained without recourse to the postulate of heterogeneous catalysis.

Hughes, *et al.*,⁷ have commented that to invoke the participation of "undissociated silver nitrate molecules" in the reaction is "a convenient theory since nobody claims to know the concentration of these molecules." The situation has now changed, however, and some confidence can be placed in ion pair concentrations obtained from conductance measurements analyzed by recently refined conductance equations.⁹ It is, moreover, only the variation of ion-pair concentration with over-all concentration which is required

to test the hypothesis and this quantity is not very sensitive to the value of the association constant taken. In the following discussion association constants for silver nitrate in ethanol-water mixtures which have been calculated from conductance measurements in this laboratory¹⁰ will be used.

Kinetic Analysis

Since the reaction rate is affected by both the silver and nitrate ion concentrations, the over-all kinetic process might tentatively be written⁸



with the nitrate ion participating in the transition complex essentially as formulated by Kornblum.¹¹

Defining the rate of reaction as the rate of decrease of stoichiometric silver nitrate concentration, and ignoring the effect of reaction products

$$-dc/dt = k'c^3\gamma^2f_{\pm}^2 \quad (2)$$

where c is the stoichiometric concentration of silver nitrate and alkyl halide (taken equal) at any time t , γ is the degree of dissociation of silver nitrate, and f_{\pm} is the mean ionic activity coefficient.

Since eq. 1 can hardly represent a single kinetic step, it may be split into a postulated association equilibrium between two of the three species, and the rate-determining step proper may be taken as the reaction between the result of this association and the remaining species. Since silver nitrate ion pairs are known to exist in solution (especially at low dielectric constant), it seems reasonable to interpret eq. 1 as $(\text{AgNO}_3) + \text{RI} \rightarrow \text{transition state}$, where parentheses are used to indicate an ion pair. This leads at once to the kinetic expression

$$-dc/dt = kc^2(1 - \gamma) \quad (3)$$

(1) M. J. Jaycock and G. D. Parfitt, *Trans. Faraday Soc.*, **57**, 791 (1961).

(2) K. A. Burke and F. G. Donnan, *J. Chem. Soc.*, **85**, 555 (1904).

(3) F. G. Donnan and K. A. Burke, *Z. physik. Chem.*, **69**, 148 (1909).

(4) F. G. Donnan and H. E. Potts, *J. Chem. Soc.*, **97**, 1882 (1910).

(5) E. Melendez-Andreu, *Ann. Chim. (Paris)*, **7**, 695 (1962).

(6) G. Senter, *J. Chem. Soc.*, **97**, 346 (1910).

(7) E. D. Hughes, C. K. Ingold, and S. Masterman, *ibid.*, 1236 (1937).

(8) G. S. Hammond, M. F. Hawthorne, J. H. Waters, and B. M. Graybill, *J. Am. Chem. Soc.*, **82**, 704 (1960).

(9) R. M. Fuoss, *ibid.*, **81**, 2659 (1959).

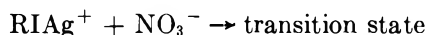
(10) G. D. Parfitt and A. L. Smith, *Trans. Faraday Soc.*, **59**, 257 (1963).

(11) N. Kornblum, R. A. Smiley, R. K. Blackwood, and D. C. Iffland, *J. Am. Chem. Soc.*, **77**, 6269 (1955).

but, since $K_A = (1 - \gamma)/c\gamma^2f_{\pm}^2$, where K_A is the association constant for the silver nitrate equilibrium, eq. 3 reduces to

$$-dc/dt = kK_Ac^3\gamma^2f_{\pm}^2$$

which is equivalent to eq. 2. An alternative interpretation of eq. 1 as



will also lead to expressions equivalent to eq. 2 and 3.

In hydroxylic solvents nitric acid appears as a product of the reaction yielding nitrate ions which will participate in the reaction. Then

$$K_A = (1 - \gamma)/\gamma f_{\pm}^2(c\gamma + c'\gamma') \quad (4)$$

where the primed symbols refer to nitric acid. In the simple case that the reaction is supposed to produce nitric acid in stoichiometric quantities (actually 70% or more in ethanol-water mixtures³) and K_A' is assumed equal to K_A (in fact, $K_A' < K_A$ in ethanol), then $\gamma = \gamma'$ and $c' = c_0 - c$, where the subscript 0 refers to initial quantities, yielding, from eq. 4, $1 - \gamma = K_Ac_0\gamma^2f_{\pm}^2$. Since, under the assumed simple conditions, the ionic strength remains constant, the activity coefficient is also constant, leading to $1 - \gamma = \text{constant}$, which, combined with eq. 3, gives

$$-dc/dt = k''c^2 \quad (5)$$

where $k'' = k(1 - \gamma)_0$ so that a given reaction would follow a simple second-order equation in stoichiometric concentrations. A plot of c^{-1} vs. t is now linear and of slope k'' whereas eq. 3 predicts that such a plot is concave to the time axis of slope, at any time, of $k(1 - \gamma)$. Even though the simple conditions assumed above do not fully apply, some straightening of the c^{-1} vs. t plot will enable initial slopes (independent of products) and, hence, k values to be obtained more accurately.

The addition of the nitrate of an indifferent cation will, on the assumed mechanism, increase the reaction rate by increasing the concentration of silver nitrate ion pairs. Equation 4 again applies, and, for nitrates such as KNO_3 ¹⁰ and NH_4NO_3 , the K_A value for the added nitrate may be taken equal to that for silver nitrate without great error.

Comparison of Kinetic Analysis with Experimental Data

Burke and Donnan² found that, for the reaction between silver nitrate and both ethyl and butyl iodides in ethanolic solution, the (apparent) second-order rate constant, k'' , calculated from $-dc/dt = k''c^2$, remained almost constant in the course of any one reaction but varied with the initial concentration of

reactants (at equal concentrations) according to $k'' = (\text{constant})c_0^{0.53}$. Thus, application of eq. 5 predicts that a plot of $\log(1 - \gamma)_0$ vs. $\log c_0$ will have a slope of 0.53. Such a plot, using γ -values calculated from conductance data¹⁰ over the range $c_0 < 20 \text{ mM}$, is shown in Figure 1. The result is a curve of slope varying between 0.4 and 0.6, which is in good agreement with the experiments of Burke and Donnan. If the value of K_A from conductance data (210 M^{-1}) is in error, it is most probable that association has been overestimated.¹² Reduction of K_A to 8 M^{-1} , as found¹⁰ in the 70 wt. % ethanol-water mixture, only causes an increase in $d \log(1 - \gamma)_0/d \log c_0$ to ~ 0.7 .

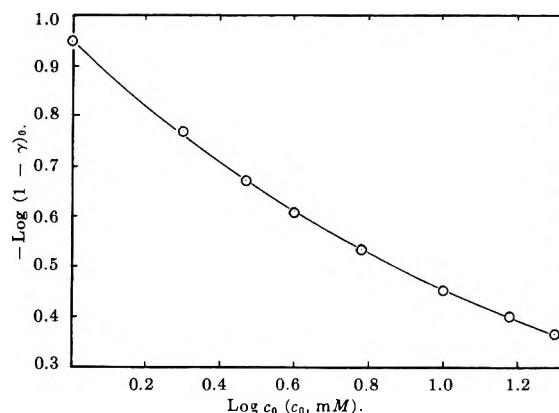


Figure 1. Plot of $\log(1 - \gamma)_0$ vs. concentration c_0 (mM) for silver nitrate in ethanol; γ is the degree of dissociation of silver nitrate.

Burke and Donnan also studied the effect of adding ammonium nitrate to the initial reaction mixture. In the range of concentrations for which values are available, they found that the value of k'' for a reaction initially 12.5 mM, with respect to ethyl iodide, silver nitrate, and ammonium nitrate, was greater than that found in the absence of ammonium nitrate by a factor of 1.2. If the ammonium nitrate is taken to have approximately the same value of K_A as silver nitrate, this factor is expected, on the ion pair mechanism, to be the ratio of the $(1 - \gamma)$ value at 25 mM to that at 12.5 mM, which, from the data quoted¹⁰ and plotted in Figure 1, is $0.46/0.38 = 1.2$. Calcium nitrate caused smaller increases in rate, as expected in view of increased ionic strength and association effects introduced by the divalent cation.

For reactions in solvents containing significant amounts of water where the nitric acid is appreciably ionized, the virtual constancy of k'' for a given reac-

(12) R. L. Kay and J. L. Dye, *Proc. Natl. Acad. Sci. U. S.*, **49**, 5 (1963).

tion is explained immediately by eq. 5: In pure ethanol the limited dissociation of nitric acid, together with the side reaction producing ethyl nitrate rather than nitric acid to the extent of $\sim 30\%$, makes the virtual constancy of k'' more difficult to explain, though the ionization of the nitric acid is still sufficient to make the reaction difficult to follow conductometrically.¹³

In the case of nonhydroxylic solvents, such as acetonitrile, where no nitric acid is produced, the value of k'' does, as expected, decrease during the course of reaction.⁸ Furthermore, when silver lactate replaces silver nitrate in ethanol-water mixtures, the value of k'' again decreases as the reaction proceeds,⁴ which is exactly as expected in view of the weak nature of lactic acid.

The ion-pair mechanism predicts that the reaction rate will decrease as the dielectric constant is raised in moving from ethanol to water as solvent, by the ratio of the $(1 - \gamma)$ values in the two solvents which is ~ 80 (γ in water calculated from an extrapolated K_A value¹⁰ and stoichiometric activity coefficients¹⁴).

As observed, the reaction with methyl or ethyl iodide³ is only decreased by a factor of ~ 7 ; the rate does not change monotonously, but it is not expected that the silver nitrate ion pair will remain equally reactive in conditions of competitive solvation obtaining in mixtures of polar solvents.

The recent work of Melendez-Andreu⁵ using an acetone-water mixture provides good support for the proposed mechanism involving the silver nitrate ion pair. The reactions of alkyl bromides, from methyl to n -hexyl, with silver nitrate and perchlorate were studied and found (by means of the Leffler plot¹⁵) to be of the same mechanism for all the bromides in all the solvent mixtures. The reaction with silver nitrate is particularly rapid in acetone, and it is significant that silver nitrate is a particularly weak electrolyte in this solvent. Silver perchlorate, which is not as weak in acetone,¹⁶ reacts much more slowly, even though in water-rich mixtures, where the two electrolytes are both strong, the rates are very similar. It is evident that the rapid rate of the silver nitrate reaction in acetone cannot be due to a high reactivity of the silver ion in this solvent and also can hardly be due to the increased nucleophilic character of a desolvated nitrate ion since the transport number for this ion in silver nitrate in acetone (0.58) is little different from that in water (0.54) and less than that in ethanol (0.61). The considerable association of silver nitrate in acetone, which may be due to stabilization of the ion pair itself in this solvent,¹⁷ explains the high reaction rate, at once, if the ion pair is the reacting species.

We conclude, therefore, that the suggestion of

Donnan as to the mechanism of the silver nitrate-alkyl halide reaction was essentially correct for many solvents despite later criticisms.

(13) A. G. Walton, Thesis, University of Nottingham, 1960.

(14) R. Parsons, "Handbook of Electrochemical Constants," Butterworth and Co., Ltd., London, 1959.

(15) J. E. Leffler, *J. Org. Chem.*, **20**, 1202 (1955).

(16) V. S. Griffiths, K. S. Lawrence, and M. L. Pearce, *J. Chem. Soc.*, 3998 (1958).

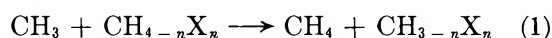
(17) W. R. Gilkerson, *J. Chem. Phys.*, **25**, 1199 (1956).

The Reaction of Methyl Radicals with Methyl and Methylene Fluoride

by G. O. Pritchard, J. T. Bryant,
and R. L. Thommarson

Department of Chemistry, University of California, Santa Barbara, California 93018 (Received July 29, 1964)

Raal and Steacie¹ have observed a significant decrease in the activation energy for H atom abstraction by methyl radicals with increasing halogenation of methane



For X = chlorine, and $n = 1, 2,$ and 3 , they obtained values of E_1 of 9.4, 7.2, and 5.8 kcal. mole⁻¹, respectively. For X = fluorine, and $n = 1$ and 2 , E_1 was found to decrease from 8.7 to 6.2 kcal. mole⁻¹. A similar trend was obtained with methyl and methylene bromide. They conclude that there is a progressive decline in the magnitude of the C-H bond strength with increasing halogenation, leading to an enhanced "activity" of hydrogen atoms in substituted methanes.

While this generalization is correct for chloromethanes,² it is certainly not correct for fluoromethanes.² We³ have found E_1 using CF_3H to be 10.2 ± 0.2 kcal. mole⁻¹, and the most likely value^{3,4} for $D(\text{CF}_3-\text{H})$ is close to 105 kcal. mole⁻¹. We have therefore re-determined E_1 for CFH_3 and CF_2H_2 .

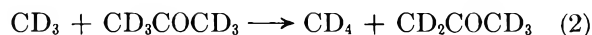
(1) F. A. Raal and E. W. R. Steacie, *J. Chem. Phys.*, **20**, 578 (1952).

(2) C. T. Mortimer, "Reaction Heats and Bond Strengths," Pergamon Press, London, 1962, pp. 132-134.

(3) G. O. Pritchard and R. L. Thommarson, *J. Phys. Chem.*, **68**, 568 (1964).

(4) E. Whittle, private communication; from unpublished bromination experiments. This is some 4 kcal. lower than the previous value, see P. Corbett, A. M. Tarr, and E. Whittle, *Trans. Faraday Soc.*, **59**, 1609 (1963).

The experimental method was identical with that described previously for the CF_3H experiments,³ in which reaction 1 competed with



The fluoromethanes were obtained commercially and purified by repeated low temperature fractionation. Their mass spectra indicated no detectable impurities and they were coincident with the previously published spectra for the two compounds.⁵ In the CFH_3 experiments, the pressure of CFH_3 was approximately 8 cm., and that of the ketone about 3 cm. In the CF_2H_2 experiments, the respective pressures were 5 and 3.5 cm. The data for CF_2H_2 are collected in Table I. The $\text{CD}_3\text{H}/\text{CD}_4$ ratios have been corrected for the d_5 impurity in the acetone- d_6 .

Table I: Data for the Competitive System:
 $\text{CD}_3 + \text{CH}_2\text{F}_2 \longrightarrow \text{CD}_3\text{H} + \text{CHF}_2$ (1) and
 $\text{CD}_3 + \text{CD}_3\text{COCD}_3 \longrightarrow \text{CD}_4 + \text{CD}_2\text{COCD}_3$ (2)

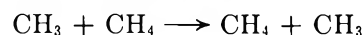
Temp., °C.	$\frac{[\text{CH}_2\text{F}_2]}{[\text{acetone-}d_6]}$	$\frac{[\text{CD}_3\text{H}]}{[\text{CD}_4]}$	$\frac{k_2}{k_1}$
122	1.03	1.22	1.19
143	1.72	1.64	1.29
164	1.69	1.52	1.37
177	1.48	1.29	1.44
198	1.12	0.98	1.47
222	1.73	1.30	1.57
239	1.55	1.08	1.70
268	2.11	1.29	1.83
301	1.36	0.82	1.91

A least-squares treatment of the Arrhenius plot for CF_2H_2 gives $k_2/k_1 = 5.5 \exp[-1200/RT]$. Taking $E_2 = 11.4 \pm 0.2$ kcal. mole⁻¹ (assuming zero activation energy for CD_3 radical recombination), we obtain E_1 (for CF_2H_2) = 10.2 ± 0.2 kcal. mole⁻¹. An average of 17 runs with CFH_3 in the temperature range 193 to 331° yielded $k_2/k_1 = 3.2 \pm 0.2$ (the ratio being 3.18 at 193° and 3.41 at 331°). This scatter was not particularly satisfactory, but it seems valid to equate E_1 (for CFH_3) with $E_2 = 11.4 \pm 0.2$ kcal. mole⁻¹. It is apparent that the activation energies given by Raal and Steacie¹ for these two reactions are markedly in error. Trotman-Dickenson⁶ has remarked that the results may be unreliable because complicating side reactions probably occurred. The differences in the two sets of determinations are well beyond the limit of being low by 1 kcal. mole⁻¹, an effect which has been observed when acetone- d_6 is used as the radical source.⁷

However, we must comment that below 200° we were unable to obtain reproducible data with the CFH_3 system. This was despite repeated careful checks on the purity of the compounds and the condition of the quartz reaction cell. Periodic blank runs with acetone- d_6 alone consistently gave reproducible $\text{CD}_3\text{H}/\text{CD}_4$ ratios. From 200° down to ~100° we obtained generally decreasing values of k_2/k_1 , which were very scattered. These indicated that $E_2 - E_1 = \sim 2.7 \pm 0.5$ kcal. mole⁻¹, which yields $E_1 = 8.7 \pm 0.7$ kcal. mole⁻¹, in complete, but probably fortuitous, agreement with Raal and Steacie's figure¹ for this reaction. These authors also obtained their result in the temperature range 125 to 211°. Our data from the CF_2H_2 system were completely reproducible over the entire temperature range, and a comparison of the results derived from the three fluoromethane systems strongly suggests that we disregard the data obtained below 200° in the CFH_3 system. The cause of the discrepancy is not obvious; it is plausible that an undetected trace impurity of a substance containing very labile H atoms is responsible.

Taking the value for the pre-exponential factor⁶ $A_2 = 6.3 \times 10^{11}$ mole⁻¹ cc. sec.⁻¹ gives normal steric factors for the two reactions of about 10^{-3} .

We intend to present data on reaction -1 for CFH_2 and CF_2H radicals. Our initial work⁸ on the photolysis of $(\text{CFH}_2)_2\text{CO}$ indicates that the reactivity of CFH_2 radicals with regard to H atom abstraction lies between that of CF_3 and CH_3 radicals. The activation energies for the two reactions



are about 10 and 14 kcal. mole⁻¹, respectively.⁹ We may therefore postulate that reaction 1 for CFH_3 and CF_2H_2 will be close to being thermoneutral, and that $D(\text{CFH}_2\text{-H})$ and $D(\text{CF}_2\text{H-H})$ will not be very different from $D(\text{CH}_3\text{-H})$.

Acknowledgments. We are very grateful to Dr. Whittle for communication of his results prior to publication, and to the National Science Foundation for support of this work.

(5) J. R. Majer, *Advan. Fluorine Chem.*, **2**, 55 (1961).

(6) A. F. Trotman-Dickenson, "Gas Kinetics," Butterworth and Co. Ltd., London, 1955, p. 202.

(7) H. O. Pritchard and G. O. Pritchard, *Can. J. Chem.*, **41**, 3042 (1963).

(8) G. O. Pritchard, M. Venugopalan, and T. F. Graham, *J. Phys. Chem.*, **68**, 1786 (1964).

(9) G. O. Pritchard and G. H. Miller, *J. Chem. Phys.*, **35**, 1135 (1961).

γ -Radiation-Induced Isomerization of Cyclohexanone to 5-Hexenal in the Liquid Phase^{1a}

by Ajit Singh and Gordon R. Freeman

Department of Chemistry, University of Alberta, Edmonton, Alberta, Canada (Received July 29, 1964)

When liquid cyclohexanone is irradiated with Co^{60} γ -rays, the compound isomerizes to 5-hexenal with a yield of 0.85 G unit.^{1b} The present communication includes evidence that the lowest triplet state of cyclohexanone is a precursor of or a reactant in the isomerization reaction.

Experimental

The techniques were similar to those described earlier.^{1b}

Various solutions of benzene and of 2,3-dimethyl-1,3-butadiene (DMB) in cyclohexanone were irradiated to a dose of $5.92 \pm 0.12 \times 10^{-4}$ e.v./e⁻, which is about 1.9×10^{20} e.v./ml., with Co^{60} γ -rays. The total dose was kept constant in units of e.v./e⁻ so that the cyclohexanone in all solutions received the same dose. The dose rate was 5×10^{18} e.v./ml. hr. and the temperature of the samples was $24 \pm 3^\circ$.

Two solutions of oxygen in cyclohexanone were irradiated to the above dose and analyzed to compare the effects of oxygen and DMB on the product yields.

Results and Discussion

The effects of benzene and DMB on the yield of 5-hexenal are shown in Figure 1. For the benzene solutions, the value of $G(5\text{-hexenal})$ increases with increasing benzene concentration and passes through a maximum at an electron fraction of benzene of about 0.6. For DMB solutions, the yield of 5-hexenal drops very rapidly at first and then decreases more slowly as the electron fraction of the solute, ϵ_s , is increased beyond about 2×10^{-3} (Figures 1B and C).

Oxygen also decreases the yield of 5-hexenal (Table I), and it is a more efficient inhibitor than is DMB.

Blank analyses were made on all solutions and a very slow dark reaction between cyclohexanone and oxygen was noted.

Benzene sensitizes the formation of 5-hexenal, whereas DMB and oxygen inhibit it. Consideration of the energies of the lowest excited singlet and triplet states and the ionization potentials of the molecules involved (Table II) indicates that these effects might be due to energy transfer processes that involve the

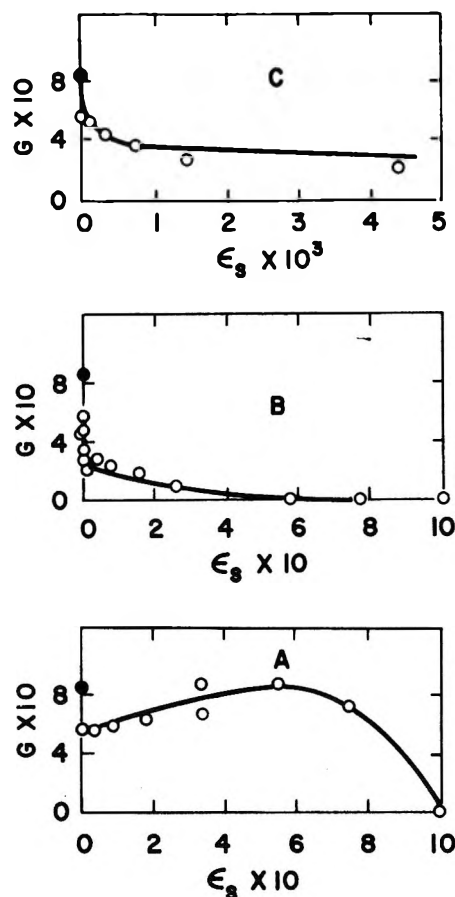


Figure 1. 5-Hexenal: ϵ_s = electron fraction of the solute; dose = $5.92 \pm 0.12 \times 10^{-4}$ e.v./e⁻. Filled points refer to yield in pure cyclohexanone at zero dose: A, benzene solutions; B and C, DMB solutions.

Table I: Oxygen Solutions (Dose = $5.92 \pm 0.12 \times 10^{-4}$ e.v./e⁻)

Pressure of O ₂ in the sample, ^a mm.	Electron fraction of O ₂ ^b	$G(5\text{-Hexenal})$	$G(\text{C}_4 \text{ hydrocarbons})$
0	0	0.56 ± 0.03	0.29 ± 0.02
71	2.5×10^{-5}	0.22 ± 0.02	0.21 ± 0.02
412	14.6×10^{-5}	0.15 ± 0.02	0.20 ± 0.02

^a Cyclohexanone, 2 ml.; oxygen, 10 ml. ^b To calculate the electron fraction of dissolved oxygen, its solubility has been assumed to be 0.2 ml./ml. of the ketone, on the basis of the values for the solubility of oxygen in some oxygenated organic compounds ("International Critical Tables").

(1) (a) This work received financial assistance from the National Research Council of Canada; (b) A. Singh and G. R. Freeman, *Can. J. Chem.*, **42**, 1869, 1877 (1964).

lowest triplet state of cyclohexanone. The ground state of oxygen is a triplet, while those of the other molecules are singlets. Thus, for reasons of spin conservation, the excited singlet states of oxygen are to be grouped with the excited triplet states of the other molecules.

Table II: Energies (in e.v.) of the Lowest Excited States and Ionization Potentials

Compound	Triplet	Singlet	Ionization potential
Cyclohexanone	2.8 ^a	4.27 ^b	9.14 ^d
Benzene	3.58 ^e	4.76 ^{b,e}	9.25 ^d
DMB	~2.6 ^f	5.4 ^b	~8.7 ^g
Oxygen	4.35 ^h	0.98 ^h 1.64 ^h	12.2 ^h

^a Estimated by comparison with the states of cyclopentanone.^{b,c}
^b C. N. R. Rao, "Ultra-Violet and Visible Spectroscopy; Chemical Applications," Butterworth and Co., Ltd., London, 1961.
^c S. R. LaPaglia and B. C. Roquette, *J. Phys. Chem.*, **66**, 1739 (1962).
^d K. Watanabe, T. Nakayama, and J. Mottl, *J. Quant. Spectry. Radiative Transfer*, **2**, 369 (1962).
^e C. Reid, "Excited States in Chemistry and Biology," Butterworth and Co., Ltd., London, 1957.
^f G. S. Hammond, N. J. Turro, and P. A. Leermakers, *J. Phys. Chem.*, **66**, 1144 (1962).
^g W. C. Price, R. Bralsford, P. V. Harris, and R. G. Ridley, *Spectrochim. Acta*, **14**, 45 (1959).
^h G. Herzberg, "Molecular Spectra and Molecular Structure. I. Spectra of Diatomic Molecules," 2nd Ed., D. Van Nostrand Co., Toronto, 1950.

The quenching effects of oxygen² and conjugated diolefins³ on triplet states have been discussed elsewhere. We suggest that the lowest triplet state of cyclohexanone is a precursor of 5-hexenal in the radiolytic system.

The yield of 5-hexenal is reduced to about a third of the initial value ($G_i = 0.85$) by about 2×10^{-3} electron fraction of DMB. The inhibition of the remaining third of the 5-hexenal requires a more than 100-fold larger concentration of DMB (Figure 1B). Oxygen is an even more efficient inhibitor than is DMB because about 3×10^{-5} electron fraction of oxygen reduces 5-hexenal to about one-fourth of the initial yield (Table I). Much larger concentrations of oxygen are required to inhibit the formation of the remaining one-fourth of the 5-hexenal (a sixfold increase in oxygen concentration causes a relatively small further decrease in the 5-hexenal yield, see Table I).

It thus appears that 5-hexenal has two precursors, one of which (roughly 70% of the total) is the lowest triplet state of cyclohexanone. The other precursor (roughly 30% of the total) has several possible identi-

ties, between which the present work does not distinguish.

The present results are consistent with either a concerted or a diradical intermediate mechanism for the isomerization of cyclohexanone to 5-hexenal. It should be mentioned that all of the evidence that has been presented in support of concerted mechanisms in the photoisomerization of cyclic ketones to open chain olefinic aldehydes⁴ can be equally well interpreted on the basis of mechanisms that involve diradical intermediates.

Kinetic Considerations. Crude values for diffusion-controlled rate constants for reactions between cyclohexanone molecules and oxygen or DMB molecules can be calculated by a method reported earlier.⁵ The value for oxygen in liquid cyclohexanone at 25° would be about 1×10^{10} l./mole sec. and that for DMB in cyclohexanone would be about half this value.

Approximately half of the precursors of 5-hexenal are quenched at a DMB concentration of $2 \times 10^{-3} M$. The average time between encounters of any given cyclohexanone molecule and a DMB molecule would be 1×10^{-7} sec. at this concentration. If the inhibition of 5-hexenal formation occurs by a diffusion-controlled reaction, the lifetime of the precursor with respect to the isomerization reaction is 10^{-7} sec. This assumes that DMB deactivates the precursor at the first encounter. A similar calculation for the oxygen solutions also indicates that the 5-hexenal precursor has a lifetime of 10^{-7} sec. It seems unlikely that a diradical would have a lifetime as great as 10^{-7} sec.,⁶ so the oxygen and DMB do not interact with diradicals in these systems. This conclusion has no bearing upon whether or not diradicals are intermediates in the formation of 5-hexenal. The conclusion is simply that if diradicals are involved, oxygen and DMB interfere with a precursor of the diradicals. This is consistent with the previous conclusion that it is the lowest triplet state of cyclohexanone that interacts with oxygen and DMB.

Other Products of C-C Bond Cleavage Reactions. Carbon monoxide, C₅ hydrocarbons, and ethylene are also products of the radiolysis of cyclohexanone.¹

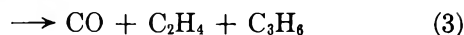
(2) R. M. Hochstrasser and F. B. Porter, *Quart. Rev. (London)*, **14**, 146 (1960).

(3) G. S. Hammond and P. A. Leermakers, *J. Phys. Chem.*, **66**, 1144, 1148 (1962).

(4) (a) R. Srinivasan, *J. Am. Chem. Soc.*, **81**, 2601 (1959); (b) *ibid.*, **83**, 4344, 4348 (1961); (c) "Advances in Photochemistry," Vol. I, W. A. Noyes, Jr., G. S. Hammond, and J. N. Pitts, Jr., Eds., Interscience Publishers, Inc., New York, N. Y., 1963, p. 83.

(5) G. R. Freeman, *J. Chem. Phys.*, **39**, 988 (1963).

(6) The period for internal rotation in the diradical would be of the order of 10^{-12} sec., so intramolecular recombination or disproportionation would probably occur in a time much less than 10^{-7} sec.



The cyclohexanone molecule requires more energy to undergo reactions 3 and 4 than it does to undergo reaction 2. It requires more energy to undergo reaction 2 than it does to undergo reaction 1. In general, the higher the energy state of a species, the shorter is its lifetime, and the smaller is the probability that the species will enter into sensitization or quenching reactions. Thus, one would expect that the yield of C_5 hydrocarbons would be less sensitive to the presence of additives than was the 5-hexenal yield. The yield of ethylene should be less sensitive than the C_5 hydrocarbon yield. The sensitivity of the CO yield should be intermediate between those of the C_5 and the ethylene yields. All these things were observed. (See Figure 2 and Table I. The effect of DMB on the C_5 yield could not be measured due to analytical difficulty.)

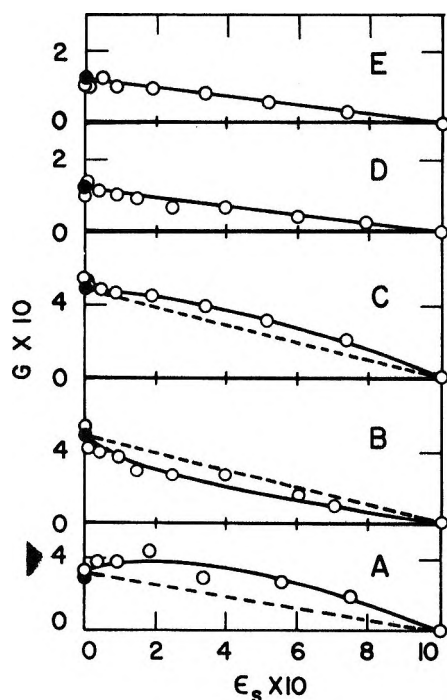


Figure 2. Other products of C-C cleavage reactions: ϵ_s = electron fraction of solute; dose = $5.92 \pm 0.12 \times 10^{-1}$ e.v./e⁻. Filled points refer to yield in pure cyclohexanone at zero dose: A, C_5 hydrocarbons from benzene solutions; B, CO from DMB solutions; C, CO from benzene solutions; D, C_2H_4 from DMB solutions; E, C_2H_4 from benzene solutions.

Effects of Charge and Nickel Ion on Proton Chemical Shifts of Glycyl Peptides

by Raj Mathur and R. Bruce Martin

Cobb Chemical Laboratory, University of Virginia, Charlottesville, Virginia (Received August 6, 1964)

Beginning with glycine and proceeding through tetraglycine, the series of glycyl peptides provides a set of compounds of known structure and increasing length upon which to study the effects of charge changes at the termini on the proton magnetic resonance spectra of pairs of equivalent protons at varying distances from the protonation sites. Such a study on this comparatively simple series would seem a prerequisite to the understanding of the effects of protonating equilibria in more complicated systems. Furthermore, since there is an ammonium group at one terminus and a carboxylic acid group at the other, effects of ionization at two different kinds of groups are simultaneously studied. In this note the proton magnetic resonance spectra of cationic, dipolar ion, and anionic glycyl peptides are reported.

When base is added to solutions containing divalent nickel ion and one equivalent of triglycine or tetraglycine, the color of the solution changes from blue to yellow. During the course of this color change, the nickel ion promotes ionization of amide hydrogens in a cooperative manner over a narrow pH range.¹ In solution, an equimolar mixture of triglycine and nickel chloride is blue and fully paramagnetic. Addition of one equivalent of base effects little change as only an ammonium hydrogen is removed, and nickel ion associates at this nitrogen. Addition of a second equivalent of base yields a solution that is half as paramagnetic as the above and half as yellow as when three equivalents of base have been added, in which case the solution exhibits little paramagnetism.² Thus increasing yellow color directly parallels loss of paramagnetism and both changes are in accord with the cooperative nature of the transition deduced from titration data. After the addition of the second equivalent of base, half of the nickel complexes possess two ionized amide hydrogens and half retain both amide

(1) R. B. Martin, M. Chamberlin, and J. T. Edsall, *J. Am. Chem. Soc.*, **82**, 495 (1960).

(2) T. D. Coyle and R. B. Martin, unpublished experiments performed in Oxford, England, in 1961. The n.m.r. method of Evans³ was used to estimate the relative paramagnetic susceptibilities on a 30-Mc. machine with solutions containing 2% *t*-butyl alcohol.

(3) D. F. Evans, *J. Chem. Soc.*, 2003 (1959).

hydrogens rather than all complexes containing ligands with one of two amide hydrogens ionized. This cooperative transition has been interpreted as a change in stereochemistry about the nickel ion from octahedral to planar. Cupric ion also promotes amide hydrogen ionization but in a normal, noncooperative manner.¹

Curiously, the magnetic susceptibility of the solid, yellow-orange, fully amide hydrogen ionized nickel triglycine complex, prepared from solutions equivalent to that mentioned above displaying almost no paramagnetism, is about 1.4 Bohr magnetons.⁴ This value is intermediate between the zero value of a low-spin complex and a value of about 2.9 Bohr magnetons for a high-spin nickel ion complex. Results of X-ray crystal structure analyses of this or similar yellow nickel ion complexes would be of considerable interest.

In this research, we attempted to obtain proton magnetic resonance solution spectra of yellow complexes of nickel ions and several amides and dipeptides. The p.m.r. solution spectra of the yellow nickel ion tetraglycine complex are reported. The existence of this type of spectra indicates that this complex is also diamagnetic. Unfortunately, we were unable to prepare yellow solutions of nickel ion and triglycine, glycinamide,¹ or glycylhistidine⁵ of sufficiently low paramagnetism so that their p.m.r. spectra could also be recorded. A spectrum was observed in yellow solutions containing histidylhistidine⁵ and nickel ion in a 6 to 1 ratio with excess base. Attempts to procure a spectrum of the complex by reducing the dipeptide to metal ion ratio yielded considerably broadened spectra.

Experimental

Proton magnetic resonance spectra were obtained with a Varian A-60 spectrometer at room temperature. About 0.5 mole of commercially obtainable materials was placed in D₂O solutions containing about 2% acetonitrile.⁶ The position of the acetonitrile reference peak is independent of added acid, base, or metal ions when the spectra are recorded immediately. In basic solutions acetonitrile eventually decomposes.

Results

Only the carbon-bound hydrogens exchange slowly enough with D₂O so that their proton magnetic resonance spectra may be recorded under the conditions of this study. Solutions (~0.5 M) were prepared with amino acid or peptide. Spectra were then taken on neutral solutions or on solutions with one equivalent plus a 5% excess of DCl or NaOD. This amount was deemed sufficient to yield predominantly the positive or negative peptide species without introducing

additional solvent effects. The spectra of the zinc-(glycinate)₂ complex were also obtained. Four equivalents of base were added to a solution containing equimolar amounts of tetraglycine and nickel chloride to give the yellow diamagnetic complex with three ionized amide hydrogens.¹ The chemical shifts downfield from acetonitrile as an internal standard in parts per million are recorded in Table I.

Table I: Proton Chemical Shifts as a Function of Charge

Compound	Charge	Chemical shifts in p.p.m. ^a
Glycine	+	1.85
	+ -	1.47
	-	1.08
Glycine + 0.5-Zn ⁺² + OH ⁻	0	1.25
Glycinamide	+	1.76
	0	1.28
Glycylglycine	+	2.03(D), 1.84(A)
	+ -	1.85(D), 1.80(A)
	-	1.71(D), 1.29(A)
Triglycine	+	2.05(D), 2.04(B), 1.91(A)
	+ -	2.03(B), 1.89(A), 1.77(D)
	-	1.95 ^b (B), 1.73(D), 1.34(A)
Tetraglycine	+	2.07(D), 2.03(B), 2.03(C), 1.93(A)
	-	2.03 ^b (C), 1.99 ^b (B), 1.77(D), 1.38(A)
Tetraglycine + Ni ⁺² + 4OH ⁻	-2	1.40(B), 1.40(C), 1.13, 1.08

^a Downfield shifts in parts per million with respect to acetonitrile as internal standard. ^b Peak disappears with time.

In the negatively charged peptides, peaks at 1.95 p.p.m. in triglycine and 2.03 and 1.99 p.p.m. in tetraglycine decrease in height over a period of several hours. The 2.03-p.p.m. peak in tetraglycine disappears more rapidly than the peak at 1.99 p.p.m. Evidently, hydrogens more downfield than about 1.9 p.p.m. in basic solutions exchange with deuterium of the solvent. Placement in alkaline solutions of D₂O provides an easy way to deuterate these compounds.

The total upfield shifts in the nickel ion complex of tetraglycine are about four times greater than can be accounted for by a simple increase of one negative charge as compared with the spectra of tetraglycine in basic solution. Since these upfield shifts are so large that peak identification is difficult, an additional ex-

(4) R. B. Martin, *Federation Proc.*, **20**, Suppl. 10, 54 (1961).

(5) R. B. Martin and J. T. Edsall, *J. Am. Chem. Soc.*, **82**, 1107 (1960).

(6) R. A. Y. Jones, A. R. Katritzky, J. N. Murrell, and N. Sheppard, *J. Chem. Soc.*, 2576 (1962).

periment was performed. The two peaks at lowest field in tetraglycinate anion were permitted nearly to disappear by exchange in excess base. Then an equivalent amount of nickel chloride was added to the solution and the spectrum was compared with that obtained from a similar but freshly prepared solution containing nickel ion which had undergone little exchange. The peak at lowest field in the first solution was markedly lower than the same peak in the second solution, a difference indicating that the two pairs of lowest field hydrogens in tetraglycinate anion are also at lowest field in the nickel complex.

If excess tetraglycine is added to a solution containing the diamagnetic nickel-tetraglycine complex, two superimposed spectra appear corresponding to the free and complexed tetraglycine. Thus the exchange of nickel ion between tetraglycine molecules is slow.

Discussion

In addition to results, Table I also contains our assignments of the pairs of methylene hydrogens to glycol residues in the peptides. The N-terminal residue is designated A and the C-terminal residue D. Residues in intermediate positions are designated B and C from the N-terminal end. Thus the successive residues from the N terminus in tetraglycine are ABCD; triglycine contains no C residue. The assignments are made on the basis of the principles mentioned below. Assignments of protons with similar chemical shifts may be reversed. All assignments are consistent with those made from studies of downfield shifts and selective broadening upon addition of metal ions to solutions containing ligand and base.^{7,8} The assignments of the double peak at 1.40 p.p.m. in the nickel solution of tetraglycinate are made on the basis of the exchange experiment. We assign the two peaks at highest field in the nickel ion complex to A and D residues, but cannot distinguish between them. Compared to tetraglycinate anion, each of the four pairs of carbon-bound hydrogens is shifted upfield in the nickel tetraglycine complex.

Except for glycine, where they are about equal, deprotonation of an ammonium group causes about twice as great an upfield shift on A protons as deprotonation of a carboxylic acid group does on D protons. The carboxylic acid proton is one atom further removed from a methylene hydrogen than is an ammonium proton. Ammonium deprotonation also exerts a somewhat greater effect on a neighboring glycol residue hydrogen than does a carboxylic acid ionization. For example, in glycyglycine or triglycine the upfield shift of the D protons on going from dipolar ion to anion is greater than the upfield shift of the A

protons on passage from cation to dipolar ion. This conclusion holds even if the assignments of A and D protons are reversed in dipolar ion glycyglycine.

Previous studies have noted the downfield shift caused by addition of a diamagnetic metal ion to a solution containing the free base form of a ligand.⁷⁻⁹ This result, expected on the basis of additional positive charge near ligand hydrogens, is verified by the 0.17-p.p.m. downfield shift on the addition of zinc ion to a solution containing glycinate anion. More to the point, however, is a comparison of the shifts caused by complexed metal ions with ligands of the same net charge as those in the complex. Thus zero net charge zinc(glycinate)₂ exhibits an upfield shift of 0.22 p.p.m. compared to dipolar ion glycine. Lesser upfield shifts have been observed in zinc and cadmium ion complexes of histidine and in the zinc ion complex of cysteine when compared with free ligand of the same net charge as that of the ligand in the complex.¹⁰

The chemical shift of the diamagnetic nickel tetraglycine complex of net charge -2 cannot be compared directly with free ligand of the same net charge. The total upfield shift for all four pairs of carbon-bound hydrogens on passing from cationic tetraglycinium ion to anionic tetraglycinate is 0.89 p.p.m. An upfield shift of about 0.45 p.p.m. might then be expected on going from a -1 to a -2 charged species of tetraglycine. To this upfield shift of about 0.45 p.p.m. might be added a value of about 0.15 p.p.m. for the effect of a diamagnetic metal ion as noted above. The total predicted upfield shift of about 0.6 p.p.m. is about one-fourth of the observed total upfield shift of 2.16 p.p.m. on passing from tetraglycinate anion to doubly negative charged nickel tetraglycine complex. Thus diamagnetic nickel ion yields a much greater upfield shift than expected from a comparison with other diamagnetic metal ions and with free ligand of the same net charge. A similar conclusion has been reached with the diamagnetic nickel(cysteinate)₂ complex on comparison with the zinc(cysteinate)₂ complex.¹⁰ Therefore, the pronounced upfield shifts induced by diamagnetic nickel ion appear to be a feature of the diamagnetic metal ion and not of the ligands involved.

Acknowledgment. We thank Dr. Thomas D. Coyle for permission to quote the results of the experiments on the paramagnetic susceptibilities of the nickel-

(7) N. C. Li, L. Johnson, and J. Shoolery, *J. Phys. Chem.*, **65**, 1902 (1961).

(8) N. C. Li, R. L. Scruggs, and E. D. Becker, *J. Am. Chem. Soc.*, **84**, 4650 (1962).

(9) R. Mathur and N. C. Li, *ibid.*, **82**, 1289 (1964).

(10) R. B. Martin and R. Mathur, in preparation.

triglycine system with 0-3 equivalents of added base. This research was supported by a grant from the National Science Foundation.

The Reduction Principle in

Linear Viscoelasticity¹

by Hershel Markovitz

Mellon Institute, Pittsburgh, Pennsylvania
(Received August 8, 1964)

The reduction principle is one of the most useful tools in experimental viscoelasticity. It is most commonly used in connection with data obtained at different temperatures and it states that there exists a simple relation between such sets of data. For example, the dynamic shear storage modulus $G'(\omega, T_0)$ and the dynamic shear loss modulus $G''(\omega, T_0)$ for a reference temperature T_0 are related to the corresponding quantities for the temperature T by expressions of the form²

$$G'(\omega, T_0) = AG'(\omega a, T) \quad (1)$$

$$G''(\omega, T_0) = AG''(\omega a, T) \quad (2)$$

where A and a are functions of the temperatures T and T_0 . The purpose of this note is to show that the phenomenological theory of linear viscoelasticity determines, in part, the nature of A and a for fluids.

It has been shown³ that at low frequencies

$$G'(\omega, T) = [\eta_0(T)]^2 J_e(T) \omega^2 \quad (3)$$

$$G''(\omega, T) = [\eta_0(T)] \omega \quad (4)$$

where $\eta_0(T)$ and $J_e(T)$ are the zero-shear viscosity and the steady-state shear creep compliance, respectively, at the temperature T . Substitution of (3) into (1) and (4) into (2) leads to two equations which can be solved for A and a

$$a = \eta_0(T_0) J_e(T_0) / \eta_0(T) J_e(T) \quad (5)$$

$$A = J_e(T) / J_e(T_0) \quad (6)$$

One of the forms commonly used for the reduced variables can be obtained by replacing $J_e(T) / J_e(T_0)$ in these expressions with $T_0 \rho_0 / T \rho$.¹ Such a substitution is compatible with various molecular theories of the linear viscoelastic behavior of dilute polymer solutions, for example, that of Rouse.^{1,4}

It has been proposed that similar reduction principles hold for other independent variables, such as concentration and molecular weight. In the latter case, one

could then be led to expect that the shift factors should be very sensitive to molecular weight distribution since J_e is.¹

(1) This work was supported by the National Science Foundation.

(2) J. D. Ferry, "Viscoelastic Properties of Polymers," John Wiley and Sons, Inc., New York, N. Y., 1961.

(3) B. D. Coleman and H. Markovitz, *J. Appl. Phys.*, **35**, 1 (1964).

(4) P. E. Rouse, Jr., *J. Chem. Phys.*, **21**, 1272 (1953).

Prediction of the Heats of Activation for Viscous Flow in Simple Nonmetallic Liquids

by J. O'M. Bockris and S. R. Richards

The Electrochemistry Laboratory, The University of Pennsylvania,
Philadelphia, Pennsylvania 19104 (Received August 28, 1964)

Two approaches are recognized in the theory of liquids: (a) numerical values of the properties of the liquid are deduced by assuming an intermolecular force law; (b) alternative models are assumed and predictions of the numerical values of experimental quantities made on their bases to ascertain which model is the most useful in representing the structure of the liquid. A difficulty in this second approach has been that usually the equations upon which the predictions are made contain an adjustable parameter, determined by calibration.

Bockris and Richards¹ applied a version of the theory of holes originated by Fürth,² to predict values of equilibrium properties in simple molten salts. The holes considered differ significantly from those of "quasi-lattice" hole models: their sizes are thermally distributed. They can be regarded as arising from density fluctuations in the liquid.³

Bockris and Hooper⁴ deduced an equation for the self-diffusion coefficient on this basis. It is easy to convert this equation into one for viscosity. The result is

$$\eta = 1.03 \frac{kT\rho}{(m\gamma)^{1/2}} \exp\left(-\frac{\Delta S^*}{R}\right) \exp\left(\frac{\Delta H^*}{RT}\right) \quad (1)$$

where ρ is the density and γ is the surface tension of the liquid, and m is the mean mass of the ions in the

(1) J. O'M. Bockris and N. E. Richards, *Proc. Roy. Soc. (London)*, **A241**, 44 (1957).

(2) R. Fürth, *Proc. Cambridge Phil. Soc.*, **37**, 252 (1941).

(3) R. A. Swalin, *Acta Met.*, **7**, 736 (1959).

(4) J. O'M. Bockris and G. W. Hooper, *Discussions Faraday Soc.*, **32**, 218 (1961).

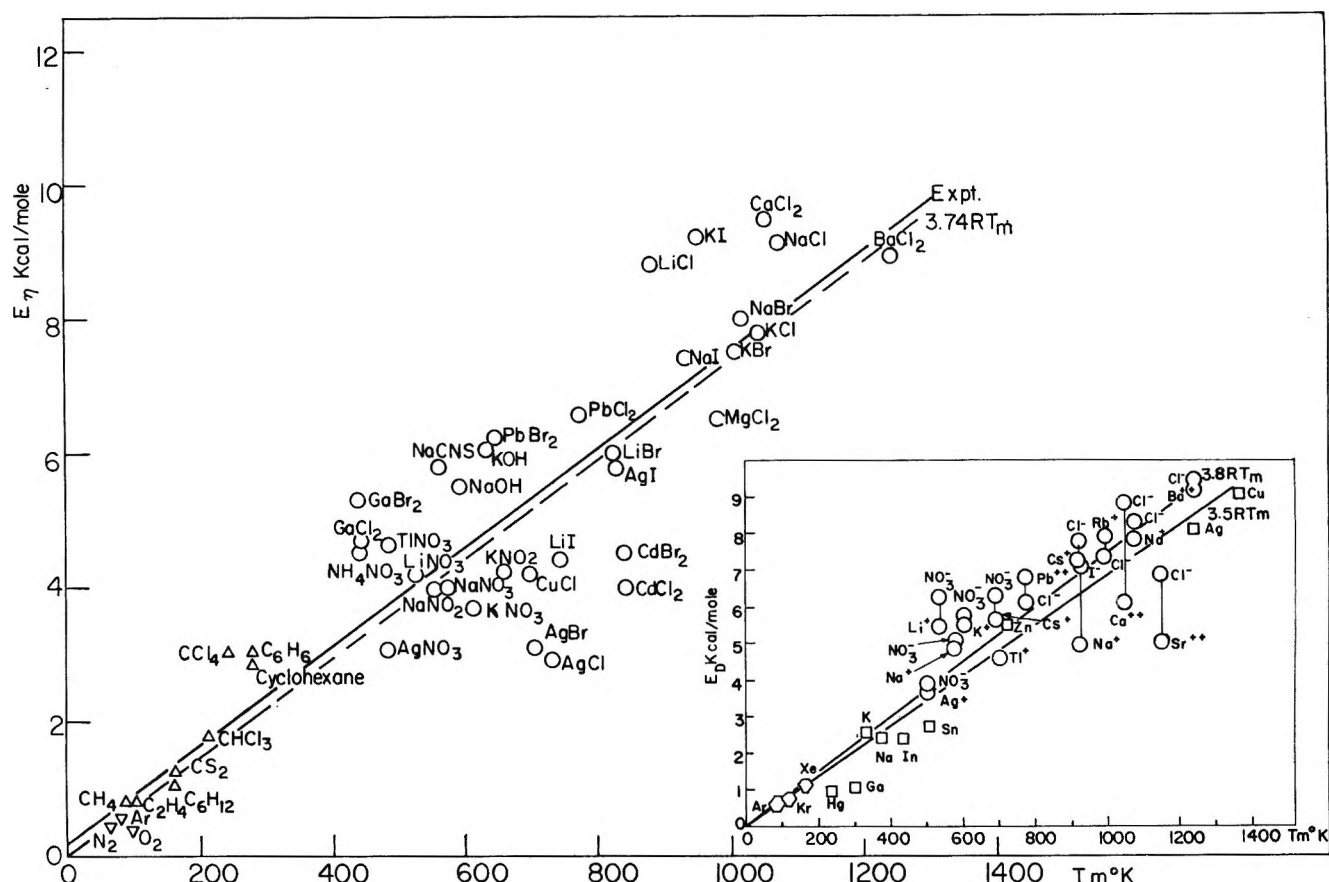


Figure 1. Energies of activation for viscous flow vs. melting temperature. Sources of data: for liquid gases and hydrocarbons, R. H. Ewell and H. Eyring, *J. Chem. Phys.*, **5**, 726 (1937); for molten salts, J. P. Frame, E. Rhodes, and A. R. Ubbelohde, *Trans. Faraday Soc.*, **55**, 2039 (1959); H. Bloom and E. Heymann, *Proc. Roy. Soc. (London)*, **A188**, 392 (1947); J. O'M. Bockris, E. H. Crook, H. Bloom, and N. E. Richards, *ibid.*, **A255**, 558 (1960); A. Klemm in "Molten Salt Chemistry," M. Blander, Ed., Interscience Publishers, Inc., New York, N. Y., 1964, Chapter 8. Inset: energies of activation for self-diffusion vs. melting temperature [after L. Nanis and J. O'M. Bockris, *J. Phys. Chem.*, **67**, 2865 (1963)].

molten salt. ΔS^* denotes the entropy of activation, and ΔH^* is given by

$$\Delta H^* = \Delta H_H + \Delta H_J^* \quad (2)$$

where ΔH_H is the heat content change in the formation of a mole of holes, and ΔH_J^* is the heat of activation for the movement of a particle from one site to another. ΔH_J^* is very much less than ΔH^* (see below), and the value of ΔH_H is that of Bockris and Hooper,⁴ namely $3.74RT_m$. Hence, for viscous flow

$$\Delta H^* \approx 3.74RT_m \quad (3)$$

The relation arises *independently of adjustable parameters*. It is compared with experimental heats of activation for viscous flow at constant pressure, E_η , for a large variety of liquids in Figure 1.

Analysis of the data shown in Figure 1 reveals that the line of best fit is

$$E_\eta = 7.32T_m + 220 \quad (4)$$

where E_η is in cal. mole⁻¹. The intercept value is within the limits of error of measurements of E_η . The regression coefficient of eq. 4 is 0.90. Liquefied gases and organic liquids of low molecular weight or near spherical symmetry fit the relation; E_η values for the molten metals fall below the line. As pointed out by Grosse,⁵ the latter group of liquids obey better a nonlinear relation in T_m given by

$$E_\eta = 0.431T_m^{1.348} \quad (5)$$

On the other hand, eq. 3 is obeyed for self-diffusion in the molten metals. Thus, while the mechanism for self-diffusion in the molten metals appears to be the same as that for fused salts (since both obey eq. 3), the same does not seem to be confirmed for viscous flow.

The equation deduced does not apply to associated

(5) A. V. Grosse, *J. Inorg. Nucl. Chem.*, **25**, 317 (1963).

liquids, because viscous flow in these is determined in rate not by the availability of holes, but by the breaking of bonds in the associated structure.⁶

Equation 3 would not be expected to be exact because it involves the approximation $\Delta H_f^* = 0$. In accordance with this, it is seen from Figure 1 that the experimental values tend to be a little higher than the prediction of eq. 3. Recent work⁷ in this laboratory on the heat of activation for self-diffusion in molten salts at constant volume (*i.e.*, $\Delta \bar{H}_f^*$) has shown that this is about $1/6$ of that at constant pressure in the case of molten sodium nitrate.

The agreement recorded here between the predicted and observed heats of activation for viscous flow strongly supports the hole model. Indeed, it became difficult to escape from this model for ionic liquids after the confrontation of the disparity between the volume change on melting and the free volume⁴ and after reliable knowledge became available⁸⁻¹¹ that the internuclear distance decreases upon fusion while the corresponding volume change is (*e.g.*, for the alkali halides) large and positive.

The model rested here produces successful predictions of both equilibrium^{1,11,12} and transport properties in ionic liquids.^{4,7,12,13} The latter are the only calculations in the field hitherto published which do not use adjustable parameters. It is pertinent to note that the work of Reiss, *et al.*,¹⁴ which gives rise to successful calculations of surface tension,¹⁵ compressibility,¹⁶ and interionic distance,¹⁷ also involves a consideration of the work of hole formation.

Acknowledgment. The authors are grateful to the Atomic Energy Commission for support of this work under Contract No. AT30-1-1769.

- (6) J. O'M. Bockris and D. C. Lowe, *Proc. Roy. Soc. (London)*, **A226**, 423 (1954).
 (7) M. K. Nagarajan, L. Nanis, and J. O'M. Bockris, *J. Phys. Chem.*, **68**, 2726 (1964).
 (8) V. I. Danilov and S. Ya. Krasnitskii, *Dokl. Akad. Nauk SSSR*, **101**, 661 (1955).
 (9) J. Zarzycki, *Compt. rend.*, **244**, 758 (1957); *J. phys. radium*, **18**, 65A (1957); **19**, 13A (1958).
 (10) H. A. Levy, P. A. Agron, M. A. Bredig, and M. D. Danford, *Ann. N. Y. Acad. Sci.*, **79**, 762 (1960).
 (11) J. O'M. Bockris, A. A. Pilla, and J. L. Barton, *Rev. Chim.*, **7**, 59 (1962).
 (12) H. Bloom and J. O'M. Bockris, "Fused Salts," B. R. Sundheim, Ed., McGraw-Hill Book Co., Inc., New York, N. Y., 1964, Chapter 1.
 (13) J. O'M. Bockris, S. Yoshikawa, and S. R. Richards, *J. Phys. Chem.*, **68**, 1838 (1964).
 (14) H. Reiss, H. L. Frisch, E. Helfand, and J. L. Lebowitz, *J. Chem. Phys.*, **32**, 119 (1960).
 (15) H. Reiss and S. W. Mayer, *ibid.*, **34**, 2001 (1961).
 (16) S. W. Mayer, *J. Phys. Chem.*, **67**, 216C (1963).
 (17) F. H. Stillinger, *J. Chem. Phys.*, **35**, 1581 (1961).

The Proton Nuclear Magnetic Resonance Spectrum of 2,2'-Bipyridine

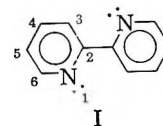
by F. Axtell Kramer, Jr., and Robert West

Department of Chemistry, University of Wisconsin, Madison 6, Wisconsin (Received August 29, 1964)

The proton n.m.r. spectrum of the important ligand 2,2'-bipyridine (α, α' -dipyridyl, I) has been described previously only in general terms.¹ This paper reports a detailed interpretation of the spectrum of this compound in dichloromethane solution (Figure 1), determined on a Varian A-60 n.m.r. spectrometer. This compound provides an unusual example of a very complicated spectrum which is nevertheless fully analyzable as repeated AX patterns by simple first-order spin-spin splitting theory.

Four nonequivalent protons, numbered as shown for I, are present on each ring of the 2,2'-bipyridine molecule. The n.m.r. spectrum at low resolution consists of two triplets, centered at 433 and 464 c.p.s., respectively, downfield from tetramethylsilane (τ 2.78 and 2.27), and two doublets at 502 and 514 c.p.s. downfield (τ 1.64 and 1.44). Under high resolution, these multiplets show further splitting and a total of 30 lines are observed.

Coupling by protons on adjacent carbon atoms is expected to be much larger than for more remote protons. On this basis, the principal splitting should



give doublets for protons 3 and 6 and triplets (or quartets) for protons 4 and 5. Much work has been done on the n.m.r. spectra of pyridine^{2,3} and substituted pyridines,¹⁻⁴ which establishes that protons in the 3- and 5-positions to the nitrogen are the more shielded and quite generally appear at higher field. Moreover, in 2-substituted pyridines, the position of the 3-proton is dependent on the substituent at the 2-position, and electronegative 2-substituents are ex-

- (1) M. Freymann and R. Freymann, *Arch. Sci. (Geneva)*, **13**, 506 (1960); M. Freymann, R. Freymann, and D. Libermann, *Compt. rend.*, **250**, 2185 (1960).
 (2) E. B. Baker, *J. Chem. Phys.*, **23**, 1981 (1955).
 (3) H. J. Bernstein and W. G. Schneider, *ibid.*, **24**, 469 (1956); H. J. Bernstein, J. A. Pople, and W. G. Schneider, *Can. J. Chem.*, **35**, 65 (1957); W. G. Schneider, H. J. Bernstein, and J. A. Pople, *ibid.*, **35**, 1487 (1957).
 (4) W. Brügel, *Z. Elektrochem.*, **66**, 159 (1962).

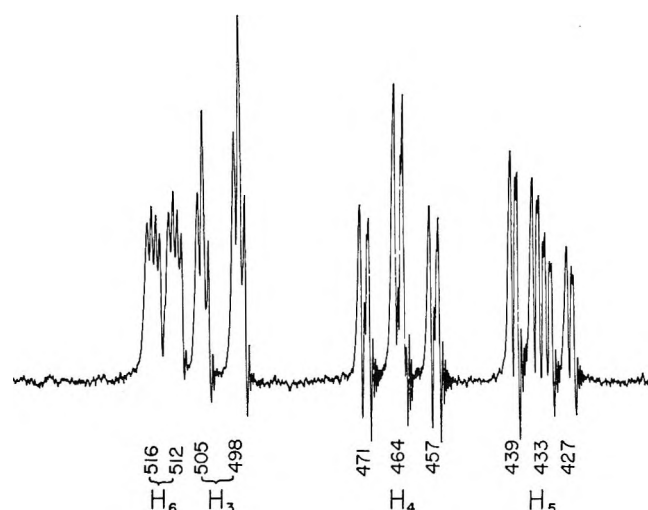


Figure 1. Proton n.m.r. spectrum of 2,2'-bipyridine, 15% w/w. in dichloromethane, determined on a Varian A-60 spectrometer, 250-cycle sweep width. Units are c.p.s. downfield from tetramethylsilane.

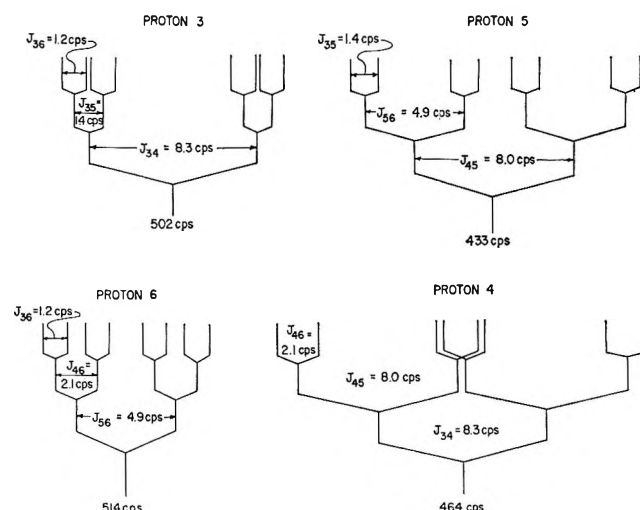


Figure 2. Diagrams of splitting patterns and spin-spin coupling constants for protons in 2,2'-bipyridine.

pected to deshield the 3-proton.⁴ Therefore, the triplet at 433 c.p.s. is assigned to proton 5. This assignment is consistent with the spectrum observed for 4,4',6,6'-tetramethyl-2,2'-bipyridine, which we find has ring proton resonances at 407 and 483 c.p.s., attributed to the 5- and 3-protons, respectively.

Assignments for the other protons follow logically and uniquely once the triplet at 433 c.p.s. has been assigned to proton 5. The other triplet at 464 c.p.s. can be assigned to the 4-proton. Because the principal J splitting for the triplet at 464 c.p.s. is equal to that of the doublet at 502 c.p.s., the latter is assigned to the 3-proton. Only the doublet at 514 c.p.s. remains, which must be assigned to proton 6. The consistency of these assignments is verified by the equivalence of the principal splitting for the peaks assigned to protons 5 and 6. Our assignment agrees with that made earlier for I¹; it is also consistent with studies of substituted pyridines, which show that the 6-proton usually appears at lowest field.²⁻⁴

Splitting constants between nearest neighbor protons can now be evaluated: from the doublet for proton 3, $J_{34} = 8.3$ c.p.s.; from the doublet for proton 6, $J_{66} = 4.9$ c.p.s.; and from the triplet for proton 4, $J_{45} = 8.0$ c.p.s. The multiplet splittings for proton 5 are consistent with these values. Coupling between protons on nonadjacent carbon atoms is also observed, giving further first-order splitting. Thus the resonance for proton 4 appears as a triplet of doublets. The doubling is due to coupling with proton 6, and from this splitting, $J_{46} = 2.1$ c.p.s. Similar reasoning allows evaluation of J_{35} as 1.4 c.p.s. and J_{36} as 1.2 c.p.s.

The complete assignment is indicated in Figure 2.

For a system of four widely separated nonequivalent protons, each coupling to one another unequally, first-order theory predicts an eight-line pattern for each proton, or a total of 32 lines. The spectrum of I is simplified, and the analysis is aided by the near-equality of J_{34} and J_{45} , and of J_{35} and J_{36} (Figure 2). At 250 c.p.s. sweep width, 28 lines are observed (Figure 1): a doublet of quartets for proton 6, a pair of separated triplets for proton 3, a quartet of doublets for proton 5, and two overlapping triplets for proton 4. At 50 c.p.s. sweep width, the resonance for proton 4 is further resolvable; the central two peaks each acquire a shoulder, giving an eight-line pattern as predicted. No further fine structure could be found. All other lines in the spectrum were unusually sharp and well-separated.

Acknowledgment. The authors thank the Atomic Energy Commission for support of this research under Contract No. AT (11-1)-1164.

Dielectric Relaxation of Mixtures of Dipolar Liquids^{1a}

by Surendra K. Garg^{1b} and Prasad K. Kadaba

Department of Electrical Engineering, University of Kentucky, Lexington, Kentucky (Received September 5, 1964)

The present investigation relates mostly to the relaxation mechanism of systems composed of two polar liquids of known structure in the microwave region,

and was undertaken to check the validity of the conclusions arrived at by Schallamach² on dipolar mixtures at radiofrequencies. He assumed that the dielectric relaxation mechanism cannot be directly connected with individual molecules but is a disturbance of an appreciable region in the liquid, involving a volume nearly large enough to be representative in its composition of the bulk concentration. On this basis, any liquid, even if a mixture of two polar components, should have only one relaxation time. Schallamach's conclusions were at variance with the theories of Debye,^{3a} Kauzmann,^{3b} and others. Also, the relatively large amount of experimental evidence reported by various workers in the literature on dilute solutions of single polar liquids in nonpolar solvents⁴ has led to the conclusion that, in the phenomenon of dielectric relaxation, the molecules retain their identity and so give a separate relaxation time for each molecular species present. Unlike the earlier work of one of the authors⁵ which was restricted to purely nonassociated liquids, the present investigation on mixtures involves both associated and nonassociated liquids. In the present investigation, some of the dielectric constant measurements have been made using a generalized approach wherein the sample is treated as a four-terminal dissipative network.

Experimental

The loss factor *vs.* temperature measurements were done at a frequency of $16,200 \pm 1$ Mc. as read on a high *Q* resonant cavity frequency meter. Primarily a reflection method based upon the variation in the reflection coefficient of a uniform layer of the dielectric⁶ was used. The other details of our experimental setup are described in an earlier paper⁵ with particular emphasis to automation of the experimental data. Since the dielectric sample is located in a wave guide propagating a single mode, one can adopt a generalized approach to the problem of dielectric measurement by treating the sample as a four-terminal dissipating network. In this method the liquid cell is terminated in a movable short circuit and for different positions of the short circuit the input impedances of the network are plotted on a reflection plane. The circle which gives the best fit is drawn through the measured points.⁷ From the complex plane plot, the determinant of the admittance representation Y_e is obtained. Setting $Y_e = G_e + jB_e$, the real and imaginary parts of the dielectric constant are, respectively

$$\epsilon' = \frac{G_e + (\lambda_g/\lambda_c)^2}{1 + (\lambda_g/\lambda_c)^2}$$

$$\epsilon'' = - \frac{B_e}{1 + (\lambda_g/\lambda_c)^2}$$

where λ_g is the wave length in the guide and λ_c is the cutoff wave length. This method has the advantage that it can be used over a wide range of loss measure-

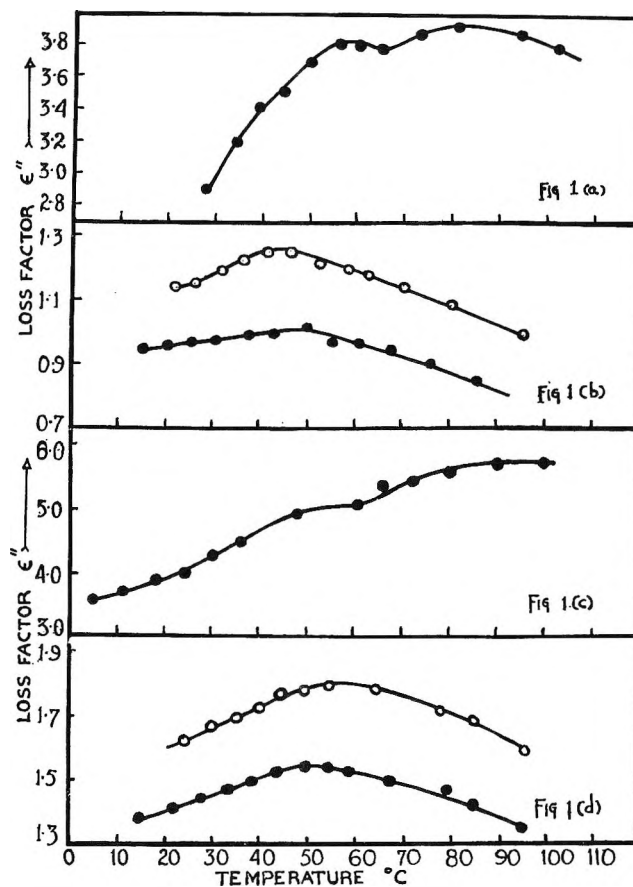


Figure 1. Loss factor *vs.* temperature of solutions in *n*-dodecane: (a) 0.35 mole fraction each of nitrobenzene and *o*-nitrotoluene; (b) O, nitrobenzene, mole fraction 0.35, and ●, *o*-nitrotoluene, mole fraction 0.35; (c) 0.45 mole fraction each of nitrobenzene and *o*-nitrotoluene; (d) O, nitrobenzene, mole fraction 0.45, and ●, *o*-nitrotoluene, mole fraction 0.45. Frequency of measurement, $16,200 \pm 1$ Mc./sec.

(1) (a) This work was supported by a grant from the National Science Foundation; (b) Postdoctoral Research Fellow.

(2) A. Schallamach, *Trans. Faraday Soc.*, **42**, 180 (1946).

(3) (a) P. Debye, "Polar Molecules," Chemical Catalog Co., Inc., New York, N. Y., 1929; (b) W. Kauzmann, *Rev. Mod. Phys.*, **14**, 1 (1942).

(4) J. G. Powles and C. P. Smyth, "Physical Methods of Organic Chemistry," Vol. I, 2nd Ed., Part III, Chapter XXXV, Interscience Publishers, Inc., New York, N. Y., 1954.

(5) P. K. Kadaba, *J. Phys. Chem.*, **62**, 887 (1958).

(6) W. H. Surber, Jr., *J. Appl. Phys.*, **19**, 514 (1948).

(7) "Handbook of Microwave Measurements," Polytechnic Institute of Brooklyn, Microwave Research Institute, 1955, Section X, pp. 5-40.

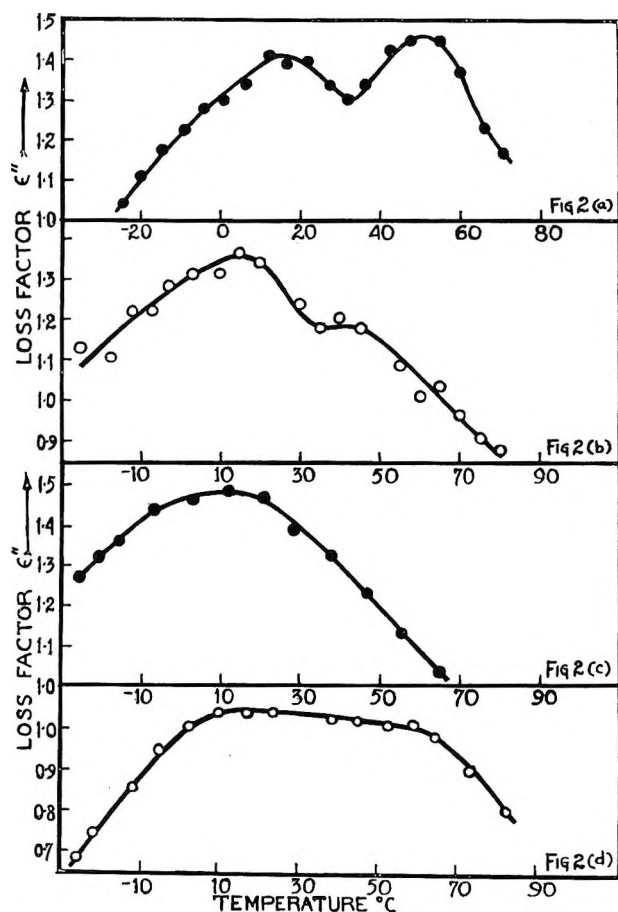


Figure 2. Loss factor vs. temperature of: (a) $\frac{2}{5}$ by volume of chlorobenzene and $\frac{3}{5}$ of bromobenzene; (b) $\frac{3}{5}$ by volume of chlorobenzene and $\frac{2}{5}$ of bromobenzene; (c) chlorobenzene; (d) bromobenzene. Frequency of measurement, $16,200 \pm 1$ Mc./sec.

ments. Some of the measurements reported in this investigation were done using this latter method, the data being processed by means of an IBM 1620 computer. The values of the dielectric constant obtained by the above two methods were self-consistent within the limits of experimental errors. In all the measurements reported in this paper, the accuracy in the determination of ϵ' was 1% and in the determination of ϵ'' , 3%.

Materials. The various chemicals used were obtained from Matheson Coleman and Bell Co. and were of C.P. grade.

Results and Discussion

Loss factor-temperature curves of solutions in *n*-dodecane of nitrobenzene and *o*-nitrotoluene are shown in Figure 1. Also shown in the same figure are the two-component mixtures with only one polar component present, the concentration of the dipolar component expressed in mole fraction being the same as that

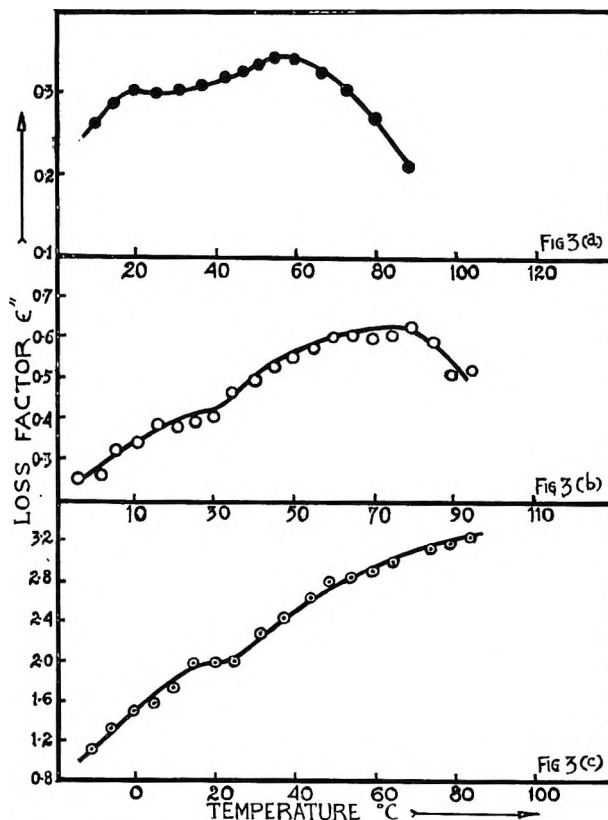


Figure 3. Loss factor vs. temperature of: (a) 0.1 mole fraction each of benzonitrile and β -isopropoxypropionitrile in *n*-dodecane; (b) mixture of diethylaniline and isoamyl alcohol at 75 wt. % diethylaniline; (c) mixture of acetic acid and pyridine at 77 wt. % pyridine. Frequency of measurement, $16,200 \pm 1$ Mc./sec.

in the ternary mixture. In the ternary mixtures, the concentrations of the individual dipolar components were adjusted to be the same. The curves for a mixture of chlorobenzene and bromobenzene at two different concentrations are shown in Figure 2. Also shown in the same figure are the curves for the individual components of the mixtures. The curves for benzonitrile and β -isopropoxypropionitrile in *n*-dodecane and the two binary mixtures diethylaniline + isoamyl alcohol and acetic acid + pyridine, both of which have rather interesting viscosity behaviors, are shown in Figure 3.

As noted earlier,⁵ the distinctness of the two maxima in all the mixtures involving two polar components is quite apparent. A comparison of the two-component curves with the curves for the ternary mixtures in Figure 1 does not reveal any particular trend toward cooperative motion of the dipoles. The change in the peaks by adding the third component in the ternary mixtures may very well be the result of a change of solvent. It may be well to point out that a preliminary

investigation of a ternary mixture of 0.2 mole fraction each of nitrobenzene and *o*-nitrotoluene in *n*-dodecane at various frequencies and at 30° gives a very good Debye circle on the Cole-Cole plot.⁸ The relaxation time, τ , corresponding to the absorption peak for this mixture is 1.9×10^{-11} sec., which is close to 1.7×10^{-11} sec. for the mixture of 0.2 mole fraction nitrobenzene in *n*-dodecane at the same temperature. The Debye circle for the ternary mixture may not be surprising as it could be the result of a simple overlap of the absorption curves of single component mixtures with very close relaxation times. In the case of the binary mixtures of chlorobenzene and bromobenzene, it is interesting to note that a change in the concentration from 60% by volume of bromobenzene to 40% does not significantly change the height or the position at which the low-temperature peak occurs, but the second peak does. Also interesting is the fact that the loss factor-temperature curve of pure bromobenzene has a rather peculiar shape. An approach was made to analyze the data in terms of the relaxation times associated with the peaks. In the case of the ternary mixture involving 0.35 mole fraction of the nitro compounds in Figure 1, for example, the relaxation time τ corresponding to the low-temperature peak is about 20% higher than the τ -values of the individual polar components in the same solvent. For the binary mixtures of chlorobenzene and bromobenzene, the relaxation times corresponding to either of the two peaks lie between the values of the individual components and tend toward the value of the relaxation time of the higher concentration component. In comparing the mixtures involving two polar components with that of the corresponding single components, it is perhaps more appropriate to compare the ratios of the relaxation times, τ , to the respective viscosities, η , instead of just the τ -values. This was done for the case of the 0.35 mole fraction mixtures of nitro compounds shown in Figures 1 (a) and (b). The viscosities at the various temperatures were measured using an Ostwald-Fenske viscometer. The τ/η value of 0.95 in units of 10^{-9} sec.-poise⁻¹ for the low-temperature peak of the composite mixture compares very well with the values 0.95 and 0.93 computed at the same temperature for the single component mixtures of nitrobenzene and *o*-nitrotoluene, respectively. The corresponding values relating to the high-temperature peak of the composite mixture, on the other hand, are 1.37 for the ternary mixtures and 0.89 and 0.91, respectively, for the single component mixtures of nitrobenzene and *o*-nitrotoluene.

The above results seem to indicate that, at least in the case of mixtures studied in the present investigation, the relaxation mechanism in dipolar liquid mixtures

may not be significantly different from that of single components.

Acknowledgments. The authors wish to thank Dr. T. J. Bhattacharyya for some of the calculations. The viscosity measurements were done by T. V. Gopalan, Research Assistant on the project.

(8) K. S. Cole and R. H. Cole, *J. Chem. Phys.*, **9**, 341 (1941).

The Mechanism of Photochromism in Metal Carbonyl Solutions

by G. R. Dobson

Department of Chemistry, University of Georgia, Athens, Georgia
(Received September 10, 1964)

Solutions of the group VI-B metal carbonyls, $M(\text{CO})_6$ ($M = \text{Cr, Mo, W}$), in many organic solvents become yellow when exposed to a strong ultraviolet source; upon removal of the source the solutions may again become colorless. El-Sayed,¹ in discussing the color changes observed upon irradiation of $\text{Mo}(\text{CO})_6$ in 1:1 ether-isopentane mixtures both at 77°K. and at room temperature, suggested that the photochromic behavior was characteristic of the species $\text{Mo}(\text{CO})_6$ rather than of the reversible formation of a weak complex between the metal carbonyl and the solvent. Among the supporting arguments advanced by El-Sayed was that for strong charge donors (D), *e.g.*, those which coordinately bond to the carbonyl through a lone pair on nitrogen, the production of the color is irreversible.

The following evidence is presented in support of the alternative explanation that the observed photochromism is the result of ultraviolet-induced complex formation between the ether and the hexacarbonyl.

A. It has been reported that ethers may form coordination complexes with the group VI-B metal carbonyls. Although spectral evidence only has been presented in support of complex formation in most cases, *e.g.*, with ethyl ether² and tetrahydrofuran,³ the complex [*bis*-(2-methoxyethyl) ether] $\text{Mo}(\text{CO})_6$,⁴ in which the ether functions as a tridentate ligand, has been characterized.

(1) M. A. El-Sayed, *J. Phys. Chem.*, **68**, 433 (1964).

(2) I. W. Stolz, G. R. Dobson, and R. K. Sheline, *Inorg. Chem.*, **2**, 323 (1963).

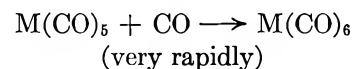
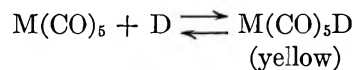
(3) W. Strohmeier and K. Gerlach, *Chem. Ber.*, **94**, 398 (1961).

(4) R. P. M. Werner and T. H. Coffield, *Chem. Ind. (London)*, 936 (1960).

B. The persistence of the yellow color is dependent upon the presence of ether, but not isopentane. Solutions of $\text{Mo}(\text{CO})_6$ in ethyl ether, when exposed to a strong ultraviolet source in a sealed cell at room temperature, remain yellow for several minutes (determined spectrophotometrically) after the completion of the irradiation. Though $\text{Mo}(\text{CO})_6$ -isopentane solutions appear yellow during irradiation, no color can be detected upon the removal of the ultraviolet source.⁵

C. Spectral evidence strongly supports complex formation. (1) The infrared spectrum in the C-O stretching region (2100–1700 cm^{-1}) for the photolysis product in an ether-isopentane mixture is that expected if a $\text{M}(\text{CO})_5\text{D}$ derivative of C_{4v} symmetry were produced, while the low-temperature spectrum reported for $\text{Mo}(\text{CO})_6$ (in saturated hydrocarbon solvents) is consistent with trigonal bipyramidal molecular symmetry (D_{3h}) analogous to the reported structure of $\text{Fe}(\text{CO})_5$.^{7,7a}

(2) The electronic spectrum of irradiated $\text{Mo}(\text{CO})_6$ in ether-isopentane is quite similar to the spectra reported for $\text{M}(\text{CO})_5\text{D}$ complexes in which D is a ligand coordinately bonded through nitrogen⁸ (Table I). The essential features of the reported spectra are independent of the metal and the donor. It is reasonable to expect that such a spectrum is characteristic of $\text{D} \rightarrow \text{M}(\text{CO})_5$ complexes regardless of the identity of the coordinating atom; the electronic spectra of different π -arene derivatives of the group VI-B metal carbonyls, for example, are quite similar.⁹



is involved, and that the process can be reversible, *i.e.*, photochromic, only when the complexing ability of the solvent is extremely poor.

Acknowledgment. Acknowledgment is made to the donors of the Petroleum Research Fund, administered by the American Chemical Society, for support of this research.

(5) At 77°K. the color imparted to irradiated $\text{M}(\text{CO})_6$ -saturated hydrocarbon glasses may persist for longer periods of time.

(6) I. W. Stolz, G. R. Dobson, and R. K. Sheline, *J. Am. Chem. Soc.*, **85**, 1013 (1963).

(7) A. W. Hansen, *Acta Cryst.*, **15**, 930 (1962).

(7a) NOTE ADDED IN PROOF. The CO stretching force constants calculated from the secular equations of F. A. Cotton and C. S. Kraihanzel (*J. Am. Chem. Soc.*, **84**, 4432 (1962)) for a postulated $\text{Mo}(\text{CO})_5$ species of C_{4v} symmetry obtained in a 1:4 methylcyclohexane-isopentane glass at 77°K.⁶ are $k_1 = 15.25$ and $k_2 = 16.31$ mdynes Å^{-1} ($k_1 = 0.33$ mdyne Å^{-1}), compared to 16.52 mdynes Å^{-1} for $\text{Mo}(\text{CO})_6$. The low values for the former suggest that the species may be a weak complex formed between $\text{Mo}(\text{CO})_5$ and an extremely poor donor, perhaps the nitrogen under which the experiments were carried out, rather than $\text{Mo}(\text{CO})_5$ itself.

(8) W. Strohmeier and K. Gerlach, *Z. physik. Chem. (Frankfurt)*, **27**, 439 (1961).

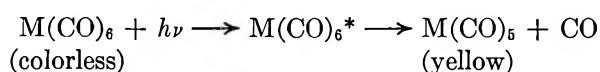
(9) R. Ercoli and A. Mangini, *Ric. Sci.*, **28**, 2136 (1958).

(10) W. Strohmeier and D. von Hobe, *Chem. Ber.*, **94**, 2031 (1961).

Table I: Comparison of Electronic Spectra for $\text{M}(\text{CO})_5\text{D}$ Complexes⁸ with that of Irradiated $\text{Mo}(\text{CO})_6$ -Ether-Isopentane Solution¹

D	M	λ_{max} , Å	
Pyridine	Cr	3900	2420
Piperidine	Cr	4200	2500
Quinoline	Cr	4130	...
Piperidine	Mo	3970	2510
Piperidine	W	4050	2470
Irradiated $\text{Mo}(\text{CO})_6$ -ether-isopentane		4095	2469

It seems most probable, therefore, that at room temperature and where color persists for a time after the completion of an ultraviolet exposure, complex formation according to the mechanism first proposed by Strohmeier¹⁰



Radiolysis of Cyanogen-Cyclohexane Mixtures

by J. A. Knight, R. A. Stokes, and David Bowen

*Nuclear Sciences Division, Engineering Experiment Station,
(Georgia Institute of Technology, Atlanta, Georgia
Received June 10, 1964)*

The radiation chemistry of cyclohexane has been the subject of a number of investigations.¹⁻¹² This is a report on the irradiation of mixtures of cyanogen and

(1) H. A. Dewhurst, *J. Phys. Chem.*, **63**, 813 (1959).

(2) T. D. Nevitt and L. P. Remsberg, *ibid.*, **64**, 969 (1960).

(3) G. R. Freeman, *J. Chem. Phys.*, **33**, 71 (1960).

(4) P. J. Dyne and J. A. Stone, *Can. J. Chem.*, **39**, 2381 (1961).

(5) P. J. Dyne and W. M. Jenkinson, *ibid.*, **39**, 2163 (1961).

(6) R. R. Williams, Jr., and W. H. Hamill, *Radiation Res.*, **1**, 158 (1954).

(7) R. H. Schuler, *J. Phys. Chem.*, **61**, 1472 (1957).

(8) G. Meshitsuka and M. Burton, *Radiation Res.*, **10**, 499 (1959).

(9) L. J. Forrestal and W. H. Hamill, *J. Am. Chem. Soc.*, **83**, 1535 (1961).

cyclohexane. The radiation-induced cyanogenation of organic compounds has been reported.¹³ In the presence of cyanogen, the yields of hydrogen, cyclohexene, and dicyclohexyl were decreased with increasing concentrations of cyanogen. Cyclohexyl cyanide was formed with $G \sim 25$ under optimum conditions, which indicates a chain process. The results from the irradiation of the cyanogen-cyclohexane mixtures are similar in many respects to the results reported for chlorinated solutes in cyclohexane.¹² The polymerization of cyanogen by α -particles from radon¹⁴ and by soft X-rays¹⁵ has been investigated. Cyclohexane was selected for this study as its radiation chemistry has been extensively investigated and the number of possible cyano products is small.

Experimental

Materials. The cyclohexane was Phillips research grade and was used without further purification. Cyanogen was obtained from The Matheson Co. Cyclohexyl cyanide was prepared as previously described.¹⁶

Irradiations. The cyclohexane was degassed by repeating several times the cycle of freezing, evacuation, and melting under vacuum. For pure samples of cyclohexane, the irradiation tube was then sealed under vacuum. For mixtures of cyanogen-cyclohexane, the required amount of cyanogen was measured in a gas buret and transferred to the irradiation tube, which was cooled in liquid nitrogen. The tube was then sealed. In all samples 10 ml. of cyclohexane was used. The samples were irradiated in the center hole of a 12-kcurie Cs¹³⁷ facility.¹⁷ Dosimetry measurements with the ferrous ion dosimeter were made so that essentially the same geometry was obtained as in the irradiations, and an electron density correction was applied. The dose rate was 6.1×10^{19} e.v./(g. hr.). For the calculation of G values for the mixtures, it was assumed that the dose absorbed was due to the cyclohexane.

Analytical. The radiolysis products were analyzed with gas chromatographic units having thermistor detectors. Hydrogen was determined using a 1.52-m. column of silica gel with argon as the carrier gas. Cyclohexene, other C₆ products, and cyanogen were determined with a 3.66-m. column of 25% (by weight) tri-*m*-cresyl phosphate and a 2.44-m. column of 25% triacetin. Cyclohexyl cyanide, dicyclohexyl, and other high molecular products were determined with a 2.74-m. column of 15% Ucon LB-550X and with a 3.05-m. column of 15% Apiezon L grease. The solid support was 50-60 mesh, acid-washed Chromosorb P, and the carrier gas was helium. The gas chromatographic

units were calibrated for thermal response for substances which were analyzed quantitatively, except as noted in the tables. For hydrogen, cyanogen, and cyclohexane, pure samples of known volume were used. For cyclohexene, other C₆ products, dicyclohexyl, and cyclohexyl cyanide, individual dilute solutions of known concentrations of each in cyclohexane were used. Hamilton microliter syringes were used for all sampling and calibration work, and all peak areas were measured with a planimeter. The samples were attached immediately after irradiation to the vacuum apparatus, and after evacuation the break-seal was broken. After equilibration, gas samples were taken for gas chromatographic analysis. The irradiated samples were removed and capped immediately. Samples of the liquid for gas chromatographic analysis were then taken through a rubber septum in the cap.

Results and Discussion

The G values for the radiolysis products from pure cyclohexane are given in Table I, and those from the cyanogen-cyclohexane mixtures are given in Table II.

Cyanogen-Cyclohexane. Cyclohexyl cyanide, the only cyano product detected, was formed with a G of ~ 25 . In the early stages of the study, it was found that the quantity of cyclohexyl cyanide in the irradiated sample decreased with time after irradiation. It was also found that either washing the irradiated sample with 5% potassium hydroxide solution or the addition of a potassium hydroxide pellet would prevent the decrease of cyclohexyl cyanide with time after irradiation, and the G value was increased 1 to 2 units over the untreated sample. The exact nature of the post-irradiation effect is not clear. The fact that the decrease in cyclohexyl cyanide is prevented by a base indicates that the effect may be attributable to some radiolytic acidic material.

The high G value for cyclohexyl cyanide indicates that a chain process is involved. This suggestion of a chain process is also supported by the fact that cyclohexyl cyanide could not be detected by the usual gas

- (10) J. A. Stone and P. J. Dyne, *Radiation Res.*, **17**, 353 (1962).
- (11) J. R. Nash and W. H. Hamill, *J. Phys. Chem.*, **66**, 1097 (1962).
- (12) J. A. Stone and P. J. Dyne, *Can. J. Chem.*, **42**, 669 (1964).
- (13) J. A. Knight, C. J. Bryan, and R. A. Stokes, *Intern. J. Appl. Radiation Isotopes*, **14**, 239 (1962).
- (14) S. C. Lind, D. C. Bardwell, and J. H. Perry, *J. Am. Chem. Soc.*, **48**, 1561 (1926).
- (15) D. C. Bardwell and D. K. Taylor, *Radiation Res.*, **11**, 432 (1959).
- (16) D. S. Breslow and C. R. Hauser, *J. Am. Chem. Soc.*, **67**, 686 (1945).
- (17) R. C. Palmer and R. W. Carter, *Intern. J. Appl. Radiation Isotopes*, **9**, 123 (1960).

Table I: Radiolysis Products from Cyclohexane

Product	<i>G</i> values ^a
Gases (total) ^{b,c}	5.8
<i>n</i> -Hexane	0.16
Hexene-1	0.50
Unknown 1 ^d	0.35
Methylcyclopentane	0.45
Cyclohexene ^c	3.16
Unknown 2 ^d	0.12
Dicyclohexyl ^c	2.06
Unknown 3 ^{c,d}	0.25

^a The *G* values are initial values with the exception of *n*-hexane which is the *G* value obtained with a dose of 1.22×10^{20} e.v./g. ^b Total gases were determined volumetrically, and no analysis was made to determine the composition of the radiolytic gases from pure cyclohexane. The major component of the gases is hydrogen, which is equal to or greater than 96% of the total radiolytic gases (ref. 1) and corresponds to a *G* value of 5.57 for hydrogen. ^c Dyne and Stone (ref. 4) reported for hydrogen, $G_i = 5.55$; cyclohexene, $G_i = 3.27$; dicyclohexyl, $G_i = 1.95$; unknown 3, identified by Dyne and Stone as cyclohexylhexene-1, $G_i = 0.25$. ^d Based on retention times, unknown 1 is most likely a C₆ unsaturated hydrocarbon; unknown 2, a C₉ hydrocarbon; and unknown 3, which appears immediately after dicyclohexyl on the gas chromatogram, a C₁₂ hydrocarbon. The calibration for *n*-hexane was used for the calculation of *G* values for unknown 1, and the calibration for dicyclohexyl was used for unknowns 2 and 3.

Table II: Radiolysis Products from Cyanogen-Cyclohexane Mixtures

Product ^a	<i>G</i> values ^b			
	6.69 ^c	8.92 ^c	17.84 ^c	26.76 ^c
Hydrogen	4.60	4.26	4.01	3.95
<i>n</i> -Hexane	0.04	0.05	0.05	0.04
Hexene-1	0.43	0.44	0.37	0.37
Unknown 1	0.06	0.07	0.05	0.02
Methylcyclopentane	0.11	0.10	0.07	0.07
Cyclohexene	1.58	1.45	1.36	1.25
Dicyclohexyl	0.42	0.39	0.38	0.37
Cyclohexyl cyanide				
Untreated sample	23.6	24.2	23.5	22.0
KOH pellet-treated sample	25.5	25.5	25.4	24.8
Cyanogen disappearance ^d	36.1	36.4	37.0	38.1

^a No evidence of unknowns 2 and 3 (see Table I) in the irradiated mixtures. ^b Dose equal to 1.22×10^{20} e.v./g. All samples contained 10 ml. of cyclohexane. ^c Moles of cyanogen $\times 10^4$ initially present. ^d Calculated on basis of total energy absorbed by system.

chromatographic method in a sample of irradiated cyclohexane which was 0.089 *M* in cyanogen and ~ 0.04 *M* in iodine.

Hydrogen cyanide was considered to be a very likely radiolytic product. Therefore, analyses were made for hydrogen cyanide by several different techniques. With hydrogen cyanide test paper, it was estimated that the *G* value for hydrogen cyanide is less than 0.1. It seems evident that, if hydrogen cyanide is formed in significant quantity in any of the processes, it is also consumed by some other process.

The simplest reaction in a chain process to account for the formation of cyclohexyl cyanide would be



If the above reaction accounts for the formation of cyclohexyl cyanide, then the fate of the cyanide radical is a matter of speculation. If the reaction is propagated by the cyanide radical abstracting a hydrogen atom from cyclohexane to yield a cyclohexyl radical and hydrogen cyanide, then *G* for hydrogen cyanide should be ~ 25 . However, this is not the case as the *G* value for hydrogen cyanide was estimated to be less than 0.1. Even though hydrogen cyanide polymerizes with $G \sim 33$ in the presence of α -particles¹⁴ and with $G = 42$ in the presence of soft X-rays,¹⁵ it would not be directly affected by the radiation to the extent required to account for its disappearance. It is possible that, if hydrogen cyanide is formed, it is consumed in some undefined process. Since approximately 3 moles of cyanogen was consumed for every mole of cyanogen converted completely to cyclohexyl cyanide, there is the possibility that a polymeric form of cyanogen is involved in reaction 1 of the chain process in the formation of cyclohexyl cyanide rather than cyanogen. The abstraction of a hydrogen atom from cyclohexane by a polymeric cyanogen radical would not require the formation of hydrogen cyanide, and, therefore, this would account for the negligible yield of hydrogen cyanide. Evidence for polymerization of cyanogen is to be found in the high *G* value for the disappearance of cyanogen, which had a value of ~ 37 , and in the insoluble dark brownish material that was formed in each irradiated mixture. The product formed by the action of α -particles¹⁴ was described as a black polymer. The formation and nature of the polymeric form of cyanogen is a matter of speculation. Even though the polymerization of cyanogen by α -particles¹⁴ and soft X-rays¹⁵ with *G* values of 22 and 27, respectively, has been reported, the cyanogen in the cyclohexane solutions should not be affected directly to the extent required for formation of a polymer form. It is possible that an energy-transfer process is operative which yields excited cyanogen molecules that initiate the formation of polymeric cyanogen. The evidence is not sufficient to

permit a definite choice of one mechanism over the other for the formation of cyclohexyl cyanide.

The yields of hydrogen, cyclohexene, and dicyclohexyl were reduced in the presence of cyanogen, and the yields of all the minor products showed some decrease with increasing concentration of cyanogen. The hydrocarbon radiolysis products from the cyanogen-cyclohexane mixtures were qualitatively the same as those from pure cyclohexane except for unknowns 2 and 3, which were not detected as products in the mixtures. The yield of hydrogen decreased with increasing concentration of cyanogen up to approximately 0.1 *M* and appeared to have reached a limiting value of $G \sim 4$ at the higher concentrations. Other substances, such as cyclohexane,^{1,2} benzene,^{3,5,10} iodine,^{5,7-9} carbon tetrachloride,¹² and chloroform,¹² also decrease the hydrogen yield by varying amounts. Hydrogen is generally considered to be produced simultaneously by a unimolecular process and a bimolecular process^{1,5}; a third undefined process also has been suggested to account for a portion of the hydrogen.² Even though a number of investigations have been devoted to the effects of solutes on the hydrogen yield from cyclohexane, the processes have not been completely elucidated. The effects of solutes have been attributed to H-atom scavenging, electron attachment, energy transfer, and quenching. From the available data, cyanogen is the least efficient of the various solutes in decreasing the hydrogen yield, being slightly less efficient than benzene¹⁰ and cyclohexene.⁴ The similarity of the results from this work with those from γ -irradiated benzene-cyclohexane mixtures and carbon tetrachloride-cyclohexane mixtures suggests that the effect of cyanogen may be of the same nature as that suggested for benzene¹⁰ and carbon tetrachloride.¹²

The yield of cyclohexene showed a rapid decrease to $G = 1.58$ at 0.067 *M* and then a more gradual decrease with increasing concentration to $G = 1.25$ at 0.268 *M*. The dicyclohexyl yield decreased sharply to $G = 0.42$ at 0.067 *M* and then decreased only slightly to $G \sim 0.38$ at the higher concentrations. The effect of cyanogen in decreasing the yields of cyclohexene and dicyclohexyl is very similar to the effects of benzene¹⁰ and chlorinated solutes,¹² with the yields of cyclohexene agreeing with those from chloroform-cyclohexane solutions and with the yields of dicyclohexyl agreeing with those from cyclohexane solutions of chloroform and carbon tetrachloride. The efficiencies of the different solutes vary, and for each solute there are residual yields of cyclohexene and dicyclohexyl. The formation of cyclohexene has been attributed to the disproportionation of cyclohexyl radicals and to the unimolecular decomposition of some form of the excited cyclohexane mole-

cule; the formation of dicyclohexyl has been attributed to the combination of cyclohexyl radicals.¹ In addition, other modes of formation for cyclohexene and dicyclohexyl have been suggested.^{2,12} A portion of the decrease in the yields of cyclohexene and dicyclohexyl can be ascribed to the radical scavenging action of the solute; in this case, cyanogen or a polymeric form of cyanogen. For cyclohexene, a part of the decrease has been attributed to interaction of the solute with some form of an excited cyclohexane molecule, thereby preventing its unimolecular decomposition to hydrogen and cyclohexene.¹² Since the yields of cyclohexene from cyanogen-cyclohexane solutions are in agreement with the yields reported for the solutes, chloroform and carbon tetrachloride,¹² the cyanogen could interact in a similar manner. The residual yields of cyclohexene and dicyclohexyl in the presence of cyanogen may be due to chain termination steps and/or to reactions of cyclohexyl radicals in the same solvent cage. If cyclohexyl cyanide is formed in a chain process as suggested above, then the disproportionation and combination of cyclohexyl radicals would constitute two chain termination steps to yield cyclohexene and dicyclohexyl. As suggested by Hardwick,¹⁸ some or all of the yields of cyclohexene and dicyclohexyl at the higher concentrations of solute may be due to the disproportionation and combination reactions of the cyclohexyl radicals formed together in the same solvent cage.

Acknowledgment. This work was supported in part by the United States Atomic Energy Commission.

(18) T. J. Hardwick, *J. Phys. Chem.*, **64**, 1623 (1960).

Activity Coefficients of Cadmium Chloride in Mixed Aqueous Solution with Benzyltrimethylammonium Chloride¹

by E. Lyndol Harris

*Department of Chemistry, McMurry College, Abilene, Texas
(Received August 8, 1964)*

Because of an anticipated need for such data in connection with another project, activity coefficients were determined for cadmium chloride in aqueous solutions

(1) This investigation was supported by Public Health Service Research Grant GM-09728, from the Division of General Medical Sciences.

with benzyltrimethylammonium chloride by the e.m.f. method at total stoichiometric ionic strengths of 1.0, 0.5, and 0.2 *m*. These were the ionic strengths used by Leifer, Argersinger, and Davidson² in determining the activity coefficients of both cadmium chloride and hydrochloric acid in mixed aqueous solutions. Harned and Gary³ had earlier reported the activity coefficients of hydrochloric acid in cadmium chloride solutions of total stoichiometric ionic strength of 5.0.

Experimental

A concentrated stock solution of cadmium chloride was prepared from Baker's Analyzed reagent and de-ionized water. Standardization was by gravimetric determination of cadmium as sulfate and was verified by gravimetric determination of chloride. The stock solution of benzyltrimethylammonium chloride was Matheson 60% aqueous solution and was standardized by gravimetric determination of chloride. Mixed solutions of stoichiometric ionic strength of 1.0 *m* were prepared from the stock solutions, using weight burets. Portions of the 1.0 *m* solutions were deoxygenated by bubbling of nitrogen under reduced pressure and were transferred to flushed e.m.f. cells with nitrogen pressure. Solution compositions in the prepared cells were corrected for loss of water.

The e.m.f. cell used may be represented by



The cadmium amalgam, approximately 8% cadmium by weight, was prepared, stored, and transferred to the cells under nitrogen. The silver-silver chloride electrodes were prepared by the thermal method.⁴ The standard potentials used were 0.35163 and -0.22246 abs. v., respectively. Cell measurements were made with a Leeds and Northrup Type K-3 potentiometer in conjunction with an electronic null indicator. Cells were made up in triplicate and were kept at $25 \pm 0.05^\circ$ during the measurements. Deviations from the average of triplicate measurements were of the order of 0.05, 0.1, and 0.2 mv. for ionic strengths 1.0, 0.5, and 0.2, respectively, except that for small X_2 at 0.2 *m* ionic strength, deviations >0.5 mv. were obtained for some cells.

Results

The results of the cell measurements are recorded in Table I, along with the calculated values of the logarithms of the stoichiometric mean ionic activity coefficients of cadmium chloride in the solutions. The latter have been adjusted by short interpolation to the

appropriate ionic strength in cases where the ionic strength differed significantly from its intended value.

Table I: Cell Measurements and Calculated Activity Coefficients of CdCl_2

Total stoichiometric ionic strength, $I = 3m_2 + m_1$	Ionic strength fraction of CdCl_2 , $X_2 = \frac{3m_2}{I}$	Measured cell potential, E , in abs. v.	$-\log \gamma_2$
1.0063	0.09969	0.70800	1.006
0.9882	0.19805	0.69851	0.989
1.0072	0.3020	0.69222	0.967
0.9985	0.3951	0.68855	0.955
1.0000	0.4998	0.68510	0.939
1.0010	0.5991	0.68269	0.926
0.9935	0.6997	0.68052	0.911
1.0119	0.8064	0.67936	0.905
0.9991	0.9002	0.67896	0.904
1.0000	1.0000	0.67906	0.905
0.5093	0.09969	0.71407	0.778
0.4877	0.19805	0.70664	0.774
0.5052	0.3020	0.70185	0.778
0.4992	0.3951	0.69870	0.768
0.5000	0.4998	0.69620	0.763
0.5002	0.5991	0.69412	0.754
0.5235	0.6997	0.69192	0.752
0.5002	0.8064	0.69200	0.747
0.4995	0.9002	0.69185	0.748
0.5002	1.0000	0.69180	0.749
0.2004	0.09969	0.73235	0.582
0.1999	0.19805	0.72391	0.576
0.1998	0.3020	0.71945	0.577
0.2003	0.3951	0.71707	0.579
0.1999	0.4998	0.71510	0.578
0.2000	0.5991	0.71308	0.570
0.1992	0.6997	0.71249	0.571
0.1973	0.8064	0.71214	0.569
0.2001	0.9002	0.71113	0.568
0.2001	1.0000	0.71110	0.569

The effect of benzyltrimethylammonium chloride on the activity coefficient of cadmium chloride is considerably different from that of hydrochloric acid in solutions of analogous composition,² particularly at the higher solution concentrations. This behavior could be of some interest because of the relationship of benzyltrimethylammonium chloride to the common type of anion-exchange resin, although the concentrations of the quaternary ammonium ion within these resins usually are much higher than those recorded here.

(2) L. Leifer, W. J. Argersinger, Jr., and A. W. Davidson, *J. Phys. Chem.*, **66**, 1321 (1962).

(3) H. S. Harned and R. Gary, *ibid.*, **63**, 2086 (1959).

(4) D. J. G. Ives and G. J. Janz, "Reference Electrodes," Academic Press, New York, N. Y., 1961, Chapter 4.

An Infrared Study of Complexes of Ethylamine with Ethylammonium and Copper Ions in Montmorillonite¹

by V. C. Farmer and M. M. Mortland

Soil Science Department, Michigan State University, East Lansing, Michigan (Received July 10, 1964)

In the course of investigations on the nature of the interactions between nitrogenous compounds and soil clays, Mortland and Barake² noted that the infrared spectrum of ethylamine adsorbed from the vapor on hydrogen montmorillonite differed markedly from that of ethylammonium ions introduced into montmorillonite by exchange from solution. To elucidate the cause of these differences, a study has been made of the products formed when ethylamine is adsorbed on films of ethylammonium and copper montmorillonite; adsorption of ethylamine on hydrogen and calcium montmorillonite² has also been re-examined.

Experimental

Montmorillonite H-25 from Upton, Wyo., supplied by Ward's Natural Science Establishment was used in this work. Homoionic clays were prepared by treating the <0.5- μ fraction with the chloride salts of ethylammonium, copper(II), and calcium in excess of the cation-exchange capacity. After flocculation had taken place, the supernatant liquid was siphoned off and distilled water was added to bring it to the original volume and the chloride salts again were added. This process was repeated three times at the end of which no more salts were added but the clays were allowed to settle and were redispersed in distilled water until the clays showed signs of not flocculating, at which time they were placed in dialysis bags and dialyzed against distilled water until the conductivity of the dialyzate approached that of distilled water.

Thin films (2–5 mg./cm.²) of ethylammonium and copper montmorillonite were prepared by evaporating suspensions in dishes of aluminum foil. Since copper ions reacted with the aluminum surface, it was necessary to line the dishes with polyethylene film, held in place by a smear of vacuum grease. The films, which could be readily stripped from these surfaces, were mounted in an evacuable brass cell fitted with sodium chloride windows. After evacuation by rotary pump for 15 min., the films were exposed to ethylamine vapor (50 cm. pressure) for 30 min. (ethylammonium) or 2 hr. (copper). The longer period was necessary to displace water coordinated to the copper ion and held

against vacuum. Excess ethylamine was then frozen out in a bath of liquid nitrogen, and the films were degassed for 30 min. by a rotary vacuum pump with a liquid nitrogen trap. Infrared spectra were recorded with the beam normal to the films on a Beckman IR7 spectrophotometer. Samples for chemical analysis were treated with ethylamine vapor for 2 hr. and then evacuated 2 hr. X-Ray diffraction patterns were obtained on the same films used for the infrared studies.

Results and Interpretation

The intense blue color which developed on treating copper montmorillonite with ethylamine indicated the formation of a copper-ethylamine complex, and this was confirmed in the infrared spectrum (curve 3 of Figure 1), which showed complete displacement of coordinated water by ethylamine. The complex was stable to atmospheric moisture. After 2 days in air there was some decrease in ethylamine absorption but no evidence for the absorption of coordinated water or hydroxyl which would be expected if amine were displaced by water from the complex. The decrease in nitrogen content over the 2 days (Table I) is ascribed to the loss of interlayer ethylamine which is not coordinated to the cation. The final nitrogen content (160 mequiv./100 g.) is just below that expected for a full complement of the square-planar complex ion $\text{Cu}(\text{EtNH}_2)_4^{2+}$, that is, 180 mequiv./100 g. A planar geometry is required by the X-ray spacings, reported below.

Table I: Nitrogen Content of Ethylamine-Treated Montmorillonites

Exchangeable cation	mequiv. of N/100 g. of hydrogen montmorillonite	
	Initially	After 2 days
EtNH_3^+	230	92
Cu^{2+}	235	160
Ca^{2+}	210	140

Coordination of ethylamine causes shifts in its absorption bands from the position observed for the free amine in CCl_4 solution.³ The NH_2 scissoring vibration, at 1626 cm^{-1} in solution, is displaced to 1590 cm^{-1} on coordination, and CH deformation vibra-

(1) Authorized for publication by the Director as Journal Article No. 3402 of the Michigan Agricultural Experimental Station, East Lansing, Mich. This work was supported by National Science Foundation Project GP1978.

(2) M. M. Mortland and N. Barake, *Trans. 8th Intern. Congr. Soil Sci.*, in press.

(3) L. Segal and F. V. Egerton, *Appl. Spectry.*, 15, 112 (1961).

(curve 1) was replaced by weaker absorption bands (curve 2) resembling those of coordinated ethylamine (curve 3).

The only features in the spectrum of the ethylamine-ethylammonium complex which can be ascribed to the proton involved in hydrogen bonding between the components of the dimer are the absorption band at 1642 cm^{-1} and a very broad featureless absorption extending from 3300 cm^{-1} to at least 1200 cm^{-1} . This pattern of absorption does not match any of those discussed by Hadzi and co-workers⁵⁻⁷ in their studies on strong hydrogen bonds, but appear to be intermediate between those given by strong bonding with a double potential minimum and those given by symmetrical hydrogen bonds with a single minimum. The former have two broad but discrete maxima near 2500 and 1800 cm^{-1} , while the latter generally give a very broad intense band extending from 1600 to 400 cm^{-1} , and sometimes also a more discrete maximum near 1600 cm^{-1} .

The ethylamine-ethylammonium complex was stable against the vacuum of a rotary pump, but ethylamine was displaced by water vapor at room humidity. During this process the broad shoulder of the complex near 1560 cm^{-1} shifted to lower frequency and developed into the 1515- cm^{-1} band of the hydrated ethylammonium ion. This change was complete within 24 hr. for ethylammonium montmorillonite, and the nitrogen analysis after 2 days (Table I) confirmed the loss of all excess ethylamine. This result must be contrasted with that of Kinter and Diamond,⁸ who found air-dry ethylammonium-saturated montmorillonite to have a carbon content 1.6 times that expected on the basis of the exchange capacity. Perhaps acetone, which was used to wash their preparations, was retained by their samples. The ethylamine-ethylammonium complex formed by treating hydrogen and calcium montmorillonite with ethylamine was more stable; both nitrogen analysis (Table I) and infrared spectra still showed the presence of perturbing ethylamine after 2 days.

The lattice 001 spacing for the copper-ethylamine montmorillonite was 12.9 Å. The same spacing was observed in all the ethylamine-clay systems studied including ethylammonium itself. When the complexes were well developed, as indicated by infrared, the X-ray patterns always showed sharp 001 peaks and rationality of the higher orders.

An attempt was made to determine the orientation of the ethylamine molecules in the copper-amine complex by observing changes in the intensity of infrared absorption bands when the clay film was positioned at

45° to the infrared beam. The method of preparation of the films leads to a well-oriented sample with the 001 planes of the clay mineral predominantly in the plane of the film. Only absorption bands with a component perpendicular to the clay sheets should be enhanced on positioning the film at an angle to the beam.

Bands found to be enhanced in intensity included those at 1472 and 1456 cm^{-1} (both by 12%), the NH_2 scissoring vibration at 1590 cm^{-1} (by 11%), and the broad NH stretching vibration at 3313 cm^{-1} (by 14%). The C-H stretching vibrations near 2900 cm^{-1} and the bands in the 1350-1400- cm^{-1} region were unaffected in intensity. None of these absorption bands can have its dipole change perpendicular to the plane of the clay sheets; a three- or fourfold increase in intensity would be expected for such bands.⁹ The increase in intensity of the broad NH stretching vibration at 3313 cm^{-1} is consistent with hydrogen bonding of the NH_2 group to the silicate sheet; the presence of a weaker, sharper NH stretching vibration at 3367 cm^{-1} suggests that the amino group is oriented so that only one of the protons is involved in hydrogen bonding, the other being free. Such an orientation of the amino group would tend to force the methylene group attached to it out of the plane of the copper ion and its coordinated nitrogen atoms, and the enhancement of the bands at 1472 and 1456 cm^{-1} gives some support for this belief. Although the asymmetric CH_3 deformation vibrations are also expected in this region, it seems likely that at least one of these absorption bands corresponds to the CH_2 scissoring vibration, as the copper-ethylenediamine complex¹⁰ has CH_2 scissoring vibrations at 1475 and 1463 cm^{-1} . The dipole change of this scissoring vibration is along the bisector of the H-C-H angle and therefore in the plane of the N-C-C skeleton. The observed enhancement of these absorption bands indicates that this plane is at an angle to the plane of the clay sheets. The absorption bands in the 1350-1400- cm^{-1} region include CH_3 symmetrical deformation vibrations and CH_2 wagging vibrations,¹⁰ both of which have dipole changes in the general direction of

(5) R. Blinc, D. Hadzi, and A. Novak, *Z. Elektrochem.*, **64**, 567 (1960).

(6) D. Hadzi, *J. Chem. Soc.*, 5128 (1962).

(7) D. Hadzi, A. Novak, and J. E. Gordon, *J. Phys. Chem.*, **67**, 1118 (1963).

(8) E. B. Kinter and S. Diamond, *Clays Clay Minerals*, **10**, 174 (1963).

(9) J. M. Serratos, A. Hidalgo, and J. M. Vinas, *Nature*, **195**, 486 (1962).

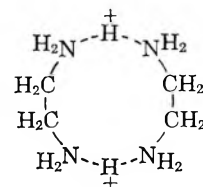
(10) D. B. Powell and N. Sheppard, *Spectrochim. Acta*, **17**, 68 (1961).

the long axis of the molecule. As these bands are insensitive to orientation, it can be concluded that the ethylamine molecule is oriented with its long axis approximately parallel to the silicate sheets and that the methylene group is displaced out of the plane of the copper and nitrogen atoms.

Discussion

A few salts involving cations of the type $[B_2 \cdot H]^+$ are known in which the two molecules of base, B, are joined by a symmetrical hydrogen bond, giving the typical infrared absorption pattern. These, however, involve oxygen atoms of the base, as in diacetamide hydrochloride,¹¹ and di(picoline oxide) salts.^{5,12} The ethylamine-ethylammonium complex shows some unusual features, which could possibly correspond to a symmetrical bond between nitrogen atoms. No reports of salts involving an ethylamine-ethylammonium complex are known to the authors. The stability of such salts depends on crystal structure considerations in addition to strength of hydrogen bonding. Expanding-layer minerals provide favorable sites to accommodate large cations of this type. *n*-Alkylamines with more than six carbon atoms are taken up from solutions of their salts by montmorillonite in amounts which are in excess of its exchange capacity.¹³ The forces involved are normally considered to be principally van der Waals, but the present work clearly indicates that hydrogen bonding may play an important part.

The results obtained here for ethylamine on clay have also been found by others for ethylenediamine. Fripiat, *et al.*,¹⁴ observed that when ethylenediamine was added in amounts less than the exchange capacity of acid montmorillonite, the NH_3^+ symmetric deformation band was clearly evident at 1531 cm.^{-1} . They also observed that ethylenediamine added in excess of the exchange capacity resulted in the suppression of the 1531-cm.^{-1} NH_3^+ symmetrical deformation band and the appearance of the NH_2 deformation vibration at 1597 cm.^{-1} . These results may be accounted for by strong hydrogen bonding between NH_2 and NH_3^+ as suggested here for the ethylamine system. Fripiat, *et al.*,¹⁴ noted a progressive diminution of the NH_3^+ symmetric deformation band from 50 to 100 mmoles/100 g. of clay, the band being totally suppressed at the higher level. This may be accounted for by strong hydrogen bonding between NH_2 and NH_3^+ to give a dimer as

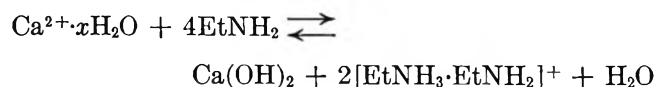


At maximum levels of diamine (150 moles/100 g. of clay), a trimer may be formed of the structure: $NH_2-(CH_2)_2NH_3^+ \cdot NH_2(CH_2)_2NH_3^+ \cdot NH_2(CH_2)_2NH_2$.

The ideas suggested here are not in contradiction to those of proton delocalization suggested by Fripiat, *et al.*,¹⁴ but are perhaps more descriptive of the actual bonds formed.

The vibrations of the NH_4^+ ion in montmorillonite are not so strongly perturbed by the presence of ammonia as was found here for the ethylamine-ethylammonium system. Adsorption of ammonia⁴ on ammonium montmorillonite causes the NH_4^+ stretching vibration at 3270 cm.^{-1} to broaden, intensify, and shift to 2791 cm.^{-1} , while the deformation vibration at 1430 cm.^{-1} shifts to 1462 cm.^{-1} . Clearly, the ammonium ion preserves its identity, although its vibrations are modified by the strong hydrogen bonding.

Although the results of the present study lead to a reinterpretation of the spectra reported by Mortland and Barake,² their conclusion that ethylammonium ions are formed when ethylamine is adsorbed on both hydrogen and calcium montmorillonite remains correct, and has been confirmed in the course of the present work. On exposure to the atmosphere, excess ethylamine was lost from the treated hydrogen montmorillonite to give the normal ethylammonium absorption pattern. Both ethylamine and ethylammonium were lost, under these conditions, from the calcium system on long exposure, leaving only a weak ethylammonium absorption at 1510 cm.^{-1} . A weak, broad band also appeared at 1413 cm.^{-1} , probably due to some calcium carbonate formed in the alkaline system on exposure to atmospheric CO_2 . The loss of ethylammonium can be ascribed to a reversal of the reaction by which it is formed, *i.e.*



(11) N. Albert and R. M. Badger, *J. Chem. Phys.*, **29**, 1193 (1958).
 (12) M. Szafran, *Bull. Acad. Polon. Sci., Ser. Sci. Chim.*, **11** (3), 111 (1963).

(13) C. T. Cowan and D. White, *Trans. Faraday Soc.*, **54**, 691 (1958).

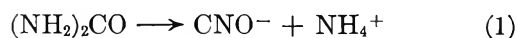
(14) J. J. Fripiat, A. Servais, and A. Leonard, *Bull. soc. chim. France*, 635 (1962).

Kinetics of Base-Catalyzed Hydrolysis of Urea

by K. R. Lynn¹

*Australian Atomic Energy Research Establishment,
Lucas Heights, N.S.W., Australia (Received July 20, 1964)*

The hydrolysis of urea in both water and aqueous mineral acids has been thoroughly investigated²; in the latter solvent ureolysis is not directly subject to catalysis by hydrogen ion, and in both solvents the decomposition of urea produces cyanate and ammonium ions.



In acid solutions, cyanate is rapidly converted to ammonia and carbon dioxide.³

Although ureolysis in the presence of hydroxide ion has been the subject of several reports,⁴ the kinetic laws pertaining to the reaction have not been unambiguously elucidated, nor the thermodynamic parameters determined. However, cyanate and ammonia are the products of the reaction, which, the data collected⁴ suggest, does not proceed in a simple bimolecular process first order in each reactant. Because the ureolysis may have relevance as a model system for a study of the urease-catalyzed hydrolysis proceeding in this laboratory, it has been re-examined.

Experimental

Reagents. The urea, which was used without further purification, was of Analytical grade, as were the sodium hydroxide, hydrochloric acid, and sodium chloride employed. Nessler's reagent was prepared by the conventional procedure.

Method. Solutions of urea in sodium hydroxide of known molarity were prepared immediately before use. Aliquots (1 or 2 ml.) were sealed in Jena or Pyrex glass tubes which were then immersed in a constant ($\pm 0.03^\circ$) temperature bath at zero time and removed therefrom at measured intervals. Reaction was quenched by chilling the samples in iced water; they were then shattered under hydrochloric acid of such strength as to provide an acidic medium for the residual urea and the products of the ureolysis. After a time sufficient to allow conversion of any cyanate formed^{4,5} to ammonium ion and carbon dioxide (during which period further hydrolysis of urea would be negligible^{2,3}), the acid solution was diluted to a concentration convenient for treatment with Nessler's solution and sub-

sequent measurement of the resulting color at 4100 Å. in a Unicam-SP600 spectrophotometer using cells of 1-cm. light path.

Results and Discussion

Pseudo-first-order rate constants were estimated graphically from the absorption measurements made as described above. Reaction was allowed to proceed in sodium hydroxide solutions ranging in concentration from 1 to 2 *M* for up to 70% of completion and no deviations from linearity were discerned in the pseudo-first-order plots. Re-formation of urea from its decomposition products in strong base was not found in this work nor by Warner.⁴ A fourfold increase in the concentration of urea, from 0.1 to 0.4 *M*, caused a small drop in the experimental rate constant for hydrolysis in 2 *M* sodium hydroxide at 50.0° (0.97×10^{-6} sec.⁻¹ to 0.95×10^{-6} sec.⁻¹) which was within the limit of the combined errors of the analytical procedure used.

Hydrolysis of urea in 2 *M* hydroxide at 60° for twenty times the "half-time" of reaction yielded only 96% of the expected amount of ammonia; a white powder, probably a polymer formed from cyanate, was also found in the reaction vessels. For this reason, ureolysis was usually allowed to proceed to only 20–40% of completion.

A typical set of pseudo-first-order rate constants from reaction in base ranging in concentration from 1 to 2 *M*, at 60°, are listed in Table I. Although the errors are somewhat larger than those expected from kinetics measurements, this may be attributed to the analytical procedure used; Shaw,² who also employed Nesslerization for assay, found comparable errors in rate measurements of ureolysis. Usually, three separate experiments, performed in duplicates containing seven to ten samples each, were made at each temperature at which the reaction was investigated.

When the rate constants collected over the full range of base concentrations and temperatures studied (1–2 *M*, 33–70°) were plotted as a function of hydroxide ion concentration, a series of curves was obtained which indicated more rapid reaction at higher concentrations of base than simple first-order dependence on that solution parameter would allow. This effect could not be attributed to the difference in ionic strength between

(1) Radiation Biology Division, NRC, c/o Atomic Energy of Canada Limited, Chalk River, Ont., Canada.

(2) W. H. R. Shaw and J. J. Bordeaux, *J. Am. Chem. Soc.*, **77**, 4729 (1955).

(3) A. R. Amell, *ibid.*, **78**, 6234 (1956).

(4) R. C. Warner, *J. Biol. Chem.*, **142**, 705 (1942).

(5) M. W. Lister, *Can. J. Chem.*, **33**, 426 (1955).

Table I: Pseudo-First-Order Rate Constants for Hydrolysis of 0.1 M Urea in Sodium Hydroxide at 60.0°

OH ⁻ , M	$k_{\text{exptl.}}^a \text{ sec.}^{-1} \times 10^{-6}$
1.0	1.02 ± 0.04
1.25	1.40 ± 0.03
1.50	1.79 ± 0.04
1.75	2.22 ± 0.13
2.0	2.69 ± 0.17

^a Errors appended are standard deviations.

solutions at 1 and 2 M base, for adjustment of those at the former concentration to 2 M with sodium chloride caused no measurable alteration in the rate of hydrolysis at 50° ($k_{\text{exptl}} = 0.320 \times 10^{-6} \text{ sec.}^{-1}$ for each experiment).

If base-catalyzed ureolysis proceeds with both uni- and bimolecular participation of hydroxide ion, then

$$v = k_1[\text{urea}] + k_2[\text{urea}][\text{OH}^-] + k_3[\text{urea}][\text{OH}^-]^2 \quad (2)$$

where v is the over-all velocity of reaction and k_1 is the specific rate constant for the hydrolysis in water, k_2 is that for reaction first order in both urea and hydroxide ion concentrations, and k_3 is that for reaction first order in substrate and second order with respect to base concentration. Consequently

$$(k_{\text{exptl}} - k_1)/[\text{OH}^-] = k_2 + k_3[\text{OH}^-] \quad (3)$$

where k_{exptl} is the experimentally determined pseudo-first-order rate constant for the base-catalyzed ureolysis.

When the left-hand side of eq. 3 was plotted as a function of hydroxide ion concentration, using values of k_{exptl} determined in this work and the data of Shaw and Bordeaux² for evaluation of k_1 , straight lines of intercept k_2 and k_3 were calculated using least-squares procedures, and the results are collected in Table II.

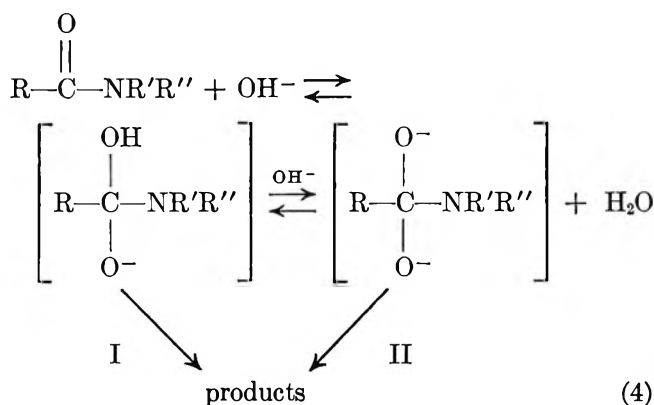
Bieschler and Taft have shown⁶ that the pseudo-first-order rate constants obtained for the hydrolysis

Table II: Evaluation of the Rate Constants k_2 and k_3

T , °C.	$k_2,^a \text{ l. mole}^{-1} \text{ sec.}^{-1} \times 10^{-7}$	$k_3,^a \text{ l.}^2 \text{ mole}^2 \text{ sec.}^{-1} \times 10^{-7}$
33.0	0.32 ± 0.02	0.19 ± 0.02
40.0	0.55 ± 0.08	0.47 ± 0.05
49.9	0.75 ± 0.06	2.01 ± 0.05
56.1	3.63 ± 0.36	2.74 ± 0.24
60.0	4.28 ± 0.30	4.14 ± 0.20
70.0	20.52 ± 3.72	7.42 ± 0.24

^a Errors appended are standard deviations.

of N-methylanilides of trifluoroacetic and other acids fit an equation analogous in form with that of (2), the term for the uncatalyzed reaction ($k_1[\text{amide}]$) being negligible in their systems. The equation was interpreted⁶ with the reaction route described by



Supporting evidence for this mechanism was adduced from a variety of reactions.⁶ More recently, Bender and Thomas⁷ have reported ¹⁸O-exchange studies which show that the initial step of eq. 4 must be represented by a rate, not a pre-equilibrium process for the anilides examined. It is also relevant to note that the hydrolysis of monochloroacetamide in sodium hydroxide has lately been shown⁸ to proceed *via* both intermediates I and II.

Arrhenius energies of activation for the reactions uni- and bimolecular in base were estimated, using least-squares procedures, as 21.59 and 21.49 kcal./mole, respectively. The corresponding entropies of activation are -20.0 and -21.4 e.u. The pairs of thermodynamic parameters are almost identical, a situation similar to that obtaining for the hydrolysis of monochloroacetamide.⁸ The Arrhenius energy of activation calculated from the experimental data of Warner,⁴ which were available for only two temperatures, is in good agreement with those reported above. Furthermore, interpolation of data reported⁴ previously at 66° in the Arrhenius plots for this work shows that there is close agreement between the rate constants found there and those of this study, even though entirely different methods of analysis were employed.

The route by which ureolysis in sodium hydroxide solution proceeds is described by eq. 4 in which R = NH₂ and R' = R'' = H. For this reaction, little stabilization of either intermediate I or II would be ex-

(6) S. S. Bieschler and R. W. Taft, *J. Am. Chem. Soc.*, **79**, 4927 (1957).

(7) M. L. Bender and R. J. Thomas, *ibid.*, **83**, 4183 (1961).

(8) F. Kezdy and A. Bruylants, *Bull. soc. chim. Belges*, **69**, 602 (1960).

pected; the large negative values of ΔS^* found verify that expectation. However, no definition of the rate-determining step(s) can be made at this time.

Acknowledgment. The author is indebted to Mr. H. E. Smith for competent technical assistance.

Depolarization of Scattered Light by Optically Active Systems

by P. F. Mijnlief and H. Zeldenrust

*Koninklijke/Shell-Laboratorium, Amsterdam, Holland
(Received July 29, 1964)*

In the present note, we wish to draw attention to a complication arising in light scattering measurements on optically active systems. In particular, it will be shown that the value of the measured depolarization of the scattered light ($\rho_{u,m}$) depends on the dimensions of the light scattering cell; in order to obtain from $\rho_{u,m}$ the depolarization (ρ_u) characteristic for the system investigated, a correction for this artifact has to be applied. This is important in the interpretation¹ of measured depolarizations as well as in molecular weight determinations. In the latter case one needs the isotropic scattering (I_{is}) and this is obtained by multiplying the measured scattering (I_m) by a Cabannes factor, which for unpolarized incident light is given by

$$\frac{6 - 7\rho_u}{6 + 6\rho_u}$$

Let us consider the scattering by a solute molecule and let the solute be optically active. In general, the light scattered in any direction will have an electrical vector with components along all of three perpendicular axes; if the x axis is the direction of the incident beam and if we are observing along the y axis, then only the components along the x and z axes make contributions, I_x and I_z , to I_m .

Now, if the solution is optically active, both I_x and I_z when "leaving" the measuring cell will have rotated around the y axis by an angle α ; the value of α depends on the distance traveled through the cell and on the specific rotation and concentration of the solute. Then the original I_x must be replaced by a new vector having the components $I_{x,x} = I_x \cos^2 \alpha$, and $I_{x,z} = I_x \sin^2 \alpha$; similarly, I_z has given rise to components $I_{z,z} = I_z \cos^2 \alpha$ and $I_{z,x} = I_z \sin^2 \alpha$. Consequently, the observed depolarization $\rho_{u,m}$ is given by

$$\rho_{u,m} = \frac{I_{x,x} + I_{z,z}}{I_{x,z} + I_{z,x}} = \frac{I_x \cos^2 \alpha + I_z \sin^2 \alpha}{I_x \sin^2 \alpha + I_z \cos^2 \alpha} = \frac{\rho_u + tg^2 \alpha}{\rho_u tg^2 \alpha + 1} \quad (1)$$

So even if ρ_u is zero, $\rho_{u,m}$ will be finite, viz., equal to $tg^2 \alpha$.

To check the validity of eq. 1, we measured for two wave lengths, 5461 and 4358 Å., the depolarization in an aqueous sucrose solution of concentration 0.5 g./cm.³ at 23°. The instrument used was that described by Coumou²; in one set of experiments the center of the incident beam (beam width, 2 mm.) was at 3 mm. and in another at a 17-mm. distance from the side wall. By inserting the relevant α -values into eq. 1, ρ_u was calculated from $\rho_{u,m}$. The results are given in Table I. It is seen that ρ_u , unlike $\rho_{u,m}$, is within the experimental error independent of the distance traveled by the scattered light through the cell, as it should be.

Table I: Correction of Depolarization in Sucrose Solution

Wave length, Å.	Beam dis- tance from side wall, mm.	$\rho_{u,m}$	α , deg.	ρ_u
5461	3	0.040	1.16	0.040
5461	17	0.052	6.60	0.039
4358	3	0.031	1.92	0.030
4358	17	0.066	10.88	0.029

Sucrose solutions are sometimes used for calibrating light scattering instruments.³ Scattering of light by such solutions was studied by Maron and Lou⁴ and by Stigter,⁵ but these authors fail to mention the rotation effect discussed above. Both publications^{4,5} compare τ_m , the turbidity derived from light scattering, with τ_{th} , the turbidity calculated from thermodynamic data. The latter quantity should be equal to τ_{is} , the turbidity for isotropic scattering. As τ_m is the total scattering, it must be converted into τ_{is} by applying the relation

$$\tau_{is} = \tau_m \times \frac{6 - 7\rho_u}{6 + 6\rho_u} \quad (2)$$

For an easier comparison with the papers discussed, we use the symbol τ for a quantity loosely called

- (1) W. Prins, *J. Phys. Chem.*, **65**, 369 (1961).
- (2) D. J. Coumou, *J. Colloid Sci.*, **15**, 408 (1960).
- (3) L. H. Princen, Thesis, University of Utrecht, 1959.
- (4) S. H. Maron and R. L. H. Lou, *J. Phys. Chem.*, **59**, 231 (1955).
- (5) D. Stigter, *ibid.*, **64**, 114 (1960).

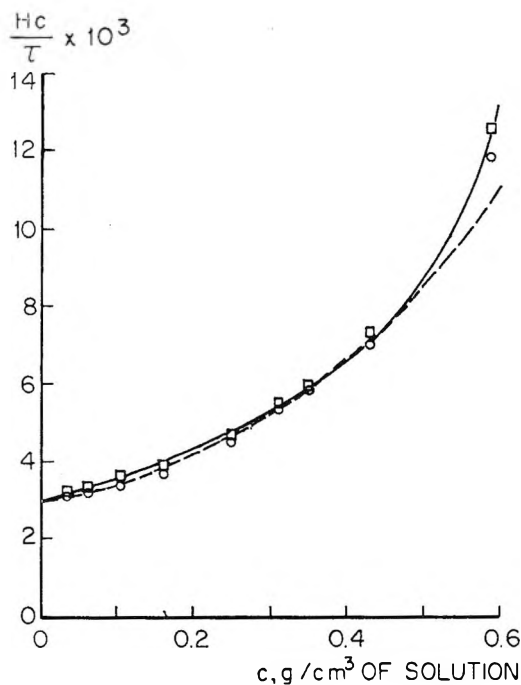


Figure 1. Light scattering by aqueous sucrose solutions at 25°: full curve, Hc/τ_{th} (Maron and Lou⁴); dashed curve, Hc/τ_{th} (Stigter⁵); O, Hc/τ_{is} (Maron and Lou, ⁴ λ 5461 Å.); □, Hc/τ_{is} (Maron and Lou, ⁴ λ 4358 Å.).

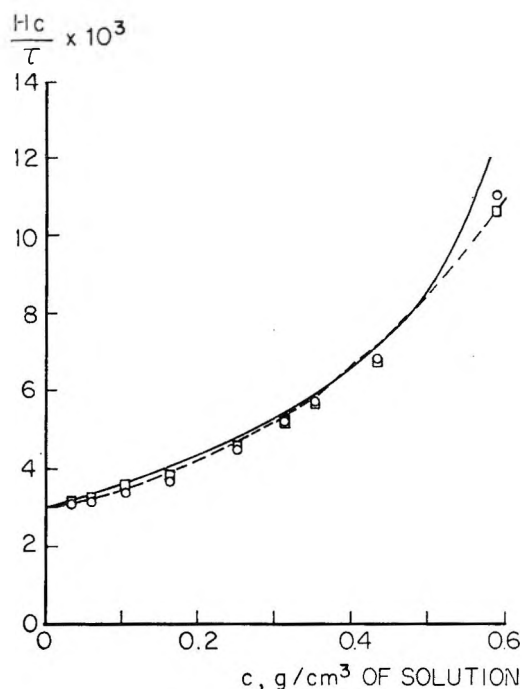


Figure 2. Legend as in Figure 1, but τ_{is} calculated by using ρ_u instead of $\rho_{u,m}$.

"turbidity." In fact, this "turbidity" is nothing but R_{90} , the Rayleigh ratio, multiplied by $16\pi/3$; as was stressed by Prins,¹ it differs from the real turbidity of the solution by a factor $(1 + \frac{1}{2}\rho_u)/(1 + \rho_u)$.

Maron and Lou⁴ claim a reasonable agreement between τ_{th} from osmotic pressure and τ_{is} ; according to Stigter,⁵ who suggests some corrections in the method for calculating τ_{th} from osmotic pressure, however, the former quantity is, at the highest concentration studied, larger than the latter. In Figure 1 Maron and Lou's⁴ Figure 4 is reproduced; the τ on the ordinate is equivalent either to τ_{th} or to τ_{is} . Furthermore Stigter's⁵ theoretical curve has been added; this curve was derived, taking into account his slightly different way of plotting, from Stigter's Figure 4.

We also draw attention to the differences between the experimental results for the two wave lengths used. As τ_{is} only depends on the thermodynamic properties of the system, it should be insensitive for the particular wave length used to measure its value.

We suspected that the latter discrepancies were due to the use of $\rho_{u,m}$ -values, instead of ρ_u -values, for converting τ_m into τ_{is} . We therefore multiplied the values of Hc/τ_{is} of Figure 1 by the factor

$$\frac{6 + 6\rho_u/6 + 6\rho_{u,m}}{6 - 7\rho_u/6 - 7\rho_{u,m}}$$

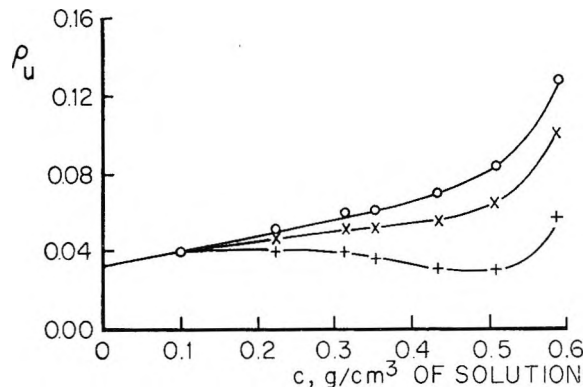


Figure 3. Depolarization of scattered light by sucrose solutions at 25°: O, $\rho_{u,m}$ (Maron and Lou, ⁴ λ 4358 and 5461 Å.); X, ρ_u , λ 5461 Å.; +, ρ_u , λ 4358 Å.

thus obtaining new values, free from the "optical activity effect," which are plotted in Figure 2. The ρ_u -values were derived from Maron and Lou's $\rho_{u,m}$ -values with the aid of eq. 1. Figure 3 gives both $\rho_{u,m}$ and ρ_u as a function of sucrose concentration; the values of α employed were those for a 4×4 -cm. light scattering cell in conformity with the experimental setup.⁶

(6) S. H. Maron and R. L. H. Lou, *J. Polymer Sci.*, **14**, 29, 273 (1954).

Figure 2 shows that now at the highest sucrose concentration the experimental light scattering turbidity is nearer to Stigter's thermodynamic value. In addition, the experimental turbidities for the two wave lengths are closer together now, especially at the higher concentrations where $\rho_{u,m}$ measurements become more accurate.

In general, the effect discussed will not be very important in turbidity measurements. As shown by Table I and Figure 3, however, attention should be paid to it if one is concerned with the interpretation of the depolarization itself.

Acknowledgment. We gratefully acknowledge valuable discussions with Dr. D. Coumou of this laboratory.

Electric Moment of Isonicotinamide in Benzene and Dioxane Solutions¹

by William P. Purcell and Judith A. Singer

Department of Pharmaceutical and Medicinal Chemistry, College of Pharmacy, University of Tennessee, Memphis, Tennessee (Received August 3, 1964)

We recently reported the dipole moments of some selected N-alkyl-substituted nicotinamides² measured in benzene solution, and the calculated values for the corresponding amide group moments. Nicotinamide and the monosubstituted derivatives were so insoluble in benzene that we were forced to measure very dilute solutions. The compounds are soluble in dioxane, but the increase in problems of association between solvent and solute molecules makes this an unattractive solvent.³ As a result, we have applied the mixed benzene-dioxane solvent technique, described by Estok, *et al.*,³⁻⁶ to isonicotinamide, a molecule which fits into our series² and one which has low solubility in benzene.

Experimental

Reagent. Isonicotinamide (research grade, Aldrich

(1) This investigation is being supported by the National Science Foundation (GB-2381/B-15989), U. S. Public Health Service Grant MH-04379 and by a grant from the Geschickter Fund for Medical Research, Inc. Computer facilities were provided through U. S. Public Health Grant FR-1.

(2) W. P. Purcell, *J. Phys. Chem.*, **68**, 2666 (1964).
 (3) G. K. Estok and C. H. Stembridge, *J. Am. Chem. Soc.*, **76**, 4316 (1954).
 (4) G. K. Estok and S. P. Sood, *J. Phys. Chem.*, **61**, 1445 (1957).
 (5) G. K. Estok, S. P. Sood, and C. H. Stembridge, *ibid.*, **62**, 1464 (1958).
 (6) G. K. Estok and S. P. Sood, *ibid.*, **66**, 1372 (1962).

Table I: Dielectric Constants and Refractive Indices of Isonicotinamide Solutions Measured at 25° in Benzene, Dioxane, and Mixtures of Benzene and Dioxane

Dioxane-benzene mixture, mole % dioxane	$w_2 \times 10^3$	ϵ	n_D	$w_2 \times 10^3$	ϵ	n_D	$w_2 \times 10^3$	ϵ	n_D
0.00	0.0000	2.2750	1.4976	0.2014	2.2766	1.4977	0.2282	2.2772	1.4978
61.43	0.0000	2.2414	1.4430	1.1982	2.2596	1.4434	1.8531	2.2696	1.4435
71.34	0.0000	2.2275	1.4345	3.0080	2.2520	1.4347	4.0066	2.2628	1.4351
78.06	0.0000	2.2088	1.4202	1.5430	2.2386	1.4207	2.2192	2.2628	1.4209
82.22	0.0000			1.8482			5.6893		
100.00	0.0000			0.8722	2.2088	1.4207	1.7007	2.2382	1.4213
100.00	0.0000			3.2757			4.6357		
							2.7089	2.2541	1.4218
							8.3482	2.2724	1.4222
							2.7089	2.2724	
							6.5434		
							2.2782	2.2795	1.4447
							2.2726	2.2856	1.4451
							2.0841	2.2856	
							0.3242	2.2795	
							0.4803	2.2795	
							0.5997	2.2802	
							14.252	2.2987	
							4.4782	2.2987	
							9.7615	1.4358	
							3.7798	1.4357	
							10.127	1.4218	
							13.342	1.4222	

Table II: Slopes, Orientation Polarizations at Infinite Dilution, Observed Moments, and Amide Group Moments of Isonicotinamide at 25°

Solvent	Technique	α	γ	$P_{2,m}$, cc./mole	μ , D.	m_2 , D.
Benzene	Pure solvent	8.952	0.8937	184.6	3.00 ± 0.09	2.88
Benzene	Mixed benzene-dioxane solvent	12.232	0.1736	276.7	3.68	3.77
Dioxane	Pure solvent	16.784	0.4322	328.1	4.01	4.19
Dioxane	Pure solvent			311.3 ^a	3.88 ^a	4.03
Dioxane	Mixed benzene-dioxane solvent	17.120	0.3943	334.8	4.05	4.23

^a D. G. Leis and B. C. Curran, *J. Am. Chem. Soc.*, **67**, 79 (1945).

Chemical Co., Inc.) was recrystallized five times from ethyl acetate; m.p. 148.9–149.4° (lit.⁷ m.p. 155°) and was dried under vacuum in an Abderhalden pistol.

Solvents. The compound was measured in dilute benzene solution using Spectroquality benzene (Matheson Coleman and Bell), in dilute *p*-dioxane solution using Spectroquality *p*-dioxane (Matheson Coleman and Bell), and in dilute mixed benzene-*p*-dioxane solutions, using the above mentioned solvents.

Apparatus. The dielectric constants, ϵ , and refractive indices, n_D , as a function of the weight fraction, w_2 , of the solute were measured at 25° as previously described.² The data are given in Table I.

Calculations. The dipole moments in pure benzene and in pure dioxane solution were calculated from the equations and methods described by Smith.⁸ The dipole moment in pure benzene was also calculated from the equations and methods described by Halverstadt and Kumler⁹ and Guggenheim,¹⁰ and the standard error of this value was calculated from the equation used by Kumler,¹¹ which takes into account only errors in the dielectric constant measurement. The dipole moments measured in mixed solvent were calculated from a modification of the method described by Estok, *et al.*^{3–6} The value α_∞ (slope of ϵ vs. w_2 in hypothetically pure benzene or dioxane solution) was calculated exactly as described by these authors; a corresponding value, γ_∞ (slope of n_D^2 vs. w_2 in hypothetically pure benzene or dioxane solution) was calculated in an analogous manner. These values were then used to calculate the dipole moment by the Smith method.⁸ Least-squares analyses were applied to determine all slopes and intercepts used in the calculations.

Results and Discussion

Table II gives the slopes of the dielectric constant and square of the refractive index with concentration, the orientation polarization calculated from Smith's modification⁸ of the Guggenheim method,¹⁰ the dipole moments in Debye units, and the amide group mo-

ments, m_2 . The amide group moments were calculated from eq. 1 which is a special case of Eyring's equation¹²

$$\mu^2 = m_1^2 + m_2^2 - 2m_1m_2 \cos \theta \cos \phi \quad (1)$$

assuming free rotation or symmetrical rotational energy barriers.¹³ We used $m_1 = 2.28$ (the observed value for pyridine measured in benzene solution²) for the benzene values, $m_1 = 2.22$ (the observed value for pyridine measured in dioxane solution^{14,15}) for the dioxane values, $\theta = 180^\circ$, and $\phi = 110^\circ$ (from Bates and Hobbs¹⁶).

There is no literature value for the moment of isonicotinamide measured in benzene, but the dioxane value, 3.88, reported by Leis and Curran¹⁴ can be compared with our value, 4.01. The benzene value, 3.00, measured in the pure solvent is 0.68 D. lower than that measured by the mixed solvent technique. The latter moment, 3.68, agrees exactly with the moment, 3.68, of isonicotinamide calculated from eq. 1 reported earlier.² The agreement between the mixed solvent, 4.05, and the pure solvent, 4.01, for the dioxane values is very good.

The large difference between the two moments for isonicotinamide in benzene can be interpreted in terms of the formation of dimers of zero moment⁶ with pure benzene as the solvent, thus lowering the observed moment in this medium. The excellent agreement be-

(7) K. W. Merz and H. Stolte, *Arch. Pharm.*, **293**, 92 (1960).

(8) J. W. Smith, *Trans. Faraday Soc.*, **46**, 394 (1950).

(9) I. F. Halverstadt and W. D. Kumler, *J. Am. Chem. Soc.*, **64**, 2988 (1942).

(10) E. A. Guggenheim, *Trans. Faraday Soc.*, **45**, 714 (1949).

(11) W. D. Kumler, A. Lewis, and J. Meinwald, *J. Am. Chem. Soc.*, **83**, 4591 (1961).

(12) H. Eyring, *Phys. Rev.*, **39**, 746 (1932).

(13) H. B. Thompson, *J. Phys. Chem.*, **64**, 280 (1960).

(14) D. G. Leis and B. C. Curran, *J. Am. Chem. Soc.*, **67**, 79 (1945).

(15) J. Barassin and H. Lumbroso, *Bull. soc. chim. France*, **492** (1961).

(16) W. W. Bates and M. E. Hobbs, *J. Am. Chem. Soc.*, **73**, 2151 (1951).

tween the observed mixed solvent moment and calculated moment, and between the value of m_2 , 3.77, and the moment of benzamide, 3.77⁴ (the group moment values, m_2 (Table II), represent the $-\text{CONH}_2$ group attached to the aromatic ring and, therefore, might be compared with the benzamide moment) in benzene using mixed solvent techniques indicates that this technique apparently circumvents the problems of association to a large extent.⁶ The mixed solvent moment for benzamide in dioxane is 3.88,⁴ which should be compared with our m_2 value, 4.23; the agreement here is not so good as that of the benzene values from mixed solvent techniques.

The larger moment found in dioxane as compared with benzene is in keeping with other experimental measurements and has been discussed in detail elsewhere.¹⁷ For example, associated molecules, when diluted with dioxane, break into single molecules (*via* the formation of hydrogen bonds to the dioxane oxygen atoms), whereas nonpolar solvents lack the ability to disrupt these associations.¹⁸ In addition, Woodbrey and Rogers¹⁹ found that the energy barriers restricting internal rotation about the central C-N bond in N,N-disubstituted amides increased with increasing polarity of the solvent in which the amide was measured. This would indicate greater contribution of the resonance form $\text{O}^-\text{C}=\text{N}^+$ in the more polar solvents, a corresponding increase in m_2 , and, therefore, an increase in the observed moment; this explains qualitatively the increase in moment measured in dioxane over that measured in benzene (the moment of dioxane is 0.4,²⁰ whereas the moment of benzene is 0²⁰).

Assuming that the mixed solvent moment in benzene, 3.68, is virtually free of association problems,⁶ the number of dimers in pure benzene solution was calculated from eq. 2,²¹ where μ_{obsd} is the observed moment,

$$\mu^2_{\text{obsd}} = C_{\text{unassociated}} \mu^2_{\text{unassociated}} + C_{\text{dimer}} \mu^2_{\text{dimer}} \quad (2)$$

3.00, in pure benzene, $C_{\text{unassociated}}$ is the fraction of unassociated molecules with moment ($\mu_{\text{unassociated}}$), 3.68, and C_{dimer} is the fraction of the isonicotinamide molecules in the dimer configuration having zero (μ_{dimer}) moment. The values obtained are 66% unassociated, 34% in the dimer form.

(17) C. P. Smyth, "Dielectric Behavior and Structure," McGraw-Hill Book Co., Inc., New York, N. Y., 1955, p. 329.

(18) P. A. Geary and J. G. Miller, *J. Electrochem. Soc.*, **97**, 54 (1950).

(19) J. C. Woodbrey and M. T. Rogers, *J. Am. Chem. Soc.*, **84**, 13 (1962).

(20) A. L. McClellan, "Tables of Experimental Dipole Moments," W. H. Freeman and Co., San Francisco, Calif., 1963.

(21) C. P. Smyth, ref. 17, p. 293.

The Infrared Spectra of Perfluorocyclopropane and *cis*- and *trans*-Perfluorobutene-2¹

by Julian Hecklen, Francis Wachi, and Vester Knight

Aerospace Corporation, El Segundo, California
(Received August 4, 1964)

We wish to report the infrared spectra in the NaCl region of three simple fluorocarbons. The preparation and purification procedure of the compounds cyclo-C₃F₆, *cis*-C₄F₈-2, and *trans*-C₄F₈-2 is described by Greene and Wachi.² For the *cis* and *trans* compounds, it was necessary that we perform the purification procedure twice for complete separation. The spectra were obtained on a Perkin-Elmer 21 infrared spectrometer and the bands and their relative intensities are listed in Table I.

The infrared spectrum of cyclo-C₃F₆ has not been previously reported. The molecular symmetry is D_{3h}, and the only allowed infrared fundamental vibrations are the two A₂' and the four E' bands. The two intense bands at 1368 and 1272 cm.⁻¹ must consist mainly of C-F stretching motions. Thus, one of these is an A₂' band and the other an E' band; it is not clear which is which. However, there are some indications to suggest that the 1368-cm.⁻¹ band has A₂' symmetry and the 1272-cm.⁻¹ band has E' symmetry. The A₂' band involves the asymmetric stretching motion of the CF₂ group, whereas the E' band involves the symmetric stretching motion. Usually, the asymmetric mode has higher frequency, which corresponds to the assignments of cyclo-C₃H₆.³ Furthermore, if the 2532-cm.⁻¹ band is the overtone of the 1272-cm.⁻¹ band, then the latter band must be of E' symmetry as the overtones of A₂' bands are symmetry forbidden. The disturbing feature is that asymmetric bands are usually more intense, but our assignment requires the reverse.

The strong band at 859 cm.⁻¹ undoubtedly corresponds to the CF₂ deformation of E' symmetry. The two bending frequencies associated with the motion of the CF₂ groups relative to the carbon skeleton lie below 650 cm.⁻¹ and are not observed. The E' ring-deformation frequency of cyclopropyl compounds usually lies within 25 cm.⁻¹ of 1025 cm.⁻¹.⁴ No such band ap-

(1) This work was supported by the U. S. Air Force under Contract No. AF 04(695)-269.

(2) S. A. Greene and F. M. Wachi, *Anal. Chem.*, **35**, 928 (1963).

(3) (a) H. H. Günthard, R. C. Lord, and T. K. McCubbin, Jr., *J. Chem. Phys.*, **25**, 768 (1956); (b) H. E. Duckworth, *Can. J. Phys.*, **34**, 1448 (1956).

Table I: Infrared Frequencies

ν , cm. ⁻¹	Relative intensity	ν , cm. ⁻¹	Relative intensity
Cyclo-C ₃ F ₆			
859	s	1172	vw
932	w	1272	vs
978	w	1368	s
1111	w	2532	w
1135	w		
<i>cis</i> -C ₄ F ₈ -2			
719	vs	1224	vs
726	sh	1245	vs
760	m	1287	m
766	m	1350	vs
905	vw	1389	m
952	vs	1481	vw
956	sh	1524	vw
1064	sh	1562	w
1111	vs	1686	sh
1156	sh	1724	s
1166	sh	1779	m
1193	vs		
<i>trans</i> -C ₄ F ₈ -2			
682	vs	1387	m
696	sh	1424	m
712	m	1451	vw
730	vw	1499	m
760	m	1527	w
875	sh	1560	w
878	sh	1582	m
882	s	1751	w
890	sh	1848	m
945	m	1953	w
982	m	2000	w
1070-1105	m	2053	m
1149	sh	2105	w
1163	sh	2353	m
1193	vs	2512	w
1242	vs	2652	w
1292	vs	2932	w
1321	sh	3003	w

^a s = strong, m = medium, w = weak, v = very, sh = shoulder.

pears in our spectrum; thus, from this point of view, cyclo-C₃F₆ must be considered atypical. We tentatively assign the 978-cm.⁻¹ band to this mode.

The weak band at 2532 cm.⁻¹ must be either a combination or an overtone of C-F stretching modes. Only seven such possibilities are consistent with the symmetry selection rules; these are the overtones of the E' or E'' bands or the five combinations A₁' × A₂'', E' × A₁', E'' × A₂'', E' × E', and E' × E''. The overtone of the E' band seems very attractive as 2532 is almost twice 1272, a result that would be expected if anharmonicity were considered.

The infrared spectrum has been reported for mixtures of *cis*- and *trans*-C₄F₈-2^{5,6} but not for the pure geometric isomers. If the internal rotations of the CF₃ groups are nearly free, then the *trans* and *cis* compounds have C_{2h} and C_{2v} symmetry, respectively. Table II gives the symmetry classes and approximate descriptions of the vibrations.

Table II: Vibrations of *cis*- and *trans*-C₄F₈-2

Description	<i>trans</i> symmetry	<i>cis</i> symmetry
In-plane motions		
C=C stretch	A _g	A ₁
C-F stretch	A _g	A ₁
C-C stretch	A _g	A ₁
CF ₃ symmetric stretch	A _g	A ₁
CF ₃ asymmetric stretch	A _g	A ₁
C-F bend	A _g	A ₁
C-C bend	A _g	A ₁
CF ₃ symmetric bend	A _g	A ₁
CF ₃ asymmetric bend	A _g	A ₁
CF ₂ coupling wag	A _g	A ₁
C-F stretch	B _u	B ₁
C-C stretch	B _u	B ₁
CF ₃ symmetric stretch	B _u	B ₁
CF ₃ asymmetric stretch	B _u	B ₁
C-F bend	B _u	B ₁
C-C bend	B _u	B ₁
CF ₃ symmetric bend	B _u	B ₁
CF ₃ asymmetric bend	B _u	B ₁
CF ₂ coupling wag	B _u	B ₁
Out-of-plane motions		
CF ₂ asymmetric stretch	A _u	A ₂
Skeletal bend	A _u	A ₂
Skeletal bend	A _u	A ₂
CF ₃ asymmetric bend	A _u	A ₂
CF ₃ coupling wag	A _u	A ₂
CF ₃ asymmetric stretch	B _g	B ₂
Skeletal bend	B _g	B ₂
CF ₃ asymmetric bend	B _g	B ₂
CF ₂ coupling wag	B _g	B ₂

For the *trans* molecule, all the *gerade* vibrations are symmetry forbidden in the infrared spectrum. Thus, there are five stretching modes that should be active. Three of these are surely the intense bands at 1193, 1242, and 1292 cm.⁻¹. The band at 882 cm.⁻¹ also might correspond principally to stretching motions. At least one (and maybe two) of the stretching bands is not readily discernible; it is probably completely or

(4) L. J. Bellamy, "The Infrared Spectra of Complex Molecules," John Wiley and Sons, Inc., New York, N. Y., 1958, p. 29.

(5) T. J. Brice, J. D. La Zerte, L. J. Hals, and W. H. Pearson, *J. Am. Chem. Soc.*, **75**, 2698 (1953).

(6) R. N. Haszeldine, *J. Chem. Soc.*, 4423 (1952).

partially obscured by the other bands. All the observed overtone bands must be combinations of *gerade* and *ungerade* bands. As a result, the C=C stretch must participate in the overtone bands at 2932 and 3003 cm.⁻¹ (except in the unlikely event that they are triple combinations). If the intense bands at 1242 and 1292 cm.⁻¹ are the other participating bands, then the differences are 1711 and 1690 cm.⁻¹, respectively, in reasonably close agreement. Allowing for some anharmonicity sets the C=C stretching frequency at 1710 ± 20 cm.⁻¹, which correlates nicely with the corresponding frequency in the *cis* molecule.

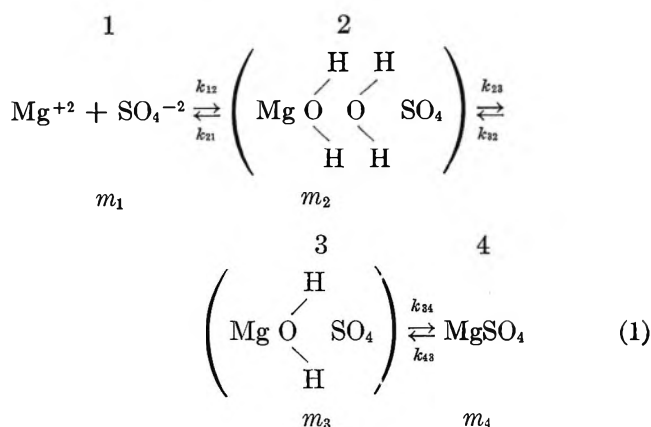
For *cis*-C₄F₈-2, all bands are allowed in the infrared spectrum, though some may be weak. The band at 1724 cm.⁻¹ is the double-bond stretch. Of the remaining ten stretching modes, at least five are observed, at 1111, 1193, 1224, 1245, and 1350 cm.⁻¹. The band at 952 cm.⁻¹ is also likely to contain considerable stretching motion. The other four stretching motions either are weak bands or are completely or partially obscured.

Multistate Dissociation and the Effect of Pressure on the Equilibrium on Magnesium Sulfate¹

by F. H. Fisher

University of California, San Diego, Marine Physical Laboratory of the Scripps Institution of Oceanography, San Diego, California 92152 (Received August 8, 1964)

Eigen and Tamm² have proposed a four-state model for the dissociation of MgSO₄ in order to explain ultrasonic absorption in aqueous solutions of this salt. The model is shown in eq. 1, where the free ions which would affect the electrical conductivity of solutions are those in state 1.



The conventional molal equilibrium constant is

$$K_m = \frac{m_1^2 \pi^f}{m_2 + m_3 + m_4} = \frac{m \gamma_{\pm}^2}{1 - \alpha} \quad (2)$$

where *m* is the molality of the salt, *m_i* is the molal concentrations of the respective states, *α* is the degree of dissociation, and $\gamma_{\pm}^2 = \alpha^2 f_{\pm}^2 = \alpha^2 \pi^f$.

Eigen and Tamm^{2b} proposed two sets of parameters to describe the four-state model. Work on the effect of pressure on sound absorption in MgSO₄ solutions favors one of the sets of parameters and these values are set forth below

$$K_{12} = 0.04 = \frac{m_1^2 \pi^f}{m_2} = \frac{k_{21}}{k_{12}}, \quad \Delta V_{12} = 0 \quad (3)$$

$$K_{23} = 1 = \frac{m_2}{m_3} = \frac{k_{32}}{k_{23}}, \quad \Delta V_{23} = -18 \text{ cc./mole} \quad (4)$$

$$K_{34} = 9 = \frac{m_3}{m_4} = \frac{k_{43}}{k_{34}}, \quad \Delta V_{34} = -3 \text{ cc./mole} \quad (5)$$

Calculation

Using eq. 2, 3, 4, and 5, it is possible to show

$$K_m = \frac{K_{12} K_{23} K_{34}}{1 + K_{34} + K_{23} K_{34}} \quad (6)$$

From the Van't Hoff equation

$$\left(\frac{\partial \ln K_{ij}}{\partial p} \right)_{T,m} = - \frac{\Delta V_{ij}}{RT} \quad (7)$$

the effect of pressure on the *K_{ij}* can be calculated using the above parameters. The effect of pressure on π^f is negligible at low concentrations. Using the equation

$$\left(\frac{\partial \ln f_{\pm}^2}{\partial p} \right) = \frac{\Delta V^*}{RT} \quad (8)$$

the value of ΔV^* is of the order of 0.2 cc./mole at *m* = 0.02.³ Values of the parameters as a function of pressure are given in Table I. This is carried up to only the pressures at which ultrasonic absorption has been measured.⁴

In conductivity experiments and in the Fuoss theory of ion association, only a two-state model has been used to calculate the effects of pressure on equilibrium according to the equation

(1) This paper represents results of research sponsored by the Office of Naval Research under contract Nonr 2216 (05).

(2) (a) M. Eigen and K. Tamm, *Z. Elektrochem.*, **66**, 93 (1962); (b) *ibid.*, **66**, 107 (1962).

(3) F. H. Fisher, *J. Phys. Chem.*, **66**, 1607 (1962).

(4) F. H. Fisher, *J. Acoust. Soc. Am.*, to be published.

$$\left(\frac{\partial \ln K_m}{\partial p}\right)_{T,m} = \frac{-\Delta V^0}{RT} \quad (9)$$

where ΔV^0 represents the difference in partial molal volumes between products and reactants. However, from eq. 6 it is seen that ΔV^0 is a composite of all volume changes involved in the four-state model; that is

$$-\frac{\Delta V^0}{RT} = \left(\frac{\partial \ln K_m}{\partial p}\right)_{T,m} = \frac{\partial \ln \left[\frac{K_{12}K_{23}K_{34}}{1 + K_{34} + K_{23}K_{34}} \right]}{\partial p} \quad (10)$$

From a plot of $RT \log K_m$ (calculated from the Eigen and Tamm model) vs. pressure, the slope of this curve $\Delta V^0 = -7.7$ cc./mole. This is in excellent agreement with the experimental value of $\Delta V^0 = -7.3$ cc./mole obtained by Fisher³ from conductivity experiments and with the value $\Delta V^0 = -7.4$ cc./mole calculated by Hamann⁵ from the ion association theory of Fuoss.

Discussion

From the close agreement of the values evaluated by three independent methods, it appears that acoustic and conductivity data on aqueous solutions of MgSO_4 can be interpreted in a quantitative manner on the basis of a four-state dissociation model. It is seen how different values of the ΔV_{ij} describing each step of the dissociation reaction must be considered in order to relate the multistate model to conductivity measurements.

As Eigen and Tamm point out, their values of the K_{ij} are only known to within $\pm 50\%$ and the ΔV_{ij} to within $\pm 20\%$ based on their ultrasonic experiments at atmospheric pressure. Eigen and Tamm show that adiabatic and isothermal ΔV_{ij} can be taken as numerically equal in aqueous solutions since the enthalpy correction term is negligible. It is seen that one of their four-state models is consistent with both acoustic and conductivity data as a function of pressure.

Table I: Pressure Dependence of Equilibrium Constants of MgSO_4 Based on Four-State Eigen and Tamm Model

P , p.s.i.	K_m	K_{12}	K_{23}	K_{34}
14.7	0.019	0.04	1	9.0
5,000	0.021	0.04	1.28	9.4
10,000	0.024	0.04	1.65	9.8
15,000	0.026	0.04	2.13	10.24

Acknowledgment. The author wishes to thank Mr. Douglas Davis for his assistance with the calculations.

(5) S. D. Hamann, *J. Acoust. Soc. Am.*, **68**, 375 (1964).

Dissociation Studies in High Dielectric Solvents.

II. Conductance of Some 2-2 Salts in Formamide at 25°

by Gyan P. Johari¹ and P. H. Tewari

Department of Chemistry, University of Gorakhpur, Gorakhpur, U. P., India (Received September 8, 1964)

Recent conductance studies²⁻⁵ have demonstrated that the Fuoss-Onsager extended theory⁶ adequately explains the conductance behavior of some high-charge symmetrical salts. Several high-charge symmetrical salts have been found unassociated in aqueous solutions,²⁻⁴ thus establishing a base line for a reasonable estimation of association constants in other solvents by this method. Since ion association depends on coulombic interaction, we would expect less association in media of high dielectric constants. Dawson⁷ and his co-workers have found that the conductance data for many electrolytes in such solvents give anabatic phoreograms, and Kohlrausch plots represent the conductance data fairly satisfactorily for 1-1 salts to much higher concentrations than in water. We have undertaken the study of some 2-2 salts in formamide to see if a high dielectric constant would relegate ion association to any extent. Conductance of MgSO_4 , NiSO_4 , and $\text{Cu(en)}_2\text{SO}_4$ has been measured in formamide at 25°. A study of the sulfates of Cu, Zn, and Mn could not be successfully done on account of the chemical interaction of the salt with formamide.

Experimental

Bis(ethylenediamine)cupric sulfate was prepared by mixing a warm aqueous solution of CuSO_4 (British Drug Houses Analar grade) and pure ethylenediamine.

(1) Grateful acknowledgment is made to the University Grants Commission, New Delhi, for the grant of a fellowship to G. P. J.

(2) G. Atkinson, M. Yokoi, and C. J. Hallada, *J. Am. Chem. Soc.*, **83**, 1570 (1961).

(3) G. Atkinson and G. J. Hallada, *ibid.*, **83**, 3759 (1961).

(4) G. Atkinson and M. Yokoi, *ibid.*, **83**, 4367 (1961).

(5) G. Atkinson and S. Petrucci, *J. Phys. Chem.*, **67**, 337 (1963).

(6) R. M. Fuoss and F. Accassina, "Electrolytic Conductance," Interscience Publishers, Inc., New York, N. Y., 1959.

The salt was precipitated with ethanol and redissolved in water. The product was recrystallized five times from conductivity water. The pure salt was dried over CaCl_2 at 25° to its dihydrate. Analysis for the sulfate was performed by estimating it as BaSO_4 and for Cu^{2+} as CuCNS by decomposing a definite amount of the salt with HCl and then precipitating as CuCNS . *Anal.* Calcd. for $\text{Cu}(\text{en})_2\text{SO}_4 \cdot 2\text{H}_2\text{O}$: Cu, 20.11; SO_4 , 30.41. Found: Cu, 19.93; SO_4 , 30.23.

$\text{MgSO}_4 \cdot 7\text{H}_2\text{O}$ and $\text{NiSO}_4 \cdot 6\text{H}_2\text{O}$, Judex A.R. grade, were recrystallized twice from conductivity water and dried over the partially dehydrated salt.

Solvent. Formamide (E. Merck, Germany) was shaken with quicklime, decanted, and fractionally distilled. This was repeated twice. The distilled formamide was kept over anhydrous sodium sulfate. This, on fractionating through a 20-cm. column at a

The final value of the cell constant was obtained from measurement on 10–14 independently prepared aqueous KCl solutions, using the L.Z.F. method.⁸

The solutions were prepared directly into the cells by a weight dilution method from the stock solutions. Before each run, the cells were cleaned with fuming nitric acid, rinsed with conductivity water, steamed out for 0.5 hr., and dried at 110° in an oven. The molarity of the solutions was calculated assuming the density to be equal to that of the pure solvent. Each run was repeated with a different stock solution and a different solvent batch. The conductances of the solutions were obtained by subtracting the conductance of the solvent of the same batch determined separately in a cell at the same time.

The resistances were measured at $25 \pm 0.005^\circ$ at 1000 cycles. No change in resistance with frequency was recorded during a check measurement up to 10,000 cycles.

Equipment. The bridge equipment consisted of two Leeds and Northrup Kohlrausch slide wires (Model 4258), a Hewlett-Packard (Model 200 AB) variable frequency oscillator with a transformer and amplifier, one Leeds and Northrup 10,000-ohm decade resistance box (inductance compensated and graduated in 0.1-ohm intervals), and two variable capacity condensers of 1000 and 500 pf. The bridge arrangement was made according to Jones design with Wagner's grounding device. The ratio arms R_5 and R_6 were made with the Kohlrausch slide wire. A pair of Leeds and Northrup headphones was used as the null detecting device.

Table I: Concentration and Equivalent Conductance Data^a

$\text{MgSO}_4 \cdot 7\text{H}_2\text{O}$		$\text{NiSO}_4 \cdot 6\text{H}_2\text{O}$		$\text{Cu}(\text{en})_2\text{SO}_4 \cdot 2\text{H}_2\text{O}$	
$c \times 10^4$	Λ	$c \times 10^4$	Λ	$c \times 10^4$	Λ
1.2646	27.236	2.4067	30.262	2.5530	30.409
2.3376	26.891	2.5980	30.110	4.1337	29.828
2.6099	26.808	3.6573	29.697	5.7498	29.489
5.0861	26.201	5.7750	29.220	8.3918	28.996
8.1822	25.536	7.4610	28.875	12.4420	28.259
9.4591	25.259	10.309	28.420	18.352	27.490
13.838	24.574	12.850	28.021	19.374	27.278
19.352	23.789	16.611	27.465		
		21.322	26.942		

^a Units: c , moles/l.; Λ , equivalent conductance.

Table II: Derived Parameters for the Data

Salt	Λ^0	aJ	$\sigma\Lambda$	$\Lambda^0\eta$	S	E	J
MgSO_4	28.385 ± 0.023	1.80 ± 0.15	0.022	0.9373	86.90	262.9	402.8
NiSO_4	31.677 ± 0.024	2.49 ± 0.12	0.033	1.0457	90.40	304.2	541.6
$\text{Cu}(\text{en})_2\text{SO}_4$	31.952 ± 0.024	2.26 ± 0.12	0.032	1.0549	90.71	307.6	504.9

pressure of <0.1 mm. (at $54\text{--}56^\circ$) gave a solvent of conductance $1\text{--}2 \times 10^{-5}$ mho. This was further subjected to fractional freezing. Two or three cycles of fractional freezing gave a sample of sufficiently low conductance. The solvent used in the preparation of solutions had a specific conductance of $2\text{--}4 \times 10^{-6}$ mho, a density of 1.1295, and a viscosity of 0.03302 poise at 25° .

Resistances were measured in 500-ml. erlenmeyer flask-type cells with lightly platinized electrodes. Three such cells were used for measurements.

Results and Discussions

In Table I are summarized the equivalent conductance and concentration data of the three salts in formamide. The data were analyzed by the Fuoss–Onsager equation⁶ for unassociated electrolytes in the form

$$\Lambda = \Lambda^0 - Sc^{1/2} + Ec \log c + Jc$$

(7) L. R. Dawson, T. M. Newell, and W. J. McCreery, *J. Am. Chem. Soc.*, **76**, 6024 (1954); L. R. Dawson, E. D. Wilhoit, and P. G. Sears, *ibid.*, **79**, 5906 (1957).

(8) J. E. Lind, J. J. Zwolenik, and R. M. Fuoss, *ibid.*, **81**, 1557 (1959).

on an IBM 7090 computer using a Fortran program similar to that described by Kay.⁹ (Higher terms in $c^{3/2}$ were neglected and the Einstein correction term in the viscosity was set to zero.)

The results of the analysis are given in Table II, where Λ^0 is the limiting equivalent conductance, a_J is the ion size parameter from J terms in the equation, $\sigma\Lambda$ is the standard deviation in $\Delta\Lambda$ units of the data from the equation, and $\Lambda^{0\eta}$ is the Walden product.

The data for the three salts fit the equation for unassociated dielectrolytes satisfactorily. The a_J values obtained, however, are unexpectedly small, showing a greater variance for MgSO_4 . This may be due to slight association or else one has to take into account the viscosity correction which was set to zero. However, on treating the data as an associated electrolyte, a negative a and K were obtained. The calculated crossover parameters^{2,3} from J and E are much different from the observed values. The smaller values of a_J and the nonconformity of calculated and observed crossover parameters suggest the need for a mixed solvent technique as an attempt to determine whether any small degree of association is taking place. Besides this, it may further give an idea whether any specific ion-solvent interaction is operating to reduce the ion association. We have started a broad program of studying several high-charge salts in a formamide-dioxane mixture.

Acknowledgment. The authors wish to thank Dr. R. P. Rastogi, Head of the Chemistry Department, for providing the necessary facilities, and Dr. G. Atkinson of the University of Maryland for data processing.

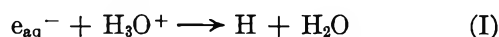
(9) R. L. Kay, *J. Am. Chem. Soc.*, **82**, 2099 (1960).

Isotope Effects in the Radiolysis and Photolysis of $\text{H}_2\text{O}-\text{D}_2\text{O}$ Mixtures^{1a}

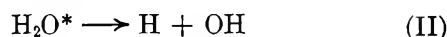
by M. Anbar^{1b} and D. Meyerstein

Chemistry Department, Stanford University, Stanford, California, and the Soreq Research Establishment, Rehovoth, Israel
(Received September 14, 1964)

The origin of hydrogen atoms formed in the radiolysis of neutral aqueous solutions was the subject of a number of studies.²⁻⁹ It has been suggested that these hydrogen atoms are formed by the reaction



occurring in the spur.^{3,4,6,7} On the other hand, it was proposed that they are formed through the dissociation of excited water molecules.^{2,5,8,9}



Measurement of the isotope effects in the formation of hydrogen from radiolyzed solutions has been previously applied in the elucidation of the primary reactions involved.^{3,6,10} Reaction I was shown to produce hydrogen atoms in acid solution.¹¹ It was of interest, therefore, to compare the isotope effect in the formation of hydrogen atoms from neutral and acid solutions. This isotope effect was also compared with the effect in the photolysis of acid aqueous iodide solutions, where reaction I was shown to take place.¹²

The isotopic composition of the hydrogen was determined using a C.E.C. 21-401 mass spectrometer. No correction for the fractionation in the mass spectrometer was included, but this should be the same for all the results and is smaller than 10%. In a $\text{H}_2\text{O}:\text{D}_2\text{O}$ 1:1 mixture, the isotope effect (α_M) on the formation of the molecular hydrogen is equal to the ratio $(\text{H}/\text{D})_{\text{evolved}}$. The isotope effect (α_A) in the formation of H atoms was calculated using the data of the "molecular" experiments, by subtracting from the measured values of masses 2 and 3 the contribution of molecular hydrogen, which is proportional to the value of mass 4 (as no mass 4 can be obtained by hydrogen abstracting from 2-propanol). The ratio between the remaining masses 2 and 3 is equal to $G_{\text{H}}/G_{\text{D}} = \alpha_A$. For the experiment with deuterated formate, it is supposed that no mass 2 was obtained from the radical yield (this introduces a small error as the compound was only 98% D). $G_{\text{H}}/G_{\text{H}_2}$ was calculated by dividing the sum of masses 2 and 3 after subtracting the proportional value of mass 4 by the sum of masses 4 plus the subtracted values. α_A' , the isotope effect in the formation of H atoms in photochemistry, is equal to the ratio of masses 2 and 3.

(1) (a) Based on experiments carried out at the Isotope Department, the Weizmann Institute of Science; (b) on sabbatical leave from the Weizmann Institute of Science.

(2) J. T. Allan and G. Scholes, *Nature*, **187**, 2188 (1960).

(3) C. Lifshitz, *Can. J. Chem.*, **40**, 1903 (1962).

(4) J. Rabani and G. Stein, *J. Chem. Phys.*, **37**, 1865 (1962).

(5) E. Hayon, *Nature*, **196**, 533 (1962).

(6) C. Lifshitz, *Can. J. Chem.*, **41**, 2175 (1963).

(7) S. Gordon, E. J. Hart, M. S. Matheson, J. Rabani, and J. K. Thomas, *Discussions Faraday Soc.*, **36**, 193 (1963).

(8) M. Anbar and D. Meyerstein, *J. Phys. Chem.*, **68**, 1713 (1964).

(9) M. Anbar and D. Meyerstein, *ibid.*, **68**, 3184 (1964).

(10) J. Jortner and G. Stein, *Intern. J. Appl. Radiation Isotopes*, **7**, 198 (1960).

(11) M. S. Matheson, *Radiation Res. Suppl.*, **4**, 1 (1964).

(12) J. Jortner, M. Ottolenghi, and G. Stein, *J. Phys. Chem.*, **66**, 2029 (1962).

All the other experimental details were identical with those previously described.^{8,9} The results are given in Table I.

Table I: Isotope Effects in the Formation of Hydrogen from Radiolyzed and Photolyzed Aqueous Solutions^a

Solute	pH	Radiolysis ^b			Photoly-
		α_M	α_A^d	G_H/G_{H_2}	sis ^e
KBr ($10^{-3} M$)	6	2.29	2.61	1.69	..
			2.26 ^e	1.58 ^e	..
			2.35 ^f	0.68 ^f	..
KBr ($10^{-3} M$) + H ₂ SO ₄ ($10^{-2} N$)	2	2.28	3.57	8.7	3.77
			2.76 ^e	2.76 ^e	..
KBr ($10^{-3} M$) + H ₂ SO ₄ (0.1 N)	1	2.34	3.60	8.7	..
KBr ($10^{-3} M$) + H ₂ SO ₄ (1.0 N)	0	2.30	3.44	10.0	..
KBr ($10^{-3} M$) + NH ₄ Cl (1.0 M) + K ₂ HPO ₄ ($2 \times 10^{-4} M$)	7.5	2.29	4.15	2.17	4.33

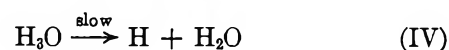
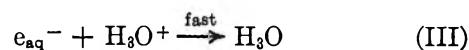
^a All solutions were evacuated and contained 1:1 hydrogen and deuterium. ^b Radiolysis with Co⁶⁰ γ -rays, dose rate 7500 r./min., total dose 1 Mrad. ^c Photolysis with a low-pressure mercury resonance lamp, these solutions contained 0.15 M KI and 0.1 M 2-propanol. ^d These solutions contained 0.1 M 2-propanol. ^e These solutions contained, in addition to the 2-propanol, 0.1 M acetone. ^f These solutions contained 0.05 M deuterated formate instead of 2-propanol.

The results for the atomic isotope effect (α_A) clearly show that the isotope effect for the residual hydrogen, in neutral solutions, is significantly lower than that in acid solutions. The effect of acetone (a good electron scavenger) in neutral solutions is small, whereas at pH 2 it causes a substantial decrease in the isotope effect.

These results prove that the atomic hydrogen is formed by two different mechanisms: "the residual hydrogen" is produced with an isotope effect of approximately 2.3, and hydrogen atoms in acid solution are formed through reaction I with an isotope effect larger than 3.6. This is in full agreement with Hayon's conclusion that in acid solution there are two mechanisms for the formation of hydrogen atoms.¹³ Further, it corroborates the conclusion that the residual hydrogen is formed mainly through reaction II.^{8,9} An alternative interpretation of the difference in the isotope effects is that reaction I takes place before H₃O⁺ reaches isotopic equilibration with the solvent. This would make it enriched in deuterium by a factor of 1.4,¹⁴ and diminish α_A by the same factor. This would mean that the recombination reaction I takes place within less than 1×10^{-11} sec. from the moment

of formation of H₃O⁺, which is the time of the H₃O⁺-H₂O equilibration.¹⁵ This is not plausible as the specific rate of reaction I is only $2.3 \times 10^{10} M^{-1} \text{sec.}^{-1}$ and the concentration of e_{aq}⁻ even in the "spur" is at least two orders of magnitude smaller than that of H₂O.

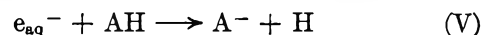
The isotope effect in reaction I is too large to be attributed to a diffusion isotope effect. This implies that the H₃O-activated complex does not decompose in the first vibration into H and H₂O. Thus reaction I may consist of two consecutive steps



This conclusion corroborates earlier suggestions that H₃O has a relatively long lifetime.^{16,17}

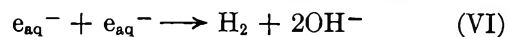
The isotope effect in photochemistry indicates that the kinetic behavior of e_{aq}⁻ formed photochemically from iodide solutions is identical with that formed by ionizing radiation.

It is of interest to note that the reaction of e_{aq}⁻ with a Brønsted acid AH (AH = NH₄⁺ or H₂PO₄⁻)¹⁸



involves an isotope effect larger than that of reaction I, a fact which was previously shown for the case of phosphate.³

The results for the "molecular" hydrogen show that the isotope effect on its formation is not changed in the pH range 0 to 6, in accord with earlier results.⁶ This fact throws some doubt on the accepted mechanism for the formation of molecular hydrogen *via* reaction VI.



In the presence of 1 M H₃O⁺, which is an efficient scavenger of e_{aq}⁻, the mechanism of H₂ formation should be partially changed to e_{aq}⁻ + H₃O⁺ → H + H₂O followed by H + H → H₂, resulting in an increased isotope effect in the formation of H₂. No such increase was observed, however. It should be noted that the molecular isotope effect is comparable with that of the residual hydrogen and the dependence upon the deuterium concentration is also similar.^{3,6} This might indicate that both species are formed through similar

(13) E. Hayon, *J. Phys. Chem.*, **68**, 1242 (1964).

(14) V. Gold, *Proc. Chem. Soc.*, 141 (1963).

(15) S. Meiboom, *J. Chem. Phys.*, **34**, 375 (1961).

(16) J. L. Magee, *Radiation Res. Suppl.*, **4**, 20 (1964).

(17) J. K. Thomas, *ibid.*, **4**, 111 (1964).

(18) J. Jortner, M. Ottolenghi, J. Rabani, and G. Stein, *J. Chem. Phys.*, **37**, 2488 (1962).

processes. This similarity may be fortuitous, however, as it has been shown that atomic and molecular hydrogen have different precursors,^{8,9} and that reactants like $\text{Co}(\text{NH}_3)_6^{+3}$ affect the yield of molecular hydrogen without diminishing the yield of atomic hydrogen in neutral solution.¹⁹ It may be concluded, therefore, that the origin of the "molecular" hydrogen in radiolyzed water remains an open question.

Acknowledgments. The authors wish to thank Dr. F. S. Klein for helpful discussions.

(19) M. Anbar and D. Meyerstein, *J. Phys. Chem.*, submitted.

Pure Acetic Acid and Acetic Anhydride and the Electrical Conductance and Dielectric Constant of This System^{1a,b}

by R. Thomas Myers

Department of Chemistry, Kent State University,
Kent, Ohio 44240 (Received September 16, 1964)

Research was contemplated using acetic acid as solvent. Acetic anhydride was used in the purification of the acid, as described below. Consequently, it seemed proper to study the effect of added acetic anhydride on the properties of the acid. The density, electrical conductance, and dielectric constant of the system acetic acid-acetic anhydride are reported below, along with novel—but very simple—methods of purifying these substances.

Experimental

Purification of the Acetic Acid. The first step was to determine the water content of the stock supply of reagent grade acetic acid by a calorimetric method similar to that of Greathouse, *et al.*² In order to avoid the rise of temperature upon addition of the perchloric acid catalyst (due to reaction of the water therein with the acetic anhydride) a solution of perchloric acid in acetic acid was used as catalyst. The catalyst solution consisted of 6 ml. of 70% perchloric acid dissolved in 39 ml. of acetic acid to which was then added in small portions slightly more than the theoretical amount of acetic anhydride (14.0 ml.). A typical run was carried out as follows. To 200.0 ml. of acetic acid in the calorimeter (a common silvered vacuum bottle) was added 8.0 ml. of anhydride. The liquids were mixed by swirling the bottle and the temperature was estimated to the nearest 0.01° on a thermometer calibrated in 0.1° steps.

Then 2.0 ml. of the catalyst solution was added and a temperature-time curve drawn. The straight portion of this curve was extrapolated back to zero time and the temperature rise computed. This can be duplicated to within about 0.03° in separate runs. The heat capacity of the calorimeter was determined by adding to the stock acetic acid a known amount of water and repeating the experiment. This gives two equations in two unknowns (the amount of water in the stock acetic acid and the heat capacity of the calorimeter). Using the heat of reaction and specific heat data given by Greathouse, the two equations can be solved simultaneously.

Then, knowing the water content of the stock solution, the pure acetic acid is prepared by adding the theoretical amount (plus a 2% excess) of acetic anhydride necessary to react with the water in the stock solution. The reaction is catalyzed by the addition of 1 g. of anhydrous 5-sulfosalicylic acid/l. This solution is kept overnight at about 100°, then distilled at total take-off through a 1-m. column, packed with glass helices and insulated with 2.5 cm. of glass fiber insulation. This new and simple process will result in acetic acid with a specific conductance of $0.6 \times 10^{-8} \text{ ohm}^{-1} \text{ cm.}^{-1}$, provided it is distilled directly into the conductance cell.

Purification of Acetic Anhydride. The acetic anhydride is purified by a novel azeotropic distillation process. Toluene is added to reagent grade acetic anhydride and the mixture is distilled through a 38-cm. column with silvered evacuated jacket, packed with glass helices or Heli-Pak,³ at a reflux ratio of 30:1. The first material to come off is the acetic acid-toluene azeotrope, boiling at 100.6° and containing 28% acetic acid.⁴ Next, toluene distills at 110.8°, and finally acetic anhydride. (Within the limits of accuracy of the experiment the acetic anhydride-toluene system is non-azeotropic at 730 mm.). At this stage the reflux ratio is changed to 20:1. Acetic anhydride of a specific conductance of about 0.5×10^{-8} can be obtained if distilled directly into the conductivity cell. The distillate reaches this low conductance after about half of the charge has distilled.

Conductance Measurements. The conductance cell was a Washburn type with a cell constant of 0.0161

(1) (a) Presented in part at the 138th National Meeting of the American Chemical Society, New York, N. Y., Sept. 1960 (Abstracts of Papers, p. 58S); (b) partially supported by the Directorate of Chemical Sciences of the Air Force Office of Scientific Research, under Contract No. AF 49 (638)-631.

(2) L. H. Greathouse, H. J. Janssen, and C. H. Hagdill, *Anal. Chem.*, **28**, 357 (1956).

(3) Obtained from Podbielniak, Inc., Chicago, Ill.

(4) L. H. Horsley, "Azeotropic Data," American Chemical Society, Washington, D. C., 1952, p. 48.

cm.⁻¹. The bridge utilized a Leeds and Northrup shielded ratio box with Wagner ground, a 1 to 111,111-ohm General Radio Company decade resistor, with a 100-kilohm resistor in parallel. The accuracy of resistance readings is considered to be about 0.1%.

Dielectric Constant Measurements. The dielectric constant was measured at 1 Mc., using a sample holder similar in design and dimensions to the one described by Smyth and co-workers.⁵ In view of the extremely corrosive nature of the liquids used in the investigation, the inner parts of the copper cell were gold-plated and given a dispersion coating of Teflon about 0.1 mm. thick. This latter, although offering very good resistance to corrosion, had the effect of making the calibration curve nonlinear, and the cell slightly variable in capacity. The cell was calibrated using Spectrograde liquids from Eastman: CCl₄, C₆H₆, CHCl₃, CH₂Cl₂, (CH₂Cl)₂, C₅H₅N, (CH₃)₂CHOH, CH₃COCH₃, and CH₃-OH. The capacitance was measured by use of a Twin-T impedance measuring circuit from General Radio Co.

Preparation of Mixtures. Mixing of solutions was accomplished by direct distillation into a small flask attached by ground joints to the distillation apparatus. The samples were weighed and then transferred through ground joints to the conductance cell. After conductance measurement the liquid was poured into the dielectric constant cell. Of course, some contact with air was unavoidable at this stage, but the effect of traces of absorbed moisture on the dielectric constant is much less than on the conductance. When density measurements were made, the liquid was transferred to the pycnometer from the conductance cell *via* ground joints.

All measurements were carried out at 25 ± 0.02°, as judged by a thermometer calibrated by the U. S. Bureau of Standards.

Results

The results for electrical conductance and dielectric constant are shown in Figure 1. The density and refractive index of mixtures are given in Table I. The data for density are in perfect qualitative agreement with the results of Drucker and Kassel⁶ at 15°. Refractive index data apparently are not available.

Discussion

The fact that the procedure described for removal of water from acetic acid yields a material of such low conductance certainly indicates that water is the chief volatile impurity in present-day reagent grade acid.

The situation with respect to acetic anhydride is more complicated. After the acetic acid-toluene azeotrope

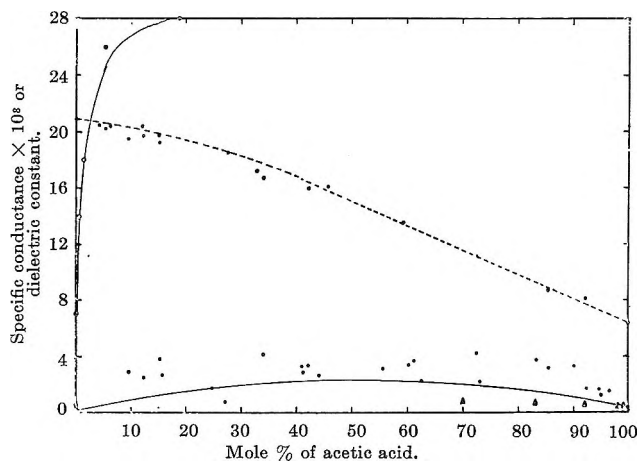


Figure 1. Specific conductance and dielectric constant of acetic acid-acetic anhydride mixtures: upper left curve, conductance data of Hoover; lower curve, conductance data of present study and of Brun (\blacktriangle); middle curve, dielectric constant.

Table I: Density and Refractive Index of Acetic Acid-Acetic Anhydride Mixtures

Mole fraction of AcOH	d_{25}^4	n_D^{25}
0	1.0747	1.3878
0.0619	1.0738	1.3874
0.1203	1.0724
0.1215	1.0733	1.3871
0.1513	1.0717	1.3862
0.3400	1.0679	1.3842
0.4208	1.0656	1.3826
0.5933	1.0607	1.3799
0.8533	1.0498	1.3738
0.9212	1.0478	1.3724
1.0000	1.0435	1.3704

and the excess toluene have come over, the anhydride which distills has a high electrical conductance, around 5×10^{-8} ohm⁻¹ cm.⁻¹. As this product which first distills over stands in the conductance cell there is a gradual increase in conductance, with a constant value reached in about 24 hr. This is true also of the mixtures of this first distillate with acetic acid. Neither this high conductance nor the increase in conductance can be due to dissolving adsorbed water from the cell, because the same result is obtained when the cell has stood for a long time with pure acetic anhydride.

However, as the distillation proceeds, the conductance of the distillate becomes less and less, reaching an

(5) W. P. Conner, R. P. Clarke, and C. P. Smyth, *J. Am. Chem. Soc.*, **64**, 1379 (1942).

(6) J. Timmermans, "Physico-Chemical Constants of Binary System," Vol. 2, Interscience Publishers, Inc., New York, N. Y., 1959, p. 625.

almost constant value after about half of the charge has distilled. A product has been obtained with a conductance as low as $0.3 \times 10^{-8} \text{ ohm}^{-1} \text{ cm.}^{-1}$. This product of low conductance does not exhibit the phenomenon of increasing conductance on standing in the conductance cell which is shown by the product in the early stage of distillation, either by itself or mixed with the acetic acid. The previous facts indicate that the conducting impurity is volatile, with a boiling point just slightly lower than that of the anhydride. Qualitative experiments show that this impurity is not water, acetic acid, 2,4-pentanedione, or ethylidene diacetate. The increasing conductance on standing indicates that a chemical reaction involving the impurity is occurring. Except for the very slightly probable simultaneous distillation of two impurities, the only probable single substance is one involving a keto-enol isomerization. At this time diketene, or some reaction product of diketene, is suspected. This problem is being investigated further.

In any event, the conductance found for pure acetic anhydride is about one order of magnitude less than most values previously reported.⁷ Likewise, the conductances of mixtures of the acid and anhydride are about one order of magnitude less than previous values.⁷

An unusual phenomenon was the relatively enormous increase in conductance when the first fractions of acetic anhydride (of about $5 \times 10^{-8} \text{ ohm}^{-1} \text{ cm.}^{-1}$) were mixed with pure acetic acid. Conductances of these mixtures were as high as 50×10^{-8} and were in essential agreement with the results of Hoover. The conductance of these mixtures increases slowly for about 24 hr. The indication is that a chemical reaction is occurring between acetic acid and an impurity in the anhydride.

The presence of an ionic solute in supposedly "pure" acetic anhydride (and the enormous increase in conductance caused by this impurity on addition of acetic acid) is reason to question a great deal of the data reported in the literature using acetic anhydride as solvent.

The conductance data reported here essentially verify the results of Brun,⁸ with the exception that the conducting impurity in acetic anhydride appears to be volatile, whereas Brun's method of distillation indicates that the impurity is nonvolatile.

Acknowledgment. A large amount of the data was obtained by Mr. Donald Knapp and Miss Viola M. L. Sun.

(7) For a good summary, see T. B. Hoover and A. W. Hutchinson, *J. Am. Chem. Soc.*, **83**, 3400 (1961).

(8) T. S. Brun, *Univ. i Bergen Arbok, Naturvitenskap. Rekke*, No. 12, 1 (1952).

On the Polarizability of Rare Gas Atoms

by Ralph L. Amey

Douglas Aircraft Company, Inc., Missile and Space Systems Division, Santa Monica, California (Received October 6, 1964)

Calculations of several authors^{1,2} indicate that the effective polarizability, α , of an atom may decrease with increasing density, contrary to the predictions of the dielectric theory derived for very low densities.³ These predictions have been experimentally verified in the case of liquefied rare gases and methane.^{4,5} ten Seldam and de Groot, employing an isolated, compressed atom model, unaffected by fluctuations in α , as well as by any attractive forces between atoms, demonstrated a decrease in α at high pressures. Jansen and Mazur showed that α remains a molecular constant for a harmonic oscillator but that, when a more realistic model is considered, the effective polarizability becomes a function of temperature and density. In the latter calculation, their employment of large intermolecular distances, corresponding to lower densities, is equivalent to the use of a potential softer than that of the harmonic oscillator.

In this note are presented calculations based on two rather simple potential energy models. The first is that of a harmonic oscillator, bounded at the points $X = \pm X_0$ by an infinite potential barrier

$$V(X) = \infty \quad [X < -X_0, X > X_0] \\ = \frac{1}{2} kX^2 \quad [-X_0 \leq X \leq X_0]$$

The second is that of a particle in the potential field

$$V(X) = V_0 \tan^2 \left(\frac{\pi X}{a} \right) \quad \left[-\frac{a}{2} \leq X \leq \frac{a}{2} \right]$$

In the first case the boundary condition changes the normalization constant, N_n , of the harmonic oscillator through the orthogonality calculations so that it now appears as

$$N_n = \left[A_n + 2^n n! \int_{-a}^a e^{-\xi^2} d\xi \right]^{-1/2}$$

where

(1) C. A. ten Seldam and S. R. de Groot, *Physica*, **18**, 905 (1952).

(2) L. Jansen and P. Mazur, *ibid.*, **21**, 193 (1955).

(3) J. G. Kirkwood, *J. Chem. Phys.*, **4**, 592 (1936).

(4) R. L. Amey and R. H. Cole, *ibid.*, **40**, 146 (1964).

(5) G. O. Jones and B. L. Smith, *Phil. Mag.*, **5**, 355 (1960); C. M. Knobler, C. P. Abbiss, and C. J. Pings, *J. Chem. Phys.*, **41**, 2200 (1964).

$$A_n = -2e^{-a^2} \left[\sum_{i=0}^{n-1} \frac{2^i n!}{(n-i)!} H_{n-i} H_{n-i-1} \right]_0^a$$

The quantity in brackets is to be evaluated at $\xi = 0$ and $\xi = a$, and $H_n(\xi)$ is the n th Hermite polynomial defining the wave function $\Psi_n = N_n H_n(\xi) \exp(-1/2\xi^2)$ in terms of the dimensionless parameter $\xi = g^{1/2} X$, where $g^{1/2} = (4\pi^2 m v_0 / h)^{1/2}$ and $a = g^{1/2} x_0$.

If $-eXF_0$ is considered as a perturbation on the harmonic oscillator system owing to the electric field, then the field contributes initially to the second-order perturbation term, ΔW .

Since $-\partial W / \partial F_0 = m = \alpha F_0$, where m is the induced electric moment, an expression for the polarizability is obtained

$$\alpha = \frac{e^2}{2k} \times \left[\frac{2^{n+1} n! \int_{-a}^a \exp(-\xi^2) d\xi - (4n^2 A_{n-1} - A_{n+1})}{A_n + 2^n n! \int_{-a}^a \exp(-\xi^2) d\xi} \right] \quad (1)$$

It is observed that for $A = 0$, eq. 1 reduces to the usual result for the harmonic oscillator case, $\alpha = e^2/k$. It is also seen that, for the lowest level where $n = 0$, one obtains

$$\alpha_{n=0} = \frac{e^2}{k} \left[1 - \frac{2a \exp(-a^2)}{\int_{-a}^a \exp(-\xi^2) d\xi} \right] \quad (2)$$

and that, for all values of a , α will be less than e^2/k , the normal harmonic oscillator value. By thus putting a bound on the permissible region of the particle, one finds that the polarizability of the particle is decreased. This is equivalent to using a harder potential function at small distances of separation. For a maximum displacement of $\sim 1 \text{ \AA}$, this decrease is about 2%.

In the second case, where $V(X) = V_0 \tan^2(\pi X/a)$, the function is asymptotic to $X = \pm a/2$, and, in the region near $X = 0$, it approximates the harmonic oscillator function. The behavior of a particle in such an environment is obtained from solution of the corresponding Schrödinger equation. The wave function is expressed in terms of Gegenbauer polynomials, $C_n^\beta(\sin Z)$,⁶⁻⁸ and is given by $\Psi_n(Z) = N_n (\cos Z)^\beta C_n^\beta(\sin Z)$, where $\beta = 1/2 + \sqrt{v + 1/4}$, $v = 2a^2 m V_0 / \pi^2 \hbar^2$, and $Z = \pi X/a$.

If Z_0 is kept undetermined, N_n then may be written as

$$N_n = \left[A_n + (-2)^n \frac{G_n \Gamma(\beta + n)}{\Gamma(\beta)} \times \int_{-Z_0}^{Z_0} (\cos Z)^{2\beta + 2n - 1} dZ \right]^{-1/2}$$

where

$$A_n = \left[\sum_{j=0}^{n-1} (-2)^j (\cos Z)^{2\beta - 1} \times \frac{G_n \Gamma(\beta + j)}{G_{n-j-1} \Gamma(\beta)} C_{n-j}^{\beta+j} C_{n-j-1}^{\beta+j+1} \right]_{-Z_0}^{Z_0}$$

and

$$G_n = \frac{(-2)^n \Gamma(\beta + n) \Gamma(2\beta + n)}{n! \Gamma(\beta) \Gamma(2\beta + 2n)}$$

If the system is perturbed by a force of the form $-eF_0 \sin Z$ (for small values of Z , $-eF_0 \sin Z \cong -eF_0 Z$), it is possible, as in the previous case, to derive an expression for α . When V is large and $n = 0$, the ground-state value for α is given by

$$\alpha_{n=0} \cong \frac{e^2 a^2}{2\pi^2 \beta^2} \left[1 - \frac{2 \sin Z_0 (\cos Z_0)^{2\beta - 1}}{\int_{-Z_0}^{Z_0} (\cos Z)^{2\beta - 1} dZ} \right] \quad (3)$$

The second term within the brackets is a function which increases slightly with decreasing values of Z_0 . Hence, $\alpha_{n=0}$ decreases as Z_0 diminishes from its maximum value of $\pi/2$. At $\pi/2$, the second term vanishes, and α reduces to $e^2 a^2 / 2\pi^2 \beta^2$, corresponding to a harmonic oscillator.

In both types of calculation, the polarizability appears to be sensitive to changes in boundary conditions. This is best seen in the second example where the function is restricted naturally by its asymptotic character.

It is gratifying that such simple calculations as these reflect the experimental observations.⁴ It appears that a more realistic model might utilize a potential harder than the harmonic oscillator at small intermolecular distances and softer at large separations.^{9,10}

Since changes in the electron cloud configuration will occur in high density regions, modification of the accompanying wave functions will be required to maintain orthogonality conditions. It is believed that such a treatment is necessary in order to represent satisfactorily the microscopic dielectric behavior at high and low densities.

Acknowledgment. Grateful appreciation is expressed for the many helpful discussions the author had with Drs. R. H. Cole and R. A. Willett.

(6) M. Abramowitz and I. Stegun, Ed., "Handbook of Mathematical Functions," National Bureau of Standards, Washington, D. C., 1964, p. 771.

(7) A. Erdeli, et al., Ed., "Higher Transcendental Functions," Vol. 1, and 2, McGraw-Hill Book Co., Inc., New York, N. Y., 1953, Chapters 3 and 10.

(8) P. M. Morse, Ed., "Methods of Theoretical Physics," Vol. 1 and 2, McGraw-Hill Book Co., Inc., New York, N. Y., 1953, Chapters 6 and 12.

(9) G. J. Oudemans and R. H. Cole, *J. Chem. Phys.*, **31**, 843 (1959).

(10) D. R. Johnston, et al., *ibid.*, **33**, 1310 (1960).

The Conductance of Some Alkali Metal Salts in Hydrogen Cyanide

by R. H. Davies

Department of Chemistry, University College, Swansea, Wales

and E. G. Taylor

Thompson Chemical Laboratory, Williams College, Williamstown, Massachusetts (Received September 24, 1964)

In an attempt to take advantage of the recent modification of the Onsager conductance equation, we have measured the conductance of some alkali metal salts in hydrogen cyanide to higher concentrations than used in an earlier investigation¹ and have made most of the

Table I: Conductance of Salts in HCN at 18 and 25°

18°		25°	
10 ^c	Λ	10 ^c	Λ
NH ₄ Cl		NH ₄ Cl	
69.62	351.4	68.62	372.3
41.36	361.0	40.76	381.9
22.56	367.8	15.74	392.9
15.97	371.4		
LiBr		LiBr	
135.4	314.5	133.4	333.2
93.25	320.5	29.16	353.7
51.16	328.2	5.644	363.3
29.59	333.5		
NaCl		NaCl	
77.20	317.9	76.07	338.2
50.62	323.8	49.89	344.1
30.04	328.8	29.60	349.2
19.45	331.4	19.16	352.3
KCl		KCl	
148.7	329.2	146.5	349.0
95.05	336.6	93.65	356.4
47.09	344.4	46.40	364.7
29.56	348.5	29.13	368.9
RbCl		RbCl	
122.6	336.2	120.8	356.3
68.82	343.6	67.82	363.9
32.96	350.8	32.48	371.3
18.31	354.7		
CsCl		CsCl	
148.7	339.5	141.7	359.7
96.87	345.8	95.47	366.1
50.02	353.3	49.30	373.4
28.87	357.7	28.45	378.4
Cesium Picrate		Cesium Picrate	
91.67	272.5	90.33	289.7
49.15	279.1	24.95	302.0
25.32	284.4	9.800	308.2
17.16	286.5		

measurements at 25° as well as at 18°. The details have been reported in a recent note.² The salts used were of the highest quality available (RbCl and CsCl were of spectroscopic grade) and were recrystallized prior to use as well as between runs.

In calculating concentrations from the weight data, the following values of a ($\times 10^4$) were used in obtaining the densities of the solutions: LiBr, NaCl, KCl, 7.5; RbCl, 7.7; CsCl, 7.6.

Typical conductance data for the salts are summarized in Table I.

Table II: Limiting Equivalent Conductances of Salts in HCN

	18°	25°
NH ₄ Cl	384.5	407.5
LiBr	349	370.8
NaCl	344.2	366.0
KCl	363.5	385.4
RbCl	366.6	388.5
CsCl	372.5	394.3
Cesium picrate	297.6	316.5

Values of Λ_0 (Table II) have been obtained by extrapolation from plots of $\Lambda' (\Lambda + Sc^{1/2} - Ec \ln c)$ vs. c .

As stated in the earlier note, the relatively low precision precludes one attaching quantitative significance to the slopes (J) of the plots, but it is worth noting that the values of the slopes for NH₄Cl, LiBr, and NaCl at 18 and 25° are negative (less than -300), while that for KCl at 18° is almost zero. In view of the catabatic behavior noted earlier¹ for both lithium and ammonium salts, it seems likely that the inclusion of an association term in the J function is responsible for negative values of the slopes. The remaining slopes have positive and reasonable values.

Approximate values of limiting ionic conductances based on values taken for the Bu₄N⁺ ion at 18 and 25° as 90 and 96, respectively,² are presented in Table III.

Table III: Limiting Equivalent Ionic Conductances in HCN at 18 and 25°

	18°	25°
NH ₄ ⁺	168	180
Li ⁺	133	142
Na ⁺	127	138
K ⁺	148	158
Rb ⁺	150	161
Cs ⁺	156	167

(1) J. E. Coates and E. G. Taylor, *J. Chem. Soc.*, 1245, 1495 (1936).

(2) R. H. Davies and E. G. Taylor, in press.